UNDERSTANDING BRAIN AGING

EDITED BY: Hans J. Grabe, Reinhold Schmidt, Stephanie Debette and Mohamad Habes
PUBLISHED IN: Frontiers in Aging Neuoscience and Frontiers in Psychiatry

frontiers Research Topics

ISSN 1664-8714
ISBN 978-2-88971-151-2
DOI 10.3389/978-2-88971-151-2

About Frontiers

Frontiers is more than just an open-access publisher of scholarly articles: it is a pioneering approach to the world of academia, radically improving the way scholarly research is managed. The grand vision of Frontiers is a world where all people have an equal opportunity to seek, share and generate knowledge. Frontiers provides immediate and permanent online open access to all its publications, but this alone is not enough to realize our grand goals.

Frontiers Journal Series

The Frontiers Journal Series is a multi-tier and interdisciplinary set of open-access, online journals, promising a paradigm shift from the current review, selection and dissemination processes in academic publishing. All Frontiers journals are driven by researchers for researchers; therefore, they constitute a service to the scholarly community. At the same time, the Frontiers Journal Series operates on a revolutionary invention, the tiered publishing system, initially addressing specific communities of scholars, and gradually climbing up to broader public understanding, thus serving the interests of the lay society, too.

Dedication to Quality

Each Frontiers article is a landmark of the highest quality, thanks to genuinely collaborative interactions between authors and review editors, who include some of the world's best academicians. Research must be certified by peers before entering a stream of knowledge that may eventually reach the public - and shape society; therefore, Frontiers only applies the most rigorous and unbiased reviews.
Frontiers revolutionizes research publishing by freely delivering the most outstanding research, evaluated with no bias from both the academic and social point of view. By applying the most advanced information technologies, Frontiers is catapulting scholarly publishing into a new generation.

What are Frontiers Research Topics?

Frontiers Research Topics are very popular trademarks of the Frontiers Journals Series: they are collections of at least ten articles, all centered on a particular subject. With their unique mix of varied contributions from Original Research to Review Articles, Frontiers Research Topics unify the most influential researchers, the latest key findings and historical advances in a hot research area! Find out more on how to host your own Frontiers Research Topic or contribute to one as an author by contacting the Frontiers Editorial Office: frontiersin.org/about/contact

UNDERSTANDING BRAIN AGING

Topic Editors:
Hans J. Grabe, University of Greifswald, Germany
Reinhold Schmidt, Medical University of Graz, Austria
Stephanie Debette, Université de Bordeaux, France
Mohamad Habes, The University of Texas Health Science Center at San Antonio, United States

Citation: Grabe, H. J., Schmidt, R., Debette, S., Habes, M., eds. (2022). Understanding Brain Aging. Lausanne: Frontiers Media SA.
doi: 10.3389/978-2-88971-151-2

Table of Contents

frontiers in Psychiatry

ORIGINAL RESEARCH
published: 26 July 2019
doi: 10.3389/fpsyt.2019.00524

Brain Peak Width of Skeletonized Mean Diffusivity (PSMD) and Cognitive Function in Later Life

Ian J. Deary[1,2], Stuart J. Ritchie[1,2,3], Susana Muñoz Maniega[2,4,5], Simon R. Cox[1,2,5], Maria C. Valdés Hernández[2,4,5,6], Michelle Luciano[1,2], John M. Starr[2,7†], Joanna M. Wardlaw[2,4,5,6] and Mark E. Bastin[2,4,5]*

[1] Department of Psychology, University of Edinburgh, Edinburgh, United Kingdom, [2] Centre for Cognitive Ageing and Cognitive Epidemiology, University of Edinburgh, Edinburgh, United Kingdom, [3] Social, Genetic and Developmental Psychiatry Research Centre, Institute of Psychiatry, Psychology and Neuroscience, King's College London, London, United Kingdom, [4] Brain Research Imaging Centre, Division of Neuroimaging Sciences, University of Edinburgh, Edinburgh, United Kingdom, [5] Scottish Imaging Network, A Platform for Scientific Excellence (SINAPSE), University of Edinburgh, Edinburgh, United Kingdom, [6] Edinburgh Dementia Research Centre, Dementia Research Institute, University of Edinburgh, Edinburgh, United Kingdom, [7] Alzheimer Scotland Dementia Research Centre, University of Edinburgh, Edinburgh, United Kingdom

OPEN ACCESS

Edited by:
Mohamad Habes, University of Pennsylvania, United States

Reviewed by:
Anil Man Tuladhar, Radboud University Nijmegen Medical Centre, Netherlands
Owen Williams, National Institute on Aging (NIA), United States

***Correspondence:**
Ian J. Deary
i.deary@ed.ac.uk

[†]Deceased

Specialty section:
This article was submitted to Aging Psychiatry, a section of the journal Frontiers in Psychiatry

Received: *02 April 2019*
Accepted: *03 July 2019*
Published: *26 July 2019*

Citation:
Deary IJ, Ritchie SJ, Muñoz Maniega S, Cox SR, Valdés Hernández MC, Luciano M, Starr JM, Wardlaw JM and Bastin ME (2019) Brain Peak Width of Skeletonized Mean Diffusivity (PSMD) and Cognitive Function in Later Life. Front. Psychiatry 10:524. doi: 10.3389/fpsyt.2019.00524

It is suggested that the brain's peak width of skeletonized water mean diffusivity (PSMD) is a neuro-biomarker of processing speed, an important aspect of cognitive aging. We tested whether PSMD is more strongly correlated with processing speed than with other cognitive domains, and more strongly than other structural brain MRI indices. Participants were 731 Lothian Birth Cohort 1936 members, mean age = 73 years (SD = 0.7); analytical sample was 656–680. Cognitive domains tested were as follows: processing speed (5 tests), visuospatial (3), memory (3), and verbal (3). Brain-imaging variables included PSMD, white matter diffusion parameters, hyperintensity volumes, gray and white matter volumes, and perivascular spaces. PSMD was significantly associated with processing speed (–0.27), visuospatial ability (–0.23), memory ability (–0.17), and general cognitive ability (–0.25); comparable correlations were found with other brain-imaging measures. In a multivariable model with the other imaging variables, PSMD provided independent prediction of visuospatial ability and general cognitive ability. This incremental prediction, coupled with its ease to compute and possibly better tractability, might make PSMD a useful brain biomarker in studies of cognitive aging.

Keywords: aging, cognition, processing speed, structural MRI, diffusion MRI, white matter, PSMD

INTRODUCTION

Cognitive functions such as processing speed, visuospatial reasoning, and some aspects of memory decline, on average, as people grow older, with deleterious effects on people's quality of life (1–3). Processing speed has a special place among the cognitive domains; it has been suggested as a foundation for long-standing differences in, and aging of, other cognitive domains (4–9). With regard to understanding of cognitive aging, detailed attention has been advocated in the study of the psychometric aspects of processing speed and its potential neurobiological correlates (10). Therefore, understanding the neurobiological foundations of people's differences in, and aging of, processing speed and other cognitive domains is a research priority (5, 11).

Even among those with no overt disease, brain-imaging-derived biomarkers of brain deterioration correlate with performance on cognitive tests. Such markers include cerebral tissue volumes and brain atrophy, and indicators of white matter health and so-called cerebral small vessel disease (12–17). Cerebral small vessel disease is an important contributor to vascular-based cognitive deterioration (18). Recognizing that, a brain imaging marker named "peak width of skeletonized [water] mean diffusivity" (PSMD) was developed and studied with respect to its association with processing speed (19). PSMD is based on skeletonization and histogram analysis of diffusion tensor magnetic resonance imaging (DT-MRI) data. PSMD was examined in comparison with other brain imaging markers in patients with inherited and sporadic cerebral small vessel disease, and in patients with Alzheimer's disease and healthy controls (19). PSMD was reported to be associated with processing speed in all samples. The authors reported that it correlated with speed more strongly than other brain imaging markers such as brain volume, volume of white matter hyperintensities, and volume of lacunes.

However, although a special association between PSMD and the cognitive domain of processing speed was emphasized by Baykara et al. (19), no other cognitive domains were examined in their study. The Trail Making Test—measured in most of their samples—is associated with general fluid cognitive ability as well as processing speed (20–22). Therefore, PSMD might correlate with cognitive abilities more generally. As Schmidt (23) explained, all cognitive domains correlate positively together, and, therefore, associations with any one domain might represent an association with general cognitive function rather than, or in addition to, a domain-specific relationship. Before concluding that PSMD is a special neuro-biomarker of the important cognitive domain of processing speed, formal tests of whether PSMD correlates more strongly with processing speed, general cognitive ability, or other cognitive domains are needed. We sought to accomplish this in the present study.

Our present study includes experimental and psychophysical measures of processing speed in addition to more widely used paper-and-pencil assessments of speed. The former, arguably, rely less on acculturalized learning than do the paper-and-pencil-tests, and they are reckoned to be purer measures of speed (6, 24). Therefore, our study affords the examination of relatively specific tests of processing speed. Correlations of the different processing speed tests with PSMD are compared with those from a wide variety of other cognitive measures tapping broad cognitive domains. We also compare PSMD–cognitive function correlations with other structural brain imaging biomarkers' cognitive correlations to test whether its association with processing speed and other cognitive domains is especially strong. Here, we run these analyses in a narrow-age sample of mostly healthy, community-dwelling older people: the Lothian Birth Cohort 1936 (LBC1936).

MATERIALS AND METHODS

Participants

All participants were members of the LBC1936 (25–27). This started (LBC1936, Wave 1) as a sample of 1,091 people who were recruited between 2004 and 2007 at about 70 years of age. All lived independently in the community, were generally healthy, and travelled to a clinical research facility for assessment. Most of them had taken part in the Scottish Mental Survey 1947 at age 11 years. At Wave 1, they undertook extensive cognitive, medical, biomarker, psycho-social, and other assessments. The assessments were repeated at Wave 2, about 3 years later at mean age 73 years, with the addition of a detailed structural brain MRI scan (28). Of the 886 who returned at Wave 2, over 700 agreed to undertake a brain scan. All variables described below were collected at Wave 2, unless otherwise noted. Ethical approval for the LBC1936 study came from the Multi-Centre Research Ethics Committee for Scotland (MREC/01/0/56; 07/MRE00/58) and the Lothian Research Ethics Committee (LREC/2003/2/29). All participants, who were volunteers and received no financial or other reward, completed a written consent form before any testing took place.

Cognitive Tests

The cognitive test data used here are from Wave 2, at mean age 73 years. All participants had already taken the same cognitive test battery at age 70 years, ensuring that they were familiar with the tests.

Processing Speed

Because processing speed was the key cognitive variable mentioned in relation with PSMD (19), it is apposite that the LBC1936 has been assessed for processing speed in detail. There were five tests of processing speed: two were paper-and-pencil psychometric tests; two were experimental, reaction time tests; and one was a psychophysical test. The psychometric tests were from the Wechsler Adult Intelligence Test-III^{UK}: Digit Symbol and Symbol Search (29). The reaction time tests were simple reaction time (8 practice trials, 20 test trials) and 4-choice reaction time (8 practice trials, 40 test trials), assessed on a stand-alone device that was used in the UK's Health and Lifestyle Study (24). The psychophysical test was inspection time, assessed using a bespoke computer program (30). The inspection time task required the participant to indicate which of two briefly presented parallel vertical lines was longer; no speeded response was required, and only the correctness of the response was recorded. Stimuli were backward-masked. There were 150 trials, with 10 trials at each of 15 durations, ranging from 6 ms to 200 ms. Durations were presented at random, using a method of constant stimuli.

Visuospatial Ability

This was assessed using Matrix Reasoning and Block Design from the Wechsler Adult Intelligence Test-III^{UK} (29) and Spatial Span (total score of forward and backward) from the Wechsler Memory Scales-III^{UK} (29).

Verbal Memory

This was assessed using Verbal Paired Associates (total score) and Logical Memory (immediate and delayed total score) from the Wechsler Memory Scales-III^{UK} (29) and Backward Digit Span from the Wechsler Adult Intelligence Test-III^{UK} (29).

Crystallized Ability

This was assessed using the National Adult Reading Test (31), the Wechsler Test of Adult Reading (32), and a phonemic verbal fluency test (using the letters C, F, and L) (25).

Demographic and Health-Related Variables

The participant's own occupational social class was based on their most prestigious job prior to retirement and assessed on a six-point scale from manual to professional (33). Education was assessed as the number of years of full-time education. These were assessed at Wave 1. Smoking was assessed at interview and classed as never, ex-, or current. The Mini-Mental State Examination (34) was used as a screen for cognitive pathology and not used as part of the cognitive test battery. Participants reported if they had a history of hypertension, cardiovascular disease, or diabetes.

Magnetic Resonance Imaging

All MRI data were acquired using a GE Signa Horizon HDxt 1.5 T clinical scanner (General Electric, Milwaukee, WI, USA) using a self-shielding gradient set with a maximum gradient strength of 33 mT/m and an 8-channel phased-array head coil. The full details of the imaging protocol can be found in the LBC1936 imaging protocol paper (28). Briefly, the DT-MRI examination consisted of seven T_2-weighted (b = 0 s mm^{-2}) and sets of diffusion-weighted (b = 1,000 s mm^{-2}) single-shot spin-echo echo-planar (EP) volumes acquired with diffusion gradients applied in 64 non-collinear directions (35). Volumes were acquired in the axial plane, with a field of view of 256 × 256 mm, contiguous slice locations, and image matrix and slice thickness designed to give 2-mm isotropic voxels. The repetition and echo time for each EP volume were 16.5 s and 98 ms, respectively. DT-MRI data were converted from DICOM (http://dicom.nema.org) to NIfTI-1 (http://nifti.-nimh.nih.gov/nifti-1) format using the TractoR package (http://www.tractor-mri.org.uk) (36). FSL tools (http://www.fmrib.ox.ac.uk/fsl) (37) were then used to extract the brain, remove bulk motion and eddy-current-induced distortions by registering all subsequent volumes to the first T_2-weighted EP volume (38), estimate the water diffusion tensor, and calculate parametric maps of mean diffusivity (MD) and fractional anisotropy (FA) from its eigenvalues using DTIFIT (39).

Peak Width of Skeletonized Water MD

Automatic calculation of PSMD followed the procedure described by Baykara et al. (19) using the freely available script they provided (http://www.psmd-marker.com). Briefly, the DT-MRI data were processed using the standard Tract-based Spatial Statistics (TBSS) (40) pipeline available in FSL with histogram analysis performed on the resulting white matter MD skeletons. First, all participants' FA volumes were linearly and non-linearly registered to the standard space FMRIB 1-mm FA template. Second, a white matter skeleton was created from the mean of all registered FA volumes. This was achieved by searching for maximum FA values in directions perpendicular to the local tract direction in the mean FA volume. An FA threshold of 0.2 was applied to the mean FA skeleton to exclude predominantly non-white matter voxels. Third, MD volumes were projected onto the mean FA skeleton and further thresholded at an FA value of 0.3 to reduce CSF partial volume contamination using the skeleton mask provided by Baykara et al. (19). Finally, PSMD was calculated as the difference between the 95th and 5th percentiles of the voxel-based MD values within each subject's MD skeleton.

Other Structural Brain Imaging Variables

The estimation of, respectively, normal-appearing gray and white matter volumes, brain atrophy (intra-cranial volume minus total brain volume), general FA and general MD derived from quantitative tractography, white matter hyperintensity (WMH) volume, and visually rated perivascular spaces (41) from LBC1936 Wave 2 have all been described previously, as, mostly, have their associations with cognitive functions (11, 42–48). They are included in the present paper in order to compare their cognitive associations alongside those of PSMD, not as new results in themselves. Briefly, general FA and general MD were calculated using confirmatory factor analyses that estimated a latent factor from the (respective) FA or MD values of each of 12 broad white matter tracts (see Ref. 45 for a list). Each model included residual correlations between the left and right versions of the bilateral tracts.

Statistical Analysis

All analyses were run in the *lavaan* package for R (49). Scores on each multi-test cognitive domain (processing speed, visuospatial ability, verbal memory, and crystallized ability) were derived from separate confirmatory factor analyses assessed using structural equation models based on the analytic sample. Scores on general cognitive ability were derived from a hierarchical confirmatory factor analysis where the score on the general cognitive factor represented the shared variance among the four cognitive domains. Associations between brain imaging parameters and cognitive test scores were conducted using linear regression, with p values adjusted for the false discovery rate (FDR) (50) as indicated in results tables. To test whether the relation of each cognitive test or domain with PSMD was significantly different from its relation with the other brain-derived variables, we used Williams's test for differences in dependent correlations (implemented using the *psych* package in R) (51); we treated the standardized regression betas as correlations for this purpose. For each test, we accounted for the dependency (correlation) between the brain variables. Before inclusion in the analysis, we adjusted all variables for sex and age (in days) at the time of testing/scanning by regressing them on these two covariates and saving the residuals.

As an additional multivariable analysis, we ran a set of structural equation models in which all eight of the brain measures were entered simultaneously as predictors of the latent cognitive scores. This allowed us to test whether PSMD was incrementally significant beyond the more conventionally studied micro- and macro-structural brain measures. For the general FA and MD factors, we extracted the factor scores to use as predictors, but

still estimated the cognitive factors as latent variables. As with the previous analyses, all variables were corrected for sex and age. Note that we already reported a similar analysis in this sample (46). However, the previous analysis did not include PSMD, and its aim was to discover how much of the variance in cognitive domains could be accounted for with structural brain variables. In the present analysis, the aim was novel, i.e., to test whether PSMD had an incremental contribution in predicting cognitive variation, in a situation where several structural brain variables were included simultaneously.

Finally, a reviewer suggested that we run an additional analysis that controlled for educational attainment and depressive symptoms. We did so, using the participants' age-73 total score on the depression subscale of the Hospital Anxiety and Depression Scale (HADS) (52) and their self-reported total years of formal, full-time education, reported at age 70, as additional covariates in the model. That is, these variables were included in the regressions along with age and sex from which we saved residuals for further analysis.

RESULTS

Summary demographic, medical, brain imaging, and cognitive descriptive results are shown in **Table 1**. The total number of subjects who agreed to brain imaging was 731 (388 men), and between 656 and 680 of them provided brain imaging data that were able to be used to compute variables for use in this study. Their mean age was 72.7 years (SD = 0.72). About 47% had a history of hypertension, 27% had a history of cardiovascular disease, and 10% had a history of diabetes. Further, up to 35% had Fazekas WMH scores of 2 or 3 in peri-ventricular or deep white matter, an elevated rate given their age (see Ref. 53). Their mean Mini-Mental State Examination score was 28.8 (SD = 1.4).

The age- and sex-adjusted correlations between the brain imaging measures used in this study are shown in **Supplementary Table 1**. PSMD correlated—in terms of absolute standardized effect sizes—above 0.5 with general FA and MD and WMH volume, about 0.3 with atrophy and perivascular spaces, and below 0.2 with gray and white matter volumes.

TABLE 1 | Characteristics of the Lothian Birth Cohort 1936 study sample. Numbers are mean and SD or *N* and %.

Variable category	Variable	Mean (SD) or *N* (%)	Total *N*
Demographic characteristics	Age (years)	72.68 (0.72)	866
	Sex; male, female	388, 343	1,091
	Adult social class	3.49 (1.21)	1,091
	Education (years)	10.79 (1.14)	1,091
	Smoking (never, ex-, current)	343, 327, 61	866
	Mini-Mental State examination	28.76 (1.41)	865
Medical conditions	Hypertension (%)	362 (46.9%)	866
	Cardiovascular disease (%)	198 (27.1%)	866
	Diabetes (%)	77 (10.5%)	866
	Hypercholesterolemia (%)	356 (41%)	866
	Depression (mean HADS score)	2.62 (2.22)	865
Structural brain imaging measures	PSMD	3.17×10^{-4} (5.01×10^{-5})	672
	General FA	0.00 (1.00)	664
	General MD	0.00 (1.00)	664
	WMH volume (cm^3)	12.23 (12.18)	656
	Gray matter volume (cm^3)	472.43 (44.68)	657
	White matter volume (cm^3)	476.89 (50.55)	657
	Perivascular spaces	3.51 (1.10)	680
Processing speed tests	Wechsler Digit Symbol	56.29 (12.42)	862
	Wechsler Symbol Search	24.62 (6.19)	862
	Simple reaction time (s)	0.27 (0.05)	865
	4-choice reaction time (s)	0.65 (0.09)	865
	Inspection time	111.37 (11.75)	838
Visuospatial ability	Wechsler Matrix Reasoning	13.36 (4.92)	863
	Wechsler Block Design	34.00 (10.07)	864
	Wechsler Spatial Span	14.75 (2.77)	861
Verbal memory	Wechsler Verbal Paired Associates	27.18 (9.57)	843
	Wechsler Logical Memory	74.53 (17.92)	864
	Wechsler Digit Span Backward	7.86 (2.32)	866
Crystallized ability	National Adult Reading Test	34.36 (8.16)	864
	Wechsler Test of Adult Reading	41.01 (6.96)	864
	Phonemic verbal fluency	43.22 (12.95)	865

General FA and MD were latent variables created using full-information maximum-likelihood estimation from 12 white matter tract measurements; the total N given is the highest possible n. HADS, Hospital Anxiety and Depression Scale (total depression score was used for this analysis).

For clarity in understanding the results reported below, all significant associations were in the direction indicating that healthier brains had better performance in processing speed and other cognitive domains. "Healthier brains" had lower PSMD, higher general FA, lower general MD, lower WMH volume, higher gray and white matter volumes, lower atrophy, and fewer perivascular spaces.

PSMD and Other Brain Imaging Variables Versus Processing Speed

We first examined the associations between the five tests of processing speed and PSMD and the other brain imaging measures (**Table 2**). Higher PSMD (representing less healthy white matter) was significantly associated with worse scores on all five measures of processing speed; the absolute standardized betas were between 0.11 and 0.23 (mean = 0.17). Those with higher PSMD had lower scores on Digit Symbol, Symbol Search, and inspection time, and slower simple and 4-choice reaction times. Therefore, PSMD does correlate significantly, in the expected direction, with these five methodologically varied tests of processing speed.

Normal-appearing gray and white matter volumes and brain atrophy had similar associations to PSMD with the five processing speed measures (**Table 2**); 11 of their 15 betas were larger in effect size (though not significantly larger) than those of PSMD. Associations between WMH volume and the processing speed tests were similar to those of PSMD, though mostly slightly lower. General FA and MD had significant associations with all five of the processing speed measures, with similar betas to those between PSMD and speed measures, though the majority were slightly lower. Perivascular spaces had non-significant associations with the five processing speed measures, and all were notably lower than those with PSMD. We repeated these analyses, omitting participants with a Mini-Mental State Examination score below 24; the results were very similar (**Supplementary Table 2**).

We tested the effect sizes of the associations between PSMD and individual processing speed tests to find out formally whether they were significantly stronger or weaker than those between other brain imaging variables and the same test. **Table 2** shows these results. Apart from perivascular spaces, where PSMD always had stronger associations with processing speed measures, PSMD had significantly stronger associations than other brain variables in only 1 of 30 comparisons.

PSMD and Other Brain Imaging Variables' Associations With Four Cognitive Domains and General Cognitive Ability

Next, we examined the possibility that PSMD showed significantly stronger associations with processing speed than with other cognitive domains, and whether they were significantly stronger or weaker associations compared to other brain imaging variables. We ascertained the associations between PSMD and other brain imaging measures and the four cognitive domains (each of which comprised multiple cognitive tests) and general cognitive ability (the variance shared by the four cognitive domains) (**Table 3**). Higher PSMD was significantly associated, at similar effect sizes, with poorer processing speed (standardized beta = −0.27), visuospatial ability (−0.23), and general cognitive ability (−0.25). The association with verbal memory was significant but lower (−0.17), and the association with crystallized ability was small and non-significant (−0.07).

TABLE 2 | The association between structural brain imaging parameters and individual tests of processing speed.

	Wechsler Digit Symbol			Wechsler Symbol Search			Simple reaction time			4-choice reaction time			Inspection time		
	β	SE	p_{adj}	β	SE	p_{adj}	β	SE	p_{adj}	β	SE	p_{adj}	β	SE	p_{adj}
PSMD	−.226	.037	1.01×10^{-8}	−.155	.038	5.74×10^{-5}	.108	.037	.003	.169	.037	1.04×10^{-5}	−.200	.037	3.02×10^{-7}
General FA	.188	.041	1.70×10^{-5}	.119	.042	.005	−.147	.044	.001	−.189	.042	1.70×10^{-5}	.172	.042	8.14×10^{-5}
General MD	−.143*	.041	.003	−.092	.042	.028	.121	.043	.008	.113	.043	.010	−.162	.042	5.05×10^{-4}
WMH volume	−.200	.037	5.55×10^{-7}	−.164	.038	3.13×10^{-5}	.044	.037	.234	.140	.037	2.12×10^{-4}	−.172	.039	2.45×10^{-5}
Gray matter volume	.259	.037	2.62×10^{-11}	.257†	.037	3.60×10^{-11}	−.047	.037	.204	−.164	.037	1.48×10^{-5}	.147	.039	2.05×10^{-4}
White matter volume	.292	.036	2.55×10^{-14}	.257†	.037	3.30×10^{-11}	−.119	.037	.001	−.215	.036	7.45×10^{-9}	.174	.039	1.07×10^{-5}
Atrophy	.268	.037	4.05×10^{-12}	.215	.038	3.16×10^{-8}	−.109	.037	.003	−.180	.037	1.42×10^{-6}	.220	.038	3.16×10^{-8}
Perivascular spaces	−.033*	.038	0.646	.005*	.039	.899	.059	.037	.276	.005*	.038	.899	−.093*	.039	.085

All variables are adjusted for sex and age on the day of testing or MRI scanning. p_{adj} values are FDR-adjusted within each brain variable (that is, by rows of this table).
**Significantly (absolutely) lower than the β for PSMD; †Significantly (absolutely) higher than the β for PSMD. Standardized regression coefficients are reported throughout.*

For all five of the cognitive variables, normal-appearing gray and white matter volumes and brain atrophy had stronger associations than PSMD (**Table 3**). The associations of WMH volume were somewhat lower than those of PSMD, and all but the association with crystallized ability were significant. General FA and MD had significant associations with all cognitive domains, except between MD and crystallized ability, and the betas were mostly slightly lower than those between PSMD and cognitive domains. Perivascular spaces had no significant associations with any cognitive domain.

We repeated these analyses, omitting participants with a Mini-Mental State Examination score below 24; the results were very similar (**Supplementary Table 3**). Additional analyses show the associations between the various structural brain imaging measures and the individual tests from the cognitive domains of Visuospatial ability, Memory, and Crystallized ability (**Supplementary Tables 4**, **5**, and **6**, respectively).

We tested the effect sizes of the associations between PSMD and each cognitive domain and general cognitive ability to find out formally whether they were significantly stronger or weaker than those between other brain imaging variables and the same cognitive variable. **Table 3** shows these results. There were 35 comparisons: in 11 of these, PSMD had stronger associations with cognitive domains and general cognitive ability, and in five of these, the PSMD associations were significantly weaker. For processing speed, PSMD was a significantly stronger associate than general MD and perivascular spaces, and significantly weaker than white matter volume. Therefore, although PSMD does correlate significantly, in the expected direction, with these cognitive measures, it did not exhibit the largest association among all brain measures in any cognitive domain.

Multivariable Models to Test PSMD's Incremental Contribution to Predicting Variance in Cognitive Domains and General Cognitive Ability

The results of the multivariable models, where all brain variables were entered together to predict variance in cognitive domain scores and general cognitive ability, are shown in **Table 4**. In these models, PSMD had a statistically significant association with visuospatial ability and with the general cognitive ability factor, but not with processing speed, verbal memory, or crystallized ability. No one brain measure consistently emerged as a statistically significant predictor for each cognitive ability. Gray matter volume, white matter volume, and atrophy were all independently significant alongside PSMD in predicting general cognitive ability. The general FA and MD variables were not independently significant in any of the models, indicating that variation in the cognitive abilities was better measured by either the macrostructural indices (except perivascular spaces, which were also not significant in any model), or by PSMD.

Analyses With Additional Covariates

As suggested by a referee on an earlier version of this paper, we re-ran the main analyses with the additional controls of educational attainment and depressive symptoms (that is, alongside age and sex). We report the relevant results in **Supplementary Tables 7**, **8**, and **9** (which are the equivalents of

TABLE 3 | The association between structural brain imaging parameters and domains of cognitive ability and general cognitive ability.

	Processing speed			Visuospatial ability			Verbal memory			Crystallized ability			General cognitive ability		
	β	SE	p_{adj}	β	SE	p_{adj}	β	SE	p_{adj}	β	SE	p_{adj}	β	SE	p_{adj}
PSMD	−.273	.040	4.64×10^{-11}	−.235	.042	3.66×10^{-8}	−.168	.045	2.37×10^{-4}	−.072	.040	.070	−.250	.041	2.57×10^{-9}
General FA	.238	.046	1.07×10^{-6}	.174*	.048	4.44×10^{-4}	.116	.050	.021	.100	.043	.021	.204	.047	2.89×10^{-5}
General MD	−.178*	.046	5.76×10^{-4}	−.163*	.047	.002	−.117	.050	.025	.003*	.043	.951	−.148*	.047	.003
WMH volume	−.247	.042	1.39×10^{-8}	−.132*	.044	.004	−.137	.046	.004	−.048	.040	.231	−.184*	.043	4.19×10^{-5}
Gray matter volume	.315	.039	6.42×10^{-16}	.310	.041	4.46×10^{-14}	.201	.044	3.97×10^{-6}	.253†	.037	7.12×10^{-12}	.357†	.038	3.95×10^{-20}
White matter volume	.364†	.037	3.94×10^{-22}	.280	.042	1.64×10^{-11}	.175	.045	8.82×10^{-5}	.239†	.037	1.21×10^{-10}	.348	.038	2.45×10^{-19}
Atrophy	.331	.039	5.89×10^{-22}	.277	.042	5.63×10^{-11}	.200	.045	1.06×10^{-5}	.169†	.038	1.33×10^{-5}	.320	.039	9.88×10^{-16}
Perivascular spaces	.038*	.043	.638	−.054*	.044	.638	−.008*	.045	.867	.043	.040	.638	−.020*	.043	.798

*All variables are adjusted for sex and age on the day of testing or MRI scanning. p_{adj} values are FDR-adjusted within each brain variable (that is, by rows of this table). *Significantly (absolutely) lower than the β for PSMD; †Significantly (absolutely) higher than the β for PSMD. Standardized regression coefficients are reported throughout.*

TABLE 4 | Multivariable models predicting latent cognitive factors from all brain variables, entered simultaneously.

	Processing speed			Visuospatial ability			Verbal memory			Crystallized ability			General cognitive ability		
	β	SE	p_{adj}	β	SE	p_{adj}	β	SE	p_{adj}	β	SE	p_{adj}	β	SE	p_{adj}
PSMD	0.093	0.060	0.240	**–0.184**	**0.063**	**0.024**	–0.095	0.068	0.416	–0.043	0.058	0.525	**–0.146**	**0.060**	**0.032**
General FA	–0.010	0.051	0.969	–0.066	0.055	0.365	–0.045	0.058	0.534	0.037	0.050	0.525	–0.026	0.052	0.813
General MD	0.002	0.052	0.969	–0.053	0.055	0.447	–0.043	0.059	0.534	0.067	0.051	0.470	–0.008	0.052	0.880
WMH volume	**0.140**	**0.053**	**0.021**	0.034	0.057	0.548	–0.076	0.060	0.416	–0.008	0.052	0.872	–0.062	0.054	0.406
Gray matter volume	–0.035	0.059	0.788	**0.173**	**0.062**	**0.024**	0.099	0.069	0.416	0.125	0.057	0.112	**0.149**	**0.059**	**0.032**
White matter volume	**–0.223**	**0.055**	**1.83 × 10^{-4}**	0.120	0.059	0.084	0.047	0.064	0.534	0.132	0.053	0.104	**0.170**	**0.056**	**0.008**
Atrophy	**–0.220**	**0.048**	**3.69 × 10^{-5}**	0.122	0.052	0.051	0.124	0.056	0.224	0.056	0.047	0.470	**0.171**	**0.049**	**0.004**
Perivascular spaces	–0.023	0.042	0.788	–0.030	0.045	0.548	0.028	0.048	0.552	0.032	0.042	0.525	0.016	0.043	0.816
R^2	0.229			0.159			0.082			0.081			0.214		

Values in bold had significant p_{adj} values. p_{adj} values were FDR-adjusted within each multivariable model (i.e., within columns of this table).

Tables 2, **3**, and **4** in this main article, respectively). The addition of these covariates made little substantive difference to the results: effect sizes were changed at the second or third decimal place. In the multivariable analysis, some of the effect sizes were made slightly larger, though broadly the picture remained similar to that described above for the main analyses.

DISCUSSION

In this large sample of community-dwelling older people with a narrow age range around 73 years, we extended the previously reported (19) link between PSMD and processing speed to include necessary comparisons with a variety of more specific processing speed tests, other correlated cognitive domains, and other brain measures. In the present study, higher PSMD correlated significantly with poorer performance on five methodologically diverse tests of processing speed: two were psychometric, paper-and-pencil tests; two were experimental, reaction time tests; and one was a psychophysical test, requiring no fast motor response. Higher PSMD correlated significantly with poorer performance on the latent cognitive domain of processing speed, composed of tests of all three types. However, PSMD was not the exclusive or strongest associate of processing speed: normal-appearing gray and white matter volumes and brain atrophy were often slightly stronger, and WMH volume and tractography-based general FA and MD had slightly lower, but still significant associations. Moreover, PSMD did not have an especially strong association with processing speed compared with other cognitive domains; it correlated at similar levels with visuospatial ability and general cognitive ability, though less strongly with verbal memory and crystallized ability. In multivariable analyses, PSMD contributed predictive power, incremental to that of other structural brain imaging variables, to visuospatial ability and general cognitive ability.

If PSMD's association with processing speed had been higher than those of other structural brain indices, and/or if PSMD has been especially strong in associating with the domain of processing speed by comparison with other cognitive domains, then there would have been strong evidence for arguing that PSMD stands out among brain imaging parameters in being especially associated with this important cognitive domain. Rather, the visuospatial cognitive domain and general cognitive ability were highlighted as having a heightened relationship with PSMD; that is, PSMD explained additional variance in these variables that was independent of the other brain imaging predictors. Because of its ease of computation and tractability, PSMD might be preferred over imaging measures that are burdensome to compute and which are more general properties of the brain. However, global measures of GM and WM volume can be obtained from a T1 alone, and their automated measurement can also be undertaken in an automated fashion. That is, both PSMD's convenience and link to more specific brain biology might be used to argue in its favor; the average magnitude of water molecular diffusion in the center of common white matter pathways provides information on individual variations in white matter microstructure and the specific methods reduce the likelihood of influences of partial volume effects, rather than simply "how much" of a tissue type an individual possesses. Furthermore, code for performing PSMD is freely available and based on the commonly used TBSS pipeline, making it an accessible biomarker of white matter structure.

The similar association of PSMD with other cognitive domains might not necessarily detract from the claim that it is a marker of processing speed. This is because processing speed has long been seen as somewhat special among the cognitive domains. It has been argued that faster processing speed might provide a foundation for better cognitive performance in higher cognitive domains and for less cognitive decline in them (4, 8, 9). This is because the tests of processing speed are arguably simpler than those of other cognitive domains, often being referred to as

elementary cognitive tests. Thus, if links to underlying biological processes are clearer for PSMD compared with other structural brain markers, and for processing speed compared with other cognitive domains, then it may be argued that PSMD is *primus inter* (apparent) *pares* for the brain indices examined here.

The study has the strengths of testing a large and age- and culturally homogeneous sample, all on the same brain scanner. The homogeneity of the sample is advantageous in that it means that there is not a "culture" variable within the sample that would need to be taken into account, with lowering of power, and as a possible source of different sizes of association. Processing speed was tested thoroughly, at three levels of description (psychometric, experimental, and psychophysical). Other important cognitive domains that show age-related mean decline—visuospatial reasoning and memory—and crystallized ability were assessed using multiple, well-validated tests. Also, recognizing that all cognitive domains correlate strongly, a general cognitive ability variable, capturing their shared variance, was included. The study has some limitations. The homogeneity of age and cultural background means that we are not able to generalize beyond those. Neither can we generalize beyond their status as relatively healthy, community-dwelling individuals, though we note that markers of small vessel disease indicated some pathology exceeding the expectations for their age. It is possible that samples with a broader range of brain pathology might show stronger brain imaging–cognitive domain associations, and possibly a pattern that brings out more of PSMD's distinctiveness. For example, PSMD was associated with general cognitive ability and executive function in patients with WMLs but not in healthy controls (54). The original PSMD-validation study (19) had the advantage of multiple clinical and healthy groups, but its limitations included that most of its samples did not have a relatively specific test of processing speed and there were insufficient tests of other cognitive domains.

The present study assessed the usefulness of PSMD as a biomarker of cognitive function in older age. We found the predicted association with processing speed, but it was not exclusive or special with respect to other structural brain indices, or with respect to other cognitive domains. To sum up, we found that a) PSMD did not show especially high associations with processing speed when compared with other cognitive domains and b) other brain imaging variables correlated as highly or higher with cognitive variables—including processing speed—as did PSMD. However, those are not the only considerations. In the Introduction, we referred to the special status that some researchers consider processing speed to have with respect to its being a foundation for individual differences in cognitive ability and cognitive aging. We also pointed out that PSMD might have tractability, i.e., that it might be a more specific brain biomarker than other imaging measures. Therefore, PSMD's specificity and processing speed's possible special status among cognitive domains make the PSMD–processing speed association worth exploring and explaining in a wider range of clinical and non-clinical populations. For instance, there is recent evidence of PSMD's association with speed tests in multiple sclerosis patients (55). Future research should also seek to clarify the nature of any distinctive relationships between PSMD with visuospatial and general cognitive abilities.

DATA AVAILABILITY

The datasets generated for this study are available on request to the corresponding author.

ETHICS STATEMENT

All subjects gave written informed consent in accordance with the Declaration of Helsinki. The protocol was approved by the Multi-Centre Research Ethics Committee for Scotland (MREC/01/0/56; 07/MRE00/58) and the Lothian Research Ethics Committee (LREC/2003/2/29).

AUTHOR CONTRIBUTIONS

ID drafted the manuscript and conceived the study aims; SR performed statistical analysis in discussion with ID; SM, SC, and MH processed the imaging data; ID, JS, JW, and MB supervised the larger cohort study. All authors commented on/edited the manuscript draft.

ACKNOWLEDGMENTS

The work was undertaken as part of the Cross Council and University of Edinburgh Centre for Cognitive Ageing and Cognitive Epidemiology (CCACE; http://www.ccace.ed.ac.uk). This work was supported by a Research into Ageing programme grant (to ID and JS) and the Age UK-funded Disconnected Mind project (http://www.disconnectedmind.ed.ac.uk; to ID, JS, and JW), with additional funding from the UK Medical Research Council (MRC; to ID, JS, JW, MB, SR, and SC). JW is supported by the Scottish Funding Council through the SINAPSE Collaboration (http://www.sinapse.ac.uk). CCACE (MRC MR/K026992/1) is funded by the Biotechnology and Biological Sciences Research Council and MRC. The image acquisition and analysis were performed at the Brain Research Imaging Centre, University of Edinburgh (http://www.bric.ed.ac.uk). The authors thank the research team members who collected, processed, collated, and checked cognitive, medical, and brain imaging data. We thank Dr Natalie Royle for her work on some of the non-PSMD brain imaging variables used in the present study. This manuscript has been released as a preprint at https://www.biorxiv.org/content/10.1101/385013v1.

SUPPLEMENTARY MATERIAL

The Supplementary Material for this article can be found online at: https://www.frontiersin.org/articles/10.3389/fpsyt.2019.00524/full#supplementary-material

REFERENCES

1. Tucker-Drob EM. Global and domain-specific changes in cognition throughout adulthood. *Dev Psychol* (2011) 47:331–43. doi: 10.1037/a0021361
2. Salthouse TA. Contributions of the individual differences approach to cognitive ageing. *J Gerontol B Psychol Sci Soc Sci* (2017) 72:7–15. doi: 10.1093/geronb/gbw069
3. Institute of Medicine. *Cognitive aging: Process in understanding and opportunities for action*. Washington, DC: The National Academies Press (2015).
4. Salthouse TA. The processing-speed theory of adult age differences in cognition. *Psychol Rev* (1996) 103:403–28. doi: 10.1037/0033-295X.103.3.403
5. Salthouse TA. Aging and measures of processing speed. *Biol Psychol* (2000) 54:35–54. doi: 10.1016/S0301-0511(00)00052-1
6. Deary IJ. *Looking down on human intelligence; from psychometric to the brain*. Oxford, UK: Oxford University Press (2000).
7. Deary IJ, Johnson W, Starr JM. Are processing speed tests biomarkers of cognitive ageing? *Psychol Aging* (2010) 25:219–28. doi: 10.1037/a0017750
8. Verhaeghen P. *The elements of cognitive ageing; meta-analysis of age-related differences in processing speed and their consequences*. Oxford, UK: Oxford University Press (2014). doi: 10.1093/acprof:oso/9780195368697.003.0010
9. Ritchie SJ, Tucker-Drob EM, Deary IJ. A strong link between speed of visual discrimination and cognitive ageing. *Curr Biol* (2014) 24:R681–R683. doi: 10.1016/j.cub.2014.06.012
10. Salthouse TA, Madden DJ. Information processing speed and aging. In: DeLuca J, Kalmar JH, editors. *Information processing speed in clinical populations*. New York: Taylor and Francis (2008). p. 221–42.
11. Penke L, Munoz Maniega A, Bastin ME, Valdes Hernandez MC, Murray C, Royle NA, et al. Brain white matter tract integrity as a neural foundation for general intelligence. *Mol Psychiatry* (2012) 17:1026–30. doi: 10.1038/mp.2012.66
12. Arvanitakis Z, Fleischman DA, Arfanakis K, Leurgans SE, Barnes LL, Bennett DA. Association of white matter hyperintensities and grey matter volume with cognition in older individuals without cognitive impairment. *Brain Struct Funct* (2016) 221:2135–46. doi: 10.1007/s00429-015-1034-7
13. Cremers LGM, de Groot M, Hofman A, Krestin GP, van der Lugt A, Niessen WJ, et al. Altered tract-specific white matter microstructure is related to poorer cognitive performance: the Rotterdam study. *Neurobiol Aging* (2016) 39:108–17. doi: 10.1016/j.neurobiolaging.2015.11.021
14. Dong C, Nabizadeh N, Caunca M, Cheung YK, Rundek T, Elkind MSV, et al. Cognitive correlates of white matter lesion load and brain atrophy. *Neurology* (2015) 85:441–9. doi: 10.1212/WNL.0000000000001716
15. Gazes Y, Bowman FD, Razlighi QR, O'Shea D, Stern Y, Habeck C. White matter tract covariance patterns predict age-declining cognitive abilities. *NeuroImage* (2016) 125:53–60. doi: 10.1016/j.neuroimage.2015.10.016
16. Liu H, Yang Y, Xia Y, Zhu W, Leak RK, Wei Z, et al. Aging of cerebral white matter. *Ageing Res Rev* (2017) 34:64–76. doi: 10.1016/j.arr.2016.11.006
17. Salthouse TA, Habeck C, Razlighi Q, Barulli D, Gazes Y, Stern Y. Breadth and age-dependency of relations between cortical thickness and cognition. *Neurobiol Aging* (2015) 36:3020–8. doi: 10.1016/j.neurobiolaging.2015.08.011
18. Shi Y, Wardlaw JM. Update on cerebral small vessel disease: a dynamic whole-brain disease. *Stroke Vasc Neurol* (2016) 1:83–92. doi: 10.1136/svn-2016-000035
19. Baykara E, Gesierich B, Adam R, Tuladhar AM, Biesbroek JM, Koek HL, et al. A novel imaging marker for small vessel disease based on skeletonization of white matter tracts and diffusion histograms. *Ann Neurol* (2016) 80:581–92. doi: 10.1002/ana.24758
20. Salthouse TA. What cognitive abilities are involved in trail-making performance? *Intelligence* (2011) 39:222–32. doi: 10.1016/j.intell.2011.03.001
21. MacPherson SE, Cox SR, Dickie DA, Karama S, Starr JM, Evans AC, et al. Processing speed and the relationship between Trail Making Test-B performance, cortical thinning and white matter microstructure in older adults. *Cortex* (2017) 95:92–13.
22. MacPherson SE, Allerhand M, Cox SR, Deary IJ. Individual differences in cognitive processes underlying Trail Making Test-B performance in old age: the Lothian Birth Cohort 1936. *Intelligence* (2019) 75:23–32.
23. Schmidt FL. Beyond questionable research methods: the role of omitted relevant research in the credibility of research. *Arch Sci Psychol* (2017) 5:32–41. doi: 10.1037/arc0000033
24. Deary IJ, Der G, Ford G. Reaction times and intelligence differences: a population-based cohort study. *Intelligence* (2001) 29:389–99. doi: 10.1016/S0160-2896(01)00062-9
25. Deary IJ, Gow AJ, Taylor MD, Corley J, Brett C, Wilson V, et al. The Lothian Birth Cohort 1936: a study to examine influences on cognitive ageing from age 11 to age 70 and beyond. *BMC Geriatr* (2007) 7:28. doi: 10.1186/1471-2318-7-28
26. Deary IJ, Gow AJ, Pattie A, Starr JM. Cohort profile: the Lothian Birth Cohorts of 1921 and 1936. *Int J Epidemiol* (2012) 41:1576–84. doi: 10.1093/ije/dyr197
27. Taylor A, Pattie A, Deary IJ. Cohort profile update: the Lothian Birth Cohorts of 1921 and 1936. *Int J Epidemiol* (2018) 47:1042. doi: 10.1093/ije/dyy022
28. Wardlaw JM, Bastin ME, Valdes Hernandez MC, Maniega SM, Royle NA, Morris Z, et al. Brain ageing, cognition in youth and old age, and vascular disease in the Lothian Birth Cohort 1936: rationale, design and methodology of the imaging protocol. *Int J Stroke* (2011) 6:547–59. doi: 10.1111/j.1747-4949.2011.00683.x
29. Wechsler D. *WAIS-IIIUK administration and scoring manual*. London, UK: Psychological Corporation (1998).
30. Deary IJ, Simonotto E, Meyer M, Marshall A, Marshall I, Goddard N, et al. The functional anatomy of inspection time: an event-related fMRI study. *NeuroImage* (2004) 22:1466–79. doi: 10.1016/j.neuroimage.2004.03.047
31. Nelson HE, Willison JR. *National Adult Reading Test (NART) Test Manual (Part II)*. Windsor, UK: NFER-Nelson (1991).
32. Holdnack JA. *WTAR: Wechsler Test of Adult Reading manual*. San Antonio, TX: Psychological Corporation (2001).
33. Office of Population and Census Surveys. *Classification of occupations*. London, UK: Her Majesty's Stationery Office (1980).
34. Folstein MF, Folstein SE, McHugh PR. Mini-Mental State: a practical method for grading the cognitive state of patients for the clinician. *J Psychiatr Res* (1975) 12:189–98. doi: 10.1016/0022-3956(75)90026-6
35. Jones DK, Williams SC, Gasston D, Horsfield MA, Simmons A, Howard R. Isotopic resolution diffusion tensor imaging with whole brain acquisition in a clinically acceptable time. *Hum Brain Mapp* (2002) 15:216–30. doi: 10.1002/hbm.10018
36. Clayden JD, Maniega SM, Storkey AJ, King MD, Bastin ME, Clark CA. TractoR: magnetic resonance imaging and tractography with R. *J Stat Softw* (2011) 44:1–18. doi: 10.18637/jss.v044.i08
37. Smith SM, Jenkinson M, Woolrich MW, Beckmann CF, Behrens TE, Johansen-Berg H, et al. Advances in functional and structural MR image analysis and implementation as FSL. *NeuroImage* (2004) 23:S208–S219. doi: 10.1016/j.neuroimage.2004.07.051
38. Jenkinson M, Smith S. A global optimisation method for robust affine registration of brain images. *Med Imag Anal* (2001) 5:143–56. doi: 10.1016/S1361-8415(01)00036-6
39. Basser PJ, Pierpaoli C. Microstructural and physiological features of tissues elucidated by quantitative-diffusion-tensor MRI. *J Magn Reson* (1996) 292:155–70. doi: 10.1016/j.jmr.2011.09.022
40. Smith SM, Jenkinson M, Johansen-Berg H, Rueckert D, Nichols TE, Mackay CE, et al. Tract-based spatial statistics: voxelwise analysis of multi-subject diffusion data. *NeuroImage* (2006) 31:1487–505. doi: 10.1016/j.neuroimage.2006.02.024
41. Potter GM, Chappell FM, Morris Z, Wardlaw JM. Cerebral perivascular spaces visible on magnetic resonance imaging: development of a qualitative rating scale and its observer reliability. *Cerebrovasc Dis* (2015) 39:224–31. doi: 10.1159/000375153
42. Royle NA, Booth T, Valdes Hernandez MC, Penke L, Murray C, Gow AJ, et al. Estimated maximal and current brain volume predict cognitive ability in old age. *Neurobiol Aging* (2013) 34:2726–33. doi: 10.1016/j.neurobiolaging.2013.05.015
43. Valdes Hernandez MC, Booth T, Murray C, Gow AJ, Penke L, Morris Z, et al. Brain white matter damage in aging and cognitive ability in youth and older age. *Neurobiol Aging* (2013) 34:2740–7. doi: 10.1016/j.neurobiolaging.2013.05.032
44. Booth T, Bastin ME, Penke L, Maniega SM, Murray C, Royle NA, et al. Brain white matter tract integrity and cognitive abilities in community-dwelling older people: the Lothian Birth Cohort 1936. *Neuropsychology* (2013) 27:595–607. doi: 10.1037/a0033354

45. Ritchie SJ, Bastin ME, Tucker-Drob EM, Maniega SM, Engelhardt LE, Cox SR, et al. Coupled changes in brain white matter microstructure and fluid intelligence in later life. *J Neurosci* (2015a) 35:8672–82. doi: 10.1523/JNEUROSCI.0862-15.2015
46. Ritchie SJ, Booth T, Valdes Hernandez M, Corley J, Maniega SM, Gow AJ, et al. Beyond a bigger brain: multivariable structural brain imaging and intelligence. *Intelligence* (2015b) 51:47–56. doi: 10.1016/j.intell.2015.05.001
47. Ritchie SJ, Dickie DA, Cox SR, Valdes Hernandez MC, Corley J, Royle NA, et al. Brain volumetric changes and cognitive ageing during the eighth decade of life. *Hum Brain Mapp* (2015c) 36:4910–25. doi: 10.1002/hbm.22959
48. Aribisala BS, Riha R, Valdes Hernandez M, Maniega SM, Cox S, Radakovic R, et al. The association of sleep duration and quality with brain perivascular spaces, white matter hyperintensities and brain atrophy. Sleep Med. (In Press).
49. Rosseel Y. An R package for structural equation modelling. *J Stat Softw* (2012) 48:1–36. doi: 10.18637/jss.v048.i02
50. Benjamini Y, Hochberg Y. Controlling the false discover rate: a practical and powerful approach to multiple testing. *J R Stat Soc Series B Stat Methodol* (1995) 57:289–300. doi: 10.1111/j.2517-6161.1995.tb02031.x
51. Revelle W. *psych: procedures for personality and psychological research*. Evanston, Illinois, USA: Northwestern University (2018).
52. Zigmond AS, Snaith RP. The hospital anxiety and depression scale. *Acta Psychiatr Scand* (1983) 67:361–70. doi: 10.1111/j.1600-0447.1983.tb09716.x
53. Wardlaw JM, Allerhand M, Doubal FN, Valdes Hernandez M, Morris Z, Gow AJ, et al. Vascular risk factors, large artery atheroma and brain white matter hyperintensities. *Neurology* (2014) 82:1331–8. doi: 10.1212/WNL.0000000000000312
54. Wei N, Deng Y, Yao L, Jia W, Wang J, Shi Q, et al. A neuroimaging marker based on diffusion tensor imaging and cognitive impairment due to cerebral white matter lesions. *Front Neurol* (2019) 10:81. doi: 10.3389/fneur.2019.00081
55. Vinciguerra C, Giorgio A, Zhang J, Di Donato I, Stromillo ML, Tappa Brocci R, et al. Peak width of skeletonized mean diffusivity (PSMD) as marker of widespread white matter tissue damage in multiple sclerosis. *Mult Scler Relat Disord* (2019) 27:294–7. doi: 10.1016/j.msard.2018.11.011

Conflict of Interest Statement: The authors declare that the research was conducted in the absence of any commercial or financial relationships that could be construed as a potential conflict of interest.

frontiers in Aging Neuroscience

ORIGINAL RESEARCH
published: 02 August 2019
doi: 10.3389/fnagi.2019.00202

A Metabolic Obesity Profile Is Associated With Decreased Gray Matter Volume in Cognitively Healthy Older Adults

*Frauke Beyer[1,2], Shahrzad Kharabian Masouleh[1,3], Jürgen Kratzsch[4], Matthias L. Schroeter[1,5], Susanne Röhr[6], Steffi G. Riedel-Heller[6], Arno Villringer[1,2,5] and A. Veronica Witte[1,2,5]**

[1] Department of Neurology, Max Planck Institute for Human Cognitive and Brain Sciences, Leipzig, Germany, [2] Subproject A1, CRC 1052 "Obesity Mechanisms", University of Leipzig, Leipzig, Germany, [3] Institute of Neuroscience and Medicine (INM-7: Brain and Behaviour), Research Centre Jülich, Jülich, Germany, [4] Institute of Laboratory Medicine, Clinical Chemistry and Molecular Diagnostics, University of Leipzig, Leipzig, Germany, [5] Clinic for Cognitive Neurology, University of Leipzig, Leipzig, Germany, [6] Institute of Social Medicine, Occupational Health and Public Health (ISAP), University of Leipzig, Leipzig, Germany

Obesity is a risk factor for cognitive decline and gray matter volume loss in aging. Studies have shown that different metabolic factors, e.g., dysregulated glucose metabolism and systemic inflammation, might mediate this association. Yet, even though these risk factors tend to co-occur, they have mostly been investigated separately, making it difficult to establish their joint contribution to gray matter volume structure in aging. Here, we therefore aimed to determine a metabolic profile of obesity that takes into account different anthropometric and metabolic measures to explain differences in gray matter volume in aging. We included 748 elderly, cognitively healthy participants (age range: 60 – 79 years, BMI range: 17 – 42 kg/m^2) of the LIFE-Adult Study. All participants had complete information on body mass index, waist-to-hip ratio, glycated hemoglobin, total blood cholesterol, high-density lipoprotein, interleukin-6, C-reactive protein, adiponectin and leptin. Voxelwise gray matter volume was extracted from T1-weighted images acquired on a 3T Siemens MRI scanner. We used partial least squares correlation to extract latent variables with maximal covariance between anthropometric, metabolic and gray matter volume and applied permutation/bootstrapping and cross-validation to test significance and reliability of the result. We further explored the association of the latent variables with cognitive performance. Permutation tests and cross-validation indicated that the first pair of latent variables was significant and reliable. The metabolic profile was driven by negative contributions from body mass index, waist-to-hip ratio, glycated hemoglobin, C-reactive protein and leptin and a positive contribution from adiponectin. It positively covaried with gray matter volume in temporal, frontal and occipital lobe as well as subcortical regions and cerebellum. This result shows that a metabolic profile characterized by high body fat, visceral adiposity and systemic inflammation is associated with reduced gray matter volume and potentially reduced executive function

OPEN ACCESS

Edited by:
Hans J. Grabe, University of Greifswald, Germany

Reviewed by:
Nils Opel, University of Münster, Germany
Deborah Janowitz, Universitätsmedizin Greifswald, Germany

***Correspondence:**
A. Veronica Witte
witte@cbs.mpg.de

Received: *17 April 2019*
Accepted: *17 July 2019*
Published: *02 August 2019*

Citation:
Beyer F, Kharabian Masouleh S, Kratzsch J, Schroeter ML, Röhr S, Riedel-Heller SG, Villringer A and Witte AV (2019) A Metabolic Obesity Profile Is Associated With Decreased Gray Matter Volume in Cognitively Healthy Older Adults. Front. Aging Neurosci. 11:202. doi: 10.3389/fnagi.2019.00202

in older adults. We observed the highest contributions for body weight and fat mass, which indicates that factors underlying sustained energy imbalance, like sedentary lifestyle or intake of energy-dense food, might be important determinants of gray matter structure in aging.

Keywords: obesity, leptin – adiponectin, aging, metabolic risk, multivariate analysis, VBM

INTRODUCTION

Obesity is associated with adverse health consequences (World Health Organization [WHO], 2000). In particular, several studies have suggested that higher body mass index (BMI) in mid- and late life is associated with impairment in cognitive function (Debette et al., 2011; Smith et al., 2011; Singh-Manoux et al., 2012) and leads to a higher risk for dementia (Baumgart et al., 2015; Emmerzaal et al., 2015).

Potential mediators, among others, include metabolic risk factors, e.g., dysregulated glucose metabolism and chronic inflammation (Shaw et al., 2017; Corlier et al., 2018; Warren et al., 2018). Yet, these factors often co-occur and their individual role is difficult to establish. Consequently, the neurobiological mechanisms that link obesity and higher risk for cognitive decline in aging remain poorly understood.

Recent neuroimaging studies have provided neurobiological evidence of an association between the most common anthropometric measure of obesity, BMI, and decreased gray matter volume (GMV) (Gustafson et al., 2004; Enzinger et al., 2005; Taki et al., 2012; Bobb et al., 2014; Debette et al., 2014; Kharabian Masouleh et al., 2016).

Further studies have shown that waist-to-hip ratio (WHR), an indicator of visceral adiposity, might be a better predictor of GMV loss compared to BMI (Debette et al., 2010; Debette et al., 2014; Janowitz et al., 2015). This finding is in analogy with the increased cardiovascular risk associated with visceral fat accumulation (Lee et al., 2008).

Visceral adiposity often goes along with dyslipidemia, e.g., increased levels of triglycerides and low-density lipoproteins along with reduced levels of high-density lipoproteins (Klop et al., 2013). While dyslipidemia increases the risk for cardiovascular disease, its association with brain structure is still unclear (Assessment, 2009). Some studies showed that higher levels of total cholesterol and lower levels of high-density lipoprotein are associated with reduced GMV or cortical thickness (Ward et al., 2010; Walhovd et al., 2014), yet other studies have failed to replicate these findings (Leritz et al., 2011; Cox et al., 2019).

A vast amount of literature suggests that disturbances in glucose metabolism, ranging from hyperglycemia and insulin resistance to manifest diabetes, are associated with decreased GMV in middle-aged and older adults (Benedict et al., 2012; Kerti et al., 2013; Moran et al., 2013; Biessels and Reijmer, 2014; Reitz et al., 2016; Shaw et al., 2017; Repple et al., 2018). Insulin resistance might be one mediator of this association given the role of insulin in memory facilitation and regulation of amyloid-β (Craft, 2005; Blázquez et al., 2014; Cheke et al., 2017) in the brain. Accordingly, several studies have reported lower GMV in key memory regions like hippocampus and temporal lobe related to disturbances in glucose regulation (Benedict et al., 2012; Cherbuin et al., 2012; Kerti et al., 2013).

Systemic inflammation is another important metabolic factor with potential implications for brain health. Visceral adipose tissue secrets inflammatory cytokines which have been shown to impair the blood-brain-barrier and might thereby promote neuro-inflammation (Yaffe et al., 2004; Hsuchou et al., 2012). Accordingly, previous neuroimaging studies showed that circulating levels of pro-inflammatory cytokines such as C-reactive protein (CRP) and interleukin-6 (IL6) predict gray matter volume decline (Marsland et al., 2008; Papenberg et al., 2016; Corlier et al., 2018).

Other obesity-related metabolic factors that might have direct or indirect effects on brain function are adipose-tissue derived signaling hormones like leptin and adiponectin.

Leptin has multiple effects in the brain beyond its known role in the hypothalamic control of food intake. For instance, leptin signaling in the hippocampus plays an important role for memory (Paz-Filho et al., 2010; Irving and Harvey, 2013). First evidence from neuroimaging indicated that higher leptin levels might be neuroprotective and help to maintain memory function in older adults, mediated by hippocampus structure (Lieb et al., 2009; Narita et al., 2009; Witte et al., 2016). However, in obesity, leptin is often chronically elevated resulting in central resistance to the effects of the molecule (Myers et al., 2008).

Adiponectin is an adipokine originally known for its insulin-sensitizing and anti-inflammatory properties in the periphery (Lihn et al., 2005). Moreover, it was also suggested to exert beneficial effects on brain function, e.g., by modulating glucose metabolism (Cisternas et al., 2018) but to date, neuroimaging studies have not shown a consistent association of adiponectin and GMV (García-Casares et al., 2016; Hayakawa et al., 2018).

Taken together, different mechanisms might link obesity and related metabolic disturbances with brain health and cognitive function in aging. Most studies so far have focused on single, mostly anthropometric measures of obesity without taking into account related metabolic factors. Here, we use a multivariate method, called partial least squares correlation (PLSC) to derive informative patterns of covariation between anthropometric (overall and visceral adiposity) and metabolic measures (markers of energy metabolism, systemic inflammation and adipose-tissue derived hormones) of obesity and GMV in a sample of cognitively healthy older adults (McIntosh et al., 1996). PLSC is well-suited for data sets with highly correlated variables (e.g., neuroimaging data) and allows to jointly model behavioral and neuroimaging data. In particular, we chose PLSC over other multivariate methods such as canonical correlation analysis as it performs better in terms of predictive power when a high number of voxel are investigated (Grellmann et al., 2015).

We hypothesized a metabolic profile, which highlights detrimental aspects of obesity-related metabolic dysregulation to be associated with a pattern of GMV loss including medio-temporal areas (Cherbuin et al., 2012; Cheke et al., 2017). Furthermore, we aimed to explore the association of this profile with cognitive function.

MATERIALS AND METHODS

Sample Selection

The study sample was selected from the LIFE-Adult study (Loeffler et al., 2015). The study was carried out in accordance with the Declaration of Helsinki and approved by the institutional ethics board of the Medical Faculty of the University of Leipzig. All subjects gave written informed consent.

We included 1222 older participants (≥60 years) with head magnetic resonance imaging (MRI) and without stroke, major brain pathology, cancer in the last 12 months or intake of centrally active medication. Out of these, we selected all participants with complete anthropometric and blood plasma measurements.

We measured body weight, height, waist and hip circumference with a precision of 0.01 kg and 0.1 cm, respectively, and calculated BMI and WHR.

Markers of long-term glucose metabolism (HbA1c), lipid metabolism (total cholesterol and high-density lipoprotein, HDL), systemic inflammation (CRP and IL6) were obtained after overnight fasting according to standard procedures (Loeffler et al., 2015).

Immunoreactive leptin and adiponectin concentrations were measured from fasted serum samples using immunoreactive kits (sensitive ELISA, Mediagnost, Reutlingen).

We excluded participants who scored below 27 in the Mini Mental State Examination (MMSE) (O'Bryant et al., 2008) to obtain a cognitively healthy sample. From these 754 participants, six had to be excluded due to failed MRI preprocessing.

We log-transformed IL6, CRP, adiponectin and leptin values to ensure normality and regressed age and sex from all predictors prior to PLSC.

Magnetic Resonance Imaging

Anatomical T1-weighted images were acquired using a 3 Tesla Siemens Verio MRI scanner (Siemens Healthcare, Erlangen, Germany) with a 3D MPRAGE protocol (inversion time, 900 ms; repetition time, 2300 ms; echo time, 2.98 ms; flip angle, 9°; field of view, 256 mm × 240 mm × 176 mm; voxel size, 1 mm × 1 mm × 1 mm).

We performed voxel-based morphometry (VBM) implemented in SPM 12 to obtain voxelwise estimates of GMV. First, a study-specific template was created from 1186 healthy participants of the LIFE-Adult study aged 60 years or older using DARTEL. After non-linear, iterative registration of the white and gray matter segmentations to this template, the resulting flowfields were applied to the gray matter segmentation. Finally, the images were modulated by the amount of spatial distortion and smoothed with a Gaussian kernel of 8 mm FWHM.

As we were interested in the association of GMV, metabolic and anthropometric measures, we aimed to remove the confounding effect of age, sex and total intra-cranial volume (TIV). Therefore, we regressed age, sex and TIV from the GMV using SPM's implementation of the General Linear Model. To limit the number of voxels included in the analysis, we only included voxels with gray matter probability of 0.3 and larger in the averaged GMV image. The number of voxels included per participant was 295365.

Statistical Analysis

PLSC Analysis

After preprocessing, the anthropometric and metabolic measures were organized in a matrix X with dimensions $N \times p$. The GMV data was stored in a matrix Y with dimensions $N \times v$. Here, N is the number of participants, p the number of anthropometric and metabolic measures and v the number of GMV voxels. The data matrices were columnwise centered and normalized to eliminate influence of variance differences between measures.

PLSC aims to create latent variables (LV) from the two data sets that maximize their pairwise correlation (Krishnan et al., 2011).

$$maximize(Cov(Xu, Yv)) = maximize(u^T X \times Yv)$$

The solution of this maximization problem is obtained by singular value decomposition (SVD). This operation decomposes the $p \times v$ matrix $X^T Y$ into three matrices $U(p \times R)$, $V(v \times R)$ and $\Delta(R \times R)$ (Abdi, 2007). R is the rank of $X^T Y$, e.g., maximally R pairs of latent variables can be extracted (here $R = 9$).

$$X^T Y = U \Delta V^T$$

U contains the R left singular vectors, Δ is a R-by-R diagnoal matrix containing the R singular values and V contains the R right singular vectors. The singular vectors, or weights, define the latent variables as linear combinations of the original data.

Specifically, $L_x = Xu$ are the LV describing the anthropometric and metabolic measures and $L_y = Yv$ are the latent variables describing the GMV. The first pair of LV explains the largest possible correlation between the two data sets; the second pair reveals the largest possible correlation under the constraint that the latent variables are uncorrelated to the first pair, and so on. In the following, the weights defining the obesity LV are referred to as metabolic profile and the obesity and GMV LV are called metabolic and brain score, respectively.

Statistical Inference

Significance of the resulting decomposition was tested with two approaches: classical permutation-bootstrap inference (Efron and Tibshirani, 1986; McIntosh and Lobaugh, 2004) and a cross-validation framework (Smith et al., 2015).

In the permutation-bootstrap inference, we first determined the significance of the pairs of LV, starting with a full decomposition, e.g., the maximal number of 9 LV pairs. We randomly permuted the rows of the obesity data matrix X while leaving the row order of the imaging data matrix Y unchanged. This process was repeated 2000 times and for each

permutation, the SVD was performed and null-distributions of singular values were built for the pairs of LV. Based on these distributions, a *p*-value was attributed to the original, unpermuted singular values.

$$p = \frac{N(permutedsingularvalue > originalsingularvalue)}{N_{permutations}}$$

A pair of LV was considered significant at a level of $\alpha = 0.05$. The amount of explained covariance was calculated as the singular value of the significant LV pair divided by the sum of all singular values.

When we considered a pair of latent variables generalizable based on the permutation-derived *p*-value, the reliability of the individual weights was estimated by using bootstrap sampling with replacement. We bootstrapped 2000 times from the participants data in the *X* and *Y* matrices and calculated the SVD. Dividing the weights by their standard error derived from bootstrapping yielded a Z-like score, which indicated stable weights when $Z > 2.3$ (Krishnan et al., 2011).

In order to visualize most stable regions, we performed a cluster-forming procedure using FSL's cluster-command with an arbitrary threshold of $Z > 5$.

We also implemented a cross-validation framework according to Smith et al. (2015). First, we randomly selected 80% of the sample for a training set (N∼499) and 20% for a test set (N∼149). Then, we estimated the SVD in the training set and calculated the LV for the test data set by multiplying the resulting weights for brain and obesity-related measures with the raw values of the test data set. This yielded a metabolic and a brain score for each individual. Then, we calculated the correlation of metabolic and brain scores across participants for the test set. In order to establish a null distribution, we randomly permuted the metabolic data matrix within the test set and reprojected the weights derived from the training set onto the permuted raw data ($N = 1000$). Then we compared the correlation of the resulting "random" scores to the original correlation and derived a *p*-value.

We repeated this procedure twenty times, e.g., twenty different training-test datasets, and calculated the average correlation of the true projection, the average correlation of the random projections and the number of significant permutation tests.

The analyses were implemented in python 2.7, based on previously published scripts for PLSC[1]. All code is openly available under https://github.com/fBeyer89/metabolic_VBM_PLSC.

Comparison of BMI and Metabolic Score

We assessed whether a LV based on anthropometric and metabolic measures was a better predictor of GMV than BMI alone. To do so, we compared two models predicting the total GMV, adjusted for intracranial volume, derived by Freesurfer segmentation software, version 5.3.0. Model 1 comprised age, sex and BMI as predictors, and Model 2 additionally included the metabolic score. The model comparison was performed with the function anova in R version 3.2.3.

[1]https://libraries.io/github/chrisfilo/pypls

Sensitivity Analyses

We performed sensitivity analyses using the permutation-bootstrap approach (9 LV, 2000 permutations, 2000 bootstraps) to assess the effect of different confounding factors.

First, we excluded $N = 240$ participants with IL6 values below the detection threshold (<1.5 pg/ml) to ensure that the skewed distribution arising from this threshold did not affect the result. Then, we repeated the analysis excluding 25 participants with markedly high CRP values (>10 mg/l, Macy et al., 1997). Similarly, we repeated the analysis excluding one participant with an outlier value in adiponectin (<average value – 5σ).

Medication intake, specifically antidiabetic and antihyperlipidemic treatment, might have confounded the laboratory measures of HbA1c and total cholesterol/HDL in our analysis. Therefore, we derived medication-adjusted HbA1c and total cholesterol/HDL values by regressing out the intake of antidiabetic or antihyperlipidemic treatment. A binary definition of antidiabetic treatment was used based on self-reported diagnosis or medication intake. For antihyperlipidemic treatment we only took into account self-reported medication intake. Then, we repeated the permutation-bootstrap analysis (9 LV, 2000 permutations, 2000 bootstraps) with the medication-adjusted HbA1c and total cholesterol/HDL values.

Higher BMI is closely linked to higher blood pressure, which is itself linked to GMV differences (Beauchet et al., 2013). Therefore, we investigated the contribution of systolic blood pressure to the metabolic score. We performed another permutation-bootstrap analysis (10 LV, 2000 permutations, 2000 bootstraps) with the previous metabolic and anthropometric measures and additionally including systolic blood pressure, adjusted for age and sex. This measure was available in $N = 740$ participants.

Cognitive Function

Cognitive function was assessed with the Consortium to Establish a Registry for Alzheimer's Disease (CERAD) neuropsychological test battery. We calculated three composite scores for executive function, memory and processing speed according to previous studies (Kharabian Masouleh et al., 2016; Zhang et al., 2018).

Verbal fluency tests "Animals" and "S"-words and the ratio of Trail-making Test (TMT) parts B and A were used to define executive function (Zexecutive = z(number of Animals VF) + z(number of S-words VF) – z(TMT(part B - part A)/part A)/3).

Memory was based on the 10-item CERAD word learning task. The composite score was calculated from the number of learnt words over three consecutive learning trials, the number of correctly recalled words after a delay of about 5 min and the number of correctly recognized word from a list of 20 mixed words [Z memory = (z(number of learned words) + z(number of recalled words) + z(number of recognized words)/3)].

Processing speed was estimated by the inverse value of the time needed to complete TMT part A [Z processing = -z(TMT part A)].

One participant missed data for the TMT.

RESULTS

Demographics

See **Table 1** for demographic and obesity-related characteristics of the study and **Supplementary Figure S7** for bivariate correlations of the anthropometric and metabolic measures used for PLS analysis.

Main Analysis

In the main analysis, we included BMI, WHR, HbA1c, total cholesterol, HDL, CRP, IL6, adiponectin and leptin as anthropometric and metabolic measures, and VBM-based GMV as brain morphometric measure.

Based on the permutation-bootstrap approach, the first two pairs of LV were significant (LV1: $p < 0.001$, LV2: $p = 0.0075$) and explained 44.9%/14.6% of the covariance of anthropometric, metabolic and GMV measures, respectively.

The first pair of LV represents an association of higher metabolic risk and lower GMV in different regions of the brain. The metabolic profile was mainly driven by positive contributions of BMI, WHR, HbA1c, CRP and leptin and a negative contribution of adiponectin. BMI (0.50), leptin (0.39), and CRP (0.33) had the highest weights (see **Figure 1**). These contributions were stable based on the bootstrapped Z-value of $Z > 2.3$.

For the GMV, a distributed pattern in temporal, frontal and occipital lobe as well as subcortical regions and cerebellum had reliable negative weights ($Z > 2.3$) (see **Figure 2**, upper row). Based on an arbitrary threshold of $Z > 5$, thalamus, left cerebellum (Crus VI), bilateral insular cortex, left amygdala/hippocampus, right temporal pole, right planum polare and right postcentral gyrus were identified as most reliable regions (see **Table 2** and **Figure 2**, lower row).

The correlation of the GMV and metabolic LV was $r = 0.246$ ($p < 0.001$, $N = 748$).

TABLE 1 | Demographics of the sample.

	Mean	Standard deviation	Minimum	Maximum
Age [years]	68.4	4.8	60.00	79.00
Sex [males/females]		416/332 (55.6%/44.4%)		
BMI [kg/m2]	27.7	4.1	16.8	42.3
WHR	0.96	0.08	0.73	1.17
HbA1c [%]	5.53	0.59	3.84	12.38
Diabetes diagnosis or intake of anti-diabetic medication [no/yes]		642/106 (85.8/14.2%)		
Total Cholesterol [mmol/l]	5.86	1.08	2.26	10.76
HDL [mmol/l]	5.85	1.10	1.66	10.76
Anti-hyperlipidemic medication [no/yes]		565/183 (75.5%/24.5%)		
CRP [mg/l]	2.95	7.40	0.16	146.92
IL6 [pg/ml]	3.76	3.88	1.50	64.74
Adiponectin [ng/ml]	7710.4	4662.6	2.0	34744.5
Leptin [ng/ml]	12.187	12.135	0.000	88.290
Systolic blood pressure [mmHg]	134.44	16.24	86.33	195.67

Given is mean ± standard deviation (min, max). BMI, body mass index; WHR, waist-to-hip ratio; HbA1c, glycated hemoglobin; HDL, high-density lipoprotein; IL6, interleukin-6; CRP, C-reactive protein.

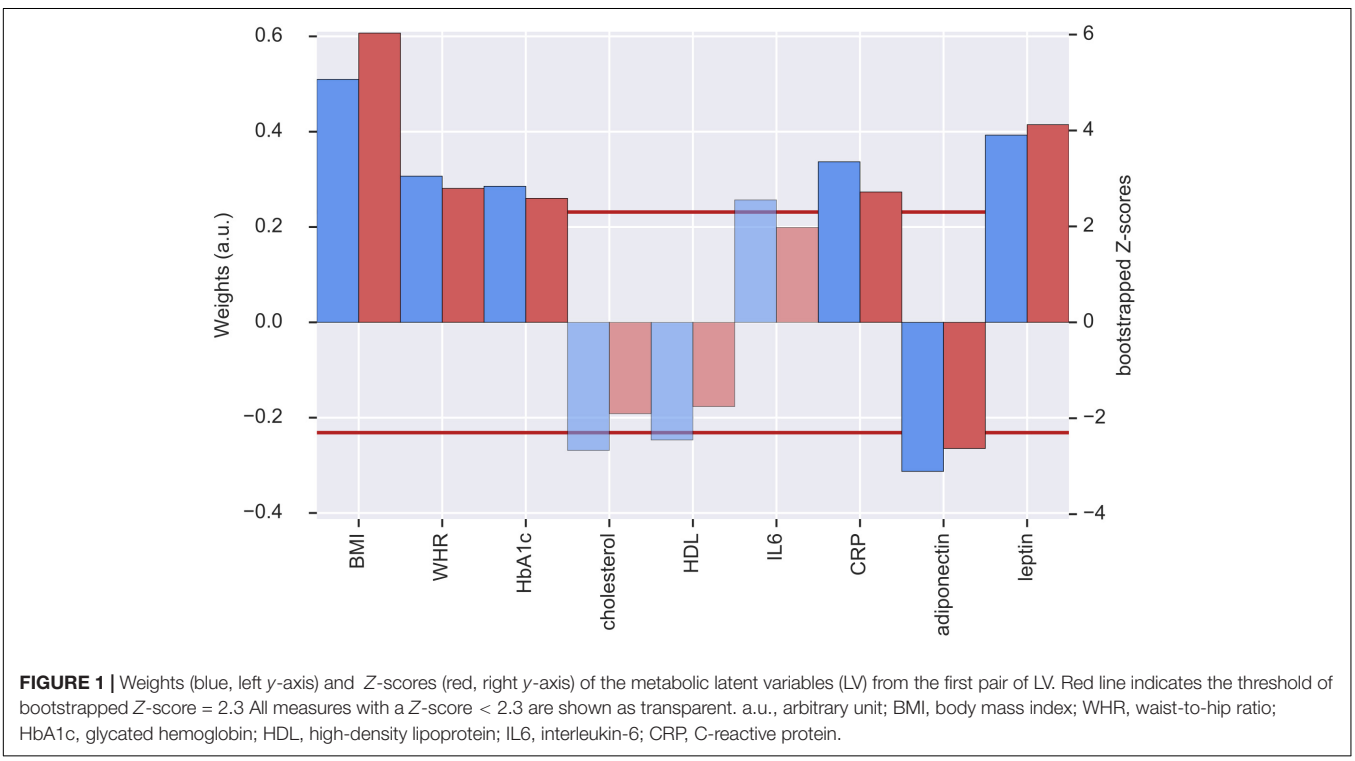

FIGURE 1 | Weights (blue, left y-axis) and Z-scores (red, right y-axis) of the metabolic latent variables (LV) from the first pair of LV. Red line indicates the threshold of bootstrapped Z-score = 2.3 All measures with a Z-score < 2.3 are shown as transparent. a.u., arbitrary unit; BMI, body mass index; WHR, waist-to-hip ratio; HbA1c, glycated hemoglobin; HDL, high-density lipoprotein; IL6, interleukin-6; CRP, C-reactive protein.

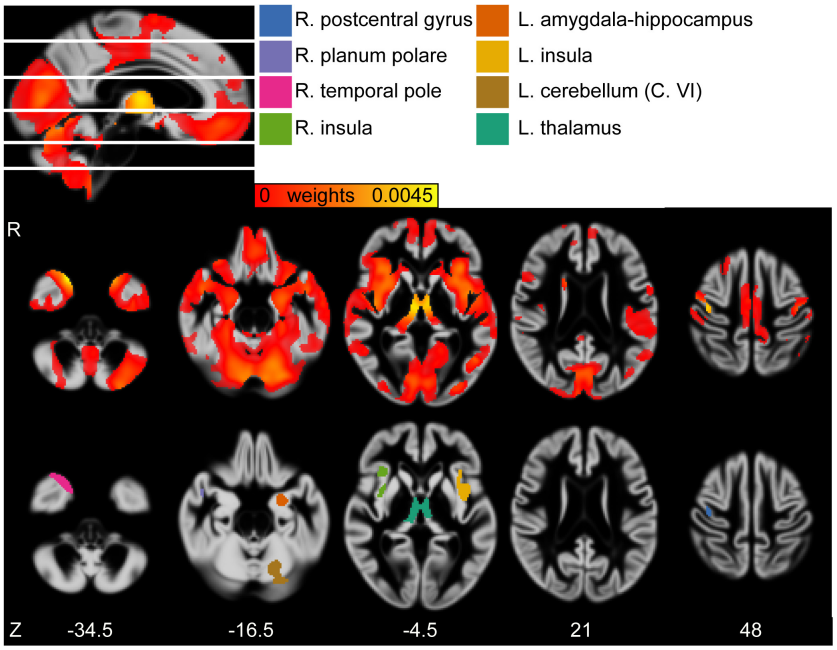

FIGURE 2 | (First row) Sagittal view of the gray matter volume (GMV) weight map of first latent variables (LV). White lines indicate axial slices shown in second row. **(Second row)** Axial view of GMV weight map of first LV. **(Third row)** Axial view of clusters derived from bootstrapped $Z > 5$. MNI-coordinates are given in mm for axial orientation (Z). Legend refers to clusters shown in third row. L, left; R, right.

The second pair of LV had positive and reliable weights for total cholesterol and HDL (see **Figure 3**). Three clusters of reliable, positive weights were found in the posterior cingulate and bilateral lateral occipital cortex (see **Figure 4**). The correlation of the second pair of latent variables was $r = 0.22$ ($p < 0.001$, $N = 748$).

We applied a cross-validation framework to assess the reliability of the first two pairs of LV.

The mean and standard deviation of the correlation between the first LV in the test data sets was 0.241 ± 0.074 ($N = 149$). Out of 20 training-test data sets, the first LV did not reach nominal significance of $p < 0.05$ in two data sets where p-values were 0.13 and 0.094.

The mean and standard deviation of the correlation between the second LV in the test data sets was 0.10 ± 0.07 ($N = 149$). Out of 20 training-test data sets, the second LV did not reach nominal significance of $p < 0.05$ in thirteen data sets.

While in the permutation-bootstrap approach the amount of variance explained in the original dataset was significant, the correlation of the second pair of LV was not stable in the cross-validation approach. In PLSC, the second pair of LV is constrained by its orthogonality to the first pair. This means that the second pair of LV represented an orthogonal mode of variation within the anthropometric and metabolic measures that might, given the relative low amount of variance explained (∼15%), have a limited interpretation. For the following analysis, we thus focus on the results for the first pair of LV.

TABLE 2 | Significant clusters of gray matter volume (GMV) weight map of the first set of latent variables (LV) according to multivariate partial least squares correlation (PLSC) analysis, according to bootstrapped Z with an arbitrary threshold of $Z > 5$.

Region	Number of voxels	MNI coordinates of peak voxel (X,Y,Z)	Bootstrapped Z at peak voxel	Weight at peak voxel
Thalamus (Th.)	1408	55, 71, 57	6.94	0.0045
Left cerebellum (Crus VI)	756	68, 40, 40	5.83	0.0037
Left insular cortex	419	83, 84, 50	5.9	0.0031
Left amygdala/ hippocampus	353	75, 80, 35	5.66	0.0031
Right insular cortex	347	37, 84, 50	5.53	0.0032
Right temporal pole	343	46, 90, 26	7.27	0.0044
Right planum polare	139	30, 80, 43	5.82	0.0034
Right Postcentral gyrus	101	34, 71, 80	6.3	0.0039

Comparison of BMI and Metabolic Score

In Model 1, age, sex and BMI were all significant predictors of total GMV adjusted for TIV (see **Table 3**). Yet, model 2 which additionally included the metabolic score, predicted total GMV slightly better (see **Table 3**, model comparison: $F = 4.1$, $p < 0.042$). This indicates metabolic measures explain additional variance compared to anthropometry when investigating GMV differences related to higher BMI.

Sensitivity Analysis

We performed sensitivity analysis to detect possible confounding effects on the first pair of LV.

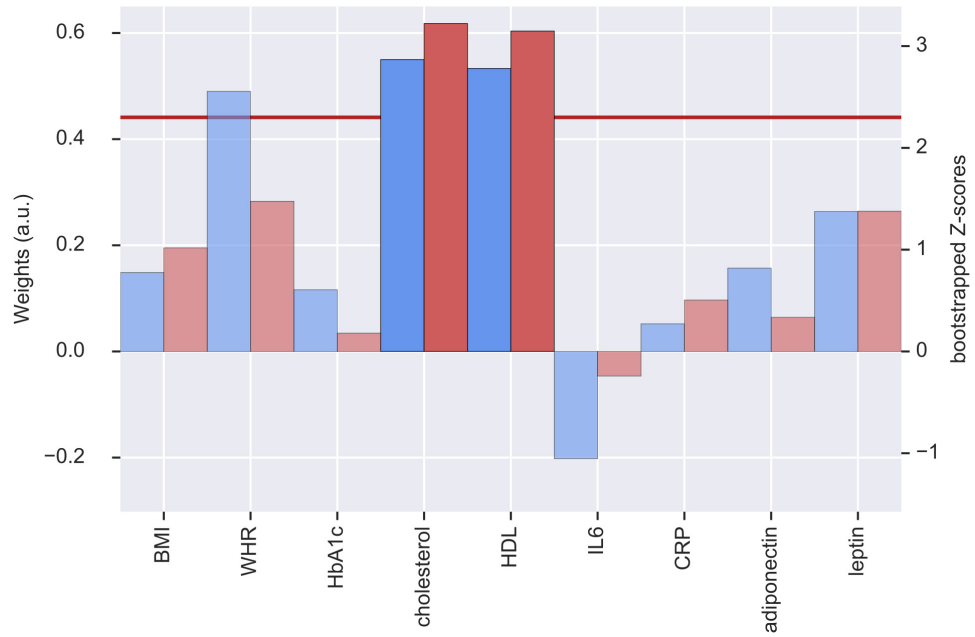

FIGURE 3 | Weights (blue, left *y*-axis) and *Z*-scores (red, right *y*-axis) of the metabolic latent variables (LV) from the second pair of LV. Red line indicates the threshold of bootstrapped *Z*-score = 2.3. All measures with a *Z*-score < 2.3 are shown as transparent. a.u., arbitrary unit; BMI, body mass index; WHR, waist-to-hip ratio; HbA1c, glycated hemoglobin; HDL, high-density lipoprotein; IL6, interleukin-6; CRP, C-reactive protein.

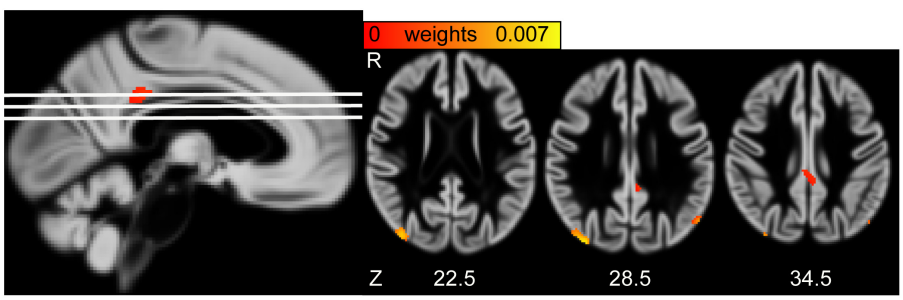

FIGURE 4 | (Left) Sagittal view of the gray matter volume (GMV) saliency weight map of second latent variables (LV). White lines indicate axial slices shown on the right. **(Right)** Axial view of GMV weight map of second LV. MNI-coordinates are given in mm for axial orientation (Z). R, Right.

IL6 Below Detection Threshold

When excluding participants with IL6 values below the detection threshold, the first pair of LV was similar to the main analysis ($p < 0.001$, explained covariance = 0.41). BMI and leptin had negative weights. Adiponectin had a stable positive contribution as well as HDL and cholesterol which reached the threshold of $Z > 2.3$ in this analysis (see **Supplementary Figure S1**). WHR and CRP did not contribute reliably to the metabolic score of the first LV. The weights of the GMV score remained essentially unchanged.

Outliers in CRP and Adiponectin

Here, we excluded participants with markedly high CRP values (>10 mg/l, $N = 25$) who might have had an acute infection or another reason for elevated CRP at the time of the assessment. The first pair of LV were very similar to the main analysis, except that the bootstrapped Z-value of CRP dropped to 2.26 below the pre-defined threshold of 2.3 (see **Supplementary Figure S2**). The pattern of the GMV score was essentially unchanged.

When removing one participant with an outlying value in adiponectin ($N = 1$), we did not see any differences in the metabolic and GMV scores (see **Supplementary Figure S3**).

Systolic Blood Pressure as Additional Predictor

We added systolic blood pressure as another important cardiovascular risk factor to see whether it explained additional variance in the obesity-GMV association. There was no reliable contribution of systolic blood pressure to the first obesity LV (see **Supplementary Figure S4**) but the positive contribution of total cholesterol and HDL to the metabolic score became significant.

The GMV score did not change.

TABLE 3 | Statistics according to linear regression models predicting total gray matter volume (GMV).

Total GMV adjusted for head size	Model 1 (R^2_{adj} = 0.207)			Model 2 (R^2_{adj} = 0.213)		
	st. β	*T*	*p*	st. β	*T*	*p*
Age	−0.27	−8.3	< 0.0001	−0.27	−8.3	< 0.0001
Sex	0.30	9.3	< 0.0001	0.31	9.4	< 0.0001
BMI	−0.17	−5.4	< 0.0001	−0.09	−1.73	0.084
Metabolic score (LV1)				0.11	2.1	0.042

Model 1 included age, sex, and body mass index (BMI). Model 2 additionally included the metabolic score from the first set of latent variables (LV) according to multivariate partial least squares analysis (see text for details). st. β, standardized ß-coefficient of the linear regression; R^2_{adj}, adjusted R^2.

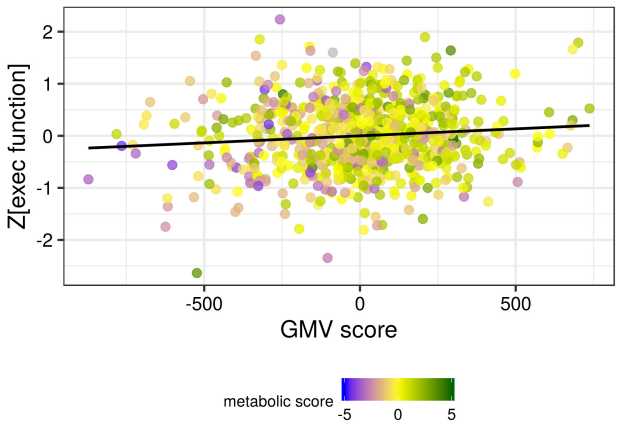

FIGURE 5 | The gray matter volume (GMV) score was positively associated with the sum score of executive function. A higher metabolic score (corresponding to lower BMI and indicated by the color coding shown in the legend) was associated with both higher GMV score and higher executive function. Black line indicates the locally smoothed average.

Analysis Adjusting for Intake of Antidiabetic and Antihyperlipidemic Medication

To see whether the observed mode of covariation was driven by manifest metabolic disease, like diabetes or hyperlipidemia, we regressed the treatment of those conditions from the respective variables HbA1c and total cholesterol/HDL. After this correction, HbA1c did not contribute to the first obesity LV anymore, indicating that the heightened levels of HbA1c in diabetic patients might have driven the involvement of HbA1c in the first obesity LV (see **Supplementary Figure S5**). The weights of the GMV LV were unchanged.

Association of the Metabolic Score and Cognitive Function

We performed linear regression to determine the association of the brain and metabolic scores and three sum scores of cognitive function.

For executive function, we found a significant positive association of brain and metabolic score with the sum score (standardized β_{ob} = 0.084, p = 0.021; standardized β_{brain} = 0.098, p = 0.007). Higher score on the brain LV and higher score in the metabolic LV (with negative loadings of BMI and WHR) both predicted better executive function (see **Figure 5**). When excluding one participant with outlying value in adiponectin, the pattern was even more pronounced (see **Supplementary Figure S6**).

No association between brain or metabolic LV was found for the memory sum score.

Processing speed was positively associated with the brain LV but not the metabolic LV (standardized β_{ob} = −0.019, p = 0.59; standardized β_{brain} = 0.132, p < 0.001).

DISCUSSION

In this study, we showed that a metabolic profile of obesity predicted lower GMV in a large population-based sample of older adults. Higher BMI, WHR, leptin, HbA1c, CRP and lower adiponectin levels were jointly associated with reduced GMV in cortical, subcortical and cerebellar brain regions, including the thalamus, insular cortex and temporal pole. We used two inference schemes and performed sensitivity analysis for potential confounding of outliers, detection thresholds and medication intake. Higher scores in the metabolic score and the GMV score predicted better executive function performance.

The Metabolic Profile

The metabolic profile of the first LV represents common metabolic dysregulations in obesity (Van Gaal et al., 2006).

Leptin and BMI had the highest weights in the metabolic profile. BMI is the ratio of body weight to height and an indirect estimate of body fat (Frankenfield et al., 2001). Yet, due to age-related changes in body composition, BMI might lack sensitivity to detect individuals with excess body fat in the older population (Romero-Corral et al., 2008; Stenholm et al., 2008). Here, leptin levels are a more accurate estimator of total body fat, as they increase with the amount of overall adipose tissue in the body (Considine et al., 1996; Ostlund et al., 1996).

In the present sample, the high weights of leptin and BMI in the profile indicate that the overall amount of adipose tissue is a strong predictor of reduced GMV in older adults. This suggests that factors underlying a sustained energy imbalance, like sedentary lifestyle or intake of energy-dense food, might be important determinants of gray matter structure in aging (Erickson et al., 2010; Dingess et al., 2017; Kreutzer et al., 2017).

Considering the central effects of leptin, it is also possible that leptin levels are directly associated with brain structure. Yet, previous studies showed mixed results in that both lower and higher leptin levels predicted reduced GMV in older individuals (Narita et al., 2009; Rajagopalan et al., 2013). To reconcile these contradictory findings it is important to consider the BMI distribution of the study population. Obesity goes along with elevated leptin levels and leptin resistance, which may lead to central deficiency and impaired beneficial action of this hormone in the brain (Paz-Filho et al., 2010). Therefore, both low and chronically elevated leptin levels might be associated with

structural brain differences, especially in the hippocampus (Lieb et al., 2009; Witte et al., 2016).

In line with the literature, adiponectin was inversely related to leptin and BMI in the metabolic profile of LV1 (Havel, 2002). As adiponectin might have positive effects on brain function related to its insulin-sensitizing and anti-inflammatory properties (Lihn et al., 2005), reduced levels of adiponectin might indirectly contribute to reduced GMV.

Smaller weights were found for WHR and CRP in the metabolic profile. WHR – in contrast to BMI and leptin – reflects the distribution of adipose tissue and is considered a measure of visceral adiposity. Having a higher amount of visceral adipose tissue is linked to a higher risk for cardiovascular disease (Lee et al., 2008) due to specific functions of this fat tissue. Visceral fat tissue releases pro-inflammatory cytokines, like IL6, and short-chain fatty acids, factors involved in the development of the metabolic syndrome and arteriosclerosis (Després and Lemieux, 2006; Bergman Richard et al., 2012; Item and Konrad, 2012). In line with these findings, the inflammation marker CRP contributed to the metabolic profile, even though the association is attenuated when excluding participants with extremely elevated CRP-levels. This points to the low specificity of CRP which is a measure of both localized and systemic inflammation and might therefore be confounded by participants with acute infections in the sample.

IL6, a pro-inflammatory cytokine secreted by visceral adipose tissue (Fontana et al., 2007), had no significant weight in the metabolic profile although it added to the profile in a similar direction as CRP. This might be due to the reduced sensitivity of the laboratory assessment and the resulting skewed distribution. When excluding participants with IL6 values below the detection threshold, CRP no longer contributed to the metabolic profile. This indicates that in participants with IL6 values below the detection threshold, relevant variance regarding inflammatory processes is captured in the high-sensitivity CRP we assessed.

Overall, the contribution of WHR and CRP to the metabolic profile shows that beyond increased whole-body fat mass (measured by BMI and leptin), visceral adipose tissue and related systemic inflammation play a role in obesity-related GMV reductions. Pro-inflammatory cytokines can cross the blood-brain barrier (Hsuchou et al., 2012) and thereby promote inflammatory reactions in the central nervous system (Erickson et al., 2012; Spielman et al., 2014). One example is the chronic activation of microglia, that triggers the production of reactive oxygen species (ROS) and pro-inflammatory cytokines, and may lead to neuronal loss (Spielman et al., 2014; Colonna and Butovsky, 2017).

Long-term glucose marker HbA1C had a significant and reliable weight in the metabolic profile, indicating that disturbed glucose and insulin metabolism is another pathway linking obesity to reduced GMV. High blood glucose levels enchain the production of advanced glycation end-products (AGEs) which trigger the production of ROS and may lead to inflammatory reactions (Yan et al., 2008). Thereby, elevated glucose levels might damage vasculature or enhance neuroinflammation (Yan et al., 2008). Insulin resistance may also damage the brain, given the importance of insulin for neuromodulatory and –protective processes as well as memory and cognition (Craft and Watson, 2004; Blázquez et al., 2014).

Our sample included around 100 individuals with diabetes and when we adjusted for intake of antidiabetic medication, HbA1c no longer contributed to the metabolic profile. This result indicates that the contribution of HbA1c might have been driven by GMV difference in diabetic patients. In line with this interpretation, pronounced GMV differences have been reported in diabetic patients while more subtle associations, mostly limited to the hippocampus, have been reported in the range of normal glucose metabolism (Benedict et al., 2012; Moran et al., 2013; Shaw et al., 2017).

Regarding the lipid metabolism, we did not find a stable contribution of total or HDL cholesterol to the metabolic profile in the main analysis. Still, we found that total and HDL cholesterol positively covaried with the metabolic profile, this effect was more pronounced when we excluded participants with IL6 below the detection threshold or included systolic blood pressure. In the literature, no or negative associations have been reported for total cholesterol and GMV (Enzinger et al., 2005; Chen et al., 2006; Walhovd et al., 2014) while one study found a positive association of HDL and GMV (Ward et al., 2010). Adjusting for intake of lipid-lowering medication did not change the result. Interestingly, in our sample, total cholesterol and HDL were highly correlated, and against our expectations, total cholesterol was negatively correlated with BMI (standardized $\beta = -0.13$, $p < 0.001$, adjusted for age and sex). This might explain why the lipid measures were not reliably included into the profile.

Chronically elevated blood pressure is commonly found in older age and strongly associated with obesity. Elevated blood pressure is a strong predictor of brain damage, in form of lacunar infarcts, white matter hyperintensities and GMV loss (Beauchet et al., 2013; Suzuki et al., 2017; Haight et al., 2018). Still, systolic blood pressure did not contribute to the metabolic profile when it was included along with the other predictors. We noticed that BMI was weakly negatively associated with systolic blood pressure in this sample (standardized $\beta = -0.075$, $p = 0.04$, adjusted for age and sex) which might explain why systolic blood pressure was not included into the profile.

The GMV Pattern Associated With the Metabolic Profile

We found a consistent association of the metabolic profile and lower GMV in thalamus, bilateral insular cortex, left amygdala-hippocampus, temporal pole and the cerebellum. These findings are in line with the literature where mostly negative associations between obesity and GMV are reported (Willette and Kapogiannis, 2015). More specifically, a recent meta-analysis reported BMI-associated reductions of GMV in temporal pole and cerebellum (Garcia-Garcia et al., 2018). The cerebellum not only contributes to the planning of motor actions but also plays an important role for cognition (Buckner et al., 2011). Importantly, atrophy patterns related to neurodegenerative disease reflect cerebellar-cortical connectivity patterns, e.g., the cerebellar regions which are functionally

connected to the default mode network show atrophy in Alzheimer's disease (Guo et al., 2016). It is therefore plausible that obesity-associated metabolic factors, associated with differences in specific brain networks, might also contribute to cerebellar atrophy (Haight et al., 2015; Beyer et al., 2017; Kharabian Masouleh et al., 2018).

Differences in thalamic, insula and amygdalar-hippocampal GMV have not been reported in the meta-analysis, but were found in univariate analysis of obesity-related factors such as CRP (Corlier et al., 2018), HbA1c (Reitz et al., 2016), and BMI (Kharabian Masouleh et al., 2016). The current study investigated the univariate association of BMI and GMV in a partly overlapping sample with Kharabian Masouleh et al. (2016) (N = 412 or 55% overlap with the present sample) and found similar clusters in thalamus, parahippocampal gyrus and temporal lobe. These regions show a decline in GMV over the adult life span, and possibly, obesity and related metabolic factors enhance this effect, as proposed by the increased brain age observed in white matter of obese participants (Storsve et al., 2014; He et al., 2015; Ronan et al., 2016).

In contrast to previous studies, the metabolic profile was not predominantly associated with frontal GMV in our analysis. Still, medial orbitofrontal and superior frontal cortex were reliably ($Z > 2.3$) linked to the metabolic profile. Studies suggested that reduced GMV in obesity might not only be a consequence but also a potential genetic risk factor for developing obesity (Opel et al., 2017). Thus, genetic factors, among others, might have contributed to the observed GMV differences in our study. Possible mediators include executive functions and impulsive behavior which might impact eating behavior and thereby lead to weight gain (Chuang et al., 2015). However, as our analysis did not include genetic or behavioral traits, in addition to its cross-sectional design, interpretation of causes and consequences underlying GMV differences is limited.

Expanding the study by Kharabian Masouleh et al. (2016), we used a multivariate strategy to characterize the association of obesity and GMV in older adults. Accordingly, the individual metabolic profile score explained more variance in total GMV than BMI alone. This analysis was independent of the actual pattern of GMV associated with the metabolic score. Yet, the overall amount of variance in total GMV explained by the metabolic score is relatively small (∼3%) compared to the variance explained by age and sex (∼18%).

Cognitive Function

Regarding the relevance of our findings for cognitive function, exploratory analyses suggested that executive function was gradually decreased along the axis of the first obesity-brain LV. Both lower metabolic LV and higher GMV LV were associated with increased performance in the domain of executive function. This result expands previous findings of reduced executive function related to increased BMI reported in a partly overlapping sample by Kharabian Masouleh et al. (2016), and shows that reduced GMV in distributed brain regions might mediate this effect.

We did not find an association of memory performance and the GMV pattern of the first LV. While there was no direct association of BMI and memory performance, (Kharabian Masouleh et al., 2016) found an indirect effect, mediated by GMV in frontal and thalamic clusters. Our analysis was possibly not suited to replicate this region-specific association between brain and cognition, given that we derived a wide-spread GMV pattern which, among others, included frontal and thalamic clusters.

We found a positive association of the GMV pattern and processing speed, but not obesity-related LV and processing speed. This might reflect the fact that both executive function and processing speed sum scores are derived from the trail-making-test, and therefore are partly collinear.

These exploratory results are largely in line with the literature, where mid-life obesity has been linked to reduced cognitive function in various cognitive domains (van den Berg et al., 2009; Prickett et al., 2015). More specifically, our results support the view that executive function might be more affected by vascular risk factors than other cognitive domains, such as verbal memory (Wolf et al., 2007; Debette and Markus, 2010) and that metabolic disturbances linearly add to obesity-related cognitive decline (Singh-Manoux et al., 2012).

Strengths and Limitations of the Current Study

Strengths of this study include a large, well-characterized participants sample and a comprehensive multivariate analysis employing two validation schemes. Additionally, we performed sensitivity analysis and assessed cognitive function of the participants with a standardized neuropsychological test battery.

The main limitation of this study is that we cannot draw causal inferences based on our cross-sectional data.

We reported a relatively specific metabolic profile and a widespread pattern of GMV loss. Yet, due to our multivariate approach we cannot conclude whether certain metabolic factors, e.g., pro-inflammatory cytokines, mediate the association or if they have independent effects on GMV loss. Furthermore, we cannot test regionally specific associations of single metabolic factors with GMV loss. This problem might be partly overcome by using sparse PLSC techniques in future studies (Monteiro et al., 2016). Introducing a sparsity constraint to the PLSC decomposition reduces the number of features, e.g., voxels, and forces many features to have zero weights. This may aid interpretability especially for high-dimensional MRI data. Another drawback of the PLSC approach was the limited interpretability of higher-order latent variables which are constrained to be orthogonal to previous LV (Krishnan et al., 2011).

CONCLUSION

Taken together, we provided evidence that a metabolic obesity profile characterized by increased body fat, visceral adiposity and systemic inflammation was associated with a widespread pattern of decreased GMV. The brain-obesity covariation was stable in two validation schemes and predicted executive function in a large sample of older adults without diagnosis of cognitive impairment. We suggest that this unfavorable metabolic profile

might contribute to reduced executive function via damage to the gray matter in widespread brain regions.

Following our study, further research is needed to establish the causal relationship between obesity, decreased gray matter volume and cognitive function in aging. Our results indicated a main contribution of overall fat mass and visceral adiposity, which should be tested in longitudinal studies. Given the importance of lifestyle factors in mid-life for cognitive function later in life, these studies might benefit from considering body weight trajectories or using cumulative measures of metabolic burden such as "obesity pack years" (Abdullah et al., 2011; Pedditizi et al., 2016).

Furthermore, investigating measures of brain health beyond gray matter structure, such as imaging markers of cerebral small vessel disease and white matter microstructure, might help to understand the complete picture linking obesity, cardiovascular risk and cognitive decline in aging.

DATA AVAILABILITY

The datasets generated for this study are available on request to the corresponding author.

ETHICS STATEMENT

This study was carried out in accordance with the Declaration of Helsinki and approved by the institutional ethics board of the Medical Faculty of the University of Leipzig. All subjects gave written informed consent.

AUTHOR CONTRIBUTIONS

FB developed the research question, performed the analysis, created the figures, and drafted the manuscript. SM refined the research question, helped with the analysis, and revised the manuscript. JK conducted the biomarker analysis and revised the manuscript. MS designed the study and revised the manuscript. SR designed the study, implemented the cognitive testing, and revised the manuscript. SR-H and AV designed the study and revised the manuscript. AW refined the research question, discussed the data analysis, and drafted and revised the manuscript.

FUNDING

This work was supported by the grants from the European Union, the European Regional Development Fund, the Free State of Saxony within the framework of the excellence initiative, the LIFE–Leipzig Research Center for Civilization Diseases, University of Leipzig (Project Numbers: 713-241202, 14505/2470, 14575/2470, and 100329290). The authors also received grants from the German Research Foundation, contract grant number CRC 1052 "Obesity mechanisms" Project A1, A. Villringer/M. Stumvoll, SCHR 774/5-1 to MS, and WI 3342/3-1 to AW. This work was also supported by the Max Planck Society.

ACKNOWLEDGMENTS

We would like to thank all the participants and staff of the LIFE-Adult study – especially Ulrike Scharrer, Annett Wiedermann, and Kerstin Wirkner and her team.

SUPPLEMENTARY MATERIAL

The Supplementary Material for this article can be found online at: https://www.frontiersin.org/articles/10.3389/fnagi.2019.00202/full#supplementary-material

REFERENCES

Abdi, H. (2007). "Singular value decomposition (SVD) and generalized singular value decompositon (GSVD)," in *Encyclopedia of Measurement and Statistics*, ed. N. Salkind (Thousand Oaks, CA: Sage), 907–912.

Abdullah, A., Wolfe, R., Stoelwinder, J. U., De Courten, M., Stevenson, C., Walls, H. L., et al. (2011). The number of years lived with obesity and the risk of all-cause and cause-specific mortality. *Int. J. Epidemiol.* 40, 985–996. doi: 10.1093/ije/dyr018

Assessment, R. (2009). Major lipids, apolipoproteins, and risk of vascular disease. *JAMA* 302, 1993–2000. doi: 10.1001/jama.2009.1619

Baumgart, M., Snyder, H. M., Carrillo, M. C., Fazio, S., Kim, H., and Johns, H. (2015). Summary of the evidence on modifiable risk factors for cognitive decline and dementia: a population-based perspective. *Alzheimers Dement.* 11, 718–726. doi: 10.1016/j.jalz.2015.05.016

Beauchet, O., Celle, S., Roche, F., Bartha, R., Montero-Odasso, M., Allali, G., et al. (2013). Blood pressure levels and brain volume reduction: a systematic review and meta-analysis. *J. Hypertens.* 31, 1502–1516. doi: 10.1097/HJH.0b013e32836184b5

Benedict, C., Brooks, S. J., Kullberg, J., Burgos, J., Kempton, M. J., Nordenskjöld, R., et al. (2012). Impaired insulin sensitivity as indexed by the homa score is associated with deficits in verbal fluency and temporal lobe gray matter volume in the elderly. *Diabetes Care* 35, 488–494. doi: 10.2337/dc11-2075

Bergman Richard, N., Kim Stella, P., Catalano Karyn, J., Hsu Isabel, R., Chiu Jenny, D., Kabir, M., et al. (2012). why visceral fat is bad: mechanisms of the metabolic syndrome. *Obesity* 14, 16S–19S. doi: 10.1038/oby.2006.277

Beyer, F., Kharabian Masouleh, S., Huntenburg, J. M., Lampe, L., Luck, T., Riedel-Heller, S. G., et al. (2017). Higher body mass index is associated with reduced posterior default mode connectivity in older adults. *Hum. Brain Mapp.* 38, 3502–3515. doi: 10.1002/hbm.23605

Biessels, G. J., and Reijmer, Y. D. (2014). Brain changes underlying cognitive dysfunction in diabetes: what can we learn from MRI? *Diabetes* 63, 2244–2252. doi: 10.2337/db14-0348

Blázquez, E., Velázquez, E., Hurtado-Carneiro, V., and Ruiz-Albusac, J. M. (2014). Insulin in the brain: its pathophysiological implications for states related with central insulin resistance, type 2 diabetes and Alzheimer's Disease. *Front. Endocrinol.* 5:161. doi: 10.3389/fendo.2014.00161

Bobb, J. F., Schwartz, B. S., Davatzikos, C., and Caffo, B. (2014). Cross-sectional and longitudinal association of body mass index and brain volume. *Hum. Brain Mapp.* 35, 75–88. doi: 10.1002/hbm.22159

Buckner, R. L., Krienen, F. M., Castellanos, A., Diaz, J. C., and Yeo, B. T. T. (2011). The organization of the human cerebellum estimated by intrinsic

functional connectivity. *J. Neurophysiol.* 106, 2322–2345. doi: 10.1152/jn.00339.2011

Cheke, L. G., Bonnici, H. M., Clayton, N. S., and Simons, J. S. (2017). Obesity and insulin resistance are associated with reduced activity in core memory regions of the brain. *Neuropsychologia* 96, 137–149. doi: 10.1016/j.neuropsychologia.2017.01.013

Chen, X., Wen, W., Anstey, K. J., and Sachdev, P. S. (2006). Effects of cerebrovascular risk factors on gray matter volume in adults aged 60–64 years: a voxel-based morphometric study. *Psychiatry Res. Neuroimaging* 147, 105–114. doi: 10.1016/j.pscychresns.2006.01.009

Cherbuin, N., Sachdev, P., and Anstey, K. J. (2012). Higher normal fasting plasma glucose is associated with hippocampal atrophy: the path study. *Neurology* 79, 1019–1026. doi: 10.1212/wnl.0b013e31826846de

Chuang, Y. F., Tanaka, T., Beason-Held, L. L., An, Y., Terracciano, A., Sutin, A. R., et al. (2015). FTO genotype and aging: pleiotropic longitudinal effects on adiposity, brain function, impulsivity and diet. *Mol. Psychiatr.* 20, 140–147. doi: 10.1038/mp.2014.49

Cisternas, P., Martinez, M., Ahima, R. S., Wong, G. W., and Inestrosa, N. C. (2018). Modulation of glucose metabolism in hippocampal neurons by adiponectin and resistin. *Mol. Neurobiol.* 56, 3024-3037. doi: 10.1007/s12035-018-1271-x

Colonna, M., and Butovsky, O. (2017). Microglia function in the central nervous system during health and neurodegeneration. *Annu. Rev. Immunol.* 35, 441–468. doi: 10.1146/annurev-immunol-051116-052358

Considine, R. V., Sinha, M. K., Heiman, M. L., Kriauciunas, A., Stephens, T. W., Nyce, M. R., et al. (1996). Serum Immunoreactive-leptin concentrations in normal-weight and obese humans. *N. Engl. J. Med.* 334, 292–295. doi: 10.1056/nejm199602013340503

Corlier, F., Hafzalla, G., Faskowitz, J., Kuller, L. H., Becker, J. T., Lopez, O. L., et al. (2018). Systemic inflammation as a predictor of brain aging: contributions of physical activity, metabolic risk, and genetic risk. *NeuroImage* 172, 118–129. doi: 10.1016/j.neuroimage.2017.12.027

Cox, S. R., Lyall, D. M., Ritchie, S. J., Bastin, M. E., Harris, M. A., Buchanan, C. R., et al. (2019). Associations between vascular risk factors and brain MRI indices in UK biobank. *bioRxiv* 511253. doi: 10.1093/eurheartj/ehz100

Craft, S. (2005). Insulin resistance syndrome and Alzheimer's disease: age- and obesity-related effects on memory, amyloid, and inflammation. *Neurobiol. Aging* 26(Suppl. 1), 65–69. doi: 10.1016/j.neurobiolaging.2005.08.021

Craft, S., and Watson, G. S. (2004). Insulin and neurodegenerative disease: shared and specific mechanisms. *Lancet Neurol.* 3, 169–178. doi: 10.1016/s1474-4422(04)00681-7

Debette, S., Beiser, A., Hoffmann, U., Decarli, C., O'donnell, C. J., Massaro, J. M., et al. (2010). Visceral fat is associated with lower brain volume in healthy middle-aged adults. *Ann. Neurol.* 68, 136–144. doi: 10.1002/ana.22062

Debette, S., and Markus, H. S. (2010). The clinical importance of white matter hyperintensities on brain magnetic resonance imaging: systematic review and meta-analysis. *BMJ* 341, c3666. doi: 10.1136/bmj.c3666

Debette, S., Seshadri, S., Beiser, A., Au, R., Himali, J. J., Palumbo, C., et al. (2011). Midlife vascular risk factor exposure accelerates structural brain aging and cognitive decline. *Neurology* 77, 461–468. doi: 10.1212/WNL.0b013e318227b227

Debette, S., Wolf, C., Lambert, J.-C., Crivello, F., Soumaré, A., Zhu, Y.-C., et al. (2014). Abdominal obesity and lower gray matter volume: a Mendelian randomization study. *Neurobiol. Aging* 35, 378–386. doi: 10.1016/j.neurobiolaging.2013.07.022

Després, J.-P., and Lemieux, I. (2006). Abdominal obesity and metabolic syndrome. *Nature* 444, 881–887.

Dingess, P. M., Darling, R. A., Kurt Dolence, E., Culver, B. W., and Brown, T. E. (2017). Exposure to a diet high in fat attenuates dendritic spine density in the medial prefrontal cortex. *Brain Struct. Funct.* 222, 1077–1085. doi: 10.1007/s00429-016-1208-y

Efron, B., and Tibshirani, R. (1986). Bootstrap methods for standard errors, confidence intervals, and other measures of statistical accuracy. *Stat. Sci.* 1:77. doi: 10.1214/ss/1177013817

Emmerzaal, T. L., Kiliaan, A. J., and Gustafson, D. R. (2015). 2003-2013: a decade of body mass index, Alzheimer's disease, and dementia. *J. Alzheimers Dis.* 43, 739–755. doi: 10.3233/JAD-141086

Enzinger, C., Fazekas, F., Matthews, P. M., Ropele, S., Schmidt, H., Smith, S., et al. (2005). Risk factors for progression of brain atrophy in aging: six-year follow-up of normal subjects. *Neurology* 64, 1704–1711. doi: 10.1212/01.wnl.0000161871.83614.bb

Erickson, K. I., Raji, C. A., Lopez, O. L., Becker, J. T., Rosano, C., Newman, A. B., et al. (2010). Physical activity predicts gray matter volume in late adulthood: the cardiovascular health study. *Neurology* 75, 1415–1422. doi: 10.1212/WNL.0b013e3181f88359

Erickson, M. A., Dohi, K., and Banks, W. A. (2012). Neuroinflammation: a Common Pathway in CNS diseases as mediated at the blood-brain barrier. *Neuroimmunomodulation* 19, 121–130. doi: 10.1159/000330247

Fontana, L., Eagon, J. C., Trujillo, M. E., Scherer, P. E., and Klein, S. (2007). Visceral fat adipokine secretion is associated with systemic inflammation in obese humans. *Diabetes* 56, 1010–1013. doi: 10.2337/db06-1656

Frankenfield, D. C., Rowe, W. A., Cooney, R. N., Smith, J. S., and Becker, D. (2001). Limits of body mass index to detect obesity and predict body composition. *Nutrition* 17, 26–30. doi: 10.1016/s0899-9007(00)00471-8

García-Casares, N., García-Arnés, J. A., Rioja, J., Ariza, M. J., Gutiérrez, A., Alfaro, F., et al. (2016). Alzheimer's like brain changes correlate with low adiponectin plasma levels in type 2 diabetic patients. *J. Diabetes Complicat.* 30, 281–286. doi: 10.1016/j.jdiacomp.2015.12.001

Garcia-Garcia, I., Michaud, A., Dadar, M., Zeighami, Y., Neseliler, S., Collins, D. L., et al. (2018). Neuroanatomical differences in obesity: meta-analytic findings and their validation in an independent dataset. *Int. J. Obes.* 43, 943–951. doi: 10.1038/s41366-018-0164-4

Grellmann, C., Bitzer, S., Neumann, J., Westlye, L. T., Andreassen, O. A., Villringer, A., et al. (2015). Comparison of variants of canonical correlation analysis and partial least squares for combined analysis of MRI and genetic data. *Neuroimage* 107, 289–310. doi: 10.1016/j.neuroimage.2014.12.025

Guo, C. C., Tan, R., Hodges, J. R., Hu, X., Sami, S., and Hornberger, M. (2016). Network-selective vulnerability of the human cerebellum to Alzheimer's disease and frontotemporal dementia. *Brain* 139, 1527–1538. doi: 10.1093/brain/aww003

Gustafson, D., Lissner, L., Bengtsson, C., Bjorkelund, C., and Skoog, I. (2004). A 24-year follow-up of body mass index and cerebral atrophy. *Neurology* 63, 1876–1881. doi: 10.1212/01.wnl.0000141850.47773.5f

Haight, T., Nick Bryan, R., Erus, G., Hsieh, M.-K., Davatzikos, C., Nasrallah, I., et al. (2018). White matter microstructure, white matter lesions, and hypertension: an examination of early surrogate markers of vascular-related brain change in midlife. *NeuroImage Clin.* 18, 753–761. doi: 10.1016/j.nicl.2018.02.032

Haight, T. J., Bryan, R. N., Erus, G., Davatzikos, C., Jacobs, D. R., D'esposito, M., et al. (2015). Vascular risk factors, cerebrovascular reactivity, and the default-mode brain network. *NeuroImage* 115, 7–16. doi: 10.1016/j.neuroimage.2015.04.039

Havel, P. J. (2002). Control of energy homeostasis and insulin action by adipocyte hormones: leptin, acylation stimulating protein, and adiponectin. *Curr. Opin. Lipidol.* 13, 51–59. doi: 10.1097/00041433-200202000-00008

Hayakawa, Y. K., Sasaki, H., Takao, H., Yoshikawa, T., Hayashi, N., Mori, H., et al. (2018). The relationship of waist circumference and body mass index to grey matter volume in community dwelling adults with mild obesity. *Obes. sci. pract.* 4, 97–105. doi: 10.1002/osp4.145

He, Q., Chen, C., Dong, Q., Xue, G., Chen, C., Lu, Z.-L., et al. (2015). Gray and white matter structures in the midcingulate cortex region contribute to body mass index in Chinese young adults. *Brain Struct. Funct.* 220, 319–329. doi: 10.1007/s00429-013-0657-9

Hsuchou, H., Kastin, A. J., Mishra, P. K., and Pan, W. (2012). C-reactive protein increases BBB permeability: implications for obesity and neuroinflammation. *Cell. Physiol. Biochem.* 30, 1109–1119. doi: 10.1159/000343302

Irving, A. J., and Harvey, J. (2013). Leptin regulation of hippocampal synaptic function in health and disease. *Philos. Trans. R. Soc. Lond. Series B Biol. sci.* 369, 20130155–20130155. doi: 10.1098/rstb.2013.0155

Item, F., and Konrad, D. (2012). Visceral fat and metabolic inflammation: the portal theory revisited. *Obes. Rev.* 13, 30–39. doi: 10.1111/j.1467-789X.2012.01035.x

Janowitz, D., Wittfeld, K., Terock, J., Freyberger, H. J., Hegenscheid, K., Völzke, H., et al. (2015). Association between waist circumference and gray matter volume in 2344 individuals from two adult community-based samples. *NeuroImage* 122, 149–157. doi: 10.1016/j.neuroimage.2015.07.086

Kerti, L., Witte, A. V., Winkler, A., Grittner, U., Rujescu, D., and Flöel, A. (2013). Higher glucose levels associated with lower memory and reduced hippocampal microstructure. *Neurology* 81, 1746–1752. doi: 10.1212/01.wnl.0000435561.00234.ee

Kharabian Masouleh, S., Arelin, K., Horstmann, A., Lampe, L., Kipping, J. A., Luck, T., et al. (2016). Higher body mass index in older adults is associated with lower gray matter volume: implications for memory performance. *Neurobiol Aging* 40, 1–10. doi: 10.1016/j.neurobiolaging.2015.12.020

Kharabian Masouleh, S., Beyer, F., Lampe, L., Loeffler, M., Luck, T., Riedel-Heller, S. G., et al. (2018). Gray matter structural networks are associated with cardiovascular risk factors in healthy older adults. *J. Cereb. Blood Flow Metab.* 38, 360–372. doi: 10.1177/0271678X17729111

Klop, B., Elte, J. W. F., and Cabezas, M. C. (2013). Dyslipidemia in obesity: mechanisms and potential targets. *Nutrients* 5, 1218–1240. doi: 10.3390/nu5041218

Kreutzer, C., Peters, S., Schulte, D. M., Fangmann, D., Türk, K., Wolff, S., et al. (2017). Hypothalamic inflammation in human obesity is mediated by environmental and genetic factors. *Diabetes* 66, 2407–2415. doi: 10.2337/db17-0067

Krishnan, A., Williams, L. J., McIntosh, A. R., and Abdi, H. (2011). Partial least squares (PLS) methods for neuroimaging: a tutorial and review. *Neuroimage* 56, 455–475. doi: 10.1016/j.neuroimage.2010.07.034

Lee, C. M. Y., Huxley, R. R., Wildman, R. P., and Woodward, M. (2008). Indices of abdominal obesity are better discriminators of cardiovascular risk factors than BMI: a meta-analysis. *J. Clin. Epidemiol.* 61, 646–653. doi: 10.1016/j.jclinepi.2007.08.012

Leritz, E. C., Salat, D. H., Williams, V. J., Schnyer, D. M., Rudolph, J. L., Lipsitz, L., et al. (2011). Thickness of the human cerebral cortex is associated with metrics of cerebrovascular health in a normative sample of community dwelling older adults. *NeuroImage* 54, 2659–2671. doi: 10.1016/j.neuroimage.2010.10.050

Lieb, W., Beiser, A. S., Vasan, R. S., Tan, Z. S., Au, R., Harris, T. B., et al. (2009). Association of plasma leptin levels with incident Alzheimer disease and MRI measures of brain aging. *JAMA* 302, 2565–2572. doi: 10.1001/jama.2009.1836

Lihn, A. S., Pedersen, S. B., and Richelsen, B. (2005). Adiponectin: action, regulation and association to insulin sensitivity. *Obes. Rev.* 6, 13–21. doi: 10.1111/j.1467-789x.2005.00159.x

Loeffler, M., Engel, C., Ahnert, P., Alfermann, D., Arelin, K., Baber, R., et al. (2015). The LIFE-Adult-Study: objectives and design of a population-based cohort study with 10,000 deeply phenotyped adults in Germany. *BMC Public Health* 15:691. doi: 10.1186/s12889-015-1983-z

Macy, E. M., Hayes, T. E., and Tracy, R. P. (1997). Variability in the measurement of C-reactive protein in healthy subjects: implications for reference intervals and epidemiological applications. *Clin. Chem.* 43, 52–58.

Marsland, A. L., Gianaros, P. J., Abramowitch, S. M., Manuck, S. B., and Hariri, A. R. (2008). Interleukin-6 covaries inversely with hippocampal grey matter volume in middle-aged adults. *Biol. Psychiatr.* 64, 484–490. doi: 10.1016/j.biopsych.2008.04.016

McIntosh, A. R., Lobaugh, N. J. (2004). Partial least squares analysis of neuroimaging data: applications and advances. *Neuroimage* 23, S250–S263. doi: 10.1016/j.neuroimage.2004.07.020

McIntosh, A. R., Bookstein, F. L., Haxby, J. V., and Grady, C. L. (1996). Spatial Pattern Analysis of functional brain images using partial least squares. *NeuroImage* 3, 143–157. doi: 10.1006/nimg.1996.0016

Monteiro, J. M., Rao, A., Shawe-Taylor, J., Mourão-Miranda, J., and Alzheimer's Disease, I. (2016). A multiple hold-out framework for sparse partial least squares. *J. Neurosci. Methods* 271, 182–194. doi: 10.1016/j.jneumeth.2016.06.011

Moran, C., Phan, T. G., Chen, J., Blizzard, L., Beare, R., Venn, A., et al. (2013). Brain atrophy in type 2 diabetes. *Diabetes Care* 36, 4036. doi: 10.2337/dc13-0143

Myers, M. G., Cowley, M. A., and Münzberg, H. (2008). Mechanisms of leptin action and leptin resistance. *Annu. Rev. Physiol.* 70, 537–556. doi: 10.1146/annurev.physiol.70.113006.100707

Narita, K., Kosaka, H., Okazawa, H., Murata, T., and Wada, Y. (2009). Relationship between plasma leptin level and brain structure in elderly: a voxel-based morphometric study. *Biol. Psychiatr.* 65, 992–994. doi: 10.1016/j.biopsych.2008.10.006

O'Bryant, S. E., Humphreys, J. D., Smith, G. E., Ivnik, R. J., Graff-Radford, N. R., Petersen, R. C., et al. (2008). Detecting dementia with the mini-mental state examination in highly educated individuals. *Arch. Neurol.* 65, 963–967. doi: 10.1001/archneur.65.7.963

Opel, N., Redlich, R., Kaehler, C., Grotegerd, D., Dohm, K., Heindel, W., et al. (2017). Prefrontal gray matter volume mediates genetic risks for obesity. *Mol. Psychiatr.* 22, 703–710. doi: 10.1038/mp.2017.51

Ostlund, R. E. Jr., Yang, J. W., Klein, S., and Gingerich, R. (1996). Relation between plasma leptin concentration and body fat, gender, diet, age, and metabolic covariates. *J. Clin. Endocrinol. Metab.* 81, 3909–3913. doi: 10.1210/jc.81.11.3909

Papenberg, G., Ferencz, B., Mangialasche, F., Mecocci, P., Cecchetti, R., Kalpouzos, G., et al. (2016). Physical activity and inflammation: effects on gray—matter volume and cognitive decline in aging. *Hum. Brain Mapp.* 37, 3462–3473. doi: 10.1002/hbm.23252

Paz-Filho, G., Wong, M., and Licinio, J. (2010). The procognitive effects of leptin in the brain and their clinical implications. *Int. J. Clin. Pract.* 64, 1808–1812. doi: 10.1111/j.1742-1241.2010.02536.x

Pedditizi, E., Peters, R., and Beckett, N. (2016). The risk of overweight/obesity in mid-life and late life for the development of dementia: a systematic review and meta-analysis of longitudinal studies. *Age Ageing* 45, 14–21. doi: 10.1093/ageing/afv151

Prickett, C., Brennan, L., and Stolwyk, R. (2015). Examining the relationship between obesity and cognitive function: a systematic literature review. *Obes. Res. Clin. Pract.* 9, 93–113. doi: 10.1016/j.orcp.2014.05.001

Rajagopalan, P., Toga, A. W., Jack, C. R., Weiner, M. W., and Thompson, P. M. (2013). Fat-mass-related hormone, plasma leptin, predicts brain volumes in the elderly. *Neuroreport* 24, 58–62. doi: 10.1097/WNR.0b013e32835c5254

Reitz, C., Guzman Vanessa, A., Narkhede, A., Decarli, C., Brickman Adam, M., and Luchsinger José, A. (2016). Relation of dysglycemia to structural brain changes in a multiethnic elderly cohort. *J. Am. Geriatr. Soc.* 65, 277–285. doi: 10.1111/jgs.14551

Repple, J., Karliczek, G., Meinert, S., Foerster, K., Grotegerd, D., Goltermann, J., et al. (2018). Variation of HbA1c affects cognition and white matter microstructure in healthy, young adults. *bioRxiv* 507186.

Romero-Corral, A., Somers, V. K., Sierra-Johnson, J., Thomas, R. J., Collazo-Clavell, M. L., Korinek, J., et al. (2008). Accuracy of body mass index in diagnosing obesity in the adult general population. *Int. J. Obes.* 32, 959–966. doi: 10.1038/ijo.2008.11

Ronan, L., Alexander-Bloch, A. F., Wagstyl, K., Farooqi, S., Brayne, C., Tyler, L. K., et al. (2016). Obesity associated with increased brain age from midlife. *Neurobiol. Aging* 47, 63–70. doi: 10.1016/j.neurobiolaging.2016.07.010

Shaw, M. E., Nettersheim, J., Sachdev, P. S., Anstey, K. J., and Cherbuin, N. (2017). Higher fasting plasma glucose is associated with increased cortical thinning over 12 years: the path through life study. *Brain Topography* 30, 408–416. doi: 10.1007/s10548-017-0544-4

Singh-Manoux, A., Czernichow, S., Elbaz, A., Dugravot, A., Sabia, S., Hagger-Johnson, G., et al. (2012). Obesity phenotypes in midlife and cognition in early old age. *Neurology* 79, 755–762. doi: 10.1212/WNL.0b013e3182661f63

Smith, E., Hay, P., Campbell, L., and Trollor, J. N. (2011). A review of the association between obesity and cognitive function across the lifespan: implications for novel approaches to prevention and treatment. *Obes. Rev.* 12, 740–755. doi: 10.1111/j.1467-789x.2011.00920.x

Smith, S. M., Nichols, T. E., Vidaurre, D., Winkler, A. M., Behrens, T. E. J., Glasser, M. F., et al. (2015). A positive-negative mode of population covariation links brain connectivity, demographics and behavior. *Nat. Neurosci.* 18, 1565–1567. doi: 10.1038/nn.4125

Spielman, L. J., Little, J. P., and Klegeris, A. (2014). Inflammation and insulin/IGF-1 resistance as the possible link between obesity and neurodegeneration. *J. Neuroimmunol.* 273, 8–21. doi: 10.1016/j.jneuroim.2014.06.004

Stenholm, S., Harris, T. B., Rantanen, T., Visser, M., Kritchevsky, S. B., and Ferrucci, L. (2008). Sarcopenic obesity-definition, etiology and consequences. *Curr. Opin. Clin. Nutrit. Metab. Care* 11, 693–700. doi: 10.1097/MCO.0b013e328312c37d

Storsve, A. B., Fjell, A. M., Tamnes, C. K., Westlye, L. T., Overbye, K., Aasland, H. W., et al. (2014). Differential longitudinal changes in cortical thickness, surface area and volume across the adult life span: regions of accelerating

and decelerating change. *J. Neurosci.* 34, 8488–8498. doi: 10.1523/JNEUROSCI.0391-14.2014

Suzuki, H., Gao, H., Bai, W., Evangelou, E., Glocker, B., O'regan, D. P., et al. (2017). Abnormal brain white matter microstructure is associated with both pre-hypertension and hypertension. *PLoS One* 12:e0187600. doi: 10.1371/journal.pone.0187600

Taki, Y., Kinomura, S., Sato, K., Inoue, K., Goto, R., Okada, K., et al. (2012). Relationship between body mass index and gray matter volume in 1,428 healthy individuals. *Obesity* 16, 119–124. doi: 10.1038/oby.2007.4

van den Berg, E., Kloppenborg, R. P., Kessels, R. P. C., Kappelle, L. J., and Biessels, G. J. (2009). Type 2 diabetes mellitus, hypertension, dyslipidemia and obesity: a systematic comparison of their impact on cognition. *Biochim. Biophys. Acta Mol. Basis Dis.* 1792, 470–481. doi: 10.1016/j.bbadis.2008.09.004

Van Gaal, L. F., Mertens, I. L., and Christophe, E. (2006). Mechanisms linking obesity with cardiovascular disease. *Nature* 444, 875–880. doi: 10.1038/nature05487

Walhovd, K. B., Storsve, A. B., Westlye, L. T., Drevon, C. A., and Fjell, A. M. (2014). Blood markers of fatty acids and vitamin D, cardiovascular measures, body mass index, and physical activity relate to longitudinal cortical thinning in normal aging. *Neurobiol. Aging* 35, 1055–1064. doi: 10.1016/j.neurobiolaging.2013.11.011

Ward, M. A., Bendlin, B. B., Mclaren, D. G., Hess, T. M., Callagher, C. L., Kastman, E. K., et al. (2010). Low HDL cholesterol is associated with lower gray matter volume in cognitively healthy adults. *Front. Aging Neurosci.* 2:29. doi: 10.3389/fnagi.2010.00029

Warren, K. N., Beason-Held, L. L., Carlson, O., Egan, J. M., An, Y., Doshi, J., et al. (2018). Elevated markers of inflammation are associated with longitudinal changes in brain function in older adults. *J. Gerontol. Series A* 73, 770–778. doi: 10.1093/gerona/glx199

Willette, A. A., and Kapogiannis, D. (2015). Does the brain shrink as the waist expands? *Ageing Res. Rev.* 20, 86–97. doi: 10.1016/j.arr.2014.03.007

Witte, A. V., Köbe, T., Graunke, A., Schuchardt, J. P., Hahn, A., Tesky, V. A., et al. (2016). Impact of leptin on memory function and hippocampal structure in mild cognitive impairment. *Hum. Brain Mapp.* 37, 4539–4549. doi: 10.1002/hbm.23327

Wolf, P. A., Beiser, A., Elias, M. F., Au, R., Vasan, R. S., and Seshadri, S. (2007). Relation of obesity to cognitive function: importance of central obesity and synergistic influence of concomitant hypertension. The Framingham Heart Study. *Curr Alzheimer Res.* 4, 111–116. doi: 10.2174/156720507780362263

World Health Organization [WHO] (2000). *Obesity: Preventing and Managing the Global Epidemic*. Geneva: World Health Organization.

Yaffe, K., Kanaya, A., Lindquist, K., Simonsick, E. M., Harris, T., Shorr, R. I., et al. (2004). The metabolic syndrome, inflammation, and risk of cognitive decline. *JAMA* 292, 2237–2242.

Yan, S. F., Ramasamy, R., and Schmidt, A. M. (2008). Mechanisms of disease: advanced glycation end-products and their receptor in inflammation and diabetes complications. *Nat. Clin. Pract. Endocrinol. Amp Metab.* 4, 285–293. doi: 10.1038/ncpendmet0786

Zhang, R., Beyer, F., Lampe, L., Luck, T., Riedel-Heller, S. G., Loeffler, M., et al. (2018). White matter microstructural variability mediates the relation between obesity and cognition in healthy adults. *NeuroImage* 172, 239–249. doi: 10.1016/j.neuroimage.2018.01.028

Conflict of Interest Statement: The authors declare that the research was conducted in the absence of any commercial or financial relationships that could be construed as a potential conflict of interest.

frontiers in Aging Neuroscience

ORIGINAL RESEARCH
published: 13 November 2019
doi: 10.3389/fnagi.2019.00307

Distinct Disruptive Patterns of Default Mode Subnetwork Connectivity Across the Spectrum of Preclinical Alzheimer's Disease

Chen Xue[1,2†], Baoyu Yuan[3†], Yingying Yue[4], Jiani Xu[2], Siyu Wang[2], Meilin Wu[2], Nanxi Ji[2], Xingzhi Zhou[2], Yilin Zhao[2], Jiang Rao[5,6], Wenjie Yang[5,6], Chaoyong Xiao[1,6] and Jiu Chen[2,6]**

[1]Department of Radiology, The Affiliated Brain Hospital of Nanjing Medical University, Nanjing, China, [2]Institute of Neuropsychiatry, The Affiliated Brain Hospital of Nanjing Medical University, Fourth Clinical College of Nanjing Medical University, Nanjing, China, [3]Department of Neurology, Affiliated ZhongDa Hospital, School of Medicine, Southeast University, Nanjing, China, [4]Department of Psychosomatics and Psychiatry, ZhongDa Hospital, School of Medicine, Southeast University, Nanjing, China, [5]Department of Rehabilitation, The Affiliated Brain Hospital of Nanjing Medical University, Nanjing, China, [6]Institute of Brain Functional Imaging, Nanjing Medical University, Nanjing, China

OPEN ACCESS

Edited by:
Hans J. Grabe,
University of Greifswald, Germany

Reviewed by:
Brunno Machado De Campos,
Campinas State University, Brazil
Qiang Wei,
First Affiliated Hospital of Anhui Medical University, China
Jiaojian Wang,
University of Pennsylvania, United States

***Correspondence:**
Chaoyong Xiao
xchaoyong@163.com
Jiu Chen
ericcst@aliyun.com

†These authors have contributed equally to this work and share first authorship

Received: 09 July 2019
Accepted: 25 October 2019
Published: 13 November 2019

Citation:
Xue C, Yuan B, Yue Y, Xu J, Wang S, Wu M, Ji N, Zhou X, Zhao Y, Rao J, Yang W, Xiao C and Chen J (2019) Distinct Disruptive Patterns of Default Mode Subnetwork Connectivity Across the Spectrum of Preclinical Alzheimer's Disease. Front. Aging Neurosci. 11:307. doi: 10.3389/fnagi.2019.00307

Background: The early progression continuum of Alzheimer's disease (AD) has been considered to advance through subjective cognitive decline (SCD), non-amnestic mild cognitive impairment (naMCI), and amnestic mild cognitive impairment (aMCI). Altered functional connectivity (FC) in the default mode network (DMN) is regarded as a hallmark of AD. Furthermore, the DMN can be divided into two subnetworks, the anterior and posterior subnetworks. However, little is known about distinct disruptive patterns in the subsystems of the DMN across the preclinical AD spectrum. This study investigated the connectivity patterns of anterior DMN (aDMN) and posterior DMN (pDMN) across the preclinical AD spectrum.

Methods: Resting-state functional magnetic resonance imaging (rs-fMRI) was used to investigate the FC in the DMN subnetworks in 20 healthy controls (HC), eight SCD, 11 naMCI, and 28 aMCI patients. Moreover, a correlation analysis was used to examine associations between the altered connectivity of the DMN subnetworks and the neurocognitive performance.

Results: Compared to the HC, SCD patients showed increased FC in the bilateral superior frontal gyrus (SFG), naMCI patients showed increased FC in the left inferior parietal lobule (IPL), and aMCI patients showed increased FC in the bilateral IPL in the aDMN; while SCD patients showed decreased FC in the precuneus, naMCI patients showed increased FC in the left middle temporal gyrus (MTG), and aMCI patients also showed increased FC in the right middle frontal gyrus (MFG) in the pDMN. Notably, the FC between the ventromedial prefrontal cortex (vmPFC) and the left MFG and the IPL in the aDMN was associated with episodic memory in the SCD and aMCI groups. Interestingly, the FC between the posterior cingulated cortex (PCC) and several regions in the pDMN was associated with other cognitive functions in the SCD and naMCI groups.

Conclusions: This study demonstrates that the three preclinical stages of AD exhibit distinct FC alternations in the DMN subnetworks. Furthermore, the patient group data showed that the altered FC involves cognitive function. These findings can provide novel insights for tailored clinical intervention across the preclinical AD spectrum.

Keywords: amnestic mild cognitive impairment, non-amnestic mild cognitive impairment, subjective cognitive decline, default mode network, functional connectivity

INTRODUCTION

Mild cognitive impairment (MCI), which is divided into amnestic mild cognitive impairment (aMCI) and non-amnestic mild cognitive impairment (naMCI; Grundman et al., 2004; Kim et al., 2015; Makovac et al., 2018), is regarded as the intermediate stage between healthy aging and dementia. Neuroimaging studies have demonstrated that aMCI, characterized by memory decline, has a high probability of developing into Alzheimer's disease (AD) dementia (Rossetto et al., 2018; Chen et al., 2019a). Moreover, several previous studies have indicated that naMCI might be an intermediate stage between health and aMCI/AD (Lee et al., 2018; Oltra-Cucarella et al., 2018). Furthermore, subjective cognitive decline (SCD), as an earlier stage of MCI, refers to the elderly with a normal cognitive performance level and no objective signs of cognitive impairment who subjectively think they are cognitively impaired (Funaki et al., 2019; Hu et al., 2019). Thus, converging evidence suggests that the development of AD may partly progress through a continuum from SCD to MCI and eventually to AD (Berger-Sieczkowski et al., 2019). This could mean that SCD, naMCI, and aMCI can be considered as a spectrum of preclinical AD, which may have a different topography of pathological involvement during different disease stages. Therefore, it is of great significance to promote our understanding of abnormal patterns across the preclinical AD spectrum, and it is particularly important to provide a tailored clinical intervention across the preclinical AD spectrum.

In recent years, resting state functional magnetic resonance imaging (rs-fMRI) has become the main means of cognitive research, while the default mode network (DMN) has been the most studied network (Cai et al., 2017; Banks et al., 2018). The DMN, anatomically distributed in different areas of the brain, can be divided into two subnetworks, the anterior and posterior subnetworks. The anterior subnetwork (the anterior DMN, aDMN) is mainly composed of the ventromedial prefrontal cortex (vmPFC), which is involved in self-referential mental idealization, and the posterior subnetwork (the posterior DMN, pDMN), which consists of the posterior cingulated cortex (PCC) and is involved in episodic memory retrieval (Yang et al., 2017; Wang et al., 2018). Some studies have shown that amyloid deposition is most likely to occur in the medial prefrontal cortex and PCC, which belong to the DMN (Wang et al., 2013). Further results have indicated that regions belonging to the DMN were affected early in the process of developing to AD, and functional connectivity (FC) changes in the DMN have been reported as predictors of AD conversion (Crockett et al., 2017; Scherr et al., 2019). In addition, the altered FC of the DMN is related to the change of cognitive performance (Joshi et al., 2018). Notably, the study of altered FC in DMN subnetworks might provide a pattern to explain the pathophysiology of AD.

Several neuroimaging studies have indicated increased FC in the DMN in SCD patients compared to healthy controls (HC), especially between pDMN and the medial temporal memory system (MTMS; Verfaillie et al., 2018). In naMCI, there tends to be a change in connectivity between the hippocampus and the PCC, and the PCC is an important area in the DMN (Dunn et al., 2014; Prieto Del Val et al., 2016). Furthermore, there is no statistical difference in the DMN intra-connectivity between naMCI and aMCI (Dunn et al., 2014). To our knowledge, there have been no studies of specific default mode subnetworks in naMCI. Additionally, in aMCI, some investigations have found increased FC in the aDMN and decreased FC in the pDMN (Wu et al., 2016); the increased FC in the aDMN was considered to be a compensatory addition of cognitive function to sustain task performance (Qi et al., 2010; Damoiseaux et al., 2012; Dunn et al., 2014). Taken together, these observations suggest that the patterns of impairment in the anterior and posterior subnetworks in these patients seem to differ. However, prior studies have focused on the specific diseases, and very little is known about whether there is a progression of the DMN subnetwork impairment pattern across the preclinical AD spectrum or potentially a corresponding progression of cognitive impairment.

Therefore, the objective of the current study is to analyze changes in the FC patterns of the DMN subnetworks across the preclinical AD spectrum, including SCD, naMCI, and aMCI, and to further investigate the relationship between the disruptive patterns of the DMN subnetworks and cognitive function. We hypothesized that there exists a distinct alteration of the DMN subnetworks in the three preclinical stages of AD and that the altered patterns in the aDMN and pDMN may contribute to different levels of cognitive impairment across the preclinical AD spectrum (Yuan et al., 2016b).

MATERIALS AND METHODS

Subjects

The present study recruited 79 elderly individuals: 21 HC, 10 SCD, 15 naMCI, and 33 aMCI individuals were selected to participate in our research from hospitals, communities, and a broadcasting station. However, 12 of the participants were excluded due to no MRI data ($n = 10$) and excessive head motion (cumulative translation or rotation >3.0 mm or 3.0°, $n = 2$). As a result, the study included 67 subjects in total (20 HC, 8 SCD, 11 naMCI, and 28 aMCI). The study participants had to

meet the following criteria: (1) 40–80 years old; (2) secondary school education or higher; (3) right-handedness; (4) Han Chinese language speakers; (5) no history of serious diseases that could influence cerebral function, such as severe brain injury, brain tumor, brain hemorrhage, brain infarction, white matter disease, neurologic, psychiatric, and systemic illnesses; and (6) no history of psychoactive medications (Dillen et al., 2017; Vecchio et al., 2018).

The inclusion criteria for HC were: (1) no memory complaints; (2) normal cognitive performance of age- and education-matched volunteers; and (3) Clinical Dementia Rating (CDR) = 0 (Chen et al., 2016b; Gu et al., 2018; Yan et al., 2018).

The inclusion criteria for SCD were based on the published SCD criteria proposed by the Subjective Cognitive Decline Initiative (SCD-I): (1) always complained of memory problems; (2) Subjective Cognitive Decline Questionnaire (SCD-Q) $>$ 5; (3) normal cognitive performance of age- and education-matched norms; and (4) CDR = 0 (Dillen et al., 2017; Yan et al., 2018; Cedres et al., 2019).

The inclusion criteria for naMCI were: (1) normal overall cognitive function as evidenced by: CDR = 0.5, Mini-Mental State Examination (MMSE) score $\geqq$ 26, the Montreal Cognitive Assessment (MoCA) $\geqq$ 26, Mattis Dementia Rating Scale-2 (MDRS-2) $\geqq$ 120, and Hamilton Depression Rating Scale (HAMD) $\leqq$ 7; and (2) objective impairment in at least one cognitive domain except memory function, including visual spatial function, executive function, and information processing speed (Dunn et al., 2014).

The inclusion criteria for aMCI were: (1) patients complained of memory impairment of at least 3 months or relatives confirmed that the memory impairment had lasted for more than 3 months; (2) objective memory performance documented by an Auditory Verbal Memory Test-delayed recall (AVLT-DR) score within $\leqq$ 1.5 standard deviation (SD) of same age- and education-adjusted norms; (3) normal overall cognitive function as described for naMCI; and (4) not demented (Dunn et al., 2014; Chen et al., 2019b; Huang et al., 2019; Zhang et al., 2019).

The study was approved by the responsible Human Participants Ethics Committee of the Affiliated Brain Hospital of Nanjing Medical University. Written informed consent was obtained from all participants.

Neurocognitive Assessments

All participants underwent comprehensive and standard neurocognitive assessments to evaluate their cognitive function, including general cognitive functions, episodic memory, executive function, information processing speed, and visual spatial domains (Gu et al., 2017; Gao et al., 2018). These assessments include the MMSE, the ADL, the MDRS-2, the MoCA, the SCD-Q, the CDR, the Hachinski Ischemic Scale (HIS), the HAMD, the Auditory Verbal Learning Test (AVLT; including the AVLT-immediate, the AVLT-5 min delay, and the AVLT-20 min delay), the Rey Complex Figure Test (CFT) delay, the Logical Memory Test (LMT), the CFT, the Clock-Drawing Test (CDT), the Boston Naming Test, the Category Verbal Fluency Test (including the CVFT-animals and the CVFT-objects), the Symbol Digit Modalities Test, the part A and B of the Trail Making Test (TMT), the Digit Span Test (including the DS forward and the DS backward), part A, B, and C of the Stroop Test, and the Semantic Similarity Test. These scales are widely used in cognitive assessment, verified by two senior neuropsychologists and evaluated by experienced clinicians.

MRI Data Acquisition

All magnetic resonance imaging (MRI) data were acquired using a 3.0 Tesla Verio Siemens scanner with an 8-channel head-coil in the Affiliated Brain Hospital of Nanjing Medical University. Resting-state functional images were collected when participants were instructed to rest with their eyes open, to not fall asleep, and to not think of anything in particular. The gradient-echo echo-planar imaging (GRE-EPI) sequence included 240 volumes (Chen et al., 2016a). The parameters were: repetition time (TR) = 2,000 ms, echo time (TE) = 30 ms, number of slices = 36, thickness = 4.0 mm, gap = 0 mm, matrix = 64 × 64, flip angle (FA) = 90°, field of view (FOV) = 220 mm × 220 mm, acquisition bandwidth = 100 kHz, and voxel size = 3.4 × 3.4 × 4 mm^3. The imaging took approximately 8 min.

High-resolution T1-weighted images were acquired by 3D magnetization-prepared rapid gradient-echo (MPRAGE) sequence (Chen et al., 2016a). The parameters were: TR = 1,900 ms, TE = 2.48 ms, inversion time (TI) = 900 ms, number of slices = 176, thickness = 1.0 mm, gap = 0.5 mm, matrix = 256 × 256, FA = 9°, FOV = 256 mm × 256 mm, and voxel size = 1 × 1 × 1 mm^3. The imaging took approximately 4.26 min.

Image Preprocessing

All fMRI data were preprocessed by MATLAB2013b[1] and Data Processing and Analysis for Brain Imaging (DPABI), which is based on Statistical Parametric Mapping (SPM8)[2]. The first 10 volumes were discarded to reduce the instability of the MRI signal. Corrections were performed for the intra-volume acquisition time differences among slices and inter-volume motion effects during the scan. Participants with excessive head motion (cumulative translation or rotation $>$3.0 mm or 3.0°) were excluded. Then, we chose affine regularization in European segmentation and nuisance covariate regression with 24 motion parameters, a global signal, a white matter signal, and a cerebrospinal fluid signal (Fox et al., 2009). Data were filtered at 0.01–0.08 Hz to reduce the effect of the low-frequency drift and high-frequency physiological noise, such as breathing and heartbeats (Chen et al., 2016a). Next, to spatially normalize the fMRI data, we used T1 image unified segmentation and resampled to an isotropic voxel size of 3 mm. At last, spatial smoothing using a 6-mm full-width half-maximum Gaussian kernel (Cha et al., 2013) and detrending were applied to reduce spatial noise and differences in anatomical structures among subjects. Stringent quality assurance measures were performed as described in previous studies to reduce the impact of head motion on the rsfMRI results (Power et al., 2012; Van Dijk et al., 2012).

[1] http://www.mathworks.com/products/matlab/
[2] https://www.fil.ion.ucl.ac.uk/spm/

TABLE 1 | Demographics and clinical measures of HC and patients with SCD, naMCI, and aMCI.

	HC	SCD	naMCI	aMCI	*F*-values (χ^2)	*p*-values
	n = 21	*n* = 10	*n* = 15	*n* = 33		
Age (years)	57.52 (8.072)	63.10 (8.774)	63.87 (8.568)	66.03 (8.579)*	4.388	0.007
Gender (male/female)	7/14	4/10	6/9	11/22	6.696	0.01
Education level (years)	12.05 (2.747)	13.85 (1.827)	10.60 (2.694)**	11.06 (3.358)	3.086	0.032
FD	0.0856 (0.04929)	0.0663 (0.04287)	0.1181 (0.05258)	0.0908 (0.07461)	1.074	0.367
MMSE scores	28.81 (1.209)	27.70 (1.160)	28.27 (1.710)	26.88 (2.027)*	6.156	0.001
MDRS-2	141.00 (2.915)	138.80 (3.393)	137.07 (3.432)	134.82 (7.970)*	5.193	0.003
MoCA	26.20 (2.624)	25.00 (3.432)	24.14 (2.931)	22.40 (3.379)*	5.357	0.002
SCD-Q	3.07 (1.591)	6.05 (0.725)*	4.36 (2.161)	5.45 (1.690)*	9.033	<0.001
Composite *Z* scores of each cognitive domain						
Episodic memory	0.4953 (0.58422)	0.5788 (0.48495)	0.3315 (0.53204)	−0.6245 (0.54907)*/**/****	25.373	<0.001
Information processing speed	0.4525 (0.75906)	0.4152 (0.46834)	−0.4064 (0.65820)*/**	−0.2252 (0.77552)*	6.535	0.001
Executive function	0.4511 (0.72800)	0.4369 (0.50400)	−0.2714 (0.48974)*/**	−0.2493 (0.61376)*/**	7.974	<0.001
Visuospatial function	0.2642 (0.56747)	0.4183 (0.44671)	−0.1231 (0.68174)	−0.2438 (1.01123)	2.79	0.046

*Numbers are given as means (standard deviation, SD) unless stated otherwise. Scores reflect the number of correct items unless stated otherwise. Significant group differences were found at p < 0.05 (ANOVA test and Multivariable general linear model), Bonferroni corrected. FD, framewise displacement; MMSE, Mini-Mental State Exam; MDRS-2, Mattis Dementia Rating Scale-2; MoCA, the Montreal Cognitive Assessment test; SCD-Q, Subjective Cognitive Decline Questionnaire. *Compared to HC, **compared to SCD, ****compared to naMCI; HC, healthy controls; SCD, subjective cognitive decline; aMCI, amnestic mild cognitive impairment; naMCI, non-amnestic mild cognitive impairment.*

Functional Connectivity Analysis

A seed-based FC analysis was performed to explore the alternation of DMN subnetworks. To identify the seed region in the present study, two 10-mm spherical regions of interest centered in the vmPFC (MNI space: 0, 52, −6, Brodmann area 10) and PCC (MNI space: 0, −53, 26, Brodmann area 31) were created (Zhang and Raichle, 2010; Yuan et al., 2016b). Individual mean time series were extracted based on the coregistered seed region as the reference time series, and then a voxel-wise cross-correlation analysis was carried out between the seed region and the whole brain within the gray matter (GM) mask. We used a Fisher's r-to-z transformation to improve the normality of the correlation coefficients. Then, we obtained the vmPFC subnetwork (aDMN) and the PCC subnetwork (pDMN).

Statistical Analyses

The Statistical Package for the Social Sciences (SPSS) software version 22.0 (IBM, Armonk, New York, NY, USA) was used for statistical analyses. The analysis of variance (ANOVA), the multimodal general linear model (GLM), and the chi-square test were conducted to compare the demographic and neurocognitive data among groups, including the HC, SCD, naMCI, and aMCI. The Bonferroni correction was used for *post hoc* comparisons. The *P*-value was set as <0.05 for significant differences.

A one-way ANOVA analysis was performed to compare the differences in FC in both the aDMN and pDMN among four groups after controlling for the effects of age, gender, level of education, and GM volumes. As suggested in a previous study, the non-parametric permutation test can precisely control the false positive rate in the cluster-level inference; therefore, we set the permutation times at 1,000 (Smith and Nichols, 2009). The corrected *p*-value < 0.05 was set for statistical significance and the cluster size >200 voxels (5,400 mm^3) was applied for multiple comparisons at the voxel level. The two-sample *T*-test was used for *post hoc* comparisons with the mask resulted from ANOVA analyses after controlling for the effects of age, gender, level of education, and GM volumes. We set the significance level with a family-wise error (TFCE-FWE) corrected cluster $p < 0.05$ and the cluster size >10 voxels (270 mm^3). The FCs of significantly altered regions were extracted with a Resting-State fMRI Data Analysis Toolkit (REST)[3] and were later used for correlation analyses. The correlation analyses were conducted to reveal the relationships between the altered FCs of the DMN and cognitive domains after controlling for the effects of age, gender, and level of education ($p < 0.05$, Bonferroni-corrected).

It is worth mentioning that, we grouped the neuropsychological tests into four cognitive domains (Gu et al., 2017; Gao et al., 2018). Episodic memory data were mainly derived from AVLT-20-min DR, LMT-20-min DR, and CFT-20-min DR. The information processing speed dates were mainly acquired from DSST, TMT-A, Stroop A, and Stroop B. Visuospatial function data were mainly extracted from the CFT and CDT. Executive function data were mainly obtained from VFT, DST-backward, TMT-B, Stroop C, and Semantic Similarity. The individual raw score of each neuropsychological test was transformed to normalized *Z* scores. Subsequently, the normalized *Z* score was averaged to calculate the composite *Z* score of each cognitive domain (Xie et al., 2012; Chen et al., 2016b; Yuan et al., 2016b).

RESULTS

Demographic and Neurocognitive Characteristics

The demographic and neurocognitive information of all participants, including 21 HC (mean age 57.52 ± 8.072), 10 SCD (mean age 63.10 ± 8.774), 15 naMCI (mean age 63.87 ± 8.568), and 33 aMCI (mean age 66.03 ± 8.579) individuals, can be found in **Table 1**. As expected, our results showed significant differences in cognitive performance.

[3]http://resting-fmri.sourceforge.net

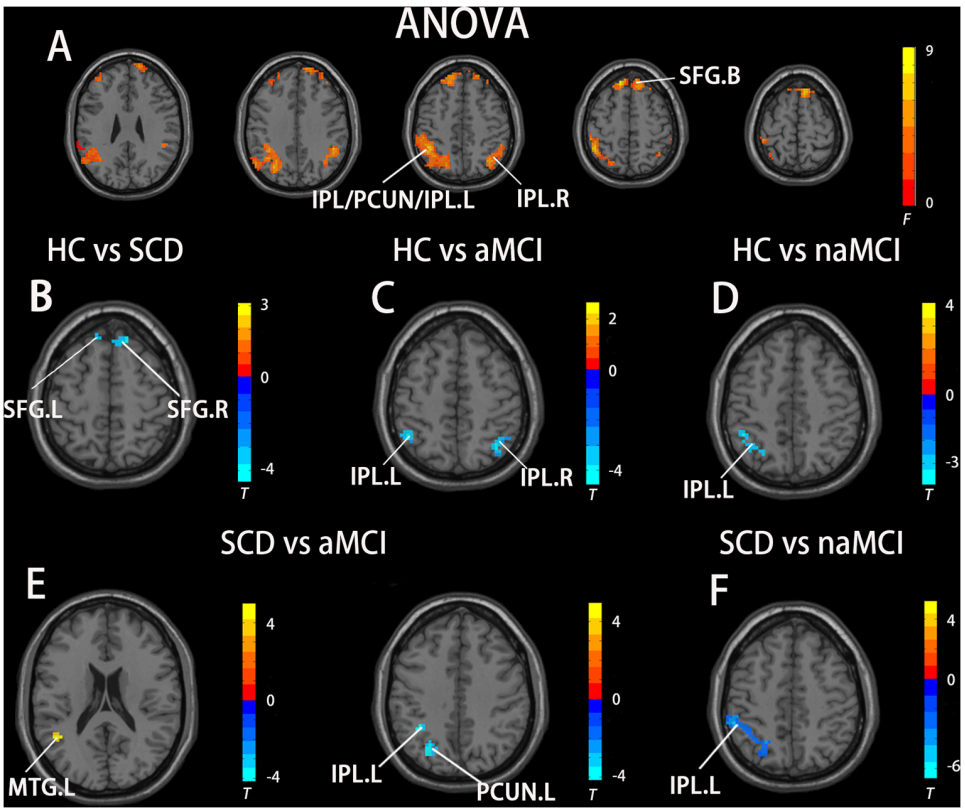

FIGURE 1 | Brain regions exhibiting significant differences in functional connectivity (FC) of the anterior default mode network (DMN) subnetwork [the ventromedial prefrontal cortex (vmPFC) subnetwork] based on analysis of variance (ANOVA) analysis and two-sample *T*-tests. Age, gender, and years of education were used as covariates for all these results. **(A)** Brain regions showing significant differences in FC of the anterior DMN subnetwork between HC, patients with SCD, patients with naMCI, and patients with Alzheimer's disease (AD; $p < 0.05$, the cluster size > 200 voxels). **(B–F)** The results of *post hoc* two-sample *T*-tests in voxel-wise analysis (TFCE-FWE corrected, cluster size $\geq$ 10, $p < 0.05$). aMCI, amnestic mild cognitive impairment; naMCI, non-amnestic mild cognitive impairment; SCD, subjective cognitive decline; HC, healthy controls; IPL, inferior parietal lobule; PCUN, precuneus; SFG, superior frontal gyrus; MTG, middle temporal gyrus; L, left; R, right.

Compared to HC, the aMCI group exhibited significantly lower MMSE, MDRS-2, MoCA scores, episodic memory, information processing speed, executive function, and visuospatial function, though it exhibited significantly higher SCD-Q scores; the naMCI group exhibited significantly lower information processing speed and executive function. Compared to SCD group, the aMCI group exhibited significantly lower episodic memory and executive function; the naMCI group exhibited significantly lower information processing speed, executive function, and education level. Compared to naMCI group, the aMCI group exhibited significantly lower episodic memory scores. Last, the SCD group had the highest SCD-Q scores (all $p < 0.05$).

Altered FC Patterns of DMN Subnetworks in Patients with SCD, naMCI, and aMCI

In the aDMN subnetwork, the ANOVA analysis showed five significantly altered brain regions among the groups, including the bilateral inferior parietal lobule (IPL), left precuneus (PCUN), left middle temporal gyrus (MTG), and bilateral superior frontal gyrus (SFG). Compared to the HC, the SCD patients showed significantly increased FC in the bilateral SFG, the naMCI individuals showed increased FC in the left IPL, and the aMCI patients showed increased FC in the bilateral IPL. Compared to the SCD group, the aMCI group showed increased FC in the left IPL, left MTG, and left PCUN, while the naMCI group showed increased FC in the left IPL. It is worth noting that, compared to the HC, the SCD, naMCI, and aMCI groups all showed increased FC in the aDMN (TFCE-FWE corrected, cluster size $\geq$ 10, $p < 0.05$). All results are after controlling the effects of age, gender, level of education, and GM volumes (see **Figure 1** and **Table 2**).

In the pDMN subnetwork, the ANOVA analysis showed 11 significantly altered brain regions among the groups, including the bilateral cerebellum posterior lobe (CPL), right inferior temporal gyrus (ITG), right lingual gyrus (LG), left inferior frontal gyrus (IFG), left MTG, right middle frontal gyrus (MFG), right precentral gyrus (PRG), right superior temporal gyrus (STG), and bilateral PCUN. Compared to the HC, the SCD patients showed decreased FC in the right PCUN, the naMCI individuals showed increased FC in the left MTG, and the aMCI patients showed increased FC in the left MFG. Compared to the SCD group, the naMCI group showed increased FC in the left

TABLE 2 | The differences in functional connectivity in the ventromedial prefrontal cortex (vmPFC) subnetwork.

Region(aal)	Peak MNI coordinate			F/t	Cluster number
	x	*y*	*z*		
ANOVA					
L Inferior Parietal Lobule/Precuneus/Middle Temporal Gyrus	−45	−51	51	8.7072	1,178
R Inferior Parietal Lobule	48	−45	36	7.3382	263
B Superior Frontal Gyrus	12	24	66	8.1821	498
SCD>HC					
L Superior Frontal Gyrus	−12	36	51	4.4635	20
R Superior Frontal Gyrus	12	33	54	4.1155	33
aMCI>HC					
R Inferior Parietal Lobule	36	−66	45	4.5565	122
L Inferior Parietal Lobule	−45	−51	51	4.0654	23
naMCI>HC					
L Inferior Parietal Lobule	−42	−45	42	3.931	82
aMCI>SCD					
L Middle Temporal Gyrus	−45	−51	21	4.9974	15
L Precuneus	−27	−60	33	4.1604	62
L Inferior Parietal Lobule					
naMCI>SCD	−36	−45	42	4.0831	68
L Inferior Parietal Lobule	−45	−45	57	6.6488	262

The x, y, z coordinates are the primary peak locations in the MNI space. Cluster size > 200 voxels in ANOVA analysis, $p < 0.05$; Cluster size > 10 voxels in two-sample T-test, $p < 0.05$, TFCE-FWE corrected.

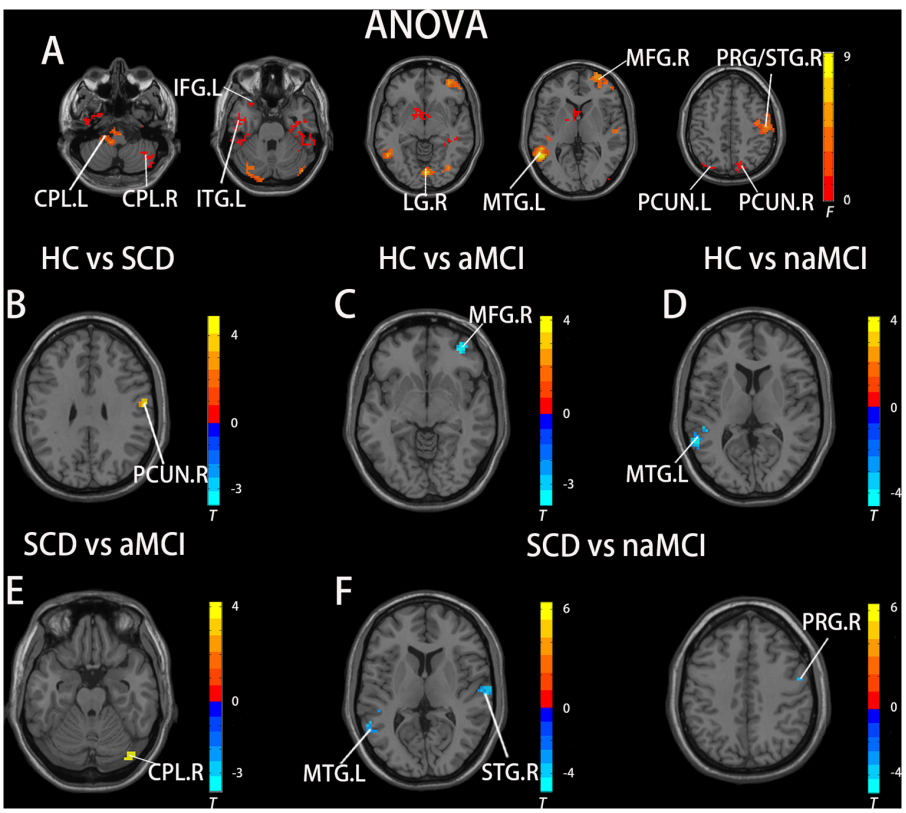

FIGURE 2 | Brain regions exhibiting significant differences in FC of the posterior DMN subnetwork [the posterior cingulated cortex (PCC) subnetwork] based on ANOVA analysis and two-sample *T*-tests. Age, gender, and years of education were used as covariates for all these results. **(A)** Brain regions showing significant differences in FC of the posterior DMN subnetwork between HC, patients with SCD, patients with naMCI, and patients with AD ($p < 0.05$, the cluster size > 200 voxels). **(B–F)** The results of *post hoc* two-sample *T*-tests in voxel-wise analysis (TFCE-FWE corrected, cluster size ≥ 10, $p < 0.05$). aMCI, amnestic mild cognitive impairment; naMCI, non-amnestic mild cognitive impairment; SCD, subjective cognitive decline; HC, healthy controls; CPL, cerebellum posterior lobe; ITG, inferior temporal gyrus; LG, lingual gyrus; IFG, inferior frontal gyrus; MTG, middle temporal gyrus; MFG, middle frontal gyrus; PRG, precentral gyrus; STG, superior temporal gyrus; PCUN, precuneus; L, left; R, right.

TABLE 3 | The differences in functional connectivity in the posterior cingulated cortex (PCC) subnetwork.

Region(aal)	Peak MNI coordinate			F/t	Cluster number
	x	*y*	*z*		
ANOVA					
L Cerebellum Posterior Lobe	−12	−39	−51	6.7851	211
R Cerebellum Posterior Lobe	51	−60	−51	0.22507	425
L Inferior Temporal Gyrus	−48	−3	−48	0.23658	212
R Lingual Gyrus	−3	−81	−6	7.5879	314
L Inferior Frontal Gyrus	−27	18	−27	0.21662	281
L Middle Temporal Gyrus	−57	−51	3	9.2035	380
R Middle Frontal Gyrus	30	66	6	6.9772	248
R Precentral Gyrus/Superior Temporal Gyrus	54	−18	48	5.364	404
R Precuneus	−15	−81	54	0.21035	290
L Precuneus	−15	−93	36	0.18706	210
HC>SCD					
R Precuneus	57	−12	30	4.9182	19
aMCI>HC					
R Middle Frontal Gyrus	36	48	−6	3.8891	69
naMCI>HC					
L Middle Temporal Gyrus	−60	−51	9	4.5979	87
SCD>aMCI					
R Cerebellum Posterior Lobe	42	−78	−21	4.2026	24
naMCI>SCD					
L Middle Temporal Gyrus	−51	−48	−3	5.0983	130
R Superior Temporal Gyrus	57	−15	3	4.6523	50
R Precentral Gyrus	54	0	45	4.434	19

The x, y, z coordinates are the primary peak locations in the MNI space. Cluster size > 200 voxels in ANOVA analysis, $p < 0.05$; Cluster size > 10 voxels in two-sample T-test, $p < 0.05$, TFCE-FWE corrected.

MTG, right STG, and right PCG, while the aMCI group showed decreased FC in the right CPL. Notably, compared to the HC, the SCD group showed decreased FC, while both the naMCI and aMCI groups showed increased FC in the pDMN (TFCE-FWE corrected, cluster size ≥ 10, $p < 0.05$). All results are after controlling the effects of age, gender, level of education, and GM volumes (see **Figure 2** and **Table 3**).

Behavioral Significance of the Disrupted Functional Connectivity of DMN Subnetworks

A correlation analysis was conducted between regions with altered FC and cognitive domains (Bonferroni corrected, $p < 0.05$). In the groups consisting of SCD and aMCI, the analysis showed that the altered FC between the vmPFC and the left IPL in the aDMN is negatively correlated with episodic memory ($r = -0.5002$, $p = 0.0019$), while the altered FC between the vmPFC and the left MTG is positively correlated with episodic memory ($r = 0.6419$, $p = < 0.0001$). In the groups that contained SCD and naMCI, the analysis showed significant negative correlation in the pDMN. Altered FC between the PCC and the right STG was negatively correlated to both executive function ($r = -0.6732$, $r = 0.0016$) and information processing speed ($r = -0.5894$, $p = 0.0017$). Altered FC between the PCC and the right PRG was negatively correlated with executive function ($r = -0.7070$, $p = 0.0007$), and altered FC between the PCC and the left MTG was negatively correlated with information processing speed ($r = -0.5894$, $p = 0.0079$). Age, gender, and years of education were used as covariates for all these results. There was no statistically significant correlation (Bonferroni corrected, $p < 0.05$) between the cognition domains and the remaining areas (see **Figure 3**).

DISCUSSION

The present study aimed to investigate changes in FC of the anterior and posterior DMN between different groups (HC, SCD, naMCI, and aMCI) and to explore how this altered FC influences cognitive function. Corresponding with our hypothesis, our study presents two main findings. First, the FC of the anterior and posterior subnetworks in the DMN was damaged in the SCD, naMCI, and aMCI groups after controlling the effects of age, gender, level of education, and GM volumes. Second, the correlation analyses demonstrated that the altered connectivity patterns of the DMN subnetworks were associated with impaired cognitive function. Moreover, our study further confirms that the aDMN and pDMN are functionally independent, and the altered subnetworks have different effects on cognitive function.

The current study indicates that there is significantly altered FC in the SCD, naMCI, and aMCI groups in/between the anterior DMN and the posterior DMN, thereby proving the heterogeneity of the DMN (Damoiseaux et al., 2012; Yuan et al., 2016b). Compared to the HC, the naMCI and aMCI groups showed increased FC both in the aDMN and pDMN, while the SCD group showed increased FC in the aDMN and decreased FC in the pDMN. Over the years, alterations in FC in the DMN have been a focal point of many studies, but few investigations have examined changes in FC in the specific DMN subnetworks.

Our findings in the three preclinical stages of AD demonstrate a widespread alteration of FC in the DMN, and further illustrate

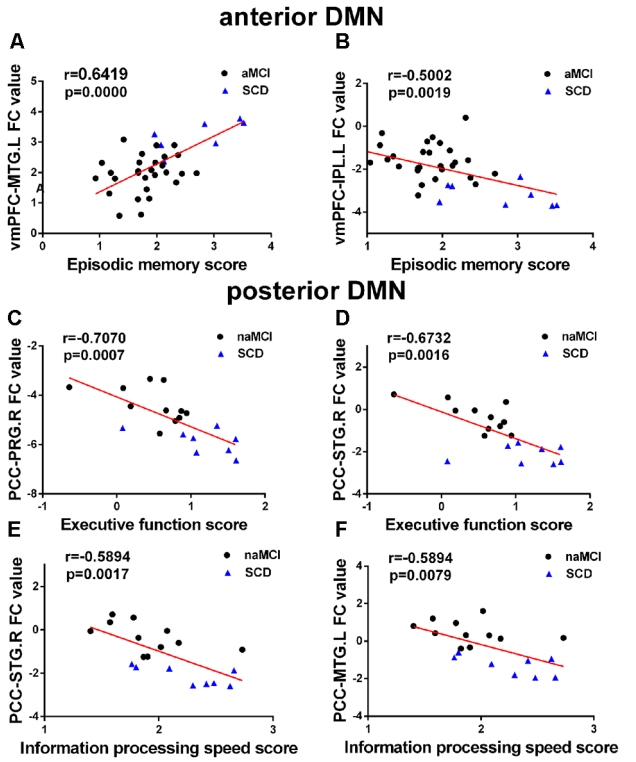

FIGURE 3 | (A–F) Significant associations between altered FC and cognitive function including episodic memory, executive function, and information processing speed in anterior DMN (aDMN) and posterior DMN (pDMN) (Bonferroni corrected, $p < 0.05$). Age, gender, and years of education were used as covariates for all these results. aMCI, amnestic mild cognitive impairment; naMCI, non-amnestic mild cognitive impairment; SCD, subjective cognitive decline; vmPFC, ventral medial prefrontal cortex; PCC, posterior cingulate cortex; MTG, middle temporal gyrus; PRG, precentral gyrus; STG, superior temporal gyrus; IPL, inferior parietal lobule; L, left; R, right.

that AD is a disconnection syndrome (Palesi et al., 2016). Specifically, our results indicate that patients with aMCI have significantly increased FC between the vmPFC and bilateral IPL (Cai et al., 2017), while naMCI patients have significantly increased FC between the vmPFC and left IPL compared with the HC. The IPL is a heterogeneous brain area with a role in multiple-modality functions including sensory motor processing, salience detection, executive control, and especially episodic memory (Wang et al., 2012, 2016, 2017; Yuan et al., 2016a). Therefore, our findings might indicate that the right IPL is one of the brain areas that is responsible for episodic memory. It is worth noting that the SCD group showed increased FC between the vmPFC and the bilateral SFG in the aDMN, while it showed decreased FC between the PCC and the right precuneus in the pDMN compared to the HC, proving that the changes in FC precede the appearance of clinical manifestations (Hayes et al., 2017). Notably, the alterations in the precuneus may begin as early as approximately 10–20 years before the onset of clinical symptoms of dementia (Bateman et al., 2012). Furthermore, the only significantly decreased FC revealed by our study is the FC between the PCC and the right precuneus in the SCD group compared with the HC, suggesting that the right precuneus might be the first damaged area in the DMN and that the increased FC between the vmPFC and the bilateral SFG might be a compensatory response. However, no altered FC was found between the PCC and the precuneus in the naMCI and aMCI groups compared to the HC, which might represent a characteristic change in the SCD patients. The PCC-precuneus plays a vital role in the DMN, and they are among the brain regions most prone to AD because of their connective, metabolic, and vascular characteristics (Cha et al., 2013; Prieto Del Val et al., 2016; Wu et al., 2016; Wang et al., 2019). In addition, the present study shows that the naMCI group exhibited increased FC between the PCC and the left MTG, while the aMCI group showed increased FC between the PCC and the right MFG compared to the HC (Liang et al., 2011; Cha et al., 2013). The MFG region consists of a caudal and rostral area, the latter including a part of the dorsal lateral prefrontal cortex, which is responsible for working memory and executive cognitive functions (Barbey et al., 2013). A previously published study reported that the MFG is an important area and that increased FC in the right MFG might be a compensation mechanism (Cha et al., 2013). Interestingly, the aMCI group showed decreased FC between the PCC and the right CPL compared to the SCD group, while both the SCD and aMCI groups showed no significant differences when compared to the HC. The cerebellum is involved not only in movement and balance but also in advanced cognitive functions (Gottwald et al., 2003). The decreased FC between the PCC and the cerebellum suggests a potential effect on the cerebellar-related cognitive functions in aMCI; this finding is in accordance with our previous studies (Chen et al., 2015, 2019b; Yang et al., 2017). Taken together, the increased FC between the vmPFC and the left IPL and between the PCC and the right MFG and the left MTG could serve as a biomarker for identifying patients with naMCI and aMCI. In addition, the altered FC between the PCC and the precuneus could be a potential biomarker of SCD.

The present study indicates that the SCD group showed increased FC in the aDMN and decreased FC in the pDMN, while the naMCI and aMCI groups showed increased FC both in the aDMN and the pDMN. We speculate that memory damage in the SCD patients is not obvious and that there may be a decrease in FC in the pDMN. With the progressive decline of cognitive ability, FC in the naMCI and aMCI patients gradually increases, which may be indicative of compensatory activity (Qi et al., 2010). We can conclude that SCD is the intermediate stage between healthy elderly and MCI, and both naMCI and aMCI are the preclinical stages of AD. Additionally, the results of the present study show that the DMN is an important intrinsic network to differentiate between the healthy elderly, SCD, naMCI, and aMCI (Wang et al., 2013).

The present study showed observably positive and negative correlations between FC and cognitive domain scores in patients with SCD, naMCI, and aMCI. In the anterior DMN subnetwork, a noteworthy finding was that the episodic memory score negatively correlated with the increased FC between the vmPFC and the left IPL in the SCD and aMCI patients; this finding confirms previously published articles stating that altered FC is associated with memory deficits in patients with aMCI

(Bai et al., 2009; Ofer et al., 2018). Furthermore, the finding indicates that the increased FC between the vmPFC and the left IPL may be an attempt to combat the induced functional decline and the negative association with episodic memory, and this may be reflective of compensatory attempts (Bai et al., 2009; Zhang et al., 2016). It is worth noting that the increased FC in the aDMN between the vmPFC and the left MTG in SCD patients is positively correlated with episodic memory, suggesting that episodic memory in SCD patients is not impaired. This could be important evidence that the SCD is an intermediate stage between healthy elderly and MCI. In the posterior DMN, we found that the FC in the left MTG, the right PRG, and the right STG is significantly negatively correlated with cognitive function, including the information processing speed and the executive function score. It has been reported that the left MTG is significantly related to MMSE scores, and this could reflect the progression of AD (Cha et al., 2013).

In terms of subnetworks, our findings show that episodic memory is significantly correlated with the altered aDMN, while information processing speed and executive function are negatively correlated with the pDMN. These results indicate that the aDMN mainly controls the episodic memory function, while the pDMN is primarily responsible for other cognitive functions except for memory.

LIMITATIONS

There are two major limitations in our present study. First, significant differences in age and education levels were present among the four groups and this potentially negatively affected our results. However, to avoid the effects of these confounding factors, we performed all statistical analyses with age, education level, and gender as covariates. Therefore, we believe that our results are credible.

Second, the study had a cross-sectional design and a small sample size, which may prevent us from detecting smaller effect sizes and may lead to some null results. We will continue to recruit volunteers to participate in this study and perform regular follow up in the future. We will try to avoid all possibilities of potential bias in our data and to further confirm our results.

CONCLUSION

This study demonstrates that SCD, naMCI, and aMCI are three preclinical stages of AD and that they exhibit distinct alternations in the FC of DMN subnetworks. Furthermore, the patient group data showed that the altered FC affects cognition, including episodic memory, executive function, and information processing speed. These results can provide novel insights for tailored clinical intervention across the preclinical AD spectrum.

DATA AVAILABILITY STATEMENT

The datasets analyzed in this manuscript are not publicly available. Requests to access the datasets should be directed to ericcst@aliyun.com.

ETHICS STATEMENT

The studies involving human participants were reviewed and approved by the responsible Human Participants Ethics Committee of the Affiliated Brain Hospital of Nanjing Medical University. The patients/participants provided their written informed consent to participate in this study. Written informed consent was obtained from the individual(s) for the publication of any potentially identifiable images or data included in this article.

AUTHOR CONTRIBUTIONS

CXu, BY, CXi and JC: designed the study. CXu, BY, CXi, JC, YY, JX, SW, MW, NJ, XZ, YZ, JR and WY: collected the data. CXu and BY: analyzed the data and prepared the manuscript.

FUNDING

This study was supported by the National Natural Science Foundation of China (No. 81701675, 81701671); the Key Project supported by the Medical Science and Technology Development Foundation, Nanjing Department of Health, Nanjing Municipality Health Bureau (No. JQX18005); the Cooperative Research Project of Southeast University-Nanjing Medical University (No. 2018DN0031); the Key Research and Development Plan (Social Development) Project of Jiangsu Province (No. BE2018608); the Disciplinary group of Psychology and Neuroscience, Xinxiang Medical University (No. 2016PN-KFKT-01); the Scientific Research Program of Jiangsu Provincial Commission of Health and Family Planning (No. H2017007); the Innovation and Entrepreneurship Training Program for College Students in Jiangsu Province, Nanjing Medical University (No. 201810312061X).

REFERENCES

Bai, F., Zhang, Z., Watson, D. R., Yu, H., Shi, Y., Yuan, Y., et al. (2009). Abnormal functional connectivity of hippocampus during episodic memory retrieval processing network in amnestic mild cognitive impairment. *Biol. Psychiatry* 65, 951–958. doi: 10.1016/j.biopsych.2008.10.017

Banks, S. J., Zhuang, X., Bayram, E., Bird, C., Cordes, D., Caldwell, J. Z. K., et al. (2018). Default mode network lateralization and memory in healthy aging and Alzheimer's disease. *J. Alzheimers Dis.* 66, 1223–1234. doi: 10.3233/jad-180541

Barbey, A. K., Koenigs, M., and Grafman, J. (2013). Dorsolateral prefrontal contributions to human working memory. *Cortex* 49, 1195–1205. doi: 10.1016/j.cortex.2012.05.022

Bateman, R. J., Xiong, C., Benzinger, T. L., Fagan, A. M., Goate, A., Fox, N. C., et al. (2012). Clinical and biomarker changes in dominantly inherited Alzheimer's disease. *N. Engl. J. Med.* 367, 795–804. doi: 10.1056/NEJMoa1202753

Berger-Sieczkowski, E., Gruber, B., Stögmann, E., and Lehrner, J. (2019). Differences regarding the five-factor personality model in patients with subjective cognitive decline and mild cognitive impairment. *Neuropsychiatr.* 33, 35–45. doi: 10.1007/s40211-018-0292-z

Cai, S., Chong, T., Peng, Y., Shen, W., Li, J., von Deneen, K. M., et al. (2017). Altered functional brain networks in amnestic mild cognitive impairment: a resting-state fMRI study. *Brain Imaging Behav.* 11, 619–631. doi: 10.1007/s11682-016-9539-0

Cedres, N., Machado, A., Molina, Y., Diaz-Galvan, P., Hernández-Cabrera, J. A., Barroso, J., et al. (2019). Subjective cognitive decline below and above the age of 60: a multivariate study on neuroimaging, cognitive, clinical, and demographic measures. *J. Alzheimers Dis.* 68, 295–309. doi: 10.3233/jad-180720

Cha, J., Jo, H. J., Kim, H. J., Seo, S. W., Kim, H. S., Yoon, U., et al. (2013). Functional alteration patterns of default mode networks: comparisons of normal aging, amnestic mild cognitive impairment and Alzheimer's disease. *Eur. J. Neurosci.* 37, 1916–1924. doi: 10.1111/ejn.12177

Chen, J., Chen, G., Shu, H., Chen, G., Ward, B. D., Wang, Z., et al. (2019a). Predicting progression from mild cognitive impairment to Alzheimer's disease at the individual basis using CARE index across different independent cohorts. *Aging* 11, 2185–2201. doi: 10.18632/aging.101883

Chen, J., Shu, H., Wang, Z., Zhan, Y., Liu, D., Liu, Y., et al. (2019b). Intrinsic connectivity identifies the sensory-motor network as a main cross-network between remitted late-life depression- and amnestic mild cognitive impairment-targeted networks. *Brain Imaging Behav.* doi: 10.1007/s11682-019-00098-4

Chen, J., Duan, X., Shu, H., Wang, Z., Long, Z., Liu, D., et al. (2016a). Differential contributions of subregions of medial temporal lobe to memory system in amnestic mild cognitive impairment: insights from fMRI study. *Sci. Rep.* 6:26148. doi: 10.1038/srep26148

Chen, J., Shu, H., Wang, Z., Zhan, Y., Liu, D., Liao, W., et al. (2016b). Convergent and divergent intranetwork and internetwork connectivity patterns in patients with remitted late-life depression and amnestic mild cognitive impairment. *Cortex* 83, 194–211. doi: 10.1016/j.cortex.2016.08.001

Chen, J., Shu, H., Wang, Z., Liu, D., Shi, Y., Zhang, X., et al. (2015). The interaction of APOE genotype by age in amnestic mild cognitive impairment: a voxel-based morphometric study. *J. Alzheimers Dis.* 43, 657–668. doi: 10.3233/jad-141677

Crockett, R. A., Hsu, C. L., Best, J. R., and Liu-Ambrose, T. (2017). Resting state default mode network connectivity, dual task performance, gait speed and postural sway in older adults with mild cognitive impairment. *Front. Aging Neurosci.* 9:423. doi: 10.3389/fnagi.2017.00423

Damoiseaux, J. S., Prater, K. E., Miller, B. L., and Greicius, M. D. (2012). Functional connectivity tracks clinical deterioration in Alzheimer's disease. *Neurobiol. Aging* 33, 828.e19–830.e30. doi: 10.1016/j.neurobiolaging.2011.06.024

Dillen, K. N. H., Jacobs, H. I. L., Kukolja, J., Richter, N., von Reutern, B., Onur, O. A., et al. (2017). Functional disintegration of the default mode network in prodromal Alzheimer's disease. *J. Alzheimers Dis.* 59, 169–187. doi: 10.3233/jad-161120

Dunn, C. J., Duffy, S. L., Hickie, I. B., Lagopoulos, J., Lewis, S. J., Naismith, S. L., et al. (2014). Deficits in episodic memory retrieval reveal impaired default mode network connectivity in amnestic mild cognitive impairment. *Neuroimage Clin.* 4, 473–480. doi: 10.1016/j.nicl.2014.02.010

Fox, M. D., Zhang, D., Snyder, A. Z., and Raichle, M. E. (2009). The global signal and observed anticorrelated resting state brain networks. *J. Neurophysiol.* 101, 3270–3283. doi: 10.1152/jn.90777.2008

Funaki, K., Nakajima, S., Noda, Y., Wake, T., Ito, D., Yamagata, B., et al. (2019). Can we predict amyloid deposition by objective cognition and regional cerebral blood flow in patients with subjective cognitive decline? *Psychogeriatrics* 19, 325–332. doi: 10.1111/psyg.12397

Gao, L., Chen, J., Gu, L., Shu, H., Wang, Z., Liu, D., et al. (2018). Effects of gender and apolipoprotein E on novelty MMN and P3a in healthy elderly and amnestic mild cognitive impairment. *Front. Aging Neurosci.* 10:256. doi: 10.3389/fnagi.2018.00256

Gottwald, B., Mihajlovic, Z., Wilde, B., and Mehdorn, H. M. (2003). Does the cerebellum contribute to specific aspects of attention? *Neuropsychologia* 41, 1452–1460. doi: 10.1016/s0028-3932(03)00090-3

Grundman, M., Petersen, R. C., Ferris, S. H., Thomas, R. G., Aisen, P. S., Bennett, D. A., et al. (2004). Mild cognitive impairment can be distinguished from Alzheimer disease and normal aging for clinical trials. *Arch. Neurol.* 61, 59–66. doi: 10.1001/archneur.61.1.59

Gu, L. H., Chen, J., Gao, L. J., Shu, H., Wang, Z., Liu, D., et al. (2017). The effect of apolipoprotein E ε4 (APOE ε4) on visuospatial working memory in healthy elderly and amnestic mild cognitive impairment patients: an event-related potentials study. *Front. Aging Neurosci.* 9:145. doi: 10.3389/fnagi.2017.00145

Gu, L. H., Chen, J., Gao, L. J., Shu, H., Wang, Z., Liu, D., et al. (2018). Cognitive reserve modulates attention processes in healthy elderly and amnestic mild cognitive impairment: an event-related potential study. *Clin. Neurophysiol.* 129, 198–207. doi: 10.1016/j.clinph.2017.10.030

Hayes, J. M., Tang, L., Viviano, R. P., van Rooden, S., Ofen, N., and Damoiseaux, J. S. (2017). Subjective memory complaints are associated with brain activation supporting successful memory encoding. *Neurobiol. Aging* 60, 71–80. doi: 10.1016/j.neurobiolaging.2017.08.015

Hu, X., Teunissen, C., Spottke, A., Heneka, M. T., Düzel, E., Peters, O., et al. (2019). Smaller medial temporal lobe volumes in individuals with subjective cognitive decline and biomarker evidence of Alzheimer's disease-Data from three memory clinic studies. *Alzheimers Dement.* 15, 185–193. doi: 10.1016/j.jalz.2018.09.002

Huang, K. L., Hsiao, I. T., Kuo, H. C., Hsieh, C. J., Hsieh, Y. C., Wu, Y. M., et al. (2019). Correlation between visual association memory test and structural changes in patients with Alzheimer's disease and amnestic mild cognitive impairment. *J. Formos. Med. Assoc.* 118, 1325–1332. doi: 10.1016/j.jfma.2018.12.001

Joshi, H., Bharath, S., John, J. P., Sadanand, S., Saini, J., Kumar, K., et al. (2018). Resting state functional connectivity abnormalities and delayed recall performance in patients with amnestic mild cognitive impairment. *Brain Imaging Behav.* doi: 10.1007/s11682-018-9974-1

Kim, S. R., Kim, S., Baek, M. J., and Kim, H. (2015). Abstract word definition in patients with amnestic mild cognitive impairment. *Behav. Neurol.* 2015:580246. doi: 10.1155/2015/580246

Lee, J. S., Cho, S. K., Kim, H. J., Kim, Y. J., Park, K. C., Lockhart, S. N., et al. (2018). Prediction models of cognitive trajectories in patients with nonamnestic mild cognitive impairment. *Sci. Rep.* 8:10468. doi: 10.1038/s41598-018-28881-1

Liang, P., Wang, Z., Yang, Y., Jia, X., and Li, K. (2011). Functional disconnection and compensation in mild cognitive impairment: evidence from DLPFC connectivity using resting-state fMRI. *PLoS One* 6:e22153. doi: 10.1371/journal.pone.0022153

Makovac, E., Serra, L., Di Domenico, C., Marra, C., Caltagirone, C., Cercignani, M., et al. (2018). Quantitative magnetization transfer of white matter tracts correlates with diffusion tensor imaging indices in predicting the conversion from mild cognitive impairment to Alzheimer's disease. *J. Alzheimers Dis.* 63, 561–575. doi: 10.3233/jad-170995

Ofer, I., Jacobs, J., Jaiser, N., Akin, B., Hennig, J., Schulze-Bonhage, A., et al. (2018). Cognitive and behavioral comorbidities in Rolandic epilepsy and their relation with default mode network's functional connectivity and organization. *Epilepsy Behav.* 78, 179–186. doi: 10.1016/j.yebeh.2017.10.013

Oltra-Cucarella, J., Delgado, S., Duque, P., Pérez-Vicente, J. A., and Cabello-Rodríguez, L. (2018). Encoding deficits in low-educated individuals with non-amnestic mild cognitive impairment. Analysis of memory processes using the item specific deficit approach. *Psychiatry Res.* 268, 211–216. doi: 10.1016/j.psychres.2018.07.026

Palesi, F., Castellazzi, G., Casiraghi, L., Sinforiani, E., Vitali, P., Gandini Wheeler-Kingshott, C. A., et al. (2016). Exploring patterns of alteration in Alzheimer's disease brain networks: a combined structural and functional connectomics analysis. *Front. Neurosci.* 10:380. doi: 10.3389/fnins.2016.00380

Power, J. D., Barnes, K. A., Snyder, A. Z., Schlaggar, B. L., and Petersen, S. E. (2012). Spurious but systematic correlations in functional connectivity MRI networks arise from subject motion. *Neuroimage* 59, 2142–2154. doi: 10.1016/j.neuroimage.2011.10.018

Prieto Del Val, L., Cantero, J. L., and Atienza, M. (2016). Atrophy of amygdala and abnormal memory-related α oscillations over posterior cingulate predict conversion to Alzheimer's disease. *Sci. Rep.* 6:31859. doi: 10.1038/srep31859

Qi, Z., Wu, X., Wang, Z., Zhang, N., Dong, H., Yao, L., et al. (2010). Impairment and compensation coexist in amnestic MCI default mode network. *Neuroimage* 50, 48–55. doi: 10.1016/j.neuroimage.2009.12.025

Rossetto, F., Castelli, I., Baglio, F., Massaro, D., Alberoni, M., Nemni, R., et al. (2018). Cognitive and affective theory of mind in mild cognitive impairment and Parkinson's disease: preliminary evidence from the italian version of the yoni task. *Dev. Neuropsychol.* 43, 764–780. doi: 10.1080/87565641.2018.1529175

Scherr, M., Utz, L., Tahmasian, M., Pasquini, L., Grothe, M. J., Rauschecker, J. P., et al. (2019). Effective connectivity in the default mode network is distinctively disrupted in Alzheimer's disease-A simultaneous resting-state FDG-PET/fMRI study. *Hum. Brain Mapp*. doi: 10.1002/hbm.24517

Smith, S. M., and Nichols, T. E. (2009). Threshold-free cluster enhancement: addressing problems of smoothing, threshold dependence and localisation in cluster inference. *Neuroimage* 44, 83–98. doi: 10.1016/j.neuroimage.2008.03.061

Van Dijk, K. R., Sabuncu, M. R., and Buckner, R. L. (2012). The influence of head motion on intrinsic functional connectivity MRI. *Neuroimage* 59, 431–438. doi: 10.1016/j.neuroimage.2011.07.044

Vecchio, F., Miraglia, F., Iberite, F., Lacidogna, G., Guglielmi, V., Marra, C., et al. (2018). Sustainable method for Alzheimer dementia prediction in mild cognitive impairment: electroencephalographic connectivity and graph theory combined with apolipoprotein E. *Ann. Neurol.* 84, 302–314. doi: 10.1002/ana.25289

Verfaillie, S. C. J., Pichet Binette, A., Vachon-Presseau, E., Tabrizi, S., Savard, M., Bellec, P., et al. (2018). Subjective cognitive decline is associated with altered default mode network connectivity in individuals with a family history of Alzheimer's disease. *Biol. Psychiatry Cogn. Neurosci. Neuroimaging* 3, 463–472. doi: 10.1016/j.bpsc.2017.11.012

Wang, J., Becker, B., Wang, L., Li, H., Zhao, X., and Jiang, T. (2019). Corresponding anatomical and coactivation architecture of the human precuneus showing similar connectivity patterns with macaques. *Neuroimage* 200, 562–574. doi: 10.1016/j.neuroimage.2019.07.001

Wang, J., Fan, L., Zhang, Y., Liu, Y., Jiang, D., Zhang, Y., et al. (2012). Tractography-based parcellation of the human left inferior parietal lobule. *Neuroimage* 63, 641–652. doi: 10.1016/j.neuroimage.2012.07.045

Wang, C., Pan, Y., Liu, Y., Xu, K., Hao, L., Huang, F., et al. (2018). Aberrant default mode network in amnestic mild cognitive impairment: a meta-analysis of independent component analysis studies. *Neurol. Sci.* 39, 919–931. doi: 10.1007/s10072-018-3306-5

Wang, Y., Risacher, S. L., West, J. D., McDonald, B. C., Magee, T. R., Farlow, M. R., et al. (2013). Altered default mode network connectivity in older adults with cognitive complaints and amnestic mild cognitive impairment. *J. Alzheimers Dis.* 35, 751–760. doi: 10.3233/jad-130080

Wang, J., Xie, S., Guo, X., Becker, B., Fox, P. T., Eickhoff, S. B., et al. (2017). Correspondent functional topography of the human left inferior parietal lobule at rest and under task revealed using resting-state fMRI and coactivation based parcellation. *Hum. Brain Mapp.* 38, 1659–1675. doi: 10.1002/hbm.23488

Wang, J., Zhang, J., Rong, M., Wei, X., Zheng, D., Fox, P. T., et al. (2016). Functional topography of the right inferior parietal lobule structured by anatomical connectivity profiles. *Hum. Brain Mapp.* 37, 4316–4332. doi: 10.1002/hbm.23311

Wu, Y., Zhang, Y., Liu, Y., Liu, J., Duan, Y., Wei, X., et al. (2016). Distinct changes in functional connectivity in posteromedial cortex subregions during the progress of Alzheimer's disease. *Front. Neuroanat.* 10:41. doi: 10.3389/fnana.2016.00041

Xie, C., Bai, F., Yu, H., Shi, Y., Yuan, Y., Chen, G., et al. (2012). Abnormal insula functional network is associated with episodic memory decline in amnestic mild cognitive impairment. *Neuroimage* 63, 320–327. doi: 10.1016/j.neuroimage.2012.06.062

Yan, T., Wang, W., Yang, L., Chen, K., Chen, R., and Han, Y. (2018). Rich club disturbances of the human connectome from subjective cognitive decline to Alzheimer's disease. *Theranostics* 8, 3237–3255. doi: 10.7150/thno.23772

Yang, H., Wang, C., Zhang, Y., Xia, L., Feng, Z., Li, D., et al. (2017). Disrupted causal connectivity anchored in the posterior cingulate cortex in amnestic mild cognitive impairment. *Front. Neurol.* 8:10. doi: 10.3389/fneur.2017.00010

Yuan, B., Chen, J., Gong, L., Shu, H., Liao, W., Wang, Z., et al. (2016a). Mediation of episodic memory performance by the executive function network in patients with amnestic mild cognitive impairment: a resting-state functional MRI study. *Oncotarget* 7, 64711–64725. doi: 10.18632/oncotarget.11775

Yuan, B., Xie, C., Shu, H., Liao, W., Wang, Z., Liu, D., et al. (2016b). Differential effects of APOE genotypes on the anterior and posterior subnetworks of default mode network in amnestic mild cognitive impairment. *J. Alzheimers Dis.* 54, 1409–1423. doi: 10.3233/jad-160353

Zhang, D., and Raichle, M. E. (2010). Disease and the brain's dark energy. *Nat. Rev. Neurol.* 6, 15–28. doi: 10.1038/nrneurol.2009.198

Zhang, Y., Simon-Vermot, L., Araque Caballero, M. A., Gesierich, B., Taylor, A. N. W., Duering, M., et al. (2016). Enhanced resting-state functional connectivity between core memory-task activation peaks is associated with memory impairment in MCI. *Neurobiol. Aging* 45, 43–49. doi: 10.1016/j.neurobiolaging.2016.04.018

Zhang, K., Wang, J., Peng, G., Liu, P., He, F., Zhu, Z., et al. (2019). Effect of cognitive training on episodic memory retrieval in amnestic mild cognitive impairment patients: study protocol for a clinical randomized controlled trial. *Trials* 20:26. doi: 10.1186/s13063-018-3143-0

Conflict of Interest: The authors declare that the research was conducted in the absence of any commercial or financial relationships that could be construed as a potential conflict of interest.

frontiers in Aging Neuroscience

ORIGINAL RESEARCH
published: 09 January 2020
doi: 10.3389/fnagi.2019.00355

Relationship Between Risk Factors and Brain Reserve in Late Middle Age: Implications for Cognitive Aging

*Bryan J. Neth[1], Jonathan Graff-Radford[1], Michelle M. Mielke[1,2], Scott A. Przybelski[2], Timothy G. Lesnick[2], Christopher G. Schwarz[3], Robert I. Reid[4], Matthew L. Senjem[3,4], Val J. Lowe[3], Mary M. Machulda[5], Ronald C. Petersen[1], Clifford R. Jack Jr.[3], David S. Knopman[1] and Prashanthi Vemuri[3]**

[1] Department of Neurology, Mayo Clinic, Rochester, MN, United States, [2] Department of Health Sciences Research, Mayo Clinic, Rochester, MN, United States, [3] Department of Radiology, Mayo Clinic, Rochester, MN, United States, [4] Department of Information Technology, Mayo Clinic, Rochester, MN, United States, [5] Department of Psychiatry and Psychology, Mayo Clinic, Rochester, MN, United States

Background: Brain reserve can be defined as the individual variation in the brain structural characteristics that later in life are likely to modulate cognitive performance. Late midlife represents a point in aging where some structural brain imaging changes have become manifest but the effects of cognitive aging are minimal, and thus may represent an ideal opportunity to determine the relationship between risk factors and brain imaging biomarkers of reserve.

Objective: We aimed to assess neuroimaging measures from multiple modalities to broaden our understanding of brain reserve, and the late midlife risk factors that may make the brain vulnerable to age related cognitive disorders.

Methods: We examined multimodal [structural and diffusion Magnetic Resonance Imaging (MRI), FDG PET] neuroimaging measures in 50–65 year olds to examine the associations between risk factors (Intellectual/Physical Activity: education-occupation composite, physical, and cognitive-based activity engagement; General Health Factors: presence of cardiovascular and metabolic conditions (CMC), body mass index, hemoglobin A1c, smoking status (ever/never), CAGE Alcohol Questionnaire (>2, yes/no), Beck Depression Inventory score), brain reserve measures [Dynamic: genu corpus callosum fractional anisotropy (FA), posterior cingulate cortex FDG uptake, superior parietal cortex thickness, AD signature cortical thickness; Static: intracranial volume], and cognition (global, memory, attention, language, visuospatial) from a population-based sample. We quantified dynamic proxies of brain reserve (cortical thickness, glucose metabolism, microstructural integrity) and investigated various protective/risk factors.

Results: Education-occupation was associated with cognition and total intracranial volume (static measure of brain reserve), but was not associated with any of the dynamic neuroimaging biomarkers. In contrast, many general health factors were associated with

OPEN ACCESS

Edited by:
Hans J. Grabe,
University of Greifswald, Germany

Reviewed by:
Diana López-Barroso,
University of Málaga, Spain
Ines Moreno-Gonzalez,
University of Málaga, Spain

****Correspondence:***
Prashanthi Vemuri
vemuri.prashanthi@mayo.edu

Received: *27 June 2019*
Accepted: *05 December 2019*
Published: *09 January 2020*

Citation:
Neth BJ, Graff-Radford J, Mielke MM, Przybelski SA, Lesnick TG, Schwarz CG, Reid RI, Senjem ML, Lowe VJ, Machulda MM, Petersen RC, Jack CR Jr, Knopman DS and Vemuri P (2020) Relationship Between Risk Factors and Brain Reserve in Late Middle Age: Implications for Cognitive Aging. Front. Aging Neurosci. 11:355. doi: 10.3389/fnagi.2019.00355

the dynamic neuroimaging proxies of brain reserve, while most were not associated with cognition in this late middle aged group.

Conclusion: Brain reserve, as exemplified by the four dynamic neuroimaging features studied here, is itself at least partly influenced by general health status in midlife, but may be largely independent of education and occupation.

Keywords: brain reserve, cognitive aging, multimodal imaging, resilience, dynamic

INTRODUCTION

Brain health is difficult to quantify – other than the absence of cognitive or neurological disease or pathology. The health of other organs is more easily measureable. For example, cardiac health can be described in terms of left ventricular ejection fraction, cardiac index, or burden of coronary artery disease (Mosterd and Hoes, 2007; Paulus et al., 2007; Jefferson et al., 2010). Renal health can be monitored by glomerular filtration rate or serum creatinine (Traynor et al., 2006). There are established thresholds or stages of disease severity for both congestive heart failure and chronic kidney disease (Coresh et al., 2007; Mosterd and Hoes, 2007). In contrast, although several fundamental components of brain health have been described, such as brain reserve and cognitive reserve or resilience, they have not been widely quantified and utilized.

The focus of the current study is on the concept of "brain reserve" or "neurobiological capital," defined as individual brain variation that may lead to resistance or ability to cope with pathology (Stern et al., 2018). The traditionally used proxies of brain reserve include total intracranial volume, premorbid brain tissue volume, and head circumference (Stern et al., 2018), which are static or fixed in nature. Although each of these measures are a gross measure of the brain anatomic capital, these measures are not sufficient to define the overall brain reserve. Because midlife and late middle age represent a critical period where prominent aging-related brain changes begin (Debette et al., 2011; Ritchie et al., 2015), identifying alterations to brain reserve in this period will enhance the understanding of early changes in cognitive and brain aging. Furthermore, studying brain reserve in late middle age may provide insights into mechanisms of resilience that could contribute to a better accepted model of overall brain health (Arenaza-Urquijo and Vemuri, 2018; Stern et al., 2018, 2019). See **Figure 1** for a model of brain reserve throughout life.

The main objective of this study was to broaden our understanding of brain reserve, protective/risk factors, and cognition in late middle age adult participants (age 50–65 years) without cognitive impairment. We focused on this age group because it is an age range during which both neuronal structure and functional alterations are observed but with few clinical symptoms (Giorgio et al., 2010; Jagust, 2013). We aimed to: (1) examine protective/risk factors of brain reserve measures and cognition; and (2) identify optimal neuroimaging measures related to global and domain-specific cognition that may best serve as dynamic neuroimaging biomarkers of brain reserve.

MATERIALS AND METHODS

Selection of Participants

Study participants were from the Mayo Clinic Study of Aging (MCSA) (Roberts et al., 2008), an epidemiologic study of Mild Cognitive Impairment (MCI) and dementia among community-dwelling residents of Olmsted County, Minnesota. We included 537 late middle age participants (age 50–65 years) who had available Magnetic Resonance Imaging (MRI) data. A subset of 454 participants also had ^{18}F-fluorodeoxyglucose positron emission tomography (FDG PET). All participants were cognitively unimpaired based upon a clinical adjudication at the clinical visit corresponding to the imaging visit. The MCSA was approved by the Mayo Clinic and Olmsted Medical Center Institutional Review Boards and all participants provided written informed consent.

Measures of Brain Reserve

We utilized four dynamic or modifiable neuroimaging measures from three imaging modalities that are related to cognitive aging and dementia as proxies of overall brain reserve: genu corpus callosum fractional anisotropy (FA), posterior cingulate cortex FDG uptake, superior parietal cortex thickness, and AD signature cortical thickness. We term these proxies of brain reserve as dynamic because they are not constant or fixed across the adult lifespan like traditional brain reserve measures such as intracranial volume.

Diffusion tensor imaging (DTI) is a method utilized to quantify water diffusion throughout white matter tracts in the brain, with FA being one diffusion metric to assess white matter integrity (Le Bihan et al., 2001). Lower FA is related to less microstructural integrity of the white matter, and lower FA has been shown to be related to lower cognition in community-dwelling older adults (Vernooij et al., 2009) and throughout the Alzheimer's spectrum (Bozzali et al., 2002; Zhang et al., 2007; Chua et al., 2008). Microstructural integrity of the genu corpus callosum as assessed by FA has been shown to be related of systemic vascular and cerebrovascular health (Vemuri et al., 2018), and is potentially an earlier surrogate of cerebrovascular health than white mater hyperintensities. There are intrinsic differences in myelination, axonal density, or even time to maturity of specific white matter tracks (Kochunov et al., 2012; Sexton et al., 2014) that uniquely differentiate the genu from other white matter tracks. Metabolism in the posterior cingulate cortex, one of the most metabolic brain regions, has been shown to preferentially decline early in preclinical Alzheimer's disease

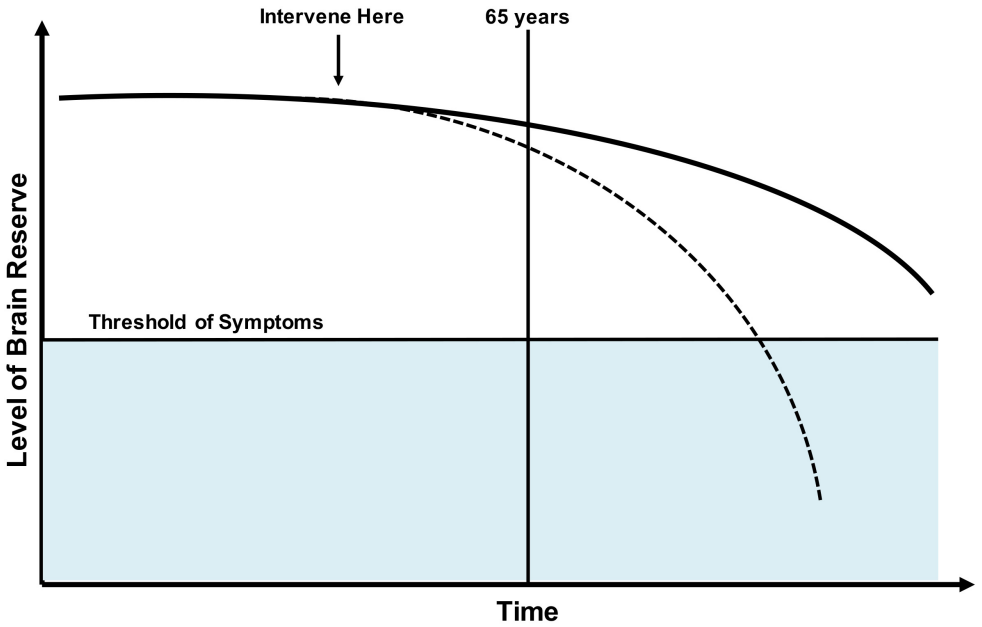

FIGURE 1 | Model of brain reserve throughout the lifespan. Dotted line: Various factors may decrease brain reserve making likelihood of age-related cognitive disorders more likely. Solid line: Normal trajectory without onset of clinical symptoms. It would be ideal to study and intervene on factors that negatively influence brain reserve prior to onset of decline, with hopes of preventing or delaying onset of clinical disease.

and is lower in APOE E4 carriers (Cunnane et al., 2011; Protas et al., 2013; Leech and Sharp, 2014). Given the higher baseline glucose uptake of the posterior cingulate cortex relative to other brain regions and the disease-related metabolic decline of the posterior cingulate cortex, it may uniquely serve as proxy of brain health. Superior parietal cortex thickness has recently been related to systemic vascular health, such that greater thickness was associated with a higher number of vascular conditions. Greater thickness has been posited to be a compensatory response to early pathology (Vemuri et al., 2018). Reports have described higher parietal volume in amyloid positive participants (Johnson et al., 2014), and greater compensatory superior parietal cortical thickness in those with lower CSF amyloid prior to atrophy that coincides with increased CSF p-tau (Fortea et al., 2014). With the significant impact of systemic vascular health on the brain and potential influence of amyloid and tau on the superior parietal lobule, we believe superior parietal cortical thickness uniquely contributes to a more comprehensive view of brain health. We chose to include Alzheimer's disease signature cortical thickness as a measure of brain reserve because it has been validated as a measure of neurodegeneration and is likely a better measure than other traditionally used proxies of age and disease related neurodegeneration, like hippocampal volume, as it is not confounded by head size (Jack et al., 2015).

Structural and Diffusion MRI

All MRI images were acquired on 3T GE MRI (GE Medical Systems, Milwaukee, WI, United States) using a Sagittal 3D magnetization prepared rapid acquisition gradient recalled echo (MP-RAGE) sequence. Repetition time (TR) was ≈2300 ms, echo time (TE) ≈3 ms, and inversion time (TI) = 900 ms. Voxel dimensions were ≈1.20 × 1.015 × 1.015 mm.

Cortical thickness measurements were computed using Freesurfer v5.3 and total intracranial volume was computed using a previously published method (Schwarz et al., 2016) on standard structural magnetization-prepared rapid acquisition gradient echo (MPRAGE) scans. We considered the dynamic measures of superior parietal cortex thickness and composite measure of cortical thickness from AD vulnerable regions (average of thickness in entorhinal cortex, inferior temporal, middle temporal, fusiform) (Jack et al., 2015). As a comparison to these measures, we have also performed analyses with the static measure of total intracranial volume.

The details of DTI acquisition and processing are discussed in our recent publication (Vemuri et al., 2018). We considered genu of the corpus callosum microstructural integrity as quantified by FA from DTI.

FDG PET

The acquisition, processing, and summary measure details for FDG PET scans acquired on the MCSA study participants are previously described (Jack et al., 2015). Computed tomography scan was obtained for attenuation correction and FDG PET images were obtained 30–40 min after tracer injection. We considered posterior cingulate cortex glucose metabolism from FDG PET.

Selection of Protective and Risk Factors

We examined a broad range of protective and risk factors including traditionally viewed proxies for resilience (e.g., education, intellectual and physical activities)

(Stern et al., 2018), and overall proxies of health (e.g., chronic or comorbid conditions).

Intellectual and Physical Activities

We utilized an education-occupation composite measure that incorporates years of education and job level score that is based on the participant's primary occupation (Vemuri et al., 2015). We assessed physical and cognitive-based activity using a questionnaire that quantified the average activity in each domain during the last 12 months (Vemuri et al., 2012). In our sample of 50–65 years old participants, these represent self-reported measures of physical and cognitive-based activities at late middle age. A complete list of activities queried on the questionnaires are previously published (Vemuri et al., 2012).

General Health Measures

Given the relationships found between overall health and cognitive aging and/or age-related disease (Whitmer et al., 2005, 2008; Yaffe et al., 2006; Crooks et al., 2008; Craft, 2009; Byers and Yaffe, 2011), we included measures that are not routinely studied in the context of cognitive resilience. The presence of cardiovascular and metabolic conditions (CMC) is a measure composed of health system data, ICD-9 and ICD-10 codes of seven common conditions related to systemic health: hypertension, hyperlipidemia, cardiac arrhythmias, coronary artery disease, congestive heart failure, diabetes mellitus, and stroke (Vemuri et al., 2017, 2018). The CMC composite score is an additive measure of the absence or presence of each condition, with a range score of 0–7 (Vemuri et al., 2017, 2018). With increasing use of electronic medical records for research data, this metric may be derived from already collected data and serve as an overall metric of systemic cardiovascular/metabolic disease burden. In addition to CMC, we also studied body mass index [BMI, mass (kg)/height (m^2)] (Calle et al., 1999), hemoglobin A1c (average blood glucose of around the last 90–120 days) (Rohlfing et al., 2002), ever-smoking (dichotomous), score on the CAGE Alcohol Questionnaire >2 (dichotomous) (Ewing, 1984), and continuous score on the Beck Depression Inventory (Beck et al., 1996).

Measures of Cognition

As previously described, cognitive tests were administered by a psychometrist and included nine tests covering four domains: memory [WMS-R Logical Memory-II (delayed), WMS-R Visual Reproduction-II (delayed), AVLT (delayed)], attention (TMT: Part B, WAIS-R Digit Symbol), language (BNT, category fluency), and visuospatial (WAIS-R Picture Completion, WAIS-R Block Design) (Roberts et al., 2008). Individual test scores from each domain were converted into *z*-scores, which were then averaged to make domain-specific *z*-scores. Global cognition was estimated from the average of the four domain-specific *z*-scores and then itself converted into a *z*-score for analyses.

Statistical Analyses

We performed multivariable linear regression to examine the relationship between: (1) protective/risk factors and brain reserve measures, (2) brain reserve measures and cognition, (3) protective/risk factors and cognition. Next, to relate both brain reserve measures and protective/risk factors independently to cognition, each brain reserve measure and protective/risk factor was used as a predictor in regression models. All analyses were adjusted for age, sex, and the presence of an APOE E4 allele. We also performed *t*-test and chi-square analyses to assess for mean differences between sexes in cross-sectional protective/risk factors, brain reserve measures, and cognition. SAS University Edition was utilized for analyses. A $p < 0.05$ was considered statistically significant.

RESULTS

Participant characteristics are shown in **Table 1**. Our sample included 537 participants with a mean age of 58.7 years. There were nearly identical number of females and males (269 and 268). Of the 537 participants, 29.1% had an APOE4 allele. Mean education was 15.2 years with a range between 9–20 years.

Table 2 shows descriptive statistics between females and males. There were no differences in age, education years, APOE4 status between males and females. Females had higher global cognition, memory, attention, language performance; males had higher visuospatial skills. Females had higher posterior cingulate FDG and superior parietal thickness, despite lower intracranial volume and genu FA. Females had lower presence of CMC and higher self-reported cognitive activity engagement. There were no sex differences in body mass index, HbA1c, smoking status, Beck Depression Inventory score, or CAGE score.

Relationship Between Protective/Risk Factors and Brain Reserve Measures

A regression heatmap from analyses adjusted for age, sex, and APOE E4 can be found in **Figure 2A**, and complete regression output can be found in **Table 3A**. A higher education-occupation composite score was associated with higher posterior cingulate cortex FDG uptake and greater intracranial volume. More physical activity was associated with higher genu FA and posterior cingulate cortex FDG uptake. We found no associations between cognitive-based activity and any of the brain reserve measures.

A higher number of CMC and higher Beck Depression Inventory scores were associated with lower posterior cingulate cortex FDG uptake and AD signature region thickness. Being an ever-smoker (relative to never-smoker) was associated with lower genu FA, AD signature region thickness, and superior parietal cortex thickness. CAGE Alcohol Questionnaire score >2 was associated with lower AD signature region thickness and superior parietal cortex thickness. Higher body mass index was related to lower posterior cingulate cortex FDG uptake and superior parietal cortex thickness, and higher HbA1c was negatively related to lower posterior cingulate cortex FDG uptake.

Relationship Between Brain Reserve Measures and Cognition

We found that higher brain reserve measures were associated with better global and domain-specific cognition. A regression

TABLE 1 | Descriptive statistics for total sample.

Variable	All (n = 537)
Age (years)	58.7 (4.3)
Education (years)	15.2 (2.2)
Educ-occ composite	13.1 (2.2)
Global cognition (Z-score)	0.75 (0.77)
Memory (Z-score)	0.62 (0.88)
Attention (Z-score)	0.66 (0.74)
Language (Z-score)	0.50 (0.87)
Visuospatial (Z-score)	0.61 (0.84)
Genu corpus callosum (FA)	0.62 (0.04)
Posterior cingulate (FDG)	1.96 (0.16)
AD ROI (Thick)	2.98 (0.12)
Superior parietal (Thick)	2.04 (0.13)
Intracranial volume	1488.5 (161.7)
CMC	1.0 (1.1)
BMI	29.3 (5.6)
HbA1c	5.6 (0.7)
BDI score	4.1 (4.8)
Physical activity	6.7 (4.6)
Cognitive activity	21.1 (8.6)
Sex: F/M (%)	269 (50)/268 (50)
Smoke: No/Yes (%)	324 (60)/213 (40)
CAGE > 2: No/Yes (%)	500 (93)/37 (7)
APOE4: −/+ (%)	370 (71)/152 (29)

Mean (Standard Deviation) for continuous variables. Count (%) for dichotomous variables.

heatmap from adjusted analyses can be found in **Figure 2B**, and complete regression output can be found in **Table 3B**. Higher intracranial volume was associated with better global cognition and visuospatial ability; higher genu FA with better global cognition, attention, and visuospatial ability; higher posterior cingulate cortex FDG uptake with better global cognition and attention; and higher superior parietal thickness with better visuospatial ability. There were no significant associations between AD signature region thickness and cognition in multivariable models.

Relationship Between Protective/Risk Factors and Cognition

Education-occupation composite score and cognitive-based activity engagement in the last 12 months were associated with better global and domain-specific cognition across all domains. Physical activity engagement in the last 12 months was associated with better global cognition and better cognition in attention, language, and visuospatial ability domain, but not memory. A regression heatmap from adjusted analyses can be found in **Figure 2C**, and complete regression output can be found in **Table 3C**.

Being an ever-smoker (relative to non-smoker) was associated with worse cognition across all domains. A greater number of depressive symptoms was associated with worse performance in global cognition and on tests of memory and attention. Higher body mass index was associated with worse global cognition and language. We found no relationship between HbA1c or CAGE Alcohol Questionnaire score >2 and global or domain-specific cognition.

DISCUSSION

We examined the relationships between protective/risk factors and imaging proxies of brain reserve in a late midlife cohort. Our major finding was that several general health factors were associated with worsening of the four dynamic neuroimaging biomarkers, in a manner that was not complicated by concomitant associations of declines in cognition and at least some of the general health factors. Depression and smoking showed associations with the dynamic neuroimaging proxies of reserve but also cognition, precluding any claims about their indirect relationships to brain reserve. Education-occupation was not associated with any of the dynamic brain imaging measures, but was associated with the static brain reserve proxy of total intracranial volume.

Brain reserve, as exemplified by the four dynamic imaging features studied here, is itself at least partly under the influence of general health status in midlife, but remarkably is largely independent of education and occupation. Health issues such as CMC, BMI, glycemic control and alcohol use that arise in midlife may have indirect effects on risks for later life cognition by influencing brain structure and function beginning in midlife or even earlier. Thus, white matter integrity in the genu corpus callosum, posterior cingulate cortex FDG, and cortical thickness are influenced by midlife health factors that in later life moderate the effects of age-related neurodegenerative and cerebrovascular diseases.

Several features distinguish this study from most published reports on resilience and brain reserve. First, we worked to strengthen our understanding of brain reserve by examining a broader set of dynamic biomarkers of brain reserve from multiple neuroimaging modalities. Traditional measures of brain reserve include premorbid brain volume, intracranial volume, or head circumference, which are fixed throughout the adult life (Stern et al., 2018). While these measures have been shown to be related to cognition, they are gross measures of overall brain reserve and do not encapsulate the likely modifiable nature of brain reserve. In this study, the static measure of intracranial volume that was used as a comparison region was only related to education-occupation and not to the other potential protective/risk factors that we identified. Whereas three of the four the dynamic brain reserve measures we used were associated with multiple general health factors. Importantly, our work builds upon recent studies that have started to expand our view of brain reserve with the incorporation of glucose metabolism, white matter integrity, and patterns of gray matter volume and cortical thickness (Querbes et al., 2009; Smith et al., 2010; Arenaza-Urquijo et al., 2013; Ewers et al., 2013; Morbelli et al., 2013; Malpetti et al., 2017; Pettigrew et al., 2017; Laubach et al., 2018). As shown in our results, the incorporation of carefully selected dynamic neuroimaging measures associated with cognitive aging may provide additional

TABLE 2 | Descriptive statistics by sex.

Variable	Female (n = 269)	Male (n = 268)	p-value
Age (years)	58.7 (4.3)	58.7 (4.2)	ns
Education (years)	15.1 (2.2)	15.3 (2.2)	ns
Educ-occ composite	12.8 (2.3)	13.3 (2.1)	0.0195
Global cognition (Z-score)	0.83 (076)	0.68 (0.77)	0.0297
Memory (Z-score)	0.78 (0.84)	0.45 (0.88)	<0.0001
Attention (Z-score)	0.79 (0.75)	0.53 (0.70)	<0.0001
Language (Z-score)	0.60 (0.89)	0.39 (0.84)	0.0049
Visuospatial (Z-score)	0.45 (0.80)	0.78 (0.85)	<0.0001
Genu corpus callosum (FA)	0.62 (0.04)	0.63 (0.04)	0.0269
Posterior cingulate (FDG)	2.00 (0.16)	1.92 (0.16)	<0.0001
AD ROI (Thick)	2.98 (0.12)	2.98 (0.12)	ns
Superior parietal (Thick)	2.06 (0.12)	2.03 (0.13)	0.0013
Intracranial volume	1381.3 (112.9)	1596.1 (128.4)	<0.0001
CMC	1.0 (1.1)	1.3 (1.2)	0.0003
BMI	29.3 (6.6)	29.3 (4.5)	ns
HbA1c	5.5 (0.6)	5.6 (0.8)	ns
BDI score	4.1 (4.7)	4.7 (4.9)	ns
Physical activity	6.6 (4.3)	6.8 (4.8)	ns
Cognitive activity	23.3 (8.6)	18.9 (8.1)	<0.0001
Smoke: No/Yes (%)	170 (63)/99 (37)	154 (57)/114 (43)	ns
CAGE > 2: No/Yes (%)	255 (94)/14 (6)	245 (91)/23 (9)	ns
APOE4: −/+ (%)	187 (72)/74 (28)	183 (70)/78 (30)	ns

Mean (Standard Deviation) for continuous variables. Count (%) for dichotomous variables. p-values for t-test and chi-square of differences in group means.

tools for the study of brain reserve; however, this will require future studies in independent samples.

Second, we studied a broad array of protective/risk factors that may impact brain health. Many studies on resilience use education, occupation, or lifestyle-social activity engagement as the sole proxy of cognitive resilience (Stern, 2009, 2012; Stern et al., 2018). While these contribute to the lower susceptibility to pathology, other factors may be additive in our understanding of cognitive resilience and brain health (Clare et al., 2017); notably: smoking, alcohol intake, and systemic vascular and metabolic health (Wolf et al., 1988; Ott et al., 1998; Thomas and Rockwood, 2001; Craft, 2009). The general health factors we examined were largely associated with lower brain reserve, as assessed by the four dynamic neuroimaging measures. By studying factors other than education, intellectual and physical activities as factors that influence cognitive resilience, we have the opportunity to better define which factors positively or negatively impact brain health and cognitive aging. This is of fundamental significance given the aging population throughout the world and an incomplete understanding of what factors lead to the complex, age-related cognitive disorders, like Alzheimer's.

Third, our study was comprised of a late midlife sample (50–65 years) of participants without clinical signs of cognitive impairment. To date, many studies concerning resilience or brain reserve have focused on older adults. This is logical when working to assess resilience and brain reserve as pathologic differences may be more evident in that population; however, it is likely the brain changes that promote cognitive decline and age-related cognitive disorders begins earlier in life (see **Figure 1**). While we are currently unaware of exactly when these changes begin, pathology studies have shown very low prevalence of neurodegenerative and cerebrovascular pathologies before the age of 65 (Nelson et al., 2012). We would advocate for the study of protective/risk factors that influence resilience, brain reserve, and overall brain health throughout life to further our understanding.

Although it's increasingly apparent that sex differences may impact brain health (Mielke et al., 2014; Chêne et al., 2015; Zagni et al., 2016), we still have an inadequate understanding of how sex impacts brain health throughout life and the propensity to develop age-related cognitive disorders. Although our study was not specifically designed to assess for sex differences, in our sample females scored higher on all cognitive domains except for visuospatial ability relative to age and education matched males. Moreover, despite having significantly lower total intracranial volume, females had no differences in AD region thickness, with higher superior parietal thickness and posterior cingulate FDG relative to males.

Strengths and Limitations

The investigation of a narrow sample of the population (50–65 years) is a key strength of this work because this is a critical range where early brain and cognitive changes are observed without significant burden of cerebrovascular disease and neurodegenerative disorders. The large sample size (n = 537) with nearly identical number of females/males in late middle age that has been well characterized with demographic

FIGURE 2 | (A) Regression Heatmap for Protective/Risk Factors × Brain Reserve Measures. Adjusted analyses shown in figure. Shades of green indicate positive relationships between Protective/Risk Factors and Brain Reserve Measures. Shades of red indicate negative relationships between Protective/Risk Factors and Brain Reserve Measures. Complete regression output with Beta and SE can be found in **Table 3A**. **(B)** Regression Heatmap for Brain Reserve Measures × Cognitive Measures. Adjusted analyses shown in figure. Shades of green indicate positive relationships between Brain Reserve Measures and Cognitive Measures. There were no negative relationships between Brain Reserve and Cognitive Measures. Complete regression output with Beta and SE can be found in **Table 3B**. **(C)** Regression Heatmap for Protective/Risk Factors × Cognitive Measures. Adjusted analyses shown in figure. Shades of green indicate positive relationships between Protective/Risk Factors and Cognitive Measures. Shades of red indicate negative relationships between Protective/Risk Factors and Cognitive Measures. Complete regression output with Beta and SE can be found in **Table 3C**.

data and neuroimaging measures obtained at a single site strengthen our findings.

Several limitations include the homogeneity of our population-based sample relative to the United States and worldwide that may limit the applicability of findings. However, previous reports support the generalizability of our sample (Rocca et al., 2012; Sauver et al., 2012). The cross-sectional design of the study limits our ability to assess the relationship between protective/risk factors and brain reserve measures to the development of MCI, dementia, or cognitive change. While we found associations between brain reserve measures and cognition, these relationships will likely be best assessed in a longitudinal study where change in cognition and other clinical outcomes may be examined. Despite these limitations our study of a unique sample helps contribute to the understanding of cognitive aging and overall brain health in late midlife.

Future Directions

Further work is needed to validate the findings of this study in an independent sample. Future studies will benefit from the development of composite risk scores and composite measures for brain health that can be used in tracking brain and cognitive aging throughout life. A longitudinal study would help to better assess cognitive decline (change in cognitive outcomes) and risk for development of MCI and dementia. It may be helpful to perform voxel-wise analyses of potential brain reserve measures. Lastly, we may work to stratify cognitively normal participants by CSF and/or PET amyloid and tau status to determine if this impacts the relationship between protective/risk factors and

TABLE 3 | Full regression output including Beta, SE, and *p*-values for tested relationships, emboldened results are significant.

(A)

Unadjusted	Educ-Occ			Phys Act			Cog Act			CMC			BMI			HbA1c			BDI			Smoke			CAGE		
Risk × BR	**B**	**SE**	**p**	**B**	**SE**	**p**	**B**	**SE**	**p**	**B**	**SE**	**p**	**B**	**SE**	**p**	**B**	**SE**	**p**	**B**	**SE**	**p**	**B**	**SE**	**p**	**B**	**SE**	**p**
GCC (FA)	0.00108	0.0007	0.1362	**0.0008**	**0.0003**	**0.01780**	−0.00025	0.0002	0.1744	**−0.00347**	**0.0014**	**0.01060**	−0.00023	0.0003	0.4138	−0.00153	0.0024	0.5255	−0.00026	0.0003	0.4312	**−0.00683**	**0.0032**	**0.03520**	−0.00512	0.0063	0.4148
PCC (FDG)	0.00481	0.0035	0.168	**0.0046**	**0.0017**	**0.00620**	**0.00240**	**0.0009**	**0.00720**	**−0.03078**	**0.0064**	**0.00001**	**−0.00285**	**0.0014**	**0.03550**	**−0.04327**	**0.0112**	**0.00010**	**−0.00415**	**0.0016**	**0.01150**	**−0.03349**	**0.0157**	**0.03330**	−0.00012	0.0304	0.9969
AD ROI (Thick)	0.00321	0.0024	0.19	0.0023	0.0012	0.0502	−0.00021	0.0006	0.7337	**−0.02029**	**0.0045**	**0.00001**	**−0.00259**	**0.0010**	**0.00680**	−0.00838	0.0081	0.3022	**−0.00319**	**0.0011**	**0.00430**	**−0.03970**	**0.0108**	**0.00030**	**−0.05290**	**0.0211**	**0.01230**
SupPar (Thick)	0.00255	0.0025	0.314	0.0001	0.0012	0.9613	0.00105	0.0006	0.1035	−0.00384	0.0047	0.4184	0.00173	0.0010	0.0809	−0.00654	0.0084	0.4353	−0.00069	0.0012	0.5499	**−0.02731**	**0.0112**	**0.01550**	**−0.07410**	**0.0216**	**0.00070**
ICV (Vol)	**14.53234**	**3.1316**	**0.00001**	1.7694	1.5417	0.2516	**−2.21202**	**0.8103**	**0.00650**	10.88245	5.9642	0.0686	−1.92489	1.2462	0.123	−6.35487	10.6098	0.5495	0.27990	1.4600	0.848	−1.28664	14.2745	0.9282	33.04846	27.5332	0.2305

Adjusted	Educ-Occ			Phys Act			Cog Act			CMC			BMI			HbA1c			BDI			Smoke			CAGE		
Risk × BR	**B**	**SE**	**p**	**B**	**SE**	**p**	**B**	**SE**	**p**	**B**	**SE**	**p**	**B**	**SE**	**p**	**B**	**SE**	**p**	**B**	**SE**	**p**	**B**	**SE**	**p**	**B**	**SE**	**p**
GCC (FA)	0.00091	0.0007	0.2006	**0.0007**	**0.0003**	**0.04770**	−0.00012	0.0002	0.5285	−0.00242	0.0014	0.0806	−0.00019	0.0003	0.4906	−0.00112	0.0024	0.6352	−0.00035	0.0003	0.2799	**−0.00621**	**0.0032**	**0.04990**	−0.00543	0.0061	0.375
PCC (FDG)	0.00756	0.0033	0.02380	**0.0045**	**0.0016**	**0.00580**	0.00137	0.0009	0.1243	**−0.02128**	**0.0064**	**0.00100**	**−0.00280**	**0.0013**	**0.03050**	**−0.03754**	**0.0108**	**0.00060**	**−0.00398**	**0.0016**	**0.01100**	−0.02530	0.0150	0.0929	0.00935	0.0290	0.7475
AD ROI (Thick)	0.00323	0.0024	0.1867	0.0020	0.0012	0.0842	−0.00018	0.0006	0.7814	**−0.01840**	**0.0047**	**0.00010**	**−0.00252**	**0.0009**	**0.00820**	−0.00701	0.0081	0.3871	**−0.00327**	**0.0011**	**0.00320**	**−0.03778**	**0.0108**	**0.00050**	**−0.05173**	**0.0210**	**0.01400**
SupPar (Thick)	0.00336	0.0025	0.1797	−0.0001	0.0012	0.9073	0.00064	0.0007	0.3265	0.00214	0.0049	0.6606	0.00179	0.0010	0.0665	−0.00394	0.0083	0.6348	−0.00056	0.0011	0.6276	**−0.02319**	**0.0111**	**0.03770**	**−0.06849**	**0.0213**	**0.00140**
ICV (Vol)	**9.67513**	**2.3652**	**0.00001**	1.2796	1.1553	0.2685	1.08832	0.6315	0.0854	−2.91924	4.6813	0.5332	−1.81222	0.9321	0.0524	−14.39758	8.0080	0.0728	−1.13769	1.0918	0.2979	−13.81308	10.7057	0.1975	5.07107	20.6777	0.8064

(B)

Unadjusted	GCC			PCC			AD ROI			SupPar			ICV		
BR × Cog	**B**	**SE**	**p**	**B**	**SE**	**p**	**B**	**SE**	**p**	**B**	**SE**	**p**	**B**	**SE**	**p**
Global	**2.80062**	**0.9010**	**0.00200**	**0.9593**	**0.2262**	**0.00001**	0.45760	0.2720	0.0931	0.44047	0.2621	0.0934	0.00003	0.0002	0.8902
Memory	1.08056	1.0296	0.2944	**0.6980**	**0.2449**	**0.00460**	0.23238	0.3054	0.4471	−0.11163	0.2964	0.7066	**−0.00074**	**0.0002**	**0.00160**
Attention	**2.24928**	**0.8604**	**0.00920**	**1.0748**	**0.2169**	**0.00001**	0.40709	0.2576	0.1146	**0.63481**	**0.2478**	**0.01070**	−0.00026	0.0002	0.1876
Language	**2.02338**	**1.0206**	**0.04790**	**0.7009**	**0.2514**	**0.00550**	0.14444	0.3050	0.636	0.29686	0.2955	0.3156	−0.00009	0.0002	0.7143
Visuospatial	**3.60372**	**0.9785**	**0.00030**	0.2285	0.2447	0.351	**0.68096**	**0.2952**	**0.02150**	**0.63359**	**0.2838**	**0.02600**	**0.00129**	**0.0002**	**0.00001**

Adjusted	GCC			PCC			AD ROI			SupPar			ICV		
BR × Cog	**B**	**SE**	**p**	**B**	**SE**	**p**	**B**	**SE**	**p**	**B**	**SE**	**p**	**B**	**SE**	**p**
Global	**2.11878**	**0.9084**	**0.02010**	**0.6834**	**0.2342**	**0.00370**	0.37298	0.2730	0.1725	0.21459	0.2605	0.4104	**0.00054**	**0.0003**	**0.04660**
Memory	1.05430	1.0379	0.3102	0.4135	0.2547	0.25466	0.13757	0.3017	0.6486	−0.39130	0.2949	0.1851	−0.00013	0.0003	0.6776
Attention	**1.93948**	**0.8550**	**0.02370**	**0.7098**	**0.2224**	**0.00150**	0.22823	0.2487	0.3593	0.35902	0.2425	0.1393	0.00050	0.0003	0.0511
Language	1.86428	1.0403	0.0737	0.4275	0.2617	0.1031	0.05065	0.3040	0.8677	0.09951	0.2976	0.7382	**0.00061**	**0.0003**	**0.0496**
Visuospatial	**2.36245**	**0.9787**	**0.01610**	0.2611	0.2494	0.2955	0.52470	0.2874	0.0685	**0.68476**	**0.2784**	**0.01420**	**0.00105**	**0.0003**	**0.00030**

(C)

Unadjusted	Educ-Occ			Phys Act			Cog Act			CMC			BMI			HbA1c			BDI			Smoke			CAGE		
Risk × Cog	**B**	**SE**	**p**	**B**	**SE**	**p**	**B**	**SE**	**p**	**B**	**SE**	**p**	**B**	**SE**	**p**	**B**	**SE**	**p**	**B**	**SE**	**p**	**B**	**SE**	**p**	**B**	**SE**	**p**
Global	**0.13989**	**0.0143**	**0.00001**	**0.0274**	**0.0074**	**0.00020**	**0.02990**	**0.0037**	**0.00001**	**−0.06770**	**0.0287**	**0.01880**	**−0.01272**	**0.0060**	**0.03440**	0.01142	0.0505	0.8211	**−0.02037**	**0.0069**	**0.00350**	**−0.39435**	**0.0668**	**0.00001**	−0.06607	0.1332	0.62
Memory	**0.10201**	**0.0168**	**0.00001**	0.0155	0.0084	0.0655	**0.02460**	**0.0043**	**0.00001**	−0.03664	0.0326	0.2615	−0.01009	0.0067	0.1349	0.00809	0.0568	0.8868	**−0.02636**	**0.0079**	**0.00080**	**−0.32235**	**0.0763**	**0.00001**	−0.29116	0.1487	0.0508
Attention	**0.09022**	**0.0142**	**0.00001**	**0.0233**	**0.0070**	**0.00100**	**0.02630**	**0.0036**	**0.00010**	**−0.09937**	**0.0271**	**0.00030**	−0.01030	0.0057	0.0706	−0.01955	0.0485	0.6868	**−0.02044**	**0.0066**	**0.00200**	**−0.33217**	**0.0638**	**0.00001**	−0.06403	0.1271	0.6147
Language	**0.14679**	**0.0162**	**0.00001**	**0.0260**	**0.0083**	**0.00180**	**0.03322**	**0.0042**	**0.00001**	−0.04264	0.0324	0.189	**−0.01393**	**0.0067**	**0.03850**	0.00327	0.0574	0.9546	−0.01463	0.0079	0.0638	**−0.35482**	**0.0759**	**0.00001**	−0.00463	0.1482	0.14823331
Visuospatial	**0.11419**	**0.0161**	**0.00001**	**0.0189**	**0.0081**	**0.01940**	**0.01202**	**0.0043**	**0.00500**	−0.01840	0.0314	0.5581	−0.00248	0.0066	0.7058	0.05340	0.0549	0.3309	−0.00166	0.0076	0.8283	**−0.26879**	**0.0740**	**0.00030**	0.06110	0.1455	0.6747

Adjusted	Educ-Occ			Phys Act			Cog Act			CMC			BMI			HbA1c			BDI			Smoke			CAGE		
Risk × Cog	**B**	**SE**	**p**	**B**	**SE**	**p**	**B**	**SE**	**p**	**B**	**SE**	**p**	**B**	**SE**	**p**	**B**	**SE**	**p**	**B**	**SE**	**p**	**B**	**SE**	**p**	**B**	**SE**	**p**
Global	**0.14417**	**0.0138**	**0.00001**	**0.0251**	**0.0072**	**0.00050**	**0.03064**	**0.0038**	**0.00001**	−0.02388	0.0295	0.4185	**−0.01250**	**0.0058**	**0.03270**	0.03165	0.0494	0.5221	**−0.02046**	**0.0068**	**0.00270**	**−0.36405**	**0.0655**	**0.00001**	−0.02553	0.1302	0.8446
Memory	**0.11046**	**0.0164**	**0.00001**	0.0144	0.0082	0.0808	**0.02132**	**0.0044**	**0.00001**	0.00635	0.0335	0.8497	−0.00985	0.0066	0.1361	0.02933	0.0558	0.5996	**−0.02483**	**0.0077**	**0.00140**	**−0.29354**	**0.0752**	**0.00010**	−0.24288	0.1461	0.0969
Attention	**0.09696**	**0.0136**	**0.00001**	**0.0237**	**0.0068**	**0.00050**	**0.02472**	**0.0035**	**0.00001**	−0.05286	0.0275	0.0551	−0.01014	0.0054	0.0621	0.00615	0.0464	0.8948	**−0.02001**	**0.0063**	**0.00160**	**−0.29355**	**0.0615**	**0.00001**	−0.06364	0.1248	0.6102
Language	**0.15326**	**0.0160**	**0.00001**	**0.0248**	**0.0082**	**0.00270**	**0.03292**	**0.0043**	**0.00001**	−0.00844	0.0337	0.8024	**−0.01367**	**0.0066**	**0.04000**	0.02159	0.0569	0.7046	−0.01386	0.0078	0.0765	**−0.33347**	**0.0755**	**0.00001**	0.02981	0.1469	0.8393
Visuospatial	**0.10693**	**0.0156**	**0.00001**	**0.0160**	**0.0078**	**0.04080**	**0.01919**	**0.0042**	**0.00001**	−0.00635	0.0317	0.8412	−0.00167	0.0063	0.7926	0.05236	0.0532	0.3254	−0.00468	0.0074	0.5271	**−0.26906**	**0.0716**	**0.00020**	0.03224	0.1407	0.8189

Results from unadjusted analyses and analyses adjusted for age, sex, and APOE4-status are provided. ***(A)*** *Protective/Risk Factors × Brain Reserve Measures,* ***(B)*** *Brain Reserve Measures × Cognitive Measures,* ***(C)*** *Protective/Risk Factors × Cognitive Measures. Bold values denote statistical significance at a threshold of* $p < 0.05$.

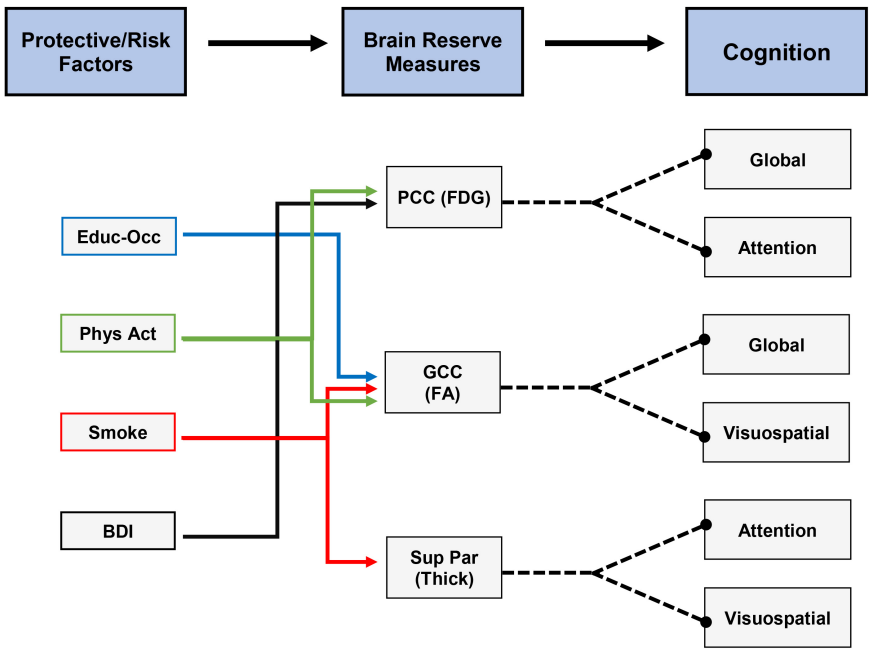

FIGURE 3 | Hypothetical depiction of connections between protective/risk factors, brain reserve measures, and cognitive measures. All depicted relationships were significant in our analyses. Note: the cross-sectional design of our study limits the ability to directly connect each protective/risk factor to cognitive measures as mediated by individual brain reserve measures.

dynamic brain reserve measures. Interestingly, in a study of 52 cognitively normal participants, those with lower CSF amyloid and higher education had lower FDG PET uptake, while those with higher CSF amyloid and higher education had higher FDG PET uptake (Ewers et al., 2013). This suggests that protective factors may be differentially related to dynamic brain reserve measures depending on baseline amyloid burden.

To better visualize potential connections between protective/risk factors, brain reserve measures, and cognition, we have compiled a flow diagram, indicating the significant relationships we found. **Figure 3** is a hypothetical depiction of these relationships where both protective/risk factors and brain reserve measures were related to the same cognitive outcome. For example, being an ever-smoker was related to lower genu FA and lower superior parietal cortex thickness, which were related to worse global cognition, visuospatial ability, and attention. Thus, it may be possible for smoking to negatively affect cognition via impact on genu FA and superior parietal cortex thickness. As seen in this figure, future work would ideally focus on expanding our understanding of individual and combined factors that augment brain reserve measures and ultimately lead to discernable clinical outcomes (i.e., cognition, functional status). Further longitudinal analyses and data across the lifespan will allow us to understand the pathways proposed.

CONCLUSION

In conclusion, we found that education-occupation was associated with cognition and the static brain reserve measure of total intracranial volume, but was not associated with any of the dynamic neuroimaging biomarkers. In contrast, many general health factors were associated with the dynamic neuroimaging proxies of brain reserve, while most were not associated with cognition in this late middle aged group. Brain reserve, as exemplified by the four dynamic neuroimaging features studied here, is itself at least partly under the influence of general health status in midlife, but remarkably is largely independent of education and occupation.

While an incomplete study of the factors that influence brain health and cognitive aging, this work contributes to the growing data that noticeable neuroimaging and cognitive relationships can be found in late midlife. We must continue to build a more comprehensive view of cognitive resilience and brain reserve to better understand the factors that make the brain vulnerable to age-related cognitive disorders.

DATA AVAILABILITY STATEMENT

The datasets generated for this study are available on request to the corresponding author.

ETHICS STATEMENT

The studies involving human participants were reviewed and approved by the Mayo Clinic and Olmsted Medical Center Institutional Review Boards. The patients/participants provided their written informed consent to participate in this study.

AUTHOR CONTRIBUTIONS

BN conceptualized the study, was responsible for the analysis and owns primary authorship. JG-R conceptualized the study and critically revised the manuscript for intellectual content. MiM, CS, RR, VL, MS, MaM, RP, CJ, and DK critically revised the manuscript for intellectual content. SP and TL were responsible for the analysis and the critical revision of manuscript for intellectual content. PV conceptualized the study and owns primary authorship.

FUNDING

This work was supported by NIH grants U01 AG006786 (PI: RP), R01 AG056366 (PI: PV), R01 NS097495 (PI: PV), P50 AG016574 (PI: RP), R37 AG011378 (PI: CJ), R01 AG041851 (PIs: CJ and DK), R01 AG034676 (Rochester Epidemiology Project), the Gerald and Henrietta Rauenhorst Foundation grant, the Millis Family, the Alexander Family Alzheimer's Disease Research Professorship of the Mayo Foundation, Alzheimer's Association (Zenith Fellows Award), Liston Award, Elsie and Marvin Dekelboum Family Foundation, Schuler Foundation, and Opus building NIH grant C06 RR018898.

ACKNOWLEDGMENTS

We thank all the study participants and staff in the Mayo Clinic Study of Aging, Mayo Alzheimer's Disease Research Center, and Aging Dementia Imaging Research laboratory at the Mayo Clinic.

REFERENCES

Arenaza-Urquijo, E. M., Landeau, B., La Joie, R., Mevel, K., Mezenge, F., Perrotin, A., et al. (2013). Relationships between years of education and gray matter volume, metabolism and functional connectivity in healthy elders. *Neuroimage* 83, 450–457. doi: 10.1016/j.neuroimage.2013.06.053

Arenaza-Urquijo, E. M., and Vemuri, P. (2018). Resistance vs resilience to Alzheimer disease: clarifying terminology for preclinical studies. *Neurology* 90, 695–703. doi: 10.1212/WNL.0000000000005303

Beck, A. T., Steer, R. A., and Brown, G. K. (1996). *Manual for the Beck Depression Inventory-II*. San Antonio, TX: Psychological Corporation. 490–498.

Bozzali, M., Falini, A., Franceschi, M., Cercignani, M., Zuffi, M., Scotti, G., et al. (2002). White matter damage in Alzheimer's disease assessed in vivo using diffusion tensor magnetic resonance imaging. *J. Neurol. Neurosurg. Psychiatry* 72, 742–746.

Byers, A. L., and Yaffe, K. (2011). Depression and risk of developing dementia. *Nat. Rev. Neurol.* 7, 323–331. doi: 10.1038/nrneurol.2011.60

Calle, E. E., Thun, M. J., Petrelli, J. M., Rodriguez, C., and Heath, C. W. Jr. (1999). Body-mass index and mortality in a prospective cohort of US adults. *N. England J. Med.* 341, 1097–1105.

Chêne, G., Beiser, A., Au, R., Preis, S. R., Wolf, P. A., Dufouil, C., et al. (2015). Gender and incidence of dementia in the framingham heart study from mid-adult life. *Alzheimers Dement.* 11, 310–320. doi: 10.1016/j.jalz.2013.10.005

Chua, T. C., Wen, W., Slavin, M. J., and Sachdev, P. S. (2008). Diffusion tensor imaging in mild cognitive impairment and Alzheimer's disease: a review. *Curr. Opin. Neurol.* 21, 83–92. doi: 10.1097/WCO.0b013e3282f4594b

Clare, L., Wu, Y.-T., Teale, J. C., Macleod, C., Matthews, F., Brayne, C., et al. (2017). Potentially modifiable lifestyle factors, cognitive reserve, and cognitive function in later life: a cross-sectional study. *PLoS Med.* 14:e1002259. doi: 10.1371/journal.pmed.1002259

Coresh, J., Selvin, E., Stevens, L. A., Manzi, J., Kusek, J. W., Eggers, P., et al. (2007). Prevalence of chronic kidney disease in the United States. *JAMA* 298, 2038–2047.

Craft, S. (2009). The role of metabolic disorders in Alzheimer Disease and vascular dementia. *Arch. Neurol.* 66, 300–305. doi: 10.1001/archneurol.2009.27

Crooks, V. C., Lubben, J., Petitti, D. B., Little, D., and Chiu, V. (2008). Social network, cognitive function, and dementia incidence among elderly women. *Am. J. Public Health* 98, 1221–1227. doi: 10.2105/AJPH.2007.115923

Cunnane, S., Nugent, S., Roy, M., Courchesne-Loyer, A., Croteau, E., Tremblay, S., et al. (2011). Brain fuel metabolism, aging, and Alzheimer's disease. *Nutrition* 27, 3–20.

Debette, S., Seshadri, S., Beiser, A., Au, R., Himali, J., Palumbo, C., et al. (2011). Midlife vascular risk factor exposure accelerates structural brain aging and cognitive decline. *Neurology* 77, 461–468. doi: 10.1212/WNL.0b013e318227b227

Ewers, M., Insel, P. S., Stern, Y., Weiner, M. W., and Alzheimer's Disease Neuroimaging Intitative. (2013). Cognitive reserve associated with FDG-PET in preclinical Alzheimer disease. *Neurology* 80, 1194–1201. doi: 10.1212/WNL.0b013e31828970c2

Ewing, J. A. (1984). Detecting alcoholism: the CAGE questionnaire. *JAMA* 252, 1905–1907.

Fortea, J., Vilaplana, E., Alcolea, D., Carmona-Iragui, M., Sánchez-Saudinos, M. B., Sala, I., et al. (2014). Cerebrospinal fluid β-amyloid and phospho-tau biomarker interactions affecting brain structure in preclinical Alzheimer disease. *Ann. Neurol.* 76, 223–230. doi: 10.1002/ana.24186

Giorgio, A., Santelli, L., Tomassini, V., Bosnell, R., Smith, S., De Stefano, N., et al. (2010). Age-related changes in grey and white matter structure throughout adulthood. *Neuroimage* 51, 943–951. doi: 10.1016/j.neuroimage.2010.03.004

Jack, CR Jr, Wiste, H. J., Weigand, S. D., Knopman, D. S., Mielke, M. M., Vemuri, P., et al. (2015). Different definitions of neurodegeneration produce similar amyloid/neurodegeneration biomarker group findings. *Brain* 138, 3747–3759. doi: 10.1093/brain/awv283

Jagust, W. (2013). Vulnerable neural systems and the borderland of brain aging and neurodegeneration. *Neuron* 77, 219–234. doi: 10.1016/j.neuron.2013.01.002

Jefferson, A. L., Himali, J. J., Beiser, A. S., Au, R., Massaro, J. M., Seshadri, S., et al. (2010). Cardiac index is associated with brain aging: the framingham heart study. *Circulation* 122, 690–697. doi: 10.1161/CIRCULATIONAHA.109.905091

Johnson, S. C., Christian, B. T., Okonkwo, O. C., Oh, J. M., Harding, S., Xu, G., et al. (2014). Amyloid burden and neural function in people at risk for Alzheimer's disease. *Neurobiol. Aging* 35, 576–584. doi: 10.1016/j.neurobiolaging.2013.09.028

Kochunov, P., Williamson, D., Lancaster, J., Fox, P., Cornell, J., Blangero, J., et al. (2012). Fractional anisotropy of water diffusion in cerebral white matter across the lifespan. *Neurobiol. Aging* 33, 9–20. doi: 10.1016/j.neurobiolaging.2010.01.014

Laubach, M., Lammers, F., Zacharias, N., Feinkohl, I., Pischon, T., Borchers, F., et al. (2018). Size matters: grey matter brain reserve predicts executive functioning in the elderly. *Neuropsychologia* 119, 172–181. doi: 10.1016/j.neuropsychologia.2018.08.008

Le Bihan, D., Mangin, J. F., Poupon, C., Clark, C. A., Pappata, S., Molko, N., et al. (2001). Diffusion tensor imaging: concepts and applications. *J. Magn. Reson. Imaging* 13, 534–546.

Leech, R., and Sharp, D. J. (2014). The role of the posterior cingulate cortex in cognition and disease. *Brain* 137, 12–32.

Malpetti, M., Ballarini, T., Presotto, L., Garibotto, V., Tettamanti, M., Perani, D., et al. (2017). Gender differences in healthy aging and Alzheimer's dementia: a 18F-FDG-PET study of brain and cognitive reserve. *Hum. Brain Mapp.* 38, 4212–4227. doi: 10.1002/hbm.23659

Mielke, M. M., Vemuri, P., and Rocca, W. A. (2014). Clinical epidemiology of Alzheimer's disease: assessing sex and gender differences. *Clin. Epidemiol.* 6, 37–48.

Morbelli, S., Perneczky, R., Drzezga, A., Frisoni, G. B., Caroli, A., Van Berckel, B. N., et al. (2013). Metabolic networks underlying cognitive reserve in prodromal

Alzheimer disease: a European Alzheimer disease consortium project. *J. Nucl. Med.* 54, 894–902. doi: 10.2967/jnumed.112.113928

Mosterd, A., and Hoes, A. W. (2007). Clinical epidemiology of heart failure. *Heart* 93, 1137–1146.

Nelson, P. T., Alafuzoff, I., Bigio, E. H., Bouras, C., Braak, H., Cairns, N. J., et al. (2012). Correlation of Alzheimer disease neuropathologic changes with cognitive status: a review of the literature. *J. Neuropathol. Exp. Neurol.* 71, 362–381. doi: 10.1097/NEN.0b013e31825018f7

Ott, A., Slooter, A., Hofman, A., Van Harskamp, F., Witteman, J., Van Broeckhoven, C., et al. (1998). Smoking and risk of dementia and Alzheimer's disease in a population-based cohort study: the rotterdam study. *Lancet* 351, 1840–1843.

Paulus, W. J., Tschöpe, C., Sanderson, J. E., Rusconi, C., Flachskampf, F. A., Rademakers, F. E., et al. (2007). How to diagnose diastolic heart failure: a consensus statement on the diagnosis of heart failure with normal left ventricular ejection fraction by the heart failure and echocardiography associations of the european society of cardiology. *Eur. Heart J.* 28, 2539–2550.

Pettigrew, C., Soldan, A., Zhu, Y., Wang, M.-C., Brown, T., Miller, M., et al. (2017). Cognitive reserve and cortical thickness in preclinical Alzheimer's disease. *Brain Imaging Behav.* 11, 357–367.

Protas, H. D., Chen, K., Langbaum, J. B., Fleisher, A. S., Alexander, G. E., Lee, W., et al. (2013). Posterior cingulate glucose metabolism, hippocampal glucose metabolism, and hippocampal volume in cognitively normal, late-middle-aged persons at 3 levels of genetic risk for Alzheimer disease. *JAMA Neurol.* 70, 320–325.

Querbes, O., Aubry, F., Pariente, J., Lotterie, J.-A., Démonet, J.-F., Duret, V., et al. (2009). Early diagnosis of Alzheimer's disease using cortical thickness: impact of cognitive reserve. *Brain* 132, 2036–2047. doi: 10.1093/brain/awp105

Ritchie, K., Ritchie, C. W., Yaffe, K., Skoog, I., and Scarmeas, N. (2015). Is late-onset Alzheimer's disease really a disease of midlife? *Alzheimers Dement.* 1, 122–130.

Roberts, R. O., Geda, Y. E., Knopman, D. S., Cha, R. H., Pankratz, V. S., Boeve, B. F., et al. (2008). The mayo clinic study of aging: design and sampling, participation, baseline measures and sample characteristics. *Neuroepidemiology* 30, 58–69. doi: 10.1159/000115751

Rocca, W. A., Yawn, B. P., Sauver, J. L. S., Grossardt, B. R., and Melton, L. J. (2012). History of the rochester epidemiology project: half a century of medical records linkage in a US population. *Mayo Clin. Proc.* 87, 1202–1213. doi: 10.1016/j.mayocp.2012.08.012

Rohlfing, C. L., Wiedmeyer, H.-M., Little, R. R., England, J. D., Tennill, A., and Goldstein, D. E. (2002). Defining the relationship between plasma glucose and HbA1c: analysis of glucose profiles and HbA1c in the diabetes control and complications trial. *Diabetes Care* 25, 275–278.

Sauver, J. L. S., Grossardt, B. R., Leibson, C. L., Yawn, B. P., Melton, III, L. J., and Rocca, W. A. (2012). Generalizability of epidemiological findings and public health decisions: an illustration from the rochester epidemiology project. *Mayo Clin. Proc.* 87, 151–160. doi: 10.1016/j.mayocp.2011.11.009

Schwarz, C. G., Gunter, J. L., Wiste, H. J., Przybelski, S. A., Weigand, S. D., Ward, C. P., et al. (2016). A large-scale comparison of cortical thickness and volume methods for measuring Alzheimer's disease severity. *Neuroimage Clin.* 11, 802–812. doi: 10.1016/j.nicl.2016.05.017

Sexton, C. E., Walhovd, K. B., Storsve, A. B., Tamnes, C. K., Westlye, L. T., Johansen-Berg, H., et al. (2014). Accelerated changes in white matter microstructure during aging: a longitudinal diffusion tensor imaging study. *J. Neurosci.* 34, 15425–15436. doi: 10.1523/JNEUROSCI.0203-14.2014

Smith, C. D., Chebrolu, H., Andersen, A. H., Powell, D. A., Lovell, M. A., Xiong, S., et al. (2010). White matter diffusion alterations in normal women at risk of Alzheimer's disease. *Neurobiol. Aging* 31, 1122–1131. doi: 10.1016/j.neurobiolaging.2008.08.006

Stern, Y. (2009). Cognitive reserve. *Neuropsychologia* 47, 2015–2028. doi: 10.1016/j.neuropsychologia.2009.03.004

Stern, Y. (2012). Cognitive reserve in ageing and Alzheimer's disease. *Lancet Neurol.* 11, 1006–1012. doi: 10.1016/S1474-4422(12)70191-6

Stern, Y., Arenaza-Urquijo, E. M., Bartrés-Faz, D., Belleville, S., Cantilon, M., Chetelat, G., et al. (2018). Whitepaper: defining and investigating cognitive reserve, brain reserve, and brain maintenance. *Alzheimers Dement.* doi: 10.1016/j.jalz.2018.07.219 [Epub ahead of print].

Stern, Y., Chetelat, G., Habeck, C., Arenaza-Urquijo, E. M., Vemuri, P., Estanga, A., et al. (2019). Mechanisms underlying resilience in ageing. *Nat. Rev. Neurosci.* 20:246.

Thomas, V. S., and Rockwood, K. J. (2001). Alcohol abuse, cognitive impairment, and mortality among older people. *J. Am. Geriatr. Soc.* 49, 415–420.

Traynor, J., Mactier, R., Geddes, C. C., and Fox, J. G. (2006). How to measure renal function in clinical practice. *BMJ* 333, 733–737.

Vemuri, P., Lesnick, T. G., Przybelski, S. A., Graff-Radford, J., Reid, R. I., Lowe, V. J., et al. (2018). Development of a cerebrovascular magnetic resonance imaging biomarker for cognitive aging. *Ann. Neurol.* 84, 705–716. doi: 10.1002/ana.25346

Vemuri, P., Lesnick, T. G., Przybelski, S. A., Knopman, D. S., Lowe, V. J., Graff-Radford, J., et al. (2017). Age, vascular health, and Alzheimer disease biomarkers in an elderly sample. *Ann. Neurol.* 82, 706–718. doi: 10.1002/ana.25071

Vemuri, P., Lesnick, T. G., Przybelski, S. A., Knopman, D. S., Preboske, G. M., Kantarci, K., et al. (2015). Vascular and amyloid pathologies are independent predictors of cognitive decline in normal elderly. *Brain* 138, 761–771. doi: 10.1093/brain/awu393

Vemuri, P., Lesnick, T. G., Przybelski, S. A., Knopman, D. S., Roberts, R. O., Lowe, V. J., et al. (2012). Effect of lifestyle activities on Alzheimer disease biomarkers and cognition. *Ann. Neurol.* 72, 730–738.

Vernooij, M. W., Ikram, M. A., Vrooman, H. A., Wielopolski, P. A., Krestin, G. P., Hofman, A., et al. (2009). White matter microstructural integrity and cognitive function in a general elderly population. *JAMA Psychiatry* 66, 545–553. doi: 10.1001/archgenpsychiatry.2009.5

Whitmer, R. A., Gustafson, D. R., Barrett-Connor, E., Haan, M. N., Gunderson, E. P., and Yaffe, K. (2008). Central obesity and increased risk of dementia more than three decades later. *Neurology* 71, 1057–1064. doi: 10.1212/01.wnl.0000306313.89165.ef

Whitmer, R. A., Sidney, S., Selby, J., Johnston, S. C., and Yaffe, K. (2005). Midlife cardiovascular risk factors and risk of dementia in late life. *Neurology* 64, 277–281.

Wolf, P. A., D'agostino, R. B., Kannel, W. B., Bonita, R., and Belanger, A. J. (1988). Cigarette smoking as a risk factor for stroke: the framingham study. *JAMA* 259, 1025–1029.

Yaffe, K., Blackwell, T., Whitmer, R. A., Krueger, K., and Barrett Connor, E. (2006). Glycosylated hemoglobin level and development of mild cognitive impairment or dementia in older women. *J. Nutr. Health Aging* 10, 293–295.

Zagni, E., Simoni, L., and Colombo, D. (2016). Sex and gender differences in central nervous system-related disorders. *Neurosci. J.* 2016:2827090. doi: 10.1155/2016/2827090

Zhang, Y., Schuff, N., Jahng, G.-H., Bayne, W., Mori, S., Schad, L., et al. (2007). Diffusion tensor imaging of cingulum fibers in mild cognitive impairment and Alzheimer disease. *Neurology* 68, 13–19.

Conflict of Interest: DK serves on a Data Safety Monitoring Board for the DIAN study, is an investigator in clinical trials sponsored by Biogen, Inc., Lilly Pharmaceuticals, and the University of Southern California. MiM served as a consultant to Eli Lilly and received unrestricted research grants from Biogen, Inc. and Lundbeck. VL consults for Bayer Schering Pharma, Piramal Life Sciences, and Merck Research and receives research support from GE Healthcare, Siemens Molecular Imaging, and AVID Radiopharmaceuticals. RP consults for Roche, Inc., Merck, Inc., Genentech, Inc., and Biogen, Inc., GE Healthcare, and Eisai, Inc., and receives royalties from Oxford University Press for the publication of Mild Cognitive Impairment. CJ consults for Lily and serves on an independent data monitoring board for Roche but he receives no personal compensation from any commercial entity. None of the relationships are relevant to the content in the manuscript.

The remaining authors declare that the research was conducted in the absence of any commercial or financial relationships that could be construed as a potential conflict of interest.

frontiers in Psychiatry

ORIGINAL RESEARCH
published: 14 January 2020
doi: 10.3389/fpsyt.2019.00953

A Biomarker for Alzheimer's Disease Based on Patterns of Regional Brain Atrophy

Stefan Frenzel[1], Katharina Wittfeld[1,2], Mohamad Habes[3], Johanna Klinger-König[1], Robin Bülow[4], Henry Völzke[5], Hans Jörgen Grabe[1,2] for the Alzheimer's Disease Neuroimaging Initiative[†]*

[1] Department of Psychiatry and Psychotherapy, University Medicine Greifswald, Greifswald, Germany, [2] German Center for Neurodegenerative Diseases (DZNE), Greifswald, Germany, [3] Center for Biomedical Image Computing and Analytics, University of Pennsylvania, Philadelphia, PA, United States, [4] Institute of Diagnostic Radiology and Neuroradiology, University Medicine Greifswald, Greifswald, Germany, [5] Institute for Community Medicine, University Medicine Greifswald, Greifswald, Germany

OPEN ACCESS

Edited by:
Gabriele Sani,
Sapienza University of Rome,
Italy

Reviewed by:
Xiaosong He,
University of Pennsylvania,
United States
Deana Davalos,
Colorado State University,
United States

***Correspondence:**
Stefan Frenzel
stefan.frenzel@uni-greifswald.de

[†]*Data used in preparation of this article were obtained from the Alzheimer's Disease Neuroimaging Initiative (ADNI) database (adni.loni.usc.edu). As such, the investigators within the ADNI contributed to the design and implementation of ADNI and/or provided data but did not participate in analysis or writing of this report. A complete listing of ADNI investigators can be found at: http://adni.loni.usc.edu/wp-content/uploads/how_to_apply/ADNI_Acknowledgement_List.pdf*

Specialty section:
This article was submitted to Aging Psychiatry, a section of the journal Frontiers in Psychiatry

Received: *21 October 2019*
Accepted: *03 December 2019*
Published: *14 January 2020*

Citation:
Frenzel S, Wittfeld K, Habes M, Klinger-König J, Bülow R, Völzke H, Grabe HJ (2020) A Biomarker for Alzheimer's Disease Based on Patterns of Regional Brain Atrophy. Front. Psychiatry 10:953. doi: 10.3389/fpsyt.2019.00953

Introduction: It has been shown that Alzheimer's disease (AD) is accompanied by marked structural brain changes that can be detected several years before clinical diagnosis *via* structural magnetic resonance (MR) imaging. In this study, we developed a structural MR-based biomarker for *in vivo* detection of AD using a supervised machine learning approach. Based on an individual's pattern of brain atrophy a continuous AD score is assigned which measures the similarity with brain atrophy patterns seen in clinical cases of AD.

Methods: The underlying statistical model was trained with MR scans of patients and healthy controls from the Alzheimer's Disease Neuroimaging Initiative (ADNI-1 screening). Validation was performed within ADNI-1 and in an independent patient sample from the Open Access Series of Imaging Studies (OASIS-1). In addition, our analyses included data from a large general population sample of the Study of Health in Pomerania (SHIP-Trend).

Results: Based on the proposed AD score we were able to differentiate patients from healthy controls in ADNI-1 and OASIS-1 with an accuracy of 89% (AUC = 95%) and 87% (AUC = 93%), respectively. Moreover, we found the AD score to be significantly associated with cognitive functioning as assessed by the Mini-Mental State Examination in the OASIS-1 sample after correcting for diagnosis, age, sex, age·sex, and total intracranial volume (Cohen's $f^2 = 0.13$). Additional analyses showed that the prediction accuracy of AD status based on both the AD score and the MMSE score is significantly higher than when using just one of them. In SHIP-Trend we found the AD score to be weakly but significantly associated with a test of verbal memory consisting of an immediate and a delayed word list recall (again after correcting for age, sex, age·sex, and total intracranial volume, Cohen's $f^2 = 0.009$). This association was mainly driven by the immediate recall performance.

Discussion: In summary, our proposed biomarker well differentiated between patients and healthy controls in an independent test sample. It was associated with measures of

cognitive functioning both in a patient sample and a general population sample. Our approach might be useful for defining robust MR-based biomarkers for other neurodegenerative diseases, too.

Keywords: Alzheimer's disease, machine learning, dementia, magnetic resonance imaging, FreeSurfer

INTRODUCTION

Alzheimer's disease (AD) is a neurodegenerative disorder and accounts for an estimated 60 to 80 percent of cases of dementia (1, 2). Dementia is characterized by memory impairments, disordered cognition, language problems, and changes in behaviour, which seriously impair a person's ability to live independently. In advanced AD the person loses basic body functions like walking and swallowing and requires around the clock-care. According the World Health Organization (WHO) the incidence of dementia worldwide will reach about 135 million people in 2050 and will become a major challenge for health-care systems of western countries (3).

The hallmark pathology of AD is the progressive accumulation of amyloid beta protein and tau protein in the brain which is accompanied by death of neurons (1, 4). Macroscopically this is reflected in atrophy of specific brain regions which can be assessed *via* structural magnetic resonance (MR) imaging. At an early stage, the mild cognitive impairment phase, there typically is an atrophy only of the temporal lobe. With progression of the disease other cortical and subcortical regions, notably the hippocampus, become affected too (5–7). These structural changes have been shown to be detectable several years before the clinical diagnosis of AD (8, 9) which led to the development of imaging-based biomarkers of AD based on machine learning (10–16). Biomarkers based on structural MR imaging have been shown to differentiate well between cases of AD and cognitively healthy controls (17) and some of them have been shown to be sensitive at the preclinical stage (18). However, most of these biomarkers have been investigated in single cohorts only.

Since structural brain changes are detectable several years before clinical diagnosis MR-based biomarkers for AD are highly relevant for general population studies, too. However, the investigation of such biomarkers has gained attention only recently within the context of general brain ageing (19–21). In this study, we developed an MR-based biomarker for the *in vivo* assessment of AD based on a supervised machine learning approach. Based on an individual's pattern of brain atrophy a continuous score is assigned which measures the similarity with brain atrophy patterns seen in clinical cases of AD. The underlying statistical model is trained using data from the Alzheimer's Disease Neuroimaging Initiative (ADNI) (22) and validation is performed in an independent patient sample from the Open Access Series of Imaging Studies (OASIS) (23). Finally, our proposed biomarker is investigated in general population data from the Study of Health in Pomerania (SHIP-Trend) (24).

MATERIALS AND METHODS

Sample Description

Alzheimer's Disease Neuroimaging Initiative (ADNI)

Data used in the preparation of this article were obtained from the Alzheimer's Disease Neuroimaging Initiative (ADNI) database (adni.loni.usc.edu). The ADNI was launched in 2003 as a public-private partnership, led by Principal Investigator Michael W. Weiner, MD. The primary goal of ADNI has been to test whether serial magnetic resonance (MR) imaging, positron emission tomography (PET), other biological markers, and clinical and neuropsychological assessment can be combined to measure the progression of mild cognitive impairment (MCI) and early Alzheimer's disease (AD). For up-to-date information, see www.adni-info.org. T1-weighted structural MR scans from 413 participants of the ADNI-1 screening sample were considered in this study. Images were acquired using multiple scanners with a field strength of 1.5T (25, 26). The detailed MR protocol can be found in the supplement. Since the ADNI scans were used to train the AD classifier additional quality control of the image processing was performed as explained below. The final sample comprised N = 374 individuals with 165 diagnosed with AD and 209 cognitively healthy controls (CN) (see **Table 1**).

Open Access Series of Imaging Studies (OASIS)

To validate the AD classifier we used data from the Open Access Series of Imaging Studies (OASIS-1) which is a cross-sectional collection of MR scans of N = 416 individuals aged 18 to 96 (23) (see **Table 1**). One hundred of the participants older than 60 have been clinically diagnosed with very mild to moderate AD. More information can be found at www.oasis-brains.org. Details of the MR protocol can be found in the supplement. All images were screened for artefacts, acquisition problems, and processing errors and images with severe flaws were excluded by the OASIS investigators. No additional quality control was performed by the authors. 235 participants (100 AD, 135 CN) completed the Mini-Mental State Examination (MMSE). The MMSE is a 30-point questionnaire that is used extensively to screen for dementia (27).

TABLE 1 | Basic demographic characteristics of all three samples.

	ADNI-1 screening	OASIS-1	SHIP-Trend
N	374	416	1,973
Females	186 (49%)	254 (61%)	1,038 (53%)
AD	165 (44%)	100 (24%)	–
Age [y]	75.7 (6.3)	52.9 (25.0)	51.3 (14.0)
Intracranial Volume [dl]	15.4 (1.7)	14.8 (1.6)	15.9 (1.6)

Study of Health in Pomerania (SHIP-Trend)

The Study of Health in Pomerania (SHIP) was designed to assess the prevalence of common risk factors and diseases in a population of northeast Germany randomly drawn from local registers (24). 4,308 subjects participated at baseline between 1997 and 2001. In parallel to the original SHIP study a new independent sample was drawn and examinations of similar extent were undertaken (SHIP-Trend). In this study, T1-weighted structural MR images of the head from 2,154 participants of SHIP-Trend were considered (28). Details of the MR protocol can be found in the supplement. Scans with very poor technical quality, (e.g. frontal darkening) were excluded (N = 84). In addition, scans showing structural abnormalities (e.g. tumors, cysts) and cases of cerebral stroke were excluded as well (N = 93). The image processing pipeline (see below) failed to process 4 scans. The final sample comprised N = 1973 individuals (see **Table 1**).

Of those, 1,955 participants completed a word list recall (WLR) test during the face-to-face interview as part of the standard SHIP-Trend protocol. The WLR test consists of eight items which needed to be recalled immediately (immediate WLR, 0 to 8 points) and after a 20 min delay (delayed WLR with distractor words, -8 to 8 points). The total WLR score was computed as sum of both tests. The WLR is part of the Nuremberg Gerontopsychological Inventory (29).

MR Image Segmentation With Freesurfer

Cortical reconstruction and volumetric segmentation of all three data sets were performed with the FreeSurfer image analysis suite version 5.3 ("recon-all"), which is documented and freely available for download online (http://surfer.nmr.mgh.harvard.edu).

Briefly, this processing includes removal of non-brain tissue using a hybrid watershed/surface deformation procedure (30), automated Talairach transformation, segmentation of subcortical white matter and deep gray matter volumetric structures (including hippocampus, amygdala, caudate, putamen, ventricles) (31–33), intensity normalization (34), tessellation of the gray matter white matter boundary, automated topology correction (35, 36), and surface deformation following intensity gradients to optimally place the gray/white and gray/cerebrospinal fluid borders at the location where the greatest shift in intensity defines the transition to the other tissue class (37–39).

Once the cortical models are complete, individual images are being registered to a spherical atlas which is based on individual cortical folding patterns to match cortical geometry across subjects (40), and the cerebral cortex is being parcelled into 68 units with respect to gyral and sulcal structure (41, 42). Cortical white matter, i.e. white matter up to 5mm below the gray matter boundary, is also being parcelled into 68 units by assigning each white matter voxel the label of the closest cortical voxel (43). FreeSurfer also gives an estimate of the total intracranial volume (eTIV) which was not used to train the AD classifier but as a covariate in subsequent statistical analyses.

Although being part of the standard FreeSurfer output several brain regions were excluded from the analyses. The 5th ventricle was excluded because it was not detected in all scan (zero volume). In addition, the brain stem and optic chiasm were excluded as well. In total, 169 out of 172 brain regions of gray matter, white matter, and the ventricular system were considered (see **Figure 1**). The complete list of regions can be found in the **Supplementary Material**.

Alzheimer's Disease Classifier

Based on the ADNI-1 screening sample a binary classifier was trained with diagnoses as dependent variable. In order to minimize the influence of image segmentation errors on the classifier, we performed an additional statistical quality control of each feature. More specifically, we removed all scans with brain

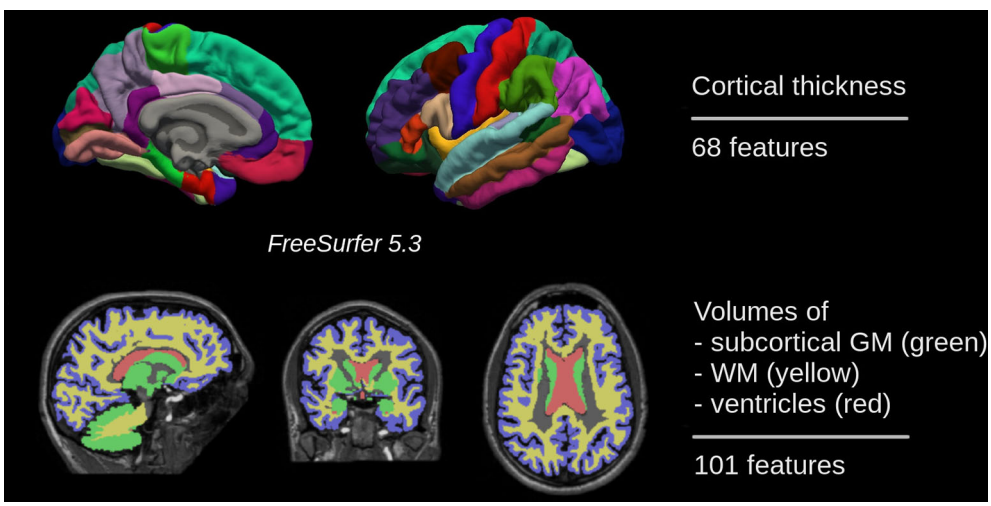

FIGURE 1 | In total, 169 features of gray matter, white matter, and the ventricular system were used for training a binary classifier which distinguishes between individuals with Alzheimer's disease and cognitively normal ones.

measurements deviating more than four standard deviations from the mean value after adjusting for age, sex, age·sex, eTIV, and diagnosis (N = 39). All features were standardized to zero mean and unit variance. We then used L2-penalized (ridge) logistic regression to train the binary classifier which optimally separates individuals with AD from CN (44). The AD score was defined as the linear predictors of the logistic model, i.e. it is given by log[p/(1-p)] with p denoting the probability of having AD.

Prediction of AD scores in OASIS-1 and SHIP-Trend were based on a classifier trained on the whole ADNI-1 sample. The corresponding model coefficients can be found in the supplement. The penalization parameter λ was selected from the set $\{2^{-8}, 2^{-7}, \ldots, 2\}$ by 20-fold cross-validation with 20 repetitions ($\lambda = 0.125$) anduni-modality of the tuning curve was checked by visual inspection (see **Supplementary Material**). In order to assess the classification accuracy within ADNI-1 we used leave-one-out cross-validation, i.e. each individual's AD score was calculated using a model trained on all others. The optimal λ was estimated within a second loop in order to strictly separate training and test data (again by 20-fold cross-validation with 20 repetitions).

Voxel-Based Morphometry

For SHIP-Trend we additionally performed voxel-based morphometry (VBM) analyses with SPM12 (Welcome Trust Centre for Neuroimaging, University College London) and CAT12 [developed by Christian Gaser, University of Jena, Germany, http://www.neuro.uni-jena.de, e.g. (45)] in order to map the contribution of distinct brain regions to the AD score.

All images were bias-corrected, spatially normalized by using the high-dimensional DARTEL normalization, segmented into the different tissue classes, modulated for non-linear warping and affine transformations, and smoothed by a Gaussian kernel of 8 mm FWHM. The homogeneity of gray matter images was checked using the covariance structure of each image with all other images (outliers ≥3 standard deviations from the mean), as implemented in the check data quality function in the CAT12 toolbox. To mask irrelevant brain areas of the smoothed gray and white matter segmentations we used the Masking Toolbox from Gerard Ridgway to define explicit masks for the gray and white matter VBM analyses. Specifically, we used the MATLAB script "make_majority_mask.m" to generate a gray matter mask with an absolute threshold of 0.1 and a consensus fraction of 80% and a white matter mask with an absolute threshold of 0.2 and a consensus fraction of 90%.

The statistical threshold for significant voxels was set to a family-wise error (FWE) corrected peak-level p-values $P_{peak,FWE} < 0.025$ as we conducted a two-sided test and looked at positive and negative associations with the FSAD score while correcting for age, sex, age·sex, and total intracranial volume. Again, age was modeled by restricted cubic splines with four knots located at the 0.05, 0.33, 0.66, and 0.95 age quantiles.

Statistical Analysis

All statistical analyses were performed with R 3.6 (46). The classifier was implemented using the *glmnet* package (47). Association analyses of the AD score with the basic covariates age, sex, age·sex, eTIV, and diagnosis were performed by ordinary least-squares multivariable regression. For SHIP-Trend we used restricted cubic splines (48) with four knots located at the 0.05, 0.33, 0.66, and 0.95 quantile in order to account for the non-linear dependency of the AD score on chronological age. Effects of single variables were assessed either by t-tests with robust variance estimates or ANOVA of type 2.

RESULTS

Prior to training the AD classifier we checked the ADNI-1 screening sample for possible imbalances with respect to age, sex, and intracranial volume. We did not find significant differences between patients and controls with respect to age (t = -0.55, P = 0.58), sex (Fisher's Exact Test, P = 0.84), and estimated intracranial volume (t = 0.15, P = 0.88).

Prediction of Diagnoses in ADNI-1 and OASIS-1 Based on the AD Score

At first, classification performance within the ADNI-1 screening sample was investigated. Classification accuracy was assessed by leave-one-out cross-validation, i.e. each individual's AD score was calculated using a model trained on all others. The resulting scores are shown in **Figure 2A**. Individuals with an AD score larger than zero and smaller than zero were classified as AD and CN, respectively, and these classifications were compared with the known diagnoses. The overall accuracy was 89% with the 95% confidence interval (CI) (85.7%, 92.2%). Sensitivity (true positive rate) and specificity (true negative rate) was 91% and 87%, respectively. The receiver operating characteristic (ROC) curves were obtained by systematic variation of the classification threshold and area under the curve (AUC) was calculated as 95% with 95% CI (93.5%, 97.6%).

Using the ADNI-1 sample a model was trained and AD scores were calculated for the OASIS-1 sample. The resulting scores are shown in **Figure 2B**, left panel. Again, individuals with an AD score larger than zero and smaller than zero were classified as AD and CN, respectively. The overall accuracy was 87% with 95% CI (83.2%, 90.0%). Sensitivity and specificity were 89% and 79%, respectively. The AUC was calculated as 93% with 95% CI (90.0%, 95.7%).

Association Analyses in ADNI-1 and OASIS-1

We performed association analyses of the AD score with the basic covariates diagnosis, age, sex, age·sex, and intracranial volume by means of multivariable regression. For the ADNI-1 sample the percentage of variation explained (R^2) was 72%. As expected, the AD score was significantly larger in those diagnosed with AD (t = 30, $P < 2{\cdot}10^{-16}$, see **Figure 2A**). In addition, there was a significant effect of age (t = 2.5, P = 0.012). No significant effects of sex (t = 1.1, P = 0.29), age·sex (t = -0.89, P = 0.37), or intracranial volume (t = 1.4, P = 0.17) were found.

For the OASIS-1 sample the multivariable regression of the AD score yielded $R^2 = 55\%$. Again, we found a significant effect of diagnosis of AD (t = 9.7, $P < 2{\cdot}10^{-16}$), and age (t = 8.5, $P = 4.9{\cdot}10^{-16}$).

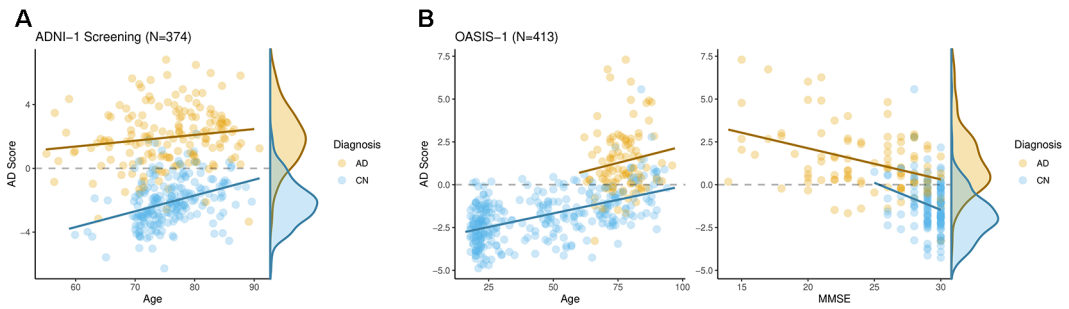

FIGURE 2 | The AD score differentiated well individuals with Alzheimer's disease from cognitively normal ones both in ADNI-1 **(A)** and OASIS-1 **(B)**. Moreover, it was significantly associated with cognitive functioning as assessed by the Mini-Mental State Examination within both groups in OASIS-1.

In addition, there was a significant effect of sex with females having slightly larger AD scores (t = 2.2, P = 0.025). No significant effects of age·sex (t = -0.75, P = 0.45), or intracranial volume (t = 0.55, P = 0.57) were found.

When analyzing the OASIS-1 subsample with MMSE scores available (N = 235, 100 AD, 135 CN) we again found significant effects of diagnosis (t = 9.3, P < $2.2{\cdot}10^{-16}$), and age (t = 5.7, P = $3.9{\cdot}10^{-8}$). No significant effects were found for sex (t = 0.97, P = 0.33), age·sex (t = -0.61, P = 0.54), and intracranial volume (t = 0.80, P = 0.42). The total R^2 was 45%. Adding the MMSE score to the model increased the R^2 to 51% and the corresponding marginal effect was significant (t = -4.1, P = $4.9{\cdot}10^{-5}$, Cohen's $f^2 = 0.13$), i.e. on average individuals with low MMSE scores had larger AD scores when correcting for all basic covariates including diagnosis.

Prediction of Diagnoses Using Both the AD Score and the MMSE Score in OASIS-1

In order to compare the diagnostic utility of the AD score with the MMSE we aimed to predict diagnoses in the OASIS-1 subsample with MMSE scores available. For this we used standard logistic regression models with different sets of predictors and compared the corresponding classification accuracies. Note that we did not separate the training and test set since we aimed to compare different sets of predictors rather than obtaining objective accuracy estimates. Using a basic model containing age, sex, and its interaction, we were able to predict AD diagnoses with an accuracy of 61% (AUC = 70%). Adding either the MMSE score or the AD score improved the accuracy to 82% (AUC = 91%) and 82% (AUC = 90%), respectively. When adding both the MMSE score and the AD score the resulting accuracy improved even further to 87% (AUC = 94%). The accuracy of the combined model was significantly better than one of the two previous ones ($\chi_1^2 = 29$, P = $8{\cdot}10^{-8}$; $\chi_1^2 = 53$, P = $3{\cdot}10^{-13}$).

General Population Data From the SHIP Sample

AD scores were calculated for the SHIP-Trend sample (N = 1973, see **Table 1**) using a model trained on the whole ADNI-1 screening sample. Again, we performed association analyses of the AD score with the basic covariates age, sex, age·sex, and intracranial volume by means of multivariable regression. Since the AD score was clearly non-linearly related to age (see **Figure 3A**) we decided to include age by restricted cubic splines. ANOVA of type 2 was used to assess the effects of each variable. We found significant associations with age (F = 170, P < $2{\cdot}10^{-16}$) and age·sex (F = 3.7, P = 0.010). No significant effects of sex (F = 0.40, P = 0.53), or intracranial volume (t = 2.5, P = 0.11) were found. The R^2 was 22%.

The AD score was significantly associated with the total WLR score (F = 4.1, P = 0.037, Cohen's $f^2 = 0.009$, adjusted for all basic covariates, see **Figure 3B**). Additional analyses showed that the AD score was more strongly associated with the immediate WLR score (F = 4.9, P = 0.026) than the delayed WLR recall (F = 1.8, P = 0.17).

In order to map the contributions of distinct brain regions to the AD score in greater detail we performed VBM analyses with both gray and white matter segmentations in SHIP-Trend. The results are visualized in **Figure 4**. Using the gray matter segmentation we found a large cluster that was negatively associated with the AD score. The peak voxel was located in the left medial temporal gyrus. The cluster stretched over the medial temporal gyrus, the inferior temporal gyrus, the fusiform gyrus, and the precuneus in both hemispheres, among others. Using the white matter segmentation we also found a large cluster that was negatively associated with the AD score. It comprised the medial temporal lobe, the periventricular area, and the corpus callosum, among others. Interestingly, it also includes a large portion of the brain stem which was not included in the feature set used for constructing the AD score.

DISCUSSION

In this study, we developed a structural MR imaging-based biomarker for the *in vivo* detection of Alzheimer's disease. It was based on 169 regional brain features of gray matter, white matter, and the ventricular system derived from the image processing pipeline FreeSurfer. L2-penalized logistic regression was used to define a binary classifier which optimally separates individuals with AD from cognitively normal ones. For the ADNI-1 screening sample the cross-validated classification

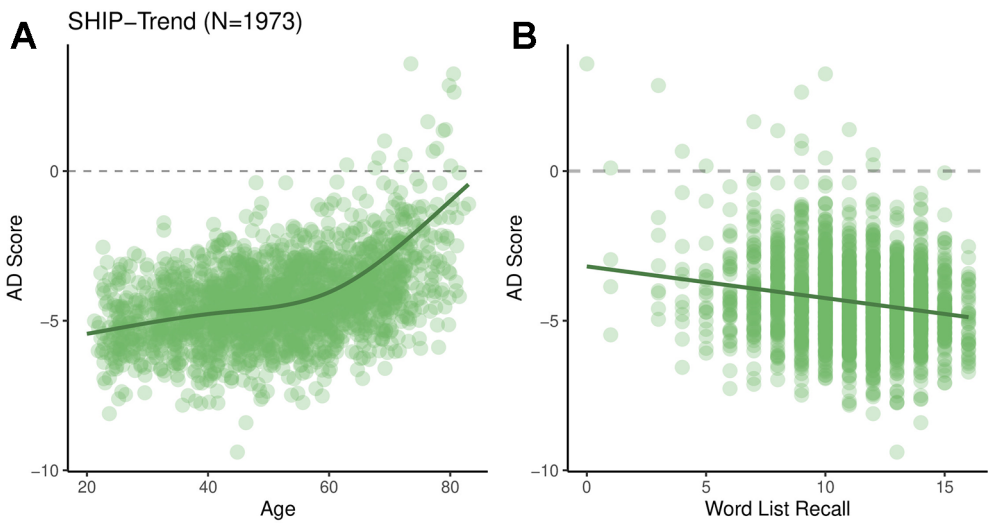

FIGURE 3 | AD scores for the SHIP-Trend sample plotted against chronological age **(A)** and the overall word list recall score **(B)**.

accuracy was 89% and AUC was 95%. These results are on par with other classification studies involving structural MR images (17). However, most classification studies were based on only one sample. Here, the classifier was trained using the ADNI-1 screening sample and AD scores were predicted in the independent sample OASIS-1. We found our classifier to also perform well with an accuracy of 87% and AUC being 93%.

For obtaining regional brain features we used the freely available image segmentation pipeline FreeSurfer. FreeSurfer has been shown to give reliable volumetric estimates independent of scanner platforms and protocols with the exception of the magnetic field strength which has been found to introduce additional bias (49). In our study, however, all scans were acquired with 1.5T. Since FreeSurfer is available under an open source license for the GNU/Linux operating system it can be run within typical high performance computing environments with little to no additional adaptations. This facilitates the application to large imaging data sets which are being used increasingly for the investigation of neurodegenerative disorders. Moreover, future improvements of the image processing algorithms used within FreeSurfer will likely improve any derived biomarkers, too.

On the other hand there is strong evidence for at least three distinct subtypes of AD with respect to regional brain atrophy (50, 51). Hence, it is unclear whether further improvements of the classification accuracy of structural MRI markers with respect a single diagnostic category (AD diagnosis) can be expected. Instead, the relation of MRI markers measures and measures of cognitive functioning, which ultimately impairs the affected individual's quality of life, seems to be more appropriate. Here, we studied the association of the AD score with MMSE scores in a subsample of OASIS-1. We found a significant association after correcting for diagnosis, age, sex, age·sex, and total intracranial volume (Cohen's $f^2 = 0.13$, see **Figure 2B**). The AD score was associated with cognitive functioning in AD patients (adjusted for age, sex, and intracranial volume) which indicates it to be a measure of the progression of AD. Interestingly, it was also associated with the MMSE in cognitive normal individuals after correcting for age, sex, and intracranial volume, indicating that it captures subclinical pathology (atrophy), too.

This was supported by the association analyses in the general population sample SHIP-Trend where we found the AD score to be significantly associated with the WLR consisting of an immediate and a delayed recall (again after correcting for age, sex, age·sex, and total intracranial volume, Cohen's $f^2 = 0.009$). This association was mainly driven by the immediate recall. Indeed, there seems to be a deficit in semantic memory years before AD diagnosis while AD patients show impairments in multiple cognitive domains (52). Such a deficit in semantic memory could explain the association with the WLR performance in SHIP-Trend.

However, the association between the AD score and cognitive functioning in non-demented individuals could also be partially driven by other psychiatric diseases. One example for this is depression which is known to be associated with decreased hippocampal volume and impaired memory. Since depression has a much higher life-time prevalence than AD it is potentially highly relevant for population-based studies. Whether the AD score proposed here is indeed associated with a specific profile of cognitive dysfunction in non-demented individuals needs to be investigated in future studies.

One limitation of our method is that AD scores of single individuals can only be interpreted within populations after adjusting for confounding variables like age. In all data sets the AD score was positively associated with age. In SHIP-Trend this association was non-linear with the slope increasing around the age of 60 (see **Figure 3A**). However, this should not be interpreted as progression of some sort of AD-related subclinical pathology, but rather statistical artefact of the spatial overlap of

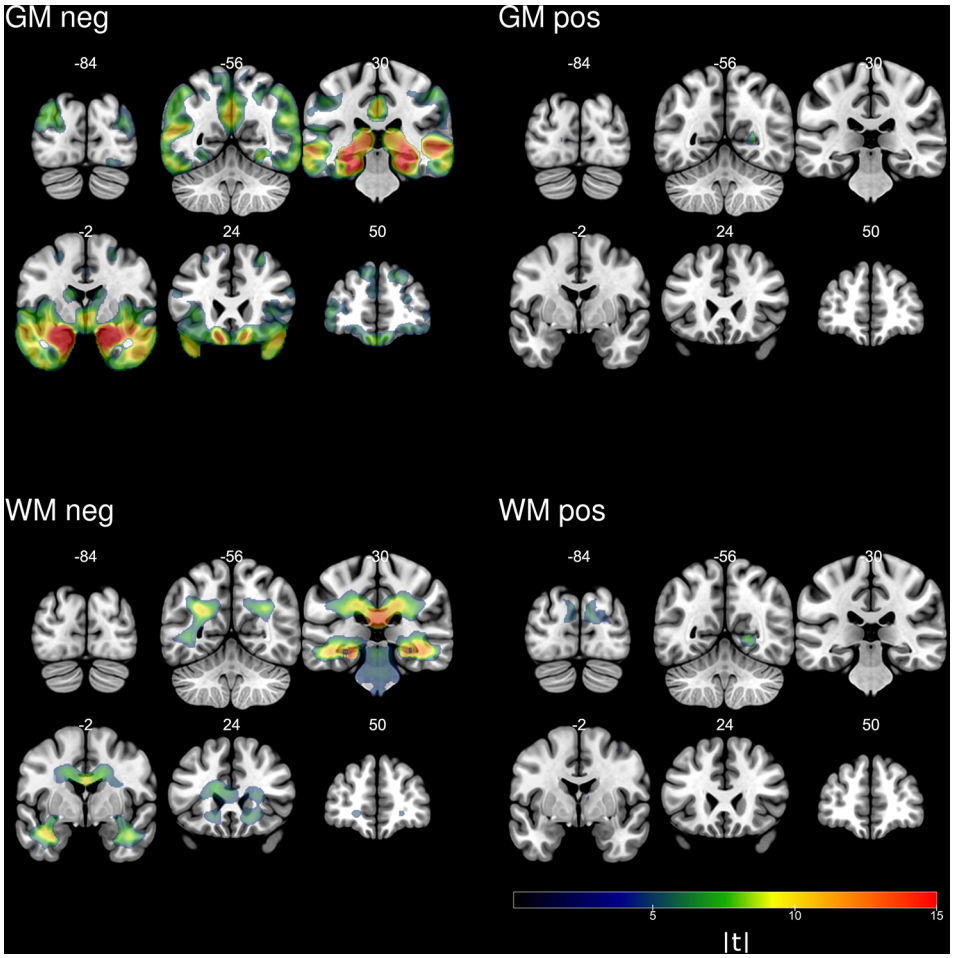

FIGURE 4 | Absolute values of the t-statistics of voxel-based analyses of the AD score in SHIP-Trend.

general age-related atrophy and AD-related atrophy. Even if the model coefficients of the AD classifier were randomly drawn there would still be a significant association of the resulting AD score with chronological age. Since age is a potential confounding variable thorough adjustment of the analyses is needed. Most of the time this requires non-linear modelling with polynomials or splines.

In summary, our proposed AD score well differentiated between patients and healthy controls in an independent test sample. It was associated with measures of cognitive functioning both in a patient sample and a general population sample. Thus, our approach might be useful for defining robust MR-based biomarkers for other neurodegenerative diseases, too.

DATA AVAILABILITY STATEMENT

Data used in the preparation of this article were obtained from the Alzheimer's Disease Neuroimaging Initiative (ADNI) database (adni.loni.usc.edu) and the Open Access Series of Imaging Studies. Request should be made to the corresponding author: stefan.frenzel@uni-greifswald.de.

ETHICS STATEMENT

The studies involving human participants were reviewed and approved by Institutional Review Board of University Medicine Greifswald ("Ethikkomission an der Universitätsmedizin Greifswald"). The patients/participants provided their written informed consent to participate in this study. Written informed consent was obtained from the individual(s) for the publication of any potentially identifiable images or data included in this article.

AUTHOR CONTRIBUTIONS

SF performed all statistical analysis, and wrote the manuscript. SF, JK-K, MH, and HG designed the study. SF, MH, and KW

processed the MR imaging data. KW conducted the VBM analyses. RB and HV contributed essentially to the data collection.

ACKNOWLEDGMENTS

Data collection and sharing for this project was in part funded by the Alzheimer's Disease Neuroimaging Initiative (ADNI) (National Institutes of Health Grant U01 AG024904) and DOD ADNI (Department of Defense award number W81XWH-12-2-0012). ADNI is funded by the National Institute on Aging, the National Institute of Biomedical Imaging and Bioengineering, and through generous contributions from the following: AbbVie, Alzheimer's Association; Alzheimer's Drug Discovery Foundation; Araclon Biotech; BioClinica, Inc.; Biogen; Bristol-Myers Squibb Company; CereSpir, Inc.; Cogstate; Eisai Inc.; Elan Pharmaceuticals, Inc.; Eli Lilly and Company; EuroImmun; F. Hoffmann-La Roche Ltd and its affiliated company Genentech, Inc.; Fujirebio; GE Healthcare; IXICO Ltd.; Janssen Alzheimer Immunotherapy Research & Development, LLC.; Johnson & Johnson Pharmaceutical Research & Development LLC.; Lumosity; Lundbeck; Merck & Co., Inc.;Meso Scale Diagnostics, LLC.; NeuroRx Research; Neurotrack Technologies; Novartis Pharmaceuticals Corporation; Pfizer Inc.; Piramal Imaging; Servier; Takeda Pharmaceutical Company; and Transition Therapeutics. The Canadian Institutes of Health Research is providing funds to support ADNI clinical sites in Canada. Private sector contributions are facilitated by the Foundation for the National Institutes of Health (www.fnih.org). The grantee organization is the Northern California Institute for Research and Education, and the study is coordinated by the Alzheimer's Therapeutic Research Institute at the University of Southern California. ADNI data are disseminated by the Laboratory for Neuro Imaging at the University of Southern California.

For this study, we also used data from the Open Access Series of Imaging Studies (OASIS) Cross-Sectional: Principal Investigators: D. Marcus, R, Buckner, J, Csernanskny J. Morris; P50 AG05681, P01 AG03991, P01 AG026276, R01 AG021910, P20 MH071616, U24 RR021382.

The Study of Health in Pomerania (SHIP) is part of the Community Medicine Research net (CMR) (http://www.medizin.uni-greifswald.de/icm) of the University Medicine Greifswald, which is supported by the German Federal State of Mecklenburg-West Pomerania. MRI scans in SHIP-Trend have been supported by a joint grant from Siemens Healthineers, Erlangen, Germany, and the Federal State of Mecklenburg-West Pomerania.

This study was further supported by the EU-JPND Funding for BRIDGET (FKZ:01ED1615).

SUPPLEMENTARY MATERIAL

The Supplementary Material for this article can be found online at: https://www.frontiersin.org/articles/10.3389/fpsyt.2019.00953/full#supplementary-material

REFERENCES

1. Alzheimer's Association. 2016 Alzheimer's disease facts and figures. *Alzheimers Dement* (2016) 12:459–509. doi: 10.1016/j.jalz.2016.03.001
2. Barker WW, Luis CA, Kashuba A, Luis M, Harwood DG, Loewenstein D, et al. Relative frequencies of alzheimer disease, lewy body, vascular and frontotemporal dementia, and hippocampal sclerosis in the State of Florida brain bank. *Alzheimer Dis Assoc Disord* (2002) 16:203. doi: 10.1097/00002093-200210000-00001
3. Prince MJ, Guerchet MM, Prina M. *The Epidemiology and Impact of Dementia: Current State and Future Trends*. Geneva, Switzerland: WHO Thematic Briefing (2015).
4. Hardy JA, Higgins GA. Alzheimer's disease: the amyloid cascade hypothesis. *Science* (1992) 256(5054):184–5. doi: 10.1126/science.1566067
5. Frisoni GB, Fox NC, Jack CRJr., Scheltens P, Thompson PM. The clinical use of structural MRI in Alzheimer disease. *Nat Rev Neurol* (2010) 6:67–77. doi: 10.1038/nrneurol.2009.215
6. Thompson PM, Hayashi KM, Zubicaray G, de, Janke AL, Rose SE, Semple J, et al. Dynamics of gray matter loss in Alzheimer's Disease. *J Neurosci* (2003) 23:994–1005. doi: 10.1523/JNEUROSCI.23-03-00994.2003
7. Tondelli M, Wilcock GK, Nichelli P, De Jager CA, Jenkinson M, Zamboni G. Structural MRI changes detectable up to ten years before clinical Alzheimer's disease. *Neurobiol Aging* (2012) 33, 825:e25–825.e36.
8. Jack CR, Shiung MM, Weigand SD, O'Brien PC, Gunter JL, Boeve BF, et al. Brain atrophy rates predict subsequent clinical conversion in normal elderly and amnestic MCI. *Neurology* (2005) 65:1227–31.
9. Twamley EW, Ropacki SAL, Bondi MW. Neuropsychological and neuroimaging changes in preclinical Alzheimer's disease. *J Int Neuropsychol Soc* (2006) 12:707–35. doi: 10.1017/S1355617706060863
10. Beheshti I, Demirel H. Feature-ranking-based Alzheimer's disease classification from structural MRI. *Magnet Resonance Imaging* (2016) 34:252–63. doi: 10.1016/j.mri.2015.11.009
11. Davatzikos C, Xu F, An Y, Fan Y, Resnick SM. Longitudinal progression of Alzheimer's-like patterns of atrophy in normal older adults: the SPARE-AD index. *Brain* (2009) 132:2026–35.
12. Duchesne S, Caroli A, Geroldi C, Barillot C, Frisoni GB, Collins DL. MRI-based automated computer classification of probable AD versus normal controls. *IEEE Trans Med Imaging* (2008) 27:509–20.
13. Fan Y, Resnick SM, Wu X, Davatzikos C. Structural and functional biomarkers of prodromal Alzheimer's disease: a high-dimensional pattern classification study. *NeuroImage* (2008) 41:277–85.
14. Klöppel S, Stonnington CM, Chu C, Draganski B, Scahill RI, Rohrer JD, et al. Automatic classification of MR scans in Alzheimer's disease. *Brain* (2008) 131:681–9.
15. Li H, Habes M, Wolk DA, Fan Y, Alzheimer's Disease Neuroimaging Initiative and the Australian Imaging Biomarkers and Lifestyle Study of Aging. A deep learning model for early prediction of Alzheimer's disease dementia based on hippocampal magnetic resonance imaging data. *Alzheimers Dement* (2019) 15:1059–70.
16. Salvatore C, Cerasa A, Battista P, Gilardi MC, Quattrone A, Castiglioni I. Magnetic resonance imaging biomarkers for the early diagnosis of Alzheimer's disease: a machine learning approach. *Front Neurosci* (2015) 9:307.
17. Rathore S, Habes M, Iftikhar MA, Shacklett A, Davatzikos C. A review on neuroimaging-based classification studies and associated feature extraction methods for Alzheimer's disease and its prodromal stages. *NeuroImage* (2017) 155:530–48.
18. Davatzikos C, Bhatt P, Shaw LM, Batmanghelich KN, Trojanowski JQ. Prediction of MCI to AD conversion, via MRI, CSF biomarkers, and pattern classification. *Neurobiol Aging* (2011) 32, 2322:e19–27.
19. Cole JH, Ritchie SJ, Bastin ME, Valdés Hernández MC, Muñoz Maniega S, Royle N, et al. Brain age predicts mortality. *Mol Psychiatry* (2018) 23:1385–92. doi: 10.1038/mp.2017.62

20. Habes M, Janowitz D, Erus G, Toledo JB, Resnick SM, Doshi J, et al. Advanced brain aging: relationship with epidemiologic and genetic risk factors, and overlap with Alzheimer disease atrophy patterns. *Trans Psychiatry* (2016) 6: e775. doi: 10.1038/tp.2016.39
21. Janowitz D, Habes M, Toledo JB, Hannemann A, Frenzel S, Terock J, et al. Inflammatory markers and imaging patterns of advanced brain aging in the general population. *Brain Imaging Behav* (2019).
22. Petersen RC, Aisen PS, Beckett LA, Donohue MC, Gamst AC, Harvey DJ, et al. Alzheimer's Disease Neuroimaging Initiative (ADNI). *Neurology* (2010) 74:201–9.
23. Marcus DS, Wang TH, Parker J, Csernansky JG, Morris JC, Buckner RL. Open Access Series of Imaging Studies (OASIS): cross-sectional MRI data in young, middle aged, nondemented, and demented older adults. *J Cognit Neurosci* (2007) 19:1498–507.
24. Völzke H, Alte D, Schmidt CO, Radke D, Lorbeer R, Friedrich N, et al. Cohort profile: the study of health in Pomerania. *Int J Epidemiol* (2011) 40:294–307.
25. Jack CR, Bernstein MA, Fox NC, Thompson P, Alexander G, Harvey D, et al. The Alzheimer's disease neuroimaging initiative (ADNI): MRI methods. *J Magnet Resonance Imaging* (2008) 27:685–91.
26. Wyman BT, Harvey DJ, Crawford K, Bernstein MA, Carmichael O, Cole PE, et al. Standardization of analysis sets for reporting results from ADNI MRI data. *Alzheimer's Dementia: J Alzheimer's Assoc* (2013) 9:332–7.
27. Folstein MF, Folstein SE, McHugh PR. "Mini-mental state": a practical method for grading the cognitive state of patients for the clinician. *J Psychiatr Res* (1975) 12:189–98.
28. Hegenscheid K, Kühn JP, Völzke H, Biffar R, Hosten N, Puls R. Whole-body magnetic resonance imaging of healthy volunteers: pilot study results from the population-based SHIP study. *Rofo* (2009) 181:748–59.
29. Oswald WD, Fleischmann UM. Psychometrics in aging and dementia: advances in geropsychological assessments. *Arch Gerontol Geriatr* (1985) 4:299–309.
30. Ségonne F, Dale AM, Busa E, Glessner M, Salat D, Hahn HK, et al. A hybrid approach to the skull stripping problem in MRI. *Neuroimage* (2004) 22:1060–75.
31. Fischl B, Salat DH, Busa E, Albert M, Dieterich M, Haselgrove C, et al. Whole brain segmentation: automated labeling of neuroanatomical structures in the human brain. *Neuron* (2002) 33:341–55.
32. Fischl B, Salat DH, van der Kouwe AJW, Makris N, Ségonne F, Quinn BT, et al. Sequence-independent segmentation of magnetic resonance images. *Neuroimage* (2004a) 23 Suppl 1:S69–84.
33. Han X, Fischl B. Atlas renormalization for improved brain MR image segmentation across scanner platforms. *IEEE Trans Med Imaging* (2007) 26:479–86.
34. Sled JG, Zijdenbos AP, Evans AC. A nonparametric method for automatic correction of intensity nonuniformity in MRI data. *IEEE Trans Med Imaging* (1998) 17:87–97.
35. Fischl B, Liu A, Dale AM. Automated manifold surgery: constructing geometrically accurate and topologically correct models of the human cerebral cortex. *IEEE Trans Med Imaging* (2001) 20:70–80.
36. Ségonne F, Pacheco J, Fischl B. Geometrically accurate topology-correction of cortical surfaces using nonseparating loops. *IEEE Trans Med Imaging* (2007) 26:518–29.
37. Dale AM, Sereno MI. Improved localizadon of cortical activity by combining EEG and MEG with MRI cortical surface reconstruction: a linear approach. *J Cognit Neurosci* (1993) 5:162–76.
38. Dale AM, Fischl B, Sereno MI. Cortical surface-based analysis. I. Segmentation and surface reconstruction. *Neuroimage* (1999) 9:179–94.
39. Fischl B, Dale AM. Measuring the thickness of the human cerebral cortex from magnetic resonance images. *Proc Natl Acad Sci USA* (2000) 97:11050–5. doi: 10.1073/pnas.200033797
40. Fischl B, Sereno MI, Tootell RBH, Dale AM. High-resolution intersubject averaging and a coordinate system for the cortical surface. *Hum Brain Mapp* (1999) 8:272–84. doi: 10.1002/(SICI)1097-0193(1999)8:4<272::AID-HBM10>3.0.CO;2-4
41. Desikan RS, Ségonne F, Fischl B, Quinn BT, Dickerson BC, Blacker D, et al. An automated labeling system for subdividing the human cerebral cortex on MRI scans into gyral based regions of interest. *Neuroimage* (2006) 31:968–80.
42. Fischl B, van der Kouwe A, Destrieux C, Halgren E, Ségonne F, Salat DH, et al. Automatically parcellating the human cerebral cortex. *Cereb Cortex* (2004b) 14:11–22.
43. Salat DH, Greve DN, Pacheco JL, Quinn BT, Helmer KG, Buckner RL, et al. Regional white matter volume differences in nondemented aging and Alzheimer's disease. *Neuroimage* (2009) 44:1247–58. doi: 10.1016/j.neuroimage.2008.10.030
44. Hastie T, Tibshirani R, Friedman JH. *The Elements of Statistical Learning: Data Mining, Inference, and Prediction*. Berlin, Germany: Springer Science & Business Media (2001).
45. Penny WD, Friston KJ, Ashburner JT, Kiebel SJ, Nichols TE. *Statistical Parametric Mapping: The Analysis of Functional Brain Images*. Amsterdam, Netherlands: Elsevier (2011).
46. Team T. (2008). The R project for statistical computing. http://www.r-Project.Org.
47. Friedman J, Hastie T, Tibshirani R. Regularization paths for generalized linear models via coordinate descent. *J Stat Softw* (2010) 33:1–22. doi: 10.18637/jss.v033.i01
48. Harrell F. *Regression Modeling Strategies: With Applications to Linear Models, Logistic and Ordinal Regression, and Survival Analysis*. Basel, Switzerland: Springer International Publishing (2015).
49. Han X, Jovicich J, Salat D, van der Kouwe A, Quinn B, Czanner S, et al. Reliability of MRI-derived measurements of human cerebral cortical thickness: the effects of field strength, scanner upgrade and manufacturer. *Neuroimage* (2006) 32:180–94. doi: 10.1016/j.neuroimage.2006.02.051
50. Varol E, Sotiras A, Davatzikos C, and the Alzheimer's Disease Neuroimaging Initiative. HYDRA: revealing heterogeneity of imaging and genetic patterns through a multiple max-margin discriminative analysis framework. *Neuroimage* (2017) 145:346–64. doi: 10.1016/j.neuroimage.2016.02.041
51. Whitwell JL, Dickson DW, Murray ME, Weigand SD, Tosakulwong N, Senjem ML, et al. Neuroimaging correlates of pathologically defined subtypes of Alzheimer's disease: a case-control study. *Lancet Neurol* (2012) 11:868–77.
52. Adlam A-LR, Bozeat S, Arnold R, Watson P, Hodges JR. Semantic knowledge in mild cognitive impairment and mild Alzheimer's Disease. *Cortex* (2006) 42:675–84. doi: 10.1016/s0010-9452(08)70404-0

Conflict of Interest: HG has received travel grants and speakers honoraria from Fresenius Medical Care and Janssen Cilag. He has received research funding from the German Research Foundation (DFG), the German Ministry of Education and Research (BMBF), the DAMP Foundation, Fresenius Medical Care, the EU "Joint Programme Neurodegenerative Disorders (JPND)".

The remaining authors declare that the research was conducted in the absence of any commercial or financial relationships that could be construed as a potential conflict of interest.

The reviewer XH declared a shared affiliation, with no collaboration, with one of the authors MH to the handling editor.

frontiers in Aging Neuroscience

ORIGINAL RESEARCH
published: 15 January 2020
doi: 10.3389/fnagi.2019.00368

Aging Disrupts the Circadian Patterns of Protein Expression in the Murine Hippocampus

Paula Adler[1,2,3], Cheng-Kang Chiang[1,2,3†], Janice Mayne[1,2,3], Zhibin Ning[1,2,3], Xu Zhang[1,2,3], Bo Xu[1,2,3], Hai-Ying Mary Cheng[4,5] and Daniel Figeys[1,2,3,6]*

[1] Shanghai Institute of Materia Medica–University of Ottawa Joint Research Centre on Systems and Personalized Pharmacology, University of Ottawa, Ottawa, ON, Canada, [2] Ottawa Institute of Systems Biology, University of Ottawa, Ottawa, ON, Canada, [3] Department of Biochemistry, Microbiology and Immunology, University of Ottawa, Ottawa, ON, Canada, [4] Department of Biology, University of Toronto Mississauga, Mississauga, ON, Canada, [5] Department of Cell and Systems Biology, University of Toronto, Toronto, ON, Canada, [6] Canadian Institute for Advanced Research, Toronto, ON, Canada

Aging is associated with cognitive decline and dysregulation of the circadian system, which modulates hippocampal-dependent memory as well as biological processes underlying hippocampal function. While circadian dysfunction and memory impairment are common features of aging and several neurodegenerative brain disorders, how aging impacts the circadian expression patterns of proteins involved in processes that underlie hippocampal-dependent memory is not well understood. In this study, we profiled the hippocampal proteomes of young and middle-aged mice across two circadian cycles using quantitative mass spectrometry in order to explore aging-associated changes in the temporal orchestration of biological pathways. Of the ∼1,420 proteins that were accurately quantified, 15% (214 proteins) displayed circadian rhythms in abundance in the hippocampus of young mice, while only 1.6% (23 proteins) were rhythmic in middle-aged mice. Remarkably, aging disrupted the circadian regulation of proteins involved in cellular functions critical for hippocampal function and memory, including dozens of proteins participating in pathways of energy metabolism, neurotransmission, and synaptic plasticity. These included processes such as glycolysis, the tricarboxylic acid cycle, synaptic vesicle cycling, long-term potentiation, and cytoskeletal organization. Moreover, aging altered the daily expression rhythms of proteins implicated in hallmarks of aging and the pathogenesis of several age-related neurodegenerative brain disorders affecting the hippocampus. Notably, we identified age-related alterations in the rhythmicity of proteins involved in mitochondrial dysfunction and loss of proteostasis, as well as proteins involved in the pathogenesis of disorders such as Alzheimer's disease and Parkinson's disease. These insights into aging-induced changes in the hippocampal proteome provide a framework for understanding how the age-dependent circadian decline may contribute to cognitive impairment and the development of neurodegenerative diseases during aging.

Keywords: aging, circadian, proteomics, hippocampus, mass spectrometry, neurodegenerative diseases

OPEN ACCESS

Edited by:
Hans J. Grabe,
University of Greifswald, Germany

Reviewed by:
Christian Griñán-Ferré,
Bosch i Gimpera Foundation, Spain
Zhigang Liu,
Northwest A&F University, China

****Correspondence:***
Daniel Figeys
dfigeys@uottawa.ca

†Present address:
Cheng-Kang Chiang,
Department of Chemistry, National Dong Hwa University, Shoufeng, Taiwan

Received: *19 June 2019*
Accepted: *16 December 2019*
Published: *15 January 2020*

Citation:
Adler P, Chiang C-K, Mayne J, Ning Z, Zhang X, Xu B, Cheng H-YM and Figeys D (2020) Aging Disrupts the Circadian Patterns of Protein Expression in the Murine Hippocampus. Front. Aging Neurosci. 11:368. doi: 10.3389/fnagi.2019.00368

INTRODUCTION

Circadian regulation of various physiological and behavioral processes is critical to maintaining homeostasis and organismal health (Bass and Lazar, 2016; Chaix et al., 2016). In mammals, the suprachiasmatic nucleus (SCN) acts as a central pacemaker to entrain an organism's internal clock using environmental cues such as the daily light/dark cycle, and in turn synchronizes peripheral oscillators located in other brain regions and organs (Liu et al., 2007; Dibner et al., 2010). Circadian disturbances occur during aging and are associated with cognitive decline and several brain disorders, including neurodegenerative diseases (Kondratov, 2007; Kondratova and Kondratov, 2012; Musiek and Holtzman, 2016). Moreover, the circadian clock influences processes involved in hallmarks of aging, underscoring its significance in maintaining physiological integrity (Kondratov, 2007; Lopez-Otin et al., 2013; Fonseca Costa and Ripperger, 2015; Chaix et al., 2016). Disruption of the temporal coordination of clock-controlled processes may therefore contribute to functional decline during aging (Kondratov, 2007; Hood and Amir, 2017). Furthermore, given the interplay between the circadian system and the aging process, and that aging is a major risk factor for several neurodegenerative diseases, the effects of aging on circadian rhythms could have important implications for the pathogenesis of these disorders (Kondratov, 2007; Musiek and Holtzman, 2016). Yet, how aging affects the circadian orchestration of biological processes in the brain remains largely unexplored (Hatanaka et al., 2017).

Several molecular and cellular mechanisms underlying synaptic plasticity and hippocampal function, as well as hippocampal-dependent memory itself, have previously been shown to be clock-regulated and disrupted by clock dysregulation (Smarr et al., 2014; Hannou et al., 2018; Snider et al., 2018). Circadian clocks modulate the expression or activity of diverse proteins involved in processes contributing to hippocampal function, such as neurotransmission, long-term potentiation (LTP), and energy metabolism (Chiang et al., 2017; Hannou et al., 2018; Greco and Sassone-Corsi, 2019). These include proteins such as calcium/calmodulin-dependent protein kinase II (CaMKII), glycogen synthase kinase 3β (GSK3β), the GluA1 AMPA receptor (AMPAR) subunit, synaptic vesicle glycoprotein 2A (SV2A), and isocitrate dehydrogenase (IDH) (Chiang et al., 2014, 2017; Neufeld-Cohen et al., 2016; Hannou et al., 2018; Snider et al., 2018). Moreover, circadian dysfunction and cognitive decline are common features of aging and multiple age-related neurodegenerative disorders, and accumulating evidence suggests that aging- and disease-related circadian disruption contributes to memory impairment (Kondratova and Kondratov, 2012; Musiek and Holtzman, 2016). However, the mechanisms underlying the association between declines in circadian function and memory during aging remain elusive. The identification of age-related changes in the circadian regulation of processes underlying memory function in the hippocampus might therefore open new avenues to correct dysregulated rhythms and thereby prevent or reverse cognitive decline.

Systems biology approaches are uniquely positioned to provide insight into the ubiquitous role of the circadian clock in physiology and to identify links among diverse temporally regulated processes (Hughes et al., 2017; Millius and Ueda, 2017). We have previously shown that the clock regulates key biological processes at the proteomic and phosphoproteomic levels in the SCN and hippocampus of young mice (Chiang et al., 2014, 2017). However, the impact of aging on the hippocampus has not yet been investigated at the global proteomic level from a circadian perspective. In this study, we compared young and middle-aged mice using a quantitative mass spectrometry (MS)-based approach to profile the hippocampal circadian proteome across two consecutive days, in order to dissect changes in the temporal orchestration of biological pathways during aging. We show that aging disrupts the circadian regulation of proteins involved in cellular functions critical for hippocampal function and memory, notably energy metabolism, neurotransmission, and synaptic plasticity. Furthermore, aging altered the daily expression rhythms of proteins implicated in various processes linked to neurodegenerative diseases as well as hallmarks of aging, such as mitochondrial dysfunction and loss of proteostasis. Collectively, our findings provide further evidence supporting the contribution of the age-dependent circadian decline to the development of neurodegenerative diseases and cognitive deterioration over time.

MATERIALS AND METHODS

Animals and Tissue Collection

Male C57BL/6J mice were purchased from the Jackson Laboratory (Bar Harbor, ME, United States; Stock #000664) and aged to 9–10 weeks (young group) or 44–52 weeks (middle-aged group). Mice were group housed in polycarbonate cages with *ad libitum* access to food and water and entrained to a 12-h light:12-h dark (LD) schedule (lights on at 6:00 a.m., lights off at 6:00 p.m.) from 5 weeks of age (young group) or 28 weeks of age (middle-aged group) before being transferred to constant darkness (DD). After 2 days in constant darkness, mice were sacrificed at 4-h intervals over 2 days starting at circadian time (CT) 2 on the third day of DD, where CT was defined by the zeitgeber time (ZT) of the previous LD schedule (Chiang et al., 2014, 2017). Sample sizes were as follows: three mice per age group were sacrificed at each CT, except for CT18 and 22 (four mice per age group at each CT), CT42 (four young mice and two middle-aged mice), and CT46 (four young mice). Mice were sacrificed by cervical dislocation under dim red light and the hippocampi were quickly excised. Tissues were immediately flash frozen in liquid nitrogen and stored at −80°C until further processing. All animal experiments were conducted at the Ottawa Hospital Research Institute and approved by the University of Ottawa Animal Care Committee in compliance with institutional and Canadian Council on Animal Care guidelines.

Proteomic Analysis of Hippocampal Tissues

Protein extracts from hippocampal tissues of individual mice were obtained by homogenization in lysis buffer using a pellet pestle and sonication (three 10 s pulses with 30 s on ice

between each pulse). The lysis buffer contained 4% (w/v) sodium dodecyl sulfate (SDS) in 50 mM ammonium bicarbonate (ABC; pH 8.2) supplemented with complete protease and phosphatase inhibitor cocktails (Roche; Mississauga, ON, Canada). Protein concentrations were determined using the DC Protein Assay (Bio-Rad; Mississauga, ON, Canada), and hippocampal lysates were loaded onto 30-kDa molecular weight cutoff Microcon filters (MilliporeSigma; Oakville, ON, Canada). Proteins were reduced by incubating samples with 20 mM dithiothreitol (DTT; MilliporeSigma; Oakville, ON, Canada) for 30 min at 37°C with agitation (245 rpm) and subsequently alkylated with 20 mM 2-iodoacetamide (IAA; MilliporeSigma; Oakville, ON, Canada) for 30 min in darkness at room temperature. Protein digestion was performed by incubation with 40:1 (w/w, protein:enzyme) trypsin (Worthington Biochemical Corporation; Lakewood, NJ, United States) overnight at 37°C with agitation (245 rpm). Prior to strong cation exchange (SCX) fractionation of hippocampal samples, peptides were diluted with 0.1% (v/v) formic acid (FA) and the pH adjusted with trifluoroacetic acid (TFA) to 3.0. Step elution of peptides was performed using in-house-made SCX columns (10-μm SCX beads, Polymer Laboratories) and subsequent addition of buffers (20 mM boric acid, 20 mM phosphoric acid, and 20 mM acetic acid) at pH 5, 6, 8, 10, and 12. Samples were desalted using in-house-made C18 desalting cartridges (C18 beads: ReproSil-Pur C18-AQ, 10 μm; Dr. Maisch GmbH, Germany) and dessicated using a SpeedVac prior to being resuspended in 0.1% (v/v) FA for liquid chromatography tandem MS (LC–MS/MS) analysis.

LC–MS/MS Analysis

Four microliters of resuspended peptides (equivalent to 2 μg of proteins) from each sample were analyzed by an online reverse-phase LC–MS/MS platform consisting of an Eksigent NanoLC 425 System (AB SCIEX) coupled with an Orbitrap Elite mass spectrometer (Thermo Fisher Scientific, San Jose, CA, United States) via a nano-electrospray source. Prior to MS analysis, peptide mixtures were separated by reverse-phase chromatography using an in-house packed ReproSil-Pur C18-AQ column (75 μm internal diameter × 15 cm, 1.9 μm, 200 Å pore size; Dr. Maisch GmbH, Germany) over a 120-min gradient of 5–30% buffer B [acetonitrile (ACN) with 0.1% (v/v) FA] at a flow rate of 300 nl/min. The Orbitrap Elite instrument was operated in the data-dependent mode to simultaneously measure survey scan MS spectra (350–1,800 m/z, R = 60,000 defined at m/z 400). Up to the 20 most intense peaks were isolated and fragmented with collision-induced dissociation (CID). System controlling and data collection were carried out using Xcalibur software version 2.2 (Thermo Scientific).

Mass Spectrometry Data Processing

Mass spectrometry raw files were processed with MaxQuant (version 1.5.2.8) using the integrated Andromeda search engine and UniProt FASTA database from mouse (*Mus musculus*; 2013_05). The search included variable modifications for methionine oxidation (M) and acetylation (protein N-term) as well as fixed modification for carbamidomethylation (C). Trypsin/P was set as the cleavage specificity with up to two missed cleavages allowed. The false discovery rate (FDR) cutoffs were set at 0.01 at the peptide and protein levels and the minimum peptide length was set at 7. Identification across different replicates and adjacent fractions was achieved by enabling the "match between runs" option with a matching time window of 5 min.

Bioinformatic and Statistical Analyses

Initial bioinformatic analysis was performed with Perseus (version 1.5.5.3). Following logarithmic ($\log_{10}$) transformation of label-free quantification (LFQ) intensities, the raw proteomic dataset was filtered to include only proteins quantified in a minimum of two biological replicates per time point in either young or middle-aged mice. Using these filtered datasets, circadian rhythmicity in protein abundance over the 12 CTs was determined using the Perseus periodicity algorithm (period = 23.6 h) (Robles et al., 2014) with q-value < 0.25 (Mauvoisin et al., 2014). Heatmaps displaying temporal expression profiles of circadian proteins ordered by phase were generated using the logarithmized LFQ intensities after z-score normalization. Gene Ontology (GO) and Kyoto Encyclopedia of Genes and Genomes (KEGG) pathway functional annotations and enrichment analyses were implemented using DAVID (version 6.8; one-sided Fisher's exact test $p \leq 0.05$ relative to the backgrounds of accurately quantified proteins in our datasets was considered significant) in order to assess changes in GO biological processes, GO cellular components, and KEGG pathways. Protein–protein interaction networks were created using the STRING database (Szklarczyk et al., 2015) (confidence score cutoff = 70%) and visualized with Cytoscape (version 3.4.0) to include the phases and q-values of rhythmic proteins.

Data Availability Statement

The mass spectrometry proteomics data have been deposited to the ProteomeXchange Consortium via the PRIDE partner repository with the dataset identifier PXD013364. Note that a stable isotope labeling by amino acids in cell culture (SILAC) spike-in was introduced during sample preparation but not used for quantification.

RESULTS

Aging Disrupts the Hippocampal Circadian Proteome

To examine how aging alters the regulation of rhythmic processes in the hippocampus, we used a quantitative MS-based approach to analyze total protein extracts from hippocampal tissues harvested from young and middle-aged mice over two consecutive circadian cycles (see the section "Materials and Methods"; **Figure 1A**). Samples were processed individually to yield three to four biological replicates at each of the 12 time points for each age group, and relative protein abundances were determined using LFQ. This MS-based analysis identified a total of 4,433 proteins, of which 1,426 and 1,416 were quantified in a minimum of two biological replicates at each time point

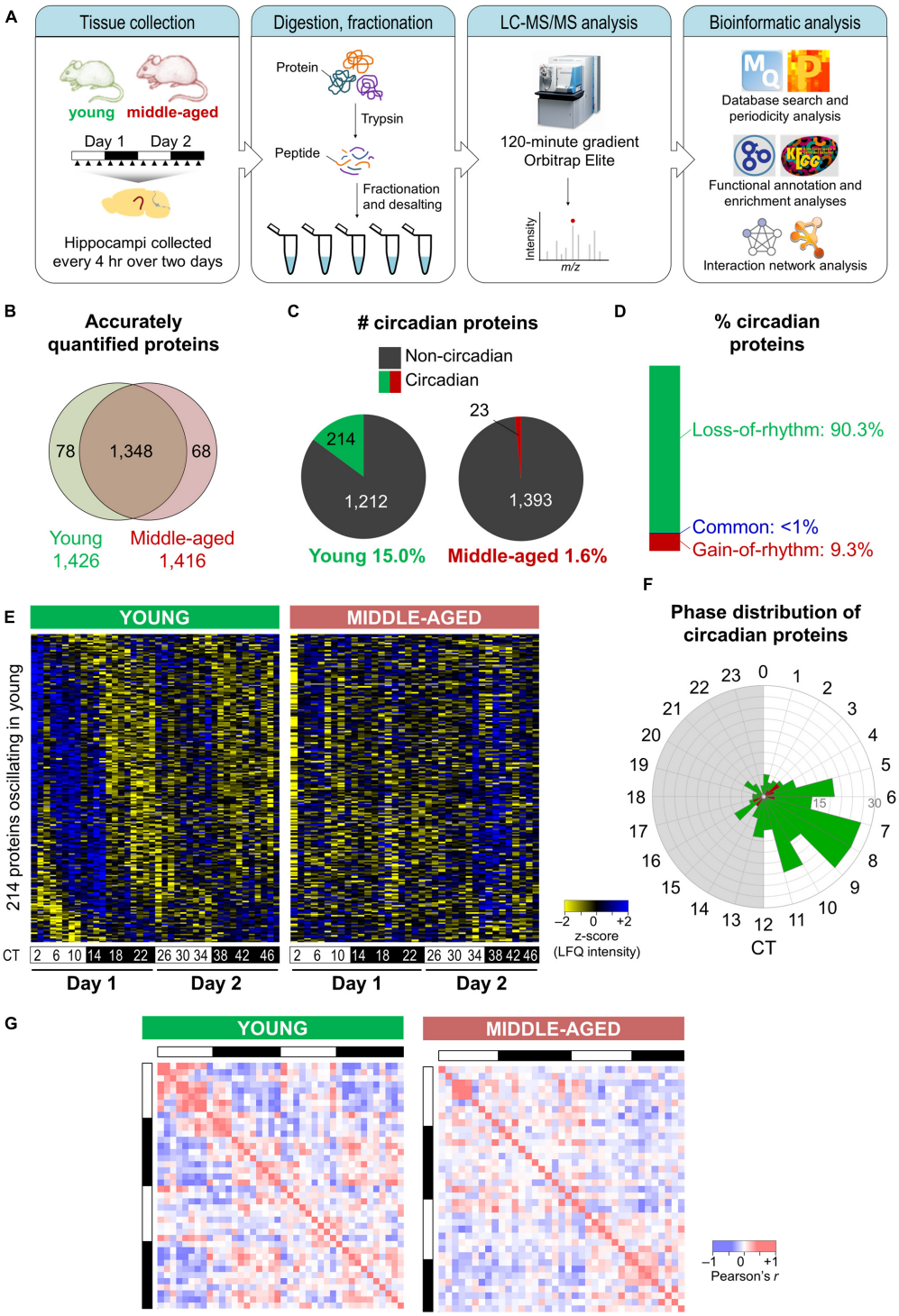

FIGURE 1 | Aging disrupts the hippocampal circadian proteome. **(A)** Experimental design and workflow of the MS-based analysis of proteins extracted from hippocampal tissues of young (9–10 weeks old) and middle-aged (44–52 weeks old) C57BL/6J mice. Samples were collected every 4 h over 2 days, and proteins extracted from tissues of individual mice were digested with trypsin, fractionated, and analyzed by an Orbitrap Elite mass spectrometer. **(B)** Proteome coverage: Venn diagram displaying the number of proteins quantified in at least two biological replicates per time point in young or middle-aged mice and overlap between ages. **(C)** Circadian proteins detected in young or middle-aged mice using the Perseus periodicity algorithm (period = 23.6 h; q-value < 0.25). **(D)** Percent distribution of circadian proteins based on changes in rhythmicity during aging. **(E)** Heatmaps displaying z-score normalized abundances ($\log_{10}$ LFQ intensities) of circadian proteins detected in young mice and their temporal expression profiles in young mice (left) and middle-aged mice (right). **(F)** Phase distribution of circadian proteins detected in young mice (green) or middle-aged mice (red). **(G)** Correlation heatmaps across 48 h in young mice (left) and middle-aged mice (right) for circadian proteins detected in young mice. Pearson correlation coefficients are shown as red (positive) or blue (negative).

in the hippocampus of young mice and middle-aged mice, respectively (**Figure 1B**). We used these stringently filtered datasets of reliably quantified proteins for downstream analysis (**Supplementary Data 1, 2**).

Proteins displaying circadian oscillations in their abundances were identified using the Perseus periodicity analysis algorithm (period = 23.6 h) (Robles et al., 2014) and a FDR value cutoff of 0.25 (Mauvoisin et al., 2014) in young and middle-aged mice. Abundance for 236 proteins changed as a function of circadian timing at either age (**Supplementary Data 3, 4**). As expected, the core circadian clock proteins were not accurately quantified in our datasets due to their low abundance in total protein extracts (Millius and Ueda, 2017). A total of 214 proteins displayed circadian rhythmicity in the hippocampus of young mice (15.0% of reliably quantified proteins), while in middle-aged mice a total of 23 rhythmic proteins were identified (1.6% of reliably quantified proteins) (**Figure 1C**). Overall, there were fewer rhythmic proteins identified in the middle-aged group, reflective of the age-related decline in the circadian system. Strikingly, ∼90% of circadian proteins detected at either age displayed a loss of rhythmicity during aging (i.e., oscillated exclusively in young mice) (**Figure 1D**), suggesting that aging is associated with widespread disruption in the temporal regulation of cellular functions in the hippocampus.

Although most age-related changes involved a loss of rhythmicity in middle-aged mice, ∼9% of all circadian proteins detected did not oscillate in young mice but gained rhythmicity during aging (**Figure 1D**). These included proteins involved in specific processes known to play roles in aging, such as apoptosis and the cellular stress response (**Supplementary Figure 1**). Consistent with our results, two previous studies have identified sets of transcripts that gained rhythmicity during aging in the human prefrontal cortex and in heads of *Drosophila melanogaster*, notably genes involved in stress response functions (Chen et al., 2016; Kuintzle et al., 2017). Moreover, proteins that have been linked to neurodegenerative diseases were among those displaying rhythmic abundances in the hippocampus of middle-aged mice (**Supplementary Table 1**). For instance, histone deacetylase 1 (HDAC1) as well as one of its target proteins, histone H3, gained rhythmicity during aging. Interestingly, histone acetylation regulates memory function as well as transcription of clock genes, and age-related changes in hippocampal-dependent memory have previously been linked to epigenetic modulation of the clock gene *Per1* through HDAC3 (Kwapis et al., 2018). Thus, aging might result in altered circadian epigenetic regulation of clock genes and other genes that affect hippocampal function.

Rhythmic proteins displayed a variety of temporal abundance profiles in the hippocampus of young mice (left panel in **Figure 1E**), with the phases of peak expression clustering in the afternoon (**Figure 1F**), while in middle-aged mice all but one of these proteins were no longer detected as oscillating (right panel in **Figure 1E**). Furthermore, aging resulted in loss of positive and negative correlations among rhythmic proteins detected in young mice across the day/night cycle (**Figure 1G**). Together, our findings indicate that there are widespread aging-induced changes in the daily patterns of protein expression in the hippocampus.

Age-Related Changes in the Circadian Regulation of Biological Functions

To explore the functional relevance of these age-related changes, we examined biological pathways and processes using KEGG and GO analyses to identify functional terms over-represented among proteins displaying loss of rhythmicity in abundance during aging (**Figure 2**). Overall, pathways involved in basic cellular metabolism, circadian entrainment, synaptic function, and neurodegenerative diseases were among those enriched (**Figure 2A**). Several enriched processes have previously been characterized as circadian in young mammalian models, including the tricarboxylic acid (TCA) cycle, dendritic spine organization, and regulation of DNA repair (Smarr et al., 2014; Chaix et al., 2016; Neufeld-Cohen et al., 2016). Biological processes involved in neurotransmission, synaptic plasticity, mitochondrial function, redox homeostasis, and proteostasis were also highly represented among proteins displaying age-related loss of circadian rhythmicity (**Figure 2B**).

Furthermore, protein–protein interaction network analysis of proteins displaying loss of rhythmicity in the hippocampus during aging revealed interactions among proteins involved in energy metabolism, mitochondrial function, cytoskeletal organization, translation, and G-protein signaling (**Supplementary Figure 2**). Given that many of these affected processes are critical for normal hippocampal function and have been implicated in neurodegenerative brain disorders, their altered circadian regulation might contribute to aging- and disease-associated decline in hippocampal function and memory. For instance, dysfunction of G-protein-coupled neurotransmission occurs in the brain during aging and may predispose older individuals to developing age-related neurodegenerative disorders (Mattson and Arumugam, 2018).

The effects of aging on rhythmic biological functions were complemented by results from a GO analysis of cellular components. In young mice, rhythmic proteins participated in diverse processes involved in the structure and function of various intracellular organelles, with the mitochondrion and cytoskeleton being two major sites of circadian regulation (**Figure 2C**). Proteins localized to the mitochondrion (including the mitochondrial inner membrane, ATP synthase complex, and pyruvate dehydrogenase complex) and synapse (including synaptic vesicles, terminal boutons, and septin cytoskeleton) displayed loss of circadian oscillations in abundance, reflective of the pathways related to mitochondrial energy metabolism, neurotransmission, and synaptic plasticity (**Figures 2A,B**).

Interestingly, some of the most highly enriched GO functional terms included myelination, myelin sheath, and oligodendrocyte differentiation (**Figures 2B,C**), which might suggest another mechanism through which aging disrupts cognitive function. Consistent with this hypothesis and our results showing that proteins involved in these functions peak during the daytime in young mice, it has previously been reported that genes involved in myelination and promoting proliferation of oligodendrocyte

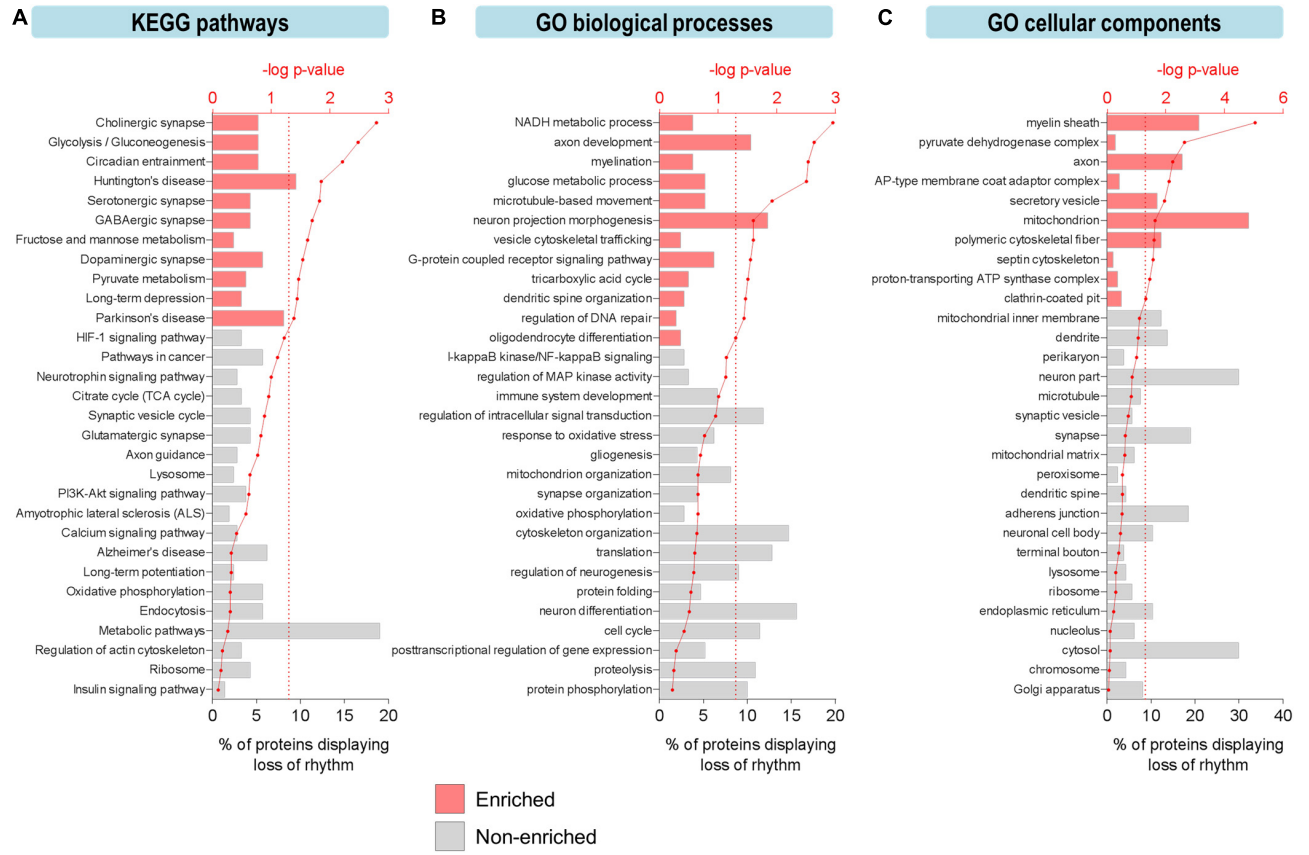

FIGURE 2 | Aging leads to loss of circadian oscillations in specific biological functions in the hippocampus. **(A–C)** Functional analysis of proteins displaying loss of circadian rhythmicity with aging. Enriched ontology terms corresponding to **(A)** KEGG pathways, **(B)** GO biological processes, and **(C)** GO cellular components are shown with colored bars ($p \leq 0.05$, Fisher's exact test relative to background of accurately quantified proteins in our dataset).

precursor cells (OPCs) are transcribed preferentially during sleep in mice (Bellesi et al., 2013). Furthermore, OPCs demonstrate daily rhythms in proliferation in the hippocampus of young mice (Matsumoto et al., 2011) and sleep loss has been shown to disrupt myelin formation (Bellesi et al., 2018). While previous work has shown that myelination is compromised in the aged human brain and especially in people with cognitive deficits (Mattson and Arumugam, 2018), our results suggest that age-related changes in the circadian regulation of myelination may also contribute to cognitive decline during aging via neural circuit dysfunction and impaired communication between different brain regions.

We also noted age-related changes in rhythmic abundances of multiple proteins involved in regulating protein phosphorylation (**Figure 2B**), indicating that temporal control of post-translational modifications such as phosphorylation may be altered and associated with cognitive decline during aging. Interestingly, we found that the phases of peak expression of circadian proteins clustered in the afternoon, at the same time as the peak in rhythmic phosphoproteins we have previously reported (Chiang et al., 2017). Moreover, aging-associated changes in the daily expression profiles of kinases such as CaMKII and GSK3β (**Supplementary Figure 3**) might contribute to the age-related declines in hippocampal-dependent memory and local clock function (Kon et al., 2014; Besing et al., 2017). GSK3β, which phosphorylates and regulates BMAL1 and REV-ERBα (Reischl and Kramer, 2011), has previously been shown to play important roles in modulating synaptic plasticity as well as the molecular clock in the hippocampus of young mice (Besing et al., 2017). Wang et al. (2017) previously reported that GSK3β peaks in nuclear activity/abundance in the livers of young mice during the day, consistent with our hippocampal study. In addition, other proteins involved in clock function displayed a loss of rhythmicity in the hippocampus of middle-aged mice (**Supplementary Figure 3**), highlighting the age-dependent decline in local clock function at the molecular level. Taken together, our findings indicate that there is widespread disruption in the circadian regulation of biological processes and pathways critical for normal hippocampal function during aging.

Aging Disrupts the Circadian Regulation of Energy Metabolism

Dysregulated energy metabolism is a hallmark of brain aging and its exacerbation underlies the molecular pathogenesis of several age-related neurodegenerative disorders, including Alzheimer's disease (AD), amyotrophic lateral sclerosis (ALS), Parkinson's

disease (PD), and Huntington's disease (HD) (Camandola and Mattson, 2017; Mattson and Arumugam, 2018). We therefore further examined the effects of aging on the circadian regulation of energy metabolism in the hippocampus, focusing on proteins involved in glucose metabolism as well as the downstream pyruvate metabolism, TCA cycle, and oxidative phosphorylation pathways.

The relative enrichment among proteins displaying loss of rhythmicity during aging of pathways such as glycolysis, pyruvate metabolism, and the TCA cycle (**Figures 2A,B**) is consistent with previous studies from our lab and others demonstrating that several components of these pathways exhibit diurnal rhythms in protein abundance in the brain as well as peripheral organs of young mice (Chiang et al., 2014, 2017; Neufeld-Cohen et al., 2016). We found over 20 proteins participating in critical energy metabolism pathways that displayed loss of rhythmicity in the hippocampus during aging (**Figure 3A**). In young mice, these rhythmic proteins peaked in a coordinated manner during the day (**Figure 3B**), and at the same time that circadian proteins involved in oxidative phosphorylation peak in the SCN of young mice (Chiang et al., 2014). Interestingly, many of the rhythmic proteins catalyzing steps in glycolysis and the TCA cycle in young mice are NAD^+-dependent enzymes, suggesting a potential mechanism by which circadian oscillations in NAD^+ could couple energy production in the brain to the daily light/dark cycle (Peek et al., 2013). Importantly, phosphofructokinase (PFK) and the regulatory subunit of isocitrate dehydrogenase 3 (IDH3) were rhythmic in young mice but not middle-aged mice. Given that these enzymes catalyze the rate-limiting steps of glycolysis and the TCA cycle, respectively, aging may have a significant impact on the dynamics of these pathways and therefore energy production in the hippocampus. These results suggest that the dysregulation of energy metabolism that occurs in the brain during aging extends to its temporal regulation, and disrupted circadian rhythms in energy metabolism pathways might contribute to age-related impairments in hippocampal function and memory.

Aging Disrupts the Circadian Regulation of Synaptic Structure and Function

Circadian modulation of hippocampal-dependent memory at the molecular level can occur through clock regulation of multiple neuronal and synaptic components, including synaptic vesicle proteins, receptors, transporters, and intracellular signaling cascades (Hannou et al., 2018; Rawashdeh et al., 2018; Snider et al., 2018). Thus, we were interested in examining the impact of aging on the circadian rhythmicity of proteins involved in synaptic plasticity and function in the hippocampus, given that changes in the regulation of these processes may contribute to age-related memory impairment.

We first examined the effects of aging on synaptic vesicle cycling, which has previously been shown to be rhythmic and important for circadian gene expression in the SCN (Deery et al., 2009). Strikingly, middle-aged mice displayed a loss of circadian oscillations in the abundances of over 10 proteins involved in this pathway, which were rhythmic in the hippocampus of young mice (**Figure 4A**). These included syntaxin binding protein 1 (also known as Munc18-1), SV2A, and endophilin A1, which we and others have previously shown to be clock-regulated at the protein or mRNA level in the brains of young mice (Chiang et al., 2014; Hannou et al., 2018). Interestingly, we also found that the GluA1 AMPAR subunit, along with other proteins regulating AMPAR phosphorylation and trafficking, such as CaMKII and protein kinase C γ, displayed loss of rhythmicity in the hippocampus during aging. Previous work has demonstrated that glutamate receptor trafficking is regulated by clock-gated signaling pathways, in line with our results (Snider et al., 2018). In addition, multiple cytoskeletal components and regulators lost rhythmicity in middle-aged mice, including actin regulators such as RHOA and Rho GDP-dissociation inhibitor (RhoGDI), whose interaction is known to be clock-regulated (Ma et al., 2018). Several proteins involved in the organization of microtubules and the septin cytoskeleton were also found to display loss of circadian oscillations in the hippocampus of middle-aged mice, suggesting that aging could lead to disruption of synaptic plasticity through multiple neuronal cytoskeleton components given that synaptic plasticity is affected by cytoskeletal remodeling (Gordon-Weeks and Fournier, 2014).

While circadian rhythmicity of proteins involved in synaptic structure and function was largely lost in middle-aged mice, these proteins peaked in a coordinated manner during the day in the hippocampus of young mice (**Figure 4B**), consistent with previous work demonstrating that processes supporting synaptic plasticity peak during sleep in mice (Eckel-Mahan et al., 2008). Thus, the age-related dampening in rhythmicity of proteins involved in the synaptic vesicle cycle, LTP and AMPAR regulation, and cytoskeleton organization might lead to compromised synaptic structure and function in the hippocampus of middle-aged mice, which could in turn result in impaired hippocampal-dependent memory during aging.

Disruption of Rhythmic Proteins Involved in Hallmarks of Aging and Neurodegenerative Diseases

Mitochondrial dysfunction, a hallmark of aging, may contribute to age-associated damage and has been implicated in cognitive impairment as well as the pathogenesis of several neurodegenerative diseases (Lopez-Otin et al., 2013; Mattson and Arumugam, 2018). We were therefore interested in examining whether the age-related decline in efficiency of mitochondrial energy metabolism and antioxidant defense mechanisms extends to their circadian regulation in the hippocampus (Green et al., 2011). As discussed above, circadian rhythms of mitochondrial proteins involved in energy metabolism were particularly affected during aging, with over 20 proteins displaying age-related loss of rhythmicity (**Figure 3**). These proteins included IDH3, which catalyzes the rate-limiting step of the TCA cycle, as well as several subunits belonging to electron transport chain complexes (**Figures 3**, **5**). In young mice, proteins involved in mitochondrial respiration peaked during the day along with many antioxidant enzymes, notably superoxide dismutase 1 (SOD1) and peroxiredoxins (PRDX3 and PRDX6). Interestingly,

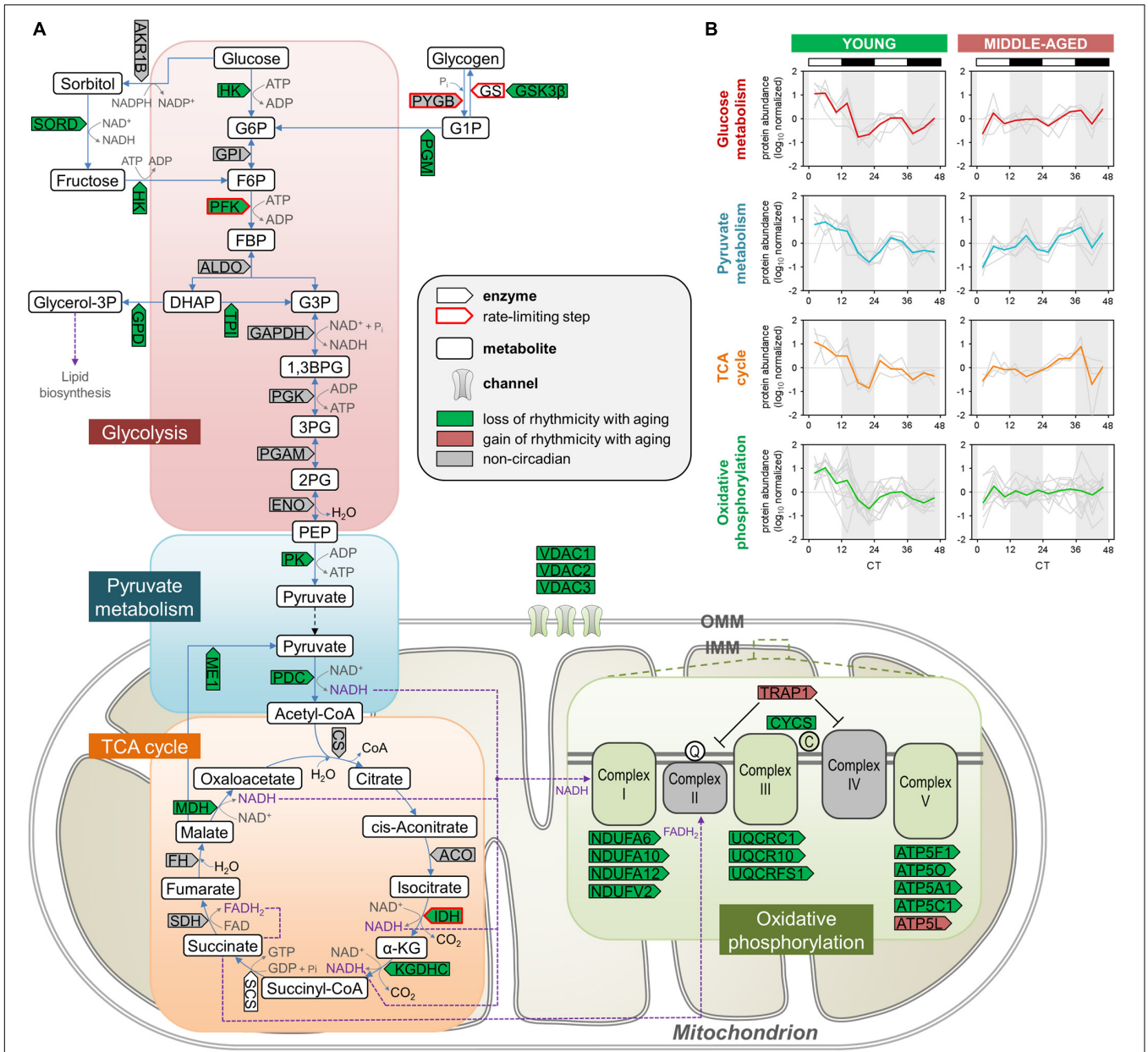

FIGURE 3 | Aging disrupts the circadian regulation of proteins involved in energy metabolism in the hippocampus. **(A)** Schematic depiction of proteins involved in energy metabolism, including glycolysis, pyruvate metabolism, the TCA cycle, and oxidative phosphorylation. Proteins that displayed loss or gain of circadian rhythmicity in abundance during aging are highlighted in color. Proteins that were reliably quantified, but not detected as circadian at either age, are shown in gray. **(B)** Temporal abundance profiles of rhythmic proteins identified in young mice involved in energy metabolism.

we found that these and other antioxidant enzymes displayed loss of rhythmic abundances during aging (**Figure 5**). We also found that all three voltage-dependent anion-selective channels (VDACs) lost their rhythmic expression in middle-aged mice, which could impact both mitochondrial function and synaptic plasticity in the hippocampus (Levy et al., 2003; **Figure 5**). Thus, aging-induced changes in the circadian rhythms of proteins involved in mitochondrial function and reactive oxygen species (ROS) homeostasis provide additional potential mechanisms through which aging may lead to an increased susceptibility to brain disorders characterized by mitochondrial dysfunction, including neurodegenerative diseases such as AD and PD (Mattson and Arumugam, 2018).

Genomic instability and epigenetic alterations, two primary hallmarks of aging, are linked to clock function through circadian regulation of proteins involved in ROS homeostasis and epigenetic modification. Given that mitochondrial respiration is a major intracellular source of ROS (Mattson and Arumugam, 2018), and that both oxidative phosphorylation and the cellular response to oxidative stress display circadian rhythmicity

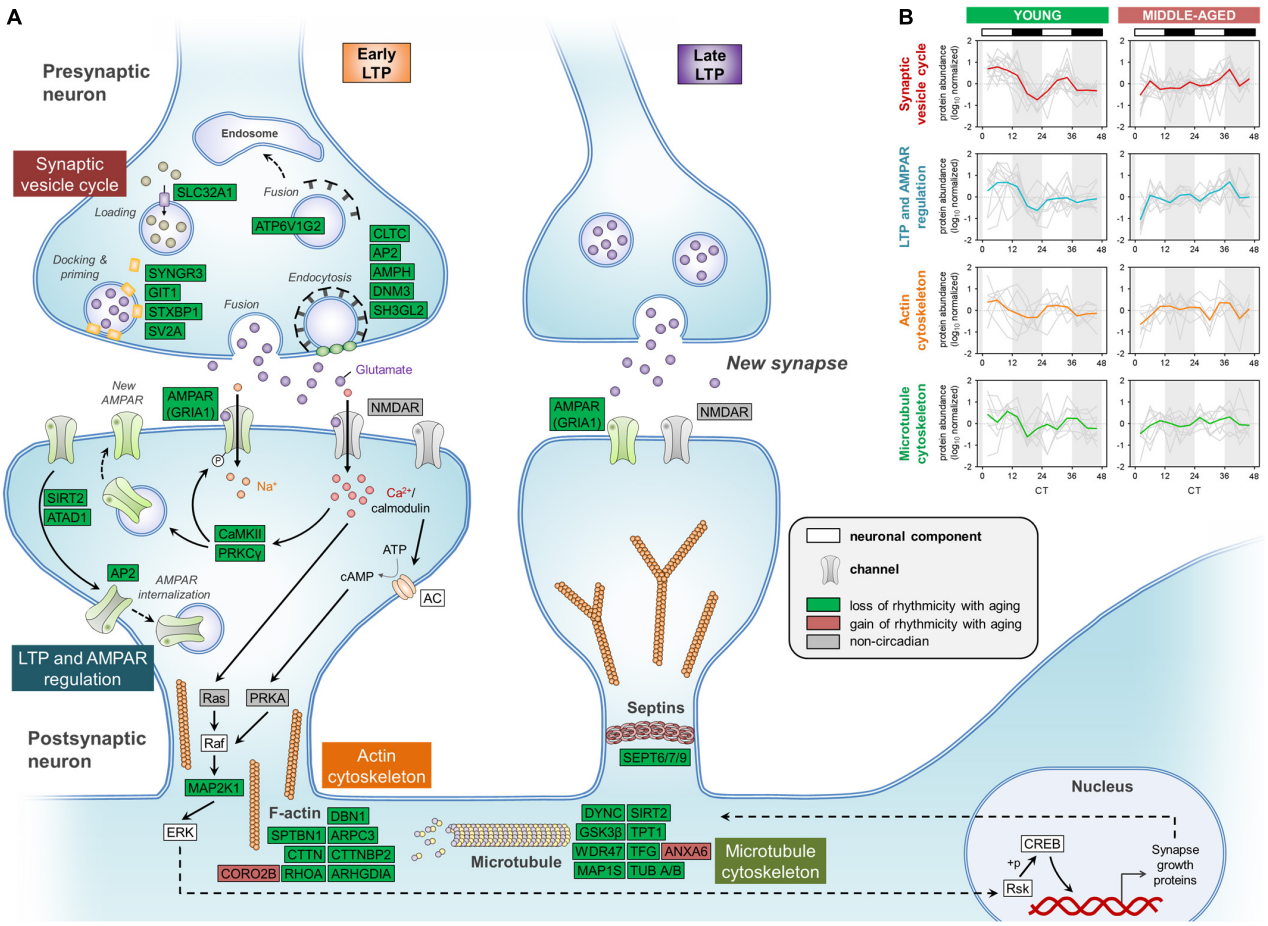

FIGURE 4 | Aging disrupts the circadian regulation of proteins involved in synaptic function in the hippocampus. **(A)** Schematic depiction of proteins involved in synaptic structure and function, including the synaptic vesicle cycle, LTP and AMPAR regulation, and the cytoskeleton. Proteins that displayed loss or gain of circadian rhythmicity in abundance during aging are highlighted in color. Proteins that were reliably quantified, but not detected as circadian at either age, are shown in gray. **(B)** Temporal abundance profiles of rhythmic proteins identified in young mice involved in synaptic structure and function.

(Chaix et al., 2016), age-related changes in the temporal control of proteins participating in these two processes (as discussed above) may lead to alterations in the accumulation of genetic damage. Genomic instability can also result from disruption of nuclear lamins, such as lamin B1 (Lopez-Otin et al., 2013). Levels of lamin B1 decline during aging (Lopez-Otin et al., 2013) and exhibited a loss of rhythmicity in the hippocampus of middle-aged mice (**Figure 5**), suggesting that this disruption could lead to aberrations in the nuclear lamina and contribute to genome instability during aging. We also found age-dependent changes in the rhythmicity of three proteins involved in epigenetic modification, specifically post-translational modification of histones. These include HDAC1, sirtuin 2 (SIRT2), and acidic leucine-rich nuclear phosphoprotein 32 (ANP32A), which are all involved in regulating histone acetylation levels (**Figure 5**). Age-related changes in the circadian regulation of proteins involved in maintaining genomic and epigenetic stability might therefore result in transcriptional alterations and increased DNA damage, which could in turn stimulate accelerated aging and lead to increased disease risk.

Loss of protein homeostasis, another primary hallmark of aging, is linked to various age-related diseases (Lopez-Otin et al., 2013). While diurnal rhythms in protein synthesis, processing, and degradation have previously been described in several organs in young mammals (Panda et al., 2002; Robles et al., 2014), the impact of aging on the rhythmicity of these processes is less well characterized. We found that the daily abundance profiles of rhythmic proteins participating in protein synthesis, folding, and degradation were altered during aging (**Figure 5** and **Supplementary Figure 2**). These proteins included the molecular chaperones calreticulin, heat shock proteins 60 and 70 (HSP60 and HSP70), and T-complex protein 1 (TCP-1) subunits, as well as valosin-containing protein (VCP), which also regulates ubiquitin-dependent protein degradation (Dai and Li, 2001). Our results suggest that the temporal control of protein homeostasis in the hippocampus is altered during aging, which may in turn impact the core circadian clock transcriptional–translational feedback loop and thus affect oscillations in other local clock-controlled genes (Takahashi, 2017).

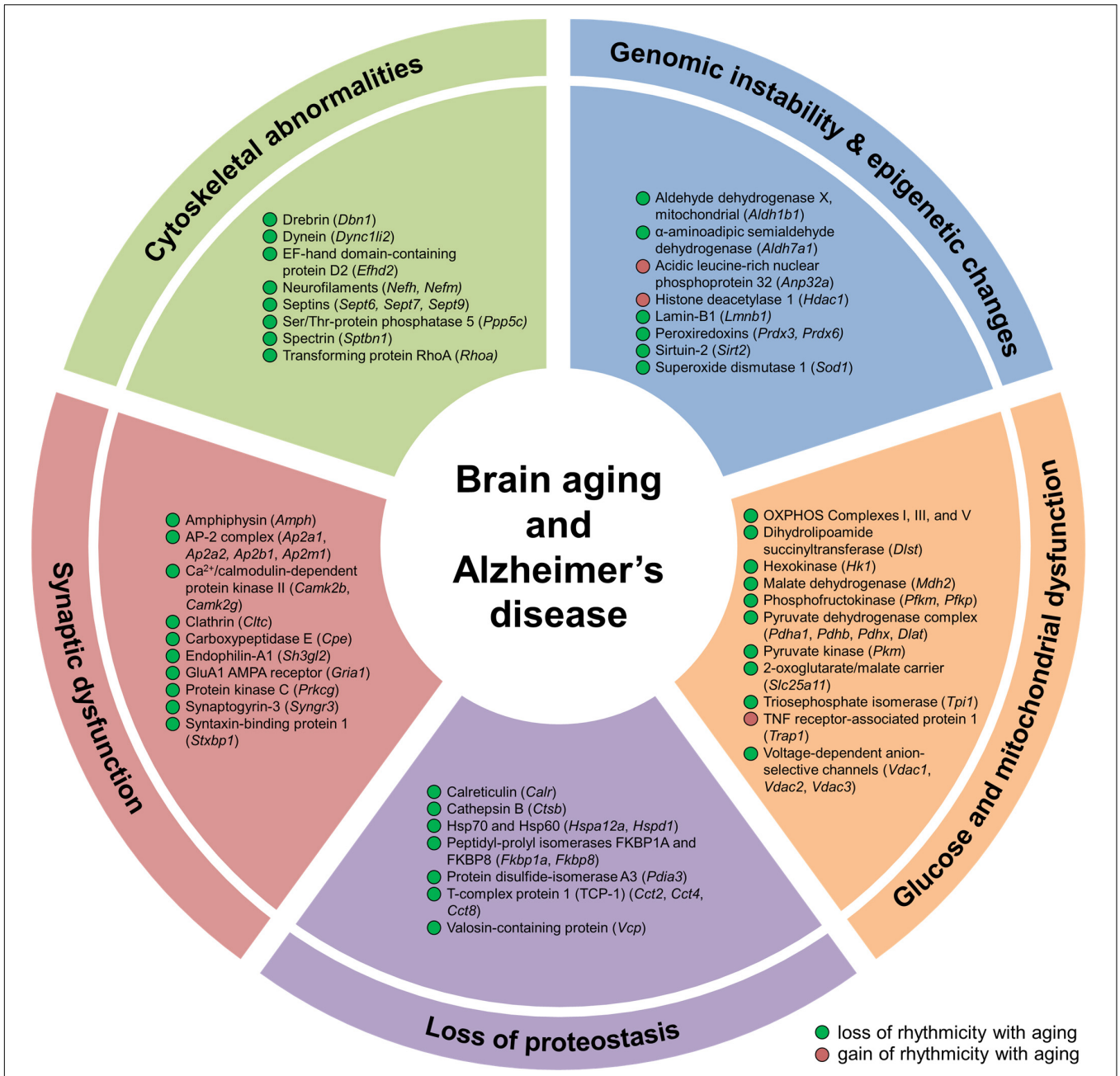

FIGURE 5 | Aging alters hippocampal circadian oscillations of proteins implicated in Alzheimer's disease and hallmarks of aging. Proteins displaying changes in rhythmicity during aging and involved in hallmarks of aging and Alzheimer's disease pathogenesis: genomic instability, epigenetic alterations, loss of proteostasis, glucose and mitochondrial dysfunction, synaptic dysfunction, and cytoskeletal abnormalities.

To further explore links between age-related disorders and changes in circadian rhythmicity of biological functions during aging, we examined disease-associated pathways containing proteins whose abundance was under circadian regulation in the hippocampus. We found rhythmic proteins associated with the pathogenesis of several age-related neurodegenerative diseases affecting the brain (**Supplementary Table 1**). In addition to proteins involved in the hallmarks of aging discussed above that are known to play roles in the pathogenesis of AD, such as mitochondrial dysfunction and loss of proteostasis, several other proteins displaying age-related changes in rhythmicity in the hippocampus were also associated with AD. These included proteins involved in synaptic dysfunction and cytoskeletal abnormalities, such as synaptic vesicle proteins, cytoskeleton components and regulators, and enzymes that regulate protein phosphorylation (**Figure 5** and **Supplementary Table 1**). Several proteins linked to AD and involved in the synaptic vesicle cycle were found to display loss of rhythmicity in the hippocampus

during aging, including amphiphysin, AP-2 complex subunits, clathrin heavy chain, endophilin-A1, synaptogyrin-3, and syntaxin-binding protein 1 (**Figures 4**, **5** and **Supplementary Table 1**). Additional proteins involved in synaptic function and dysregulated in AD included the GluA1 AMPAR subunit, CaMKII, and protein kinase C γ, which all displayed loss of rhythmicity during aging (**Figure 4** and **Supplementary Table 1**). Moreover, several cytoskeletal proteins and regulators known to be implicated in AD pathogenesis were found to lose rhythmicity during aging, including neurofilaments, septins, and actin regulators such as drebrin and RHOA (**Supplementary Table 1** and **Figures 4**, **5**). Our data indicate that age-dependent changes in circadian regulation of various processes are associated with and might contribute to AD pathogenesis.

While decline in hippocampal function is a prominent feature of AD, it also occurs in several other neurodegenerative disorders, namely PD (Camicioli et al., 2003), HD (Spargo et al., 1993), ALS (Takeda et al., 2009), and frontotemporal dementia (FTD) (Laakso et al., 2000). We were therefore also interested in identifying age-related hippocampal alterations in the rhythmicity of proteins involved in these diseases. We found that several proteins believed to play major roles in the pathogenesis of these diseases displayed changes in circadian regulation in the hippocampus during aging, notably TDP-43, SOD1, and TNF receptor-associated protein 1 (TRAP1) (**Supplementary Table 1**). TDP-43, which gained rhythmicity during aging, has been identified as the major pathological protein in both ALS and FTD (Mackenzie and Rademakers, 2008). Moreover, SOD1 displayed a loss of rhythmicity during aging, and mutations in *SOD1* and the TDP-43 gene *TARDBP* are known to occur in familial ALS (Millecamps et al., 2010). The mitochondrial chaperone TRAP1, also known as HSP75, gained rhythmicity in the hippocampus of middle-aged mice and has been linked to familial PD arising due to mutations in *PTEN induced putative kinase 1* (*PINK1*) (Pridgeon et al., 2007). Interestingly, the protective role of PINK1 against oxidative stress is mediated through phosphorylation of TRAP1 and inhibition of the mitochondrial release of cytochrome c (Pridgeon et al., 2007), another protein that displayed loss of rhythmicity in the hippocampus during aging (**Supplementary Table 1**). Taken together, these results provide further evidence for the association of age-related circadian disruption in the brain with the pathogenesis of neurodegenerative diseases. Furthermore, our findings highlight the widespread aging-associated alterations in temporal regulation of biological processes implicated in aging and age-related brain disorders.

DISCUSSION

Given the regulation of hippocampal physiology and function by the circadian clock, the age-dependent decline of the circadian system may contribute to cognitive decline over time and development of aging-associated neurodegenerative disorders. Previous large-scale studies of circadian rhythms, while mainly restricted to examining rhythmic processes in young model organisms at the transcriptomic level, have greatly contributed to our understanding of the circadian system's role in modulating various processes in a tissue-specific manner (Zhang et al., 2014; Millius and Ueda, 2017). Proteomic analyses, which incorporate additional mechanisms of circadian regulation at the post-transcriptional level, have been performed on the brain and peripheral organs of young mice to reveal large-scale coordination of biological processes by the clock (Millius and Ueda, 2017). However, how aging modifies clock-controlled processes has only recently begun to be explored at the transcriptomic level in the liver and stem cells of mice (Sato et al., 2017; Solanas et al., 2017), while the effects in the brain are largely unknown. A large-scale characterization of hippocampal circadian rhythms in protein abundances at different ages would therefore provide insight into age-related perturbations in the timing of cellular functions and could facilitate future studies on the molecular mechanisms of aging- and disease-associated cognitive impairment. Further studies are needed to identify age-related alterations in circadian rhythms of protein abundance in peripheral organs as well as other brain regions, particularly the central pacemaker in the SCN.

In this study, we used a quantitative MS-based approach to analyze hippocampal tissues from young and middle-aged mice and to explore the effects of aging on circadian regulation at the proteomic level. Middle-aged mice demonstrate impaired learning and memory (Shoji et al., 2016), indicating that age-dependent hippocampal proteomic alterations might contribute to cognitive decline at this age. We found that there is widespread disruption of the circadian orchestration of protein expression rhythms in the hippocampus during aging, reflective of the age-related decline in the circadian system. Notably, we have shown that aging leads to a loss of temporal coordination of pathways critical for normal hippocampal function, including energy metabolism, neurotransmission, and synaptic plasticity.

Rhythmic proteins involved in energy metabolism and synaptic vesicle cycling peaked in a coordinated manner during the day in young mice, complementing previous work showing that the synaptic vesicle cycle is the main source of activity-driven metabolic demand at synapses (Rangaraju et al., 2014). Importantly, these pathways lost rhythmicity in the hippocampus of middle-aged mice, suggesting that aging is associated with a disruption in the temporal coupling between energy demand and production, which could lead to impaired synaptic function. High rates of energy production in the brain are required to support neuronal and glial activities, with neurons relying on glucose as their main energy source (Camandola and Mattson, 2017). Moreover, reduced hippocampal energy metabolism (particularly glucose metabolism) has been associated with cognitive impairment and AD (Mattson and Arumugam, 2018). Circadian regulation of energy metabolism and synchronization among local brain clocks might contribute to sustaining daily cycles in brain function, such as increases in memory consolidation and synaptic rewiring during sleep (Kyriacou and Hastings, 2010). Synaptic plasticity must be supported during sleep, when consolidation of memories is hypothesized to preferentially occur (Kondratova and Kondratov, 2012). In line with this

hypothesis, circadian oscillations in signal transduction events underlying LTP in the hippocampus have previously been shown to peak during the day in young mice, and disruption of these rhythms results in impaired hippocampal-dependent memory (Eckel-Mahan et al., 2008). Thus, disruption of the temporal coordination of energy production, which supports these functions in the hippocampus, might contribute to age-related cognitive impairment.

The progressive functional deterioration that characterizes aging is a primary risk factor for various age-related disorders, including neurodegenerative diseases (Kondratova and Kondratov, 2012). Interestingly, sleep and circadian disturbances are shared clinical features of several neurodegenerative diseases, and a growing body of evidence indicates that disruption of circadian rhythms contributes directly to their pathogenesis (Kondratova and Kondratov, 2012; Musiek and Holtzman, 2016). Given that these disorders involve an exacerbation of aging-associated circadian dysfunction and hallmarks of aging (Mattson and Arumugam, 2018; Musiek and Holtzman, 2016), identifying changes in the daily cycles of biological functions in the brain during normal aging might contribute to a better understanding of the pathogenesis of these diseases. We found that proteins displaying age-related alterations in rhythmicity in the hippocampus of mice were involved in various hallmarks of aging, including mitochondrial dysfunction, genomic instability, epigenetic alterations, and loss of protein homeostasis. A recent study identified age-dependent changes in dynamics of the oxidative stress response in the hippocampus of aged mice (Lacoste et al., 2017), consistent with our results. We also found rhythmic hippocampal proteins involved in the pathogenesis of several aging-associated neurodegenerative diseases affecting the brain, indicating that age-related alterations in circadian regulation are associated with and might contribute to the pathogenesis of these diseases.

Age-dependent changes in the temporal regulation of proteins involved in local hippocampal clock function, such as proteins involved in regulating protein phosphorylation and turnover, provide novel potential mechanisms through which aging may be associated with alterations in physiological circadian rhythms. Additional studies are needed to characterize the effects of aging on the circadian rhythms of post-translational modifications of proteins, given that our results implicate enzymes regulating protein acetylation and phosphorylation in hallmarks of aging and age-related functional decline. This is plausible given that we and others have previously shown the relevance of rhythmic protein phosphorylation in the hippocampus of young mice (Chiang et al., 2017; Snider et al., 2018).

Our study represents the first large-scale proteomic analysis of aging in mammals from a circadian perspective, and our findings provide a framework for understanding the links between age-related cognitive decline, neurodegenerative disorders, and the circadian clock. Circadian disruption is associated with hippocampal-dependent memory impairment, and it is conceivable that aging-induced alterations in the circadian regulation of processes critical for hippocampal function could contribute to this decline. Our results build upon previous studies examining the circadian proteomes of brain, liver, and heart tissues from young mice (Millius and Ueda, 2017) and the circadian transcriptomes of various central and peripheral tissues from young mice (Zhang et al., 2014) and baboons (Mure et al., 2018). Furthermore, a growing number of recent studies are exploring the effects of aging (Sato et al., 2017), environmental and genetic circadian disruption (Archer et al., 2014; Martino and Young, 2015), and various diets (Sato et al., 2017; Tognini et al., 2017) on the circadian regulation of cellular functions in humans and mice. Our dataset may therefore also serve as a resource to the circadian biology community for future studies investigating the effects of environmental and genetic modifications or potential therapeutic interventions on hippocampal function in mammals.

DATA AVAILABILITY STATEMENT

The mass spectrometry proteomics data have been deposited to the ProteomeXchange Consortium via the PRIDE partner repository with the dataset identifier PXD013364.

ETHICS STATEMENT

The animal study was reviewed and approved by the University of Ottawa Animal Care Committee.

AUTHOR CONTRIBUTIONS

H-YC and DF conceived the study. C-KC, JM, ZN, XZ, BX, H-YC, and DF designed the study. PA, C-KC, JM, ZN, XZ, BX, and H-YC performed the experiments. PA, C-KC, ZN, and XZ analyzed the data. PA, JM, ZN, C-KC, XZ, BX, and DF interpreted the data. PA drafted the manuscript. All authors edited and approved the manuscript.

FUNDING

This work was supported by funding from the Canada Research Chair Program and from the University of Ottawa.

ACKNOWLEDGMENTS

DF acknowledges a Canada Research Chair in Proteomics and Systems Biology. PA acknowledges support from an Alzheimer Society of Canada Biomedical Doctoral Award. The authors thank Jasmine I. Moore for help with mouse colony maintenance and tissue collection.

SUPPLEMENTARY MATERIAL

The Supplementary Material for this article can be found online at: https://www.frontiersin.org/articles/10.3389/fnagi.2019.00368/full#supplementary-material

REFERENCES

Archer, S. N., Laing, E. E., Moller-Levet, C. S., van der Veen, D. R., Bucca, G., Lazar, A. S., et al. (2014). Mistimed sleep disrupts circadian regulation of the human transcriptome. *Proc. Natl. Acad. Sci. U.S.A.* 111, E682–E691. doi: 10.1073/pnas.1316335111

Bass, J., and Lazar, M. A. (2016). Circadian time signatures of fitness and disease. *Science* 354, 994–999. doi: 10.1126/science.aah4965

Bellesi, M., Haswell, J. D., de Vivo, L., Marshall, W., Roseboom, P. H., Tononi, G., et al. (2018). Myelin modifications after chronic sleep loss in adolescent mice. *Sleep* 41, zsy034. doi: 10.1093/sleep/zsy034

Bellesi, M., Pfister-Genskow, M., Maret, S., Keles, S., Tononi, G., and Cirelli, C. (2013). Effects of sleep and wake on oligodendrocytes and their precursors. *J. Neurosci.* 33, 14288–14300. doi: 10.1523/JNEUROSCI.5102-12.2013

Besing, R. C., Rogers, C. O., Paul, J. R., Hablitz, L. M., Johnson, R. L., McMahon, L. L., et al. (2017). GSK3 activity regulates rhythms in hippocampal clock gene expression and synaptic plasticity. *Hippocampus* 27, 890–898. doi: 10.1002/hipo.22739

Camandola, S., and Mattson, M. P. (2017). Brain metabolism in health, aging, and neurodegeneration. *EMBO J.* 36, 1474–1492. doi: 10.15252/embj.201695810

Camicioli, R., Moore, M. M., Kinney, A., Corbridge, E., Glassberg, K., and Kaye, J. A. (2003). Parkinson's disease is associated with hippocampal atrophy. *Mov. Disord.* 18, 784–790. doi: 10.1002/mds.10444

Chaix, A., Zarrinpar, A., and Panda, S. (2016). The circadian coordination of cell biology. *J. Cell Biol.* 215, 15–25. doi: 10.1083/jcb.201603076

Chen, C. Y., Logan, R. W., Ma, T., Lewis, D. A., Tseng, G. C., Sibille, E., et al. (2016). Effects of aging on circadian patterns of gene expression in the human prefrontal cortex. *Proc. Natl. Acad. Sci. U.S.A.* 113, 206–211. doi: 10.1073/pnas.1508249112

Chiang, C. K., Mehta, N., Patel, A., Zhang, P., Ning, Z., Mayne, J., et al. (2014). The proteomic landscape of the suprachiasmatic nucleus clock reveals large-scale coordination of key biological processes. *PLoS Genet.* 10:e1004695. doi: 10.1371/journal.pgen.1004695

Chiang, C. K., Xu, B., Mehta, N., Mayne, J., Sun, W. Y., Cheng, K., et al. (2017). Phosphoproteome profiling reveals circadian clock regulation of posttranslational modifications in the murine hippocampus. *Front. Neurol.* 8:110. doi: 10.3389/fneur.2017.00110

Dai, R. M., and Li, C. C. (2001). Valosin-containing protein is a multi-ubiquitin chain-targeting factor required in ubiquitin-proteasome degradation. *Nat. Cell Biol.* 3, 740–744. doi: 10.1038/35087056

Deery, M. J., Maywood, E. S., Chesham, J. E., Sladek, M., Karp, N. A., Green, E. W., et al. (2009). Proteomic analysis reveals the role of synaptic vesicle cycling in sustaining the suprachiasmatic circadian clock. *Curr. Biol.* 19, 2031–2036. doi: 10.1016/j.cub.2009.10.024

Dibner, C., Schibler, U., and Albrecht, U. (2010). The mammalian circadian timing system: organization and coordination of central and peripheral clocks. *Annu. Rev. Physiol.* 72, 517–549. doi: 10.1146/annurev-physiol-021909-135821

Eckel-Mahan, K. L., Phan, T., Han, S., Wang, H., Chan, G. C., Scheiner, Z. S., et al. (2008). Circadian oscillation of hippocampal MAPK activity and cAmp: implications for memory persistence. *Nat. Neurosci.* 11, 1074–1082. doi: 10.1038/nn.2174

Fonseca Costa, S. S., and Ripperger, J. A. (2015). Impact of the circadian clock on the aging process. *Front. Neurol.* 6:43. doi: 10.3389/fneur.2015.00043

Gordon-Weeks, P. R., and Fournier, A. E. (2014). Neuronal cytoskeleton in synaptic plasticity and regeneration. *J. Neurochem.* 129, 206–212. doi: 10.1111/jnc.12502

Greco, C. M., and Sassone-Corsi, P. (2019). Circadian blueprint of metabolic pathways in the brain. *Nat. Rev. Neurosci.* 20, 71–82. doi: 10.1038/s41583-018-0096-y

Green, D. R., Galluzzi, L., and Kroemer, G. (2011). Mitochondria and the autophagy-inflammation-cell death axis in organismal aging. *Science* 333, 1109–1112. doi: 10.1126/science.1201940

Hannou, L., Roy, P. G., Ballester Roig, M. N., and Mongrain, V. (2018). Transcriptional control of synaptic components by the clock machinery. *Eur. J. Neurosci.* [Epub ahead of print]. doi: 10.1111/ejn.14294

Hatanaka, F., Ocampo, A., and Izpisua Belmonte, J. C. (2017). Keeping the rhythm while changing the lyrics: circadian biology in aging. *Cell* 170, 599–600. doi: 10.1016/j.cell.2017.07.039

Hood, S., and Amir, S. (2017). The aging clock: circadian rhythms and later life. *J. Clin. Invest.* 127, 437–446. doi: 10.1172/JCI90328

Hughes, M. E., Abruzzi, K. C., Allada, R., Anafi, R., Arpat, A. B., Asher, G., et al. (2017). Guidelines for genome-scale analysis of biological rhythms. *J. Biol. Rhythms* 32, 380–393. doi: 10.1177/0748730417728663

Kon, N., Yoshikawa, T., Honma, S., Yamagata, Y., Yoshitane, H., Shimizu, K., et al. (2014). CaMKII is essential for the cellular clock and coupling between morning and evening behavioral rhythms. *Genes Dev.* 28, 1101–1110. doi: 10.1101/gad.237511.114

Kondratov, R. V. (2007). A role of the circadian system and circadian proteins in aging. *Ageing Res. Rev.* 6, 12–27. doi: 10.1016/j.arr.2007.02.003

Kondratova, A. A., and Kondratov, R. V. (2012). The circadian clock and pathology of the ageing brain. *Nat. Rev. Neurosci.* 13, 325–335. doi: 10.1038/nrn3208

Kuintzle, R. C., Chow, E. S., Westby, T. N., Gvakharia, B. O., Giebultowicz, J. M., and Hendrix, D. A. (2017). Circadian deep sequencing reveals stress-response genes that adopt robust rhythmic expression during aging. *Nat. Commun.* 8:14529. doi: 10.1038/ncomms14529

Kwapis, J. L., Alaghband, Y., Kramar, E. A., Lopez, A. J., Vogel Ciernia, A., White, A. O., et al. (2018). Epigenetic regulation of the circadian gene Per1 contributes to age-related changes in hippocampal memory. *Nat. Commun.* 9:3323. doi: 10.1038/s41467-018-05868-0

Kyriacou, C. P., and Hastings, M. H. (2010). Circadian clocks: genes, sleep, and cognition. *Trends Cogn. Sci.* 14, 259–267. doi: 10.1016/j.tics.2010.03.007

Laakso, M. P., Frisoni, G. B., Kononen, M., Mikkonen, M., Beltramello, A., Geroldi, C., et al. (2000). Hippocampus and entorhinal cortex in frontotemporal dementia and Alzheimer's disease: a morphometric MRI study. *Biol. Psychiatry* 47, 1056–1063. doi: 10.1016/s0006-3223(99)00306-6

Lacoste, M. G., Ponce, I. T., Golini, R. L., Delgado, S. M., and Anzulovich, A. C. (2017). Aging modifies daily variation of antioxidant enzymes and oxidative status in the hippocampus. *Exp. Gerontol.* 88, 42–50. doi: 10.1016/j.exger.2016.12.002

Levy, M., Faas, G. C., Saggau, P., Craigen, W. J., and Sweatt, J. D. (2003). Mitochondrial regulation of synaptic plasticity in the hippocampus. *J. Biol. Chem.* 278, 17727–17734. doi: 10.1074/jbc.M212878200

Liu, A. C., Lewis, W. G., and Kay, S. A. (2007). Mammalian circadian signaling networks and therapeutic targets. *Nat. Chem. Biol.* 3, 630–639. doi: 10.1038/nchembio.2007.37

Lopez-Otin, C., Blasco, M. A., Partridge, L., Serrano, M., and Kroemer, G. (2013). The hallmarks of aging. *Cell* 153, 1194–1217. doi: 10.1016/j.cell.2013.05.039

Ma, T. J., Zhang, Z. W., Lu, Y. L., Zhang, Y. Y., Tao, D. C., Liu, Y. Q., et al. (2018). CLOCK and BMAL1 stabilize and activate RHOA to promote F-actin formation in cancer cells. *Exp. Mol. Med.* 50:130. doi: 10.1038/s12276-018-0156-4

Mackenzie, I. R., and Rademakers, R. (2008). The role of transactive response DNA-binding protein-43 in amyotrophic lateral sclerosis and frontotemporal dementia. *Curr. Opin. Neurol.* 21, 693–700. doi: 10.1097/WCO.0b013e3283168d1d

Martino, T. A., and Young, M. E. (2015). Influence of the cardiomyocyte circadian clock on cardiac physiology and pathophysiology. *J. Biol. Rhythms* 30, 183–205. doi: 10.1177/0748730415575246

Matsumoto, Y., Tsunekawa, Y., Nomura, T., Suto, F., Matsumata, M., Tsuchiya, S., et al. (2011). Differential proliferation rhythm of neural progenitor and oligodendrocyte precursor cells in the young adult hippocampus. *PLoS One* 6:e27628. doi: 10.1371/journal.pone.0027628

Mattson, M. P., and Arumugam, T. V. (2018). Hallmarks of brain aging: adaptive and pathological modification by metabolic states. *Cell Metab.* 27, 1176–1199. doi: 10.1016/j.cmet.2018.05.011

Mauvoisin, D., Wang, J., Jouffe, C., Martin, E., Atger, F., Waridel, P., et al. (2014). Circadian clock-dependent and -independent rhythmic proteomes implement distinct diurnal functions in mouse liver. *Proc. Natl. Acad. Sci. U.S.A.* 111, 167–172. doi: 10.1073/pnas.1314066111

Millecamps, S., Salachas, F., Cazeneuve, C., Gordon, P., Bricka, B., Camuzat, A., et al. (2010). SOD1, ANG, VAPB, TARDBP, and FUS mutations in familial amyotrophic lateral sclerosis: genotype-phenotype correlations. *J. Med. Genet.* 47, 554–560. doi: 10.1136/jmg.2010.077180

Millius, A., and Ueda, H. R. (2017). Systems biology-derived discoveries of intrinsic clocks. *Front. Neurol.* 8:25. doi: 10.3389/fneur.2017.00025

Mure, L. S., Le, H. D., Benegiamo, G., Chang, M. W., Rios, L., Jillani, N., et al. (2018). Diurnal transcriptome atlas of a primate across major neural and peripheral tissues. *Science* 359:eaao0318. doi: 10.1126/science.aao0318

Musiek, E. S., and Holtzman, D. M. (2016). Mechanisms linking circadian clocks, sleep, and neurodegeneration. *Science* 354, 1004–1008. doi: 10.1126/science.aah4968

Neufeld-Cohen, A., Robles, M. S., Aviram, R., Manella, G., Adamovich, Y., Ladeuix, B., et al. (2016). Circadian control of oscillations in mitochondrial rate-limiting enzymes and nutrient utilization by PERIOD proteins. *Proc. Natl. Acad. Sci. U.S.A.* 113, E1673–E1682. doi: 10.1073/pnas.1519650113

Panda, S., Antoch, M. P., Miller, B. H., Su, A. I., Schook, A. B., Straume, M., et al. (2002). Coordinated transcription of key pathways in the mouse by the circadian clock. *Cell* 109, 307–320. doi: 10.1016/s0092-8674(02)00722-5

Peek, C. B., Affinati, A. H., Ramsey, K. M., Kuo, H. Y., Yu, W., Sena, L. A., et al. (2013). Circadian clock NAD+ cycle drives mitochondrial oxidative metabolism in mice. *Science* 342:1243417. doi: 10.1126/science.1243417

Pridgeon, J. W., Olzmann, J. A., Chin, L. S., and Li, L. (2007). PINK1 protects against oxidative stress by phosphorylating mitochondrial chaperone TRAP1. *PLoS Biol.* 5:e172. doi: 10.1371/journal.pbio.0050172

Rangaraju, V., Calloway, N., and Ryan, T. A. (2014). Activity-driven local ATP synthesis is required for synaptic function. *Cell* 156, 825–835. doi: 10.1016/j.cell.2013.12.042

Rawashdeh, O., Parsons, R., and Maronde, E. (2018). Clocking in time to gate memory processes: the circadian clock is part of the ins and outs of memory. *Neural Plast.* 2018:6238989. doi: 10.1155/2018/6238989

Reischl, S., and Kramer, A. (2011). Kinases and phosphatases in the mammalian circadian clock. *FEBS Lett.* 585, 1393–1399. doi: 10.1016/j.febslet.2011.02.038

Robles, M. S., Cox, J., and Mann, M. (2014). In-vivo quantitative proteomics reveals a key contribution of post-transcriptional mechanisms to the circadian regulation of liver metabolism. *PLoS Genet.* 10:e1004047. doi: 10.1371/journal.pgen.1004047

Sato, S., Solanas, G., Peixoto, F. O., Bee, L., Symeonidi, A., Schmidt, M. S., et al. (2017). Circadian reprogramming in the liver identifies metabolic pathways of aging. *Cell* 170, 664.e11–677.e11. doi: 10.1016/j.cell.2017.07.042

Shoji, H., Takao, K., Hattori, S., and Miyakawa, T. (2016). Age-related changes in behavior in C57BL/6J mice from young adulthood to middle age. *Mol. Brain* 9:11. doi: 10.1186/s13041-016-0191-9

Smarr, B. L., Jennings, K. J., Driscoll, J. R., and Kriegsfeld, L. J. (2014). A time to remember: the role of circadian clocks in learning and memory. *Behav. Neurosci.* 128, 283–303. doi: 10.1037/a0035963

Snider, K. H., Sullivan, K. A., and Obrietan, K. (2018). Circadian regulation of hippocampal-dependent memory: circuits, synapses, and molecular mechanisms. *Neural Plast.* 2018:7292540. doi: 10.1155/2018/7292540

Solanas, G., Peixoto, F. O., Perdiguero, E., Jardi, M., Ruiz-Bonilla, V., Datta, D., et al. (2017). Aged stem cells reprogram their daily rhythmic functions to adapt to stress. *Cell* 170, 678.e20–692.e20. doi: 10.1016/j.cell.2017.07.035

Spargo, E., Everall, I. P., and Lantos, P. L. (1993). Neuronal loss in the hippocampus in Huntington's disease: a comparison with HIV infection. *J. Neurol. Neurosurg. Psychiatry* 56, 487–491. doi: 10.1136/jnnp.56.5.487

Szklarczyk, D., Franceschini, A., Wyder, S., Forslund, K., Heller, D., Huerta-Cepas, J., et al. (2015). STRING v10: protein-protein interaction networks, integrated over the tree of life. *Nucleic Acids Res.* 43, D447–D452. doi: 10.1093/nar/gku1003

Takahashi, J. S. (2017). Transcriptional architecture of the mammalian circadian clock. *Nat. Rev. Genet.* 18, 164–179. doi: 10.1038/nrg.2016.150

Takeda, T., Uchihara, T., Arai, N., Mizutani, T., and Iwata, M. (2009). Progression of hippocampal degeneration in amyotrophic lateral sclerosis with or without memory impairment: distinction from Alzheimer disease. *Acta Neuropathol.* 117, 35–44. doi: 10.1007/s00401-008-0447-2

Tognini, P., Murakami, M., Liu, Y., Eckel-Mahan, K. L., Newman, J. C., Verdin, E., et al. (2017). Distinct circadian signatures in liver and gut clocks revealed by ketogenic diet. *Cell Metab.* 26, 523.e5–538.e5. doi: 10.1016/j.cmet.2017.08.015

Wang, J., Mauvoisin, D., Martin, E., Atger, F., Galindo, A. N., Dayon, L., et al. (2017). Nuclear proteomics uncovers diurnal regulatory landscapes in mouse liver. *Cell Metab.* 25, 102–117. doi: 10.1016/j.cmet.2016.10.003

Zhang, R., Lahens, N. F., Ballance, H. I., Hughes, M. E., and Hogenesch, J. B. (2014). A circadian gene expression atlas in mammals: implications for biology and medicine. *Proc. Natl. Acad. Sci. U.S.A.* 111, 16219–16224. doi: 10.1073/pnas.1408886111

Conflict of Interest: The authors declare that the research was conducted in the absence of any commercial or financial relationships that could be construed as a potential conflict of interest.

frontiers in Aging Neuroscience

REVIEW
published: 21 January 2020
doi: 10.3389/fnagi.2019.00367

Functional Near-Infrared Spectroscopy to Study Cerebral Hemodynamics in Older Adults During Cognitive and Motor Tasks: A Review

Cristina Udina[1,2,3], Stella Avtzi[4], Turgut Durduran[4,5], Roee Holtzer[6,7], Andrea L. Rosso[8], Carmina Castellano-Tejedor[1,2,3], Laura-Monica Perez[1,2], Luis Soto-Bagaria[1,2] and Marco Inzitari[1,2,3]*

[1] Parc Sanitari Pere Virgili, Barcelona, Spain, [2] RE-FiT Barcelona Research Group, Vall d'Hebrón Institute of Research, Barcelona, Spain, [3] Department of Medicine, Universitat Autònoma de Barcelona, Barcelona, Spain, [4] Institut de Ciències Fotòniques, The Barcelona Institute of Science and Technology, Barcelona, Spain, [5] Institució Catalana de Recerca i Estudis Avançats, Barcelona, Spain, [6] Ferkauf Graduate School of Psychology, Yeshiva University, New York, NY, United States, [7] Department of Neurology, Albert Einstein College of Medicine, New York, NY, United States, [8] Department of Epidemiology, Graduate School of Public Health, University of Pittsburgh, Pittsburgh, PA, United States

The integrity of the frontal areas of the brain, specifically the prefrontal cortex, are critical to preserve cognition and mobility in late life. Prefrontal cortex regions are involved in executive functions and gait control and have been related to the performance of dual-tasks. Dual-task performance assessment may help identify older adults at risk of negative health outcomes. As an alternative to neuroimaging techniques that do not allow assessment during actual motion, functional Near-Infrared Spectroscopy (fNIRS) is a non-invasive technique that can assess neural activation through the measurement of cortical oxygenated and deoxygenated hemoglobin levels, while the person is performing a motor task in a natural environment as well as during cognitive tasks. The aim of this review was to describe the use of fNIRS to study frontal lobe hemodynamics during cognitive, motor and dual-tasks in older adults. From the 46 included publications, 20 studies used only cognitive tasks, three studies used motor tasks and 23 used dual-tasks. Our findings suggest that fNIRS detects changes in frontal activation in older adults (cognitively healthy and mild cognitive impairment), especially while performing cognitive and dual-tasks. In both the comparison between older and younger adults, and in people with different neurological conditions, compared to healthier controls, the prefrontal cortex seems to experience a higher activation, which could be interpreted in the context of proposed neural inefficiency and limited capacity models. Further research is needed to establish standardized fNIRS protocols, study the cerebral hemodynamic in different neurological and systemic conditions that might influence cortical activation and explore its role in predicting incident health outcomes such as dementia.

Keywords: functional Near-Infrared Spectroscopy, gait, dual task, motor task, cognition, older adults, prefrontal cortex, cerebral hemodynamics

OPEN ACCESS

Edited by:
Hans J. Grabe,
University of Greifswald, Germany

Reviewed by:
Dafin F. Muresanu,
Iuliu Haţieganu University of Medicine and Pharmacy, Romania
Sarah Anne Fraser,
University of Ottawa, Canada

****Correspondence:***
Cristina Udina
cudina@perevirgili.cat

Received: *20 June 2019*
Accepted: *16 December 2019*
Published: *21 January 2020*

Citation:
Udina C, Avtzi S, Durduran T, Holtzer R, Rosso AL, Castellano-Tejedor C, Perez L-M, Soto-Bagaria L and Inzitari M (2020) Functional Near-Infrared Spectroscopy to Study Cerebral Hemodynamics in Older Adults During Cognitive and Motor Tasks: A Review. Front. Aging Neurosci. 11:367. doi: 10.3389/fnagi.2019.00367

INTRODUCTION

The worldwide aging of the population makes tackling aging-associated disability an urgent priority. Cognitive impairment and mobility disability are key contributors to dementia and loss of independence in the activities of daily living and have a synergistic effect (Verghese et al., 2014). The integrity of the frontal areas of the brain, specifically the PFC, are critical to preserve cognition and mobility in late life (Beauchet et al., 2016). PFC regions carry out executive functions, i.e., higher order cognitive functions essential to plan and execute complex goal-directed actions, which are also key for motor control in older adults (Inzitari et al., 2007). The loss of integrity in frontal or prefrontal regions, either due to neurodegeneration, cerebrovascular disease or due to their interactions, contributes to the development of dementia (Burgmans et al., 2009; Kisler et al., 2017) and mobility impairments (De Laat et al., 2011). The PFC has also been implicated in performance of DT (Sala et al., 1995; Dux et al., 2006; Filmer et al., 2013), that are motor tasks performed simultaneously with a secondary, usually a cognitive task. DT increases the cognitive demand of walking and potentially results in a decrease in task performance in one or both tasks relative to when the tasks are performed separately as ST. DT performance assessment may help identify older adults at higher risk of incident cognitive decline (Ceïde et al., 2018; Rosso et al., 2019), disability, frailty and mortality (Verghese et al., 2012). One of the goals of the study of cognitive aging is to elucidate neural mechanisms that underlie the ability of the aging brain to cope with decline in cognitive functions and efficiency. Several hypothesis have been described and there is still no consensus regarding definitions of several concepts (Cabeza et al., 2018). Two of the previously described hyphotheses are: the "neural inefficiency hypothesis" (Rypma and D'Esposito, 2000; Holtzer et al., 2009) or "compensation by upregulation" (Cabeza et al., 2018), according to which older adults show increased activity of the same networks recruited by younger counterparts in order to meet behavioral demands, and the "capacity limitation hypothesis" (Cabeza, 2004; Holtzer et al., 2009) which postulates that older adults, while recruiting the same brain networks as young adults, would show a reduced activation compared to their younger counterparts (Holtzer et al., 2009; Stern, 2009).

Classic clinical and epidemiological studies have based their assessment of PFC on a static, structural basis, mainly through magnetic resonance imaging (MRI) techniques, which have shown a contribution of both cortical frontal and PFC volumes (Rosano et al., 2008; Weinstein et al., 2012) and subcortical alterations to executive dysfunction/dementia (Jokinen et al., 2009) and mobility limitations (Baezner et al., 2008). In addition, functional neuroimaging techniques, such as functional MRI (fMRI), allow the study of PFC by assessing the hemodynamic changes due to neurovascular coupling that are triggered by its neural activation (Buchbinder, 2016). fMRI studies assess whole brain function with a relatively high spatial resolution, are non-invasive and the most used technique to date to assess neural activity during specific task activation (Rosen and Savoy, 2012). Several fMRI studies have demonstrated the relevance of PFC for executive functions (Wager et al., 2004; Venkatraman et al., 2010; Yaple et al., 2019) and DT (Szameitat et al., 2002; Dux et al., 2006; Jurado and Rosselli, 2007). Limitations of both MRI and fMRI include their relatively high cost, unsuitability for many older adults due to metal implants in the body, claustrophobia or inability to lie still for long periods. Further, due to the nature of the scanner, the tasks are carried out in unnatural environments which may alter their relevance to the real-world and do not allow functional analysis of brain activity during locomotion. Imagined gait has been used as a way to study the neural correlates of locomotion with fMRI (Zwergal et al., 2012; Blumen et al., 2014); however, it is not entirely clear how well this mimics brain activation during actual walking. Other options, although they do not allow online assessment of gait either, include PET studies after walk trials with administration of fludeoxyglucose-18 tracer (la Fougère et al., 2010). We refer the reader to Holtzer et al. (2014) for a comprehensive review on neuroimaging of locomotion in aging.

Emerging alternatives to fMRI, based on near-infrared diffuse optical techniques, allow measurements in more realistic environments and during motion (Boas et al., 2014; Scholkmann et al., 2014). Accumulating evidence supports the use of these techniques for the study of frontal hemodynamic and metabolic changes (Agbangla et al., 2017; Gramigna et al., 2017). These diffuse optical techniques such as fNIRS (Durduran et al., 2010; Ferrari and Quaresima, 2012) allow the study of tissue composition by emitting near-infrared light (∼650–950 nm) into biological tissue and collecting the photons that undergo multiple scattering and absorption (i.e., diffuse) and emerge few centimeters away from the injection point (Delpy and Cope, 1997; Durduran et al., 2010). At these wavelengths the main absorbers in tissues, i.e., O_2Hb and HHb, differentially absorb light in a wavelength dependent manner. Therefore, most common fNIRS methods can relate changes in the detected light intensity at different wavelengths to changes in oxygenated and deoxygenated hemoglobin concentrations by utilizing the modified Beer-Lambert law (Scholkmann et al., 2014). This is a signal similar to the blood oxygen level dependent (BOLD) signal from fMRI but can be obtained by portable (even wearable) instrumentation and flexible fiber-optic probes. The majority of the systems are using source and detector probes placed on the scalp of the head. The most common source-detector separations are of few centimeters. Able to detect signal coming from superficial cortical layers (Ferrari and Quaresima, 2012), fNIRS measurement is based on the neurovascular coupling (oxygen consumption to meet energy demands in activated cerebral areas cause an increase in blood flow resulting in an increase of O_2Hb and decrease of HHb) and both the analysis and acquisition methods are still being developed with O_2Hb changes appearing more reliable as a marker of brain activation since it has shown high reproducibility and stability over time (Plichta et al., 2006) and has the highest correlation to fMRI BOLD measures (Strangman et al., 2002). fNIRS studies usually

Abbreviations: AD, Alzheimer's disease; DT, dual-task; fNIRS, Functional Near-Infrared Spectroscopy; HHb, deoxygenated hemoglobin; MCI, mild cognitive impairment; NGA, Neurological Gait Abnormalities; O_2Hb, oxygenated hemoglobin; PD, Parkinson's disease; PFC, prefrontal cortex; ST, single task; VF, verbal fluency.

consist of a combination of resting periods, to assess baseline brain activity, and different kinds of tasks. Brain activation is then calculated by comparing hemoglobin measurements at baseline and during the task, although there is a high heterogeneity in data processing and analysis methods. Regarding its advantages, fNIRS is a lower cost modality than fMRI, usable at point-of-care, and allows measurements during mobility tasks. These advantatges allow the potential use of the technique to assess cerebral blood flow and oxygenation with application in different pathologies (e.g., stroke, psychiatric disorders,. . .) resulting thus in continuous growth on relevant literature (Noda et al., 2017; Giacalone et al., 2019). However, the main limitations of most fNIRS devices include: (i) the limited penetration depth, allowing only the interrogation of superficial layers of the cortex in the adult brain, (ii) the assessment of a limited portion of the cortical surface with often a low spatial resolution with the probes that are attached to the scalp, not allowing complete whole-brain imaging, (iii) issues with extracerebral contamination from superficial tissues (i.e., cutaneous or skull perfusion) and (iv) motion artifacts.

Recent studies have expanded the use of fNIRS in the assessment of PFC of older adults during cognitive or motor tests (Verghese et al., 2017). These studies show changes in PFC hemodynamics during the execution of cognitive or motor tasks, and also report differences according to the person's age and cognitive function. However, these findings are still preliminary and it is not yet clear if there is a specific pattern according to age or cognitive status, nor about how these differences should be interpreted. Recently published reviews have assessed the results of studies on fNIRS during cognitive tasks (Herold et al., 2018) or dual tasks (Gramigna et al., 2017; Herold et al., 2017; Leone et al., 2017; Vitorio et al., 2017; Stuart et al., 2018; Kahya et al., 2019) and some of them have chosen to focus on specific clinical profiles (Gramigna et al., 2017; Vitorio et al., 2017) or on methodological aspects such as fNIRS signal processing (Herold et al., 2017, 2018; Vitorio et al., 2017). To the best of our knowledge, our review is the first to focus specifically on older adults regardless of their clinical profile and to assess, from a clinical point of view, studies using only cognitive or motor tasks, as well as DTs.

The aim of this review is to describe, through an updated literature search, the use of optical techniques, specifically fNIRS, to study brain hemodynamics, with a focus on frontal regions, in relation to cognitive and physical function in normal and pathological older adult populations.

METHODS

This is a narrative review. We performed, however, a search using pre-set criteria, to make sure that we considered all the relevant articles on the topic. We included manuscripts that have aimed to study frontal and prefrontal lobe hemodynamics (excluding those focusing on other brain regions) using fNIRS to measure oxygenated and deoxygenated hemoglobin levels during cognitive, motor and DTs in older adults. Articles were included if the mean age of the sample or a separately analyzed subgroup was 60 years or older. Review articles, studies assessing change in cerebral hemodynamics after an intervention, those not written in English and those that do not describe the age of the participants in the manuscript were excluded. In order to focus on most recent literature, we limited the publication date to the previous 5 years. The last search was performed on August 29th, 2018.

The article selection was performed in three phases (review of titles, abstracts, and full-texts). Two independent reviewers (CU and MI) reviewed the titles and abstracts resulting from the search, in order to assess potential inclusion. From the selected articles, we performed a full manuscript review to assess if the article met the eligibility criteria. Discrepancies were solved through consensus.

RESULTS

General Description

As depicted in the flow-chart (**Figure 1**), after removing duplicates, our search resulted in 134 items. After excluding records by title and abstract screening (n = 46), 89 full-text articles were assessed for eligibility. Studies not meeting the above described eligibility criteria such as sample/subgroup mean age (n = 19), the aim/topic focus of our review (n = 6) (i.e., use of NIRS to monitor cancer treatment), methodological aspects of the design of studies (n = 6) (i.e., different location of the probes or NIRS measures performed to assess the effect of an intervention) and review articles (n = 11), were excluded. We finally included 46 articles in our review.

Of the 46 included articles, 13 included a mix of younger and older participants (Heilbronner and Münte, 2013; Ohsugi et al., 2013; Beurskens et al., 2014; Müller et al., 2014; Oboshi et al., 2014; Hernandez et al., 2016; Bierre et al., 2017; Mirelman et al., 2017; Rosso et al., 2017; Hawkins et al., 2018) whereas 29 included only older adults (Doi et al., 2013; Heinzel et al., 2013, 2015; Niu et al., 2013; Clark et al., 2014; Vermeij et al., 2014; Dupuy et al., 2015; Holtzer et al., 2015, 2016, 2017a,b, 2018a,b; Laguë-Beauvais et al., 2015; Al-Yahya et al., 2016; Maidan et al., 2016, 2017; Mahoney et al., 2016; Nieuwhof et al., 2016; Osofundiya et al., 2016; Takeuchi et al., 2016; Uemura et al., 2016; Yeung et al., 2016a,b; Chen et al., 2017; Huppert et al., 2017; Verghese et al., 2017; Yap et al., 2017; Halliday et al., 2018; Katzorke et al., 2018; Lucas et al., 2018; Mori et al., 2018; Thumm et al., 2018). Moreover, 26 studies included only cognitively normal participants (Heilbronner and Münte, 2013; Heinzel et al., 2013, 2015; Ohsugi et al., 2013; Beurskens et al., 2014; Clark et al., 2014; Müller et al., 2014; Oboshi et al., 2014; Vermeij et al., 2014; Holtzer et al., 2015, 2016, 2017a,b, 2018a,b; Osofundiya et al., 2016; Bierre et al., 2017; Chen et al., 2017; Huppert et al., 2017; Mirelman et al., 2017; Rosso et al., 2017; Verghese et al., 2017; Halliday et al., 2018; Lucas et al., 2018), seven compared participants with different cognitive status [without cognitive impairment, with MCI or with mild AD] (Doi et al., 2013; Niu et al., 2013; Al-Yahya et al., 2016; Uemura et al., 2016; Yeung et al., 2016a,b; Yap et al., 2017; Katzorke et al., 2018), three studies focused on older adults with previous history of stroke (Al-Yahya et al., 2016; Hawkins et al., 2018; Mori et al., 2018), five assessed

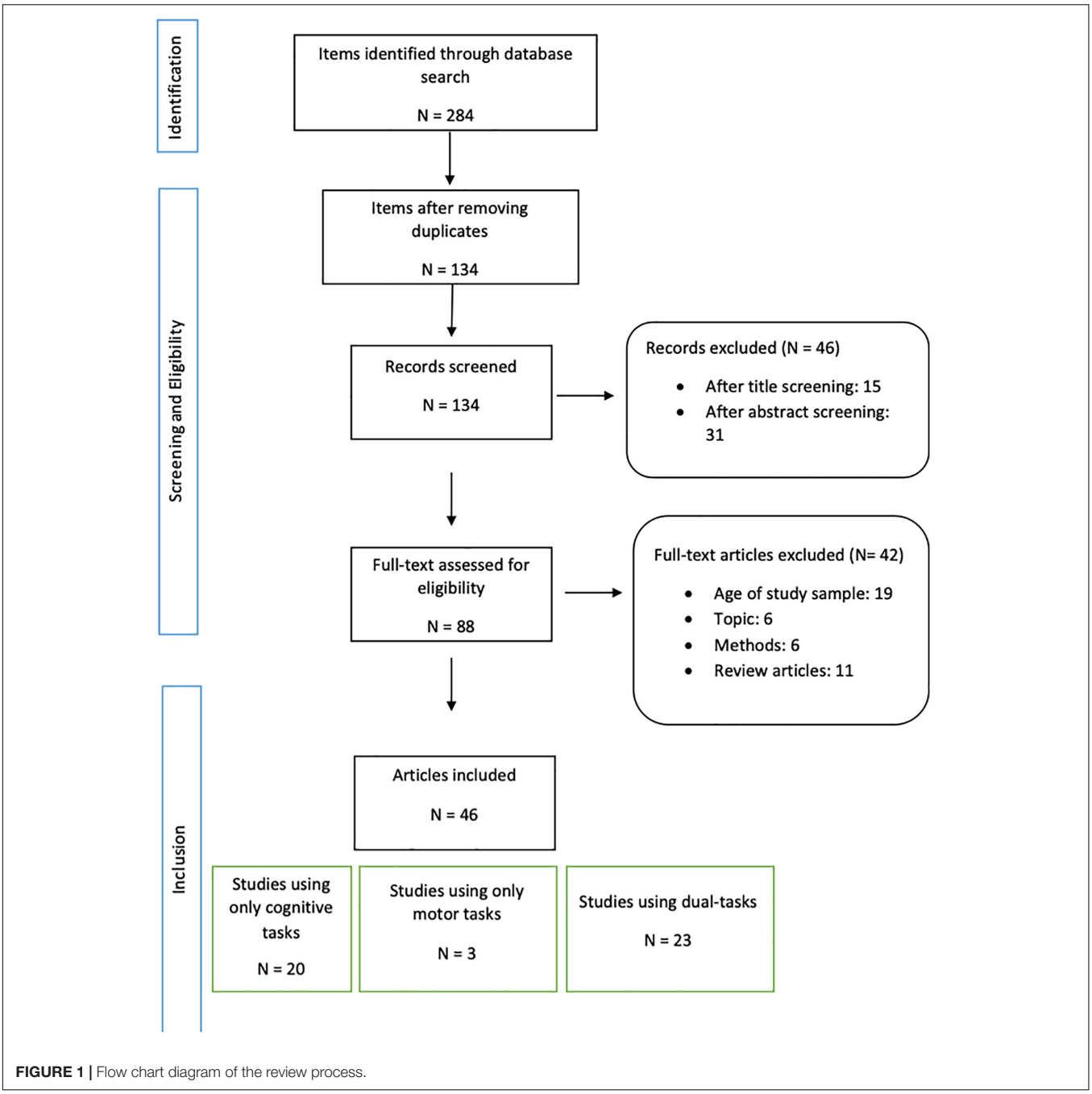

FIGURE 1 | Flow chart diagram of the review process.

patients with parkinsonian syndromes (Mahoney et al., 2016; Maidan et al., 2016, 2017; Nieuwhof et al., 2016; Thumm et al., 2018) and two with Multiple Sclerosis (Hernandez et al., 2016; Chaparro et al., 2017).

Looking at the older adults subgroups that were included in the studies, there was a wide range of mean ages, from 61 ± 4 (Hernandez et al., 2016) to 88.1 ± 6 (Huppert et al., 2017). The largest sample size was 1052 participants (Heinzel et al., 2015) while a sample of 12 older adults was the smallest (Nieuwhof et al., 2016). Most source populations were community-dwelling but two studies included older adults living in nursing home (Osofundiya et al., 2016; Huppert et al., 2017). Ten studies did not describe the participant setting (Niu et al., 2013; Oboshi et al., 2014; Al-Yahya et al., 2016; Uemura et al., 2016; Maidan et al., 2017; Mirelman et al., 2017; Rosso et al., 2017; Katzorke et al., 2018; Mori et al., 2018; Thumm et al., 2018).

The majority, 29 studies, used O_2Hb to assess brain activation while nine studies (Heilbronner and Münte, 2013; Beurskens et al., 2014; Müller et al., 2014; Al-Yahya et al., 2016; Hyodo et al., 2016; Nieuwhof et al., 2016; Rosso et al., 2017; Halliday et al., 2018; Katzorke et al., 2018) used both O_2Hb and HHb and one used only Total Hb (Huppert et al., 2017). Two studies calculated

the Total Oxygenation Index (O_2Hb/Total Hb x 100) in order to assess brain hemodynamics (Clark et al., 2014; Bierre et al., 2017). In the following paragraphs, we will use the term activation to refer to changes in these hemoglobin indices.

Twenty-three studies measuring single cognitive or motor tasks performed intra-group comparisons of the cerebral activation during different tasks and the rest periods (see articles listed in **Tables 1**, **2A**), whereas the other 23 studies compared cerebral hemodynamics between single and DT (see articles listed in **Table 2B**). Twenty-four studies performed comparisons of cerebral activation patterns between different groups (either young vs. old, MCI vs. cognitively normal, healthy vs. stroke etc.) (Heilbronner and Münte, 2013; Niu et al., 2013; Ohsugi et al., 2013; Beurskens et al., 2014; Müller et al., 2014; Oboshi et al., 2014; Laguë-Beauvais et al., 2015; Al-Yahya et al., 2016; Hernandez et al., 2016; Maidan et al., 2016, 2017; Mahoney et al., 2016; Osofundiya et al., 2016; Takeuchi et al., 2016; Uemura et al., 2016; Yeung et al., 2016a,b; Bierre et al., 2017; Mirelman et al., 2017; Rosso et al., 2017; Yap et al., 2017; Hawkins et al., 2018; Katzorke et al., 2018; Mori et al., 2018).

Some studies, beyond assessing frontal hemodynamics, investigated the influence of other clinical characteristics in the reported frontal activation findings (Albinet et al., 2014; Dupuy et al., 2015; Hyodo et al., 2016; Osofundiya et al., 2016; Holtzer et al., 2016, 2017a,b, 2018a; Verghese et al., 2017; Halliday et al., 2018; Lucas et al., 2018) (see **Table 3**).

Studies Assessing the Effect of Cognitive Tasks

We found 20 articles assessing cerebral activation during cognitive tasks (**Table 1**). The most frequent cognitive task was VF (Heinzel et al., 2013, 2015; Yeung et al., 2016a; Yap et al., 2017; Katzorke et al., 2018). Generally, VF tests ask the participants to produce the maximum number of words starting with a specific letter (phonemic) or belonging to a pre-specified semantic category (semantic). Three studies used N-back tests (Niu et al., 2013; Vermeij et al., 2014; Yeung et al., 2016b), which assess working memory function. N-back tasks are usually designed as conditions with increasing working-memory load: 0-back (subject has to detect if the presented stimulus is the one described as target), 1-back (the subject has to remember if the presented stimulus was presented on the previous position) and 2-back conditions (the participant must be able to remember if the stimulus is the same presented 2 positions before). From the twelve remaining studies, eleven used different tests of executive functions (i.e., Stroop, symbol digit coding and shifting attention test, Go/No go inhibition task, Trail Making Test part B, etc.) (Heilbronner and Münte, 2013; Albinet et al., 2014; Müller et al., 2014; Oboshi et al., 2014; Dupuy et al., 2015; Laguë-Beauvais et al., 2015; Hyodo et al., 2016; Bierre et al., 2017; Huppert et al., 2017; Halliday et al., 2017, 2018) and one used an episodic memory task (Uemura et al., 2016).

Cognitively Healthy Older Adults

Regarding the studies that assessed frontal hemodynamics in cognitively healthy older adults, two studies by Heinzel et al. (2015) showed different activation patterns while performing VF tasks: one showed an increased activation and another found a decreased activation on bilateral inferior frontal junction in healthy older adults while middle frontal gyri and supramarginal gyri showed an increased activation (interpreted as compensatory mechanisms) (Heinzel et al., 2013). Cognitively healthy older adults showed an increased prefrontal activation while performing a working memory task with visual recognition (Oboshi et al., 2014) as well as with increasing working memory load during a N-back task (Vermeij et al., 2014). Studies using other executive function tests, found an increase in frontal lobe activation during executive function tasks (Heilbronner and Münte, 2013; Albinet et al., 2014; Müller et al., 2014; Bierre et al., 2017; Huppert et al., 2017). One study, instead of reporting only the mean values of O_2Hb, addressed the association between O_2Hb variability and behavioral results during an executive function task (Halliday et al., 2017). They reported that within-person O_2Hb variability was associated with better accuracy and faster performance but between-person variability was associated with slower performance.

Comparison of Healthy Old Versus Young Adults

Healthy older adults showed higher frontal activation than younger persons while performing a visuomotor task with increasing executive function demand (Bierre et al., 2017). Moreover, a different activation pattern during executive function tests between age groups was observed. According to Heilbronner and Münte (2013), in older adults, activation shifted rostrally on the left hemisphere and dorsally on the right hemisphere during the inhibition task, while Müller et al. (2014) reported an additional activation in left medial and lateral PFC during the TMT-B (while more ventral activation was evidenced in younger counterparts). The effect of prioritization of a stimulus was assessed in one study (Laguë-Beauvais et al., 2015) where the participants were asked to prioritize one of two stimuli displayed (priority block) or to give the same priority to both stimuli (equal block). A change in the activation pattern between the priority and equal conditions was found only in the older adults group, with a less lateralized pattern (bilateral dorsolateral PFC activation) when not prioritizing either stimuli.

Comparison by Cognitive Status

Regarding the studies assessing older adults with different cognitive status, three studies using VF tasks reported an increased activation during the task in MCI (Yeung et al., 2016a; Yap et al., 2017) and mild AD (Yap et al., 2017) while Katzorke et al. (2018) found a decreased activation during VF in MCI patients. Yap et al. (2017) compared the activation pattern in cognitively healthy older adults, MCI and mild AD and found the highest O_2Hb increase in MCI older adults followed by healthy and AD participants, although the difference was not statistically significant. Increasing working memory load led to lower frontal lobe activation during a N-back task in MCI, compared to healthy controls (Niu et al., 2013; Yeung et al., 2016b). Only one study measured PFC activation during encoding and retrieval of episodic memory, and it found a decreased activation on bilateral dorsolateral cortex during memory retrieval in amnestic MCI (Uemura et al., 2016).

Studies Assessing the Effect of Motor Tasks

All the studies that used isolated motor tasks in order to assess PFC hemodynamics (n = 3) enrolled older adults with parkinsonian syndromes but were heterogeneous regarding the motor tasks paradigm (**Table 2A**). The reported results were also heterogeneous. According to Mahoney et al. (2016), older adults with parkinsonian syndromes showed higher PFC activation while performing a postural control task (compared to participants with mild parkinsonian signs or without these). Participants with PD walking on a straight walkway showed an increased PFC activation, compared to the baseline, and a

TABLE 1 | Summary of the studies assessing fNIRS measures during cognitive tasks in older adults.

First author (Journal, year), Country	Sample size (N) Clinical characteristics of the sample (mean age ± SD) NIRS optodes localization	Paradigm description	Main fNIRS results
Verbal fluency			
Heinzel (Neurobiol Aging, 2013), Germany (Heinzel et al., 2013)	*N* = 325 Healthy (64.6 ± 7.3). Prefrontal, temporal and parietal.	Tasks: – Phonetic verbal fluency. – Semantic verbal fluency. – Control task: reciting week days. Three trials: 30 s each. Rest: 30 sec after each trial.	With increasing age: ⇓: Lower activation on bilateral inferior frontal junction during verbal fluency. Increased bilateral activation at middle frontal gyri and supramarginal gyri.
Heinzel (PLoS One 2015), Germany (Heinzel et al., 2015)	*N* = 1052 Healthy (65.2 ± 6.8). Prefrontal, parietal and fronto-temporal.	Tasks: – Phonetic verbal fluency. – Semantic verbal fluency. – Control task: reciting week days. Three trials: 30 s each. Rest: 30 sec after each trial.	⇑: Increased activation during both verbal fluencies (compared to control task). Stronger response in phonological than semantic (increased activation in right prefrontal and bilateral inferior parietal regions extending toward postcentral gyri and decreased in bilateral fronto-temporal areas).
Yeung (Front Aging Neurosci., 2016), China (Yeung et al., 2016a)	*N* = 52 MCI (69.1 ± 6.2); Healthy (68.8 ± 6.1). Prefrontal.	Tasks: – Semantic verbal fluency. Two task blocks, 60 s each. Rest: repeat "1, 2, 3, 4" out loud. Before and after VF task.	⇑: Increased O_2Hb bilaterally during verbal fluency in both groups. No significant group differences. Control group showed left lateralization of frontal lobe activation (whereas MCI group did not).
Yap (Front Aging Neurosci., 2017), Malaysia (Yap et al., 2017)	*N* = 61 Healthy (72.6 ± 8.5); MCI (73.1 ± 8.2); Mild AD (74.7 ± 10). Prefrontal and part of temporal.	Task: – Semantic verbal fluency (60 s). Rest: 20 s before and after task.	⇑: Highest O_2Hb increase during task was observed in MCI followed by healthy and mild AD.
Katzorke (Psychiatry Res Neuroimaging, 2018), Germany (Katzorke et al., 2018)	*N* = 110 Healthy (74.2 ± 1.6); MCI (74.0 ± 1.6). Fronto-temporal.	Tasks: – Letter verbal fluency. – Semantic verbal fluency. – Control (weekdays). Three trials per task: 30 sec each. Rest: 30 s after each task.	⇓: Decreased PFC activation during semantic verbal fluency in MCI compared to healthy controls (but not during phonological verbal fluency).
N-back tasks			
Niu (CNS Neurosci Ther., 2013), China (Niu et al., 2013)	*N* = 24 MCI (64.8 ± 7.2); healthy (63.5 ± 5.3). Frontal, parietal and temporal.	Task: – Digit N-back task (0-back and 1-back conditions). Three blocks in each condition: 20 trials for each block followed by 1000 ms interstimulus period. Rest: No rest time specified.	⇓: MCI participants showed lower O_2Hb concentrations in the left dorsolateral PFC, right supplementary motor area and left superior temporal regions compared to control group.
Vermeij (Front Aging Neurosci., 2014), Netherlands (Vermeij et al., 2014)	*N* = 18 Healthy older adults (70.8 ± 5.0). Prefrontal.	Task: – Spatial N-back (0-back, 1-back and 2-back conditions). 60 trials (500 ms each) with 3000 ms interval between trials. Rest: Initial 1 min-baseline (staring at screen).	⇑: Increased working-memory load associated increased prefrontal activation and decreased performance.

(Continued)

TABLE 1 | Continued

First author (Journal, year), Country	Sample size (N) Clinical characteristics of the sample (mean age ± SD) NIRS optodes localization	Paradigm description	Main fNIRS results
Yeung (Dement Geriatr Cogn Disord., 2016), China (Yeung et al., 2016b)	*N* = 52 MCI (69.1 ± 6.3); cognitively normal (68.8 ± 6.1). Frontal.	Task: – Digit N-back task (0-back and 2-back conditions). 20 trials (1000 ms each) followed by 1000 ms interval between trials. Rest: 30 s between blocks.	⇓: MCI group did not show frontal activation. Tended to reduce activation with high working memory load. ⇑: Control group: frontal activation in high working memory load (2-back condition).
Other tests for executive functions			
Heilbronner (Neuroimage, 2013), Germany (Heilbronner and Münte, 2013)	*N* = 35. Healthy older adults (68 ± 1.4); younger adults group (23.1 ± 0.4). Frontotemporal.	Task: – Cognitive Go/No Go inhibition task: Go stimulus: press button; No Go stimulus: inhibit pressing button. 1083 stimuli in 5 trials. Rest: Rest in a self-paced manner.	⇑: Older adults showed activation in frontal areas. Compared to young participants, activation shifted rostrally (left hemisphere) and dorsally (right hemisphere) in older adults.
*** Albinet** (Front Aging Neurosci., 2014), France (Albinet et al., 2014)	*N* = 40 Healthy old adults: high-fit (67.32 ± 4.48); low-fit (68.88 ± 3.87) Prefrontal	Task: – Random Number Generation: participants asked to say random number when heard a tone. Fast pace (tone/1 s) and slow pace (tone/1.5 s). Two trials of 100 responses at each pace. – Control: count in order from one to nine.	⇑: Increasing activation in relation to task difficulty. High-fit group showed greater increase in O_2Hb.
Müller (Neuropsychologia, 2014), Germany (Müller et al., 2014)	*N* = 40 Older adults (70.9 ± 3.5); younger adults (25.7 ± 3.0). PFC, motor and premotor regions.	Task: – Adapted version of Trail Making Test (TMT) A and B. – Control task: retrace 90 interconnected circles. Each test presented three times (30 s each). Rest: 30 s after each test.	⇑: Older adults showed bilateral ventrolateral and dorsolateral prefrontal and premotor cortex activation during TMT-B (more channels active in the right hemisphere). Additional activation in medial and lateral PFC in elderly (younger participants show more ventral PFC, especially in the left hemisphere).
Oboshi (PLoS One, 2014), Japan (Oboshi et al., 2014)	*N* = 120 Healthy older adults (71.0 ± 6.4); younger adults (21.7 ± 3.3). Prefrontal.	Task: – Visual working memory task. Six blocks (28.8 s each). Rest: 30 s.	⇑: Older adults: O_2Hb increase during working memory task. Young adults: Higher O_2Hb increase during pre-task (compared to elderly). Both groups: lower activation during pre-task is associated with higher O_2Hb change during working memory task.
*** Dupuy** (Front Hum Neurosci., 2015), Canada (Dupuy et al., 2015)	*N* = 58 Healthy older adults (62.9 ± 5.4); young adults (24.6 ± 3.6). Prefrontal.	Task: – Modified Stroop-task with two conditions: naming (identify the color of the ink); executive or incongruent (color of the ink not matching the color-word displayed). Four trial-blocks (60 s each). Rest: 60 s between blocks.	⇑: High-fit women showed increased activation in right inferior frontal gyrus (independent of age group).
*** Hyodo** (Neuroimage, 2015), Japan (Hyodo et al., 2016)	*N* = 60 Healthy older adults (70.3 ± 3.2). Prefrontal.	Task: – Modified Stroop-task: participants asked to decide if word is printed in the color written below the word (neutral and incongruent conditions). 60 trials (30 neutral and 30 incongruent trials). Rest: 9–13 s interstimulus interval.	Higher fitness levels and left-lateralized PFC activation related to shorter Stroop interference time. Higher fitness associated with more left-lateralized activation.

(Continued)

TABLE 1 | Continued

First author (Journal, year), Country	Sample size (N) Clinical characteristics of the sample (mean age ± SD) NIRS optodes localization	Paradigm description	Main fNIRS results
Laguë-Beauvais (Brain and Cognition, 2015), Canada (Laguë-Beauvais et al., 2015)	*N* = 35 Healthy older adults (63.47 ± 3.67); young adults (23.94 ± 2.32). Prefrontal.	Task: – Color task: identify color of an "X" on screen (by typing on keyboard). – Letter task: identify "K" or "L" on screen (by typing on keyboard). • Conditions: – Single pure: only an "X" or letter is displayed to perform one of the tasks. – Dual mixed: both an "X" and a letter are displayed and have to be answered. These are performed under the instruction to prioritize the letter over the color task (Priority Block) or to give the same priority to both tasks (Equal Block). Rest: staring at fixation cross on screen (1000 ms).	Priority condition: – Older adults: activation in the left dorsolateral prefrontal cortex and bilateral ventrolateral cortex during DT. – Young adults: dual mixed trials showed greater changes in more frontal areas, especially right sided. Equal condition: – Older adults: dual mixed trials engaged bilateral dorsolateral prefrontal cortex, compared to single trials. – Young adults: no differences between activation during dual mixed and single trials. Single trials showed change in activation in right posterior dorsolateral prefrontal cortex for HHb. The activation change between priority and equal conditions was found only in older adults.
Bierre (J Gerontol A Biol Sci Med Sci., 2017), New Zealand (Bierre et al., 2017)	*N* = 72 Healthy older adults (66 ± 3.8); young adults (21.9 ± 2.7). Frontal.	Task: – Visuomotor tasks (increasing executive demand): 1) Basic visuomotor performance. 2) Adding inhibition. 3) Adding need to switch between tasks. Rest: 2 min (sitting).	⇑: Older adults showed increased O_2Hb in relation to increasing task difficulty. Older adults showed higher O_2Hb compared to younger adults
Halliday (Neurophoton., 2017), Canada (Halliday et al., 2017)	*N* = 25 Healthy older adults (75.88 ± 3.28) Prefrontal.	Task: – Computerized cognitive task: Multi-Source Interference Task (congruent and incongruent condition). Fifteen trials in a 30 s block. Rest: 60 s baseline before task. 20 s between blocks.	Greater mean O_2Hb during congruent (easier) task associated with faster performance and during incongruent (more difficult) task, with slower performance. Greater O_2Hb variability at within-person level associated with better accuracy and faster performance. Greater O_2Hb variability at between-person level associated with slower performance.
Huppert (PLoS One, 2017), USA (Huppert et al., 2017)	*N* = 19 Older adults (88.1 ± 6.0). Frontal.	Tasks: – Stroop Test. – Symbol Digit Coding. – Shifting Attention Test. Rest: 30 s (quiet sitting baseline).	⇑: Left Broadmann's area (BA) 10 (right superior frontal) activation during Symbol Digit Coding and Shifting Attention Test. Right BA-10, right BA-45 and left BA-10 activated during Stroop test.
* **Halliday** (J Clin Exp Neuropsychol., 2018), Canada (Halliday et al., 2018)	*N* = 27 Older adults (76.1 ± 3.3). Prefrontal.	Task: – Computerized cognitive task: Multi-Source Interference Task (congruent and incongruent condition). Fifteen trials in a 30 s block (total of 4 blocks for each condition). Rest: No rest time specified.	⇑: Fallers: activation during congruent and incongruent task; recruited additional tissue to perform at similar level. Non-fallers: no active channels during congruent task; little activation during incongruent task (medial right prefrontal cortex).
Memory test			
Uemura (Int J Geriatr Psychiatry, 2016), Japan (Uemura et al., 2016)	*N* = 130 Amnestic MCI (71.8 ± 43); healthy older adults (71.7 ± 3.9). Prefrontal.	Task: – Encoding and retrieval of 10 words (20–30 s respectively). Repeat vowels: Pre-task (10 s), rest after task (20–30 s) and post-task (10 s).	⇓: Reduced activation in bilateral dorsolateral cortex during memory retrieval in amnestic MCI. No significant group effects during encoding.

*AD, Alzheimer's Disease; DT, dual-task; fNIRS, Functional Near-Infrared Spectroscopy; HHb, deoxygenated hemoglobin; MCI, Mild Cognitive Impairment; O_2Hb, oxygenated hemoglobin; PFC, Prefrontal Cortex; ST, single task; SD, Standard Deviation; VF, Verbal Fluency. *Articles assessing modulation of health characteristics on brain activation (**Table 3**).*

TABLE 2 | Summary of the studies assessing fNIRS measures during motor and/or dual-tasks in older adults.

First author (Journal, year), Country	Sample size (N) Clinical characteristics of the sample (mean age ± SD) NIRS optodes localization	Paradigm description	Main fNIRS results
(2A) Motor tasks			
Mahoney (Brain Res., 2016), USA (Mahoney et al., 2016)	*N* = 269 Parkinsonian syndrome (81.2 ± 5.9); Mild parkinsonian signs (77.5 ± 6.7); healthy adults (74.4 ± 6.1). Prefrontal.	Task: – Postural control while standing and silently counting for 10 sec.	⇑: Parkinsonian syndromes: increased prefrontal activation to maintain postural control (compared to the other two groups).
Maidan (Brain Topogr., 2017), Israel (Maidan et al., 2017)	*N* = 49 PD without cognitive impairment or freezing of gait (72.8 ± 1). Frontal.	Task: – Walk with turns: 30-m walk and 180° turn. – Five trials: 20 s of quiet standing between walk and turn. Rest: 20 s before and after each walk (quiet standing).	⇑: Increased activation during walking and decrease during turns (compared to baseline). ⇑: Older adults with lower gait speed (<1 m/sec): higher activation during turns (compared to older adults with normal gait speed).
Thumm (Gait Posture, 2018), Israel (Thumm et al., 2018)	*N* = 20 PD (69.8 ± 6.4). Prefrontal.	Task: – 30-m over-ground vs. treadmill walking. – Five trials (30 s each). Rest: 20 s quiet standing.	⇓: Lower activation during treadmill walking (compared to over-ground walking).
(2B) Dual-tasks			
Doi (Aging Clin Exp Res., 2013), Japan (Doi et al., 2013)	*N* = 16 Older adults with MCI (75.4 ± 7.2). Prefrontal.	Tasks: – ST: 10-m walk. – DT: 10-m walk + phonetic verbal fluency. – Three trials in each condition (20 s each). Rest: 10 s pre-task and 30 s post-task (standing).	⇑: Increased prefrontal activation during DT walking compared to ST walking.
Ohsugi (BMC Neurosc., 2013), Japan (Ohsugi et al., 2013)	*N* = 35 Healthy older adults (77.9 ± 5.3) vs. young (26 ± 3.6). Prefrontal.	Tasks: – ST: seated stepping while forward counting from 0. – ST: serial 7-subtraction from 100. – DT: stepping + subtraction. – Each task repeated three times (30 s each). Rest: 30 s (self-paced counting).	⇑: Higher O_2Hb values during DT compared to stepping as ST. ST count showed higher activation compared to stepping. ⇑: Older adults: higher O_2Hb levels during DT compared to younger adults.
Beurskens (Int J Physchophysiol., 2014), Germany (Beurskens et al., 2014)	*N* = 25 Healthy older adults (71.0 ± 3.8) vs. younger adults (24.5 ± 3.3). Prefrontal.	Tasks: – ST: treadmill walk. – ST: checking boxes on paper. – ST: reciting alternate alphabet. – DT: walk + check. – DT: walk + alphabet. Each task: 30 s and repeated twice. Rest: seated (duration is not specified).	⇓: Older adults: lower activation during walk + check compared to ST walk. No significant difference between walk + alphabet vs. walk. Young: no significant difference in activation during ST vs. DT. ⇑: Higher activation in younger adults compared to older adults during visually demanding dual-task (walk + check).
Clark (Front Aging Neurosci., 2015) (Clark et al., 2014)	*N* = 16 Older adults with mild mobility difficulties (77.2 ± 5.6). Prefrontal.	Tasks: – ST: 90-meter walk (5 × 18 m). – Walk + phonetic verbal fluency. – Walk + dimmed light. – Walk + carrying tray. – Walk + 6 obstacles negotiation. – Walk + weighted vest. Rest: 1 min quite standing between tasks.	⇑: Increased activation during DT walk + verbal fluency, walk + vest, walk + obstacles. Although not significative, there was a trend toward increase during DT walk carrying tray and walk with dimmed light.

(Continued)

TABLE 2 | Continued

First author (Journal, year), Country	Sample size (N) Clinical characteristics of the sample (mean age ± SD) NIRS optodes localization	Paradigm description	Main fNIRS results
Holtzer (Neuroimage, 2015), USA (Holtzer et al., 2015)	*N* = 348 Healthy older adults (76.8 ± 6.8). Prefrontal.	Tasks: – ST: Walk 3 loops on 14-feet walkway. – ST: 30 s reciting alternate alphabet. – DT: Walk + alphabet. Rest: 10 s standing still and counting silently before tasks.	⇑: Bilateral increases in O_2Hb during DT compared to normal walk. In ST walk, after an initial increase, O_2Hb levels decrease in the course of the walk. While during the DT walk, O_2Hb remains elevated during the task.
Al-Yahya (Neurorehabil Neural Repair, 2016), UK (Al-Yahya et al., 2016)	*N* = 19 Chronic stroke (66.2 ± 8.3); healthy controls (56.2 ± 9.5). Prefrontal.	Tasks: – ST: feet tapping. – ST: backward count. – DT: feet tap + count. Five trials (30 s for each task). Rest: 25–45 s in a pseudo-random order after each task.	⇑: Higher O_2Hb during DT compared to ST in stroke participants compared to healthy controls.
Hernández (J Neurol Sci., 2016), USA (Hernandez et al., 2016)	*N* = 16 Multiple Sclerosis (57 ± 5); healthy controls (61 ± 4). Prefrontal.	Tasks: – ST: Walk 3 loops on walkway. – ST: 30 s reciting alternate alphabet. – DT: Walk + alphabet. Rest: 10 s standing still and counting silently before tasks.	⇑: Higher O_2Hb levels in MS compared to healthy controls in walking tasks. Larger increase in O_2Hb from ST walk to DT in MS compared to healthy controls.
* **Holtzer** (Brain Topogr, 2016), USA (Holtzer et al., 2016)	*N* = 236 Healthy older adults (75.5 ± 6.5). Prefrontal.	Tasks: – ST: Walk 3 loops on 14-feet electronic walkway. – ST: Reciting alternate alphabet (30 s). – DT: Walk + alphabet. Rest: 10 s standing still and counting silently before tasks.	⇑: Normal gait: Higher O_2Hb levels in DT compared to ST walk. ⇓: Central NGA: attenuated changes in PFC O_2Hb levels from ST to DT compared to peripheral NGA and normal gait group. ⇑: Peripheral NGA showed greatest increase in O_2Hb during DT.
Maidan (Neurorehabil Neural Repair, 2016) (Maidan et al., 2016)	*N* = 106 PD (71.6 ± 0.9); healthy older adults (70.4 ± 0.9). Prefrontal.	Tasks: – ST: Walk on 30-m walkway (30 s). – DT: Walk + serial subtractions. – DT: Walk + obstacles. 5 trials each task. Rest: 1 min before whole paradigm starts and 20 s standing before and after tasks.	⇑: Increased frontal activation during DT walking compared with ST walking in healthy group. ⇓: In PD, HbO_2 levels did not increase during DT. ⇑: In PD, HbO_2 increased during walk + obstacle compared with ST walking. ⇑: Higher increase in activation during ST walking in PD compared to healthy controls. No significant difference between groups during DT walks.
Nieuwhof (Pilot Feasibility Stud., 2016), Netherlands (Nieuwhof et al., 2016)	*N* = 12 Parkinson's Disease (70.1 ± 5.4). Prefrontal.	Tasks: – DT: Walk + counting forward. – DT: Walk + serial 3 or 7-substraction. – DT: Walk + reciting digit spans. Five blocks (with 3 tasks each); 40 s each task. Rest: 20 s still-standing before/after task and 1–2 min random rest (while listening to instructions). At least 1 min stand before block.	⇑ All tasks increased O_2Hb during task compared to rest.
*** Osofundiya** (Clin Biomech., 2016), USA (Osofundiya et al., 2016)	*N* = 20 Cognitively healthy older adults: obese (80.5 ± 6.8) vs. non-obese (80.6 ± 7.5). Prefrontal	Tasks: – ST: walk (30 s). – DT: walk + reciting alphabet (30 s). – DT: walk and step on targets on walkway (precision walk). Two blocks: 4 trials (30 s each) per block. Rest: quiet sitting (30 s) before start; 10 s quiet standing between trials; 2 min seating between blocks.	⇑: Higher PFC activation during DT and precision walk compared to ST walk. ⇑: Obesity associated greater activation in all tasks but specially during precision walking.

(Continued)

TABLE 2 | Continued

First author (Journal, year), Country	Sample size (N) Clinical characteristics of the sample (mean age ± SD) NIRS optodes localization	Paradigm description	Main fNIRS results
Takeuchi (BMC Neurosci., 2016), Japan (Takeuchi et al., 2016)	*N* = 31 Healthy older adults (71.7 ± 3.3); young adults (25.9 ± 4.4) Prefrontal.	Task: – ST: walk for 30 s around a 2.5 m-radius circle – ST: smartphone-based touch game (sitting). Participants instructed to touch in ascending order a set of numbers on screen. – DT: walk + touch. Rest: not described.	No difference between young vs. old in PFC activation during DT. Less PFC lateralization in older adults to suppress DT cost in gait performance.
Chaparro (J Neuroeng Rehabil., 2017), USA (Chaparro et al., 2017)	*N* = 22 Healthy older adults (63.1 ± 4.4); multiple sclerosis (56.2 ± 5.1) Prefrontal.	Task: – ST: alternate alphabet reciting (standing) – ST: Normal walk – DT: walk while reciting alternate alphabet Walk: 30 s warm-up walk; 30 s test; 15 s deceleration Rest: 10 s before each task (quiet standing). Protocol performed with and without partial body weight support	⇑: Higher activation during DT compared to normal walk. ⇑: MS older adults: larger increase in O_2Hb during all tasks in all conditions compared to healthy older adults (especially during DT without partial body weight support).
Chen (Gait Posture, 2017), USA (Chen et al., 2017)	*N* = 90 Healthy older adults (78 ± 15.5). Prefrontal.	Tasks: – ST: Walk 3 loops on 14ft electronic walkway. – DT: Walk + alternate alphabet reciting. – ST: Walk with obstacle negotiation. – DT: Walk with obstacle + alternate alphabet reciting. Rest: 10 s standing still and counting silently before tasks.	⇑: Higher activation during DT compared to ST in both normal walk and walk with obstacles. ⇑: Participants with slower gait showed higher increase in O_2Hb during walk with obstacles compared to unobstructed walk (relative to participants with normal gait).
* **Holtzer** (Eur J Neurosci., 2017), USA (Holtzer et al., 2017a)	*N* = 318 Healthy older adults (76.6 ± 6.7). Prefrontal.	Tasks: – ST: Walk (3 loops on 14-feet electronic walkway). – ST: Reciting alternate alphabet (30 s). – DT: Walk + alphabet. Rest: 10 s standing still and counting silently before tasks.	⇓: Higher levels of perceived task-related stress associated attenuation of brain activation from ST to DT.
*** Holtzer** (J Gerontol A Biol Sci Med Sci., 2017), USA (Holtzer et al., 2017b)	*N* = 314 Healthy older adults (76.8 ± 6.7). Prefrontal.	Tasks: – ST: Walk 3 loops on 14-feet electronic walkway. – ST: Reciting alternate alphabet (30 s). – DT: Walk + alphabet. Rest: 10 s standing still and counting silently before tasks.	⇑: Increased O_2Hb levels during DT walking compared with ST walking. ⇓: Higher levels of subjective fatigue attenuated the increase in O_2Hb from ST to DT walking.
Mirelman (Brain Cogn., 2017), Israel (Mirelman et al., 2017)	*N* = 43. Healthy older adults (69.7 ± 5.8); younger adults (30.9 ± 3.7). Prefrontal.	Tasks: – ST: Walk on 30-m walkway. – DT: Walk + serial subtraction. – DT: Walk + obstacles. Three loops on walkway for 30 s for each task. Rest: 20 s quiet standing before/after tasks.	⇑: Older participants increased O_2Hb during DT compared to ST walk and during ST walk compared to rest periods. ⇑: Young adults: Activation during DT compared to ST walk. No increase in O_2Hb during ST walking (compared to rest). ⇑: Older adults showed higher O_2Hb levels in all tasks compared to younger participant.

(Continued)

TABLE 2 | Continued

First author (Journal, year), Country	Sample size (N) Clinical characteristics of the sample (mean age ± SD) NIRS optodes localization	Paradigm description	Main fNIRS results
Rosso (Gait Posture, 2017), USA (Rosso et al., 2017)	*N* = 16 Healthy older adults (74 ± 5); younger adults (24 ± 3). Left prefrontal, temporal, and motor.	Tasks: – ST: Attention task (seated). – ST: Postural control (standing). – DT: Postural control + attention task. Three trials of each task (121 s each). Rest: 30 s sitting or standing before and after each task.	⇑: Older adults had greater activation of prefrontal and temporal regions compared to younger adults.
* **Verghese** (Neurology, 2017), USA (Verghese et al., 2017)	*N* = 166 Healthy older adults (74.9 ± 6.1). Prefrontal.	Tasks: – ST: Walk 3 loops on 14-feet walkway. – ST: Reciting alternate alphabet (30 s). – DT: Walk + alphabet. Rest: 10 s standing still and counting silently before tasks.	⇑: DT walk showed higher PFC activation than ST walk. Higher PFC activation levels on fNIRS during DT predicted incident falls.
Mori (Gait Posture, 2018), Japan (Mori et al., 2018)	*N* = 28 Post-stroke (>6 months) with hemiparesis (61.1 ± 9.3); healthy controls (66.3 ± 13.3). Prefrontal.	Tasks: – ST: Serial subtractions of 3 (standing). – DT: Walk around a circle with 2.5 m radius + serial subtractions of 3. 3 trials. Rest: 60 s (repeat sequence of numbers 1–10).	⇓: Stroke participants: Lower PFC activation during DT compared to healthy participants.
Hawkins (Hum Mov Sci., 2018), USA (Hawkins et al., 2018)	*N* = 48 Post-stroke (>4 years) with hemiparesis (58.0 ± 9.3); older adults with mild gait deficits (77.2 ± 5.6); young healthy adults (22.4 ± 3.2). Prefrontal.	Tasks: – ST: Walk on an 18-m oval-shaped course. – DT: Walk + obstacle negotiation. – DT: Walk + phonetic verbal fluency. Rest: quiet standing (duration not specified).	⇑: Elderly vs. young: Higher O_2Hb increase during normal walk and obstacle negotiation in the early time period. In the late time period, higher PFC activation during normal walk (but not with obstacles). ⇑: Stroke participants: Higher O_2Hb increase during normal walk and obstacle negotiation compared to young participants. Greater activation during obstacle negotiation compared to elderly in the late time period. O_2Hb increase was highest in the post-stroke group, followed by older and young adults.
* **Holtzer** (Brain Cogn., 2018), USA (Holtzer et al., 2018a)	*N* = 315 Healthy old (76.8 ± 6.7). Prefrontal.	Tasks: – ST: Walk 3 loops on 14-feet walkway. – ST: Reciting alternate alphabet (30 s). – DT: Walk + alphabet. Rest: 10 s standing still and counting silently before tasks.	⇑: Participants without diabetes: increased O_2Hb levels during DT compared to ST walk. ⇓: Diabetes: attenuated increase in O_2Hb levels from ST walk to DT (compared to non-diabetics).
* **Lucas** (J Gerontol A Biol Sci Med Sci., 2018), USA (Lucas et al., 2018)	*N* = 55 Healthy older adults (74.7 ± 4.9). Prefrontal.	Tasks: – ST: Walk 3 loops on 20-feet walkway. – DT: Walk + reciting alternate alphabet. Rest: 10 s standing still and counting silently before tasks.	⇑: Higher PFC activation during DT compared to ST. ⇑: Poorer white matter integrity associates greater increase in O_2Hb levels during DT.

*AD, Alzheimer's disease; DT, dual-task; fNIRS, Functional Near-Infrared Spectroscopy; MCI, Mild Cognitive Impairment; NGA, Neurological Gait Abnormalities; O_2Hb, oxygenated hemoglobin; PD, Parkinson's disease; PFC, Prefrontal Cortex; ST, single task; SD, Standard Deviation; VF, Verbal Fluency. *Articles assessing modulation of health characteristics on brain activation (**Table 3**).*

decrease when performing 180° turns (Maidan et al., 2017). However, when comparing older adults with different gait speed, participants with gait speed lower than 1m/sec showed higher activation during turns, compared to those with normal gait speed. Thumm et al. reported lower O_2Hb levels while walking on a treadmill vs. over-ground walking in PD participants (Thumm et al., 2018).

Studies Assessing the Effect of Dual Tasking

Twenty-three articles assessed PFC hemodynamics while performing DT (**Table 2B**). Studies included in this review used walking (Doi et al., 2013; Beurskens et al., 2014; Clark et al., 2014; Holtzer et al., 2015, 2016, 2017a,b, 2018a,b; Maidan et al., 2016; Nieuwhof et al., 2016; Takeuchi et al.,

TABLE 3 | Studies assessing effect modification by different health characteristics on PFC activation.

First author (Journal, year) (reference)	Clinical variables
Halliday et al. (J Clin Exp Neuropsychol., 2017) (Halliday et al., 2018)	Fallers versus non-fallers
Holtzer et al. (Brain Topogr, 2016) (Holtzer et al., 2016)	Neurological Gait Abnormalities
Osofundiya (Clin Biomech., 2016) (Osofundiya et al., 2016)	Obesity
Holtzer et al. (Eur J Neurosci, 2017) (Holtzer et al., 2017a)	Levels of perceived task-related stress
Holtzer et al. (J Gerontol A Biol Sci Med Sci., 2017) (Holtzer et al., 2017b)	Fatigue
Verghese et al. (Neurology, 2017) (Verghese et al., 2017)	Longitudinal association with falls
Holtzer et al. (Brain Cogn., 2018) (Holtzer et al., 2018a)	Diabetes
Lucas et al. (J Gerontol A Biol Sci Med Sci., 2018) (Lucas et al., 2018)	Relation with white matter integrity
Hyodo et al. (Neuroimage, 2015) (Hyodo et al., 2016)	Fitness levels
Albinet (Front Aging Neurosci., 2014) (Albinet et al., 2014)	
Dupuy (Front Hum Neurosci., 2015) (Dupuy et al., 2015)	

2016; Chaparro et al., 2017; Chen et al., 2017; Mirelman et al., 2017; Verghese et al., 2017; Hawkins et al., 2018; Lucas et al., 2018; Mori et al., 2018), feet tapping (Al-Yahya et al., 2016), stepping (Ohsugi et al., 2013) and postural control (Rosso et al., 2017) as the motor task and VF (Doi et al., 2013; Clark et al., 2014; Hawkins et al., 2018), calculation (Ohsugi et al., 2013; Al-Yahya et al., 2016; Maidan et al., 2016; Nieuwhof et al., 2016; Mirelman et al., 2017; Mori et al., 2018), alphabet (Beurskens et al., 2014; Holtzer et al., 2015, 2016, 2017a,b, 2018; Chaparro et al., 2017; Chen et al., 2017; Verghese et al., 2017; Lucas et al., 2018), digit span (Nieuwhof et al., 2016), visual (Beurskens et al., 2014) or attention (Takeuchi et al., 2016; Rosso et al., 2017) tasks as the added cognitive tasks. Other studies used challenging factors while walking such as obstacle negotiation or carrying a tray as the secondary task to assess DT performance (Clark et al., 2014; Maidan et al., 2016; Osofundiya et al., 2016; Chen et al., 2017; Mirelman et al., 2017; Hawkins et al., 2018).

Cognitively Healthy Older Adults

The vast majority of studies reported an increase in PFC activation in cognitively healthy older adults while performing several types of DT compared to a ST (Ohsugi et al., 2013; Clark et al., 2014; Holtzer et al., 2015, 2017a,b; Maidan et al., 2016; Osofundiya et al., 2016; Chen et al., 2017; Mirelman et al., 2017; Verghese et al., 2017; Lucas et al., 2018). Only one article reported lower O_2Hb levels during walking while performing a visual check task compared to ST walk in the older adults group (Beurskens et al., 2014).

Comparison of Cognitively Healthy Older Versus Younger Adults

Older older adults showed higher PFC activation during DT in most studies, compared to younger participants (Ohsugi et al., 2013; Mirelman et al., 2017; Rosso et al., 2017; Hawkins et al., 2018). Only one study reported lower activation in older adults, compared to younger older adults, during a walk and visual check DT (Beurskens et al., 2014) and Takeuchi et al. (2016) did not find significant differences between age groups.

Other Clinical Conditions

The effect of dual tasking in older adults with MCI was assessed in one of the included studies, which found an increased activation during DT compared to ST walking (Doi et al., 2013). Frontal hemodynamics has also been studied in stroke patients, although these studies included participants with heterogeneous clinical characteristics (mainly the time after the stroke event) and DT paradigms (i.e., Task protocols). Compared to healthy controls, patients with stroke history showed higher activation during counting while feet tapping (Al-Yahya et al., 2016) but a lower activation during counting while walking in another study (Mori et al., 2018). Walking while negotiating obstacles caused a higher activation in stroke patients compared to younger adults (Hawkins et al., 2018). PD patients show an increase in frontal activation during DT that involve walking and counting or reciting digit spans compared to the resting baseline periods (Nieuwhof et al., 2016). Middle-aged Multiple Sclerosis older adults show increased PFC activation during ST and DT walking and larger increases in O_2Hb levels from ST to DT when compared to healthy older adults (Hernandez et al., 2016; Chaparro et al., 2017). Multiple Sclerosis participants show an especially larger increase in activation (compared to healthy counterparts) when not provided with partial body weight support (Chaparro et al., 2017).

Association Between Activation and Clinical Variables

Other studies assessed how different variables modulate the PFC activation during cognitive, motor tasks and DT (**Table 3**). Publications from the "Central Control of Mobility in Aging" (CCMA) study, including community-dwelling older adults without dementia, found that activation of PFC during DT, compared to ST, was lower in participants with central NGA compared to peripheral NGA or with normal gait. In fact, the highest O_2Hb increase during DT was showed by participants with peripheral NGA (Holtzer et al., 2016). Also in participants from the CCMA study, higher levels of self-perceived stress and fatigue were associated with attenuation of brain activation patterns (lower increase in O_2Hb levels from ST to DT walking) (Holtzer et al., 2017a,b). Participants with diabetes from the same study showed lower PFC activation during DT, compared to non-diabetics (Holtzer et al., 2018a), while obese cognitively healthy older adults from a different study showed higher activation, especially during a precision walking task, compared to non-obese counterparts (Osofundiya et al., 2016). When combining fNIRS with cerebral microstructural white matter integrity assessment, using MRI with Diffusion Tensor Imaging (DTI), altered white matter integrity was associated to higher O_2Hb levels during DT walk compared to normal walk in the CCMA study (Lucas et al., 2018). Using data from the

same study, Verghese et al. (2017) revealed higher risk of incident falls in older adults with higher levels of PFC activation during DT. It is important to note that this is the only article included in our review that assessed the relationship between PFC hemodynamic and outcomes in a longitudinal manner. Furthermore, in a separate sample, fallers compared to non-fallers (history of falls in the previous 2 years) had higher activation while performing executive function tasks (Halliday et al., 2018). The effect of fitness level on frontal activation during executive functions tasks among cognitively healthy participants was addressed in three studies. Although they assessed the level of fitness with different instruments, it seems that higher levels of fitness might produce larger increases in prefrontal activation (Albinet et al., 2014). Two of these studies used two different versions of modified Stroop tasks and while one found a more left-lateralized activation in the high-fit participants (Hyodo et al., 2016), the other study found an increased activation in right inferior frontal gyrus in the high-fit group (Dupuy et al., 2015).

DISCUSSION

Summary and Interpretation of Findings

Our review identified 46 articles that reported the assessment of frontal and PFC hemodynamics in older adults using fNIRS during cognitive, motor and DTs.

This has revealed a quite homogeneous pattern of activation of the PFC in cognitively healthy older adults during cognitive and DTs compared to rest and to single-task conditions, respectively. This supports the use of fNIRS investigations to detect changes in frontal hemodynamics in older adults.

Cognitively healthy older adults, compared to younger ones, show a higher activation during executive function tasks and DTs (Ohsugi et al., 2013; Bierre et al., 2017; Mirelman et al., 2017; Rosso et al., 2017; Hawkins et al., 2018). However, one study reported lower activation during walking while performing a visual check task compared to ST walk in the older adults group and compared to the younger group (Beurskens et al., 2014). The results in older adults with various degrees of cognitive impairment are more heterogeneous. Overall, MCI older adults show increased PFC activation during VF tasks (Yeung et al., 2016a; Yap et al., 2017) and during DT compared to ST (Doi et al., 2013). However, gradually increasing working memory load causes a lower activation compared to healthy controls (Niu et al., 2013; Yeung et al., 2016b).

These findings are in line with previously proposed hypotheses, such as the "neural inefficiency theory" (Rypma and D'Esposito, 2000; Holtzer et al., 2009), according to which older adults show increased activity of the same networks recruited by younger counterparts in order to meet behavioral demands. On the other hand, the lower activation in the healthy old subgroup relative to younger adults could be interpreted as an inability to meet the increased cognitive demands during the more complex DT (Beurskens et al., 2014) and is supported by the "capacity limitation hypothesis" (Cabeza, 2004; Holtzer et al., 2009). This theory might also explain the decrease in activation in MCI older adults with increasing working memory load (Niu et al., 2013; Yeung et al., 2016b). Importantly, neural inefficiency and capacity limitation theories are not mutually exclusive and likely both play a role in determining activation levels.

Regarding the studies focusing on older adults with other specific diseases, the findings support an activation of PFC during gait as ST (Maidan et al., 2017) and DT (Nieuwhof et al., 2016) in adults with PD (compared to rest periods). The only study that assessed PFC during postural control found a higher activation in participants with parkinsonian syndromes relative to healthier controls (Mahoney et al., 2016). This could be interpreted in the context of the neural inefficiency theory, where adults with impaired postural mechanisms as seen in PD (Baltadjieva et al., 2006; Benítez-Rivero et al., 2013), need a higher PFC activation to maintain postural control. Similar results, of higher activation than healthy controls, were obtained in Multiple Sclerosis participants (Hernandez et al., 2016; Chaparro et al., 2017) whereas stroke patients reported more heterogeneous results. This might be due to different clinical characteristics of the samples and of the DT paradigms (Al-Yahya et al., 2016; Hawkins et al., 2018; Mori et al., 2018).

Studies that investigated the effect of several clinical variables on the PFC activation during DT found a higher activation in participants with peripheral NGA, lower stress and fatigue levels, obesity, non-diabetics and altered white matter integrity in MRI. The only study that assessed prediction of longitudinal outcomes of frontal hemodynamics, found a higher risk of falls associated with higher PFC activation. However, most of these findings come from a single sample. According to the results from three studies, higher levels of fitness might produce larger increases in prefrontal activation during executive functions tasks in healthy older adults (Albinet et al., 2014; Dupuy et al., 2015; Hyodo et al., 2016).

Overall, our findings suggest that fNIRS studies are able to detect changes in frontal and PFC activation in older adults (both cognitively healthy and MCI), especially while performing cognitive and DTs that are believed to engage the frontal areas of the brain. In particular, in both the comparison between older and younger adults, and in people with different neurological conditions, compared to healthier controls, the PFC seems to experience a higher activation, which could be interpreted in the context of proposed neural inefficiency and limited capacity models.

Methodological Aspects and Limitations

Main limitations of the fNIRS technique arise either due to physical or technological constraints of the setups, due to analysis methods, or due to the nature of the study itself. It is well known that the recorded signal contains information not only from brain activation due to a specific stimulus or task but is also affected by extra-cerebral (skull and scalp perfusion) as well as systemic parameters (heart and respiratory rate, blood pressure, Mayer waves). Nowadays, the fNIRS community

has made not only technological improvements but also has developed an abundance of methods to attempt to overcome the abovementioned limitations (Tachtsidis and Scholkmann, 2016). Current instrumentation provides the ability of using multiple source detector pairs that cover a wide range of tissue penetration depth, giving the possibility to record short channel preparation and regress out signal coming from superficial tissue layers when using continuous wave light sources (Yücel et al., 2015). On the other hand, emerging methods that employ pulsed light sources [time-resolved NIRS (TRS)], allow for the possibility to discriminate between intra- and extra cerebral signals (Torricelli et al., 2014). These methods were prohibitively complex but have recently begun to become practical (Pifferi et al., 2016). In this context, to cover a large imaging area, multiple channels can be used in combination with MRI, thus overcoming the lack of anatomical information and allow for localization of the origin of NIRS signal (Okamoto et al., 2004). Another technical limitation, could originate from the differential path length factor (DPF), used in modified Beer-Lambert law (Cope and Delpy, 1988), that could lead in cross-talk between oxygenated and deoxygenated hemoglobin measurements and false calculations (Hoshi, 2007). Regarding the analysis methods of the acquired fNIRS signal, to date, there is no standard method established (Pfeifer et al., 2018). Some of the most common strategies include the use of low-pass filters to remove heart rate or instrumental noise and high pass filters to extract low frequency systemic noise. Signal analysis methods are also heterogeneous in the current literature (Kirilina et al., 2012; Zhang et al., 2016). Furthermore, in functional studies and especially in motor and DT, motion artifacts play an important role, therefore, motion correction processes are widely used, covering a wide range of proposed methods (Wavelet filtering, Kalman filtering, spline interpolation, etc.) (Cooper et al., 2012; Brigadoi et al., 2014). In general, for more accurate results when designing an fNIRS experimental protocol or analysis method, it is crucial to take into account, potential particularities that each studied population might have.

The heterogeneity in task protocols, methodology and small sample sizes in most of the included articles may limit the interpretation of the findings, although the studies with larger samples show promising results in similar directions. The great majority of the reviewed articles measured activation only over frontal areas, avoiding the assessment of possible compensatory activations in distant areas of the brain (Stern, 2005; Holtzer et al., 2009). This may be mainly due to the simplicity of the application over hairless areas and can be overcome with better probe designs.

Furthermore, differences in cerebral activation patterns detected by fNIRS could be actually related to structural alterations, as recently reported in an MRI-fNIRS study (Wagshul et al., 2019) where higher activation in healthy older adults during DT was related to reduced cortical volumes, especially in bilateral superior and rostral-middle frontal cortex. More evidence is needed supporting this concept.

Other gaps and limitations might limit the generalizability of the results produced by the studies published to date. Regarding studies reporting the results of the motor task alone (not as dual task), the studies are limited to older adults with Parkinson syndromes. The samples are also very heterogeneous regarding the mean age ranges and other clinical characteristics. In most of the included studies, inclusion criteria take into account age and cognitive function, but individuals of the samples or within the comparison groups might be heterogeneous regarding aspects which might affect the cerebral neurovascular coupling and metabolism, such as cardiovascular risk load, atherosclerosis, small vessels disease etc.

Our work is not exempt from limitations. In particular, the non-systematic search strategy might lead to possible missing relevant published literature on the topic. However, we consider our pre-defined search strategy sufficiently comprehensive to include the most if not all relevant ones.

Clinical Implications and Future Directions

Our findings support the potential role of fNIRS in research and clinical practice to study cognition and mobility in aging. As mentioned, fNIRS is a non-invasive technique, which can assess brain regions involved in executive functions, which are key to goal-oriented behaviors and preserved cognitive and motor functions. In particular, fNIRS allows to obtain relevant information regarding neural activation while the person is performing a real motor task in a natural environment, in a relatively inexpensive way. However, further research is needed to confirm those findings and to establish standardized protocols (for tasks protocols and fNIRS data acquisition and processing). Further research should also focus more on cerebral hemodynamic in different neurological diseases and on the influence of systemic conditions (e.g., vascular risk factors such as diabetes and hypertension) on brain activation patterns as assessed with fNIRS. Furthermore, fNIRS-derived brain activation patterns can be utilized as predictors of incident health outcomes including but not limited to dementia.

A recent study demonstrated that within session training resulted in improved DT walking that was coupled with reduced activation in the PFC among healthy older adults suggesting improved neural efficiency due to practice (Holtzer et al., 2018b). Moreover, the presence of fear of falling delayed practice-related improvements in PFC efficiency during DT walking (Holtzer et al., 2019). These findings suggest that fNIRS can be used to quantify neuroplasticity, monitor improvement in PFC efficiency due to practice and detect the effect of clinically relevant variables such as fear of falling on brain function and efficiency during active walking. Hence, it is appropriate to consider the inclusion of fNIRS at least as a secondary outcome measure in clinical trials designed to assess the effect of treatment on brain neuroplasticity and efficiency as well as for the development and monitoring of rehabilitation/training programs.

CONCLUSION

In conclusion, our review supports the use of fNIRS as a neuroimaging technique to study changes in the hemodynamic

response in the frontal cortex during cognitively demanding tasks and during active walking under single and DT conditions in older adults. From a pathophysiological perspective this approach might help characterize the evolution of functional impairments in different neurological diseases in older adults as well as in healthy aging.

AUTHOR CONTRIBUTIONS

CU and MI designed the concept of this manuscript, reviewed abstracts and full-text publications to assess eligibility, and wrote the first draft of the manuscript. CU extracted the relevant data from the included publications to write the manuscript. SA, TD, RH, AR, CC-T, L-MP, and LS-B contributed in the redaction and revision of the manuscript.

FUNDING

This work was partially supported through the MEDPHOTAGE project (DTS16/00099) which was supported by the "Instituto de Salud Carlos III" (ISCIII) and "Fondo Europeo de Desarrollo Regional (FEDER)" through the "Desarrollo Tecnológico en Salud" (DTS) program (Spain).

REFERENCES

Agbangla, N. F., Audiffren, M., and Albinet, C. T. (2017). Use of near-infrared spectroscopy in the investigation of brain activation during cognitive aging: a systematic review of an emerging area of research. *Ageing Res. Rev.* 38, 52–66. doi: 10.1016/j.arr.2017.07.003

Albinet, C. T., Mandrick, K., Bernard, P. L., Perrey, S., and Blain, H. (2014). Improved cerebral oxygenation response and executive performance as a function of cardiorespiratory fitness in older women: a FNIRS study. *Front. Aging Neurosci.* 6:272. doi: 10.3389/fnagi.2014.00272

Al-Yahya, E., Johansen-Berg, H., Kischka, U., Zarei, M., Cockburn, J., and Dawes, H. (2016). Prefrontal cortex activation while walking under dual-task conditions in stroke. *Neurorehabil. Neural Repair* 30, 591–599. doi: 10.1177/1545968315613864

Baezner, H., Blahak, C., Poggesi, A., Pantoni, L., Inzitari, D., Chabriat, H., et al. (2008). Association of gait and balance disorders with age-related white matter changes: the LADIS study. *Neurology* 70, 935–942. doi: 10.1212/01.wnl.0000305959.46197.e6

Baltadjieva, R., Giladi, N., Gruendlinger, L., Peretz, C., and Hausdorff, J. M. (2006). Marked alterations in the gait timing and rhythmicity of patients with de novo Parkinson's disease. *Eur. J. Neurosci.* 24, 1815–1820. doi: 10.1111/j.1460-9568.2006.05033.x

Beauchet, O., Allali, G., Annweiler, C., and Verghese, J. (2016). Association of motoric cognitive risk syndrome with brain volumes: results from the GAIT study. *J. Gerontol. A Biol. Sci. Med. Sci.* 71, 1081–1088. doi: 10.1093/gerona/glw012

Benítez-Rivero, S., Marín-Oyaga, V. A., García-Solís, D., Huertas-Fernández, I., García-Gómez, F. J., Jesús, S., et al. (2013). Clinical features and 123 I-FP-CIT SPECT imaging in vascular parkinsonism and Parkinson's disease. *J. Neurol. Neurosurg. Psychiatry* 84, 122–129. doi: 10.1136/jnnp-2012-302618

Beurskens, R., Helmich, I., Rein, R., and Bock, O. (2014). Age-related changes in prefrontal activity during walking in dual-task situations: a FNIRS study. *Int. J. Psychophysiol.* 92, 122–128. doi: 10.1016/j.ijpsycho.2014.03.005

Bierre, K. L., Lucas, S. J. E., Guiney, H., Cotter, J. D., and Machado, L. (2017). Cognitive difficulty intensifies age-related changes in anterior frontal hemodynamics: novel evidence from near-infrared spectroscopy. *J. Gerontol. A Biol. Sci. Med. Sci.* 72, 181–188. doi: 10.1093/gerona/glw061

Blumen, H. M., Holtzer, R., Brown, L. L., Gazes, Y., and Verghese, J. (2014). Behavioral and neural correlates of imagined walking and walking-while-talking in the elderly. *Hum. Brain Mapp.* 35, 4090–4104. doi: 10.1002/hbm.22461

Boas, D. A., Elwell, C. E., Ferrari, M., and Taga, G. (2014). Twenty years of functional near-infrared spectroscopy: introduction for the special issue. *Neuroimage* 85, 1–5. doi: 10.1016/j.neuroimage.2013.11.033

Brigadoi, S., Ceccherini, L., Cutini, S., Scarpa, F., Scatturin, P., Selb, J., et al. (2014). Motion artifacts in functional near-infrared spectroscopy: a comparison of motion correction techniques applied to real cognitive data. *Neuroimage* 85, 181–191. doi: 10.1016/j.neuroimage.2013.04.082

Buchbinder, B. R. (2016). *Functional Magnetic Resonance Imaging. In Pathobiology of Human Disease: A Dynamic Encyclopedia of Disease Mechanisms*, 1st Edn. Amsterdam: Elsevier.

Burgmans, S., van Boxtel, M. P. J., Smeets, F., Vuurman, E. F. P. M., Gronenschild, E. H. B. M., Verhey, F. R. J., et al. (2009). Prefrontal cortex atrophy predicts dementia over a six-year period. *Neurobiol. Aging* 30, 1413–1419. doi: 10.1016/j.neurobiolaging.2007.11.028

Cabeza, R. (2004). Task-independent and task-specific age effects on brain activity during working memory, visual attention and episodic retrieval. *Cereb. Cortex* 14, 364–375. doi: 10.1093/cercor/bhg133

Cabeza, R., Albert, M., Belleville, S., Craik, F. I. M., Duarte, A., Grady, C. L., et al. (2018). Maintenance, reserve and compensation: the cognitive neuroscience of healthy ageing. *Nat. Rev. Neurosci.* 19, 701–710. doi: 10.1038/s41583-018-0068-2

Ceïde, M. E., Ayers, E. I., Lipton, R., and Verghese, J. (2018). Walking while talking and risk of incident dementia. *Am. J. Geriatr. Psychiatry* 26, 580–588. doi: 10.1016/j.jagp.2017.12.009

Chaparro, G., Balto, J. M., Sandroff, B. M., Holtzer, R., Izzetoglu, M., Motl, R. W., et al. (2017). Frontal brain activation changes due to dual-tasking under partial body weight support conditions in older adults with multiple sclerosis. *J. Neuroeng. Rehabil.* 14, 1–10. doi: 10.1186/s12984-017-0280-8

Chen, M., Pillemer, S., England, S., Izzetoglu, M., Mahoney, J. R., and Holtzer, R. (2017). Neural correlates of obstacle negotiation in older adults: an FNIRS study. *Gait Posture* 58, 130–135. doi: 10.1016/j.gaitpost.2017.07.043

Clark, D. J., Rose, D. K., Ring, S. A., and Porges, E. C. (2014). Utilization of central nervous system resources for preparation and performance of complex walking tasks in older adults. *Front. Aging Neurosci.* 6:217. doi: 10.3389/fnagi.2014.00217

Cooper, R. J., Selb, J., Gagnon, L., Phillip, D., Schytz, H. W., Iversen, H. K., et al. (2012). A systematic comparison of motion artifact correction techniques for functional near-infrared spectroscopy. *Front. Neurosci.* 6:147. doi: 10.3389/fnins.2012.00147

Cope, M., and Delpy, D. T. (1988). System for long-term measurement of cerebral blood and tissue oxygenation on newborn infants by near infra-red transillumination. *Med. Biol. Eng. Comput.* 26, 289–294. doi: 10.1007/BF02447083

De Laat, K. F., Tuladhar, A. M., Van Norden, A. G. W., Norris, D. G., Zwiers, M. P., and De Leeuw, F. E. (2011). Loss of white matter integrity is associated with gait disorders in cerebral small vessel disease. *Brain* 134, 73–83. doi: 10.1093/brain/awq343

Delpy, D. T., and Cope, M. (1997). Quantification in tissue near–infrared spectroscopy. *Philos. Trans. R. Soc. Lond. B Biol. Sci.* 352, 649–659. doi: 10.1098/rstb.1997.0046

Doi, T., Makizako, H., Shimada, H., Park, H., Tsutsumimoto, K., Uemura, K., et al. (2013). Brain activation during dual-task walking and executive function among older adults with mild cognitive impairment: a FNIRS study. *Aging Clin. Exp. Res.* 25, 539–544. doi: 10.1007/s40520-013-0119-5

Dupuy, O., Gauthier, C. J., Fraser, S. A., Desjardins-Crèpeau, L., Desjardins, M., Mekary, S., et al. (2015). Higher levels of cardiovascular fitness are associated

with better executive function and prefrontal oxygenation in younger and older women. *Front. Hum. Neurosci.* 9:66. doi: 10.3389/fnhum.2015.00066

Durduran, T., Choe, R., Baker, W. B., and Yodh, A. G. (2010). Diffuse optics for tissue monitoring and tomography. *Rep. Prog. Phys.* 73:076701. doi: 10.1088/0034-4885/73/7/076701

Dux, P. E., Ivanoff, J., Asplund, C. L., and Marois, R. (2006). Isolation of a central bottleneck of information processing with time-resolved FMRI. *Neuron* 52, 1109–1120. doi: 10.1016/j.neuron.2006.11.009

Ferrari, M., and Quaresima, V. (2012). A brief review on the history of human functional near-infrared spectroscopy (fnirs) development and fields of application. *Neuroimage* 63, 921–935. doi: 10.1016/j.neuroimage.2012.03.049

Filmer, H. L., Mattingley, J. B., and Dux, P. E. (2013). Improved multitasking following prefrontal TDCS. *Cortex* 49, 2845–2852. doi: 10.1016/j.cortex.2013.08.015

Giacalone, G., Zanoletti, M., Re, R., Germinario, B., Contini, D., Spinelli, L., et al. (2019). Time-Domain Near-Infrared Spectroscopy In Acute Ischemic Stroke Patients. *Neurophotonics* 6:015003. doi: 10.1117/1.NPh.6.1.015003

Gramigna, V., Pellegrino, G., Cerasa, A., Cutini, S., Vasta, R., Olivadese, G., et al. (2017). Near-infrared spectroscopy in gait disorders: is it time to begin? *Neurorehabil. Neural Repair* 31, 402–412. doi: 10.1177/1545968317693304

Halliday, D. W. R., Hundza, S. R., Garcia-Barrera, M. A., Klimstra, M., Commandeur, D., Lukyn, T. W., et al. (2018). Comparing executive function, evoked hemodynamic response, and gait as predictors of variations in mobility for older adults. *J. Clin. Exp. Neuropsychol.* 40, 151–160. doi: 10.1080/13803395.2017.1325453

Halliday, D. W. R., Mulligan, B. P., Garrett, D. D., Schmidt, S., Hundza, S. R., Garcia-Barrera, M. A., et al. (2017). Mean and variability in functional brain activations differentially predict executive function in older adults: an investigation employing functional near-infrared spectroscopy. *Neurophotonics* 5:011013. doi: 10.1117/1.nph.5.1.011013

Hawkins, K. A., Fox, E. J., Daly, J. J., Rose, D. K., Christou, E. A., and McGuirk, T. E. (2018). Prefrontal over-activation during walking in people with mobility deficits: interpretation and functional implications. *Hum. Mov. Sci.* 59, 46–55. doi: 10.1016/j.humov.2018.03.010

Heilbronner, U., and Münte, T. F. (2013). Rapid event-related near-infrared spectroscopy detects age-related qualitative changes in the neural correlates of response inhibition. *Neuroimage* 65, 408–415. doi: 10.1016/j.neuroimage.2012.09.066

Heinzel, S., Metzger, F. G., Ehlis, A. C., Korell, R., Alboji, A., Haeussinger, F. B., et al. (2013). Aging-related cortical reorganization of verbal fluency processing: a functional near-infrared spectroscopy study. *Neurobiol. Aging* 34, 439–450. doi: 10.1016/j.neurobiolaging.2012.05.021

Heinzel, S., Metzger, F. G., Ehlis, A. C., Korell, R., Alboji, A., Haeussinger, F. B., et al. (2015). Age and vascular burden determinants of cortical hemodynamics underlying verbal fluency. *PLoS One* 10:e0138863. doi: 10.1371/journal.pone.0138863

Hernandez, M. E., Holtzer, R., Chaparro, G., Jean, K., Balto, J. M., Sandroff, B. M., et al. (2016). Brain activation changes during locomotion in middle-aged to older adults with multiple sclerosis. *J. Neurol. Sci.* 370, 277–283. doi: 10.1016/j.jns.2016.10.002

Herold, F., Wiegel, P., Scholkmann, F., and Müller, N. (2018). Applications of functional near-infrared spectroscopy (FNIRS) neuroimaging in exercise–cognition science: a systematic, methodology-focused review. *J. Clin. Med.* 7:466. doi: 10.3390/jcm7120466

Herold, F., Wiegel, P., Scholkmann, F., Thiers, A., Hamacher, D., and Schega, L. (2017). Functional near-infrared spectroscopy in movement science: a systematic review on cortical activity in postural and walking tasks. *Neurophotonics* 4:041403. doi: 10.1117/1.nph.4.4.041403

Holtzer, R., Epstein, N., Mahoney, J. R., Izzetoglu, M., and Blumen, H. M. (2014). Neuroimaging of mobility in aging: a targeted review. *J. Gerontol. A Biol. Sci. Med. Sci.* 69, 1375–1388. doi: 10.1093/gerona/glu052

Holtzer, R., George, C. J., Izzetoglu, M., and Wang, C. (2018a). The effect of diabetes on prefrontal cortex activation patterns during active walking in older adults. *Brain Cogn.* 125, 14–22. doi: 10.1016/j.bandc.2018.03.002

Holtzer, R., Izzetoglu, M., Chen, M., and Wang, C. (2018b). Distinct FNIRS-Derived HbO2 trajectories during the course and over repeated walking trials under single- and dual-task conditions: implications for within session learning and prefrontal cortex efficiency in older adults. *J. Gerontol. A* 74, 1076–1083. doi: 10.1093/gerona/gly181

Holtzer, R., Kraut, R., Izzetoglu, M., and Ye, K. (2019). The effect of fear of falling on prefrontal cortex activation and efficiency during walking in older adults. *Geroscience* 41, 89–100. doi: 10.1007/s11357-019-00056-4

Holtzer, R., Mahoney, J. R., Izzetoglu, M., Wang, C., England, S., and Verghese, J. (2015). Online fronto-cortical control of simple and attention-demanding locomotion in humans. *Neuroimage* 112, 152–159. doi: 10.1016/j.neuroimage.2015.03.002

Holtzer, R., Rakitin, B. C., Steffener, J., Flynn, J., Kumar, A., and Stern, Y. (2009). Age effects on load-dependent brain activations in working memory for novel material. *Brain Res.* 1249, 148–161. doi: 10.1016/j.brainres.2008.10.009

Holtzer, R., Schoen, C., Demetriou, E., Mahoney, J. R., Izzetoglu, M., Wang, C., et al. (2017a). Stress and gender effects on prefrontal cortex oxygenation levels assessed during single and dual-task walking conditions. *Eur. J. Neurosci.* 45, 660–670. doi: 10.1111/ejn.13518

Holtzer, R., Verghese, J., Allali, G., Izzetoglu, M., Wang, C., and Mahoney, J. R. (2016). Neurological gait abnormalities moderate the functional brain signature of the posture first hypothesis. *Brain Topogr.* 29, 334–343. doi: 10.1007/s10548-015-0465-z

Holtzer, R., Yuan, J., Verghese, J., Mahoney, J. R., Izzetoglu, M., and Wang, C. (2017b). Interactions of subjective and objective measures of fatigue defined in the context of brain control of locomotion. *J. Gerontol. A Biol. Sci. Med. Sci.* 72, 417–423. doi: 10.1093/gerona/glw167

Hoshi, Y. (2007). Functional near-infrared spectroscopy: current status and future prospects. *J. Biomed. Optics* 12:062106. doi: 10.1117/1.2804911

Huppert, T. J., Karim, H., Lin, C., Alqahtani, B. A., Greenspan, S. L., and Sparto, P. J. (2017). Functional imaging of cognition in an old-old population: a case for portable functional near-infrared spectroscopy. *PLoS One* 12:e0184918. doi: 10.1371/journal.pone.0184918

Hyodo, K., Dan, I., Kyutoku, Y., Suwabe, K., Byun, K., Ochi, G., et al. (2016). The association between aerobic fitness and cognitive function in older men mediated by frontal lateralization. *Neuroimage* 125, 291–300. doi: 10.1016/j.neuroimage.2015.09.062

Inzitari, M., Baldereschi, M., Di Carlo, A., Di Bari, M., Marchionni, N., Scafato, E., et al. (2007). Impaired attention predicts motor performance decline in older community-dwellers with normal baseline mobility: results from the italian longitudinal study on aging (ILSA). *J. Gerontol. A Biol. Sci. Med. Sci.* 62, 837–843. doi: 10.1093/gerona/62.8.837

Jokinen, H., Kalska, H., Ylikoski, R., Madureira, S., Verdelho, A., Van Der Flier, W. M., et al. (2009). Longitudinal cognitive decline in subcortical ischemic vascular disease -the ladis study. *Cerebrovasc. Dis.* 27, 384–391. doi: 10.1159/000207442

Jurado, M. B., and Rosselli, M. (2007). The elusive nature of executive functions: a review of our current understanding. *Neuropsychol. Rev.* 17, 213–233. doi: 10.1007/s11065-007-9040-z

Kahya, M., Moon, S., Ranchet, M., Vukas, R. R., Lyons, K. E., Pahwa, R., et al. (2019). Brain activity during dual task gait and balance in aging and age-related neurodegenerative conditions: a systematic review. *Exp. Gerontol.* 128:110756. doi: 10.1016/j.exger.2019.110756

Katzorke, A., Zeller, J. B. M., Müller, L. D., Lauer, M., Polak, T., Deckert, J., et al. (2018). Decreased hemodynamic response in inferior frontotemporal regions in elderly with mild cognitive impairment. *Psychiatry Res. Neuroimaging* 274, 11–18. doi: 10.1016/j.pscychresns.2018.02.003

Kirilina, E., Jelzow, A., Heine, A., Niessing, M., Wabnitz, H., Brühl, R., et al. (2012). The physiological origin of task-evoked systemic artefacts in functional near infrared spectroscopy. *Neuroimage* 61, 70–81. doi: 10.1016/j.neuroimage.2012.02.074

Kisler, K., Nelson, A. R., Montagne, A., and Zlokovic, B. V. (2017). Cerebral blood flow regulation and neurovascular dysfunction in alzheimer disease. *Nat. Rev. Neurosci.* 18, 419–434. doi: 10.1038/nrn.2017.48

la Fougère, C., Zwergal, A., Rominger, A., Förster, S., Fesl, G., Dieterich, M., et al. (2010). Real versus imagined locomotion: a [18F]-FDG PET-FMRI comparison. *Neuroimage* 50, 1589–1598. doi: 10.1016/j.neuroimage.2009.12.060

Laguë-Beauvais, M., Fraser, S. A., Desjardins-Crépeau, L., Castonguay, N., Desjardins, M., Lesage, F., et al. (2015). Shedding light on the effect of priority instructions during dual-task performance in younger and older adults: a FNIRS study. *Brain Cogn.* 98, 1–14. doi: 10.1016/j.bandc.2015.05.001

Leone, C., Feys, P., Moumdjian, L., D'Amico, E., Zappia, M., and Patti, F. (2017). Cognitive-motor dual-task interference: a systematic review of neural correlates. *Neurosci. Biobehav. Rev.* 75, 348–360. doi: 10.1016/j.neubiorev.2017.01.010

Lucas, M., Wagshul, M. E., Izzetoglu, M., and Holtzer, R. (2018). Moderating effect of white matter integrity on brain activation during dual-task walking in older adults. *J. Gerontol. A* 74, 435–441. doi: 10.1093/gerona/gly131

Mahoney, J. R., Holtzer, R., Izzetoglu, M., Zemon, V., Verghese, J., and Allali, G. (2016). The role of prefrontal cortex during postural control in parkinsonian syndromes a functional near-infrared spectroscopy study. *Brain Res.* 1633, 126–138. doi: 10.1016/j.brainres.2015.10.053

Maidan, I., Bernad-Elazari, H., Giladi, N., Hausdorff, J. M., and Mirelman, A. (2017). When is higher level cognitive control needed for locomotor tasks among patients with Parkinson's disease? *Brain Topogr.* 30, 531–538. doi: 10.1007/s10548-017-0564-0

Maidan, I., Nieuwhof, F., Bernad-Elazari, H., Reelick, M. F., Bloem, B. R., Giladi, N., et al. (2016). The role of the frontal lobe in complex walking among patients with Parkinson's disease and healthy older adults: an FNIRS study". *Neurorehabil. Neural Repair* 30, 963–971. doi: 10.1177/1545968316650426

Mirelman, A., Maidan, I., Bernad-Elazari, H., Shustack, S., Giladi, N., and Hausdorff, J. M. (2017). Effects of aging on prefrontal brain activation during challenging walking conditions. *Brain Cogn.* 115, 41–46. doi: 10.1016/j.bandc.2017.04.002

Mori, T., Takeuchi, N., and Izumi, S. (2018). Prefrontal cortex activation during a dual task in patients with stroke. *Gait Posture* 59, 193–198. doi: 10.1016/j.gaitpost.2017.09.032

Müller, L. D., Guhn, A., Zeller, J. B. M., Biehl, S. C., Dresler, T., Hahn, T., et al. (2014). Neural correlates of a standardized version of the trail making test in young and elderly adults: a functional near-infrared spectroscopy study. *Neuropsychologia* 56, 271–279. doi: 10.1016/j.neuropsychologia.2014.01.019

Nieuwhof, F., Reelick, M. F., Maidan, I., Mirelman, A., Hausdorff, J. M., and Olde Rikkert, M. G. M. (2016). Measuring prefrontal cortical activity during dual task walking in patients with Parkinson's disease: feasibility of using a new portable FNIRS device. *Pilot Feasibility Stud.* 2, 1–11. doi: 10.1186/s40814-016-0099-2

Niu, H., Li, X., Chen, Y., Ma, C., Zhang, J., and Zhang, Z. (2013). Reduced frontal activation during a working memory task in mild cognitive impairment: a non-invasive near-infrared spectroscopy study. *CNS Neurosci. Ther.* 19, 125–131. doi: 10.1111/cns.12046

Noda, T., Nakagome, K., Setoyama, S., and Matsushima, E. (2017). Working memory and prefrontal/temporal hemodynamic responses during post-task period in patients with schizophrenia: a multi-channel near-infrared spectroscopy study. *J. Psychiatr. Res.* 95, 288–298. doi: 10.1016/j.jpsychires.2017.09.001

Oboshi, Y., Kikuchi, M., Shimizu, Y., Yoshimura, Y., Hiraishi, H., Okada, H., et al. (2014). Pre-task prefrontal activation during cognitive processes in aging: a near-infrared spectroscopy study. *PLoS One* 9:e098779. doi: 10.1371/journal.pone.0098779

Ohsugi, H., Ohgi, S., Shigemori, K., and Schneider, E. B. (2013). Differences in dual-task performance and prefrontal cortex activation between younger and older adults. *BMC Neurosci.* 14:10. doi: 10.1186/1471-2202-14-10

Okamoto, M., Dan, H., Shimizu, K., Takeo, K., Amita, T., Oda, I., et al. (2004). Multimodal assessment of cortical activation during apple peeling by NIRS and FMRI. *Neuroimage* 21, 1275–1288. doi: 10.1016/j.neuroimage.2003.12.003

Osofundiya, O., Benden, M. E., Dowdy, D., and Mehta, R. K. (2016). Obesity-specific neural cost of maintaining gait performance under complex conditions in community-dwelling older adults. *Clin. Biomech.* 35, 42–48. doi: 10.1016/j.clinbiomech.2016.03.011

Pfeifer, M. D., Scholkmann, F., and Labruyère, R. (2018). Signal processing in functional near-infrared spectroscopy (fnirs): methodological differences lead to different statistical results. *Front. Hum. Neurosci.* 11:641. doi: 10.3389/fnhum.2017.00641

Pifferi, A., Contini, D., Dalla Mora, A., Farina, A., Spinelli, L., and Torricelli, A. (2016). New frontiers in time-domain diffuse optics, a review. *J. Biomed. Optics* 21:091310. doi: 10.1117/1.JBO.21.9.091310

Plichta, M. M., Herrmann, M. J., Baehne, C. G., Ehlis, A. C., Richter, M. M., Pauli, P., et al. (2006). Event-related functional near-infrared spectroscopy (FNIRS): are the measurements reliable? *Neuroimage* 31, 116–124. doi: 10.1016/j.neuroimage.2005.12.008

Rosano, C., Aizenstein, H., Brach, J., Longenberger, A., Studenski, S., and Newman, A. B. (2008). Gait measures indicate underlying focal gray matter atrophy in the brain of older adults. *J. Gerontol. A Biol. Sci. Med. Sci.* 63, 1380–1388. doi: 10.1093/gerona/63.12.1380

Rosen, B. R., and Savoy, R. L. (2012). FMRI at 20: has it changed the world? *Neuroimage* 62, 1316–1324. doi: 10.1016/j.neuroimage.2012.03.004

Rosso, A. L., Cenciarini, M., Sparto, P. J., Loughlin, P. J., Furman, J. M., and Huppert, T. J. (2017). Neuroimaging of an attention demanding dual-task during dynamic postural control. *Gait Posture* 57, 193–198. doi: 10.1016/j.gaitpost.2017.06.013

Rosso, A. L., Metti, A. L., Faulkner, K., Redfern, M., Yaffe, K., Launer, L., et al. (2019). Complex walking tasks and risk for cognitive decline in high functioning older adults. *J. Alzheimers Dis.* 71, S65–S73. doi: 10.3233/JAD-181140

Rypma, B., and D'Esposito, M. (2000). Isolating the neural mechanisms of age-related changes in human working memory. *Nat. Neurosci.* 3, 509–515. doi: 10.1038/74889

Sala, S., Baddeley, A., Papagno, C., and Spinnler, H. (1995). Dual-task paradigm: a means to examine the central executive. *Ann. N. Y. Acad. Sci.* 769, 161–172. doi: 10.1111/j.1749-6632.1995.tb38137.x

Scholkmann, F., Kleiser, S., Jaako Metz, A., Zimmermann, R., Mata Pavia, J., Wolf, U., et al. (2014). A review on continuous wave functional near-infrared spectroscopy and imaging instrumentation and methodology. *Neuroimage* 85, 6–27. doi: 10.1016/j.neuroimage.2013.05.004

Stern, Y. (2005). Brain networks associated with cognitive reserve in healthy young and old adults. *Cereb. Cortex* 15, 394–402. doi: 10.1093/cercor/bhh142

Stern, Y. (2009). Cognitive reserve. *Neuropsychologia* 47, 2015–2028. doi: 10.1016/j.neuropsychologia.2009.03.004

Strangman, G., Culver, J. P., Thompson, J. H., and Boas, D. A. (2002). A quantitative comparison of simultaneous bold FMRI and NIRS recordings during functional brain activation. *Neuroimage* 17, 719–731. doi: 10.1006/nimg.2002.1227

Stuart, S., Vitorio, R., Morris, R., Martini, D. N., Fino, P. C., and Mancini, M. (2018). Cortical activity during walking and balance tasks in older adults and in people with Parkinson's disease: a structured review. *Maturitas* 113, 53–72. doi: 10.1016/j.maturitas.2018.04.011

Szameitat, A. J., Schubert, T., Müller, K., Von Yves, and Cramon, D. (2002). Localization of executive functions in dual-task performance with FMRI. *J. Cogn. Neurosci.* 14, 1184–1199. doi: 10.1162/089892902760807195

Tachtsidis, I., and Scholkmann, F. (2016). False positives and false negatives in functional near-infrared spectroscopy: issues, challenges, and the way forward. *Neurophotonics* 3:031405. doi: 10.1117/1.NPh.3.3.031405

Takeuchi, N., Mori, T., Suzukamo, Y., Tanaka, N., and Izumi, S. (2016). Parallel processing of cognitive and physical demands in left and right prefrontal cortices during smartphone use while walking. *BMC Neurosci.* 17:9. doi: 10.1186/s12868-016-0244-0

Thumm, P. C., Maidan, I., Brozgol, M., Shustak, S., Gazit, E., Shema Shiratzki, S., et al. (2018). Treadmill walking reduces pre-frontal activation in patients with Parkinson's disease. *Gait Posture* 62, 384–387. doi: 10.1016/j.gaitpost.2018.03.041

Torricelli, A., Contini, D., Pifferi, A., Caffini, M., Re, R., Zucchelli, L., et al. (2014). Time domain functional nirs imaging for human brain mapping. *Neuroimage* 85, 28–50. doi: 10.1016/j.neuroimage.2013.05.106

Uemura, K., Shimada, H., Doi, T., Hakizako, H., Tsutsumimoto, K., Park, H., et al. (2016). Reduced prefrontal oxygenation in mild cognitive impairment during memory retrieval. *Int. J. Geriatr. Psychiatry* 31, 583–591. doi: 10.1002/gps.4363

Venkatraman, V. K., Aizenstein, H., Guralnik, J., Newman, A. B., Glynn, N. W., Taylor, C., et al. (2010). Executive control function, brain activation and white matter hyperintensities in older adults. *Neuroimage* 49, 3436–3442. doi: 10.1016/j.neuroimage.2009.11.019

Verghese, J., Annweiler, C., Ayers, E., Barzilai, N., Beauchet, O., Bennett, D. A., et al. (2014). Motoric cognitive risk syndrome: multicountry prevalence and dementia risk. *Neurology* 83, 718–726. doi: 10.1212/WNL.0000000000000717

Verghese, J., Holtzer, R., Lipton, R. B., and Wang, C. (2012). Mobility stress test approach to predicting frailty, disability, and mortality in high-functioning older adults. *J. Am. Geriatr. Soc.* 60, 1901–1905. doi: 10.1111/j.1532-5415.2012.04145.x

Verghese, J., Wang, C., Ayers, E., Izzetoglu, M., and Holtzer, R. (2017). Brain activation in high-functioning older adults and falls: prospective cohort study. *Neurology* 88, 191–197. doi: 10.1212/WNL.0000000000003421

Vermeij, A., van Beek, A. H. E. A., Reijs, B. L. R., Claassen, J. A. H. R., and Kessels, R. P. C. (2014). An exploratory study of the effects of spatial working-memory load on prefrontal activation in low- and high-performing elderly. *Front. Aging Neurosci.* 6:303. doi: 10.3389/fnagi.2014.00303

Vitorio, R., Stuart, S., Rochester, L., Alcock, L., and Pantall, A. (2017). FNIRS response during walking — artefact or cortical activity? A systematic review. *Neurosci. Biobehav. Rev.* 83, 160–172. doi: 10.1016/j.neubiorev.2017.10.002

Wager, T. D., Jonides, J., and Reading, S. (2004). Neuroimaging studies of shifting attention: a meta-analysis. *Neuroimage* 22, 1679–1693. doi: 10.1016/j.neuroimage.2004.03.052

Wagshul, M. E., Lucas, M., Ye, K., Izzetoglu, M., and Holtzer, R. (2019). Multi-modal neuroimaging of dual-task walking: structural MRI and FNIRS analysis reveals prefrontal grey matter volume moderation of brain activation in older adults. *Neuroimage* 189, 745–754. doi: 10.1016/j.neuroimage.2019.01.045

Weinstein, A. M., Voss, M. W., Prakash, Chaddock, L., Szabo, A., White, S. M., et al. (2012). The association between aerobic fitness and executive function is mediated by prefrontal cortex volume. *Brain Behav. Immun.* 26, 811–819. doi: 10.1016/j.bbi.2011.11.008

Yap, K. H., Ung, W., Ebenezer, E. G. M., Nordin, N., Chin, P., Sugathan, S., et al. (2017). Visualizing hyperactivation in neurodegeneration based on prefrontal oxygenation: a comparative study of mild Alzheimer's disease, mild cognitive impairment, and healthy controls. *Front. Aging Neurosci.* 9:287. doi: 10.3389/fnagi.2017.00287

Yaple, Z. A., Stevens, W. D., and Arsalidou, M. (2019). Meta-analyses of the n-back working memory task: FMRI evidence of age-related changes in prefrontal cortex involvement across the adult lifespan. *Neuroimage* 196, 16–31. doi: 10.1016/j.neuroimage.2019.03.074

Yeung, M. K., Sze, S. L., Woo, J., Kwok, T., Shum, D. H. K., Yu, R., et al. (2016a). Altered frontal lateralization underlies the category fluency deficits in older adults with mild cognitive impairment: a near-infrared spectroscopy study. *Front. Aging Neurosci.* 8:59. doi: 10.3389/fnagi.2016.00059

Yeung, M. K., Sze, S. L., Woo, J., Kwok, T., Shum, D. H., Yu, R., et al. (2016b). Reduced frontal activations at high working memory load in mild cognitive impairment: near-infrared spectroscopy. *Dement. Geriatr. Cogn. Disord.* 42, 278–296. doi: 10.1159/000450993

Yücel, M. A., Selb, J., Aasted, C. M., Petkov, M. P., Becerra, L., Borsook, D., et al. (2015). Short separation regression improves statistical significance and better localizes the hemodynamic response obtained by near-infrared spectroscopy for tasks with differing autonomic responses. *Neurophotonics* 2:035005. doi: 10.1117/1.NPh.2.3.035005

Zhang, X., Noah, J. A., and Hirsch, J. (2016). Separation of the global and local components in functional near-infrared spectroscopy signals using principal component spatial filtering. *Neurophotonics* 3:015004. doi: 10.1117/1.NPh.3.1.015004

Zwergal, A., Linn, J., Xiong, G., Brandt, T., Strupp, M., and Jahn, K. (2012). Aging of human supraspinal locomotor and postural control in FMRI. *Neurobiol. Aging* 33, 1073–1084. doi: 10.1016/j.neurobiolaging.2010.09.022

Conflict of Interest: The authors declare that the research was conducted in the absence of any commercial or financial relationships that could be construed as a potential conflict of interest.

frontiers in Aging Neuroscience

BRIEF RESEARCH REPORT
published: 21 January 2020
doi: 10.3389/fnagi.2019.00364

Brain Gray Matter Volume Associations With Abnormal Gait Imagery in Patients With Mild Cognitive Impairment: Results of a Cross-Sectional Study

Olivier Beauchet[1,2,3,4]*, *Maxime Montembeault*[5,6] *and Gilles Allali*[7]

[1]*Department of Medicine, Division of Geriatric Medicine, Sir Mortimer B. Davis—Jewish General Hospital and Lady Davis Institute for Medical Research, McGill University, Montreal, QC, Canada,* [2]*Dr. Joseph Kaufmann Chair in Geriatric Medicine, Faculty of Medicine, McGill University, Montreal, QC, Canada,* [3]*Centre of Excellence on Longevity, McGill Integrated University Health Network, Montreal, QC, Canada,* [4]*Lee Kong Chian School of Medicine, Nanyang Technological University, Singapore, Singapore,* [5]*Centre de Recherche de l'Institut Universitaire de Gériatrie de Montréal, Montréal, QC, Canada,* [6]*Département de Psychologie, Université de Montréal, Montréal, QC, Canada,* [7]*Department of Neurology, Geneva University Hospital and University of Geneva, Geneva, Switzerland*

Individuals with mild cognitive impairment (MCI) have worse gait performance compared to cognitive healthy individuals (CHI). The discrepancy between imagined and performed timed up and go test (TUG), known as the TUG delta time, is a marker of brain gait control impairment in individuals with MCI. The study aims to examine the association between the TUG delta time and brain gray matter (GM) volumes in CHI and individuals with MCI. A total of 326 participants, 156 CHI and 170 MCI, with TUG delta time and a brain T1-weighted magnetic resonance imaging (MRI) were selected in this cross-sectional study. Individuals with MCI were older and had greater (i.e., worst performance) performed TUG and TUG delta time compared to CHI. The GM volume association with TUG delta time was examined in CHI and MCI assuming that increased TUG delta time would be associated with locally decreased GM volumes. No significant association was found in CHI, whereas TUG delta time was negatively associated with the GM volume of the right medial temporal lobe in individuals with MCI.

Keywords: MRI, aged, brain, motricity, EPI-epidemiology

OPEN ACCESS

Edited by:
Mohamad Habes, University of Pennsylvania, United States

Reviewed by:
Laura Eva Jonkman, VU University Medical Center, Netherlands
Dafin F. Muresanu, Iuliu Hatieganu University of Medicine and Pharmacy, Romania

***Correspondence:**
Olivier Beauchet
olivier.beauchet@mcgill.ca

Received: *13 June 2019*
Accepted: *11 December 2019*
Published: *21 January 2020*

Citation:
Beauchet O, Montembeault M and Allali G (2020) Brain Gray Matter Volume Associations With Abnormal Gait Imagery in Patients With Mild Cognitive Impairment: Results of a Cross-Sectional Study. Front. Aging Neurosci. 11:364. doi: 10.3389/fnagi.2019.00364

INTRODUCTION

Individuals with mild cognitive impairment (MCI) have worse gait performance compared to cognitive healthy individuals (CHI; Bahureksa et al., 2017; Beauchet et al., 2018). Impairment in gait control at a brain level explains in large part poor gait performance in individuals with MCI (Beauchet et al., 2018). The mental chronometry applied to the timed up and go test (TUG)—the time needed for standing up, walking 3 m, turning, walking back and sitting down—is used to examine impairment in gait control in individuals with MCI (Beauchet et al., 2014). It has been shown that individuals with MCI executed the imagined TUG more quickly than the performed TUG, but not CHI (Beauchet et al., 2014). The discrepancy between imagined and performed TUG, known as TUG delta time, has been proposed as a marker of impairment in gait control at a brain level in individuals with MCI (Beauchet et al., 2010, 2014).

No imaging study has examined the association of TUG delta time and brain regions in CHI and individuals with MCI. The hippocampus is a key brain region involved in gait control (Seidler et al., 2010). Decreased hippocampal volume has been reported in individuals with MCI (Tabatabaei-Jafari et al., 2015). Performed TUG has been negatively associated with brain volume reduction in total gray matter (GM) and in the hippocampus in non-demented older adults (Allali et al., 2016). Because both increased TUG delta time and decreased hippocampal volume have been separately reported in individuals with MCI, we hypothesized that increased TUG delta time will be associated with decreased hippocampal volume. The study aims to examine the association between TUG delta time and brain GM volumes in CHI and individuals with MCI.

MATERIALS AND METHODS

A total of 326 participants—156 CHI and 170 MCI—referred to the memory clinic of Angers University Hospital (France) were recruited in the "Gait and Alzheimer Interactions Tracking" (GAIT) study. All participants with TUG delta time and a brain T1-weighted magnetic resonance imaging (MRI) were selected in this cross-sectional study. Exclusion criteria were an acute medical illness in the past month, neurological and psychiatric diseases other than cognitive impairment, and medical conditions affecting gait, dementia, and morphological (i.e., dilatation of ventricular system compatible with a diagnosis of normal pressure hydrocephalus) or vascular abnormalities (i.e., stroke) on the brain MRI. Cognitive status (i.e., CHI and MCI) was defined during a multidisciplinary meeting. Information on cognitive performances, physical examination findings, blood tests, and the brain MRI were used. Mini Mental State Examination (MMSE; Folstein et al., 1975), Frontal Assessment Battery (FAB; Dubois et al., 2000), Alzheimer's Disease Assessment Scale–Cognitive subscale (ADAS-cog; Rosen et al., 1984), Trail Making Test (TMT) parts A and B (Brown et al., 1958), French version of the Free and Cued Selective Reminding Test (Grober et al., 1988; Van der Linden et al., 2004), and Instrumental Activities of Daily Living scale (IADL; Pérès et al., 2006) were the cognitive test used for the assessment of cognitive performance. Participants who had normal neuropsychological and functional performances were considered as cognitively healthy. MCI was defined according to the criteria detailed by Dubois et al. (2010). Participants with any form of MCI, amnestic or non-amnestic and affecting single or multiple domains, were pooled together. Brain imaging was performed with a 1.5 and 3 Tesla MRI scanner (Magnetom Avanto, Siemens Medical Solutions, Erlangen, Germany) following a scanning protocol previously described (Allali et al., 2019). The structural images were processed using voxel-based morphometry (VBM) implemented in SPM12, as previously described (Allali et al., 2019). Overall, the traditional VBM pre-processing steps were conducted, including the creation of study-specific template using the diffeomorphic anatomical registration using exponentiated lie algebra (DARTEL) approach. Angers Ethical Committee (France) approved the study protocol and the recruited participants gave their written informed consent.

The participants' characteristics were summarized using means and standard deviations or frequencies and percentages, as appropriate. Unpaired *t*-test or Chi-square test was used for the comparisons between CHI and MCI. Whole-brain VBM analyses were conducted to determine the correlations between GM volume association with TUG delta time in CHI and MCI. TUG delta time was entered as a covariate of interest in a multiple regression statistical model including both CHI and MCI individuals entered separately, assuming that increased TUG delta time would be associated with regional decreased GM volumes. Each model was adjusted by age, sex, total intracranial volume, white matter abnormalities and type of MRI. The significance of each effect of interest was determined using the theory of Gaussian fields. Statistical threshold of P-value < 0.05 family-wise error (FWE) cluster-corrected was used for all analyses. In addition to correcting for multiple comparisons, a correction for non-stationary smoothness was applied using the implementation of this method in the VBM5 toolbox, which is necessary to avoid false positives or decreased sensitivity when using cluster-size tests (Hayasaka et al., 2004).

RESULTS

As shown in **Table 1**, individuals with MCI were older ($P = 0.001$), had greater performed TUG ($P = 0.001$) and TUG delta time ($P \leq 0.001$) compared to CHI. There was more male in MCI compared to CHI ($P = 0.044$). There was no significant difference for the other characteristics. The associations of brain GM volumes with TUG delta time are shown in **Table 2** and **Figure 1**. No significant association at the cluster-corrected threshold was found in CHI, whereas TUG delta time was negatively associated with a large medial temporal cluster including the right entorhinal cortex, the amygdala, the parahippocampal gyrus, the insula, and the hippocampus ($P \leq 0.05$ cluster-corrected) in individuals with MCI. TUG delta time was not associated with GM volume in this region in CHI even when considering the results with an uncorrected threshold.

DISCUSSION

The main finding is that increased TUG delta time was negatively associated with the GM volume of the right medial temporal lobe in individuals with MCI, but not in CHI. This association suggests that TUG delta time may be an appropriate marker of gait control in individuals with MCI; this discrepancy between imagined and performed TUG (i.e., worst gait control) being associated with a decreased GM volume (i.e., worst brain structure) in a key brain region for gait control. This result is consistent with a previous association found between increased gait variability (i.e., worst gait performance) and low hippocampal volume in individuals with MCI and mild dementia (Seidler et al., 2010; Beauchet et al., 2019). Atrophy of the hippocampus is a morphological characteristic of individuals with MCI (Tabatabaei-Jafari et al., 2015). This brain region is a key region involved in memorization and

TABLE 1 | Clinical characteristics of participants (n = 326).

	Participants		*P*-value*
	CHI (n = 156)	MCI (n = 170)	
Age (years), mean ± SD	70.4 ± 3.7	70.0 ± 5.1	**0.001**
Male, *n* (%)	81 (51.9)	107 (62.9)	**0.044**
High educational level‡, *n* (%)	4 (2.6)	3 (1.8)	0.619
TUG			
Realized (s), mean ± SD	9.5 ± 1.9	10.4 ± 3.1	**0.001**
Imagined (s), mean ± SD	7.3 ± 2.6	6.8 ± 3.0	0.159
Delta time (%)	30.1 ± 27.5	44.4 ± 33.8	**<0.001**
3 Tesla MRI scanner, *n* (%)	60 (38.5)	70 (41.2)	0.617
Total cranial volume (cm^3), mean ± SD	1,543.1 ± 254.0	1,565.4 ± 323.1	0.494
Total white matter abnormality‖ volume (cm^3), mean ± SD	391.4 ± 372.7	454.2 ± 664.3	0.302

*MCI, mild cognitive impairment; CHI, cognitively healthy individuals; SD, Standard deviation; *comparisons based on unpaired t-test or Chi-square test, as appropriate; ‡high school and above; ‖defined as MRI signal abnormalities (i.e. T1 hypointensities) and measured using FreeSurfer software; P-value significant (i.e. <0.05) indicated in bold.*

TABLE 2 | Association between gray matter volumes and delta timed up and go time in individuals cognitively healthy and with mild cognitive impairment.

Group of individuals	Cluster/peak regions	Side	*x*	*y*	*z*	Extent	*T*-value*
MCI	Entorhinal cortex	R	21	1	−42	1,024	3.98
	Amygdala	R	31	1	−14	sc	3.77
	Parahippocampal gyrus	R	21	3	−31	sc	3.23
	Insula	R	29	11	−14	sc	3.19
	Hippocampus	R	24	−1	−22	sc	3.15

*MCI, mild cognitive impairment; R, Right; L, Left; sc, same cluster; model adjusted by age, sex, total intracranial volume, white matter abnormalities and type of MRI; *P ≤ 0.05 cluster-corrected.*

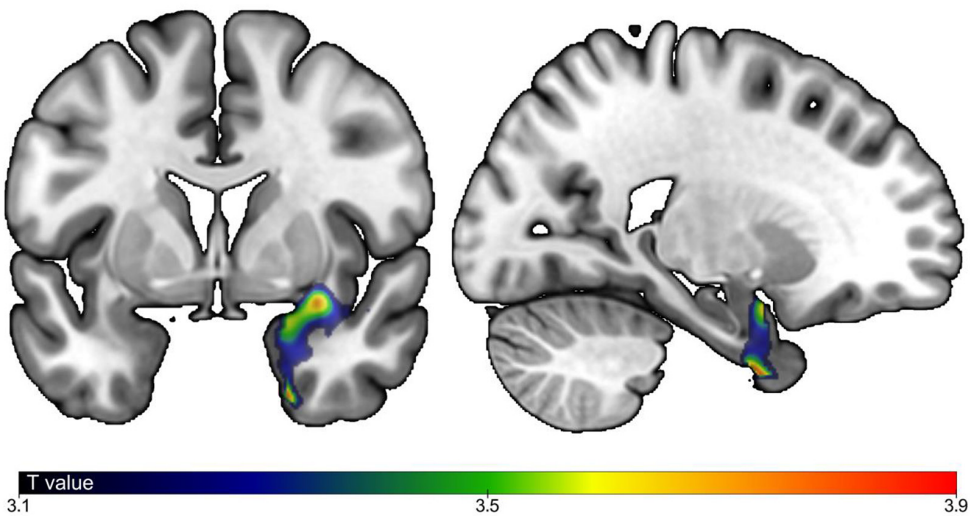

FIGURE 1 | Correlations between brain gray matter (GM) volumes and timed up and go delta time. Correlation between GM regions and gait speed with *P*-Value ≤ 0.05, cluster corrected). Strength of positive association in individuals with mild cognitive impairment (MCI) shown in blue (lowest) to red (highest). Model adjusted by age, sex, total intracranial volume, white matter abnormalities and type of magnetic resonance imaging (MRI).

in navigation defined as the ability to move safely in the environment (Tabatabaei-Jafari et al., 2015). TUG delta time may be assimilated as a marker of navigation, low value being an expression of safe navigation and good gait control (Beauchet et al., 2010, 2014). In contrast, increased TUG delta time means inability to navigate appropriately, and this abnormality is associated with abnormality of the brain region controlling navigation. Interestingly, our results were only significant for the right hemisphere. In previous studies focusing on spatial navigation, the right hemisphere and more specifically, the right hippocampus, has been more consistently reported to be related to navigation than the left. For example, in the investigation of navigation skills of London taxi drivers, the correlation between time taxi driving and hippocampal GM volume was right lateralized (Maguire et al., 2006). However, the left hippocampus has been also associated with navigation (Ghaem et al., 1997). The cross-sectional design of this study cannot afford information about the causality of the association

between decreased GM volume of the medial temporal lobe and increased TUG delta time, which is the main limitation of our study. Further research needs to examine this association with an observational, prospective, and cohort design with the objective to better understand brain control disorganization in patients with MCI.

DATA AVAILABILITY STATEMENT

The datasets analyzed in this article are not publicly available. Requests to access the datasets should be directed to olivier.beauchet@mcgill.ca.

ETHICS STATEMENT

The studies involving human participants were reviewed and approved by Angers Hospital ethic committe. The patients/participants provided their written informed consent to participate in this study.

AUTHOR CONTRIBUTIONS

All authors listed have made substantial, direct and intellectual contribution to the work, and approved it for publication.

FUNDING

The study was financially supported by the French Ministry of Health (Projet Hospitalier de Recherche Clinique national n°2009-A00533-54).

ACKNOWLEDGMENTS

We acknowledge all participants included in the present study.

REFERENCES

Allali, G., Annweiler, C., Predovan, D., Bherer, L., and Beauchet, O. (2016). Brain volume changes in gait control in patients with mild cognitive impairment compared to cognitively healthy individuals; GAIT study results. *Exp. Gerontol.* 76, 72–79. doi: 10.1016/j.exger.2015.12.007

Allali, G., Montembeault, M., Brambati, S. M., Bherer, L., Blumen, H. M., Launay, C. P., et al. (2019). Brain structure covariance associated with gait control in aging. *J. Gerontol. A Biol. Sci. Med. Sci.* 74, 705–713. doi: 10.1093/gerona/gly123

Bahureksa, L., Najafi, B., Saleh, A., Sabbagh, M., Coon, D., Mohler, M. J., et al. (2017). The impact of mild cognitive impairment on gait and balance: a systematic review and meta-analysis of studies using instrumented assessment. *Gerontology* 63, 67–83. doi: 10.1159/000445831

Beauchet, O., Annweiler, C., Assal, F., Bridenbaugh, S., Herrmann, F. R., Kressig, R. W., et al. (2010). Imagined timed up and go test: a new tool to assess higher-level gait and balance disorders in older adults? *J. Neurol. Sci.* 294, 102–106. doi: 10.1016/j.jns.2010.03.021

Beauchet, O., Blumen, H. M., Callisaya, M. L., De Cock, A. M., Kressig, R. W., Srikanth, V., et al. (2018). Spatiotemporal gait characteristics associated with cognitive impairment: a multicenter cross-sectional study, the intercontinental "gait, cognition and decline" initiative. *Curr. Alzheimer Res.* 15, 273–282. doi: 10.2174/1567205014666170725125621

Beauchet, O., Launay, C. P., Sejdić, E., Allali, G., and Annweiler, C. (2014). Motor imagery of gait: a new way to detect mild cognitive impairment? *J. Neuroeng. Rehabil.* 11:66. doi: 10.1186/1743-0003-11-66

Beauchet, O., Launay, C. P., Sekhon, H., Montembeault, M., and Allali, G. (2019). Association of hippocampal volume with gait variability in pre-dementia and dementia stages of Alzheimer disease: results from a cross-sectional study. *Exp. Gerontol.* 115, 55–61. doi: 10.1016/j.exger.2018.11.010

Brown, E. C., Casey, A., Fisch, R. I., and Neuringer, C. (1958). Trail making test as a screening device for the detection of brain damage. *J. Consult. Psychol.* 22, 469–474. doi: 10.1037/h0039980

Dubois, B., Feldman, H. H., Jacova, C., Cummings, J. L., Dekosky, S. T., Barberger-Gateau, P., et al. (2010). Revising the definition of Alzheimer's disease: a new lexicon. *Lancet Neurol.* 9, 1118–1127. doi: 10.1016/S1474-4422(10)70223-4

Dubois, B., Slachevsky, A., Litvan, I., and Pillon, B. (2000). The FAB: a frontal assessment battery at bedside. *Neurology* 55, 1621–1626. doi: 10.1212/wnl.55.11.1621

Folstein, M. F., Folstein, S. E., and McHugh, P. R. (1975). "Mini-mental state". *J. Psychiatr. Res.* 12, 189–198. doi: 10.1016/0022-3956(75)90026-6

Ghaem, O., Mellet, E., Crivello, F., Tzourio, N., Mazoyer, B., Berthoz, A., et al. (1997). Mental navigation along memorized routes activates the hippocampus, precuneus and insula. *Neuroreport* 8, 739–744. doi: 10.1097/00001756-199702100-00032

Grober, E., Buschke, H., Crystal, H., Bang, S., and Dresner, R. (1988). Screening for dementia by memory testing. *Neurology* 38, 900–903. doi: 10.1212/wnl.38.6.900

Hayasaka, S., Phan, K. L., Liberzon, I., Worsley, K. J., and Nichols, T. E. (2004). Nonstationary cluster-size inference with random field and permutation methods. *Neuroimage* 22, 676–687. doi: 10.1016/j.neuroimage.2004.01.041

Maguire, E. A., Woollett, K., and Spiers, H. J. (2006). London taxi drivers and bus drivers: a structural MRI and neuropsychological analysis. *Hippocampus* 16, 1091–1101. doi: 10.1002/hipo.20233

Pérès, K., Chrysostome, V., Fabrigoule, C., Orgogozo, J. M., Dartigues, J. F., and Barberger-Gateau, P. (2006). Restriction in complex activities of daily living in MCI: impact on outcome. *Neurology* 67, 461–466. doi: 10.1212/01.wnl.0000228228.70065.f1

Rosen, W. G., Mohs, R. C., and Davis, K. L. (1984). A new rating scale for Alzheimer's disease. *Am. J. Psychiatry* 141, 1356–1364. doi: 10.1176/ajp.141.11.1356

Seidler, R. D., Bernard, J. A., Burutolu, T. B., Fling, B. W., Gordon, M. T., Gwin, J. T., et al. (2010). Motor control and aging: links to age-related brain structural, functional and biochemical effects. *Neurosci. Biobehav. Rev.* 34, 721–733. doi: 10.1016/j.neubiorev.2009.10.005

Tabatabaei-Jafari, H., Shaw, M. E., and Cherbuin, N. (2015). Cerebral atrophy in mild cognitive impairment: a systematic review with meta-analysis. *Alzheimers. Dement. Amst.* 1, 487–504. doi: 10.1016/j.dadm.2015.11.002

Van der Linden, M., Coyette, F., Poitrenaud, F., Kalafat, M., Calicis, F., and Adam, F. L. (2004). "épreuve de rappel libre/rappel indicé à 16 items (RL/RI-16)," in *L'évaluation Des Troubles de la Mémoire*, eds M. Van der Liden, S. Adam, A. Agniel, and C. Baisset Mouly (Marseille: Solal), 112–120.

Conflict of Interest: The authors declare that the research was conducted in the absence of any commercial or financial relationships that could be construed as a potential conflict of interest.

frontiers in Aging Neuroscience

ORIGINAL RESEARCH
published: 31 January 2020
doi: 10.3389/fnagi.2020.00008

Functional Connectivity of the Anterior and Posterior Hippocampus: Differential Effects of Glucose in Younger and Older Adults

Riccarda Peters[1]*, *David J. White*[1], *Brian R. Cornwell*[2] and *Andrew Scholey*[1]

[1]Centre for Human Psychopharmacology, Swinburne University of Technology, Melbourne, VIC, Australia, [2]Centre for Mental Health, Swinburne University of Technology, Melbourne, VIC, Australia

The hippocampus features structurally and functionally distinct anterior and posterior segments. Relatively few studies have examined how these change during aging or in response to pharmacological interventions. Alterations in hippocampal connectivity and changes in glucose regulation have each been associated with cognitive decline in aging. A distinct line of research suggests that administration of glucose can lead to a transient improvement in hippocampus-dependent memory. Here, we probe age, glucose and human cognition with a special emphasis on resting-state functional connectivity (rsFC) of the hippocampus along its longitudinal axis to the rest of the brain. Using a randomized, placebo-controlled, double-blind, crossover design 32 healthy adults (16 young and 16 older) ingested a drink containing 25 g glucose or placebo across two counter balanced sessions. They then underwent resting-state functional magnetic resonance imaging (rs-fMRI) and cognitive testing. There was a clear dissociation in the effects of glucose by age. Magnitude change in rsFC from posterior hippocampus (pHPC) to medial frontal cortex (mPFC) was correlated with individual glucose regulation and gains in performance on a spatial navigation task. Our results demonstrate that glucose administration can attenuate cognitive performance deficits in older adults with impaired glucose regulation and suggest that increases in pHPC-mPFC rsFC are beneficial for navigation task performance in older participants.

Keywords: resting-state fMRI, glucose, spatial navigation, hippocampus, aging, cognition

OPEN ACCESS

Edited by:
Hans J. Grabe,
University of Greifswald, Germany

Reviewed by:
Talitha Best,
Central Queensland University, Australia
Xiao-Xin Yan,
Central South University, China
Yuka Kotozaki,
Tohoku University, Japan

***Correspondence:**
Riccarda Peters
riccarda.peters@gmail.com

Received: *03 October 2019*
Accepted: *13 January 2020*
Published: *31 January 2020*

Citation:
Peters R, White DJ, Cornwell BR and Scholey A (2020) Functional Connectivity of the Anterior and Posterior Hippocampus: Differential Effects of Glucose in Younger and Older Adults. Front. Aging Neurosci. 12:8. doi: 10.3389/fnagi.2020.00008

INTRODUCTION

Increasing the levels of available glucose, by the administration of a glucose drink, has been shown to improve cognitive performance in both younger and older adults in the minutes and hours following the drink (Smith et al., 2011). The effects of glucose have been reported to be comparable to those observed after administration of pharmaceutical cognitive enhancers (Riby, 2004).

Converging evidence suggests a relationship between the effect of glucose on tasks which are predominantly related to hippocampal function such as episodic memory and spatial memory (Riby, 2004; Smith et al., 2011).

The hippocampus is known to be important in the formation and recollection of memory (Moscovitch et al., 2005) and is a key brain hub for episodic memory, operating in the context of a large-scale network (Nyberg et al., 2000). Resting-state functional connectivity (rsFC) analysis, including using functional magnetic resonance imaging (fMRI), has proved to be a powerful tool to help unravel the functional architecture of brain networks (Raichle et al., 2001). One of the most common findings in studies of age-related rsFC is an association between advancing age and decreased functional connectivity within the default mode network (Ferreira and Busatto, 2013) and overall reductions in functional connectivity between the hippocampus and the rest of the brain (Geerligs et al., 2015).

It is increasingly recognized that there is a structural and functional dissociation between anterior and posterior segments of the hippocampus (Strange et al., 1999). This includes distinct patterns of rsFC displayed by anterior (aHPC) and posterior parts (pHPC) of the hippocampus (Wagner et al., 2016). The functional relevance of these networks and age-related changes therein are largely unknown. There is mixed evidence regarding the association between pHPC and aHPC connectivity and performance on cognitive tasks, and the functional differentiation of aHPC and pHPC is yet to be clearly defined. An episodic-spatial dichotomy of anterior and posterior hippocampal segments has been proposed, with pHPC being related to spatial memory functions and aHPC to episodic memory functions (Persson et al., 2018).

Much of the work on the influence of glucose on neurocognitive performance has focused on age-related effects (van der Zwaluw et al., 2015). Senescence is accompanied by changes in glucose metabolism (Blesa et al., 1997), specifically poorer glucose regulation. These changes in glucose regulation have been linked to age-related cognitive decline (Korol and Gold, 1998; Awad et al., 2004) and Alzheimer's disease (Watson and Craft, 2003).

While cognitive domains implicated in the glucose facilitation effect have been argued to preferentially enhance hippocampus-dependent tasks, relatively limited research has directly explored underlying neurophysiological mechanisms in the human brain. Several event-related potential (ERP) studies support the involvement of the hippocampus (Smith et al., 2009; Brown and Riby, 2013; Scholey et al., 2015). Further evidence for the involvement of the hippocampus in the effect stems from a study using fMRI (Parent et al., 2011).

To the best of our knowledge, no study to date has considered the anterior-posterior division of the hippocampus in the study of the glucose facilitation effect. Furthermore, rsfMRI has not been directed to compare the modulation of cognition and resting-state connectivity in younger and older adults. The present study addresses these gaps in the literature. Here, we describe the outcomes of a placebo-controlled, double-blind, crossover neuroimaging study investigating the relationship between age, glucose and human cognition with a special emphasis on the connectivity of the hippocampus along its anterior-posterior axis to the rest of the brain.

MATERIALS AND METHODS

Participants

A total of 32 healthy right-handed participants from Melbourne, Australia, were recruited for this randomized, double-blind, crossover trial. Half of this group ($n = 16$, eight women) consisted of younger subjects (mean ± SD: age 25.8 ± 3.2 years, range 21–30) and the other half ($n = 16$, eight women) consisted of older subjects (mean ± SD: age 68.6 ± 6.54, range 55–78). The participants were recruited *via* flyers, online advertising and from a database. All participants provided informed consent and received a small monetary compensation for their participation. The study was approved by the Swinburne University Ethics committee and all procedures were performed in accordance with the principles of the 1974 Declaration of Helsinki.

Inclusion criteria included normal or corrected-to-normal vision and hearing, no major physical illness and had no history of neurological/psychiatric illness or head trauma. Further exclusion criteria were a diagnosis of diabetes mellitus, a history of hypersensitivity to glucose, heart disease or high blood pressure, smoking, substance abuse, intolerance to artificial sweeteners, pregnancy, claustrophobia, metal implants or any other contraindications to MRI.

Participants were excluded if they reported health conditions that would affect food metabolism including the following: food allergies, kidney disease, liver disease and/or gastrointestinal diseases (e.g., irritable bowel syndrome, coeliac disease, peptic ulcers).

Subjects were also excluded if they were taking any medication, herbal extracts, vitamin supplements or illicit drugs which might reasonably be expected to interfere with blood glucose levels within 4 weeks prior to and during the study. In order to study associations with glucoregulation, the study included a range of fasting blood glucose levels (mmol/l). Fasting levels above 6 mmol/l were presumed to reflect fasting compliance with compromised glucoregulation as long as they were noted consistently across visits. Where fasting levels above six were not noted across both visits, the subject was excluded from the analysis as this was taken as evidence of non-compliance with fasting.

During the testing session, participants could be excluded if they scored lower than 25 on the Mini-Mental State Exam (MMSE; Folstein et al., 1975). Participant enrolment and inclusion pathways are depicted in a CONSORT flow diagram in the **Supplementary Figure S1.1**. All testing occurred at the Centre for Human Psychopharmacology at Swinburne University.

Procedure

Participants attended the Centre for Human Psychopharmacology on three occasions a screening visit and two experimental sessions (with the experimental sessions balanced for treatment order). At the screening visit, informed consent was obtained, and eligibility was confirmed. Socio-demographic and morphometric data were collected (see **Table 1**). The session also served to familiarize participants

TABLE 1 | Demographics.

	Young	Older	*P*-value
N (female)	16 (8)	16 (8)	-
Age (years)	25.0 ± 3.5	68.3 ± 6.4	-
BMI (m/kg^2)	23.0 ± 4.5	25.0 ± 4.01	0.224
Education (years)	17.0 ± 2.0	15.4 ± 3.6	0.117
MMSE	29.8 ± 0.3	29.2 ± 1.0	0.025*

*Note: for BMI, education and MMSE numbers represent: mean (standard deviation), significant results are marked *at 0.05 level.*

with the cognitive tasks they would encounter during the study days.

The two experimental sessions started between 8.30 am and 10 am and were scheduled between 2 and 14 days, apart. Participants were asked to abstain from food and drink (except water) after 10 pm before testing (to achieve a 12-h overnight fast). Participants were questioned on compliance and excluded in case of non-compliance. Fasting blood glucose levels were measured *via* capillary fingerprick using a Freestyle Optium Blood Glucose Sensor and Optium Blood Glucose Test Strips (Abbott Diabetes Care Limited, Witney, UK) according to the manufacturer's instructions. Following baseline glucose measurement, participants were asked to complete self-report questionnaires measuring mood and appetite. The self-report questionnaires were administered after each blood glucose measurement throughout the testing day and will be described elsewhere. They then received the treatment drink which consisted of 25 g glucose (Glucodin Pure Glucose Powder) mixed with 150 ml of water and 20 ml of sugar-free cordial in the glucose condition, and two tablets (30 mg) sodium saccharine (Hermesetas©) mixed with 150 mL of water and 20 ml sugar-free cordial in the placebo condition. It has previously been shown that the two drinks are indistinguishable in taste and mouthfeel (Scholey et al., 2001; Scholey and Fowles, 2002). There is evidence that the glucose facilitation effect follows an inverted U-shape dose-response curve in humans (Parsons and Gold, 1992), and 25 g has been reported as the optimal dose for memory enhancement (Riby, 2004).

Participants were randomly assigned to a treatment sequence that counterbalanced the order of treatments within age groups and gender. To ensure blinding, randomization and preparation of the drink were performed by a disinterested third party with no other involvement in the study. Blood glucose was measured again 20 min, 120 min, and 150 min post-ingestion by a person who was not the experimenter to maintain blinding (unblinding occurred only after data analyses were completed).

MRI scanning commenced 30 min post-ingestion. This interval was selected to ensure that blood glucose levels would be maximally elevated during MRI scanning (Korol and Gold, 1998). Anatomical (T1) images were acquired first, followed by a seven-minute resting-state scan (**Figure 1**).

Cognitive Testing

Cognitive testing took place after MRI scanning (120 min post-ingestion; **Figure 1**). Two cognitive tests focusing on different domains of memory were used, as follows.

Working Memory

Working memory performance was assessed using the mental arithmetic Serial Sevens task. It involves the serial subtraction of seven from a given number. Previous work has shown that performance on this to be enhanced by glucose administration (Scholey et al., 2001). Standard instructions were displayed on a computer monitor, informing the participant to count backward in sevens from the given starting number, as quickly and accurately as possible, using the numeric keypad to enter each response. Performance was assessed using the number of correct subtractions within 2 min.

Spatial Learning and Memory

Spatial learning performance was measured using a virtual analog of the Morris Water Maze (vMWM; Morris, 1981). The latter has been used extensively in rodents to study hippocampal-dependent spatial navigation. The vMWM has been validated for use in humans (Cornwell et al., 2008).

Participants were instructed to try to find a platform in a virtual pool environment presented on a computer screen. The platform was visible on some trials and hidden ("submerged") on others (**Figure 2**).

Probe trials were administered in which the platform was removed unbeknownst to participants. In this case, participants started from a novel position in the pool in order to assess spatial memory performance beyond immediate training experience. The platform was then moved to a new location and participants completed an additional set of hidden platform trials along with a second probe trial. The dependent measure was heading error (square-root transformed) or angular deviation from a straight path to the platform's location on the probe trials.

For detailed task descriptions see section 2 in **Supplementary Material**.

MRI Acquisition

Participants underwent MRI scanning on both testing days, following the same protocol. fMRI data were acquired using a 3-Tesla Siemens Magnetom Trio scanner (Siemens, Erlangen, Germany) at Swinburne University of Technology, Melbourne, Australia with a 32-channel head coil. To minimize head movement comfortable padding was placed around the participants' head and participants were instructed to lie as still as possible. Structural high-resolution 3D T1-weighted magnetization prepared rapid acquisition gradient echo (MP-RAGE) anatomical images for anatomical reference were collected at the start of the scanning session (1 mm isotropic MP-RAGE, TR = 1,900 ms, TE = 2.52 ms, flip angle = 9°). Following the anatomical image, the participant underwent 7 min 15 sec resting-state fMRI (rsfMRI), during which they were instructed to keep their eyes open and look at a fixation cross. Functional data were obtained continuously with an interleaved multi band sequence (multiband acceleration factor = 6, bandwidth = 1,860 Hz/Px, TR = 870 ms, TE = 30 ms, echo spacing = 0.69 ms, flip angle = 55°, field of view = 192 mm, voxel resolution = 2 × 2 × 2 mm, slice orientation = transversal, number of slices = 66,500 volumes

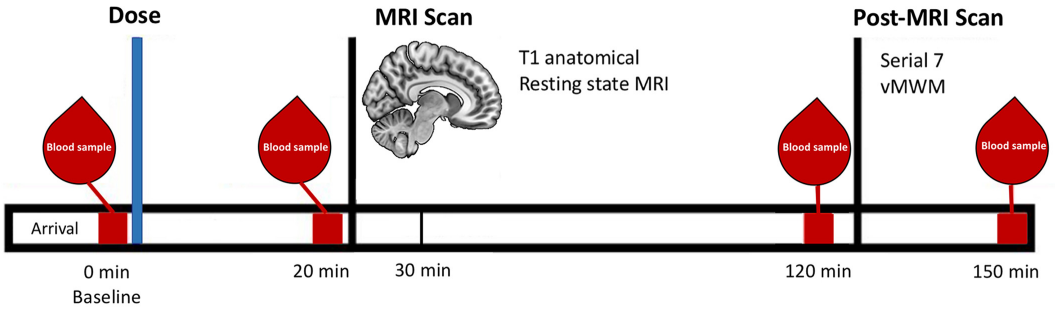

FIGURE 1 | Schematic representation of the testing timeline for the treatment visits.

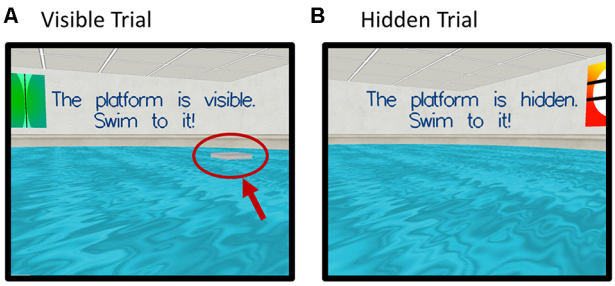

FIGURE 2 | Screenshots of the virtual Morris Water Maze Task (vMWM) which was presented to the participants on a computer screen. Panel **(A)** depicts a trial where the platform is visible (red arrow and circle were added retrospectively and are not part of the actual display). Panel **(B)** depicts a trial where the platform is hidden ("submerged").

per session). MRI scanning took 60 min in total and also included two task-related fMRI scans and a spectroscopy sequence that will be reported elsewhere.

Resting-State Analysis

Functional and structural images were processed using the CONN toolbox Version 17f (Whitfield-Gabrieli and Nieto-Castanon, 2012[1]) for Statistical Parametric Mapping Software (SPM12; Wellcome Department of Imaging Science, Functional Imaging Laboratory, University College London) run under Matlab R2014a. Preprocessing steps were conducted using the default preprocessing pipeline for volume-based analysis (to MNI space; realignment and unwarping, ART-based identification of outlier scans for scrubbing, simultaneous gray matter (GM), white matter (WM), and cerebrospinal fluid (CSF) segmentation and normalization into standard MNI space (Montreal Neurological Institute, Montréal, QC, Canada).

To remove confounding effects from the BOLD time series the anatomical CompCor strategy (Behzadi et al., 2007) was used as implemented in the CONN toolbox. Physiological and other spurious sources of noise were estimated and regressed out of the BOLD functional data in the denoising step (simultaneous option). Five principal components were extracted from both WM and CSF, as well as 12 motion regressors (six head motion parameters + six first-order temporal derivatives) derived from spatial motion correction, which were used as temporal covariates and removed from the BOLD functional data using linear regression.

The resulting residual BOLD time series were band-pass filtered with a frequency window of 0.008 Hz–0.2 Hz.

In addition to the above steps controlling for motion, an analysis of motion across groups and conditions was conducted. Framewise displacement (FD; maximum total and averages scan-to-scan) was calculated according to Power et al. (2012) between-sessions and between-groups (see section 3.1 in **Supplementary Material**). As FD was higher for younger adults than older adults at both treatment sessions, and FD also differed between sessions in the younger group, all group-level analyses included average framewise displacement as a covariate at the second level.

Seed Based Connectivity Analysis

To assess rsFC of the hippocampus, four seed regions were defined based on coordinates which have been used in previous research (Wagner et al., 2016) to facilitate comparisons of results. Four ROIs were created in MarsBar toolbox[2] and defined as spheres with a 5 mm radius around the anterior and posterior part of the hippocampus on the left (anterior: $x = -28$, $y = -12$, $z = -20$; posterior: $x = -28$, $y = -24$, $z = -12$) and right side (anterior: $x = 28$, $y = -12$, $z = -20$; posterior: $x = 32$, $y = -24$, $z = -12$). The resting-state BOLD signal time-series of each hippocampal region of interest was extracted and correlated against voxels of the rest of the brain for each session of each subject. Fisher z transformation was applied.

Statistical Analysis

Blood glucose level and cognitive outcomes were assessed by mixed-design ANOVA, with treatment as a repeated-measures factor and age as a between-subjects factor (IBM SPSS Statistics, Version 24). Blood glucose levels had additional repeated measures factor of assessment time within sessions. Glucose

[1]http://www.nitrc.org/projects/conn

[2]http://marsbar.sourceforget.net/

tolerance was assessed as an incremental area under the curve (iAUC) using the trapezoidal rule (Le Floch et al., 1990) based on the four blood glucose measurements taken at baseline, 20 min, 120 min and 150 min post glucose administration. Higher iAUC values reflect higher circulating glucose levels, indicative of poorer glucoregulatory ability.

Functional connectivity analyses used whole-brain voxel-wise mixed within-subject (glucose, placebo) and between-subject (younger, older) second-level models, using the partitioned variance approach implemented in CONN, in order to test for treatment × age-group interactions. All rsFC analyses used a cluster-extent FWE-corrected p-value < 0.05, obtained using non-parametric statistics with 5,000 permutations at a cluster-defining threshold of $p < 0.001$.

To explore the relationship between changes in rsFC and performance on cognitive measures, *post hoc* Pearson's correlation coefficient analyses were carried out using SPSS.

RESULTS

Data from two participants of the young group (one male, one female) was omitted from the analysis because they showed significantly higher fasting glucose levels at a single session compared to the other session. The higher fasting glucose levels could indicate non-compliance to the fasting regime, therefore they were excluded from further analysis.

Blood Glucose Levels

Blood glucose levels throughout both testing sessions for each group are depicted in **Figure 3A**, which also presents the timing of the experimental measures. There were no between-group differences in baseline blood glucose levels between the younger and older group either at glucose ($T_{(1,28)} = 0.59$, $P = 0.954$) nor placebo visit ($T_{(1,28)} = -0.878$, $P = 0.387$).

A 2 (Age: young/old) × 2 (Treatment: Glucose/Placebo) × 4 (Timepoint: 0, 20, 120, 150 min) ANOVA was conducted. The rmANOVA analysis of glucose levels omitted data from one young participant who had a missing post-dose blood glucose assessment at the placebo visit.

There was a significant main effect of Treatment ($F_{(1,27)} = 25.18$ $P < 0.001$, $\eta^2 = 0.485$), a main effect of Time point ($F_{(1.567,27)} = 59.43$, $P < 0.001$, $\eta^2 = 0.688$, Greenhouse-Geisser) and a significant Treatment × Timepoint interaction ($F_{(1.843,27)} = 19.43$, $P < 0.001$, $\eta^2 = 0.644$, Greenhouse–Geisser). There was also a main effect of Age ($F_{(1,27)} = 9.076$, $P = 0.006$, $\eta^2 = 0.252$). The older group showed a greater increase of blood glucose levels in response to glucose ingestion than the younger group ($T_{(1,28)} = -2.99$, $P = 0.006$).

There was also a significant difference in blood glucose levels 20 min post-ingestion at the placebo visit ($T_{(1,27)} = -3.72$, $P = 0.001$). Glucose levels decreased in the younger group.

Using blood glucose iAUC at the glucose visit as a measure of glucoregulatory efficiency, older participants had significantly higher iAUC than younger participants ($T_{(1,28)} = -3.403$, $P = 0.002$), indicative of poorer glucose regulation in the older sample (**Figure 3B**).

Resting-State

A significant Treatment × Age-group interaction in rsFC was observed between left pHPC and a cluster within in the medial frontal cortex (mPFC) encompassing areas in anterior cingulate, paracingulate gyrus and superior frontal gyrus [Brodmann Area (BA) 32 and 8; MNI peak (+08 +26 +30; **Table 2** and **Figure 4A**)]. There were no main effects of condition or group.

Post hoc t-tests revealed that glucose (compared to placebo) significantly increased left pHPC-mPFC connectivity in older

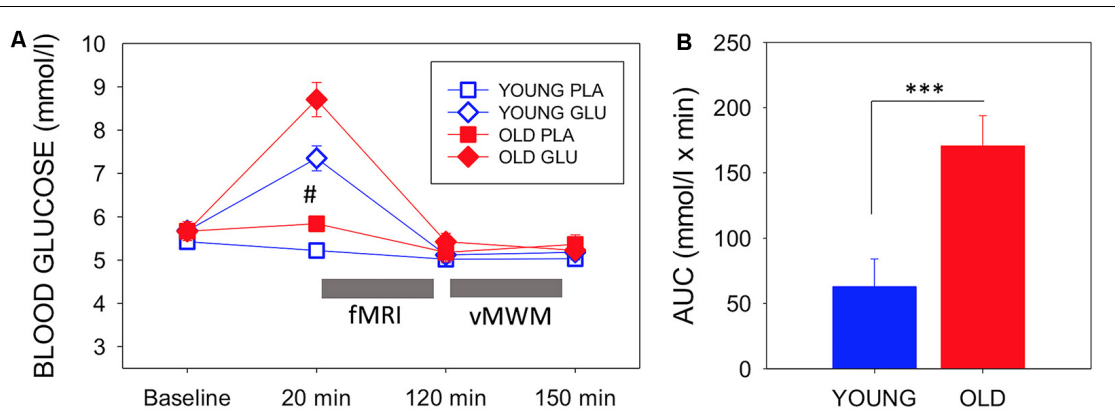

FIGURE 3 | (A) Mean (with SEM) blood glucose levels at baseline, pre-magnetic resonance imaging (MRI) (20 min post-dose), post-MRI (120 min post-dose), and end of testing (150 min post-dose) for each group and each visit. Circles depict younger adults, while squares depict older adults. Filled symbols represent measures taken on glucose visit, while open symbols represent measures at the placebo visit. #Indicates a significant difference between drink condition and significant difference between ages in both drink conditions (p-values see text). Timing of fMRI and virtual Morris Water maze (vMWM) are indicated in relation to glucose measurements. **(B)** Blood glucose incremental area under the curve as a measure of glucoregulatory efficiency, bars depict mean (with SEM). Older adults had significantly higher incremental area under the curve (iAUC) than younger adults ($T_{(1,28)} = -3.403$, $P = 0.002$), indicating poorer glucose regulation. ***$P < 0.005$.

TABLE 2 | Whole-brain voxel-wise rmANOVA of resting-state functional connectivity (rsFC) with left posterior hippocampus.

Cluster *p* (FWE-corr)	Cluster size *k* voxels	Peak *t*	MNI co-ord (peak) *x*	*y*	*z*	Peak region
0.044	96	−6.39	8	26	30	Paracingulate gyrus R

Treatment × age-group interaction (young > older; Glucose > Placebo) for left posterior hippocampus (pHPC) seed (two-sided contrast; 5,000 permutations, FWE-corrected) to cluster in mPFC (encompassing anterior cingulate, paracingulate gyrus and superior frontal gyrus). The table displays cluster size p-value (FWE-corr), cluster size (k), Peak t-value, Montreal Neurological Imaging (x, y, z) peak coordinates, peak region (Harvard-Oxford Atlas), R = right hemisphere.

participants, $T_{(1,15)} = 5.13$, $P < 0.001$), whereas the reverse was observed in young participants, $T_{(1,13)} = -3.6$, $P = 0.003$ (**Figure 2B**).

This analysis was repeated using individual pHPC volume as a covariate. The cluster in the same area remained significant although smaller in size [MNI peak (+04 +24 +44); $\text{Voxels}_{(k)} = 58$]; see section 3.2 in **Supplementary Material**, **Supplementary Table S3.2**). No significant differences were observed from any of the other seed ROIs (right pHPC, or left and right aHPC).

Further *post hoc* tests showed that younger participants exhibited higher rsFC between left pHPC and mPFC relative to older participants under placebo conditions, $T_{(1,28)} = 3.54$, $P = 0.001$; and that older participants exhibited significantly greater left pHPC-mPFC connectivity relative to the younger group after glucose ingestion alone, $T_{(1,28)} = -2.75$, $P = 0.01$ (**Figure 4B**).

To relate the present finding to individual glucose regulation, *post hoc* Pearson correlation using iAUC at the glucose treatment visit and rsFC connectivity were performed. Change in pHPC-mPFC rsFC was correlated with individual glucose regulation across the whole sample ($r = 0.39$, $P = 0.04$; **Figure 4C**).

Task Performance

Data from two additional participants (one young, one old) was omitted from the analysis of the vMWM due to missing data. There was a significant Treatment × Age-group interaction for performance on the vMWM task ($F_{(1,26)} = 8.64$, $P = 0.007$) as depicted in **Figure 5A**. *Post hoc* pairwise comparisons revealed that while the older group showed significantly worse performance compared to the younger group under placebo ($T_{(1,26)} = -3.42$, $P = 0.02$), there was no group difference after glucose administration ($T_{(1,26)} = 0.35$, $P = 0.73$). No Treatment by

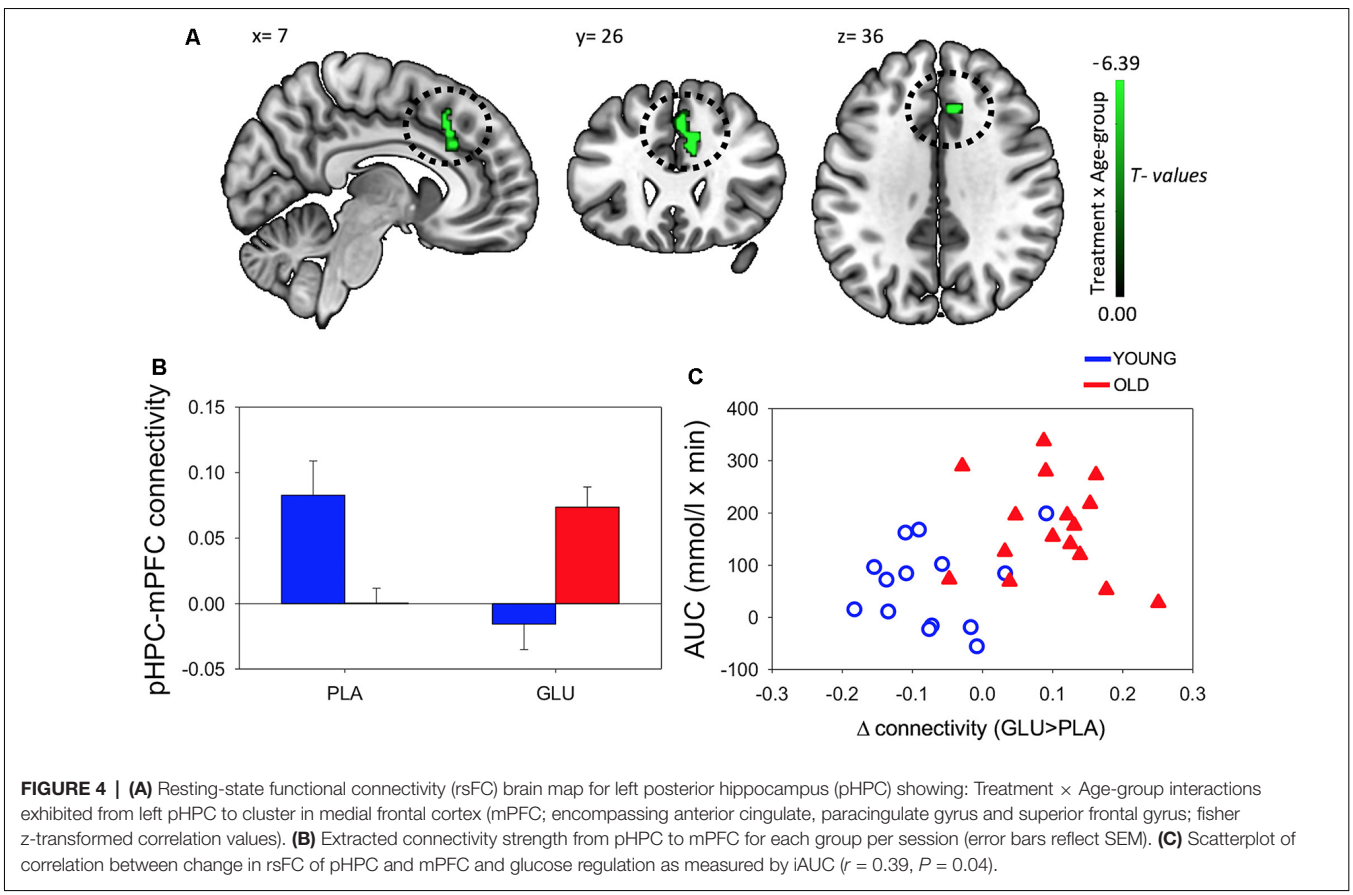

FIGURE 4 | **(A)** Resting-state functional connectivity (rsFC) brain map for left posterior hippocampus (pHPC) showing: Treatment × Age-group interactions exhibited from left pHPC to cluster in medial frontal cortex (mPFC; encompassing anterior cingulate, paracingulate gyrus and superior frontal gyrus; fisher z-transformed correlation values). **(B)** Extracted connectivity strength from pHPC to mPFC for each group per session (error bars reflect SEM). **(C)** Scatterplot of correlation between change in rsFC of pHPC and mPFC and glucose regulation as measured by iAUC ($r = 0.39$, $P = 0.04$).

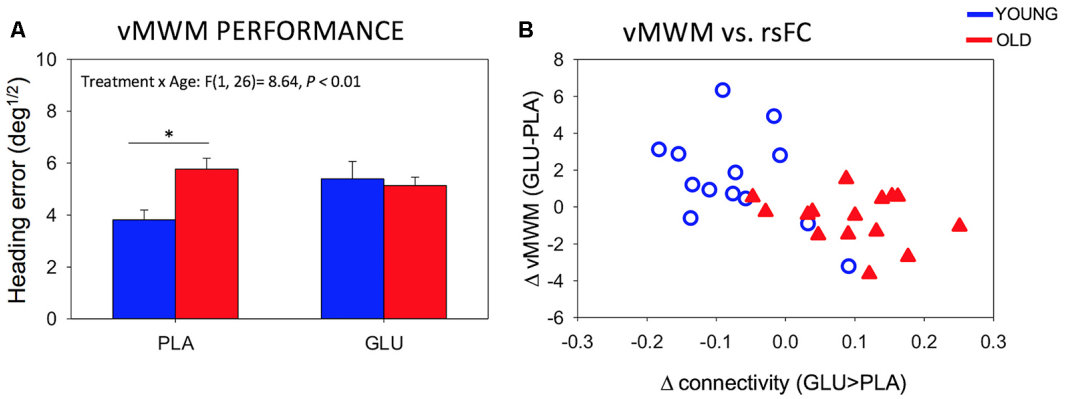

FIGURE 5 | (A) Behavioral performance on the vMWM task for younger and older subjects following placebo and glucose drink. Bars depict mean Heading error ($deg^{1/2}$; with SEM). Smaller values reflect better performance $^*P < 0.05$. **(B)** Scatterplot of change in rsFC of left posterior hippocampus to mPFC and change in performance on the spatial navigation task (heading error; $r = -0.56$, $P = 0.002$).

age-group interactions were found in the Serial Sevens (correct; $F_{(1,28)} = 1.38$, $P = 0.25$).

We further probed the relationship between significant changes in left pHPC-mPFC rsFC and change in performance on the spatial navigation task. Change in rsFC magnitude between left pHPC and mPFC was correlated with changes in spatial memory performance ($r = -0.56$, $P = 0.002$). The negative correlation reflects greater connectivity after glucose to be associated with smaller heading errors (averaged across the two probe trials) after glucose ingestion. Specifically, in older participants, glucose increased functional connectivity between the left posterior hippocampus and mPFC and that the magnitude of this functional connectivity change correlated with the change in performance (**Figure 5B**).

DISCUSSION

The aim of the present study was to investigate age-related differences in changes in rsFC in response to a glucose load from the anterior and posterior segments of the hippocampus, comparing a group of younger and a group of older adults. Further, we wanted to investigate if these changes are linked to individual glucose regulation and how they relate to memory performance on two different memory tasks.

After the ingestion of a 25 g glucose drink, we observed changes in functional connectivity of the pHPC to a cluster in the mPFC. In older participants, glucose increased rsFC between pHPC and mPFC. Furthermore, the change in connectivity was related to glucoregulatory ability. Participants with poorer glucose regulation, as indicated by greater circulating glucose following administration, benefited most from the glucose load. In younger participants we observed the opposite pattern of connectivity change. Moreover, the change in the magnitude of rsFC was correlated with gains in performance on a spatial memory task.

Here, we demonstrate age-dependent, acute modulation of pHPC connectivity, suggesting that connectivity of the posterior segment of the hippocampus is differentially susceptible to an acute glucose load in older individuals.

This study is the first to compare the effects of glucose on rsFC and cognition in both younger and older individuals. There is a general consensus that glucose enhancement is more effective in older compared to younger adults (Macpherson et al., 2015). This effect has been partially attributed to an age-related decline in glucose regulation. Our findings indicate that pHPC-mPFC connectivity increases were more marked as glucoregulation worsened in older participants (see **Figure 4C**). Our results suggest that these connectivity changes may contribute to previously reported demonstrations that glucose more readily attenuates age-related cognitive performance decrements in elderly adults with impaired glucose regulation (Kaplan et al., 2000; Messier et al., 2003).

The hippocampus has been hypothesized as a key structure in the glucose facilitation effect (Smith et al., 2011). Our results show the potential importance of considering subdivisions of the hippocampus along its anterior-posterior axis in neuropharmacological studies.

The hippocampus and surrounding temporal lobes have long been recognized to be an important node for the processing of spatial information (for a review, see Howard et al., 2005). The results of the present study support the role of the posterior segment of the hippocampus in spatial memory performance. This relationship has recently been demonstrated in a rsfMRI study by Persson et al. (2018), who predicted spatial memory performance from pHPC, but not aHPC, rsFC. Our results are also consistent with reports of positive associations between posterior hippocampal activation and virtual navigation performance (Maguire et al., 1998; Hartley et al., 2003; Cornwell et al., 2008).

Growing evidence points to the importance of the mPFC, including the anterior cingulate cortex (ACC), in spatial memory. Interactions between mPFC and hippocampus have been proposed to be critical to successful encoding and retrieval of spatial information (Wirt and Hyman, 2017). The present results show that increases in pHPC-mPFC rsFC are beneficial

to navigation task performance, thus contributing to the growing amount of literature emphasizing the importance of information sharing between these two areas in spatial memory.

The post-glucose performance of the older participants was similar to that of the younger group. Conversely, in the younger group performance decreased slightly. In young adults, the glucose facilitation effect is most readily observed under increased task difficulty (Kennedy and Scholey, 2000; Scholey et al., 2001) and divided attention (Sünram-Lea et al., 2002; Scholey et al., 2009). It is thus possible that the task demands in this study were not high enough to elicit an effect in the younger group. It is also the case that there are a number of studies where glucose modulation did not affect behavioral task performance (Knott et al., 2001; Riby, 2004), and there are isolated reports of decreased task performance after glucose ingestion (Scholey et al., 2015). This may be a manifestation of complex interactions between glucose levels and task demands which make the effect more fragile in younger adults.

The reason for the difference between blood glucose levels 20 min post-ingestion of the placebo drink are unknown, but they may reflect better glucoregulation as reflected intact insulin signaling after (false) nutritional load in the young group. Anticipatory hormonal response to flavoring (without glucose) has been observed before (Scholey and Kennedy, 2004).

There were some limitations to this study. The sample sizes were relatively small, and future studies with larger sample sizes are needed in order to investigate the glucose facilitation effect especially with regard to mediating variables such as gender. There is research suggesting that gender might be a contributing factor in the atrophy of the hippocampus (Pruessner et al., 2001) as well as a factor in the glucose facilitation effect (Craft et al., 1994). Even though gender-matched cohorts were used in the current study, larger sample sizes are necessary to increase the power to detect potential gender differences. Future studies investigating the effects of gender and other mediating variables are encouraged.

The consumption of glucose results not only in increases in glucose levels but also increases in systemic insulin and gut peptides, such as glucagon-like peptide-1 (GLP-1), cholecystokinin (CCK) and peptide tyrosine-tyrosine (PYY; Zanchi et al., 2017). In the current investigation we did collect endocrine data, which limits the interpretation of results. As the timing of cognitive task was 2 h post glucose ingestion it could be argued that the effect was driven by changes in insulin levels. Cognitive enhancing properties of insulin have been revealed in previous investigations (Benedict et al., 2004; Krug et al., 2010). A recommendation for future studies is, therefore, to include measurements of insulin and gut peptides to examine the cognitive enhancing mechanism of glucose ingestion in more detail.

We used a hypothesis-driven seed-based analysis to investigate the role of the anterior and posterior segments of the hippocampus in the glucose facilitation effect. This kind of analysis is influenced by the seed coordinates chosen. The seed coordinates for the anterior and posterior hippocampus in the present study were determined based on other investigations (Wagner et al., 2016) to facilitate comparisons between studies. However other researchers have used different seed coordinates for anterior and posterior hippocampus (e.g., Damoiseaux et al., 2016) which may affect the results.

CONCLUSION

This is the first study investigating the functional connectivity of aHPC and pHPC after glucose load in young and elderly adults.

The results of the present study indicate the possibility that the pHPC is especially sensitive to pharmacological interventions, as we have shown that a simple glucose load modulates its connectivity and enhances cognitive performance in older adults.

The results also suggest that glucose modulated functional connectivity and cognitive performance more readily in older adults with impaired glucose regulatory ability. We further demonstrated the functional relevance of the changes in functional connectivity by relating gains in performance on a spatial memory task to increase in pHPC-mPFC connectivity.

DATA AVAILABILITY STATEMENT

The data that support the findings of this study are available on reasonable request from the corresponding author (RP). The SPMs of all reported contrasts (and their unthresholded versions) are available at: https://neurovault.org/collections/TRYHPFXR/.

ETHICS STATEMENT

The studies involving human participants were reviewed and approved by Swinburne University Ethics committee. The patients/participants provided their written informed consent to participate in this study.

AUTHOR CONTRIBUTIONS

AS and DW designed the experiment and supervised all aspects of the study. BC and RP contributed to the design of the study. RP collected and analyzed the data. DW and BC contributed to data analysis. RP prepared the manuscript. DW, AS and BC helped to draft and revise the manuscript. All authors have read and approved the manuscript.

FUNDING

The study was partially supported by a scanning grant from Swinburne Neuroimaging (SNI) Facility, supported by the National Imaging Facility (NIF) under the National Collaborative Researcher Infrastructure Strategy (NCRIS). This manuscript has been released as a Pre-Print at bioRxiv.org and can be found here: doi: https://doi.org/10.1101/482455 (Peters et al., 2018).

SUPPLEMENTARY MATERIAL

The Supplementary Material for this article can be found online at: https://www.frontiersin.org/articles/10.3389/fnagi.2020.00008/full#supplementary-material.

REFERENCES

Awad, N., Gagnon, M., and Messier, C. (2004). The relationship between impaired glucose tolerance, type 2 diabetes and cognitive function. *J. Clin. Exp. Neuropsychol.* 26, 1044–1080. doi: 10.1080/13803390490514875

Behzadi, Y., Restom, K., Liau, J., and Liu, T. T. (2007). A component based noise correction method (CompCor) for BOLD and perfusion based fMRI. *NeuroImage* 37, 90–101. doi: 10.1016/j.neuroimage.2007.04.042

Benedict, C., Hallschmid, M., Hatke, A., Schultes, B., Fehm, H. L., Born, J., et al. (2004). Intranasal insulin improves memory in humans. *Psychoneuroendocrinology* 29, 1326–1334. doi: 10.1016/j.psyneuen.2004.04.003

Blesa, R., Mohr, E., Miletich, R., Randolph, C., Hildebrand, K., Sampson, M., et al. (1997). Changes in cerebral glucose metabolism with normal aging. *Eur. J. Neurol.* 4, 8–14. doi: 10.1111/j.1468-1331.1997.tb00294.x

Brown, L. A., and Riby, L. M. (2013). Glucose enhancement of event-related potentials associated with episodic memory and attention. *Food Funct.* 4, 770–776. doi: 10.1039/c3fo30243a

Cornwell, B. R., Johnson, L. L., Holroyd, T., Carver, F. W., and Grillon, C. (2008). Human hippocampal and parahippocampal theta during goal-directed spatial navigation predicts performance on a virtual Morris water maze. *J. Neurosci.* 28, 5983–5990. doi: 10.1523/JNEUROSCI.5001-07.2008

Craft, S., Murphy, C., and Wemstrom, J. (1994). Glucose effects on complex memory and nonmemory tasks: the influence of age, sex, and glucoregulatory response. *Psychobiology* 22, 95–105.

Damoiseaux, J. S., Viviano, R. P., Yuan, P., and Raz, N. (2016). Differential effect of age on posterior and anterior hippocampal functional connectivity. *NeuroImage* 133, 468–476. doi: 10.1016/j.neuroimage.2016.03.047

Ferreira, L. K., and Busatto, G. F. (2013). Resting-state functional connectivity in normal brain aging. *Neurosci. Biobehav. Rev.* 37, 384–400. doi: 10.1016/j.neubiorev.2013.01.017

Folstein, M. F., Folstein, S. E., and McHugh, P. R. (1975). "Mini-mental state". A practical method for grading the cognitive state of patients for the clinician. *J. Psychiatr. Res.* 12, 189–198. doi: 10.1016/0022-3956(75)90026-6

Geerligs, L., Renken, R. J., Saliasi, E., Maurits, N. M., and Lorist, M. M. (2015). A brain-wide study of age-related changes in functional connectivity. *Cereb. Cortex* 25, 1987–1999. doi: 10.1093/cercor/bhu012

Hartley, T., Maguire, E. A., Spiers, H. J., and Burgess, N. (2003). The well-worn route and the path less traveled: distinct neural bases of route following and wayfinding in humans. *Neuron* 37, 877–888. doi: 10.1016/s0896-6273(03)00095-3

Howard, M. W., Fotedar, M. S., Datey, A. V., and Hasselmo, M. E. (2005). The temporal context model in spatial navigation and relational learning: toward a common explanation of medial temporal lobe function across domains. *Psychol. Rev.* 112, 75–116. doi: 10.1037/0033-295x.112.1.75

Kaplan, R. J., Greenwood, C. E., Winocur, G., and Wolever, T. M. (2000). Cognitive performance is associated with glucose regulation in healthy elderly persons and can be enhanced with glucose and dietary carbohydrates. *Am. J. Clin. Nutr.* 72, 825–836. doi: 10.1093/ajcn/72.3.825

Kennedy, D. O., and Scholey, A. B. (2000). Glucose administration, heart rate and cognitive performance: effects of increasing mental effort. *Psychopharmacology* 149, 63–71. doi: 10.1007/s002139900335

Knott, V., Messier, C., Mahoney, C., and Gagnon, M. (2001). Glucose and glucoregulatory modulation of memory scanning, event-related potentials and EEG in elderly subjects. *Neuropsychobiology* 44, 156–166. doi: 10.1159/000054936

Korol, D. L., and Gold, P. E. (1998). Glucose, memory, and aging. *Am. J. Clin. Nutr.* 67, 764S–771S. doi: 10.1093/ajcn/67.4.764S

Krug, R., Benedict, C., Born, J., and Hallschmid, M. (2010). Comparable sensitivity of postmenopausal and young women to the effects of intranasal insulin on food intake and working memory. *J. Clin. Endocrinol. Metab.* 95, E468–E472. doi: 10.1210/jc.2010-0744

Le Floch, J.-P., Escuyer, P., Baudin, E., Baudon, D., and Perlemuter, L. (1990). Blood glucose area under the curve: methodological aspects. *Diabetes Care* 13, 172–175. doi: 10.2337/diacare.13.2.172

Macpherson, H., Roberstson, B., Sünram-Lea, S., Stough, C., Kennedy, D., and Scholey, A. (2015). Glucose administration and cognitive function: differential effects of age and effort during a dual task paradigm in younger and older adults. *Psychopharmacology* 232, 1135–1142. doi: 10.1007/s00213-014-3750-8

Maguire, E. A., Burgess, N., Donnett, J. G., Frackowiak, R. S., Frith, C. D., and O2Keefe, J. (1998). Knowing where and getting there: a human navigation network. *Science* 280, 921–924. doi: 10.1126/science.280.5365.921

Messier, C., Tsiakas, M., Gagnon, M., Desrochers, A., and Awad, N. (2003). Effect of age and glucoregulation on cognitive performance. *Neurobiol. Aging* 24, 985–1003. doi: 10.1016/s0197-4580(03)00004-6

Morris, R. G. (1981). Spatial localization does not require the presence of local cues. *Learn. Motiv.* 12, 239–260. doi: 10.1016/0023-9690(81)90020-5

Moscovitch, M., Rosenbaum, R. S., Gilboa, A., Addis, D. R., Westmacott, R., Grady, C., et al. (2005). Functional neuroanatomy of remote episodic, semantic and spatial memory: a unified account based on multiple trace theory. *J. Anat.* 207, 35–66. doi: 10.1111/j.1469-7580.2005.00421.x

Nyberg, L., Persson, J., Habib, R., Tulving, E., McIntosh, A. R., Cabeza, R., et al. (2000). Large scale neurocognitive networks underlying episodic memory. *J. Cogn. Neurosci.* 12, 163–173. doi: 10.1162/089892900561805

Parent, M. B., Krebs-Kraft, D. L., Ryan, J. P., Wilson, J. S., Harenski, C., and Hamann, S. (2011). Glucose administration enhances fMRI brain activation and connectivity related to episodic memory encoding for neutral and emotional stimuli. *Neuropsychologia* 49, 1052–1066. doi: 10.1016/j.neuropsychologia.2011.02.013

Parsons, M. W., and Gold, P. E. (1992). Glucose enhancement of memory in elderly humans: an inverted-U dose-response curve. *Neurobiol. Aging* 13, 401–404. doi: 10.1016/0197-4580(92)90114-d

Persson, J., Stening, E., Nordin, K., and Söderlund, H. (2018). Predicting episodic and spatial memory performance from hippocampal resting-state functional connectivity: evidence for an anterior-posterior division of function. *Hippocampus* 28, 53–66. doi: 10.1002/hipo.22807

Peters, R., White, D. J., Cornwell, B. R., and Scholey, A. (2018). Functional connectivity of the anterior and posterior hippocampus: differential effects of glucose in younger and older adults. *bioRxiv* [Preprint]. doi: 10.1101/482455

Power, J. D., Barnes, K. A., Snyder, A. Z., Schlaggar, B. L., and Petersen, S. E. (2012). Spurious but systematic correlations in functional connectivity MRI networks arise from subject motion. *NeuroImage* 59, 2142–2154. doi: 10.1016/j.neuroimage.2011.10.018

Pruessner, J. C., Collins, D. L., Pruessner, M., and Evans, A. C. (2001). Age and gender predict volume decline in the anterior and posterior hippocampus in early adulthood. *J. Neurosci.* 21, 194–200. doi: 10.1523/JNEUROSCI.21-01-00194.2001

Raichle, M. E., MacLeod, A. M., Snyder, A. Z., Powers, W. J., Gusnard, D. A., and Shulman, G. L. (2001). A default mode of brain function. *Proc. Natl. Acad. Sci. U S A* 98, 676–682. doi: 10.1073/pnas.98.2.676

Riby, L. M. (2004). The impact of age and task domain on cognitive performance: a meta-analytic review of the glucose facilitation effect. *Brain Impair.* 5, 145–165. doi: 10.1375/brim.5.2.145.58253

Scholey, A., Camfield, D., Macpherson, H., Owen, L., Nguyen, P., Stough, C., et al. (2015). Hippocampal involvement in glucose facilitation of recognition memory: event-related potential components in a dual-task paradigm. *Nutr. Aging* 3, 9–20. doi: 10.3233/nua-140042

Scholey, A. B., and Fowles, K. A. (2002). Retrograde enhancement of kinesthetic memory by alcohol and by glucose. *Neurobiol. Learn. Mem.* 78, 477–483. doi: 10.1006/nlme.2002.4065

Scholey, A. B., and Kennedy, D. O. (2004). Cognitive and physiological effects of an "energy drink": an evaluation of the whole drink and of glucose, caffeine and herbal flavouring fractions. *Psychopharmacology* 176, 320–330. doi: 10.1007/s00213-004-1935-2

Scholey, A. B., Harper, S., and Kennedy, D. O. (2001). Cognitive demand blood glucose. *Physiol. Behav.* 73, 585–592. doi: 10.1016/s0031-9384(01)00476-0

Scholey, A. B., Sünram-Lea, S. I., Greer, J., Elliott, J., and Kennedy, D. O. (2009). Glucose administration prior to a divided attention task improves tracking performance but not word recognition: evidence against differential memory enhancement? *Psychopharmacology* 202, 549–558. doi: 10.1007/s00213-008-1387-1

Smith, M. A., Riby, L. M., Eekelen, J. A., and Foster, J. K. (2011). Glucose enhancement of human memory: a comprehensive research review of the glucose memory facilitation effect. *Neurosci. Biobehav. Rev.* 35, 770–783. doi: 10.1016/j.neubiorev.2010.09.008

Smith, M. A., Riby, L. M., Sünram-Lea, S. I., van Eekelen, J., and Foster, J. K. (2009). Glucose modulates event-related potential components of recollection and familiarity in healthy adolescents. *Psychopharmacology* 205, 11–20. doi: 10.1007/s00213-009-1509-4

Strange, B., Fletcher, P., Henson, R., Friston, K., and Dolan, R. (1999). Segregating the functions of human hippocampus. *Proc. Natl. Acad. Sci. U S A* 96, 4034–4039. doi: 10.1073/pnas.96.7.4034

Sünram-Lea, S. I., Foster, J. K., Durlach, P., and Perez, C. (2002). Investigation into the significance of task difficulty and divided allocation of resources on the glucose memory facilitation effect. *Psychopharmacology* 160, 387–397. doi: 10.1007/s00213-001-0987-9

van der Zwaluw, N. L., van de Rest, O., Kessels, R. P., and de Groot, L. C. (2015). Effects of glucose load on cognitive functions in elderly people. *Nutr. Rev.* 73, 92–105. doi: 10.1093/nutrit/nuu002

Wagner, G., Gussew, A., Köhler, S., de la Cruz, F., Smesny, S., Reichenbach, J. R., et al. (2016). Resting state functional connectivity of the hippocampus along the anterior-posterior axis and its association with glutamatergic metabolism. *Cortex* 81, 104–117. doi: 10.1016/j.cortex.2016.03.022

Watson, G. S., and Craft, S. (2003). The role of insulin resistance in the pathogenesis of Alzheimer's disease. *CNS Drugs* 17, 27–45. doi: 10.2165/00023210-200317010-00003

Whitfield-Gabrieli, S., and Nieto-Castanon, A. (2012). Conn: a functional connectivity toolbox for correlated and anticorrelated brain networks. *Brain Connect.* 2, 125–141. doi: 10.1089/brain.2012.0073

Wirt, R. A., and Hyman, J. M. (2017). Integrating spatial working memory and remote memory: interactions between the medial prefrontal cortex and hippocampus. *Brain Sci.* 7:E43. doi: 10.3390/brainsci7040043

Zanchi, D., Depoorter, A., Egloff, L., Haller, S., Mählmann, L., Lang, U. E., et al. (2017). The impact of gut hormones on the neural circuit of appetite and satiety: a systematic review. *Neurosci. Biobehav. Rev.* 80, 457–475. doi: 10.1016/j.neubiorev.2017.06.013

Conflict of Interest: DW has received research funding and/or consultancy/speaker honoraria from Abbott Nutrition, Arla Foods, Bayer Healthcare, and Neurobrands. AS has received research funding and/or consultancy/travel/speaker fees from Abbott Nutrition, Australian Research Council, Arla Foods, Australian Wine Research Institute, Barilla, Bayer, Biotechnology and Biological Sciences Research Council, Blackmores, Cognis, Cyvex, Dairy Health Innovation Consortium, Danone, DuPont, European Commission Framework 5 Research and Innovation initiative, GlaxoSmithKline, Ginsana, Kemin Foods, Martek, Masterfoods, National Health and Medical Research Council, Naturex, Nestlé, Neurobrands, Novartis, Nutricia-Danone, Red Bull, Sanofi, Sen-Jam Pharmaceuticals, Verdure Sciences, Unilever, Wrigley Science Institute.

The remaining authors declare that the research was conducted in the absence of any commercial or financial relationships that could be construed as a potential conflict of interest.

frontiers in Psychiatry

ORIGINAL RESEARCH
published: 07 February 2020
doi: 10.3389/fpsyt.2020.00033

Genetic Burden for Late-Life Neurodegenerative Disease and Its Association With Early-Life Lipids, Brain, Behavior, and Cognition

*Sander Lamballais[1], Ryan L. Muetzel[1,2], Mohammad Arfan Ikram[1], Henning Tiemeier[2,3], Meike W. Vernooij[1,4], Tonya White[2,4] and Hieab H. H. Adams[1,4,5]**

[1] Department of Epidemiology, Erasmus MC University Medical Center Rotterdam, Rotterdam, Netherlands, [2] Department of Child and Adolescent Psychiatry and Psychology, Erasmus MC University Medical Center Rotterdam, Rotterdam, Netherlands, [3] Department of Social and Behavioral Science, Harvard T. H. Chan School of Public Health, Boston, MA, United States, [4] Department of Radiology and Nuclear Medicine, Erasmus MC University Medical Center Rotterdam, Rotterdam, Netherlands, [5] Department of Clinical Genetics, Erasmus MC University Medical Center Rotterdam, Rotterdam, Netherlands

OPEN ACCESS

Edited by:
Mohamad Habes, University of Pennsylvania, United States

Reviewed by:
Gilberto Sousa Alves, Federal University of Ceara, Brazil
Sara L. Weisenbach, Stony Brook Medicine, United States

****Correspondence:***
Hieab H. H. Adams
h.adams@erasmusmc.nl

Specialty section:
This article was submitted to Aging Psychiatry, a section of the journal Frontiers in Psychiatry

Received: *19 October 2019*
Accepted: *10 January 2020*
Published: *07 February 2020*

Citation:
Lamballais S, Muetzel RL, Ikram MA, Tiemeier H, Vernooij MW, White T and Adams HHH (2020) Genetic Burden for Late-Life Neurodegenerative Disease and Its Association With Early-Life Lipids, Brain, Behavior, and Cognition. Front. Psychiatry 11:33. doi: 10.3389/fpsyt.2020.00033

Background: Genetics play a significant role in the etiology of late-life neurodegenerative diseases like Alzheimer's disease, Parkinson's disease, and frontotemporal dementia. Part of the individual differences in risk for these diseases can be traced back decades before the onset of disease symptoms. Previous studies have shown evidence for plausible links of apolipoprotein E (APOE), the most important genetic marker for Alzheimer's disease, with early-life cognition and neuroimaging markers. We aimed to assess whether genome-wide genetic burden for the aforementioned neurodegenerative diseases plays a role in early-life processes.

Methods: We studied children from the Generation R Study, a prospective birth cohort. APOE genotypes and polygenic genetic burdens for Alzheimer's disease, Parkinson's disease, and frontotemporal dementia were obtained through genome-wide genotyping. Non-verbal intelligence was assessed through cognitive tests at the research center around the age of 6 years, and educational attainment through a national school performance test around the age of 11 years. The Child Behavior Checklist was administered around the age of 10 years, and data from the anxious/depressed, withdrawn/depressed, and the internalizing behavior problems scales were used. Children participated in a neuroimaging study when they were 10 years old, in which structural brain metrics were obtained. Lipid serum profiles, which may be influenced by APOE genotype, were assessed from venal blood obtained around the age of 6 years. The sample size per analysis varied between 1,641 and 3,650 children due to completeness of data.

Results: We did not find evidence that APOE genotype or the polygenic scores impact on childhood nonverbal intelligence, educational attainment, internalizing behavior, and global brain structural measures including total brain volume and whole brain fractional anisotropy (all $p > 0.05$). Carriership of the APOE ε2 allele was associated with lower and

APOE ε4 with higher low-density lipoprotein cholesterol concentrations when compared to APOE ε3/ε3 carriers.

Conclusion: We found no evidence that genetic burden for late-life neurodegenerative diseases associates with early-life cognition, internalizing behavior, or global brain structure.

Keywords: polygenic risk scores, Alzheimer's disease, Parkinson's disease, frontotemporal dementia, cognition, neuroimaging, lipid profiles, internalizing behavior

INTRODUCTION

Genetic factors play a significant role in the etiology of late-life neurodegenerative diseases like Alzheimer's disease (AD) (1, 2), Parkinson's disease (PD) (3), and frontotemporal dementia (FTD) (4). With the exception of rare Mendelian forms of diseases, cases arise due to multifactorial processes where many genetic variants confer risk of neurodegeneration, in combination with non-genetic factors. The clinical onset of the aforementioned diseases tends to be preceded by years of deterioration of cognition and brain structure (5–7) as well as an increased incidence of depressive and psychiatric symptoms (8–10). For AD, these differences may even extend decades before the onset of disease (11–13), which could partly be explained by individual differences in the genetic burden for AD. As the genome is stable throughout life, the genes implicated in late-life neurodegenerative disease may already lead to subtle differences during childhood.

The apolipoprotein E epsilon 4 allele (APOE ε4) is the strongest common genetic variant for AD (14–16). The APOE gene plays a role in lipoprotein metabolism, and has been shown to affect lipid serum profiles during adulthood (17–21), and potentially during childhood (22, 23). As APOE also increases the risk for AD, its role in early-life cognition and brain markers has also been studied. The studies on APOE ε4 and cognition during adolescence and early adulthood have reported mixed results, with some reporting lower cognitive function, some higher, and most reporting no difference (24). Additionally, a number of studies showed that APOE ε4 may relate to lower brain volumes during infancy and childhood, particularly in regions affected in AD such as the hippocampus (25–30). Overall, APOE ε4 may associate with early-life processes, but this needs to be elucidated further.

With the advent of genome-wide association studies (GWAS) there has been an increase in the number of genes identified for neurodegenerative disease. GWAS has led to the discovery of at least 30 new genetic loci for AD (1, 2), at least genetic 24 loci for PD (3), and at least 3 loci for FTD (4). The disease burden per locus can be combined into a single score, known as polygenic risk scores (PGRS), to assess the genetic burden a person has for that disease (31). The genetic burden for AD, PD, and FTD may relate to early-life processes, which can be studied using PGRS. However, few studies exist that assesses the effect of such PGRS on early-life markers.

To obtain a more comprehensive overview of the relevance in early-life of genes related to late-life neurodegenerative disease we performed a comprehensive study within the Generation R birth cohort. We assessed the APOE genotype and created PGRS for AD, PD, and FTD. Given the existing literature we hypothesized that these genetic predispositions to late-life neurodegenerative disorders associate with early-life non-verbal intelligence quotient (IQ), educational attainment, internalizing behavior, and neuroimaging markers, and that APOE and the AD PGRS associate with lipid profiles.

METHODS

Participants

The data was obtained from the Generation R cohort, a prospective birth cohort based in Rotterdam, the Netherlands (32). Pregnant women in Rotterdam were at their first prenatal visit approached to participate. A total of 9,901 children were born as part of the Generation R cohort and were invited to participate in questionnaires and research center visits beginning in 2002 to the present day.

DNA was sequenced from blood obtained from the umbilical cord or with blood samples collected around 6 years of age, and genetic data was available for 5,725 children. In the case of sibling pairs (n = 235 pairs) we included the oldest sibling. This led to a sample of 5,490 children. The focus of the current study was on cognitive function, brain structure, and blood lipid profiles. Non-verbal IQ was measured at approximately 6 years (n = 3,650) and educational attainment at 11 years of age (n = 1,641). The Childhood Behavior Checklist (CBCL) was administered around the age of 10 years with data for the anxious/depressed scale (n = 1,867), the withdrawn/depressed scale (n = 1,862), and the internalizing problems scale (n = 1,859) used for this study. Magnetic resonance imaging (MRI) of the brain was done when the children were approximately 10 years of age, collecting both T_1-weighted (n = 1,962) and diffusion-weighted images (n = 1,832). Blood lipid profiles were determined with blood samples obtained around the age of 6 years (n = 2,749). A flow chart of the study population is shown in **Supplementary Figure 1**.

Ethics Statement

The study was conducted in accordance with the guidelines as proposed in the World Medical Association Declaration of Helsinki and was approved by the Medical Ethics Committee of the Erasmus MC. Written informed consent was obtained from primary caregivers on behalf of the child.

Genotyping, Apolipoprotein E ε4, and Polygenic Risk Scores

DNA sample collection, genotype calling procedures, and subsequent quality control have been described elsewhere (33, 34). In brief, samples were either collected from cord blood at birth (Illumina 610K Quad Chip) or from venipuncture at a visit to the research center when children were between the age of 5 and 8 years (Illumina 660K Quad Chip). Single nucleotide polymorphisms were filtered for minor allele frequency < 0.01, Hardy-Weinberg disequilibrium p < .00001, and missing rate > 0.05. To be able to account for population stratification, we calculated the first 10 genomic components using the multi-dimensional scaling function of PLINK (34, 35).

APOE carriership status was assessed from the genotyped data and based on the nucleotide combinations of two single nucleotide polymorphisms: rs429348 and rs7412. A thymine at both locations is classified as APOE ε2, one thymine and one cytosine as APOE ε1 or APOE ε3, and both cytosines as APOE ε4. As APOE ε1 and APOE ε3 cannot be distinguished we classified both as APOE ε3. We considered APOE ε3/ε3 to be the reference category as this is the most prevalent genotype.

PGRS for AD, PD, and FTD were calculated using PRSice-2 (36). The scores were based on summary statistics from the largest GWAS for each respective neurodegenerative disease (3, 4, 37). PGRS are generally calculated for different thresholds of statistical significance in the summary statistics. As we did not have an *a priori* hypothesis on the optimal threshold, we calculated PGRS based on single nucleotide polymorphisms below the following p-value thresholds: 0.000001, 0.000005, 0.00001, 0.000005, 0.00001, 0.00005, 0.0001, 0.0005, 0.01, 0.05, 0.1, 0.5, and 1.0. Strand flips were corrected and we used clumping to build the score using independent loci.

Non-Verbal Intelligence Quotient and Educational Attainment

Two measures for cognitive function were available. The first was an assessment of non-verbal IQ at the research visit around the age of 6 years. Participants completed two subtests of the Snijders-Oomen Non-Verbal Intelligence Test-Revised (SON-R 2½-7) (38): "Mosaics," a spatial visualization task, and "Categories," an abstract reasoning task. The raw scores were converted to IQ scores using age and sex-specific norms. As both tasks specifically assess non-verbal cognition, we considered these scores as non-verbal IQ scores. The correlation between IQ derived from the whole test battery and IQ derived from just the "Mosaics" and "Categories" tests has been shown to be high (r = 0.86) (39).

The measure of cognitive function was the educational attainment score obtained at the age of 11 years. The "Centraal Instituut voor Toetsontwikkeling" (CITO) test is administered in the majority primary schools in the Netherlands and is completed during the final year of primary school. The CITO test generally consists of two main skill domains: language and mathematics. The raw test scores for both domains were obtained for most Generation R children that took the CITO test during the years 2014 to 2017 and that were still part of Generation R at the time. As the test difficulty tends to vary slightly each year we summed the raw domain scores to a total score for each child, standardized the scores for all children within a given year, and finally combined the stratified distributions into one distribution. This method yielded standardized scores that were comparable across testing years.

Child Behavior Checklist

Behavioral problems were assessed using the CBCL for ages 6 to 18 (40). The CBCL is a validated and reliable 113-item inventory that uses caregiver-reported information to assess behavioral problems in children. The procedure and specific characteristics for Generation R have been described elsewhere (41). For this study we considered mother-reported data on the anxious/depressed, the withdrawn/depressed, and the internalizing problems scales.

Image Acquisition and Processing

Image acquisition has been described elsewhere (41). In brief, structural brain MR images were obtained on a single 3T GE Discovery MR750w MRI system (General Electric, Milwaukee, WI, USA) utilizing an eight-channel receive-only head coil. T_1-weighted images were collected using a three-dimensional (3D) inversion recovery-prepared fast spoiled gradient recalled sequence (T_R = 8.77 ms, T_E = 3.4 ms, T_I = 600 ms, flip angle = 10°, field of view = 220 x 220 mm, acquisition matrix = 220 x 220, slice thickness = 1 mm, number of slices = 230, bandwidth = 25 kHz). Diffusion-weighted images consisted of three b_0 volumes and 35 diffusion directions using an echo planar imaging sequence (T_R = 12,500 ms, T_E = 72 ms, field of view = 240 x 240 mm, acquisition matrix = 120 x 120, slice thickness = 2 mm, number of slices = 65, b = 900 s/mm^2).

T_1-weighted images were processed through the FreeSurfer analysis suite, version 6.0.0 (42). The procedure has been described elsewhere (43). Briefly, non-brain tissue was removed, voxel intensities were normalized for B1 inhomogeneity, whole-brain tissue segmentation was performed, and a surface-based model of the cortex was reconstructed. For each participant we obtained metrics for total brain volume, cortical gray matter volume, cerebrospinal fluid volume, and mean cortical thickness. For analyses of APOE status and the AD PGRS we additionally focused on volumes of the hippocampus, the entorhinal cortex, the middle temporal gyrus, and the parahippocampal gyrus. For the PD PGRS we also considered volumes of the nucleus accumbens, the caudate nucleus, the globus pallidi, and the putamen. Finally, for the FTD PGRS we also looked at the frontal and the temporal lobes, and in particular the volume, the mean thickness, and the surface area. For all lateralized structures we took the mean of both sides.

Diffusion tensor imaging (DTI) images were processed through the FMRIB Software Library (FSL), version 5.0.9 (44). The full procedure is described elsewhere (43). Briefly, non-brain tissue was removed and images were corrected for eddy-current artifacts and translations/rotations resulting from head motion. Diffusion tensors were fitted at each voxel using the RESTORE method from the Camino diffusion MRI toolkit (45). We further performed probabilistic white matter fiber tractography in native

space for each participant using the FSL plugin AutoPtx to identify connectivity distributions of a number of well-known fiber bundles (46). Average fractional anisotropy and mean diffusivity values were then computed for each white matter tract. Global measures for fractional anisotropy and mean diffusivity were obtained by performing factor analyses on the tract-specific values (47).

Lipid Profiles

Lipid profiles of the children were assessed from venous blood acquired during the research visits around the age of 6 years after a 30 min fast. Serum total cholesterol, high-density lipoprotein cholesterol (HDL-c), and triglyceride concentrations were derived with the Roche cobas 8000 analyzer (Roche Diagnostics GmbH, Penzberg, Germany), and low-density lipoprotein cholesterol (LDL-c) was estimated using the Friedewald equation (48). We considered these lipids in relation to APOE status and the AD PGRS as the APOE gene plays a significant role in lipid metabolism (49), whereas we did not have such a prior expectation for PD and FTD.

Statistical Analysis

Statistical analyses were performed with the R statistical package, version 3.5.2 (R 50). We used multiple linear regression for all outcomes, correcting for age at outcome measurement, sex of the child, maternal education (low, intermediate, or high), and the first 10 genomic components. The latter was done to take into account the underlying genetic structure of the population. The serum lipid models were additionally adjusted for body mass index (BMI) at the time of the venous puncture. The volumetric neuroimaging models, i.e. cortical volume, cerebrospinal fluid (CSF) volume, and the disease-specific regional brain volumes, were additionally adjusted for total brain volume. Furthermore, we applied square-root transformations to the CBCL scales to better satisfy the linearity assumption of linear regression.

Polygenic burden may only affect those whose burden is above a certain threshold, thus leading to non-linearity of an association. We assessed this through two approaches: 1) dichotomization of the top PGRS decile *versus* the rest of the population, 2) fitting restrictive cubic splines on the PGRSs to assess any non-linearity in the association.

Use of PGRS in the Generation R Study requires a critical consideration of ethnicity. The GWAS from which we used the summary statistics were based on populations of European ancestry. Findings from GWAS and by extension PGRS are specific to the ethnicity of the original study population. The Generation R study is based in the city of Rotterdam, where about half of all individuals are of non-European ancestry. We focused our main findings on the complete population, but we additionally stratified our analyses for European ancestry to check for any effects related specifically to ethnicity. We additionally performed sensitivity analyses where we did not correct for the first 10 genomic components, to see whether improper correction for population stratification is relevant for studies on APOE and studies on AD, PD, and FTD PGRS (51).

Multiple testing correction was considered on three levels: 1) the PGRS for AD, PD, or FTD, 2) the PGRS thresholds, and 3) the outcome measures. We did not expect dependence among the PGRS of the neurodegenerative diseases. Therefore, we applied a Bonferroni correction across AD, PD, and FTD. As the PGRS thresholds were strongly intercorrelated as well as some of the outcome measures, we applied a false discovery rate (FDR) correction within a given disease. The p-values reported below are those after the FDR correction.

RESULTS

Population Characteristics

Table 1 shows the characteristics of the total study population and stratified by European ancestry and non-European ancestry. Overall, the most common APOE genotypes were ε3/ε3 (64.9%), ε2/ε3 (11.5%), and ε3/ε4 (19.1%), whereas the other genotypes were much less common, i.e. ε2/ε2 (0.5%), ε2/ε4 (2.3%), and ε4/ε4 (1.6%). These numbers were similar for those with European and non-European ancestry.

Apolipoprotein E and Polygenic Risk Scores for Alzheimer's Disease

Figures 1 and **2** display the results of the associations of all relevant outcomes with APOE genotype and AD PGRS, respectively. Neither APOE genotype nor any AD PGRS associated with non-verbal IQ during the 6-year visit or the CITO score at 11 years (all $p_{corrected} > 0.05$). The APOE genotype and AD PGRS also did not relate to global brain metrics such as total brain volume and CSF volume, nor with the connectivity metrics global fractional anisotropy and mean diffusivity (all $p_{corrected} > 0.05$). APOE genotype and the AD PGRS also did not associate with region-specific metrics for the hippocampus, the entorhinal cortex, the medial temporal gyrus, and the parahippocampal region. Finally, APOE genotype and AD PGRS did not show any statistically significant associations with the CBCL scales anxious/depressed or withdrawn/depressed, nor with the internalizing problems scale (all $p_{corrected} > 0.05$).

The APOE genotype associated with serum lipid profiles. Compared to the APOE ε3/ε3 genotype, those with APOE ε2/ε3 had lower total cholesterol concentrations ($\beta = -0.32$, SE = 0.06, $p_{corrected} < 0.001$), lower LDL-c concentrations ($\beta = -0.57$, SE = 0.06, $p_{corrected} < 0.001$), and higher HDL-c concentrations ($\beta = 0.22$, SE = 0.06, $p_{corrected} = 0.01$). The APOE ε2/ε2 followed the exact same pattern but with even larger differences.

Compared to the APOE ε3/ε3 genotype those with ε3/ε4 had higher total cholesterol concentrations ($\beta = 0.19$, SE = 0.05, $p_{corrected} = 0.003$), higher LDL-c concentrations ($\beta = 0.16$, SE = 0.05, $p_{corrected} < 0.001$), and lower HDL-c concentrations ($\beta = 0.26$, SE = 0.05, $p_{corrected} = 0.02$). These differences were similar and larger when comparing the APOE ε3/ε3 genotype with the APOE ε4/ε4 genotype.

Triglycerides were higher in all genotypes compared to APOE ε3/ε3, although none of these were statistically significance (all $p_{corrected} > 0.05$).

The AD PGRS also associated with serum lipid profiles, but only at stricter PGRS thresholds, i.e. PGRS thresholds below 0.001.

TABLE 1 | Characteristics of the study population.

Characteristics	All	European ancestry	Non-European ancestry
	(N = 5,490)	(N = 2,651)	(N = 2,839)
APOE genotype (%)			
ε2/ε2	0.5	0.5	0.6
ε2/ε3	11.5	10.4	12.6
ε2/ε4	2.3	2.5	2.1
ε3/ε3	64.9	60.6	69.0
ε3/ε4	19.1	21.6	16.8
ε4/ε4	1.6	2.2	1.1
Visit around 6 years			
Non-verbal IQ (mean, SD)	101 (15)	105 (14)	97 (15)
Total cholesterol (mean, SD) (mmol/L)	4.2 (0.6)	4.2 (0.6)	4.3 (0.7)
HDL-c (mean, SD) (mmol/L)	1.3 (0.3)	1.3 (0.3)	1.4 (0.3)
LDL-c (mean, SD) (mmol/L)	2.4 (0.6)	2.3 (0.6)	2.4 (0.6)
Triglycerides[a] (geometric mean, SD) (mmol/L)	1.0 (0.5)	1.1 (0.5)	1.5 (0.5)
Visits at 10 and 11 years			
CITO score, standardized (mean, SD)	0.0 (1.0)	0.2 (0.9)	−0.3 (1.1)
Total brain volume (mean, SD) (cm^3)	1,200 (118)	1,225 (113)	1,168 (116)
Cortical volume (mean, SD) (cm^3)	574 (59)	588 (56)	556 (59)
Cerebrospinal fluid volume (mean, SD) (cm^3)	0.9 (0.2)	0.9 (0.2)	0.9 (0.2)
Mean cortical thickness (mean, SD) (mm)	2.67 (0.08)	2.68 (0.08)	2.67 (0.08)
Global FA, standardized (mean, SD)	0.00 (1.00)	0.11 (0.97)	−0.15 (1.02)
Global MD, standardized (mean, SD)	0.00 (1.00)	−0.03 (0.98)	0.04 (1.03)
Anxious/depressed scale (mean, SD)	2.2 (2.7)	2.2 (2.7)	2.2 (2.6)
Withdrawn/depressed scale (mean, SD)	1.1 (1.6)	1.1 (1.5)	1.1 (1.8)
Internalizing problems scale (mean, SD)	4.7 (5.0)	4.5 (4.8)	5.1 (5.4)

APOE, apolipoprotein epsilon.
IQ, intelligence quotient.
HDL-c, high density lipoprotein cholesterol.
LDL-c, low density lipoprotein cholesterol.
FA, fractional anisotropy.
MD, mean diffusivity.
[a]*Triglyceride serum values were log-transformed.*

However, these associations disappeared upon including the APOE genotype as a covariate (all $p_{corrected} > 0.05$). Furthermore, the results did not differ when using the top-decile PGRS dichotomization rather than the continuous PGRS, or when modeling cubic splines.

Polygenic Risk Scores for Parkinson's Disease and Frontotemporal Dementia

The results for the PD and FTD PGRS are shown in **Figures 3** and **4**, respectively. We found no support for associations of scores at any threshold with non-verbal IQ, educational attainment, internalizing behavior scales, or neuroimaging markers. Furthermore, we did not find evidence for associations of the PD scores with the volumes of the nucleus accumbens (ß for PGRS at 0.05 threshold = −0.08, $SE_{0.05} = 0.12$, $p_{corrected} = 1.00$), the caudate nucleus ($ß_{0.05} = 0.03$, $SE_{0.05} = 0.12$, $p_{corrected} = 1.00$), the globus pallidus ($ß_{0.05} = -0.07$, $SE_{0.05} = 0.13$, $p_{corrected} = 1.00$), or the putamen ($ß_{0.05} = -0.13$, $SE_{0.05} = 0.12$, $p_{corrected} = 1.00$). Similarly, we did not observe any associations of the FTD scores with the volumes of the frontal ($ß_{0.05} = -0.00$, $SE_{0.05} = 0.03$, $p_{corrected} = 1.00$) or temporal lobes ($ß_{0.05} = 0.01$, $SE_{0.05} = 0.03$, $p_{corrected} = 1.00$).

Population Structure

All analyses were performed in all available participants, and were controlled for the first 10 genomic components. We further stratified the analyses for European *versus* non-European ancestry (**Figures 5A, D**, **Supplementary Figure 2**), and the effect estimates were generally similar. We additionally reran the analyses without correcting for the genomic components, and this led to stark changes in the results (**Figures 5B, E**, **Supplementary Figure 3**). The higher the PGRS threshold, the more statistically significant findings were present in the analyses not corrected for genomic components compared to when we did correct for genomic components. We further split the uncorrected analyses for European *versus* non-European ancestry, to see whether one of these groups was driving the sudden change in findings (**Figures 5C, F**, **Supplementary Figure 4**). Within the uncorrected analyses for individuals of non-European ancestry we find an inflation of the number of statistically significant findings, whereas this was not the case for individuals of European ancestry.

DISCUSSION

None of the measures for genetic burden for AD, PD, or FTD were associated with childhood non-verbal IQ, educational attainment, internalizing behavior, global brain structure, or disease-specific regional brain structures. Although genetic burden for late-life neurodegenerative disease has been linked to brain structure and cognitive function during late-life, we find no evidence that these affect the same processes during early life. Furthermore, we provided clear evidence that the APOE genotype affects lipid profiles during childhood. Finally, we showed that improper control of the ethnic structure of the population through genomic components can lead to false positive associations when considering PGRS for AD, PD, and FTD.

We found no support for the link between AD genetic burden and global, hippocampal. and temporal regions although previous studies have provided evidence for such links during infancy (28, 29), childhood (25, 30, 52, 53), and early adulthood (27, 54–61). The support for such associations does seem stronger in studies during early adulthood than during childhood. This suggests that the genetic burden for AD becomes more relevant with age, and that there are cumulative processes at play which may only become apparent after early-life. For example, the pathological burden in APOE ε4 carriers may be increased due to accumulation of lipoprotein (62, 63),

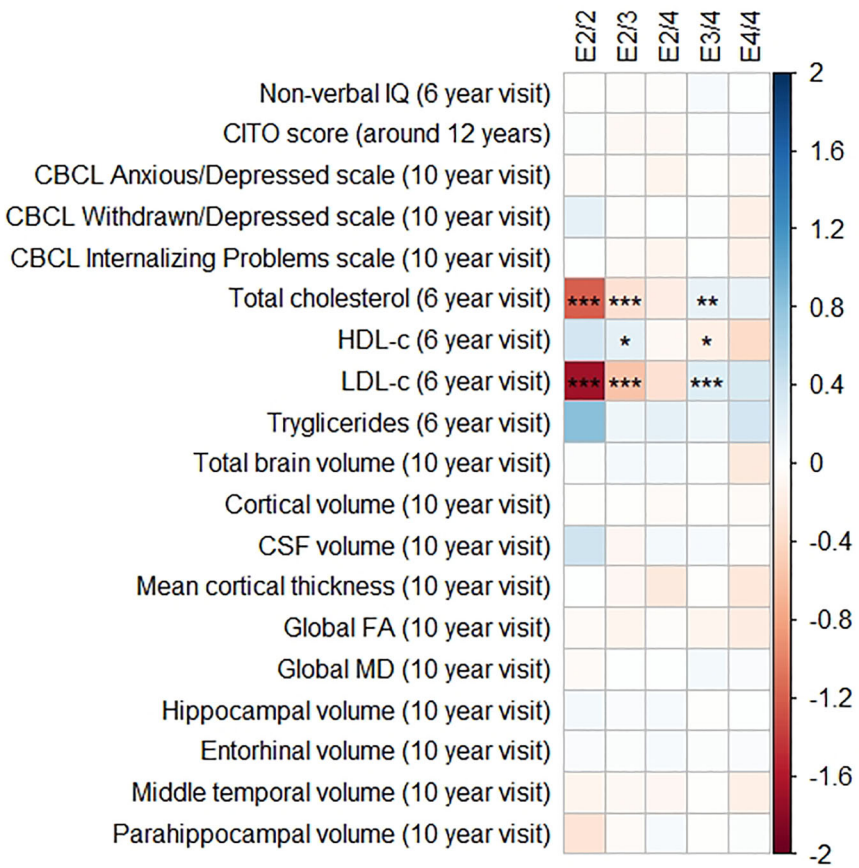

FIGURE 1 | Heatmap showing the regression coefficients between apolipoprotein E (APOE) genotype and all phenotypes. The E3/3 genotype is used as a reference for the other genotypes. All coefficients are standardized. The reported p-values were corrected for multiple testing. IQ, intelligence quotient; CBCL, Child Behavior Checklist; HDL, high-density lipoprotein; LDL, low-density lipoprotein; CSF, cerebrospinal fluid; FA, fractional anisotropy; MD, mean diffusivity; * = 0.05; ** = 0.01; *** = 0.001.

reduced neuronal reparative capacity (64, 65), and altered responses to neuroinflammatory processes (66).

Interpreting the role of APOE in childhood brain development is further complicated by the inconsistency of findings. Shaw and colleagues found in children and adolescents that APOE ε4 carriers had thinner entorhinal cortices than non-carriers (25). Chang and colleagues also studied children and adolescents, but they found that ε4 carriers had larger hippocampi than non-carriers (30). Additionally, they report that ε4 carriers compared to non-carriers had larger volumes for the cuneus, the temporal pole, the lateral occipital pole, and the medial orbitofrontal cortex. The two studies that report that APOE affects brain structure in infants show that ε4 carriers have smaller hippocampi than non-carriers (28, 29). Furthermore, they report that APOE affects regions that are very different from those reported by Chang and colleagues (30). More recently, Axelrud and colleagues reported that the AD PGRS relates to hippocampal volume in Brazilian children aged 6 to 14 years old (53). However, the source GWAS on which the PGRS in the latter study was based was performed in a population of European ancestry (37). As we have shown, using the AD PGRS in populations of non-European ancestry leads to false positive findings. Indeed, Axelrud and colleagues could not replicate their findings in a separate Canadian population of 1,024 adolescents. In summary, previous findings have been inconsistent, which suggests that AD genetic burden may only affect early-life brain structure under specific circumstances or that the effect is unlikely to be clinically relevant.

We did not find evidence in our study to suggest that AD genetic burden affects cognitive functioning during childhood. Previous studies on this topic report mixed results, but several larger studies also did not find evidence for such a link. Taylor and colleagues studied cognition in the Avon Longitudinal Study of Parents and Children (ALSPAC) study (23). The only pattern observed was that APOE ε4 carriers performed better on cognitive tests than those with a APOE ε3/ε3 genotype, although not statistically significant. In our study we found no evidence to support this. More recently, Weissberger and colleagues meta-analyzed data from 9,234 individuals aged 2 to 40 years old and found no association of APOE ε4 carriership with intelligence, attention, executive function, language, memory, processing speed, and visuospatial abilities (67). In our study we confirmed this finding at two timepoints in childhood (around 6 years of age

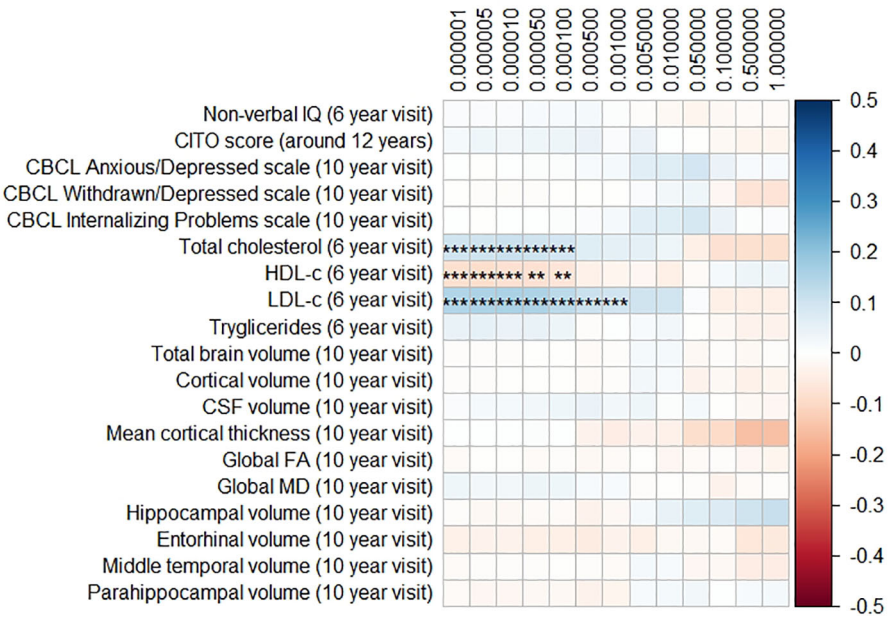

FIGURE 2 | Heatmap showing the regression coefficients between the Alzheimer's disease (AD) polygenic risk score (PGRS) and all phenotypes. Each score is based on a different threshold for inclusion of single-nucleotide polymorphisms (SNPs) into the score. All coefficients are standardized. The reported p-values were corrected for multiple testing. IQ, intelligence quotient; CBCL, Child Behavior Checklist; HDL, high-density lipoprotein; LDL, low-density lipoprotein; CSF, cerebrospinal fluid; FA, fractional anisotropy; MD, mean diffusivity; ** = 0.01; ** = 0.001.

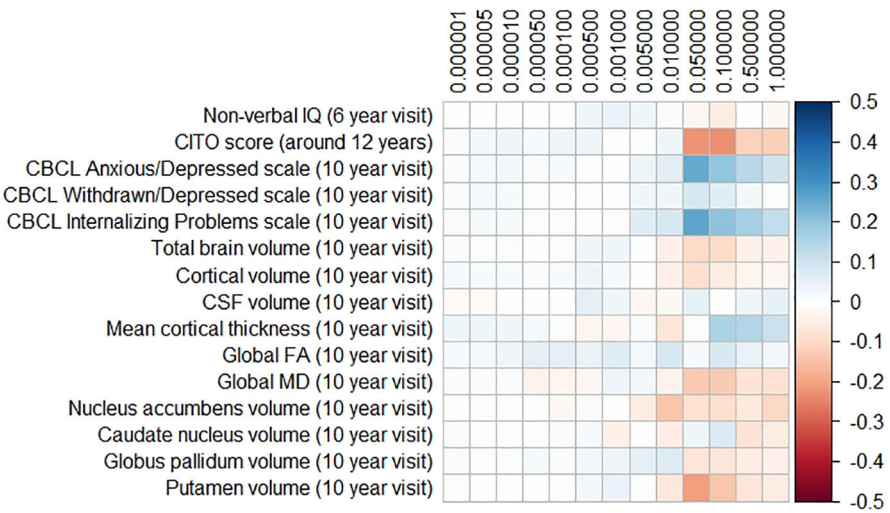

FIGURE 3 | Heatmap showing the regression coefficients between the Parkinson's disease (PD) polygenic risk score (PGRS) and all phenotypes. Each score is based on a different threshold for inclusion of single-nucleotide polymorphisms (SNPs) into the score. All coefficients are standardized. The reported p-values were corrected for multiple testing. None of the associations were statistically significant after correction. IQ, intelligence quotient; CBCL, Child Behavior Checklist; HDL, high-density lipoprotein; LDL, low-density lipoprotein; CSF, cerebrospinal fluid; FA, fractional anisotropy; MD, mean diffusivity.

and around 11 years of age), and we also extend the findings to APOE ε2 genotypes and to broader AD genetic burden. Taken together, the literature and this study suggest that AD genetic burden does not affect cognition during early life.

The role of the APOE gene in serum lipid profiles during early life has been studied before. In 2011, a study by Taylor and colleagues assessed the relation between APOE status and serum lipid profiles in 2,875 children aged 8 to 11 years from the ALSPAC

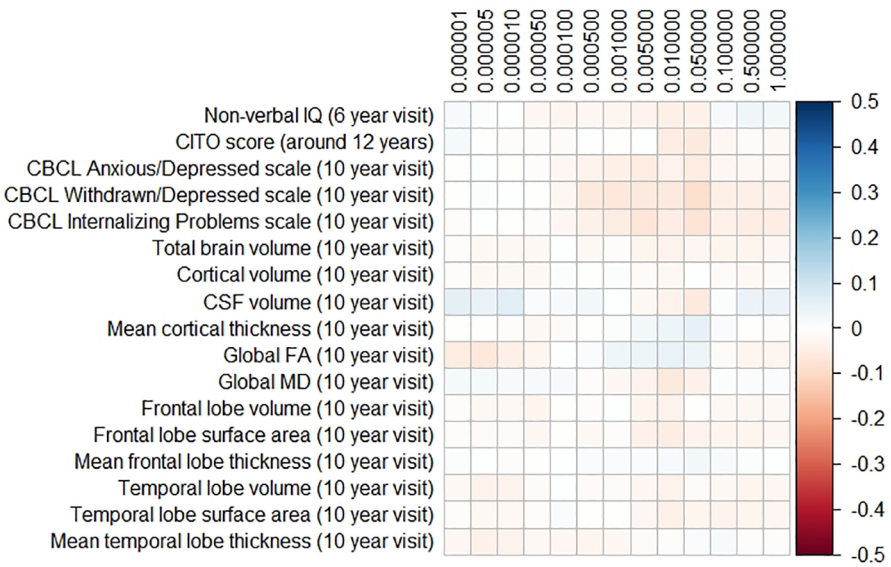

FIGURE 4 | Heatmap showing the regression coefficients between the frontotemporal dementia (FTD) polygenic risk score (PGRS) and all phenotypes. Each score is based on a different threshold for inclusion of single-nucleotide polymorphisms (SNPs) into the score. All coefficients are standardized. The reported p-values were corrected for multiple testing. None of the associations were statistically significant after correction. IQ, intelligence quotient; CBCL, Child Behavior Checklist; HDL, high-density lipoprotein; LDL, low-density lipoprotein; CSF, cerebrospinal fluid; FA, fractional anisotropy; MD, mean diffusivity.

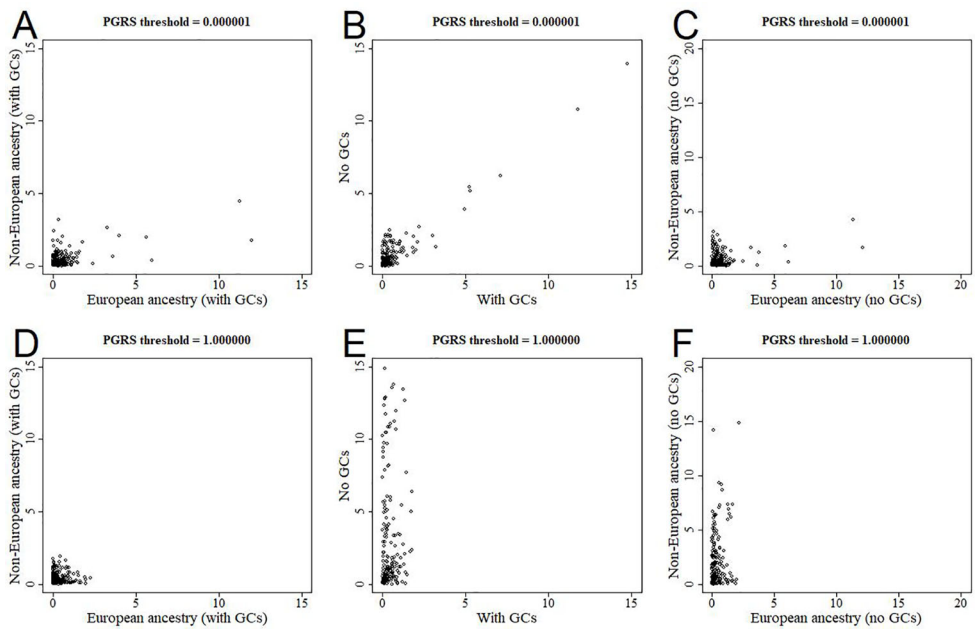

FIGURE 5 | Scatterplots of log-transformed p-values when comparing different analyses. The results are shown for polygenic risk score (PGRS) thresholds 0.000001 (top row) and 1.000000 (bottom row). Comparisons are shown for European *versus* non-European **(A, D)**, correcting for genomic components or not **(B, E)**, and European *versus* non-European when not correcting for genomic components **(C, F)**. GC, genomic component.

cohort, a prospective birth cohort study (23). They showed that carriership of APOE ε2 was associated with reduced cholesterol and increased triglyceride levels compared to APOE ε3/ε3, whereas APOE ε4 carriers had both elevated cholesterol and triglyceride levels. In 1997, Kallio and colleagues showed that cord blood from 42 APOE ε4 carriers contained higher concentrations of cholesterol than 13 carriers of APOE ε2 (22). In addition, LDL levels rose steeper during the first year of life in the APOE ε4 carriers than in

the APOE ε2 carriers. In our study we had similar findings for ε2/ε3 and ε3/ε4 but not for ε2/ε2 and ε4/ε4 genotypes, likely because those genotypes were uncommon within the current study population. Our findings further consolidate the causal role of APOE genotype in serum lipid levels even during early life.

We found no evidence that PD and FTD genetic burden influences early-life processes. However, the etiology and pathogenesis of PD and FTD are poorly understood, and less is known on the preclinical disease stage compared to AD. It is therefore not clear how genetic burden for PD or FTD would influence early-life processes. As both syndromes can occur through dominant autosomal inheritance, it should be possible to investigate families of PD or FTD patients to identify such processes. However, we were unable to identify any such study in the literature. Another route would be to look at healthy carriers of known genetic risk variants for either PD or FTD to identify affected processes. For example, the G2019S mutation in the LRRK2 gene, the gene most widely associated with Parkinson's disease, has been studied in healthy controls. Different studies found this gene to be associated with lower executive functioning (68), changes in gait (69), olfactory dysfunction (70). However, all these studies were small and exploratory. To the best of our knowledge, no studies focusing on FTD candidate genes in healthy controls are available. Further work is needed to elucidate whether PD and FTD genetic burden play a role in other domains during early-life, for example brain function rather than brain structure.

The etiology of AD, PD, and FTD extend beyond lipid profiles, the brain, behavior, and cognition, thus raising the question which other processes could be relevant during childhood. For example, cerebrospinal fluid markers levels such as Tau and phosphorylated Tau are affected by APOE ε4 carriership in demented individuals (71–74). In addition, APOE protein levels in cerebrospinal fluid, but not blood serum, depend on the APOE genotype (75). Another avenue for further research are inflammatory markers such as C-reactive protein, interleukin-6, and α1-antichymotrypsin, which have shown predictive value for the onset of all-cause dementia (76). Further assessment of endophenotypes closely related to specific gene function may provide more stable findings related to early life.

Our findings may have been limited by several aspects of the study design. First, we relied on cross-sectional data. Brain growth follows non-linear trajectories, reaching a peak at around the age when the children in our study underwent neuroimaging (77). The genetic burdens for neurodegenerative disease may affect the trajectories of brain development, which would only be detectable through longitudinal studies. Alternatively, the genetic burden for late-life neurodegenerative disease may not express until later in childhood or adolescence, and the study population may simply be too young for the research questions at hand. Second, the number of individuals with ε2/ε2 or ε4/ε4 genotypes was relatively low, thus we were likely underpowered to establish any small effects for those genotypes. Third, we administered a limited number of cognitive tests around the age of 6, limiting our investigation to non-verbal IQ. AD is generally characterized by a loss of memory function, for which we did not have an adequate test in children.

Our study also had clear strengths. The size of our study population ensured sufficient power to detect relatively small effects related to the common APOE genotypes and the AD, PD, and FTD PGRS. Furthermore, we provide an unambiguous case for proper control of population stratification, which was only possible due to the large proportion of participants of non-European ancestry. Finally, the Generation R study is a representative sample from the general population, which vastly improves the generalizability to a community-dwelling population of European descent.

In conclusion, we found no evidence to support the role of genetic burden for late-life neurodegenerative disease in early-life cognitive performance, internalizing behavior, and brain metrics. APOE genotype was related to blood lipid profiles. Genetic burden for AD, PD, and FTD did not relate to cognition or brain structure. These findings suggest that the etiology of late-life neurodegenerative disease becomes only relevant later in life.

DATA AVAILABILITY STATEMENT

The datasets for this article are not automatically publicly available due to legal and informed consent restrictions. Reasonable requests to access the datasets should be directed to the Director of the Generation R Study, Vincent Jaddoe (generationr@erasmusmc.nl), in accordance with the local, national and European Union regulations.

AUTHOR CONTRIBUTIONS

SL, RM, TW, and HA designed the project. SL analyzed the data. SL and HA interpreted the results and drafted the article. All authors contributed to manuscript revision, and read and approved the submitted version. All authors agree to be accountable for all of the published work.

FUNDING

The work was supported by the European Research Council (ERC) under the European Union's Horizon 2020 research and innovation program (project: ORACLE, grant agreement No: 678543, and project JPco-fuND, grant agreement No: 643417), the ZonMw (grant numbers 912.11.021 and 916.19.151), and the Sophia Foundation (grant S18-20). The general design of Generation R Study is made possible by financial support from the Erasmus Medical Center, Rotterdam, the Erasmus University Rotterdam, the Netherlands Organization for Health Research and Development (ZonMw), the Netherlands Organisation for Scientific Research (NWO), the Ministry of Health, Welfare and Sport, and the Ministry of Youth and Families.

ACKNOWLEDGMENTS

The Generation R Study is conducted by the Erasmus Medical Center in close collaboration with the School of Law and Faculty of Social Sciences of the Erasmus University Rotterdam, the Municipal Health Service Rotterdam area, Rotterdam, the Rotterdam Homecare Foundation, Rotterdam, and the

Stichting Trombosedienst & Artsenlaboratorium Rijnmond (STAR-MDC), Rotterdam. We gratefully acknowledge the contribution of children and parents, general practitioners, hospitals, midwives, and pharmacies in Rotterdam.

SUPPLEMENTARY MATERIAL

The Supplementary Material for this article can be found online at: https://www.frontiersin.org/articles/10.3389/fpsyt.2020.00033/full#supplementary-material

SUPPLEMENTARY FIGURE 1 | Flow chart of the study population.

SUPPLEMENTARY FIGURE 2 | Scatterplots of log-transformed p-values when comparing analyses in the European versus non-European samples when correcting for genomic components.

SUPPLEMENTARY FIGURE 3 | Scatterplots of log-transformed p-values when comparing analyses corrected for genomic components versus not.

SUPPLEMENTARY FIGURE 4 | Scatterplots of log-transformed p-values when comparing analyses in the European versus non-European samples when not correcting for genomic components.

REFERENCES

1. Jansen IE, Savage JE, Watanabe K, Bryois J, Williams DM, Steinberg S, et al. Genome-wide meta-analysis identifies new loci and functional pathways influencing Alzheimer's disease risk. *Nat Genet* (2019) 51:404–13. doi: 10.1038/s41588-018-0311-9
2. Kunkle BW, Grenier-Boley B, Sims R, Bis JC, Damotte V, Naj AC, et al. Genetic meta-analysis of diagnosed Alzheimer's disease identifies new risk loci and implicates Abeta, tau, immunity and lipid processing. *Nat Genet* (2019) 51:414–30. doi: 10.1038/s41588-019-0358-2
3. Nalls MA, Pankratz N, Lill CM, Do CB, Hernandez DG, Saad M, et al. Large-scale meta-analysis of genome-wide association data identifies six new risk loci for Parkinson's disease. *Nat Genet* (2014) 46:989–93. doi: 10.1038/ng.3043
4. Ferrari R, Hernandez DG, Nalls MA, Rohrer JD, Ramasamy A, Kwok JB, et al. Frontotemporal dementia and its subtypes: a genome-wide association study. *Lancet Neurol* (2014) 13:686–99. doi: 10.1016/S1474-4422(14)70065-1
5. Jack CRJr., Knopman DS, Jagust WJ, Petersen RC, Weiner MW, Aisen PS, et al. Tracking pathophysiological processes in Alzheimer's disease: an updated hypothetical model of dynamic biomarkers. *Lancet Neurol* (2013) 12:207–16. doi: 10.1016/S1474-4422(12)70291-0
6. Postuma RB, Berg D. Prodromal Parkinson's Disease: The Decade Past, the Decade to Come. *Mov Disord* (2019) 34:665–75. doi: 10.1002/mds.27670
7. Staffaroni AM, Cobigo Y, Goh SM, Kornak J, Bajorek L, Chiang K, et al. Individualized atrophy scores predict dementia onset in familial frontotemporal lobar degeneration. *Alzheimers Dement* (2020) 1:37–48. doi: 10.1016/j.jalz.2019.04.007
8. Barnes DE, Yaffe K, Byers AL, Mccormick M, Schaefer C, Whitmer RA. Midlife vs late-life depressive symptoms and risk of dementia: differential effects for Alzheimer disease and vascular dementia. *Arch Gen Psychiatry* (2012) 69:493–8. doi: 10.1001/archgenpsychiatry.2011.1481
9. Cherbuin N, Kim S, Anstey KJ. Dementia risk estimates associated with measures of depression: a systematic review and meta-analysis. *BMJ Open* (2015) 5:e008853. doi: 10.1136/bmjopen-2015-008853
10. Almeida OP, Hankey GJ, Yeap BB, Golledge J, Flicker L. Depression as a modifiable factor to decrease the risk of dementia. *Transl Psychiatry* (2017) 7:e1117. doi: 10.1038/tp.2017.90
11. Elias MF, Beiser A, Wolf PA, Au R, White RF, D'agostino RB. The preclinical phase of alzheimer disease: A 22-year prospective study of the Framingham Cohort. *Arch Neurol* (2000) 57:808–13. doi: 10.1001/archneur.57.6.808
12. Albanese E, Launer LJ, Egger M, Prince MJ, Giannakopoulos P, Wolters FJ, et al. Body mass index in midlife and dementia: Systematic review and meta-regression analysis of 589,649 men and women followed in longitudinal studies. *Alzheimers Dement (Amst)* (2017) 8:165–78. doi: 10.1016/j.dadm.2017.05.007
13. Li G, Larson EB, Shofer JB, Crane PK, Gibbons LE, Mccormick W, et al. Cognitive Trajectory Changes Over 20 Years Before Dementia Diagnosis: A Large Cohort Study. *J Am Geriatr Soc* (2017) 65:2627–33. doi: 10.1111/jgs.15077
14. Strittmatter WJ, Saunders AM, Schmechel D, Pericak-Vance M, Enghild J, Salvesen GS, et al. Apolipoprotein E: high-avidity binding to beta-amyloid and increased frequency of type 4 allele in late-onset familial Alzheimer disease. *Proc Natl Acad Sci U S A* (1993) 90:1977–81. doi: 10.1073/pnas.90.5.1977
15. Corneveaux JJ, Myers AJ, Allen AN, Pruzin JJ, Ramirez M, Engel A, et al. Association of CR1, CLU and PICALM with Alzheimer's disease in a cohort of clinically characterized and neuropathologically verified individuals. *Hum Mol Genet* (2010) 19:3295–301. doi: 10.1093/hmg/ddq221
16. Stocker H, Mollers T, Perna L, Brenner H. The genetic risk of Alzheimer's disease beyond APOE epsilon4: systematic review of Alzheimer's genetic risk scores. *Transl Psychiatry* (2018) 8:166. doi: 10.1038/s41398-018-0221-8
17. Lin SK, Kao JT, Tsai SM, Tsai LY, Lin MN, Lai CJ, et al. Association of apolipoprotein E genotypes with serum lipid profiles in a healthy population of Taiwan. *Ann Clin Lab Sci* (2004) 34:443–8.
18. Alvim RO, Freitas SR, Ferreira NE, Santos PC, Cunha RS, Mill JG, et al. APOE polymorphism is associated with lipid profile, but not with arterial stiffness in the general population. *Lipids Health Dis* (2010) 9:128. doi: 10.1186/1476-511X-9-128
19. El-Lebedy D, Raslan HM, Mohammed AM. Apolipoprotein E gene polymorphism and risk of type 2 diabetes and cardiovascular disease. *Cardiovasc Diabetol* (2016) 15:12. doi: 10.1186/s12933-016-0329-1
20. Kritharides L, Nordestgaard BG, Tybjaerg-Hansen A, Kamstrup PR, Afzal S. Effect of APOE epsilon Genotype on Lipoprotein(a) and the Associated Risk of Myocardial Infarction and Aortic Valve Stenosis. *J Clin Endocrinol Metab* (2017) 102:3390–9. doi: 10.1210/jc.2017-01049
21. Shatwan IM, Winther KH, Ellahi B, Elwood P, Ben-Shlomo Y, Givens I, et al. Association of apolipoprotein E gene polymorphisms with blood lipids and their interaction with dietary factors. *Lipids Health Dis* (2018) 17:98. doi: 10.1186/s12944-018-0744-2
22. Kallio MJ, Salmenpera L, Siimes MA, Perheentupa J, Gylling H, Miettinen TA. Apoprotein E phenotype determines serum cholesterol in infants during both high-cholesterol breast feeding and low-cholesterol formula feeding. *J Lipid Res* (1997) 38:759–64.
23. Taylor AE, Guthrie PA, Smith GD, Golding J, Sattar N, Hingorani AD, et al. IQ, educational attainment, memory and plasma lipids: associations with apolipoprotein E genotype in 5995 children. *Biol Psychiatry* (2011) 70:152–8. doi: 10.1016/j.biopsych.2010.10.033
24. O'donoghue MC, Murphy SE, Zamboni G, Nobre AC, Mackay CE. APOE genotype and cognition in healthy individuals at risk of Alzheimer's disease: A review. *Cortex* (2018) 104:103–23. doi: 10.1016/j.cortex.2018.03.025
25. Shaw P, Lerch JP, Pruessner JC, Taylor KN, Rose AB, Greenstein D, et al. Cortical morphology in children and adolescents with different apolipoprotein E gene polymorphisms: an observational study. *Lancet Neurol* (2007) 6:494–500. doi: 10.1016/S1474-4422(07)70106-0
26. Filippini N, Macintosh BJ, Hough MG, Goodwin GM, Frisoni GB, Smith SM, et al. Distinct patterns of brain activity in young carriers of the APOE-ε4 allele *Distinct patterns Brain act In young carriers APOE-epsilon allele4. Proc Natl Acad Sci U S A* (2009) 106:7209–14. doi: 10.1073/pnas.0811879106
27. O'dwyer L, Lamberton F, Matura S, Tanner C, Scheibe M, Miller J, et al. Reduced hippocampal volume in healthy young ApoE4 carriers: an MRI study. *PloS One* (2012) 7:e48895. doi: 10.1371/journal.pone.0048895
28. Dean DC3rd, Jerskey BA, Chen K, Protas H, Thiyyagura P, Roontiva A, et al. Brain differences in infants at differential genetic risk for late-onset Alzheimer disease: a cross-sectional imaging study. *JAMA Neurol* (2014) 71:11–22. doi: 10.1001/jamaneurol.2013.4544
29. Knickmeyer RC, Wang J, Zhu H, Geng X, Woolson S, Hamer RM, et al. Common variants in psychiatric risk genes predict brain structure at birth. *Cereb Cortex* (2014) 24:1230–46. doi: 10.1093/cercor/bhs401
30. Chang L, Douet V, Bloss C, Lee K, Pritchett A, Jernigan TL, et al. Gray matter maturation and cognition in children with different APOE epsilon genotypes. *Neurology* (2016) 87:585–94. doi: 10.1212/WNL.0000000000002939
31. Khera AV, Chaffin M, Aragam KG, Haas ME, Roselli C, Choi SH, et al. Genome-wide polygenic scores for common diseases identify individuals with

risk equivalent to monogenic mutations. *Nat Genet* (2018) 50:1219–24. doi: 10.1038/s41588-018-0183-z
32. Kooijman MN, Kruithof CJ, Van Duijn CM, Duijts L, Franco OH, Van IMH, et al. The Generation R Study: design and cohort update 2017. *Eur J Epidemiol* (2016) 31:1243–64. doi: 10.1007/s10654-016-0224-9
33. Jaddoe VW, Bakker R, Van Duijn CM, Van Der Heijden AJ, Lindemans J, Mackenbach JP, et al. The Generation R Study Biobank: a resource for epidemiological studies in children and their parents. *Eur J Epidemiol* (2007) 22:917–23. doi: 10.1007/s10654-007-9209-z
34. Medina-Gomez C, Felix JF, Estrada K, Peters MJ, Herrera L, Kruithof CJ, et al. Challenges in conducting genome-wide association studies in highly admixed multi-ethnic populations: the Generation R Study. *Eur J Epidemiol* (2015) 30:317–30. doi: 10.1007/s10654-015-9998-4
35. Purcell S, Neale B, Todd-Brown K, Thomas L, Ferreira MA, Bender D, et al. PLINK: a tool set for whole-genome association and population-based linkage analyses. *Am J Hum Genet* (2007) 81:559–75. doi: 10.1086/519795
36. Euesden J, Lewis CM, O'reilly PF. PRSice: Polygenic Risk Score software. *Bioinformatics* (2015) 31:1466–8. doi: 10.1093/bioinformatics/btu848
37. Lambert JC, Ibrahim-Verbaas CA, Harold D, Naj AC, Sims R, Bellenguez C, et al. Meta-analysis of 74,046 individuals identifies 11 new susceptibility loci for Alzheimer's disease. *Nat Genet* (2013) 45:1452–8. doi: 10.1038/ng.2802
38. Tellegen PJ, Winkel M, Wijnberg-Williams B, Laros JA. *SON-R 2,5-7: Snijder-Oomen niet-verbale intelligentietest*. Amsterdam: Hogrefe Uitgevers (2005).
39. Langeslag SJ, Schmidt M, Ghassabian A, Jaddoe VW, Hofman A, Van Der Lugt A, et al. Functional connectivity between parietal and frontal brain regions and intelligence in young children: the Generation R study. *Hum Brain Mapp* (2013) 34:3299–307. doi: 10.1002/hbm.22143
40. Achenbach TM, Rescorla LA. *Manual for the ASEBA preschool forms and profiles*. Burlington, VT: University of Vermont, Research center for children, youth (2000).
41. White T, Muetzel RL, El Marroun H, Blanken LME, Jansen P, Bolhuis K, et al. Paediatric population neuroimaging and the Generation R Study: the second wave. *Eur J Epidemiol* (2018) 33:99–125. doi: 10.1007/s10654-017-0319-y
42. Fischl B. FreeSurfer. *Neuroimage* (2012) 62:774–81. doi: 10.1016/j.neuroimage.2012.01.021
43. Muetzel RL, Blanken LME, Van Der Ende J, El Marroun H, Shaw P, Sudre G, et al. Tracking Brain Development and Dimensional Psychiatric Symptoms in Children: A Longitudinal Population-Based Neuroimaging Study. *Am J Psychiatry* (2018) 175:54–62. doi: 10.1176/appi.ajp.2017.16070813
44. Jenkinson M, Beckmann CF, Behrens TE, Woolrich MW, Smith SM. Fsl. *Neuroimage* (2012) 62:782–90. doi: 10.1016/j.neuroimage.2011.09.015
45. Chang LC, Jones DK, Pierpaoli C. RESTORE: robust estimation of tensors by outlier rejection. *Magn Reson Med* (2005) 53:1088–95. doi: 10.1002/mrm.20426
46. De Groot M, Vernooij MW, Klein S, Ikram MA, Vos FM, Smith SM, et al. Improving alignment in Tract-based spatial statistics: evaluation and optimization of image registration. *Neuroimage* (2013) 76:400–11. doi: 10.1016/j.neuroimage.2013.03.015
47. Muetzel RL, Mous SE, Van Der Ende J, Blanken LM, Van Der Lugt A, Jaddoe VW, et al. White matter integrity and cognitive performance in school-age children: A population-based neuroimaging study. *Neuroimage* (2015) 119:119–28. doi: 10.1016/j.neuroimage.2015.06.014
48. Friedewald WT, Levy RI, Fredrickson DS. Estimation of the concentration of low-density lipoprotein cholesterol in plasma, without use of the preparative ultracentrifuge. *Clin Chem* (1972) 18:499–502.
49. Huang Y, Mahley RW. Apolipoprotein E: structure and function in lipid metabolism, neurobiology, and Alzheimer's diseases. *Neurobiol Dis* (2014) 72:3–12. doi: 10.1016/j.nbd.2014.08.025
50. Core Team R. *R: A language and environment for statistical computing*. Vienna, Austria: R Foundation for Statistical Computing (2016).
51. Hellwege JN, Keaton JM, Giri A, Gao X, Velez Edwards DR, Edwards TL. Population Stratification in Genetic Association Studies. *Curr Protoc Hum Genet* (2017) 18;95:1.22.1–1.22.23. doi: 10.1002/cphg.48
52. Quiroz YT, Schultz AP, Chen K, Protas HD, Brickhouse M, Fleisher AS, et al. Brain Imaging and Blood Biomarker Abnormalities in Children With Autosomal Dominant Alzheimer Disease: A Cross-Sectional Study. *JAMA Neurol* (2015) 72:912–9. doi: 10.1001/jamaneurol.2015.1099
53. Axelrud LK, Santoro ML, Pine DS, Talarico F, Gadelha A, Manfro GG, et al. Polygenic Risk Score for Alzheimer's Disease: Implications for Memory Performance and Hippocampal Volumes in Early Life. *Am J Psychiatry* (2018) 175:555–63. doi: 10.1176/appi.ajp.2017.17050529
54. Alexopoulos P, Richter-Schmidinger T, Horn M, Maus S, Reichel M, Sidiropoulos C, et al. Hippocampal volume differences between healthy young apolipoprotein E epsilon2 and epsilon4 carriers. *J Alzheimers Dis* (2011) 26:207–10. doi: 10.3233/JAD-2011-110356
55. Heise V, Filippini N, Ebmeier KP, Mackay CE. The APOE varepsilon4 allele modulates brain white matter integrity in healthy adults. *Mol Psychiatry* (2011) 16:908–16. doi: 10.1038/mp.2010.90
56. Alexander GE, Bergfield KL, Chen K, Reiman EM, Hanson KD, Lin L, et al. Gray matter network associated with risk for Alzheimer's disease in young to middle-aged adults. *Neurobiol Aging* (2012) 33:2723–32. doi: 10.1016/j.neurobiolaging.2012.01.014
57. Dibattista AM, Stevens BW, Rebeck GW, Green AE. Two Alzheimer's disease risk genes increase entorhinal cortex volume in young adults. *Front Hum Neurosci* (2014) 8:779. doi: 10.3389/fnhum.2014.00779
58. Konishi K, Bhat V, Banner H, Poirier J, Joober R, Bohbot VD. APOE2 Is Associated with Spatial Navigational Strategies and Increased Gray Matter in the Hippocampus. *Front Hum Neurosci* (2016) 10:349. doi: 10.3389/fnhum.2016.00349
59. Mormino EC, Sperling RA, Holmes AJ, Buckner RL, De Jager PL, Smoller JW, et al. Polygenic risk of Alzheimer disease is associated with early- and late-life processes. *Neurology* (2016) 87:481–8. doi: 10.1212/WNL.0000000000002922
60. Foley SF, Tansey KE, Caseras X, Lancaster T, Bracht T, Parker G, et al. Multimodal Brain Imaging Reveals Structural Differences in Alzheimer's Disease Polygenic Risk Carriers: A Study in Healthy Young Adults. *Biol Psychiatry* (2017) 81:154–61. doi: 10.1016/j.biopsych.2016.02.033
61. Nao J, Sun H, Wang Q, Ma S, Zhang S, Dong X, et al. Adverse Effects of the Apolipoprotein E epsilon4 Allele on Episodic Memory, Task Switching and Gray Matter Volume in Healthy Young Adults. *Front Hum Neurosci* (2017) 11:346. doi: 10.3389/fnhum.2017.00346
62. Hanson AJ, Bayer-Carter JL, Green PS, Montine TJ, Wilkinson CW, Baker LD, et al. Effect of apolipoprotein E genotype and diet on apolipoprotein E lipidation and amyloid peptides: randomized clinical trial. *JAMA Neurol* (2013) 70:972–80. doi: 10.1001/jamaneurol.2013.396
63. Heinsinger NM, Gachechiladze MA, Rebeck GW. Apolipoprotein E Genotype Affects Size of ApoE Complexes in Cerebrospinal Fluid. *J Neuropathol Exp Neurol* (2016) 75:918–24. doi: 10.1093/jnen/nlw067
64. Ignatius MJ, Gebicke-Harter PJ, Skene JH, Schilling JW, Weisgraber KH, Mahley RW, et al. Expression of apolipoprotein E during nerve degeneration and regeneration. *Proc Natl Acad Sci U S A* (1986) 83:1125–9. doi: 10.1073/pnas.83.4.1125
65. Arendt T, Schindler C, Bruckner MK, Eschrich K, Bigl V, Zedlick D, et al. Plastic neuronal remodeling is impaired in patients with Alzheimer's disease carrying apolipoprotein epsilon 4 allele. *J Neurosci* (1997) 17:516–29. doi: 10.1523/JNEUROSCI.17-02-00516.1997
66. Tzioras M, Davies C, Newman A, Jackson R, Spires-Jones T. Invited Review: APOE at the interface of inflammation, neurodegeneration and pathological protein spread in Alzheimer's disease. *Neuropathol Appl Neurobiol* (2019) 45:327–46. doi: 10.1111/nan.12529
67. Weissberger GH, Nation DA, Nguyen CP, Bondi MW, Han SD. Meta-analysis of cognitive ability differences by apolipoprotein e genotype in young humans. *Neurosci Biobehav Rev* (2018) 94:49–58. doi: 10.1016/j.neubiorev.2018.08.009
68. Thaler A, Mirelman A, Gurevich T, Simon E, Orr-Urtreger A, Marder K, et al. Lower cognitive performance in healthy G2019S LRRK2 mutation carriers. *Neurology* (2012) 79:1027–32. doi: 10.1212/WNL.0b013e3182684646
69. Mirelman A, Gurevich T, Giladi N, Bar-Shira A, Orr-Urtreger A, Hausdorff JM. Gait alterations in healthy carriers of the LRRK2 G2019S mutation. *Ann Neurol* (2011) 69:193–7. doi: 10.1002/ana.22165
70. Saunders-Pullman R, Stanley K, Wang C, San Luciano M, Shanker V, Hunt A, et al. Olfactory dysfunction in LRRK2 G2019S mutation carriers. *Neurology* (2011) 77:319–24. doi: 10.1212/WNL.0b013e318227041c
71. Tapiola T, Lehtovirta M, Ramberg J, Helisalmi S, Linnaranta K, Riekkinen PSr., et al. CSF tau is related to apolipoprotein E genotype in early Alzheimer's disease. *Neurology* (1998) 50:169–74. doi: 10.1212/WNL.50.1.169
72. Koch G, Di Lorenzo F, Loizzo S, Motta C, Travaglione S, Baiula M, et al. CSF tau is associated with impaired cortical plasticity, cognitive decline and

astrocyte survival only in APOE4-positive Alzheimer's disease. *Sci Rep* (2017) 7:13728. doi: 10.1038/s41598-017-14204-3
73. Van Harten AC, Jongbloed W, Teunissen CE, Scheltens P, Veerhuis R, Van Der Flier WM. CSF ApoE predicts clinical progression in nondemented APOEepsilon4 carriers. *Neurobiol Aging* (2017) 57:186–94. doi: 10.1016/j.neurobiolaging.2017.04.002
74. Hohman TJ, Dumitrescu L, Barnes LL, Thambisetty M, Beecham G, Kunkle B, et al. Sex-Specific Association of Apolipoprotein E With Cerebrospinal Fluid Levels of Tau. *JAMA Neurol* (2018) 75:989–98. doi: 10.1001/jamaneurol.2018.0821
75. Cruchaga C, Kauwe JS, Nowotny P, Bales K, Pickering EH, Mayo K, et al. Cerebrospinal fluid APOE levels: an endophenotype for genetic studies for Alzheimer's disease. *Hum Mol Genet* (2012) 21:4558–71. doi: 10.1093/hmg/dds296
76. Darweesh SKL, Wolters FJ, Ikram MA, De Wolf F, Bos D, Hofman A. Inflammatory markers and the risk of dementia and Alzheimer's disease: A meta-analysis. *Alzheimers Dement* (2018) 14:1450–9. doi: 10.1016/j.jalz.2018.02.014
77. Shaw P, Kabani NJ, Lerch JP, Eckstrand K, Lenroot R, Gogtay N, et al. Neurodevelopmental trajectories of the human cerebral cortex. *J Neurosci* (2008) 28:3586–94. doi: 10.1523/JNEUROSCI.5309-07.2008

Conflict of Interest: The authors declare that the research was conducted in the absence of any commercial or financial relationships that could be construed as a potential conflict of interest.

frontiers in Aging Neuroscience

ORIGINAL RESEARCH
published: 19 February 2020
doi: 10.3389/fnagi.2020.00028

Feature Selection and Combination of Information in the Functional Brain Connectome for Discrimination of Mild Cognitive Impairment and Analyses of Altered Brain Patterns

Xiaowen Xu[1], Weikai Li[2], Jian Mei[3], Mengling Tao[1], Xiangbin Wang[1], Qianhua Zhao[4,5], Xiaoniu Liang[4,5], Wanqing Wu[4,5], Ding Ding[4,5] and Peijun Wang[1]**

[1] Department of Medical Imaging, Tongji Hospital, Tongji University School of Medicine, Shanghai, China, [2] College of Computer Science and Technology, Nanjing University of Aeronautics and Astronautics, Nanjing, China, [3] Physical Education College, Soochow University, Suzhou, China, [4] Institute of Neurology, Huashan Hospital, Fudan University, Shanghai, China, [5] National Clinical Research Center for Aging and Medicine, Huashan Hospital, Fudan University, Shanghai, China

Mild cognitive impairment (MCI) is often considered a critical time window for predicting early conversion to Alzheimer's disease (AD). Brain functional connectome data (i.e., functional connections, global and nodal graph metrics) based on resting-state functional magnetic resonance imaging (rs-fMRI) provides numerous information about brain networks and has been used to discriminate normal controls (NCs) from subjects with MCI. In this paper, Student's *t*-tests and group-least absolute shrinkage and selection operator (group-LASSO) were used to extract functional connections with significant differences and the most discriminative network nodes, respectively. Based on group-LASSO, the middle temporal, inferior temporal, lingual, posterior cingulate, and middle frontal gyri were the most predominant brain regions for nodal observation in MCI patients. Nodal graph metrics (within-module degree, participation coefficient, and degree centrality) showed the maximum discriminative ability. To effectively combine the multipattern information, we employed the multiple kernel learning support vector machine (MKL-SVM). Combined with functional connectome information, the MKL-SVM achieved a good classification performance (area under the receiving operating characteristic curve = 0.9728). Additionally, the altered brain connectome pattern revealed that functional connectivity was generally decreased in the whole-brain network, whereas graph theory topological attributes of some special nodes in the brain network were increased in MCI patients. Our findings demonstrate that optimal feature selection and combination of all connectome features (i.e., functional connections, global and nodal graph metrics) can achieve good performance in discriminating NCs from MCI subjects. Thus, the combination of functional connections and global and nodal graph metrics of brain networks can predict the occurrence of MCI and contribute to the early clinical diagnosis of AD.

Keywords: resting-state functional magnetic resonance imaging, functional connectivity, graph theory, multiple kernel learning, mild cognitive impairment

OPEN ACCESS

Edited by:
Mohamad Habes, University of Pennsylvania, United States

Reviewed by:
Han Zhang, The University of North Carolina at Chapel Hill, United States
Sandhitsu Das, University of Pennsylvania, United States

****Correspondence:***
Ding Ding
dingding@huashan.org.cn
Peijun Wang
tongjipjwang@vip.sina.com

Received: *31 May 2019*
Accepted: *28 January 2020*
Published: *19 February 2020*

Citation:
Xu X, Li W, Mei J, Tao M, Wang X, Zhao Q, Liang X, Wu W, Ding D and Wang P (2020) Feature Selection and Combination of Information in the Functional Brain Connectome for Discrimination of Mild Cognitive Impairment and Analyses of Altered Brain Patterns. Front. Aging Neurosci. 12:28. doi: 10.3389/fnagi.2020.00028

INTRODUCTION

Alzheimer's disease (AD) is a progressive neurodegenerative disorder characterized by loss of memory and cognitive decline (Blennow et al., 2006). With the aging of the global population, there will be an estimated 115 million AD patients in the world by 2050, with an average of 1 new AD patient every 33 s (Ijaopo, 2017). Mild cognitive impairment (MCI) is an intermediate stage that precedes early AD. Evidence indicates that about 15% of MCI patients progress to AD per year (Petersen et al., 1999; Grundman et al., 2004). Therefore, MCI is regarded as the critical time window for early prediction of conversion to AD (Manly et al., 2008).

Components of the brain functional connectome, including functional connections and graph theory topological metrics, have become important imaging markers for exploring brain networks and predicting the classification of neurodegenerative diseases (Biswal et al., 2010; Wang et al., 2013; Filippi et al., 2018). The functional connectome systematically depicts global graph metrics (i.e., small world, modularity, global efficiency), nodal graph metrics (i.e., degree, participant coefficient, shortest path length), and functional connections of the network. It provides a novel approach for revealing altered brain network patterns (delEtoile and Adeli, 2017; Khazaee et al., 2017; Filippi et al., 2018). Given the large numbers of network features in the brain connectome, the Student's *t*-test (Qiao et al., 2016; Li W. et al., 2019) and sparse methods such as least absolute shrinkage and selection operator (LASSO) have been applied to select the critical features of brain networks (Wee et al., 2014; Li Y. et al., 2019). Nodal graph metrics naturally have a group topology (i.e., a node corresponds to a group of node-graph theoretical attributes). Group-LASSO is a regression-analysis method for group-feature selection and regularization that can be adopted to select nodal graph metrics (Liu et al., 2019) and maintain significant discrimination of nodal features.

In recent years, machine learning approaches with data-driven algorithms have been used to combine and classify brain features. Some classifiers such as support vector machines (SVMs) (Prasad et al., 2015; Khazaee et al., 2016), Naïve Bayes (Zhuo et al., 2018) and deep neural networks (Themistocleous et al., 2018) are applied to discriminate normal controls from subjects with MCI. However, most of these methods focus on a single modality of imaging, the functional connectome, or graph theory attributes separately, resulting in relatively poor classification performance (Suk et al., 2014). Therefore, the multimodal brain network (i.e., functional connections and graph theory topological metrics) should be used to provide a comprehensive and insightful understanding of the brain network in patients with MCI. Combined with information from different attributes, multiple kernel learning SVM (MKL-SVM) (Niu et al., 2017) can partially alleviate the high-dimensional curve of multiple features and measure the contributions of different features to the classification. These proposed methods could help select critical features and discriminate normal controls from subjects with diseases.

The main purposes of the present study were to select discriminative features of the brain connectome (i.e., functional connections, global graph metrics, and nodal graph metrics) and develop a classification of MCI based on different attributes of the brain network. Altered patterns of discriminative features were further analyzed using the proposed methods. By combining the group-LASSO model and MKL-SVM, we (i) identified the most discriminative nodal features of the brain connectome and predominant brain regions in MCI patients, (ii) achieved accurate and automatic classification of MCI patients and normal controls (NCs), and (iii) analyzed the changed patterns in the brain network.

MATERIALS AND METHODS

Participants

Participants with MCI and NCs were recruited to establish a registry at Huashan Hospital. Each participant underwent a comprehensive evaluation, including clinical interview, neuropsychological assessment, laboratory tests, and multimodal magnetic resonance imaging (MRI) examinations of the brain. MCI was defined according to the following criteria (Petersen, 2004): (i) cognitive concern/complaint by the subject, nurse, or physician, with a Clinical Dementia Rating (CDR) = 0.5; (ii) objective impairment in $\geq$1 cognitive domain based on 1.5 standard deviations (SDs) below the mean using the norms obtained in the pilot study; (iii) basic normal functional activities (determined by CDR and daily living activity assessment); (iv) absence of dementia according to the Diagnostic and Statistical Manual of Mental Disorders, 4th edition (Rabe-Jablonska and Bienkiewicz, 1994). The inclusion criteria of NCs were: (i) no neurology-related or cerebral vascular diseases (e.g., Parkinson's disease, intracranial aneurysms, or cerebral tumors); (ii) no severe mental retardation or schizophrenia; (iii) no severe problems in speaking, vision, or hearing; (iv) able to actively participate in the neuropsychological assessment. In the present study, 105 participants (41 MCI patients and 64 NCs) were selected. Two patients with MCI and four NCs were excluded due to incomplete data in resting state-functional MRI (rs-fMRI) and severe head motion at some time points. Finally, data from 99 individuals (39 MCI patients and 60 NCs) were included in the subsequent statistical analyses. The clinical and demographic data of these 99 participants were summarized. The study protocol was approved by the Ethics Committee of Huashan Hospital of Fudan University (Shanghai, China). Written informed consent was obtained from each participant (or his/her legal representative). In addition, we adopted the Alzheimer's Disease Neuroimaging Initiative (ADNI)[1] dataset as an independent test dataset to verify the performance of the pre-trained model.

Data Acquisition

Rs-fMRI and structural MR images were acquired on a 3T MR scanner (Magnetom® Verio; Siemens, Munich, Germany) using a 32-channel head coil. Before imaging, all participants were

[1]http://adni.loni.usc.edu/

instructed to keep their eyes closed (but not to fall asleep), think of nothing, and move as little as possible during data acquisition. Three-dimensional (3D) T1-weighted sagittal images were acquired using magnetization-prepared rapid gradient echo with the following parameters: repetition time (TR) = 2530 ms, echo time (TE) = 2.34 ms, flip angle = 7°, inversion time (TI) = 1100 ms, matrix = 256 × 256, slice number = 192, thickness = 1.0 mm, and voxel size = 1 × 1 × 1 mm^3. The scan lasted 6 min 03 s. The parameters of the rs-fMRI protocol were as follows: axial acquisition, TR = 2000 ms, TE = 30 ms, flip angle = 90°, slice thickness = 3.8 mm, slice number = 31, field of view = 220 × 220 mm^2, matrix size = 64 × 64, and voxel size = 3.4 × 3.4 × 3.8 mm^3. Each scan collected 240 volumes with a scan time of 8 min 06 s. The ADNI dataset was acquired on the 3T Philips with the following scan parameters: TR = 3000 ms, TE = 30 mm, flip angle = 80°, slice thickness = 3.3 mm, slice number = 48, matrix size = 64 × 64, and measurements = 140.

Image Preprocessing

Preprocessing procedures were carried out using Data Processing Assistant for Resting-State fMRI (DPARSF)[2] and Statistical Parametric Mapping (SPM12)[3]. The first 10 time points were not used to ensure stabilization of the initial signal and adaptation of participants to the environment. Timing correction to the last slice was conducted. Realignment for compensation of head-movement effects was achieved using a six-parameter rigid-body spatial transformation. All spatial movement was <3 mm of displacement and <3° of rotation in any direction, and no participant was excluded. Next, rs-fMRI images were co-registered to the high-resolution 3D-T1 structural images. Normalization of 3D-T1 structural MRI images to Montreal Neurological Institute (MNI) space was undertaken by non-linear warping based on Diffeomorphic Anatomical Registration Through Exponentiated Lie Algebra (DARTEL). Then, rs-fMRI images were spatially normalized to the MNI space using the parameters derived from the normalization of structural images and simultaneously resampled into 3-mm isotropic voxels. All normalized fMRI images were smoothed with a 6-mm, full-width at half-maximum Gaussian kernel. Linear detrending and band-pass filtering at 0.01–0.1 Hz were carried out to control low-frequency drift and high-frequency physiological noise. Finally, nuisance covariates were regressed out, including the Friston 24-motion parameter model (six head-motion parameters, six head-motion parameters one time point before, and the 12 corresponding squared items), global mean, white matter, and cerebrospinal fluid signals.

Brain Network Construction

The average time series within each region based on the 264 putative functional area atlas were separately extracted to construct the connectivity brain network (Power et al., 2011). The Pearson's correlation coefficients of all pairs of 264 regions of interest (ROIs) were applied separately to define the edges of functional connections. Thus, the functional connectivity matrix (adjacency matrix) was constructed (Li et al., 2017). The final functional connection networks produced N*(N-1)/2 edges, where N corresponded to the number of nodes in the networks. Considering the ambiguous interpretation of negative correlations, we restricted the analysis to positive correlations and set the negative correlation coefficients as zero. A thresholding method based on network sparsity was adopted to remove the less significant connections and to retain the topological properties of graph theory by setting an appropriate threshold for network sparsity (Dai et al., 2019). Sparsity thresholds (ranging from 0.02 to 0.5, with steps of 0.01) were set to acquire a binary undirected network (Chang et al., 2016). To avoid ambiguity, we used the area under the curve (AUC; i.e., the sum value of 49 values of the corresponding node attributes) as input for the node attribute to train the classifier.

Computation of Graph Metrics

Based on binary undirected matrices, we systematically analyzed the global and local properties of the functional brain network with the Graph Theoretical Network Analysis Toolbox (GRETNA)[4] based on Statistical Parametric Mapping (SPM8; see text footnote 3) with MATLAB R2013b. Global metrics [i.e., clustering coefficient (C_p), characteristic path length (L_p), normalized clustering coefficient (γ), normalized characteristic path length (λ), small-world σ, global efficiency (E_{global})], and nodal properties (i.e., degree centrality, nodal efficiency, betweenness centrality, shortest path length) were applied to characterize the different patterns of connections in the brain network (**Table 1**; Wang et al., 2015). The modularity (Q) of a brain network quantified the efficiency of segmenting a network into modules (Newman, 2006). A modified greedy optimization algorithm was used as follows:

$$Q = \sum_{i=1}^{N_m} [l_i/L - (d_i/2L)^2]$$

where N_m represents the number of modules, L is the total number of edges in the brain network, and l_i is the number of within-module edges in module i; d_i represents the sum of the linked edges at each node within module i. Modified greedy optimization was applied to detect the modular structure (Newman, 2004).

[2]http://restfmri.net/forum/index.php

[3]http://www.fil.ion.ucl.ac.uk/spm

[4]www.nitrc.org/projects/gretna/

TABLE 1 | Global and local graph metrics of the brain connectome.

Global graph metrics	Local graph metrics
Clustering coefficient C_p	Betweenness centrality
Characteristic path length L_p	Degree centrality
Normalized clustering coefficient γ	Nodal clustering coefficient
Normalized characteristic path length λ	Local efficiency
Small-world σ	Shortest path length
Network efficiency	Participant coefficient
Modularity	Within-module degree

At the module level, the intra-module connectivity density (D_s) and intermodule connectivity density ($D_{s,t}$) were calculated as follows:

$$D_s = \frac{2\sum_{i,j\in s}\varepsilon_{i,j}}{N_s(N_S-1)}$$

where N_S is the number of nodes within module s, and $\varepsilon_{i,j}$ are the edges within module *s*.

$$D_{s,t} = \frac{\sum_{i\in s,j\in t}\varepsilon_{i,j}}{N_s * N_t}$$

where N_s is the number of nodes within module *s*, N_t represent the number of nodes within module *t*, and ε_{ij} is the number of edges between module *s* and module *t*.

Moreover, at the nodal level, within-module degree (WD) and the participation coefficient (PC) were measured as follows:

$$WD_i = \frac{e_i - \bar{e}_s}{\sigma_s}$$

where e_i is the nodal degree of node *i* within module s, $\bar{e}_s$ is the average nodal degree of all nodes in module s, and σ_s is the standard deviation of the nodal degree within the module of all nodes in module s.

$$PC_i = 1 - \sum_{s=1}^{N_m}\left(\frac{k_{i,s}}{k_i}\right)^2$$

where N_m is the number of modules and $k_{i,s}$ is the number of connections between node *i* and module *s*. k_i represents the number of connections of node *i* to all other nodes within the N_m modules.

Nodes with a degree of 2 standard deviations higher than the mean of the degree of all nodes were identified as hub nodes (Rubinov and Sporns, 2010). Small-world attributes were applied to characterize an optimized balance between functional segregation and integration of the network.

Statistical Analyses

For demographics and clinical characteristics, two-sample Student's *t*-tests were carried out except for sex, which was tested by the chi-square test. $P < 0.05$ indicated a significant difference in the demographic data. First, functional connections and global and local metrics were regressed to remove potential effects of the covariates age, sex, and education duration. Then, differences pertaining to graph theory metrics between MCI patients and NCs were compared based on two-sample Student's *t*-tests. A procedure to ascertain the false discovery rate was performed to further correct for multiple comparisons. To localize the specific pairs of regions in which functional connections were altered in MCI patients, we used a network-based statistic (NBS) approach (Zalesky et al., 2010). A corrected *P*-value was calculated for each component using the null distribution of the maximal connected component size, which was empirically derived using a non-parametric permutation approach (10,000 permutations) (Zuo et al., 2012). $P < 0.01$ indicated a significant difference.

Feature Selection for Nodal Graph Metrics

As mentioned above, the brain was divided into 264 nodes based on the 264 putative functional area atlas (Power et al., 2011), and each node corresponded to seven local graph metrics (i.e., betweenness centrality, degree centrality, nodal clustering coefficient, local efficiency, shortest path length, participant coefficient, within-module degree). Thus, the nodal graph metrics naturally have a group topology, that is, a node corresponds to a group of node-graph theoretical attributes. Given the natural group attributes, we used group-LASSO as the feature-selection scheme for nodal graph metrics.

$$min_W \sum_{i=1}^{nSub} log\left(1 + exp\left(-y_i \times \left(\sum_{j=1}^{nROI}\sum_{k=1}^{7} w_{(j,k)}x_{(j,k)} + c\right)\right)\right) + \lambda\sum_{j=1}^{nROI}\|w_{jk}\|_q,$$

where y_i is the label of the *i*-th participant, and $w_{(j,k)}$ and $x_{(j,k)}$ are the weight and value of the *j*-th ROI and *k*-th Nodal Graphic Metric, respectively. Note that $x_{(j,k)}$ is normalized by Fisher Z-transformation to avoid scale imbalance. We used the SLEP toolbox[5] to calculate $w_{(j,k)}$ with a default setting of $\lambda = 1$.

Classification

Combination of information provides an effective way to integrate multiple views of biomarkers (i.e., connections and graph metrics). The simplest way is to overlay the data directly, but this approach can be inappropriate due to the high-dimensional curve and small number of samples. Moreover, a modality with more dimensions can submerge a modality with fewer dimensions. To overcome this challenge, we used MKL-SVM for information combination because the kernel trick can partially alleviate the high-dimensional curve. MKL-SVM was conducted as shown below.

Suppose that there are n training samples with connection values and graph metrics. For x_i^m, m = 1,2,3, which correspond to the connection value, the nodal graph metrics and global graph metrics respectively. y represent the correcponding class label of the *i*-th sample. MKL-SVM solves the following primal problem:

$$\min_w \frac{1}{2}\sum_{m=1}^{2}\beta_m\|w^m\|^2 + C\sum_{i=1}^{2}\xi_i$$

$$\text{s.t. } y_i\left(\sum_{m=1}^{2}\beta_m(w^m)^T\phi^m(x_i^m) + b\right) \geq 1 - \xi_i$$

$$\xi_i \geq 0, \quad i = 1, 2$$

where ϕ^m represents a mapping from the original space to the Represent Hilbert Kernel Space (RHKS), w^m represents the normal vector of the hyperplane in RHKS, and β_m denotes the

[5]www.yelab.net/software/SLEP

corresponding combining weight on the m-th modality. Then, the dual form of MKL-SVM can be represented as:

$$\max_{\alpha} \sum_{i=1}^{n} \alpha_i - \frac{1}{2} \sum_{i,j} \alpha_i \alpha_j y_i y_j \sum_{m=1}^{2} \beta_m k^m(x_i^m, y_i^m)$$

$$\text{s.t.} \sum_{i=1}^{n} \alpha_i y_i = 0$$

$$0 \leq \alpha_i \leq C, i = 1, 2$$

where $k^m(x_i^m, y_i^m) = \phi^m(x_i^m)^T \phi^m(x_j^m)$ and is the kernel matrix on the m-th modality. After we trained the model, we tested the new samples $x = \{x_1, x_2, \ldots, x_M\}$. The kernel between the new test sample and the i-th training sample on the m-th modality is defined as $k^m(x_i^m, x^m) = \phi^m(x_i^m)^T \phi^m(x^m)$. In the end, the predictive level based on MKL-SVM can be formulated as follows:

$$f(x_1, x_2, \ldots, x_M) = \text{sign}\left(\sum_{i=1}^{n} y_i \alpha_i \sum_{m=1}^{M} \beta_m k^m(x_i^m, x^m) + b \right)$$

The proposed formulation of MKL-SVM is similar to but different from existing multi-kernel learning methods because β_m is selected based on the cross-validation scheme on the grid-searching space with constraints $\sum_m \beta_m = 1$. The range of c was 2^−5 to 2^5. All data-processing and classification procedures used in our study are shown in **Figure 1**. Due to the small sample size, we used the leave-one-out cross-validation (LOOCV) strategy to verify the performance of the methods, in which only one subject is left out for testing while the others are used to train the models and obtain the optimal parameters. For the choice of optimal parameters, an inner LOOCV was conducted on the training data using a grid-search strategy. Moreover, in order to verify the performance of the proposed model, we also tested the model on the independent ADNI dataset.

RESULTS

Demographics and Clinical Characteristics

The demographic data and clinical characteristics of all participants are summarized in **Table 2**. There were no significant differences in sex, age, or education level between the MCI and NC groups ($P > 0.05$ for all). However, the MCI group had significantly lower scores on the Mini Mental State Examination ($P < 0.001$) than the NC group. We also selected 50 samples (27 MCI and 23 NCs) from the independent ADNI dataset. The details of their demographic and clinical characteristics are listed in **Table 3**.

Significant Differences of Functional Connections in Brain-Network

The mean connection strengths of the whole brain network were compared between MCI and NC. A total of 3072 connections with significant differences were extracted between the MCI and NC groups within the range of fully sparse values from 0.02 to 0.5 ($P < 0.01$) using Student's t-tests. After permutation of NBS,

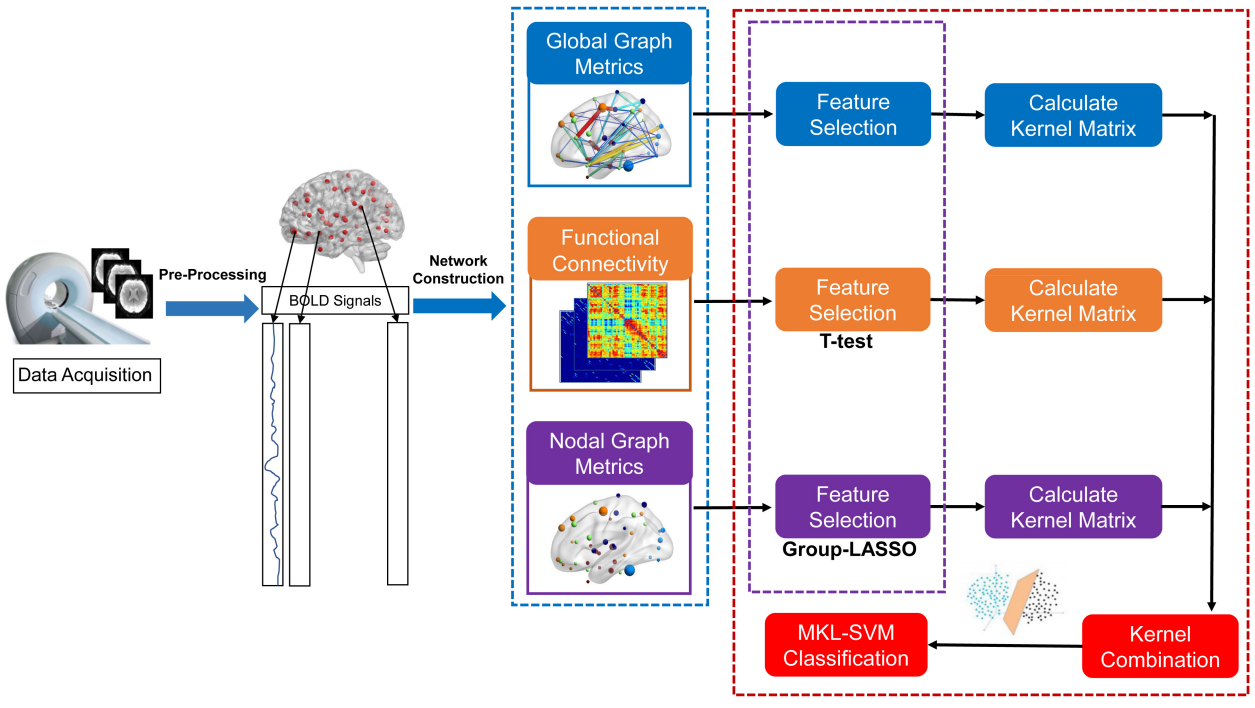

FIGURE 1 | Data-processing and classification procedures employed in our study.

TABLE 2 | Demographics and clinical characteristics of MCI patients and NCs in the current study.

Characteristic	MCI (*n* = 39)	NCs (*n* = 60)	*P*
Male/female, *n*	25/14	30/30	0.168[a]
Age, years, mean ±SD	74.00 ± 7.67	71.25 ± 7.08	0.071[b]
Education, years, mean ±SD	10.97 ± 4.29	12.42 ± 3.58	0.074[b]
MMSE, mean ±D	26.77 ± 2.33	28.28 ± 1.35	<0.001[b]
Hippocampal volume ($\times 10^3$ mm^3)	6.80 ± 0.87	7.43 ± 0.69	0.002[b]

MMSE, Mini mental state examination. [a]The P-value was obtained by using the chi-square test. [b]The P-value was obtained by using a two-sample t-test.

TABLE 3 | Demographics and clinical characteristics of the ADNI dataset.

Characteristic	MCI (*n* = 27)	NCs (*n* = 23)	*P*
Male/female, *n*	13/14	11/12	0.982[a]
Age, years, mean ±SD	70.11 ± 8.17	75.22 ± 6.82	0.021[b]
MMSE, mean ±SD	25.33 ± 1.07	27.17 ± 1.30	<0.001[b]

MMSE, Mini mental state examination. [a]The P-value was obtained by using the chi-square test. [b]The P-value was obtained by using a two-sample t-test.

we retained the most significant 100 connections with the lowest *P*-values (**Figure 2**). We projected them into the corresponding subnetworks and found that the most discriminative network connections were mainly distributed in the default mode network (DMN), subcortical network, frontoparietal task control network, dorsal attention network, and visual network. Compared with NCs, patients with MCI had significantly lower functional connection strength in brain-network connections ($P < 0.01$).

Global Graph Metrics of the Functional Brain Connectome

The global graph metrics of the MCI and NC groups showed the small-world topological attributes. That is, the functional brain networks had larger clustering coefficients and almost identical shortest path lengths compared with the matched random networks. With increasing connection density, C_p increased, whereas L_p, γ, λ, and small-world σ decreased in the MCI and NC groups. Statistical analysis revealed that the C_p of MCI patients was higher than that in the NC group, whereas λ and small-world σ were lower in the MCI group compared with the NC group ($P < 0.01$). However, these differences were only observed at a few network thresholds (**Figure 3**).

Nodal Graph Metrics of the Functional Brain Connectome

Two strategies were developed to investigate the discriminative features of nodal graph metrics and nodes based on local network parameters. On the one hand, we analyzed the most predominant brain regions with the greatest number of significant differences in nodal graph metrics. Before group-LASSO, 212 significantly different nodes were observed between MCI and NC groups ($P < 0.01$). However, after feature selection by group-LASSO,

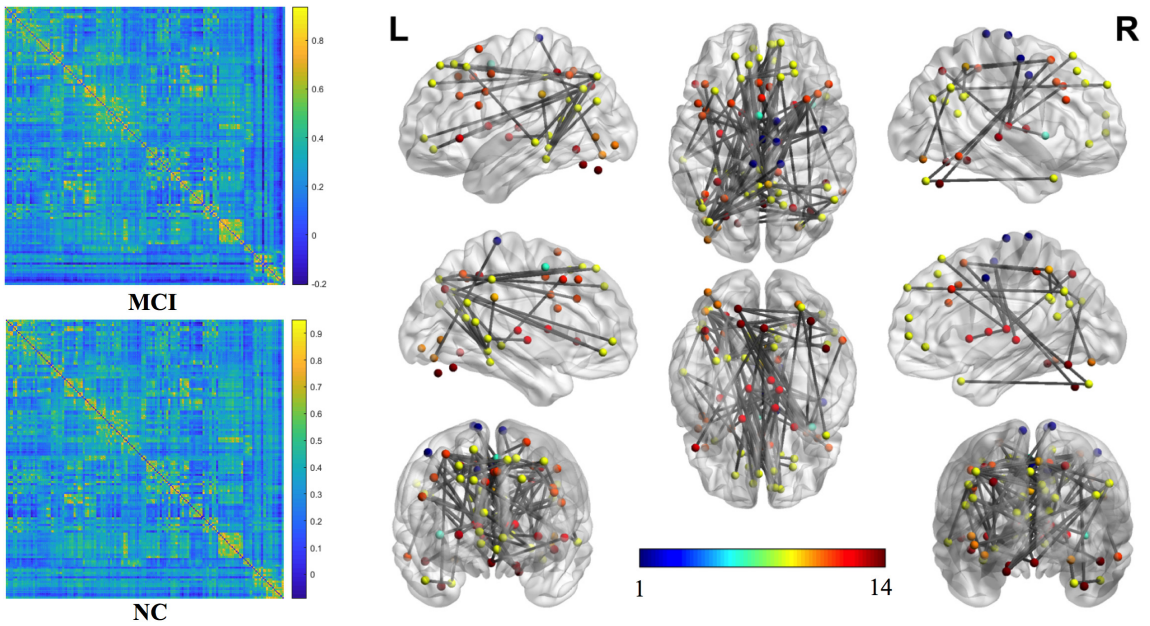

FIGURE 2 | The most significant 100 connections mapped on the ICBM 152 template using the BrainNet Viewer software package (http://nitrc.org/projects/bnv/). The connectivity matrices of the fully connected network of MCI patients and NCs are shown. The 100 most significant connections were retained, with gray indicating a reduction in connectivity strength. Plots in this figure were created by BrainNet Viewer (http://nitrc.org/projects/bnv/). The color-bar numbers represent the subnetworks with reference to the 264 putative functional area atlas proposed by Power et al. (2011). The details are: 1 sensory/somatomotor hand network; 2 sensory/somatomotor mouth network; 3 cingulo-opercular task control network; 4 auditory network; 5 default mode network; 6 memory retrieval network; 7 visual network; 8 frontoparietal task control network; 9 salience network; 10 subcortical network; 11 ventral attention network; 12 dorsal attention network; 13 cerebellar network; 14 unknown network.

we selected the nodal graph metrics from 76 ROIs as inputs. These 76 ROIs were considered as the extremely predominant nodes for discriminating MCI patients from NCs, and each ROI had ≥4 and ≤7 nodal topological metrics with significant differences. The locations of nodes in the 264 atlas were labeled according to the AAL_90 atlas (**Figure 4** and **Table 4**). On the other hand, we identified the distinguishing features for each nodal graph theory attribute using the feature selection of group-LASSO (**Table 5**). The top-20 nodal graph topological features with maximum discriminative ability are listed in **Table 6**. Therefore, the most predominant brain regions with the greatest numbers of significant nodal graph measures and the most discriminative nodal graph features were distributed mainly in the temporal, cingulate, superior frontal, lingual, and parietal gyri, which corresponded to the DMN, dorsal attention network, and cingulo-opercular task network.

According to the definition of "hubs," we identified hub nodes in MCI patients and NCs. **Figure 5** shows the hub nodes in each group. In MCI patients and NCs, the common hub regions were mainly located in the left middle temporal gyrus, right precuneus, left median cingulate gyrus, left cuneus, and paracingulate gyri. More importantly, some hub nodes were present only in MCI patients and absent in NCs: the left paracentral lobule, right paracentral lobule, left postcentral gyrus, and right cuneus. Simultaneously, there were also some hub nodes in NCs but not in MCI patients. These regions were located on the left Heschl, right superior temporal, left inferior occipital, and left middle occipital gyri. Hub nodes play critical roles in maintaining high-level cognitive functions by coordinating overall information flow and supporting the integrity of the brain connectome (Wang et al., 2013). The similar distributions suggested preservation of hubs in MCI.

Further comparisons of the predominant brain regions mentioned above revealed that MCI patients had significantly lower values of betweenness centrality and degree centrality and significantly higher values for the nodal shortest path in the frontal lobe (e.g., bilateral superior frontal gyrus), temporal lobe (e.g., bilateral inferior temporal gyrus), limbic lobe (e.g., left median cingulate and paracingulate gyri), and parietal lobe (e.g., left inferior parietal gyrus) compared with the NC group

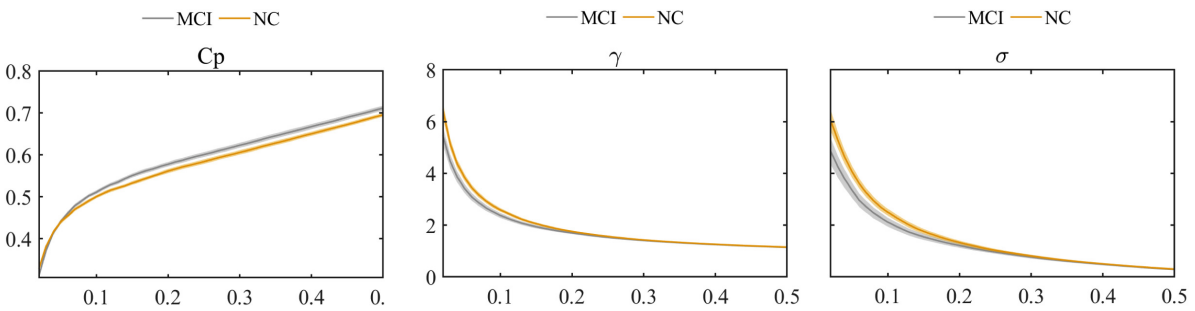

FIGURE 3 | Comparison of clustering coefficient (C_p), normalized clustering coefficient (γ), and small-world σ between MCI and NC groups.

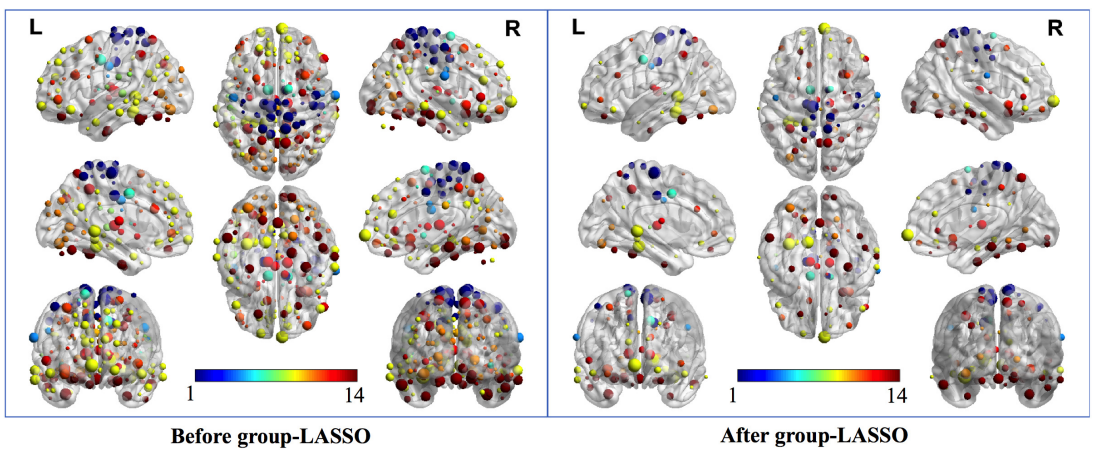

FIGURE 4 | The most predominant nodes for discriminating MCI patients from NCs. Before group-LASSO, 212 significantly different nodes were present between MCI and NC groups ($P < 0.01$). After feature selection by group-LASSO, the 76 most highly discriminative nodes were reserved. The color-bar numbers represent the subnetworks with reference to the 264 putative functional area atlas proposed by Power et al. (2011). The details are: 1 sensory/somatomotor hand network; 2 sensory/somatomotor mouth network; 3 cingulo-opercular task control network; 4 auditory network; 5 default mode network; 6 memory retrieval network; 7 visual network; 8 frontoparietal task control network; 9 salience network; 10 subcortical network; 11 ventral attention network; 12 dorsal attention network; 13 cerebellar network; 14 unknown network.

TABLE 4 | Top 20 most predominant nodes (brain regions) with the greatest number of significant differences in nodal graph metrics.

ROI number	Corresponding AAL area	Sub-network	Number of nodal metrics
77	Lingual_L	Default mode	7
126	Fusiform_L	Default mode	7
4	Temporal_Inf_L	Unknown	7
116	Temporal_Mid_R	Default mode	7
22	Precuneus_R	Sensory/somatomotor	6
17	Paracentral_Lobule_L	Sensory/somatomotor	6
251	Precuneus_R	Dorsal attention	6
259	Parietal_Inf_L	Dorsal attention	6
75	Frontal_Mid_Orb_R	Default mode	6
92	Cingulum_Post_R	Default mode	6
224	Thalamus_L	Subcortical	6
225	Thalamus_R	Subcortical	6
53	Supp_Motor_Area_R	Cingulo-opercular task	6
211	Insula_R	Salience	6
203	Cingulum_Mid_R	Salience	6
124	ParaHippocampal_L	Default mode	6
139	Frontal_Inf_Orb_R	Default mode	5
51	Cingulum_Mid_L	Cingulo-opercular task	5
172	Fusiform_L	Visual	5
263	Parietal_Sup_L	Dorsal attention	5

AAL, the automated anatomical labeling atlas.

($P < 0.01$ for all). Nevertheless, in the occipital lobe (e.g., left lingual and left fusiform gyri), the MCI group showed significantly higher values of betweenness centrality and degree centrality and significantly lower values of nodal shortest path, which was opposite to the pattern of nodal graph metrics in the brain lobes mentioned above (**Figure 6**).

Classification

After feature selection of functional connections with Student's *t*-tests and nodal graph metrics by group-LASSO, MKL-SVM was carried out to combine the brain connectome information. We evaluated the classification performance of different methods with a set of quantitative measures – accuracy, sensitivity, and specificity – which were defined as follows:

$$Accuracy = \frac{TP + TN}{TP + FP + TN + FN},$$

$$Sensitivity = \frac{TP}{TP + FN},$$

$$Specificity = \frac{TN}{TN + FP},$$

where TP, TN, FP, and FN denote the number of true-positive, true-negative, false-positive, and false-negative values, respectively. The area under the receiver operating characteristic curve (AUC) was calculated as a performance measure for binary classification of the MCI and NC groups. In particular, LOOCV was employed in this study due to the small sample size, which provided an optimistic estimate of the classification accuracy since all except one of the subjects are used to train the classifier. For other approaches such as k-fold cross-validation, only N-k (N is the total number of participants in the dataset) participants are included during the training process, resulting in poorer performance due to the small dataset (Wee et al., 2012). For the functional connections (C), global metrics (G), and nodal metrics (N) of the brain network, we obtained AUCs of 0.9605, 0.7290, and 0.9576, respectively (**Table 7**). We also performed classification experiments by combining functional connections (C), global metrics (G), nodal metrics (N), global metrics (G), and nodal metrics (N). The results showed that despite the low classification performance of single global graph metrics, they still effectively increased the classification performance of nodal graph metrics and functional connections. For a direct combination of connections, global metrics, and nodal metrics, we obtained 87.88% accuracy and

TABLE 5 | Number of discriminative features for each nodal graph metrics from the feature-selection step of LASSO.

Nodal graph metric	Number of selected features
Betweenness centrality	33
Degree centrality	46
Nodal clustering coefficient	48
Nodal local efficiency	19
Nodal shortest path length	44
Participant coefficient	70
Within-module degree	81

TABLE 6 | Top 20 features corresponding to nodal graph metrics with maximum discriminative ability.

Nodal graph measure	ROI number	Corresponding AAL area	Subnetwork
Within-module degree	124	ParaHippocampal_L	Default mode
Within-module degree	89	Precuneus_R	Default mode
Within-module degree	191	Parietal_Sup_L	Frontoparietal task
Degree centrality	77	Lingual_L	Default mode
Participant coefficient	9	Temporal_Inf_R	Uncertain
Within-module degree	92	Cingulum_Post_R	Default mode
Degree centrality	225	Thalamus_R	Subcortical
Participant coefficient	118	Temporal_Mid_L	Default mode
Participant coefficient	75	Frontal_Mid_Orb_R	Default mode
Nodal clustering coefficient	75	Frontal_Mid_Orb_R	Default mode
Nodal shortest path length	75	Frontal_Mid_Orb_R	Default mode
Participant coefficient	17	Paracentral_Lobule_L	Sensory/somatomotor
Degree centrality	224	Thalamus_L	Subcortical
Nodal shortest path length	9	Temporal_Inf_R	Uncertain
Participant coefficient	83	Temporal_Inf_L	Default mode
Degree centrality	126	Fusiform_L	Default mode
Betweenness centrality	77	Lingual_L	Default mode
Nodal clustering coefficient	77	Lingual_L	Default mode
Betweenness centrality	51	Cingulum_Mid_L	Cingulo-opercular task
Nodal local efficiency	92	Cingulum_Post_R	Default mode

AAL, the automated anatomical labeling atlas.

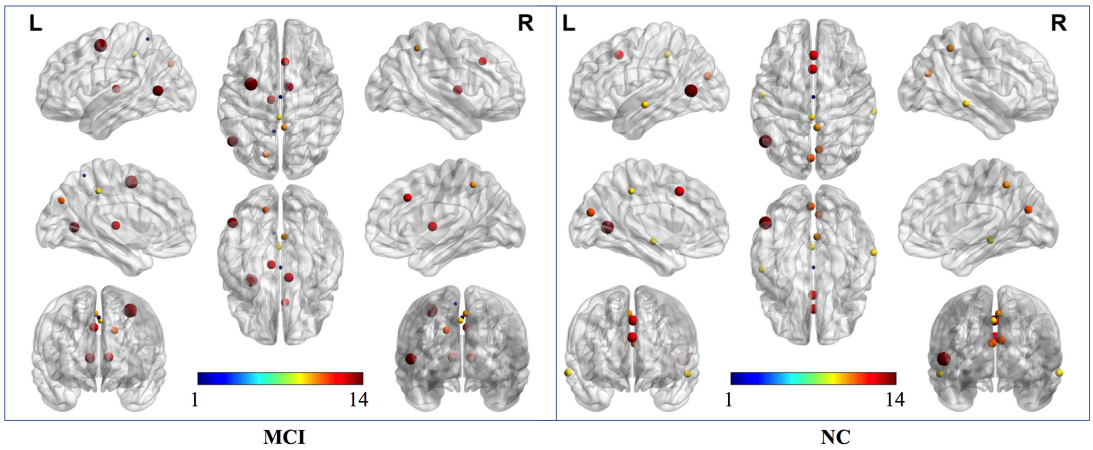

FIGURE 5 | Hub nodes of MCI and NC groups in the brain. The color-bar numbers represent the subnetworks with reference to the 264 putative functional area atlas proposed by Power et al. (2011). The details are: 1 sensory/somatomotor hand network; 2 sensory/somatomotor mouth network; 3 cingulo-opercular task control network; 4 auditory network; 5 default mode network; 6 memory retrieval network; 7 visual network; 8 frontoparietal task control network; 9 salience network; 10 subcortical network; 11 ventral attention network; 12 dorsal attention network; 13 cerebellar network; 14 unknown network.

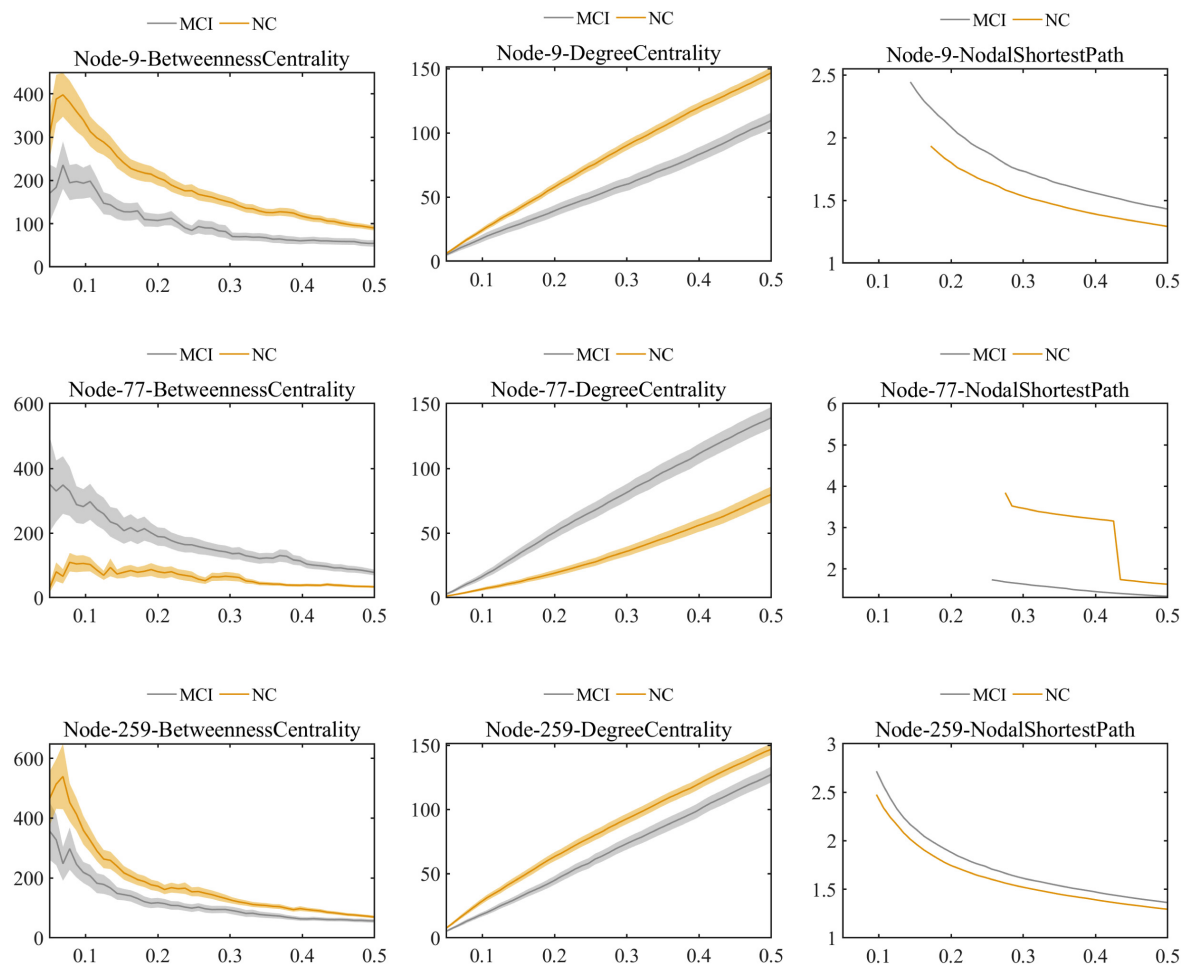

FIGURE 6 | Comparison of values of nodal graph metrics between MCI patients and NCs. Betweenness centrality, degree centrality, and nodal shortest path length of Node 9 (right inferior temporal gyrus). Betweenness centrality, degree centrality and nodal shortest path length of Node 259 (left inferior parietal). Betweenness centrality, degree centrality, and nodal shortest path length of Node 77 (left lingual gyrus).

TABLE 7 | The evaluation of classification performance corresponding to different functional connectome features.

Method	Accuracy (%)	Sensitivity (%)	Specificity (%)	AUC
Connection (C)	85.86	82.05	88.33	0.9605
Global Metrics (G)	73.74	69.23	76.67	0.7290
Nodal Metrics (N)	87.88	82.05	91.67	0.9576
MKL_CG	86.87	82.05	90.00	0.9329
MKL_CN	90.91	84.62	95.00	0.9581
MKL_GN	89.90	84.62	93.33	0.9371
C + G + N	87.88	92.31	85.00	0.9666
MKL_CGN	92.93	89.74	95.00	0.9728
Hippocampal (H)	72.73	71.67	74.36	0.7005
MKL_CH	86.86	84.62	88.33	0.9509
MKL_GH	76.77	73.33	82.05	0.8117
MKL_NH	89.90	87.18	91.67	0.9647

MKL-SVM, multiple kernel learning support vector machine.

an AUC of 0.9666, which meant that simple combination did not effectively improve the classification performance. Finally, the combination of all connectome features based on MKL-SVM achieved the best classification performance, with 92.93% accuracy, 95.00% specificity, and an AUC of 0.9728. Moreover, the weight values (β) of functional connections, global metrics, and nodal metrics were 0.3, 0.01, and 0.6, respectively, indicating that the node attributes contributed most to the classification (**Figure 7**). It should be noted that MKL-SVM both combines the information of functional connectivity and graph theory attributes and provides a method to merge more useful information for MCI identification. Therefore, we also combined the traditional unimodal marker of hippocampal volume with the brain connectome; the results are listed in **Table 7**. Our results suggest that the AUC of the hippocampal volume was 0.7005, and the AUCs of the combination of hippocampal volume with functional connectivity, global graph theory attributes, or node graph theory attributes were 0.9509, 0.8117, and 0.9647, respectively. In addition, the independent ADNI dataset was then employed to verify the generalization of the pre-trained model. The all connectome features combination based on MKL-SVM achieved classification performance with 66.00% accuracy, 70.37% sensitivity, and 60.87% specificity.

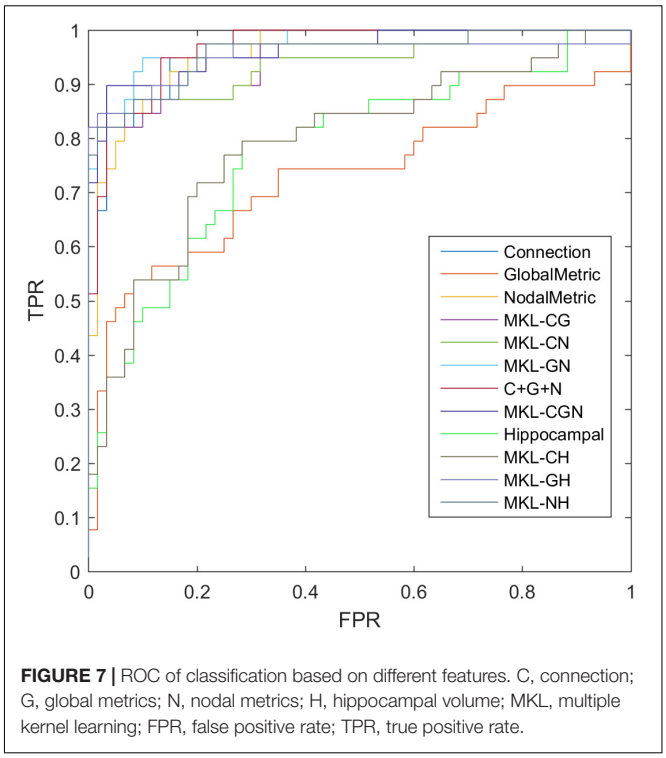

FIGURE 7 | ROC of classification based on different features. C, connection; G, global metrics; N, nodal metrics; H, hippocampal volume; MKL, multiple kernel learning; FPR, false positive rate; TPR, true positive rate.

DISCUSSION

In the present study, we selected discriminative features from different attributes of the brain connectome (i.e., functional connections, global graph metrics, and nodal graph metrics) and combined the information to train a classifier for distinguishing subjects with MCI from NCs. Based on the feature selection and combination of the proposed methods, we further described the altered patterns of the best distinguishing features of MCI through group comparison, aiming to further clarify disease pathogenesis. Our detailed results are listed as follows. First, the most predominant brain regions and most discriminative nodal graph metrics for discriminating NCs from MCI were selected by the group-LASSO. Second, the information combination strategy (MKL-SVM) effectively improved the classification performance, and the nodal graph metrics of the connectome contributed most to the classification. Finally, the altered functional brain connectome pattern in MCI patients included a general decrease in functional connections in the whole brain network, whereas nodal topological attributes in some local brain regions were increased.

The Most Predominant Brain Regions and Discriminative Nodal Graph Metrics

The nodal graph metrics have a natural group topology; that is, a node corresponds to a group of node-graph theoretical attributes. Thus, we used group-LASSO as the feature-selection scheme for nodal graph metrics. It effectively extracted the group-structure information of nodal attributes. The most predominant brain regions (with seven significantly different nodal topological metrics) were mainly distributed in the left lingual, left fusiform, left inferior temporal, and right middle temporal gyri. These brain regions showed significant changes in nodal graph metrics and so could be regarded as the most sensitive observation areas for nodal topological attributes in MCI patients. Also, within-module degree, degree centrality, and participation coefficient showed the most significant discriminative ability among the selected nodal graph metrics. The corresponding brain regions with the three most discriminative nodal metrics considerably overlapped with the hub nodes found in MCI patients. Overall, our results emphasize the importance of analyzing the attributes of intra-modules and hub nodes for early discrimination of NCs from subjects with MCI.

By projecting brain regions with significant differences of functional connections and graph metrics in the brain network to subnetworks, we found that the differences between MCI patients and NCs were distributed mainly in the DMN, dorsal attention network, cingulo-opercular task network, and frontoparietal task network. Of these, the DMN had the most significant discriminative ability. Studies have verified the correlations between these subnetworks and cognitive functions in the human brain, corresponding to spatial attention (Rolle et al., 2017), visual attention (Wirth et al., 2017), and executive function (Talpos and Shoaib, 2015).

In this study, the DMN carried the most distinguishing information, which was verified by the proposed feature selection methods. Previous studies showed that the DMN is involved in episodic memory and is considered the major cognitive domain impaired in the early stage of AD (Meskaldji et al., 2016; Dillen et al., 2017). Besides validating the discriminative ability of the DMN for discriminating NCs from MCI, we accurately located the predominant brain regions (middle temporal, inferior temporal, lingual, posterior cingulate, and middle frontal gyri) in the DMN and the corresponding nodal graph metrics. These results may facilitate the early and accurate diagnosis of MCI. They also demonstrate the repeatability and verifiability of the proposed methods, which is an important contribution of our work.

Fusion Classification of MKL-SVM and Identification of Maximum Contribution

Group-LASSO is valid for nodal feature selection because it can retain significant features with the most discriminative ability while avoiding data redundancy. We carried out reduction of nodal features according to group-LASSO and selected optimal features to achieve the best performance for discriminating NCs from MCI. This is an effective way to integrate multiple views of biomarkers for AD classification. The simplest way is to directly splice the data. Studies using multivariate pattern analysis [e.g., linear discriminate analysis (Alam et al., 2017), artificial neural networks (Quintana et al., 2012), and random forest (Sarica et al., 2017)] have been undertaken to identify MCI using complex network characteristics. However, those approaches could be inappropriate due to the high-dimensional curves and small samples. Information with higher dimensions can submerge the low-dimension information. To overcome these challenges, we employed MKL-SVM for information combination. MKL (Niu et al., 2017) is a sparse machine-learning method that allows identification of the most relevant classification sources. The results suggested that the performance of classification by combining multiple brain connectome features was better than that of individual connectome features. The weight value (β) of functional connections, global metrics, and nodal metrics emphasized that nodal graph attributes had the greatest contribution to classification. It also indicated that MCI patients had significant changes in nodal properties. More surprisingly, although global metrics showed the worst classification performance, they can still provide important information about functional connections and nodal metrics. After combining functional connections and global metrics (C + G), functional connections and nodal metrics (C + N), and global metrics and nodal metrics (G + N), the results indicated that classification performance was effectively improved by combining the information of global metrics.

To verify this significant improvement, the Delong test was applied (DeLong et al., 1988). We found that the proposed method significantly outperformed the global graph attributes, functional connection, and nodal graph attributes under the 95% confidence interval with P-values of 0.0002, 0.0227, and 0.0419, respectively. Although MKL-SVM did not yield significant improvements compared to the feature concatenation method (P = 0.1627), it still had two advantages. First, MKL-SVM could address the imbalanced dimension issue across modalities to some extent and better embody the contribution of different information sources to distinguish MCI patients from NCs. Second, experimental results demonstrated that the proposed method outperformed the single modality of the functional connectome in the brain network. It should also be noted that both methods are simple attempts to verify information effectiveness.

The classification results based on the traditional marker of hippocampal volume suggested that the combination of hippocampal volume and connectome features could also improve classification accuracy. The MKL-SVM can be used to combine multiple features of the brain connectome and effectively integrate multimodal information to discriminate NCs from patients with MCI.

During validation of the proposed model, the classification performance of the independent ADNI dataset was not as good as the pre-trained sample. This may be due to heterogeneity in scanning machines, parameters, and physiological structures between western and eastern samples, which obviously violates the independently identically distribution assumption of SVM.

Altered Pattern of the Brain Network Connectome in MCI

At the global brain level, we found that MCI patients had weaker functional connections in the brain network, which was consistent with previous functional network studies of AD (Li et al., 2016) and MCI (Wang et al., 2013; Lee et al., 2016). Some results demonstrated that these abnormal functional connections were directly related to the global topological attributes of brain networks (Wang et al., 2013). In our study, we first found that patients with MCI and NCs fit the features of a small-world network in a global network topology. That is, the brain network supported rapid, real-time integration of information across separate sensory brain regions to confer resilience against pathology and maximize efficiency with minimal cost for effective information processing between brain regions (Sporns and Zwi, 2004; Achard and Bullmore, 2007; Sporns, 2011). Further comparison suggested that the value of small-world σ in MCI patients was lower than that in NCs, indicating "economic small-world" disruption (Liao et al., 2017) (i.e., reduction of the segregation and integration functions of effective information in the brain network). Moreover, we found changes in the

functional segregation of brain networks in MCI patients (increased C_p). C_p is a measure of local network connectivity (Bullmore and Sporns, 2009) that reflects the efficiency of local information transfer and the ability to defend against random attacks against a network. A higher value of C_p represents a more concentrated clustering of local connections and a stronger capacity for processing local information. It is notable that previous studies reported decreased C_p in AD patients (Zhao et al., 2012). The reason for this difference might be related to the compensatory change of segregation function in the transition stage of MCI. Therefore, our results suggested that functional connections in the whole-brain network were generally decreased, whereas the network segregation of local information processing was increased.

At the local brain level, further analyses of the hub nodes and nodes with the most discriminative ability for MCI showed that MCI patients had significantly lower values of betweenness centrality and degree centrality and higher values of nodal shortest path in some brain regions (the frontal, temporal, limbic, and parietal lobes) compared with NCs. These data suggested that the network integration and local transmission capability of these lobes were decreased in MCI patients. However, in critical nodes in the occipital lobe, the increased betweenness/degree centrality and decreased shortest path indicated enhanced integration function and greater local transmission efficiency. We speculated that enhanced variation of these nodal graph metrics in some occipital nodes suggests compensation to maintain high-level cognitive performance despite the pathological process of amyloid accumulation during the earliest phases of AD. This functional variation in the occipital lobe was also mentioned in previous studies. For example, Dai et al. found that the left fusiform gyrus exhibited higher functional connections in the AD group (Dai et al., 2015). Bokde et al. (2010) found significantly greater activation in the right middle occipital gyrus during the location-matching task.

Therefore, the altered brain connectome patterns in our study revealed that functional connections generally decreased in the whole brain network but increased for nodal graph topological attributes of local brain regions. This might suggest functional compensation in some brain regions to maintain normal cognitive function in the early stage of AD.

Limitations and Future Directions

There are still several limitations that need to be considered further. First, the class imbalance issue. Although there are several approaches (e.g., resampling or reweighting) to overcome imbalance, taking them makes it difficult to estimate whether the improvement of performance is based on these adjustments or on the proposed methods. In the future, we plan to investigate high-quality data with more balanced samples for feature selection and classification or develop a more robust algorithm that improves classification accuracy and generalization.

Second, we assessed a small sample size. The optimization of parameters and hyperparameters inevitably leads to overfitting for small samples. To avoid this issue, we empirically chose parameters with a default setting of lambda = 1 and $C = 1$ instead of optimized parameters and hyperparameters. In the future, we will conduct parameter optimization based on a larger sample size.

Third, we must consider the generalization of the model. For the independent ADNI dataset, classification performance was not as good as observed for the pre-trained sample, which suggests a limitation in modal generalization for different centers. We intend to improve the classification performance of multicenter data sources by combining domain adaptation.

Finally, our cross-validation approach may have been insufficient. Evaluation of classification by *k*-fold cross-validation might be more precise when sufficient data are available. Therefore, in the future, it is necessary to compare the results obtained by different cross-validation methods (i.e., LOOCV and *k*-fold cross-validation).

CONCLUSION

In the present study, the discriminative features of functional connections and nodal graph metrics were selected by Student's *t*-tests and group-LASSO, respectively. The combination of all connectome information using MKL-SVM achieved the best classification performance (AUC = 0.9728). In addition, the altered brain connectome pattern revealed that functional connectivity was generally decreased in the whole-brain network, whereas graph theory topological attributes of some special nodes were increased in MCI patients. Our findings demonstrate that optimal feature selection and the combination of all connectome features could achieve good performance for discriminating NCs from MCI. The combination of functional connections and global and nodal graph metrics of brain networks can predict the occurrence of MCI and contribute to the early clinical diagnosis of AD.

DATA AVAILABILITY STATEMENT

All datasets generated for this study are included in the article/supplementary material.

ETHICS STATEMENT

The studies involving human participants were reviewed and approved by the Ethics Committee of Huashan Hospital within Fudan University (Shanghai, China). The patients/participants provided their written informed consent to participate in this study.

AUTHOR CONTRIBUTIONS

XX and PW designed the study. QZ diagnosed patients. XL and WW administered the neuropsychological tests. XW acquired the MRI data. XX, WL, and JM analyzed and interpreted the results of the data. XX and MT drafted the manuscript. DD and PW revised the manuscript. All authors contributed equally to this work and approved the final manuscript.

FUNDING

This work was partially supported by the National Natural Science Foundation of China (Grant Nos. 81830059, 81571655, and 81771889), the Shanghai Municipal Commission of Health and Family Planning Smart Medical Special Research Project (Grant No. 2018ZHYL0105), the Fundamental Research Funds for the Central Universities (Grant No. 22120190219), Natural Science Foundation Project of CQCSTC (cstc2018jcyjA2756), Shanghai Municipal Planning Commission of Science and Research Fund (201740010), Shanghai Municipal Science and Technology Major Project (No. 2018SHZDZX01), and ZJLab.

REFERENCES

Achard, S., and Bullmore, E. (2007). Efficiency and cost of economical brain functional networks. *PLoS Comput. Biol.* 3:e17. doi: 10.1371/journal.pcbi.0030017

Alam, S., Kwon, G. R., Kim, J. I., and Park, C. S. (2017). Twin SVM-based classification of Alzheimer's disease using complex dual-tree wavelet principal coefficients and LDA. *J. Healthc. Eng.* 2017:8750506. doi: 10.1155/2017/8750506

Biswal, B. B., Mennes, M., Zuo, X. N., Gohel, S., Kelly, C., Smith, S. M., et al. (2010). Toward discovery science of human brain function. *Proc. Natl. Acad. Sci. U.S.A.* 107, 4734–4739. doi: 10.1073/pnas.0911855107

Blennow, K., de Leon, M. J., and Zetterberg, H. (2006). Alzheimer's disease. *Lancet* 368, 387–403. doi: 10.1016/S0140-6736(06)69113-7

Bokde, A. L., Lopez-Bayo, P., Born, C., Ewers, M., Meindl, T., Teipel, S. J., et al. (2010). Alzheimer disease: functional abnormalities in the dorsal visual pathway. *Radiology* 254, 219–226. doi: 10.1148/radiol.2541090558

Bullmore, E., and Sporns, O. (2009). Complex brain networks: graph theoretical analysis of structural and functional systems. *Nat. Rev. Neurosci.* 10, 186–198. doi: 10.1038/nrn2575

Chang, T. Y., Huang, K. L., Ho, M. Y., Ho, P. S., Chang, C. H., Liu, C. H., et al. (2016). Graph theoretical analysis of functional networks and its relationship to cognitive decline in patients with carotid stenosis. *J. Cereb. Blood Flow Metab.* 36, 808–818. doi: 10.1177/0271678X15608390

Dai, Z., Lin, Q., Li, T., Wang, X., Yuan, H., Yu, X., et al. (2019). Disrupted structural and functional brain networks in Alzheimer's disease. *Neurobiol. Aging* 75, 71–82. doi: 10.1016/j.neurobiolaging.2018.11.005

Dai, Z., Yan, C., Li, K., Wang, Z., Wang, J., Cao, M., et al. (2015). Identifying and mapping connectivity patterns of brain network hubs in Alzheimer's disease. *Cereb. Cortex* 25, 3723–3742. doi: 10.1093/cercor/bhu246

delEtoile, J., and Adeli, H. (2017). Graph theory and brain connectivity in Alzheimer's disease. *Neuroscientist* 23, 616–626. doi: 10.1177/1073858417702621

DeLong, E. R., DeLong, D. M., and Clarke-Pearson, D. L. (1988). Comparing the areas under two or more correlated receiver operating characteristic curves: a nonparametric approach. *Biometrics* 44, 837–845.

Dillen, K. N. H., Jacobs, H. I. L., Kukolja, J., Richter, N., von Reutern, B., Onur, O. A., et al. (2017). Functional disintegration of the default mode network in prodromal Alzheimer's disease. *J. Alzheimers Dis.* 59, 169–187. doi: 10.3233/JAD-161120

Filippi, M., Basaia, S., Canu, E., Imperiale, F., Magnani, G., Falautano, M., et al. (2018). Changes in functional and structural brain connectome along the Alzheimer's disease continuum. *Mol. Psychiatry* 25, 230–239. doi: 10.1038/s41380-018-0067-8

Grundman, M., Petersen, R. C., Ferris, S. H., Thomas, R. G., Aisen, P. S., Bennett, D. A., et al. (2004). Mild cognitive impairment can be distinguished from Alzheimer disease and normal aging for clinical trials. *Arch. Neurol.* 61, 59–66. doi: 10.1001/archneur.61.1.59

Ijaopo, E. O. (2017). Dementia-related agitation: a review of non-pharmacological interventions and analysis of risks and benefits of pharmacotherapy. *Transl. Psychiatry* 7:e1250. doi: 10.1038/tp.2017.199

Khazaee, A., Ebrahimzadeh, A., and Babajani-Feremi, A. (2016). Application of advanced machine learning methods on resting-state fMRI network for identification of mild cognitive impairment and Alzheimer's disease. *Brain Imaging Behav.* 10, 799–817. doi: 10.1007/s11682-015-9448-7

Khazaee, A., Ebrahimzadeh, A., Babajani-Feremi, A., and Alzheimer's Disease Neuroimaging Initiative, (2017). Classification of patients with MCI and AD from healthy controls using directed graph measures of resting-state fMRI. *Behav. Brain Res.* 322(Pt B), 339–350. doi: 10.1016/j.bbr.2016.06.043

Lee, E. S., Yoo, K., Lee, Y. B., Chung, J., Lim, J. E., Yoon, B., et al. (2016). Default mode network functional connectivity in early and late mild cognitive impairment: results from the Alzheimer's disease neuroimaging initiative. *Alzheimer. Dis. Assoc. Disord.* 30, 289–296. doi: 10.1097/WAD.0000000000000143

Li, W., Qiao, L., Zhang, L., Wang, Z., and Shen, D. (2019). Functional brain network estimation with time series self-scrubbing. *IEEE J. Biomed. Health Inform.* 23, 2494–2504. doi: 10.1109/JBHI.2019.2893880

Li, W., Wang, Z., Zhang, L., Qiao, L., and Shen, D. (2017). Remodeling Pearson's correlation for functional brain network estimation and autism spectrum disorder identification. *Front. Neuroinform.* 11:55. doi: 10.3389/fninf.2017.00055

Li, Y., Liu, J., Gao, X., Jie, B., Kim, M., Yap, P. T., et al. (2019). Multimodal hyper-connectivity of functional networks using functionally-weighted LASSO for MCI classification. *Med. Image Anal.* 52, 80–96. doi: 10.1016/j.media.2018.11.006

Li, Y., Wang, X., Li, Y., Sun, Y., Sheng, C., Li, H., et al. (2016). Abnormal resting-state functional connectivity strength in mild cognitive impairment and its conversion to Alzheimer's disease. *Neural Plast.* 2016:4680972. doi: 10.1155/2016/4680972

Liao, X., Vasilakos, A. V., and He, Y. (2017). Small-world human brain networks: perspectives and challenges. *Neurosci. Biobehav. Rev.* 77, 286–300. doi: 10.1016/j.neubiorev.2017.03.018

Liu, X., Cao, P., Wang, J., Kong, J., and Zhao, D. (2019). Fused group lasso regularized multi-task feature learning and its application to the cognitive performance prediction of Alzheimer's disease. *Neuroinformatics* 17, 271–294. doi: 10.1007/s12021-018-9398-5

Manly, J. J., Tang, M. X., Schupf, N., Stern, Y., Vonsattel, J. P., and Mayeux, R. (2008). Frequency and course of mild cognitive impairment in a multiethnic community. *Ann. Neurol.* 63, 494–506. doi: 10.1002/ana.21326

Meskaldji, D. E., Preti, M. G., Bolton, T. A., Montandon, M. L., Rodriguez, C., Morgenthaler, S., et al. (2016). Prediction of long-term memory scores in MCI based on resting-state fMRI. *Neuroimage Clin.* 12, 785–795. doi: 10.1016/j.nicl.2016.10.004

Newman, M. E. (2004). Fast algorithm for detecting community structure in networks. *Phys. Rev. E* 69(Pt 2):066133. doi: 10.1103/PhysRevE.69.066133

Newman, M. E. (2006). Finding community structure in networks using the eigenvectors of matrices. *Phys. Rev. E* 74(Pt 2):036104. doi: 10.1103/PhysRevE.74.036104

Niu, W., Xia, K., Zu, B., and Bai, J. (2017). Efficient multiple kernel learning algorithms using low-rank representation. *Comput. Intell. Neurosci.* 2017:3678487. doi: 10.1155/2017/3678487

Petersen, R. C. (2004). Mild cognitive impairment as a diagnostic entity. *J. Intern. Med.* 256, 183–194. doi: 10.1111/j.1365-2796.2004.01388.x

Petersen, R. C., Smith, G. E., Waring, S. C., Ivnik, R. J., Tangalos, E. G., and Kokmen, E. (1999). Mild cognitive impairment: clinical characterization and outcome. *Arch. Neurol.* 56, 303–308.

Power, J. D., Cohen, A. L., Nelson, S. M., Wig, G. S., Barnes, K. A., Church, J. A., et al. (2011). Functional network organization of the human brain. *Neuron* 72, 665–678. doi: 10.1016/j.neuron.2011.09.006

Prasad, G., Joshi, S. H., Nir, T. M., Toga, A. W., Thompson, P. M., and Alzheimer's Disease Neuroimaging Initiative, (2015). Brain connectivity and novel network measures for Alzheimer's disease classification. *Neurobiol. Aging* 36(Suppl. 1), S121–S131. doi: 10.1016/j.neurobiolaging.2014.04.037

Qiao, L., Zhang, H., Kim, M., Teng, S., Zhang, L., and Shen, D. (2016). Estimating functional brain networks by incorporating a modularity prior. *Neuroimage* 141, 399–407. doi: 10.1016/j.neuroimage.2016.07.058

Quintana, M., Guardia, J., Sanchez-Benavides, G., Aguilar, M., Molinuevo, J. L., Robles, A., et al. (2012). Using artificial neural networks in clinical neuropsychology: high performance in mild cognitive impairment and Alzheimer's disease. *J. Clin. Exp. Neuropsychol.* 34, 195–208. doi: 10.1080/13803395.2011.630651

Rabe-Jablonska, J., and Bienkiewicz, W. (1994). Anxiety disorders in the fourth edition of the classification of mental disorders prepared by the American Psychiatric Association: diagnostic and statistical manual of mental disorders (DMS-IV – options book). *Psychiatr. Pol.* 28, 255–268.

Rolle, C. E., Anguera, J. A., Skinner, S. N., Voytek, B., and Gazzaley, A. (2017). Enhancing spatial attention and working memory in younger and older adults. *J. Cogn. Neurosci.* 29, 1483–1497. doi: 10.1162/jocn_a_01159

Rubinov, M., and Sporns, O. (2010). Complex network measures of brain connectivity: uses and interpretations. *Neuroimage* 52, 1059–1069. doi: 10.1016/j.neuroimage.2009.10.003

Sarica, A., Cerasa, A., and Quattrone, A. (2017). Random forest algorithm for the classification of neuroimaging data in Alzheimer's disease: a systematic review. *Front. Aging Neurosci.* 9:329. doi: 10.3389/fnagi.2017.00329

Sporns, O. (2011). The human connectome: a complex network. *Ann. N. Y. Acad. Sci.* 1224, 109–125. doi: 10.1111/j.1749-6632.2010.05888.x

Sporns, O., and Zwi, J. D. (2004). The small world of the cerebral cortex. *Neuroinformatics* 2, 145–162. doi: 10.1385/ni:2:2:145

Suk, H. I., Lee, S. W., Shen, D., and Alzheimers Disease Neuroimaging, I. (2014). Subclass-based multi-task learning for Alzheimer's disease diagnosis. *Front Aging Neurosci.* 6:168. doi: 10.3389/fnagi.2014.00168

Talpos, J., and Shoaib, M. (2015). Executive function. *Handb. Exp. Pharmacol.* 228, 191–213. doi: 10.1007/978-3-319-16522-6_6

Themistocleous, C., Eckerstrom, M., and Kokkinakis, D. (2018). Identification of mild cognitive impairment from speech in Swedish using deep sequential neural networks. *Front. Neurol.* 9:975. doi: 10.3389/fneur.2018.00975

Wang, J., Wang, X., Xia, M., Liao, X., Evans, A., and He, Y. (2015). GRETNA: a graph theoretical network analysis toolbox for imaging connectomics. *Front. Hum. Neurosci.* 9:386. doi: 10.3389/fnhum.2015.00386

Wang, J., Zuo, X., Dai, Z., Xia, M., Zhao, Z., Zhao, X., et al. (2013). Disrupted functional brain connectome in individuals at risk for Alzheimer's disease. *Biol. Psychiatry* 73, 472–481. doi: 10.1016/j.biopsych.2012.03.026

Wee, C. Y., Yap, P. T., Zhang, D., Denny, K., Browndyke, J. N., Potter, G. G., et al. (2012). Identification of MCI individuals using structural and functional connectivity networks. *Neuroimage* 59, 2045–2056. doi: 10.1016/j.neuroimage.2011.10.015

Wee, C. Y., Yap, P. T., Zhang, D., Wang, L., and Shen, D. (2014). Group-constrained sparse fMRI connectivity modeling for mild cognitive impairment identification. *Brain Struct. Funct.* 219, 641–656. doi: 10.1007/s00429-013-0524-8

Wirth, M., Isaacowitz, D. M., and Kunzmann, U. (2017). Visual attention and emotional reactions to negative stimuli: the role of age and cognitive reappraisal. *Psychol. Aging* 32, 543–556. doi: 10.1037/pag0000188

Zalesky, A., Fornito, A., and Bullmore, E. T. (2010). Network-based statistic: identifying differences in brain networks. *Neuroimage* 53, 1197–1207. doi: 10.1016/j.neuroimage.2010.06.041

Zhao, X., Liu, Y., Wang, X., Liu, B., Xi, Q., Guo, Q., et al. (2012). Disrupted small-world brain networks in moderate Alzheimer's disease: a resting-state fMRI study. *PLoS One* 7:e33540. doi: 10.1371/journal.pone.0033540

Zhuo, Z., Mo, X., Ma, X., Han, Y., and Li, H. (2018). Identifying aMCI with functional connectivity network characteristics based on subtle AAL atlas. *Brain Res.* 1696, 81–90. doi: 10.1016/j.brainres.2018.04.042

Zuo, X. N., Ehmke, R., Mennes, M., Imperati, D., Castellanos, F. X., Sporns, O., et al. (2012). Network centrality in the human functional connectome. *Cereb. Cortex* 22, 1862–1875. doi: 10.1093/cercor/bhr269

Conflict of Interest: The authors declare that the research was conducted in the absence of any commercial or financial relationships that could be construed as a potential conflict of interest.

frontiers in Aging Neuroscience

ORIGINAL RESEARCH
published: 25 February 2020
doi: 10.3389/fnagi.2020.00039

Dysfunction of Inferior Parietal Lobule During Sensory Gating in Patients With Amnestic Mild Cognitive Impairment

Chia-Hsiung Cheng[1,2,3,4]*, *Fu-Jung Hsiao*[5], *Yu-Wei Hsieh*[1,2,6] and *Pei-Ning Wang*[5,7,8]*

[1]Department of Occupational Therapy, Graduate Institute of Behavioral Sciences, College of Medicine, Chang Gung University, Taoyuan, Taiwan, [2]Healthy Aging Research Center, Chang Gung University, Taoyuan, Taiwan, [3]Department of Psychiatry, Chang Gung Memorial Hospital, Linkou, Taiwan, [4]Laboratory of Brain Imaging and Neural Dynamics (BIND Lab), Chang Gung University, Taoyuan, Taiwan, [5]Brain Research Center, National Yang-Ming University, Taipei, Taiwan, [6]Department of Physical Medicine and Rehabilitation, Chang Gung Memorial Hospital, Linkou, Taiwan, [7]Division of General Neurology, Department of Neurological Institute, Taipei Veterans General Hospital, Taipei, Taiwan, [8]Department of Neurology, National Yang-Ming University, Taipei, Taiwan

Patients with amnestic mild cognitive impairment (aMCI) demonstrate significant cognitive deficits, especially in the memory aspect. The memory deficiency might be attributed to the difficulties in the inhibitory function to suppress redundant stimuli. Sensory gating (SG) refers to the attenuation of neural responses to the second identical stimulus in a paired-click paradigm, in which auditory stimuli are delivered in pairs with inter-stimulus intervals (ISI) of 500 ms and inter-pair intervals of 6–8 s. It is considered as an electrophysiological signal to reflect the brain's automatic response to gate out repetitive sensory inputs. However, there has been no study systematically investigating SG function in aMCI patients. Thus, the present study used magnetoencephalography (MEG) to record neuromagnetic responses to a paired-click paradigm in 23 healthy controls (HC) and 26 aMCI patients. The Stimulus 2/Stimulus 1 (S2/S1) amplitude ratio was used to represent the SG function. Compared to HC, aMCI patients showed M50 SG deficits in the left inferior frontal gyrus (IFG) and right inferior parietal lobule (IPL). M100 SG defects were also observed in the right IPL. Based on the ROIs showing significant between-group SG differences, we found that a more deficient M50 SG function in the right IPL was associated with poorer performance in the immediate recall of Logic Memory (LM), Chinese Version Verbal Learning Test (CVVLT) and Digit Span Backward (DSB) Test. Furthermore, the M50 SG ratios of the right IPL together with the neuropsychological performance of LM and CVVLT demonstrated very good accuracy in the discrimination of aMCI from HC. In conclusion, compared to HC, aMCI patients showed a significant SG deficit in the right IPL, which was correlated with the auditory short-term memory function. We suggest the combination of SG in the right IPL, LM and CVVLT to be sensitive indicators to differentiate aMCI patients from HC.

Keywords: sensory gating, mild cognitive impairment, aging, inhibitory control, magnetoencephalography (MEG)

OPEN ACCESS

Edited by:
Hans J. Grabe,
University of Greifswald, Germany

Reviewed by:
Yang Jiang,
University of Kentucky, United States
Can Sheng,
Tsinghua University, China

***Correspondence:**
Chia-Hsiung Cheng
ch.cheng@mail.cgu.edu.tw;
chiahsiung.cheng@gmail.com
Pei-Ning Wang
pnwang@vghtpe.gov.tw

Received: *11 June 2019*
Accepted: *06 February 2020*
Published: *25 February 2020*

Citation:
Cheng C-H, Hsiao F-J, Hsieh Y-W and Wang P-N (2020) Dysfunction of Inferior Parietal Lobule During Sensory Gating in Patients With Amnestic Mild Cognitive Impairment. Front. Aging Neurosci. 12:39. doi: 10.3389/fnagi.2020.00039

INTRODUCTION

Amnestic mild cognitive impairment (aMCI) is considered as an intermediate phase between normal aging and Alzheimer's disease (AD; Feldman et al., 2004; Petersen et al., 2014). Despite the intact function of activities of daily living, patients with aMCI are characterized by declined performance on standardized cognitive tests, particularly in the aspects of learning and memory. Inhibitory function plays a vital role in the memory performance since successful encoding and/or consolidation requires not only enhancement of task-relevant representations, but also suppression of task-irrelevant representations (Hasher and Zacks, 1988; Gazzaley et al., 2008; Chadick et al., 2014). Using functional magnetic resonance imaging (MRI), it has been shown that older adults demonstrated a relatively preserved capacity in the cortical enhancement of task-relevant stimuli, while a significant deficit in the top-down inhibition of cortical activities related to task-irrelevant stimuli (Gazzaley et al., 2005). Such a top-down inhibitory deficit was also found to be correlated with working memory performance (Gazzaley et al., 2005, 2008). In addition to top-down inhibitory function, bottom-up inhibition is a more fundamental ability in the early-stage information processing and may have an impact on the subsequent cognitive operations.

Sensory gating (SG) refers to the ability of the brain to automatically (i.e., bottom-up) inhibit the responses to the repetitive or redundant sensory inputs (Boutros and Belger, 1999; Cheng et al., 2015, 2016a, 2018). It has been proposed to serve as a protective mechanism against sensory inundation in the central nervous system (Patterson et al., 2008; Earls et al., 2016). SG is typically assessed in a paired-click paradigm in which two identical auditory stimuli are presented with an inter-stimulus interval (ISI) of 500 ms and an inter-pair interval of 6–8 s. Quantitatively, the amplitude ratio of the second stimulus (S2) over the first stimulus (S1; S2/S1) is calculated to reflect the SG function. A lower ratio reflects better performance in inhibiting irrelevant information (Cheng et al., 2016b, 2017b). In the electrophysiological recordings of auditory evoked potentials (AEPs), P50 (or its magnetic counterpart, M50) and N100 (or its magnetic counterpart, M100) are the two major components to assess SG. Since paired-click paradigm is a well-established and solid method, a number of clinical investigations have been conducted in patients with schizophrenia, and the results suggested a significant SG deficit either in the prodromal (Hsieh et al., 2012; van Tricht et al., 2015), acute (Devrim-Uçok et al., 2008; Oranje et al., 2013), or chronic (Brockhaus-Dumke et al., 2008; Micoulaud-Franchi et al., 2015) stage.

There have been some studies examining the SG function in neurodegenerative diseases, including dementia (Jessen et al., 2001; Cancelli et al., 2006; Thomas et al., 2010; Cheng et al., 2012; Josef Golubic et al., 2017). For example, Thomas and colleagues, recruiting 19 patients with probable AD and 17 healthy older adults, have revealed a significant P50 SG deficit in AD patients than in control subjects (Thomas et al., 2010). This result was similar to earlier reports in which mild AD (Cancelli et al., 2006) and moderate AD (Jessen et al., 2001) were studied. Regarding the association of SG function and neuropsychological assessments, a higher SG ratio (i.e., poorer inhibitory function) was reported to correlate with a more deficient performance on working memory, verbal fluency, and global cognitive function when AD and healthy older subjects were pooled together (Thomas et al., 2010; Josef Golubic et al., 2017). However, other studies failed to detect such a relationship (Jessen et al., 2001; Cancelli et al., 2006). Although previous studies have shown a deficit of SG in AD patients, there is no study, to the best of our knowledge, systematically investigating SG function by using paired-stimulus paradigm in patients with aMCI.

Considering the methodological issue, all of the aforementioned studies have applied electroencephalography (EEG) to compare SG ratios between AD and healthy controls (HC). With the limitation of electrode number and different conductivities of structures, it is less possible for EEG to probe the SG function at the source level. Magnetoencephalography (MEG), in contrast, has a better spatial resolution than EEG (Hari et al., 2010; Baillet, 2017) and therefore possesses a greater potential to disentangle the neural substrates underlying SG deficits. In addition, compared to the focal source modeling, the minimum norm estimate (MNE) is a distributed source imaging method, which can display a number of activated sources even when they overlap in time (Hämäläinen and Ilmoniemi, 1994). Thus, MNE has been considered to be a preferred strategy when analyzing multi-source evoked responses (Lin et al., 2006).

To be more specific, the goals of the present study were 3-fold. First, we attempted to test whether M50 and M100 SG ratios at the cortical level would be higher (i.e., worse function) in the patients with aMCI than those in the healthy older controls. Second, we sought to examine whether the regions exhibiting SG deficits would be associated with deteriorated neuropsychological performance, particularly those related to auditory short-term memory function because the memory impairment is the major clinical manifestation in aMCI patients. Finally, in order to differentiate aMCI from normal aging at the individual level, we further examined whether the SG ratio or its combination with short-term memory tests could serve as good indicators.

MATERIALS AND METHODS

Participants

A total of 23 community-dwelling elderly adults (nine males, mean age = 69.04 ± 1.77 years) were recruited as the HC group. A total of 26 aMCI patients (14 males, mean ages = 69.96 ± 1.78 years) were enrolled from the outpatient memory clinic of the Department of Neurology, Taipei Veterans General Hospital. Each subject was interviewed by the neurologist (P-NW) to obtain a clinical history and neuropsychological performance. MRI and laboratory examinations were used to rule out tumors, strokes, severe white matter diseases. All participants had no history of epilepsy, alcoholism, major psychiatric illness, poly-pharmacy, or other systematic diseases that potentially affect cognitive function. The aMCI patients fulfilled the Peterson criteria (Petersen et al., 1999). They had objective

memory impairment, MMSE ≥24, normal basic daily living activities, and without dementia (Wang et al., 2014). All of the subjects also reported no hearing impairment and normal or corrected-to-normal vision. Most of them were right-handed (handedness >80%) as evaluated by the Edinburg Inventory (Oldfield, 1971).

The present study was approved by the Institutional Review Board of Taipei Veterans General Hospital (Taipei, Taiwan), and was performed in accordance with approved guidelines and regulations. All the participants gave written informed consent after detailed descriptions of experimental procedures.

Neuropsychological Testing

All the studying subjects underwent thorough neuropsychological assessments, including: (1) Mini-Mental State Examination (MMSE), with the proposed cutoff score between HC and dementia of 23/24 (Kochhann et al., 2010); (2) Chinese Version Verbal Learning Test (CVVLT), in which the proposed cutoff point of total score between HC and dementia was 20/21 (Chang et al., 2010); (3) Logic Memory (LM) Test of Wechsler Memory Scale, which has been shown to be a sensitive measure for detecting MCI and AD (Rabin et al., 2009); (4) Boston Naming Test, whose normative data from geriatric performance has been established (Jefferson et al., 2007); (5) Rey-Osterrieth Complex Figure Test, with the proposed cutoff score delayed recall subscale between HC and MCI of 18/19 (Takayama, 2010); (6) Trail Making Test Part A and B, whose psychometric properties have also been established in Chinese version (Wei et al., 2018); (7) Digit Span Forward and Backward Test (Muangpaisan et al., 2010); and (8) Verbal Fluency Test, with the proposed cutoff score between HC and those with cognitive impairments (MCI and mild dementia) of 16/17 (Alegret et al., 2018). Apolipoprotein E ε4 (APOE 4) genotyping was also performed in all subjects. The detailed demographic and neuropsychological data were presented in **Table 1**.

TABLE 1 | Demographic variables and neuropsychological measures (mean ± SEM).

	HC (*n* = 23)	aMCI (*n* = 26)	*P*-values
Sex (male/female)	9/14	14/12	0.30
Age (years)	69.04 ± 1.77	69.96 ± 1.78	0.72
Education (years)	13.04 ± 0.72	11.12 ± 0.77	0.08
APOE 4 (yes/no)	5/18	4/21[a]	0.72
MMSE	28.83 ± 0.22	28.35 ± 0.25	0.16
STM	2.48 ± 0.15	2.27 ± 0.13	0.30
CVVLT			
Total	31.00 ± 0.73	25.88 ± 0.84	<0.001
Delayed	8.26 ± 0.19	6.46 ± 0.30	<0.001
WMS Logic memory			
Immediate	15.78 ± 0.80	10.04 ± 0.78	<0.001
Delayed	14.96 ± 0.84	7.81 ± 0.77	<0.001
CFT			
Copy	32.48 ± 0.52	31.69 ± 0.66	0.36
Immediate	25.15 ± 1.25	19.52 ± 1.46	0.006
Delayed	24.74 ± 1.34	18.38 ± 1.44	0.002
VFT-animal	19.26 ± 0.92	15.46 ± 1.01	0.008
BNT			
Spontaneous	27.09 ± 0.54	26.85 ± 0.54	0.75
Semantic cues	0.39 ± 0.15	0.19 ± 0.10	0.26
Phonemic cues	1.52 ± 0.29	1.46 ± 0.31	0.89
Digit Span Test			
Forward	8.39 ± 0.24	8.00 ± 0.21	0.23
Backward	5.61 ± 0.34	4.65 ± 0.27	0.03
Trail Making Test			
Part A (s)	16.83 ± 3.49	12.92 ± 0.85	0.29
Part B (s)	36.74 ± 5.65	48.23 ± 5.48	0.15

SEM, standard error of the mean; HC, healthy control; aMCI, amnestic mild cognitive impairment; STM, short-term memory; CVVLT, Chinese Version Verbal Learning Test; WMS-Logic memory, Wechsler Memory Scale-Logic memory; CFT, Rey-Osterrieth Complex Figure Test; VFT-animal, Verbal Fluency Test-animal; BNT, Boston Naming Test.
[a]The blood test from one aMCI patient was not valid.

MEG Recordings

During MEG recordings, a paired-stimulus paradigm was presented to the subjects by means of Presentation software (version 11.3, Neurobehavioral System Inc., Davis, CA, USA). Stimuli consisted of a series of pairs of identical click-like tones (800 Hz, ISI = 500 ms, inter-pair interval = 6 s) and were binaurally delivered at the intensity of 60–70 dB through plastic earphones. Subjects were instructed to watch a silent, emotionally-neutral movie with subtitles and to ignore the auditory stimuli.

AEFs were recorded with a whole-head 306-channel MEG (Vectorview, Elekta-Neuromag, Helsinki, Finland). The sampling rate and online bandpass filter were set at 1,000 Hz and (0.1, 200) Hz, respectively. The head position in relation to MEG sensors was measured by four head position indicators (HPIs) attached to known sites on the scalp. The sites of three fiducial points (i.e., nasion, left and right preauricular points) and scalp surface were localized with a 3-D digitizer to allow alignment of the MEG and MRI coordinate systems. Electrooculograms (EOGs) attached above the left orbit and below the right orbit were used to monitor eye movements. In addition, heartbeats were recorded by electrocardiograms (ECGs). At least 100 pairs were collected from each participant for further analysis.

MEG Data Analysis

In order to reduce the artifacts originating inside the device and external interferences outside the sensors, we applied MaxFilter from the Neuromag software system (Taulu et al., 2004; Taulu and Simola, 2006). Furthermore, all the acquired raw data contaminated by eye blinks and heartbeats were removed by using signal space projections (SSP), with the default setting in the Brainstorm software (Tadel et al., 2011).

The averaged AEFs were then offline filtered with a bandpass (1, 30) Hz, with a 100-ms baseline correction. The M50 peak was defined as the maximal response between 30 and 80 ms after the stimulus onset, and the M100 peak was defined as the maximal response between 70 and 160 ms after the stimulus onset.

The source activities of neuromagnetic data were analyzed by using depth-weighted MNE (Hämäläinen and Ilmoniemi, 1994) implemented in the Brainstorm software. The forward problem of MEG measures was resolved by the overlapping-sphere model (Huang et al., 1999), which estimates the strength of electrical dipoles located at the cortical surfaces. The noise covariance in the source estimation was calculated directly from the recordings. For each participant, the cortical-constraint MNE was computed over a set of ∼15,000 dipoles distributed

over the cortical envelope. Based on the prior knowledge from literature and our grand-averaged MNE results, a cluster of 30 vertices of 4–5 cm^2 were manually selected to define regions of interest (ROIs) for M50 and M100, including bilateral superior temporal gyrus (STG; Edgar et al., 2003; Cheng et al., 2017a), bilateral middle temporal gyrus (MTG; Boutros et al., 2013; Cheng et al., 2015), bilateral inferior frontal gyrus (IFG; Garcia-Rill et al., 2008; Bak et al., 2014), and bilateral inferior parietal lobule (IPL; Boutros et al., 2013; Cheng et al., 2015). Although these anatomical structures cover a relatively wide area of cortical surfaces, the maximal activation cluster of each ROI in response to S1 was used as the center of the scout for both M50 and M100 from each participant. This method allowed us to extract the largest amplitudes of M50 and M100 to calculate SG ratios in each ROI.

In order to obtain the MNE source maps with a better signal-to-noise ratio, the time-resolved magnitude of each dipole was normalized to its baseline, yielding *z*-score values at each cortical location. The *z* scores were rectified to produce absolute magnitude changes above baseline levels. The peak response to S1 and S2 were extracted from each participant at the identified ROIs, and the SG ratio was derived from S2/S1 in the M50 and M100 components.

Statistical Analysis

All the data were presented as mean ± standard error of the mean (SEM). All variables included in the final analysis were normally distributed as verified by the Kolmogorov-Smirnov test ($Z < 1.168$, $p > 0.131$). The differences of SG ratios (M50 and M100) between HC and aMCI groups were compared by means of independent *t*-test in each identified ROI. Based on the ROIs with significant between-group differences, partial correlations, with age, gender and years of education as covariates, were used to further investigate the relationship between SG ratios and auditory short-term memory assessments, such as CVVLT, Digit Span Backward (DSB), and immediate recall of LM Test. Finally, we applied receiver operator characteristic (ROC) curve analysis to test if the SG ratio or its combination with auditory short-term memory tests could differentiae aMCI from HC. For the area under the curve (AUC), AUC between 0.5 and 0.7 was considered less accurate, AUC between 0.7 and 0.9 was considered moderately accurate, and AUC above 0.9 was considered very accurate (Greiner et al., 2000). A *p*-value < 0.05 (two-tailed) was considered to be statistically significant. In the correlational analysis, *p*-values were corrected for multiple comparisons by the *Benjamini and Hochberg approach* (Benjamini and Hochberg, 1995).

RESULTS

The two study groups did not significantly differ by age, gender, years of education, APOE 4 carrier distribution and MMSE scores. However, the patients with aMCI performed worse than HC in most of the neuropsychological tests, including CVVLT, LM Test of Wechsler Memory Scale, Rey-Osterrieth Complex Figure Test, Verbal Fluency Test, and DSB Test (**Table 1**).

The upper panel of **Figure 1** displays the grand-averaged AEFs to paired-click stimulation in the HC ($n = 23$) and aMCI ($n = 26$) groups. Compared to S1, neuromagnetic responses to S2 were reduced in both M50 and M100 components, either in the HC or aMCI subjects. The lower panel of **Figure 1** shows the MNE source maps of M50 and M100 components. In addition to the temporal cortex, several regions of parietal and frontal cortices were activated to paired-click stimulation.

We further compared the SG ratios between the two groups in the identified ROIs (**Figure 2**). There were no significant differences in the STG and MTG. However, we found that compared to HC, patients with aMCI demonstrated conspicuously higher M50 SG ratios in the left IFG ($t = 2.063$, $p = 0.045$) and right IPL ($t = 3.726$, $p = 0.001$). As for M100 SG, a significant between-group difference was also found in the right IPL ($t = 3.550$, $p = 0.001$).

Since the significant between-group differences were found in the left IFG and right IPL, we further investigated whether SG ratios in these ROIs would show associations with neuropsychological assessments in which auditory short-term memory function was involved. M50 SG ratios of the left IFG and M100 SG ratios of right IPL did not show any significant correlation with neuropsychological performance after the correction of multiple comparisons. M50 SG ratios in the right IPL were significantly correlated with scores of LM (immediate recall, $r = -0.436$, adjusted $p = 0.006$), CVVLT ($r = -0.372$, adjusted $p = 0.011$), and DSB ($r = -0.292$, adjusted $p = 0.049$; **Figure 3**).

The AUC of M50 SG ratio of the right IPL was 0.791 (sensitivity = 0.846, specificity = 0.609), considered moderately accurate. Furthermore, this M50 SG ratio in combination with LM scores (AUC = 0.891, sensitivity = 0.885, specificity = 0.783) or CVVLT scores (AUC = 0.870, sensitivity = 0.846, specificity = 0.870) improved the discrimination ability (**Figure 4**). It was notable that the M50 SG ratio together with LM and CVVLT scores reached a very accurate ability in the discrimination of aMCI from HC (AUC = 0.915, sensitivity = 0.923, specificity = 0.783). **Table 2** shows the detailed results of the ROC curve analysis.

DISCUSSION

This study compared the pre-attentive SG function between HC and aMCI at the source level and attempted to determine whether the SG ratios would be correlated with neuropsychological tests in which auditory short-term memory was involved. Our data yielded three major findings. First, compared to HC, patients with aMCI demonstrated deficient SG function in the left IFG and right IPL. Based on the aforementioned ROIs showing obvious between-group differences, M50 SG ratios of the right IPL were significantly correlated with the performance of short-term memory tests. Finally, ROC curve analysis revealed that the combination of the M50 SG ratio in the right IPL, LM and CVVLT had very good accuracy in differentiating aMCI from HC.

SG deficits have been evident in patients with AD (Jessen et al., 2001; Cancelli et al., 2006; Thomas et al., 2010; Cheng

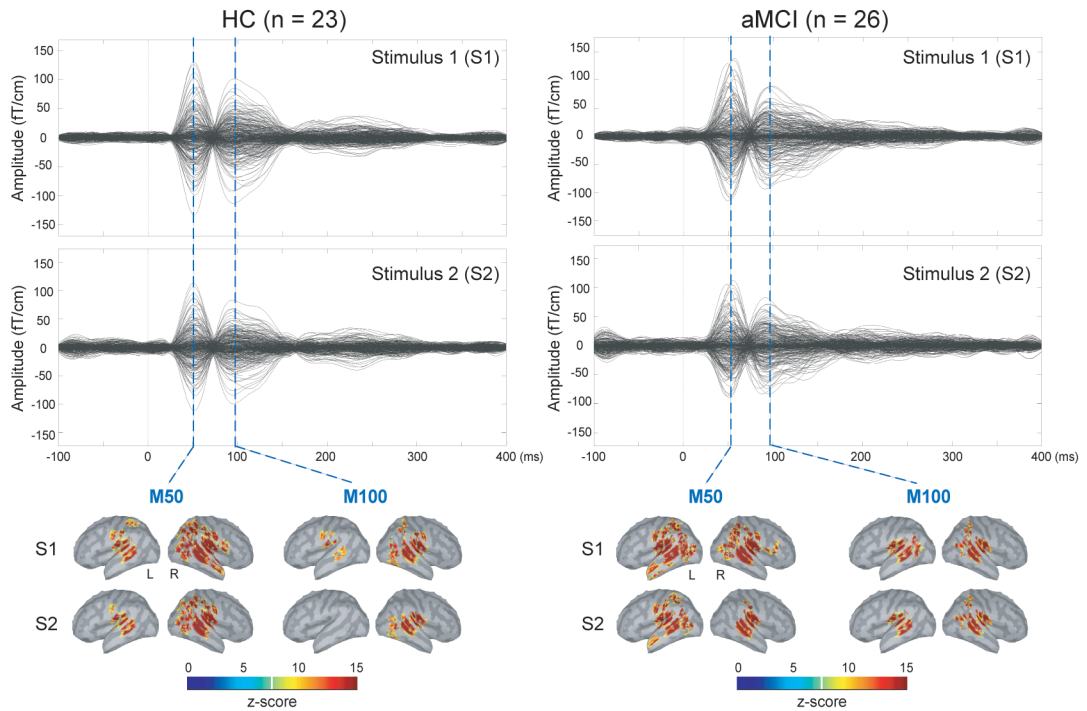

FIGURE 1 | Upper panel: grand-averaged sensor waveforms of the auditory paired-stimulus paradigm in healthy controls (HC) and patients with amnestic mild cognitive impairment (aMCI). Lower panel: spatiotemporal dynamics of minimum norm estimate (MNE) regarding the M50 and M100 components. The cortical surfaces have been smoothed for better visualization (dark gray, sulci; light gray, gyri). L, left hemisphere; R, right hemisphere.

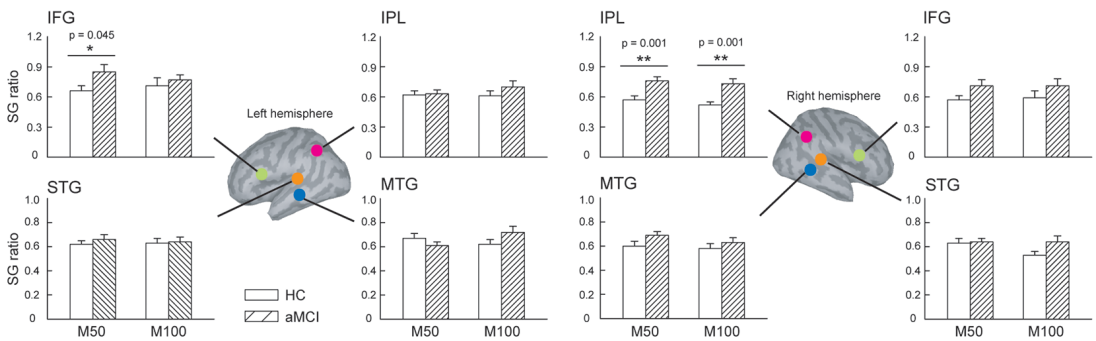

FIGURE 2 | The regions of interest (ROIs) were manually identified in the bilateral superior temporal gyrus (STG), middle temporal gyrus (MTG), inferior frontal gyrus (IFG), and inferior parietal lobule (IPL) to study sensory gating (SG). Compared to HC, patients with aMCI demonstrated significantly higher M50 SG in the left IFG and right IPL. As for the M100 component, aMCI patients also showed an elevated SG ratio. These results suggest a deficit of inhibitory function in this clinical population. $^{*}p < 0.05$, $^{**}p < 0.01$.

et al., 2012), whereas the relevant investigation on aMCI is extremely scarce. One of the major reasons is possibly due to the insensitivity of the recording instruments. In the previous EEG studies, midline electrodes, such as Fz or Cz, were analyzed to reflect the electrophysiological activities from the summation of temporal and frontal sources. Mastoid electrodes, on the other hand, were considered as a pure indicator of the temporal generators when the auditory evoked potentials were studied (Kujala and Näätänen, 2001; Cooper et al., 2006). However, the SG deficiency in the aMCI, compared to the control subjects, might not be obvious enough that can be detected by EEG electrodes. The advantage of MEG in its superior spatial resolution covers the weakness of EEG in the aspect of source localization. Our current MEG data, to some extent, supported this account since we did not find the significant between-group SG differences in the bilateral STG and MTG, both of which were considered as main neural generators of SG (Edgar et al., 2003; Cheng et al., 2017a).

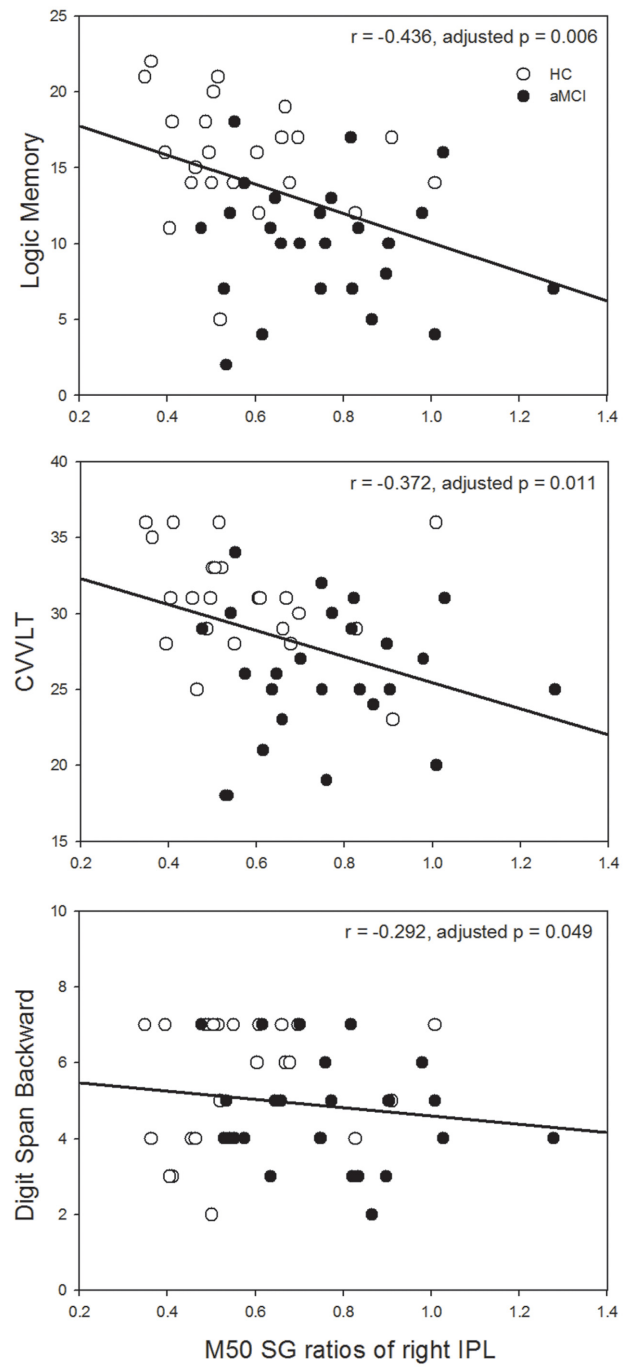

FIGURE 3 | Higher M50 SG ratios in the right IPL were significantly associated with the worse performance of the Logic Memory (LM) Test (immediate recall), Chinese Version Verbal Learning Test (CVVLT), and Digit Span Backward (DSB) Test. HC, healthy control; aMCI, amnestic mild cognitive impairment.

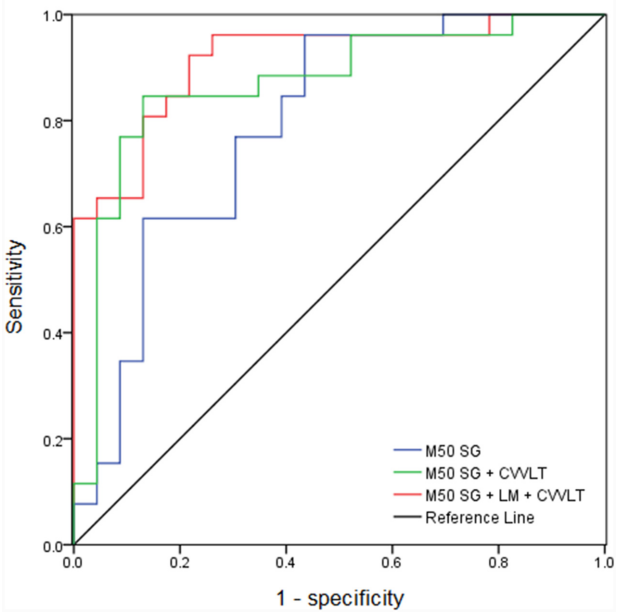

FIGURE 4 | Receiver operator characteristic (ROC) curves of M50 SG ratio in the right IPL alone and its combination with scores of CVVLT and immediate recall of LM.

Instead, compared to the HC, aMCI showed a deficient SG function in the left IFG and right IPL. These findings suggested that reduced SG function in aMCI was attributed to the information processing deficits in the relatively higher-order centers (e.g., IFG and IPL), rather than basic sensory centers (e.g., STG and MTG).

Regarding the reduced M50 SG function of the IFG in aMCI patients, there are two plausible accounts to interpret our data. A prevailing contention is the inhibitory deficit hypothesis due to frontal dysfunction (Hasher and Zacks, 1988; Alain and Woods, 1999; Stothart and Kazanina, 2016). Compared to the younger adults, the elderly have been reported to demonstrate significantly larger P50 and/or N100 amplitudes to repetitive auditory stimulation (Chao and Knight, 1997). Furthermore, subjects with prefrontal damages showed an enhancement of P50 and/or N100 amplitudes to frequent auditory stimuli (Knight, 1984; Alho et al., 1994). Another account is the predictive coding hypothesis (Garrido et al., 2009; Grotheer and Kovács, 2016). SG or repetition suppression is an indicator of error minimization occurring when bottom-up sensory inputs from the level below (e.g., temporal cortex) coincide with the top-down predictions from the level above (e.g., frontal cortex; Friston, 2005; Auksztulewicz and Friston, 2016). Upon repetitive stimulation, the predictive error is reduced by adjusting synaptic activities within and between multiple hierarchical levels. By using a paired-stimulus paradigm, our data indicated that compared to the HC, aMCI patients exhibited higher SG ratios in the IFG, suggesting such inhibitory deficit may be indicative of a deficiency of top-down processing according to the predictive coding hypothesis.

The neurophysiological meanings regarding the reduced M50 and M100 SG of the IPL in aMCI patients remain extremely elucidative. First of all, it should be noted that the IPL is involved in the SG function. Using the grid and strip electrodes on the cerebral cortex, Boutros and colleagues

TABLE 2 | ROC curve analysis with the combination of different variables.

	AUC	Sensitivity	Specificity
M50 SG	0.791	0.846	0.609
M50 SG + LM	0.891	0.885	0.783
M50 SG + CVVLT	0.870	0.846	0.870
M50 SG + DSB	0.834	0.885	0.739
M50 SG + LM + CVVLT	0.915	0.923	0.783
M50 SG + LM + DSB	0.893	0.885	0.739
M50 SG + CVVLT + DSB	0.891	0.885	0.826
M50 SG + LM + CVVLT + DSB	0.916	0.885	0.826

ROC, receiver operator characteristic; M50 SG, M50 sensory gating ratio in the right inferior parietal lobule; LM, Logic Memory; CVVLT, Chinese Version Verbal Learning Test, DSB, Digit Span Backward; AUC, area under the curve.

have reported that in addition to the temporal lobe, the parietal cortex was part of neural circuits underlying P50 SG (Boutros et al., 2013) and N100 SG (Boutros et al., 2011). Our previous MEG study, by identifying a number of ROIs, has also found that S2-evoked M100 amplitude was significantly lower than S1-evoked M100 amplitude in the IPL among the younger adults (Cheng et al., 2015). The functional role of the IPL may be related to the monitoring of the information originating from other sensory cortex (Balslev et al., 2006; Schnell et al., 2007). In our previous MEG study, we did not observe age-related M100 SG differences in the IPL, suggesting healthy aging does not interfere with this function. However, when the pathological aging occurred, such as aMCI, SG was apparently deteriorated and could be detected at the basis of group comparisons. In addition, it should be noted that the AD-related pathologies occur a couple of years prior to the clinical manifestations. Also, the preclinical state can be longer than 2–3 years. Subjective cognitive decline (SCD), a self-perceived worsening in cognitive capacity along with normal performance on standardized cognitive assessments, has gained much attention over the past decade. It will be of clinical importance for future studies to investigate whether older adults with SCD show an altered auditory SG ability compared to those without SCD.

Based on the ROIs showing significant between-group SG differences, we further explored the relationships between SG and auditory short-term memory tests. Although there were several studies investigating the correlations between SG and all kinds of neuropsychological tests (Smith et al., 2010; Thomas et al., 2010; Hamilton et al., 2018), the present study only selected those in which auditory short-term memory was assessed since these cognitive assessments and SG were tested through the auditory modality. We found that M50 SG ratios of the right IPL were significantly correlated with the performance of short-term memory function (**Figure 3**). These results were consistent with previous studies showing that lower P50 SG and/or N100 SG ratios (i.e., better SG function) were related to better performance of attention and working memory in patients with schizophrenia (Smith et al., 2010; Hamilton et al., 2018). As for the AD patients, gating deficit has been related to the poor performance of DSB when healthy elderly and AD subjects were pooled together (Thomas et al., 2010). The novel result of the present study was that such an association was specifically observed in the IPL. Previous studies have applied regional homogeneity (ReHo) to measure local coherence of spontaneous brain activity and found that compared to HC, aMCI patients demonstrated reduced ReHo in the IPL (Zhang et al., 2012; Yuan et al., 2016). By analyzing the n-back working memory paradigm, a previous coordinate-based meta-analysis has shown that bilateral IPL was consistently activated across all the studies (Wang et al., 2019). In addition, a delicate study tracking cognitive changes over 6 months with longitudinal functional MRI data revealed a significant correlation between performance changes in free recall and brain activation changes in the IPL (McLaren et al., 2012). Taken together, our results suggest the critical role of IPL, particularly the right hemisphere, in the relationship between neurophysiological SG function and short-term memory performance.

We considered M50 SG in the right IPL as an acceptable neurophysiological indicator (AUC = 0.791, sensitivity = 0.846, specificity = 0.609) in differentiating aMCI from HC. A previous study applying another electrophysiological signal, called mismatch negativity (MMN), has revealed a similar accurate level as ours. More specifically, they found the MMN amplitude, but not latency, to be a reasonable biomarker (AUC = 0.76 for the first evaluation and AUC = 0.82 for the second evaluation; Lindín et al., 2013) for the discrimination between aMCI and middle-aged controls. In our present study, M50 SG ratios of the right IPL together with the LM and CVVLT further improved the discriminative accuracy. We suggest the combination of SG of the right IPL, LM and CVVLT to be sensitive indicators to differentiate aMCI patients from HC.

Conceptually, it is interesting to discuss the similarities/differences of the terminologies including SG and repetition priming (RP). Generally speaking, the aforementioned terms refer to the same phenomenon that the neural responses would be reduced after the repeated stimuli. However, based on different experimental paradigms or academic fields, there are somewhat different descriptions and meanings. The RP is usually studied with the semantic judgment task or working memory task, in which the subjects are required to respond to targets (Olichney et al., 2000, 2008; Yang et al., 2014; Broster et al., 2018). A stronger repetition effect (e.g., higher accuracy rate or shortened reaction time to the subsequently repeated stimuli, reduced amplitude after the repeated stimuli, etc.) indicates better memory-related performance since the N400 and/or P600 components are measured (Olichney et al., 2000, 2008; Yang et al., 2014). The SG is usually studied with the auditory (Smith et al., 2013; Rosburg, 2018) and somatosensory (Kisley and Cornwell, 2006; Cheng and Lin, 2013) paired-click paradigms, in which the subjects do not require to make a behavioral response. A lower ratio, that is more neural suppression to the repeated stimuli, indicates better SG function. Due to the independence of the behavioral requirement, SG has been widely studied in the clinical populations who have difficulties in maintaining attention and motivation. In our present study, aMCI and HC did not show significant differences of SG ratios in the primary sensory cortex (i.e., STG) but in the IPL, which was consistent with a previous report showing that patients with AD demonstrated spared repetition effect in the

primary visual cortex (Broster et al., 2018). These findings also supported the prevailing notion that during neurodegenerative processes, most of the cortices (frontal cortices, parietal cortices, cingulate regions) apart from primary cortices have experienced major pathophysiological changes.

Several limitations of the present study must be acknowledged. First, the sample size was relatively small, which might impede us to find significant differences of APOE 4 carrier distribution between HC and aMCI. Previous large-scale studies have suggested that compared to the healthy older adults, the prevalence of APOE 4 was increased in patients with aMCI (van der Flier et al., 2008; Edmonds et al., 2015). Second, the individual's hearing threshold was not collected in this study. Despite self-reportedly no obvious hearing impairments from our participants, we could not rule out the possibilities of hearing acuity on central auditory processes due to aging. However, it has been shown no significant age-related differences in hearing threshold at 1,000 Hz (Horváth et al., 2009). All of our subjects were older adults, which represented a more homogeneous sample in terms of auditory acuity. It was also important to note that the frequency we used in the present study was 800 Hz so that all the participants could successfully register the auditory inputs. Finally, the significant associations between neurophysiological function and neuropsychological performance did not allow us to infer their causality. Future research, which investigates whether the changes of SG will show concomitant changes along with the neuropsychological performance, is needed.

In conclusion, compared to HC, aMCI patients exhibited SG deficits, particularly in the right IPL. Such a deficiency was also related to the immediate recall of auditory memory tests. Our data further highlighted the importance of the combination of SG ratios and short-term memory tests in the discrimination between HC and aMCI.

DATA AVAILABILITY STATEMENT

All datasets generated for this study are included in the article.

ETHICS STATEMENT

The studies involving human participants were reviewed and approved by Institutional Review Board of Taipei Veterans General Hospital (Taipei, Taiwan). The patients/participants provided their written informed consent to participate in this study.

AUTHOR CONTRIBUTIONS

C-HC and P-NW conceived and design the work and wrote the article. C-HC acquired the data. C-HC, F-JH, and Y-WH analyzed the data and participated in the discussion and provided the comments. All of the authors have read and approved the manuscript.

FUNDING

This work was supported by Chang Gung Memorial Hospital (CMRPD1E0291, CMRPD1E0292, CMRPD1E0293, CMRPD1E0294), Chang Gung University (BMRPE25), Healthy Aging Research Center, Chang Gung University from the Featured Areas Research Center Program within the Framework of the Higher Education Sprout Project by the Ministry of Education (MOE) in Taiwan (EMRPD1I0451), Ministry of Science and Technology (MOST-104-2314-B-182-001-MY2, MOST-105-2628-B-182-004-MY3), and the Brain Research Center, National Yang-Ming University from The Featured Areas Research Center Program within the Framework of the Higher Education Sprout Project by the Ministry of Education (MOE) in Taiwan.

ACKNOWLEDGMENTS

We thank Chih-Che Chou (IBRU, Taipei Veterans General Hospital) for the technical assistance in MEG signal calibration.

REFERENCES

Alain, C., and Woods, D. L. (1999). Age-related changes in processing auditory stimuli during visual attention: evidence for deficits in inhibitory control and sensory memory. *Psychol. Aging* 14, 507–519. doi: 10.1037/0882-7974.14.3.507

Alegret, M., Peretó, M., Pérez, A., Valero, S., Espinosa, A., Ortega, G., et al. (2018). The role of verb fluency in the detection of early cognitive impairment in Alzheimer's disease. *J. Alzheimers Dis.* 62, 611–619. doi: 10.3233/JAD-170826

Alho, K., Woods, D. L., Algazi, A., Knight, R. T., and Naatanen, R. (1994). Lesions of frontal cortex diminish the auditory mismatch negativity. *Electroencephalogr. Clin. Neurophysiol.* 91, 353–362. doi: 10.1016/0013-4694(94)00173-1

Auksztulewicz, R., and Friston, K. (2016). Repetition suppression and its contextual determinants in predictive coding. *Cortex* 80, 125–140. doi: 10.1016/j.cortex.2015.11.024

Baillet, S. (2017). Magnetoencephalography for brain electrophysiology and imaging. *Nat. Neurosci.* 20, 327–339. doi: 10.1038/nn.4504

Bak, N., Rostrup, E., Larsson, H. B., Glenthoj, B. Y., and Oranje, B. (2014). Concurrent functional magnetic resonance imaging and electroencephalography assessment of sensory gating in schizophrenia. *Hum. Brain Mapp.* 35, 3578–3587. doi: 10.1002/hbm.22422

Balslev, D., Nielsen, F. A., Lund, T. E., Law, I., and Paulson, O. B. (2006). Similar brain networks for detecting visuo-motor and visuo-proprioceptive synchrony. *NeuroImage* 31, 308–312. doi: 10.1016/j.neuroimage.2005.11.037

Benjamini, Y., and Hochberg, Y. (1995). Controlling the false discovery rate: a practical and powerful approach to multiple testing. *J. R. Statist. Soc. B* 57, 289–300. doi: 10.1111/j.2517-6161.1995.tb02031.x

Boutros, N. N., and Belger, A. (1999). Midlatency evoked potentials attenuation and augmentation reflect different aspects of sensory gating. *Biol. Psychiatry* 45, 917–922. doi: 10.1016/s0006-3223(98)00253-4

Boutros, N. N., Gjini, K., Eickhoff, S. B., Urbach, H., and Pflieger, M. E. (2013). Mapping repetition suppression of the P50 evoked response to the human cerebral cortex. *Clin. Neurophysiol.* 124, 675–685. doi: 10.1016/j.clinph.2012.10.007

Boutros, N. N., Gjini, K., Urbach, H., and Pflieger, M. E. (2011). Mapping repetition suppression of the N100 evoked response to the human cerebral cortex. *Biol. Psychiatry* 69, 883–889. doi: 10.1016/j.biopsych.2010.12.011

Brockhaus-Dumke, A., Schultze-Lutter, F., Mueller, R., Tendolkar, I., Bechdolf, A., Pukrop, R., et al. (2008). Sensory gating in schizophrenia: P50 and N100 gating in antipsychotic-free subjects at risk, first-episode and chronic patients. *Biol. Psychiatry* 64, 376–384. doi: 10.1016/j.biopsych.2008.02.006

Broster, L. S., Li, J., Wagner, B., Smith, C. D., Jicha, G. A., Schmitt, F. A., et al. (2018). Spared behavioral repetition effects in Alzheimer's disease linked to an altered neural mechanism at posterior cortex. *J. Clin. Exp. Neuropsychol.* 40, 761–776. doi: 10.1080/13803395.2018.1430230

Cancelli, I., Cadore, I. P., Merlino, G., Valentinis, L., Moratti, U., Bergonzi, P., et al. (2006). Sensory gating deficit assessed by P50/Pb middle latency event related potential in Alzheimer's disease. *J. Clin. Neurophysiol.* 23, 421–425. doi: 10.1097/01.wnp.0000218991.99714.ee

Chadick, J. Z., Zanto, T. P., and Gazzaley, A. (2014). Structural and functional differences in medial prefrontal cortex underlie distractibility and suppression deficits in ageing. *Nat. Commun.* 5:4223. doi: 10.1038/ncomms5223

Chang, C. C., Kramer, J. H., Lin, K. N., Chang, W. N., Wang, Y. L., Huang, C. W., et al. (2010). Validating the Chinese version of the verbal learning test for screening Alzheimer's disease. *J. Int. Neuropsychol. Soc.* 16, 244–251. doi: 10.1017/S1355617709991184

Chao, L. L., and Knight, R. T. (1997). Prefrontal deficits in attention and inhibitory control with aging. *Cereb. Cortex* 7, 63–69. doi: 10.1093/cercor/7.1.63

Cheng, C. H., Baillet, S., and Lin, Y. Y. (2015). Region-specific reduction of auditory sensory gating in older adults. *Brain Cogn.* 101, 64–72. doi: 10.1016/j.bandc.2015.10.004

Cheng, C. H., Chan, P. S., Liu, C. Y., and Hsu, S. C. (2016a). Auditory sensory gating in patients with bipolar disorders: a meta-analysis. *J. Affect. Disord.* 203, 199–203. doi: 10.1016/j.jad.2016.06.010

Cheng, C. H., Chan, P. Y., Niddam, D. M., Tsai, S. Y., Hsu, S. C., and Liu, C. Y. (2016b). Sensory gating, inhibition control and gamma oscillations in the human somatosensory cortex. *Sci. Rep.* 6:20437. doi: 10.1038/srep20437

Cheng, C. H., and Lin, Y. Y. (2013). Aging-related decline in somatosensory inhibition of the human cerebral cortex. *Exp. Brain Res.* 226, 145–152. doi: 10.1007/s00221-013-3420-9

Cheng, C. H., Lin, M. Y., and Yang, S. H. (2018). Age effect on automatic inhibitory function of the somatosensory and motor cortex: an MEG study. *Front. Aging Neurosci.* 10:53. doi: 10.3389/fnagi.2018.00053

Cheng, C. H., Niddam, D. M., Hsu, S. C., Liu, C. Y., and Tsai, S. Y. (2017a). Resting GABA concentration predicts inhibitory control during an auditory Go-Nogo task. *Exp. Brain Res.* 235, 3833–3841. doi: 10.1007/s00221-017-5101-6

Cheng, C. H., Tsai, S. Y., Liu, C. Y., and Niddam, D. M. (2017b). Automatic inhibitory function in the human somatosensory and motor cortices: an MEG-MRS study. *Sci. Rep.* 7:4234. doi: 10.1038/s41598-017-04564-1

Cheng, C. H., Wang, P. N., Hsu, W. Y., and Lin, Y. Y. (2012). Inadequate inhibition of redundant auditory inputs in Alzheimer's disease: an MEG study. *Biol. Psychol.* 89, 365–373. doi: 10.1016/j.biopsycho.2011.11.010

Cooper, R. J., Todd, J., McGill, K., and Michie, P. T. (2006). Auditory sensory memory and the aging brain: a mismatch negativity study. *Neurobiol. Aging* 27, 752–762. doi: 10.1016/j.neurobiolaging.2005.03.012

Devrim-Uçok, M., Keskin-Ergen, H. Y., and Uçok, A. (2008). P50 gating at acute and post-acute phases of first-episode schizophrenia. *Prog. Neuropsychopharmacol. Biol. Psychiatry* 32, 1952–1956. doi: 10.1016/j.pnpbp.2008.09.018

Earls, H. A., Curran, T., and Mittal, V. (2016). A meta-analytic review of auditory event-related potential components as endophenotypes for schizophrenia: perspectives from first-degree relatives. *Schizophr. Bull.* 42, 1504–1516. doi: 10.1093/schbul/sbw047

Edgar, J. C., Huang, M. X., Weisend, M. P., Sherwood, A., Miller, G. A., Adler, L. E., et al. (2003). Interpreting abnormality: an EEG and MEG study of P50 and the auditory paired-stimulus paradigm. *Biol. Psychol.* 65, 1–20. doi: 10.1016/s0301-0511(03)00094-2

Edmonds, E. C., Delano-Wood, L., Clark, L. R., Jak, A. J., Nation, D. A., McDonald, C. R., et al. (2015). Susceptibility of the conventional criteria for mild cognitive impairment to false-positive diagnostic errors. *Alzheimers Dement.* 11, 415–424. doi: 10.1016/j.jalz.2014.03.005

Feldman, H., Scheltens, P., Scarpini, E., Hermann, N., Mesenbrink, P., Mancione, L., et al. (2004). Behavioral symptoms in mild cognitive impairment. *Neurology* 62, 1199–1201. doi: 10.1212/01.wnl.0000118301.92105.ee

Friston, K. (2005). A theory of cortical responses. *Philos. Trans. R. Soc. Lond. B Biol. Sci.* 360, 815–836. doi: 10.1098/rstb.2005.1622

Garcia-Rill, E., Moran, K., Garcia, J., Findley, W. M., Walton, K., Strotman, B., et al. (2008). Magnetic sources of the M50 response are localized to frontal cortex. *Clin. Neurophysiol.* 119, 388–398. doi: 10.1016/j.clinph.2007.10.027

Garrido, M. I., Kilner, J. M., Kiebel, S. J., Stephan, K. E., Baldeweg, T., and Friston, K. J. (2009). Repetition suppression and plasticity in the human brain. *NeuroImage* 48, 269–279. doi: 10.1016/j.neuroimage.2009.06.034

Gazzaley, A., Clapp, W., Kelley, J., McEvoy, K., Knight, R. T., and D'Esposito, M. (2008). Age-related top-down suppression deficit in the early stages of cortical visual memory processing. *Proc. Natl. Acad. Sci. U S A* 105, 13122–13126. doi: 10.1073/pnas.0806074105

Gazzaley, A., Cooney, J. W., Rissman, J., and D'Esposito, M. (2005). Top-down suppression deficit underlies working memory impairment in normal aging. *Nat. Neurosci.* 8, 1298–1300. doi: 10.1038/nn1543

Greiner, M., Pfeiffer, D., and Smith, R. D. (2000). Principles and practical application of the receiver-operating characteristic analysis for diagnostic tests. *Prev. Vet. Med.* 45, 23–41. doi: 10.1016/s0167-5877(00)00115-x

Grotheer, M., and Kovács, G. (2016). Can predictive coding explain repetition suppression? *Cortex* 80, 113–124. doi: 10.1016/j.cortex.2015.11.027

Hämäläinen, M. S., and Ilmoniemi, R. J. (1994). Interpreting magnetic fields of the brain: minimum norm estimates. *Med. Biol. Eng. Comput.* 32, 35–42. doi: 10.1007/bf02512476

Hamilton, H. K., Williams, T. J., Ventura, J., Jasperse, L. J., Owens, E. M., Miller, G. A., et al. (2018). Clinical and cognitive significance of auditory sensory processing deficits in schizophrenia. *Am. J. Psychiatry* 175, 275–283. doi: 10.1176/appi.ajp.2017.16111203

Hari, R., Parkkonen, L., and Nangini, C. (2010). The brain in time: insights from neuromagnetic recordings. *Ann. N Y Acad. Sci.* 1191, 89–109. doi: 10.1111/j.1749-6632.2010.05438.x

Hasher, L., and Zacks, R. (1988). Working memory, comprehension and aging: a review and a new view. *Psychol. Learn. Motiv.* 22, 193–225. doi: 10.1016/s0079-7421(08)60041-9

Horváth, J., Czigler, I., Birkas, E., Winkler, I., and Gervai, J. (2009). Age-related differences in distraction and reorientation in an auditory task. *Neurobiol. Aging* 30, 1157–1172. doi: 10.1016/j.neurobiolaging.2007.10.003

Hsieh, M. H., Shan, J. C., Huang, W. L., Cheng, W. C., Chiu, M. J., Jaw, F. S., et al. (2012). Auditory event-related potential of subjects with suspected pre-psychotic state and first-episode psychosis. *Schizophr. Res.* 140, 243–249. doi: 10.1016/j.schres.2012.06.021

Huang, M. X., Mosher, J. C., and Leahy, R. M. (1999). A sensor-weighted overlapping-sphere head model and exhaustive head model comparison for MEG. *Phys. Med. Biol.* 44, 423–440. doi: 10.1088/0031-9155/44/2/010

Jefferson, A. L., Wong, S., Gracer, T. S., Ozonoff, A., Green, R. C., and Stern, R. A. (2007). Geriatric performance on an abbreviated version of the Boston naming test. *Appl. Neuropsychol.* 14, 215–223. doi: 10.1080/09084280701509166

Jessen, F., Kucharski, C., Fries, T., Papassotiropoulos, A., Hoenig, K., Maier, W., et al. (2001). Sensory gating deficit expressed by a disturbed suppression of the P50 event-related potential in patients with Alzheimer's disease. *Am. J. Psychiatry* 158, 1319–1321. doi: 10.1176/appi.ajp.158.8.1319

Josef Golubic, S., Aine, C. J., Stephen, J. M., Adair, J. C., Knoefel, J. E., and Supek, S. (2017). MEG biomarker of Alzheimer's disease: absence of a prefrontal generator during auditory sensory gating. *Hum. Brain Mapp.* 38, 5180–5194. doi: 10.1002/hbm.23724

Kisley, M. A., and Cornwell, Z. M. (2006). Gamma and beta neural activity evoked during a sensory gating paradigm: effects of auditory, somatosensory and cross-modal stimulation. *Clin. Neurophysiol.* 117, 2549–2563. doi: 10.1016/j.clinph.2006.08.003

Knight, R. T. (1984). Decreased response to novel stimuli after prefrontal lesions in man. *Electroencephalogr. Clin. Neurophysiol.* 59, 9–20. doi: 10.1016/0168-5597(84)90016-9

Kochhann, R., Varela, J. S., Lisboa, C. S. M., and Chaves, M. L. F. (2010). The mini mental state examination: review of cutoff points adjusted for schooling in a large southern Brazilian sample. *Dement. Neuropsychol.* 4, 35–41. doi: 10.1590/S1980-57642010dn40100006

Kujala, T., and Näätänen, R. (2001). The mismatch negativity in evaluating central auditory dysfunction in dyslexia. *Neurosci. Biobehav. Rev.* 25, 535–543. doi: 10.1016/s0149-7634(01)00032-x

Lin, F. H., Belliveau, J. W., Dale, A. M., and Hamalainen, M. S. (2006). Distributed current estimates using cortical orientation constraints. *Hum. Brain Mapp.* 27, 1–13. doi: 10.1002/hbm.20155

Lindín, M., Correa, K., Zurron, M., and Diaz, F. (2013). Mismatch negativity (MMN) amplitude as a biomarker of sensory memory deficit in amnestic mild cognitive impairment. *Front. Aging Neurosci.* 5:79. doi: 10.3389/fnagi.2013.00079

McLaren, D. G., Sreenivasan, A., Diamond, E. L., Mitchell, M. B., Van Dijk, K. R., Deluca, A. N., et al. (2012). Tracking cognitive change over 24 weeks with longitudinal functional magnetic resonance imaging in Alzheimer's disease. *Neurodegener. Dis.* 9, 176–186. doi: 10.1159/000335876

Micoulaud-Franchi, J. A., Faugere, M., Boyer, L., Cermolacce, M., Richieri, R., Faget, C., et al. (2015). Association of metabolic syndrome with sensory gating deficits in patients with chronic schizophrenia. *Psychoneuroendocrinology* 57, 125–133. doi: 10.1016/j.psyneuen.2015.04.005

Muangpaisan, W., Intalapaporn, S., and Assantachai, P. (2010). Digit span and verbal fluency tests in patients with mild cognitive impairment and normal subjects in Thai-community. *J. Med. Assoc. Thai.* 93, 224–230.

Oldfield, R. C. (1971). The assessment and analysis of handedness: the Edinburgh inventory. *Neuropsychologia* 9, 97–113. doi: 10.1016/0028-3932(71)90067-4

Olichney, J. M., Taylor, J. R., Gatherwright, J., Salmon, D. P., Bressler, A. J., Kutas, M., et al. (2008). Patients with MCI and N400 or P600 abnormalities are at very high risk for conversion to dementia. *Neurology* 70, 1763–1770. doi: 10.1212/01.wnl.0000281689.28759.ab

Olichney, J. M., Van Petten, C., Paller, K. A., Salmon, D. P., Iragui, V. J., and Kutas, M. (2000). Word repetition in amnesia. Electrophysiological measures of impaired and spared memory. *Brain* 123, 1948–1963. doi: 10.1093/brain/123.9.1948

Oranje, B., Aggernaes, B., Rasmussen, H., Ebdrup, B. H., and Glenthoj, B. Y. (2013). P50 suppression and its neural generators in antipsychotic-naive first-episode schizophrenia before and after 6 months of quetiapine treatment. *Schizophr. Bull.* 39, 472–480. doi: 10.1093/schbul/sbr183

Patterson, J. V., Hetrick, W. P., Boutros, N. N., Jin, Y., Sandman, C., Stern, H., et al. (2008). P50 sensory gating ratios in schizophrenics and controls: a review and data analysis. *Psychiatry Res.* 158, 226–247. doi: 10.1016/j.psychres.2007.02.009

Petersen, R. C., Caracciolo, B., Brayne, C., Gauthier, S., Jelic, V., and Fratiglioni, L. (2014). Mild cognitive impairment: a concept in evolution. *J. Intern. Med.* 275, 214–228. doi: 10.1111/joim.12190

Petersen, R. C., Smith, G. E., Waring, S. C., Ivnik, R. J., Tangalos, E. G., and Kokmen, E. (1999). Mild cognitive impairment: clinical characterization and outcome. *Arch. Neurol.* 56, 303–308. doi: 10.1001/archneur.56.3.303

Rabin, L. A., Pare, N., Saykin, A. J., Brown, M. J., Wishart, H. A., Flashman, L. A., et al. (2009). Differential memory test sensitivity for diagnosing amnestic mild cognitive impairment and predicting conversion to Alzheimer's disease. *Neuropsychol. Dev. Cogn. B Aging Neuropsychol. Cogn.* 16, 357–376. doi: 10.1080/13825580902825220

Rosburg, T. (2018). Auditory N100 gating in patients with schizophrenia: a systematic meta-analysis. *Clin. Neurophysiol.* 129, 2099–2111. doi: 10.1016/j.clinph.2018.07.012

Schnell, K., Heekeren, K., Schnitker, R., Daumann, J., Weber, J., Hesselmann, V., et al. (2007). An fMRI approach to particularize the frontoparietal network for visuomotor action monitoring: detection of incongruence between test subjects' actions and resulting perceptions. *NeuroImage* 34, 332–341. doi: 10.1016/j.neuroimage.2006.08.027

Smith, A. K., Edgar, J. C., Huang, M., Lu, B. Y., Thoma, R. J., Hanlon, F. M., et al. (2010). Cognitive abilities and 50- and 100-msec paired-click processes in schizophrenia. *Am. J. Psychiatry* 167, 1264–1275. doi: 10.1176/appi.ajp.2010.09071059

Smith, D. M., Grant, B., Fisher, D. J., Borracci, G., Labelle, A., and Knott, V. J. (2013). Auditory verbal hallucinations in schizophrenia correlate with P50 gating. *Clin. Neurophysiol.* 124, 1329–1335. doi: 10.1016/j.clinph.2013.02.004

Stothart, G., and Kazanina, N. (2016). Auditory perception in the aging brain: the role of inhibition and facilitation in early processing. *Neurobiol. Aging* 47, 23–34. doi: 10.1016/j.neurobiolaging.2016.06.022

Tadel, F., Baillet, S., Mosher, J. C., Pantazis, D., and Leahy, R. M. (2011). Brainstorm: a user-friendly application for MEG/EEG analysis. *Comput. Intell. Neurosci.* 2011:879716. doi: 10.1155/2011/879716

Takayama, Y. (2010). A delayed recall battery as a sensitive screening for mild cognitive impairment: follow-up study of memory clinic patients after 10 years. *J. Med. Dent. Sci.* 57, 177–184.

Taulu, S., Kajola, M., and Simola, J. (2004). Suppression of interference and artifacts by the signal space separation method. *Brain Topogr.* 16, 269–275. doi: 10.1023/b:brat.0000032864.93890.f9

Taulu, S., and Simola, J. (2006). Spatiotemporal signal space separation method for rejecting nearby interference in MEG measurements. *Phys. Med. Biol.* 51, 1759–1768. doi: 10.1088/0031-9155/51/7/008

Thomas, C., vom Berg, I., Rupp, A., Seidl, U., Schroder, J., Roesch-Ely, D., et al. (2010). P50 gating deficit in Alzheimer dementia correlates to frontal neuropsychological function. *Neurobiol. Aging* 31, 416–424. doi: 10.1016/j.neurobiolaging.2008.05.002

van der Flier, W. M., Pijnenburg, Y. A., Schoonenboom, S. N., Dik, M. G., Blankenstein, M. A., and Scheltens, P. (2008). Distribution of APOE genotypes in a memory clinic cohort. *Dement. Geriatr. Cogn. Disord.* 25, 433–438. doi: 10.1159/000124750

van Tricht, M. J., Nieman, D. H., Koelman, J. T., Mensink, A. J., Bour, L. J., van der Meer, J. N., et al. (2015). Sensory gating in subjects at ultra high risk for developing a psychosis before and after a first psychotic episode. *World J. Biol. Psychiatry* 16, 12–21. doi: 10.3109/15622975.2012.680911

Wang, P. N., Chou, K. H., Chang, N. J., Lin, K. N., Chen, W. T., Lan, G. Y., et al. (2014). Callosal degeneration topographically correlated with cognitive function in amnestic mild cognitive impairment and Alzheimer's disease dementia. *Hum. Brain Mapp.* 35, 1529–1543. doi: 10.1002/hbm.22271

Wang, H., He, W., Wu, J., Zhang, J., Jin, Z., and Li, L. (2019). A coordinate-based meta-analysis of the n-back working memory paradigm using activation likelihood estimation. *Brain Cogn.* 132, 1–12. doi: 10.1016/j.bandc.2019.01.002

Wei, M., Shi, J., Li, T., Ni, J., Zhang, X., Li, Y., et al. (2018). Diagnostic accuracy of the chinese version of the trail-making test for screening cognitive impairment. *J. Am. Geriatr. Soc.* 66, 92–99. doi: 10.1111/jgs.15135

Yang, J. C., Chi, L., Teichholtz, S., Schneider, A., Nanakul, R., Nowacki, R., et al. (2014). ERP abnormalities elicited by word repetition in fragile X-associated tremor/ataxia syndrome (FXTAS) and amnestic MCI. *Neuropsychologia* 63, 34–42. doi: 10.1016/j.neuropsychologia.2014.08.001

Yuan, X., Han, Y., Wei, Y., Xia, M., Sheng, C., Jia, J., et al. (2016). Regional homogeneity changes in amnestic mild cognitive impairment patients. *Neurosci. Lett.* 629, 1–8. doi: 10.1016/j.neulet.2016.06.047

Zhang, Z., Liu, Y., Jiang, T., Zhou, B., An, N., Dai, H., et al. (2012). Altered spontaneous activity in Alzheimer's disease and mild cognitive impairment revealed by regional homogeneity. *NeuroImage* 59, 1429–1440. doi: 10.1016/j.neuroimage.2011.08.049

Conflict of Interest: The authors declare that the research was conducted in the absence of any commercial or financial relationships that could be construed as a potential conflict of interest.

frontiers in Aging Neuroscience

ORIGINAL RESEARCH
published: 26 February 2020
doi: 10.3389/fnagi.2020.00020

Age-Related Decreases in Interhemispheric Resting-State Functional Connectivity and Their Relationship With Executive Function

Jizheng Zhao[1,2,3], Peter Manza[4], Corinde Wiers[4], Huaibo Song[1,2,3], Puning Zhuang[1,2,3], Jun Gu[5], Yinggang Shi[1], Gene-Jack Wang[4] and Dongjian He[1,2,3]**

[1] College of Mechanical and Electronic Engineering, Northwest A&F University, Yangling, China, [2] Key Laboratory of Agricultural Internet of Things, Ministry of Agriculture, Yangling, China, [3] Shaanxi Key Laboratory of Agricultural Information Perception and Intelligent Service, Yangling, China, [4] Laboratory of Neuroimaging, National Institute on Alcohol Abuse and Alcoholism, Bethesda, MD, United States, [5] Department of Endocrinology, First Affiliated Hospital of Hebei North University, Zhangjiakou, China

Age-related alterations of functional brain networks contribute to cognitive decline. Current theories indicate that age-related intrinsic brain functional reorganization may be a critical marker of cognitive aging. Yet, little is known about how intrinsic interhemispheric functional connectivity changes with age in adults, and how this relates to critical executive functions. To address this, we examined voxel-mirrored homotopic connectivity (VMHC), a metric that quantifies interhemispheric communication, in 93 healthy volunteers (age range: 19–85) with executive function assessment using the Delis-Kaplan Executive Function System (D-KEFS) scales. Resting functional MRI data were analyzed to assess VMHC, and then a multiple linear regression model was employed to evaluate the relationship between age and the whole-brain VMHC. We observed age-related reductions in VMHC of ventromedial prefrontal cortex (vmPFC) and hippocampus in the medial temporal lobe subsystem, dorsal anterior cingulate cortex and insula in salience network, and inferior parietal lobule in frontoparietal control network. Performance on the color-word inhibition task was associated with VMHC of vmPFC and insula, and VMHC of vmPFC mediated the relationship between age and CWIT inhibition reaction times. The percent ratio of correct design scores in design fluency test correlated positively with VMHC of the inferior parietal lobule. The current study suggests that brain interhemispheric functional alterations may be a promising new avenue for understanding age-related cognitive decline.

Keywords: executive function, voxel-mirrored homotopic connectivity, Delis-Kaplan executive function system, mediation analysis, medial temporal lobe subsystem, salience network, frontoparietal control network

OPEN ACCESS

Edited by:
Hans J. Grabe,
University of Greifswald, Germany

Reviewed by:
Qinghua He,
Southwest University, China
Zsigmond Tamás Kincses,
University of Szeged, Hungary

****Correspondence:***
Gene-Jack Wang
gene-jack.wang@nih.gov
Dongjian He
hdj168@nwsuaf.edu.cn

Received: *21 September 2019*
Accepted: *21 January 2020*
Published: *26 February 2020*

Citation:
Zhao J, Manza P, Wiers C, Song H, Zhuang P, Gu J, Shi Y, Wang G-J and He D (2020) Age-Related Decreases in Interhemispheric Resting-State Functional Connectivity and Their Relationship With Executive Function. Front. Aging Neurosci. 12:20. doi: 10.3389/fnagi.2020.00020

INTRODUCTION

Cognitive function is altered with age (Ulman, 2014; Harrington et al., 2017). In particular, its decline with age affects quality of life and life satisfaction in older adults (Reuter-Lorenz and Park, 2010; Ferreira and Busatto, 2013). Executive functions broadly consist of inhibition, working memory, and cognitive flexibility (Diamond, 2013). Studies on cognitive performance in healthy

elder groups have indicated that increasing age is associated with multifaceted impairments of executive function (Ulman, 2014; Harrington et al., 2017). For example, aging is associated with impairment in cognitive performance in verbal fluency, category fluency, and category switching tests (Harrington et al., 2017). In addition, many studies have used the color-word Stroop task and found that response inhibition performance, or the ability to stop unwanted or inappropriate responses, declines with age (Ivnik et al., 1996; Klein et al., 1997; Troyer et al., 2006; Adólfsdóttir et al., 2016; Anderson and Craik, 2017; Harrington et al., 2017).

Resting-state functional MRI (rs-fMRI) imaging technology permits studying age-related intrinsic brain alterations *in vivo*. Accumulating studies have shown age-related regional functional connectivity (FC) decreases in brain regions within default mode (DMN), salience (SN), and frontoparietal control (FPCN) networks (Grady, 2012; Li et al., 2015). The most common FC reductions within DMN have been reported in medial prefrontal cortex and posterior cingulate cortex (PCC/precuneus) (Bluhm et al., 2008; Damoiseaux et al., 2008; Koch et al., 2010; Allen et al., 2011; Wu et al., 2011; Tomasi and Volkow, 2012; Grady et al., 2016). Age increase is also generally associated with decreases in intra-network FC within the bilateral insula and dorsal anterior cingulate cortex (dorsal ACC) (Keiichi et al., 2012; He et al., 2014; Zhang et al., 2014). FPCN shows numerically lower intra-network FC in older adults compared to young adults (Elman et al., 2014; Geerligs et al., 2014a; Grady et al., 2016). Further, the FC reduction within FPCN has been shown in middle-aged (41–60 years) compared to young (21–40 years) individuals (Siman-Tov et al., 2017). The reduced network covariation is in line with the idea that increasing age is accompanied by decreasing connectivity within functional brain systems (Chan et al., 2014; Geerligs et al., 2014a; Grady et al., 2016). Moreover, inter-network FC patterns have shown alterations with aging, including reductions in the segregation of DMN, SN, and FPCN (Chan et al., 2014; Geerligs et al., 2014a), and enhancements in FC strength between DMN and FPCN with age (Geerligs et al., 2014a; Grady et al., 2016). Thus, rs-fMRI may be a powerful tool to investigate age-related brain functional reorganization.

Neuropsychology studies have indicated that the age-related intrinsic functional reorganizations of DMN, SN, and FPCN are associated with impaired executive function. Age-related reductions in FC between MPFC and PCC/precuneus correlated with loss of executive function, memory, and processing speed (Andrews-Hanna et al., 2007). A higher number of Stroop errors correlated with reduced FC within the DMN and SN in cognitively normal elders (Duchek et al., 2013). In older adults, the strength of network covariation of the left insula and dorsal ACC in SN correlated significantly with executive functions measured by Frontal Assessment Battery (FAB) and Kohs Block-Design Test (Keiichi et al., 2012). Further, FC between SN and frontal cortex successfully predicted response inhibition as assessed by the Stroop test (La Corte et al., 2016). The between-network connectivity of the FPCN is enhanced in older subjects, and its strength is positively correlated with associative memory performance (Grady et al., 2016). These findings on intrinsic brain functional reorganizations shed light on the neural mechanisms underlying age-related executive function decline.

Theories on the relationship between age and neurocognition suggest a hemispheric asymmetry reduction for older adults (HAROLD model) in response to cognitive tasks (Cabeza, 2002; Manuela et al., 2013). For example, elders were shown to recruit a more bilateral frontal pattern within the task-related network to achieve successful performance during working memory (Sala-Llonch et al., 2012) and inhibitory control (Colcombe et al., 2005) tasks, while younger groups recruited the right-lateralized frontal regions (Colcombe et al., 2005; Sala-Llonch et al., 2012). This reduced lateralization pattern in frontal cortex suggests that functional reorganization occurs across hemispheres with age, and therefore, these changes may be measurable outside of the task state (e.g., alterations in resting-state FC or in structural changes). In support of this idea, a study on white matter integrity has shown that age-related changes are prominently seen in the anterior corpus callosum (Frederiksen and Waldemar, 2012), which is involved in information transformation across the right and the left brain hemisphere. For example, the changes of anterior corpus callosum are suggested to be accompanied by alterations of interhemispheric FC pattern of frontal cortex for healthy young participants (Qiu et al., 2017). However, little is known about the age-related alterations of interhemispheric FC pattern and whether such interhemispheric functional alterations contribute to age-related executive function change.

In the rs-fMRI literature, voxel-mirrored homotopic connectivity (VMHC) offers a metric to evaluate interhemispheric FC (Zuo et al., 2010), which measures integrity of information communication between brain hemispheres. Abnormal VMHC patterns in widespread cortical and subcortical networks have been reported in studies on cocaine addiction (Kelly et al., 2011), mild cognitive impairment (MCI) (Luo et al., 2018), Alzheimer's disease (Wang et al., 2015; Li et al., 2018), and schizophrenia (Hoptman et al., 2012), indicating that VMHC is a reliable neural marker for brain functional reorganization. This abnormal VMHC has been associated with impaired executive functioning in individuals with MCI (Luo et al., 2018) and Alzheimer's disease (Li et al., 2018), suggesting that altered VMHC might associate with executive function change. Taken together, the VMHC-based rs-fMRI analysis may provide additional information beyond classical FC metrics for understanding neural mechanisms of age-related executive function alteration. To our best knowledge, only one study has explored the relationship between VMHC and age (Zuo et al., 2010). This study included 7- to 85-year-old healthy participants, and focused on the developmental trajectories of brain inter-hemisphere FC in the lifespan (Zuo et al., 2010). However, the age-related homotopic FC alterations in adult and its associations with executive functions have not yet been examined.

We examined whether homotopic FC measured with VMHC changes with age in adults aged 19–85. Furthermore, we tested whether any age-related alterations of VMHC would be associated with executive function, as assessed by Delis-Kaplan Executive Function System (D-KEFS) scales. Finally, we employed a mediation analysis to identify whether interhemispheric connectivity is a possible neural mechanism underlying age-related cognitive decline.

MATERIALS AND METHODS

Participants

For the current study, Nathan Klein Institute (NKI) data (Nooner et al., 2012) (demographic and executive function data, resting functional and structural MRI images) were downloaded from http://fcon_1000.projects.nitrc.org/indi/pro/nki.html. The NKI data included 207 subjects. First, subjects with a history of psychiatric disorders or medical conditions were excluded. For example, subjects with Beck Depression Inventory (BDI) (Beck et al., 1988) scores higher than 15, indicating mild-severe depression, were excluded. Forty-one healthy children and adolescents (age < 18) were excluded from the current study. For the 105 healthy adults, there were two subjects without D-KEFS scores (Homack et al., 2005) and three subjects without resting functional MRI data. Six subjects were excluded due to large head movements (mean framewise displacement >0.4 mm) (Power et al., 2014). One subject with extensive large color-word inhibition scores in D-KEFS test (105, which exceeded three standard deviations from the mean) was excluded. The final sample consisted of 93 healthy adults subjects (female: 45, male: 48; age range: 19–85, mean = 42.65 ± 1.93 SE years; 31 subjects aged 19–29, 11 subjects aged 30–39, 22 subjects aged 40–49, 8 subjects aged 50–59, 9 subjects aged 60–69, 9 subjects aged 70–79, 3 subjects aged 80–85) who completed resting-state MRI, structural scans, and the D-KEFS test. For the final sample, there was no subject with hypertension or diabetes, and systolic blood pressure was less than 140 mmHg. There was no subject taking daily medications. There was no subject with past or current mental disorder or substance abuse disorder. Handedness was assessed with the Edinburgh Handedness Inventory (Oldfield, 1971), height and weight of participant were measured on the day before the MRI scan, and then BMI was calculated. **Table 1** provided the subjects' demographic information.

Executive Function Measurements

For the NKI data, five tests from D-KEFS were conducted to assess executive function, namely, Color-Word Interference (CWIT), Verbal Fluency, Design Fluency, Sorting, and Twenty Questions Tests. Detailed task descriptions can be found in Swanson (2005) and Mace et al. (2018). In brief, CWIT required participants to name the color or word in congruent and incongruent conditions. For example, when the word "green" was printed in red ink, participants were asked to process task-relevant color information (ink) and inhibit pre-potent processing of conflicting task-irrelevant information (word meaning). CWIT data included scores of word naming, color naming, and color-word inhibition. For the Verbal Fluency Test, participants were asked to name uniquely as many words as possible in 60 s by letter or category for altering categories. Data included scores of letter fluency, category fluency, category switching fluency, and category switching accuracy. On the Design Fluency Test, participants were instructed to draw unique geometric designs in dots arrays within 60 s. The paradigm consists of three conditions: connection of filled dots, connection of empty dots, and alternating connections between filled and unfilled dots. Data included scores of filled dots design, empty dots design, switching design, and total percent ratio of correct design. The Sorting Test asked participants to sort items into categories and describe the applied categorization rules and included two card sets. The number of correct sorts was computed and included scores of free sort confirmed sorts, free sort description, and sort recognition description. Twenty Questions Test asked participants to guess the objects from 30 common objects, and the participants were instructed to ask as few "yes" or "no" questions as possible. It included scores of initial abstraction, total questions asked, and total weighted achievement. The MRI scans were conducted at 9:00 am, and D-KEFS test was conducted at 12:30 pm on the same day.

TABLE 1 | Demographic characteristics.

	Range	Mean ± SE
Age (years)	19–85	42.65 ± 1.93
Gender	F45/M48	
Handedness	Right 79/Left 12, one subject was unknown, one subject was ambidextrous	
BMI (kg/m^2)	16.3–40	26.16 ± 0.50
BDI_Total	0–12	2.43 ± 0.33

MRI Data

All participants provided written informed consent and were scanned according to procedures approved by the local Institutional Review Board (IRB) at the NKI. The data were shared with the approval of the IRB at the NKI. All subjects gave written informed consent in accordance with the Declaration of Helsinki.

Resting functional images were acquired using a Siemens MAGNETOM Tim Trio 3.0 T scanner. There were 260 functional MRI images (lasting for 10.83 min) with a gradient echo-planar sequence (TR = 2.5 s; TE = 35 ms; flip angle = 80°; FOV: 256 × 256; in-plane resolution = 3 mm × 3 mm, slice thickness: 3 mm). Structural MRI scans were acquired with the same Siemens MAGNETOM Tim Trio 3.0 T scanner using T1-weighted MPRAGE sequence (TR = 2.5 s; TE = 3.5 ms; TI = 1200 ms; FOV: 256 × 256; slice thickness: 1 mm; flip angle: 8°; matrix size: 256 × 256; 200 Transverse slices).

MRI Preprocessing

Functional data were analyzed using Data Processing & Analysis for Brain Imaging (DPABI) toolbox (Yan et al., 2016). Image preprocessing included slice-time correction, image realignment, skull stripping, coregistration between functional and structural images, spatial normalization to the stereotactic space of the Montreal Neurological Institute (MNI), and resampling to 3-mm isotropic voxels and smoothing with a Gaussian kernel of 6-mm FWHM. Head motion correction was conducted based on a "scrubbing" approach (Power et al., 2014). Specifically, if the framewise displacement (FD) was larger than 0.5 mm, the corresponding volume was linearly interpolated using its temporal neighbors (Power et al., 2014). In addition, the mean FD value was used as a regressor in the group-level regression model

and partial correlation analyses to control the possible motion influence. Multiple linear regression was performed to remove nuisances including the mean signal fluctuations in the whole brain, ventricles, and white matter, and the six head realignment parameters and their derivatives. Detrending and a temporal band-pass filtering (0.01–0.08 Hz) were subsequently conducted to minimize temporal drifts and white noise.

VMHC measurements assumed symmetric morphology between each brain hemisphere. To minimize differences in the geometric configuration of the cerebral hemispheres, we averaged 93 normalized T1 images to create a group-mean T1 image. This image was averaged with its left-right mirrored version to generate a group-specific symmetrical template. Each individual T1 image was non-linearly registered to the standard template, and the identical transformation was then applied to the resting-state functional images. VMHC was obtained by calculation of Pearson's correlation coefficient between the time series of each voxel and that of its symmetrical interhemispheric counterpart. Voxels medial of $x = \pm 4$ were excluded, to minimize the blurring effect across the midline (Kelly et al., 2011).

Correlation Analysis of D-KEFS Scores and Age

Partial correlations were conducted on each D-KEFS score and age, with gender, handedness, and body mass index (BMI) as covariates. Bonferroni correction was carried out for multiple comparisons, and level of significance was set at $P < 0.0025$ (0.05/18 for 18 D-KEFS scores). Finally, scores of color-word inhibition, category switching fluency and category switching accuracy, the percent ratio of correct design, and sort recognition description were significantly correlated with age. Then, the correlations of these five scores and age-related interhemispheric FC were examined.

Statistical Analyses on Resting fMRI Data

Statistical analyses were performed using SPM12 (Welcome Department of Cognitive Neurology, London, United Kingdom)[1]. Multiple linear regression model was used to assess the association between age and VMHC metrics. The subject's BMI, gender, handedness, mean FD, and total intracranial volume (TICV) were included as covariates. Statistical significance was based on a familywise error (FWE) correction for multiple comparisons at the cluster level ($P_{FWE} < 0.05$) with a minimum cluster size of $k = 30$ voxels and a cluster-defining threshold $P < 0.001$, in line with current reporting guidelines (Eklund et al., 2016; Flandin and Friston, 2019).

ROI-Based Analysis

When the significant age-related statistics brain mapping was acquired, regions of interest (ROI) were defined by spheres with 6-mm radius and center at the local peak voxel in statistics brain mapping. Mean regional values were calculated for each subject. Then, group-level partial correlations were conducted on age-related regional VMHC values and scores of color-word inhibition, category switching fluency and category switching accuracy, the percent ratio of correct design, and sort recognition description respectively, with BMI, gender, handedness, mean FD, and TICV as covariates. Bonferroni correction was carried out for multiple comparisons, and level of significance was set at $P < 0.0008$ (0.05/12/5 for 12 pairs of mirrored regions in VMHC results by five D-KEFS scores).

In order to test whether shifting with one TR lag of time courses from the opposite hemisphere affected VMHC, Pearson correlation coefficients were calculated between time courses of brain regions in the left hemisphere lagging one TR and time courses of their mirrored brain regions in the right hemisphere without lag (termed FCs_leftlag), between time courses of brain regions in the left hemisphere without lag and time courses of their mirrored brain regions in the right hemisphere lagging one TR (termed FCs_rightlag), as well as between time courses of brain regions in the bilateral hemisphere both without lag (termed FCs_nolag). Three two-way ANOVA of FC types (specially, FCs_leftlag and FCs_nolag, FCs_rightlag and FCs_nolag, FCs_leftlag and FCs_rightlag) by region (12 pairs of mirrored brain regions) were conducted to examine the effect of time course lag.

Mediation Analysis

For all age-related brain regions, we examined whether interhemispheric functional coupling of these regions mediated the relationship between age and these five scores respectively. We tested our mediation hypothesis with Multilevel Mediation and Moderation Toolbox (Wager et al., 2008), with age, BMI, gender, handedness, FD, and TICV as covariates. Bonferroni-correction was carried out for multiple comparisons, and level of significance was set at $P < 0.0008$ (0.05/12/5 for 12 pairs of mirrored regions in VMHC results by five D-KEFS scores).

RESULTS

Behavioral Results

Table 2 shows the range, mean, and standard error of 18 D-KEFS scores, as well as their partial correlations with age. Age was significantly associated with scores of category switching fluency ($r = -0.347$, $P = 0.001$) and category switching accuracy ($r = -0.361$, $P = 0.001$), percent ratio of correct design ($r = -0.352$, $P = 0.001$), and sort recognition description ($r = -0.321$, $P = 0.002$). Age was positively correlated with color-word inhibition reaction times ($r = 0.462$, $P < 0.001$). **Supplementary Figure S1** shows the scatter plots of age and these five D-KEFS scores.

VMHC Results

There was no brain region in which VMHC correlated positively with age. Age correlated negatively with VMHC between bilateral putamen, insula (BA 13), hippocampus, superior temporal gyrus (BA 22), globus pallidus, paracentral lobule (BA 3), precentral gyrus (BA 4), perigenual and dorsal anterior cingulate gyrus

[1] http://www.fil.ion.ucl.ac.uk/spm

TABLE 2 | Descriptive analysis on D-KEFS scores, and the partial correlations of each D-KEFS scores and age, with gender, handedness, and body mass index (BMI) as covariates.

Task	Scores	Range	Mean ± SE	Correlation with Age *R* (*P*)
Verbal Fluency	Letter Fluency	18–67	42.67 ± 1.15	0.094 (0.382)
	Category Fluency	18–63	42.73 ± 0.95	−0.217 (0.042)
	Category Switching Fluency	7–20	13.17 ± 0.30	**−0.347 (0.001)**
	Category Switching Accuracy	3–19	11.41 ± 0.34	**−0.361 (0.001)**
Design Fluency	Empty Dots Design	2–18	10.65 ± 0.34	−0.139 (0.197)
	Filled Dots Design	4–20	10.27 ± 0.35	−0.113 (0.292)
	Alternating Design	14–50	32.63 ± 0.81	0.214 (0.045)
	Percent Ratio of Correct Design	34–100	82.49 ± 1.45	**−0.352 (0.001)**
Color Word Interference	Word Naming	12–33	20.66 ± 0.45	0.145 (0.177)
	Color Naming	16–45	27.12 ± 0.54	0.262 (0.014)
	Color-word Inhibition	26–95	50.88 ± 1.32	**0.462 (<0.001)**
Sorting	Free Sort Confirmed Sorts	2–53	9.60 ± 0.55	−0.167 (0.121)
	Recognition Sorts	16–63	36.73 ± 1.16	**−0.321 (0.002)**
	Description Sorts	8–59	34.66 ± 1.12	−0.205 (0.056)
Twenty Questions Tests	Total Questions Asked	16–46	26.62 ± 0.61	0.051 (0.634)
	Total Weighted Achievement	7–20	15.12 ± 0.28	−0.080 (0.457)
	Initial Abstraction	7–60	29.09 ± 1.31	−0.027 (0.801)

Significant correlations were showed in bold fonts.

(pgACC and dorsal ACC, BA 24), ventromedial prefrontal cortex (vmPFC, BA 10), and inferior parietal lobule (IPL, BA 39) (see **Table 3** and **Figure 1**).

ROI-Based Analysis

CWIT inhibition reaction times correlated negatively with VMHC in the insula ($r = -0.41$, $P = 0.00007$), vmPFC ($r = -0.46$, $P = 0.000006$), hippocampus ($r = -0.39$, $P = 0.0002$), and superior temporal gyrus ($r = -0.37$, $P = 0.0004$). The percent ratio of correct design scores correlated positively with VMHC in the IPL ($r = 0.36$, $P = 0.0006$) (**Supplementary Figure S2** shows scatter plots of the significant correlations above). The result showed that FCs_nolag was significantly larger than FCs_leftlag [$F(1,20) = 204.208$, $P < 0.001$] and FCs_rightlag [$F(1,20) = 214.208$, $P < 0.001$]. There was no significant difference between the FCs_leftlag and FCs_rightlag [$F(1,20) = 1.987$, $P = 0.174$].

TABLE 3 | The foci of brain areas showed intrinsic activity associating with age ($P_{FWE} = 0.05$, family-wise error correction) when controlling for gender, handedness, body mass index (BMI), FD, and total intracranial volume (TICV).

Region	BA	Voxel	*Z*	MNI		
				X	*Y*	*Z*
Brain regions that VMHC showed negative correlation with age						
Putamen	–	2733	7.08	± 27	−3	9
Insula	BA 13		6.02	± 36	21	6
Hippocampus	BA 28		5.72	± 24	−15	−21
Superior Temporal Gyrus	BA 22		5.42	± 54	−9	−15
Globus Pallidus	–		5.23	± 24	15	6
Paracentral Lobule	BA 3	129	5.53	± 21	−30	60
Precentral Gyrus	BA 4	131	4.94	± 45	−9	48
Anterior Cingulate	BA 24	149	4.96	± 12	33	21
Anterior Cingulate	BA24		4.35	± 6	6	42
Medial Frontal Gyrus	BA 10	36	4.48	± 6	54	−9
Medial Frontal Gyrus	BA 10		4.47	± 6	48	−18
Inferior Parietal Lobule	BA 40	47	4.22	± 60	−39	45

BA, Brodmann area; –, no BA covered.

Mediation Analysis

Table 4 shows all estimated mediation models. When multiple comparisons were considered, mediation analyses showed that VMHC in vmPFC significantly mediated the relationship between age and CWIT inhibition reaction time (vmPFC: $ab = 0.122$, $P = 0.0003$, confidence interval (CI): [0.041, 0.262]) (see **Figure 2**).

At an uncorrected level, VMHC in insula, hippocampus, and precentral gyrus also mediated the relationship between age and CWIT inhibition reaction time (insula: $ab = 0.128$. $P = 0.027$, CI: [0.015, 0.276]); hippocampus: $ab = 0.125$. $P = 0.026$, CI: [0.013, 0.277]; precentral gyrus: $ab = 0.102$. $P = 0.014$, CI: [0.016, 0.245]). Moreover, VMHC in IPL, pgACC, globus pallidus, and putamen mediated the relationship between age and the percent ratio of correct design scores, respectively (IPL: $ab = -0.106$, $P = 0.014$, CI: [−0.221, −0.040]; pgACC: $ab = 0.100$, $P = 0.015$, CI: [0.022, 0.206]; globus pallidus: $ab = 0.156$, $P = 0.016$, CI: [0.028, 0.290]; putamen: $ab = 0.149$, $P = 0.025$, CI: [0.021, 0.295]).

DISCUSSION

Little is known regarding the influence of age on brain homotopic functional coupling and how this reorganization might be associated with age-related executive function alterations. In line with FC-based rs-fMRI studies on normal aging, here we observed age-associated reduction of interhemispheric FC

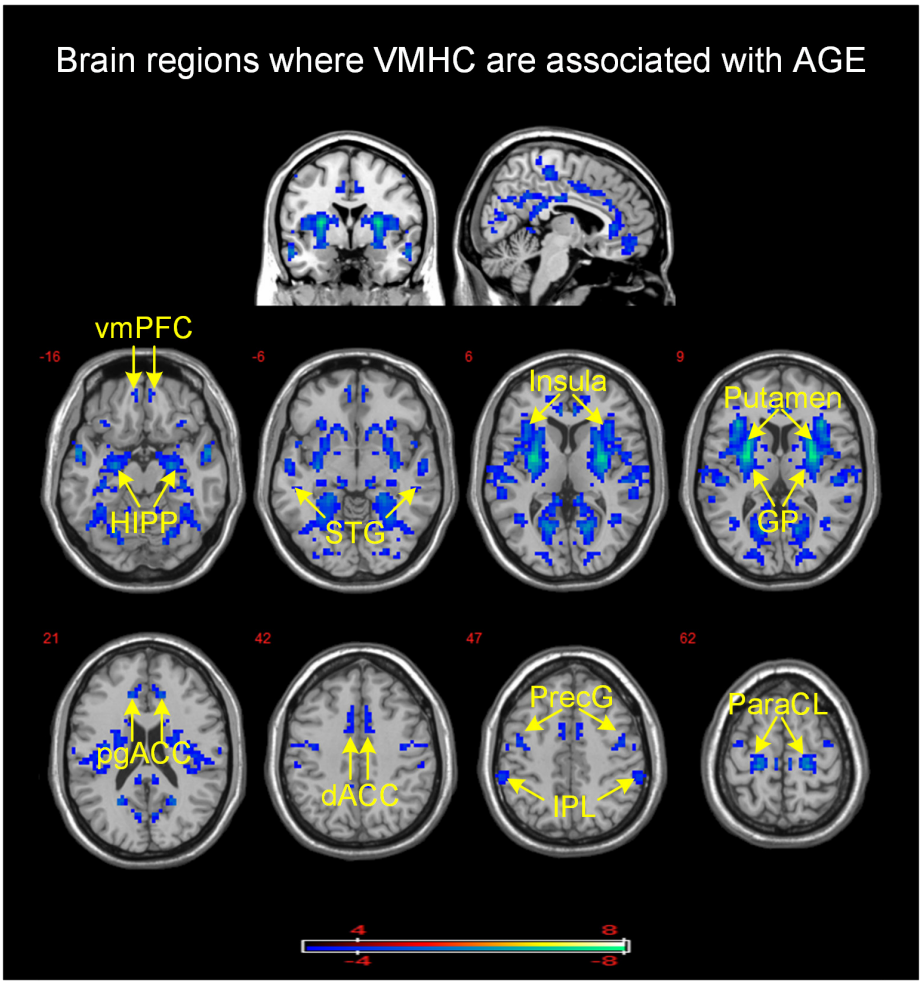

FIGURE 1 | Brain mapping of VMHC demonstrated a significant association with age (P_{FWE} = 0.05, family-wise error correction). VMHC was negatively associated with age in brain regions with cool color. Color bar provides *T* values. vmPFC, ventromedial prefrontal cortex; HIPP, hippocampus; STG, superior temporal gyrus; GP, globus pallidus; pgACC, perigenual anterior cingulate cortex; dACC, dorsal anterior cingulate cortex; PreG, precentral gyrus; IPL, inferior parietal lobule; ParaCL, paracentral lobule.

of medial temporal lobe subsystem (vmPFC and pgACC and hippocampus) within DMN, dACC and insula within SN, and IPL within FPCN. Further, we showed that response inhibition performance was associated with reduced interhemispheric functional coupling of medial temporal lobe subsystem of DMN and insula in SN, and correct design scores were associated with functional coupling of bilateral IPL of FPCN. Our findings extend previous studies on age-related intrinsic functional network reorganization (Damoiseaux et al., 2008; Keiichi et al., 2012; Chan et al., 2014; Grady et al., 2016) and indicate that the alterations of interhemispheric functional coupling might also at least partly underlie age-related executive function change.

Age-Related Executive Function Alterations

In the current study, age was negatively associated with performance in color-word inhibition (reaction time), category switching task (fluency and accuracy), design fluency (percent ratio of correct design), and sort recognition tasks. Performance on these tasks assesses higher executive function, such as inhibitory control, cognitive flexibility, and conceptual reasoning. The previous cross-sectional (Ivnik et al., 1996; Klein et al., 1997; Harrington et al., 2017) and longitudinal studies (Adólfsdóttir et al., 2016) of the Stroop task have indicated a negative relationship between response inhibition and age after controlling for basic word naming and color naming conditions. This negative relationship between category switching performance and age seems to corroborate the previous study indicating significant age-related effects in category switching task (Wecker et al., 2005; Lanting et al., 2009). Moreover, older adults were found to complete significantly fewer designs than middle-aged adults in design fluency task (Ready, 2010; Sanders and Schmitter-Edgecombe, 2012). Age has also been negatively associated with scores of sort recognition (Mattioli et al., 2014). These results reiterate the viewpoint that higher executive function is vulnerable to aging.

TABLE 4 | Mediation models on the relationship between age and D-KEFS scores.

D-KEFS task *(Y)*	Brain region *(M)*		Path a (*X* – > *M*)	Path b (*M* - > *Y*)	Path c'(a – > Y)	Path c (*a* - > *Y*)	Mediation path *ab*
CWIT inhibition scores	Hippocampus (±24, −15, −21)	Beta	−0.005	−25.012	0.209	0.335	0.125
		P	0.0003	0.046	0.006	0.00003	0.026
		CI	[−0.007, −0.003]	[−48.716, −3.061]	[0.051, 0.394]	[0.181, 0.512]	[0.013, 0.277]
	Insula (±36, 21, 6)	Beta	−0.005	−27.078	0.206	0.334	0.128
		P	0.0003	0.032	0.007	0.00002	0.027
		CI	[−0.006, −0.003]	[−51.450, −2.091]	[0.057, 0.393]	[0.183, 0.518]	[0.015, 0.276]
	Precentral Gyrus (±45, −9, 48)	Beta	−0.004	−24.826	0.232	0.334	0.102
		P	0.001	0.048	0.003	0.00002	0.014
		CI	[−0.006, −0.003]	[−48.027, −4.394]	[0.082, 0.387]	[0.181, 0.510]	[0.016, 0.245]
	vmPFC (±6, 48,−18)	**Beta**	**−0.003**	**−37.276**	**0.213**	**0.335**	**0.122**
		P	**0.0009**	**0.0009**	**0.0005**	**0.00002**	**0.0003**
		CI	**[−0.005,−0.001]**	**[−57.702,−17.681]**	**[0.092, 0.356]**	**[0.180, 0.517]**	**[0.041, 0.262]**
The percent ratio of correct design scores	Inferior Parietal Lobule (±60, −39, 45)	Beta	−0.004	29.821	−0.146	−0.251	−0.106
		P	0.0001	0.002	0.105	0.0007	0.014
		CI	[−0.005, −0.002]	[10.700, 52.456]	[−0.332, 0.018]	[−0.422, −0.109]	[−0.221, −0.040]
	Anterior Cingulate Cortex (±12, 33, 21)	Beta	−0.003	−33.278	−0.350	−0.250	0.100
		P	3.04E-06	0.019	0.0006	0.001	0.015
		CI	[−0.004, −0.002]	[−60.171, −4.815]	[−0.545, −0.182]	[−0.424, −0.105]	[0.022, 0.206]
	Globus Pallidus (±24, 15, 6)	Beta	−0.004	−41.254	−0.407	−0.251	0.156
		P	0.0001	0.002	0.0004	0.001	0.016
		CI	[−0.005, −0.003]	[−69.503, −5.897]	[−0.610, −0.183]	[−0.430, −0.107]	[0.028, 0.290]
	Putamen (±27, −3, 9)	Beta	−0.005	−29.378	−0.400	−0.251	0.149
		P	0.0009	0.023	0.001	0.002	0.025
		CI	[−0.006, −0.004]	[−53.794, −3.423]	[−0.646, −0.162]	[−0.423, −0.106]	[0.021, 0.295]
Sort recognition description scores	Hippocampus (±24, −15, −21)	Beta	−0.005	−20.805	−0.266	−0.168	0.098
		P	0.0002	0.020	0.0004	0.013	0.015
		CI	[−0.006, −0.003]	[−40.696, −2.551]	[−0.410, −0.123]	[−0.295, −0.037]	[0.019, 0.210]
	Putamen (±27, −3, 9)	Beta	−0.005	−27.758	−0.307	−0.168	0.139
		P	0.001	0.012	0.0003	0.0166	0.005
		CI	[−0.006, −0.004]	[−49.604, −7.309]	[−0.481, −0.143]	[−0.302, −0.040]	[0.039, 0.262]

In the model, age was the independent variable, each D-KEFS score was set to be the dependent variable. VMHC of brain regions significantly associated with age and D-KEFS score was set to be mediator, respectively. Path "a" was the effect of independent variable on mediator, Path "b" was the effect of mediator on dependent variable with independent variable as covariates. Path "c"' was the direct effect of independent variable on dependent variable with mediator being taken into consideration. Path "c" was the direct effect of independent variable on dependent variable without mediator being taken into consideration. Mediation path "ab" was the effect of mediator on the relationship of the independent variable on the dependent variable. Gender, handedness, body mass index (BMI), FD, and total intracranial volume (TICV) were included as covariates. CI, confidence interval. The model with significant mediation effect was showed in bold fonts.

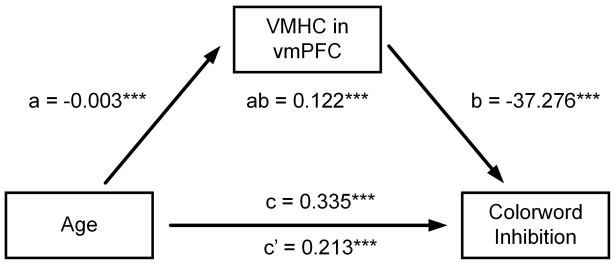

FIGURE 2 | Mediation models on the relationship between age and CWIT inhibition reaction times. The relationship between age and CWIT inhibition reaction time was attenuated after controlling for VMHC of bilateral vmPFC. However, the direct effect of age on CWIT inhibition reaction time was still significant. Their relationship was therefore partly mediated by VMHC of bilateral vmPFC. ***$P < 0.001$.

Age-Related Interhemispheric FC Alterations

In the current study, age correlated negatively with VMHC of vmPFC, pgACC, and hippocampus areas that belong to the medial temporal lobe subsystem of DMN (Andrews-Hanna et al., 2010). The medial temporal lobe subsystem has been associated with episodic judgments about the personal future, among other high-level executive functions (Andrews-Hanna et al., 2010). Damoiseaux et al. (2008) have employed ICA and showed that network covariation of the anterior part of DMN inversely correlated with age. Further, FC density of the vmPFC is decreased with age (Tomasi and Volkow, 2012). Previous FC studies have indicated that the DMN may be one of the brain networks most vulnerable to aging. Our results thus extend prior work indicating that age affects the interhemispheric functional coupling of the medial temporal lobe subsystem of DMN.

We observed that VHMC of bilateral dACC and insula attenuated with aging, both of which were key components of SN. The insula is involved in detecting and selecting salient stimuli by combining endogenous and exogenous information, and mediating interactions with other neurocognitive systems (Seeley et al., 2007; Tim et al., 2007; Sridharan et al., 2008). A body of studies have shown reduction of intra-network FC of dACC and insula with aging (Keiichi et al., 2012; He et al., 2014; Zhang et al., 2014). The inter-network FC profiles between SN and visual network, as well as the SN and the anterior part of the DMN, are powerful predictors of age (Keiichi et al., 2012). These results are in line with the notion that SN is one of the brain networks most vulnerable to aging (La Corte et al., 2016). However, relatively few studies have examined the interhemispheric FC strength of SN. There is one study showing that FC strength of the bilateral insula negatively correlates with age (Keiichi et al., 2012). Our findings confirm these results, and further indicate that interhemispheric functional coupling of dACC decrease with age increase, suggesting that these effects extend to other nodes of the SN.

In the current study, VMHC of IPL (belonging to FPCN) correlated negatively with age. IPL is involved in adaptive cognitive control decision-making processes (Vincent et al., 2008). With regard to neurocognitive aging, IPL has shown an asymmetric response pattern in cognitive tasks for older and younger adults: younger adults utilize the left IPL more than older adults when ignoring irrelevant stimuli on 1-back memory task (Campbell et al., 2012). However, older adults show stronger activation of the right IPL during target detection than young adults (Geerligs et al., 2014b). These two studies may emphasize the adapting response of IPL to external cognitive control task for older adults. Grady et al. (2016) have employed a graph theory method to show that, in older adults, the bilateral IPL are functionally stronger connected with brain cortices in the dorsal attention network than with classic brain regions in FPCN, indicating the functional reorganization of parietal regions for older adults. The current study added to this literature in that IPL showed reorganization of interhemispheric functional coupling in older adults. However, Madhyastha and Grabowski, 2014 find that the FC between bilateral IPL is not correlated with age in older subjects (aged 56–89), possibly because FC between bilateral IPL is vulnerable to age at an early stage (Siman-Tov et al., 2017).

The Relationship of Age-Related VMHC Alterations and Executive Function

CWIT inhibition scores (reaction time) correlated negatively with VMHC in vmPFC. The vmPFC is implicated in governing goal-directed learning (Valentin et al., 2007; Sanne et al., 2009) and decision-making (Sanne et al., 2009; Reber et al., 2017) for outcome valuation. Previous fMRI studies have also suggested that vmPFC is more heavily recruited during the processing of incongruent trials in a spatial Stroop task, and its activation has shown correlations with the efficiency of top-down cognitive control (Araneda et al., 2018). fMRI studies have documented an association between diminished activity in vmPFC and poor performance on the Stroop task in pathological gamblers (Potenza et al., 2003) and individuals with binge eating disorder (Balodis et al., 2013), suggesting a pivotal role of vmPFC in cognitive control. In line with this, the negative association between VMHC of vmPFC and CWIT inhibition reaction times confirms the key role of vmPFC in cognitive control, suggesting that the functional coordination of vmPFC is also a sensitive neural marker to age-related change in response to inhibition performance. One possible explanation is that inhibition requires a decision that is congruent on a complex goal rather than an immediate response to stimuli; this process may depend on the encoding of goal values by vmPFC (Reber et al., 2017). In addition, we showed that VMHC of bilateral vmPFC mediated the influence of age increase on CWIT inhibition reaction time, indicating that age-related functional alterations of vmPFC might be part of the neural mechanism underlying age-related decline of response inhibition (Andrews-Hanna et al., 2007).

CWIT inhibition reaction time also correlated with VMHC of the bilateral insula. The right insula has been emphasized by its prominent role in saliency processing and initiating attentional control during executive control behaviors (Eckert et al., 2009, 2010). The bilateral insula have been indicated as common regions that are recruited in Go/NoGo, Flanker

and Stimulus-response compatibility tasks (Morelli et al., 2015). Their task-related activation levels are shown to correlate with behavioral performance (Eckert et al., 2010; Morelli et al., 2015), such as Stroop performance (Leung et al., 2000; Potenza et al., 2003; Zysset and Schroeter, 2007; Balodis et al., 2013). One rs-fMRI study finds a positive association between FC of the bilateral insula with categorical verbal fluency test scores (Keiichi et al., 2012). In line with these studies, our findings show that insular VMHC numerically mediated the relationship between age and CWIT inhibition performance, suggesting that functional coupling of bilateral insula is, at least partly, involved in neural mechanisms underlying age-related decline in response inhibition.

In the current study, percent ratio of correct design scores correlated positively with VMHC of IPL. A body of literature has implicated that IPL is commonly involved in executive function tasks, such as working memory, response inhibition, interference control, and sustained attention (Langner and Eickhoff, 2013; Cieslik et al., 2015; Krall et al., 2015). Moreover, an accumulating literature has shown that performance in design fluency task is positively associated with bilateral IPL gray matter volume (Kramer et al., 2007; Possin et al., 2012). Furthermore, interhemispheric IPL connectivity has shown to be reduced in patients after pediatric arterial ischemic stroke, and D-KEFS category fluency correlated positively with the interhemispheric IPL connection in both these patients and healthy controls (Kornfeld et al., 2018). In line with the study above, we also found that age-related reductions in connectivity of bilateral IPL contributed to attenuation of performance in design fluency task. Successful design fluency task complement has been shown to require processing of abundant bottom visual and motor information under top-down cognitive control (Yana et al., 2010). IPL comprises multimodal neurons for integration of auditory, sensory, visual, and motor information (Daniel et al., 2015) and receipt top-down regulation of dACC for cognitive control (Harding et al., 2015), which is a candidate brain region to be involved in design fluency task. In line with this point, VMHC of IPL mediated the relationship between age and the percent ratio of correct design scores (at trend level), suggesting that IPL function plays a pivotal role in age-related performance alteration of design fluency task. Our findings extend previous ones that found age-related functional reorganization of FPCN contributing to cognitive ability decline, suggesting that the alterations of interhemispheric functional coupling of posterior parietal cortex might also contribute to age-related performance decline in design cognition.

Limitations

In the current study, there are some limitations that should be noted. First, previous studies have indicated that aging influences the brain in multiple ways, such as alteration of cortical thickness, gray matter volume, and functional organization. The current study shed light on alterations of interhemispheric communication with aging, but in future work, it will be important to study other kinds of brain FC to investigate more comprehensive patterns of age-related brain functional reorganization. For example, one could employ connectome-based individualized prediction modeling (Jiang et al., 2018). Second, we did not perform test–retest examination on independent data due to unavailability of a similar resting fMRI data with similar age range and executive function test. Future studies are thus needed to replicate our findings.

CONCLUSION

The current study highlights age-related interhemispheric FC alterations and explores the links between these alterations and executive function. Aging was associated with interhemispheric FC alterations of brain areas belonging to medial temporal lobe subsystem of DMN, insula, and dorsal ACC of SN, and IPL of FPCN. Further, interhemispheric FC alterations contributed to age-related executive function change. Our findings provide new evidence for theories of age-related cognitive decline.

DATA AVAILABILITY STATEMENT

The datasets generated for this study are available on request to the corresponding author.

ETHICS STATEMENT

The studies involving human participants were reviewed and approved by the local Institutional Review Board (IRB) at the NKI. The patients/participants provided their written informed consent to participate in this study.

AUTHOR CONTRIBUTIONS

JZ, HS, PZ, JG, and YS analyzed the data and performed the statistical analysis. JZ, PM, CW, and G-JW wrote the first draft of the manuscript. G-JW and DH contributed to the conception and design of the study.

FUNDING

This work was supported by the National Natural Science Foundation of China under Grant No. 81601563 (JZ), Key Industrial Innovation Chain Project in Agricultural Domain (Grant No. 2019ZDLNY02-05) (JZ), and in part by Intramural Research Program of the United States National Institute of Alcohol Abuse and Alcoholism (PM, CW, GJ-W, Y01AA3009).

SUPPLEMENTARY MATERIAL

The Supplementary Material for this article can be found online at: https://www.frontiersin.org/articles/10.3389/fnagi.2020.00020/full#supplementary-material

REFERENCES

Adólfsdóttir, S., Wollschlaeger, D., Wehling, E., and Lundervold, A. J. (2016). Inhibition and switching in healthy aging: a longitudinal study. *J. Int. Neuropsychol. Soc.* 23, 90–97. doi: 10.1017/s1355617716000898

Allen, E., Erhardt, E., Damaraju, E., Gruner, W., Segall, J., Silva, R., et al. (2011). A baseline for the multivariate comparison of resting-state networks. *Front. Syst. Neurosci.* 5:2. doi: 10.3389/fnsys.2011.00002

Anderson, N. D., and Craik, F. I. (2017). 50 years of cognitive aging theory. *J. Gerontol.* 72, 1–6. doi: 10.1093/geronb/gbw108

Andrews-Hanna, J. R., Reidler, J. S., Sepulcre, J., Poulin, R., and Buckner, R. L. (2010). Functional-anatomic fractionation of the brain's default network. *Neuron* 65, 550–562. doi: 10.1016/j.neuron.2010.02.005

Andrews-Hanna, J. R., Snyder, A. Z., Vincent, J. L., Lustig, C., Head, D., Raichle, et al. (2007). Disruption of large-scale brain systems in advanced aging. *Neuron* 56, 924–935. doi: 10.1016/j.neuron.2007.10.038

Araneda, R., Renier, L., Dricot, L., Decat, M., Ebnerkarestinos, D., Deggouj, N., et al. (2018). A key role of the prefrontal cortex in the maintenance of chronic tinnitus: an fMRI study using a Stroop task. *Neuroimage Clin.* 17, 325–334. doi: 10.1016/j.nicl.2017.10.029

Balodis, I. M., Molina, N. D., Kober, H., Worhunsky, P. D., White, M. A., Sinha, R., et al. (2013). Divergent neural substrates of inhibitory control in binge eating disorder relative to other manifestations of obesity. *Obesity* 21, 367–377. doi: 10.1002/oby.20068

Duchek, J. M., Balota, D. A., Thomas, J. B., Snyder, A. Z., Rich, P., and Benzinger, T. L. (2013). Relationship between stroop performance and resting state functional connectivity in cognitively normal older adults. *Neuropsychology* 27, 516–528. doi: 10.1037/a0033402

Beck, A. T., Steer, R. A., and Carbin, M. G. (1988). Psychometric properties of the beck depression inventory: twenty-five years of evaluation. *Clin. Psychol. Rev.* 8, 77–100. doi: 10.1016/0272-7358(88)90050-5

Bluhm, R. L., Osuch, E. A., Lanius, R. A., Boksman, K., Neufeld, R. W., Théberge, J., et al. (2008). Default mode network connectivity: effects of age, sex, and analytic approach. *Neuroreport* 19, 887–891. doi: 10.1097/wnr.0b013e328300ebbf

Cabeza, R. (2002). Hemispheric asymmetry reduction in older adults: the HAROLD model. *Psychol. Aging* 17, 85–100. doi: 10.1037/0882-7974.17.1.85

Campbell, K. L., Grady, C. L., Ng, C., and Hasher, L. (2012). Age differences in the frontoparietal cognitive control network: implications for distractibility. *Neuropsychologia* 50, 2212–2223. doi: 10.1016/j.neuropsychologia.2012.05.025

Chan, M. Y., Park, D. C., Savalia, N. K., Petersen, S. E., and Wig, G. S. (2014). Decreased segregation of brain systems across the healthy adult lifespan. *Proc. Natl. Acad. Sci. U.S.A.* 111:E4997.

Cieslik, E. C., Mueller, V. I., Eickhoff, C. R., Langner, R., and Eickhoff, S. B. (2015). Three key regions for supervisory attentional control: evidence from neuroimaging meta-analyses. *Neurosci. Biobehav. Rev.* 48, 22–34. doi: 10.1016/j.neubiorev.2014.11.003

Colcombe, S. J., Kramer, A. F., Erickson, K. I., and Paige, S. (2005). The implications of cortical recruitment and brain morphology for individual differences in inhibitory function in aging humans. *Psychol. Aging* 20, 363–375. doi: 10.1037/0882-7974.20.3.363

Damoiseaux, J. S., Beckmann, C. F., Arigita, E. J. S., Barkhof, F., Scheltens, P., Stam, C. J., et al. (2008). Reduced resting-state brain activity in the "default network" in normal aging. *Cereb. Cortex* 18, 1856–1864. doi: 10.1093/cercor/bhm207

Daniel, Z., Vladimir, L., Friston, K. J., and Joseph, C. (2015). Sensory processing and the rubber hand illusion–an evoked potentials study. *J. Cogn. Neurosci.* 27, 573–582. doi: 10.1162/jocn_a_00705

Diamond, A. (2013). Executive functions. *Annu. Rev. Psychol.* 64, 135–168.

Eckert, M. A., Menon, V., Walczak, A., Ahlstrom, J., Denslow, S., and Horwitz, A. (2010). At the heart of the ventral attention system: the right anterior insula. *Hum. Brain Mapp.* 30, 2530–2541. doi: 10.1002/hbm.20688

Eckert, M. A., Menon, V., Walczak, A., Ahlstrom, J., Denslow, S., Horwitz, A., et al. (2009). At the heart of the ventral attention system: the right anterior insula. *Hum. Brain Mapp.* 30, 2530–2541. doi: 10.1002/hbm.20688

Eklund, A., Nichols, T. E., and Knutsson, H. (2016). Cluster failure: why fMRI inferences for spatial extent have inflated false-positive rates. *Proc. Natl. Acad. Sci. U.S.A.* 113:7900. doi: 10.1073/pnas.1602413113

Elman, J. A., Madison, C. M., Baker, S. L., Vogel, J. W., Marks, S. M., Crowley, S., et al. (2014). Effects of beta-amyloid on resting state functional connectivity within and between networks reflect known patterns of regional vulnerability. *Cereb. Cortex* 26, 695–707. doi: 10.1093/cercor/bhu259

Ferreira, L. K., and Busatto, G. F. (2013). Resting-state functional connectivity in normal brain aging. *Neurosci. Biobehav. Rev.* 37, 384–400. doi: 10.1016/j.neubiorev.2013.01.017

Flandin, G., and Friston, K. J. (2019). Analysis of family-wise error rates in statistical parametric mapping using random field theory. *Hum. Brain Mapp.* 40, 2052–2054. doi: 10.1002/hbm.23839

Frederiksen, K. S., and Waldemar, G. (2012). *Corpus callosum* in aging and neurodegenerative diseases. *Neurodegener. Dis. Manag.* 2, 493–502. doi: 10.2217/nmt.12.52

Geerligs, L., Renken, R. J., Saliasi, E., Maurits, N. M., and Lorist, M. M. (2014a). A brain-wide study of age-related changes in functional connectivity. *Cereb. Cortex* 25, 1987–1999. doi: 10.1093/cercor/bhu012

Geerligs, L., Saliasi, E., Maurits, N. M., Renken, R. J., and Lorist, M. M. (2014b). Brain mechanisms underlying the effects of aging on different aspects of selective attention. *Neuroimage* 91, 52–62. doi: 10.1016/j.neuroimage.2014.01.029

Grady, C. (2012). The cognitive neuroscience of ageing. *Nat. Rev. Neurosci.* 13, 491–505. doi: 10.1038/nrn3256

Grady, C., Sarraf, S., Saverino, C., and Campbell, K. (2016). Age differences in the functional interactions among the default, frontoparietal control, and dorsal attention networks. *Neurobiol. Aging* 41, 159–172. doi: 10.1016/j.neurobiolaging.2016.02.020

Harding, I. H., Yücel, M., Harrison, B. J., Pantelis, C., and Breakspear, M. (2015). Effective connectivity within the frontoparietal control network differentiates cognitive control and working memory. *Neuroimage* 106, 144–153. doi: 10.1016/j.neuroimage.2014.11.039

Harrington, K. D., Lim, Y. Y., Ames, D., Hassenstab, J., Rainey-Smith, S., Robertson, J., et al. (2017). Using robust normative data to investigate the neuropsychology of cognitive aging. *Arch. Clin. Neuropsychol.* 32, 142–154. doi: 10.1093/arclin/acw106

He, X., Qin, W., Liu, Y., Zhang, X., and Yu, C. (2014). Abnormal salience network in normal aging and in amnestic mild cognitive impairment and Alzheimer's disease. *Hum. Brain Mapp.* 35, 3446–3464. doi: 10.1002/hbm.22414

Homack, S., Lee, D., and Riccio, C. A. (2005). Test review: delis-kaplan executive function system. *J. Clin. Exp. Neuropsychol.* 27, 599–609. doi: 10.1080/13803390490918444

Hoptman, M. J., Zuo, X. N., D'Angelo, D., Mauro, C. J., Butler, P. D., Milham, M. P., et al. (2012). Decreased interhemispheric coordination in schizophrenia: a resting state fMRI study. *Schizophr. Res.* 141, 1–7. doi: 10.1016/j.schres.2012.07.027

Ivnik, R. J., Malec, J. F., Smith, G. E., Tangalos, E. G., and Petersen, R. C. (1996). Neuropsychological tests' norms above age 55: COWAT, BNT, MAE token, WRAT-R reading, AMNART, STROOP, TMT, and JLO. *Clin. Neuropsychol.* 10, 262–278. doi: 10.1080/13854049608406689

Jiang, R., Calhoun, V. D., Zuo, N., Lin, D., Li, J., Fan, L., et al. (2018). Connectome-based individualized prediction of temperament trait scores. *Neuroimage* 183, 366–374. doi: 10.1016/j.neuroimage.2018.08.038

Keiichi, O., Masaki, I., and Shuhei, Y. (2012). Decreased functional connectivity by aging is associated with cognitive decline. *Cogn. Neurosci. J.* 24, 2186–2198. doi: 10.1162/jocn_a_00269

Kelly, C., Zuo, X. N., Gotimer, K., Cox, C. L., Lynch, L., Brock, D., et al. (2011). Reduced interhemispheric resting state functional connectivity in cocaine addiction. *Biol. Psychiatry* 69, 684–692. doi: 10.1016/j.biopsych.2010.11.022

Klein, M., Ponds, R. W. H. M., Houx, P. J., and Jolles, J. (1997). Effect of test duration on age-related differences in stroop interference. *J. Clin. Exp. Neuropsychol.* 19, 77–82. doi: 10.1080/01688639708403838

Koch, W., Teipel, S., Mueller, S., Buerger, K., Bokde, A. L. W., Hampel, H., et al. (2010). Effects of aging on default mode network activity in resting state fMRI: does the method of analysis matter? *Neuroimage* 51, 280–287. doi: 10.1016/j.neuroimage.2009.12.008

Kornfeld, S., Yuan, R., Biswal, B. B., Grunt, S., Kamal, S., Delgado Rodriguez, J. A., et al. (2018). Resting-state connectivity and executive functions after pediatric arterial ischemic stroke. *Neuroimage Clin.* 17, 359–367. doi: 10.1016/j.nicl.2017.10.016

Krall, S. C., Rottschy, C., Oberwelland, E., Bzdok, D., Fox, P. T., Eickhoff, S. B., et al. (2015). The role of the right temporoparietal junction in attention and

social interaction as revealed by ALE meta-analysis. *Brain Struct. Funct.* 220, 587–604. doi: 10.1007/s00429-014-0803-z

Kramer, J. H., Lovingly, Q., David, D., John, N., Rosen, H. J., Cathra, H., et al. (2007). Magnetic resonance imaging correlates of set shifting. *J. Int. Neuropsychol. Soc.* 13, 386–392.

La Corte, V., Sperduti, M., Malherbe, C., Vialatte, F., Lion, S., Gallarda, T., et al. (2016). Cognitive decline and reorganization of functional connectivity in healthy aging: the pivotal role of the salience network in the prediction of age and cognitive performances. *Front. Aging Neurosci.* 8:204. doi: 10.3389/fnagi.2016.00204

Langner, R., and Eickhoff, S. B. (2013). Sustaining attention to simple tasks: a meta-analytic review of the neural mechanisms of vigilant attention. *Psychol. Bull.* 139, 870–900. doi: 10.1037/a0030694

Lanting, S., Haugrud, N., and Crossley, M. (2009). The effect of age and sex on clustering and switching during speeded verbal fluency tasks. *J. Int. Neuropsychol. Soc.* 15, 196–204. doi: 10.1017/S1355617709090237

Leung, H. C., Skudlarski, P., Gatenby, J. C., Peterson, B. S., and Gore, J. C. (2000). An event-related functional MRI study of the stroop color word interference task. *Cereb. Cortex* 10, 552–560. doi: 10.1093/cercor/10.6.552

Li, H. J., Hou, X. H., Liu, H. H., Yue, C. L., Lu, G. M., and Zuo, X. N. (2015). Putting age-related task activation into large-scale brain networks: a meta-analysis of 114 fMRI studies on healthy aging. *Neurosci. Biobehav. Rev.* 57, 156–174. doi: 10.1016/j.neubiorev.2015.08.013

Li, K. C., Luo, X., Zeng, Q. Z., Xu, X. J., Huang, P. Y., Shen, Z. J., et al. (2018). Distinct patterns of interhemispheric connectivity in patients with early- and late-onset Alzheimer's disease. *Front Aging Neurosci.* 10:261. doi: 10.3389/fnagi.2018.00261

Luo, X., Li, K., Zeng, Q., Huang, P., Jiaerken, Y., Qiu, T., et al. (2018). Decreased bilateral FDG-PET uptake and inter-hemispheric connectivity in multi-domain amnestic mild cognitive impairment patients: a preliminary study. *Front. Aging Neurosci.* 10:161. doi: 10.3389/fnagi.2018.00161

Mace, R. A., Waters, A. B., Sawyer, K. S., Turrisi, T., and Gansler, D. A. (2018). Components of executive function predict regional prefrontal volumes. *bioRxiv [Preprint]*

Madhyastha, T. M., and Grabowski, T. J. (2014). Age-related differences in the dynamic architecture of intrinsic networks. *Brain Connect.* 4, 231–241. doi: 10.1089/brain.2013.0205

Manuela, B., Laura, D., Gabriella, B., Maurizio, S., and Eraldo, P. (2013). Reassessing the HAROLD model: is the hemispheric asymmetry reduction in older adults a special case of compensatory-related utilisation of neural circuits? *Exp. Brain Res.* 224, 393–410. doi: 10.1007/s00221-012-3319-x

Mattioli, F., Stampatori, C., Bellomi, F., Scarpazza, C., Galli, P., Guarneri, C., et al. (2014). Assessing executive function with the D-KEFS sorting test: normative data for a sample of the Italian adult population. *Neurol. Sci.* 35, 1895–1902. doi: 10.1007/s10072-014-1857-7

Morelli, S. A., Sacchet, M. D., and Zaki, J. (2015). Common and distinct neural correlates of personal and vicarious reward: a quantitative meta-analysis. *Neuroimage* 112, 244–253. doi: 10.1016/j.neuroimage.2014.12.056

Nooner, K. B., Colcombe, S., Tobe, R., Mennes, M., Benedict, M., Moreno, A., et al. (2012). The NKI-rockland sample: a model for accelerating the pace of discovery science in psychiatry. *Front. Neurosci.* 6:152. doi: 10.3389/fnins.2012.00152

Oldfield, R. C. (1971). The assessment and analysis of handedness: the Edinburgh inventory. *Neuropsychologia* 9, 97–113. doi: 10.1016/0028-3932(71)90067-4

Possin, K. L., Chester, S. K., Victor, L., Alan, B., Rosen, H. J., Miller, B. L., et al. (2012). The frontal-anatomic specificity of design fluency repetitions and their diagnostic relevance for behavioral variant frontotemporal dementia. *J. Int. Neuropsychol. Soc.* 18, 834–844. doi: 10.1017/s1355617712000604

Potenza, M. N., Hoi-Chung, L., Blumberg, H. P., Peterson, B. S., Fulbright, R. K., Lacadie, C. M., et al. (2003). An FMRI Stroop task study of ventromedial prefrontal cortical function in pathological gamblers. *Am. J. Psychiatry* 160, 1990–1994. doi: 10.1176/appi.ajp.160.11.1990

Power, J. D., Mitra, A., Laumann, T. O., Snyder, A. Z., Schlaggar, B. L., and Petersen, S. E. (2014). Methods to detect, characterize, and remove motion artifact in resting state fMRI. *Neuroimage* 84, 320–341. doi: 10.1016/j.neuroimage.2013.08.048

Qiu, Y. W., Jiang, G. H., Ma, X. F., Su, H. H., Lv, X. F., and Zhuo, F. Z. (2017). Aberrant interhemispheric functional and structural connectivity in heroin-dependent individuals. *Addict. Biol.* 22, 1057–1067. doi: 10.1111/adb.12387

Ready, R. E. (2010). Emotion and executive functioning: the effect of normal mood states on fluency tasks. *J. Clin. Exp. Neuropsychol.* 32, 225–230. doi: 10.1080/13803390902902458

Reber, J., Feinstein, J. S., O'Doherty, J. P., Liljeholm, M., Adolphs, R., and Tranel, D. (2017). Selective impairment of goal-directed decision-making following lesions to the human ventromedial prefrontal cortex. *Brain* 140, 1743–1756. doi: 10.1093/brain/awx105

Reuter-Lorenz, P. A., and Park, D. C. (2010). Human neuroscience and the aging mind: a new look at old problems. *J. Gerontol. B Psychol. Sci. Soc. Sci.* 65, 405–415. doi: 10.1093/geronb/gbq035

Sala-Llonch, R., Arenaza-Urquijo, E. M., Valls-Pedret, C., Vidal-Piñeiro, D., Bargalló, N., Junque, C., et al. (2012). Dynamic functional reorganizations and relationship with working memory performance in healthy aging. *Front. Hum. Neurosci.* 6:152. doi: 10.3389/fnhum.2012.00152

Sanders, C., and Schmitter-Edgecombe, M. (2012). Identifying the nature of impairment in planning ability with normal aging. *J. Clin. Exp. Neuropsychol.* 34, 724–737. doi: 10.1080/13803395.2012.670210

Sanne, D. W., Corlett, P. R., Aitken, M. R., Anthony, D., and Fletcher, P. C. (2009). Differential engagement of the ventromedial prefrontal cortex by goal-directed and habitual behavior toward food pictures in humans. *J. Neurosci.* 29, 11330–11338. doi: 10.1523/jneurosci.1639-09.2009

Seeley, W., Menon, V., Af, Keller, J., Glover, G., Kenna, H., et al. (2007). Dissociable intrinsic connectivity networks for salience processing and executive control. *J. Neurosci.* 27, 2349–2356. doi: 10.1523/jneurosci.5587-06.2007

Siman-Tov, T., Bosak, N., Sprecher, E., Paz, R., Eran, A., Aharon-Peretz, J., et al. (2017). Early age-related functional connectivity decline in high-order cognitive networks. *Front. Aging Neurosci.* 8:330. doi: 10.3389/fnagi.2016.00330

Sridharan, D., Levitin, D. J., and Menon, V. (2008). A critical role for the right fronto-insular cortex in switching between central-executive and default-mode networks. *Proc. Natl. Acad. Sci. U.S.A.* 105, 12569–12574. doi: 10.1073/pnas.0800005105

Swanson, J. (2005). The delis-kaplan executive function system: a review. *Can. J. Sch. Psychol.* 20, 117–128. doi: 10.1177/0829573506295469

Tim, H., Marcia, C., Benjamin, P., Martin, J., Nicholas, G., Masud, H., et al. (2007). The role of the ventrolateral frontal cortex in inhibitory oculomotor control. *Brain* 130(Pt 6), 1525–1537. doi: 10.1093/brain/awm064

Tomasi, D., and Volkow, N. D. (2012). Aging and functional brain networks. *Mol. Psychiatry* 17, 549–558. doi: 10.1038/mp.2011.81

Troyer, A. K., Larry, L., and Esther, S. (2006). Aging and response inhibition: normative data for the Victoria Stroop Test. *Aging Neuropsychol. Cogn.* 13, 20–35. doi: 10.1080/138255890968187

Ulman, L. (2014). Human cognitive aging: corriger la fortune? *Science* 6209, 572–578. doi: 10.1126/science.1254403

Valentin, V. V., Anthony, D., and O'Doherty, J. P. (2007). Determining the neural substrates of goal-directed learning in the human brain. *J. Neurosci.* 27, 4019–4026. doi: 10.1523/jneurosci.0564-07.2007

Vincent, J. L., Itamar, K., Snyder, A. Z., Raichle, M. E., and Buckner, R. L. (2008). Evidence for a frontoparietal control system revealed by intrinsic functional connectivity. *J. Neurophysiol.* 100, 3328–3342. doi: 10.1152/jn.90355.2008

Wager, T. D., Davidson, M. L., Hughes, B. L., Lindquist, M. A., and Ochsner, K. N. (2008). Prefrontal-subcortical pathways mediating successful emotion regulation. *Neuron* 59, 1037–1050. doi: 10.1016/j.neuron.2008.09.006

Wang, Z., Wang, J., Zhang, H., Mchugh, R., Sun, X., Li, K., et al. (2015). Interhemispheric functional and structural disconnection in Alzheimer's disease: a combined resting-state fMRI and DTI study. *PLoS One* 10:e0126310. doi: 10.1371/journal.pone.0126310

Wecker, N. S., Kramer, J. H., Hallam, B. J., and Delis, D. C. (2005). Mental flexibility: age effects on switching. *Neuropsychology* 19, 345–352. doi: 10.1037/0894-4105.19.3.345

Wu, J.-T., Wu, H.-Z., Yan, C.-G., Chen, W.-X., Zhang, H.-Y., He, Y., et al. (2011). Aging-related changes in the default mode network and its anti-correlated networks: a resting-state fMRI study. *Neurosci. Lett.* 504, 62–67. doi: 10.1016/j.neulet.2011.08.059

Yan, C.-G., Wang, X.-D., Zuo, X.-N., and Zang, Y.-F. (2016). DPABI: data processing & analysis for (resting-state) brain imaging. *Neuroinformatics* 14, 339–351. doi: 10.1007/s12021-016-9299-4

Yana, S., Kraybill, M. L., and Gidley Larson, J. C. (2010). Understanding design fluency: motor and executive contributions. *J. Int. Neuropsychol. Soc.* 16, 26–37. doi: 10.1017/s1355617709990804

Zhang, H.-Y., Chen, W.-X., Jiao, Y., Xu, Y., Zhang, X.-R., and Wu, J.-T. (2014). Selective vulnerability related to aging in large-scale resting brain networks. *PLoS One* 9:e108807. doi: 10.1371/journal.pone.0108807

Zuo, X.-N., Kelly, C., Di Martino, A., Mennes, M., Margulies, D. S., Bangaru, S., et al. (2010). Growing together and growing apart: regional and sex differences in the lifespan developmental trajectories of functional homotopy. *J. Neurosci.* 30, 15034–15043. doi: 10.1523/jneurosci.2612-10.2010

Zysset, S., and Schroeter, M. L. (2007). Stroop interference, hemodynamic response and aging: an event-related fMRI study. *Neurobiol. Aging* 28, 937–946. doi: 10.1016/j.neurobiolaging.2006.05.008

Conflict of Interest: The authors declare that the research was conducted in the absence of any commercial or financial relationships that could be construed as a potential conflict of interest.

frontiers in Psychiatry

ORIGINAL RESEARCH
published: 28 February 2020
doi: 10.3389/fpsyt.2020.00100

Leukocyte Telomere Length Is Related to Brain Parenchymal Fraction and Attention/Speed in the Elderly: Results of the Austrian Stroke Prevention Study

Piyush Gampawar[1], *Reinhold Schmidt*[2] *and Helena Schmidt*[1]*

[1] Research Unit-Genetic Epidemiology, Gottfried Schatz Research Centre for Cell Signalling, Metabolism and Aging, Molecular Biology and Biochemistry, Medical University Graz, Graz, Austria, [2] Department of Neurology, Clinical Division of Neurogeriatrics, Medical University Graz, Graz, Austria

There are controversial results if leukocyte telomere length (LTL) is related to structural brain changes and cognitive decline in aging. Here, we investigated the association between LTL and 1) global MRI correlates of brain aging such as brain parenchymal fraction (BPF) and white matter hyperintensities (WMH) load and Fazekas score as well as 2) global (g-factor) and domain-specific cognition such as attention/speed, conceptualization, memory, and visuopractical skills. In total, 909 participants of the Austrian Stroke Prevention Study with LTL, MRI, and cognitive tests were included. There were 388 (42.7%) men, and the mean age was 65.9 years. Longer LTL was significantly associated with larger BPF ($\beta = 0.43$, $p < 0.001$), larger WMH load ($\beta = 0.03$, $p = 0.04$), and score ($\beta = 0.05$, $p = 0.04$) after adjusting for age, sex, vascular risk factors, and ApoE4 carrier status. The effect on BPF was more significant in the subgroups of women ($\beta = 0.51$, $p = 0.001$), age >65 years ($\beta = 0.58$, $p = 0.002$), BMI ≥ 25 ($\beta = 0.40$, $p = 0.004$), education ≤10 years ($\beta = 0.42$, $p = 0.002$), hypertensives ($\beta = 0.51$, $p = 0.001$), cardiovascular disease (CVD) ($\beta = 0.58$, $p = 0.005$), non-diabetics ($\beta = 0.42$, $p < 0.001$), and Apoe4 non-carriers ($\beta = 0.49$, $p < 0.001$). The effect on WMH was significant within the hypertensives (load: $\beta = 0.04$, $p = 0.02$), non-diabetics (load:$\beta = 0.03$, $p = 0.01$; score: $\beta = 0.06$, $p = 0.02$), in those with education ≤10 years (load: $\beta = 0.03$, $p = 0.04$; score: $\beta = 0.07$, $p = 0.02$), in ApoE4 non-carriers (load: $\beta = 0.03$, $p = 0.02$; score: $\beta = 0.07$, $p = 0.01$) and in subjects without CVD (score: $\beta = 0.06$, $p = 0.05$). We only observed a significant association between LTL and the cognitive domain of attention/speed, which was confined to the subgroups of BMI ≥ 25 ($\beta = 0.04$, $p = 0.05$) and education ≤10 years ($\beta = 0.04$, $p = 0.05$). The effect of LTL on attention/speed was partly mediated in both subgroups by BPF ($\beta = 0.02$, 95% CI = 0.01:0.03) when tested by bootstrapping. Our results support a strong protective role of longer LTL on global brain volume which in turn may contribute to better cognitive functions, especially in the attention/speed domain in the elderly.

Keywords: telomeres, leukocyte telomere length, brain aging, cognition, brain parenchymal fraction, white matter hyperintensities, attention/speed

OPEN ACCESS

Edited by:
Francesco Ernesto Pontieri, Sapienza University of Rome, Italy

Reviewed by:
Fabrizio Piras, Santa Lucia Foundation (IRCCS), Italy
Alessio Squassina, University of Cagliari, Italy

***Correspondence:**
Helena Schmidt
helena.schmidt@medunigraz.at

Specialty section:
This article was submitted to Aging Psychiatry, a section of the journal Frontiers in Psychiatry

Received: *21 October 2019*
Accepted: *06 February 2020*
Published: *28 February 2020*

Citation:
Gampawar P, Schmidt R and Schmidt H (2020) Leukocyte Telomere Length Is Related to Brain Parenchymal Fraction and Attention/Speed in the Elderly: Results of the Austrian Stroke Prevention Study. Front. Psychiatry 11:100. doi: 10.3389/fpsyt.2020.00100

INTRODUCTION

Telomeres are nucleoprotein protective caps at the end of the chromosomes containing repeating hexamer, TTAGGG, sequences. They shorten during mitosis due to the inability of the DNA polymerase to complete replication, and due to oxidative stress, they are particularly prone to. During life, there are two phases of accelerated telomere attrition 1) during development up to puberty due to the high number of cell divisions and 2) during aging due to a high level of oxidative stress (1). Telomere shortening destabilizes the genome and leads to the senescence of the affected cells. Cellular senescence is part of the aging process at the organismal level as well (2). In human epidemiological studies, leukocyte telomere length (LTL) is used as a biological marker of aging (3). LTL also reflects the telomere length of other cell types within the body, which is called synchrony. The heritability estimate of LTL is approximately 60%, while that of LTL shortening approximately 30%. Shorter LTL is related to the presence of vascular risk factors such as smoking, obesity, physical inactivity, poor diet, hypertension, and type 2 diabetes mellitus (2, 3). It is associated with age-related chronic vascular and degenerative diseases, especially with Alzheimer's disease and stroke (2, 4). Shorter LTL is also related to all-cause mortality in the elderly (5).

The role of telomeres in normal brain aging is debated. LTL, as well as LTL attrition, has been associated with structural brain changes on magnetic resonance imaging (MRI), including both regional and global brain volumes as well as with white matter hyperintensities (WMH) (6, 7). Results are particularly inconsistent with the effect of short LTL on cognitive function and decline. No relationship was observed in the Dallas Heart Study (DHS) including 2606 subjects between LTL and cognition (8), while recently 2 large meta-analyses studies found an association between longer LTL and higher level of general cognition (9) as well as better cognitive performance and better memory, speed, and executive function (10). Also, longitudinal studies reported associations between LTL attrition and cognitive decline (11).

Studies investigating the effect of LTL on both brain structure and cognitive function in a simultaneous way at the population level are so far largely missing. Here, we tested the hypothesis that longer LTL is related to 1) better structural preservation of the brain such as larger brain parenchymal fraction (BPF) and less WMH, 2) better cognitive performances including g-factor and composite scores for attention/speed, conceptualization, memory, visuopractical skills. We tested the hypothesis in a large cohort of normal elderly participating in the Austrian Stroke Prevention Study (ASPS) (12). We explored if the effect of LTL on brain phenotypes is modified by the presence of risk factors such as sex, age, hypertension, body mass index (BMI), education, diabetes, cardiovascular disease (CVD), and ApoE4 carrier status using subgroup analyses. We also performed mediation analyses to asses if the observed significant effects of LTL on cognition are mediated by structural brain changes (**Figure 1**). To our knowledge, this is the first study finding evidence that the protective effect of LTL on the brain is highly significant at the structural level and that this, in turn, may transform into better cognition in the attention/speed domain.

METHODS

Participants

In the present study, we included 909 participants from the ASPS, a community-dwelling cohort study in the elderly population in the city of Graz, Austria, who underwent LTL measurements along with MRI and cognitive tests (12). The study was approved by the Medical Ethics Committee of Karl-Franzens University of Graz. Written informed consent was obtained from all study participants. The mean age of the participants was 65.9 ± 8 years (range: 46–90), 42.7% were males, 69.4% hypertensives, 10.9% diabetics, and 40% had CVD. The mean years of education were 11.3 ± 2.6 (range: 9–18 years). There were 28.3% former smokers and 11% current smokers in the study sample. In total, 898 participants had the ApoE4 genotypes, with 0.8% being homozygous and 19.3% heterozygous carriers.

LTL Measurement

All 909 participants had LTL measurements. A detailed description of the method was published previously (13). In brief, DNA was extracted from EDTA whole peripheral blood using the phenol-chloroform method. Two quantitative polymerase chain reactions were used to measure telomere repeat copy (T) and single-copy gene (*36B4*) (S). We normalized the relative LTL (T/S ratio) using reference DNA pooled from 24 subjects, and the final T/S ratio was calculated according to Cawthon's modified method (14). The median of relative LTL was 0.61 (range: 0.05–2.60). The median of LTL was 0.61 (IQR: 0.47 to 0.82).

Brain MRI

All MRI scans were performed on 1.5T scanners using proton density- and T2-weighted sequences. All punctate early confluent and confluent WMH in the deep and subcortical white matter and periventricular WMHs irregularly extending into the deep white matter were marked and outlined on a transparency that was overlaid on the proton density scan. Periventricular caps, pencil-thin lining, and periventricular halos were not included for WMH load measurement as these changes are considered to be of non-ischemic origin. Independent from visual analysis, WMH load measurements were done on proton density-weighted images on an UltraSPARC workstation (Sun Microsystems, Santa Clara, CA) by a trained operator using DISPImage. The operators used a hardcopy overlaid by the transparency, with each single lesion outlined by the experienced readers as reference. Every single lesion was segmented on the computer image, and its area was provided by the semi-automated thresholding algorithm implemented in DISPImage. Each hyperintensity volume was calculated by multiplying the area by slice thickness. Total

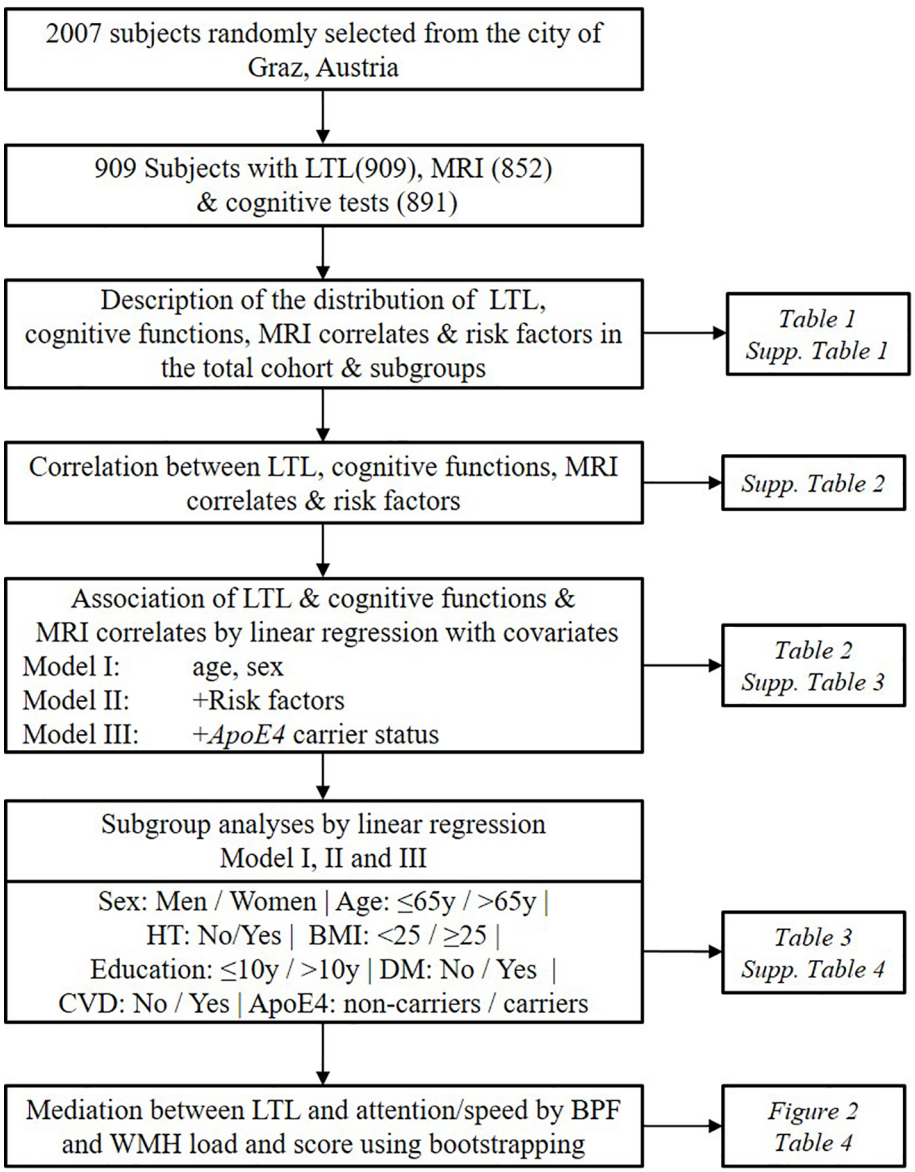

FIGURE 1 | Workflow of the study design. The current study cohort is a subsample of the Austrian Stroke Prevention Study. Risk factors include hypertension, diabetes, cardiovascular diseases, body mass index, education, high-density lipoprotein, and smoking status. LTL, Leukocyte Telomere Length; HT, Hypertension; DM, Diabetes Mellitus; CVD, Cardiovascular Disease; BPF, Brain Parenchymal Fraction; WMH, White Matter Hyperintensities.

WMH load in cubic millimetres was the sum of volumes of single lesions in a given study participant. WMH load was available from 827 participants. WMH score was based on the Fazekas scale on deep white matter changes where a score of 0 is an absence of any white matter change, 1 is punctate foci, 2 is beginning confluence of foci, and 3 is large confluent areas (15). WMH score was available in 852 participants. Brain volume was calculated from the T2-weighted spin-echo sequence using automated structural image evaluation of atrophy[1]. BPF is the ratio of brain parenchymal volume to total intracranial volume (16). BPF was available in 739 subjects.

Cognitive Testing

For cognitive evaluation, participants went through a group of tests to assess performance in the domains of attention/speed, conceptualization, memory, and visuopractical skills. In detail, information on the conduction of these tests is published previously (12). The measures of the cognitive performance were converted into z-scores by normalizing to the mean of the group. G-factor, which is the first unrotated component of

[1] SIENEX, part of FMRIB Software Library; https://fsl.fmrib.ox.ac.uk/fsl/fslwiki/

principal component analysis performed on the results of the battery of cognitive tests, was used as a measure of global cognition (17).

Covariate Analyses

Hypertension was coded as a categorical variable, and a participant considered as hypertensive when there was a history of hypertension or hypertension medication or mean systolic blood pressure ≥ 140 mm of Hg or mean diastolic pressure ≥ 90 mm of hg. Diabetes was defined as a history of diabetes, use of antidiabetic treatment, or fasting blood sugar level >140 mg/dl. Cardiovascular disease assumed to be present if there was evidence of cardiac abnormalities known to be a source for cerebral embolism, evidence of coronary heart disease, appropriate ECG findings, or if an individual presented signs of left ventricular hypertrophy on echocardiogram or ECG (12). Education was measured in years of schooling, meaning the number of years a person attended school including university and higher education programs. Smoking status was assigned after asking each participant whether they ever smoked or if they are currently smoking. It was coded in the form of never, former, or current smoker. Participants were genotyped for the presence of E4 allele using PCR-RFLP and graded as heterozygous (presence of one allele), homozygous (presence of two alleles), or absence of E4 allele (18).

Statistical Analyses

The statistical analysis was performed using IBM SPSS statistics version 25[2]. The normal distribution of the variables was tested using the Kolmogorov-Smirnov test and by visual inspection of histograms. LTL measurement was transformed into z-scores relative to the mean of the whole group. The z-transformation was done by subtracting the mean LTL of the cohort from the observed value of that individual and dividing by the standard deviation. This was done to interpret the relative position of a particular individual under the LTL distribution curve of the cohort. The skewed distribution of WMH load was converted into normal distribution by log transformation after adding 1 to the volume. BPF was converted into percentage by multiplying the value of fraction by 100 to facilitate the interpretation of the results from linear regression. Cognitive tests had a normal distribution. One outlier with a value of -5.95 within the attention/speed domain was removed.

Co-variates for multiple linear regression models were selected based on their correlation with outcome variables and LTL (Pearson's correlation $p < 0.1$) and/or based on previous reports on their association with the phenotypes. Linear regression models were used to test the effect of LTL on brain morphological measures and cognition in the presence of age, sex, risk factors such as hypertension, diabetes, cardiovascular disease, BMI, HDL, years of education, smoking, and ApoE4 genotypes. Model I was adjusted for age and sex, Model II, additionally for hypertension, diabetes, cardiovascular disease, BMI, education, HDL, and smoking status, and Model III for ApoE4 carrier status. We formally tested the collinearity amongst independent variables by calculating variance inflation factors. The variance inflation factor for all independent variables was <1.5, indicating almost no correlation between them.

Subgroup Analyses

We divided our cohort into subgroups based on sex (men/women), age (≤ 65y/ > 65y), hypertension (normotensives/hypertensives), BMI (normal weight: < 25 Kg/m^2/overweight: ≥25 kg/m^2), education (basic education ≤ 10y/ > 10y mid to high education), diabetes (No/Yes), CVD (No/Yes), and ApoE4 carrier status (No/Yes).

The continuous variables age and BMI were used as covariates in the subgroup analyses within the respective subgroups of age ≤ 65y/ > 65y and, BMI < 25 /BMI ≥25), while years of education was omitted due to only minimal variation left after stratifying on educational status (basic education≤ 10 years subgroup included 250 persons with 9 years and 366 with 10 years of schooling; mid-high education subgroup > 10 years 213 with 13 years and 80 with 18 years of education). We also did not include ApoE4carrier status as covariate in the ApoE stratified analyses for the same reason (7 subjects homozygous, 173 heterozygous for the ApoE4 allele, and 718 non-carriers.)

Due to a large number of statistical tests performed owing to the explorative strategy of this study, we performed the Benjamini-Hochberg procedure to control the false discovery rate (FDR). We used a FDR of 0.05 to calculate the Benjamini-Hochberg critical value and provide the adjusted p-values for each test.

We formally tested if the effect of LTL is modulated by the risk factors by using the interaction terms namely (gender × zLTL), (age × zLTL), (hypertension × zLTL), (BMI × zLTL), (education × zLTL), (DM × zLTL), (CVD × zLTL), and (ApoE4 status × zLTL) in the model III of regression.

Mediation Analysis

In order to test if the effect of LTL (independent variable) on attention/speed (dependent variable) is mediated either by BPF or WMH, we used bootstrapping (PROCESS macro version 3.4)[3]. We applied model III including age, sex, risk factors such as hypertension, diabetes, cardiovascular disease, BMI, HDL, years of education, smoking, and ApoE4 genotypes as covariates. Bootstrapping gives the estimates of direct and indirect effects. The extent of the effect which was mediated through BPF or WMH was calculated by repeating the sampling procedure 5000 times. Effect sizes, as well as 95% confidence intervals (95%CI), are given. Significant mediation is present when 95%CI does not include the value of zero.

RESULTS

Description of the Participants

In total, there were 909 participants with LTL (909), MRI (852), and cognitive tests (891). The mean age was 65.9 years. There were 388 (42.7%) men, 631(69.4%) hypertensives, 99(10.9%) diabetics and 364 (40%) with CVD within the cohort. The proportion of ApoE4 carriers

[2]IBM Corp. Released 2017. IBM SPSS Statistics for Windows, Version 25.0. Armonk, NY: IBM Corp.

[3]The process macro for SPSS and SAS; http://processmacro.org/index.html

was 20.1% (**Table 1**, **Supplementary Table 1**). The correlation between LTL and age was negative (r = -0.092, p = 0.006), and participants with CVD had significantly lower LTL (β = -0.136, p = 0.046) than their counterparts (**Supplementary Table 2**). There were no significant differences on LTL by sex, hypertension, BMI, diabetes, education and ApoE4 carrier status (**Supplementary Table 1**). BPF was smaller in individuals with age >65y ($p = 2.92 \times 10^{-42}$), hypertension ($p = 9.19\times10^{-7}$), DM ($p = 7.8 \times 10^{-4}$), and CVD (p = 0.03). WMH load was higher in women (p = 0.002), > 65y ($p = 2.7 \times 10^{-40}$), hypertensives ($p = 7.2 \times 10^{-14}$), in those with ≤10y of education (p = 0.02), diabetics (p = 0.008), CVD (p = 0.001), and in ApoE4 carriers (p = 0.04). Similarly, WMH score were significantly higher in the subgroups of women (p = 0.03), > 65 y ($p = 1.5\times10^{-32}$), hypertensives ($p = 2.7\times10^{-9}$), diabetics (p = 0.01), and CVD (p = 0.04) but not in education ≤10y (p = 0.3) and Apoe4 carriers (p = 0.6). The g-factor was significantly lower in all high-risk groups, and also domain specific cognitive scores followed a similar trend. No significant difference was present for conceptualization by sex, for attention/speed and conceptualization by BMI and for visuopractical skills by education (**Supplementary Table 1**).

LTL Versus MRI Correlates and Cognitive Functions

Total Cohort

We found significant correlations between LTL and BPF (r = 0.169, $p = 3.71\times10^{-6}$) and attention/speed (r = 0.0081, p = 0.018) (**Supplementary Table 2**). Next, we investigated the association between LTL and MRI as well as cognitive functions by linear regression using 3 models by adjusting for age and sex (Model I), additionally for risk factors such as hypertension, diabetes, CVD, BMI, education, HDL and smoking status (Model II), and adding ApoE4 carrier status (Model III). The results for all analyses in detail are shown in **Supplementary Table 3**. Significant associations were observed between LTL and BPF in Model I (β = 0.44, $p = 1.3\times10^{-4}$), II (β = 0.43, $p = 2.1\times10^{-4}$), and III (β = 0.43, $p = 2.1\times10^{-4}$). The effect of LTL on WMH load as well as the WMH score was significant in Model II (β = 0.02, p = 0.04, β = 0.05, p = 0.04, respectively), and III (β = 0.02, p = 0.04, β = 0.05, p = 0.04 respectively). Results of the regression analyses using Model III for all MRI and cognitive variables are given in **Table 2**. LTL explained 1.2% of the variation in BPF and 0.4% of the variation in WMH load and score. There was no significant association between LTL and any of the cognitive measures in the total cohort in any of the multivariable models (**Table 2** and **Supplementary Table 3**).

Subgroups

In order to further explore the association, we repeated the linear regression models in subgroups divided by sex, age, hypertension, BMI, education, diabetes, CVD, and by ApoE4 carrier status. Statistically significant results are presented in **Table 3**, while results of the stratified analyses in total are presented in **Supplementary Table 4**. The effect of LTL was highly significant on BPF within the subgroups of women (β = 0.51, p = 0.001), in individuals with age >65y (β = 0.58, p = 0.002), hypertension (β = 0.51, $p = 7.0 \times 10^{-4}$), BMI ≥ 25(β = 0.40, p = 0.004), education ≤ 10y (β = 0.42, p = 0.002), CVD (β = 0.33, p = 0.02), in non-diabetics (β = 0.42, $p = 4.0 \times 10^{-4}$), and Apoe4 non-carriers (β = 0.49, $p = 1.1 \times 10^{-4}$). Although the effect of LTL on BPF in the overweight subjects (BMI ≥ 25) was comparable to that in the normal weight individuals (BMI < 25), in the obese

TABLE 1 | Characteristics of the study population.

	Total (n)
Social demographic factors	
Age (years)	65.9 ± 8.0 (909)
Sex (Male)	388 (42.7%)
Risk factors	
Hypertension	631 (69.4%)
SBP (mm of Hg)	143.8 ± 22.8 (908)
DBP (mm of Hg)	87.6 ± 10.0 (908)
Diabetes Mellitus	99 (10.9%)
CVD	364 (40.0%)
BMI (kg/m^2)	26.9 ± 4.1 (909)
Education	11.1 ± 2.6 (909)
TC (mg/dl)	227.87 ± 40.4 (909)
HDL (mg/dl)	56.5 ± 17.2 (901)
Smoking	
Never	551 (60.7%)
Former	257 (28.3%)
Current	100 (11.0%)
ApoE4	
No allele	718 (80.0%)
Heterozygous	173 (19.3%)
Homozygous	7 (0.8%)
Predictor	
LTL	0.61(0.47-0.82) (909)
MRI correlates	
BPF (%)	78.7 ± 3.9 (739)
WMH load (mm^3)	0.8(0.2-3.1) (827)
WMH Score	
0	157 (18.4%)
1	503 (59.0%)
2	123 (14.4%)
3	69 (8.1%)
Cognitive functions	
Attention/Speed	0.03 ± 0.53 (853)
Conceptualization	0.06 ± 0.59 (858)
Memory	0.01 ± 1.01 (860)
Visuopractical Skills	0.00 ± 0.93 (891)
g factor	0.01 ± 1.01 (823)

The independent sample t-test was performed for normally distributed continuous variables, Mann-Whitney U test for skewed variables, and the chi-square test for categorized variables to compare the groups.

For normally distributed variables, mean ± SD, for skewed variables median (IQR), and categorical variables, numbers of observations (%) in the category are given.

SBP, Systolic Blood Pressure; DBP, Diastolic Blood Pressure; CVD, Cardiovascular Diseases; BMI, Body Mass Index; TC, Total Cholesterol; HDL, High-Density Lipoprotein; LTL, Leukocyte Telomere Length; BPF, Brain Parenchymal Fraction; WMH, White Matter Hyperintensities; SD, Standard Deviation; IQR, Inter-Quartile Range.

TABLE 2 | Linear regression analysis of the association of leukocyte telomere length (LTL) with magnetic resonance imaging (MRI) correlates and cognitive functions.

	β	SE	*p*	Partial R^2
BPF	0.429	0.115	**0.0002**	0.012
WMH load	0.024	0.012	**0.037**	0.004
WMH Score	0.052	0.025	**0.037**	0.004
Attention/Speed	0.025	0.017	0.149	0.002
Conceptualization	0.017	0.019	0.382	0.001
Memory	-0.015	0.029	0.610	0.000
Visuopractical Skills	0.010	0.024	0.668	0.000
g factor	0.009	0.026	0.738	0.000

The results are shown from linear regression after adjusting for age, sex, risk factors, and ApoE4 genotypes (Model III). Bold shows significance level of <0.05.
BPF, Brain Parenchymal Fraction; WMH, White Matter Hyperintensities, β-Effect size, SE-Standard Error.

TABLE 3 | Stratified analyses of the significant association of leukocyte telomere length (LTL) with magnetic resonance imaging (MRI) correlates and cognitive functions.

	β	SE	p	Partial R^2	β	SE	p	Partial R^2
BPF	Men (313)				Women (426)			
	0.330	0.174	0.058	0.008	0.505	0.155	**0.001**	0.016
	≤65 years (352)				>65 years (387)			
	0.350	0.142	**0.014**	0.013	0.583	0.186	**0.002**	0.016
	Normotensive (231)				Hypertensive (508)			
	0.348	0.187	0.064	0.011	0.505	0.148	0.001	0.015
	BMI <25 (266)				BMI ≥25 (473)			
	0.502	0.202	**0.013**	0.014	0.403	0.140	**0.004**	0.012
	Education ≤10 (505)				Education >10 (234)			
	0.424	0.138	**0.002**	0.012	0.418	0.213	0.051	0.011
	No DM (662)				DM (77)			
	0.418	0.117	**0.000**	0.013	0.250	0.575	0.665	0.002
	No CVD (437)				CVD (302)			
	0.328	0.140	**0.020**	0.008	0.584	0.207	**0.005**	0.017
	Apoe4 non-carriers (589)				Apoe4 carriers (140)			
	0.485	0.125	**0.000**	0.016	0.149	0.299	0.620	0.001
WMH load	Normotensive (258)				Hypertensive (596)			
	-0.003	0.015	0.860	0.000	0.038	0.016	**0.017**	0.008
	Education ≤10 (564)				Education >10 (263)			
	0.029	0.014	**0.039**	0.006	0.018	0.022	0.406	0.002
	No DM (737)				DM (90)			
	0.031	0.012	**0.008**	0.007	-0.076	0.048	0.115	0.021
	Apoe4 non-carriers (589)				Apoe4 carriers (140)			
	0.029	0.013	**0.020**	0.006	-0.001	0.030	0.975	0.000
WMH Score	Education ≤10 (578)				Education >10 (274)			
	0.069	0.030	**0.021**	0.008	0.023	0.047	0.633	0.001
	No DM (760)				DM (92)			
	0.061	0.026	**0.018**	0.006	-0.049	0.102	0.633	0.002
	No CVD (508)				CVD (344)			
	0.060	0.031	**0.049**	0.006	0.042	0.044	0.343	0.002
	Apoe4 non-carriers (674)				Apoe4 carriers (167)			
	0.070	0.027	**0.010**	0.008	-0.019	0.062	0.760	0.000
Attention /Speed	BMI <25 (308)				BMI ≥25 (546)			
	0.001	0.034	0.974	0.000	0.039	0.019	**0.048**	0.006
	Education ≤10 (581)				Education >10 (273)			
	0.044	0.022	**0.048**	0.005	-0.031	0.025	0.208	0.005

The results are shown from linear regression after adjusting for age, sex, risk factors, and ApoE4 genotypes (Model III) in subgroups. Bold shows significance level of <0.05. For each subgroup, number of participants is given in the brackets.
BPF, Brain Parenchymal Fraction ;WMH, White Matter Hyperintensities; BMI, Body Mass Index; DM, Diabetes Mellitus; CVD, Cardiovascular Disease, β-Effect size, SE-Standard Error.

individuals (BMI ≥ 30) the effect of LTL on BPF was three times as high as in non-obese (BMI < 30) (**Supplementary Table 5**). The effect of LTL was significant on both WMH load and WMH score in ≤10y of education, non-diabetics (β = 0.03, p = 0.04, β = 0.03, p = 0.008, β = 0.06, p = 0.02, β = 0.06, p = 0.02), and Apoe4 non-carriers (β = 0.03, p = 0.02, β = 0.07, p = 0.01). On WMH load the effect was in addition significant in hypertensives (β = 0.04, p = 0.02) and on WMH score in subjects without CVD (β = 0.06, p = 0.05). The effect of LTL on cognition was significant only in the attention/speed domain within the subgroup of those with BMI ≥ 25 (β = 0.04, p = 0.05) and ≤10y of education (β = 0.04, p = 0.05). When testing formally for interaction between LTL and the risk factors on MRI and cognitive phenotypes, none of the interaction terms reached statistical significance (p > 0.05).

By controlling for multiple testing using FDR, the significant association between LTL and BPF within subgroups of women (p = 0.005), individuals with age >65y (p = 0.006), hypertension (p = 0.004), BMI ≥ 25 (p = 0.009), education ≤ 10y (p = 0.006), CVD (p = 0.010), in non-diabetics (p = 0.003), and Apoe4 non-carriers (0.002) persisted. Yet, the associations between LTL and WMH load, WMH score and attention/speed domains within respective subgroups became non-significant (p > 0.05).

Using bootstrapping, we investigated if the significant effects of LTL on attention/speed were mediated by BPF in the subgroup of BMI ≥ 25 and education ≤10y or by WMH load/score in those ≤10y of education using model III. We found significant mediation by BPF in both subgroups (effect = 0.02, 95%CI 0.01-0.03 for both subgroups) while the mediation effect by WMH load/score was not significant (load: effect = -0.01, 95%CI -0.02-0.001; score: effect = -0.03, 95%CI -0.01-0.001) (**Figure 2** and **Table 4**).

DISCUSSION

Summary

In summary, we found a highly significant association between LTL and BPF in the elderly. The association was independent of age, sex, the presence of vascular risk factors, and ApoE4 allele. The effect was stronger in women and in individuals with a higher risk for cerebrovascular disease and dementia such as those older than 65 years, hypertensives, overweight (BMI ≥ 25), having education less than 10 years, and CVD. In the case of ApoE4, the effect of LTL on BPF was significantly stronger in non-carriers. LTL had no significant effect on cognition except for the domain of attention/speed within the subgroups of basic education and overweight. The association between LTL and attention/speed was significantly mediated by BPF in these subgroups.

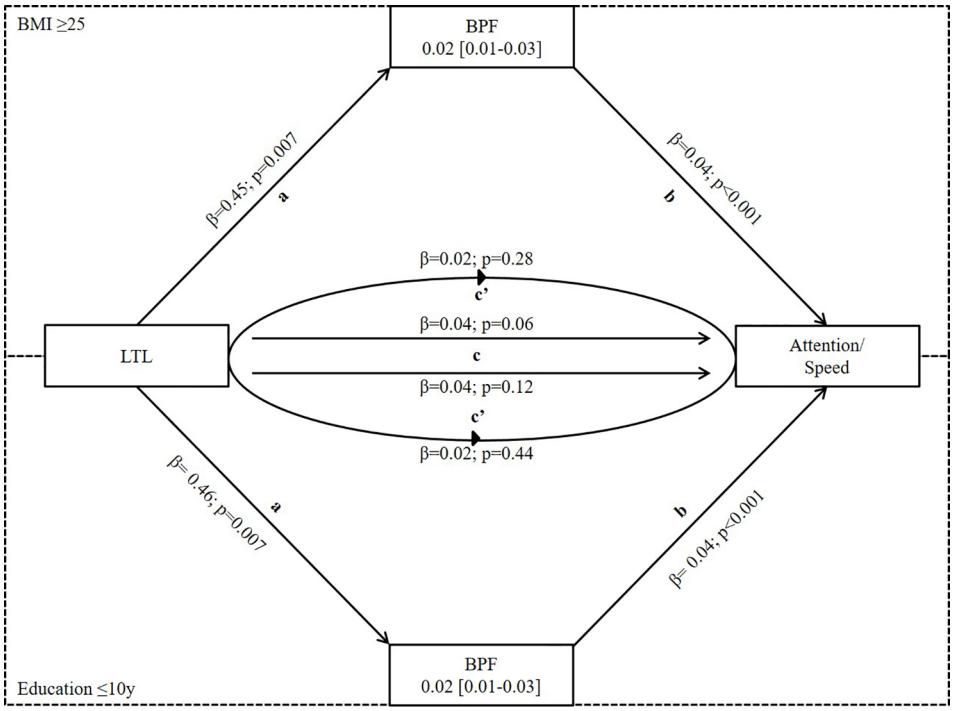

FIGURE 2 | Mediation analysis of LTL on attention/speed *via* BPF in subgroups of BMI≥ 25 and Education ≤ 10y where LTL was significantly associated with both BPF and attention/speed. Mediation is calculated after adjusting for covariates from Model III of linear regression. a- effect of LTL on BPF, b-effect of BPF on attention/speed, c-total effect of LTL on attention/speed, and c'-direct effect of LTL on attention/speed when controlled for BPF. It shows partial mediation because total effect (c) of LTL on attention/speed is reduced in the presence of BPF (c'). LTL, Leukocyte Telomere Length; BPF, Brain Parenchymal Fraction.

TABLE 4 | Mediation analyses.

Subgroups	Effect (β)	SE	CI Lower	CI Upper
		BPF		
BMI ≥25	0.019	0.006	0.007	0.033
Education ≤10	0.019	0.006	0.008	0.032
		WMH load		
Education ≤ 10	-0.008	0.005	-0.019	0.001
		WMH Score		
Education ≤ 10	-0.0029	0.0026	-0.0088	0.0013

The effect size of the mediation calculated using bootstrapping is shown here. We use the 5000 bootstrap samples. When the confidence interval of the effect size does not include zero, it shows a significant effect.

BPF, Brain Parenchymal Fraction; WMH, White Matter Hyperintensities; BMI, Body Mass Index; SE, Standard Error; CI, 95% Confidence Interval.

LTL and MRI Correlates

There are only a few studies available, which investigated brain size in relation to LTL. Their results are contradictory. The so-far largest study, the DHS with 1960 subjects including non-Hispanic whites, blacks, Hispanics, and other ethnicities, found a highly significant association with total cerebral volume and volume of the cerebral white and grey matter (6). LTL explained 1.3% of the cerebral volume, which is very close to that, what we observed for LTL in the case of BPF (partial R^2 = 1.2%) (**Table 2**). In both studies, this corresponded about 1/20 of the proportion explained by age (partial R^2 = 20 in DHS and R^2 = 24 in ASPS). This pinpoints to a robust and reproducible effect of LTL on brain size, even in diverse populations. In our cohort, the effect of LTL on BPF was especially strong in the high-risk groups. The effect size of LTL in women, individuals older than 65 years, hypertensives, and those with cardiovascular disease was approximately twice as large as in their counterparts. The highest protective effect of LTL was seen in the subgroups of obese people where the effect size was three times as high as in their counterpart (BMI < 30). These results suggest an especially important protective role for longer telomeres when the brain is exposed to damaging factors. Similar subgroup-specific results were reported by the Swedish subsample of the CASCADE where the effect of LTL on subcortical atrophy was stronger in those above the median age of 69.6 years (19). Importantly, in the case of ApoE, those who did not carry the E4 allele, the effect of LTL on BPF was more than three times as high (p = 0.0001) as in carriers (p = 0.6). This was a surprising finding and might indicate a different mechanism linking LTL to BPF in this subgroup as in the traditional high-risk groups.

For both WMH load and score, we observed an unexpected positive association with LTL, meaning longer telomeres were related to more lesions in the total cohort as well as in some subgroups (**Supplementary Tables 3** and **4**). The significance and the effect sizes were moderate but became more significant and, larger when adjusting for vascular risk factors and ApoE4 carrier status in addition to age and sex. In contrary, a recent

study (7) on 369 American Indians found a significant association between shorter LTL and an increase in WMH loads. Also, the Swedish subsample of CASCADE reported shorter LTL being associated with periventricular WMH particularly in participants above the age of 69.6 years (19), We did not see the differential effect by age, rather was the association significant within hypertensives, non-diabetics, and those with education less than 10 years. Most likely, the differences between the subgroups were at least partly due to differences in sample sizes. Relevantly different effect sizes were only observed for WMH load in hypertensives vs normotensives and ApoE4 non-carriers vs carriers. Presently we have no biological explanation for the detrimental effect of longer telomeres on WMH load and score. They may represent chance findings, as after performing FDR for adjusting for multiple comparisons, the significance does not persist.

LTL and Cognition

In our study, we applied a comprehensive evaluation of cognitive functions within the domains of attention/speed, conceptualization, memory, and visuopractical skills, and built the composite score of g-factor as a measure of global cognitive function. LTL had a very specific effect on cognition with longer telomeres being associated with better performances only in the attention/speed domain. However, this effect was only observed in those with overweight and education less than 10 years. In these groups, the effect sizes were also much larger than in their counterparts. Previously population-based cohort studies reported divergent findings. While in DHS, there was no association observed within 2,606 participants between LTL and cognition (8), Zhan et al. reported that longer LTL was related to better general cognition in a meta-analyses including four prospective cohorts (N = 5,955) when adjusted for age. This association became insignificant when additional adjustment for risk factors was done. In the largest meta-analyses so far performed in European ancestry cohorts (N = 17,052) (10) longer LTL was associated with better cognitive performance, including memory, executive function, and importantly similarly to our study with speed.

Effect Mediation by BPF on Attention/Speed

The effect of LTL was significant on both BPF and attention/speed in subjects with overweight and education less than 10 years. Within these subgroups, we found evidence that about half of the effect by LTL on cognition was mediated by BPF. Our results for the first time support the hypothesis that longer telomeres protect the brain, and this transforms to better cognitive performance especially within the attention/speed domain. Attention/speed is considered as a basic cognitive function, which declines with age linearly, and its decline also affects other cognitive domains (20, 21). In our cohort, BPF was only significantly related to attention/speed but not to other cognitive domains or to g-factor when tested by linear regression using model III.

Working Hypothesis

Figure 3 presents our working hypothesis on the relation between LTL and structural and functional brain changes associated with aging. In this model, we hypothesize that longer LTL plays a causal and protective role in the process of brain aging. Mendelian randomization studies suggested a causal role for telomeres for Alzheimer's Disease (22, 23). Its effect on BPF might be mediated by two major pathways, one linked to the development of the brain up to puberty and the second related to aging. These are the two phases when telomere attrition is accelerated, and major inter-individual differences in telomere length develop (3). In the first pathway, we hypothesize that those inheriting longer telomeres or loosing less of their telomere during growth, develop a larger brain translating to higher brain reserve. Indeed, faster LTL attrition in younger life was associated with poorer global cognitive function as well as worse performance in domains including processing speed in midlife (24). We further hypothesize that the effect modulators acting already early in life such as female sex, lower education, and ApoE4 non-carrier status, mainly act on this developmental pathway (Modulators I). In the second pathway, we hypothesize that in those with longer LTL, the process of brain aging is slowed down, and brain parenchyma is longer preserved. In addition, during aging, the brain is challenged by risk factors such as old age, hypertension, overweight and CVD (Modulators II). Those, however, who enter the process of aging with a larger brain reserve are better protected against atrophy and cognitive decline. This is in line with the findings of Brickman et al. (2011), showing that for any given level of cognitive function, those with higher reserve -derived by latent variable analyses have higher WMH load (25). A difference, which especially gets measurable when risk factors are present. Our data presently only supports the connection between longer LTL, larger BPF, and better performances in attention/speed (marked bold in **Figure 3**). However, it will be important to further investigate in larger studies if better attention/speed further translates to better cognitive functions in other domains as well. Also, the microstructural substrate of the hypothesized larger brain reserve by more advanced MRI such as DTI needs to be followed up (26). The peak width of skeletonized mean diffusivity was reported to be strongly linked to attention/speed (27). Clearly, also, the association between LTL and WMH load needs further investigation.

Strengths and Weaknesses

The strength of our study is the large sample size within a well-established population-based cohort with LTL, MRI, and comprehensive measures on cognitive functions. This also allowed us to explore the effect of LTL on the brain by stratifying on subgroups based on the presence and absence of relevant risk factors and define significant effect modulators. Yet, in some subgroups such as those with DM, the sample size was still probably too small to reach statistical power for meaningful testing. By performing mediation analyses between LTL, BPF and cognition, we found the first evidence that the beneficial

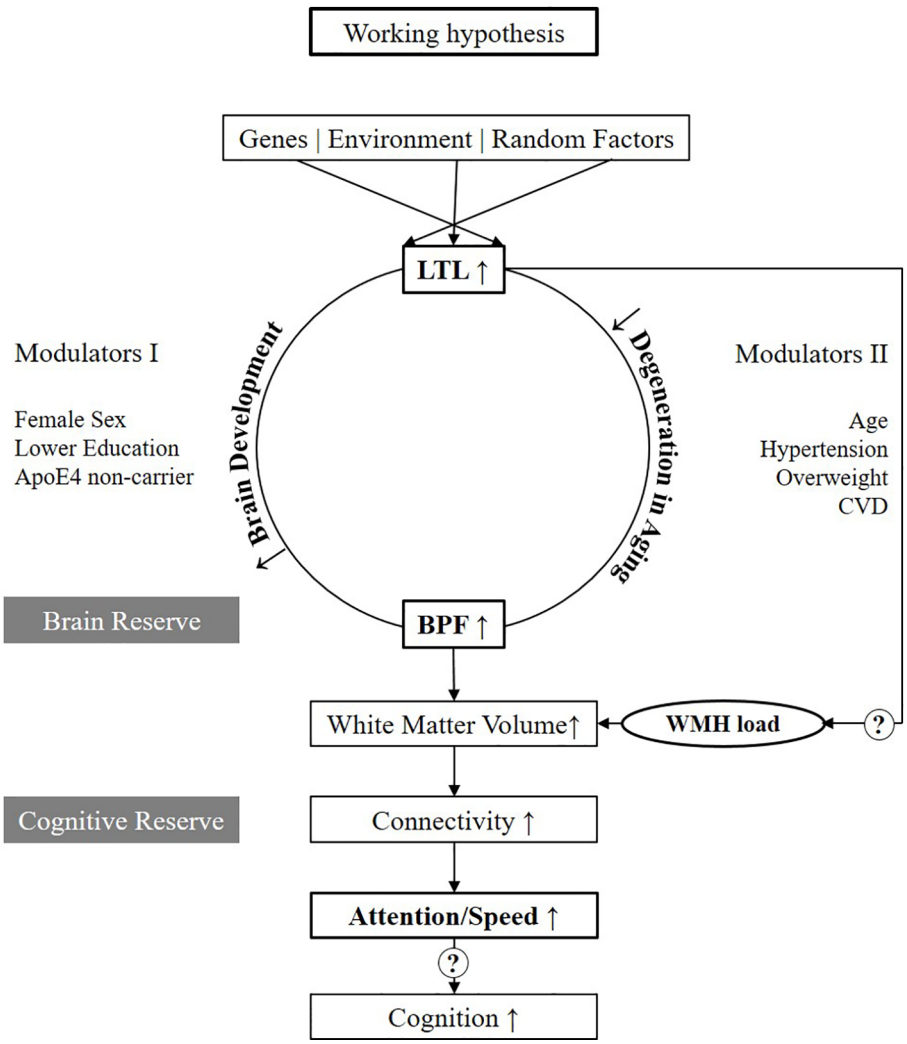

FIGURE 3 | Working hypothesis. Variables in bold are those which are tested in the present study. LTL, Leukocyte Telomere Length; BPF, Brain Parenchymal Fraction; WMH, White Matter Hyperintensities; CVD, Cardiovascular disease.

effect of LTL on BPF transforms into a positive effect on attention/speed. Certainly, using this explorative strategy, we performed multiple tests. Altogether we ran the 3 models within 16 subgroups for all MRI and cognitive phenotypes. Indeed, when adjusting for multiple testing by using FDR, significant results were only present for BPF ($p < 0.05$) but not for WMH ($p = 0.1$) or attention/speed ($p = 0.2$). A weakness of the study is its cross-sectional setting, which makes causal interference difficult as well as the possibility for residual confounding in spite to test for a wide range of possible confounders. Since this study was based on the original ASPS cohort, only 1.5T MRI was available. In the future, we, therefore, will expand our study to the ASPS-Family cohort with available 3T MRI scans in order to deepen our understanding of microstructural changes involved in the brain effect of LTL.

CONCLUSION

Our results support a significant protective role of longer LTL on the brain in the normal elderly. Longer LTL is associated with a larger brain and with better cognitive functioning in the attention/speed domain. The effect is largely confined to women and to the high-risk groups of older than 65 years, overweight, hypertensives and those having education less than 10 years. We found for the first time evidence that the protective effect of LTL on the brain may transform into better cognition as up to 50% of its effect on attention/speed was mediated by BPF. Our results pinpoint to a possible role of longer LTL in the maintenance of better brain and cognitive reserve in the elderly, which might be especially important when the brain is challenged by risk factors.

DATA AVAILABILITY STATEMENT

The datasets generated for this study are available on request to the corresponding author.

ETHICS STATEMENT

The studies involving human participants were reviewed and approved by the ethics committee of Medical University of Graz. The patients/participants provided their written informed consent to participate in this study.

AUTHOR CONTRIBUTIONS

PG—Data analyses and writing the manuscript. RS—Critically reading the manuscript and principal investigator of ASPS study. HS—Study design, data analyses, writing the manuscript and obtained funding for the project.

FUNDING

The research reported in this article was funded by the Austrian National Bank Anniversary Fund, P15435, City Graz, Graz, Austria and, the Austrian Ministry of Science under the aegis of the EU Joint Programme—Neurodegenerative Disease Research—www. jpnd.eu. The project is supported through the following funding organizations under the aegis of EU Joint Programme—Neurodegenerative Disease Research—www.jpnd.eu: Australia, National Health and Medical Research Council, Austria, Federal Ministry of Science, Research and Economy; Canada, Canadian Institutes of Health Research; France, French National Research Agency; Germany, Federal Ministry of Education and Research; Netherlands, The Netherlands Organisation for Health Research and Development; United Kingdom, Medical Research Council. This project has received funding from the European Union's Horizon 2020 research and innovation program under grant agreement no. 643417. PhD position for PG is supported through the PhD program "Molecular Medicine" of Medical University of Graz, Graz, Austria.

ACKNOWLEDGMENTS

We acknowledge the efforts of Michael Schallert for measuring the leukocyte telomere length.

SUPPLEMENTARY MATERIAL

The Supplementary Material for this article can be found online at: https://www.frontiersin.org/articles/10.3389/fpsyt.2020.00100/full#supplementary-material

REFERENCES

1. Reichert S, Stier A. Does oxidative stress shorten telomeres *in vivo*? A review. *Biol Lett* (2017) 13(12):20170463. doi: 10.1098/rsbl.2017.0463
2. Blackburn EH, Epel ES, Lin J. Human telomere biology: A contributory and interactive factor in aging, disease risks, and protection. *Science* (2015) 350:1193–8. doi: 10.1126/science.aab3389
3. Sanders JL, Newman AB. Telomere length in epidemiology: A biomarker of aging, age-related disease, both, or neither? *Epidemiol Rev* (2013) 35:112–31. doi: 10.1093/epirev/mxs008
4. Haycock PC, Heydon EE, Kaptoge S, Butterworth AS, Thompson A, Willeit P. Leucocyte telomere length and risk of cardiovascular disease: Systematic review and meta- Analysis. *BMJ* (2014) 349:g4227. doi: 10.1136/bmj.g4227
5. Wang Q, Zhan Y, Pedersen NL, Fang F, Hägg S. Telomere Length and All-Cause Mortality: A Meta-analysis. *Ageing Res Rev* (2018) 48:11–20. doi: 10.1016/j.arr.2018.09.002
6. King KS, Kozlitina J, Rosenberg RN, Peshock RM, McColl RW, Garcia CK. Effect of Leukocyte Telomere Length on Total and Regional Brain Volumes in a Large Population-Based Cohort. *JAMA Neurol* (2014) 71:1247. doi: 10.1001/jamaneurol.2014.1926
7. Suchy-Dicey AM, Muller CJ, Madhyastha TM, Shibata D, Cole SA, Zhao J, et al. Telomere Length and Magnetic Resonance Imaging Findings of Vascular Brain Injury and Central Brain Atrophy. *Am J Epidemiol* (2018) 187:1231–9. doi: 10.1093/aje/kwx368
8. Kaja R, Reyes SM, Rossetti HC, Brown ES. Association between telomere length and cognitive ability in a community-based sample. *Neurobiol Aging* (2019) 75:51–3. doi: 10.1016/j.neurobiolaging.2018.11.006
9. Zhan Y, Clements MS, Roberts RO, Vassilaki M, Druliner BR, Boardman LA, et al. Association of telomere length with general cognitive trajectories: a meta-analysis of four prospective cohort studies. *Neurobiol Aging* (2018) 69:111–6. doi: 10.1016/j.neurobiolaging.2018.05.004
10. Hägg S, Zhan Y, Karlsson R, Gerritsen L, Ploner A, van der Lee SJ, et al. Short telomere length is associated with impaired cognitive performance in European ancestry cohorts. *Transl Psychiatry* (2017) 7:e1100. doi: 10.1038/tp.2017.73
11. Devore EE, Prescott J, De Vivo I, Grodstein F. Relative telomere length and cognitive decline in the Nurses' Health Study. *Neurosci Lett* (2011) 492:15–8. doi: 10.1016/j.neulet.2011.01.041
12. Schmidt R, Fazekas F, Kapeller P, Schmidt H, Hartung H-P. MRI white matter hyperintensities: Three-year follow-up of the Austrian Stroke Prevention Study. *Neurology* (1999) 53:132–2. doi: 10.1212/WNL.53.1.132
13. Sen A, Marsche G, Freudenberger P, Schallert M, Toeglhofer AM, Nagl C, et al. Association between higher plasma lutein, zeaxanthin, and vitamin C concentrations and longer telomere length: Results of the Austrian Stroke Prevention Study. *J Am Geriatr Soc* (2014) 62:222–9. doi: 10.1111/jgs.12644
14. Cawthon RM. Telomere measurement by quantitative PCR. *Nucleic Acids Res* (2002) 30:47e–47. doi: 10.1093/nar/30.10.e47
15. Fazekas F, Chawluk JB, Alavi A. MR signal abnormalities at 1.5 T in Alzheimer's dementia and normal aging. *Am J Neuroradiol* (1987) 8:421–6. doi: 10.2214/ajr.149.2.351
16. Sen A, Gider P, Cavalieri M, Freudenberger P, Farzi A, Schallert M, et al. Association of cardiorespiratory fitness and morphological brain changes in the elderly: Results of the Austrian stroke prevention study. *Neurodegener Dis* (2012) 10:135–7. doi: 10.1159/000334760
17. Freudenberger P, Petrovic K, Sen A, Töglhofer AM, Fixa A, Hofer E, et al. Fitness and cognition in the elderly The Austrian Stroke Prevention Study. *Neurology* (2016) 86: (5):418–24. doi: 10.1212/WNL.0000000000002329
18. Schmidt H, Schmidt R, Fazekas F, Semmler J, Kapeller P, Reinhart B, et al. Apolipoprotein E4allele in the normal elderly: neuropsychologic and brain MRI correlates. *Clin Genet* (1996) 50:293–9. doi: 10.1111/j.1399-0004.1996.tb02377.x
19. Wikgren M, Karlsson T, Söderlund H, Nordin A, Roos G, Nilsson L-G, et al. Shorter telomere length is linked to brain atrophy and white matter hyperintensities. *Age Ageing* (2014) 43:212–7. doi: 10.1093/ageing/aft172

20. Finkel D, Reynolds CA, McArdle JJ, Pedersen NL. Age changes in processing speed as a leading indicator of cognitive aging. *Psychol Aging* (2007) 22:558–68. doi: 10.1037/0882-7974.22.3.558
21. Hagenaars SP, Harris SE, Davies G, Hill WD, Liewald DCM, Ritchie SJ, et al. Shared genetic aetiology between cognitive functions and physical and mental health in UK Biobank (N=112 151) and 24 GWAS consortia. *Mol Psychiatry* (2016) 21:1624–32. doi: 10.1038/mp.2015.225
22. Zhan Y, Song C, Karlsson R, Tillander A, Reynolds CA, Pedersen NL, et al. Telomere length shortening and Alzheimer disease-A mendelian randomization study. *JAMA Neurol* (2015) 72:1202–3. doi: 10.1001/jamaneurol.2015.1513
23. Kuźma E, Hannon E, Zhou A, Lourida I, Bethel A, Levine DA, et al. Which risk factors causally influence dementia? A systematic review of mendelian randomization studies. *J Alzheimer's Dis* (2018) 64:181–93. doi: 10.3233/JAD-180013
24. Cohen-Manheim I, Doniger GM, Sinnreich R, Simon ES, Pinchas R, Aviv A, et al. Increased attrition of leukocyte telomere length in young adults is associated with poorer cognitive function in midlife. *Eur J Epidemiol* (2016) 31:147–57. doi: 10.1007/s10654-015-0051-4
25. Brickman AM, Siedlecki KL, Muraskin J, Manly JJ, Luchsinger JA, Yeung LK, et al. White matter hyperintensities and cognition: testing the reserve hypothesis. *Neurobiol Aging* (2011) 32:1588–98. doi: 10.1016/j.neurobiolaging.2009.10.013
26. Staffaroni AM, Tosun D, Lin J, Elahi FM, Casaletto KB, Wynn MJ, et al. Telomere attrition is associated with declines in medial temporal lobe volume and white matter microstructure in functionally independent older adults. *Neurobiol Aging* (2018) 69:68–75. doi: 10.1016/j.neurobiolaging.2018.04.021
27. Deary IJ, Ritchie SJ, Muñoz Maniega S, Cox SR, Valdés Hernández MC, Luciano M, et al. Brain Peak Width of Skeletonized Mean Diffusivity (PSMD) and cognitive function in later life. *Front Psychiatry* (2019) 10:3389. doi: 10.3389/fpsyt.2019.00524

Conflict of Interest: The authors declare that the research was conducted in the absence of any commercial or financial relationships that could be construed as a potential conflict of interest.

frontiers in Psychiatry

ORIGINAL RESEARCH
published: 28 February 2020
doi: 10.3389/fpsyt.2020.00075

Prevalence, Incidence, Influence Factors, and Cognitive Characteristics of Amnestic Mild Cognitive Impairment Among Older Adult: A 1-Year Follow-Up Study in China

Wei Li[1,2], *Lin Sun*[1,2*†] *and Shifu Xiao*[1,2*†]

[1] *Department of Geriatric Psychiatry, Shanghai Mental Health Center, Shanghai Jiao Tong University School of Medicine, Shanghai, China,* [2] *Alzheimer's Disease and Related Disorders Center, Shanghai Jiao Tong University, Shanghai, China*

Background: The risk and protective factors of amnestic mild cognitive impairment (aMCI) and its prevalence as well as incidence among old adult in Chinese community are still unclear.

Methods: We carried out this 1-year longitudinal study to survey a random sample of 3,246 community elders aged 60 and over in China. All subjects were required to complete a comprehensive clinical assessment, physical examination and several neuropsychological tests at baseline and follow-up. What's more, we also collected their lifestyle information by a standardized questionnaire.

Results: We found that the prevalence of aMCI was 17.1%, while the incidence of aMCI among Chinese old adult was 70.57 per 1,000 person-years. By using Cox regression analysis, we found that male sex (p = 0.001, OR = 0.489, 95%CI 0.319~0.751) and reading (p = 0.023, OR = 0.533, 95%CI 0.310~0.917) were protective factors for against aMCI. Old adult who developed aMCI in the future showed multiple cognitive impairments (such as immediate memory, associative learning memory and executive function) in their early stage, and Wechsler's Block Design (p = 0.027, OR = 0.969, 95%CL 0.943~0.996) could predict whether subjects would turn into aMCI in the future.

Conclusions: The present study suggests that aMCI is a considerable health problem in China. Executive dysfunction may be an indicator of future development of aMCI in the old normal adult.

Keywords: Chinese, amnestic mild cognitive impairment, prevalence, incidence, executive function

OPEN ACCESS

Edited by:
Reinhold Schmidt,
Medical University of Graz, Austria

Reviewed by:
David Facal,
University of Santiago de Compostela, Spain
Ellen E. Lee,
University of California, San Diego, United States
Maria Donata Orfei,
IMT School for Advanced Studies Lucca, Italy

****Correspondence:***
Lin Sun
xiaosuan2004@126.com
Shifu Xiao
xiaoshifu@msn.com

†These authors have contributed equally to this work

Specialty section:
This article was submitted to Aging Psychiatry, a section of the journal Frontiers in Psychiatry

Received: *22 November 2019*
Accepted: *30 January 2020*
Published: *28 February 2020*

Citation:
Li W, Sun L and Xiao S (2020) Prevalence, Incidence, Influence Factors, and Cognitive Characteristics of Amnestic Mild Cognitive Impairment Among Older Adult: A 1-Year Follow-Up Study in China. Front. Psychiatry 11:75. doi: 10.3389/fpsyt.2020.00075

INTRODUCTION

Mild cognitive impairment (MCI) is an intermediate phase between normal ageing and early dementia, and is associated with increased risk of Aizheimer's disease (AD) (1). MCI is characterized by cognition impairment, especially in memory, but has no significant impact on daily life (2). MCI can be further divided into four subtypes: amnestic MCI-single domain (sa-MCI), amnestic MCI-multiple domains (ma-MCI), nonamnestic MCI-single domain (sna-MCI), and nonamnestic MCI-multiple domains (mna-MCI) (3), among which, amnestic mild cognitive impairment (including sa-MCI and ma-MCI), characterized by diminished delayed free recall ability, is the subtype most correlated with AD (4). And the autopsy results show that the pathological characteristic of aMCI is consistent with the stage preceding AD (5). According to previous studies, 10–15% of aMCI will be converted to AD (6), while the nonamnestic MCI will develop into dementia with Lewy bodies or frontotemporal dementia (7).

Determining the MCI and subtype prevalence is essential to develop preventive approaches for old adult (5). However, at present, the prevalence of MCI is difficult to calculate, as it depends on the precise diagnostic criteria (8). For example, a systematic review reports that the prevalence of MCI ranges widely from 0.5% to 42% (5). Nevertheless, since AD increases double every 5 years after age 65 (9), it is important to evaluate adults with aMCI from several years before that age. So far, there are only two studies involving the prevalence of aMCI in China, Our previous study found that the prevalence of aMCI among old adult in Shanghai community was 22.3%, and the incidence (per 1,000 person-years) was 96.9 (10), while another study carried out in Tianjin showed that the prevalence of MCI was 11.33% (11). So our conclusions are not consistent, and this may be due to different inclusion criteria (we included subjects aged 60 and over, and their subjects aged 65 and over) and assessment tools (we used MOCA to assess the global cognitive function of the subjects, while they used MMSE, and the greater sensitivity of the MOCA (vs MMSE) might contribute to a higher rate of aMCI in Shanghai).

Due to the inconsistent conclusions and regional differences in the previous studies, we conducted a 1-year follow-up study across the country [including 20 target communities (18 urban and 2 rural) located in the eastern, mid, and western parts of China] to explore the prevalence, incidence, influence factors as well as cognitive characteristics of aMCI among the old adult in Chinese communities. The 2014 World Alzheimer Report pointed out that low education in early life, hypertension in midlife as well as diabetes and smoking across the life course were associated with dementia (12), therefore, we speculate that the above factors may also affect the aMCI.

MATERIALS AND METHODS

Calculation of Sample Size

Accumulated evidence suggests that the prevalence of MCI (Pexp) is between 10% and 20% (10, 13, 14). Based on the sample size calculation formula: $N = (1.96/d)^2 \times (Pexp) \times (1-Pexp)$, ($d = \pm 3\%$), we determined that the sample size for this study should be no less than 785 (15).

Participants

This follow-up study was a collaborative effort of 15 institutions located in the eastern, middle and western parts of China, which was conducted from March 2011 to July 2012. Each institution identified one or more target communities, and 20 target communities (18 urban and 2 rural) entered in this project. Finally, a total of 15,304 individuals, aged 60 and over, registered in the 2010 national census as permanent residents of these communities, were put into a database. The inclusion criteria were as follows: (1) 60 years and older; (2) permanent residents; (3) without evidence of serious physical illness, such as cancer and acute myocardial infarction; (4) without serious mental illness, such as mental retardation and schizophrenia; and (5) agreed to participate in the study. Exclusion criteria were as follows: (1) less than 60 years old; (2) external population; (3) acute stress state; (4) serious physical illness or mental illness; (5) refused to participate in the study; Then, we randomly selected 3,246 old adult people as the potential participants (among these selected, 111 participants were excluded for incomplete data, and there was no bias due to missing data). Among these groups, illiteracy accounted for 17.1%, primary education accounted for 25.5%, junior high school accounted for 24.7%, senior high school or technical secondary school accounted for 15.7%, junior college accounted for 6.4%, university or above accounted for 10.6%. And the sampling process has been outlined in detail in our previous studies (1).

Aims of the Project

a. Estimate the prevalence of aMCI among the old adult in Chinese communities.
b. Develop a screening program for aMCI that uses a mathematical algorithm which integrates both biological and psychological measures.
c. Implement screening procedures in a consultative network including psychiatrists, clinical psychologists and community physicians to determine the sensitivity and specificity of the algorithm for identifying prodromal cases of aMCI.
d. Develop China-specific, standardized treatment protocols for non-pharmacological treatment of aMCI (using cognitive training).
e. Establish norms for brain volumes and other measures obtained from magnetic resonance imaging (MRI) as well as a bank of biological samples.

Ethical approval was issued by Shanghai Mental Health Centre, and all the participants had signed an informed consent before the study was initiated.

Clinical Assessment

Amnesic Mild Cognitive Impairment

The diagnosis of MCI was based on the diagnosis standard of Petersen (16): (1) self- or informant -reported cognitive

complain; (2) objective memory impairment; (3) preserved independence in functional abilities; and (4) absence of dementia. And if people with MCI performed poorly in episodic memory, they were considered as amnestic MCI (aMCI), while if they performed poorly in other cognitive areas rather than memory, they were considered as non-amnestic MCI (naMCI) (17).

Subjective Memory Decline

The diagnosis of subjective memory decline (SCD) was based on a conceptual framework of criteria for identification of SCD (18): (1)self -reported cognitive decline; 2 the onset age was more than 60 years old; (2) the presence of subjective memory decline had persisted for ≥6 months; (3) objective cognitive score in normal range.

Dementia

The diagnosis of dementia was based on the Diagnostic and Statistical Manual of mental disorders, Fourth Edition (DSM-IV) (19). When dementia was diagnosed, participants would be further classified into three subtypes: Alzheimer disease (AD), vascular dementia (VD), and mixed dementia (MD). Diagnostic criteria for AD were based on the criteria issued by the National Institute of Neurological and Communicative Disorders and Stroke–Alzheimer's Disease and Related Disorders Association (20). Diagnostic criteria for VD were based on the reports of the NINDS-AIREN International Workshop (21). And MD included other types of dementia (such as frontotemporal dementia, alcoholic dementia, dementia with Lewy bodies, Parkinson's disease with dementia, etc) that could not be diagnosed.

Cognitively Unimpaired (CU)

Participants were considered to be cognitively unimpaired if there were: (a) without subjective memory or other cognitive complaints; (b) without evidence by extensive clinical evaluation or history of memory or other cognitive decline; (c) global Clinical Dementia Rating Scale (CDR) (22) score of 0 rated by the clinician; (d) objective cognitive score in normal range (23).

Neuropsychological Tests

Cognitive Assessment

A series of neuropsychological tests, including the Mini- mental State Examination (MMSE) (24), the Montreal Cognitive Assessment (MoCA) (25), Digit Span (26), Associative Learning Test (ALT), Visual Identification Test (VIT), Verbal Fluency (VF), Auditory Verbal Learning Test (AVLT) (27), Wechsler Adult Intelligence Scale (WAIS)-III Block Design, and Wechsler Adult Intelligence Scale (WAIS)-III picture completion were used to assess the cognitive function of subjects. And neuropsychiatric Inventory (NPI) (28) was used to evaluate psychiatric and somatic symptoms. The diagnosis of aMCI in the present study was characterized by MMSE scores higher than, or equal to, 25, 21, or 18 for participants who had a middle school or higher education, an elementary school education, or no education, respectively (29).

Quality of Life Assessment

The quality of life of participants will be assessed utilizing the Life Event Scale (LES), and the Social Support Rating Scale (SSRS) (1).

MR Image Acquisition and Processing

Brain structure image was acquired by using a Siemens Magnetom Verio 3.0T scanner (Siemens, Munich, Germany). The parameters of T1-weighted 3D magnetization prepared rapid gradient echo (MPRAGE) sequences were as follows: TE = 2.98 ms, TR = 2,300 ms,; matrix size = 240 × 256; flip angle of 9 degree, field of view (FOV) = 240 × 256 mm; slice thickness = 1.2 mm. Volumetric data was assessed by automated procedures, which have been described by Wolz R et al. (30). For each subject, volume and asymmetry with various brain areas as well as the brain size index were extracted (by using FreeSurfer).

Laboratory Tests

Peripheral blood samples (5 ml) were collected between 7 and 9 am after an overnight fast. A regular blood panel was carried out to measure hemoglobin, white blood cells, red blood cells, neutrophil granulocytes, mean cell volume, and platelets. Biochemical tests assessed bilirubin, creatinine, potassium, chloride, sodium, glucose, triglyceride, cholesterol, total proteins, alanine transaminase, aspartate transaminase, blood urea nitrogen, high density lipoprotein, low density lipoprotein, apolipoprotein A, apolipoprotein B, and lipoprotein. Separated serum and plasma (200 ul each) were stored in -70°C freezers.

All subjects were obliged to finish a baseline examination including a review of their medical history, physical and neurological examinations, neuropsychological tests, laboratory tests, and MRI scans. Based on clinical evaluation and neuropsychological test, 535 participants were diagnosed as aMCI, 75 as vascular MCI(vMCI), 23 as subjective cognitive impairment (SCD), 110 as Aizheimer's disease(AD), 65 as vascular dementia (VD), 17 as mixed dementia (MD), 2218 as cognitively unimpaired (CU), 14 as depression(DD), as well as 78 were unable to diagnose (such as anxiety, obsession, alcohol dependence, syphilis, and so on, due to the small proportion of the above diseases, we did not include them in the statistics). Next, we followed up 2,218 cognitively unimpaired aging people for 1 year, and repeated the baseline survey (follow-up evaluation). **Figure 1** describes our research process.

Social Population Information

Social population information was gathered by self-reported. And the following data, such as name, age, gender, years of education, daily living information (smoking, drinking alcohol, drinking tea, taking exercise, hobby, reading, playing music, surfing the internet), and history of disease(depression, diabetes, and hypertension) were collected by standardized questionnaire. In terms of daily living information, taking reading as an example, participants were asked the following question "Do you read?" If the answer is "yes," the participants were further asked to report their frequency of participation, such as "almost every day," "sometimes," or "never" (31). In the present study, we defined reading almost every day as reading.

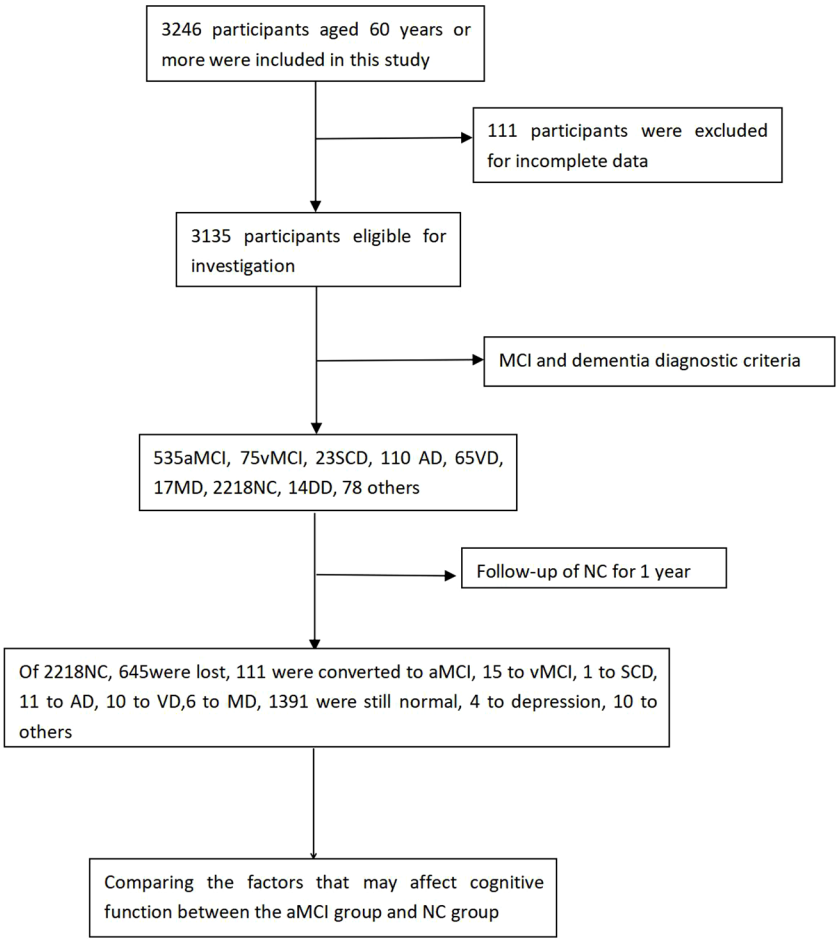

FIGURE 1 | Flow diagram of the study population in the project. aMCI, vMCI, SCD, AD, VD, MD, NC, DD stand for amnestic mild cognitive impairment, Vascular mild cognitive impairment, Subjective cognitive impairment, Alzheimer disease, Vascular dementia, mixed dementia, normal control, depression, respectively.

STATISTICAL ANALYSIS

The continuous variables were presented as mean± SD, while categorical variables were expressed as the frequency (%). The prevalence of aMCI was calculated by splitting the total number of cases diagnosed (n = 535) at baseline by the total number of participants (n = 3135, 111 persons were excluded for missing diagnoses). The incidence for aMCI (expressed as the number of cases per 1,000 person-years) was established by dividing the numbers of newly diagnosed cases at the 1-year follow-up visit. And the influence factors of aMCI were analyzed by Cox logistic regression (whether the cognitively unimpaired aging people changed into aMCI were taken as state variable and age as time variable). Finally, we randomly selected 111 cognitively unimpaired aging people who were not converted to aMCI (matched with age, sex, and education of those who were converted to aMCI) and compared the baseline and follow up neuropsychological tests between the two groups by using independent sample t-test (normally distributed data) or Mann-Whitney U(non-normally distributed data). Then, Cox regression analysis (111 pairs) was used to screen which neuropsychological test was most helpful to predict aMCI. And LSD-t test was used to correct multiple comparisons. Statistical analysis was performed by using SPSS version 22.0 and a p-value < 0.05 was regarded as significant.

RESULTS

Characteristics of the Total Sample

A total of 3,246 nationally representative people (with 1,473 males, 45.4%), completed the survey. Their age range was 60–99, with an average age of 71.58 ± 8.061. Of them, 111 were excluded because of missing data. And there was no significant difference ($p > 0.05$) in age, gender and education between the excluded population and the study population.

Characteristics of the Old Normal Adult Who Were Followed Up

2218 old adult people (1,074 males, age:70.14 ± 7.535) with cognitively unimpaired were followed up for one year. Among them, 645 (29.1%) lost their visits, 111(5.0%) changed into aMCI, 15(0.7%) into vMCI, 1(0.0) into SCD, 11 (0.5%) into AD, 10 (0.5%) into VD, 6 (0.3%) into MD, 4(0.2%) into depression, 10 (0.5%) into others, while 1,391(62.7%) were still cognitively unimpaired (**Figure 1**). **Supplementary Table 1** shows the general demographic differences between the lost population and the follow-up population. Next, we compared the general demographic data of normal -normal group and normal-aMCI group, and we found that the average age (75.30 ± 7.123) of the normal-aMCI group was significantly higher than that (69.82 ± 7.336) of the normal-normal group, while the years of education (6.17 ± 5.500) of the normal-aMCI group were lower than that (9.83 ± 4.876) of the normal-normal group. What's more, the normal-aMCI group had a higher proportion of depression, and a lower proportion of male, hobby, reading, playing music, and surfing the internet compared with the normal-normal group ($p < 0.05$). In addition, the volume of left and right hippocampus of the normal-aMCI group was lower ($p < 0.05$) than that of the normal-normal group. However, there was no significant difference ($p > 0.05$) between the two groups in NPI total score and subtest. **Table 1** presents the results.

Then we brought the above variables into Cox regression equation, and the results showed that male sex ($p = 0.001$, OR = 0.489, 95%CI: 0.319~0.751) and reading ($p = 0.023$, OR = 0.533, 95%CI: 0.310~0.917) were the protective factors for the development of aMCI (**Table 2** shows the related results).

Cognitive Characteristics of the Old Normal Adult Who Were Followed Up

Next, we compared the cognitive characteristics between the two groups of people. In order to eliminate the influence of age, gender, and education on cognitive function, for each eligible case, a control subject matched for age, gender and education had been randomly selected from the subjects with cognitively unimpaired. So 111 pairs of cognitively unimpaired aging people matched in gender, age, and education were selected to participate in the final assessment. And we found that the baseline raw scores of Normal- aMCI group on Digit Span, Auditory verbal learning tests, Associative learning test, Verbal fluency, Wechsler Adult Intelligence Scale (WAIS)-III Block Design, and Wechsler Adult Intelligence Scale (WAIS)-III picture completion were lower than those of Normal-normal group ($p < 0.05$), while there was no statistical differences ($p > 0.05$) in MMSE, MoCA, Visual identification test and Delayed memory between two groups (**Table 3**). One year later, we re-evaluated all subjects and found that the scores of MMSE, MOCA, Digit Span, Auditory verbal learning tests, Associative learning test, Visual identification test, Verbal fluency, Delayed memory, Wechsler Adult Intelligence Scale (WAIS)-III Block Design, and Wechsler Adult Intelligence Scale (WAIS)-III picture completion of Normal-aMCI group were significantly lower ($p < 0.05$) than those in the Normal-normal group (**Table 4**). By using Cox regression analysis and cluster analysis, (whether the subjects were converted to aMCI as a grouping variable and age as time variable, 111 pairs), we found that the baseline scores of Wechsler's Block Design (p=0.027, OR=0.969, 95%CL 0.943~0.996) could predict whether subjects would turn into aMCI in the future (**Table 5**).

TABLE 1 | Demographic, health, and disease-related for Normal-aMCI and Normal-Normal group.

Characteristics	Normal-aMCI (N=111)	Normal-Normal (n=1,391)	t/ X^2	P-value
Age, y	75.30 ± 7.123	69.82 ± 7.336	7.214	<0.001*
Education, y	6.17 ± 5.500	9.83 ± 4.876	-6.633	<0.001*
Male,n (%)	37(33.3)	694(49.9)	11.283	0.001*
Smoking,n (%)	27(24.3)	408(29.3)	1.253	0.279
Drinking alcohol,n (%)	16(14.4)	288(20.7)	2.519	0.140
Drinking tea,n (%)	50(45.0)	727(52.3)	2.146	0.167
Taking exercise,n (%)	80(72.1)	1,068(76.8)	1.264	0.295
Hobby,n (%)	53(5.4)	931(66.9)	16.742	<0.001*
Reading,n (%)	23(20.7)	477(34.3)	8.525	0.003*
Playing music, n (%)	17(15.3)	368(26.5)	6.693	0.009*
Surfing the internet, n (%)	6(5.4)	174(12.5)	4.918	0.023*
Depression, n (%)	10(9.0)	60(4.3)	5.101	0.033*
Diabetes, n (%)	14(12.6)	208(15.0)	0.447	0.580
Hypertension, n (%)	58(52.3)	646(46.4)	1.394	0.277
Right hippocampus, mm^3	3453.37 ± 433.25	3,886.07 ± 458.32	-3.432	0.001*
Left hippocampus, mm^3	3348.45 ± 331.05	3,653.17 ± 468.51	-3.126	0.017*
NPI	2.56 ± 7.087	2.24 ± 6.786	0.468	0.640
Delusion	1.81 ± 0.580	1.70 ± 0.711	1.884	0.062
Hallucination	1.82 ± 0.575	1.70 ± 0.710	1.686	0.092
Aggressive	1.82 ± 0.575	1.70 ± 0.710	1.686	0.092
Depression/dysthymia	1.77 ± 0.598	1.69 ± 0.712	1.260	0.208
Anxiety	1.79 ± 0.590	1.69 ± 0.712	1.426	0.154
Euphoria	1.82 ± 0.575	1.70 ± 0.710	1.667	0.096
Apathy	1.82 ± 0.575	1.71 ± 0.869	1.241	0.215
Disinhibition	1.82 ± 0.575	1.70 ± 0.710	1.667	0.096
Irritability/emotional instability	1.81 ± 0.564	1.72 ± 0.880	1.064	0.287
Abnormal motor behavior	1.82 ± 0.575	1.70 ± 0.710	1.667	0.096
Sleep/night behavior	1.80 ± 0.585	1.69 ± 0.713	1.555	0.120
Appetite and eating disorders	1.82 ± 0.575	1.71 ± 0.753	1.500	0.134

*$p < 0.05$.

TABLE 2 | Risk and protective factors for patients with aMCI.

Variables	B	S.E.	Wald Score	df	p	OR	The 95% CI of OR Lower limit	Upper limit
Male	-0.715	0.219	10.672	1	0.001	0.489	0.319	0.751
Reading	-0.629	0.277	5.168	1	0.023	0.533	0.310	0.917

TABLE 3 | Results of global cognitive functioning tests and neuropsychological tests in different cognitive domains in aMCI subjects and cognitively normal controls (baseline).

Neuropsychological test	Normal-aMCI (n = 111)	Normal-normal (n = 111)	t or Z	p-value
Age, y	75.30 ± 7.123	73.56 ± 8.623	1.511	0.133
Education, y	6.17 ± 5.550	7.36 ± 4.472	-1.671	0.096
Male, n (%)	37(33.3)	38(34.2)	0.020	1.000
Neuropsychological tests				
MMSE	25.28 ± 3.467	26.00 ± 4.439	-1.348	0.179
MoCA	20.13 ± 4.886	21.24 ± 6.011	-1.519	0.130
Digit Span	12.436 ± 4.165	14.266 ± 3.458	-3.535	<0.001*
Auditory verbal learning Test	35.596 ± 11.446	40.314 ± 15.044	-2.175	0.031*
Associative learning test	5.42 ± 3.821	6.87 ± 4.095	-2.629	0.009*
Visual identification test	15.00 ± 4.000	15.71 ± 4.483	-1.216	0.225
Verbal fluency	23.56 ± 7.874	26.88 ± 10.932	-2.530	0.012*
Delayed memory	15.50 ± 9.078	17.09 ± 10.139	-1.213	0.227
Wechsler's picture completion	8.02 ± 3.391	9.10 ± 4.418	-2.209	0.044*
Wechsler's Block Design	21.72 ± 8.142	24.50 ± 9.934	-2.251	0.025*

DISCUSSION

In this study, we found that the prevalence of aMCI among the old adult in Chinese communities was 17.1%, similar to the prevalence found in Lima, Peru (the mean age of the 352 participants was 70.91 ± 7.07 years, three quarters (82.9%) were women, and the mean number of years of education was 11.9 ± 3.7 years) (32) and Tremembé, Brazil (this study included 630 individuals [mean age, 71.3 y (±7.99); mean years of education, 4.9 (±4.54); 397 (63.0%) were women]) (33). With the unification of diagnostic standards and tools for aMCI in the world, the prevalence of aMCI in different ethnic groups tends to be the same. And other studies conducted in China also showed that the prevalence of aMCI was between 14.2% and 22.3% (14, 34), so our findings were consistent. As far as I know, this is the first nationwide study involving the incidence of aMCI in China. And we found that the incidence of aMCI among individuals age 60 and over in 20 Chinese communities was 70.57 per 1,000 person-years, which was similar to what found in other studies , for example, Ravaglia G et al. (34) followed up 745 old adult Italian participants [mean age: 77.4 ± 8.0; 398(54.0%) were women, 256 (29.6%) had less than 3 years of education] without dementia for 4 years, and found 155 changed into MCI, so the incidence rate of MCI was 76.8 (95% CI = 66.8 - 88.4) per 1,000 person-years. However, Katz MJ (35) et al surveyed 1944 adults aged 70 or older (Bronx residents, 1168 dementia free at baseline; mean age, 78.8 y; average follow-up, 3.9 y), and found that the incidence of aMCI was 38/1000 person-years. And the disparity was likely due to investigation methods (our study only investigated the overall incidence of aMCI, but did not focus on age and gender specificity). What's more, the lack of epidemiological studies in China and the potential over-diagnosis of this entity should also be considered (32).

TABLE 4 | Results of global cognitive functioning tests and neuropsychological tests in different cognitive domains in aMCI subjects and cognitively normal controls (follow-up).

Neuropsychological test	Normal-aMCI (n = 111)	Normal-normal (n = 111)	t or Z	p-value
MMSE	23.30 ± 4.753	25.81 ± 3.912	-4.302	<0.001*
MoCA	17.63 ± 5.702	21.80 ± 5.763	-5.421	<0.001*
Digit Span	11.873 ± 3.931	14.380 ± 3.874	-4.743	<0.001*
Auditory verbal learning Test	30.252 ± 13.039	37.476 ± 14.429	-3.770	<0.001*
Associative learning test	4.24 ± 4.021	6.18 ± 4.396	-3.312	0.001*
Visual identification test	12.93 ± 5.197	16.27 ± 4.350	-5.105	<0.001*
Verbal fluency	21.24 ± 9.321	27.13 ± 10.400	-4.315	<0.001*
Delayed memory	12.23 ± 9.236	16.44 ± 9.531	-3.198	0.002*
Wechsler's picture completion	7.10 ± 3.880	9.72 ± 4.041	-4.874	<0.001*
Wechsler's Block Design	20.50 ± 9.095	24.54 ± 9.885	-3.099	0.002*

TABLE 5 | Neuropsychological tests that can be used to predict aMCI.

Variables	B	S.E	Wald	df	p	OR	95% CI
Wechsler's Block Design	-0.031	0.014	4.917	1	0.027	0.969	0.943~0.996

Previous studies indicated that 35%–75% of patients with aMCI would experience at least one neuropsychiatric symptom (NPS), such as delusions, aggressiveness, anxiety, depression, aberrant motor behavior, and eating problems (36). And the present of NPS was proved to be associated with decreased quality of life, increased hospital stay, as well as decreased survival (37). What's more, the presence of NPS among aMCI patients would also increase the risk of progression to dementia (38, 39). In the present study, we used NPI to investigate the NPS of normal old adult people, and found that the total and subtest scores of NPI in normal-aMCI group were significant higher than that in the normal-normal group, although the difference was not statistically significant ($p > 0.05$). Therefore, we speculated that mental symptoms would gradually increase with the deterioration of cognitive symptoms. However, due to the serious missing of data, we were unable to count the prevalence of NPS in the aMCI and AD population, which was also a major limitation of this study.

By using Cox regression analysis, we confirmed that male sex ($p = 0.001$, OR = 0.489, 95%CI 0.319~0.751) and reading ($p = 0.023$, OR = 0.533, 95%CI 0.310~0.917) were protective factors for against aMCI. Evidence from epidemiological studies has indicated a lower prevalence of AD in males than in age-matched females (40), independent of race, culture, and diagnostic criteria used (41). In populations over the age of 65, men are half as likely to suffer from AD as women (42). However, a meta- analysis of fifty-six studies also showed that there were no statistically significant sex

differences in the prevalence or incidence of amnestic MCI (43). Therefore, a larger sample of longitudinal studies is needed to specifically explore the gender differences in aMCI. There are several mechanisms to explain the difference in AD prevalence between men and women, first, compared to female with AD, male AD patients tend to have a better score on a variety of neuropsychological tasks, greater hippocampal volumes, less total brain atrophy and temporal lobe degeneration (44). In our present study, we also found that the volume of left (3,945.76 ± 470.139) and right hippocampus(3,724.5 ± 452.619) in normal old men was significantly larger ($p < 0.001$) than that (left hippocampus:3,671.84 ± 474.656; right hippocampus:3,504.96 ± 383.105) in women; second, estrogens can affect the prevalence of AD in women, but not in men (45); third, women often live longer than men, since age is the strongest risk factor for sporadic AD (46), as a result, women have a higher risk of AD; Fourth, risk factors (e.g., apolipoprotein E [APOE] genotype, type 2 diabetes, metabolic syndrome, obesity) that are equally common in women and men but are more common or have a stronger effect in one sex or gender group (46). Fifth, females often show higher frontal cortex cholinergic activity whereas males have higher activity in the hippocampus (47).

In addition, we also found that reading was an important factor for preventing aMCI, which was consistent with the findings of Wang YP (the research method is similar to ours) (48). So our conclusions were consistent. It is worth noting that there was a low rate of illiteracy in the present study, since people with higher socioeconomic status/education may also be more likely to read (49), the relationship between reading and aMCI needs further study.

Next, we explored the cognitive characteristics of people who would develop into aMCI in the future. And found that the old adult who would develop into aMCI in the future would show multiple cognitive impairments (such as immediate memory, associative learning memory, and executive function) in the early stage, although their overall cognitive function was not significantly abnormal. Then, we further explored which neuropsychological test can predict the transition from normal aging to aMCI. By using Cox regression analysis and cluster analysis, (whether the subjects were converted to aMCI as a grouping variable and age as time variable, 111 pairs), we found that Wechsler's Block Design ($p = 0.027$, OR = 0.969, 95%CL 0.943~0.996) could predict whether subjects would turn into aMCI in the fucture. Although the impairment of memory is regarded as a hallmark of aMCI, recent studies (50, 51) have demonstrated that executive dysfunction may also be present. And Johns et al. (51) found that aMCI would show deficits in at least one sub-domain of executive function, independent of whether they were of a single domain or multiple domain subtype. Therefore, we inferred that executive dysfunction might be an indicator of future transition to aMCI, which was harmonious with Chapman's findings (they also found that speed executive functioning was a strong predictor of MCI conversion to AD) (52).

LIMITATIONS

We have to admit that there are some limitations in our research. First, we did not specifically discuss the relationship between the different subtypes of aMCI and cognitive function. Second, longitudinal data from larger samples was needed to verify the above conclusions. Third, although we also collected the social activities and exchange information of the participants, we did not include them in the final statistics due to the serious lack of data. Fourth, neuropsychiatric symptoms were a common accompaniment of dementia or aMCI (53), however, we did not concentrate on them in this study.

CONCLUSIONS

In summary, using the nationwide community-based data, we found out that the prevalence and incidence aMCI among the old adult in Chinese communities was 17.1% and 70.57 per 1,000 person-years, respectively. And male sex and reading are protective factors for against aMCI. In addition, the old adult who will develop aMCI in the future will show multiple cognitive impairments (such as immediate memory, associative learning memory and executive function) in the early stage, and executive dysfunction might be an indicator of future transition to aMCI.

DATA AVAILABILITY STATEMENT

The datasets analyzed in this article are not publicly available. Requests to access the datasets should be directed to xiaoshifu@msn.com.

ETHICS STATEMENT

The studies involving human participants were reviewed and approved by Shanghai Mental Health Centre. The patients/participants provided their written informed consent to participate in this study. Written informed consent was obtained from the individual(s) for the publication of any potentially identifiable images or data included in this article.

AUTHOR CONTRIBUTIONS

WL wrote this article. LS analyzed the data. SX was the project leader.

FUNDING

This work was supported by grants from the Shanghai Jiao Tong University Technological Innovation Special Fund (YG2016MS38), the Cultivation of Multidisciplinary Interdisciplinary Project in Shanghai Jiaotong University (YG2019QNA10), and the Shanghai Mental Health Center Clinical Research Center (CRC2017ZD02).

SUPPLEMENTARY MATERIAL

The Supplementary Material for this article can be found online at: https://www.frontiersin.org/articles/10.3389/fpsyt.2020.00075/full#supplementary-material

TABLE S1 | Demographic, health, and disease-related for the follow up and lost population.

REFERENCES

1. Xiao S, Li J, Tang M, Chen W, Bao F, Wang H, et al. Methodology of China's national study on the evaluation, early recognition, and treatment of psychological problems in the elderly: the China Longitudinal Aging Study (CLAS). *Shanghai Arch Psychiatry* (2013) 25(2):91–8. doi: 10.3969/j.issn.1002-0829.2013.02.005
2. Albert MS, DeKosky ST, Dickson D, Dubois B, Feldman HH, Fox NC, et al. The diagnosis of mild cognitive impairment due to Alzheimer's disease: recommendations from the National Institute on Aging-Alzheimer's Association workgroups on diagnostic guidelines for Alzheimer's disease. *Alzheimer's Dement* (2011) 7(3):270–9. doi: 10.1016/j.jalz.2011.03.008
3. Petersen RC, Morris JC. Mild cognitive impairment as a clinical entity and treatment target. *Arch Neurol* (2005) 62(7):1160–3. doi: 10.1001/archneur.62.7.1160
4. De Simone MS, Perri R, Fadda L, Caltagirone C, Carlesimo GA. Predicting progression to Alzheimer's disease in subjects with amnestic mild cognitive impairment using performance on recall and recognition tests. *J Neurol* (2019) 266(1):102–11. doi: 10.1007/s00415-018-9108-0
5. Petersen RC, Parisi JE, Dickson DW, Johnson KA, Knopman DS, Boeve BF, et al. Neuropathologic features of amnestic mild cognitive impairment. *Arch Neurol* (2006) May63(5):665–72. doi: 10.1001/archneur.63.5.665
6. Petersen RC, Stevens JC, Ganguli M, Tangalos EG, Cummings JL, DeKosky ST. Practice parameter: early detection of dementia: mild cognitive impairment (an evidence-based review). Report of the Quality Standards Subcommittee of the American Academy of Neurology. *Neurology* (2001) 56(9):1133–42. doi: 10.1212/WNL.56.9.1133
7. Zhao Z, Lu J, Jia X, Chao W, Han Y, Jia J. Selective changes of resting-state brain oscillations in aMCI: an fMRI study using ALFF. *Biomed. Res. Int.* (2014) 2014:92–108. doi: 10.1155/2014/920902
8. Ward A, Arrighi HM, Michels S, Cedarbaum JM. Mild cognitive impairment: disparity of incidence and prevalence estimates. *Alzheimer's Dement* (2012) 8(1):14–21. doi: 10.1016/j.jalz.2011.01.002
9. Cid-Fernandez S, Lindin M, Diaz F. The importance of age in the search for ERP biomarkers of aMCI. *Biol Psychol* (2019) 142:108–15. doi: 10.1016/j.biopsycho.2019.01.015
10. Hao L, Wang X, Zhang L, Xing Y, Guo Q, Hu X, et al. Prevalence, risk factors, and complaints screening tool exploration of subjective cognitive decline in a large cohort of the Chinese population. *J Alzheimer's Dis* (2017) 60(2):371–88. doi: 10.3233/JAD-170347
11. Ma F, Wu T, Zhao J, Ji L, Song A, Zhang M, et al. Prevalence of mild cognitive impairment and its subtypes among Chinese older adults: role of vascular risk factors. *Dement Geriatric Cogn Disord* (2016) 41(5-6):261–72. doi: 10.1159/000446507
12. Wajman JR, Mansur LL, Yassuda MS. Lifestyle patterns as a modifiable risk factor for late-life cognitive decline: a narrative review regarding dementia prevention. *Curr Aging Sci* (2018) 11(2):90–9. doi: 10.2174/1874609811666181003160225
13. Xue J, Li J, Liang J, Chen S. The prevalence of mild cognitive impairment in china: a systematic review. *Aging Dis* (2018) 9(4):706–15. doi: 10.14336/AD.2017.0928
14. Hu C, Yu D, Sun X, Zhang M, Wang L, Qin H. The prevalence and progression of mild cognitive impairment among clinic and community populations: a systematic review and meta-analysis. *Int Psychogeriatrics* (2017) 29(10):1595–608. doi: 10.1017/S1041610217000473
15. Su X, Shang L, Xu Q, Li N, Chen J, Zhang L, et al. Prevalence and predictors of mild cognitive impairment in Xi'an: a community-based study among the elders. *PLoS One* (2014) 9(1):657–75. doi: 10.1371/journal.pone.0083217
16. Petersen RC, Doody R, Kurz A, Mohs RC, Morris JC, Rabins PV, et al. Current concepts in mild cognitive impairment. *Arch Neurol* (2001) 58(12):1985–92. doi: 10.1001/archneur.58.12.1985
17. Petersen RC, Caracciolo B, Brayne C, Gauthier S, Jelic V, Fratiglioni L. Mild cognitive impairment: a concept in evolution. *J Internal Med* (2014) 275(3):214–28. doi: 10.1111/joim.12190
18. Abdulrab K, Heun R. Subjective memory impairment. A review of its definitions indicates the need for a comprehensive set of standardised and validated criteria. *Eur Psychiatry* (2008) 23(5):321–30. doi: 10.1016/j.eurpsy.2008.02.004
19. Reisberg B. Diagnostic criteria in dementia: a comparison of current criteria, research challenges, and implications for DSM-V. *J Geriatric Psychiatry Neurol* (2006) 19(3):137–46. doi: 10.1177/0891988706291083
20. McKhann G, Drachman D, Folstein M, Katzman R, Price D, Stadlan EM. Clinical diagnosis of Alzheimer's disease: report of the NINCDS-ADRDA Work Group under the auspices of Department of Health and Human Services Task Force on Alzheimer's Disease. *Neurology* (1984) 34(7):939–44. doi: 10.1212/WNL.34.7.939
21. Roman GC, Tatemichi TK, Erkinjuntti T, Cummings JL, Masdeu JC, Garcia JH, et al. Vascular dementia: diagnostic criteria for research studies. Report of the NINDS-AIREN International Workshop. *Neurology* (1993) 43(2):250–60. doi: 10.1212/WNL.43.2.250
22. Morris JC. The Clinical Dementia Rating (CDR): current version and scoring rules. *Neurology* (1993) 43(11):2412–4. doi: 10.1212/WNL.43.11.2412-a
23. Loewenstein DA, Curiel RE, Wright C, Sun X, Alperin N, Crocco E, et al. Recovery from proactive semantic interference in mild cognitive impairment and normal aging: relationship to atrophy in brain regions vulnerable to alzheimer's disease. *J Alzheimer's Dis* (2017) 56(3):1119–26. doi: 10.3233/JAD-160881
24. O'Bryant S, Humphreys JG, Ivnik R, Graff-Radford N, Petersen R, Lucas J. Detecting dementia with the mini-mental state examination in highly educated individuals. *Arch Neurol* (2008) 65(7):963–7. doi: 10.1001/archneur.65.7.963
25. Gil L, DSC R, Gil F, Romero SJ, Pretelt BF. Validation of the Montreal Cognitive Assessment (MoCA) in Spanish as a screening tool for mild cognitive impairment and mild dementia in patients over 65 years old in Bogotá, Colombia. *Int J Geriatric Psychiatry* (2014) 30(6):655–63. doi: 10.1002/gps.4199
26. Leung JLM, Lee GTH, Lam YH, Chan RCC, Wu JYM. The use of the Digit Span Test in screening for cognitive impairment in acute medical inpatients. *Int Psychogeriatrics* (2011) 23(10):1569–74. doi: 10.1017/S1041610211000792
27. Xia H, Zhang ZX, Li-Yong WU, Shi LL, Zhao XH. Validity of auditory verbal learning test in diagnosis of alzheimer's disease. *Acta Academiae Med Sinicae* (2012) 34(3):262–6.
28. Cummings JL, Mega M, Gray K, Rosenberg-Thompson S, Carusi DA, Gornbein J. The neuropsychiatric inventory: comprehensive assessment of psychopathology in dementia. *Neurology* (1994) 44(12):2308–14. doi: 10.1212/WNL.44.12.2308
29. Wang T, Xiao S, Chen K, Yang C, Dong S, Cheng Y, et al. Prevalence, incidence, risk and protective factors of amnestic mild cognitive impairment in the elderly in Shanghai. *Curr Alzheimer Res* (2017) 14(4):460–6.
30. Wolz R, Schwarz AJ, Yu P, Cole PE, Rueckert D, Jack CR, et al. Robustness of automated hippocampal volumetry across magnetic resonance field strengths and repeat images. *Alzheimer's Dement* (2014) 10(4):430–438.e432.
31. Mao C, Li ZH, Lv YB, Cao X, Zhou B, KR B, et al. Specific leisure activities and cognitive functions among the oldest-old: the Chinese longitudinal healthy longevity survey. *J Gerontol Ser A Biol Sci Med Sci* (2019). 474:99–108. doi: 10.1093/gerona/glz086

32. Sanchez SS, Abanto J. Frequency and associated factors of amnestic mild cognitive impairment at four senior citizen clubs in Lima, Peru. (2019). *Dement. Neuropsychol.* 13: (3):321–8. doi: 10.1590/1980-57642018dn13-030009
33. Cesar KG, Brucki SM, Takada LT, Nascimento LF, Gomes CM, Almeida MC, et al. Prevalence of cognitive impairment without dementia and dementia in Tremembe, Brazil. *Alzheimer Dis Assoc Disord* (2016) 30(3):264–71. doi: 10.1097/WAD.0000000000000122
34. Rao D, Luo X, Tang M, et al. Prevalence of mild cognitive impairment and its subtypes in community-dwelling residents aged 65 years or older in Guangzhou, China. *Arch Gerontol Geriatrics* (2018) 75:70–5. doi: 10.1016/j.archger.2017.11.003
35. Katz MJ, Lipton RB, Hall CB, Zimmerman ME, Sanders AE, Verghese J, et al. Age-specific and sex-specific prevalence and incidence of mild cognitive impairment, dementia, and Alzheimer dementia in blacks and whites: a report from the Einstein Aging Study. *Alzheimer Dis Assoc Disord* (2012) 26(4):335–43. doi: 10.1097/WAD.0b013e31823dbcfc
36. Apostolova LG, Cummings JL. Neuropsychiatric manifestations in mild cognitive impairment: a systematic review of the literature. *Dementia Geriatric Cogn Disord* (2008) 25(2):115–26. doi: 10.1159/000112509
37. Kazui H, Yoshiyama K, Kanemoto H, Suzuki Y, Sato S, Hashimoto M, et al. Differences of behavioral and psychological symptoms of dementia in disease severity in four major dementias. *PLoS One* (2016) 11(8):92–103. doi: 10.1371/journal.pone.0161092
38. Rosenberg PB, Mielke MM, Appleby BS, Oh ES, Geda YE, Lyketsos CG. The association of neuropsychiatric symptoms in MCI with incident dementia and Alzheimer disease. *Am J Geriatric Psychiatry* (2013) 21(7):685–95. doi: 10.1016/j.jagp.2013.01.006
39. Forrester SN, Gallo JJ, Smith GS, Leoutsakos JM. Patterns of neuropsychiatric symptoms in mild cognitive impairment and risk of dementia. *Am J Geriatric Psychiatry* (2016) 24(2):117–25. doi: 10.1016/j.jagp.2015.05.007
40. Mielke MM, Vemuri P, Rocca WA. Clinical epidemiology of Alzheimer's disease: assessing sex and gender differences. *Clin Epidemiol* (2014) 6:37–48. doi: 10.2147/CLEP.S37929
41. Baron S, Ulstein I, Werheid K. Psychosocial interventions in Alzheimer's disease and amnestic mild cognitive impairment: evidence for gender bias in clinical trials. *Aging Ment Health* (2015) 19(4):290–305. doi: 10.1080/13607863.2014.938601
42. Hy LX, Keller DM. Prevalence of AD among whites: a summary by levels of severity. *Neurology* (2000) 55(2):198–204. doi: 10.1212/WNL.55.2.198
43. Au B, Dale-McGrath S, Tierney MC. Sex differences in the prevalence and incidence of mild cognitive impairment: a meta-analysis. *Ageing Res Rev* (2017) 35:176–99. doi: 10.1016/j.arr.2016.09.005
44. Li W, Qiu Q, Sun L, Yue L, Wang T, Li X, et al. Sex differences in obesity and cognitive function in a cognitively normal aging Chinese Han population. *Neuropsychiatr Dis Treat* (2017) 13:2405–10. doi: 10.2147/NDT.S145245
45. Pike CJ. Sex and the development of Alzheimer's disease. *J Neurosci Res* (2017) 95(1-2):671–80. doi: 10.1002/jnr.23827
46. Nebel RA, Aggarwal NT, Barnes LL, Gallagher A, Goldstein JM, Kantarci K, et al. Understanding the impact of sex and gender in Alzheimer's disease: a call to action. *Alzheimer's Dement* (2018) 14(9):1171–83. doi: 10.1016/j.jalz.2018.04.008
47. Giacobini E, Pepeu G. Sex and gender differences in the brain cholinergic system and in the response to therapy of Alzheimer disease with cholinesterase inhibitors. *Curr Alzheimer Res* (2018) 15(11):1077–84. doi: 10.2174/1567205015666180613111504
48. Wang YP, Zhai JB, Zhu F, Zhang WW, Yang XJ, Qu CY. A three-year follow-up study on the transfer of mild cognitive impairment to Alzheimer's disease among the elderly in Taiyuan city. *Zhonghua Liu Xing Bing Xue za zhi = Zhonghua Liuxingbingxue zazhi* (2011) 32(2):105–9.
49. Romeo RR, Christodoulou JA, Halverson KK, Murtagh J, Cyr AB, Schimmel C, et al. Socioeconomic status and reading disability: neuroanatomy and plasticity in response to intervention. *Cereb Cortex (N Y N.Y.: 1991).* (2018) 28(7):2297–312. doi: 10.1093/cercor/bhx131
50. Brandt J, Aretouli E, Neijstrom E, et al. Selectivity of executive function deficits in mild cognitive impairment. *Neuropsychology* (2009) 23(5):607–18. doi: 10.1037/a0015851
51. Johns EK, Phillips NA, Belleville S, et al. The profile of executive functioning in amnestic mild cognitive impairment: disproportionate deficits in inhibitory control. *J Int Neuropsychol Soc* (2012) 18(3):541–55. doi: 10.1017/S1355617712000069
52. Chapman RM, Mapstone M, McCrary JW, Gardner MN, Porsteinsson S, Sandoval TC, et al. Predicting conversion from mild cognitive impairment to Alzheimer's disease using neuropsychological tests and multivariate methods. *J Clin Exp Neuropsychol* (2011) 33(2):187–99. doi: 10.1080/13803395.2010.499356
53. Kales HC, Gitlin LN, Lyketsos CG. Assessment and management of behavioral and psychological symptoms of dementia. *BMJ (Clin Res ed.)* (2015) 350–69. doi: 10.1136/bmj.h369

Conflict of Interest: The authors declare that the research was conducted in the absence of any commercial or financial relationships that could be construed as a potential conflict of interest.

frontiers in Aging Neuroscience

ORIGINAL RESEARCH
published: 05 March 2020
doi: 10.3389/fnagi.2020.00048

Resting State Glucose Utilization and Adult Reading Test Performance

Younghwa Lee[1], Dahyun Yi[2], Eun Hyun Seo[3], Ji Young Han[4], Haejung Joung[1], Min Soo Byun[5], Jun Ho Lee[6], Jongho Jun[7] and Dong Young Lee[1,2,4,8]* for the KBASE research group[†]*

[1]Interdisciplinary Program of Cognitive Science, Seoul National University, Seoul, South Korea, [2]Institute of Human Behavioral Medicine, Medical Research Center, Seoul National University, Seoul, South Korea, [3]Premedical Science, College of Medicine, Chosun University, Gwangju, South Korea, [4]Department of Neuropsychiatry, Seoul National University Hospital, Seoul, South Korea, [5]Department of Neuropsychiatry, Seoul National University Bundang Hospital, Sungnam, South Korea, [6]Department of Geriatric Psychiatry, National Center for Mental Health, Seoul, South Korea, [7]Department of Linguistics, Seoul National University, Seoul, South Korea, [8]Department of Psychiatry and Behavioral Science, Seoul National University College of Medicine, Seoul, South Korea

Adult reading tests (ART) have been widely used in both research and clinical settings as a measure of premorbid cognitive abilities or cognitive reserve. However, the neural substrates underlying ART performance are largely unknown. Furthermore, it has not yet been examined whether the neural substrates of ART performance reflect the cortical regions associated with premorbid intelligence or cognitive reserve. The aim of the study is to identify the functional neural correlates of ART performance using 18F-fluorodeoxyglucose (FDG) positron emission tomography (PET) imaging in the cognitively normal (CN) middle- and old-aged adults. Voxel-wise analyses revealed positive correlations between glucose metabolism and ART performance in the frontal and primary somatosensory regions, more specifically the lateral frontal cortex, anterior cingulate cortex and postcentral gyrus (PCG). When conducted again only for amyloid-β (Aβ)-negative individuals, the voxel-wise analysis showed significant correlations in broader areas of the frontal and primary somatosensory regions. This is the first neuroimaging study to directly demonstrate the cerebral resting-state glucose utilization associated with ART performance. Our findings provide important evidence at the neural level that ART predicts premorbid general intelligence and cognitive reserve, as brain areas that showed significant correlations with ART performance correspond to regions that have been associated with general intelligence and cognitive reserve.

Keywords: adult reading test, cerebral glucose metabolism, cognitive reserve, beta-amyloid, cognitively normal adults

OPEN ACCESS

Edited by:
Mohamad Habes, University of Pennsylvania, United States

Reviewed by:
Nabin Koirala, Haskins Laboratories, United States
Heike Endepols, University Hospital of Cologne, Germany

****Correspondence:***
Dahyun Yi
dahyunyi@gmail.com
Dong Young Lee
selfpsy@snu.ac.kr

[†]The coinvestigators of the KBASE Research Group are listed elsewhere: http://kbase.kr/

Received: *07 November 2019*
Accepted: *11 February 2020*
Published: *05 March 2020*

Citation:
Lee Y, Yi D, Seo EH, Han JY, Joung H, Byun MS, Lee JH, Jun J and Lee DY (2020) Resting State Glucose Utilization and Adult Reading Test Performance. Front. Aging Neurosci. 12:48. doi: 10.3389/fnagi.2020.00048

INTRODUCTION

Estimation of premorbid cognitive ability is essential in both research and clinical settings to quantify and diagnose cognitive impairment. The most widely applied approach to estimating premorbid cognitive function is the use of an adult reading test (ART), which comprises of oral reading of orthographically irregular words. Premorbid intelligence can be estimated from ART based on the rationale that the reading ability of irregular word correlates strongly with measure of IQ in healthy adults (Nelson and Willison, 1991; Crawford et al., 2001; Yi et al., 2017), and is relatively resistant to cognitive declines in patients with neurological or psychiatric disorders (Sasanuma et al., 1992; McGurn et al., 2004; Matsuoka et al., 2006). It is assumed that better

performance on ART implies prior knowledge of a word's pronunciation and therefore a higher premorbid intelligence (Lezak et al., 2004). Moreover, numerous studies on Alzheimer's disease (AD) have reported that an ability to pronounce irregular words is a retained skill even in advanced stages of the disease (Sasanuma et al., 1992; McGurn et al., 2004; Matsuoka et al., 2006), suggesting that ART is able to provide a reasonable estimate of premorbid intelligence for AD patients.

ART has also been used as an index for cognitive reserve (CR)—a theoretical concept referring to the cognitive capacity to cope with brain damages (Stern et al., 2003; Lo and Jagust, 2013; Rentz et al., 2017). The concept of CR has been widely used to explain the discrepancy between the clinical manifestations and degree of brain damage or pathology (Stern et al., 2003, 2008). It is also considered as a contributing factor toward individual differences of resilience to brain pathology. In epidemiologic studies, higher intelligence has consistently been shown to be protective against the progression of AD (Snowdon et al., 1996; Whalley and Deary, 2001; Yeo et al., 2011). Moreover, high prevalence of AD-related abnormal biomarkers at a given level of cognitive performance was associated with higher scores on ART, indicating that those with higher ART scores cope better with AD pathology (McGurn et al., 2004; Vemuri et al., 2011; Rentz et al., 2017). Taken together, these findings support that performance on ART reflects CR.

While there is ample evidence demonstrating that ART provides a good estimate of intelligence and CR at the behavioral level, the neural basis of ART performance is largely unknown. Furthermore, it has not yet been identified whether ART performance reflects the neural function of the regions associated with intelligence or CR. Previous neuroimaging studies on ART focused largely on examining whether CR measured by ART helps to cope against neuropathology in individuals with cognitive impairment (Alexander et al., 1997; Vemuri et al., 2011; Rentz et al., 2017). To our knowledge, however, there are no studies to date that looked directly into the neural substrates of ART performance.

Therefore, the present study aimed to identify the neural correlates of ART performance in cognitively normal (CN) adults. To achieve this aim, the correlation between ART performance and regional cerebral glucose metabolism was examined with brain ^{18}F-fluorodeoxyglucose (FDG)-positron emission tomography (PET), which has been known to provide a reliable index of neural activity (Teipel et al., 2006; Melrose et al., 2013; Han et al., 2015). In addition, the neural correlates were reexamined in individuals without a significant level of amyloid-β (Aβ) deposition in the AD signature regions shown on ^{11}C-labelled Pittsburgh Compound B (PIB)-PET, in order to eliminate the influence of AD pathology on cerebral glucose metabolism.

MATERIALS AND METHODS

Subjects

This study included 271 healthy CN middle- and old-aged adults who participated in the Korean Brain Aging Study for the Early Diagnosis and Prediction of Alzheimer's disease (KBASE), which is an ongoing prospective cohort study established in 2014 (Byun et al., 2017). All subjects underwent comprehensive clinical and neuropsychological assessments and multi-modal brain imaging including brain FDG-PET and PiB-PET. Details of the inclusion and exclusion criteria were described previously (Byun et al., 2017). The inclusion criteria for participants with normal cognition were: (a) aged 55–90 years (inclusive); (b) Clinical Dementia Rating score of 0; and (c) no diagnosis of mild cognitive impairment or dementia. Participants who met the following criteria were excluded: (a) any present serious medical, psychiatric, or neurological disorder that could affect mental functioning; (b) presence of severe communication problems that would make a clinical examination or brain scan difficult; (c) contraindications for MRI; (d) absence of a reliable informant; (e) illiteracy; and (f) participation in another clinical trial and treatment with an investigational product.

All subjects provided written informed consent prior to the administration of the study procedure. The study protocol was approved by the Institutional Review Boards of Seoul National University Hospital (C-1401-027-547) and SNU-SMG Boramae Center, Seoul, South Korea (26-2015-60), and was conducted in accordance with the recommendations of the current version of the Declaration of Helsinki.

Clinical Assessments

All participants received standardized clinical assessments by trained psychiatrists based on the KBASE clinical assessment protocol (Byun et al., 2017) which corresponded with the Korean version of the Consortium to Establish a Registry for AD Assessment Packet (CERAD-K; Lee et al., 2002). In addition, the KBASE neuropsychological assessments (Byun et al., 2017) incorporating the CERAD-K neuropsychological battery (Lee et al., 2004) were administered to all participants by a neuropsychologist or trained psychometrists.

FDG-PET Acquisition and Preprocessing

FDG-PET scans were performed using a 3.0T Biograph mMR (PET-MR) scanner (Siemens, Germany) and 3D T1-weighted magnetic resonance imaging was simultaneously performed with PET. Details of the acquisition were described previously (Byun et al., 2017).

The FDG-PET data were preprocessed using Statistical Parametric Mapping 12 (SPM12; Institute of Neurology, University College of London, United Kingdom) implemented in Matlab 2015ba (Mathworks, Natick, MA, USA). In the first step, static FDG-PET images were co-registered to individual T1 structural images. Next, transformation parameters were calculated from the individual T1 images that were coregistered to the MNI template image. The forward parameters were used to spatially normalize individual T1 and FDG-PET images to the MNI template. The spatially normalized FDG-PET images were smoothed with a 12-mm Gaussian filter and pons were used as the reference region for intensity normalized (Minoshima et al., 1995).

PIB-PET Acquisition and Processing

All participants also underwent 3-dimensional (3D) PiB-PET using the same PET-MR machine as the FDG-PET scans.

Details of the acquisition were described previously (Byun et al., 2017). Image preprocessing for statistical analyses was performed using SPM 12 implemented in Matlab 2015b. First, the PiB images were coregistered to individual T1 structural images that were coregistered to the MNI template space, and inverse transformation parameters were obtained for spatial normalization. The inverse transformation parameters were used to transform coordinates from the automatic anatomic labeling (AAL) 116 atlas (Tzourio-Mazoyer et al., 2002) into an individual space for each subject (resampling voxel size = 1 × 0.98 × 0.98 mm) with the IBASPM software. The segmented cerebral gray matter segment image from each subject was used to mask the non-gray matter portion of the atlas.

Mean cerebral PiB uptake values were extracted using the individual AAL 116 atlas from the T1-coregistered PiB-PET images and quantitative normalization was performed using the cerebellar gray matter as the reference region (Lopresti et al., 2005). The probabilistic cerebellar atlas (Institute of Cognitive Neuroscience, UCL; Cognitive Neuroscience Laboratory, Royal Holloway) that was transformed into individual space was used to obtain mean cerebellar PiB uptakes from the cerebellar lobular regions except for the vermis. The AAL algorithm (Tzourio-Mazoyer et al., 2002) and a region-combining method (Reiman et al., 2009) were applied to determine regions of interest (ROIs) to characterize the PiB retention level in the frontal, lateral parietal, posterior cingulate-precuneus (PC-PRC), and lateral temporal regions. Each participant was classified as Aβ-positive if the standardized uptake value ratio (SUVR) value was >1.4 in at least one of the four ROIs or as Aβ-negative if the SUVR value of all four ROIs was ≤1.4 (Reiman et al., 2009; Villeneuve et al., 2015).

The Korean Adult Reading Test (KART)

The KART, the validated Korean version of ART, was administered to all participants (Yi et al., 2017). KART-estimated Wechsler Adult Intelligence Scale, 4th edition (K-WAIS-IV) full-scale IQ (FSIQ) was used as a measure for ART performance.

Statistical Analyses

Statistical analyses were performed with SPSS 22.0 and SPM12. Correlation between KART-estimated FSIQ score and regional cerebral glucose metabolism was examined using voxel-wise regression with age and gender as covariates. For explorative purposes, the statistical threshold was set at $p < 0.005$ (uncorrected) and a cluster size threshold of 1,062 voxels was applied to correct for multiple comparisons. The cluster size threshold was determined based on a cluster correction procedure in Analysis of Functional and Neural image (i.e., 3dClustSim), with 10,000 iterations of Monte Carlo simulations on anatomical cerebral mask dataset (Forman et al., 1995). The results with the statistical threshold set at $p < 0.001$ (uncorrected) and a cluster size threshold of 527 voxels based on the same cluster correction procedure as the above are presented in the **Supplementary Tables S1, S2**. In addition, the mean FDG-PET metabolism SUVR values were extracted from the clusters presenting a significant correlation with the KART-estimated FSIQ score. Partial correlation analyses controlling for age and gender were implemented with the FDG-PET SUVR data to examine the strength of the correlations between KART-performance and FDG uptake. The abovementioned analyses were performed again after excluding the Aβ-positive participants.

RESULTS

Subject Characteristics

The demographic characteristics of the study sample are summarized in **Table 1**. The sample consisted of 271 participants, of which 51.7% ($n = 140$) were female and 86.7% ($n = 235$) were Aβ-negative. Participants had a mean age of 69.0 years (SD = 8.1) and average years of education of 11.8 (SD = 4.8). The mean KART error score was 5.0 (SD = 4.9) and the mean FSIQ score estimated from the KART error score was 116.0 (SD = 9.9).

Correlation Between Regional Cerebral Glucose Metabolism and KART Performance in all CN Subjects

The voxel-wise analysis using age and gender as nuisance covariates revealed significant positive correlations between KART-estimated FSIQ score and regional cerebral glucose metabolism in the frontal and primary somatosensory regions, particularly in the left middle frontal gyrus (MFG), right anterior cingulate gyrus (ACG) and left postcentral gyrus (PCG; **Table 2**, **Figure 1A**).

In order to further examine the strength of the correlations, raw mean FDG-PET SUVR values were extracted from each cluster showing a significant association with the KART performance and partial correlation analyses were performed controlling for the effects of age and gender. There were positive and moderately significant correlations between KART-estimated IQ score and mean FDG-PET SUVR values in all clusters (whole cluster: $r = 0.21$, $p = 0.001$; left MFG: $r = 0.20$, $p = 0.001$; right ACG: $r = 0.19$, $p = 0.002$; left PCG: $r = 0.18$, $p = 0.003$; **Figure 2**).

Correlation Between Regional Cerebral Glucose Metabolism and KART Performance in Aβ-Negative CN Subjects

For Aβ-negative subsample ($n = 235$), the voxel-wise analysis showed positive correlations in more widespread clusters of the bilateral frontal and primary somatosensory regions including

TABLE 1 | Demographic characteristics.

Characteristics	CN
N	271
Age, mean (SD, range)	00069.0 (8.1, 55–87)
Female, *N* (%)	140 (51.7)
Years of education, mean (SD)	11.8 (4.8)
KART error score, mean (SD)	5.0 (4.9)
KART-estimated FSIQ, mean (SD)	116.0 (9.9)
Aβ-negative, *N* (%)	235 (86.7)

Values are mean (SD) or count. SD, standard deviation; N, count; KART-estimated FSIQ, Wechsler Adult Intelligence Scale Full-Scale IQ estimated using the KART; Aβ, amyloid-beta.

TABLE 2 | Positive correlations between regional cerebral glucose metabolism and The Korean Adult Reading Test (KART)-estimated full-scale IQ (FSIQ) score after adjusting for age and gender in all cognitively normal (CN) subjects.

Regions	BA	Coordinates (mm)			Extent voxels	*T*-value	Cluster number
		x	*y*	*z*			
L middle frontal gyrus	6/9	−21	−1	46	1,990	3.57	C1
R anterior cingulate gyrus	32	5	8	43	5,623	3.38	C2
L postcentral gyrus	3	−30	−25	46	1,545	3.35	C3

$p < 0.005$ (uncorrected) with significance of $k > 1{,}062$. Adjusted for age and gender. Coordinates are in Montreal Neurological Institute (MNI) space. Cluster numbers are labeled for each cluster (i.e., C1 denotes cluster no.1). BA, approximate Brodmann area; L, left hemisphere; R, right hemisphere.

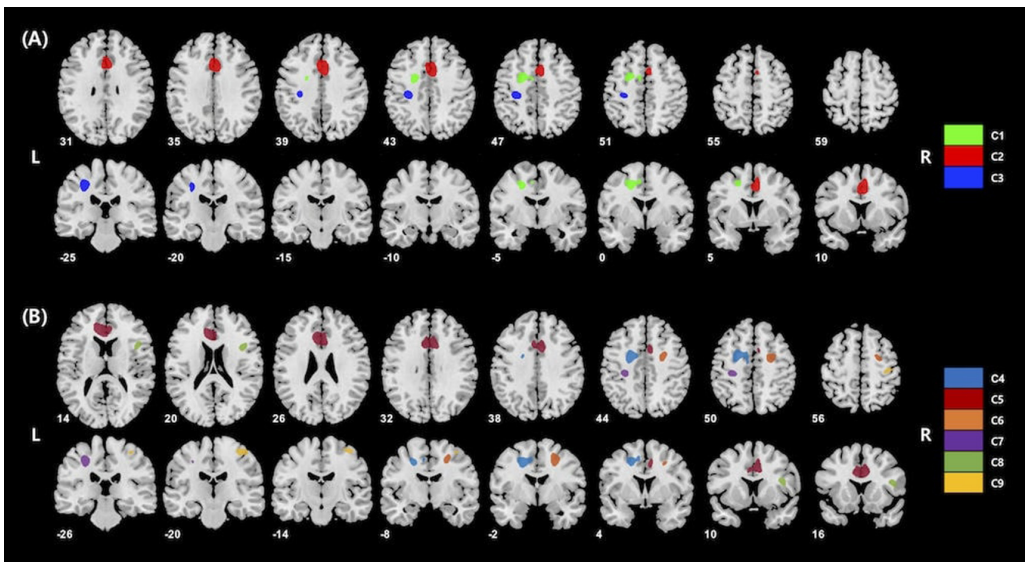

FIGURE 1 | (A) Results of whole-brain voxel-wise analysis presenting significant associations between cerebral glucose metabolism and korean adult reading test (KART)-estimated full-scale IQ (FSIQ) score in all cognitively normal (CN) subjects. Positive correlations were shown in the left middle frontal gyrus (MFG), right anterior cingulate gyrus (ACG) and left postcentral gyrus (PCG). Cluster numbers (e.g., C1) correspond to those in **Table 2**. **(B)** Results of whole-brain voxel-wise analysis presenting significant associations between cerebral glucose metabolism and KART-estimated FSIQ score in amyloid-β (Aβ)-negative CN subjects. Positive correlations were shown in the bilateral middle frontal gyri, bilateral anterior cingulate gyri, bilateral postcentral gyri and right inferior frontal gyrus (IFG). Cluster numbers correspond to those in **Table 3**.

the bilateral MFC, bilateral ACG, bilateral PCG and right inferior frontal gyrus (IFG; **Table 3**, **Figure 1B**). Particularly, additional positive correlations were found in the right lateral frontal cortex (LFC; middle and inferior frontal gyri), left ACG and right PCG after Aβ-positive subjects were excluded.

Partial correlation analyses adjusted for the effects of age and gender were repeated to see the strengths of the correlations with the raw mean FDG-PET SUVR values from these significant clusters and the KART performance. Relatively modest and significant correlations were found in all clusters (whole cluster: $r = 0.23$, $p = 0.001$; right IFG: $r = 0.19$, $p = 0.004$; left MFG: $r = 0.21$, $p = 0.001$; right MFG: $r = 0.20$, $p = 0.002$; left ACG: $r = 0.21$, $p = 0.001$; right ACG: $r = 0.21$, $p = 0.001$; left PCG: $r = 0.19$, $p = 0.003$; right PCG: $r = 0.19$, $p = 0.004$; **Supplementary Figure S1**).

DISCUSSION

The current study identified the brain regions correlated with ART performance by examining the associations between resting-state glucose metabolism and KART scores using a voxel-wise approach in CN adults. To sum up, in the whole sample including individuals both with and without significant levels of Aβ deposition, KART performance was positively correlated with regional glucose metabolism in the frontal and primary somatosensory areas—more specifically the left MFG, right ACG, and left PCG. After excluding Aβ-positive subjects, positive correlations with KART performance were found in much larger areas of the frontal and primary somatosensory regions including the bilateral MFG, right IFG, bilateral ACG and bilateral PCG. These findings suggest that the neural substrates of ART performance are located primarily in the frontal and primary somatosensory areas.

These results emphasize the involvement of the frontal and primary somatosensory areas in premorbid function, as estimated by ART. The patterns of brain metabolic impairment typical of AD begins in the precuneus and posterior cingulate cortex, spreads to parieto-temporal regions, and finally progresses to frontal and sensory cortices (Mosconi et al., 2007, 2008). The frontal and primary somatosensory regions have been

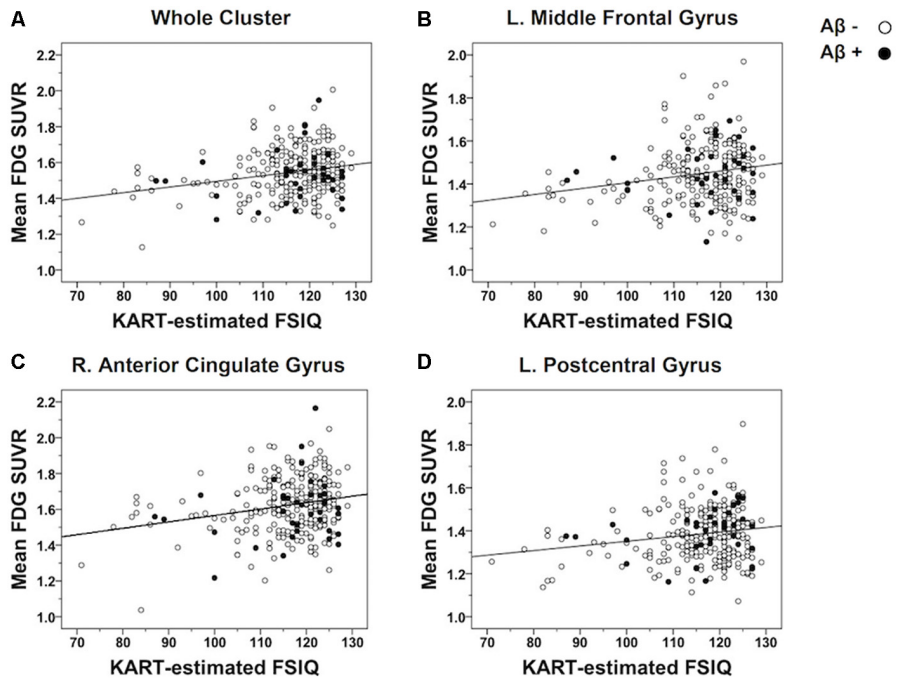

FIGURE 2 | Scatterplots demonstrating the strength of correlations between KART-estimated FSIQ score and regional glucose metabolism in all CN subjects. Mean FDG-PET SUVR values were extracted from the clusters of voxels showing a significant association with KART performance and examined the correlation with KART performance with using a partial correlation analysis adjusted for age and gender. There were positive significant correlations between KART-estimated IQ score and mean FDG-PET SUVR values in all clusters: **(A)** whole cluster; **(B)** left middle frontal gyrus; **(C)** right anterior cingulate gyrus; **(D)** left postcentral gyrus.

TABLE 3 | Positive correlations between regional cerebral glucose metabolism and KART-estimated FSIQ score after adjusting for age and gender in Aβ-negative CN subjects.

Regions	BA	Coordinates (mm)			Extent voxels	*T*-value	Cluster number
		x	*y*	*z*			
L middle frontal gyrus	6,8	−21	−2	45	3,071	3.66	C4
L anterior cingulate gyrus	32	−6	37	9	14,444	3.52	C5
R middle frontal gyrus	6	23	−4	48	1,878	3.38	C6
L postcentral gyrus	3	−29	−25	47	1,194	3.21	C7
R anterior cingulate gyrus	32	6	16	34	14,444	3.19	C5
R inferior frontal gyrus	9	42	12	19	1,092	3.01	C8
R postcentral gyrus	3	38	−20	60	1,543	2.95	C9

$p < 0.005$ (uncorrected) with significance of $k > 1,062$. Adjusted for age, and gender. Coordinates are in Montreal Neurological Institute (MNI) space. Cluster numbers are labeled for each cluster (i.e., C1 denotes cluster no.1). BA, approximate Brodmann area; L, left hemisphere; R, right hemisphere.

identified as being typically affected in the late stages of AD (Braak and Braak, 1991; Mosconi et al., 2007, 2008). Indeed, the regional neural functions that are found to be associated with KART performance are relatively less vulnerable in AD. Therefore, it may be posited that ART can predict premorbid function by reflecting the neuronal functions of regions that are relatively preserved in AD.

The largest region that showed positive correlations between glucose metabolism and KART performance was the frontal area, particularly the ACC and LFC. The ACC and LFC are components of the frontoparietal network (FPN), which has been reported to be the neural substrates of general intelligence (Margulies et al., 2007; Cole et al., 2012, 2015). The ACC, in particular, is known to support intelligence by handling and processing conflicting streams of information (Botvinick et al., 1999; Cohen et al., 2005; Brown, 2009). In addition to being recognized as a core region for intelligence, the LFC is functionally responsible for regulating the flow and integration of information between other regions (Cole et al., 2012, 2013, 2015).

The postcentral gyri, also known as the primary somatosensory cortex (SSC), were significantly associated with KART performance. While the roles of the SSC pertaining to intelligence are less clear, previous studies showed positive associations between general intelligence and cortical thickness or gray matter volumes of the SSC (Colom et al., 2009, 2013; Karama et al., 2009). Given that the SSC is involved in not only the processing of somatosensory input but also in the integration of sensory and motor signals (Borich et al., 2015), it is therefore

possible that this region supports intelligence by working in tandem with the frontal area towards high-level cognitive functions such as perceptual decision making (Colom et al., 2009, 2013; Santarnecchi et al., 2015). While the exact underlying mechanism for the involvement of SSC when performing ART is unclear, the current findings demonstrate that the same SSC region associated with general intelligence is also associated with the proxy for general intelligence.

Notably, the LFC has also been suggested as a putative neural substrate of CR, in addition to being associated with general intelligence. The neural mechanism underlying CR is largely unclear, but several possible mechanisms have been postulated including the task-invariant networks (TIN; Stern et al., 2008; Stern, 2009, 2017). The TIN, which remains active throughout multiple tasks with various levels of processing demands, has been suggested to support CR by serving as a compensatory neural network against brain pathology (Stern, 2006, 2009, 2017). The LFC has been reported to have strong connectivity with multiple TINs and is considered as the hub region of the TINs (Cole et al., 2015; Franzmeier et al., 2017b,c). Given that the TIN is reported to support CR and the hub of the TIN is thought to reside in the LFC, it can be posited that the LFC subserves CR (Franzmeier et al., 2017a,b,c). A recent resting-state fMRI study, which showed that the association between AD-related biomarkers and lower memory performance was attenuated by the global functional connectivity of the LFC in patients with mild cognitive impairment, provides support for the current findings (Franzmeier et al., 2017b). Taken together, the current findings further corroborate the possible role of the LFC—the region most significantly associated with KART performance—as the neural substrate of CR.

An additional interesting finding of the current study is that the regions associated with KART performance became larger when individuals with high levels of Aβ were excluded in the analysis. Considering the fact that accumulated AD pathology generates structural and functional changes in the brain (Perl, 2010; Beason-Held et al., 2013; Mattsson et al., 2014), the neural correlates related to ART performance may vary due to AD pathology, as also observed in the current analyses. Such variation (i.e., the inclusion of much broader regions of functional activity after excluding Aβ-positive subjects) may signify several points. First, this demonstrates that the neuronal functions may be affected by AD neuropathology even in individuals without clinical manifestation of AD. Second, it may indicate that the broader regions found after eliminating Aβ-positive subjects are a more precise representation of the neural correlates of ART performance. Last, given that the associations of the left LFC, left PCG and right ACC—the regions found in the initial analyses with the entire sample—persisted even when those with AD pathology were included, it can be inferred that ART performance is indeed resistant against AD.

In conclusion, this is the first functional neuroimaging study describing the neural substrates associated with ART performance. The positive correlation between ART performance and glucose metabolism in the frontal and primary somatosensory areas indeed corresponds to regions that have been previously reported to be associated with general intelligence and cognitive reserve. The current study provides support, at the neural level, for the use of ART as a measure of premorbid functioning in both research and clinical settings. Moreover, the identification of the neural correlates of ART performance helps to gain an understanding of the neural mechanism underlying CR. Future studies using a multimodal approach such as combining FDG-PET with task-fMRI will provide more detailed information regarding the functional neural substrates that underlie ART performance. Furthermore, future studies utilizing more advanced atlases than AAL will be informative.

DATA AVAILABILITY STATEMENT

The datasets generated for this study are available on request to the corresponding author.

ETHICS STATEMENT

The studies involving human participants were reviewed and approved by Institutional Review Boards of Seoul National University Hospital (IRB no. C-1401-027-547) and SNU-SMG Boramae Center, Seoul, South Korea (IRB no. 26-2015-60). The patients/participants provided their written informed consent to participate in this study.

AUTHOR CONTRIBUTIONS

YL, DY, and DL designed the study, acquired and interpreted the data, and were major contributors to the writing of the manuscript and critically revising the manuscript for intellectual content. ES, JH, HJ, MB, JL, and JJ acquired and analyzed the data and helped to draft the manuscript. DL served as the principal investigator and supervised the study. All authors read and approved the final manuscript.

FUNDING

This study was supported by a grant from the Ministry of Science and ICT and Future Planning, South Korea (Grant No. NRF-2014M3C7A1046042) and a grant of the Korea Health Technology R&D Project through the Korea Health Industry Development Institute (KHIDI), funded by the Ministry of Health and Welfare, South Korea (Grant No. HI18C0630 and HI19C0149). The funding source had no role in the study design, data collection, data analysis, data interpretation, writing of the manuscript, or decision to submit it for publication.

ACKNOWLEDGMENTS

We thank the study participants for their participation.

SUPPLEMENTARY MATERIAL

The Supplementary Material for this article can be found online at: https://www.frontiersin.org/articles/10.3389/fnagi.2020.00048/full#supplementary-material.

REFERENCES

Alexander, G. E., Furey, M. L., Grady, C. L., Pietrini, P., Brady, D. R., Mentis, M. J., et al. (1997). Association of premorbid intellectual function with cerebral metabolism in Alzheimer's disease: implications for the cognitive reserve hypothesis. *Am. J. Psychiatry* 154, 165–172. doi: 10.1176/ajp.154.2.165

Beason-Held, L. L., Goh, J. O., An, Y., Kraut, M. A., O'Brien, R. J., Ferrucci, L., et al. (2013). Changes in brain function occur years before the onset of cognitive impairment. *J. Neurosci.* 33, 18008–18014. doi: 10.1523/JNEUROSCI.1402-13.2013

Borich, M. R., Brodie, S. M., Gray, W. A., Ionta, S., and Boyd, L. A. (2015). Understanding the role of the primary somatosensory cortex: opportunities for rehabilitation. *Neuropsychologia* 79, 246–255. doi: 10.1016/j.neuropsychologia.2015.07.007

Botvinick, M., Nystrom, L. E., Fissell, K., Carter, C. S., and Cohen, J. D. (1999). Conflict monitoring versus selection-for-action in anterior cingulate cortex. *Nature* 402, 179–181. doi: 10.1038/46035

Braak, H., and Braak, E. (1991). Neuropathological stageing of Alzheimer-related changes. *Acta Neuropathol.* 82, 239–259. doi: 10.1007/bf00308809

Brown, J. W. (2009). Conflict effects without conflict in anterior cingulate cortex: multiple response effects and context specific representations. *NeuroImage* 47, 334–341. doi: 10.1016/j.neuroimage.2009.04.034

Byun, M. S., Yi, D., Lee, J. H., Choe, Y. M., Sohn, B. K., Lee, J. Y., et al. (2017). Korean brain aging study for the early diagnosis and prediction of Alzheimer's disease: methodology and baseline sample characteristics. *Psychiatry Investig.* 14, 851–863. doi: 10.4306/pi.2017.14.6.851

Cohen, M. X., Heller, A. S., and Ranganath, C. (2005). Functional connectivity with anterior cingulate and orbitofrontal cortices during decision-making. *Cogn. Brain Res.* 23, 61–70. doi: 10.1016/j.cogbrainres.2005.01.010

Cole, M. W., Ito, T., and Braver, T. S. (2015). Lateral prefrontal cortex contributes to fluid intelligence through multinetwork connectivity. *Brain Connect.* 5, 497–504. doi: 10.1089/brain.2015.0357

Cole, M. W., Reynolds, J. R., Power, J. D., Repovs, G., Anticevic, A., and Braver, T. S. (2013). Multi-task connectivity reveals flexible hubs for adaptive task control. *Nat. Neurosci.* 16, 1348–1355. doi: 10.1038/nn.3470

Cole, M. W., Yarkoni, T., Repovs, G., Anticevic, A., and Braver, T. S. (2012). Global connectivity of prefrontal cortex predicts cognitive control and intelligence. *J. Neurosci.* 32, 8988–8999. doi: 10.1523/JNEUROSCI.0536-12.2012

Colom, R., Burgaleta, M., Roman, F. J., Karama, S., Alvarez-Linera, J., Abad, F. J., et al. (2013). Neuroanatomic overlap between intelligence and cognitive factors: morphometry methods provide support for the key role of the frontal lobes. *NeuroImage* 72, 143–152. doi: 10.1016/j.neuroimage.2013.01.032

Colom, R., Haier, R. J., Head, K., Álvarez-Linera, J., Quiroga, M. Á., Shih, P. C., et al. (2009). Gray matter correlates of fluid, crystallized, and spatial intelligence: testing the P-FIT model. *Intelligence* 37, 124–135. doi: 10.1016/j.intell.2008.07.007

Crawford, J. R., Millar, J., and Milne, A. B. (2001). Estimating premorbid IQ from demographic variables: a comparison of a regression equation vs. clinical judgement. *Br. J. Clin. Psychol.* 40, 97–105. doi: 10.1348/014466501163517

Forman, S. D., Cohen, J. D., Fitzgerald, M., Eddy, W. F., Mintun, M. A., and Noll, D. C. (1995). Improved assessment of significant activation in functional magnetic resonance imaging (fMRI): use of a cluster-size threshold. *Magn. Reson. Med.* 33, 636–647. doi: 10.1002/mrm.1910330508

Franzmeier, N., Buerger, K., Teipel, S., Stern, Y., Dichgans, M., Ewers, M., et al. (2017a). Cognitive reserve moderates the association between functional network anti-correlations and memory in MCI. *Neurobiol. Aging* 50, 152–162. doi: 10.1016/j.neurobiolaging.2016.11.013

Franzmeier, N., Duering, M., Weiner, M., Dichgans, M., Ewers, M., and Alzheimer's Disease Neuroimaging Initiative (ADNI). (2017b). Left frontal cortex connectivity underlies cognitive reserve in prodromal Alzheimer disease. *Neurology* 88, 1054–1061. doi: 10.1212/wnl.0000000000003711

Franzmeier, N., Göttler, J., Grimmer, T., Drzezga, A., Áraque-Caballero, M. A., Simon-Vermot, L., et al. (2017c). Resting-state connectivity of the left frontal cortex to the default mode and dorsal attention network supports reserve in mild cognitive impairment. *Front. Aging Neurosci.* 9:264. doi: 10.3389/fnagi.2017.00264

Han, J. Y., Byun, M. S., Seo, E. H., Yi, D., Choe, Y. M., Sohn, B. K., et al. (2015). Functional neural correlates of figure copy and recall task performances in cognitively impaired individuals: an 18F-FDG-PET study. *Neuroreport* 26, 1077–1082. doi: 10.1097/wnr.0000000000000476

Karama, S., Ad-Dab'bagh, Y., Haier, R., Deary, I., Lyttelton, O., Lepage, C., et al. (2009). Positive association between cognitive ability and cortical thickness in a representative US sample of healthy 6 to 18 year-olds. *Intelligence* 37, 145–155. doi: 10.1016/j.intell.2008.09.006

Lee, J. H., Lee, K. U., Lee, D. Y., Kim, K. W., Jhoo, J. H., Kim, J. H., et al. (2002). Development of the korean version of the consortium to establish a registry for Alzheimer's disease assessment packet (CERAD-K): clinical and neuropsychological assessment batteries. *J. Gerontol. B Psychol. Sci. Soc. Sci.* 57, P47–P53. doi: 10.1093/geronb/57.1.p47

Lee, D. Y., Lee, K. U., Lee, J. H., Kim, K. W., Jhoo, J. H., Kim, S. Y., et al. (2004). A normative study of the CERAD neuropsychological assessment battery in the Korean elderly. *J. Int. Neuropsychol. Soc.* 10, 72–81. doi: 10.1017/s1355617704101094

Lezak, M. D., Howieson, D. B., Loring, D. W., Hannay, H. J., and Fischer, J. S. (2004). *Neuropsychological Assessment*. Oxford; New York, NY: Oxford University Press.

Lo, R. Y., Jagust, W. J., and Alzheimer's Disease Neuroimaging Initiative (2013). Effect of cognitive reserve markers on Alzheimer pathologic progression. *Alzheimer Dis. Assoc. Disord.* 27, 343–350. doi: 10.1097/WAD.0b013e3182900b2b

Lopresti, B. J., Klunk, W. E., Mathis, C. A., Hoge, J. A., Ziolko, S. K., Lu, X., et al. (2005). Simplified quantification of Pittsburgh Compound B amyloid imaging PET studies: a comparative analysis. *J. Nucl. Med.* 46, 1959–1972. doi: 10.1038/sj.jcbfm.9591524.0589

Margulies, D. S., Kelly, A. M., Uddin, L. Q., Biswal, B. B., Castellanos, F. X., and Milham, M. P. (2007). Mapping the functional connectivity of anterior cingulate cortex. *NeuroImage* 37, 579–588. doi: 10.1016/j.neuroimage.2007.05.019

Matsuoka, K., Uno, M., Kasai, K., Koyama, K., and Kim, Y. (2006). Estimation of premorbid IQ in individuals with Alzheimer's disease using Japanese ideographic script (Kanji) compound words: japanese version of national adult reading test. *Psychiatry Clin. Neurosci.* 60, 332–339. doi: 10.1111/j.1440-1819.2006.01510.x

Mattsson, N., Insel, P. S., Nosheny, R., Tosun, D., Trojanowski, J. Q., Shaw, L. M., et al. (2014). Emerging β-amyloid pathology and accelerated cortical atrophy. *JAMA Neurol.* 71, 725–734. doi: 10.1001/jamaneurol.2014.446

McGurn, B., Starr, J., Topfer, J., Pattie, A., Whiteman, M., Lemmon, H., et al. (2004). Pronunciation of irregular words is preserved in dementia, validating premorbid IQ estimation. *Neurology* 62, 1184–1186. doi: 10.1212/01.wnl.0000103169.80910.8b

Melrose, R. J., Harwood, D., Khoo, T., Mandelkern, M., and Sultzer, D. L. (2013). Association between cerebral metabolism and Rey-Osterrieth Complex Figure Test performance in Alzheimer's disease. *J. Clin. Exp. Neuropsychol.* 35, 246–258. doi: 10.1080/13803395.2012.763113

Minoshima, S., Frey, K. A., Foster, N. L., and Kuhl, D. E. (1995). Preserved pontine glucose metabolism in Alzheimer disease: a reference region for functional brain image (PET) analysis. *J. Comput. Assist. Tomogr.* 19, 541–547. doi: 10.1097/00004728-199507000-00006

Mosconi, L., Brys, M., Glodzik-Sobanska, L., De Santi, S., Rusinek, H., and de Leon, M. J. (2007). Early detection of Alzheimer's disease using neuroimaging. *Exp. Gerontol.* 42, 129–138. doi: 10.1016/j.exger.2006.05.016

Mosconi, L., Tsui, W. H., Herholz, K., Pupi, A., Drzezga, A., Lucignani, G., et al. (2008). Multicenter standardized 18F-FDG PET diagnosis of mild cognitive impairment, Alzheimer's disease, and other dementias. *J. Nucl. Med.* 49, 390–398. doi: 10.2967/jnumed.107.045385

Nelson, H. E., and Willison, J. (1991). *National Adult Reading Test (NART)*. Windsor, UK: Nfer-Nelson.

Perl, D. P. (2010). Neuropathology of Alzheimer's disease. *Mt Sinai J. Med.* 77, 32–42. doi: 10.1002/msj.20157

Reiman, E. M., Chen, K., Liu, X., Bandy, D., Yu, M., Lee, W., et al. (2009). Fibrillar amyloid-β burden in cognitively normal people at 3 levels of genetic risk for Alzheimer's disease. *Proc. Natl. Acad. Sci. U S A* 106, 6820–6825. doi: 10.1073/pnas.0900345106

Rentz, D. M., Mormino, E. C., Papp, K. V., Betensky, R. A., Sperling, R. A., and Johnson, K. A. (2017). Cognitive resilience in clinical and preclinical Alzheimer's disease: the association of amyloid and tau burden on cognitive

performance. *Brain Imaging Behav.* 11, 383–390. doi: 10.1007/s11682-016-9640-4

Santarnecchi, E., Tatti, E., Rossi, S., Serino, V., and Rossi, A. (2015). Intelligence-related differences in the asymmetry of spontaneous cerebral activity. *Hum. Brain Mapp.* 36, 3586–3602. doi: 10.1002/hbm.22864

Sasanuma, S., Sakuma, N., and Kitano, K. (1992). Reading kanji without semantics: evidence from a longitudinal study of dementia. *Cogn. Neuropsychol.* 9, 465–486. doi: 10.1080/02643299208252068

Snowdon, D. A., Kemper, S. J., Mortimer, J. A., Greiner, L. H., Wekstein, D. R., and Markesbery, W. R. (1996). Linguistic ability in early life and cognitive function and Alzheimer's disease in late life. Findings from the Nun Study. *JAMA* 275, 528–532. doi: 10.1001/jama.1996.03530310034029

Stern, Y. (2006). Cognitive reserve and Alzheimer disease. *Alzheimer Dis. Assoc. Disord.* 20, 112–117. doi: 10.1097/01.wad.0000213815.20177.19

Stern, Y. (2009). Cognitive reserve. *Neuropsychologia* 47, 2015–2028. doi: 10.1016/j.neuropsychologia.2009.03.004

Stern, Y. (2017). An approach to studying the neural correlates of reserve. *Brain Imaging Behav.* 11, 410–416. doi: 10.1007/s11682-016-9566-x

Stern, Y., Zarahn, E., Habeck, C., Holtzer, R., Rakitin, B. C., Kumar, A., et al. (2008). A common neural network for cognitive reserve in verbal and object working memory in young but not old. *Cereb. Cortex* 18, 959–967. doi: 10.1093/cercor/bhm134

Stern, Y., Zarahn, E., Hilton, H. J., Flynn, J., DeLaPaz, R., and Rakitin, B. (2003). Exploring the neural basis of cognitive reserve. *J. Clin. Exp. Neuropsychol.* 25, 691–701. doi: 10.1076/jcen.25.5.691.14573

Teipel, S. J., Willoch, F., Ishii, K., Bürger, K., Drzezga, A., Engel, R., et al. (2006). Resting state glucose utilization and the CERAD cognitive battery in patients with Alzheimer's disease. *Neurobiol. Aging* 27, 681–690. doi: 10.1016/j.neurobiolaging.2005.03.015

Tzourio-Mazoyer, N., Landeau, B., Papathanassiou, D., Crivello, F., Etard, O., Delcroix, N., et al. (2002). Automated anatomical labeling of activations in SPM using a macroscopic anatomical parcellation of the MNI MRI single-subject brain. *NeuroImage* 15, 273–289. doi: 10.1006/nimg.2001.0978

Vemuri, P., Weigand, S. D., Przybelski, S. A., Knopman, D. S., Smith, G. E., Trojanowski, J. Q., et al. (2011). Cognitive reserve and Alzheimer's disease biomarkers are independent determinants of cognition. *Brain* 134, 1479–1492. doi: 10.1093/brain/awr049

Villeneuve, S., Rabinovici, G. D., Cohn-Sheehy, B. I., Madison, C., Ayakta, N., Ghosh, P. M., et al. (2015). Existing Pittsburgh Compound-B positron emission tomography thresholds are too high: statistical and pathological evaluation. *Brain* 138, 2020–2033. doi: 10.1093/brain/awv112

Whalley, L. J., and Deary, I. J. (2001). Longitudinal cohort study of childhood IQ and survival up to age 76. *BMJ* 322:819. doi: 10.1136/bmj.322.7290.819

Yeo, R. A., Arden, R., and Jung, R. E. (2011). Alzheimer's disease and intelligence. *Curr. Alzheimer Res.* 8, 345–353. doi: 10.2174/156720511795745276

Yi, D., Seo, E. H., Han, J. Y., Sohn, B. K., Byun, M. S., Lee, J. H., et al. (2017). Development of the Korean Adult Reading Test (KART) to estimate premorbid intelligence in dementia patients. *PLoS One* 12:e0181523. doi: 10.1371/journal.pone.0181523

Conflict of Interest: The authors declare that the research was conducted in the absence of any commercial or financial relationships that could be construed as a potential conflict of interest.

frontiers in Aging Neuroscience

ORIGINAL RESEARCH
published: 09 March 2020
doi: 10.3389/fnagi.2020.00046

Functional Brain Network Connectivity Patterns Associated With Normal Cognition at Old-Age, Local β-amyloid, Tau, and APOE4

*Frances C. Quevenco[1], Jiri M. van Bergen[1], Valerie Treyer[1,2], Sandro T. Studer[1], Sonja M. Kagerer[1,3], Rafael Meyer[1], Anton F. Gietl[1], Philipp A. Kaufmann[2], Roger M. Nitsch[1,3], Christoph Hock[1,3] and Paul G. Unschuld[1,4,5]**

[1]*Institute for Regenerative Medicine (IREM), University of Zurich, Zurich, Switzerland,* [2]*Department of Nuclear Medicine, University of Zurich, Zurich, Switzerland,* [3]*Neurimmune, Schlieren, Switzerland,* [4]*Department of Psychogeriatric Medicine, Psychiatric University Hospital Zurich (PUK), Zurich, Switzerland,* [5]*Zurich Neuroscience Center (ZNZ), Zurich, Switzerland*

Background: Integrity of functional brain networks is closely associated with maintained cognitive performance at old age. Consistently, both carrier status of Apolipoprotein E ε4 allele (APOE4), and age-related aggregation of Alzheimer's disease (AD) pathology result in altered brain network connectivity. The posterior cingulate and precuneus (PCP) is a node of particular interest due to its role in crucial memory processes. Moreover, the PCP is subject to the early aggregation of AD pathology. The current study aimed at characterizing brain network properties associated with unimpaired cognition in old aged adults. To determine the effects of age-related brain change and genetic risk for AD, pathological proteins β-amyloid and tau were measured by Positron-emission tomography (PET), PCP connectivity as a proxy of cognitive network integrity, and genetic risk by APOE4 carrier status.

Methods: Fifty-seven cognitively unimpaired old-aged adults (MMSE = 29.20 ± 1.11; 73 ± 8.32 years) were administered 11C Pittsburgh Compound B and 18F Flutemetamol PET for assessing β-amyloid, and 18F AV-1451 PET for tau. Individual functional connectivity seed maps of the PCP were obtained by resting-state multiband BOLD functional MRI at 3-Tesla for increased temporal resolution. Voxelwise correlations between functional connectivity, β-amyloid- and tau-PET were explored by Biological Parametric Mapping (BPM).

Results: Local β-amyloid was associated with increased connectivity in frontal and parietal regions of the brain. Tau was linked to increased connectivity in more spatially distributed clusters in frontal, parietal, occipital, temporal, and cerebellar regions. A positive interaction was observable for APOE4 carrier status and functional connectivity with brain regions characterized by increased local β-amyloid and tau tracer retention.

OPEN ACCESS

Edited by:
Reinhold Schmidt, Medical University of Graz, Austria

Reviewed by:
Daniele Altomare, Université de Genève, Switzerland
Suzanne Lyn Baker, Lawrence Berkeley National Laboratory, United States

****Correspondence:***
Paul G. Unschuld
paul.unschuld@uzh.ch

Received: *14 August 2019*
Accepted: *10 February 2020*
Published: *09 March 2020*

Citation:
Quevenco FC, van Bergen JM, Treyer V, Studer ST, Kagerer SM, Meyer R, Gietl AF, Kaufmann PA, Nitsch RM, Hock C and Unschuld PG (2020) Functional Brain Network Connectivity Patterns Associated With Normal Cognition at Old-Age, Local β-amyloid, Tau, and APOE4. Front. Aging Neurosci. 12:46. doi: 10.3389/fnagi.2020.00046

Conclusions: Our data suggest an association between spatially differing connectivity systems and local β-amyloid, and tau aggregates in cognitively normal, old-aged adults, which is moderated by APOE4. Additional longitudinal studies may determine protective connectivity patterns associated with healthy aging trajectories of AD-pathology aggregation.

Keywords: MRI, functional connectivity, PET, beta-amyloid, tau, multiband fMRI, preclinical, aging

BACKGROUND

Aggregation of beta-amyloid (β-amyloid) and hyperphosphorylated tau are hallmarks of brain pathology associated with Alzheimer's Disease (AD). The age-related accumulation of both proteins precedes disease onset by decades (Price and Morris, 1999; Bateman et al., 2012). Recently published data indicate a sequential association between brain β-amyloid accumulation, subsequent tau change and resulting cognitive decline (Hanseeuw et al., 2019). However, the precise impact of β-amyloid and pathological tau on brain functionality is not yet completely understood. Several studies demonstrated the validity of positron-emission-tomography (PET) tracers for inferring the relationship between AD-pathology burden, and risk for severe cognitive impairment at old age (Klunk, 2011; Villemagne et al., 2011; Vos et al., 2013). Distinct effects on brain network connectivity have been shown for both β-amyloid and pathological tau burden (Hansson et al., 2017; Hoenig et al., 2018; Korthauer et al., 2018; Franzmeier et al., 2019; Hodgetts et al., 2019). Functional connectivity changes within the "default mode network" (DMN) relate to AD-pathology and precede the manifestation of cognitive disorder by years (Sorg et al., 2007; Sperling et al., 2009; Wang et al., 2013; Sorg and Grothe, 2015). Moreover, large clinical studies demonstrate an association between AD-pathology and brain functionality in non-demented old-aged adults, as reflected by functional network integrity (Jack et al., 2019; Maass et al., 2019; Ossenkoppele et al., 2019). This may be consistent with functional network change in other neurodegenerative diseases (Rektorova et al., 2012; Ross et al., 2014; Kronenbuerger et al., 2019).

Despite the consensus in the literature that AD-pathology is related to a breakdown in functional brain networks, its associations with functional connectivity are tenuous. The relationship between β-amyloid and decreased connectivity, mainly in the DMN, is well established for clinically manifest AD (Hedden et al., 2009; Sheline et al., 2010; Chhatwal et al., 2013; Wang et al., 2013). However, during aging and in the absence of cognitive disorder, both increased functional connectivity (Mormino et al., 2011; Lim et al., 2014), but also decreased network connectivity (Wang et al., 2013) has been observed to be associated with AD-pathology when assessing total β-amyloid load, and tau burden.

The posterior cingulate and precuneus (PCP) represents a central node of the DMN needed for memory processing (Sperling et al., 2009; Cieri and Esposito, 2018). β-amyloid load affects the functionality of the PCP in old aged adults with, and without cognitive impairment (Unschuld et al., 2012; Schreiner et al., 2016; Grothe et al., 2017; Quevenco et al., 2017, 2019). The Apolipoprotein E ε4 allele (APOE4) is the strongest known genetic risk factor for late-onset AD (Corder et al., 1993; Strittmatter et al., 1993; Beffert and Poirier, 1996). In the general population, APOE4 carrier status is associated with an increased risk for the presence of AD-pathology (Schipper, 2011; Verghese et al., 2011; Liu et al., 2013; Jack et al., 2019; Yamazaki et al., 2019). Consistently, brain network alterations involving the PCP are pronounced in carriers of the APOE4 genotype (Sperling et al., 2009; De Vogelaere et al., 2012).

PET using tracers 18F-Flutemetamol and Pittsburgh Compound B (PiB) by now is a well-established neuroimaging technique for measuring individual β-amyloid plaque burden (Vandenberghe et al., 2010; Klunk, 2011; Frisoni and Blennow, 2013). Moreover, PET tau tracers such as 18F AV-1451 have enabled *in vivo* assessment of pathological, hyperphosphorylated tau burden in humans (Schöll et al., 2017; Mainta et al., 2018; Villemagne et al., 2018). These advances in PET technologies allow for investigating the relationship of β-amyloid and tau, whose interactions are considered to significantly contribute to disease progression and functional decline (Selkoe and Hardy, 2016; Tosun et al., 2017; Kametani and Hasegawa, 2018) Spatial distribution patterns of both proteins diverge substantially, with β-amyloid accumulation beginning in the neocortex and progressing towards subcortical structures (Braak and Braak, 1991a), whereas tau accumulation begins in the brainstem and transentorhinal regions and spreads towards neocortical structures as the disease progresses (Braak and Braak, 1991b). Considering these earlier reports, we hypothesized that PCP functional connectivity in cognitively normal old-aged adults might reflect the interplay between β-amyloid and tau pathology on a local level. Moreover, we hypothesized, that such effects should be more pronounced in APOE4 carriers. To test these hypotheses, the relationship between local β-amyloid, local tau and PCP connectivity was investigated on a voxel-level. We used the software biological parametric mapping (BPM; Casanova et al., 2007) for generating subject-specific PET tracer retention patterns and beta-maps (Whitfield-Gabrieli and Nieto-Castanon, 2012) as a measure of individual connectivity patterns (Biswal et al., 1995), associated with AD pathology. High temporal resolution of connectivity data was achieved by using multiband functional MRI (fMRI) for the simultaneous acquisition of multiple slices (Feinberg and Setsompop, 2013; Preibisch et al., 2015).

MATERIALS AND METHODS

Study Population

For the current study, 57 old-aged cognitively unimpaired (mean MMSE = 29.20 ± 1.11), and medically healthy adults (mean age = 73 ± 8.32 years) were included from an on-going neuroimaging study at our institute, using study procedures reported earlier (van Bergen et al., 2018a; Vandenberghe et al., 2010). Written informed consent was obtained from all participants before inclusion in the study. Study procedures were carried out in accordance with the Good Clinical Practice (GCP) guidelines issued by the local ethics authority (Kantonale Ethikkommision Zürich[1]), and with the Human Research Act of Switzerland and the declaration of Helsinki (World_Medical_Association, 1991).

Inclusion criteria were age above 50 years, pre-existing PET information on cerebral amyloid deposition, German language proficiency and capacity to consent to study procedures. Exclusion criteria were: significant medication or drug abuse that might have possible effects on cognition, a history of severe allergic reaction or known allergy against components of 11C-PiB, 18-Flutemetamol, AV-1451, general MRI exclusion criteria, MRI scans with evidence of infection or infarction and severe atrophy, clinically relevant changes in red blood cell count, serious medical or neuropsychiatric illness and significant exposure to radiation.

Flutemetamol and PiB-PET for Estimation of β-amyloid Load

Individual measures of local β-amyloid burden were determined by quantification of standardized uptake values of either 18F-Flutemetamol (34 participants) or 11C-Pittsburgh Compound B (11C-PiB, 23 participants). PET was performed as reported in earlier studies of ours (Schreiner et al., 2014; Steininger et al., 2014; van Bergen et al., 2018a). A General Electric (GE) healthcare SIGNA PETMR was used for measuring 18F-Flutemetamol uptake, and a GE healthcare Discovery scanner for 11C-PiB. Average and standard deviation (SD) maps of all amyloid-PET SUVR are indicated in **Supplementary Figures S1**, **S2**. For the former, an individual dose of approximately 140 MBq of Flutemetamol was injected into the cubital vein. Time-of-flight algorithms and the required corrections were applied to reconstruct the PET images. Late-frame values (85–105 min) were referenced to the cerebellar gray matter (Vandenberghe et al., 2010) to obtain 3D volumes of Flutemetamol retention as an estimate β-amyloid load using standardized uptake value ratios (SUVR; matrix = 256 × 256 × 89, voxel size = 1.2 × 1.2 × 2.78 mm^3). For the PiB protocol, approximately 350 MBq were administered intravenously and late-frame values (50–70 min) were used to obtain mean PiB uptake in all cortical VOIs and cerebellar regions using a volume-weighted averaging procedure (Gietl et al., 2015). Identical to the Flutemetamol protocol, these were normalized and referenced to the cerebellar gray matter to obtain SUVRs as estimates of the β-amyloid load.

[1]www.kek.zh.ch

AV1451-PET for the Estimation of Tau Load

The current study also included measures of tau load, by assessing local retention of 18F-AV1451 using an established PET procedure (Chien et al., 2013). A GE healthcare SIGNA PETMR was used for measuring 18F-AV1451 uptake. Average and SD maps of all tau-PET SUVR are indicated in **Supplementary Figures S3**, **S4**. In our study, an individual dose of approximately 200 MBq of 18F-AV1451 was administered into the cubital vein. Similar to the β-amyloid procedure, time-of-flight algorithms with the necessary corrections were applied to construct the tau-PET images based on regional uptake values. For analysis, 8 × 5 min frames were acquired. These were summed to late-frame values (80–120 min) and referenced to the cerebellar gray matter for generation of SUVRs.

MRI Acquisition

MR-Images were acquired on a 3-Tesla GE Discovery 750w MR whole-body scanner (GE Medical Systems, Milwaukee, WI, USA) equipped with a 32 Channel head coil array. A 3D T1-weighted (IR-SPGR) sequence (TI = 600 ms, TE = minimum, voxel size = 1 × 1 × 1 mm^3, FOV = 256 × 256 × 256 mm^3, flip angle = 8°, scan time = 5:49 min) was used to obtain structural images for anatomical referencing and automated image segmentation at the same visit the AV1451-PET was performed for tau. The average time between MRI and β-amyloid PET was 1,138 days, with a minimum of 49 days, and a maximum of 2,414 days.

Resting-state BOLD fMRI images were acquired using a 2D Gradient Echo Mux Multiband sequence (TR = 2,000 ms, TE = 30 ms, flip angle = 70°, slice thickness = 2.4 mm, number of slices = 22, number of MUXed slices (1–8) = 3, Autocalibrating Reconstruction for Cartesian imaging (ARC) acceleration factor = 2, ARC enabling = 1, scan time = 8:32 min) to obtain individual beta maps, indicating functional connectedness of each voxel to the PCP based on BOLD synchronicity (Biswal et al., 1995; Whitfield-Gabrieli and Nieto-Castanon, 2012). Average and SD maps PCC connectivity are indicated in **Supplementary Figures S5**, **S6**.

Pre-processing of Functional Images and Obtaining PCP Seed Maps

Functional images were spatially preprocessed using an in-house script implementing functions from the SPM12 toolbox[2] with MATLAB 2016a (Mathworks, Natick, MA, USA). The following spatial preprocessing measures were covered in the script: (1) Functional image time-series were realigned using a 6-parameter rigid-body transformation for each image. (2) Anatomical (T1) scans were coregistered to the mean functional image. (3) Structural T1 images were segmented using SPM12's Segment function in order to obtain tissue probability maps to warp the functional images into normalized MNI space. (4) Functional and structural images were normalized by using the forward deformations obtained in the previous step to warp the images from native into MNI space. (5) Normalized functional images were then smoothed with an 8 mm FWHM

[2]http://www.fil.ion.ucl.ac.uk/spm/software/spm12

Gaussian kernel. Slice-time correction is not a necessity with multiband images due to the low TR, which reduces temporal differences between slices. In addition, as multiband acquires a high number of slices, the slight movement could have corrections done for the wrong slice. In order to avoid this complication, this step was omitted from spatial preprocessing. Normalized and smoothed functional and normalized T1 images were processed using the CONN v12 toolbox (Whitfield-Gabrieli and Nieto-Castanon, 2012). This toolbox uses the CompCor denoising method procedure, which regresses out nuisance regressors without including the global signal. After the denoising step, PCP seed maps were obtained using the CONN toolbox by calculating the correlation between the PCP and other regions of the brain.

Biological Parametric Mapping (BPM) for Voxel-Level Analysis

PET images were, based on their co-registered T1 image, aligned to the TAU PET/MR T1 image using the PMOD software, Version 3.8 (PMOD Technologies Limited, Zurich, Switzerland). T1 MRI images were normalized to MNI space and matrices were applied to the PET images, which were then scaled by cerebellum gray matter values derived from an intersected Hammers atlas derived gray matter region, which fit all normalized PET images. These were then smoothed with a 5 mm FWHM Gaussian kernel. Preprocessing of the functional images for BPM analysis required realignment, coregistration, segmentation and warping into MNI space and finally smoothed with an 8 mm FWHM Gaussian kernel using in-house scripts running on SPM12[2] with MATLAB 2016a (Mathworks, Natick, MA, USA). The smoothed and normalized functional images were processed using the CONN v.12 toolbox (Whitfield-Gabrieli and Nieto-Castanon, 2012). Individual Fisher r-to-z transformed beta PCP seed connectivity maps were calculated for each participant. A second level *t*-test against zero was applied on the data and multiple test correction was performed at the voxel level, using FDR (*p-FDR corrected,* $q < 0.05$ for p-uncorrected = 0.001, **Figure 1**). To limit the analysis to the gray matter, images were masked using a multi-atlas matching approach (van Bergen et al., 2018b). Regression analysis of normalized and smoothed PET and fMRI images was performed by administering BPM[3] (Casanova et al., 2007; Yang et al., 2011), a toolbox useful for exploring multimodal voxel-level correlations using the General Linear Model (GLM), running under Matlab 2010a and SPM5[4]. The common spatial resolution of the images used in the analysis was determined by the spatial modality of PET (the lowest resolution) of approximately 3 mm. BPM was used to investigate regression models for investigating the relationship between local β-amyloid PET, tau-PET and DMN connectivity, as measured by beta maps, with a BPM cluster threshold set at 100 voxels. Additionally, the potential moderating effects of APOE4 carrier status were explored by multiple regression.

[3]https://www.nitrc.org/projects/rbpm/
[4]https://www.fil.ion.ucl.ac.uk/spm/software/spm5/

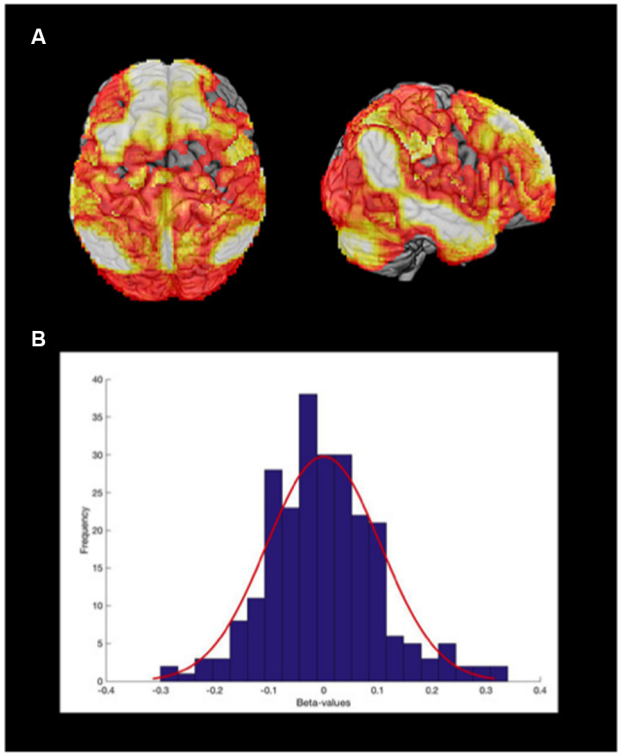

FIGURE 1 | Posterior cingulate and precuneus (PCP) connectivity seed map of sample population. **(A)** Connectivity map of the whole sample (*p-FDR* < 0.05), using the PCP as a seed, projected on a 3D brain. **(B)** The median distribution of the Fisher r-to-z transformed beta maps.

RESULTS

Neuropsychological Performance and APOE4 Carrier Frequency

All participants underwent a battery of neuropsychological tests including the Mini-Mental State Exam (MMSE), the Boston Naming, Trail-Making and the VLMT Delayed Recall test. Mini-Mental State (MMSE) scores were within the normal range (mean MMSE = 29.20 ± 1.11), and the other neuropsychological tests indicated consistently high performance of the studied population in the investigated domains (**Supplementary Table S1**). Moreover, genotyping identified 11 APOE4 carriers within the 57 study participants (19.3% of the population).

Local β-amyloid and Tau Deposits Are Associated With Locally Increased Functional Connectivity

By applying voxel-wise regression, eight positively associated clusters with a size of at least 100 voxels (Total voxels = 2,030, $T > 2.3$, $p < 0.05$) could be identified, indicating relationships between local β-amyloid load and increased PCP connectivity. Clusters were mainly located in the frontal and parietal lobe (**Figure 2A**), including the middle frontal gyrus, the anterior orbital gyrus (right), the medial orbital gyrus (right), the lateral orbital gyrus (right), the left precentral gyrus, the inferior lateral

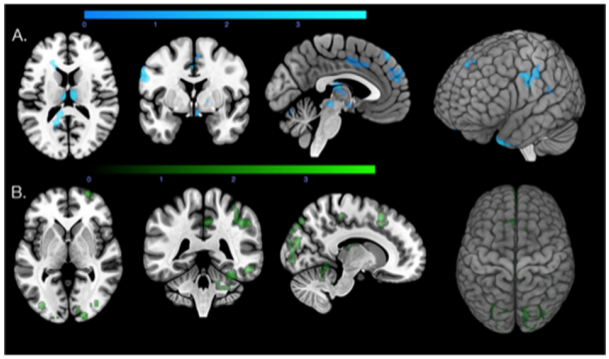

FIGURE 2 | Regions that show correlations between local β-amyloid, local tau, and increased functional connectivity. **(A)** Axial, coronal, and sagittal slices and a 3D render of the T-map ($p < 0.05$, extent threshold = 100 voxels) illustrating the regions with correlations between local β-amyloid and increased connectivity (blue). **(B)** Axial, coronal, and sagittal slices and a 3D render of the T-map ($p < 0.05$, extent threshold = 100) illustrating the regions with correlations between local tau load (green) and increased functional connectivity.

remainder of the parietal lobe (right) and other regions such as the left anterior temporal lobe (medial part) and the left cerebellum. No significant association between local β-amyloid burden and decreased PCP connectivity could be observed. Also, when applying voxel-wise regression, no significant relationship could be observed between age and gender, and PCP connectivity.

For local tau associated PCP connectivity changes, the voxel-based analysis identified 14 positively associated clusters with a minimum size of 100 voxels (Total voxels = 5,662, $T > 2.26$, $p < 0.05$) widely distributed across the brain (**Figure 2B**). Regions primarily involved were thalamus, superior frontal gyrus, middle frontal gyrus, the inferolateral remainder of the parietal lobe (right), superior parietal gyrus, the lateral remainder of the occipital lobe, posterior temporal lobe and middle and inferior temporal gyrus. Smaller clusters included the cingulate gyrus and the right cerebellum.

There were small regions of overlap (257 voxels) between local β-amyloid associated connectivity and tau-related connectivity (**Figure 3**), representing ca. 12.66% of voxels included in the β-amyloid PCP connectivity map and 4.54% of the tau PCP connectivity map. The overlap between β-amyloid and tau-related connectivity was observable in particular for the left and right cerebellum, superior frontal gyrus and the inferolateral remainder of the parietal lobe (right).

APOE4 Carrier Status Moderates the Association Between β-amyloid and Tau Load With Functional Connectivity

APOE4 carrier status was included in the regression model as a non-imaging covariate and was found to have positive moderator effects on both β-amyloid and tau-related functional connectivity properties (**Figure 4**). APOE4 carrier status and local β-amyloid load were associated with increased PCP connectivity in 14 clusters of at least 100 voxels (Total voxels = 3,666, $T > 2.80$, $p < 0.05$). In contrast to the regression model with just β-amyloid and the Fisher r-to-z beta maps, which found regions with the strongest associations in the frontal lobe, APOE4 status and local β-amyloid were associated with more widely distributed PCP connectivity changes primarily in the temporal and frontal lobe (**Figure 5A**). These included the left anterior temporal lobe (medial and lateral part), posterior temporal lobe, right middle and inferior temporal gyrus, left middle frontal gyrus, left precentral gyrus, right medial orbital gyrus, and the right anterior orbital gyrus. Other regions included in the clusters were the right thalamus, the inferolateral remainder of the parietal lobe and the left lingual gyrus in the occipital lobe.

Local tau-tracer retention and APOE4 carrier status were associated with increased PCP connectivity in 13 clusters with at least 100 voxels in size (Total voxels = 7,045, $T > 2.5$, $p < 0.05$). Similar to the findings from the local tau and connectivity regression model, regions with strong associations between increased connectivity, local tau, and APOE4 carrier status were widely distributed across

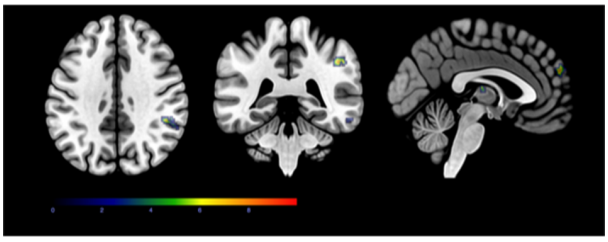

FIGURE 3 | The minor regional overlap between local β-amyloid and increased PCP connectivity and local tau and increased PCP connectivity. Axial, coronal, and sagittal slices showing the small regional overlap of regions that are associated with local β-amyloid and increased PCP connectivity ($p < 0.05$, extent threshold = 100 voxels), and local tau-load and increased PCP connectivity ($p < 0.05$, extent threshold = 100 voxels).

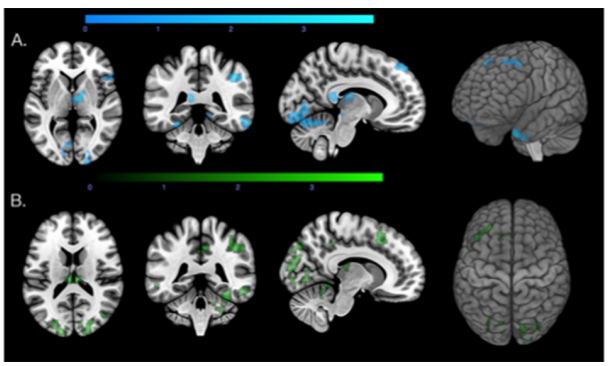

FIGURE 4 | Regions with increased connectivity associated with local β-amyloid, local tau, and Apolipoprotein E ε4 allele (APOE4) carrier status. **(A)** Axial, coronal, and sagittal slices and a 3D view of the biological parametric mapping (BPM) T-map ($p < 0.05$, extent threshold = 100) illustrating regions with associations between local β-amyloid, increased functional connectivity, moderated by APOE4 carrier status (blue). **(B)** Axial, coronal, and sagittal slices and a 3D view of the BPM T-map ($p < 0.05$, extent threshold = 100) illustrating regions that showed associations between local tau, increased connectivity, moderated by APOE4 carrier status (green).

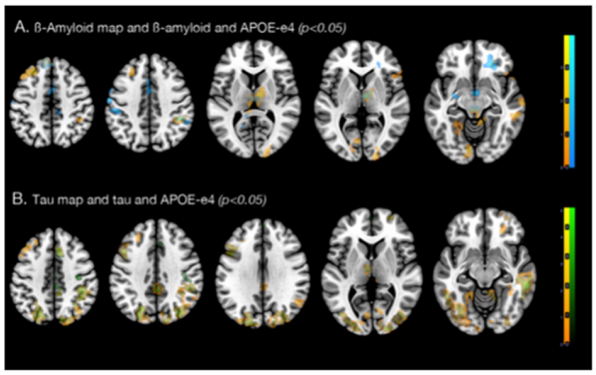

FIGURE 5 | Effects of APOE4 carrier status on regional associations between increased connectivity with **(A)** local β-amyloid, and **(B)** local tau. **(A)** Axial slices of regions with correlations between local β-amyloid and increased connectivity (blue), and local β-amyloid, APOE4 carrier status and increased PCP connectivity (orange). **(B)** Axial slices of regions associated with local tau-load and the Fisher r-to-z transformed beta-maps (green), local tau-load, APOE4 carrier status and increased PCP connectivity (orange).

the brain (**Figure 5B**). Primary regions were located in the neocortex and also include other central structures, such as the cerebellum, the thalamus and caudate nucleus. These clusters enclosed brain regions within the right superior frontal gyrus, middle frontal gyrus, superior parietal gyrus, the lateral remainder of the occipital lobe, right middle and inferior temporal gyrus, and posterior temporal lobe. Similarly as with β-amyloid, no significant association between local retention of the tau-tracer and decreased PCP connectivity could be observed.

DISCUSSION

By applying a multimodal voxel-wise regression approach to non-demented old-aged adults, we identified relationships between local β-amyloid and tau deposits with functional connectivity changes of the PCP. While local aggregation of both proteins was associated with distinct patterns of functional hyperconnectivity, the regional overlap was small. As we did find a positive moderator effect of APOE4 for both β-amyloid and tau related connectivity, we assume potential relevance for risk and progression of AD.

The majority of studies in the past have found decreased functional connectivity in the presence of AD (Sheline et al., 2010; Ouchi and Kikuchi, 2012; Song et al., 2013) and β-amyloid deposition (Sperling et al., 2010), particularly affecting the DMN and even reduction of connectivity in specific DMN nodes, such as the posterior cingulate (Weiler et al., 2014). There is however a handful of contradicting findings that observed increased connectivity and postulated that these changes may be exemplary of early-stage compensatory mechanisms in reaction to brain pathology (Mormino et al., 2011; Lim et al., 2014).

Though the reduction in connectivity is a prominent finding in the literature, our results coincide with a longitudinal PET connectivity study (Jack et al., 2013) and a recent β-amyloid and tau study (Schultz et al., 2017), that suggests that along the AD spectrum there are phases of hyper- and hypoconnectivity, with the former preceding the latter. Moreover, our findings are consistent with recent data on functional alterations associated with the presence of AD-pathology in non-demented old-aged adults (Jack et al., 2019; Maass et al., 2019; Ossenkoppele et al., 2019). Considering that the here investigated study population still had a low β-amyloid burden (*A*β−) and was cognitively relatively healthy, the observed increase in PCP connectivity may reflect the presence of pathological impairment prior to significant β-amyloid aggregation. The observed β-amyloid associated PCP connectivity was focal and significant clusters were located in the frontal and temporal lobe. Tau, however, was associated with increased activity in a wider distribution of regions across the brain. Only limited spatial overlap between PCP connectivity networks affected by β-amyloid and tau were observable. Overlap was present in the superior frontal gyrus, the cerebellum and the inferolateral remainder of the parietal lobe. While our data needs to be interpreted with caution due to the low level of PET tracer retention in an *A*β− population, possible off-target tau signal (Baker et al., 2019) and the possibility of slightly different attenuation correction due to the use of different PET scanners, our data nevertheless may accord with recent fMRI studies that suggest distinct PCP functional connectivity networks associated with β-amyloid and tau (Sepulcre et al., 2017; Franzmeier et al., 2019).

Interestingly, we found more clusters to be associated with local β-amyloid load and APOE4 carrier status than β-amyloid alone and these clusters are no longer primarily in the frontal lobe but cover many parts of the neocortex as well as other central structures, such as the cerebellum, thalamus and the caudate nucleus. While the addition of the genetic AD risk factor to the regression model better explains PCP associated increased connectivity in our data, this may be consistent with earlier reports on APOE4 associated connectivity changes in non-demented populations (Westlye et al., 2011; Wang et al., 2015; Hodgetts et al., 2019). However, this relationship was less prominent for local tau and PCP connectivity. Although adding APOE4 carrier status as an independent covariate did show some regions that were not affected with only tau alone, APOE4 effects on tau appeared less widespread. While our findings might support earlier reports on an association between APOE4 and tauopathy (Beffert and Poirier, 1996; Tiraboschi et al., 2004; Shi et al., 2017), in our study APOE4 moderated the relationship between local tau and functional connectivity to a lesser degree than β-amyloid.

Nonetheless, this observation could be a reflection of the relatively healthy status of our population, where neurodegenerative brain damage, indicated by increased tau, may still be very limited, resulting in low power for the detection of interactive effects between tau, APOE4 and functional connectivity. This may accord with the amyloid cascade hypothesis, which postulates that β-amyloid dysregulation precedes tau related neurodegeneration in preclinical stages of AD (Hardy and Selkoe, 2002). Furthermore, this study

only finds relationships between β-amyloid and tau with increased PCP connectivity. Our finding of distinct functional impacts of β-amyloid and tau might be consistent with the notion of pathogenic synergism of protein aggregates in aging and neurodegenerative disease (Nelson et al., 2012). However, our findings may also reflect other non-AD related tauopathy, which might concur with very early stages of potential β-amyloid pathology in the studied population. Possible implications for therapeutic intervention strategies against age-related cognitive decline have been reviewed recently (Pini et al., 2018).

For the current study multiband fMRI was used, allowing for increased temporal resolution of resting-state data (Feinberg and Setsompop, 2013; Preibisch et al., 2015) while maintaining reproducibility of results with conventional EPI based fMRI protocols (Smitha et al., 2018). The increase in temporal resolution made possible by multiband fMRI has been suggested to allow for novel insights in brain network dynamics (Preibisch et al., 2015).

However, the cross-sectional nature and small sample size is a limitation of our study. Furthermore, due to the small sample size, further stratification of the studied population by AD-relevant properties is not compatible with the chosen statistical analysis strategy. While we did not find effects of gender and age, these might be present in a larger study population, particularly if a wider age range is included. Also, the specific investigation of APOE4 carriers, and also limiting the analysis to individuals with high cerebral β-amyloid (*A*β+ vs. *A*β−), and effects associated with tau progression beyond the entorhinal cortex, may provide additional insights on AD pathology (Braak and Braak, 1991b; Thal et al., 2002). While it is difficult to conclude whether our findings reflect pathological stages associated with either β-amyloid or tau, recent data suggest a sequential association of pathological change in AD (Hanseeuw et al., 2019). Prospective, longitudinal studies may include trajectories of gray matter integrity, as demonstrated recently for estimating neural tissue disintegration (Koini et al., 2018). Moreover, as we investigated a relatively healthy population, information on a relationship between connectivity-properties and structural change of vulnerable brain regions is limited. At present, 18F AV-1451 has become a popular choice for *in vivo* tau imaging (Villemagne et al., 2018; Mattsson et al., 2019; Smith et al., 2019). However, AV-1451 off-target binding unrelated to tau is a frequent finding particularly at low tracer retention, as observed in our study. Here, AV-1451 off-target signal may reflect iron deposition, neuromelanin, or vascular factors (Lockhart et al., 2017). This particularly affects brain regions such as the thalamus, putamen, superior cerebellar gray, choroid plexus, but also meninges and skull, posing challenges when studying early tau accumulation, as done in the current study (Baker et al., 2019). Functional coupling between the PCP and the PCC is well known, and our finding of an association with local β-amyloid may accord with earlier reports on altered functional brain changes during aging (Steininger et al., 2014; Li et al., 2017; Liu et al., 2017; Luo et al., 2019). However, considering that no significant cerebellar β-amyloid accumulation is to be expected in cognitively healthy individuals (Thal et al., 2002), also this finding needs further replication, and for now, needs to be interpreted with caution. Another limitation is the fact that there was significant temporal delay between β-amyloid PET and MRI, while tau PET and MRI took place at once. This difference needs to be taken into account when interpreting our findings on connectivity effects associated with β-amyloid vs. tau. However, β-amyloid effects may manifest in the long term, considering that aggregation of β-amyloid has been estimated to take about 19 years from β-amyloid positivity-threshold to mean values observed in AD dementia (Roberts et al., 2017).

Moreover, although the PCP is considered to play a central role in various cognitive processes associated with the DMN (Choo et al., 2010; Teipel et al., 2015; Quevenco et al., 2017; Cieri and Esposito, 2018), PCP seed map-related effects observed in this study may nevertheless primarily reflect PCP specific pathology than general alterations of the DMN. Follow-up studies using whole-brain connectivity approaches both at rest and during cognitive tasks may thus expand findings of the current study to investigate the DMN and also other brain networks in the context of AD-risk. Here, the advent of novel blood-based biomarkers might help to further characterize processes resulting in impaired brain functionality in preclinical AD (Bacioglu et al., 2016; Mattsson et al., 2017; Zetterberg and Blennow, 2018).

In conclusion, our findings are consistent with recently published studies that describe phases of PCP hyperconnectivity during the early stages of age-related β-amyloid and tau-related aggregation (Sepulcre et al., 2017). Considering the central role of the PCP for DMN connectivity, our study suggests that APOE4 carrier status, aggregation of β-amyloid and tau closely interact regarding their effects on DMN connectivity. Additional studies are needed to clarify connectivity in the context of the sequential progression of AD pathology (Hanseeuw et al., 2019), early functional change (McLaren et al., 2012), and potential opportunities for therapeutic intervention (Pini et al., 2018). The fact that these effects are observable before the manifestation of dementia, but still are related to APOE4 carrier status, may indicate relevance for the progression of early AD-pathology (Haller et al., 2019). Thus, further longitudinal studies are needed to investigate the temporal sequence of the observed changes, and whether they are associated with accelerated disease progression. Such studies may also inform on functional connectivity in a context of resilience against the aging-related accumulation of AD pathology. Possibly protective effects of functional connectivity patterns may allow for compensating emerging brain pathology during aging, allowing for preserved cognition.

DATA AVAILABILITY STATEMENT

Openly available datasets generated for this study are included in the article/**Supplementary Material**.

ETHICS STATEMENT

The studies involving human participants were reviewed and approved by Kantonale Ethikkommission Zürich. The

patients/participants provided their written informed consent to participate in this study.

AUTHOR CONTRIBUTIONS

FQ: performed data processing, analysis and interpretation of neuroimaging data and contributed to writing of the manuscript together with PU, and has performed a final revision. JB: established the multiband fMRI protocol on the GE scanner in Schlieren, and installed the pipeline for performing multimodal analyses using Biological Parametric Mapping. Also, he performed data processing of MR- and PET-data for integrated, voxel-level analysis. SS, AG, RM, and VT: contacted participants, administered MRI and PET. AG: coordinated the study and genotyping of APOE, interaction with ethics committee and acquisition of PET-MR data. SK: revised MR-data analysis and wrote the manuscript. RM and VT: supervised data acquisition (MRI and PET). VT and PK: supervised the preparation of the 18F-tracer for measuring brain Aβ-plaque density, quality control of PET-data and analysis. RN and CH are the chairmen of the department and sponsors of the study, they provided critical revisions of the final manuscript. PU: proposed the research question, supervised all data analysis, wrote the manuscript and is corresponding author. Also, he supervised the acquisition, processing, analysis, interpretation of acquired data and has performed the final revision.

FUNDING

This work was supported by the Clinical Research Priority Program (CRPP) of the University of Zurich (UZH) on Molecular Imaging (MINZ), Zurich Neuroscience Center (ZNZ), Zurich Program for Sustainable Development of Mental Health Services, Synapsis Foundation Alzheimer Research Switzerland, the Mäxi-Foundation and with institutional support from the Institute for Regenerative Medicine (IREM), University of Zurich, Switzerland.

ACKNOWLEDGMENTS

We would like to thank all study participants for their time, enthusiasm and unsalaried commitment to this research. We thank Esmeralda Gruber (IREM) for her assistance in participant recruitment.

SUPPLEMENTARY MATERIAL

The Supplementary Material for this article can be found online at: https://www.frontiersin.org/articles/10.3389/fnagi.2020.00046/full#supplementary-material.

FIGURE S1 | Amyloid average over all PET scans performed (18F Flutemetamol and 11C PiB). Scaled from 0 to 2.8 SUVR.

FIGURE S2 | Amyloid standard deviation (SD) over all PET scans performed (18F Flutemetamol and 11C PiB). Scaled from 0 to 0.8 SUVR SD.

FIGURE S3 | Tau average over all PET scans performed (18F AV1451). Scaled from 1.0 to 2.0 SUVR.

FIGURE S4 | Tau SD over all PET scans performed (18F AV1451). Scaled from 0 to 0.6 SUVR SD.

FIGURE S5 | Beta-maps average, scaled from 0 to 1.0.

FIGURE S6 | Beta-maps SD, scaled from 0 to 0.3.

REFERENCES

Bacioglu, M., Maia, L. F., Preische, O., Schelle, J., Apel, A., Kaeser, S. A., et al. (2016). Neurofilament light chain in blood and csf as marker of disease progression in mouse models and in neurodegenerative diseases. *Neuron* 91, 56–66. doi: 10.1016/j.neuron.2016.05.018

Baker, S. L., Harrison, T. M., Maass, A., La Joie, R., and Jagust, W. J. (2019). Effect of off-target binding on ^{18}F-Flortaucipir variability in healthy controls across the life span. *J. Nucl. Med.* 60, 1444–1451. doi: 10.2967/jnumed.118.224113

Bateman, R. J., Xiong, C., Benzinger, T. L., Fagan, A. M., Goate, A., Fox, N. C., et al. (2012). Clinical and biomarker changes in dominantly inherited Alzheimer's disease. *N. Engl. J. Med.* 367, 795–804. doi: 10.1056/NEJMoa1202753

Beffert, U., and Poirier, J. (1996). Apolipoprotein E, plaques, tangles and cholinergic dysfunction in Alzheimer's disease. *Ann. N Y Acad. Sci.* 777, 166–174. doi: 10.1111/j.1749-6632.1996.tb34415.x

Biswal, B., Yetkin, F. Z., Haughton, V. M., and Hyde, J. S. (1995). Functional connectivity in the motor cortex of resting human brain using echo-planar MRI. *Magn. Reson. Med.* 34, 537–541. doi: 10.1002/mrm.1910340409

Braak, H., and Braak, E. (1991a). Demonstration of amyloid deposits and neurofibrillary changes in whole brain sections. *Brain Pathol.* 1, 213–216. doi: 10.1111/j.1750-3639.1991.tb00661.x

Braak, H., and Braak, E. (1991b). Neuropathological stageing of Alzheimer-related changes. *Acta Neuropathol.* 82, 239–259. doi: 10.1007/bf00308809

Casanova, R., Srikanth, R., Baer, A., Laurienti, P. J., Burdette, J. H., Hayasaka, S., et al. (2007). Biological parametric mapping: a statistical toolbox for multimodality brain image analysis. *NeuroImage* 34, 137–143. doi: 10.1016/j.neuroimage.2006.09.011

Chhatwal, J. P., Schultz, A. P., Johnson, K., Benzinger, T. L., Jack, C. Jr., Ances, B. M., et al. (2013). Impaired default network functional connectivity in autosomal dominant Alzheimer disease. *Neurology* 81, 736–744. doi: 10.1212/WNL.0b013e3182a1aafe

Chien, D. T., Bahri, S., Szardenings, A. K., Walsh, J. C., Mu, F., Su, M. Y., et al. (2013). Early clinical PET imaging results with the novel PHF-tau radioligand [F-18]-T807. *J. Alzheimers Dis.* 34, 457–468. doi: 10.3233/jad-122059

Choo, I. H., Lee, D. Y., Oh, J. S., Lee, J. S., Lee, D. S., Song, I. C., et al. (2010). Posterior cingulate cortex atrophy and regional cingulum disruption in mild cognitive impairment and Alzheimer's disease. *Neurobiol. Aging* 31, 772–779. doi: 10.1016/j.neurobiolaging.2008.06.015

Cieri, F., and Esposito, R. (2018). Neuroaging through the lens of the resting state networks. *Biomed Res. Int.* 2018:5080981. doi: 10.1155/2018/5080981

Corder, E. H., Saunders, A. M., Strittmatter, W. J., Schmechel, D. E., Gaskell, P. C., Small, G. W., et al. (1993). Gene dose of apolipoprotein E type 4 allele and the risk of Alzheimer's disease in late onset families. *Science* 261, 921–923. doi: 10.1126/science.8346443

De Vogelaere, F., Santens, P., Achten, E., Boon, P., and Vingerhoets, G. (2012). Altered default-mode network activation in mild cognitive impairment compared with healthy aging. *Neuroradiology* 54, 1195–1206. doi: 10.1007/s00234-012-1036-6

Feinberg, D. A., and Setsompop, K. (2013). Ultra-fast MRI of the human brain with simultaneous multi-slice imaging. *J. Magn. Reson.* 229, 90–100. doi: 10.1016/j.jmr.2013.02.002

Franzmeier, N., Rubinski, A., Neitzel, J., Kim, Y., Damm, A., Na, D. L., et al. (2019). Functional connectivity associated with tau levels in ageing, Alzheimer's, and small vessel disease. *Brain* 142, 1093–1107. doi: 10.1093/brain/awz026

Frisoni, G. B., and Blennow, K. (2013). Biomarkers for Alzheimer's: the sequel of an original model. *Lancet Neurol.* 12, 126–128. doi: 10.1016/s1474-4422(12)70305-8

Gietl, A. F., Warnock, G., Riese, F., Kalin, A. M., Saake, A., Gruber, E., et al. (2015). Regional cerebral blood flow estimated by early PiB uptake is reduced in mild cognitive impairment and associated with age in an amyloid-dependent manner. *Neurobiol. Aging* 36, 1619–1628. doi: 10.1016/j.neurobiolaging.2014.12.036

Grothe, M. J., Barthel, H., Sepulcre, J., Dyrba, M., Sabri, O., Teipel, S. J., et al. (2017). *in vivo* staging of regional amyloid deposition. *Neurology* 89, 2031–2038. doi: 10.1212/wnl.0000000000004643

Haller, S., Montandon, M. L., Rodriguez, C., Garibotto, V., Herrmann, F. R., and Giannakopoulos, P. (2019). Hippocampal volume loss, brain amyloid accumulation and APOE status in cognitively intact elderly subjects. *Neurodegener. Dis.* doi: 10.1159/000504302 [Epub ahead of print].

Hanseeuw, B. J., Betensky, R. A., Jacobs, H. I. L., Schultz, A. P., Sepulcre, J., Becker, J. A., et al. (2019). Association of amyloid and tau with cognition in preclinical Alzheimer disease: a longitudinal study. *JAMA Neurol.* doi: 10.1001/jamaneurol.2019.1424 [Epub ahead of print].

Hansson, O., Grothe, M. J., Strandberg, T. O., Ohlsson, T., Hagerstrom, D., Jogi, J., et al. (2017). Tau pathology distribution in Alzheimer's disease corresponds differentially to cognition-relevant functional brain networks. *Front. Neurosci.* 11:167. doi: 10.3389/fnins.2017.00167

Hardy, J., and Selkoe, D. J. (2002). The amyloid hypothesis of Alzheimer's disease: progress and problems on the road to therapeutics. *Science* 297, 353–356. doi: 10.1126/science.1072994

Hedden, T., Van Dijk, K. R., Becker, J. A., Mehta, A., Sperling, R. A., Johnson, K. A., et al. (2009). Disruption of functional connectivity in clinically normal older adults harboring amyloid burden. *J. Neurosci.* 29, 12686–12694. doi: 10.1523/JNEUROSCI.3189-09.2009

Hodgetts, C. J., Shine, J. P., Williams, H., Postans, M., Sims, R., Williams, J., et al. (2019). Increased posterior default mode network activity and structural connectivity in young adult APOE-epsilon4 carriers: a multimodal imaging investigation. *Neurobiol. Aging* 73, 82–91. doi: 10.1016/j.neurobiolaging.2018.08.026

Hoenig, M. C., Bischof, G. N., Seemiller, J., Hammes, J., Kukolja, J., Onur, O. A., et al. (2018). Networks of tau distribution in Alzheimer's disease. *Brain* 141, 568–581. doi: 10.1093/brain/awx353

Jack, C. R. Jr., Wiste, H. J., Therneau, T. M., Weigand, S. D., Knopman, D. S., Mielke, M. M., et al. (2019). Associations of amyloid, tau, and neurodegeneration biomarker profiles with rates of memory decline among individuals without dementia. *JAMA* 321, 2316–2325. doi: 10.1001/jama.2019.7437

Jack, C. R. Jr., Wiste, H. J., Weigand, S. D., Knopman, D. S., Lowe, V., Vemuri, P., et al. (2013). Amyloid-first and neurodegeneration-first profiles characterize incident amyloid PET positivity. *Neurology* 81, 1732–1740. doi: 10.1212/01.wnl.0000435556.21319.e4

Kametani, F., and Hasegawa, M. (2018). Reconsideration of amyloid hypothesis and tau hypothesis in Alzheimer's disease. *Front. Neurosci.* 12:25. doi: 10.3389/fnins.2018.00025

Klunk, W. E. (2011). Amyloid imaging as a biomarker for cerebral β-amyloidosis and risk prediction for Alzheimer dementia. *Neurobiol. Aging* 32, S20–S36. doi: 10.1016/j.neurobiolaging.2011.09.006

Koini, M., Duering, M., Gesierich, B. G., Rombouts, S., Ropele, S., Wagner, F., et al. (2018). Grey-matter network disintegration as predictor of cognitive and motor function with aging. *Brain Struct. Funct.* 223, 2475–2487. doi: 10.1007/s00429-018-1642-0

Korthauer, L. E., Zhan, L., Ajilore, O., Leow, A., and Driscoll, I. (2018). Disrupted topology of the resting state structural connectome in middle-aged APOE ε4 carriers. *NeuroImage* 178, 295–305. doi: 10.1016/j.neuroimage.2018.05.052

Kronenbuerger, M., Hua, J., Bang, J. Y. A., Ultz, K. E., Miao, X., Zhang, X., et al. (2019). Differential changes in functional connectivity of striatum-prefrontal and striatum-motor circuits in premanifest Huntington's disease. *Neurodegener. Dis.* 19, 78–87. doi: 10.1159/000501616

Li, R., Yin, S., Zhu, X., Ren, W., Yu, J., Wang, P., et al. (2017). Linking inter-individual variability in functional brain connectivity to cognitive ability in elderly individuals. *Front. Aging Neurosci.* 9:385. doi: 10.3389/fnagi.2017.00385

Lim, H. K., Nebes, R., Snitz, B., Cohen, A., Mathis, C., Price, J., et al. (2014). Regional amyloid burden and intrinsic connectivity networks in cognitively normal elderly subjects. *Brain* 137, 3327–3338. doi: 10.1093/brain/awu271

Liu, C. C., Kanekiyo, T., Xu, H., and Bu, G. (2013). Apolipoprotein E and Alzheimer disease: risk, mechanisms and therapy. *Nat. Rev. Neurol.* 9, 106–118. doi: 10.1038/nrneurol.2012.263

Liu, K., Yao, S., Chen, K., Zhang, J., Yao, L., Li, K., et al. (2017). Structural brain network changes across the adult lifespan. *Front. Aging Neurosci.* 9:275. doi: 10.3389/fnagi.2017.00275

Lockhart, S. N., Ayakta, N., Winer, J. R., La Joie, R., Rabinovici, G. D., and Jagust, W. J. (2017). Elevated ^{18}F-AV-1451 PET tracer uptake detected in incidental imaging findings. *Neurology* 88, 1095–1097. doi: 10.1212/wnl.0000000000003724

Luo, N., Sui, J., Abrol, A., Lin, D., Chen, J., Vergara, V. M., et al. (2019). Age-related structural and functional variations in 5,967 individuals across the adult lifespan. *Hum. Brain Mapp.* doi: 10.1002/hbm.24905 [Epub ahead of print].

Maass, A., Berron, D., Harrison, T. M., Adams, J. N., La Joie, R., Baker, S., et al. (2019). Alzheimer's pathology targets distinct memory networks in the ageing brain. *Brain* 142, 2492–2509. doi: 10.1093/brain/awz154

Mainta, I. C., Vargas, M. I., Trombella, S., Frisoni, G. B., Unschuld, P. G., and Garibotto, V. (2018). Hybrid PET-MRI in Alzheimer's disease research. *Methods Mol. Biol.* 1750, 185–200. doi: 10.1007/978-1-4939-7704-8_12

Mattsson, N., Andreasson, U., Zetterberg, H., Blennow, K., and Alzheimer's Disease Neuroimaging, I. (2017). Association of plasma neurofilament light with neurodegeneration in patients with Alzheimer disease. *JAMA Neurol.* 74, 557–566. doi: 10.1001/jamaneurol.2016.6117

Mattsson, N., Insel, P. S., Donohue, M., Jogi, J., Ossenkoppele, R., Olsson, T., et al. (2019). Predicting diagnosis and cognition with ^{18}F-AV-1451 tau PET and structural MRI in Alzheimer's disease. *Alzheimers Dement.* 15, 570–580. doi: 10.1016/j.jalz.2018.12.001

McLaren, D. G., Sreenivasan, A., Diamond, E. L., Mitchell, M. B., Van Dijk, K. R., Deluca, A. N., et al. (2012). Tracking cognitive change over 24 weeks with longitudinal functional magnetic resonance imaging in Alzheimer's disease. *Neurodegener. Dis.* 9, 176–186. doi: 10.1159/000335876

Mormino, E. C., Smiljic, A., Hayenga, A. O., Onami, S. H., Greicius, M. D., Rabinovici, G. D., et al. (2011). Relationships between β-amyloid and functional connectivity in different components of the default mode network in aging. *Cereb. Cortex* 21, 2399–2407. doi: 10.1093/cercor/bhr025

Nelson, P. T., Alafuzoff, I., Bigio, E. H., Bouras, C., Braak, H., Cairns, N. J., et al. (2012). Correlation of Alzheimer disease neuropathologic changes with cognitive status: a review of the literature. *J. Neuropathol. Exp. Neurol.* 71, 362–381. doi: 10.1097/NEN.0b013e31825018f7

Ossenkoppele, R., Iaccarino, L., Schonhaut, D. R., Brown, J. A., La Joie, R., O'Neil, J. P., et al. (2019). Tau covariance patterns in Alzheimer's disease patients match intrinsic connectivity networks in the healthy brain. *NeuroImage Clin.* 23:101848. doi: 10.1016/j.nicl.2019.101848

Ouchi, Y., and Kikuchi, M. (2012). A review of the default mode network in aging and dementia based on molecular imaging. *Rev. Neurosci.* 23, 263–268. doi: 10.1515/revneuro-2012-0029

Pini, L., Manenti, R., Cotelli, M., Pizzini, F. B., Frisoni, G. B., and Pievani, M. (2018). Non-invasive brain stimulation in dementia: a complex network story. *Neurodegener. Dis.* 18, 281–301. doi: 10.1159/000495945

Preibisch, C., Castrillon, G. J., Buhrer, M., and Riedl, V. (2015). Evaluation of multiband EPI acquisitions for resting state fMRI. *PLoS One* 10:e0136961. doi: 10.1371/journal.pone.0136961

Price, J. L., and Morris, J. C. (1999). Tangles and plaques in nondemented aging and "preclinical" Alzheimer's disease. *Ann. Neurol.* 45, 358–368. doi: 10.1002/1531-8249(199903)45:3<358::aid-ana12>3.0.co;2-x

Quevenco, F. C., Preti, M. G., van Bergen, J. M., Hua, J., Wyss, M., Li, X., et al. (2017). Memory performance-related dynamic brain connectivity indicates pathological burden and genetic risk for Alzheimer's disease. *Alzheimers Res. Ther.* 9:24. doi: 10.1186/s13195-017-0249-7

Quevenco, F. C., Schreiner, S. J., Preti, M. G., van Bergen, J. M. G., Kirchner, T., Wyss, M., et al. (2019). GABA and glutamate moderate β-amyloid related functional connectivity in cognitively unimpaired old-aged adults. *NeuroImage Clin.* 22:101776. doi: 10.1016/j.nicl.2019.101776

Rektorova, I., Krajcovicova, L., Marecek, R., and Mikl, M. (2012). Default mode network and extrastriate visual resting state network in patients with Parkinson's disease dementia. *Neurodegener. Dis.* 10, 232–237. doi: 10.1159/000334765

Roberts, B. R., Lind, M., Wagen, A. Z., Rembach, A., Frugier, T., Li, Q. X., et al. (2017). Biochemically-defined pools of amyloid-β in sporadic Alzheimer's disease: correlation with amyloid PET. *Brain* 140, 1486–1498. doi: 10.1093/brain/awx057

Ross, C. A., Aylward, E. H., Wild, E. J., Langbehn, D. R., Long, J. D., Warner, J. H., et al. (2014). Huntington disease: natural history, biomarkers and prospects for therapeutics. *Nat. Rev. Neurol.* 10, 204–216. doi: 10.1038/nrneurol.2014.24

Schipper, H. M. (2011). Presymptomatic apolipoprotein E genotyping for Alzheimer's disease risk assessment and prevention. *Alzheimers Dement.* 7, e118–e123. doi: 10.1016/j.jalz.2010.06.003

Schöll, M., Ossenkoppele, R., Strandberg, O., Palmqvist, S., Swedish BioFINDER study, Jögi, J., et al. (2017). Distinct ^{18}F-AV-1451 tau PET retention patterns in early- and late-onset Alzheimer's disease. *Brain* 140, 2286–2294. doi: 10.1093/brain/awx171

Schreiner, S. J., Kirchner, T., Wyss, M., Van Bergen, J. M., Quevenco, F. C., Steininger, S. C., et al. (2016). Low episodic memory performance in cognitively normal elderly subjects is associated with increased posterior cingulate gray matter N-acetylaspartate: a ^{1}H MRSI study at 7 Tesla. *Neurobiol. Aging* 48, 195–203. doi: 10.1016/j.neurobiolaging.2016.08.022

Schreiner, S. J., Liu, X., Gietl, A. F., Wyss, M., Steininger, S. C., Gruber, E., et al. (2014). Regional fluid-attenuated inversion recovery (FLAIR) at 7 Tesla correlates with amyloid-β in hippocampus and brainstem of cognitively normal elderly subjects. *Front. Aging Neurosci.* 6:240. doi: 10.3389/fnagi.2014.00240

Schultz, A. P., Chhatwal, J. P., Hedden, T., Mormino, E. C., Hanseeuw, B. J., Sepulcre, J., et al. (2017). Phases of hyperconnectivity and hypoconnectivity in the default mode and salience networks track with amyloid and tau in clinically normal individuals. *J. Neurosci.* 37, 4323–4331. doi: 10.1523/JNEUROSCI.3263-16.2017

Selkoe, D. J., and Hardy, J. (2016). The amyloid hypothesis of Alzheimer's disease at 25 years. *EMBO Mol. Med.* 8, 595–608. doi: 10.15252/emmm.201606210

Sepulcre, J., Sabuncu, M. R., Li, Q., El Fakhri, G., Sperling, R., and Johnson, K. A. (2017). Tau and amyloid-β proteins distinctively associate to functional network changes in the aging brain. *Alzheimers Dement.* 13, 1261–1269. doi: 10.1016/j.jalz.2017.02.011

Sheline, Y. I., Raichle, M. E., Snyder, A. Z., Morris, J. C., Head, D., Wang, S., et al. (2010). Amyloid plaques disrupt resting state default mode network connectivity in cognitively normal elderly. *Biol. Psychiatry* 67, 584–587. doi: 10.1016/j.biopsych.2009.08.024

Shi, Y., Yamada, K., Liddelow, S. A., Smith, S. T., Zhao, L., Luo, W., et al. (2017). ApoE4 markedly exacerbates tau-mediated neurodegeneration in a mouse model of tauopathy. *Nature* 549, 523–527. doi: 10.1038/nature24016

Smith, R., Wibom, M., Pawlik, D., Englund, E., and Hansson, O. (2019). Correlation of *in vivo* [^{18}F]Flortaucipir with postmortem alzheimer disease tau pathology. *JAMA Neurol.* 76, 310–317. doi: 10.1001/jamaneurol.2018.3692

Smitha, K. A., Arun, K. M., Rajesh, P. G., Joel, S. E., Venkatesan, R., Thomas, B., et al. (2018). Multiband fMRI as a plausible, time-saving technique for resting-state data acquisition: study on functional connectivity mapping using graph theoretical measures. *Magn. Reson. Imaging* 53, 1–6. doi: 10.1016/j.mri.2018.06.013

Song, X., Mitnitski, A., Zhang, N., Chen, W., Rockwood, K., and Alzheimer's Disease Neuroimaging, I. (2013). Dynamics of brain structure and cognitive function in the Alzheimer's disease neuroimaging initiative. *J. Neurol. Neurosurg. Psychiatry* 84, 71–78. doi: 10.1136/jnnp-2012-303579

Sorg, C., and Grothe, M. J. (2015). The complex link between amyloid and neuronal dysfunction in Alzheimer's disease. *Brain* 138, 3472–3475. doi: 10.1093/brain/awv302

Sorg, C., Riedl, V., Muhlau, M., Calhoun, V. D., Eichele, T., Laer, L., et al. (2007). Selective changes of resting-state networks in individuals at risk for Alzheimer's disease. *Proc. Natl. Acad. Sci. U S A* 104, 18760–18765. doi: 10.1073/pnas.0708803104

Sperling, R. A., Dickerson, B. C., Pihlajamaki, M., Vannini, P., LaViolette, P. S., Vitolo, O. V., et al. (2010). Functional alterations in memory networks in early Alzheimer's disease. *Neuromolecul. Med.* 12, 27–43. doi: 10.1007/s12017-009-8109-7

Sperling, R. A., Laviolette, P. S., O'Keefe, K., O'Brien, J., Rentz, D. M., Pihlajamaki, M., et al. (2009). Amyloid deposition is associated with impaired default network function in older persons without dementia. *Neuron* 63, 178–188. doi: 10.1016/j.neuron.2009.07.003

Steininger, S. C., Liu, X., Gietl, A., Wyss, M., Schreiner, S., Gruber, E., et al. (2014). Cortical amyloid β in cognitively normal elderly adults is associated with decreased network efficiency within the cerebro-cerebellar system. *Front. Aging Neurosci.* 6:52. doi: 10.3389/fnagi.2014.00052

Strittmatter, W. J., Saunders, A. M., Schmechel, D., Pericak-Vance, M., Enghild, J., Salvesen, G. S., et al. (1993). Apolipoprotein E: high-avidity binding to β-amyloid and increased frequency of type 4 allele in late-onset familial Alzheimer disease. *Proc. Natl. Acad. Sci. U S A* 90, 1977–1981. doi: 10.1073/pnas.90.5.1977

Teipel, S., Grothe, M. J., and Alzheimer's Disease Neuroimaging, I. (2015). Does posterior cingulate hypometabolism result from disconnection or local pathology across preclinical and clinical stages of Alzheimer's disease? *Eur. J. Nucl. Med. Mol. Imaging* 43, 526–536. doi: 10.1007/s00259-015-3222-3

Thal, D. R., Rüb, U., Orantes, M., and Braak, H. (2002). Phases of A β-deposition in the human brain and its relevance for the development of AD. *Neurology* 58, 1791–1800. doi: 10.1212/wnl.58.12.1791

Tiraboschi, P., Hansen, L. A., Masliah, E., Alford, M., Thal, L. J., and Corey-Bloom, J. (2004). Impact of APOE genotype on neuropathologic and neurochemical markers of Alzheimer disease. *Neurology* 62, 1977–1983. doi: 10.1212/01.wnl.0000128091.92139.0f

Tosun, D., Landau, S., Aisen, P. S., Petersen, R. C., Mintun, M., Jagust, W., et al. (2017). Association between tau deposition and antecedent amyloid-β accumulation rates in normal and early symptomatic individuals. *Brain* 140, 1499–1512. doi: 10.1093/brain/awx046

Unschuld, P. G., Edden, R. A., Carass, A., Liu, X., Shanahan, M., Wang, X., et al. (2012). Brain metabolite alterations and cognitive dysfunction in early Huntington's disease. *Mov. Disord.* 27, 895–902. doi: 10.1002/mds.25010

van Bergen, J. M. G., Li, X., Quevenco, F. C., Gietl, A. F., Treyer, V., Leh, S. E., et al. (2018a). Low cortical iron and high entorhinal cortex volume promote cognitive functioning in the oldest-old. *Neurobiol. Aging* 64, 68–75. doi: 10.1016/j.neurobiolaging.2017.12.014

van Bergen, J. M. G., Li, X., Quevenco, F. C., Gietl, A. F., Treyer, V., Meyer, R., et al. (2018b). Simultaneous quantitative susceptibility mapping and Flutemetamol-PET suggests local correlation of iron and β-amyloid as an indicator of cognitive performance at high age. *NeuroImage* 174, 308–316. doi: 10.1016/j.neuroimage.2018.03.021

Vandenberghe, R., Van Laere, K., Ivanoiu, A., Salmon, E., Bastin, C., Triau, E., et al. (2010). ^{18}F-flutemetamol amyloid imaging in Alzheimer disease and mild cognitive impairment: a phase 2 trial. *Ann. Neurol.* 68, 319–329. doi: 10.1002/ana.22068

Verghese, P. B., Castellano, J. M., and Holtzman, D. M. (2011). Apolipoprotein E in Alzheimer's disease and other neurological disorders. *Lancet Neurol.* 10, 241–252. doi: 10.1016/S1474-4422(10)70325-2

Villemagne, V. L., Dore, V., Burnham, S. C., Masters, C. L., and Rowe, C. C. (2018). Imaging tau and amyloid-β proteinopathies in Alzheimer disease and other conditions. *Nat. Rev. Neurol.* 14:446. doi: 10.1038/s41582-018-0021-z

Villemagne, V. L., Pike, K. E., Chetelat, G., Ellis, K. A., Mulligan, R. S., Bourgeat, P., et al. (2011). Longitudinal assessment of Aβ and cognition in aging and Alzheimer disease. *Ann. Neurol.* 69, 181–192. doi: 10.1002/ana.22248

Vos, S. J., Xiong, C., Visser, P. J., Jasielec, M. S., Hassenstab, J., Grant, E. A., et al. (2013). Preclinical Alzheimer's disease and its outcome: a longitudinal cohort study. *Lancet Neurol.* 12, 957–965. doi: 10.1016/S1474-4422(13)70194-7

Wang, L., Brier, M. R., Snyder, A. Z., Thomas, J. B., Fagan, A. M., Xiong, C., et al. (2013). Cerebrospinal fluid Aβ42, phosphorylated Tau181,

and resting-state functional connectivity. *JAMA Neurol.* 70, 1242–1248. doi: 10.1001/jamaneurol.2013.3253

Wang, J., Wang, X., He, Y., Yu, X., Wang, H., and He, Y. (2015). Apolipoprotein E ε4 modulates functional brain connectome in Alzheimer's disease. *Hum. Brain Mapp.* 36, 1828–1846. doi: 10.1002/hbm.22740

Weiler, M., Teixeira, C. V., Nogueira, M. H., de Campos, B. M., Damasceno, B. P., Cendes, F., et al. (2014). Differences and the relationship in default mode network intrinsic activity and functional connectivity in mild Alzheimer's disease and amnestic mild cognitive impairment. *Brain Connect.* 4, 567–574. doi: 10.1089/brain.2014.0234

Westlye, E. T., Lundervold, A., Rootwelt, H., Lundervold, A. J., and Westlye, L. T. (2011). Increased hippocampal default mode synchronization during rest in middle-aged and elderly APOE ε4 carriers: relationships with memory performance. *J. Neurosci.* 31, 7775–7783. doi: 10.1523/jneurosci.1230-11.2011

Whitfield-Gabrieli, S., and Nieto-Castanon, A. (2012). Conn: a functional connectivity toolbox for correlated and anticorrelated brain networks. *Brain Connect.* 2, 125–141. doi: 10.1089/brain.2012.0073

World_Medical_Association. (1991). Declaration of Helsinki. *Law Med Health Care* 19, 264–265.

Yamazaki, Y., Zhao, N., Caulfield, T. R., Liu, C. C., and Bu, G. (2019). Apolipoprotein E and Alzheimer disease: pathobiology and targeting strategies. *Nat. Rev. Neurol.* 15, 501–518. doi: 10.1038/s41582-019-0228-7

Yang, X., Beason-Held, L., Resnick, S. M., and Landman, B. A. (2011). Biological parametric mapping with robust and non-parametric statistics. *NeuroImage* 57, 423–430. doi: 10.1016/j.neuroimage.2011.04.046

Zetterberg, H., and Blennow, K. (2018). From cerebrospinal fluid to blood: the third wave of fluid biomarkers for Alzheimer's disease. *J. Alzheimers Dis.* 64, S271–S279. doi: 10.3233/JAD-179926

Conflict of Interest: RN (CEO) and CH (CMO) are members of the board of directors at Neurimmune, Schlieren, Switzerland.

The remaining authors declare that the research was conducted in the absence of any commercial or financial relationships that could be construed as a potential conflict of interest.

frontiers in Aging Neuroscience

ORIGINAL RESEARCH
published: 10 March 2020
doi: 10.3389/fnagi.2020.00061

Development of Brain Structural Networks Over Age 8: A Preliminary Study Based on Diffusion Weighted Imaging

*Zhanxiong Wu[1,2], Yun Peng[2], Sudhakar Selvaraj[3], Paul E. Schulz[4] and Yingchun Zhang[2]**

[1] School of Electronic Information, Hangzhou Dianzi University, Hangzhou, China, [2] Department of Biomedical Engineering, University of Houston, Houston, TX, United States, [3] Louis A. Faillace, MD, Department of Psychiatry and Behavioral Sciences, The McGovern Medical School of UT Health Houston, Houston, TX, United States, [4] Department of Neurology, The McGovern Medical School of UT Health Houston, Houston, TX, United States

Brain structural network changes provide key information about the aging process of the brain. Unfortunately, there has yet to be a detailed characterization of these structural networks across different age groups. Efforts to classify these networks have also been hampered by their reliance on technically limited traditional methods, which are unable to track multiple fiber orientations within a voxel and consequently are prone to false detection and artifacts. In this study, a newly developed Ensemble Average Propagator (EAP) based probabilistic tractography method was applied to construct a structural network, with the strength of the link between any two brain functional regions estimated according to the alignment of the EAP along connecting pathways. Age-related changes in the topological organization of human brain structural networks were thereby characterized across a broad age range (ages 8–75 years). The data from 48 healthy participants were divided into four age groups (Group 1 aged 8–15 years; Group 2 aged 25–35 years; Group 3 aged 45–55 years; and, Group 4 aged 65–75 years; N = 12 per group). We found that the brain structural network continues to strengthen during later adolescence and adulthood, through the first 20–30 years of life. Older adults, aged 65–75, had a significantly less optimized topological organization in their structural network, with decreased global efficiency and increased path lengths versus subjects in other groups. This study suggests that probabilistic tractography based on EAP provides a reliable method to construct macroscale structural connectivity networks to capture the age-associated changes of brain structures.

Keywords: magnetic resonance imaging, diffusion weighted imaging, ensemble average propagator, structural network, brain development

OPEN ACCESS

Edited by:
Hans J. Grabe,
University of Greifswald, Germany

Reviewed by:
Lukas Pirpamer,
Medical University of Graz, Austria
Zhen Yuan,
University of Macau, China

****Correspondence:***
Yingchun Zhang
yzhang94@uh.edu

Received: *07 August 2019*
Accepted: *20 February 2020*
Published: *10 March 2020*

Citation:
Wu Z, Peng Y, Selvaraj S, Schulz PE and Zhang Y (2020) Development of Brain Structural Networks Over Age 8: A Preliminary Study Based on Diffusion Weighted Imaging. Front. Aging Neurosci. 12:61. doi: 10.3389/fnagi.2020.00061

INTRODUCTION

Human brain structural networks are functionally modular and connect effectively through neural bundles to meet the needs for complex cognitive tasks (Schmahmann et al., 2007; Lerch et al., 2017). This neural fiber connectivity enables the communication between the various regions of the brain (Bassett et al., 2011) and its integrity is pivotal for individual health. Due to

the development of non-invasive imaging technologies, such as diffusion-weighted imaging (DWI), our knowledge of these structural pathways have vastly improved. DWI characterizes structural connectivity networks across brain regions *in-vivo* by calculating the number of streamlines or the probability of connections (Frank, 2002; Tuch et al., 2002; Anderson, 2005; Maier-Hein et al., 2017). The demonstrated connectivity patterns can then be assessed through graph-based analyses that outline the complex structural substrates of cognition (Betzel et al., 2014). This approach has been effectively employed to identify densely interconnected structural hub regions that are critical to efficient neuronal signaling and communication (van den Heuvel and Sporns, 2013).

Aging has been recognized as a significant factor affecting brain functions. Specifically, a growing body of evidence suggests that brain structure is altered as age increases. Although the fundamental cause of these age-related white matter changes has yet to be fully understood, current theories tie them to changes in the axonal diameter and myelination, synaptic pruning, and modification (Onoda et al., 2012; Dennis and Thompson, 2014; Geerligs et al., 2014; Huang et al., 2015; Grady et al., 2016). According to the "early-in-late-out" hypothesis, increases in fiber tract white matter density and axonal myelination are important for cognitive development during childhood and adolescence (Paus et al., 1999). In contrast, demyelination and a loss of nerve fibers contribute to cognitive decline (Peters, 2002). Despite these early hypotheses and studies, available data describing age-related changes in structural connectivity remains lacking (Damoiseaux, 2017).

While limited, currently available evidence suggests that old age is associated with lower connectivity and lower local efficiency (Damoiseaux et al., 2007; Gong et al., 2009; Burzynska et al., 2010; Otte et al., 2015). These studies, however, address coarsely divided age subgroups. In addition, recent evidence from Zhao et al. (2015) also suggests that the age-related trajectories of local and global structural network efficiency changes are non-linear. The use of large age ranges may then combine subjects at different stages, complicating the study of age-related structural connectivity changes that would otherwise provide useful insights for patient diagnosis and management.

Several methods have been developed to reconstruct structural connectivity networks. Previous studies have relied heavily on diffusion tensor imaging (DTI) methods to trace white matter connections (Gong et al., 2009; Betzel et al., 2014; Otte et al., 2015; Zhao et al., 2015). Conventional DTI, however, struggles to resolve complex fiber populations when they occur within a DWI voxel, as is the case when tracts cross, branch, merge, or kiss (Tuch, 2004; Hess et al., 2006; Poupon et al., 2008). As approximately one- to two-thirds of DWI voxels contain multiple fiber populations (Duarte-Carvajalino et al., 2014), structural connectivity networks reconstructed based on diffusion tensor may deviate largely from real situations. It is then necessary to develop methods capable of parsing these complex white matter structures.

In this study, age-related changes in structural connectivity were investigated using a novel Ensemble Average Propagator (EAP)-based probabilistic tractography method. Unlike DTI or orientation distribution function methods, EAP preserves the radial part of the diffusion signal and thus may accurately identify the crossing orientations of neural fascicles within a white matter voxel (Fick et al., 2014; Paquette et al., 2015). The aim of this study was to evaluate the novel EAP approach for reconstructing structural connectivity networks, using a healthy subject dataset that covered a wide range of ages.

MATERIALS AND METHODS

DWI Dataset

The lifespan datasets publicly available from the Human Connectome Project (HCP) (Marcus et al., 2011; Van Essen et al., 2013) and the OASIS3 database (Longitudinal neuroimaging, clinical, and cognitive dataset for normal aging and Alzheimer's disease[1]) were used in this study. Datasets included 48 subjects aged 8–75 years, organized into 4 age groups (**Table 1**). HCP subjects (34) underwent an abbreviated scan protocols similar to that used for the WU-Minn young adult HCP study (Feinberg et al., 2010). Data for each subject was collected using a 3T General Electric MR scanner, with a whole-body radiofrequency coil for signal excitation and a quadrature 8-channel brain coil for the reception. The HCP acquisition protocol consisted of: (1) high resolution 3D T1-weighted SPGR sequence, with TR/TE/flip angle of 9.1 ms/4.1 ms/108, acquisition matrix size = 256 × 256 × 320, and slice thickness = 1 mm; (2) DWI using a single-shot spin-echo echo-planar sequence, including 91 non-collinear encoding directions with b values of 1000, 2000, 3000 s/mm^2, TR/TE = 12700/88.3 ms, acquisition matrix size = 144 × 168 × 111, slice thickness = 2.4 mm, and voxel size = 2.4 mm × 2.4 mm × 2.4 mm, along with six additional images with no diffusion sensitization b = 0 s/mm^2 (b0, non-diffusion-weighted images). The remaining 14 subjects from the OASIS3 dataset were scanned using a Siemens TIM Trio 3T MRI scanner with 16-channel head coils and the scan protocols that included: (1) high-resolution 3D T1-weighted GR IR with TR/TE/flip angle = 2.4 s/3.16 ms/8, acquisition matrix size = 256 × 256 × 176; (2) DWI using a single-shot spin-echo echo-planar sequence with TR/TE/flip angle = 9.9 s/102 ms/90, b-values = 600, 800, 1000 s/mm^2, acquisition matrix size = 96 × 96 × 60, slice thickness = 2 mm, and voxel size = 1.98 mm × 1.98 mm × 2 mm, wherein diffusion-weighted gradients were applied along 25 directions with one

[1]www.oasis-brains.org

TABLE 1 | Lifespan datasets from HCP and OASIS3 database, including four age groups.

Age (years)	*N*	Gender
8-15	12	8 Female, 4 Male
25-35	12	5 Female, 7 Male
45-55	12	5 Female, 7 Male
65-75	12	6 Female, 6 Male

b0 image. The overall process for scanning and data analysis is summarized in **Figure 1**.

Reconstruction of the Structural Connectivity Network

Brain parcellation and reconstruction were performed using FreeSurfer (stable version 6.0.0)[2] (Fischl, 2012). Parcellations for each subject were generated in the native space, based on the collected high-resolution T1-weighted MRI images. The cerebral cortex was parcellated into 68 functional regions, 34 for each hemisphere (Desikan et al., 2006). These regions were considered as the nodes in a structural connectivity graph. Lastly, the corresponding atlas was affine registered to the DWI native space for each subject. The 68 cortical regions used to construct brain SC networks are list in **Appendix Table A1**.

The DWI dataset was first denoised following the procedure outlined by Wu et al. (2019b). The topup and eddy_openmp FSL 6.0 commands (Ubuntu Linux 16.04) were then used to correct eddy distortion and motion artifact (Andersson et al., 2003; Andersson and Sotiropoulos, 2015, 2016). Briefly, these corrections were performed by first performing an affine alignment of each DWI image to the b0 image. Next, EAPs were estimated from multi-shell DWI samples using spherical polar Fourier imaging (SPFI) (Cheng et al., 2010). According to a spherical harmonics expansion, EAPs were calculated along 726 directions evenly distributed about a spherical shell (Hess et al., 2006). Diffusion orientations contained within a white matter voxel were then extracted by detecting the local EAP peaks (Wu et al., 2018), which coincide with neural fiber tracts. Probabilistic fiber tracking was then performed to obtain the connection weights between different cortical regions (Iturria-Medina et al., 2007). Under angular constraints, the deterministic path planning algorithm was subsequently used to find all reasonable pathways between the WM voxels belonging to different ROIs. A train of consecutive WM voxels along each of the identified pathways was thereby determined, and the connection strengths of these pathways were computed by integrating their EAP alignment over a solid angle. The connection strength of each pair of WM voxels was then assigned as the connection strength with the largest connection possibility. Finally, the connection strength between each ROI pair was calculated as the sum of the connection probabilities for each pair of WM voxels within the ROIs (Wu et al., 2019a). The resulting link strength depended on the alignment of the EAP along connecting pathways, with higher strengths indicating better alignment. Evidence suggests that the link strengths determined by EAP fields may provide a more robust and suitable measure for structural connectivity network analysis than diffusion tensor and orientation distribution function (Assemlal et al., 2007; Cheng et al., 2010). To ensure that path propagations were anatomically realistic, we imposed a 90° maximum curvature threshold between every two successive path steps (Iturria-Medina et al., 2007, 2008; Sotiropoulos et al., 2010). This fiber tracking procedure yielded adjacency matrices whose elements represented the connection probabilities between each pair of parcellated cortical regions of interest.

Network graphs were created that consisted of a series of nodes connected by edges to interpret the generated adjacency matrices. Each node within a network graph represented a cortical region of interest, and the edges connecting them were assigned weights according to their determined link strength. In this study, each brain region was selected as the seed region, and its connectivity strength to each of the other 67 regions was calculated. Thus, for each subject, a 68 × 68 weighted, undirected network graph was constructed.

[2]http://www.freesurfer.net/fswiki/DownloadAndInstall

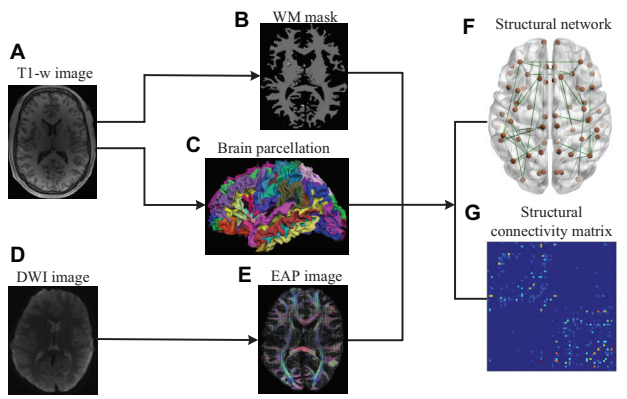

FIGURE 1 | Flowchart for the construction of structural connectivity networks based on EAP. **(A)** High-resolution T1-weighted MRI images. **(B)** White matter mask. **(C)** Cerebral cortex parcellation from T1-weighted MRI images using FreeSurfer. **(D)** DWI images. **(E)** EAPs constructed with SPFI. **(F)** Structural connectivity Networks. **(G)** Structural connectivity matrix. Before SC network construction, **(B,C)** are co-registered into DWI B0 native space in FreeSurfer.

TABLE 2 | Definitions of structural connectivity network metrics.

Network metrics	Description
$E_{glob}(G) = \frac{1}{N(N-1)} \sum_{i \neq j \in G} \frac{1}{L_{ij}}$	L_{ij} is the shortest path length between node i and j in G.
$E_{loc}(G) = \frac{1}{N} \sum_{i \in G} E_{glob}(G_i)$	G_i denotes the subgraph composed of the nearest neighbors of node i.
$L_p(G) = \frac{1}{N(N-1)} \sum_{i \neq j \in G} L_{ij}$	L_{ij} is the shortest path length between node i and j. This function quantifies the ability for information to be propagated in parallel.
$C_p = \frac{1}{N} \sum_{i \in G} C(i)$	C_p is the average of the clustering coefficient over all nodes, which indicates the extent of local interconnectivity or cliquishness in a network.
$\gamma = C_p^{SC} / C_p^{rand}$	C_p^{rand} is the mean C_p of 100 matched random networks. C_p^{SC} is the clustering coefficient empirical SC network.
$\lambda = L_p^{SC} / L_p^{rand}$	L_p^{rand} is the mean L_p of 100 matched random networks. L_p^{SC} is the shortest length of the SC networks.
$E_{nodal}(i) = \frac{1}{N-1} \sum_{i \neq j \in G} \frac{1}{L_{ij}}$	$E_{nodal}(i)$ measures the average shortest pathway length between a given node *i* and all of the other nodes in the network.

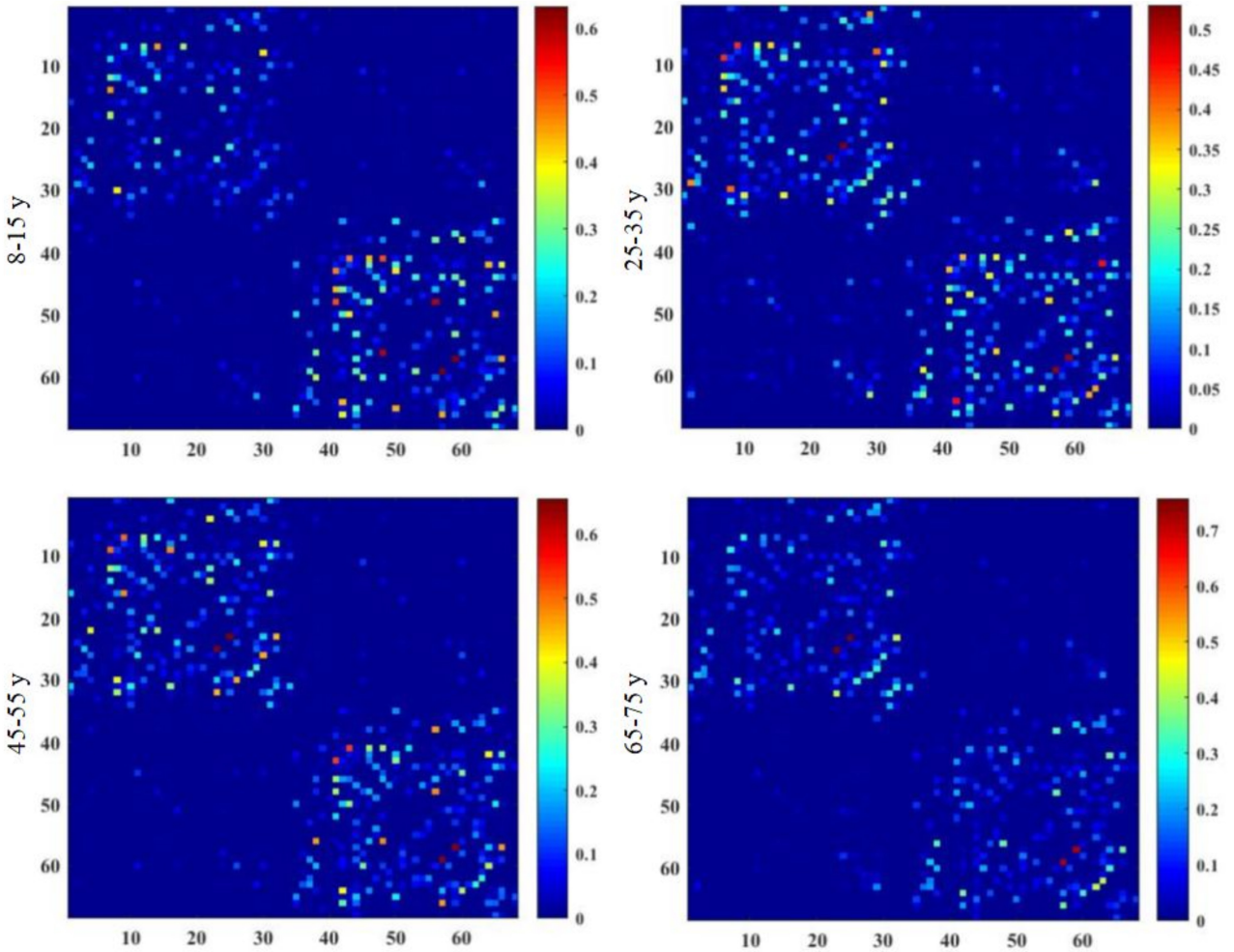

FIGURE 2 | Group-averaged structural connectivity maps of HCP lifespan subjects, which are 68 × 68 symmetric matrices. The subjects are arranged into four groups by age, including 8–15, 25–35, 45–55, and 65–75 years groups. In the maps, self-connections are excluded. The numbers on the axes of connectivity matrix are the indexes of parcellated regions.

Structural Connectivity Network Topological Analysis

A number of network metrics were adopted to quantify the topological features of the generated network graphs, including global efficiency E_{glob}, local efficiency E_{loc}, clustering coefficient C_p, regional efficiency E_{nodal}, and the small-world parameters γ and λ (Cao et al., 2013). After adjacency matrices were acquired and thresholded to remove weak connections, the enumerated network metrics were computed for each age group using the GRETNA (Wang et al., 2015) and BCT toolboxes (Rubinov and Sporns, 2010). Of particular interest here are the "small-world" parameters, which estimate the efficiency of information transfer within a defined network structure. An ideal, small-world network described by these parameters should feature a minimum path length between any pair of nodes equal to that of a comparable random network, with greater local interconnectivity or cliquishness (He et al., 2007). Lastly, the nodal efficiency metric, E_{nodal}, was used to describe regional properties. The mathematical equations for these measures are provided in **Table 2**, and detailed descriptions of each are provided by Cao et al. (2013). The weights were thresholded from 0.05 and 0.21 in intervals of 0.02 to remove spurious connections. The information from these serial measurements was integrated to calculate the area under the curve (AUC) for each metric, such that the resultant AUC values summarized the topological organization of the brain structural connectivity networks, independent of a single threshold selection. To identify the differences across age groups, we performed Kruskal–Wallis tests on the lifespan subjects. Finally, quadratic regression using least square fitting was performed to fit the AUC values of each metric.

Age-Related Changes

To further investigate age-associated structural connectivity differences, the group-wise structural connectivity hub regions were identified for each group. These are defined as regions that critically enable efficient neuronal signaling and communication

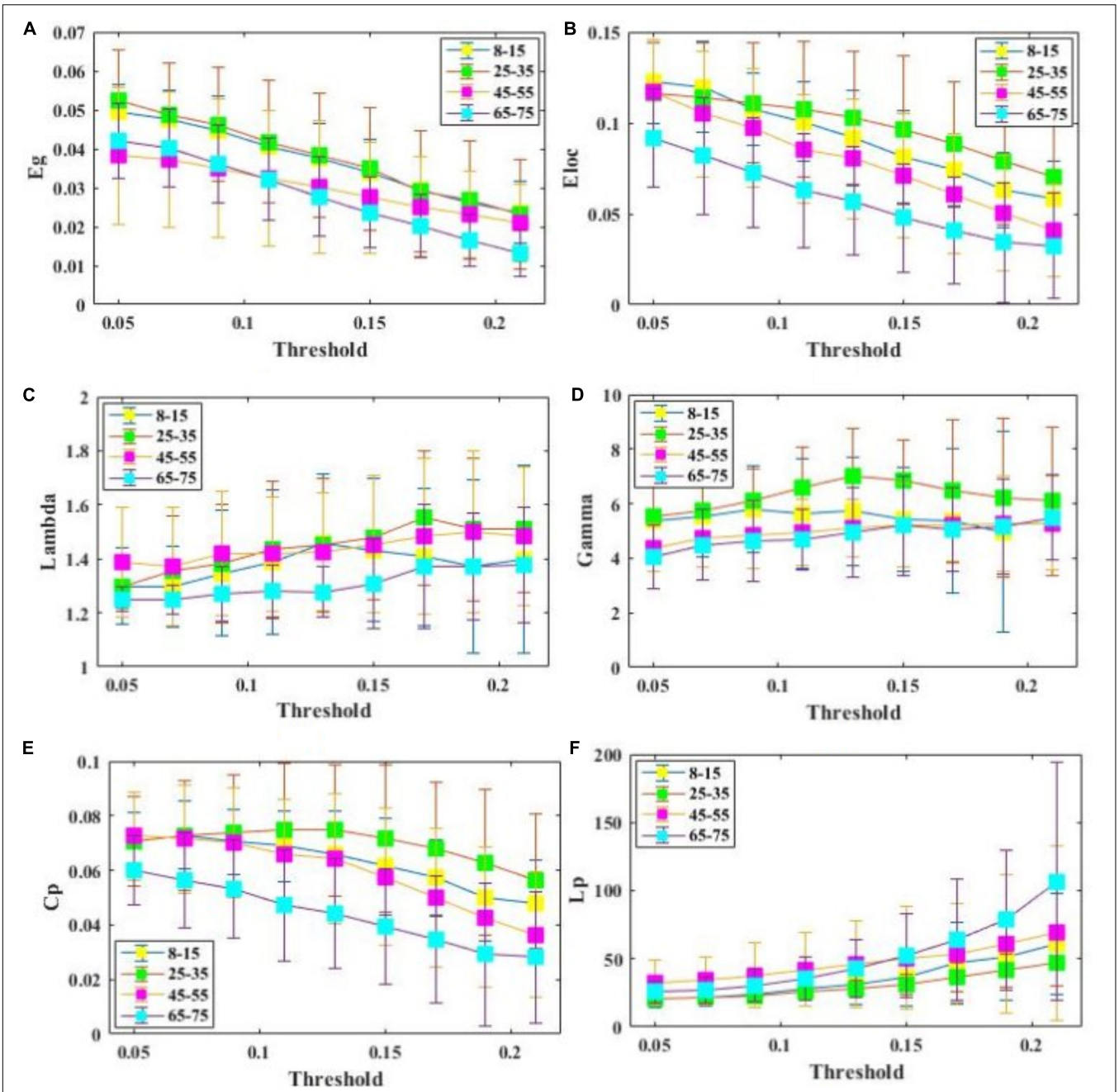

FIGURE 3 | Comparison of global and regional network metrics across 4 age groups. **(A)** Global efficiency E_{glob}, and it measures the global efficiency of parallel information transfer in a network. **(B)** Local efficiency E_{loc}, and it measures how efficient communication is among the first neighbors of a given node when it is removed. **(C)** $\lambda = L_p^{SC} / L_p^{SC} L_p^{rand}$. **(D)** $\gamma = L_p^{SC} / L_p^{rand}$. **(E)** Clustering coefficientC_p. **(F)** Characterized shortest path length of SC network L_p.

TABLE 3 | Group-wise comparisons of *AUC values* of global and local network metrics.

Age/y	aE_{glob}	aE_{loc}	aL_p	aC_p	$a\lambda$	$a\gamma$
8-15	0.0059 ± 0.0013	0.0146 ± 0.0034	5.6431 ± 1.9215	0.0101 ± 0.0021	0.2088 ± 0.0168	0.7782 ± 0.2151
25-35	0.0061 ± 0.0024	0.0126 ± 0.0049	4.8403 ± 1.1238	0.0112 ± 0.0037	0.2301 ± 0.0344	1.0163 ± 0.2300
45-55	0.0048 ± 0.0024	0.0158 ± 0.0054	7.5264 ± 1.1707	0.0095 ± 0.0035	0.2314 ± 0.0307	0.8036 ± 0.1806
65-75	0.0045 ± 0.0014	0.0092 ± 0.0045	7.9390 ± 1.4663	0.0070 ± 0.0031	0.2209 ± 0.0305	0.9345 ± 0.2775

These values were the fitted AUC values (mean ± SD).

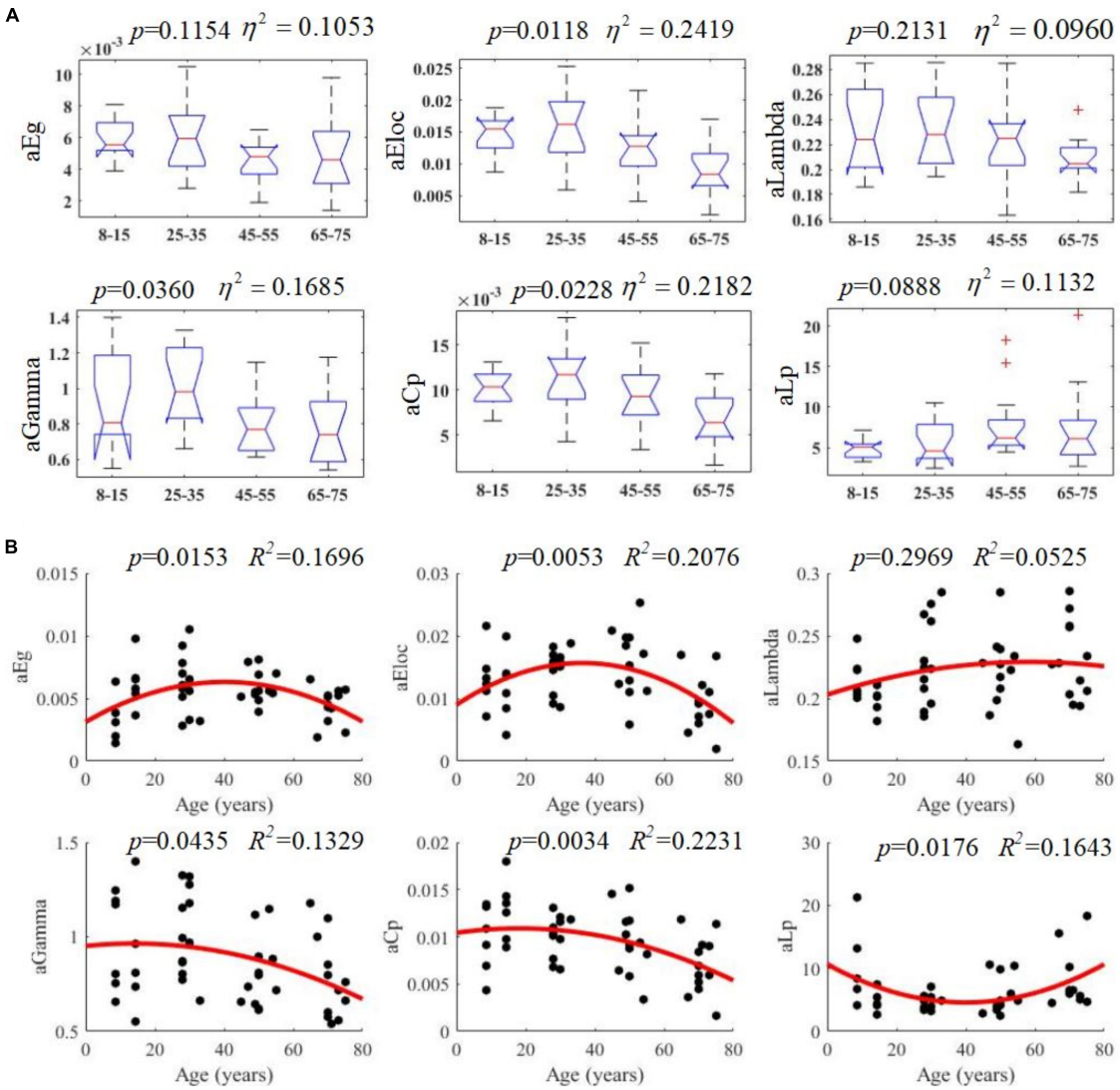

FIGURE 4 | Age-related changes in structural connectivity networks. **(A)** Kruskal–Wallis tests were performed to examine topological differences across age groups, and aEloc, aGamma and aCp can significantly differentiate age groups (p-value < 0.05). **(B)** The trajectories of aEg, aEloc, and aCp are statistically significant at p-value < 0.05.

(van den Heuvel and Sporns, 2013), integrating information to support complex cognitive functions. Network nodes were considered to be brain hubs if their nodal efficiency E_{nodal} was at least one standard deviation greater than the average nodal efficiency of the network. Group-wise backbone links were also extracted from structural connectivity networks, which were formed based on the rich club connections for high-capacity brain communication (van den Heuvel et al., 2012).

RESULTS

Brain structural connectivity networks were constructed for 48 subjects using probabilistic EAP-based tractography, including 68 nodes (**Appendix Table A1**). **Figure 2** shows the consensus structural connectivity maps for each age group. These adjacency matrices were symmetric, with self-connections excluded. The values in these maps were normalized to [0, 1], with higher values indicating stronger anatomical connectivity. Based on these adjacency matrices, group-wise topological properties were examined to find the structural connectivity differences between age groups.

Network Metrics

All examined groups showed a small-world organization, characterized by $\gamma >> 1$ and $\lambda > 1$ (**Figures 3C,D**). Compared with other groups, the subjects aged 65–75 years had significantly decreased E_{glob}, E_{loc}, and C_p, along with increased L_p (**Figures 3A,B,E,F**). The descriptive statistics for the AUC values of the thresholded graph metrics are provided in **Table 3**.

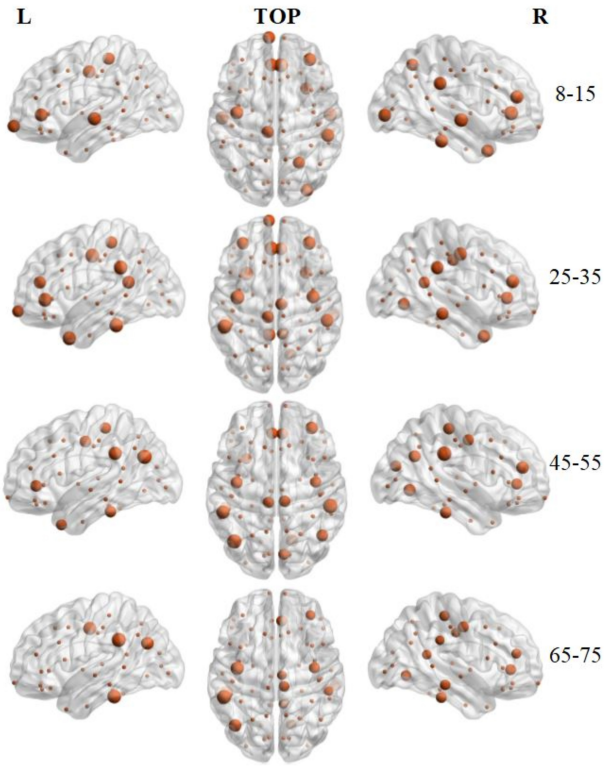

FIGURE 5 | 3D distribution of hub regions in the structural connectivity networks of the four age groups. The hub nodes are shown in brown with node sizes indicating their nodal efficiency values. The hub regions were mapped onto the cortical surface at the left, top, and right views. For the index of hub nodes, see **Table 4**. The brain graphs were visualized by using BrainNet Viewer software (Xia et al., 2013).

Kruskal–Wallis tests indicate that E_{loc},C_p, and γ significantly differentiate the four age groups (p-value < 0.05) (**Figure 4A**). All metrics show a parabolic relationship with age from childhood to old age (**Figure 4B**), although the R^2 values (5.25–22.31%) were relatively low.

Hub Regions

Hub regions were identified from the SC networks of each group. The nodes were considered as network hubs if their nodal efficiencies were at least one standard deviation greater than the average nodal efficiency of the network (Cao et al., 2013). The four age groups showed highly similar hub distributions, with core regions mainly in the frontal (region indices: 25, 59, 63) and parietal cortices (region indices: 23, 57, 64, 66) (Desikan et al., 2006), consistent with previous structural connectivity network studies on healthy adults (Sporns, 2013; van den Heuvel and Sporns, 2013). Group-wise analysis using the GRETNA toolbox then revealed that the 65–75 age group had reduced nodal efficiency in the inferior parietal (left hemisphere), inferior temporal (left hemisphere), middle temporal (left hemisphere), precuneus (left and right hemispheres), inferior parietal (right hemisphere), lateral occipital (right hemisphere), and superior parietal (right hemisphere) cortices (**Figure 5** and **Table 4**).

Backbone Links

The number of brain structural backbone links in each age group is shown across threshold values in **Figure 6**, with the specific brain backbone links for each age group at a threshold of 021 shown in **Figure 7**. Results suggest that the number of backbone links in SC networks of the 65–57 years group significantly decreased as thresholds increased (**Figure 6**). However, the average backbone connection strengths showed no significant differences between age groups (**Table 5**).

DISCUSSION

The performance of humans on formal cognitive testing and real world cognitive function declines with aging, generally peaking in the 20s and lessening thereafter. Understanding these changes will be critical for gaining insights into the age-associated risk of multiple neurodegenerative disorders and the increased sensitivity of people with aging to various insults, such as infections and brain trauma. Understanding these underlying mechanisms is a first step toward treating or preventing them. Studying structural connectivity may provide vital information for understanding these normal processes of the aging brain and hence its increased vulnerability over the lifespan.

Heretofore, many studies have relied on traditional reconstruction methods that show limited performance when applied to complex fiber populations. In this preliminary study, the performance of a novel Ensemble Average Propagator-based probabilistic tractography method was evaluated as it reconstructed the brain structural connectivity networks of 48 subjects obtained from the HCP and OASIS3 databases. The results suggest a non-linear evolution of age-dependent brain structural connectivity network properties.

The current investigation presents a novel application of the EAP. Previous EAP methods have been used to improve the diagnosis of Parkinson's disease, stroke detection, and brain tissue assessment (Banerjee et al., 2016; Brusini et al., 2016; Zucchelli et al., 2016); however, this is its first use at addressing structural connectivity. The current probabilistic method was modified from Iturria-Medina et al. (2007), extracting diffusion directions from EAP and avoiding exhaustive searches to identify the strongest paths between different ROIs.

Results obtained through this approach suggest that critical brain structural connectivity properties are conserved throughout the development process, which supports the conclusion that small-world networks are resilient to developmental alteration (Hagmann et al., 2008; Gong et al., 2009; He et al., 2009; Supekar et al., 2010). Despite retaining a small-world topology, however, the 65–75 years subjects showed decreased global efficiency, local efficiency, and increased path length (**Figure 3**). These findings may reflect structural degeneration due to neuron death or fiber breakdown. These results are supported by a recent study that reported reduced global efficiency in the functional brain networks of older adults (Damoiseaux, 2017). Another study, however, found no differences in global efficiency (Gong et al., 2009). Lack of differences may be ascribed to the use of a diffusion tensor

TABLE 4 | Hub regions distributed in SC networks of the four age groups.

8-15		25-35		45-55		65-75	
Hub regions (index)	aE_{nodal}	**Hub regions (index)**	aE_{nodal}	**Hub regions (index)**	aE_{nodal}	**Hub regions (index)**	aE_{nodal}
16	0.0082	8	0.0103	7	0.0118	7	0.0130
23	0.0087	9	0.0092	8	0.0089	8	0.0143
25	0.0088	16	0.0088	16	0.0087	23	0.0136
29	0.0091	23	0.0105	23	0.0092	30	0.0148
31	0.0084	25	0.0102	25	0.0089	42	0.0105
42	0.0087	26	0.0089	30	0.0107	43	0.0087
44	0.0086	30	0.0104	32	0.0082	46	0.0100
59	0.0097	31	0.0083	38	0.0086	48	0.0100
60	0.0089	32	0.0101	41	0.0092	50	0.0100
62	0.0081	43	0.0082	42	0.0090	56	0.0087
63	0.0093	46	0.0086	46	0.0096	57	0.0107
64	0.0087	48	0.0090	50	0.0089	59	0.0104
66	0.0082	56	0.0085	57	0.0086	60	0.0091
		57	0.0097	59	0.0084	64	0.0083
		59	0.0089	60	0.0099		
		60	0.0097	64	0.0119		
		64	0.0094				
		66	0.0089				

*The nodes were considered brain hubs if their nodal efficiencies were at least 1 SD greater than the average nodal efficiency of the network. The corresponding indexes (see **Appendix Table A1**) are listed.*

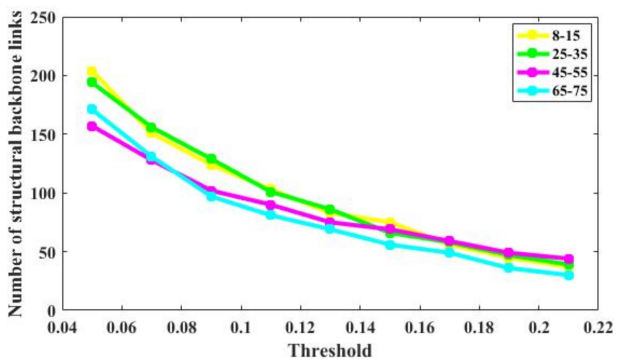

FIGURE 6 | Number of backbone links of the structural connectivity networks of the four age groups. For the 65–75 group, the number of backbone links is decreases significantly. For other groups, there are some minor differences.

model neural tracking that cannot resolve multiple fiber populations in a DWI voxel.

To examine the topological changes that occur over the lifespan here, a quadratic regression model was fit to the AUC values of each network metric (**Figure 4**). These results suggest that the lifetime development of structural cortical networks follows a non-linear trajectory. From 7 to 35 years, brain networks strengthen with growth, training, and learning. From 35 to 75 years, however, the network is gradually reduced as overall cortical connectivity declines. These results are mostly consistent with a recent study performed by Zhao et al. (2015), which found a similar non-linear trajectory of structural changes. The present study then investigated the patterns of specific network topological properties. In this way, global efficiency, local efficiency, small-worldness, and cluster coefficients were found to follow negative parabolic trajectories, while characteristic pathway lengths followed a positive parabolic trajectory.

These findings complement the negative parabolic trajectories that were uncovered for the global network properties (Zhao et al., 2015), including network strength, cost, topological efficiency, and robustness. Together, these results suggest that the overall shape of graph network trajectories is consistent and that SC network changes during development and aging are non-linear. These results, then, identify possible structural substrates underlying functional and cognitive changes during development and aging and may be important for separating pathogenic changes from normal aging processes. Some minor differences between these two studies may arise from differences in the dataset, tractography method, and brain parcellation schemes. The current EAP-based probabilistic tractography method has shown to improve fiber tracking accuracy (Descoteaux et al., 2009). Given the scarcity of data, future studies will be required to further corroborate these important findings.

To identify the hub regions, we examined the nodal efficiency of each cortical region. In the 8–15 age group, 13 regions were identified as the hubs by their large nodal efficiency E_{nodal} values. In the 25–35 and 45–55 age groups, 18 and 16 regions were identified as the hubs, respectively, and 14 regions were identified as hubs in the 65–75 age group (**Table 4**). Identified hubs were predominately located in regions of the frontal and parietal cortices that connected with multiple other cortical regions (Mesulam, 1998). This dense interconnectivity suggests their pivotal roles in the human structural cortical networks.

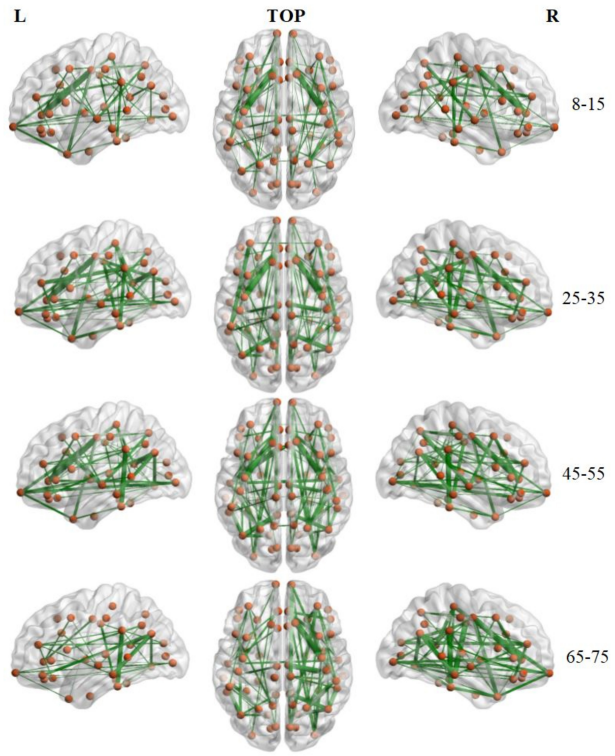

FIGURE 7 | Backbone connections of brain structural connectivity networks of four groups at the strength threshold of 0.21. The links were mapped into the brain at the left, top, and right views. The edge widths represent the connection weights between nodes. The brain graphs were visualized by using BrainNet Viewer software (Xia et al., 2013).

The findings align with several previous studies, in which these cortical regions were identified as critical nodes in both structural and functional brain networks in humans (Achard et al., 2006; He et al., 2007). Finally, it should be noted that only the 3rd and 4th age groups included data from both the OASIS3 and HCP datasets. Consequently, these groups included subjects who were scanned using different systems with different acquisition parameters. Although the overall data showed the same trends, the effect that these protocol variations may have had on network construction remains to be studied.

Backbone connections were then investigated across age groups. Although all age groups showed decreases in the backbone number as the threshold increased, the number of backbone connections in the 65–75 years group showed a particularly noteworthy reduction (**Figure 6**). The connections that survived at the highest threshold value were primarily composed of the prefrontal cortex and the insular cortex (**Figure 7**). These results suggest a strong correlation between the SC wiring within the prefrontal and insular cortex and the behavioral symptoms of old age, such as inattention and amnesia. While the adoption of a lower threshold may provide a more comprehensive snapshot of the structural network, probability-based approaches carry the possibility of identifying spurious nerve fiber connections between regions that are not biologically connected. The use of a high probability threshold may assuage this issue and suggests that present results are not dependent on an arbitrarily chosen threshold. To ensure that spurious connections were removed, a range of thresholds were applied between 0.05 and 0.21 in intervals of 0.02. Links whose connection strength fell below the chosen threshold were excluded from topological analysis ensuring that only strong connections were retained. Despite the tested range, no threshold value caused a significant change in the non-linear patterns of age-dependent brain structural connectivity networks.

The human brain undergoes both macro- and micro-scale structural changes throughout its lifespan (Lebel and Deoni, 2018). The white matter plasticity in response to learning or environmental stimuli can alter the brain's structural connectivity network, although the magnitude and time course of these changes can vary. Comprehensive lifespan studies provide valuable insight into the processes of macrostructural brain changes and have contributed to our understanding of brain development (Gong et al., 2009; Hagmann et al., 2010; Betzel et al., 2014; Otte et al., 2015; Zhao et al., 2015). The large-scale brain changes during development provide a context for studying white matter changes at the macroscopic level. The current work aimed to characterize normative brain development from 8 to 75 years, emphasizing group-wise comparative studies and statistical techniques to study structural connectivity network development. Previous studies have demonstrated consistent, rapid white matter development over the first 3 years of life, suggesting increased myelination and axonal packing (Huang et al., 2013). Results here clearly demonstrates that the structural connectivity network continually strengthens during later childhood, adolescence, and adulthood, due to white matter changes.

There are several limitations to this study. First, this study had a relatively small sample size (N = 48) and results should be interpreted in that context. Nevertheless, the parabolic patterns of functional changes observed using the novel EAP method are promising, suggesting that an EAP-based method is a reliable tool

TABLE 5 | Connection strength of backbone links at different thresholds.

	>0.05	>0.09	>0.13	>0.17	>0.21
8–15	0.1414 ± 0.0947	0.1900 ± 0.0932	0.2295 ± 0.0904	0.2660 ± 0.0892	0.3066 ± 0.0842
25–5	0.1556 ± 0.1157	0.1993 ± 0.1198	0.2457 ± 0.1225	0.2947 ± 0.1218	0.3467 ± 0.1172
45–55	0.1675 ± 0.1200	0.2207 ± 0.1183	0.2603 ± 0.1143	0.2904 ± 0.1109	0.3254 ± 0.1077
65–75	0.1409 ± 0.1050	0.1956 ± 0.1115	0.2304 ± 0.1150	0.2657 ± 0.1195	0.3154 ± 0.1303

These values are probability values (mean ± SD) of links in each group.

for future studies. These preliminary findings will require further corroboration from future studies with larger-sample sizes. Second, a probabilistic tractography method based on EAP was used to construct whole-brain neural connectivity, which is more capable of tracking complicated fiber tracts than deterministic tractography methods (Behrens et al., 2007). While this provides a better reconstruction of the brain structural network, the reliance on a probabilistic method allows for connections to be drawn between regions that are not biologically linked. Spurious connections are likely to show limited connection strength, however, so the adoption of a high probability threshold should minimize this issue, and the number of remaining connections further suggests that results were not dependent on an arbitrarily chosen threshold.

Third, the whole-brain structural connectivity networks were only derived from DWI data. The brain networks can also be studied using both structural and functional MRI data. The combination of multimodal neuroimaging techniques should add considerably to our understandings of how age-linked structural disruptions in neuronal circuits are associated with functional alterations. Lastly, subjects from the different datasets (HCP and OASIS3) were collected using different scanners and different acquisition protocols, the effects of which are currently unknown and require further study. Although T1-weighted images were denoised through a non-local SVD method (Wu et al., 2019b), alleviating the possible influences of white matter hyperintensities (WMH) on the WM segmentation, future investigations will be necessary to understand the extent to which WMHs could affect EAP calculation (Popescu et al., 2014; Valverde et al., 2014; Prados et al., 2016). Finally, several studies have suggested that the graphic metrics of whole-brain structural connectivity networks are heavily dependent on the resolution of their cortex parcellation (Wang et al., 2009). In the future, different parcellation schemes should be used in conjunction to provide a holistic investigation of topological SC network features.

CONCLUSION

Non-linear parabolic patterns of age-dependent brain structural connectivity network properties were observed across the age ranges of 8–75 years using a probabilistic Ensemble Average Propagator-based tractography method. This novel method provided a reliable method to construct macroscale structural connectivity networks that capture age-associated changes in brain structure. This study reveals new insights into age related changes in cognitive function that are observed clinically and starts the process of helping us understand where to focus our efforts at understanding the very important, age-related brain changes that markedly increase vulnerability to neurodegenerative disorders. Understanding age-related vulnerability, in turn, will help us design methods to reduce these age related risks.

DATA AVAILABILITY STATEMENT

The datasets generated for this study are available on request to the corresponding author.

ETHICS STATEMENT

Ethical review and approval was not required for the study on human participants in accordance with the local legislation and institutional requirements. The patients/participants provided their written informed consent to participate in this study.

AUTHOR CONTRIBUTIONS

ZW conducted the data analysis, result summarization, and manuscript drafting. YP contributed to study design, result preparation, and manuscript revising. SS and PS contributed to study design and manuscript revising with clinical knowledge. YZ contributed to study design, result review, manuscript revising, and finalization.

FUNDING

The research was supported by Natural Science Foundation of Zhejiang Province (LY20E070005 and LY17E070007), China, National Natural Science Foundation of China (51207038), and the University of Houston. Thirty four datasets were provided by Human Connectome Project, WU-Minn Consortium (Principal Investigators: David Van Essen and Kamil Ugurbil; 1U54MH091657) funded by the 16 NIH Institutes and Centers that support the NIH Blueprint for Neuroscience Research; and by the McDonnell Center for Systems Neuroscience at Washington University. Other 14 datasets were selected from OASIS3 project (P50 AG05681, P01 AG03991, R01 AG021910, P50 MH071616, U24 RR021382, and R01 MH56584).

REFERENCES

Achard, P., Cheng, H., De Grauwe, L., Decat, J., Schoutteten, H., Moritz, T., et al. (2006). Integration of plant responses to environmentally activated phytohormonal signals. *Science* 311, 91–94. doi: 10.1126/science.1118642

Anderson, A. W. (2005). Measurement of fiber orientation distributions using high angular resolution diffusion imaging. *Magn. Reson. Med.* 54, 1194–1206. doi: 10.1002/mrm.20667

Andersson, J. L., Skare, S., and Ashburner, J. (2003). How to correct susceptibility distortions in spin-echo echo-planar images: application to diffusion tensor imaging. *Neuroimage* 20, 870–888. doi: 10.1016/s1053-8119(03)00336-7

Andersson, J. L., and Sotiropoulos, S. N. (2015). Non-parametric representation and prediction of single-and multi-shell diffusion-weighted MRI data using Gaussian processes. *Neuroimage* 122, 166–176. doi: 10.1016/j.neuroimage.2015.07.067

Andersson, J. L., and Sotiropoulos, S. N. (2016). An integrated approach to correction for off-resonance effects and subject movement in diffusion MR imaging. *Neuroimage* 125, 1063–1078. doi: 10.1016/j.neuroimage.2015.10.019

Assemlal, H. E., Tschumperlé, D., and Brun, L. (2007). "Fiber tracking on HARDI data using robust ODF fields," in *Proceedings of the IEEE International Conference on Image Xplore*, San Antonio, TX, 133–136.

Banerjee, M., Okun, M. S., Vaillancourt, D. E., and Vemuri, B. (2016). A method for automated classification of Parkinson's disease diagnosis using an Ensemble Average Propagator template brain map estimated from diffusion MRI. *PLoS One* 11:e0155764. doi: 10.1371/journal.pone.0155764

Bassett, D. S., Brown, J. A., Deshpande, V., Carlson, J. M., and Grafton, S. T. (2011). Conserved and variable architecture of human white matter connectivity. *Neuroimage* 54, 1262–1279. doi: 10.1016/j.neuroimage.2010.09.006

Behrens, T. E., Berg, H. J., Jbabdi, S., Rushworth, M. F., and Woolrich, M. W. (2007). Probabilistic diffusion tractography with multiple fibre orientations: what can we gain? *Neuroimage* 34, 144–155. doi: 10.1016/j.neuroimage.2006.09.018

Betzel, R. F., Byrge, L., He, Y., Goñi, J., Zuo, X. N., and Sporns, O. (2014). Changes in structural and functional connectivity among resting-state networks across the human lifespan. *Neuroimage* 102, 345–357. doi: 10.1016/j.neuroimage.2014.07.067

Brusini, L., Obertino, S., Galazzo, I. B., Zucchelli, M., Krueger, G., Granziera, C., et al. (2016). Ensemble average propagator-based detection of microstructural alterations after stroke. *Int. J. Comput. Assist. Radiol. Surg.* 11, 1585–1597. doi: 10.1007/s11548-016-1442-z

Burzynska, A. Z., Preuschhof, C., Bäckman, L., Nyberg, L., Lim, S. C., Lindenberger, U., et al. (2010). Age-related differences in white matter microstructure: region-specific patterns of diffusivity. *Neuroimage* 49, 2104–2112. doi: 10.1016/j.neuroimage.2009.09.041

Cao, Q., Shu, N., An, L., Wang, P., Sun, L., Xia, M. R., et al. (2013). Probabilistic diffusion tractography and graph theory analysis reveal abnormal white matter structural connectivity networks in drug-naive boys with attention deficit/hyperactivity disorder. *J. Neurosci.* 33, 10676–10687. doi: 10.1523/jneurosci.4793-12.2013

Cheng, J., Ghosh, A., Jiang, T., and Deriche, R. (2010). "Model-free and analytical EAP reconstruction via spherical polar Fourier diffusion MRI," in *Proceedings of the International Conference on Medical Image Computing and Computer-Assisted Intervention*, (Berlin: Springer), 590–597. doi: 10.1007/978-3-642-15705-9_72

Damoiseaux, J. S. (2017). Effects of aging on functional and structural brain connectivity. *Neuroimage* 160, 32–40. doi: 10.1016/j.neuroimage.2017.01.077

Damoiseaux, J. S., Beckmann, C., Arigita, E. S., Barkhof, F., Scheltens, P., Stam, C., et al. (2007). Reduced resting-state brain activity in the "default network" in normal aging. *Cereb. Cortex* 18, 1856–1864. doi: 10.1093/cercor/bhm207

Dennis, E. L., and Thompson, P. M. (2014). Functional brain connectivity using fMRI in aging and Alzheimer's disease. *Neuropsychol. Rev.* 24, 49–62. doi: 10.1093/cercor/bhu259

Descoteaux, M., Deriche, R., Knosche, T. R., and Anwander, A. (2009). Deterministic and probabilistic tractography based on complex fibre orientation distributions. *IEEE Trans. Med. Imaging* 28, 269–286. doi: 10.1109/TMI.2008.2004424

Desikan, R. S., Ségonne, F., Fischl, B., Quinn, B. T., Dickerson, B. C., Blacker, D., et al. (2006). An automated labeling system for subdividing the human cerebral cortex on MRI scans into gyral based regions of interest. *Neuroimage* 31, 968–980. doi: 10.1016/j.neuroimage.2006.01.021

Duarte-Carvajalino, J. M., Lenglet, C., Xu, J., Yacoub, E., Ugurbil, K., Moeller, S., et al. (2014). Estimation of the CSA-ODF using Bayesian compressed sensing of multi-shell HARDI. *Magn. Reson. Med.* 72, 1471–1485. doi: 10.1002/mrm.25046

Feinberg, D. A., Moeller, S., Smith, S. M., Auerbach, E., Ramanna, S., Glasser, M. F., et al. (2010). Multiplexed echo planar imaging for sub-second whole brain FMRI and fast diffusion imaging. *PLoS One* 5:e15710. doi: 10.1371/journal.pone.0015710

Fick, R. H., Wassermann, D., Sanguinetti, G., and Deriche, R. (2014). An analytical 3D Laplacian regularized SHORE basis and its impact on EAP reconstruction and microstructure recovery. *Math. Vis.* 39, 151–165. doi: 10.1007/978-3-319-11182-7_14

Fischl, B. (2012). FreeSurfer. *Neuroimage* 62, 774–781. doi: 10.1016/j.neuroimage.2012.01.021

Frank, L. R. (2002). Characterization of anisotropy in high angular resolution diffusion-weighted MRI. *Magn. Reson. Med.* 47, 1083–1099. doi: 10.1002/mrm.10156

Geerligs, L., Renken, R. J., Saliasi, E., Maurits, N. M., and Lorist, M. M. (2014). A brain-wide study of age-related changes in functional connectivity. *Cereb. Cortex* 25, 1987–1999. doi: 10.1093/cercor/bhu012

Gong, G., Rosa-Neto, P., Carbonell, F., Chen, Z. J., He, Y., and Evans, A. C. (2009). Age-and gender-related differences in the cortical anatomical network. *J. Neurosci.* 29, 15684–15693. doi: 10.1523/JNEUROSCI.2308-09.2009

Grady, C., Sarraf, S., Saverino, C., and Campbell, K. (2016). Age differences in the functional interactions among the default, frontoparietal control, and dorsal attention networks. *Neurobiol. Aging* 41, 159–172. doi: 10.1016/j.neurobiolaging.2016.02.020

Hagmann, P., Cammoun, L., Gigandet, X., Meuli, R., Honey, C. J., Wedeen, V. J., et al. (2008). Mapping the structural core of human cerebral cortex. *PLoS Biol.* 6:e159. doi: 10.1371/journal.pbio.0060159

Hagmann, P., Sporns, O., Madan, N., Cammoun, L., Pienaar, R., Wedeen, V. J., et al. (2010). White matter maturation reshapes structural connectivity in the late developing human brain. *Proc. Natl. Acad. Sci. U.S.A.* 107, 19067–19072. doi: 10.1073/pnas.1009073107

He, Y., Chen, Z. J., and Evans, A. C. (2007). Small-world anatomical networks in the human brain revealed by cortical thickness from MRI. *Cereb. Cortex* 17, 2407–2419. doi: 10.1093/cercor/bhl149

He, Y., Wang, J., Wang, L., Chen, Z. J., Yan, C., Yang, H., et al. (2009). Uncovering intrinsic modular organization of spontaneous brain activity in humans. *PLoS One* 4:e5226. doi: 10.1371/journal.pone.0005226

Hess, C. P., Mukherjee, P., Han, E. T., Xu, D., and Vigneron, D. B. (2006). Q-ball reconstruction of multimodal fiber orientations using the spherical harmonic basis. *Magn. Reson. Med.* 56, 104–117. doi: 10.1002/mrm.20931

Huang, C. C., Hsieh, W. J., Lee, P. L., Peng, L. N., Liu, L. K., Lee, W. J., et al. (2015). Age-related changes in resting-state networks of a large sample size of healthy elderly. *CNS Neurosci. Ther.* 21, 817–825. doi: 10.1111/cns.12396

Huang, H., Shu, N., Mishra, V., Jeon, T., Chalak, L., Wang, Z. J., et al. (2013). Development of human brain structural networks through infancy and childhood. *Cereb. Cortex* 25, 1389–1404. doi: 10.1093/cercor/bht335

Iturria-Medina, Y., Canales-Rodriguez, E., Melie-Garcia, L., Valdes-Hernandez, P., Martinez-Montes, E., Alemán-Gómez, Y., et al. (2007). Characterizing brain anatomical connections using diffusion weighted MRI and graph theory. *Neuroimage* 36, 645–660. doi: 10.1016/j.neuroimage.2007.02.012

Iturria-Medina, Y., Sotero, R. C., Canales-Rodríguez, E. J., Alemán-Gómez, Y., and Melie-García, L. (2008). Studying the human brain anatomical network via diffusion-weighted MRI and Graph Theory. *Neuroimage* 40, 1064–1076. doi: 10.1016/j.neuroimage.2007.10.060

Lebel, C., and Deoni, S. (2018). The development of brain white matter microstructure. *Neuroimage* 182, 207–218. doi: 10.1016/j.neuroimage.2017.12.097

Lerch, J. P., van der Kouwe, A. J., Raznahan, A., Paus, T., Johansen-Berg, H., Miller, K. L., et al. (2017). Studying neuroanatomy using MRI. *Nat. Neurosci.* 20, 314–326. doi: 10.1038/nn.4501

Maier-Hein, K. H., Neher, P. F., Houde, J. C., Côté, M. A., Garyfallidis, E., Zhong, J., et al. (2017). The challenge of mapping the human connectome based on diffusion tractography. *Nat. Commun.* 8:1349. doi: 10.1038/s41467-017-01285-x

Marcus, D., Harwell, J., Olsen, T., Hodge, M., Glasser, M., Prior, F., et al. (2011). Informatics and data mining tools and strategies for the human connectome project. *Front. Neuroinform.* 5:4. doi: 10.3389/fninf.2011.00004

Mesulam, M. M. (1998). From sensation to cognition. *Brain* 121, 1013–1052. doi: 10.1093/brain/121.6.1013

Onoda, K., Ishihara, M., and Yamaguchi, S. (2012). Decreased functional connectivity by aging is associated with cognitive decline. *J. Cogn. Neurosci.* 24, 2186–2198. doi: 10.1162/jocn_a_00269

Otte, W. M., van Diessen, E., Paul, S., Ramaswamy, R., Rallabandi, V. S., Stam, C. J., et al. (2015). Aging alterations in whole-brain networks during adulthood mapped with the minimum spanning tree indices: the interplay of density, connectivity cost and life-time trajectory. *Neuroimage* 109, 171–189. doi: 10.1016/j.neuroimage.2015.01.011

Paquette, M., Merlet, S., Gilbert, G., Deriche, R., and Descoteaux, M. (2015). Comparison of sampling strategies and sparsifying transforms to improve compressed sensing diffusion spectrum imaging. *Magn. Reson. Med.* 73, 401–416. doi: 10.1002/mrm.25093

Paus, T., Zijdenbos, A. P., Worsley, K., Collins, L., Blumenthal, J., Giedd, J. N., et al. (1999). Structural maturation of neural pathways in children and adolescents: in vivo study. *Science* 283, 1908–1911. doi: 10.1126/science.283.5409.1908

Peters, A. (2002). The effects of normal aging on myelin and nerve fibers: a review. *J. Neurocytol.* 31, 581–593.

Popescu, V., Ran, N. C. G., Barkhof, F., Chard, D. T., Wheeler-Kingshott, C. A., and Vrenken, H. (2014). Accurate gm atrophy quantification in ms using lesion-filling with co-registered 2d lesion masks. *Neuroimage Clin.* 4, 366–373. doi: 10.1016/j.nicl.2014.01.004

Poupon, C., Rieul, B., Kezele, I., Perrin, M., Poupon, F., and Mangin, J. F. (2008). New diffusion phantoms dedicated to the study and validation of high-angular-resolution diffusion imaging (HARDI) models. *Magn. Reson. Med.* 60, 1276–1283. doi: 10.1002/mrm.21789

Prados, F., Cardoso, M. J., Kanber, B., Ciccarelli, O., and Ourselin, S. (2016). A multi-time-point modality-agnostic patch-based method for lesion filling in multiple sclerosis. *Neuroimage* 139, 376–384. doi: 10.1016/j.neuroimage.2016.06.053

Rubinov, M., and Sporns, O. (2010). Complex network measures of brain connectivity: uses and interpretations. *Neuroimage* 52, 1059–1069. doi: 10.1016/j.neuroimage.2009.10.003

Schmahmann, J. D., Pandya, D. N., Wang, R., Dai, G., D'arceuil, H. E., de Crespigny, A. J., et al. (2007). Association fibre pathways of the brain: parallel observations from diffusion spectrum imaging and autoradiography. *Brain* 130, 630–653. doi: 10.1093/brain/awl359

Sotiropoulos, S. N., Bai, L., Morgan, P. S., Constantinescu, C. S., and Tench, C. R. (2010). Brain tractography using Q-ball imaging and graph theory: improved connectivities through fibre crossings via a model-based approach. *Neuroimage* 49, 2444–2456. doi: 10.1016/j.neuroimage.2009.10.001

Sporns, O. (2013). Network attributes for segregation and integration in the human brain. *Curr. Opin. Neurobiol.* 23, 162–171. doi: 10.1016/j.conb.2012.11.015

Supekar, K., Uddin, L. Q., Prater, K., Amin, H., Greicius, M. D., and Menon, V. (2010). Development of functional and structural connectivity within the default mode network in young children. *Neuroimage* 52, 290–301. doi: 10.1016/j.neuroimage.2010.04.009

Tuch, D. S. (2004). Q-ball imaging. *Magn. Reson. Med.* 52, 1358–1372.

Tuch, D. S., Reese, T. G., Wiegell, M. R., Makris, N., Belliveau, J. W., and Wedeen, V. J. (2002). High angular resolution diffusion imaging reveals intravoxel white matter fiber heterogeneity. *Magn. Reson. Med.* 48, 577–582. doi: 10.1002/mrm.10268

Valverde, S., Oliver, A., and Lladó, X. (2014). A white matter lesion-filling approach to improve brain tissue volume measurements. *Neuroimage Clin.* 6, 86–92. doi: 10.1016/j.nicl.2014.08.016

van den Heuvel, M. P., Kahn, R. S., Goñi, J., and Sporns, O. (2012). High-cost, high-capacity backbone for global brain communication. *Proc. Natl. Acad. Sci. U.S.A.* 109, 11372–11377. doi: 10.1073/pnas.1203593109

van den Heuvel, M. P., and Sporns, O. (2013). Network hubs in the human brain. *Trends Cogn. Sci.* 17, 683–696. doi: 10.1016/j.tics.2013.09.012

Van Essen, D. C., Smith, S. M., Barch, D. M., Behrens, T. E., Yacoub, E., Ugurbil, K., et al. (2013). The WU-Minn human connectome project: an overview. *Neuroimage* 80, 62–79. doi: 10.1016/j.neuroimage.2013.05.041

Wang, J., Wang, L., Zang, Y., Yang, H., Tang, H., Gong, Q., et al. (2009). Parcellation-dependent small-world brain functional networks: a resting-state fMRI study. *Hum. Brain Mapp.* 30, 1511–1523. doi: 10.1002/hbm.20623

Wang, J., Wang, X., Xia, M., Liao, X., Evans, A., and He, Y. (2015). GRETNA: a graph theoretical network analysis toolbox for imaging connectomics. *Front. Hum. Neurosci.* 9:386. doi: 10.3389/fnhum.2015.00386

Wu, Z., Peng, Y., Xu, D., Hong, M., and Zhang, Y. (2019a). Construction of brain structural connectivity network using a novel integrated algorithm based on ensemble average propagator. *Comput. Biol. Med.* 112:103384. doi: 10.1016/j.compbiomed.2019.103384

Wu, Z., Xu, D., Potter, T., and Zhang, Y. (2019b). Denoising high angular resolution diffusion imaging data by combining singular value decomposition and non-local means filter. *J. Neurosci. Methods* 312, 105–113. doi: 10.1016/j.jneumeth.2018.11.020

Wu, Z., Yu, X., Liu, Y., and Hong, M. (2018). A PSO-Powell hybrid method to extract fiber orientations from ODF. *Comput. Math. Methods Med.* 2018:7680164.

Xia, M., Wang, J., and He, Y. (2013). BrainNet Viewer: a network visualization tool for human brain connectomics. *PLoS One.* 8:e68910. doi: 10.1371/journal.pone.0068910

Zhao, T., Cao, M., Niu, H., Zuo, X. N., Evans, A., He, Y., et al. (2015). Age-related changes in the topological organization of the white matter structural connectome across the human lifespan. *Hum. Brain Mapp.* 36, 3777–3792. doi: 10.1002/hbm.22877

Zucchelli, M., Brusini, L., Méndez, C. A., Daducci, A., Granziera, C., and Menegaz, G. (2016). What lies beneath? Diffusion EAP-based study of brain tissue microstructure. *Med. Image Anal.* 32, 145–156. doi: 10.1016/j.media.2016.03.008

Conflict of Interest: The authors declare that the research was conducted in the absence of any commercial or financial relationships that could be construed as a potential conflict of interest.

APPENDIX

The cerebral cortex was parcellated into 68 functional areas, 34 for each hemisphere. The indexes and their corresponding names of function regions are provided in **Appendix Table A1**.

TABLE A1 | Cerebral cortex was parcellated into 68 functional areas, 34 for each hemisphere.

Index	Region	Index	Region	Index	Region	Index	Region
1	lh.bankssts	18	lh.parahippocampal	35	rh.bankssts	52	rh.parahippocampal
2	lh.caudalanteriorcingulate	19	lh.parsopercularis	36	rh.caudalanteriorcingulate	53	rh.parsopercularis
3	lh.caudalmiddlefrontal	20	lh.parsorbitalis	37	rh.caudalmiddlefrontal	54	rh.parsorbitalis
4	lh.cuneus	21	lh.parstriangularis	38	rh.cuneus	55	rh.parstriangularis
5	lh.entorhinal	22	lh.pericalcarine	39	rh.entorhinal	56	rh.pericalcarine
6	lh.frontalpole	23	lh.postcentral	40	rh.frontalpole	57	rh.postcentral
7	lh.fusiform	24	lh.posteriorcingulate	41	rh.fusiform	58	rh.posteriorcingulate
8	lh.inferiorparietal	25	lh.precentral	42	rh.inferiorparietal	59	rh.precentral
9	lh.inferiortemporal	26	lh.precuneus	43	rh.inferiortemporal	60	rh.precuneus
10	lh.insula	27	lh.rostralanteriorcingulate	44	rh.insula	61	rh.rostralanteriorcingulate
11	lh.isthmuscingulate	28	lh.rostralmiddlefrontal	45	rh.isthmuscingulate	62	rh.rostralmiddlefrontal
12	lh.lateraloccipital	29	lh.superiorfrontal	46	rh.lateraloccipital	63	rh.superiorfrontal
13	lh.lateralorbitofrontal	30	lh.superiorparietal	47	rh.lateralorbitofrontal	64	rh.superiorparietal
14	lh.lingual	31	lh.superiortemporal	48	rh.lingual	65	rh.superiortemporal
15	lh.medialorbitofrontal	32	lh.supramarginal	49	rh.medialorbitofrontal	66	rh.supramarginal
16	lh.middletemporal	33	lh.temporalpole	50	rh.middletemporal	67	rh.temporalpole
17	lh.paracentral	34	lh.transversetemporal	51	rh.paracentral	68	rh.transversetemporal

The prefix of lh indicates left hemisphere, and rh represents right hemisphere. The numbers are the indexes of function regions.

frontiers in Aging Neuroscience

ORIGINAL RESEARCH
published: 17 March 2020
doi: 10.3389/fnagi.2020.00071

Longitudinal Changes in Whole-Brain Functional Connectivity Strength Patterns and the Relationship With the Global Cognitive Decline in Older Adults

Qiongge Li[1†], Chao Dong[1,2†], Tao Liu[1,3,4], Xiaodan Chen[5,6], Alistair Perry[7], Jiyang Jiang[2], Jian Cheng[3], Haijun Niu[1,4], Nicole A. Kochan[2,8], Henry Brodaty[2,9], Perminder S. Sachdev[2,8,9] and Wei Wen[2,8]*

[1] School of Biological Science and Medical Engineering, Beihang University, Beijing, China, [2] Centre for Healthy Brain Aging, School of Psychiatry, University of New South Wales, Sydney, NSW, Australia, [3] Beijing Advanced Innovation Center for Big Data-Based Precision Medicine, Beihang University, Beijing, China, [4] Beijing Advanced Innovation Center for Biomedical Engineering, Beihang University, Beijing, China, [5] National Key Laboratory of Cognitive Neuroscience and Learning, Beijing Normal University, Beijing, China, [6] Beijing Key Laboratory of Brain Imaging and Connectomics, Beijing Normal University, Beijing, China, [7] Max Planck UCL Centre for Computational Psychiatry and Aging Research, Berlin, Germany, [8] Neuropsychiatric Institute, Prince of Wales Hospital, Sydney, NSW, Australia, [9] Dementia Centre for Research Collaboration, School of Psychiatry, University of New South Wales, Sydney, NSW, Australia

OPEN ACCESS

Edited by:
Reinhold Schmidt, Medical University of Graz, Austria

Reviewed by:
Robert Langner, Heinrich Heine University Düsseldorf, Germany
Marisa Heckner, Heinrich Heine University Düsseldorf, Germany, in collaboration with reviewer RL
Andrea T. Shafer, National Institutes of Health (NIH), United States

***Correspondence:**
Tao Liu
tao.liu@buaa.edu.cn;
taoliu_nature@163.com

† These authors have contributed equally to this work

Received: *04 August 2019*
Accepted: *26 February 2020*
Published: *17 March 2020*

Citation:
Li Q, Dong C, Liu T, Chen X, Perry A, Jiang J, Cheng J, Niu H, Kochan NA, Brodaty H, Sachdev PS and Wen W (2020) Longitudinal Changes in Whole-Brain Functional Connectivity Strength Patterns and the Relationship With the Global Cognitive Decline in Older Adults. Front. Aging Neurosci. 12:71. doi: 10.3389/fnagi.2020.00071

Aging is associated with changes in brain functional patterns as well as cognition. The present research sought to investigate longitudinal changes in whole brain functional connectivity strength (FCS) and cognitive performance scores in very old cognitively unimpaired individuals. We studied 34 cognitively normal elderly individuals at both baseline and 4-year follow-up (baseline age = 78 ± 3.14 years) with resting-state functional magnetic resonance imaging (r-fMRI), structural MRI scans, and neuropsychological assessments conducted. Voxel-based whole brain FCS was calculated and we found that bilateral superior parietal and medial frontal regions showed decreased FCS, while the supplementary motor area (SMA) and insula showed increased FCS with age, along with a decrease in bilateral prefrontal cortical thickness. The changes of FCS in left precuneus were associated with an aging-related decline in global cognition. Taken together, our results suggest changes in FCS with aging with the precuneus as a hub and this may underlie changes in global cognition that accompany aging. These findings help better understand the normal aging mechanism.

Keywords: aging, functional connectivity strength, global cognition, longitudinal changes, resting-state fMRI

INTRODUCTION

Normal aging has been associated with cognitive decline, affecting various cognitive domains such as processing speed, memory, and executive function (Hedden and Gabrieli, 2004; Fjell et al., 2015, 2017). Cognitive performance which may change with age is associated with communication between brain regions, as well as extrinsic interactions between functional networks

(Fox et al., 2005; Onoda et al., 2012; Fjell et al., 2016; Perry et al., 2017). However, there are few resting-state functional magnetic resonance imaging (r-fMRI) studies investigating how age-related brain functional connectivity and their relationships with cognition evolve over time in cognitively unimpaired older adults.

Most r-fMRI studies have reported that aging-related functional connectivity decrements preferentially affect the default mode network (DMN) (Damoiseaux et al., 2008; Koch et al., 2010; Wang et al., 2010; Tomasi and Volkow, 2012) and the dorsal attentional network (DAN; Tomasi and Volkow, 2012) (for a comprehensive review, see Ferreira and Busatto, 2013). Previous longitudinal studies about functional connectivity have brought new insights into aging (Fjell et al., 2016; Salami et al., 2016). A longitudinal study found that inter-network functional connectivity between executive control network and DMN showed a U-shaped trajectory, initially increasing over time and later decreasing as participants aged (Ng et al., 2016). A recent study also found that whole-brain and DMN functional connectivity exhibited a non-linear trajectory (Staffaroni et al., 2018). However, most of the previous aging-related studies explored the aging brain by comparing resting-state functional connectivity, few have compared whole brain functional connectivity strength (FCS) which can permit a comprehensive characterization of the functional properties of each voxel (Boccaletti et al., 2006; Rubinov and Sporns, 2010). FCS is computed by summing weights of all the connections of a given voxel that exceeded a predefined optimized threshold, and it is also known as weighted degree centrality (Buckner et al., 2009). Brain regions with relatively high FCS can be regarded as functional hubs in large-scale brain networks (Buckner et al., 2009; Tomasi and Volkow, 2011; Dai et al., 2015). Furthermore, the whole brain voxel-based FCS applied in the current study can enable whole brain hub mapping but avoid parcellation-dependency (Smith et al., 2011). To the best of our knowledge, no study has yet investigated the longitudinal changes in whole brain FCS of cognitively unimpaired older individuals.

Longitudinal studies have indicated that decreased functional connectivity within DMN, particularly the precuneus/posterior cingulate cortex (PCC), was correlated with memory declines (Persson et al., 2014; Bernard et al., 2015), episodic memory, and processing speed changes (Staffaroni et al., 2018). However, the relationship between longitudinal changes of whole brain FCS and longitudinal changes of cognitive performance scores, especially global cognition, in very old cognitively unimpaired people are poorly understood. In addition, a longitudinal study over a mean follow-up interval of 8 years found that age-related decline in cortical thickness is widespread (Thambisetty et al., 2010). A recent study highlights that cortical thickness changes should be considered when evaluating the standard deviation (SD) of the BOLD signal alternations in the lifespan (Pur et al., 2019). Therefore, investigation about longitudinal FCS and cognition combined with longitudinal cortical thickness may be a useful tool to detect perturbations in brain function and structure in cognitively normal subjects.

In the current study, first, we sought to determine the FCS patterns at two time points and whether there are significant FCS changes between two time points. We then sought to verify whether the observed changes in FCS are influenced by gray matter volume. Second, we aimed to find whether 4-year FCS changes are related to the significantly decreased cognitive domains. In addition, we aimed to explore whether there are cortical thickness changes in 4-year's follow-up, which can help to understand the brain-aging mechanism.

MATERIALS AND METHODS

Participants

Participants were drawn from the Sydney Memory and Aging Study (MAS), a longitudinal study of non-demented, community-dwelling individuals aged 70–90 years old at baseline (Sachdev et al., 2010). MAS participants were recruited randomly from the eastern suburbs of Sydney, Australia, using the electoral roll, for which registration is compulsory for Australian citizens. At baseline, each of 1037 MAS participants was administered a comprehensive neuropsychological test battery, and 542 (52.3%) also had an MRI scan. Individuals were excluded if they had a Mini-Mental State Examination (MMSE) score < 24 (Folstein et al., 1975; Anderson et al., 2007), a diagnosis of dementia, mental retardation, psychotic disorder (including schizophrenia and bipolar disorder), multiple sclerosis, motor neuron disease, progressive malignancy, or inadequate English to complete assessments. Participants were classified as cognitively unimpaired if performance on all test measures was above the 6.68 percentile (-1.5 SDs) or equivalent score compared to normative published values, they were not demented, and they had normal function or minimal impairment in IADLs defined by a total average score < 3.0 on the Bayer ADL scale (Hindmarch et al., 1998). All the participants were first examined in 2005–2007, and re-examined approximately 2, 4, 6 years later, and fMRI scans were performed at 2 and 6 years in a proportion of participants. For the current study, we used these two time points as baseline and 4-year follow-up assessments. Details of the sampling methodology have been published previously (Sachdev et al., 2010). The study was approved by the Ethics Committees of the University of New South Wales and the South Eastern Sydney and Illawarra Area Health Service. Written informed consent was obtained from each participant.

For the current study, we only included participants who were classified as cognitively unimpaired from neuropsychological assessments and received r-fMRI scans at both baseline and 4-year follow-up ($N = 38$). All 38 participants had an MMSE score higher than 26. After excluding participants from non-English speaking background (NESB) (Anderson et al., 2007), imaging artifacts (including the metal artifact), and damaged image, 34 participants were finally included in the current study (demographic characteristics in **Table 1**).

Neuropsychological Assessments

All eligible participants ($N = 34$) received assessments for a comprehensive neuropsychological battery (Sachdev et al., 2010). Five cognitive domains were tested, including processing speed, executive function, language, visuo-spatial, and memory

TABLE 1 | Demographic and cognitive characteristics for the study sample.

Variable	Baseline	4-year follow-up	*P*-value
Age (mean ± SD, years)	78.27 ± 3.14	82.19 ± 3.17	<0.001*
Gender (M/F)	14/20	14/20	–
Education (mean ± SD, years)	12.54 ± 2.90	12.54 ± 2.90	–
MMSE (mean ± SD)	28.91 ± 1.00	28.82 ± 1.00	0.702

**Significant difference between baseline and 4-year follow-up. MMSE: Mini-Mental State Examination.*

(**Supplementary Table S1**). Specially, executive function in the present study includes the Controlled Oral Word Association Test (FAS) and Trail Making Test (TMT) B (**Supplementary Table S1**). FAS measures letter-based word retrieval, adherence to rule constraints. TMT B measures complex attention, set-shifting, psychomotor speed, and visual search. Raw component test scores were transformed to z scores based on sample means and SDs [z = (raw – mean)/SD], and domain composite scores were calculated by averaging z scores of component tests. Global cognition score was calculated for each participant as the average of all composite domain z scores. The signs of z scores of TMT A and TMT B were reversed, so for all composites of cognitive domains, greater positive scores represented better performance. Paired *t*-test was performed to compare the cognitive scores changes between baseline and 4-year follow-up. IBM SPSS Statistics 21 was used to analyze the behavioral data, and data were screened for univariate outliers.

Image Acquisition

Magnetic resonance imaging scans were conduct on a Philips 3T Achieva Quasar Dual scanner (Philips Medical Systems, Best, Netherlands), at NeuRA (Neuroscience Research Australia), Sydney. All participants were instructed to keep their eyes closed and think nothing when receiving resting-state fMRI scans. A T2*-weighted echo planar imaging (EPI) sequence was used, with the following parameters: repetition time (TR)/echo time (TE) = 2000/30 ms, flip angle = 90°, field of view (FOV) = 240 × 130.5 × 240 mm^3, 29 continuous axial slices, slice thickness = 4.5 mm without interslice gap, matrix size = 128 × 128, resulting in voxel size = 1.9 × 1.9 × 4.5 mm^3. During the 7-min scan of fMRI, we required 208 volumes per subject. A 3D T1-weighted structural MRI was acquire d during the same scanning session with TR/TE = 6.39/2.9 ms, flip angle = 8°, FOV = 256 × 256 × 190 mm^3, slice thickness = 1.0 without interslice gap, resulting an isotropic voxel size = 1 × 1 × 1 mm^3.

Images Processing

All the fMRI data were pre-processed and analyzed using DPABI (Yan and Zang, 2010), which is a toolbox for data processing based on Statistical Parametric Mapping (SPM12). The first 10 volumes were discarded to allow the magnetization to approach a dynamic equilibrium and for the participants to get used to the scanner noise. R-fMRI data were then corrected for slice-timing to the median reference slice and realigned for head motion correction. No subject was excluded under a head motion criterion of 3 mm and 3°. We then normalized all images to Montreal Neurological Institute (MNI) space by using EPI template and resliced with a voxel size of 3 mm × 3 mm × 3 mm to agree with the gray matter probability maps. Spatial smoothing was then applied with a 4-mm full-width half-maximum (FWHM) Gaussian Kernel. Several nuisance variables, including Friston's 24 head motion parameters (Friston et al., 1996), the averaged signal from white matter and cerebrospinal fluid tissue, were removed through multiple linear regression analysis to reduce the effects of non-neuronal signals (Fox et al., 2005). The SPM-defined cerebrospinal fluid and white matter masks were used to extract the mean signal for nuisance regression. Finally, a bandpass filter (0.01–0.1 Hz) was applied to reduce the very low frequency and high frequency noise.

FCS Estimates

Whole-brain FCS analysis was performed. First, the blood oxygen level-dependent (BOLD) time-series of each pair of voxels within a gray matter mask without cerebellum (with the number of voxels of the mask N = 45381) was calculated. The mask was generated by selecting a threshold of 0.2 on the gray matter probability map (>0.2) provided by SPM12 and extracting overlapping voxels in the automated anatomical labeling template (Tzourio-Mazoyer et al., 2002). Then only Pearson's correlation coefficients above a threshold of $r > 0.2$ were used, because the physiological basis of the negative correlations was ambiguous (Fox et al., 2009). And this threshold was typically used in previous study (Liao et al., 2013). Next, the degree strength of each voxel was defined as $\mathrm{D}(i) = \sum r_{ij}$, where $\mathrm{j} = 1 \ldots N, i \neq j$. Finally, the values of the degree map were standardized to z scores to make them comparable across subjects:

$$\mathrm{FCS}(i) = \frac{D_i - u}{\delta},\ 1 \leq i \leq N$$

where u and δ are mean and SD of the degree strength across all N nodes.

This high threshold was chosen to eliminate counting voxels that had low temporal correlation attributable to signal noise. Different threshold selections did not qualitatively change the results for cortex (see **Supplementary Figures S1, S2**). The FCS voxel-wise analysis and voxel-wise covariates were performed using DPABI and MATLAB code in-house.

Analysis of FCS Patterns at Two Time Points

We estimated the FCS patterns at this two time points before longitudinal analysis. One-sample *t*-test was performed to explore the FCS patterns at each time point (two-tailed GRF correction, voxel-wise: minimum z-value > 3.29; cluster significance: $p < 0.05$). The peak coordinates and assignation of Brodmann's area labels were performed using SPM12.

Analysis of Longitudinal Changes in FCS

To explore the 4-year changes in age-related changes of FCS, we defined longitudinal FCS changes as follow-up minus baseline (ΔFCS). The statistical significance of differences in whole

brain degree maps between baseline and 4-year follow-up were examined with 10,000 random permutations and corrected for multiple comparisons [cluster-defining threshold: $p \leq 0.01$, family-wise error (FWE) corrected: $p \leq 0.05$]. The permutation test was performed using Statistical Non-Parametric Mapping (SnPM)—a toolbox for SPM (Nichols and Holmes, 2014).

Validation Test: Longitudinal Changes in FCS With Gray Matter Volume as Additional Covariates

In order to estimate whether these results are robust, we performed this validation test. Given the controversy surrounding the idea that differences in the functional connectivity might result from a structural abnormality in gray matter volume (He et al., 2007; Oakes et al., 2007; Kathirvelu et al., 2019), we performed the analysis of voxel-based global cortical gray matter volume in SPM 12. We applied a voxel-based morphometry (VBM) protocol using the DPABI in SPM12. Gray matter, white matter, and cerebrospinal fluid were segmented on each subject's individual T1-weighted sequence using SPM12. We derived each subject's gray matter volume map at two time points fromT1 structural images using the longitudinal pre-processing pipeline. FCS differences between baseline and 4-year follow-up were re-examined using paired *t*-test by taking individual gray matter volume of two time points as additional covariates (**Supplementary Figure S3**). The analyses were carried out with multiple comparisons correction (two-tailed GRF correction, voxel-wise: minimum z-value > 3.29; cluster significance: $p < 0.05$). The Statistical Analysis sub-toolbox of DPABI was used to perform a paired *t*-test with gray matter volume as a voxel-wise covariate.

Correlation Between Changes in FCS and Changes in Cognitive Performance

At each time point, we computed the relationship between FCS and three cognitive domains which showed significantly decline in 4 years (processing speed, executive function, and global cognition), with sex, baseline age, and gray matter volume reduction as covariates. Furthermore, in order to investigate the FCS and cognition associations in longitudinal settings, we also focused on 4-year changes of FCS and the significantly decreased cognitive domain scores (processing speed, executive function, and global cognition). Decreased scores were computed as follow-up minus baseline (Δcognition). Changes in FCS were also computed as follow-up minus baseline (ΔFCS). Pearson's correlation was used to assess the relationship between ΔFCS and Δcognition, with sex, baseline age, and gray matter volume reduction as covariates. Multiple comparisons were carried out by two-tailed Gaussian random field (GRF) theory correction (voxel-wise: minimum z-value > 3.29; cluster significance: $p < 0.05$).

Cortical Thickness Measurement

To measure cortical thickness, T1-weighted images were processed with the longitudinal pipeline available in FreeSurfer (Reuter et al., 2012). Specifically, this pipeline creates an unbiased within-subject template space and image using robust, inverse consistent registration (Reuter and Fischl, 2011). The following processing steps were also included: skull stripping, Talairach transforms, atlas registration, spherical surface maps, and parcellation of cerebral cortex. Based on gyral and sulcal anatomy, the cortex was segmented into 34 different gyral and sulcal anatomy using the Desikan–Killiany Atlas (Desikan et al., 2006). For each of these regions, mean cortical thickness was calculated as the distance (in mm) between the pial and gray/white matter surfaces. FreeSurfer results were manually checked for segmentation and registration accuracy. Four-year changes in cortical thickness were investigated by vertex-based paired *t*-test obtained with general linear models (GLMs) using the QDEC toolbox in FreeSurfer [corrected with false discovery rate (FDR) < 0.05].

Even though cortical thickness may be more sensitive in explaining variability in the BOLD signal compared to GM volume, it is impossible to control for cortical thickness in a voxel-wise analysis as it is vertex-based. Therefore, to control for connectivity differences due to GM differences, VBM was used. However, since differences in the thickness of the cortical mantle may be the main driver of differences in GM volume, age-related changes in cortical thickness were also examined.

RESULTS

Neuropsychological Tests

The neuropsychological results are summarized in **Table 2**. Significant decline was found in global cognition and two cognitive domains (processing speed, executive function) in 4 years.

FCS Patterns at Two Time Points

Figure 1 shows patterns of distributions of FCS at both baseline and follow-up, highlighting the similarity of the patterns at the two time points (**Table 3**). Main clusters were located in bilateral precuneus, left calcarine, left inferior occipital, and right inferior temporal. The regions with strong connections to other brain regions were approximately bilaterally symmetrical.

Longitudinal Changes in FCS

There were significant FCS changes in five cerebral regions when comparing baseline with follow-up (**Figure 2**).

TABLE 2 | Cognitive domain scores.

Cognitive domain	Baseline	4-year follow-up	*P*-value
Processing speed	0.60 ± 0.65	0.16 ± 1.05	0.003*
Executive function	0.64 ± 0.79	0.44 ± 0.85	0.019*
Language	0.40 ± 0.76	0.42 ± 0.83	0.816
Visuo-spatial	0.35 ± 0.88	0.30 ± 0.95	0.648
Memory	0.74 ± 0.87	0.74 ± 0.81	0.983
Global cognition	0.72 ± 0.69	0.54 ± 0.88	0.023*

**Difference between baseline and 4-year follow-up is significant (P < 0.05). Data in first two columns are means ± standard deviations.*

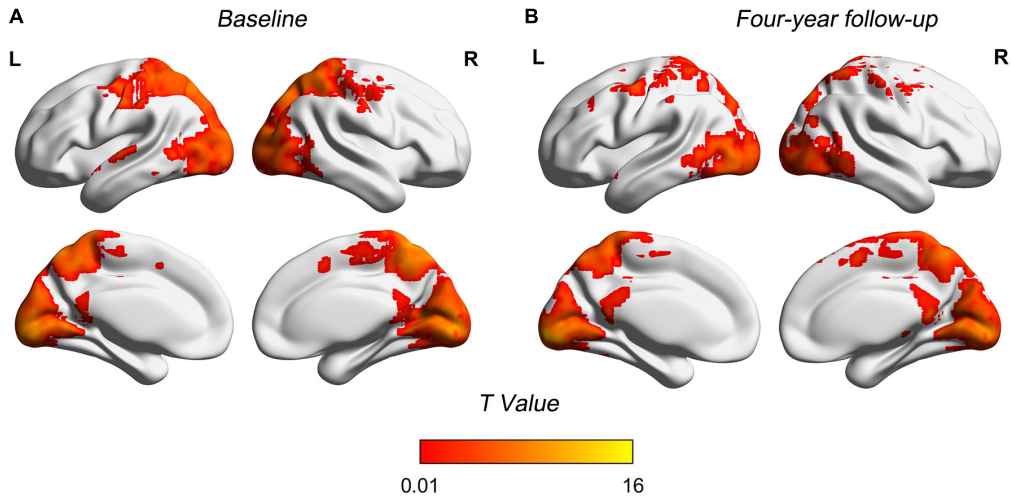

FIGURE 1 | Spatial FCS patterns of two time points. **(A)** FCS patterns in baseline. **(B)** FCS patterns in 4-year follow-up. Brain regions showing higher FCS were mainly located in precuneus, calcarine, inferior occipital, and inferior temporal. FCS maps at two time points showed similar distribution patterns. FCS, functional connectivity strength; T, statistical value; L, left bran; R, right brain.

Left supplementary motor area (SMA) (BA 6) and left insula (BA 13) showed increased FCS over time. Decreased FCS was observed in the right medial frontal (BA 11) and bilateral superior parietal lobes (BA 7) (10,000 random permutations for two-sample *t*-test, cluster-defining threshold: $p \leq 0.01$, FWE-corrected: $p \leq 0.05$). The detailed information for each cluster was summarized in **Table 4**. Moreover, in the validation test, our main findings were preserved after correcting for gray matter volume (**Supplementary Figure S3**).

Association Between ΔFCS and ΔCognition

No significant correlation between FCS and cognitive domains (processing speed, executive function, and global cognition) was found at each time point. But significant positive correlation between Δglobal cognition and ΔFCS (two-tailed GRF correction, voxel-wise: minimum z-value > 3.29; cluster significance: $p < 0.05$) was found in the left precuneus (**Figure 3**). No significant relationship was found between Δprocessing speed and ΔFCS, or Δexecutive function cognition and ΔFCS. The peak location of relationship between ΔFCS and Δglobal cognition was then used to define the seed region to further explore the connectivity patterns in the sample (**Supplementary Material**).

TABLE 3 | FCS patterns at two time points.

	Brain regions	BA	Cluster size	Peak MNI coordinates, mm			T
				x	*y*	*z*	
Baseline	Left precuneus	7	10,405	−6	−63	63	15.79
	Right precuneus	5	–	3	−54	51	14.63
	Right precuneus	7	–	6	−69	57	13.02
4-year	Left calcarine	18	9694	−9	−96	−6	14.86
follow-up	Left inferior occipital	19	–	−51	−69	−15	12.96
	Right inferior temporal	37	–	51	−60	−21	11.60

BA, Brodmann's area; MNI, Montreal Neurological Institute; T, statistical value of peak voxel; All listed clusters significant at p < 0.01.

Longitudinal Changes in Cortical Thickness

Longitudinal assessment of changes in cortical thickness revealed cortical thinning over large areas of bilateral frontal (BA 9/10/11),

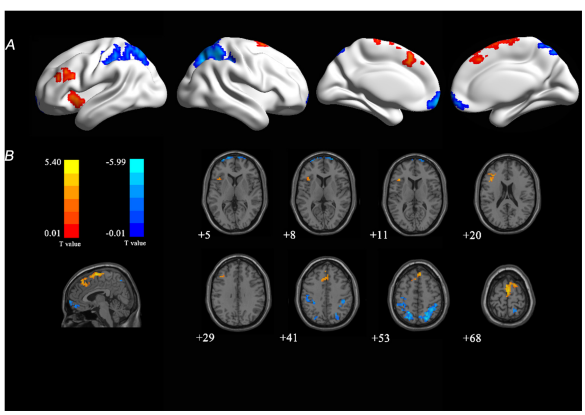

FIGURE 2 | T-statistical FCS map at 4-year follow-up compared with baseline. **(A)** Longitudinal changes were overlaid on three-dimensional standard brain. **(B)** Longitudinal changes were overlaid on two-dimensional standard brain. Warm colors (red and yellow) represent increased FCS and cool colors (blue) represent decreased FCS with age. FCS, functional connectivity strength; T, statistical value.

TABLE 4 | Regions showing significant differences in FCS with normal aging.

	Brain regions	BA	Cluster size	Peak MNI coordinates, mm			T
				x	*y*	*z*	
Increased FCS	Left SMA	6	339	−6	−3	78	5.40
	Left insula	13	189	−39	18	−6	4.16
Decreased FCS	Right superior parietal	7	395	21	−72	54	5.12
	Left superior parietal	7	320	−24	−57	54	5.39
	Right medial frontal	11	284	12	69	−3	5.99

BA, Brodmann's area; MNI, Montreal Neurological Institute; FCS, functional connectivity strength; T, statistical value of peak voxel; SMA, supplementary motor area; All listed clusters significant at $p < 0.01$.

small area of left middle cingulum (BA 23), and part of right temporal cortex (BA 20/36) ($p < 0.05$, FDR-corrected, **Figure 4**). No significant associations were found between alterations of cortical thickness and cognitive domain scores.

DISCUSSION

In this longitudinal study, we explored the changes of FCS, cortical thickness, and cognitive performance over a period of 4 years in cognitively normal old people. Most observed longitudinal FCS changes remained after correcting for longitudinal reduction in gray matter volume. In addition, the positive relationship between 4-year changes of FCS and aging-related decline in global cognition was found in left precuneus, which was then used as a seed to investigate its functional connectivity with other voxels in the brain.

Aging-related functional connectivity decrements preferentially affect DMN and the DAN (Ferreira and Busatto, 2013). In this study, we found that decreased FCS was located primarily in the DMN and DAN regions, i.e., right medial frontal and bilateral superior parietal, consistent with previous study (Tomasi and Volkow, 2012). The DMN, which has been the main focus of aging-related fMRI research, comprises a set of cortical regions that include the medial prefrontal cortex, the inferior parietal lobule, the hippocampus, and precuneus (Raichle et al., 2001; Ferreira and Busatto, 2013). Furthermore, the DMN regions, the core components of functional hubs, are involved in a variety of functional processes. The medial prefrontal cortex shows high metabolic activity at rest (Raichle et al., 2001). Medial frontal cortex was shown to play a critical role in performance monitoring and the implementation of associated adjustments in cognitive control (Ridderinkhof et al., 2004). Superior parietal regions correlate with episodic retrieval and the phenomenological experience of remembering (Wagner et al., 2005). According to our findings, the FCS in those regions decreased with aging, which may affect some related functions. Tomasi and Volkow (2012) also found that aging was associated

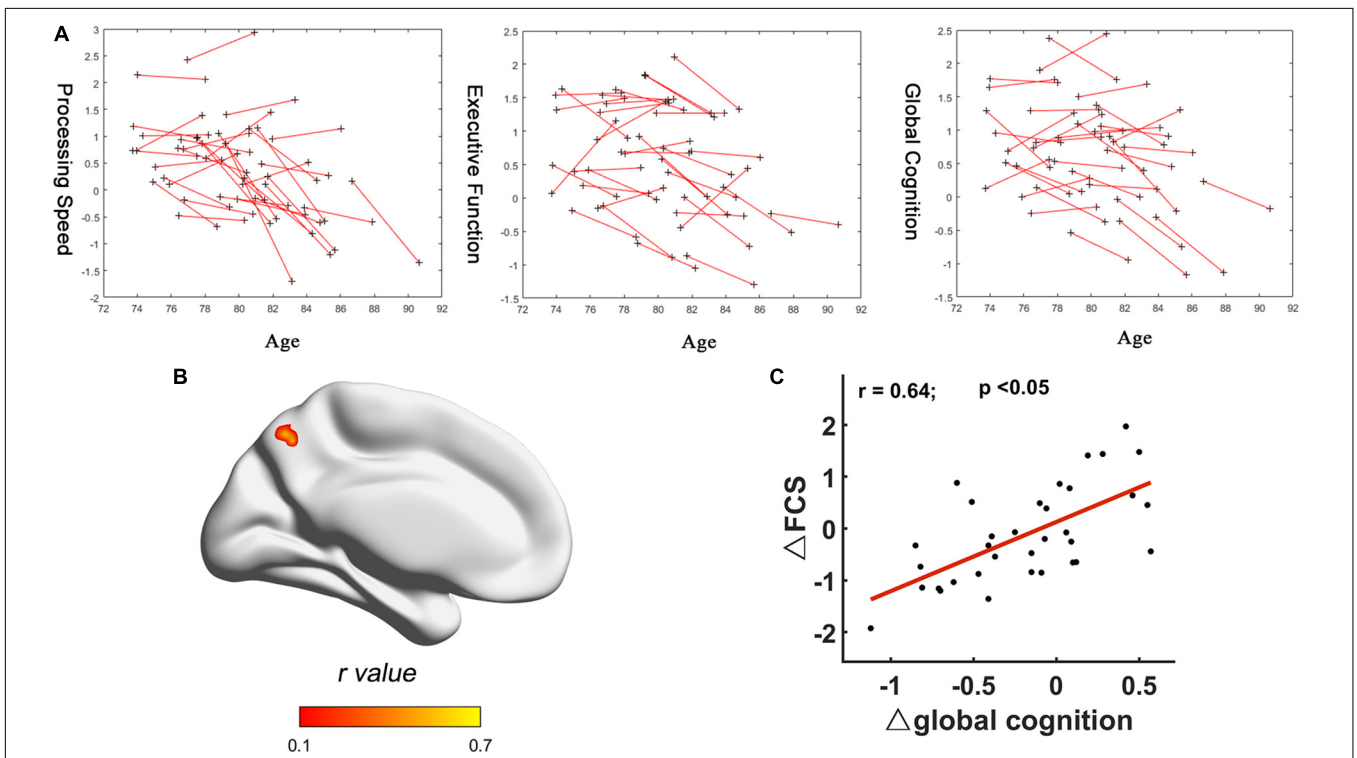

FIGURE 3 | Correlation between FCS changes and cognition changes. **(A)** Longitudinal trajectories of cognitive data: processing speed, executive function, and global cognition. **(B)** R-statistical map of association between ΔFCS and Δglobal cognition. **(C)** Scatter plot of fitted ΔFCS of peak voxel in the left precuneus versus Δglobal cognition. Each data point represents a single subject. FCS, functional connectivity strength.

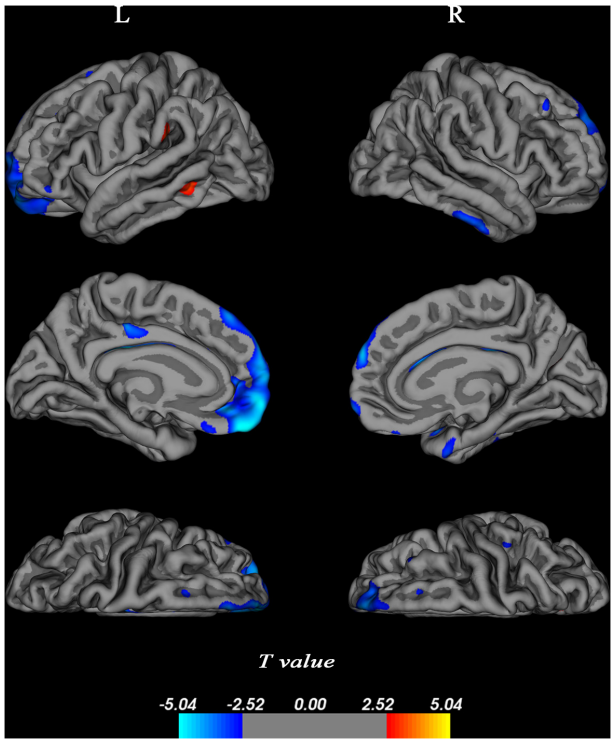

FIGURE 4 | Changes in cortical thickness over 4 years. Cortical thickness was determined using a general linear model corrected at a false discovery rate (FDR) of 0.05 and projected onto a semi-inflated brain. Decreased cortical thickness was indicated in blue, and increased cortical thickness was presented in red. L, left bran; R, right brain.

with decreased functional connectivity density, similar to FCS in the present study, in DMN. Taken together, these findings provide the longitudinal evidence that the influence of advancing age is mainly in right medial frontal and bilateral superior parietal, evidenced by disturbance of FCS in these areas.

Increased FCS with normal aging was observed in the left insula and left SMA in our study. Cauda et al. (2011) investigated functional connectivity of insula in the resting brain and reported the role of insula in sensorimotor integration and links to SMA. These findings may partly explain the synchronous changes of FCS in these two areas. A previous study found that long-range functional connectivity density in insula, somatosensory, and motor cortex increased with age (Tomasi and Volkow, 2012). Insula and SMA are related to the salience network which regulates dynamic changes in other networks (Bonnelle et al., 2012) and participates in the integration of sensory data (Seeley et al., 2007). There is growing evidence to suggest that the integrity of the salience network is necessary for the efficient regulation of activity in the DMN (Bonnelle et al., 2012). As for the findings of increased FCS in the present study, one possible explanation is that it is a compensatory increase. Another interpretation is that aging-related dedifferentiation processes (Cabeza et al., 2002) or neural strategies change in the brain. Age-related increases may reflect the use of alternative cognitive strategies with aging, or they may signal beneficial compensatory activity (Cabeza et al., 1997). These altered FCS patterns may interact with each other to keep the participants still holding a cognitively normal state across four years. The evidence for possible compensatory mechanisms is important and would also be well suited for future studies. Intriguingly, parietal and SMA not only showed relatively high FCS (**Figure 1**), but also exhibited altered FCS (**Figure 2**), which may be taken to support the hypothesis that highly connected regions would be particularly vulnerable to aging effects, related to its central role as mechanisms subtending lifetime brain plasticity (Fjell et al., 2014).

In the current study, global cognition and two of five cognitive performances (processing speed and executive function) decreased significantly over 4 years. Intriguingly, no significant correlation between FCS and these three cognitive domains (processing speed, executive function, and global cognition) was found at each time point. Only the positive relationship between Δglobal cognition and ΔFCS was found in the left precuneus. These interesting findings indicated that correlation between ΔFCS and Δglobal cognition was more significant than any correlation between FCS and cognitive scores at each time point. Previous studies have suggested that the precuneus, which is a core hub in DMN, plays an important role in a diverse array of highly integrated functions (Leech and Sharp, 2014) and is relevant for episodic memory retrieval (Greicius et al., 2004). Longitudinal studies have indicated that memory declines are related to decreased functional connectivity within DMN, particularly the precuneus/PCC (Persson et al., 2014; Bernard et al., 2015). The positive relationships indicated that more the FCS decreased in precuneus, greater the decline in global function with aging. The relationship between FCS changes and cognition changes was observed for global cognition rather than the individual domains, possibly because of the likely role of the FCS in integrating multiple cognitive functions, and the greater sensitivity of the global cognitive measure. Only one region, the precuneus, showed a significant relationship between change in brain connectivity and change in global cognition. This indicates that changes in global cognition are related to local, rather than large-scale network connectivity. We would expect higher level cognitive functions, such as global cognition, should require integration of information from different sources, and therefore benefit from global efficiency across a whole network.

To further explore the importance of precuneus in aging brain, a seed-based method was used to display the pattern of functional connectivity. The most straightforward way to examine the functional connections of a particular brain region is to correlate the resting-state time-series of the depicted brain region against the time-series of all other regions (Van Den Heuvel and Hulshoff Pol, 2010). The wide-spread connections seen by this method suggest the precuneus is a major association area which may subserve a variety of cognitive-behavioral functions, as has been previously suggested (Cavanna and Trimble, 2006). Clusters that our study depicted were not all included in DMN, but they participate in distinct functional networks which control high-level cognition. Several other studies have proposed that

precuneus is connected to brain networks that differ from DMN (Cavanna and Trimble, 2006; Margulies et al., 2009; Utevsky et al., 2014). However, the main functional connectivity clusters were located in bilateral precuneus, which showed an extensive autocorrelation. These results also suggested that the precuneus functional connectivity is relatively stabilized. In addition, precuneus is one of the regions to be affected early in AD, and it is difficult to be certain that early AD pathology is not, at least, partially responsible for this change with aging.

In the present study, we also found age-related changes in cortical thickness. There was cortical atrophy with age in the bilateral medial prefrontal, cingulum extending to PCC, and right dorsolateral temporal cortex, regions that form nodes of the default network. We also found that two small cortical areas of left middle temporal and left supramarginal gyrus were thicker in older participants, which indicates the ability of some brain regions to compensate for cortical atrophy. Alterations of cortical thickness did not exhibit any significant associations with cognitive functions. In fact, the evidence for a relation between cortical atrophy and cognitive decline is equivocal in humans (Ziegler et al., 2010; Tuladhar et al., 2015; Pini et al., 2016), and our results are consistent with this.

Several limitations of our study should be noted. First, our sample size was modest for a normal aging study. However, it is worth noting that the participants were very old (aged 78+), which can bring some new insights into longitudinal changes of normal aging in old-aged group. Larger samples may be required to detect more subtle relationships involving age, FCS, and cognition. Second, we did not explicitly evaluate the reliability the resting-state functional connectivity measures. Selective attrition and test–retest effects may influence the results (Taris and Kompier, 2003). Selective attrition adds bias but is a reliability issue. Third, tasks that were used to obtain the executive function compound score cannot present "executive function" sufficiently, as the concept of "executive function" is broad, heterogeneous, and complex. Fourth, for longitudinal FCS changes, we did not control sex and age in the longitudinal analysis, and this would be our areas of future research. Fifth, the statistical analysis was not completely identical—we used the permutation test as statistical modal in Section "Analysis of Longitudinal Changes in FCS," and parametric test (paired *t*-test) in other sections. Finally, we did not have PET imaging to investigate associations between amyloid deposition in the brain and abnormal changes in FCS. Previous studies have shown that a significant proportion of cognitive unimpaired older adults may present substantial amyloid deposition in brain (Aizenstein et al., 2008). In the future, effective multimodal neuroimaging research should be used to deeply explore normal aging mechanisms.

CONCLUSION

In conclusion, normal aging was accompanied by altered FCS and cognitive performance. Reduced FCS may affect main brain networks and explain age-related cognitive decline with aging. However, there is some evidence of increases in FCS with age, possibly playing a role in neural strategies change or compensatory mechanisms during the aging process. FCS changes are detectable with normal aging, and measures of ΔFCS are correlated with Δglobal cognition in the left precuneus. Our characterization of aging effects on brain networks is of great value to help better understand the potential aging mechanisms.

DATA AVAILABILITY STATEMENT

The datasets used and analyzed are available to other researchers subject to review of the request by the Scientific Committee of the study and ethics approval. Data are moreover already shared in COSMIC consortia.

ETHICS STATEMENT

The studies involving human participants were reviewed and approved by the Ethics Committees of the University of New South Wales and the South Eastern Sydney and Illawarra Area Health Service. The patients/participants provided their written informed consent to participate in this study. Written informed consent was obtained from the individual(s) for the publication of any potentially identifiable images or data included in this article.

AUTHOR CONTRIBUTIONS

TL, CD, and QL contributed to study design, data analyses, interpretation of the results, and manuscript writing. WW contributed to study design and interpretation of the results. HB, PS, and NK contributed to data collection and interpretation of the results. XC, AP, JJ, JC, and HN contributed to data analyses. All authors participated in manuscript revision and final approval.

FUNDING

This work was supported by the Natural Science Foundation of China (Grant No. 81871434) and the National Health and Medical Research Council (NHMRC) Program Grants of Australia (350833, 56896, and 109308).

ACKNOWLEDGMENTS

We gratefully acknowledge Prof. Yong He for helpful discussion before the starting of the project.

SUPPLEMENTARY MATERIAL

The Supplementary Material for this article can be found online at: https://www.frontiersin.org/articles/10.3389/fnagi.2020.00071/full#supplementary-material

REFERENCES

Aizenstein, H. J., Nebes, R. D., Saxton, J. A., Price, J. C., Mathis, C. A., Tsopelas, N. D., et al. (2008). Frequent amyloid deposition without significant cognitive impairment among the elderly. *Arch. Neurol.* 65, 1509–1517.

Anderson, T. M., Sachdev, P. S., Brodaty, H., Trollor, J. N., and Andrews, G. (2007). Effects of sociodemographic and health variables on Mini-Mental State Exam scores in older Australians. *Am. J. Geriatric Psychiatry* 15, 467–476. doi: 10.1097/jgp.0b013e3180547053

Bernard, C., Dilharreguy, B., Helmer, C., Chanraud, S., Amieva, H., Dartigues, J. F., et al. (2015). PCC characteristics at rest in 10-year memory decliners. *Neurobiol. Aging* 36, 2812–2820. doi: 10.1016/j.neurobiolaging.2015.07.002

Boccaletti, S., Latora, V., Moreno, Y., Chavez, M., and Hwang, D.-U. (2006). Complex networks: structure and dynamics. *Phys. Rep.* 424, 175–308.

Bonnelle, V., Ham, T. E., Leech, R., Kinnunen, K. M., Mehta, M. A., Greenwood, R. J., et al. (2012). Salience network integrity predicts default mode network function after traumatic brain injury. *Proc. Natl. Acad. Sci. U.S.A.* 109, 4690–4695. doi: 10.1073/pnas.1113455109

Buckner, R. L., Sepulcre, J., Talukdar, T., Krienen, F. M., Liu, H., Hedden, T., et al. (2009). Cortical hubs revealed by intrinsic functional connectivity: mapping, assessment of stability, and relation to Alzheimer's disease. *J. Neurosci.* 29, 1860–1873. doi: 10.1523/jneurosci.5062-08.2009

Cabeza, R., Anderson, N. D., Locantore, J. K., and Mcintosh, A. R. (2002). Aging gracefully: compensatory brain activity in high-performing older adults. *NeuroImage* 17, 1394–1402. doi: 10.1006/nimg.2002.1280

Cabeza, R., Grady, C. L., Nyberg, L., Mcintosh, A. R., Tulving, E., Kapur, S., et al. (1997). Age-related differences in neural activity during memory encoding and retrieval: a positron emission tomography study. *J. Neurosci.* 17, 391–400. doi: 10.1523/jneurosci.17-01-00391.1997

Cauda, F., D'agata, F., Sacco, K., Duca, S., Geminiani, G., and Vercelli, A. (2011). Functional connectivity of the insula in the resting brain. *Neuroimage* 55, 8–23. doi: 10.1016/j.neuroimage.2010.11.049

Cavanna, A. E., and Trimble, M. R. (2006). The precuneus: a review of its functional anatomy and behavioural correlates. *Brain* 129, 564–583. doi: 10.1093/brain/awl004

Dai, Z., Yan, C., Li, K., Wang, Z., Wang, J., Cao, M., et al. (2015). Identifying and mapping connectivity patterns of brain network hubs in alzheimer's disease. *Cereb. Cortex* 25, 3723–3742. doi: 10.1093/cercor/bhu246

Damoiseaux, J. S., Beckmann, C. F., Arigita, E. J., Barkhof, F., Scheltens, P., Stam, C. J., et al. (2008). Reduced resting-state brain activity in the "default network" in normal aging. *Cereb. Cortex* 18, 1856–1864. doi: 10.1093/cercor/bhm207

Desikan, R. S., Segonne, F., Fischl, B., Quinn, B. T., Dickerson, B. C., Blacker, D., et al. (2006). An automated labeling system for subdividing the human cerebral cortex on MRI scans into gyral based regions of interest. *Neuroimage* 31, 968–980. doi: 10.1016/j.neuroimage.2006.01.021

Ferreira, L. K., and Busatto, G. F. (2013). Resting-state functional connectivity in normal brain aging. *Neurosci. Biobehav. Rev.* 37, 384–400. doi: 10.1016/j.neubiorev.2013.01.017

Fjell, A. M., Mcevoy, L., Holland, D., Dale, A. M., Walhovd, K. B., Alzheimer's Disease, et al. (2014). What is normal in normal aging? Effects of aging, amyloid and Alzheimer's disease on the cerebral cortex and the hippocampus. *Prog. Neurobiol.* 117, 20–40. doi: 10.1016/j.pneurobio.2014.02.004

Fjell, A. M., Sneve, M. H., Grydeland, H., Storsve, A. B., De Lange, A. G., Amlien, I. K., et al. (2015). Functional connectivity change across multiple cortical networks relates to episodic memory changes in aging. *Neurobiol. Aging* 36, 3255–3268. doi: 10.1016/j.neurobiolaging.2015.08.020

Fjell, A. M., Sneve, M. H., Grydeland, H., Storsve, A. B., and Walhovd, K. B. (2017). The disconnected brain and executive function decline in aging. *Cereb. Cortex* 27, 2303–2317.

Fjell, A. M., Sneve, M. H., Storsve, A. B., Grydeland, H., Yendiki, A., and Walhovd, K. B. (2016). Brain events underlying episodic memory changes in aging: a longitudinal investigation of structural and functional connectivity. *Cereb. Cortex* 26, 1272–1286. doi: 10.1093/cercor/bhv102

Folstein, M. F., Folstein, S. E., and Mchugh, P. R. (1975). "Mini-mental state". A practical method for grading the cognitive state of patients for the clinician. *J. Psychiatr. Res.* 12, 189–198.

Fox, M. D., Snyder, A. Z., Vincent, J. L., Corbetta, M., Van Essen, D. C., and Raichle, M. E. (2005). The human brain is intrinsically organized into dynamic, anticorrelated functional networks. *Proc. Natl. Acad. Sci. U.S.A.* 102, 9673–9678. doi: 10.1073/pnas.0504136102

Fox, M. D., Zhang, D. Y., Snyder, A. Z., and Raichle, M. E. (2009). The global signal and observed anticorrelated resting state brain networks. *J. Neurophysiol.* 101, 3270–3283. doi: 10.1152/jn.90777.2008

Friston, K. J., Williams, S., Howard, R., Frackowiak, R. S., and Turner, R. (1996). Movement-related effects in fMRI time-series. *Magn. Reson Med.* 35, 346–355. doi: 10.1002/mrm.1910350312

Greicius, M. D., Srivastava, G., Reiss, A. L., and Menon, V. (2004). Default-mode network activity distinguishes Alzheimer's disease from healthy aging: evidence from functional MRI. *Proc. Natl. Acad. Sci. U.S.A.* 101, 4637–4642. doi: 10.1073/pnas.0308627101

He, Y., Wang, L., Zang, Y., Tian, L., Zhang, X., Li, K., et al. (2007). Regional coherence changes in the early stages of Alzheimer's disease: a combined structural and resting-state functional MRI study. *Neuroimage* 35, 488–500. doi: 10.1016/j.neuroimage.2006.11.042

Hedden, T., and Gabrieli, J. D. (2004). Insights into the ageing mind: a view from cognitive neuroscience. *Nat. Rev. Neurosci.* 5, 87–96. doi: 10.1038/nrn1323

Hindmarch, I., Lehfeld, H., De Jongh, P., and Erzigkeit, H. (1998). The Bayer activities of daily living scale (B-ADL). *Dementia Geriatr. Cognit. Disord.* 9, 20–26. doi: 10.1159/000051195

Kathirvelu, D., Vinupritha, P., and Kalpana, V. (2019). A computer aided diagnosis system for measurement of mandibular cortical thickness on dental panoramic radiographs in prediction of women with low bone mineral density. *J. Med. Syst.* 43:148.

Koch, W., Teipel, S., Mueller, S., Buerger, K., Bokde, A. L. W., Hampel, H., et al. (2010). Effects of aging on default mode network activity in resting state fMRI: does the method of analysis matter? *Neuroimage* 51, 280–287. doi: 10.1016/j.neuroimage.2009.12.008

Leech, R., and Sharp, D. J. (2014). The role of the posterior cingulate cortex in cognition and disease. *Brain* 137, 12–32. doi: 10.1093/brain/awt162

Liao, X.-H., Xia, M.-R., Xu, T., Dai, Z.-J., Cao, X.-Y., Niu, H.-J., et al. (2013). Functional brain hubs and their test–retest reliability: a multiband resting-state functional MRI study. *Neuroimage* 83, 969–982. doi: 10.1016/j.neuroimage.2013.07.058

Margulies, D. S., Vincent, J. L., Kelly, C., Lohmann, G., Uddin, L. Q., Biswal, B. B., et al. (2009). Precuneus shares intrinsic functional architecture in humans and monkeys. *Proc. Natl. Acad. Sci. U.S.A.* 106, 20069–20074. doi: 10.1073/pnas.0905314106

Ng, K. K., Lo, J. C., Lim, J. K. W., Chee, M. W. L., and Zhou, J. (2016). Reduced functional segregation between the default mode network and the executive control network in healthy older adults: a longitudinal study. *Neuroimage* 133, 321–330. doi: 10.1016/j.neuroimage.2016.03.029

Nichols, T., and Holmes, A. (2014). *SnPM-Statistical NonParametric Mapping: A Toolbox for SPM*. Available at: http://www.nisox.org/Software/SnPM

Oakes, T. R., Fox, A. S., Johnstone, T., Chung, M. K., Kalin, N., and Davidson, R. J. (2007). Integrating VBM into the general linear model with voxelwise anatomical covariates. *Neuroimage* 34, 500–508. doi: 10.1016/j.neuroimage.2006.10.007

Onoda, K., Ishihara, M., and Yamaguchi, S. (2012). Decreased Functional Connectivity by Aging Is Associated with Cognitive Decline. *J. Cognit. Neurosci.* 24, 2186–2198. doi: 10.1162/jocn_a_00269

Perry, A., Wen, W., Kochan, N. A., Thalamuthu, A., Sachdev, P. S., and Breakspear, M. (2017). The independent influences of age and education on functional brain networks and cognition in healthy older adults. *Hum. Brain Mapp.* 38, 5094–5114. doi: 10.1002/hbm.23717

Persson, J., Pudas, S., Nilsson, L. G., and Nyberg, L. (2014). Longitudinal assessment of default-mode brain function in aging. *Neurobiol. Aging.* 35, 2107–2117. doi: 10.1016/j.neurobiolaging.2014.03.012

Pini, L., Pievani, M., Bocchetta, M., Altomare, D., Bosco, P., Cavedo, E., et al. (2016). Brain atrophy in Alzheimer's disease and aging. *Ageing Res. Rev.* 30, 25–48.

Pur, D. R., Eagleson, R. A., De Ribaupierre, A., Mella, N., and De Ribaupierre, S. (2019). Moderating effect of cortical thickness on BOLD signal variability age-related changes. *Front. Aging Neurosci.* 11:46. doi: 10.3389/fnagi.2019.00046

Raichle, M. E., Macleod, A. M., Snyder, A. Z., Powers, W. J., Gusnard, D. A., and Shulman, G. L. (2001). A default mode of brain function. *Proc. Natl. Acad. Sci. U.S.A.* 98, 676–682.

Reuter, M., and Fischl, B. (2011). Avoiding asymmetry-induced bias in longitudinal image processing. *Neuroimage* 57, 19–21. doi: 10.1016/j.neuroimage.2011.02.076

Reuter, M., Schmansky, N. J., Rosas, H. D., and Fischl, B. (2012). Within-subject template estimation for unbiased longitudinal image analysis. *Neuroimage* 61, 1402–1418. doi: 10.1016/j.neuroimage.2012.02.084

Ridderinkhof, K. R., Ullsperger, M., Crone, E. A., and Nieuwenhuis, S. (2004). The role of the medial frontal cortex in cognitive control. *Science* 306, 443–447. doi: 10.1126/science.1100301

Rubinov, M., and Sporns, O. (2010). Complex network measures of brain connectivity: uses and interpretations. *Neuroimage* 52, 1059–1069. doi: 10.1016/j.neuroimage.2009.10.003

Sachdev, P. S., Brodaty, H., Reppermund, S., Kochan, N. A., Trollor, J. N., Draper, B., et al. (2010). The Sydney Memory and Ageing Study (MAS): methodology and baseline medical and neuropsychiatric characteristics of an elderly epidemiological non-demented cohort of Australians aged 70-90 years. *Int. Psychoger.* 22, 1248–1264. doi: 10.1017/s1041610210001067

Salami, A., Wahlin, A., Kaboodvand, N., Lundquist, A., and Nyberg, L. (2016). Longitudinal evidence for dissociation of anterior and posterior MTL resting-state connectivity in aging: links to perfusion and memory. *Cereb. Cortex* 26, 3953–3963. doi: 10.1093/cercor/bhw233

Seeley, W. W., Menon, V., Schatzberg, A. F., Keller, J., Glover, G. H., Kenna, H., et al. (2007). Dissociable intrinsic connectivity networks for salience processing and executive control. *J. Neurosci.* 27, 2349–2356. doi: 10.1523/jneurosci.5587-06.2007

Smith, S. M., Miller, K. L., Salimi-Khorshidi, G., Webster, M., Beckmann, C. F., Nichols, T. E., et al. (2011). Network modelling methods for FMRI. *Neuroimage* 54, 875–891. doi: 10.1016/j.neuroimage.2010.08.063

Staffaroni, A. M., Brown, J. A., Casaletto, K. B., Elahi, F. M., Deng, J., Neuhaus, J., et al. (2018). The longitudinal trajectory of default mode network connectivity in healthy older adults varies as a function of age and is associated with changes in episodic memory and processing speed. *J. Neurosci.* 38, 2809–2817. doi: 10.1523/jneurosci.3067-17.2018

Taris, T. W., and Kompier, M. (2003). Challenges in longitudinal designs in occupational health psychology. *Scand. J. Work, Environ. Health* 29, 1–4. doi: 10.5271/sjweh.697

Thambisetty, M., Wan, J., Carass, A., An, Y., Prince, J. L., and Resnick, S. M. (2010). Longitudinal changes in cortical thickness associated with normal aging. *Neuroimage* 52, 1215–1223. doi: 10.1016/j.neuroimage.2010.04.258

Tomasi, D., and Volkow, N. D. (2011). Association between functional connectivity hubs and brain networks. *Cereb. Cortex* 21, 2003–2013. doi: 10.1093/cercor/bhq268

Tomasi, D., and Volkow, N. D. (2012). Aging and functional brain networks. *Mol. Psychiatry* 17, 549–458.

Tuladhar, A. M., Reid, A. T., Shumskaya, E., De Laat, K. F., Van Norden, A. G., Van Dijk, E. J., et al. (2015). Relationship between white matter hyperintensities, cortical thickness, and cognition. *Stroke* 46:425. doi: 10.1161/strokeaha.114.007146

Tzourio-Mazoyer, N., Landeau, B., Papathanassiou, D., Crivello, F., Etard, O., Delcroix, N., et al. (2002). Automated anatomical labeling of activations in SPM using a macroscopic anatomical parcellation of the MNI MRI single-subject brain. *Neuroimage* 15, 273–289. doi: 10.1006/nimg.2001.0978

Utevsky, A. V., Smith, D. V., and Huettel, S. A. (2014). Precuneus is a functional core of the default-mode network. *J. Neurosci.* 34, 932–940. doi: 10.1523/jneurosci.4227-13.2014

Van Den Heuvel, M. P., and Hulshoff Pol, H. E. (2010). Exploring the brain network: a review on resting-state fMRI functional connectivity. *Eur. Neuropsychopharmacol.* 20, 519–534. doi: 10.1016/j.euroneuro.2010.03.008

Wagner, A. D., Shannon, B. J., Kahn, I., and Buckner, R. L. (2005). Parietal lobe contributions to episodic memory retrieval. *Trends Cognit. Sci.* 9, 445–453. doi: 10.1016/j.tics.2005.07.001

Wang, L., Laviolette, P., O'keefe, K., Putcha, D., Bakkour, A., Van Dijk, K. R. A., et al. (2010). Intrinsic connectivity between the hippocampus and posteromedial cortex predicts memory performance in cognitively intact older individuals. *Neuroimage* 51, 910–917. doi: 10.1016/j.neuroimage.2010.02.046

Yan, C., and Zang, Y. (2010). DPARSF: a MATLAB toolbox for "pipeline" data analysis of resting-state fMRI. *Front. Syst. Neurosci.* 4:13. doi: 10.3389/fnsys.2010.00013

Ziegler, D. A., Piguet, O., Salat, D. H., Prince, K., Connally, E., and Corkin, S. (2010). Cognition in healthy aging is related to regional white matter integrity, but not cortical thickness. *Neurobiol. Aging* 31:1912. doi: 10.1016/j.neurobiolaging.2008.10.015

Conflict of Interest: The authors declare that the research was conducted in the absence of any commercial or financial relationships that could be construed as a potential conflict of interest.

frontiers in Psychiatry

ORIGINAL RESEARCH
published: 07 April 2020
doi: 10.3389/fpsyt.2020.00255

Classification Methods Based on Complexity and Synchronization of Electroencephalography Signals in Alzheimer's Disease

Sou Nobukawa[1], Teruya Yamanishi[2], Shinya Kasakawa[2], Haruhiko Nishimura[3], Mitsuru Kikuchi[4,5] and Tetsuya Takahashi[4,6]*

[1] Department of Computer Science, Chiba Institute of Technology, Narashino, Japan, [2] AI & IoT Center, Department of Management Information Science, Fukui University of Technology, Fukui, Japan, [3] Graduate School of Applied Informatics, University of Hyogo, Kobe, Japan, [4] Research Center for Child Mental Development, Kanazawa University, Kanazawa, Japan, [5] Department of Psychiatry & Behavioral Science, Kanazawa University, Ishikawa, Japan, [6] Department of Neuropsychiatry, University of Fukui, Yoshida, Japan

OPEN ACCESS

Edited by:
Stefano L. Sensi, Università degli Studi G. d'Annunzio Chieti e Pescara, Italy

Reviewed by:
Marco Onofrj, Università degli Studi G. d'Annunzio Chieti e Pescara, Italy
Valentina Ciullo, Santa Lucia Foundation, Italy

***Correspondence:**
Sou Nobukawa
nobukawa@cs.it-chiba.ac.jp

Specialty section:
This article was submitted to Aging Psychiatry, a section of the journal Frontiers in Psychiatry

Received: *10 January 2020*
Accepted: *16 March 2020*
Published: *07 April 2020*

Citation:
Nobukawa S, Yamanishi T, Kasakawa S, Nishimura H, Kikuchi M and Takahashi T (2020) Classification Methods Based on Complexity and Synchronization of Electroencephalography Signals in Alzheimer's Disease. Front. Psychiatry 11:255. doi: 10.3389/fpsyt.2020.00255

Electroencephalography (EEG) has long been studied as a potential diagnostic method for Alzheimer's disease (AD). The pathological progression of AD leads to cortical disconnection. These disconnections may manifest as functional connectivity alterations, measured by the degree of synchronization between different brain regions, and alterations in complex behaviors produced by the interaction among wide-spread brain regions. Recently, machine learning methods, such as clustering algorithms and classification methods, have been adopted to detect disease-related changes in functional connectivity and classify the features of these changes. Although complexity of EEG signals can also reflect AD-related changes, few machine learning studies have focused on the changes in complexity. Therefore, in this study, we compared the ability of EEG signals to detect characteristics of AD using different machine learning approaches one focused on functional connectivity and the other focused on signal complexity. We examined functional connectivity, estimated by phase lag index (PLI) in EEG signals in healthy older participants [healthy control (HC)] and patients with AD. We estimated signal complexity using multi-scale entropy. Utilizing a support vector machine, we compared the identification accuracy of AD based on functional connectivity at each frequency band and complexity component. Additionally, we evaluated the relationship between synchronization and complexity. The identification accuracy of functional connectivity of the alpha, beta, and gamma bands was significantly high (AUC 1.0), and the identification accuracy of complexity was sufficiently high (AUC 0.81). Moreover, the relationship between functional connectivity and complexity exhibited various temporal-scale-and-regional-specific dependency in both HC participants and patients with AD. In conclusion, the combination of functional connectivity and complexity might reflect complex pathological process of AD. Applying a combination of both machine learning methods

to neurophysiological data may provide a novel understanding of the neural network processes in both healthy brains and pathological conditions.

Keywords: Alzheimer's disease, electroencephalography, complexity, functional connectivity, machine learning

INTRODUCTION

With a growing aging population, we are awaiting an effective treatment strategy and an early diagnosis test for Alzheimer's disease (AD) (1–4). In AD, three main anatomical changes are observed: progressive neuronal death, neurofibrillary tangles, and senile plaques in widespread brain regions; moreover, recent progress of genome wide association studies have revealed the genes associated with AD (5, 6). For diagnosis, positron emission tomography (PET) imaging and magnetic resonance imaging (MRI) are widely used to detect neurotransmitter activity deficits and deposition of amy loid beta plaques, and brain atrophy, respectively (2–4). As other plausible diagnosis methods, tests based on temporal behaviors of neural activity, which are captured by electroencephalography (EEG), magnetoencephalography (MEG), and functional magnetic resonance imaging (fMRI), have been studied (7–13). Among these methods, those based on EEG are highly effective in clinical application, because they are cost-effective, widely available, and non-invasive (14, 15). The pathological progression of AD leads to cortical disconnection; consequently, in EEG signals, it alters functional connectivity measured by the degree of synchronization between different brain regions and complex behavior produced by the interactions among wide spread brain regions (9, 11, 12, 16–23).

To evaluate the complexity in the EEG signals in patients with AD, some studies have investigated an approach focusing on deterministic chaos and fractal dimension such as correlation dimension and Lyapunov exponent (24). These studies reported reduced complexity in the neural activity of patients with AD (8, 25–30). While, EEG dynamics plays a different role at each temporal-scale, such as memory function, cognitive function, and perceptual function in the theta, beta, and gamma bands, respectively (31). Therefore, an evaluation of the complexity of temporal-scale dependency in the EEG signals of patients with AD is an effective method. For this temporal-scale-specific complexity, several types of evaluation methods have been proposed, e.g., multiscale entropy based on sample entropy for course-grained time-series (32, 33), temporal-scale-specific fractal dimension expanded from Higuchi's fractal dimension (34), and maximum Lyapunov exponent and correlation dimension in band-specific EEG signals processed by wavelet transformation (35, 36). Particularly, our previous study using multi-scale entropy demonstrated that the complexity of EEG signals in patients with AD decreases at smaller (faster) temporal scales, but increases at larger (slower) temporal scales (37). In our study with the temporal-scale-specific fractal dimension, the reduced complexity is restricted to temporal scale regions faster and slower than the alpha band scale; moreover, the complexity around the alpha band scale exhibits high correlation with cognitive decline (34). Further, Adeli and colleagues revealed that alternation of complexity appears at the delta and theta bands in the eyes-open condition and at the delta, theta, and alpha bands by maximum Lyapunov exponent and correlation dimension analysis for band-specific EEG signals (35, 36).

Measuring coherence has long been used to evaluate functional connectivity in patients with AD, and it has revealed band-specific alterations of functional connectivity (38, 39). Wada et al. reported that resting-state functional connectivity reduces in the alpha and beta bands in AD (38). Sankari et al. showed that both enhancement and reduction are observed with frequency-band and spatial dependence (39). However, the studies with traditional synchronization indexes, typified as coherence measurements, correlation and mutual information, are influenced by volume conduction and can detect spurious synchronization (40, 41). To solve this problem, indexes for phase synchronization have been proposed, such as the synchronization likelihood (42), imaginary part of coherency (43) and phase lag index (PLI) (44). These indexes achieve fine temporal and spatial resolution for functional connectivity (42–44). By using this advantage and combining it with neuroimaging modalities that have high spatio-temporal resolution, such as magnetoencephalography (MEG), the alternations in functional connectivity for the whole brain network have been revealed (45–47). Stam et al. reported that functional connectivity in patients with AD estimated by PLI of MEG signals in the alpha and beta bands decreases; moreover, the clustering coefficient and path length of functional connectivity are reduced in the alpha band, i.e., the AD network approaches toward a random network (45). Engels et al. showed through PLI analysis of EEG signals that as AD progresses, the functional connectivity in the alpha band decreases and the hub structure shifts from the posterior to other regions in higher frequency bands (46).

Furthermore, recently, machine learning methods such as clustering algorithms and classification methods such as support vector machines (SVM), have been adopted to detect changes in functional connectivity in diseases (47–54). Yu et al. applied a method used for hierarchical clustering organization in minimum spanning trees on the functional connectivity of EEG signals in AD and frontotemporal dementia; they revealed disease-specific changes in brain network efficiency [Yu etal. (47)]. Khazaee et al. applied several graph measures such as degree, betweenness centrality, and local efficiency of the functional connectivity estimated by resting-state functional magnetic resonance imaging (fMRI) and showed that it accurately identified AD (54). Thus, machine learning approaches to study functional connectivity have been successfully applied to assess AD.

In contrast to these approaches, studies using a machine learning approach based on the complexity of brain activity have rarely been reported (55), despite EEG/MEG signals having features that can be used to identify AD. Within this context, it is important to compare the accuracy of identifying AD in machine learning approaches based on functional connectivity and those based on complexity. Therefore, in this study, we examined the functional connectivity estimated by PLI in EEG signals and the complexity estimated by MSE in healthy older people [healthy control (HC)] and patients with AD. We evaluated the identification accuracy of AD by using an SVM based on functional connectivity at each frequency-band and based on the complexity component. These identified characteristics were also evaluated.

MATERIALS AND METHODS

Participants

The study consisted of 16 participants diagnosed with AD and 18 age- and sex-matched healthy control (HC) participants (34, 37). HC participants were functionally normal, independent in their daily lives, and did not take central-nervous-system-active medications. Patients with AD fulfilled the NINCDS-ADRDA work group criteria for probable AD (56), and the DSM-IV criteria for primary degenerative dementia and presenile onset. Moreover, to remove the other medical factors that induce dementia, the patients with AD were excluded based on neurological, serological, and neuroimaging [MRI and/or Computed Tomography (CT)] tests. The severity of AD in each patient was assessed by the functional assessment stages (FAST) (57) and a Japanese version of MMSE (58). The detailed information of the participants is presented in **Table 1**. Here, the sample size of the patients with AD is larger than that in our previous works (34, 37), because increasing the dataset as much as possible is required for SVM learning. All participants were medication-free, non-habitual drinkers, non-smokers, and right-handed. All participants provided informed consent before the initiation of the study. The study protocol was approved by the Ethics Committee of the Kanazawa University. All procedures of this study were performed in accordance with the Declaration of Helsinki.

TABLE 1 | Physical characteristics in healthy older participants [healthy control (HC)] and Alzheimer's disease (AD) participants.

	HC participants	AD participants	*p* values
Male/female	7/11	5/11	0.72
Age (year)	59.3 (5.3, 55–66)	57.5 (4.7, 43–64)	0.31
MMSE score	NA	15.5 (4.7, 10–26)	NA
Assessment of AD	NA	NINCDS-ADRDA work group criteria for probable AD DSM-IV criteria for primary degenerative dementia and presenile onset	NA
FAST assessment	NA	three (FAST3), seven (FAST4), and six (FAST5) patients.	NA

[Values represent mean (SD, range)]. FAST, functional assessment stages.

EEG Recordings

The method for recording and pre-processing EEG data was established as reported in our previous study (37). During EEG recording, participants were seated in an electrically shielded, sound proofed recording room, and light was controlled. Standard scalp EEG electrodes were located in accordance with the International 10–20 System. In EEG recording, we used an 18-channel electroencephalogram (EEG-4518, Nihon-Koden, Tokyo, Japan) at 16 electrodes sites: Fp1, Fp2, F3, Fz, F4, F7, F8, C3, C4, P3, Pz, P4, T5, T6, O1, and O2, referenced to physically linked ear lobe electrodes. Eye movements were tracked using bipolar electro-oculography (EOG). The EEG signals were recorded with a 200 Hz sampling frequency, a time constant of 0.3, and a 1.5 to 60 Hz bandpass filter. The line noise at 60 Hz was removed by a notch filter. The impedance of electrode/skin conductance for each electrode was carefully controlled at less than 5 kΩ. EEG signals for each participant were measured for 10–15 min under the eyes closed resting condition. Using a video monitoring system, the vigilance state of the participant was visually inspected to ensure only epochs at eyes-closed wakefulness state (and not light sleep) were measured. EEG time-series segments recorded in the eyes-closed wakefulness state were identified by visual inspection of the EEG and EOG recordings. We considered that the participant was fully awake when predominant alpha activity appeared over the posterior regions, corresponding to fast eye movements in the EOG channel (59).

The data were stored on a magnetic optical disk for off-line analysis. Other pre-processing steps (i.e., filtering, artifacts removal, or data reconstruction) were avoided, because they may destroy the intrinsic dynamics of the data; epochs without artifacts were selected after a rigorous visual inspection. To evaluate long temporal dynamics, we initially prepared a single artifact-free, 60-s (12,000 data points) continuous epoch during the eyes-closed resting condition. Additionally, against the above dataset, 1,000 data points at the beginning and end of this epoch were removed to avoid the transition effect of the 1.5 to 60 Hz bandpass filter. MSE analysis was conducted against the continuous 50-s (10,000 data points) epoch. For PLI analysis, a long epoch length prevents identification of disease-specific changes, because the value becomes small with increasing epoch length (60) and vice versa. Furthermore, using a short epoch length cannot capture behaviors with slow frequency components. To balance them, for PLI analysis the continuous 50 s (10,000 data points) was divided into 10 epochs of 5 s (61, 62).

Phase Lag Index

To measure phase synchronization, the characteristics of synchronous signals can be quantitatively estimated at different detection points by calculating the PLI. Firstly, the EEG signals were divided into 5 frequency bands: delta (2–4 Hz), theta (4–8 Hz), alpha (8–13 Hz), beta (13–30 Hz), and gamma (30–60 Hz). Each band-divided signal at time t and point α is represented by the phase $\phi a\ (t)$ and the amplitude $Aa\ (t)$ *via* the Hilbert

transform. Subsequently, the difference in the phases $\Delta\phi_{ab}(t_i)$ observed between signals with two different detecting points α and b at time t_i was written as Stam et al. (44)

$$\Delta\phi_{ab}(t_i) = \phi_a(t_i) - \phi_b(t_i), \quad (1)$$

and

$$\Delta\phi_{\mathrm{mod}}(t_i) = \Delta\phi_{ab}(t_i) \mod 2\pi . \quad (2)$$

From Eq.(2), we obtained $|\Delta\phi_{\mathrm{mod}}(t_i)| \leq \pi$. The PLI of signals between two observed points α–b for a number of signals T is defined as

$$PLI_{ab} = \left| \frac{1}{T} \sum_{i=0}^{T} \mathrm{sign}(\Delta\phi_{\mathrm{mod}}(t_i)) \right|, \quad (3)$$

where the PLI in Eq.(3) is moderately synchronous near 1.0, but is random near 0. From Eq.(1) and Eq.(2), the value of PLI in a case when signals with a common source are observed at different points becomes 0 because $\Delta\phi_{ab}(t_i)$ is 0, and $\Delta\phi_{mod}(t_i) = 0$. In addition, the observation at a point located on the opposite side of the electric dipole has $\Delta\phi_{ab}(t_i) = \pi$ in Eq.(1), where a signal source is assumed to follow the dipole model. Because this results in $\mathrm{PLI}_{ab} = 0$, the PLI also omits this signal.

We considered the averaged PLI of any electrode α through other electrodes $b = 1, 2, \cdots, K(b \neq \alpha)$, which is called the node degree (ND), from Eq.(3) as

$$NDa = \frac{1}{K-1} \sum_{b=1, b\neq a}^{K} \mathrm{PLI}_{ab}, \quad (4)$$

where, K in Eq.(4) represents the total number of electrode, and has K = 16.

Multi-Scale Entropy

In MSE analysis, the sample entropy (SampEn) is calculated by temporal-course grained time-series to evaluate the temporal scale dependency of complexity (32, 33). We define a coarse-grained time series from observed signals x_i ($i = 1, 2, \cdots, T$) over non-overlapping time segments as follows:

$$y_{j,(\tau)} = \frac{1}{\tau} \sum_{i=(j-1)\tau+1}^{j\tau} x_i, \qquad 1 \leq j \leq \frac{T}{\tau}, \quad (5)$$

where is τ a scale factor. Subsequently, the MSE can be evaluated by calculating SampEn in terms of scale factor, which is described as

$$\mathrm{SampEn}(r, m) = -\ln\left[\frac{C_{m+1}(r)}{C_m(r)}\right], \quad (6)$$

where r and m are the tolerance level and the length of the sequences, respectively. $C_m(r)$ in Eq.(6) is given as

$$C_m = \sum_{i,j\in r, i\neq j} \frac{||Y_i^m - Y_j^m||}{(T-m+1)(T-m)}, \quad (7)$$

where $||Y_i^m - Y_j^m||$ indicates that it is counted when the distance between any two vectors Y_i^m and Y_j^m as the norm is less than r, $||Y_i^m - Y_j^m|| = |y(i+l-1) - y(j+l-1)|_{l=1,\cdots,m} \leq r$ From Eq.(7), SampEn becomes 0 when the patterns remain the same and have no complexity, while SampEn becomes large when the patterns have high complexity.

Statistical Analysis

For electrode-pair-wise group comparison of PLI between HC and AD groups, an independent two-tailed t-test was used. Here, t-statistical analysis was controlled by multiple comparison. Particularly, t-values corrected to $q < 0.05, 0.01$ were applied to PLI (600 p values: 120 electrode pairs × 5 bands) according to Benjamini–Hochberg false discovery rate (FDR) correction.

For the ND of PLI, repeated measures analysis of variance (ANOVA), with group (HC vs. AD) as the between-subject factor and electrode (16 electrodes from Fp1 to O2) as the within-subject factor, was performed to test for group differences at each band (delta to gamma bands). The Greenhouse-Geisser adjustment was applied to the degrees of freedom, and α two-tailed level of 0.05 was considered as statistically significant criteria in order to avoid type I error. To assess the significant main effect of group and the electrode-wise interactions, post-hoc t-tests were utilized. To control the multiple comparison, FDR correction was applied to the t-scores of ND ($q < 0.05, 0.01$) (80 p values: 16 electrodes × 5 bands).

For SampEn, repeated measures ANOVA with group (HC vs. AD) as the between-subject factor and electrode (16 electrodes form Fp1 to O2) and temporal scale (20 temporal scales) as within-subject factors, was performed to test for group differences. The Greenhouse-Geisser adjustment and a two-tailed α level of 0.05 were used as well as ND of PLI case. To assess the significant main effect of group and the interactions for electrode-wise and temporal-scale-wise, post-hoc t-tests were utilized. For multiple comparison, FDR correction was applied for the t-scores of SampEn ($q < 0.05, 0.01$) (320 p values: 16 electrode × 20 scales).

For identification of AD, a linear SVM based on the ND of PLI and SampEn was used. As pre-process for classification, by the principal component analysis, the principal components that are required to explain at least 90% variability of all components were chosen in order of the first principal component. SVM learning was conducted using these principal components. To examine the ability to classify HC and AD groups by SVM, we used receiver operating characteristic (ROC) curves that quantify the balance between sensitivity and specificity (63). Performance was evaluated by measuring the area under the ROC curve (AUC), which is an index for the overall identification accuracy. An AUC of 1.0 corresponds to perfect discriminating ability, while an AUC of 0.5 leads to random prediction. Here, 5-fold cross-validation was used.

To evaluate the relationship between synchronization and complexity, we used Pearson's correlation coefficient R between SampEn and ND of PLI. To control the multiple comparison, FDR correction was applied these R-scores ($q < 0.05, 0.01$) (1,600 p values: 16 electrodes × 5 bands × 20 scales).

RESULTS

Phase Lag Index Analysis

Figures 1A, B show the mean PLI values for the HC and AD groups and their difference at each frequency band. *t*-tests with FDR correction in the bottom two rows of **Figure 1B** show significantly decreased PLI values in the AD group at the alpha, beta, and gamma bands. **Table 2** summarizes the repeated measures ANOVA test results for group differences in the ND of PLI. The significant group × electrode interactions and the main effect of group at alpha, beta, and gamma bands. **Figure 1C** shows a post-hoc *t*-test for the ND of PLI controlled by FDR correction and represents edges (electrode pairs) with significant group differences corresponding to **Figure 1B**. In post-hoc *t*-tests for ND, the ND of F8, Fz, P3, Pz, T5, O1, and O2 at the alpha band; the ND of electrodes except for C4, T5, P3, P4, and T6 at the beta band; and the ND of all electrodes at the gamma band passed through the criteria of $q < 0.05$ (corresponding to $p <$

TABLE 2 | Repeated measures ANOVA results for the ND of PLI comparing HC and AD groups for each band.

Frequency band	Group effect	Group × node
delta	$F = 2.18$, $p = 0.14$	$F = 0.83$, $p = 56$
theta	$F = 2.77$, $p = 0.10$	$F = 1.57$, $p = 0.13$
alpha	**$F = 5.80$, $p = 0.02$**	**$F = 3.86$, $p = 2.5 \times 10^{-3}$**
beta	**$F = 12.49$, $p = 1.2 \times 10^{-3}$**	**$F = 10.01$, $p = 0.00$**
gamma	**$F = 27.78$, $p = 9.0 \times 10^{-6}$**	**$F = 8.47$, $p = 0.00$**

For clarity, comparisons with $p < 0.05$ are shown in bold.

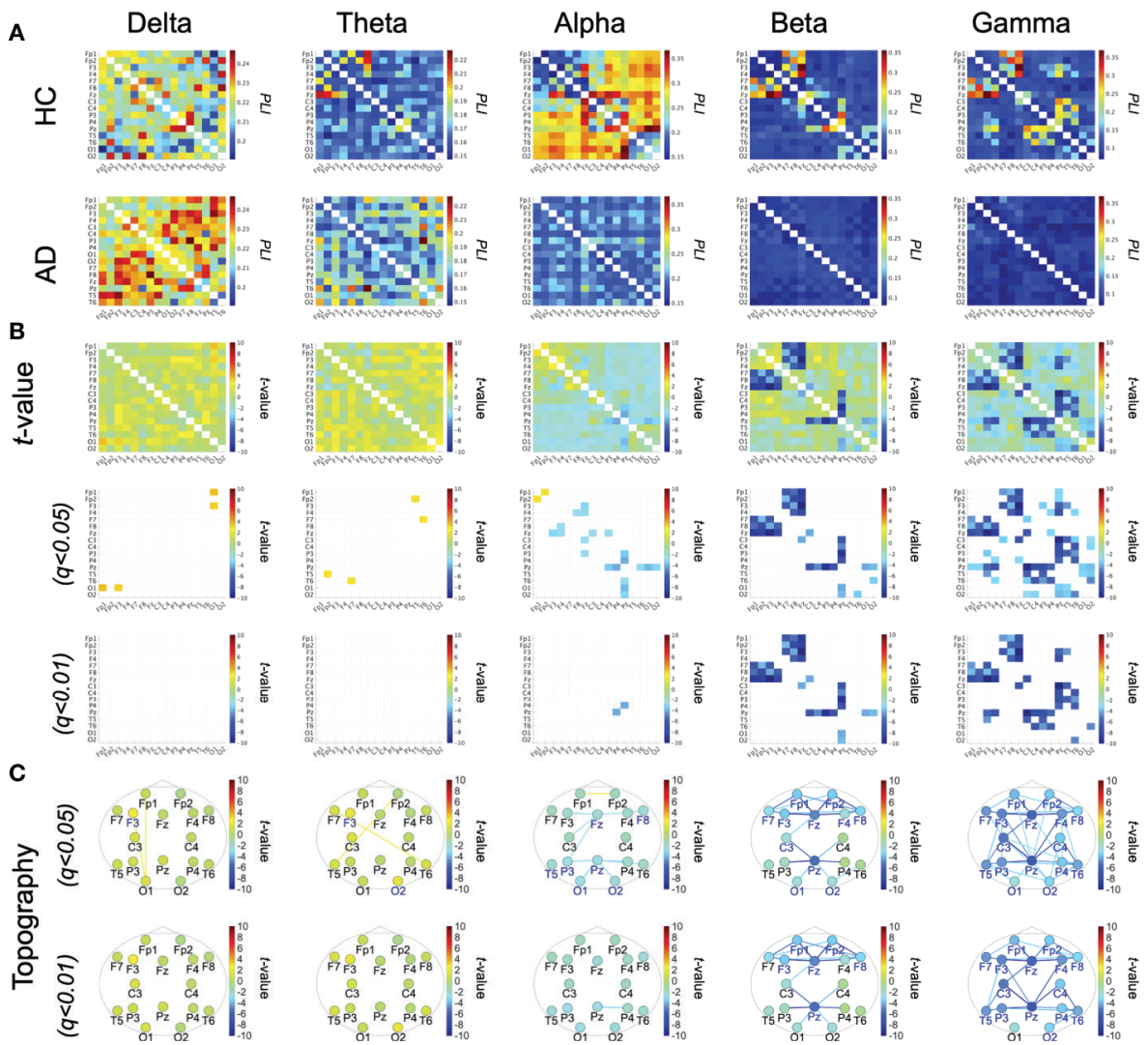

FIGURE 1 | (A) Mean values of phase lag index (PLI) in the healthy control (HC) group and the Alzheimer's disease (AD) group. **(B)** *t*-scores for differences between the HC and AD groups (top parts) and *t*-scores passing through the criteria adjusted for false discovery rate (FDR) $q < 0.05$, $q < 0.01$ (corresponding to) $p < 5.90 \times 10^{-3}$), $p < 6.73 \times 10^{-4}$, respectively) (middle and bottom parts). **(C)** *t*-scores of PLI passing through the criteria adjusted for FDR: $q < 0.05$, 0.01 across the topography. *t*-scores for node degree (ND), where colored electrode labels correspond ones for passing through the criteria after adjustment FDR $q < 0.05$, $q < 0.01$ (corresponding to $p < 0.0232$ $p < 2.51 \times 10^{-3}$, respectively). Bluer (redder) colors represent the reduction (enhancement) of ND/PLI values in AD group.

0.0232). The ND of Fp1, Fp2, F3, F8, Fz, and Pz at the beta band and the ND of all electrodes except for O1 at the gamma band passed through the criteria of $q < 0.01$ (corresponding to $p < 2.51 \times 10^{-3}$). A significant reduction of pair-wised PLI in the AD group was mainly observed at the alpha, beta, and gamma bands among widespread regions.

Multi-Scale Entropy Analysis

Table 3 represents the results of repeated measures ANOVA results for the HC and AD groups. Significant group × scale interactions without the main effect of the group were observed. **Figure 2** shows the mean values of SampEn in the HC and AD groups and the results of the post-hoc *t*-tests. The results indicate a significant reduction of SampEn in AD ($q < 0.05$ corresponding to $p < 0.0029$) in the 1-5 scale ranges at F3 [scale 2: $t = -3.85$ ($p < 5.2 \times 10^{-4}$), scale 3: $t = -3.99$ ($p = 8.35 \times 10^{-4}$), scale 4: $t = -3.54$ $p = 0.0025$], F4 [scale 2: $t = -3.82$ $p = 0.0029$, scale 3: $t = -3.79$ ($p = 0.0011$), scale 4: $t = -3.82$ ($p = 0.0011$)], Fz [scale 2: $t = -4.33$ ($p = 1.36 \times 10^{-4}$), scale 3: $t = -4.77$ ($p = 9.89 \times 10^{-5}$), scale 4: $t = -4.67$ ($p = 1.91 \times 10^{-4}$)], C3 [scale 2: $t = -3.75$ ($p = 6.94 \times 10^{-4}$), scale 3: $t = -4.48$ ($p = 2.13 \times 10^{-4}$), scale 4: $t = -4.24$ ($p = 5.07 \times 10^{-4}$)], C4 [scale 3: $t = -3.90$ ($p = 7.53 \times 10^{-4}$), scale 4: $t = -3.66$ ($p = 0.0015$)], P3 [scale 3: $t = -3.59$ ($p = 0.0011$)], P4 [scale 4: $t = -3.33$ ($p = 0.0022$)], and T6 [scale 3: $t = -3.36$ ($p = 0.0020$), scale 4: $t = -3.41$ ($p = 0.0018$)].

Classification by the ND of PLI and MSE

AD was identified by linear SVM using significant reduction of the ND of PLI at the alpha, beta, and gamma bands. **Table 4** summarizes the accuracy of the classification between HC and AD by linear SVM based on the ND of PLI. Here, the ND values of all nodes were used at each band. The high ability to identify AD was confirmed (AUC = 10).

In MSE analysis, in the scale ranges 1–5, a significant reduction of SampEn in the AD group was confirmed (see **Figure 2**). Against the mean value of SampEn in scales 1.5 at all electrodes, the linear SVM was adopted. **Table 5** shows the relatively high accuracy of identification (AUC = 81).

Correlation Between Synchronization and Complexity

To evaluate the relationship between the ND of PLI and SampEn, the correlation coefficients between SampEn and the ND of PLI in the HC and AD groups were evaluated in **Figure 3**. The results show significantly high correlation passing through the criteria of FDR ($q < 0.05$, 0.01) in the alpha, beta, gamma bands. Particularly, a high positive correlation was observed at the frontal, central, parietal regions in the scale-range ≈ 5 in alpha and beta bands in the HC case. In the AD case, this correlation was observed at F7 and F8 in the alpha band. Moreover, a significant high negative correlation was observed at F4 at scales 5 and 6 in the gamma band in the HC case. In the AD case, this negative correlation was observed in a widespread region in the scale-range $\gtrsim 10$ in alpha and beta bands. **Figure 4** shows the scatter plots between SampEn at scale 5 and the ND of PLI at alpha, beta, and gamma bands at the F3 and F4 electrode in HC and AD cases. The slopes of correlation are different in HC and AD groups (The values of slope and *R* are represented in **Figure 4**).

TABLE 3 | Repeated measures ANOVA results for Sample Entropy (SampEn) comparing HC and AD groups.

Group effect	Group × electrode	Group × scale	Group × electrode × scale
$F = 0.17$, $p = 0.68$	$F = 1.12$, $p = 0.34$	**$F = 6.67$, $p = 2.05 \times 10^{-3}$**	$F = 1.43$, $p = 0.163$

For clarity, comparisons with p < *0.05 are shown in bold.*

DISCUSSION AND CONCLUSION

In this study, we evaluated functional connectivity using PLI and complexity by measuring MSE in HC and AD groups. Significant reductions of PLI in the alpha, beta, and gamma bands and of SampEn at small (fast) temporal-scales were confirmed in AD group. Next, we classified the HC and AD groups by the linear SVM using the ND of PLI and SampEn averaged in the small temporal-scale range. We confirmed a significantly higher identification accuracy of the functional connectivity of the alpha, beta, and gamma bands (AUC: 10), and a sufficiently high identification accuracy of complexity (AUC: 81). Furthermore, we evaluated the relationship between functional connectivity and complexity, and found various temporal-scale-and-regional-specific dependencies in both HC participants and patients with AD.

Regarding functional connectivity in the EEG/MEG signals in patients with AD, many previous studies have reported a reduction in functional connectivity at the alpha, beta, and gamma bands (38, 45, 46, 64). Further, recent studies of AD pathology have revealed that the reduction in functional connectivity is caused by neuroinflammation and deposition of amyloid-β and tau proteins (65–67). Similar reductions in functional connectivity were also observed in this study. Regarding the complexity of the EEG/MEG signals in patients with AD, many studies have reported alternations of temporal behaviors (23); particularly, the reduction in the complexity of the EEG/MEG signals in patients with AD (8, 22, 25–30). Analysis of the indexes for temporal-scale-dependent complexity has shown that this reduction of complexity especially concentrates in fast wave components (34, 36). Studies of neurotransmitter changes in AD have reported that dysfunction of the gamma-aminobutyric acid (GABA) signaling system, which is caused by the deposition of amyloid- β and tau proteins, leads to reduced oscillatory gamma band activity (68–70). The impairment of gamma oscillatory activity might lead the complexity at faster temporal scales more than slower temporal scales (34, 36). The results obtained with MSE analysis are congruent with these findings.

We must consider the reason the changes in functional connectivity exhibited significant regional specificity, while the complexity did not. As a plausible explanation, it is assumed that synchronization is determined by the interaction between brain

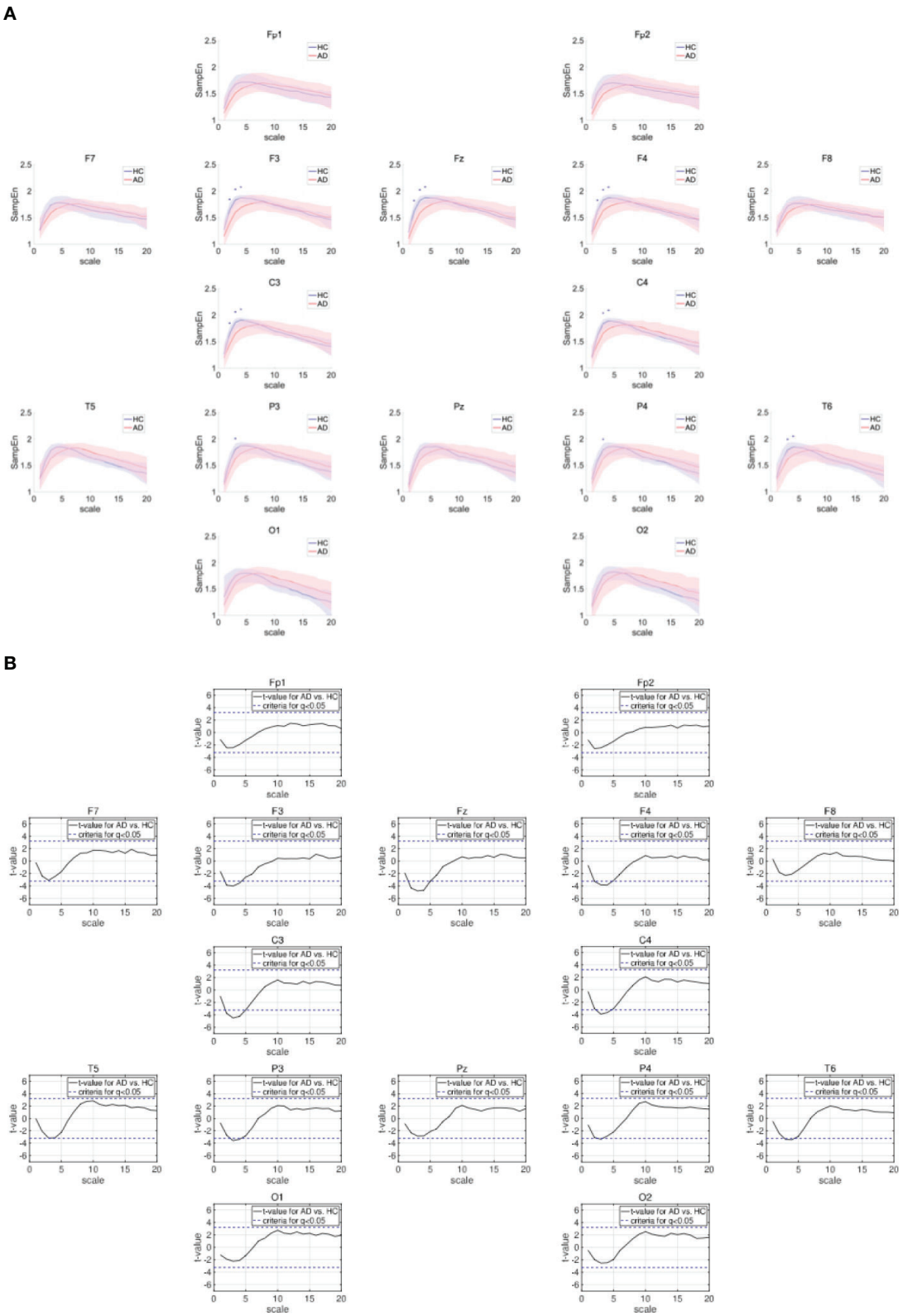

FIGURE 2 | Continued

FIGURE 2 | (A) Dependence of sample entropy (SampEn) on temporal scale. The blue + indicates the significant group difference satisfying the criteria after adjustment for FDR: $q < 0.05$ (corresponding to to $p < 0.0029$). Here, no significant group differences satisfying $q < 0.01$ were identified. **(B)** Dependence of *t*-values between SampEns for AD and ones for AD on temporal scale. Positive (negative) values indicate larger (smaller) SampEns for AD in comparison with HC. The *t*-values for criteria after adjustment FDR: $q < 0.05$ are represented by blue dashed lines ($|t| > 3.23$).

TABLE 4 | Accuracy of classification between HC and AD by ND.

	Accuracy (%)	AUC	Size of principal components
Alpha band	100	1.0	4
Beta band	100	1.0	7
Gamma band	100	1.0	6

Here, the linear support vector machine (SVM) was used as the classification method and 5-fold cross-validation. Size of principal components means the size of components required to explain at least 90% variability of all components. AUC, area under the ROC curve.

TABLE 5 | Accuracy of classification between HC and AD by SampEn. AUC, area under the ROC curve.

	Accuracy (%)	AUC	Size of principal components
Mean SampEn in scale 1–5	73.5	0.81	3

regional pairs, while the characteristics of complexity are produced by interactions among wide-spread brain regions (9). Therefore, it might be difficult when complexity exhibits regional specificity. Model-based studies regarding the relationship between complex neural behavior and topological features of the whole network support these findings (71–75). In the classification of HC and AD by SVM, the ND or the mean SampEn averaged in fast temporal-scale region at 16 electrodes were used. Higher disease-specific regional dependency might enhance the accuracy of identification of AD, because classification can be conducted in a feature space with larger dimensions. Therefore, it can be assumed that SVM based on the ND of PLI with higher regional dependency exhibited higher identification accuracy in comparison with one based on SampEn.

Furthermore, we must discuss the necessity of focusing on the complexity of EEG/MEG signals to identify AD. Cortical disconnection, which is induced by the pathological progression of AD, leads to impairment in the interaction

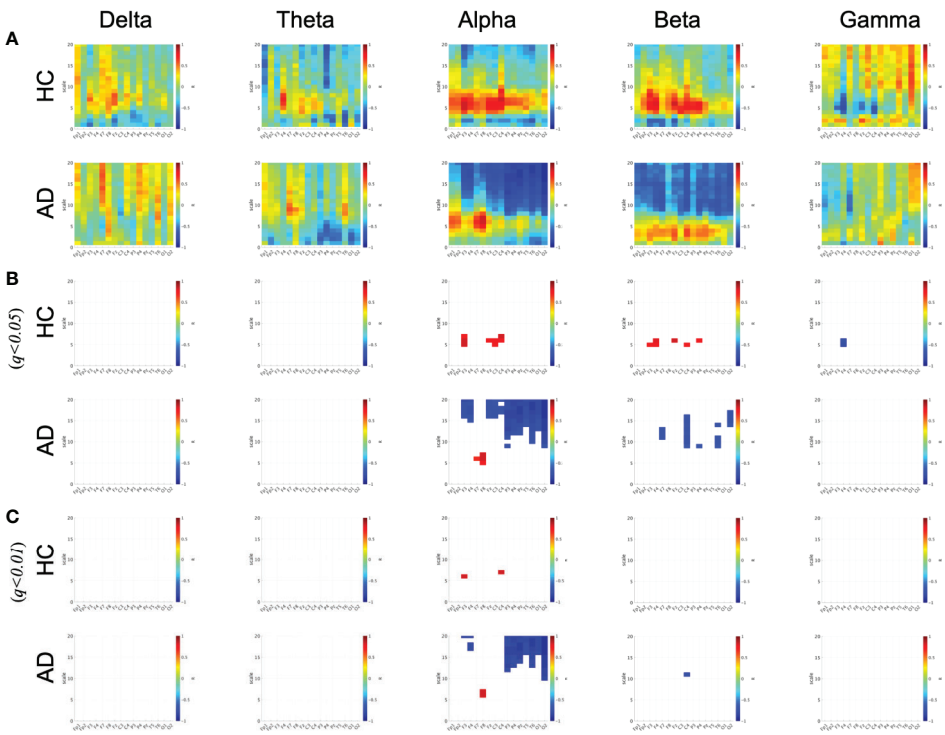

FIGURE 3 | Correlation coefficient *R* between SampEn and the ND of PLI in HC and AD cases. There are significantly high positive and negative correlations passing through criteria of FDR ($q < 0.05$, 0.01) in alpha, beta, and gamma bands in HC and AD cases. **(A)** Correlation coefficient R. **(B)** R satisfying q<0.05. **(C)** R satisfying q<0.01.

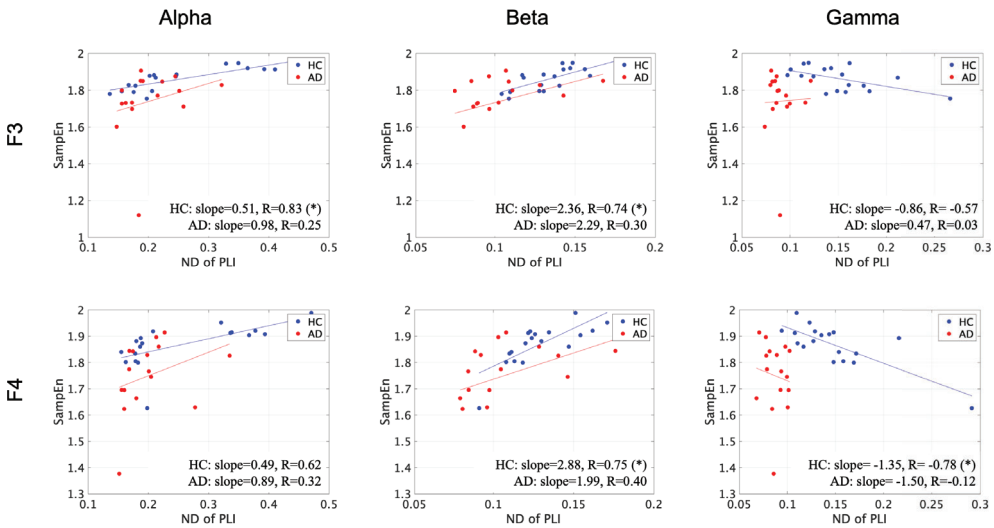

FIGURE 4 | Scatter plots between SampEn at scale 5 and ND of PLI at alpha, beta, and gamma bands at F3 and F4 electrode in HC and AD cases. Here, the solid lines indicated the linear regression lines (blue: linear regression line for HC, red: linear regression line for AD). The correlation coefficient R [R value satisfying $q < 0.05$ is represented by (*)] and slope in the linear regression were described by text in figures. The slopes of correlation are different in HC and AD groups.

between different brain regions; consequently reducing functional connectivity and complexity (9, 11, 12, 16, 17, 19–21). The positive correlation between them (see **Figure 3**) can be supported by these findings. Moreover, the slopes in these correlations were different between the HC and AD groups (see **Figure 4**). Therefore, this relationship between complexity and functional connectivity could be used for diagnosis of AD. Not only positive correlation but also negative correlation was confirmed in **Figure 3**. According to nonlinear dynamical theory, it is known that non-linear coupled oscillations exhibit enhancement of complexity by emergence of a chaotic state during the process of reducing the efficiently strong coupled strength for the state of complete synchronization [reviewed in (76). This induced enhancement is attributed to perturbations to the stable orbit from each oscillation's behavior (77, 78). Synchronization decreases during the process of decreasing coupled strength, and complexity enhances. The negative correlation observed in this study could be interpreted by this mechanism. These findings suggest that a combination of functional connectivity and complexity might reflect the complex pathological process of AD.

To investigate if the high heterogeneity of age and severity in the patients with AD affected classification, we performed repeated measures ANOVA in the AD group. For MSE analysis, the repeated measures ANOVA was performed with age [high age vs. low age (these groups were divided by median of AD age distribution = 59.5 years)] and severity (FAST scale score: 3, 4, and 5) as between-subject factors, and electrode and scale factor as within-subject factors. The results showed no significant high main effect and interactions. For the ND of PLI at each frequency band, the repeated measures ANOVA was performed with age (high age vs. low age) and severity (FAST scale score: 3, 4, and 5) as between-subject factors, and electrode as a within-subjects factor. The results showed that severity did not demonstrate any significant main effects or interaction. In contrast to the MSE case, age showed a significant high main effect in the theta [$F = 5.86$ ($p = 0.0029$)], beta [$F = 6.16$ ($p = 0.026$)], and gamma [$F = 8.9$ ($p = 9.84 \times 10^{-3}$)] bands, and a significant high interaction between age vs. electrodes at the beta [$F = 4.73$ ($p = 1.59 \times 10^{-3}$)] and gamma [$F = 5.10$ ($p = 2.41 \times 10^{-4}$)] bands. Further, in larger AD groups, the severity-dependent effect may appear in both PLI and MSE cases. Therefore, to consider these effects in classification by SVM, a larger sample size is necessary.

This study has limitations that must be considered. The data set of the HC and AD groups used in this study can completely identify AD using SVM and the ND of PLI. Therefore, the effect of enhancing identification accuracy by combining with components of SampEn cannot be evaluated. To evaluate this effect, the classification of the severity of AD (FAST 3, 4, and 5) may be appropriate. However, for this evaluation, the size of data set used in this study was too small for SVM learning. Moreover, the AD group had high heterogeneity of age and severity, which could have influenced the accuracy of the classification by SVM. However, the sample size of the AD group was too small to quantify this influence. In future studies, we will evaluate these issues using a larger data set of AD EEG signals. Another limitation of this study is that the EEG signals do not necessarily reflect neural activity directly under the electrodes; the spacial resolution of the 16 electrodes used in this study was too low to identify the complex functional connectivity structures relating to AD pathology. Therefore, the use of

neuroimaging modalities with more precise and higher spatial resolution, such as MEG and cortical source localization, may provide the necessary spatial information. Finally, data sets of other pathological conditions, such as schizophrenia and autism spectrum disorder, and healthy aging must be evaluated by the machine learning method used in this study.

In conclusion, we confirmed that the identification accuracy of SVM based on functional connectivity was significantly high, and the identification accuracy of SVM based on complexity was sufficiently high. Moreover, the combination of functional connectivity and complexity might reflect the complex pathological process of AD. Although some limitations must be considered, applying a combination of machine learning methods to neurophysiological data may provide a novel understanding of the neural network processes in both healthy brains and pathological conditions.

DATA AVAILABILITY STATEMENT

The datasets generated for this study will not be made publicly available because the informed consent did not include the declaration regarding publicity of clinical data. Requests to access the datasets should be directed to the corresponding author.

ETHICS STATEMENT

The studies involving human participants were reviewed and approved by the Ethics Committee of the Kanazawa University. The patients/participants provided their written informed consent to participate in this study.

AUTHOR CONTRIBUTIONS

SN, TY, TT, MK, and HN conceived the methods. SN, TY, SK, and TT analyzed the results, wrote the main manuscript text, and prepared all the figures. MK conducted the experiments. All authors reviewed the manuscript.

FUNDING

This work was supported by JSPS KAKENHI for Early-Career Scientists (grant number 18K18124) (SN) and for Scientific Research (C) (grant number 18K11450) (TY).

REFERENCES

1. Spalletta G, Musicco M, Padovani A, Perri R, Fadda L, Canonico V, et al. Neuropsychiatric symptoms and syndromes in a large cohort of newly diagnosed, untreated patients with Alzheimer disease. *Am J Geriatr Psychiatry* (2010) 18:1026–35. doi: 10.1097/JGP.0b013e3181d6b68d
2. McKhann GM, Knopman DS, Chertkow H, Hyman BT, Jack CRJr., Kawas CH, et al. The diagnosis of dementia due to Alzheimer's disease: Recommendations from the national institute on Aging-Alzheimer's Association workgroups on diagnostic guidelines for Alzheimer's disease. *Alzheimers Demen* (2011) 7:263–9. doi: 10.1016/j.jalz.2011.03.005
3. Sperling RA, Aisen PS, Beckett LA, Bennett DA, Craft S, Fagan AM, et al. Toward defining the preclinical stages of Alzheimer's disease: Recommendations from the national institute on Aging-Alzheimer's association workgroups on diagnostic guidelines for Alzheimer's disease. *Alzheimers Demen* (2011) 7:280–92. doi: 10.1016/j.jalz.2011.03.003
4. Ewers M, Sperling RA, Klunk WE, Weiner MW, Hampel H. Neuroimaging markers for the prediction and early diagnosis of Alzheimer's disease dementia. *Trends Neurosci* (2011) 34:430–42. doi: 10.1016/j.tins.2011.05.005
5. Sims R, Van Der Lee SJ, Naj AC, Bellenguez C, Badarinarayan N, Jakobsdottir J, et al. Rare coding variants in PLCG2, ABI3, and TREM2 implicate microglial-mediated innate immunity in Alzheimer's disease. *Nat Genet* (2017) 49:1373–84. doi: 10.1038/ng.3916
6. Yamaguchi-Kabata Y, Morihara T, Ohara T, Ninomiya T, Takahashi A, Akatsu H, et al. Integrated analysis of human genetic association study and mouse transcriptome suggests LBH and SHF genes as novel susceptible genes for amyloid-β accumulation in Alzheimer's disease. *Hum Genet* (2018) 137:521–33. doi: 10.1007/s00439-018-1906-z
7. Greicius MD, Srivastava G, Reiss AL, Menon V. Default-mode network activity distinguishes Alzheimer's disease from healthy aging: evidence from functional MRI. *Proc Natl Acad Sci* (2004) 101:4637–42. doi: 10.1073/pnas.0308627101
8. Jeong J. Eeg dynamics in patients with alzheimer's disease. *Clin Neurophysiol* (2004) 115:1490–505. doi: 10.1016/j.clinph.2004.01.001
9. Stam CJ. Nonlinear dynamical analysis of EEG and MEG: review of an emerging field. *Clin Neurophysiol* (2005) 116:2266–301. doi: 10.1016/j.clinph.2005.06.011
10. Dickerson BC, Sperling RA. Functional abnormalities of the medial temporal lobe memory system in mild cognitive impairment and Alzheimer's disease: insights from functional MRI studies. *Neuropsychologia* (2008) 46:1624–35. doi: 10.1016/j.neuropsychologia.2007.11.030
11. Yang AC, Tsai S-J. Is mental illness complex? from behavior to brain. *Prog Neuropsychopharmacol Biol Psychiatry* (2013) 45:253–7. doi: 10.1016/j.pnpbp.2012.09.015
12. Takahashi T. Complexity of spontaneous brain activity in mental disorders. *Prog Neuropsychopharmacol Biol Psychiatry* (2013) 45:258–66. doi: 10.1016/j.pnpbp.2012.05.001
13. Wang B, Niu Y, Miao L, Cao R, Yan P, Guo H, et al. Decreased complexity in Alzheimer's disease: resting-state fMRI evidence of brain entropy mapping. *Front Aging Neurosci* (2017) 9:378. doi: 10.3389/fnagi.2017.00378
14. Vecchio F, Babiloni C, Lizio R, Fallaní FDV, Blinowska K, Verrienti G, et al. Resting state cortical EEG rhythms in Alzheimer's disease: toward EEG markers for clinical applications: a review. *Suppl Clin Neurophysiol* (2013) 62:223–36. doi: 10.1016/B978-0-7020-5307-8.00015-6
15. Kulkarni N, Bairagi V. *EEG-based diagnosis of Alzheimer disease: a review and novel approaches for feature extraction and classification techniques*. (2018).
16. Delbeuck X, Van der Linden M, Collette F. Alzheimer'disease as a disconnection syndrome? *Neuropsychol Rev* (2003) 13:79–92. doi: 10.1023/a:1023832305702
17. Adeli H, Ghosh-Dastidar S, Dadmehr N. Alzheimer's disease: models of computation and analysis of EEG. *Clin EEG Neurosci* (2005) 36:131–40. doi: 10.1177/155005940503600303
18. Sperling R. Functional MRI studies of associative encoding in normal aging, mild cognitive impairment, and Alzheimer's disease. *Ann N Y Acad Sci* (2007) 1097:146–55. doi: 10.1196/annals.1379.009
19. Dauwels J, Vialatte F, Musha T, Cichocki A. A comparative study of synchrony measures for the early diagnosis of Alzheimer's disease based on EEG. *NeuroImage* (2010) 49:668–93. doi: 10.1016/j.neuroimage.2009.06.056
20. Bhat S, Acharya UR, Dadmehr N, Adeli H. Clinical neurophysiological and automated EEG-based diagnosis of the Alzheimer's disease. *Eur Neurol* (2015) 74:202–10. doi: 10.1159/000441447
21. Mammone N, Bonanno L, Salvo SD, Marino S, Bramanti P, Bramanti A, et al. Permutation disalignment index as an indirect, EEG -based, measure of brain

connectivity in MCI and AD patients. *Int J Neural Syst* (2017) 27:1750020. doi: 10.1142/S0129065717500204
22. Kulkarni N. Use of complexity based features in diagnosis of mild Alzheimer disease using EEG signals. *Int J Inf Technol* (2018) 10:59–64. doi: 10.1007/s41870-017-0057-0
23. Smailovic U, Koenig T, Laukka EJ, Kalpouzos G, Andersson T, Winblad B, et al. EEG time signature in Alzheimer´ s disease: Functional brain networks falling apart. *NeuroImage: Clin* (2019) 24:102046. doi: 10.1016/j.nicl.2019.102046
24. Kantz H, Schreiber T. *Nonlinear time series analysis* Vol. 7. (Cambridge, UK: Cambridge University Press). (2003).
25. Woyshville MJ, Calabrese JR. Quantification of occipital EEG changes in Alzheimer's disease utilizing a new metric: the fractal dimension. *Biol Psychiatry* (1994) 35:381–7. doi: 10.1016/0006-3223(94)90004-3
26. Besthorn C, Sattel H, Geiger-Kabisch C, Zerfass R, Förstl H. Parameters of EEG dimensional complexity in Alzheimer's disease. *Electroencephalography Clin Neurophysiol* (1995) 95:84–9. doi: 10.1016/0013-4694(95)00050-9
27. Jelles B, Van Birgelen J, Slaets J, Hekster R, Jonkman E, Stam C. Decrease of non-linear structure in the EEG of Alzheimer patients compared to healthy controls. *Clin Neurophysiol* (1999) 110:1159–67. doi: 10.1016/S1388-2457(99)00013-9
28. Abásolo D, Escudero J, Hornero R, Espino P, Gómez C. Fractal dimension of the EEG in´ alzheimer's disease. In: *Encyclopedia of Healthcare Information Systems*. (Pennsylvania, US: IGI Glonal). (2008). p. 603–9.
29. Smits FM, Porcaro C, Cottone C, Cancelli A, Rossini PM, Tecchio F. Electroencephalographic fractal dimension in healthy ageing and Alzheimer's disease. *PloS One* (2016) 11:e0149587. doi: 10.1371/journal.pone.0149587
30. Al-nuaimi AH, Jammeh E, Sun L, Ifeachor E. Higuchi fractal dimension of the electroencephalogram as a biomarker for early detection of alzheimer's disease. In: *Engineering in Medicine and Biology Society (EMBC), 2017 39th Annual International Conference of the IEEE*. (Seogwipo, South Korea) (2017), p. 2320–4.
31. Klimesch W, Sauseng P, Hanslmayr S, Gruber W, Freunberger R. Event-related phase reorganization may explain evoked neural dynamics. *Neurosci Biobehav Rev* (2007) 31:1003–16. doi: 10.1016/j.neubiorev.2007.03.005
32. Costa M, Goldberger AL, Peng C-K. Multiscale entropy analysis of complex physiologic time series. *Phys Rev Lett* (2002) 89:068102. doi: 10.1103/PhysRevLett.89.068102
33. Costa M, Goldberger AL, Peng C-K. Multiscale entropy analysis of biological signals. *Phys Rev E* (2005) 71:021906. doi: 10.1103/PhysRevE.71.021906
34. Nobukawa S, Yamanishi T, Nishimura H, Wada Y, Kikuchi M, Takahashi T. Atypical temporal-scale-specific fractal changes in Alzheimer's disease eeg and their relevance to cognitive decline. *Cogn Neurodyn* (2019b) 13:1–11. doi: 10.1007/s11571-018-9509-x
35. Adeli H, Ghosh-Dastidar S, Dadmehr N. A spatio-temporal wavelet-chaos methodology for EEG -based diagnosis of Alzheimer's disease. *Neurosci Lett* (2008) 444:190–4. doi: 10.1016/j.neulet.2008.08.008
36. Ahmadlou M, Adeli H, Adeli A. Fractality and a wavelet-chaos-methodology for EEG -based diagnosis of alzheimer disease. *Alzheimer Dis Assoc Disord* (2011) 25:85–92. doi: 10.1097/WAD.0b013e3181ed1160
37. Mizuno T, Takahashi T, Cho RY, Kikuchi M, Murata T, Takahashi K, et al. Assessment of EEG dynamical complexity in Alzheimer's disease using multiscale entropy. *Clin Neurophysiol* (2010) 121:1438–46. doi: 10.1016/j.clinph.2010.03.025
38. Wada Y, Nanbu Y, Kikuchi M, Koshino Y, Hashimoto T, Yamaguchi N. Abnormal functional connectivity in Alzheimer's disease: intrahemispheric EEG coherence during rest and photic stimulation. *Eur Arch Psychiatry Clin Neurosci* (1998) 248:203–8. doi: 10.1007/s004060050038
39. Sankari Z, Adeli H, Adeli A. Intrahemispheric, interhemispheric, and distal EEG coherence in Alzheimer's disease. *Clin Neurophysiol* (2011) 122:897–906. doi: 10.1016/j.clinph.2010.09.008
40. Nunez PL, Srinivasan R, Westdorp AF, Wijesinghe RS, Tucker DM, Silberstein RB, et al. EEG coherency: I: statistics, reference electrode, volume conduction, laplacians, cortical imaging, and interpretation at multiple scales. *Electroencephalogr Clin Neurophysiol* (1997) 103:499–515. doi: 10.1016/S0013-4694(97)00066-7
41. Nolte G, Holroyd T, Carver F, Coppola R, Hallett M. Localizing brain interactions from rhythmic EEG/MEG data. In: *The 26th Annual International Conference of the IEEE Engineering in Medicine and Biology Society*, vol. 1. (San Francisco, CA, USA) (2004b). p. 998–1001.
42. Stam C, Van Dijk B. Synchronization likelihood: an unbiased measure of generalized synchronization in multivariate data sets. *Physica D: Nonlin Phenom* (2002) 163:236–51. doi: 10.1016/S0167-2789(01)00386-4
43. Nolte G, Bai O, Wheaton L, Mari Z, Vorbach S, Hallett M. Identifying true brain interaction from EEG data using the imaginary part of coherency. *Clin Neurophysiol* (2004a) 115:2292–307. doi: 10.1016/j.clinph.2004.04.029
44. Stam CJ, Nolte G, Daffertshofer A. Phase lag index: assessment of functional connectivity from multi channel EEG and MEG with diminished bias from common sources. *Hum Brain Mapp* (2007) 28:1178–93. doi: 10.1002/hbm.20346
45. Stam C, De Haan W, Daffertshofer A, Jones B, Manshanden I, van Cappellen van Walsum AM, et al. Graph theoretical analysis of magnetoencephalographic functional connectivity in Alzheimer's diseasein alpha band. *Brain* (2008) 132:213–24. doi: 10.1093/brain/awn262
46. Engels MM, Stam CJ, van der Flier WM, Scheltens P, de Waal H, van Straaten EC. Declining functional connectivity and changing hub locations in Alzheimer's disease: an EEG study. *BMC Neurol* (2015) 15:145. doi: 10.1186/s12883-015-0400-7
47. Yu M, Gouw AA, Hillebrand A, Tijms BM, Stam CJ, van Straaten EC, et al. Different functional connectivity and network topology in behavioral variant of frontotemporal dementia and Alzheimer's disease: an EEG study. *Neurobiol Aging* (2016) 42:150–62. doi: 10.1016/j.neurobiolaging.2016.03.018
48. Shen H, Wang L, Liu Y, Hu D. Discriminative analysis of resting-state functional connectivity patterns of schizophrenia using low dimensional embedding of fMRI. *Neuroimage* (2010) 49:3110–21. doi: 10.1016/j.neuroimage.2009.11.011
49. Lemm S, Blankertz B, Dickhaus T, Muller K-R. Introduction to machine learning for¨ brain imaging. *Neuroimage* (2011) 56:387–99. doi: 10.1016/j.neuroimage.2010.11.004
50. Hulbert S, Adeli H. EEG/MEG-and imaging-based diagnosis of Alzheimer's disease. *Rev Neurosci* (2013) 24:563–76. doi: 10.1515/revneuro-2013-0042
51. Richiardi J, Achard S, Bunke H, Van De Ville D. Machine learning with brain graphs: Predictive modeling approaches for functional imaging in systems neuroscience. *IEEE Signal Process Mag* (2013) 30:58–70. doi: 10.1109/MSP.2012.2233865
52. Jamal W, Das S, Oprescu I-A, Maharatna K, Apicella F, Sicca F. Classification of autism spectrum disorder using supervised learning of brain connectivity measures extracted from synchrostates. *J Neural Eng* (2014) 11:046019. doi: 10.1088/1741-2560/11/4/046019
53. Zeng L-L, Shen H, Liu L, Hu D. Unsupervised classification of major depression using functional connectivity MRI. *Hum Brain Mapp* (2014) 35:1630–41. doi: 10.1002/hbm.22278
54. Khazaee A, Ebrahimzadeh A, Babajani-Feremi A. Identifying patients with Alzheimer's disease using resting-state fMRI and graph theory. *Clin Neurophysiol* (2015) 126:2132–41. doi: 10.1016/j.clinph.2015.02.060
55. Kulkarni N, Bairagi V. Extracting salient features for EEG -based diagnosis of Alzheimer's disease using support vector machine classifier. *IETE J Res* (2017) 63:11–22. doi: 10.1080/03772063.2016.1241164
56. McKhann G, Drachman D, Folstein M, Katzman R, Price D, Stadlan EM. Clinical diagnosis of Azheimer's disease: Report of the NICNDS-ADRDA work group* under the auspices of Department of Health and Human Services Task Force on Alzheimer's Disease. *Neurology* (1984) 34:939–9. doi: 10.1212/WNL.34.7.939
57. Reisberg B. Functional assessment staging (FAST). *Psychopharmacol Bull* (1988) 24:653–9. doi: 10.1037/t08620-000
58. Folstein MF, Folstein SE, McHugh PR. "mini-mental state": a practical method for grading the cognitive state of patients for the clinician. *J Psychiatr Res* (1975) 12:189–98. doi: 10.1016/0022-3956(75)90026-6
59. Wada Y, Nanbu Y, Koshino Y, Shimada Y, Hashimoto T. Inter-and intrahemispheric EEG coherence during light drowsiness. *Clin EEG Neurosci* (1996) 27:84–8. doi: 10.1177/155005949602700207

60. Fraschini M, Demuru M, Crobe A, Marrosu F, Stam CJ, Hillebrand A. The effect of epoch length on estimated EEG functional connectivity and brain network organisation. *J Neural Eng* (2016) 13:036015. doi: 10.1088/1741-2560/13/3/036015
61. Takahashi T, Yamanishi T, Nobukawa S, Kasakawa S, Yoshimura Y, Hiraishi H, et al. Band-specific atypical functional connectivity pattern in childhood autism spectrum disorder. *Clin Neurophysiol* (2017) 128:1457–65. doi: 10.1016/j.clinph.2017.05.010
62. Takahashi T, Goto T, Nobukawa S, Tanaka Y, Kikuchi M, Higashima M, et al. Abnormal functional connectivity of high-frequency rhythms in drug-naïve schizophrenia. *Clin Neurophysiol* (2018) 129:222–31. doi: 10.1016/j.clinph.2017.11.004
63. Zweig MH, Campbell G. Receiver-operating characteristic (roc) plots: a fundamental evaluation tool in clinical medicine. *Clin Chem* (1993) 39:561–77. doi: 10.1093/clinchem/39.4.561
64. Lee S-H, Park Y-M, Kim D-W, Im C-H. Global synchronization index as a biological correlate of cognitive decline in Alzheimer's disease. *Neurosci Res* (2010) 66:333–9. doi: 10.1016/j.neures.2009.12.004
65. Jagust W. Imaging the evolution and pathophysiology of alzheimer disease. *Nat Rev Neurosci* (2018) 19:687–700. doi: 10.1038/s41583-018-0067-3
66. Passamonti L, Tsvetanov K, Jones P, Bevan-Jones WR, Arnold R, Borchert RJ, et al. Neuroinflammation and functional connectivity in Alzheimer's disease: interactive influences on cognitive performance. *J Neurosci* (2019) 39:7218–26. doi: 10.1523/JNEUROSCI.2574-18.2019
67. Contreras JA, Aslanyan V, Sweeney MD, Sanders LM, Sagare AP, Zlokovic BV, et al. Functional connectivity among brain regions affected in alzheimer's disease is associated with CSF TNF-α *in* apoe4 carriers. *Neurobiol Aging* (2020) 86:112–22. doi: 10.1016/j.neurobiolaging.2019.10.013
68. Nava-Mesa MO, Jiménez-Díaz L, Yajeya J, Navarro-Lopez JD. Gabaergic neurotransmission and new strategies of neuromodulation to compensate synaptic dysfunction in early stages of Alzheimer's disease. *Front Cell Neurosci* (2014) 8:167. doi: 10.3389/fncel.2014.00167
69. Govindpani K, Calvo-Flores Guzmán B, Vinnakota C, Waldvogel HJ, Faull RL, Kwakowsky A. Towards a better understanding of gabaergic remodeling in Alzheimer's disease. *Int J Mol Sci* (2017) 18:1813. doi: 10.3390/ijms18081813
70. Calvo-Flores Guzmán B, Vinnakota C, Govindpani K, Waldvogel H, Faull R, Kwakowsky A. The GABAergic system as a therapeutic target for Alzheimer's disease. *J Neurochem* (2018) 146.6(2018):649–669. doi: 10.1111/jnc.14345
71. Ostojic S. Two types of asynchronous activity in networks of excitatory and inhibitory spiking neurons. *Nat Neurosci* (2014) 17:594. doi: 10.1038/nn.3658
72. Mastrogiuseppe F, Ostojic S. Intrinsically-generated fluctuating activity in excitatory-inhibitory networks. *PloS Comput Biol* (2017) 13:e1005498. doi: 10.1371/journal.pcbi.1005498
73. Martí D, Brunel N, Ostojic S. Correlations between synapses in pairs of neurons slow down dynamics in randomly connected neural networks. *Phys Rev E* (2018) 97:062314. doi: 10.1103/PhysRevE.97.062314
74. Park J, Ichinose K, Kawai Y, Suzuki J, Asada M, Mori H. Macroscopic cluster organizations change the complexity of neural activity. *Entropy* (2019) 21:214. doi: 10.3390/e21020214
75. Nobukawa S, Nishimura H, Yamanishi T. Temporal-specific complexity of spiking patterns in spontaneous activity induced by a dual complex network structure. *Sci Rep* (2019a) 9:1–12. doi: 10.1038/s41598-019-49286-8
76. Pikovsky A, Rosenblum M, Kurths J. *Synchronization: a universal concept in nonlinear sciences* Vol. 12. (UK: Cambridge University Press). (2003).
77. Schweighofer N, Doya K, Fukai H, Chiron JV, Furukawa T, Kawato M. Chaos may enhance information transmission in the inferior olive. *Proc Natl Acad Sci* (2004) 101:4655–60. doi: 10.1073/pnas.0305966101
78. Nobukawa S, Nishimura H. Chaotic resonance in coupled inferior olive neurons with the Llinás approach neuron model.′. *Neural Comput* (2016) 28:2505–32. doi: 10.1162/NECO_a_00894

Conflict of Interest: The authors declare that the research was conducted in the absence of any commercial or financial relationships that could be construed as a potential conflict of interest.

frontiers in Aging Neuroscience

ORIGINAL RESEARCH
published: 08 April 2020
doi: 10.3389/fnagi.2020.00090

Reduced Dynamic Complexity of BOLD Signals Differentiates Mild Cognitive Impairment From Normal Aging

Haixia Zheng[1], Keiichi Onoda[2], Atsushi Nagai[2] and Shuhei Yamaguchi[2]*

[1] Laureate Institute for Brain Research, Tulsa, OK, United States, [2] Department of Neurology, Faculty of Medicine, Shimane University, Izumo, Japan

Mild cognitive impairment (MCI) is characterized as a transitional phase between cognitive decline associated with normal aging and Alzheimer's disease (AD). Resting-state functional magnetic resonance imaging (fMRI) measuring blood oxygenation level-dependent (BOLD) signals provides complementary information considered essential for understanding disease progression. Previous studies suggested that multi-scale entropy (MSE) analysis quantifying the complexity of BOLD signals is a novel and promising method for investigating neurodegeneration associated with cognitive decline in different stages of MCI. Therefore, the current study used MSE to explore the changes in the complexity of resting-state brain BOLD signals in patients with early MCI (EMCI) and late MCI (LMCI). We recruited 345 participants' data from the Alzheimer's Disease Neuroimaging Initiative database, including 176 normal control (NC) subjects, 87 patients with EMCI and 82 patients with LMCI. We observed a significant reduction of brain signal complexity toward regularity in the left fusiform gyrus region in the EMCI group and in the rostral anterior cingulate cortex in the LMCI group. Our results extend prior work by revealing that significant reductions of brain BOLD signal complexity can be detected in different stages of MCI independent of age, sex and regional atrophy. Notably, the reduction of BOLD signal complexity in the rostral anterior cingulate cortex was significantly associated with greater risk of progression to AD. The present study thus identified MSE as a potential imaging biomarker for the early diagnosis of pre-clinical Alzheimer's disease and provides further insights into the neuropathology of cognitive decline in prodromal AD.

Keywords: mild cognitive impairment, multi-scale entropy, resting-state fMRI, BOLD complexity, imaging biomarker

OPEN ACCESS

Edited by:
Mohamad Habes, The University of Texas Health Science Center at San Antonio, United States

Reviewed by:
Martin Dyrba, German Center for Neurodegenerative Diseases (DZNE), Germany
Seungjun Ryu, Gwangju Institute of Science and Technology, South Korea
Ottavia Dipasquale, King's College London, United Kingdom

****Correspondence:***
Haixia Zheng
hzheng@laureateinstitute.org

Received: *07 October 2019*
Accepted: *17 March 2020*
Published: *08 April 2020*

Citation:
Zheng H, Onoda K, Nagai A and Yamaguchi S (2020) Reduced Dynamic Complexity of BOLD Signals Differentiates Mild Cognitive Impairment From Normal Aging. Front. Aging Neurosci. 12:90. doi: 10.3389/fnagi.2020.00090

INTRODUCTION

Mild cognitive impairment (MCI) is a condition in which individuals exhibit cognitive decline exceeding that expected with normal aging that does not notably interfere with activities of daily life (Petersen, 2004). However, previous evidence revealed that more than 50% of people with MCI progress to dementia, particularly Alzheimer's disease (AD), within 5 years (Gauthier et al., 2006). Owing to lack of effective clinical treatment for AD, early detection of individuals with

MCI is increasingly important to permit early and adequate clinical interventions to reduce the risk of progression to AD. Also, because the anatomical or functional brain changes in patients with MCI are extremely subtle and often overlap (Guerrero et al., 2014), it has been a major challenge to discriminate brain structural and functional alterations between patients with MCI and normal control (NC).

Resting-state functional magnetic resonance imaging (fMRI) studies based on blood oxygen level-dependent (BOLD) signal, which indirectly measures neural activity by detecting changes in blood oxygenation, have revealed the potential of BOLD signals as a biomarker for early detection of the neurophysiological alterations associated with MCI. This is attributable to its non-invasive and task-free nature (Ogawa et al., 1990; Deyoe et al., 1994), as well as because functional changes appear well before structural changes (Pievani et al., 2011; Teipel et al., 2015) and detectable cerebrospinal fluid amyloid-β and phosphorylated tau abnormalities (Chen et al., 2016). It has become evident that functional connectivity (FC) is altered in multiple brain regions such as the posterior cingulate cortex, thalamus, hippocampus, temporal gyrus and occipital gyrus in subjects with MCI (Weiner et al., 2017). Although FC and brain network analysis has provided valuable insights into differences between patients with MCI and NC subjects, the observations have not been consistent, and the mechanism underlying these alterations remains largely unknown. However, this linear statistical approach, which assesses the correlation of BOLD signals between brain areas, underestimates the complex and dynamic activity of the BOLD time series, thus limiting its capability and sensitivity for characterizing the complex human brain function alterations related to cognitive decline. Hence, it is critical to consider this issue while analyzing spontaneous fluctuations of resting-state BOLD signals.

Over the past few years, a non-linear statistical method named sample entropy has been introduced to study the complexity and regularity of physiological systems, as well as human brain function associated with aging and cognitive decline (Richman and Moorman, 2000; Yang et al., 2013; Smith et al., 2014). Sample entropy is a concept which originally came from information theory which proved a mathematical way of quantifying the complexity/irregularity of finite length time series (Pincus, 1991; Richman and Moorman, 2000). When applied to several coarse-sampled scales from the original time series, sample entropy can be extended to multi-scale entropy (MSE) to better capture the dynamic complexity of neural signals across multiple temporal scales (Costa et al., 2018). To date, evidence has suggested a general trend of decreasing complexity in EEG signals with aging and worse performance of memory-related tasks (Wang et al., 2016; Sheehan et al., 2018). Furthermore, both resting-state fNIRS and resting-state fMRI have observed reduced brain signal complexity in patients with AD compared with NC group across several networks, especially the default mode network (DMN) (Grieder et al., 2018; Li et al., 2018). These preliminary studies indicate that MSE can be a valid index for cognitive decline that better captures dynamic changes of BOLD signals than FC.

In the current study, we obtained BOLD rs-fMRI data from the Alzheimer's Disease Neuroimaging Initiative (ADNI), applying a non-linear approach by using MSE to probe brain function changes among healthy subjects and patients with MCI. We anticipated lower MSE values in prodromal AD than in normal aging. Accumulating evidence indicates that the pathologies and functional abnormalities involved in the development of AD-associated cognitive deterioration are complex and vary by disease state (Lee et al., 2014; Teipel et al., 2016; Weiner et al., 2017; Fletcher et al., 2018). Therefore, in an effort to investigate pre-symptomatic AD progression at different stages, patients with MCI have been classified into two subgroups based upon clinical and behavioral measures provided by ADNI at the time of the imaging study: early MCI (EMCI) and late MCI (LMCI). This enabled the investigation of AD biomarkers and potential disease-related factors in various clinical stages, which is essential for uncovering AD developmental processes and designing effective early interventions to slow disease progression.

MATERIALS AND METHODS

Subjects

The dataset used in this study was obtained from the ADNI database[1]. The ADNI was launched in 2003, and the primary goal has been to test whether imaging, other biological markers and clinical and neuropsychological assessments can be combined to measure the progression of early dementia[2]. Detailed inclusion criteria for the diagnostic categories can be found on the ADNI website[3]. Briefly, all subjects in this study aged between 55 and 90 years with Mini-Mental State Examination (MMSE) scores of 24–30 and geriatric depression scale of $\leq$5. Subjects with EMCI or LMCI had a subjective memory concern as identified by themselves or their partners, an abnormal Logical Memory II score (education-adjusted) and a clinical dementia rating (CDR) of 0.5 (memory box $\geq$0.5). The score ranges of Logical Memory II for EMCI were 9–11 for 16 years of education, 5–9 for 8–15 years and 3–6 for 0–7 years, and the ranges for LMCI were $\leq$8 for 16 years of education, 4–7 for 8–15 years and 2–3 for 0–7 years. In addition, the general cognition and functional performance of patients with EMCI or LMCI was sufficiently preserved such that a diagnosis of AD could not be made. NC subjects had no memory complaints beyond that expected by aging (verified by a partner), a normal Logical Memory II score (education-adjusted) and CDR = 0 (memory box = 0). In total, 101 patients with EMCI (73.3 years old, 52 females), 96 patients with LCMI (73.9 years old, 45 females) and 204 NC subjects (74.5 years old, 121 females) from the database were analyzed in this study. Data were selected according to the availability of resting-state fMRI datasets for patients with MCI and age-matched healthy subjects. Among these, longitudinal follow-up data for an average of 13 $\pm$ 20 months were also collected. The demographic information for the ADNI subjects is summarized in **Table 1**. There were no significant age and sex differences

[1] adni.loni.usc.edu

[2] www.adni-info.org for up-to-date information

[3] http://adni.loni.usc.edu/methods/

TABLE 1 | Demographic data.

	EMCI	LMCI	NC	statistics
N (N of analysis)	101 (87)	96 (82)	204 (176)	
Age	73.3 ± 9.0	73.9 ± 7.1	74.5 ± 9.2	n.s.
Sex (female/male)	52/49	45/51	121/83	n.s.
MMSE	28.2 ± 1.8	27.9 ± 1.8	28.9 ± 1.5	EMCI, LMCI < NC
Conversion time (months) (N)	23.6 ± 16.3 (8)	25.3 ± 14.8 (13)	–	n.s.
Follow-up duration (months)	21.4 ± 24.6	13.7 ± 19.4	8.8 ± 17.2	n.s.

The two-sample t-test for age, chi-squared test for sex and Kruskal–Wallis test for Mini-Mental State Exam (MMSE) were used. The values in parentheses for N indicate the numbers of subjects who had no excessive head movement (<4.5 mm). The values in parentheses for conversion time indicate the numbers of subjects who converted to Alzheimer's disease. NC, normal control; EMCI, early mild cognitive impairment; LMCI, late mild cognitive impairment.

between the groups. The MMSE score was significantly lower in the EMCI and LMCI groups than in the NC group.

Image Acquisition

FMRI data were acquired using Philips 3T scanners. The measurement parameters of resting-state fMRI were as follows: repetition time (TR) = 3000 ms, echo time (TE) = 30 ms, slice thickness = 3.3 mm, voxel size = 3 mm × 3 mm × 3 mm, flip angle (FA) = 80°, slice number = 48 and 140–200 time points. The structural T1 images were obtained using the following parameters: TR = 6.72 ms, TE = 3.16 ms, slice number = 171, field of view: 256 mm × 256 mm, voxel size: 1.0 mm × 1.0 mm × 1.2 mm and FA = 9°.

Pre-processing of Functional Images

Statistical Parametric Mapping (SPM12) and functional connectivity toolbox (CONN) (Whitfield-Gabrieli and Nieto-Castanon, 2012) were used for pre-processing. The functional images were re-aligned to remove any artifacts caused by head movement. Subjects who moved their heads excessively (more than 4.5 mm) were excluded from the following analysis (remaining numbers of subjects: 87 for EMCI, 82 for LMCI and 176 for NC). ANOVA confirmed there were no head movement differences among the three groups (EMCI, 1.7 ± 1.1 mm; LMCI, 1.4 ± 1.2 mm; NC, 1.5 ± 1.1 mm; $F = 1.08$, $p = 0.34$). The images were corrected for differences in image acquisition time between slices and were normalized to a Montreal Neurological Institute template space using the DARTEL method (re-sampled into 3 mm × 3 mm × 3 mm voxels). Spatial smoothing was applied with a full-width half-maximum (FWHM) equal to 8 mm. The linear trends of time courses were removed, and the effect of head movement parameters and mean BOLD signals from the whole brain, white matter and cerebrospinal fluid were removed at each voxel. Temporal filtering (0.01 Hz < f < 0.1 Hz) was applied. Finally, each voxel time series was standardized to a mean of zero and standard deviation of unity.

The analysis of the gray matter volume (GMV) was performed according to voxel-based morphometry (VBM) on Computational Anatomy Toolbox (CAT12[4]). The VBM procedure involves the segmentation of the original structural MRI images in gray matter, white matter and cerebrospinal fluid. The gray matter images were normalized to templates in stereotactic space and smoothed using a 6-mm FWHM Gaussian kernel. Gray matter mask was used to exclude voxels outside of the brain from further statistical analysis.

MSE

Richman and Moorman (2000) proposed sample entropy measuring the complexity and regularity of clinical and experimental time series data (**Figure 1**). Sample entropy estimates the randomness or irregularity of a time series by determining how often different patterns of data are found in the given time series. It is defined by the negative natural logarithm of the conditional probability that a time series data of pattern length m (the sequence length of adjacent time points to be compared), having repeated itself within a tolerance of r (similarity factor), will also repeat itself for $m + 1$ time points without allowing self-matches (Richman and Moorman, 2000). A large value of sample entropy represents unpredictability or random variation (high complexity) whereas a small value represents predictability or a more regular structure (low complexity). MSE consists of a set of sample entropy values under multiple time scales. Therefore, MSE method incorporated two procedures: First, a "coarse-graining" process was applied to the time series. For instance, time series at scale 3 was constructed by averaging every 3 data points without overlapping. For time series scale 1, the coarse-grained time series is simply the original time series (**Figure 1A**). Second, sample entropy was calculated for each coarse-grained time series scale (**Figure 1B**).

The Complexity Toolbox[5] was used to compute the MSE maps of resting-state fMRI data for each subject at each voxel. Pattern length m, distance threshold r and time scale l were set to calculate MSE. For short datasets (time series length, approximately 100), sample entropy for $r \geq 0.3$ (in the case of $m = 2$) agreed with the theoretical value (Richman and Moorman, 2000). Previous fMRI studies used the sample entropy set $m = 1$ or 2 and $r = 0.30$–0.45 (Smith et al., 2014; Yang et al., 2015, 2018; Wang et al., 2018). In the current study, MSE was calculated for each BOLD time series based on $m = 2$ and $r = 0.3$ across the range of time scales from 1 to 6.

Group level analysis was conducted by using ANCOVA with age, gender and scan duration as covariates at both the global and voxel level. The statistical criteria were a false-discovery rate (FDR) corrected $p < 0.05$ at the cluster level and uncorrected $p < 0.001$ at the voxel level. Then, we extracted individual MSE data of a sphere radius of 6 mm with the peak voxel of a significant cluster as the centre, which was for the visualization and following analysis. To investigate the effect of brain atrophy on MSE, we conducted correlation analysis between the sample entropy and GMV. As performed for the MSE data, we extracted the GMV data from the same cluster of individual subjects.

[4]http://dbm.neuro.uni-jena.de/cat/

[5]http://loft-lab.org/index-5.html

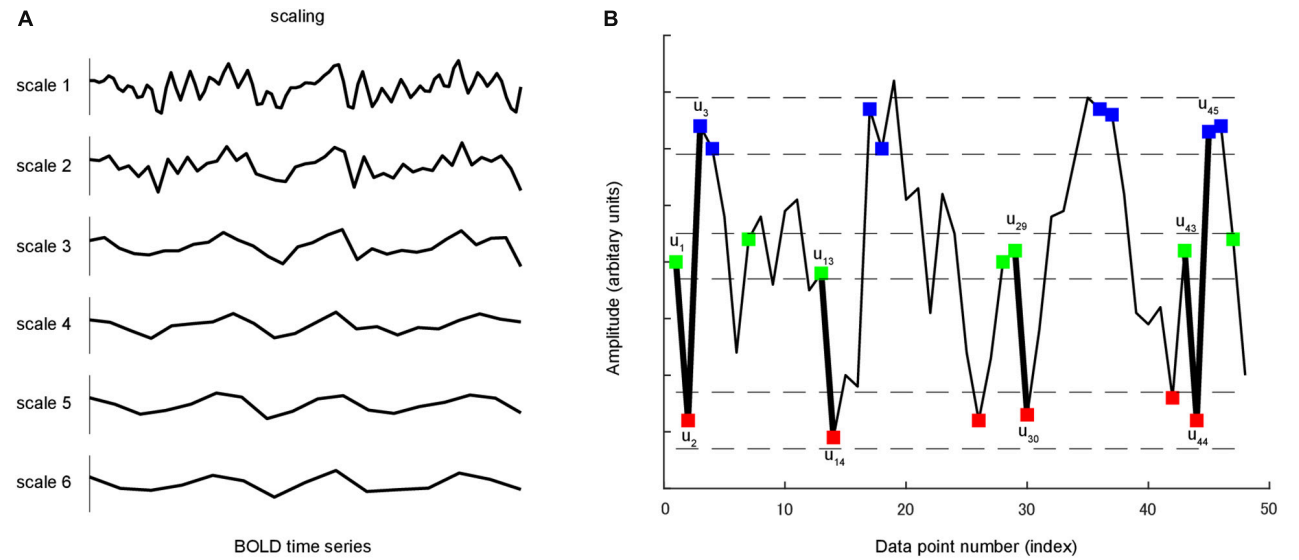

FIGURE 1 | (A) A coarse-graining process was applied to time series. For a given time series, multiple coarse-grained time series were constructed by averaging the data within non-overlapping windows of increasing length. **(B)** A time series u is shown to illustrate the procedure for calculating sample entropy. In this case, the pattern length m is 2, and the similarity criterion r is 0.3 of the standard deviation of u. Dotted horizontal lines around u_1, u_2 and u_3 represent $u_1 \pm r$, $u_2 \pm r$ and $u_3 \pm r$, respectively. Two data values match each other, that is, they are not distinguishable, if the absolute difference between them is less than r. Green, red and blue points represent points that match u_1, u_2 and u_3, respectively. Consider the m-component green-red template sequence (u_1, u_2) and (m + 1)-component green-red-blue (u_1, u_2, u_3) template sequence. For the segment shown, three green-red sequences matched the template, whereas only one green-red-blue sequence matched the template. In this case, the numbers of sequences matching the two- and three-component template are 3 and 1, respectively. These calculations were repeated for the next two- and three-component template sequences. The numbers of sequences that matched each of the two and three components were added to the previous values. This procedure was repeated for all other possible template to determine the ratio between the total numbers of two- and three-component template matches. Sample entropy is the natural logarithm of this ratio.

Cox Proportional Hazards Regression

The Cox proportional hazards regression model was used to analyze the relationship between brain entropy and time to convert to AD in consideration of censored data. For each individual, the event was considered conversion to AD. Survival time was defined as the interval between the month of MRI measurement at baseline and diagnosis at follow-up. In an effort to minimize the effect of age and gender, we used a linear regression model to regress out gender and the age at baseline scan (years). We then entered the residuals into the Cox regression model. An FDR adjusted p value < 0.05 was considered to indicate a statistical significance. Additionally, the difference of the risk of AD conversion between high entropy and low entropy groups was estimated using the Kaplan-Meier method with the log-rank test. The high-low group assignment was based on a median-split threshold. The analysis was performed using RStudio version 1.1.463 (Integrated Development for R. RStudio, Inc., Boston, MA, United States. URL[6]).

Data Availability

The datasets analyzed for this study can be found in the Alzheimer's Disease Neuroimaging Initiative (ADNI) database (adni.loni.usc.edu).

[6]http://www.rstudio.com

RESULTS

Figure 2A shows the lateral and medial views of mean MSE across groups for each scale. For scale 1 entropy value was generally higher at the middle cingulate cortex, supplementary motor cortex and posterior medial prefrontal cortex than in other brain regions. For scales 2 to 5, the temporo-parietal junction, lateral and medial prefrontal cortex, posterior cingulate cortex and primary visual cortex exhibited a relatively higher entropy value than other brain regions. Statistical group difference comparison was carried out at global and voxel level:

First, we calculated the global mean sample entropy of the whole brain for each subject and plotted it by group (**Figure 2B**). The global mean sample entropy was highest at scale 2, and it gradually decreased along with the increase of scales. ANCOVA with age, gender and scan duration as covariates was conducted to test whether global mean sample entropy differs among groups. There were no significant global mean sample entropy differences among the groups at any scale.

Next, we compared the entropy map of each scale among the groups at the voxel level. We found significant differences among the groups regarding the sample entropy at scales 2, 3, and 5 (**Figure 2C**). The analysis revealed that the left fusiform gyrus (FG) at scale 2 exhibited a significant main effect of group [(x, y, z) = (−27, −9, −42), voxel size = 49, FDR corrected $p = 0.035$]. To illustrate the group difference, we extracted the individual sample entropy of voxels within a sphere ($r = 6$ mm)

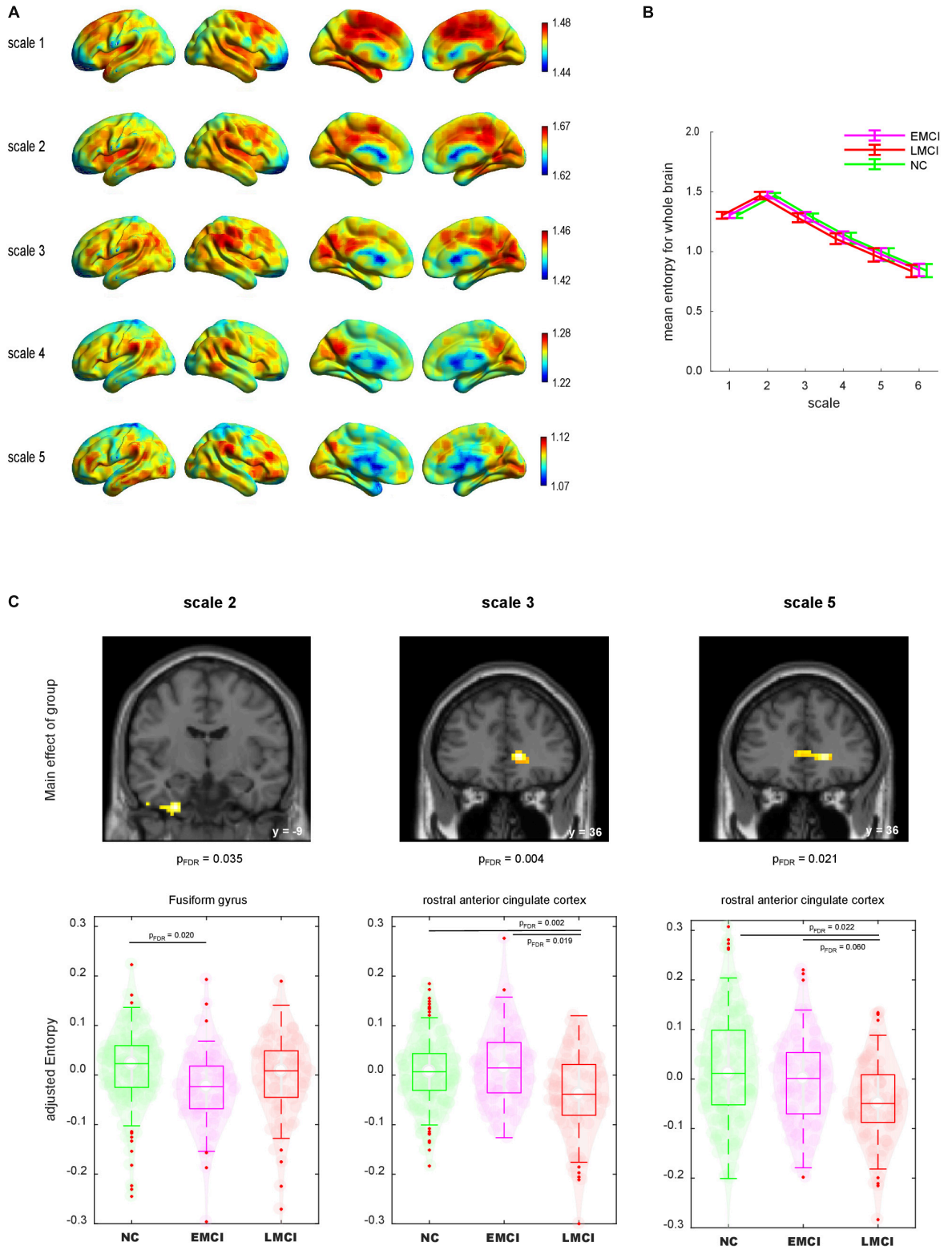

FIGURE 2 | (A) Lateral and medial views of mean maps of sample entropy for scales 1–6. The value range was different for each scale. **(B)** Mean sample entropy of the whole brain for scales 1–6. Error bar denotes standard deviation. **(C)** Group comparisons of sample entropy using whole-brain ANCOVA. Top: Brain regions displayed significant main effects of group (voxel level $p < 0.001$ and cluster level false-discovery rate corrected $p < 0.05$). Bottom: Violin plot of each individual sample entropy value. Boxes indicate the mean and interquartile. Whiskers indicate the interquartile range. NC, normal control; EMCI, early mild cognitive impairment; LMCI, late mild cognitive impairment.

with the peak as a centre and calculated the averages. The scatter plot indicated that the sample entropy was lower for the EMCI group than for the NC group. The decrease of sample entropy in the LMCI group was not significant in direct comparison. At scales 3 and 5, the rostral anterior cingulate cortex (rACC) displayed significant main effects of group [scale 2: (15, 36, 3), size = 82, FDR corrected $p = 0.004$; scale 5: (18, 36, 0), size = 65, FDR corrected $p = 0.021$]. The sample entropy of the rACC was decreased in the LMCI group, whereas the EMCI group did not display a significant decrement.

The GMV was estimated by regressing out age, gender and total intracranial volume. The entropy was estimated by regressing out age and gender. GMV in the FG and rACC did not show significant group differences ($p > 0.07$). The correlation analysis revealed no significant correlation coefficient between the sample entropy and GMV in the FG and rACC ($rs < 0.15$, $p > 0.58$, **Figure 3**).

To assess the association between these reductions in brain local BOLD signal entropy and time to progress to AD, we conducted Cox proportional hazards regression analysis. Local BOLD signal entropy was adjusted for age and gender by regressing out age and gender using a linear regression model. We found a negative association between entropy in the rACC at scale 5 and time to convert to AD with a beta coefficient of −7.11 (FDR corrected $p = 0.009$). This association was confirmed in all samples as well as the LMCI group (beta coefficient = −8.21, FDR corrected $p = 0.048$), which indicated that a smaller value of entropy in the rACC was associated with a significantly greater risk of progressing into AD. There were no statistically significant associations between entropy in other brain regions and time to convert into AD (see detailed results in **Table 2**).

To better capture the risk of reduced entropy in rACC converting to AD, we divided subjects into high and low entropy groups by using a median-split approach and estimated the difference of the risk of AD between groups. Subjects with lower BOLD signal entropy at rACC scale 5 were associated with a 3.4 times (adjusted hazard ratio was 3.4 with a 95% confidence interval of 1.2 to 9.2, $p < 0.01$, **Figure 4A**) increased risk of converting to AD compared with the high entropy group. This risk was 5.1 times if the subjects were in LMCI group (adjusted hazard ratio was 5.1 with a 95% confidence interval of 0.66 to 39, $p < 0.05$, **Figure 4B**). There was no significant difference in the EMCI group.

DISCUSSION

The results of the current analyses reveal that people with EMCI or LMCI exhibit reduced resting-state fMRI BOLD signal complexity toward the regular pattern compared with the NC group. In the EMCI group, reduced complexity was observed in the FG, whereas in the LMCI group, this reduction was found in the rACC. These alterations were not caused by gray matter atrophy. More importantly, these reductions of brain signal variability in the rACC region exceeded structural atrophy, and it was associated with a greater risk of progressing into AD.

Our findings are consistent with the literature in this area. Previous studies demonstrated a general trend of decreasing signal complexity with normal aging and cognitive decline associated with AD (Yang et al., 2013; McIntosh et al., 2014; Grieder et al., 2018; Li et al., 2018; Sheehan et al., 2018). A few study used resting-state fNIRS/fMRI to investigate neural signal complexity among NC, MCI and AD groups (Wang et al., 2017; Li et al., 2018). Consistent with our findings, a reduction of BOLD signal complexity in the FG was observed in patients with AD compared with the findings in the MCI or NC group (Wang et al., 2017). The FG is located in the ventral portion of the temporal lobe and under the parahippocampal gyrus. Although the function of the FG is unclear, it has been associated with object recognition and face perception (Baroni et al., 2017; Weiner et al., 2018). Probably limited by small sample sizes and their methods of measuring entropy that considered only the ranks of the samples and not their metrics (Bandt and Pompe, 2002), previous studies failed to find meaningful alterations in the EMCI or LMCI group compared with the NC group. Our study therefore filled this gap by using larger sample sizes and sample entropy to provide new evidence by using MSE to assess different stages of MCI. The findings of reduced BOLD signal intensity in different regions between EMCI and LMCI suggests that BOLD signal complexity changes associated with cognitive decline are stage-dependent and are sensitive for detecting very early stages of prodromal AD.

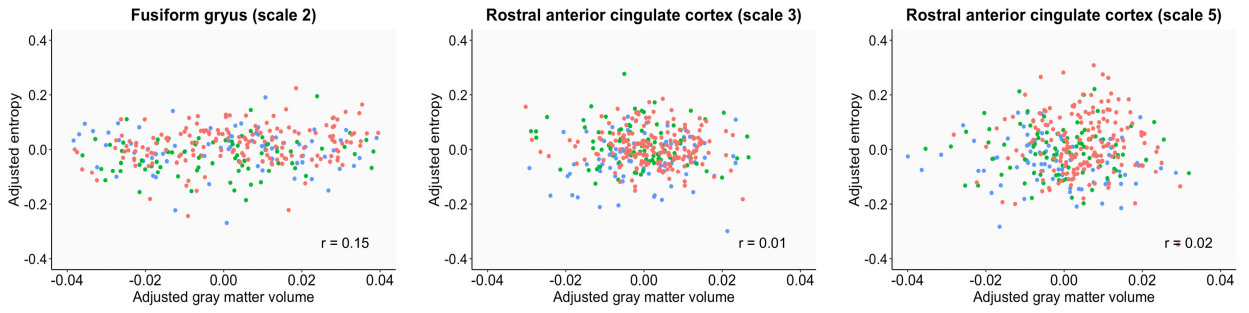

FIGURE 3 | Scatter plots between sample entropy and gray matter volume in the fusiform gyrus and rostral anterior cingulate cortex. The gray matter volume was estimated by regressing out age, gender and total intracranial volume. The entropy was estimated by regressing out age and gender. Red, normal control; Green, early mild cognitive impairment; Blue, late mild cognitive impairment.

TABLE 2 | Risk factors associated with conversion to Alzheimer's disease after adjustment using the Cox proportional hazards regression model.

	All samples				LMCI				EMCI			
RF	**BC**	**SE**	**HR**	**P**	**BC**	**SE**	**HR**	**P**	**BC**	**SE**	**HR**	**P**
FG_S2	−1.98	2.13	0.14	0.35	−0.09	3.11	1.09	0.98	−2.31	4.13	0.10	0.58
rACC_S3	−3.29	2.96	0.04	0.27	−0.27	4.03	0.76	0.95	−1.93	4.73	0.15	0.68
rACC_S5	−7.11	2.42	0.0008	0.009**	−8.21	3.83	0.0003	0.048*	−2.73	3.60	0.07	0.45

*All of the risk factor estimates were the residuals from a linear regression model which regressed out age and gender. RF, risk factor; BC, beta coefficient; SE, standard error; HR, Hazard ratio; FG_S2, entropy in the fusiform gyrus at scale 2; rACC_S3, entropy in the rostral anterior cingulate cortex at scale 3; rACC_S5, entropy in the rostral anterior cingulate cortex at scale 5; EMCI, early mild cognitive impairment; LMCI, late mild cognitive impairment; *FDR adjusted $p < 0.05$, **FDR adjusted $p < 0.01$.*

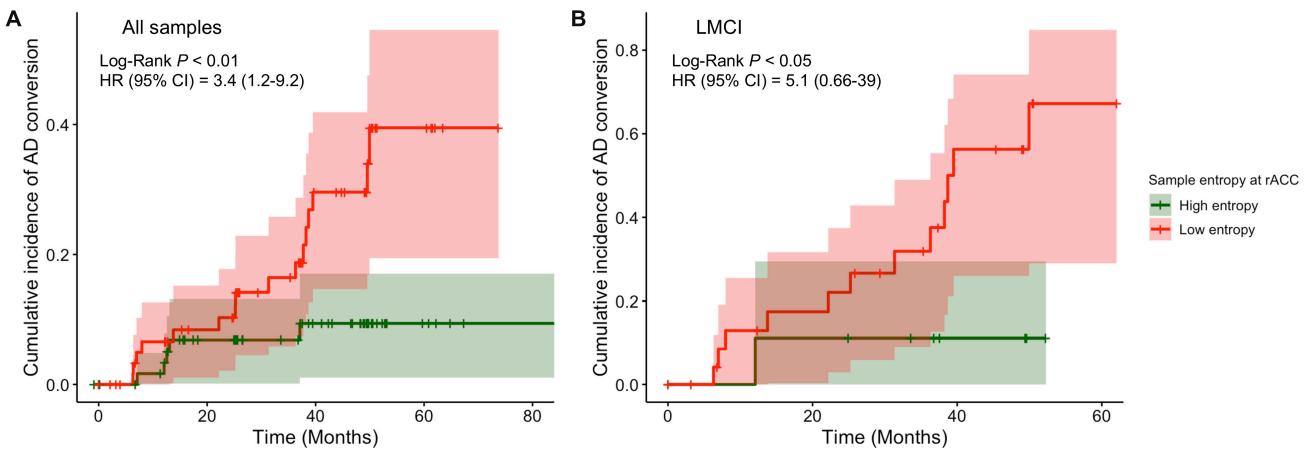

FIGURE 4 | Comparison of cumulative incidence of AD conversion under condition of high entropy and low entropy at rostral anterior cingulate cortex. **(A)** All samples were included. **(B)** Only LMCI subjects were included. AD, Alzheimer dementia; HR, hazard ratio; CI, confidence intervals.

Previous studies consistently observed lower brain signal complexity in DMN nodes in patients with AD compared with the NC subjects (Wang et al., 2017; Grieder et al., 2018; Li et al., 2018). Interestingly, we observed a trend toward decreased BOLD signal complexity with increasing cognitive decline in the rACC, which is a key component of the DMN. Although this finding did not reach significance in the EMCI group, it appears that BOLD signal variability decreases with the progression of AD. This hypothesis was supported by our finding of a correlation between the reduction of BOLD signal complexity in the rACC with the risk of progressing to AD via Cox proportional hazards regression analysis. Anatomically, the rACC has strong connections with both "emotional" limbic systems such as the anterior insular cortex and amygdala and "cognitive" systems such as the posterior cingulate cortex, prefrontal cortex and striatal brain regions (Etkin et al., 2006; Palomero-Gallagher et al., 2008; Stevens et al., 2011). Functionally, the rACC has been demonstrated to play a key role in the regulation of cognitive influences on emotional processing (Stevens et al., 2011; Szekely et al., 2017), especially when performing emotional conflict regulation tasks (Etkin et al., 2006, 2011). Moreover, strong functional connectivity between the ACC and other brain regions such as the hippocampus, frontal gyrus and temporal gyrus has been associated with excellent memory capacity in older adults, even in the presence of amyloid deposition (Lin et al., 2017). Therefore, our finding of significant MSE reduction in the rACC region in the LMCI group compared with the data in the NC group suggests that cognitive decline might be associated with disturbances of cognitive-emotional interactions in the brain. It has long been observed that progressive atrophy and glucose hypometabolism in the medial temporal lobe and cingulate cortex were associated with pre-symptomatic stages of AD (Fox et al., 2001; Knopman et al., 2013; Teipel et al., 2016). Together with the observations of a strong association of glucose metabolism with BOLD signals (Tomasi et al., 2013; Zhang et al., 2013), our evidence highlighted the involvement of rACC function in the neuropathology of cognitive decline in prodromal AD.

This study had a few potential limitations. First, previous studies suggested that the ADNI MCI criteria have a high rate of false-positive diagnostic errors (Bondi et al., 2014). This might explain why the reduction of rACC signal complexity in the EMCI group did not reach statistical significance. Further studies of MSE using MCI samples are warranted to determine if these findings are pathophysiologically relevant. Second, we evaluated cross-group and follow-up data; however, these data were incomplete because of subject dropouts or other factors such as study design and cost constraints. Although the multivariate Cox proportional hazards regression model considers censored data, future studies with well-designed longitudinal data are needed to support our interpretation. Third, MSE is a mathematical measure of BOLD signal complexity at the voxel level. The

current study and existing evidence offer very limited insight into the association between macroscopic alterations and underlying biology in the context of cognitive decline. Future work combined with other methods such as dynamic functional connectivity or fluorodeoxyglucose positron emission tomography imaging is warranted.

In sum, our study indicated that significant reductions of brain BOLD signal complexity can be detected in patients with EMCI or LMCI. These alterations were independent of age or sex, and significantly associated with greater risk of AD conversion. Our findings indicate that MSE based on resting-state BOLD signals is more sensitive than functional connectivity or structural MRI; therefore, it could represent a quantitative functional marker for cognitive decline that may be useful for early screening in older adults at risk for AD.

DATA AVAILABILITY STATEMENT

The datasets analyzed for this study can be found in the Alzheimer's Disease Neuroimaging Initiative (ADNI) database (adni.loni.usc.edu).

ETHICS STATEMENT

The studies involving human participants were reviewed and approved by the Shimane University Ethics Committee. The patients/participants provided their written informed consent to participate in this study.

AUTHOR CONTRIBUTIONS

HZ, KO, AN, and SY conceived and designed the research. HZ and KO performed research. HZ and KO analyzed the data. HZ and KO wrote the manuscript with input from AN. All authors reviewed the manuscript. SY approved the final submission.

FUNDING

This work is supported by the Impulsing Paradigm Change through disruptive Technologies (ImPACT) programme in Japan.

ACKNOWLEDGMENTS

Data collection and sharing for this project were funded by the Alzheimer's Disease Neuroimaging Initiative (ADNI) (National Institutes of Health Grant U01 AG024904 [PI: MWWeiner]) and DOD ADNI (Department of Defense award number W81XWH-12-2-0012). ADNI is funded by the National Institute on Aging (NIA) and the National Institute of Biomedical Imaging and Bioengineering (NIBIB), as well as generous contributions from the following organizations: AbbVie, Alzheimer's Association; Alzheimer's Drug Discovery Foundation; Araclon Biotech; BioClinica, Inc.; Biogen; Bristol-Myers Squibb Company; CereSpir, Inc.; Cogstate; Eisai Inc.; Elan Pharmaceuticals, Inc.; Eli Lilly and Company; EuroImmun; F. Hoffmann-La Roche Ltd. and its affiliated company Genentech, Inc.; Fujirebio; GE Healthcare; IXICO Ltd.; Janssen Alzheimer Immunotherapy Research & Development, LLC.; Johnson & Johnson Pharmaceutical Research & Development LLC.; Lumosity; Lundbeck; Merck & Co., Inc.; Meso Scale Diagnostics, LLC.; NeuroRx Research; Neurotrack Technologies; Novartis Pharmaceuticals Corporation; Pfizer Inc.; Piramal Imaging; Servier; Takeda Pharmaceutical Company; and Transition Therapeutics. The Canadian Institutes of Health Research provided funds to support ADNI clinical sites in Canada. Private sector contributions are facilitated by the Foundation for the National Institutes of Health (http://www.fnih.org). The grantee organization is the Northern California Institute for Research and Education, and the study was coordinated by the Alzheimer's Therapeutic Research Institute at the University of Southern California. ADNI data are disseminated by the Laboratory for Neuroimaging at the University of California.

REFERENCES

Bandt, C., and Pompe, B. (2002). Permutation entropy: a natural complexity measure for time series. *Phys. Rev. Lett.* 88:174102. doi: 10.1103/PhysRevLett.88.174102

Baroni, F., van Kempen, J., Kawasaki, H., Kovach, C. K., Oya, H., Howard, M., et al. (2017). Intracranial markers of conscious face perception in humans. *Neuroimage* 162, 322–343. doi: 10.1016/j.neuroimage.2017.08.074

Bondi, M. W., Edmonds, E. C., Jak, A. J., Clark, L. R., Delano-Wood, L., McDonald, C. R., et al. (2014). Neuropsychological criteria for mild cognitive impairment improves diagnostic precision, biomarker associations, and progression rates. *J. Alzheimers Dis.* 42, 275–289. doi: 10.3233/JAD-140276

Chen, G., Shu, H., Chen, G., Ward, B. D., Antuono, P. G., Zhang, Z., et al. (2016). Staging Alzheimer's disease risk by sequencing brain function and structure, cerebrospinal fluid, and cognition biomarkers. *J. Alzheimers Dis.* 54, 983–993. doi: 10.3233/JAD-160537

Costa, M., Goldberger, A. L., Peng, C.-K., and Israel, B. (2018). *Multiscale Entropy Analysis (MSE)*. Available online at: http://circ.ahajournals.org/cgi/content/full/101/23/e215 (Accessed November 13, 2018).

Deyoe, E. A., Bandettini, P., Neitz, J., Miller, D., and Winans, P. (1994). *Functional Magnetic Resonance Imaging (FMRI) of the Human Brain*. Available online at: http://www.neitzvision.com/research/publications/publications/1994-Deyoe-fMRI_of_human_brain-JNeuroMeth.pdf (accessed December 17, 2018).

Etkin, A., Egner, T., and Kalisch, R. (2011). Emotional processing in anterior cingulate and medial prefrontal cortex. *Trends Cogn. Sci.* 15, 85–93. doi: 10.1016/j.tics.2010.11.004

Etkin, A., Egner, T., Peraza, D. M., Kandel, E. R., and Hirsch, J. (2006). Resolving emotional conflict: a role for the rostral anterior cingulate cortex in modulating activity in the amygdala. *Neuron* 51, 871–882. doi: 10.1016/J.NEURON.2006.07.029

Fletcher, E., Filshtein, T. J., Harvey, D., Renaud, A., Mungas, D., and Decarli, C. (2018). Staging of amyloid β, t-tau, regional atrophy rates, and cognitive change in a nondemented cohort: results of serial mediation analyses. *Alzheimers Dement.* 10, 382–393. doi: 10.1016/j.dadm.2018.04.001

Fox, N. C., Crum, W. R., Scahill, R. I., Stevens, J. M., Janssen, J. C., and Rossor, M. N. (2001). Imaging of onset and progression of Alzheimer's disease with voxel-compression mapping of serial magnetic resonance images. *Lancet* 358, 201–205. doi: 10.1016/S0140-6736(01)05408-3

Gauthier, S., Reisberg, B., Zaudig, M., Petersen, R., Ritchie, K., Broich, K., et al. (2006). Mild cognitive impairment. *Lancet* 367, 1262–1270. doi: 10.1016/S0140-6736(06)68542-5

Grieder, M., Wang, D. J. J., Dierks, T., Wahlund, L.-O., and Jann, K. (2018). Default mode network complexity and cognitive decline in mild Alzheimer's disease. *Front. Neurosci.* 12:770. doi: 10.3389/fnins.2018.00770

Guerrero, R., Wolz, R., Rao, A. W., and Rueckert, D. (2014). Manifold population modeling as a neuro-imaging biomarker: application to ADNI and ADNI-GO. *Neuroimage* 94, 275–286. doi: 10.1016/J.NEUROIMAGE.2014.03.036

Knopman, D. S., Jack, C. R., Wiste, H. J., Weigand, S. D., Vemuri, P., Lowe, V. J., et al. (2013). Selective worsening of brain injury biomarker abnormalities in cognitively normal elderly persons with β-amyloidosis. *JAMA Neurol.* 70, 1030–1038. doi: 10.1001/jamaneurol.2013.182

Lee, S., Seo, J., Lee, J., Park, H., and Adni. (2014). Differences in early and late mild cognitive impairment tractography using a diffusion tensor MRI. *Neuroreport* 25, 1393–1398. doi: 10.1097/WNR.0000000000000279

Li, X., Zhu, Z., Zhao, W., Sun, Y., Wen, D., Xie, Y., et al. (2018). Decreased resting-state brain signal complexity in patients with mild cognitive impairment and Alzheimer's disease: a multi-scale entropy analysis. *Biomed. Opt. Express* 9:1916. doi: 10.1364/BOE.9.001916

Lin, F., Ren, P., Mapstone, M., Meyers, S. P., Porsteinsson, A., and Baran, T. M. (2017). The cingulate cortex of older adults with excellent memory capacity. *Cortex* 86, 83–92. doi: 10.1016/J.CORTEX.2016.11.009

McIntosh, A. R., Vakorin, V., Kovacevic, N., Wang, H., Diaconescu, A., and Protzner, A. B. (2014). Spatiotemporal dependency of age-related changes in brain signal variability. *Cereb. Cortex* 24, 1806–1817. doi: 10.1093/cercor/bht030

Ogawa, S., Lee, T. M., Kay, A. R., and Tank, D. W. (1990). Brain magnetic resonance imaging with contrast dependent on blood oxygenation. *Proc. Natl. Acad. Sci. U.S.A.* 87, 9868–9872. doi: 10.1073/PNAS.87.24.9868

Palomero-Gallagher, N., Mohlberg, H., Zilles, K., and Vogt, B. (2008). Cytology and receptor architecture of human anterior cingulate cortex. *J. Comp. Neurol.* 508, 906–926. doi: 10.1002/cne.21684

Petersen, R. (2004). *Mild Cognitive Impairment as a Diagnostic Entity*. Available online at: https://pdfs.semanticscholar.org/91b5/c1eadc549cc56c03f7d0212010494c8b7090.pdf (accessed November 25, 2018).

Pievani, M., de Haan, W., Wu, T., Seeley, W. W., and Frisoni, G. B. (2011). Functional network disruption in the degenerative dementias. *Lancet Neurol.* 10, 829–843. doi: 10.1016/S1474-4422(11)70158-2

Pincus, S. M. (1991). Approximate entropy as a measure of system complexity. *Proc. Natl. Acad. Sci. U.S.A.* 88, 2297–2301. doi: 10.1073/pnas.88.6.2297

Richman, J. S., and Moorman, J. R. (2000). Physiological time-series analysis using approximate entropy and sample entropy. *Am. J. Physiol. Circ. Physiol.* 278, H2039–H2049. doi: 10.1152/ajpheart.2000.278.6.H2039

Sheehan, T. C., Sreekumar, V., Inati, S. K., and Zaghloul, K. A. (2018). Signal complexity of human intracranial EEG tracks successful associative-memory formation across individuals. *J. Neurosci.* 38, 1744–1755. doi: 10.1523/JNEUROSCI.2389-17.2017

Smith, R. X., Yan, L., and Wang, D. J. J. (2014). Multiple time scale complexity analysis of resting state FMRI. *Brain Imaging Behav.* 8, 284–291. doi: 10.1007/s11682-013-9276-6

Stevens, F. L., Hurley, R. A., and Taber, K. H. (2011). Anterior cingulate cortex: unique role in cognition and emotion. *J. Neuropsychiatry Clin. Neurosci.* 23, 121–125. doi: 10.1176/jnp.23.2.jnp121

Szekely, A., Silton, R. L., Heller, W., Miller, G. A., and Mohanty, A. (2017). Differential functional connectivity of rostral anterior cingulate cortex during emotional interference. *Soc. Cogn. Affect. Neurosci.* 12, 476–486. doi: 10.1093/scan/nsw137

Teipel, S., Drzezga, A., Grothe, M. J., Barthel, H., Chételat, G., Schuff, N., et al. (2015). Multimodal imaging in Alzheimer's disease: validity and usefulness for early detection. *Lancet Neurol.* 14, 1037–1053. doi: 10.1016/S1474-4422(15)00093-9

Teipel, S., Grothe, M. J., and Alzheimer's Disease Neuroimaging Initiative for the ADN (2016). Does posterior cingulate hypometabolism result from disconnection or local pathology across preclinical and clinical stages of Alzheimer's disease? *Eur. J. Nucl. Med. Mol. Imaging* 43, 526–536. doi: 10.1007/s00259-015-3222-3

Tomasi, D., Wang, G.-J., and Volkow, N. D. (2013). Energetic cost of brain functional connectivity. *Proc. Natl. Acad. Sci. U.S.A.* 110, 13642–13647. doi: 10.1073/pnas.1303346110

Wang, B., Niu, Y., Miao, L., Cao, R., Yan, P., Guo, H., et al. (2017). Decreased complexity in Alzheimer's disease: resting-state fMRI evidence of brain entropy mapping. *Front. Aging Neurosci.* 9:378. doi: 10.3389/fnagi.2017.00378

Wang, H., McIntosh, A. R., Kovacevic, N., Karachalios, M., and Protzner, A. B. (2016). Age-related multiscale changes in brain signal variability in pre-task versus post-task resting-state EEG. *J. Cogn. Neurosci.* 28, 971–984. doi: 10.1162/jocn_a_00947

Wang, N., Wu, H., Xu, M., Yang, Y., Chang, C., Zeng, W., et al. (2018). Occupational functional plasticity revealed by brain entropy: a resting-state fMRI study of seafarers. *Hum. Brain Mapp.* 39, 2997–3004. doi: 10.1002/hbm.24055

Weiner, K. S., Natu, V. S., and Grill-Spector, K. (2018). On object selectivity and the anatomy of the human fusiform gyrus. *Neuroimage* 173, 604–609. doi: 10.1016/J.NEUROIMAGE.2018.02.040

Weiner, M. W., Veitch, D. P., Aisen, P. S., Beckett, L. A., Cairns, N. J., Green, R. C., et al. (2017). Recent publications from the Alzheimer's disease neuroimaging initiative: reviewing progress toward improved AD clinical trials. *Alzheimers Dement.* 13, e1–e85. doi: 10.1016/j.jalz.2016.11.007

Whitfield-Gabrieli, S., and Nieto-Castanon, A. (2012). Conn: a functional connectivity toolbox for correlated and anticorrelated brain networks. *Brain Connect.* 2, 125–141. doi: 10.1089/brain.2012.0073

Yang, A. C., Hong, C.-J., Liou, Y.-J., Huang, K.-L., Huang, C.-C., Liu, M.-E., et al. (2015). Decreased resting-state brain activity complexity in schizophrenia characterized by both increased regularity and randomness. *Hum. Brain Mapp.* 36, 2174–2186. doi: 10.1002/hbm.22763

Yang, A. C., Huang, C.-C., Yeh, H.-L., Liu, M.-E., Hong, C.-J., Tu, P.-C., et al. (2013). Complexity of spontaneous BOLD activity in default mode network is correlated with cognitive function in normal male elderly: a multiscale entropy analysis. *Neurobiol. Aging* 34, 428–438. doi: 10.1016/J.NEUROBIOLAGING.2012.05.004

Yang, A. C., Tsai, S.-J., Lin, C.-P., and Peng, C.-K. (2018). A strategy to reduce bias of entropy estimates in resting-state fMRI signals. *Front. Neurosci.* 12:398. doi: 10.3389/fnins.2018.00398

Zhang, J., Chu, K.-W., Hazlett, E. A., and Buchsbaum, M. S. (2013). A FDG-PET and fMRI study on glucose metabolism and hemodynamic response during visual attentional performance in schizophrenia. *Omi. J. Radiol.* 2, 1–6. doi: 10.4172/2167-7964.1000149

Conflict of Interest: The authors declare that data used in preparation of this article were obtained from the Alzheimer's Disease Neuroimaging Initiative (ADNI) database (adni.loni.usc.edu). As such, the funder and the investigators within ADNI contributed to the data collection, but did not participate in analysis, interpretation of data, the writing of this article or the decision to submit it for publication.

frontiers in Aging Neuroscience

ORIGINAL RESEARCH
published: 28 April 2020
doi: 10.3389/fnagi.2020.00102

Insula and Amygdala Atrophy Are Associated With Functional Impairment in Subjects With Presbycusis

Chama Belkhiria[1], Rodrigo C. Vergara[1,2], Simón San Martin[1], Alexis Leiva[1], Melissa Martinez[3], Bruno Marcenaro[1], Maricarmen Andrade[4], Paul H. Delano[1,5,6,7] and Carolina Delgado[1,3]**

[1] Neuroscience Department, Facultad de Medicina, Universidad de Chile, Santiago, Chile, [2] Kinesiology Department, Facultad de Artes y Educación Física, Universidad Metropolitana de Ciencias de la Educación, Santiago, Chile, [3] Neurology and Neurosurgery Department, Hospital Clínico de la Universidad de Chile, Santiago, Chile, [4] Internal Medicine Department, Clínica Universidad de los Andes, Santiago, Chile, [5] Otolaryngology Department, Hospital Clínico de la Universidad de Chile, Santiago, Chile, [6] Centro Avanzado de Ingeniería Eléctrica y Electrónica, AC3E, Universidad Técnica Federico Santa María, Valparaíso, Chile, [7] Biomedical Neuroscience Institute, Facultad de Medicina, Universidad de Chile, Santiago, Chile

OPEN ACCESS

Edited by:
Tobias Kleinjung,
University of Zurich, Switzerland

Reviewed by:
Takahito Yoshizaki,
Keio University, Japan
Josef Syka,
Institute of Experimental Medicine (ASCR), Czechia
Antonin Skoch,
Institute for Clinical and Experimental Medicine (IKEM), Czechia,
in collaboration with reviewer JS

***Correspondence:**
Carolina Delgado
cdelgado@uchile.cl
Chama Belkhiria
belkhiria.chama@gmail.com

Received: 04 August 2019
Accepted: 26 March 2020
Published: 28 April 2020

Citation:
Belkhiria C, Vergara RC, San Martin S, Leiva A, Martinez M, Marcenaro B, Andrade M, Delano PH and Delgado C (2020) Insula and Amygdala Atrophy Are Associated With Functional Impairment in Subjects With Presbycusis. Front. Aging Neurosci. 12:102. doi: 10.3389/fnagi.2020.00102

Hearing loss is an important risk factor for dementia. However, the mechanisms that relate these disorders are still unknown. As a proxy of this relationship, we studied the structural brain changes associated with functional impairment in activities of daily living in subjects with age related hearing loss, or presbycusis. One hundred eleven independent, non-demented subjects older than 65 years recruited in the ANDES cohort were evaluated using a combined approach including (i) audiological tests: hearing thresholds and cochlear function measured by pure tone averages and the distortion product otoacoustic emissions respectively; (ii) behavioral variables: cognitive, neuropsychiatric, and functional impairment in activities of daily living measured by validated questionnaires; and (iii) structural brain imaging—assessed by magnetic resonance imaging at 3 Tesla. The mean age of the recruited subjects (69 females) was 73.95 ± 5.47 years (mean ± SD) with an average educational level of 9.44 ± 4.2 years of schooling. According to the audiometric hearing thresholds and presence of otoacoustic emissions, we studied three groups: controls with normal hearing (n = 36), presbycusis with preserved cochlear function (n = 33), and presbycusis with cochlear dysfunction (n = 38). We found a significant association (R^2_D = 0.17) between the number of detected otoacoustic emissions and apathy symptoms. The presbycusis with cochlear dysfunction group had worse performance than controls in global cognition, language and executive functions, and severe apathy symptoms than the other groups. The neuropsychiatric symptoms and language deficits were the main determinants of functional impairment in both groups of subjects with presbycusis. Atrophy of insula, amygdala, and other temporal areas were related with functional impairment, apathy, and language deficits in the presbycusis with cochlear dysfunction group. We conclude

that (i) the neuropsychiatric symptoms had a major effect on functional loss in subjects with presbycusis, (ii) cochlear dysfunction is relevant for the association between hearing loss and behavioral impairment, and (iii) atrophy of the insula and amygdala among other temporal areas are related with hearing loss and behavioral impairment.

Keywords: dementia, cochlear dysfunction, apathy, activities of daily living, behavioral impairment, presbycusis, insula atrophy

INTRODUCTION

Age-related chronic disorders, including sensory, neurological, and mental syndromes are among the major contributors for disability (Prince et al., 2015). Dementia, or major neurocognitive disorder (McKhann et al., 2011; Sachdev et al., 2015), is usually defined as an acquired cognitive or behavioral impairment that causes functional loss which interferes with independence in everyday activities. Importantly, in low- and middle-income countries, dementia has emerged as the leading cause of disability in older people (Prince et al., 2015). Today, 50 million people live with dementia worldwide, and due to the population aging this number is projected to double every 20 years (World Alzheimer Report, 2016, ADI). In Alzheimer's disease (AD), non-cognitive behavioral symptoms including mood, perception, and behavioral alterations are grouped as neuropsychiatric symptoms (NPS), which are important contributors for functional impairment in elders (Lyketsos et al., 2011; de Oliveira et al., 2015).

Another common cause of disability in elders is age-related hearing loss, or presbycusis. It is the third most prevalent condition in the elderly population, reaching 80% in those older than 85 years (Cruickshanks et al., 1998; Li-Korotky, 2012). Hearing loss is defined by an increase of audiogram thresholds and has recently been recognized as a new major risk factor for dementia in those older than 55 years (Livingston et al., 2017). Several longitudinal studies have demonstrated that hearing loss increases the risk of incident all-cause dementia, with a relative risk that augments linearly with the severity of hearing loss (Lin et al., 2011; Gallacher et al., 2012; Deal et al., 2016). In addition to its association with cognitive decline, hearing loss has been related with increased risk of depressive symptoms (Brewster et al., 2018; Cosh et al., 2018). Therefore, the comorbidity of disorders that are risk factors for dementia or functional disability –such as presbycusis and NPS – is very common in the elderly, as many of them are related with the aging process (Livingston et al., 2017). Accordingly, previous studies that accounted for the variables related to functional limitations in subjects with presbycusis found that functional impairment is associated with multiple conditions, such as older age, comorbidities, cognitive impairment, and more severe hearing loss (López-Torres Hidalgo et al., 2009; Solheim et al., 2011; Sogebi et al., 2015). Even in high-functioning elderly, subjective perception of hearing loss increases the risk of intellectual impairment and loss of the social role (Tomioka et al., 2015). In addition to the behavioral changes that precede dementia, recent studies suggest that biomarkers of neurodegeneration such as brain atrophy in certain areas could predict cognitive decline and dementia (ten Kate et al., 2018). Likewise, subjects with presbycusis have gray matter atrophy in the temporal lobe (Lin et al., 2014), as well as in nodes of the default mode network (Ren et al., 2018), such as the insula and the cingulate cortex. In this sense, we recently found that subjects with presbycusis and cochlear dysfunction, as evidenced by the loss of otoacoustic emissions, have atrophy of the cingulate and temporal cortices, which were related to executive dysfunction and depressive symptoms (Belkhiria et al., 2019).

In this present study, we hypothesized that the atrophy of the temporal lobe, among other brain areas related with hearing loss, will be associated not solely with neuropsychiatric symptoms and cognitive impairment, but also with functional loss in subjects with presbycusis. Our main objective was to study structural brain changes associated with functional impairment, neuropsychiatric and cognitive variables in independent non-demented subjects with presbycusis. In addition, in line with our previous work (Belkhiria et al., 2019), we evaluated whether these associations were stronger in the group with loss of otoacoustic emissions.

MATERIALS AND METHODS

Subjects

A total of 199 adults aged ≥65 years were screened in the Auditory and Dementia study (ANDES) between 2016 and 2018 from a primary health center located in the Recoleta district in Santiago, Chile. All subjects gave written informed consent in accordance with the Declaration of Helsinki. Only 111 subjects were included in this study according to the following criteria. Inclusion criteria were to (i) be older than 65 years at the beginning of the study, (ii) possess a Mini-Mental State Examination (MMSE) score of ≥24, and (iii) demonstrate preserved functionality measured by a Pfeffer's Functional Activities Questionnaire score of <25 (Quiroga et al., 2004). Exclusion criteria were (i) having a stroke or other symptoms of neurological disorders, (ii) having dementia, (iii) presenting psychiatric disorders, (iv) displaying other causes of hearing loss different from presbycusis, (v) using hearing aids, and (vi) other causes of significant disability, such as poor vision (Snellen test ≥50/20) or severe arthrosis. All procedures were approved by the Ethical and Scientific Committee of the Clinical Hospital of the University of Chile, permission number OAIC 752/15.

Abbreviations: ADL, activity of daily living; AES, apathy evaluation scale; DPOAE, distortion product otoacoustic emissions; PCD, presbycusis with cochlear dysfunction; PCF, preserved cochlear function; PTA, pure tone average; NPS, neuropsychiatric symptoms.

Audiological Evaluations

Hearing thresholds were measured by an experienced audiologist with a clinical audiometer (AC40, Interacoustics®) in a soundproof room placed in the Otolaryngology Department of the Clinical Hospital of the University of Chile. Subjects were instructed to respond when they perceived a tone at a specific frequency and intensity. The lowest-intensity sound they could hear was registered in decibels for each frequency, including 0.125, 0.25, 0.5, 1, 2, 3, 4, 6, and 8 kHz for each ear separately. Pure tone average (PTA) hearing thresholds were calculated using 0.5, 1, 2, and 4 kHz frequencies per ear, and the PTA in the better-hearing ear was used for subsequent analyses. Subjects were classified according to the PTA of the better hearing ear into normal hearing ($\leq$20 dB) and presbycusis ($>$20 dB).

Distortion product otoacoustic emissions (DPOAE) were used as a measure of the loss of outer hair cells in both ears. DPOAE measurements were performed in the same soundproof room as audiogram evaluations using a sensitive microphone (ER10C, Etymotic Research®) fitted to the external ear canal. The acoustic stimuli were two pure tones of different frequencies (f1 and f2) that elicited a DPOAE at 2f1–f2. The difference between the intensity of f1 and f2 tones was 10 dB (65 and 55 dB SPL), while the frequency ratio of f2/f1 was fixed at 1.22. We presented eight pairs of primary tones (f1 and f2) in each ear, eliciting eight different 2f1–f2 frequencies: 707, 891, 1,122, 1,414, 1,781, 2,244, 2,828, and 3,563 Hz. The testing time for DPOAE measurements was 180 s for each ear. The detection of the DPOAEs was based on a signal to noise amplitude criterion: a DPOAE must be at least 6 dB above the average level of the noise floor sampled at several frequencies surrounding the emission frequency.

We calculated the number of DPOAE detected in the eight different frequencies in each ear (minimum = 0, maximum = 8). For the subsequent analyses we used the sum of DPOAE obtained in both ears (minimum = 0, maximum = 16). Using a bimodal distribution of the presence of DPOAE in our data (see Belkhiria et al., 2019 for more details of the DPOAE measurements). We defined the group of subjects with presbycusis and cochlear dysfunction (PCD) as those subjects that had $<$4 DPOAE in the sum of both ears, while the group with preserved cochlear function (PCF) was defined as those subjects that had four or more DPOAEs in the sum of both ears. According to the hearing threshold of the better ear and cochlear function we divided the sample into three groups: (i) Control with normal hearing and preserved cochlear function: PTA $<$ 20 dB and DPOAE in both ears $\geq$4; (ii) subjects with presbycusis and more preserved cochlear function: PTA $\geq$ 20 dB and DPOAE in both ears $\geq$ 4; and (iii) subjects with presbycusis and cochlear dysfunction PTA $\geq$ 20 dB and DPOAE in both ears $<$4. We used this approach because PTA and DPOAE measure different functions: audiogram PTA evaluates individual audition, while DPOAE measures loss of outer hair cells in both ears.

Functional Loss in Activities of Daily Living

This variable was measured by the informant using the Technology-Activities of Daily Living Questionnaire (T-ADLQ) (Muñoz-Neira et al., 2012). The T-ADLQ includes advanced activities of daily living and the use of technologies that are not usually measured in other tests. It is composed of 33 items that measure ADL of different complexity, gathered in seven subscales: self-care activities, house hold care, employment and recreation, shopping and money, travel, communication, technology. Each item is rated on a 4-point scale from 0 (no problem) to 3 (no longer capable of performing the activity). Higher scores indicate greater deterioration. For each item, a rating is provided for instances in which the patient may never have performed that activity in the past, stopped the activity prior to the onset of dementia, or for which the proxy had no information (Johnson et al., 2004).

Cognitive Assessment

A trained clinical neuropsychologist administered and scored all neuropsychological tests that were done blinded to the audiological status of the subjects. The cognitive domains were assessed using the following measures: (i) global cognitive functioning, the Chilean version of the MMSE (Quiroga et al., 2004); (ii) episodic memory, the total recall of the "Word" Chilean Spanish-version of the free and cued selective reminding test (FCSRT) (Grober et al., 1988; Delgado et al., 2016); (iii) executive function, the Frontal Assessment Battery (FAB) (Dubois et al., 2000); (iv) processing speed, the trail making test A (TMT A) (Army Individual Test Battery, 1944); (v) language, the Boston nominating test (Kaplan, 1978); and (vi) visuospatial abilities the Rey-Osterrieth complex figure test (Rey, 1959).

Behavioral and Psychological Symptoms

NPS were measured using different questionnaires: for global measurement we used the Chilean version of the Neuropsychiatric Inventory Questionnaire (NPI-Q) (Musa et al., 2017). The NPI-Q is rated by the proxy and evaluates 12 neuropsychiatric disturbances common in dementia (Musa et al., 2017). The presence and severity of each symptom was rated from 0 to 3 on the basis of scripted questions administered to the proxy. In addition, we calculated the total NPI severity score ranking from 0 to 36. Apathy was measured using the apathy evaluation scale informant version (AES-i). It consists of an 18-item questionnaire which is rated on a 4-point Likert scale from 1 (not at all characteristic) to 4 (very characteristic). Higher scores indicate higher levels of apathy (Marin et al., 1991). Significant levels of apathy were considered two standard deviations over the total group mean score. Depression was self-rated by the subjects using the Geriatric Depression Scale (GDS), which consists of 15 Yes/No answer questions. Higher scores indicate higher levels of depression, while scores over five indicate significant depressive symptoms (Yesavage et al., 1982).

Magnetic Resonance Imaging

Imaging data were acquired using a MAGNETOM Skyra 3 Tesla whole body MRI Scanner (Siemens Healthcare GmbHR, Erlangen, Germany) using a T1 MPRAGE sequence. Contiguous images across the entire brain were acquired with the following parameters: time echo (TE) = 232 ms, time repetition (TR) = 2,300 ms, flip angle = 8_, 26 slices, matrix = 256 _ 256, voxel

size = 0.94 _ 0.94 _ 0.9 mm3. We also registered T2 weighted turbo spin echo (TSE) (4,500 TR ms, 92 TE ms) and fluid attenuated inversion recovery (FLAIR) (8,000 TR ms, 94 TE ms, 2,500 TI ms) to inspect structural abnormalities. The acquisition duration was 30 min with a total of 440 images for each subject.

Image Processing and Analysis

The morphometric analysis was carried out using the software FreeSurfer version 6 running under Centos 6.0 (Gronenschild et al., 2012). A single Linux workstation was used for T1 weighted images analysis of individual subjects as suggested by Gronenschild et al. (2012). The FreeSurfer software processes cortical reconstruction (Fischl, 2012) through the following steps: volume registration with the Talairach atlas, bias field correction, initial volumetric labeling, non-linear alignment to the Talairach space, and final volume labeling. FreeSurfer's standard pipeline (i.e., recon-all) was used to produce representations of the cortical parcellation. It uses both intensity and continuity information from the entire three-dimensional MRI volume in segmentation and deformation procedures. Brain volumes were normalized by the estimated total intracranial volume (eTIV) to account for variations in head size (Buckner et al., 2004). The reliability between manual tracing and automatic volume measurements has been validated (Fischl et al., 2002). All volumes were visually inspected, and if needed, edited by a trained researcher according to standard processes. T2 FLAIR MRI dataset was not used, but all surfaces were visually inspected to ensure accuracy of registration, skull stripping, segmentation, and cortical surface reconstruction. If geometric inaccuracy in boundaries between white matter, gray matter, and cerebrospinal fluid was present in the automated white matter segmentation, then manual editing was conducted. FreeSurfer morphometric procedures have been confirmed to present good test-retest reliability across scanner manufacturers and across field strengths (Han et al., 2006; Reuter et al., 2012).

After the whole-brain analysis, we selected regions of interest that have been consistently implicated in previous neuroimaging studies relating audition, cognition, and dementia (Li et al., 2017; Ren et al., 2018; Xu X.-M. et al., 2019). To define ROI's, we used the Desikan-Killiany atlas, a gyrus-based atlas (Desikan et al., 2006) that has been commonly employed to explore cortical morphometry (Fornito et al., 2013; Jalbrzikowski et al., 2013).

Regions of Interest (ROIs)

Considering that our study explores audition, cognition, NPS and functional impairment, we looked for the main cortical and subcortical brain areas responsible for the following functions in the literature: (i) temporal cortex (e.g., superior, middle, and inferior gyri) was atrophied in a longitudinal hearing impairment study (Lin et al., 2011); (ii) cingulate cortex has been previously related with presbycusis (Husain, 2016; Belkhiria et al., 2019); (iii) amygdala atrophy has been related with neuropsychiatric symptoms in early AD (Poulin et al., 2011); and (iv) structural and functional changes of the insula have been reported in hearing loss patients (Yang et al., 2014; Li et al., 2017; Ren et al., 2018; Xu X.-M. et al., 2019). Other regions such as the hippocampus, thalamus and accumbens areas were included because of their early affection in AD (ten Kate et al., 2018).

Statistical Analysis

The Statistical Package for the Social Sciences (SPSS) version 20 for Windows (IBM Corp., Armonk, NY, United States) and R project version 3.3.3 was used for statistical analysis. The associations of hearing function (PTA of the better hearing ear and DPOAE) with neuropsychiatric symptoms, cognitive performance, and functionality in ADL (T-ADLQ) were examined using partial correlations and Poisson regressions. We first adjusted a Poisson regression to then evaluate the same model against a quasi-Poisson regression. If no substantial change was observed in deviances, the Poisson model was kept. For Poisson regression models, we presented pseudo R^2_D (Cameron and Windmeijer, 1997; Martin and Hall, 2016). We then analyzed the main determinants of functional impairment by performing multiple linear regression models including the T-ADLQ as the dependent variable, while demographics, cognitive tests, apathy, irritability, depression, sleeping disorders, and audiological measurements (DPOAE or PTA) were independent variables. As DPOAE and PTA were correlated, in order to avoid collinearity they were never tested simultaneously. In the case that both were significant regressors, we kept the best based on R^2. All variables used in regression models were standardized by z-scores, allowing comparison among regressors' coefficients. We further divided the whole group according to hearing status into controls, presbycusis with more preserved cochlear function and presbycusis with cochlear dysfunction according to the number of detectable DPOAE (as explained previously in the DPOAE method section). Cognitive, neuropsychiatric, auditory, and brain volume variables were compared between the three groups (controls, PCF, and PCD) using ANCOVA with gender, age, and years of education as covariates using Tukey *post hoc* tests for specific comparisons. Partial correlations were run between measures of functional impairment and brain volume values. A p-value < 0.05 was considered significant. All results are reported without multiple comparison corrections between tests. However, in order to limit false positive results, we included a multiple comparison correction between tests. We also corrected by the total number of statistical tests used using a Holm-Bonferroni procedure (Holm, 1979). This correction did not include *post hoc* and regressor tests.

RESULTS

Demographic Characteristics and Hearing Status

The mean age of the recruited subjects (n = 111, 69 female) was 73.95 ± 5.47 years (mean ± SD) with an average educational level of 9.44 ± 4.2 years of schooling. According to the audiometric hearing thresholds, 40 normal-hearing subjects and 71 with presbycusis participated. The average number of detected DPOAE as sum of both ears was 6.95 ± 5.56, which had a non-normal, bimodal distribution (W = 0.89, $p < 0.001$).

Based on PTA and DPOAEs results, the sample was stratified into three groups: (i) controls (36 subjects), (ii) presbycusis with more preserved cochlear function (PCF, 33 subjects), and (iii) presbycusis with cochlear dysfunction (PCD, 38 subjects). Four subjects from the control group who did not fit this classification criteria were excluded from the study. A summary of demographic data, including age, sex, education, hearing level, and cardiovascular risk factors is presented in **Table 1**.

Correlations Between Audiological, Demographic, and Behavioral Variables in the Entire Group

PTA and DPOAE numbers were significantly correlated ($r = -0.74$, $p < 0.001$), and both were correlated with age ($r = 0.36$, $p < 0.001$ and $r = -0.41$, $p < 0.001$, respectively). When age, gender, and education were included, PTA and DPOAE were correlated with the nomination score ($r = -0.29$, $p < 0.01$ and $r = 0.25$, $p < 0.01$, respectively) and with executive functions ($r = -0.3$, $p < 0.01$ and $r = 0.3$, $p < 0.01$, respectively). There was a significant association obtained through multiple Poisson regressions between apathy and the number of detectable DPOAE in both ears ($\beta = -0.015$ (± 0.003), $z = -4.16$, $p = 3.18\text{e-}05^{\#}$, $R^2_D = 0.17$) including age, gender, and years of education (**Figure 1**), while the same model, substituting PTA for DPOAE, showed 0.12% of variance [$\beta = -0.003$ (± 0.001), $z = 2.35$, $p = 0.01$, $R^2_D = 0.12$]. When performing a Poisson regression with T-ADQL as the dependent variable and DPOAE and other control variables (age, gender, and years of education), again DPOAE was a significant regressor [$\beta = -0.025$ (± 0.006), $z = -4.05$, $p = 5.09\text{e-}05^{\#}$, $R^2_D = 0.15$]. When performing the same analysis with PTA instead of DPOAE, PTA was not a significant regressor.

Comparison of Behavioral Variables Across Hearing Status Groups

The analysis of the neuropsychiatric symptoms showed that most subjects (72%) have at least one neuropsychiatric symptom. The most common neuropsychiatric symptoms were sleeping disorders (35%), irritability (32%), depressive symptoms (30%), and apathy (22%). Among these NPS, only the apathy severity scored by the AES-i showed significant differences between the three groups, with more severe apathy symptoms in the presbycusis and cochlear dysfunction groups [$F_{(2,\ 107)} = 6.03$, $p = 0.003$]. No difference was found in the depressive symptoms score [$F_{(2,\ 107)} = 0.24$, $p = 0.78$].

When comparing cognitive tests between the three groups (**Table 2**), the group of presbycusis with cochlear dysfunction showed the worst performance for global cognition [$F_{(2,\ 106)} = 5.2$, $p = 0.007$], executive function [$F_{(2,\ 106)} = 8.89$, $p = 0.0002$] and nomination [$F_{(2,\ 106)} = 3.53$, $p = 0.032$]. In the entire sample, the mean percentage of functional impairment in ADL was 9.8 ± 8 (mean $\pm$ SD) which is considered a low value. No significant differences were observed for the percentage of functional impairment between the three groups [$F_{(2,\ 107)} = 2.722$, $p = 0.07$].

TABLE 1 | Demographic description of the ANDES cohort.

Characteristic	Cohort ($n = 111$)
Age, mean (*SD*)	73.95 (5.47)
Sex, *n* (%) Female	69 (62.16)
Education, mean years (*SD*)	9.44 (4.27)
Hearing threshold, mean dB (*SD*)	26.59 (12.20)
DPOAEs, mean number (*SD*)	6.95 (5.56)
Hearing loss and cochlear status category, *n* (%)	
Normal hearing with preserved cochlear function	36 (32.43)
Presbycusis with preserved cochlear function	33 (29.72)
Presbycusis with cochlear dysfunction	38 (34.23)
Hypertension, *n* (%)	43 (38.73)
Smoking, *n* (%)	21 (18.91)
Diabetes, *n* (%)	29 (26.12)
Hearing aid use, *n* (%)	0 (0.0)

Determinants of Functional Impairment Across Hearing Status Groups

We analyzed the main determinants of functional impairment by means of multiple linear regression models. We included only the apathy and irritability severity index of the NPS variables, as they were the most prevalent and severe. We also included cognitive, audiological, and demographic data. None of these variables were significant predictors of functional loss for the control group (**Table 3**). In contrast, for PCF [$F_{(3,\ 32)} = 8.35$; $p = 0.0003^{\#}$; $R^2 = 0.38$] and PCD [$F_{(3,\ 33)} = 9.02$; $p = 0.0001^{\#}$; $R^2 = 0.40$] groups, these models were significant and explained similar variance, 38 and 40% respectively (**Table 3**). Irritability and apathy were significant predictors for PCF and PCD functionality, while nomination was a significant predictor of functionality only in the PCD group. The DPOAE number was a significant predictor for PCF functionality. Interestingly, PTA was not a significant predictor of functional loss in any of the three groups. When observing the standardized coefficients, irritability presented a higher influence on functionality for PCF compared with PCD, while apathy presented a higher contribution to functionality for PCD compared with PCF (**Table 3**). The associations between irritability, apathy, nomination, and functional impairment are shown in **Figure 2**.

Functional Impairment and Brain Volume Changes

To examine whether the main determinants of functional loss were linked to brain volume changes, we applied partial correlations for each group. Age, gender, years of education, and estimated total intracranial volume were included as covariates. In the control and PCF groups, apathy, executive functions, and language and functional abilities were not associated with brain volume changes (not shown). In the PCD group, apathy severity (measured by AES-i), nomination and the percentage of functional loss (measured by T-ADLQ) were distinctly associated with brain volume atrophy.

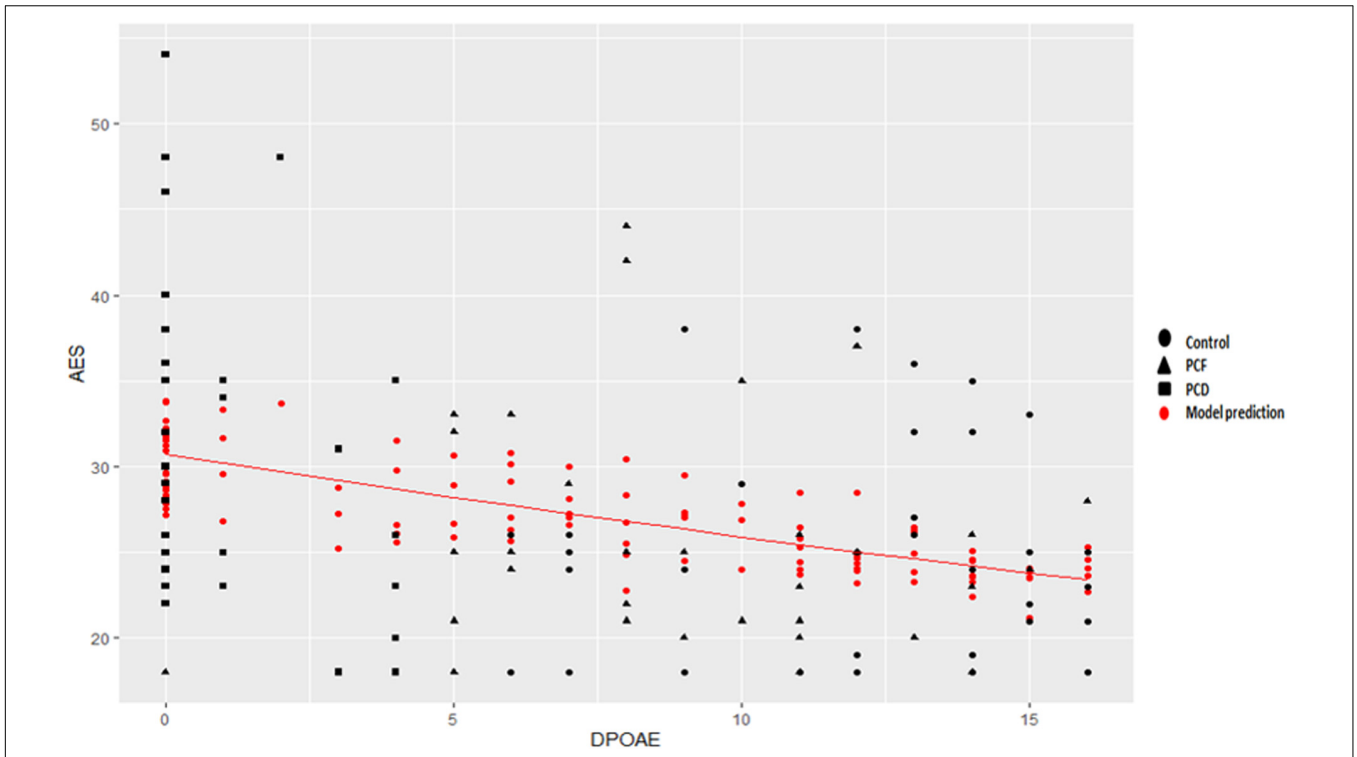

FIGURE 1 | Poisson regression between apathy symptoms and cochlear function. A significant Poisson regression, including age, gender, and education, was obtained between apathy and the number of detectable DPOAE in both ears [β = –0.015 (±0.003), z = –4.16, p = 3.18e-05$^{\#}$, R^2_D = 0.17]. Black indicates actual observations. Red dots correspond to the model's prediction, correcting for age, gender, and years of education. The Poisson regression including only DPOAE, without age, gender, or years of education, accounts for 11% of variance depicted as a red line [β = –0.016 (±0.003), z = –4.99, –0.28, p = 5.8e-07$^{\#}$, R^2_D = 0.11].

TABLE 2 | Demographic, audiological, and cognitive comparisons across hearing status groups.

	Controls	PCF	PCD	F or χ^2	*P*
	(*n* = 36)	(*n* = 33)	(*n* = 38)		
Age (years)	71.22 ± 4.9	73.64 ± 5.66$^{£}$	76.73 ± 4.6$^{¥}$	11.27	3.77E-05$^{**\#}$
Education (years)	9.72 ± 3.74	9.42 ± 4.43	9.94 ± 4.24	0.138	0.871
Sex, Female (%)	27 (75%)	20 (60%)	19 (50%)	4.912	0.086
DPOAEs (number)	12.11 ± 3.28	9.09 ± 2.87$^{£}$	0.92 ± 1.49$^{¥\$}$	182.9	<2E-16$^{**\#}$
PTA (dB)	15.05 ± 3.6	26.27 ± 4.48$^{£}$	39.21 ± 9.92$^{¥\$}$	119.3	<2E-16$^{**\#}$
Global cognition (MMSE)	28.26 ± 1.3	28.55 ± 0.86	27.60 ± 1.46$^{\$}$	5.207	0.007*
Executive functions (FAB)	14.52 ± 1.89	13.48 ± 2.41	12.51 ± 2.38$^{\$}$	8.891	0.0002$^{*\#}$
Visuospatial capacities (Rey figure)	29.33 ± 6.01	29.88 ± 5.42	30.43 ± 3.42	0.553	0.57
Processing speed (TMT A)	59.52 ± 28.99	55.85 ± 27.31	73.16 ± 58.45	2.043	0.13
Episodic memory (FCSRT-total recall)	42.85 ± 8.09	43.03 ± 6.47	43.64 ± 4.52	0.455	0.107
Nomination (Boston)	25.58 ± 2.70	25.06 ± 3.03	23.75 ± 3.5$^{¥}$	3.531	0.032*
Functional impairment (T-ADLQ)	7.94 ± 7.31	9.03 ± 7.52	12.1 ± 9.23	2.722	0.07
Neuropsychiatric symptoms (NPI-Q)	1.39 ± 1.35	1.94 ± 1.71	1.68 ± 1.87	0.941	0.394
Apathy (AES-i)	25.5 ± 5.9	25.48 ± 6.95	31.07 ± 9.14$^{¥\$}$	6.121	0.003
Depression (GDS)	3.26 ± 3.21	3.17 ± 3.21	3.71 ± 3.80	0.246	0.783

*Data were analyzed using ANCOVA for comparing variables between the three groups, corrected for age, sex, and education as corresponded. Differences of sex between groups were assessed using Chi-squared test. Mean ± SD values for age, education, sex, DPOAEs, PTA, and cognitive tests are shown for controls, presbycusis with more preserved cochlear function (PCF), and presbycusis with cochlear dysfunction (PCD). *p < 0.05, **p < 0.001 for significant ANCOVA. ¥Significant differences when comparing PCD vs. controls; $significant differences when comparing PCD vs. PCF; £significant differences when comparing PCF vs. controls; #if significant after correcting for all statistical tests applied.*

AES-i showed significant inverse correlations with bilateral volume of amygdala, insula, and inferior temporal gyrus. Nomination (Boston) score was directly correlated with left orbitofrontal, right thalamus and bilateral hippocampus, anterior cingulate, and insula volume (**Table 4**). However, the percentage of functional impairment was significantly and inversely

TABLE 3 | Determinants of functional impairment in the hearing status groups.

Regressors	Control	PCF	PCD
Regression models			
Age	n.s.	n.s.	n.s.
Education	n.s.	n.s.	n.s.
FAB	n.s.	n.s.	n.s.
Nomination (Boston)	n.s.	n.s.	$-0.35^{**\#}$
Irritability (Severity)	n.s.	$0.43^{**\#}$	$0.31^{*\#}$
Apathy (AES-i)	n.s.	$0.34^{*\#}$	$0.40^{**\#}$
DPOAE	n.s.	$-0.30^{*\#}$	n.s.
PTA	n.s.	n.s.	n.s.
Adjusted R^2	NA	0.38	0.40

*Z-score standardization regression coefficients are presented. *p < 0.05, **p < 0.01, n.s. for variables tested but further pruned from the models due to none-significant results, and # if significant after correcting for all statistical tests applied. PCF, Presbycusis with more preserved cochlear function; PCD, Presbycusis with cochlear dysfunction.*

correlated with bilateral frontotemporal regions as well as with amygdala, insula, hippocampus and nucleus accumbens volume (**Table 4**). These areas are represented in **Figure 3**.

DISCUSSION

In order to explore the mechanisms that relate presbycusis and dementia, we analyzed the structural brain changes associated with mild functional and behavioral impairment in presbycusis subjects. We found that functional loss was related with atrophy in the anterior insula and amygdala, among other temporal areas in subjects with presbycusis and cochlear dysfunction. We found a neural link relating presbycusis and mild functional impairment.

Hearing Loss and Functional Impairment

As a first step, we presented a detailed assessment of cognitive, neuropsychiatric, and audiological variables related with functional impairment in presbycusis subjects, excluding other non-neural causes of disability. We reached a significant model that explained nearly 40% of the variability of functional loss in both presbycusis groups. The variables that were significantly related with functional loss included the NPS, nomination impairment, and cochlear dysfunction (**Tables 2**, **3**). Surprisingly, hearing threshold as measured by PTA was not a significant predictor of functional impairment in any of the groups with presbycusis. One explanation could be due to our inclusion criterion of no use of hearing aids at recruitment. For this reason, there were relatively few subjects with moderate to severe hearing loss, which according to the World Health Organization (2017) probably had more severe functional impairment due to hearing loss.

On the other hand, the cochlear function, measured by the sum of the total DPOAEs detected in both ears, appeared to be significant predictor of functional loss in the PCF group, which was mainly comprised of mild presbycusis subjects. The lack of effect of DPOAE in the PCD group is probably caused by the low variability in the number of DPOAEs in this group (0.92 ± 1.49) compared to the PCF (9.09 ± 2.87) (mean $\pm$ SD) due to our classification criteria. Our findings suggest that the loss of DPOAE is a more sensitive measure for predicting functional impairment in subjects with mild presbycusis than PTA (average thresholds between 0.5 and 4 kHz). This is also supported by the behavioral analysis (**Tables 2**, **3** and **Figure 2**) showing that

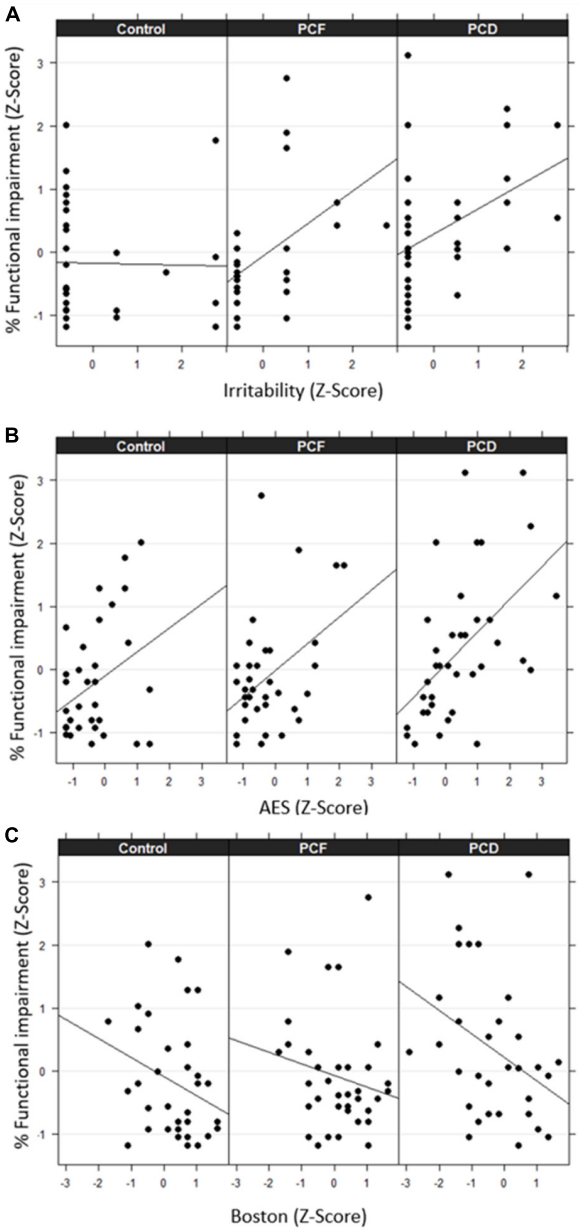

FIGURE 2 | Association between percentage of functional impairment and irritability **(A)**, apathy **(B)**, and nomination **(C)** across the three groups. Values are expressed in terms of z-scores. PCF indicates presbycusis with more preserved cochlear function, while PCD indicates presbycusis with cochlear dysfunction.

TABLE 4 | Partial correlations between brain volume and apathy severity, nomination score, and percentage of functional impairment in PCD group.

	Apathy	*p*	Nomination	*P*	Functional impairment	*P*	Apathy	*p*	Nomination	*p*	Functional impairment	*P*
	Left hemisphere						Right hemisphere					
Lateral orbitofrontal	−0.14	n.s.	0.42*	0.01	−0.34*	0.04	−0.12	n.s.	0.3	n.s.	−0.15	n.s.
Anterior cingulate	−0.08	n.s.	0.54**	0.002**	−0.21	n.s.	0.29	n.s.	0.37*	0.03	−0.24	n.s.
Posterior cingulate	−0.11	n.s.	0.15	n.s.	−0.28	n.s.	0.14	n.s.	0.28	n.s.	−0.29	n.s.
Superior temporal	−0.21	n.s.	0.17	n.s.	−0.39*	0.02	−0.11	n.s.	0.21	n.s.	−0.37*	0.03
Middle temporal	0.02	n.s.	0.21	n.s.	−0.31*	0.04	0.11	n.s.	0.12	n.s.	−0.2	n.s.
Inferior temporal	−0.34*	0.04	−0.09	n.s.	−0.39*	0.04	−0.34*	0.04	−0.09	n.s.	−0.39*	0.02
Insula	−0.3*	0.04	0.44*	0.01	−0.39*	0.02	−0.34*	0.04	0.46*	0.006	−0.46*	0.006
Amygdala	−0.31*	0.04	0.26	n.s.	−0.36*	0.03	−0.36*	0.03	0.2	n.s.	−0.51*	0.002
Hippocampus	−0.17	n.s.	0.42*	0.01	−0.46*	0.04	−0.17	n.s.	0.42*	0.01	−0.46**	0.005
Thalamus	−0.16	n.s.	−0.05	n.s.	−0.31*	0.04	−0.04	n.s.	0.35*	0.03	−0.19	n.s.
Accumbens-area	−0.13	n.s.	0.15	n.s.	−0.35*	0.04	−0.083	n.s.	0.15	n.s.	−0.27	n.s.

*Results are corrected for age, gender, years of education, and estimated total intracranial volume. n.s: $p > 0.05$, *$p < 0.05$, **$p < 0.01$, #if significant after correcting for all statistical tests applied.*

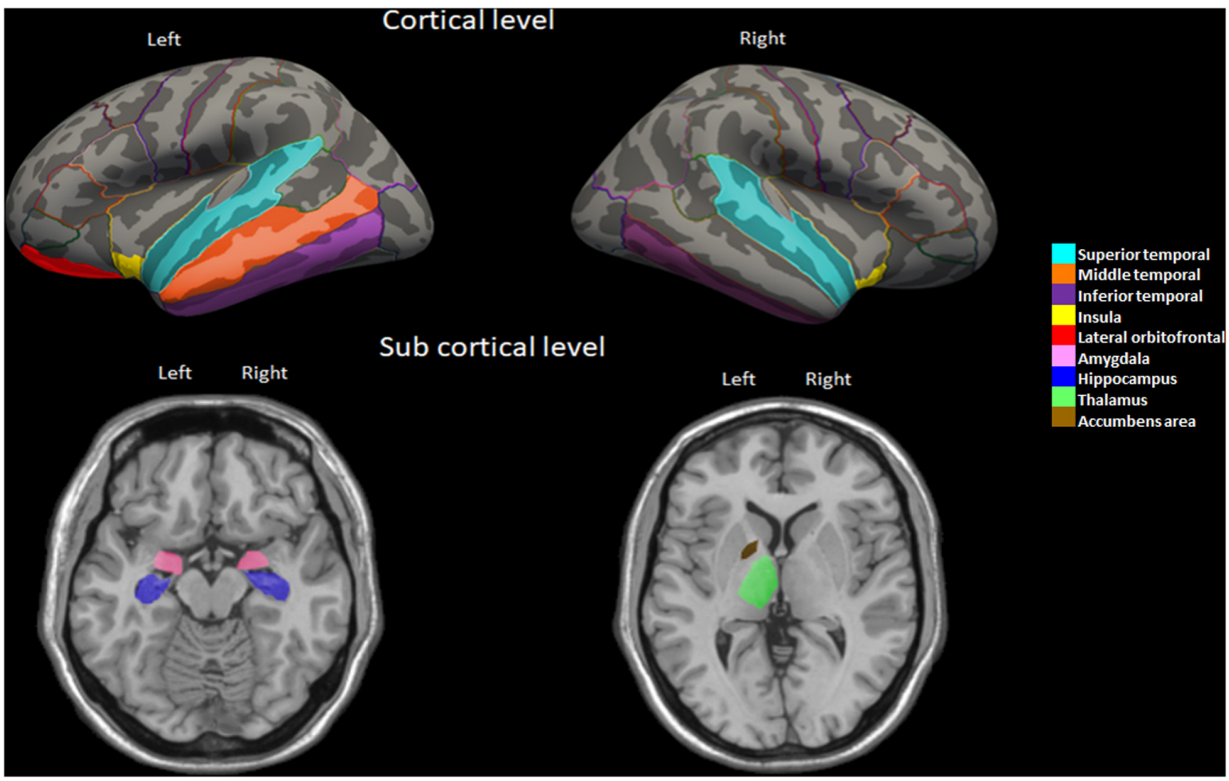

FIGURE 3 | Brain regions highlighting the significant partial correlations between volume and functional impairment in the PCD group.

the PCD group had worse performance in cognitive tests and behavioral questionnaires compared to the PCF group.

The most important determinants of functional impairment in presbycusis were the NPS, specifically apathy and irritability. Apathy is widely defined as a marked "loss of motivation" (Marin et al., 1991; Kaji and Hirata, 2011; Kirsch-Darrow et al., 2011), which has been related with functional impairment in demented (Freels et al., 1992; Lechowski et al., 2009; Clarke et al., 2011; Rog et al., 2014; You et al., 2015; Stanton and Carson, 2016; Farias et al., 2017; Lanctôt et al., 2017; Parrao et al., 2017) and non-demented elders (Freels et al., 1992; Rog et al., 2014; van Dalen et al., 2018; Delgado et al., 2019). Considering the high prevalence of presbycusis in the elderly, it is possible that hearing loss could mediate, at least partially, the association between apathy and functional impairment described in these studies. The relationship between neuropsychiatric symptoms and sensorial loss have been reported in subjects with AD and Parkinson's disease (Cramer et al., 2010; Hong et al., 2015), showing that

apathy severity was related with olfactory dysfunction (Yu et al., 2018), suggesting that the neurodegenerative process affects the limbic system, including the olfactory system (Seligman et al., 2013). In our study, interestingly, apathy severity was significantly associated with cochlear dysfunction (loss of DPOAEs). Although it is relevant to note that we found a rather weak association (R^2_D = 0.17), most of the variance was due to DPOAE instead of known related variables such as age and education or gender. **Figure 1** showed that better cochlear function (higher DPOAE number) is associated with less severe apathy symptoms (smaller AES-i score). As far as we know, this is the first study reporting an association between apathy and a pure peripheral cause of hearing loss in non-demented subjects. Also, PTA was not associated with apathy, supporting that to some extent DPOAE complements the information obtained with PTA in regards to neurodegeneration and cognitive decline (Belkhiria et al., 2019).

Structural Brain Changes Related With Functional Impairment in Presbycusis

In line with the behavioral results, we found significant correlations between functional impairment and atrophy of bilateral insula and several areas of the temporal cortex, including the bilateral hippocampus and amygdala in the PCD group but not in the PCF group. Also, there were significant associations with subcortical areas, including the left thalamus and the nucleus accumbens (**Table 4**). Among these areas, the atrophy of the bilateral insula and hippocampus was related to nomination impairment, while apathy severity was associated with atrophy of the bilateral inferior temporal cortex, insula, and amygdala (**Table 4**). Notably, the functional decline in the PCD group was related with the atrophy of areas beyond the core speech network (Peelle and Wingfield, 2016; Peelle, 2018). Some of these areas, such as the cingulate cortex and the insula, have been shown to be activated during speech understanding of acoustically degraded situations. During these conditions, subjects need to increase their listening effort to comprehend the acoustic information (Sharma and Glick, 2016; Xu X.-M. et al., 2019). The listening effort might increase the cognitive load, deteriorating cognitive processing of non-auditory stimuli in patients with presbycusis (Cardin, 2016; Husain, 2016). Accordingly, a recent study evaluating functional and structural MRI in hearing impaired patients (Xu X.-M. et al., 2019) showed that the functional connections between insula and other brain regions were significantly decreased and associated with emotional and cognitive dysregulation in these patients. In addition, a study in patients with presbycusis and structural MRI showed evidence that a thicker right insula was associated with better speech perception (Ren et al., 2018). In fact, the insula is an important hub in many brain networks, including the salience network, high-level cognitive control, attentional processes, language processing, and regulation of emotion and behavior (Craig, 2009; Bestelmeyer et al., 2014). Functional MRI studies showed insular activation in response to a wide variety of stimuli and paradigms involving sound detection, auditory temporal processing, and phonological processing (Ghaziri et al., 2018). Lesions of the insula or disconnections with the auditory cortex cause auditory impairment such as agnosia, musical anhedonia (Sihvonen et al., 2016) and hyperacusis (Boucher et al., 2015). The insula is known to have a direct, extensive and reciprocal functional connection with frontal areas involved in language processing, such as the prefrontal cortex and frontal operculum (Augustine, 1996; Jakab et al., 2012), which could explain its relation with nomination impairment in our study. In addition, the insula is atrophied in diseases with language impairment such as the progressive non-fluent aphasia (Nestor et al., 2003). In several neurodegenerative diseases such as AD, Parkinson's disease, and progressive supranuclear palsy, the atrophy of insula, anterior and posterior cingulate gyri, and frontoparietal areas have been related with apathy severity (Reijnders et al., 2010; Jeong et al., 2018; Le Heron et al., 2018).

On the other hand, the amygdala receives corticofugal projections from the auditory cortex, direct projections from subcortical regions of the ascending auditory, and from other sensorial pathways (Frühholz et al., 2014; Pérez-Valenzuela et al., 2019). It has been proposed as a key component in models of tinnitus to account for emotional distress (Jastreboff, 1990). Similar to the insula, the amygdala has been demonstrated to be especially important for decision-making by triggering autonomic responses to emotional stimuli (Clark et al., 2008).

Finally, it is important to note that the brain atrophy associated with functional impairment in presbycusis subjects with cochlear dysfunction could be related with neurodegeneration, especially considering the high prevalence of AD biomarkers in cognitively normal subjects older than 65 years (Jansen et al., 2015). In fact, recent work with animals (Park et al., 2018) showed that tau levels are elevated in the hippocampus of mice with noise-induced hearing loss, while in humans with hearing loss there are elevated Tau levels in the cerebrospinal fluid associated with brain atrophy (Xu W. et al., 2019). Thus, some of the subjects involved in our study could have a preclinical state of AD and/or another neurodegenerative process. This is supported by the view that the amygdala, hippocampus, and other temporal areas are the first atrophied regions in the early stages of AD (ten Kate et al., 2018), and that atrophy of these temporal areas has been linked to functional impairment in early stages of AD (Slachevsky et al., 2019).

CONCLUSION

We demonstrated that in independent non-demented subjects with presbycusis, cochlear dysfunction was related with neuropsychiatric symptoms, language dysfunction, and functional impairment in activities of daily living. These behavioral changes were associated with atrophy of the insula and amygdala, among other temporal areas. These regions regulate the sensorial, cognitive, and emotional processing necessary for decision making and behavior, suggesting a neural link between presbycusis and dementia. Cochlear dysfunction may be considered a biomarker of progressive functional impairment in presbycusis subjects.

LIMITATIONS

Potential limitations of this study are as follows. First, we have focused only on the volumetric measurements. Future studies could investigate the possible functional connectivity between cortical and subcortical structures and their collective contributions to functional impairment and behavioral symptoms in presbycusis. Secondly, future studies might address whether low- (<0.5 kHz) and high-frequency (>4 kHz) audiogram thresholds are associated with cognitive and brain structural changes in presbycusis. Thirdly, the cross-sectional design of the present study does not permit causal inferences. Longitudinal studies are necessary to unravel the determinants and neural mechanisms of functional impairment in presbycusis. Finally, this study used a large number of statistical tests: 7 correlations, 3 linear regressions, 4 Poisson regressions, 15 ANCOVAs, and 70 partial correlations. This naturally increases the chances of detecting effects that may not be reproducible. When using cross-statistical tests *p*-value correction, many results were significant; however, others did not pass such correction. For this reason, we advise caution on the interpretation of results, and we encourage other authors to research how PTA and DPOAE may be of help in understanding dementia and neural degeneration.

DATA AVAILABILITY STATEMENT

The raw data supporting the conclusions of this manuscript will be made available by the authors, without undue reservation, to any qualified researcher.

ETHICS STATEMENT

The studies involving human participants and all the procedures were reviewed and approved by the Ethical and Scientific Committee of the Clinical Hospital of the Universidad de Chile, permission number OAIC 752/15. The patients/participants provided their written informed consent to participate in this study.

AUTHOR CONTRIBUTIONS

CB analyzed the data and wrote the manuscript. RV and SS participated to analyze the data. AL, BM, MM, and MA performed the data acquisition. PD and CD performed experimental design, data analysis, and edited the manuscript.

FUNDING

This project was funded by Fondecyt 1161155 to PD, Proyecto Anillo ACT1403, CONICYT BASAL FB008, Proyecto ICM P09-015F, and Fundación Guillermo Puelma.

ACKNOWLEDGMENTS

We would like to thank the participants that gave their time to take part in this study and everybody who has contributed to its realization.

REFERENCES

Augustine, J. R. (1996). Circuitry and functional aspects of the insular lobe in primates including humans. *Brain Res. Brain Res. Brain Res. Rev.* 22, 229–244. doi: 10.1016/s0165-0173(96)00011-2

Belkhiria, C., Vergara, R. C., San Martín, S., Leiva, A., Marcenaro, B., Martinez, M., et al. (2019). Cingulate cortex atrophy is associated with hearing loss in presbycusis with cochlear amplifier dysfunction. *Front. Aging Neurosci.* 11:97. doi: 10.3389/fnagi.2019.00097

Bestelmeyer, P. E. G., Maurage, P., Rouger, J., Latinus, M., and Belin, P. (2014). Adaptation to vocal expressions reveals multistep perception of auditory emotion. *J. Neurosci.* 34, 8098–8105. doi: 10.1523/jneurosci.4820-13.2014

Boucher, O., Turgeon, C., Champoux, S., Ménard, L., Rouleau, I., Lassonde, M., et al. (2015). Hyperacusis following unilateral damage to the insular cortex: a three-case report. *Brain Res.* 1606, 102–112. doi: 10.1016/j.brainres.2015.02.030

Brewster, K. K., Ciarleglio, A., Brown, P. J., Chen, C., Kim, H.-O., Roose, S. P., et al. (2018). Age-related hearing loss and its association with depression in later life. *Am. J. Geriatr. Psychiatry* 26, 788–796. doi: 10.1016/j.jagp.2018.04.003

Buckner, R. L., Head, D., Parker, J., Fotenos, A. F., Marcus, D., Morris, J. C., et al. (2004). A unified approach for morphometric and functional data analysis in young, old, and demented adults using automated atlas-based head size normalization: reliability and validation against manual measurement of total intracranial volume. *Neuroimage* 23, 724–738. doi: 10.1016/j.neuroimage.2004.06.018

Cameron, A. C., and Windmeijer, F. A. G. (1997). An R-squared measure of goodness of fit for some common nonlinear regression models. *J. Econometr.* 77, 329–342. doi: 10.1016/s0304-4076(96)01818-0

Cardin, V. (2016). Effects of aging and adult-onset hearing loss on cortical auditory regions. *Front. Aging Neurosci.* 10:199. doi: 10.3389/fnins.2016.00199

Clark, L., Bechara, A., Damasio, H., Aitken, M. R. F., Sahakian, B. J., and Robbins, T. W. (2008). Differential effects of insular and ventromedial prefrontal cortex lesions on risky decision-making. *Brain* 131, 1311–1322. doi: 10.1093/brain/awn066

Clarke, D. E., Ko, J. Y., Kuhl, E. A., van Reekum, R., Salvador, R., and Marin, R. S. (2011). Are the available apathy measures reliable and valid? A review of the psychometric evidence. *J. Psychosom. Res.* 70, 73–97.

Cosh, S., Carriere, I., Daien, V., Amieva, H., Tzourio, C., Delcourt, C., et al. (2018). The relationship between hearing loss in older adults and depression over 12 years: findings from the Three-City prospective cohort study. *Int. J. Geriat.r Psychiatry* 33, 1654–1661. doi: 10.1002/gps.4968

Craig, A. D. (2009). Emotional moments across time: a possible neural basis for time perception in the anterior insula. *Philos. Trans. R. Soc. B Biol. Sci.* 364, 1933–1942. doi: 10.1098/rstb.2009.0008

Cramer, C. K., Friedman, J. H., and Amick, M. M. (2010). Olfaction and apathy in Parkinson's disease. *Parkins. Relat. Disord.* 16, 124–126.

Cruickshanks, K. J., Wiley, T. L., Tweed, T. S., Klein, B. E. K., Klein, R., Mares-Perlman, J. A., et al. (1998). Prevalence of hearing loss in older adults in beaver dam, wisconsin: the epidemiology of hearing loss study. *Am. J. Epidemiol.* 148, 879–886. doi: 10.1093/oxfordjournals.aje.a009713

de Oliveira, F. F., Wajman, J. R., Bertolucci, P. H. F., Chen, E. S., and Smith, M. C. (2015). Correlations among cognitive and behavioural assessments in patients with dementia due to Alzheimer's disease. *Clin. Neurol. Neurosurg.* 135, 27–33. doi: 10.1016/j.clineuro.2015.05.010

Deal, J. A., Betz, J., Yaffe, K., Harris, T., Purchase-Helzner, E., Satterfield, S., et al. (2016). Hearing impairment and incident dementia and cognitive decline in older adults: the health ABC study. *J. Gerontol. A Biol. Sci. Med. Sci.* 72, 703–709.

Delgado, C., Muñoz-Neira, C., Soto, A., Martínez, M., Henríquez, F., Flores, P., et al. (2016). Comparison of the psychometric properties of the "word" and "picture" versions of the free and cued selective reminding test in a spanish-speaking cohort of patients with mild Alzheimer's disease and cognitively healthy controls. *Arch. Clin. Neuropsychol.* 31, 165–175.

Delgado, C., Vergara, R. C., Martínez, M., Musa, G., Henríquez, F., and Slachevsky, A. (2019). Neuropsychiatric symptoms in Alzheimer's disease are the main determinants of functional impairment in advanced everyday activities. *J. Alzheimers Dis.* 67, 381–392. doi: 10.3233/jad-180771

Desikan, R. S., Ségonne, F., Fischl, B., Quinn, B. T., Dickerson, B. C., Blacker, D., et al. (2006). An automated labeling system for subdividing the human cerebral cortex on MRI scans into gyral based regions of interest. *NeuroImage* 31, 968–980. doi: 10.1016/j.neuroimage.2006.01.021

Dubois, B., Slachevsky, A., Litvan, I., and Pillon, B. (2000). The FAB: a frontal assessment battery at bedside. *Neurology* 55, 1621–1626. doi: 10.1212/wnl.55.11.1621

Farias, S. T., Lau, K., Harvey, D., Denny, K. G., Barba, C., and Mefford, A. N. (2017). Early functional limitations in cognitively normal older adults predict diagnostic conversion to mild cognitive impairment. *J. Am. Geriatr. Soc.* 65, 1152–1158. doi: 10.1111/jgs.14835

Fischl, B. (2012). FreeSurfer. *J. Neuroimage* 62, 774–781. doi: 10.1016/j.neuroimage.2012.01.021

Fischl, B., Salat, D. H., Busa, E., Albert, M., Dieterich, M., and Haselgrove, C. (2002). Whole brain segmentation: automated labeling of neuroanatomical structures in the human brain. *Neuron* 33, 341–355.

Fornito, A., Zalesky, A., and Breakspear, M. (2013). Graph analysis of the human connectome: promise, progress, and pitfalls. *NeuroImage* 80, 426–444. doi: 10.1016/j.neuroimage.2013.04.087

Freels, S., Cohen, D., Eisdorfer, C., Paveza, G., Gorelick, P., Luchins, D. J., et al. (1992). Functional status and clinical findings in patients with Alzheimer's disease. *J. Gerontol.* 47, M177–M182.

Frühholz, S., Trost, W., and Grandjean, D. (2014). The role of the medial temporal limbic system in processing emotions in voice and music. *Prog. Neurobiol.* 123, 1–17. doi: 10.1016/j.pneurobio.2014.09.003

Gallacher, J., Ilubaera, V., Ben-Shlomo, Y., Bayer, A., Fish, M., Babisch, W., et al. (2012). Auditory threshold, phonologic demand, and incident dementia. *Neurology* 79, 1583–1590. doi: 10.1212/wnl.0b013e31826e263d

Ghaziri, J., Tucholka, A., Girard, G., Boucher, O., Houde, J.-C., Descoteaux, M., et al. (2018). Subcortical structural connectivity of insular subregions. *Sci. Rep.* 8:8596.

Grober, E., Buschke, H., Crystal, H., Bang, S., and Dresner, R. (1988). Screening for dementia by memory testing. *Neurology* 38, 900–900. doi: 10.1212/wnl.38.6.900

Gronenschild, E. H. B. M., Habets, P., Jacobs, H. I. L., Mengelers, R., Rozendaal, N., van Os, J., et al. (2012). The effects of FreeSurfer version, workstation type, and macintosh operating system version on anatomical volume and cortical thickness measurements. *PLoS ONE* 7:e38234. doi: 10.1371/journal.pone.0038234

Han, X., Jovicich, J., Salat, D., van der Kouwe, A., Quinn, B., Czanner, S., et al. (2006). Reliability of MRI-derived measurements of human cerebral cortical thickness: the effects of field strength, scanner upgrade and manufacturer. *NeuroImage* 32, 180–194. doi: 10.1016/j.neuroimage.2006.02.051

Holm, S. (1979). An improved sequentially rejective bonferroni test procedure. *Scand. J. Stat.* 6, 65–70.

Hong, J. Y., Sunwoo, M. K., Ham, J. H., Lee, J. J., Lee, P. H., and Sohn, Y. H. (2015). Apathy and olfactory dysfunction in early Parkinson's disease. *J. Mov. Disord.* 8, 21–25. doi: 10.14802/jmd.14029

Husain, F. T. (2016). Neural networks of tinnitus in humans: elucidating severity and habituation. *Hear Res.* 334, 37–48. doi: 10.1016/j.heares.2015.09.010

Individual Test Battery, (1944). *Manual of Directions and Scoring*. Washington, DC: Adjunct General's Office.

Jakab, A., Molnár, P. P., Bogner, P., Béres, M., and Berényi, E. L. (2012). Connectivity-based parcellation reveals interhemispheric differences in the insula. *Brain Imag. Behav.* 25, 264–271. doi: 10.1007/s10548-011-0205-y

Jalbrzikowski, M., Jonas, R., Senturk, D., Patel, A., Chow, C., Green, M. F., et al. (2013). Structural abnormalities in cortical volume, thickness, and surface area in 22q11.2 microdeletion syndrome: relationship with psychotic symptoms. *NeuroImage Clin.* 3, 405–415. doi: 10.1016/j.nicl.2013.09.013

Jansen, W. J., Ossenkoppele, R., Knol, D. L., Tijms, B. M., Scheltens, P., Verhey, F. R. J., et al. (2015). Amyloid biomarker study group, et al., 2015. Prevalence of cerebral amyloid pathology in persons without dementia: a meta-analysis. *JAMA* 313, 1924–1938.

Jastreboff, P. J. (1990). Phantom auditory perception (tinnitus): mechanisms of generation and perception. *Neurosci. Res.* 8, 221–254. doi: 10.1016/0168-0102(90)90031-9

Jeong, H., Kang, I., Im, J. J., Park, J.-S., Na, S.-H., Heo, Y., et al. (2018). Brain perfusion correlates of apathy in Alzheimer's disease. *Dement Neurocogn Disord.* 17:50.

Johnson, N., Barion, A., Rademaker, A., Rehkemper, G., and Weintraub, S. (2004). The activities of daily living questionnaire: a validation study in patients with dementia. *Alzheimer Dis. Assoc. Disord.* 18, 223–230.

Kaji, Y., and Hirata, K. (2011). Apathy and anhedonia in Parkinson's disease. *ISRN Neurol.* 2011:219427.

Kaplan, E. (1978). *The Boston Naming Test*. Philadelphia, PA: Lea & Febiger.

Kirsch-Darrow, L., Marsiske, M., Okun, M. S., Bauer, R., and Bowers, D. (2011). Apathy and depression: separate factors in Parkinson's disease. *J. Int. Neuropsychol. Soc. Soc.* 17, 1058–1066. doi: 10.1017/s1355617711001068

Lanctôt, K. L., Agüera-Ortiz, L., Brodaty, H., Francis, P. T., Geda, Y. E., Ismail, Z., et al. (2017). Apathy associated with neurocognitive disorders: recent progress and future directions. *Alzheimers Dement.* 13, 84–100. doi: 10.1016/j.jalz.2016.05.008

Le Heron, C., Apps, M. A. J., and Husain, M. (2018). The anatomy of apathy: a neurocognitive framework for amotivated behaviour. *Neuropsychologia* 118, 54–67. doi: 10.1016/j.neuropsychologia.2017.07.003

Lechowski, L., Benoit, M., Chassagne, P., Vedel, I., Tortrat, D., Teillet, L., et al. (2009). Persistent apathy in Alzheimer's disease as an independent factor of rapid functional decline: the REAL longitudinal cohort study. *Int. J. Geriatr. Psychiatry* 24, 341–346. doi: 10.1002/gps.2125

Li, M., Meng, Y., Wang, M., Yang, S., Wu, H., Zhao, B., et al. (2017). Cerebral gray matter volume reduction in subcortical vascular mild cognitive impairment patients and subcortical vascular dementia patients, and its relation with cognitive deficits. *Brain Behav.* 7:e00745. doi: 10.1002/brb3.745

Li-Korotky, H.-S. (2012). Age-related hearing loss: quality of care for quality of life. *Gerontologist* 52, 265–271. doi: 10.1093/geront/gnr159

Lin, F. R., Ferrucci, L., An, Y., Goh, J. O., Doshi, J., Metter, E. J., et al. (2014). Association of hearing impairment with brain volume changes in older adults. *NeuroImage* 90, 84–92. doi: 10.1016/j.neuroimage.2013.12.059

Lin, F. R., Ferrucci, L., Metter, E. J., An, Y., Zonderman, A. B., and Resnick, S. M. (2011). Hearing loss and cognition in the baltimore longitudinal study of aging. *Neuropsychology* 25, 763–770. doi: 10.1037/a0024238

Livingston, G., Sommerlad, A., Orgeta, V., Costafreda, S. G., Huntley, J., Ames, D., et al. (2017). Dementia prevention, intervention, and care. *Lancet* 390, 2673–2734.

López-Torres Hidalgo, J., Gras, C. B., Lapeira, J. T., Verdejo, M. ÁL., del Campo, J. M., and Rabadán, F. E. (2009). Functional status of elderly people with hearing loss. *Arch. Gerontol. Geriatr.* 49, 88–92. doi: 10.1016/j.archger.2008.05.006

Lyketsos, C. G., Carrillo, M. C., Ryan, J. M., Khachaturian, A. S., Trzepacz, P., Amatniek, J., et al. (2011). Neuropsychiatric symptoms in Alzheimer's disease. *Alzheimers Dement.* 7, 532–539.

Marin, R. S., Biedrzycki, R. C., and Firinciogullari, S. (1991). Reliability and validity of the apathy evaluation scale. *Psychiatry Res.* 38, 143–162. doi: 10.1016/0165-1781(91)90040-v

Martin, J., and Hall, D. B. (2016). R2 measures for zero-inflated regression models for count data with excess zeros. *J. Statist. Comput. Simulat.* 86, 3777–3790. doi: 10.1080/00949655.2016.1186166

McKhann, G. M., Knopman, D. S., Chertkow, H., Hyman, B. T., Jack, C. R., Kawas, C. H., et al. (2011). The diagnosis of dementia due to Alzheimer's disease: recommendations from the National Institute on Aging-Alzheimer's association workgroups on diagnostic guidelines for Alzheimer's disease. *Alzheimers Dement.* 7, 263–269.

Muñoz-Neira, C., López, O. L., Riveros, R., Núñez-Huasaf, J., Flores, P., and Slachevsky, A. (2012). The technology – Activities of daily living questionnaire: a version with a technology-related subscale. *Dement Geriatr. Cogn. Disord.* 33, 361–371. doi: 10.1159/000338606

Musa, G., Henríquez, F., Muñoz-Neira, C., Delgado, C., Lillo, P., and Slachevsky, A. (2017). Utility of the neuropsychiatric inventory questionnaire (NPI-Q) in the

assessment of a sample of patients with Alzheimer's disease in Chile. *Dement Neuropsychol.* 11, 129–136. doi: 10.1590/1980-57642016dn11-020005

Nestor, P. J., Graham, N. L., Fryer, T. D., Williams, G. B., Patterson, K., and Hodges, J. R. (2003). Progressive non-fluent aphasia is associated with hypometabolism centred on the left anterior insula. *Brain* 126, 2406–2418. doi: 10.1093/brain/awg240

Park, S. Y., Kim, M. J., Kim, H. L., Kim, D. K., Yeo, S. W., and Park, S. N. (2018). Cognitive decline and increased hippocampal p-tau expression in mice with hearing loss. *Behav. Brain Res.* 342, 19–26. doi: 10.1016/j.bbr.2018.01.003

Parrao, T., Brockman, S., Bucks, R. S., Bruce, D. G., Davis, W. A., Hatch, K. K., et al. (2017). The structured interview for insight and judgment in dementia: development and validation of a new instrument to assess awareness in patients with dementia. *Alzheimers Dement. (Amst).* 7, 24–32. doi: 10.1016/j.dadm.2016.12.012

Peelle, J. E. (2018). Listening effort. *Ear Hear.* 39, 204–214.

Peelle, J. E., and Wingfield, A. (2016). The neural consequences of age-related hearing loss. *Trends Neurosci.* 39, 486–497. doi: 10.1016/j.tins.2016.05.001

Pérez-Valenzuela, C., Terreros, G., and Dagnino-Subiabre, A. (2019). Effects of stress on the auditory system: an approach to study a common origin for mood disorders and dementia. *Rev. Neurosci.* 30, 317–324. doi: 10.1515/revneuro-2018-0018

Poulin, S. P., Dautoff, R., Morris, J. C., Barrett, L. F., Dickerson, B. C., Alzheimer's Disease, et al. (2011). Amygdala atrophy is prominent in early Alzheimer's disease and relates to symptom severity. *Psychiatry Res. Neuroimag.* 194, 7–13. doi: 10.1016/j.pscychresns.2011.06.014

Prince, M. J., Wu, F., Guo, Y., Gutierrez Robledo, L. M., O'Donnell, M., Sullivan, R., et al. (2015). The burden of disease in older people and implications for health policy and practice. *Lancet* 385, 549–562. doi: 10.1016/s0140-6736(14)61347-7

Quiroga, P., Albala, C., and Klaasen, G. (2004). Validation of a screening test for age associated cognitive impairment, in Chile. *Rev. Med. Chile* 132, 467–478.

Reijnders, J. S. A. M., Scholtissen, B., Weber, W. E. J., Aalten, P., Verhey, F. R. J., and Leentjens, A. F. G. (2010). Neuroanatomical correlates of apathy in Parkinson's disease: a magnetic resonance imaging study using voxel-based morphometry. *Mov. Disord.* 25, 2318–2325. doi: 10.1002/mds.23268

Ren, F., Ma, W., Li, M., Sun, H., Xin, Q., Zong, W., et al. (2018). Gray matter atrophy is associated with cognitive impairment in patients with presbycusis: a comprehensive morphometric study. *Front. Neurosci.* 12:744. doi: 10.3389/fnins.2018.00744

Reuter, M., Schmansky, N. J., Rosas, H. D., and Fischl, B. (2012). Within-subject template estimation for unbiased longitudinal image analysis. *NeuroImage* 61, 1402–1418. doi: 10.1016/j.neuroimage.2012.02.084

Rey, A. (1959). *Test de copie d'une Figure Complexe*. Paris: Centre de Psychologie Appliquée.

Rog, L. A., Park, L. Q., Harvey, D. J., Huang, C.-J., Mackin, S., and Farias, S. T. (2014). The independent contributions of cognitive impairment and neuropsychiatric symptoms to everyday function in older adults. *Clin. Neuropsychol.* 28, 215–236. doi: 10.1080/13854046.2013.876101

Sachdev, P. S., Lipnicki, D. M., Kochan, N. A., Crawford, J. D., Thalamuthu, A., Andrews, G., et al. (2015). Cohort studies of memory in an international consortium (COSMIC). The prevalence of mild cognitive impairment in diverse geographical and ethnocultural regions: the COSMIC collaboration. *PLoS ONE* 10:e0142388. doi: 10.1371/journal.pone.0142388

Seligman, S. C., Kamath, V., Giovannetti, T., Arnold, S. E., and Moberg, P. J. (2013). Olfaction and apathy in Alzheimer's disease, mild cognitive impairment, and healthy older adults. *Aging Ment Health* 17, 564–570. doi: 10.1080/13607863.2013.768208

Sharma, A., and Glick, H. (2016). Cross-modal re-organization in clinical populations with hearing loss. *Brain Sci.* 6:4. doi: 10.3390/brainsci6010004

Sihvonen, A. J., Ripollés, P., Leo, V., Rodríguez-Fornells, A., Soinila, S., and Särkämö, T. (2016). Neural basis of acquired amusia and its recovery after stroke. *J. Neurosci.* 36, 8872–8881. doi: 10.1523/jneurosci.0709-16.2016

Slachevsky, A., Forno, G., Barraza, P., Mioshi, E., Delgado, C., Lillo, P., et al. (2019). Mapping the neuroanatomy of functional decline in Alzheimer's disease from basic to advanced activities of daily living. *J. Neurol.* 266, 1310–1322. doi: 10.1007/s00415-019-09260-w

Sogebi, O. A., Oluwole, L. O., and Mabifah, T. O. (2015). Functional assessment of elderly patients with hearing impairment: a preliminary evaluation. *J. Clin. Gerontol. Geriatr.* 6, 15–19. doi: 10.1016/j.jcgg.2014.08.004

Solheim, J., Kværner, K. J., and Falkenberg, E. S. (2011). Daily life consequences of hearing loss in the elderly. *Disabil. Rehabil.* 33, 2179–2185. doi: 10.3109/09638288.2011.563815

Stanton, B. R., and Carson, A. (2016). Apathy: a practical guide for neurologists. *Pract. Neurol.* 16, 42–47. doi: 10.1136/practneurol-2015-001232

ten Kate, M., Redolfi, A., Peira, E., Bos, I., Vos, S. J., Vandenberghe, R., et al. (2018). MRI predictors of amyloid pathology: results from the EMIF-AD multimodal biomarker discovery study. *Alzheimers Res. Ther.* 10:100.

Tomioka, K., Okamoto, N., Morikawa, M., and Kurumatani, N. (2015). Self-reported hearing loss predicts 5-year decline in higher-level functional capacity in high-functioning elderly adults: the fujiwara-kyo study. *J. Am. Geriatr. Soc.* 63, 2260–2268. doi: 10.1111/jgs.13780

van Dalen, J. W., van Wanrooij, L. L., Moll van Charante, E. P., Brayne, C., van Gool, W. A., and Richard, E. (2018). Association of apathy with risk of incident dementia. *JAMA Psychiatry* 75:1012. doi: 10.1001/jamapsychiatry.2018.1877

World Alzheimer Report, (2016). *Alzheimer's Disease International*. Available at: https://www.alz.co.uk/research/world-report-2016 (accessed 7.4.19).

World Health Organization, (2017). *WHO Grades of Hearing Impairment*. Genova: WHO.

Xu, X.-M., Jiao, Y., Tang, T.-Y., Zhang, J., Salvi, R., and Teng, G.-J. (2019). Inefficient involvement of insula in sensorineural hearing loss. *Front. Neurosci.* 13:133. doi: 10.3389/fnins.2019.00133

Xu, W., Zhang, C., Li, J.-Q., Tan, C.-C., Cao, X.-P., Tan, L., et al. (2019). Age-related hearing loss accelerates cerebrospinal fluid tau levels and brain atrophy: a longitudinal study. *Aging* 11, 3156–3169. doi: 10.18632/aging.101971

Yang, M., Chen, H.-J., Liu, B., Huang, Z.-C., Feng, Y., Li, J., et al. (2014). Brain structural and functional alterations in patients with unilateral hearing loss. *Hear Res.* 316, 37–43. doi: 10.1016/j.heares.2014.07.006

Yesavage, J. A., Brink, T. L., Rose, T. L., Lum, O., Huang, V., Adey, M., et al. (1982). Development and validation of a geriatric depression screening scale: a preliminary report. *J. Psychiatr. Res.* 17, 37–49. doi: 10.1016/0022-3956(82)90033-4

You, S. C., Walsh, C. M., Chiodo, L. A., Ketelle, R., Miller, B. L., and Kramer, J. H. (2015). Neuropsychiatric symptoms predict functional status in Alzheimer's disease. *J. Alzheimers Dis.* 48, 863–869. doi: 10.3233/jad-150018

Yu, Q., Guo, P., Li, D., Zuo, L., Lian, T., Yu, S., et al. (2018). Olfactory dysfunction and its relationship with clinical symptoms of alzheimer disease. *Aging Dis.* 9, 1084–1095.

Conflict of Interest: The authors declare that the research was conducted in the absence of any commercial or financial relationships that could be construed as a potential conflict of interest.

frontiers in Psychiatry

ORIGINAL RESEARCH
published: 04 May 2020
doi: 10.3389/fpsyt.2020.00342

Age-Related Changes of Peak Width Skeletonized Mean Diffusivity (PSMD) Across the Adult Lifespan: A Multi-Cohort Study

*Grégory Beaudet[1,2], Ami Tsuchida[1,2], Laurent Petit[1,2], Christophe Tzourio[3], Svenja Caspers[4,5], Jan Schreiber[4], Zdenka Pausova[6,7], Yash Patel[6,7], Tomas Paus[8,9], Reinhold Schmidt[10], Lukas Pirpamer[10], Perminder S. Sachdev[11,12], Henry Brodaty[11,12], Nicole Kochan[11,12], Julian Trollor[11,12], Wei Wen[11,12], Nicola J. Armstrong[13], Ian J. Deary[14], Mark E. Bastin[14,15], Joanna M. Wardlaw[14,15], Susana Munõz Maniega[14,15], A. Veronica Witte[16], Arno Villringer[16], Marco Duering[17], Stéphanie Debette[2,3,18] and Bernard Mazoyer[1,2]**

[1] Institute of Neurodegenerative Diseases (IMN), CNRS, CEA, Bordeaux, France, [2] Institute of Neurodegenerative Diseases (IMN), University of Bordeaux, Bordeaux, France, [3] Bordeaux Population Health Research Center, Inserm, Bordeaux, France, [4] Institute of Neuroscience and Medicine (INM-1), Research Centre Juelich, Juelich, Germany, [5] Institute for Anatomy I, Medical Faculty, Heinrich Heine University Dusseldorf, Dusseldorf, Germany, [6] Research Institute, The Hospital for Sick Children, Toronto, ON, Canada, [7] Department of Physiology and Nutritional Sciences, University of Toronto, Toronto, ON, Canada, [8] Bloorview Research Institute, Holland Bloorview Kids Rehabilitation Hospital, Toronto, ON, Canada, [9] Departments of Psychology and Psychiatry, University of Toronto, Toronto, ON, Canada, [10] Department of Neurology, Medical University of Graz, Graz, Austria, [11] Centre for Healthy Brain Ageing (CHeBA), School of Psychiatry, UNSW Medicine, University of New South Wales, Sydney, NSW, Australia, [12] Neuropsychiatric Institute, Neuropsychiatric Institute Prince of Wales Hospital, Randwick, NSW, Australia, [13] Mathematics and Statistics, Murdoch University, Perth, WA, Australia, [14] Centre for Cognitive Ageing and Cognitive Epidemiology, Department of Psychology, University of Edinburgh, Edinburgh, United Kingdom, [15] Brain Research Imaging Centre, Neuroimaging Sciences, The University of Edinburgh, Edinburgh, United Kingdom, [16] Departmet of Neurology, Max Planck Institute for Human Cognitive and Brain Sciences, Leipzig, Germany, [17] Institute for Stroke and Dementia Research (ISD), University Hospital, LMU Munich, Munich, Germany, [18] Department of Neurology, Bordeaux University Hospital, Bordeaux, France

OPEN ACCESS

Edited by:
Elisa Ambrosi,
Hospital of the Brothers of St. John of God, Austria

Reviewed by:
Arvind Caprihan,
Mind Research Network (MRN), United States
Fabrizio Piras,
Santa Lucia Foundation (IRCCS), Italy

***Correspondence:**
Bernard Mazoyer
bernard.mazoyer@u-bordeaux.fr

Specialty section:
This article was submitted to Aging Psychiatry, a section of the journal Frontiers in Psychiatry

Received: 06 January 2020
Accepted: 06 April 2020
Published: 04 May 2020

Citation:
Beaudet G, Tsuchida A, Petit L, Tzourio C, Caspers S, Schreiber J, Pausova Z, Patel Y, Paus T, Schmidt R, Pirpamer L, Sachdev PS, Brodaty H, Kochan N, Trollor J, Wen W, Armstrong NJ, Deary IJ, Bastin ME, Wardlaw JM, Munõz Maniega S, Witte AV, Villringer A, Duering M, Debette S and Mazoyer B (2020) Age-Related Changes of Peak Width Skeletonized Mean Diffusivity (PSMD) Across the Adult Lifespan: A Multi-Cohort Study. Front. Psychiatry 11:342. doi: 10.3389/fpsyt.2020.00342

Parameters of water diffusion in white matter derived from diffusion-weighted imaging (DWI), such as fractional anisotropy (FA), mean, axial, and radial diffusivity (MD, AD, and RD), and more recently, peak width of skeletonized mean diffusivity (PSMD), have been proposed as potential markers of normal and pathological brain ageing. However, their relative evolution over the entire adult lifespan in healthy individuals remains partly unknown during early and late adulthood, and particularly for the PSMD index. Here, we gathered and analyzed cross-sectional diffusion tensor imaging (DTI) data from 10 population-based cohort studies in order to establish the time course of white matter water diffusion phenotypes from post-adolescence to late adulthood. DTI data were obtained from a total of 20,005 individuals aged 18.1 to 92.6 years and analyzed with the same pipeline for computing skeletonized DTI metrics from DTI maps. For each individual, MD, AD, RD, and FA mean values were computed over their FA volume skeleton, PSMD being calculated as the 90% peak width of the MD values distribution across the FA skeleton. Mean values of each DTI metric were found to strongly vary across cohorts, most likely due to major differences in DWI acquisition protocols as well as pre-processing

and DTI model fitting. However, age effects on each DTI metric were found to be highly consistent across cohorts. RD, MD, and AD variations with age exhibited the same U-shape pattern, first slowly decreasing during post-adolescence until the age of 30, 40, and 50 years, respectively, then progressively increasing until late life. FA showed a reverse profile, initially increasing then continuously decreasing, slowly until the 70s, then sharply declining thereafter. By contrast, PSMD constantly increased, first slowly until the 60s, then more sharply. These results demonstrate that, in the general population, age affects PSMD in a manner different from that of other DTI metrics. The constant increase in PSMD throughout the entire adult life, including during post-adolescence, indicates that PSMD could be an early marker of the ageing process.

Keywords: ageing, white matter, neurodegeneration, MRI, diffusion, PSMD

INTRODUCTION

Parameters of water diffusion in white matter derived from diffusion-weighted imaging (DWI), such as fractional anisotropy (FA), mean, axial, and radial diffusivity (MD, AD, and RD) are well-established markers of normal brain maturation (1–5) and ageing (6–12) and have been proposed as potential tools for the investigation of various brain disorders (13–19).

More recently, peak width of skeletonized mean diffusivity (PSMD) (20), a new phenotype of white matter microstructure that can be derived from DWI, has been proposed as an imaging biomarker of small vessel disease (SVD) (20, 21) and a correlate of cognitive impairment, particularly processing speed (20–22). Recall that PSMD is the difference between the 5th and the 95th percentiles of the distribution of the voxel MD value across a skeleton of the brain white matter. Note that PSMD is a dispersion statistic, as opposed to other diffusion tensor imaging (DTI) metric, such as AD, MD, RD, and FA, that are central tendency statistics. So far, our knowledge of the PSMD distribution in healthy individuals has been limited to these three previously mentioned studies that all included people aged over 50 years. In addition, none of these studies addressed the issue of changes in PSMD across lifespan, which is critical for establishing whether PSMD could be used as an imaging marker of brain aging as well as an early predictor of age-related disorders or to serve as a tool to monitor outcomes in clinical trials. Here, we gathered and analyzed cross-sectional DTI data from 10 population-based cohort studies to establish the time course, from post-adolescence to late adulthood, of the PSMD distribution and compare it with that of more commonly used white matter water diffusion phenotypes in white matter.

MATERIALS AND METHODS

Participants

Ten independent data sets coming from cross-sectional cohort studies were gathered in the present study, namely, MRi-Share, BIL&GIN, SYS, LIFE-Adult, 1000 BRAINS, UKBiobank, ASPSF, OATS, LBC1936, MAS (see acronym definition in **Table 1** caption). All but three (LIFE-Adult, 1000BRAINS, and UKBiobank) were part of the BRIDGET Consortium (BRain Imaging, cognition, Dementia, and next generation GEnomics: a Transdisciplinary approach to search for risk and protective factors of neurodegenerative disease), supported by EU-JPND (European Union Joint Programme—Neurodegenerative Disease Research). The 10 data sets included a total of 20,005 individuals (age range, 18.1 to 92.6 years; 10,807 women and 9,198 men). **Table 1** detail sample size and age distribution for the 10 cohorts that were all of cross.

Diffusion-Weighted Image Acquisition and Preprocessing

Table 2 summarize the main characteristics of the DWI acquisition and preprocessing for the 10 cohorts. Overall, there was considerable variability between studies regarding almost all acquisition parameters, including scanner manufacturer, field strength, gradient strength, diffusion pulse sequence, resolution, and number of directions. For the present work, it was not possible to access raw DWI data at different sites in order to harmonize processing from the initial DICOM data. For this reason, DWI data sets were pre-processed with procedures specific to each site, including exclusion of data upon visual detection of major artifacts due to eddy current distortions or head motion. AD, RD, MD, and FA maps were computed by fitting the DTI model parameters in each voxel from these preprocessed DWI volumes. Additional details on DWI preprocessing and DTI parameter map computation for each data set are provided in the **Supplementary Material** section.

Derivation of DTI Metrics

Various metrics were derived from the DTI data using a script developed by Baykara et al. (http://www.psmd-marker.com) (20). This original script was designed to extract PSMD, an index of the dispersion of MD values across the white matter skeleton. Briefly, the computation included two steps: 1) WM skeletonizing using the FA map, and 2) analyzing the voxel value distribution histogram in the MD volume masked by the WM-

TABLE 1 | Basic statistics for the 10 contributing data sets.

Data set		MRi-Share	BIL&GIN	SYS	LIFE	1000 BRAINS	UKBiobank	ASPSF	OATS	LBC 1936	MAS
Sample size	**20,005**	1,824	410	512	1,906	1,209	12,397	277	386	672	412
	(% females)	72%	51%	54%	51%	44%	53%	60%	64%	47%	53%
Age (years)	mean (SD)	22.1 (2.3)	26.9 (8.0)	49.5 (5.0)	58.1 (15.1)	60.8 (13.4)	62.6 (7.4)	65.0 (11.1)	71.1 (5.1)	72.7 (0.7)	80.3 (4.6)
	range	[18.1, 34.9]	[18.1, 57.2]	[36.4, 65.4]	[19.0, 82.0]	[18.5, 85.4]	[45.1, 80.3]	[38.5, 85.6]	[65.4, 89.5]	[71.0, 74.2]	[72.7, 92.6]
TIV (cm^3)	females	1515 (104)*	1323 (93)	1348 (164)	1637 (115)	1401 (104)	1466 (203)*	1396 (110)	1369 (133)	1353 (100)	1267 (141)
mean (SD)	males	1703 (118)*	1503 (127)	1622 (131)	1831 (131)	1570 (118)	1576 (147)*	1572 (118)	1574 (138)	1537 (112)	1460 (163)
(N) per age category	**18 to 28** (2,200)	1,778	285	0	101	36	0	0	0	0	0
	28 to 38 (340)	46	84	3†	142	65	0	0	0	0	0
	38 to 48 (707)	0	24†	176	250	93	126††	38	0	0	0
	48 to 58 (4,287)	0	17†	311	218	176	3,525	40	0	0	0
	58 to 68 (6,535)	0	3†	22†	511	431	5,375	52††	144††	0	0
	68 to 78 (5,515)	0	0	0	656	358	3,351	129	195	672	154
	78 to 98 (421)	0	0	0	28†	50	20†	18†	47	0	258

MRi-Share, magnetic resonance imaging subcohort of Internet-based Students HeAlth Research Enterprise; BIL&GIN, Brain Imaging of Lateralization study at Groupe d'Imagerie Neurofonctionnelle; SYS cohort, Saguenay Youth Study; ASPSF, Austrian Stroke Prevention Study Family; OATS, Older Australian Twin Study; LBC 1936, Lothian Birth Cohort; MAS, Memory and Ageing Study; TIV, total intracranial volume estimated with Freesurfer 5.3 version except "" with FreeSurfer 6.0 version. †data subsample size < 30 (not included in the age category statistical analysis).*

TABLE 2 | Diffusion-weighted imaging acquisition the 10 contributing data sets.

Data set	MRi-Share	BIL&GIN	SYS	LIFE	1000 BRAINS	UKBiobank	ASPSF	OATS	LBC 1936	MAS
MRI scanner	SIEMENS PRISMA	PHILIPS ACHIEVA	SIEMENS	SIEMENS VERIO	SIEMENS TIM TRIO	SIEMENS SKYRA	SIEMENS TIM TRIO	PHILIPS (x2) SIEMENS(x2)	GE Signa Horizon HDxt	PHILIPS ACHIEVA Quasar Dual
B0 strength	3T	3T	1.5T	3T	3T	3T	3T	1.5T & 3T	1.5T	3T
b-gradient (s/mm^2)	1000*	1000	1000	1000	1000	1000*	1000	1000	1000	700 or 1000
Nr of directions	32	2 x 21	64	60	30	50	6 or 12	32	64	6 or 32
Voxel size (mm^3)	1.7 × 1.7 × 1.8	2 × 2 × 2	2.3 × 2.3 × 3	1.7 × 1.7 × 1.7	2 × 2 × 2	2 × 2 × 2	1.8 × 1.8 × 2.5	2.5 × 2.5 × 2.5	2 × 2 × 2	2.5 × 2.5 × 2.5
TR (ms)	3540 (multiband × 3)	8500	8000	13,800	7800	3600 (multiband ×3)	4900 or 6700	7800 or 8600	16500	7800
TE (ms)	75	81	102	100	83	92	81 or 95	68 or 96	98	68
Acquisition duration	9'45	7'45	10'	16'08	4'30	9'45	4'51 or 6'10	4'40 or 4'56	19'30	4'40

*see **Table 1** legend for the meaning of data set abbreviated names and **Supplementary Material** section for a more detailed description of these data sets.*
**Multi-shell acquisition.*

FA skeleton. The 3D brain image of FA of each individual was skeletonized using the FSL-TBSS software, part of the FMRIB Software Library (FSL) (23, 24), using the FMRIB 1 mm FA template and applying a 0.2 threshold on FA maps. Then the MD volume of the same individual was masked, keeping only voxels within the FA skeleton. Furthermore, in order to reduce contamination of the skeleton by CSF voxels, the FA-masked MD volumes were further masked by both a standard FA skeleton with a threshold of 0.3 on FA values and a custom mask (provided with the PSMD software tool) designed so as to exclude regions adjacent to the ventricles, such as the fornix. Finally, PSMD was computed as the difference between the 95th and 5th percentiles of the so-masked MD volume voxel value distribution. Here, we extended this script in order to obtain, in addition to PSMD values, estimates of the mean values of axial, radial, and mean diffusivity (AD, RD, MD, respectively) as well as of FA over the same customized skeleton. All 10 cohorts were processed separately with this customized script, and the results were sent to the Bordeaux site where they were combined for further statistical analysis.

Statistical Analyses

Age Category Definition

Due to previously reported non-linear effects of age on DTI metrics (1, 3, 8), we divided each cohort sample into subsamples of 10-year age range starting at 18 years of age, the last subsample (i.e. [78 to 98]) including all subjects older than 78 years, as there was only a small number of individuals older than 88 years. **Table 1** and **Figure 1** detail the contribution of each cohort to each age category. Because we planned running analyses at the age category by cohort by sex level, we discarded subsamples of small sizes, namely, containing less than 30 individuals.

Assessing Age-Related Changes of PSMD and Other DTI Metrics

For each of the five DTI metrics and each age category, we performed an analysis of variance including "age" as the main effect, and "sex," total intracranial volume (TIV), and "Cohort" as confounding factors. The Cohort effect was included in order to account for apparent large differences in DTI metric average values across cohorts contributing to the same age category data set (see **Figure 2**). "Sex" and "TIV" were included as covariates since mixed results have been reported regarding the impact of sex and TIV on DTI measures [(12, 25–28), see review in (3)]. In order to document differences of age effects between cohorts contributing to the same age category, we also performed an analysis of variance for each age category and each cohort, including "age," "sex," and "TIV" as effects. Moreover, we analyzed the effects of age on DTI metrics in men and women separately.

Assessing the Effects of Sex and TIV on PSMD and Other DTI Metrics

For each of the five DTI metrics and each age category, we also performed an analysis of variance including "Sex" and "TIV" as main factors and "Cohort" as confounding factors.

All statistical analyses were performed using the JMP Pro Software (version 14.3.0, SAS Institute Inc.).

RESULTS

Descriptive Statistics

Tables 3A–E provide basic statistics across age categories and cohorts for PSMD and the four other DTI metrics, while **Figure 2** illustrates their respective profiles across the adult lifespan. From both **Table 3** and **Figure 2**, it is apparent that there is considerable variability in all five DTI parameter values, and that within a given age category the variability across cohorts is larger than the variability between individuals of the same cohort (see the extreme case of AD and FA values for the LBC1936 study performed at 1.5T, for example).

Figure 3 compares the inter-individual variability of PSMD (in terms of its coefficient of variation, CV in %) within each cohort to those of the other DTI metrics, again for each age category and each cohort, revealing that PSMD CV's is in the order of 10% to 15% (with values as high as 20% for later ages) while those for AD, RD, MD, and FA are in the order of 2% to 5%. Note also that the CVs of all DTI metrics increase with age, more for PSMD than for the other parameters.

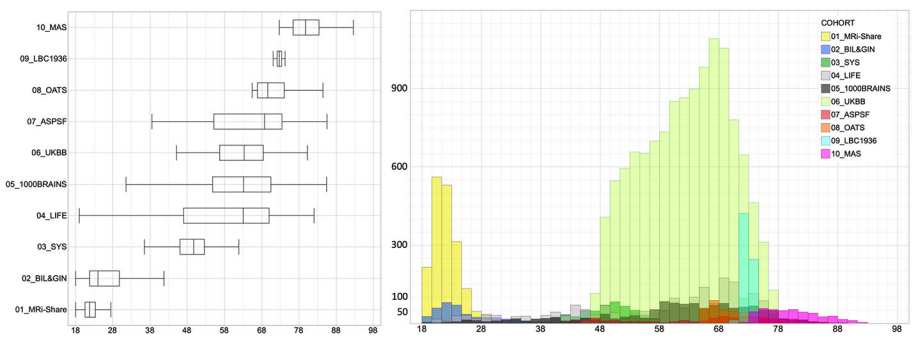

FIGURE 1 | Box-plots and histogram distribution of the age of the participants of the 10 contributing data sets.

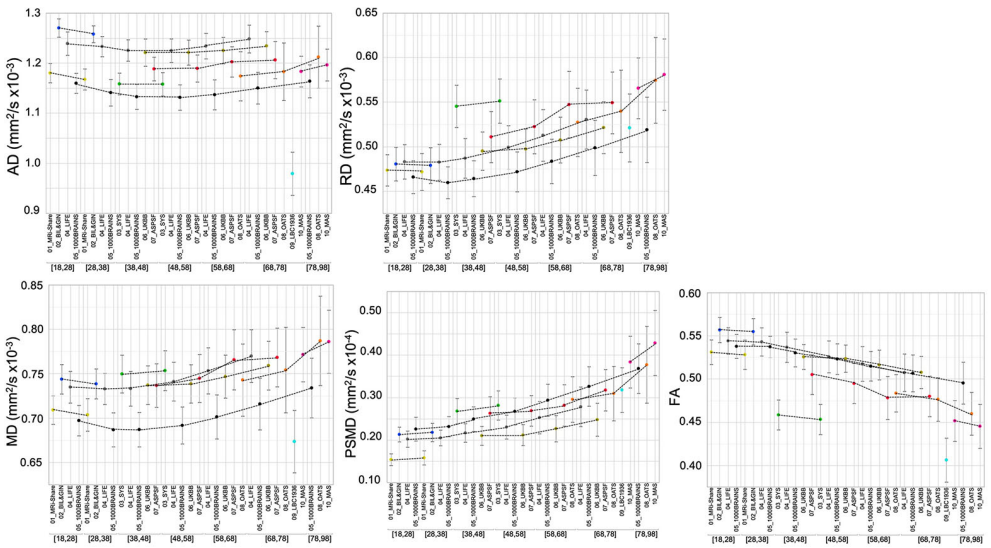

FIGURE 2 | Mean and standard deviation (bars) of the five DTI metrics for each age subcategory and each data set. The dotted lines connect values for the different age categories of the same data set.

Effects of Age on PSMD and Other DTI Metrics

The evolution of PSMD across the adult life is different from that of the other metrics (**Figure 2**). Indeed, PSMD seems to increase monotonically with age, whereas AD, RD, and MD exhibit a similar J-shape profile, initially slightly decreasing during post-adolescence before later increasing during adulthood. As for FA, it shows a reverse profile to that of AD, RD, and MD, with an initial small increase followed by a later decrease.

This apparent specific lifespan profile of PSMD was confirmed by the quantitative estimates of the effects of age on PSMD and other DTI metrics provided by the between-cohort ANOVA (see **Table 4**) and their profiles of evolution across age categories as shown in **Figure 4**. Estimates of the age effect on PSMD were indeed positive for all age categories and significant for all but the 28- to 38-year age period. This increase in PSMD accelerated during late life periods, its value being multiplied by a factor of 3 between the 58- to 68-year and the 78- to 98-year periods. By contrast, AD, RD, and MD age variation profiles were characterized by an initial small but significant decrease (negative age effect), followed by a stable period (non-significant age effect) and a final significant increase (positive age effect). What distinguished AD, RD, and MD profiles was their respective timings, the initial decrease in RD and MD being significant only for the 18 to 28 years subsample, while it extended over the 38- to 48-year period for AD. Note that since the stable period covered two periods of 10 years for all three metrics, the increase in AD was delayed by 10 years compared with RD and MD. At the same time, FA exhibited the reverse contrast consisting of an initial increase during the 18- to 28-year period followed by a stable period (28 to 38 years) before an accelerated decrease during the rest of the adult life course. The age effects on DTI metrics were not significantly different between men and women as revealed by the separate sex-specific analyses of age effects.

Effects of Sex and TIV on DTI

Amplitude of sex effects on DTI metric average values were found to be quite variable across the various cohorts for the different age categories (see **Figure 5**). When pooling all data sets, we found that sex had significant effects on all DTI parameters except on FA. Women had higher mean AD and MD values than men, who conversely had higher PSMD values than women (see **Table 5**). As for TIV, we found that it had positive effects on all DTI parameters (see **Table 5**), including PSMD, these effects being very significant ($p < 10^{-4}$) in all cases but RD ($p = 0.53$).

DISCUSSION

We will first discuss methodological issues and potential limitations in interpreting results of our study. Second, we will discuss what the present study adds to the already existing literature on age effects on classical DTI parameters. In the third part, we will focus on the original findings regarding PSMD distribution and evolution over the adult life.

Methodological Issues and Potential Limitations of the Present Study

In order to study the effects of age over the entire adult lifespan, we gathered DTI data from 20,005 individuals scanned at 10 different sites with the major objective of maximizing statistical power. By so doing, we were aware that the variability of DTI parameters derived from the entire data set would be much larger

TABLE 3A | Basic statistics of axial diffusivity (AD, in $mm^2\ s^{-1} \times 10^{-4}$) average across a white matter skeleton for each age category and each contributing data set.

Age range	MRi-Share	BIL&GIN	SYS	LIFE	1000 BRAINS	UKBiobank	ASPSF	OATS	LBC 1936	MAS
18 to 28	11.80 (0.19)	12.70 (0.18)		12.39 (0.23)	11.60 (0.20)					
	[10.87, 12.45]	[12.26, 13.18]		[11.70, 13.10]	[11.09, 11.96]					
28 to 38	11.68 (0.21)	12.58 (0.17)		12.33 (0.20)	11.41 (0.27)					
	[11.10, 12.12]	[12.14, 13.04]		[11.80, 12.90]	[10.71, 11.95]					
38 to 48		12.45 (0.21)	11.58 (0.22)	12.25 (0.21)	11.33 (0.25)	12.21 (0.27)	11.88 (0.24)			
		[12.07, 12.88]	[11.03, 12.29]	[11.60, 12.80]	[10.52, 11.89]	[10.76, 12.85]	[11.50, 12.46]			
48 to 58			11.58 (0.23)	12.25 (0.24)	11.31 (0.25)	12.21 (0.25)	11.89 (0.27)			
			[11.01, 12.38]	[11.40, 13.10]	[10.59, 12.02]	[10.18, 13.03]	[11.42, 12.68]			
58 to 68			11.67 (0.24)	12.34 (0.26)	11.37 (0.30)	12.25 (0.26)	12.03 (0.30)	11.74 (0.49)		
			[11.24, 12.21]	[11.60, 13.20]	[10.30, 12.32]	[10.52, 13.24]	[11.41, 12.76]	[10.61, 12.80]		
68 to 78				12.48 (0.28)	11.50 (0.32)	12.34 (0.29)	12.06 (0.37)	11.83 (0.58)	9.79 (0.43)	11.83 (0.31)
				[11.40, 13.40]	[10.36, 12.58]	[10.70, 13.53]	[9.69, 12.88]	[10.69, 13.18]	[8.41, 10.94]	[11.06, 12.56]
78 to 98				12.49 (0.30)	11.64 (0.33)	12.44 (0.27)		12.12 (0.62)		11.96 (0.32)
				[11.90, 13.20]	[11.07, 12.47]	[11.66, 12.83]		[10.80, 13.49]		[10.99, 13.05]

*Values are mean (S.D. and range [min, max] across the age category sample). See **Table 1** legend for the meaning of data set abbreviated names.*

than for a single-site study because of between-site differences in data acquisition protocols, such as scanner manufacturer, field strength, number and strength of diffusion-encoding gradients, image voxel size, post-processing of raw DWI data, and so on (23, 24, 29–32). Accordingly, a key issue was to reduce as much as possible the variability due to sources that were controllable so that we could maximize benefits of the very large sample size.

Concerns with DTI multi-site studies have been emphasized by several authors (33, 34) and strategies have been proposed for harmonizing DWI data before proceeding to statistical analysis of DTI parameter maps. However, it has also been reported that DTI parameters estimated over the whole white matter or large regions of interest actually exhibit high intra- and inter-scanner reproducibility, making them suitable for multisite studies without extensive harmonization (17, 35, 36). This is the approach that we implemented here as it was not possible to access raw DWI data at different sites in order to harmonize processing from the very earliest stages (see **Supplementary Materials**). In our study, harmonization was limited to the post-processing of DTI maps pre-computed by each site using the same script for generating individual skeletons and computing individual DTI parameter values across these skeletons. However, our findings indicate that it is possible to draw meaningful conclusions from such minimal harmonization by focusing on the effects of interest (age in our case) rather than the absolute values of the measurements, an approach previously used by others (37).

Multi-site studies do have some advantages as compared with single-site investigations, namely, statistical power due to very large sample size, and the ability to recruit a sufficient number of individuals over the entire life or adult lifespan. As emphasized by others, these are important features in the context of clinical studies that are often multisite in nature (17, 35). In fact, there have been several previous reports of multisite studies on DTI parameters in adults but they dealt with issues other than age effects such as methodology (17, 30, 33) and genetic effects (38, 39), for example.

In this study, we focused on the mean DTI metrics over a white matter skeleton, rather than over the entire white-matter compartment, since our primary metric of interest was PSMD, which is defined over the FSL-TBSS white matter skeleton derived from FA data. This approach should in theory minimize any partial volume effects by limiting the measurement over the core of white matter tracts. Indeed, when we compared the mean DTI metrics over the white matter skeleton with those measured over the whole white-matter compartment in two cohorts of the study (MRi-Share and BIL&GIN), mean FA values were higher and diffusivity values were lower when averaged over the white matter skeleton than when averaged over the entire white-matter compartment. However, the cross-subject variability measured as the CV of the mean DTI metrics decreased only marginally (a fraction of a percent for CVs ranging from 2% to 4%) when mean values were computed over the white matter skeleton rather than the whole white matter. In contrast, the CV of PSMD decreased markedly (on average, from 24% to 8%) when its computation was

TABLE 3B | Basic statistics of radial diffusivity (RD, in $mm^2\ s^{-1} \times 10^{-4}$) average across a white matter skeleton for each age category and each contributing data set.

Age range	MRi-Share	BIL&GIN	SYS	LIFE	1000 BRAINS	UKBiobank	ASPSF	OATS	LBC 1936	MAS
18 to 28	4.74 (0.18)	4.81 (0.19)		4.83 (0.19)	4.66 (0.18)					
	[4.15, 5.53]	[4.26, 5.44]		[4.33, 5.29]	[4.26, 5.19]					
28 to 38	4.72 (0.21)	4.79 (0.20)		4.83 (0.20)	4.60 (0.18)					
	[4.35, 5.10]	[4.45, 5.56]		[4.42, 5.36]	[4.20, 5.17]					
38 to 48		4.83 (0.22)	5.45 (0.24)	4.87 (0.22)	4.64 (0.20)	4.95 (0.22)	5.11 (0.29)			
		[4.49, 5.27]	[4.88, 6.36]	[4.35, 5.59]	[4.28, 5.27]	[4.19, 5.64]	[4.54, 5.79]			
48 to 58			5.51 (0.25)	4.99 (0.24)	4.72 (0.22)	4.97 (0.23)	5.22 (0.30)			
			[4.93, 6.54]	[4.47, 6.01]	[4.21, 5.38]	[4.17, 6.22]	[4.57, 6.05]			
58 to 68			5.58 (0.31)	5.13 (0.29)	4.84 (0.25)	5.08 (0.26)	5.47 (0.37)	5.27 (0.38)		
			[5.02, 6.27]	[4.29, 6.36]	[4.21, 5.57]	[4.34, 6.40]	[4.73, 6.59]	[4.36, 6.05]		
68 to 78				5.31 (0.33)	4.99 (0.31)	5.21 (0.29)	5.49 (0.35)	5.40 (0.46)	5.21 (0.38)	5.66 (0.34)
				[4.48, 6.73]	[4.16, 6.29]	[4.29, 7.10]	[4.85, 6.69]	[4.44, 6.77]	[4.28, 8.87]	[5.05, 6.78]
78 to 98				5.37 (0.33)	5.19 (0.37)	5.36 (0.20)		5.75 (0.48)		5.81 (0.40)
				[4.87, 6.31]	[4.69, 5.99]	[5.03, 5.69]		[4.80, 7.08]		[4.88, 7.17]

*Values are mean (S.D. and range [min, max] across the age category sample (see **Table 1** legend for the meaning of data set abbreviated names).*

TABLE 3C | Basic statistics of mean diffusivity (MD, in $mm^2\ s^{-1} \times 10^{-4}$) average across a white matter skeleton for each age category and each contributing data set.

Age range	MRi-Share	BIL&GIN	SYS	LIFE	1000 BRAINS	UKBiobank	ASPSF	OATS	LBC 1936	MAS
18 to 28	7.09 (0.16)	7.44 (0.17)		7.35 (0.18)	6.97 (0.17)					
	[6.54, 7.76]	[7.02, 7.98]		[6.89, 7.75]	[6.54, 7.34]					
28 to 38	7.04 (0.18)	7.39 (0.17)		7.33 (0.18)	6.87 (0.19)					
	[6.64, 7.38]	[7.08, 7.97]		[6.92, 7.78]	[6.43, 7.39]					
38 to 48		7.37 (0.20)	7.50 (0.21)	7.33 (0.20)	6.87 (0.19)	7.37 (0.22)	7.37 (0.25)			
		[7.05, 7.80]	[6.98, 8.17]	[6.81, 7.84]	[6.42, 7.39]	[6.38, 8.05]	[6.97, 8.01]			
48 to 58			7.53 (0.23)	7.41 (0.22)	6.92 (0.21)	7.39 (0.22)	7.45 (0.27)			
			[6.97, 8.45]	[6.89, 8.31]	[6.35, 7.58]	[6.17, 8.42]	[6.91, 8.26]			
58 to 68			7.61 (0.27)	7.53 (0.26)	7.01 (0.25)	7.47 (0.24)	7.66 (0.34)	7.43 (0.41)		
			[7.09, 8.20]	[6.82, 8.64]	[6.35, 7.78]	[6.41, 8.67]	[6.98, 8.58]	[6.55, 8.18]		
68 to 78				7.70 (0.30)	7.16 (0.29)	7.59 (0.27)	7.68 (0.33)	7.54 (0.48)	6.74 (0.35)	7.72 (0.31)
				[6.93, 8.92]	[6.30, 8.39]	[6.43, 9.23]	[6.51, 8.74]	[6.57, 8.91]	[5.79, 7.86]	[7.14, 8.71]
78 to 98				7.74 (0.31)	7.34 (0.34)	7.72 (0.20)		7.87 (0.51)		7.86 (0.36)
				[7.23, 8.61]	[6.84, 8.15]	[7.34, 8.01]		[6.92, 9.21]		[6.96, 9.06]

*Values are mean (S.D. and range [min, max] across the age category sample (see **Table 1** legend for the meaning of data set abbreviated names).*

TABLE 3D | Basic statistics of peak width skeletonized mean diffusivity (PSMD, in $mm^2\ s^{-1} \times 10^{-4}$) for each age category and each contributing data set.

Age range	MRi-Share	BIL&GIN	SYS	LIFE	1000 BRAINS	UKBiobank	ASPSF	OATS	LBC 1936	MAS
18 to 28	1.54 (0.14)	2.13 (0.17)		2.02 (0.19)	2.26 (0.28)					
	[1.20, 2.13]	[1.75, 2.78]		[1.68, 2.53]	[1.86, 3.47]					
28 to 38	1.58 (0.17)	2.18 (0.22)		2.05 (0.19)	2.32 (0.24)					
	[1.33, 2.01]	[1.75, 2.85]		[1.65, 2.63]	[1.75, 3.00]					
38 to 48		2.24 (0.18)	2.68 (0.30)	2.17 (0.22)	2.49 (0.29)	2.10 (0.22)	2.63 (0.39)			
		[1.89, 2.58]	[2.07, 4.44]	[1.64, 3.00]	[1.94, 3.46]	[1.60, 3.11]	[1.95, 3.53]			
48 to 58			2.82 (0.34)	2.31 (0.28)	2.67 (0.32)	2.12 (0.25)	2.69 (0.36)			
			[1.99, 5.12]	[1.70, 3.63]	[2.03, 4.07]	[1.49, 4.58]	[2.18, 3.70]			
58 to 68			2.92 (0.30)	2.53 (0.38)	2.94 (0.38)	2.27 (0.31)	2.82 (0.49)	2.96 (0.54)		
			[2.51, 3.57]	[1.83, 4.85]	[2.14, 5.03]	[1.56, 5.71]	[2.15, 4.54]	[2.11, 4.90]		
68 to 78				2.78 (0.47)	3.26 (0.47)	2.48 (0.39)	3.17 (0.49)	3.10 (0.64)	3.18 (0.53)	3.84 (0.61)
				[1.88, 5.26]	[2.23, 5.53]	[1.61, 6.19]	[2.15, 4.60]	[2.17, 6.66]	[2.09, 5.72]	[2.56, 6.02]
78 to 98				2.96 (0.45)	3.68 (0.58)	2.74 (0.33)		3.77 (0.90)		4.29 (0.77)
				[2.15, 3.94]	[2.83, 5.32]	[2.10, 3.45]		[2.47, 6.51]		[2.95, 7.96]

*Values are mean (S.D. and range [min, max] across the age category sample (see **Table 1** legend for the meaning of data set abbreviated names).*

TABLE 3E | Basic statistics of fractional anisotropy (FA, unitless) average across individual FA skeleton for each age range category and each contributing data set.

Age range	MRi-Share	BIL&GIN	SYS	LIFE	1000 BRAINS	UKBiobank	ASPSF	OATS	LBC 1936	MAS
18 to 28	0.53 (0.01) [0.47, 0.58]	0.56 (0.01) [0.51, 0.60]		0.54 (0.02) [0.49, 0.58]	0.54 (0.01) [0.49, 0.56]					
28 to 38	0.53 (0.02) [0.49, 0.56]	0.55 (0.02) [0.50, 0.58]		0.54 (0.02) [0.50, 0.58]	0.54 (0.01) [0.49, 0.57]					
38 to 48		0.55 (0.02) [0.52, 0.57]	0.46 (0.02) [0.39, 0.50]	0.54 (0.02) [0.48, 0.58]	0.53 (0.02) [0.48, 0.56]	0.53 (0.01) [0.49, 0.56]	0.51 (0.02) [0.46, 0.55]			
48 to 58			0.45 (0.02) [0.40, 0.50]	0.53 (0.02) [0.46, 0.57]	0.52 (0.02) [0.47, 0.58]	0.52 (0.02) [0.44, 0.57]	0.49 (0.02) [0.42, 0.54]			
58 to 68			0.45 (0.02) [0.41, 0.49]	0.52 (0.02) [0.44, 0.58]	0.51 (0.02) [0.46, 0.57]	0.52 (0.02) [0.44, 0.57]	0.48 (0.02) [0.41, 0.53]	0.48 (0.02) [0.43, 0.55]		
68 to 78				0.51 (0.02) [0.40, 0.56]	0.51 (0.02) [0.44, 0.56]	0.51 (0.02) [0.37, 0.57]	0.48 (0.02) [0.41, 0.53]	0.48 (0.03) [0.38, 0.54]	0.41 (0.03) [0.31, 0.47]	0.45 (0.02) [0.36, 0.49]
78 to 98				0.50 (0.02) [0.45, 0.54]	0.50 (0.02) [0.44, 0.53]	0.50 (0.01) [0.48, 0.52]		0.46 (0.02) [0.40, 0.51]		0.45 (0.03) [0.34, 0.51]

*Values are mean (S.D. and range [min, max] across the age category sample (see **Table 1** legend for the meaning of data set abbreviated names).*

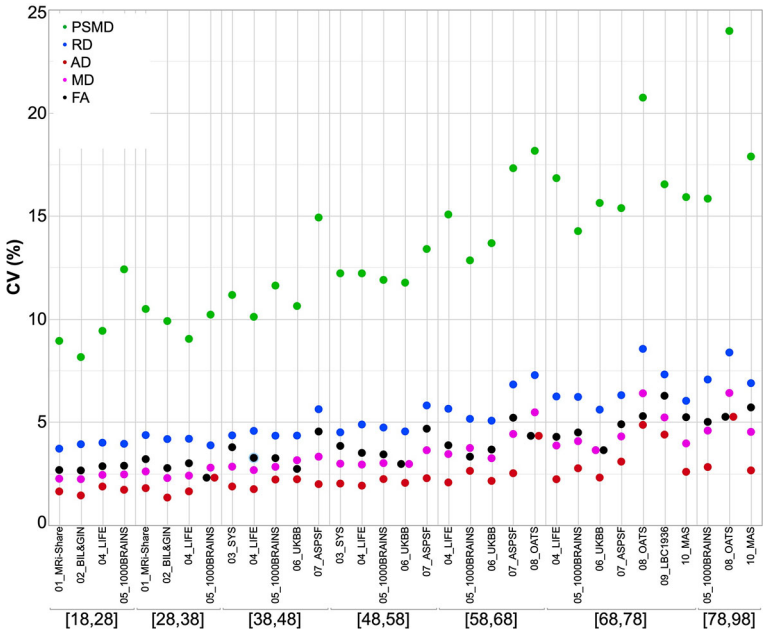

FIGURE 3 | Coefficients of variation of the five DTI metrics for each age subcategory and each data set.

TABLE 4 | ANOVA effect of age (estimate (standard error) and significance p-value) on five DTI metrics (AD, RD, MD, PSMD, and FA evaluated across individual FA skeletons).

Age range (years)	AD		RD		MD		PSMD		FA	
	estimate	p	estimate	p	estimate	p	estimate	p	estimate	p
18 to 28	−2.01 (0.20)	<0.0001	−1.06 (0.18)	<0.0001	−1.38 (0.17)	<0.0001	0.41 (0.15)	0.0058	0.30 (0.15)	0.041
28 to 38	−1.32 (0.43)	0.0023	−0.22 (0.41)·	0.59	−0.58 (0.37)	0.12	0.60 (0.42)	0.15	−0.27 (0.32)	0.40
38 to 48	−0.68 (0.37)	0.065	0.40 (0.37)	0.27	0.047 (0.33)·	0.89	1.84 (0.41)	<0.0001	−0.54 (0.27)	0.046
48 to 58	−0.11 (0.13)	0.41	0.61 (0.12)	<0.0001	0.37 (0.12)	0.0019	1.11 (0.14)	<0.0001	−0.56 (0.09)	<0.0001
58 to 68	0.95 (0.12)	<0.0001	1.46 (0.11)	<0.0001	1.29 (0.11)	<0.0001	2.18 (0.14)	<0.0001	−0.91 (0.08)	<0.0001
68 to 78	1.75 (0.19)	<0.0001	1.94 (0.18)	<0.0001	1.87 (0.17)	<0.0001	3.67 (0.24)	<0.0001	−0.97 (0.12)	<0.0001
78 to 98	2.30 (0.60)	0.0002	4.01 (0.64)	<0.0001	3.44 (0.59)	<0.0001	6.99 (0.12)	<0.0001	−2.36 (0.39)	<0.0001

Values are in $mm^2\ s^{-1}\ year^{-1} \times 10^{-6}$ for AD, RD, and MD, in $mm^2\ s^{-1}\ year^{-1} \times 10^{-7}$ for PSMD, and in $year^{-1} \times 10^{-3}$ for FA.

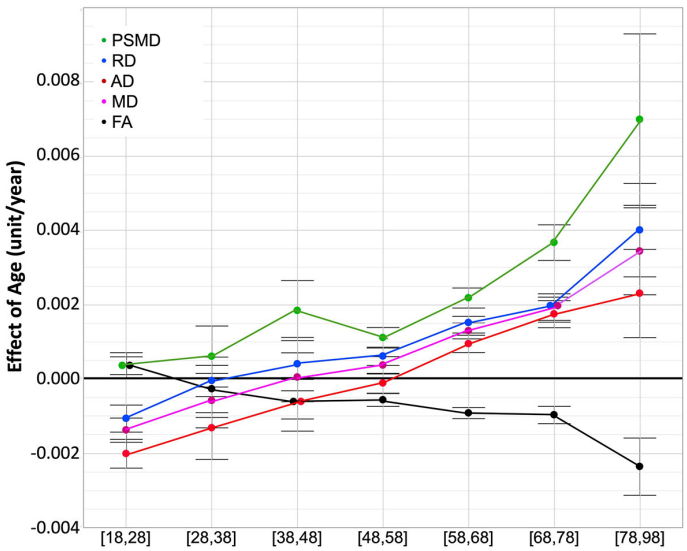

FIGURE 4 | ANOVA estimates and 95% confidence intervals of the effects of age on the five DT metrics for each age subcategory. Units are $mm^2/s/year \times 10^{-3}$ for AD, RD, and MD, $mm^2/s/year \times 10^{-4}$ for PSMD, year $\times 10^{-3}$ for FA.

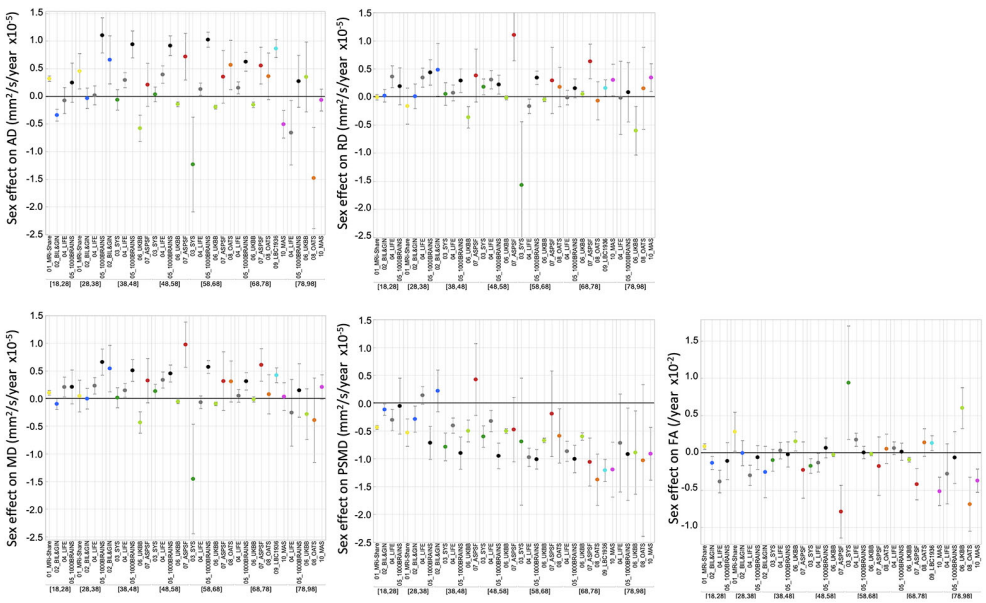

FIGURE 5 | ANOVA estimates and 95% confidence intervals of the effects of sex (females minus males) on the five DT metrics for each age subcategory and each data set.

performed on the white matter skeleton rather than on than the global white-matter mask. This demonstrates the importance of choosing a measure of MD dispersion values over a white matter skeleton for controlling between subject variability.

In the present work, we restricted the analysis to classical DTI metrics as only two of the contributing cohorts had high angular resolution and/or multi-shell acquisition schemes that could be used for estimating advanced white-matter microstructural parameters with more sophisticated models (29). Here, DWI data processing was solely based on the classical DTI model. The DTI model limitations are well known (24), and it has been shown, for example, that correction for free water has a major

TABLE 5 | ANOVA effect of sex and TIV (estimate (standard error) and significance p value) on five DTI metrics (AD, RD, MD, PSMD, and FA evaluated across individual FA skeletons).

	AD		RD		MD		PSMD		FA	
Effect	**estimate**	**p**	**estimate**	**p**	**estimate**	**p**	**estimate**	**p**	**estimate**	**p**
Sex (F-M)	1.13 (0.21)	<0.0001	0.45 (0.21)	0.032	0.68 (0.19)	0.0005	−5.34 (0.26)	<0.0001	0.04 (0.14)·	0.74
TIV	1.41 (0.12)	<0.0001	0.07 (0.12)·	0.53	0.52 (0.01)	<0.0001	1.43 (0.15)	<0.0001	0.54 (0.08)	<0.0001

Values for the effects of sex are in $mm^2\ s^{-1} \times 10^{-6}$ for AD, RD, MD, and PSMD and in $\times 10^{-3}$ for FA, and for the effects of TIV are in $mm^2\ s^{-1}\ cm^{-3} \times 10^{-6}$ for AD, RD MD, and PSMD and in $cm^{-3} \times 10^{-5}$ for FA.

impact on classical DTI parameter values (40, 41). However, although investigating advanced white-matter microstructural parameters is highly desirable, it was beyond the scope of our study: it would require additional data sets with multi-shell acquisition, especially for individuals aged 30 to 50 years or over 70 years, in order to supplement existing data (8) on the adult lifespan trajectory of these microstructural parameters.

Mixed results have been reported regarding the impact of sex and TIV on DTI measures [(12, 25–28), see review in (3)]. Here, we also observed mixed results across the different cohorts, although very significant sex effects on all DTI parameters, except FA, were uncovered when combining the entire data set. Note, however, these sex effects were of very small size (for PSMD, for example, $omega^2 = 6.7 \times 10^{-3}$ for the sex effect to be compared with 7.6×10^{-2} for the age effect), which could explain the mixed findings in the literature, and suggests further investigations are required in order to understand their biological origins. TIV effects on DTI parameters are not well established in the literature. In our study, we found that TIV was positively correlated with all DTI parameters except for RD. Similar to sex, TIV effects when significant were very small (for PSMD again, $omega^2 = 1.5 \times 10^{-3}$ for the TIV effect). Here again additional investigations are needed to understand the origins of these effects.

Finally, and importantly, it should be stressed that interpretation of the results of the present study should be taken with caution because of the cross-sectional nature of the data that we analyzed. Numerous reports have indeed pointed out the caveats of cross-sectional design for assessing effects of age and demonstrated how such design may lead to spurious findings when compared to those obtained with longitudinal data (12, 42, 43). In the present work, there was no attempt to use a single model to describe the variation of DTI parameters with age over the entire adulthood period. Rather, we selected a piecewise linear model to examine/compare age-related changes in 10-year duration consecutive time bins, thereby minimizing the generation bias between cohorts of nearby categories. Understandably, such an approach does not eradicate the intrinsic limits of our cross-sectional study. But it should be reminded that a fully longitudinal design is quasi impossible to implement in the context of lifespan research, since, in practice, measures in an individual can be repeated only a few times and at short duration intervals. As a consequence, such longitudinal studies suffer from some of the limitations of cross-sectional ones. This may explain why the results of the present study are compatible with those a previously published longitudinal study (12) in which individuals aged between 20 and 84 years were observed twice 3 years apart.

Adult Lifespan Profiles of Variation of Classical DTI Parameters AD, RD, MD, and FA

Effects of age on white-matter microstructure assessed with DTI have been intensively investigated over the past decade from a developmental perspective (4) as well as in a lifespan/ageing framework (1, 3, 5, 8, 11, 12, 27, 40). Briefly, and considering only DTI metrics estimated at the global level, AD, RD, and thus, MD were reported to follow similar U- or better J-shape age variation patterns, initially decreasing during childhood and adolescence (see (4) for review) then exhibiting an accelerated increase during the adult life (8, 12), while FA followed a reverse profile. Our own findings agree with this body of results during the adult life course. Raw data plots show J-shape profiles for AD, RD, and MD, and the reverse profile for FA, as well as acceleration of these changes during late life.

Maximum global FA values and minimum global MD, RD, and AD values have been reported to occur before the age of 40 years (1, 5, 11, 12, 27), although large variations were found when considering individual tracts (5, 26, 44, 45). Here, we found extreme values for RD, MD, and FA occurring between 28 and 38 years, well in line with these previous findings. In addition, we found that the decrease of AD in the post-adolescence period extended into adulthood by about 10 years more than for RD and MD, thereby uncovering heterochrony of AD and RD variations during adulthood. Such a heterochrony during adulthood was not detected in a previous longitudinal study (12) possibly due to an insufficient sample size and large DTI metric variability between individuals (as can be seen in Figure 7 of the mentioned report). Note that two recent studies (46, 47) have reported opposite age effects for AD (decrease) and RD (increase) with stable MD during the 18 to 55 year age period; however, as both studies used simple linear modeling due to small sample sizes, no age at extreme value could be observed. Rather, our findings are compatible with the AD-RD variation heterochrony that has been noticed earlier during childhood and adolescence at the individual tract level with stronger decrease for RD than for AD (34, 44). According to these and our findings, the AD decrease/RD increase profile (6) would occur only during mid-adulthood.

PSMD Is a Diffusion Imaging Phenotype With a Profile of Variation Across the Adult Lifespan That Differs From That of Other DTI Parameters

The distribution of PSMD values observed for the different cohorts and age categories of the present study are consistent with the few comparable data reported in the literature for older participants (no data are available in young adults). For example, Baykara et al. reported in their pioneering article a PSMD median value around 3.0 (in $mm^2\ s^{-1} \times 10^{-4}$, range [2.5, 4.9]) in a sample of healthy individuals aged 60 to 80 years drawn from the ASPF cohort [see **Table 2** of Baykara et al. (20)], values that are comparable to those reported in **Table 3D** of our study in subsamples of other cohorts of similar age category. Similarly, Wei et al. (21) recently reported a PSMD average value of $2.4 \times 10^{-4}\ mm^2\ s^{-1}$ in a sample of healthy controls aged around 60 years. In both studies, PSMD CVs were close to 10%, a value again similar to those observed in our own study. That the CV of PSMD is two to three times larger than the CVs of other DTI metrics could be expected since PSMD is a dispersion rather than a central tendency statistic. Moreover, the larger increase in PSMD CV as age advances (as compared to the other DTI metrics) indicates that this phenotype should be used with caution especially during the late life period. However, it is important to note that the CV of PSMD was found to be quite stable across cohorts with similar age ranges.

The main goal of the present study was to document the profile of PSMD evolution across age bands during adulthood. In this respect, and the proviso that the data we gathered were not longitudinal, our results show that PSMD increases continuously from post-adolescence to late adult life, that this increase is accelerating at later ages, and that this acceleration is larger than for the other DTI metrics. As there are no available data of PSMD in childhood and adolescence, it is not possible to decide whether the lifetime PSMD evolution profile is similar to those of AD, RD, MD, i.e. with a decrease during childhood that reaches the minimum value before adulthood, or if it shows continuous increase throughout the lifespan. Nevertheless, it remains the case that the continuous and accelerating increase of PSMD during adulthood is an indication that it is an adequate and potentially valuable marker of white matter ageing. In particular, it is notable that PSMD increases during early adulthood when the other DTI metrics variations appear to be still undergoing late maturational processes.

The biological mechanisms of the origin of PSMD evolution with age are at present unknown, but one can think of several reasons why PSMD may be more prone to increase with age as compared with the other metrics. First, it is important to remember that PSMD is a measure of MD values dispersion across a skeleton of white matter. As such, it will be directly affected by differences across MD values of the individual tracts. Consequently, regional heterogeneity as well as heterochrony in MD values of the fiber tracts will result in higher PSMD values more than in average MD values. Second, MD itself is a weighted average of AD (1/3) and RD (2/3) values, and thus MD value dispersion will also be affected by heterochrony in AD and RD variations with age. Overall, what possibly makes PSMD an early and sensitive imaging marker of ageing is that it captures multiple sources of heterogeneity in white matter water diffusion parameters. With this regard, it would be interesting to investigate variations in the pattern of MD dispersion at the regional level using tract-based DTI metrics since it is well established that heterochrony is a major feature of the development and aging of the different fiber tracts [see for example (5, 8, 26, 44)]. Accordingly, variations of PSMD value provide only a gross and possibly biased estimate of the white matter-microstructure dynamics. We did not implement regional analysis as our study focused on PSMD that is by definition a dispersion statistic over the entire white matter skeleton. Nevertheless, a regional approach would certainly be interesting and feasible since peak width of MD values could be measured on a white-matter skeleton at the tract level in the same manner as it has been done for other DTI metrics (see (34, 46) for example).

DATA AVAILABILITY STATEMENT

The raw data supporting the conclusions of this article will be made available by the authors, without undue reservation, to any qualified researcher.

ETHICS STATEMENT

The 10 cohort studies involving human participants were reviewed and approved by the following ethic committees: Comité de Protection des Personnes Sud-Ouest (MRi-Share), Comité d'Ethique de Basse-Normandie (BIL&GIN), Research Ethics Committee of the Chicoutimi Hospital (SYS), Ethics committee of the University of Duisburg-Essen (1000BRAINS), Ethics board of the Medical Faculty of the University of Leipzig (LIFE), North West Multi-center Research Ethics Committee (UKBiobank), Ethics Committee of the Medical University Graz (ASPS), Ethics committees of the Australian Twin Registry, University of New South Wales, University of Melbourne, Queensland Institute of Medical Research and the South-Eastern Sydney and Illawarra Area Health Service (OATS), Multi-Centre Research Ethics Committee for Scotland and the Lothian Research Ethics Committee (LBC1936), Ethics Committee of the University of New South Wales (MAS). The participants provided written informed consent to participate in these studies.

AUTHOR CONTRIBUTIONS

Study conception: BM and SD. Data collection: GB, CT, SC, ZP, TP, RS, PS, HB, NK, JT, ID, AW, AV, and BM. Data analysis: GB, LPe, SC, JS, YP, LPi, PS, WW, NA, MB, SM, AW, MD, and BM. Drafting: GB, AT, and BM. Revising the manuscript: LPe, CT,

SC, JS, ZP, YP, TP, RS, LPi, PS, WW, NA, ID, MB, JW, SM, AW, AV, MD, SD, and BM).

FUNDING

GB has been supported by an EU-ERC starting grant (SEGWAY, PI S Debette, with funding from the European Union's Horizon 2020 research and innovation program under grant agreement No 640643). AT is supported by a grant from the Fondation pour la Recherche Médicale (DIC202161236446). SC was supported by the Initiative and Networking Fund of the Helmholtz Association and the European Union's Horizon 2020 Research and Innovation Program under Grant Agreement 785907 (Human Brain Project SGA2). The BRIDGET project is supported by the Fondation Leducq (Transatlantic Network of Excellence on the Pathogenesis of SVD of the Brain) and is an EU Joint Program -Neurodegenerative Disease Research (JPND) project. The project is supported through the following funding organizations under the aegis of JPND—www.jpnd.eu: Australia, National Health and Medical Research Council, Austria, Federal Ministry of Science, Research and Economy; Canada, Canadian Institutes of Health Research; France, French National Research Agency; Germany, Federal Ministry of Education and Research; Netherlands, The Netherlands Organization for Health Research and Development; United Kingdom, Medical Research Council. This project has received funding from the European Union's Horizon 2020 research and innovation program under grant agreement No 643417. This project has also received funding from the European Research Council (ERC) under the European Union's Horizon 2020 research and innovation program under grant agreement No 640643.

SUPPLEMENTARY MATERIAL

The Supplementary Material for this article can be found online at: https://www.frontiersin.org/articles/10.3389/fpsyt.2020.00342/full#supplementary-material

REFERENCES

1. Hasan KM, Sankar A, Halphen C, Kramer LA, Brandt ME, Juranek J, et al. Development and organization of the human brain tissue compartments across the lifespan using diffusion tensor imaging. *Neuroreport* (2007) 18:1735–9. doi: 10.1097/WNR.0b013e3282f0d40c
2. Giorgio A, Watkins KE, Chadwick M, James S, Winmill L, Douaud G, et al. Longitudinal changes in grey and white matter during adolescence. *NeuroImage* (2010) 49:94–103. doi: 10.1016/j.neuroimage.2009.08.003
3. Lebel C, Gee M, Camicioli R, Wieler M, Martin W, Beaulieu C. Diffusion tensor imaging of white matter tract evolution over the lifespan. *NeuroImage* (2012) 60:340–52. doi: 10.1016/j.neuroimage.2011.11.094
4. Lebel C, Treit S. Beaulieu C. A review of diffusion MRI of typical white matter development from early childhood to young adulthood. *NMR BioMed* (2019) 32:e3778. doi: 10.1002/nbm.3778
5. Yeatman JD, Wandell BA, Mezer AA. Lifespan maturation and degeneration of human brain white matter. *Nat Commun* (2014) 5:4932. doi: 10.1038/ncomms5932
6. Bennett IJ, Madden DJ, Vaidya CJ, Howard DV, Howard JH. Age-related differences in multiple measures of white matter integrity: A diffusion tensor imaging study of healthy aging. *Hum Brain Mapp* (2010) 31:378–90. doi: 10.1002/hbm.20872
7. Bartzokis G, Lu PH, Heydari P, Couvrette A, Lee GJ, Kalashyan G, et al. Multimodal Magnetic Resonance Imaging Assessment of White Matter Aging Trajectories Over the Lifespan of Healthy Individuals. *Biol Psychiatry* (2012) 72:1026–34. doi: 10.1016/j.biopsych.2012.07.010
8. Cox SR, Ritchie SJ, Tucker-Drob EM, Liewald DC, Hagenaars SP, Davies G, et al. Ageing and brain white matter structure in 3,513 UK Biobank participants. *Nat Commun* (2016) 7:13629. doi: 10.1038/ncomms13629
9. de Lange A-MG, Bråthen ACS, Rohani DA, Fjell AM, Walhovd KB. The temporal dynamics of brain plasticity in aging. *Cereb Cort* (2018) 28:1857–65. doi: 10.1093/cercor/bhy003
10. Rathee R, Rallabandi VPS, Roy PK. Age-related differences in white matter integrity in healthy human brain: evidence from structural MRI and diffusion tensor imaging. *Magn Reson Insights* (2016) 9:9–20. doi: 10.4137/MRI.S39666
11. Westlye LT, Walhovd KB, Dale AM, Bjornerud A, Due-Tonnessen P, Engvig A, et al. Life-Span Changes of the Human Brain White Matter: Diffusion Tensor Imaging (DTI) and Volumetry. *Cereb Cortex* (2010) 20:2055–68. doi: 10.1093/cercor/bhp280
12. Sexton CE, Walhovd KB, Storsve AB, Tamnes CK, Westlye LT, Johansen-Berg H, et al. Accelerated Changes in White Matter Microstructure during Aging: A Longitudinal Diffusion Tensor Imaging Study. *J Neurosci* (2014) 34:15425–36. doi: 10.1523/JNEUROSCI.0203-14.2014
13. for the Alzheimer's Disease Neuroimaging Initiative, Chandra A, Dervenoulas G, Politis M. Magnetic resonance imaging in Alzheimer's disease and mild cognitive impairment. *J Neurol* (2019) 266:1293–302. doi: 10.1007/s00415-018-9016-3
14. Tae W-S, Ham B-J, Pyun S-B, Kang S-H, Kim B-J. Current clinical applications of diffusion-tensor imaging in neurological disorders. *J Clin Neurol* (2018) 14:129. doi: 10.3988/jcn.2018.14.2.129
15. Shen X, Adams MJ, Ritakari TE, Cox SR, McIntosh AM, Whalley HC. White matter microstructure and its relation to longitudinal measures of depressive symptoms in mid- and late life. *Biol Psychiatry* (2019) 86:759–68. doi: 10.1016/j.biopsych.2019.06.011
16. Suzuki H, Gao H, Bai W, Evangelou E, Glocker B, O'Regan DP, et al. Abnormal brain white matter microstructure is associated with both pre-hypertension and hypertension. *PloS One* (2017) 12:e0187600. doi: 10.1371/journal.pone.0187600
17. Croall ID, Lohner V, Moynihan B, Khan U, Hassan A, O'Brien JT, et al. Using DTI to assess white matter microstructure in cerebral small vessel disease (SVD) in multicentre studies. *Clin Sci* (2017) 131:1361–73. doi: 10.1042/CS20170146
18. Dekkers IA, Jansen PR, Lamb HJ. Obesity, Brain volume, and white matter microstructure at MRI: A Cross-sectional UK Biobank Study. *Radiology* (2019) 291:763–71. doi: 10.1148/radiol.2019181012
19. Zavaliangos-Petropulu A, Nir TM, Thomopoulos SI, Reid RI, Bernstein MA, Borowski B, et al. Diffusion MRI Indices and their relation to cognitive impairment in brain aging: the updated multi-protocol approach in ADNI3. *Front Neuroinform* (2019) 13:2. doi: 10.3389/fninf.2019.00002
20. Baykara E, Gesierich B, Adam R, Tuladhar AM, Biesbroek JM, Koek HL, et al. a novel imaging marker for small vessel disease based on skeletonization of white matter tracts and diffusion histograms. *Ann Neurol* (2016) 80:581–92. doi: 10.1002/ana.24758
21. Wei N, Deng Y, Yao L, Jia W, Wang J, Shi Q, et al. A Neuroimaging marker based on diffusion tensor imaging and cognitive impairment due to cerebral white matter lesions. *Front Neurol* (2019) 10:81. doi: 10.3389/fneur.2019.00081
22. Deary IJ, Ritchie SJ, Muñoz Maniega S, Cox SR, Valdés Hernández MC, Luciano M, et al. Brain Peak Width of Skeletonized Mean Diffusivity (PSMD) and cognitive function in later life. *Front Psychiatry* (2019) 10:524. doi: 10.3389/fpsyt.2019.00524
23. Barrio-Arranz G, de Luis-García R, Tristán-Vega A, Martín-Fernández M, Aja-Fernández S. Impact of MR acquisition parameters on DTI scalar indexes:

a tractography based approach. *PloS One* (2015) 10:e0137905. doi: 10.1371/journal.pone.0137905
24. Curran KM, Emsell L, Leemans A. Quantitative DTI Measures. In: Van Hecke W, Emsell L, Sunaert S, editors. *Diffusion Tensor Imaging*. New York, NY: Springer New York (2016). p. 65–87. doi: 10.1007/978-1-4939-3118-7_5
25. Sullivan EV, Adalsteinsson E, Hedehus M, Ju C, Moseley M, Lim KO, et al. Equivalent disruption of regional white matter microstructure in ageing healthy men and women. *Neuroreport* (2001) 12:99–104. doi: 10.1097/00001756-200101220-00027
26. Hasan KM, Kamali A, Abid H, Kramer LA, Fletcher JM, Ewing-Cobbs L. Quantification of the spatiotemporal microstructural organization of the human brain association, projection and commissural pathways across the lifespan using diffusion tensor tractography. *Brain Struct Funct* (2010) 214:361–73. doi: 10.1007/s00429-009-0238-0
27. Kochunov P, Glahn DC, Lancaster J, Thompson PM, Kochunov V, Rogers B, et al. Fractional anisotropy of cerebral white matter and thickness of cortical gray matter across the lifespan. *NeuroImage* (2011) 58:41–9. doi: 10.1016/j.neuroimage.2011.05.050
28. Hsu J-L, Leemans A, Bai C-H, Lee C-H, Tsai Y-F, Chiu H-C, et al. Gender differences and age-related white matter changes of the human brain: A diffusion tensor imaging study. *NeuroImage* (2008) 39:566–77. doi: 10.1016/j.neuroimage.2007.09.017
29. Alexander DC, Dyrby TB, Nilsson M, Zhang H. Imaging brain microstructure with diffusion MRI: practicality and applications. *NMR BioMed* (2019) 32:e3841. doi: 10.1002/nbm.3841
30. Helmer KG, Chou M-C, Preciado RI, Gimi B, Rollins NK, Song A, et al. Multi-site study of diffusion metric variability: characterizing the effects of site, vendor, field strength, and echo time using the histogram distance. In: Gimi B, Krol A, editors. *Proc SPIE Int Soc Opt Eng*. San Diego, California, United States: Int Soc Opt. Eng. (2016). p. 9788. doi: 10.1117/12.2217449
31. Qin W, Shui Yu C, Zhang F, Du XY, Jiang H, Xia Yan Y, et al. Effects of echo time on diffusion quantification of brain white matter at 1.5T and 3.0T. *Magn Reson Med* (2009) 61:755–60. doi: 10.1002/mrm.21920
32. Hutchinson EB, Avram AV, Irfanoglu MO, Koay CG, Barnett AS, Komlosh ME, et al. Analysis of the effects of noise, DWI sampling, and value of assumed parameters in diffusion MRI models: Cross-Model Analysis of Noise and DWI Sampling. *Magn Reson Med* (2017) 78:1767–80. doi: 10.1002/mrm.26575
33. Fortin J-P, Parker D, Tunç B, Watanabe T, Elliott MA, Ruparel K, et al. Harmonization of multi-site diffusion tensor imaging data. *NeuroImage* (2017) 161:149–70. doi: 10.1016/j.neuroimage.2017.08.047
34. Pohl KM, Sullivan EV, Rohlfing T, Chu W, Kwon D, Nichols BN, et al. Harmonizing DTI measurements across scanners to examine the development of white matter microstructure in 803 adolescents of the NCANDA study. *NeuroImage* (2016) 130:194–213. doi: 10.1016/j.neuroimage.2016.01.061
35. Grech-Sollars M, Hales PW, Miyazaki K, Raschke F, Rodriguez D, Wilson M, et al. Multi-centre reproducibility of diffusion MRI parameters for clinical sequences in the brain: Multi-centre reproducibility of diffusion MRI using clinical sequences. *NMR BioMed* (2015) 28:468–85. doi: 10.1002/nbm.3269
36. Prohl AK, Scherrer B, Tomas-Fernandez X, Filip-Dhima R, Kapur K, Velasco-Annis C, et al. Reproducibility of Structural and Diffusion Tensor Imaging in the TACERN Multi-Center Study. *Front Integr Neurosci* (2019) 13:24. doi: 10.3389/fnint.2019.00024
37. Jockwitz C, Mérillat S, Liem F, Oschwald J, Amunts K, Caspers S, et al. Generalizing age effects on brain structure and cognition: A two-study comparison approach. *Hum Brain Mapp* (2019) 40:2305–19. doi: 10.1002/hbm.24524
38. Jahanshad N, Kochunov PV, Sprooten E, Mandl RC, Nichols TE, Almasy L, et al. Multi-site genetic analysis of diffusion images and voxelwise heritability analysis: A pilot project of the ENIGMA–DTI working group. *NeuroImage* (2013) 81:455–69. doi: 10.1016/j.neuroimage.2013.04.061
39. Kochunov P, Jahanshad N, Sprooten E, Nichols TE, Mandl RC, Almasy L, et al. Multi-site study of additive genetic effects on fractional anisotropy of cerebral white matter: Comparing meta and megaanalytical approaches for data pooling. *NeuroImage* (2014) 95:136–50. doi: 10.1016/j.neuroimage.2014.03.033
40. Chad JA, Pasternak O, Salat DH, Chen JJ. Re-examining age-related differences in white matter microstructure with free-water corrected diffusion tensor imaging. *Neurobiol Aging* (2018) 71:161–70. doi: 10.1016/j.neurobiolaging.2018.07.018
41. Wu Y-C, Field AS, Whalen PJ, Alexander AL. Age- and gender-related changes in the normal human brain using hybrid diffusion imaging (HYDI). *NeuroImage* (2011) 54:1840–53. doi: 10.1016/j.neuroimage.2010.09.067
42. Fjell Anders M, Walhovd KB, Westlye LT, Østby Y, Tamnes CK, Jernigan TL, et al. When does brain aging accelerate? Dangers of quadratic fits in cross-sectional studies. *NeuroImage* (2010) 50:1376–83. doi: 10.1016/j.neuroimage.2010.01.061
43. Pfefferbaum A, Sullivan EV. Cross-sectional versus longitudinal estimates of age-related changes in the adult brain: overlaps and discrepancies. *Neurobiol Aging* (2015) 36:2563–7. doi: 10.1016/j.neurobiolaging.2015.05.005
44. Lebel C, Walker L, Leemans A, Phillips L, Beaulieu C. Microstructural maturation of the human brain from childhood to adulthood. *NeuroImage* (2008) 40:1044–55. doi: 10.1016/j.neuroimage.2007.12.053
45. Lebel C, Beaulieu C. Longitudinal Development of Human Brain Wiring Continues from Childhood into Adulthood. *J Neurosci* (2011) 31:10937–47. doi: 10.1523/JNEUROSCI.5302-10.2011
46. Kodiweera C, Alexander AL, Harezlak J, McAllister TW, Wu Y-C. Age effects and sex differences in human brain white matter of young to middle-aged adults: A DTI, NODDI, and q-space study. *NeuroImage* (2016) 128:180–92. doi: 10.1016/j.neuroimage.2015.12.033
47. Tian L, Ma L. Microstructural Changes of the Human Brain from Early to Mid-Adulthood. *Front Hum Neurosci* (2017) 11:393. doi: 10.3389/fnhum.2017.00393

Conflict of Interest: The authors declare that the research was conducted in the absence of any commercial or financial relationships that could be construed as a potential conflict of interest.

frontiers in Psychiatry

ORIGINAL RESEARCH
published: 05 May 2020
doi: 10.3389/fpsyt.2020.00360

Gray Matter Covariance Networks as Classifiers and Predictors of Cognitive Function in Alzheimer's Disease

Fabian Wagner[1], *Marco Duering*[2], *Benno G. Gesierich*[2], *Christian Enzinger*[1], *Stefan Ropele*[1], *Peter Dal-Bianco*[3], *Florian Mayer*[3], *Reinhold Schmidt*[1]* *and Marisa Koini*[1]

[1] Department of Neurology, Medical University of Graz, Graz, Austria, [2] Institute for Stroke and Dementia Research (ISD), University Hospital, LMU Munich, Munich, Germany, [3] Department of Neurology, Medical University of Vienna, Vienna, Austria

OPEN ACCESS

Edited by:
Francesco Ernesto Pontieri, Sapienza University of Rome, Italy

Reviewed by:
Sara L. Weisenbach, Stony Brook Medicine, United States
Fabrizio Piras, Santa Lucia Foundation (IRCCS), Italy

***Correspondence:**
Reinhold Schmidt
reinhold.schmidt@medunigraz.at

Specialty section:
This article was submitted to Aging Psychiatry, a section of the journal Frontiers in Psychiatry

Received: 21 October 2019
Accepted: 09 April 2020
Published: 05 May 2020

Citation:
Wagner F, Duering M, Gesierich BG, Enzinger C, Ropele S, Dal-Bianco P, Mayer F, Schmidt R and Koini M (2020) Gray Matter Covariance Networks as Classifiers and Predictors of Cognitive Function in Alzheimer's Disease. Front. Psychiatry 11:360. doi: 10.3389/fpsyt.2020.00360

The study of shared variation in gray matter morphology may define neurodegenerative diseases beyond what can be detected from the isolated assessment of regional brain volumes. We, therefore, aimed to (1) identify SCNs (structural covariance networks) that discriminate between Alzheimer's disease (AD) patients and healthy controls (HC), (2) investigate their diagnostic accuracy in comparison and above established markers, and (3) determine if they are associated with cognitive abilities. We applied a random forest algorithm to identify discriminating networks from a set of 20 SCNs. The algorithm was trained on a main sample of 104 AD patients and 104 age-matched HC and was then validated in an independent sample of 28 AD patients and 28 controls from another center. Only two of the 20 SCNs contributed significantly to the discrimination between AD and controls. These were a temporal and a secondary somatosensory SCN. Their diagnostic accuracy was 74% in the original cohort and 80% in the independent samples. The diagnostic accuracy of SCNs was comparable with that of conventional volumetric MRI markers including whole brain volume and hippocampal volume. SCN did not significantly increase diagnostic accuracy beyond that of conventional MRI markers. We found the temporal SCN to be associated with verbal memory at baseline. No other associations with cognitive functions were seen. SCNs failed to predict the course of cognitive decline over an average of 18 months. We conclude that SCNs have diagnostic potential, but the diagnostic information gain beyond conventional MRI markers is limited.

Keywords: structural covariance network, longitudinal, Alzheimer, cognition, random forest

INTRODUCTION

Alzheimer's Disease (AD) has been recognized as a disconnection syndrome (1, 2) leading to increasing cognitive deficits as the disease progresses. Resting state functional magnetic resonance imaging (rs-fMRI) has been used to study functional connectivity at rest and showed decreased connectivity in brain networks of AD patients (3–5). The default mode network (DMN) (3, 6) is

most affected (7–9). Alterations in connectivity have also been found in the salience and frontal executive networks (6, 8). In healthy subjects, DMN connectivity is inhibited while other networks increase their connectivity. AD patients lose the ability to suppress the DMN network during cognitive activity, (8) and a task-based fMRI study showed an association between de-synchronized hippocampus and DMN activity and impaired memory (10). In line with functional disconnection in AD, multi-level deficiency of white matter (WM) connectivity has been shown in DTI studies (11, 12). The authors reported a decreased fiber-count of WM and loss of connective efficiency within and between AD relevant brain areas like the hippocampus, precuneus, and temporal gyrus (11). Another study showed degeneration in 18 major WM tracts, including the fornix, cingulum, and corpus callosum (12). Connectivity between gray matter regions can also be assessed by a method called structural covariance networks (SCNs) (13). SCNs are networks found on the basis of distinct gray matter (GM) covariation patterns in remote cortical areas. In healthy subjects, SCN integrity decreases with age (14, 15), and relates to impairment of cognitive and motor functions (16, 17). In patients with mild cognitive impairment and AD, SCNs containing temporal and limbic regions as well as the precuneus were found to predict the rate of decline in memory over time (13, 18, 19).

In the present study we aimed to identify those SCNs that best discriminate between AD patients and healthy controls by utilizing twenty SCNs obtained in a group of 257 healthy aging subjects (16). We hypothesized, that networks including the temporal lobes as well as the DMN discriminate best between patients and controls. To validate the diagnostic accuracy of potentially significant identified networks, we applied them on an independent sample. The diagnostic value of SCNs was then compared to conventional MRI markers of AD including the medial temporal lobe atrophy score, total brain volume, and hippocampal volume. We also tested whether SCNs relate to cognitive functioning cross-sectionally and longitudinally.

METHODS

Sample

The data from AD patients are from the Prospective Registry on Dementia (PRODEM), a longitudinal multi-center study on disease-progression of dementia patients in Austria. The inclusion criteria were as follows: (a) dementia diagnosis according to DSM-IV criteria, (b) non-institutionalization and no need for 24-h care and (c) availability of a caregiver who is able to provide additional information on the patient. We excluded patients with co-morbidities that were likely to cause early termination from the study such as cancer. Subjects who were not able to sign an informed consent form were also excluded. For further detail see (20). The data from the *controls are from the* Austrian Stroke Prevention Study–Family (ASPS-Fam). The ASPS-Fam is a single-center, prospective study on risk factors and their effects on the brain in the normal elderly. None of our control subjects had a history of neuropsychiatric disease, including cerebrovascular attacks and dementia. All had a normal neurologic examination (21).

For the present study all PRODEM patients with (1) either possible or probable AD defined by the NINCDS-ADRDA Alzheimer's criteria (22), (2) a 3-Tesla T1-weighted 3D MRI scan, and (3) a cognitive assessment within 3 months of the imaging examination were selected. The cognitive assessment included the Mini Mental State examination (MMSE) and the "Consortium to Establish a Registry for Alzheimer's Disease"—Test battery—plus version (CERAD-Plus). In total 104 AD patients (mean age = 71.45 ± 7.97 years, range: 51–87 years, 59 females) from Graz and 28 AD patients (mean age = 73.79 ± 6.17, range: 58–82, 14 females) from Vienna were included. The Graz sample was used for statistical modeling, while the Viennese sample served as the independent validation cohort. In each center a cohort of controls was matched to each AD patient. Matching was done for age (+/− 3 years) and sex (Graz: mean age = 71.09 ± 7.38 years; range: 53–86, 59 females; Vienna: n = 28, mean age = 72.44 ± 7.18 years; range: 56–85 years, 14 female).

Eighty-two AD patients from the Graz set had a follow-up clinical and cognitive assessment that ranged between 6 and 37 months with a mean of 18 months. Patients who dropped out from the study did not differ from subjects with follow-up in terms of and the Mini Mental State Examination scores at baseline.

The study was approved by the ethics committees of the Medical Universities of Graz, Austria and Vienna, Austria. Informed consent was obtained from all subjects and/or caregivers included in the study.

MRI Protocol

Structural data were assessed using a three-dimensional, T1-weighted, magnetization prepared rapid gradient echo sequence (MPRAGE) in Graz and Vienna (Trio Tim 3.0T, manufactured by Siemens Healthcare, Erlangen, Germany) with whole brain coverage. The selected sequence parameters for PRODEM were as follows: Repetition time: 1,900/2,000 ms, inversion time: 900 ms, echo time: 2.19 ms, flip angle: 9° and a resolution of: 1 mm × 1 mm × 1 mm/1.2 mm. For ASPS-Fam, the selected sequence parameters were as follows: Repetition time: 1,900, inversion time: 900 ms, echo time: 2.19 ms, flip angle: 9° an isotropic resolution of 1 mm.

Image Analysis

Structural Covariance Networks

To prevent biasing data, all image processing steps were done independently for the Graz and Vienna cohorts of this sample. The T1 weighted images were visually checked to ensure consistent image quality for analysis. Pre-processing and SCN analyses were performed using FMRIB's Software Library (FSL) Version 5.0.9 (23). A detailed version of processing steps can be found in (14, 16, 18, 24) In brief, the brain was extracted from

non-brain tissue in the images with a semiautomatic brain extraction tool (BET) implemented in FSL (25). The extracted brains were visually checked for artefacts (remaining skull or missing part of sulci). In case of missing part of sulci, parameters for BET were changed. Remaining skull was removed by hand. Then followed tissue-type segmented into gray matter (GM), white matter (WM), and cerebrospinal fluid (CSF) using a voxel-based morphometric analysis (VBM) within the FSL framework (26). After visual inspection, the individual GM images were non-linear registered (27) to the GM MNI152 standard space (Montreal Neurological Institute, Montreal, QC, Canada) (23). By averaging the resulting images, a study-specific GM template was created to which the native GM images were non-linearly re-registered. Following, the images were modulated to correct for distortions due to non-linear transformation (26, 28). Finally, the GM images were then spatially smoothed with an isotropic Gaussian kernel with a sigma of 3 mm and concatenated to a 4D–data set. Thereafter, this 4D–data set was spatially regressed onto 20 networks obtained by Koini and colleagues (16) in a healthy sample, using spatial regression (Step 1 of the dual regression script provided by FSL) (29) to calculate individual network integrity scores. These networks included a temporal, a temporo-cerebellar, a superior temporal gyrus, a supplementary motor, a secondary somatosensory, a limbic, a fronto-parietal, a cuneal, a precuneus, a fronto-occipital, an insular including the gyrus cinguli, an occipital including the posterior cingulate cortex, six cerebellar, and an amygdala SCN. The outcome of the spatial regression consists of individual beta scores (positive and negative) per person and per SCN, representing network integrity values, which were used in the statistical analyses.

Visual and Automated Atrophy Marker

The native T1-weighted images of all subjects were visually rated by trained specialists using the medial temporal lobe atrophy (MTA)-score scale, a five-point rating scale, ranging from no atrophy (0) to maximum atrophy (4) (30). Ratings were made for both hemispheres, with a mean value calculated for statistical analyses. Automatic brain volume measurements from the native T1-weighted images of all subjects were done by using FreeSurfer (Version 5.3) (31). The brain volume and the hippocampus volumes, averaged across hemispheres, were normalized for intracranial volume.

Cognitive Assessment

The PRODEM study protocol includes the CERAD-Plus (Consortium to Establish a Registry for Alzheimer's Disease) test battery, which among others includes subtests for verbal memory and figural memory (32). Verbal memory is tested by the recall of a wordlist and figural memory is assessed by drawing geometric figures from a template and later from memory. For both subtests "savings" scores, the ratio of correctly recalled items to learned items (times 100), were available as measurement for memory retention. We also determined a composite score of CERAD-Plus subtest, the Chandler-score (33). Verbal and figural memory savings and the Chandler-score were selected as outcome variables in the cross sectional and longitudinal analyses.

Statistical Analysis

The statistical software R (version 3.5.3 on Windows 10) was used (34). Training of the classification algorithms were done solely on the cohort from Graz. For discrimination between AD patients and HC the value of the integrity score of each of the 20 SCNs was used in a random forest analysis (35) using the "cforest" function within the "party" package (36–38). 1001 condition inference trees and the associated conditional permutation importance for the SCN integrity scores were calculated (39). Numbers of random variables at the nodes ("mtry" parameter) were left at the standard of five variables. The conditional permutation importance is a measure of variable importance and is defined as a score for mean loss of accuracy in classification, if a given SCN is excluded from the random forest model. SCNs with a variable importance score of less than one were not regarded as crucial for classification. Since the random forest estimations and variable importance calculations contain steps based on randomness, the results typically vary in small ranges. To compensate for this, the calculations were repeated 100 times to build mean values and standard deviation.

Next, random forest models containing distinct combinations of crucial SCNs were compared to check if comparable classification accuracy can be achieved with sparser models. Crucial SCNs were identified and selected by variable importance as mentioned above. Accuracy, sensitivity, and specificity calculations were done with the "caret"-package (40). These models were again calculated 100 times to obtain mean accuracy, sensitivity, and specificity values. The models were then tested on the independent data set containing AD patients from Vienna and HC from the ASPS-Fam. Thereafter, a model containing the crucial SCNs was extended by the established markers MTA-score, total brain volume, and averaged hippocampus volume to measure their joint discriminative ability.

To examine the association between the SCNs integrity and cognitive ability, six multiple linear regression models were computed using the longitudinal cohort from Graz. Outcome variables were baseline (BL) values (cross-sectional) and annualized change values from BL to follow-up (FU, longitudinal) of (a) the Chandler-score, (b) the verbal memory savings, and (c) the figural memory savings. Predictors were the crucial SCNs evaluated by variable importance.

RESULTS

Diagnostic Accuracy

From the 20 template networks included in our random forest analysis (Model A), the temporal network (**Figure 1A**, **Table 1**) and the secondary somatosensory (S2) network (**Figure 1B**, **Table 1**) reached a variable importance score above one (**Figure 2**), and discriminative value.

As can be seen from **Table 2**, sensitivity, specificity, and diagnostic accuracy of the temporal SCN is 72, 77, and 74%, respectively. These values were replicated in the validation cohort. It is also shown in this table that the S2 SCN has lower

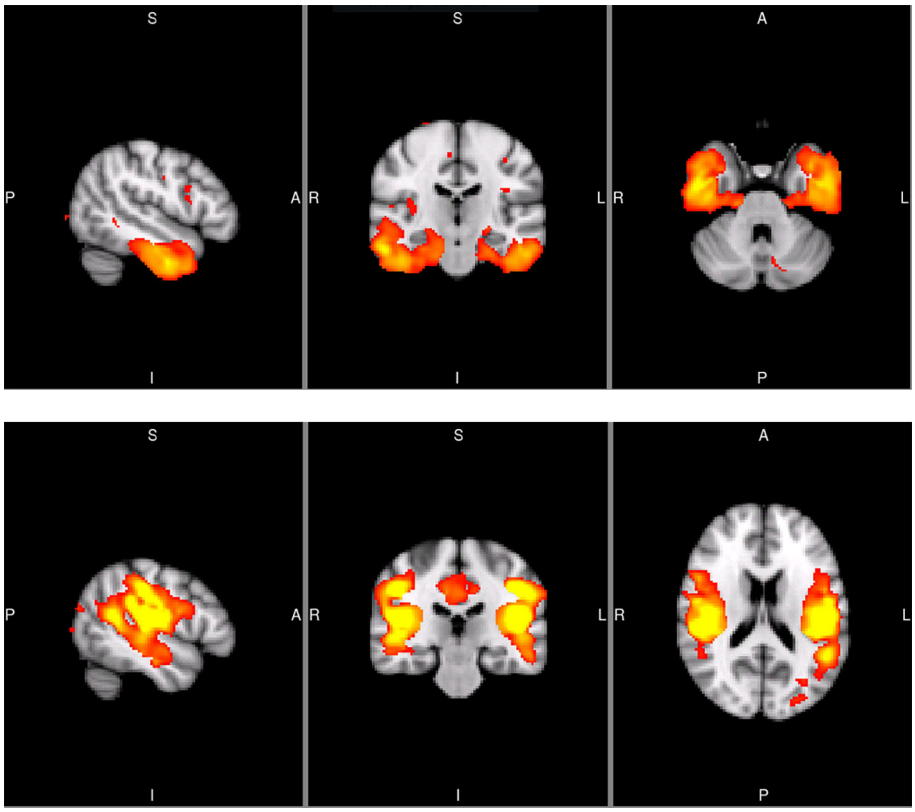

FIGURE 1 | Sagittal, coronal, and axial slices of the temporal SCN (MNI coordinates: x = –50, y = –20, z = –32) and the secondary somatosensory SCN (S2; MNI coordinates: x = –50, y = –26, z = 18). The images are taken from the Koini masks (16).

diagnostic accuracy. A combination of the S2 and temporal SCNs and even a combination of all 20 SCNs increased the diagnostic accuracy only marginally when compared to the temporal SCN alone.

In **Table 3** and **Figure 3** we show the random forest models assessing diagnostic accuracy measure for volumetric MRI markers of AD alone and for the full model including all volumetric measures and the temporal and S2 SCN. In both the Graz cohort and the Vienna validation cohort single volumetric MRI markers performed similar to SCNs. Joint use of volumetric markers and SCNs discriminated best between AD and controls with a diagnostic accuracy of 82 and 86% in the founder and validation cohort, respectively. The increase in accuracy when adding SCNs to conventional MRI volumetric measures was near zero and non-significant.

Cognition

Cross-sectionally, in AD, the temporal SCN showed a significant association with verbal memory savings (**Table 4**), explaining nine percent of the variance. No association between SCN integrity and any other test scores were found. For change in cognitive measures over time, no associations with SCN integrity were found either (**Table 4**).

DISCUSSION

Among 20 covariance networks, a temporal gray matter network and a secondary somatosensory gray matter network showed a diagnostic accuracy of 74 and 80% in two independent cohorts. AD patients were correctly identified in 76 and 83% of cases, controls were correctly identified in 78 and 75% of cases. The gray matter networks did not significantly surpass the diagnostic accuracy of traditional volumetric markers including brain volume, hippocampal volume, and MTA score. When adding the covariance networks to a model of traditional volumetric MR markers, the diagnostic accuracy remained virtually unchanged. This contrasts the view that the assessment of networks, which degenerate in synchrony, provides more diagnostic information than a simple volumetric assessment of selected brain regions known to be involved in AD (1, 41, 42).

Loss of connectivity within the temporal network was related to lower verbal memory, but neither the temporal network nor other SCNs were able to predict the slope of cognitive decline over the observational period.

The covariance networks in our study are partly overlapping with those described by Hafkemeijer and co-workers (18). The temporal gray matter network, which related to verbal memory in

TABLE 1 | Regions included in the Temporal SCN and Secondary Somatosensory SCN (16).

SCN	Voxels	MNI coordinates			Region	Hemisphere
		x	y	z		
Temporal	*10,442*	*40*	*–4*	*–40*	*Inferior temporal gyrus, anterior division*	*R*
	5,355	*–38*	*8*	*–38*	*Temporal pole*	*L*
	1,466	*0*	*20*	*40*	*Paracingulate gyrus*	*R*
	1,313	*10*	*38*	*–4*	*Cingulate gyrus, anterior division*	*R*
	1,106	*–32*	*22*	*–4*	*Insular Cortex*	*L*
Secondary Somatosensory (S2)	*9,650*	*–48*	*–26*	*16*	*Parietal operculum cortex*	*L*
	7,478	*50*	*–28*	*16*	*Parietal operculum cortex*	*R*
	1,028	*10*	*–26*	*34*	*Cingulate gyrus, posterior division*	*R*

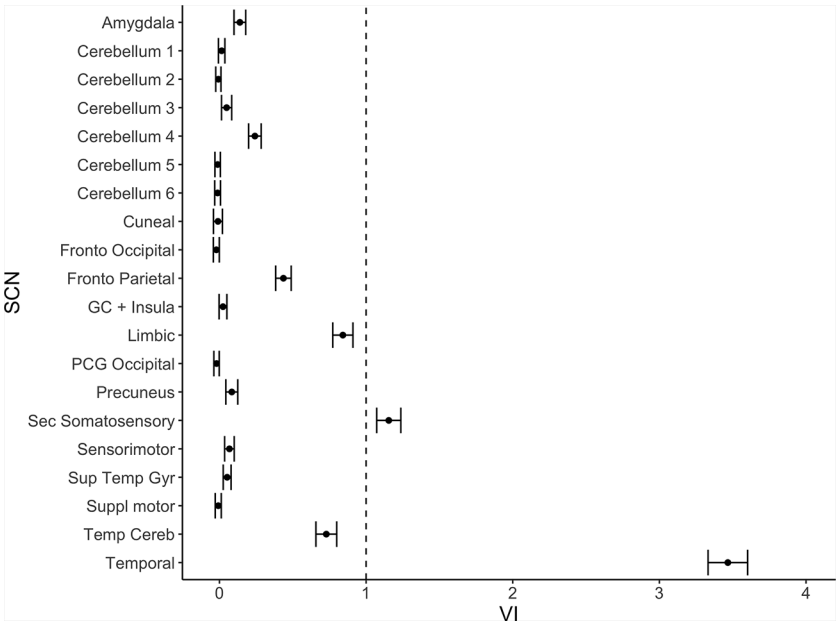

FIGURE 2 | Variable importance (mean accuracy loss) of 20 structural covariance networks (SCNs) in a random forest classification model. Exclusion of the temporal and the secondary somatosensory network show a variable importance score above one. The error bars show one standard deviation.

TABLE 2 | Accuracy, sensitivity, and specificity measures for the classification models in the original Graz sample and the independent Viennese sample.

Model	Predictors	Main sample (Graz)			Independent sample (Vienna)		
		Accuracy	Sensitivity	Specificity	Accuracy	Sensitivity	Specificity
A	*All SCNs*	77	76	78	79	83	75
B	*Temporal + S2*	74	73	75	80	85	75
C	*Temporal SCN*	74	72	77	74	75	73
D	*S2 SCN*	67	67	67	54	54	53

our study, contains connections between the anterior part of the right inferior temporal gyrus, the left temporal pole, the right paracingulate gyrus, the anterior part of the right cingulate gyrus, and the left insular cortex. These areas have been reported to be particularly affected by AD pathology (43–46). However, the inclusion of the anterior cingulate and paracingulate gyri in the temporal network is somehow unusual, but in case of the former a comparable network was also found in a study by Hafkemeijer and co-workers (14). Since there is quite some randomness in network creation depending on both sample data and parameter choice, we are unable to determine whether the inclusion of the anterior division of the cingulate gyrus and the paracingulate gyrus in the temporal SCN occurred on true biological grounds. A statistical change finding cannot be excluded with certainty. The

TABLE 3 | Accuracy, sensitivity, and specificity measures for MTA-score, normalized brain volume (BV), normalized hippocampus volume (Hc), and combined models.

	Graz AD–HC			Vienna AD–HC		
Model	**Accuracy**	**Sensitivity**	**Specificity**	**Accuracy**	**Sensitivity**	**Specificity**
MTA	77	74	81	82	82	82
BV	74	72	75	73	75	72
Hc	76	73	79	79	88	74
MTA + Hc + BV	82	80	84	88	92	84
MTA + Hc + BV + Temporal + S2	82	81	82	86	92	81

Calculations were done in the original Graz sample and the independent Viennese sample.

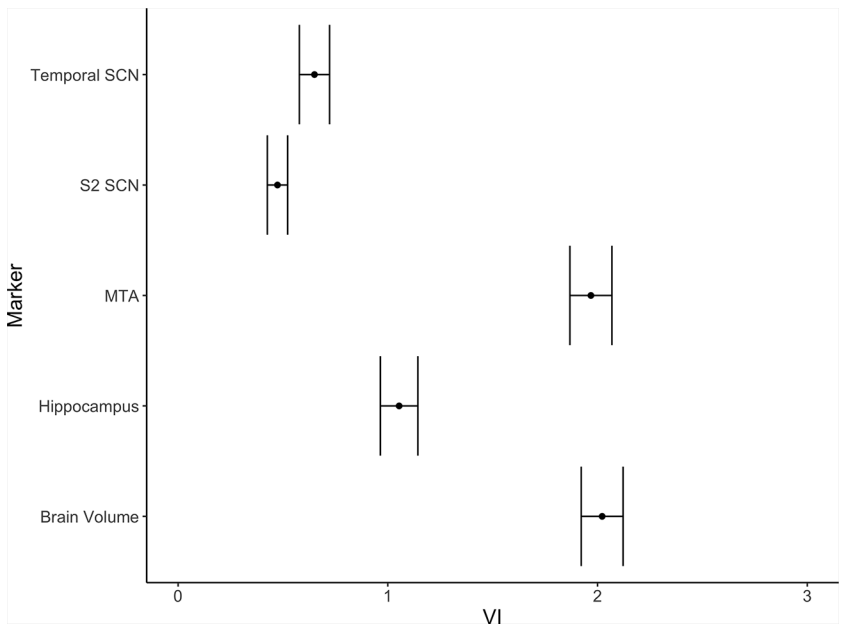

FIGURE 3 | Variable importance (mean accuracy loss) of the temporal and the S2 SCNs and three alternative markers (MTA-score, normalized brain volume, normalized hippocampus volume) in a random forest classification model. The error bars depict one standard deviation.

TABLE 4 | Multiple linear regression models to evaluate the predictive value of the SCNs for cognition.

N = 82	**Chandler-score**			**Verbal memory savings**			**Figural memory savings**		
Cross-sectional									
Variable	*B*	*SE*	*beta*	*B*	*SE*	*beta*	*B*	*SE*	*Beta*
Temporal SCN	276.34	200.33	.15	**1,060.42***	**508.55**	**.23***	−168.11	508.11	−.03
Secondary Somatosensory SCN	204.857	225.80	.10	805.79	573.23	.15	569.17	572.73	.11
R^2 (p-value)		*.04 (.17)*			***.09 (.01)****			*.01 (.61)*	
Longitudinal									
Variable	*B*	*SE*	*beta*	*B*	*SE*	*beta*	*B*	*SE*	*Beta*
Temporal SCN	−7.26	126.24	<−0.00	155.77	484.45	.03	−182.99	391.47	< .00
Secondary Somatosensory SCN	−71.78	143.45	−0.06	−902.78	570.06	−.19	87.47	441.26	< .00
R^2 (p-value)		*< .00 (.86)*			*.03 (.29)*			*< .00 (.89)*	

**significance at.05 level.*

secondary somatosensory SCN, which was the second gray matter network that discriminated AD from controls in the current study, contains connections between the parietal operculum and the posterior part of the cingulate gyrus, which is also involved in the AD pathophysiologic processes (44). Assessment of SCNs as potential MRI markers for the differential diagnosis of dementia follows the network degeneration hypothesis of Seeley and co-workers (13). It suggests disease-dependent simultaneous network degeneration of gray matter rather than isolated and successive involvement of brain areas to by typical for primary degenerative dementias including AD, behavioral variant fronto-temporal dementia, semantic dementia, progressive nonfluent aphasia, and cortico-basal syndrome. Our results are somewhat contrasting this assumption in that the potential of SCNs to discriminate between AD and controls was almost identical to that of isolated volumetric measures. So far, five studies have used SCNs as a diagnostic tool to separate AD cases from controls (18, 19, 47–49). They identified multiple SCNs that differ between AD and HC, such as the default mode network, a hippocampal network, the salience network, and the executive control network. We also found two networks, the temporal and the somatosensory SCN to contribute to the classification between patients and controls. Our study extends previous investigations by not only defining SCNs that may assist in AD diagnosis but by also assessing their diagnostic potential relative to established MR-based biomarkers. In our study SCNs did not increase the diagnostic accuracy beyond that of whole brain volume, hippocampal volume, and MTA rating. Similar assessments were not done in previous studies but are needed to better define the diagnostic potential of SCNs in clinical settings. Another reason for insignificant results may be the use of MNI152 for co-registration standard space during processing. MNI152 may not be ideal, since the brains of the elderly might significantly differ from the brains used for the MNI152 template. However, Fillmore et al. (50) and Huang et al. (51) discussed this problem and indicated that these effects are diminished in case of VBM because it results in a study specific template. This was the case in our study. As Ashburner and Friston discussed in their technical paper on VBM, a version of standard space template is needed to create this study specific template, and it is merely used for correction of global brain shape difference (26). However, we cannot completely rule out that the use of the default workflow might have had an impact on our analyses. Possibly another crucial factor for our results may be the use of SCN templates from Koini et al. (52). To our knowledge, there exist two commonly used options for template selection. One is using templates from prior studies, the other is to generate study specific templates. Bijsterbosch et al. (53) discuss these choices of network templates and associated advantages and disadvantages. They point out that the first choice is typically to create study specific network templates on the study sample. This approach increases the likelihood for finding statistical differences between investigational groups, because it represents the best fit for the sample under investigation and provides a way to control for noise in the data. This advantage may come at a price of interpretability. If we had created study specific templates, they would include both experimental groups (controls and patients) and therefore represent a form of hybrid networks rather than being specific for each comparative sample. Using data of only one of the experimental groups in template creation (controls for example) would introduce a strong bias for later statistical analyses (53). Hence, we decided to use templates from an independent healthy sample with adequate sample size, since we expected sufficient differences and a high potential for classification accuracy between patients and controls when using networks derived from healthy individuals. Another factor regarding interpretation of our results is the inclusion of imaging data from two different centers. While from the same vendor, slightly different image acquisition parameters were used at the two centers which could have affected the study results (54). It is important to note, however, that both cohorts were pre-processed independently, and although some center effects cannot be excluded with certainty, the results on the diagnostic accuracy of SCNs were almost identical at both sites. This is a clear indication for the robustness of the study's finding across centers.

Our study has several strengths. The size of the cohort is considerable, and we used an independent sample for validation of our results. The diagnostic accuracy was almost identical in both samples which underscores the robustness of our findings. A limitation of our study was the absence of imaging data at follow-up. Longitudinal change in network integrity over time may be a better diagnostic marker of AD. Moreover, although we did not find an association between SCNs at baseline and future cognitive functioning, we cannot rule out that loss of SCN integrity over time parallels cognitive decline in AD patients. In this study, we used subtests of the CERAD-Plus for assessment of verbal and figural memory. While CERAD is a well-established test battery in AD research, more extensive memory tests to reduce the possibility of measurement error may be considered.

In conclusion, we found that established volumetric markers and the visual MTA score perform similarly well in differentiating AD from healthy controls than SCNs which need extensive image postprocessing. As to whether SCNs are helpful in discriminating between different forms of dementia syndromes needs to be determined and it is likely that longitudinal assessment of SCNs can increase our understanding of the spatial and timely evolution of neurodegenerative processes.

DATA AVAILABILITY STATEMENT

The datasets for this article are not publicly available due to ethical and privacy restrictions. Information contained in the data may compromise the privacy of research participants. Requests to access the datasets should be directed to RS (reinhold.schmidt@medunigraz.at).

ETHICS STATEMENT

The studies involving human participants were reviewed and approved by Ethics committees of the Medical Universities of

Graz, Austria and Vienna, Austria. The patients/participants provided their written informed consent to participate in this study.

AUTHOR CONTRIBUTIONS

RS, MK, MD, SR, CE, and FW contributed to the conception and design of the study. FM, SR, PD-B, and RS implemented MRI as well as clinical data collection. FW, RS, MK, and BG performed the statistical analysis. FW wrote the first draft of the manuscript. RS, MK, MD, and CE wrote sections of the manuscript. All authors contributed to the manuscript revision, read and approved the submitted version.

FUNDING

This study was funded by a D-A-CH grand (German Research DF DU1626/1-1, and an Austrian Fund FWF 12889-B31) and the Austrian Science Fund (FWF, KLI 546-BBL).

REFERENCES

1. Brier MR, Thomas JB, Ances BM. Network dysfunction in Alzheimer's disease: refining the disconnection hypothesis. *Brain Connect* (2014) 4 (5):299–311. doi: 10.1089/brain.2014.0236
2. Palop JJ, Mucke L. Network abnormalities and interneuron dysfunction in Alzheimer disease. *Nat Rev Neurosci* (2016) 17(12):777–92. doi: 10.1038/nrn.2016.141
3. Greicius MD, Srivastava G, Reiss AL, Menon V. Default-mode network activity distinguishes Alzheimer's disease from healthy aging: evidence from functional MRI. *Proc Natl Acad Sci U S A* (2004) 101(13):4637–42. doi: 10.1073/pnas.0308627101
4. Buckner RL, Sepulcre J, Talukdar T, Krienen FM, Liu H, Hedden T, et al. Cortical Hubs Revealed by Intrinsic Functional Connectivity: Mapping, Assessment of Stability, and Relation to Alzheimer's Disease. *J Neurosci* (2009) 29(6):1860–73. doi: 10.1523/JNEUROSCI.5062-08.2009
5. Wang K, Liang M, Wang L, Tian L, Zhang X, Li K, et al. Altered functional connectivity in early Alzheimer's disease: A resting-state fMRI study. *Hum Brain Mapp* (2007) 28(10):967–78. doi: 10.1002/hbm.20324
6. Agosta F, Pievani M, Geroldi C, Copetti M, Frisoni GB, Filippi M. Resting state fMRI in Alzheimer's disease: Beyond the default mode network. *Neurobiol Aging* (2012) 33(8):1564–78. doi: 10.1016/j.neurobiolaging.2011.06.007
7. Hafkemeijer A, Möller C, Dopper EGP, Jiskoot LC, Schouten TM, van Swieten JC, et al. Resting state functional connectivity differences between behavioral variant frontotemporal dementia and Alzheimer's disease. *Front Hum Neurosci* (2015) 9(September):1–12. doi: 10.3389/fnhum.2015.00474
8. Brier M, Thomas JB, Snyder AZ, Benzinger TL, Zhang D. Loss of Intra- and Inter-Network Resting State Functional Connections with Alzheimer's Disease Progression. *J Neurosci* (2012) 32(26):8890–9. doi: 10.1523/JNEUROSCI.5698-11.2012.Loss
9. Klaassens BL, van Gerven JMA, van der Grond J, de Vos F, Möller C, Rombouts SARB. Diminished posterior precuneus connectivity with the default mode network differentiates normal aging from Alzheimer's Disease. *Front Aging Neurosci* (2017) 9(APR):1–13. doi: 10.3389/fnagi.2017.00097
10. Celone KA, Calhoun VD, Dickerson BC, Atri A, Chua EF, Miller SL, et al. Alterations in Memory Networks in Mild Cognitive Impairment and Alzheimer's Disease: An Independent Component Analysis. *J Neurosci* (2006) 26(40):10222–31. doi: 10.1523/JNEUROSCI.2250-06.2006
11. Wang T, Shi F, Jin Y, Yap PT, Wee CY, Zhang J, et al. Multilevel Deficiency of White Matter Connectivity Networks in Alzheimer's Disease: A Diffusion MRI Study with DTI and HARDI Models. *Neural Plast* (2016). doi: 10.1155/2016/2947136
12. Jin Y, Huang C, Daianu M, Zhan L, Dennis EL, Reid RI, et al. 3D Tract-Specific Local and Global Analysis of White Matter Integrity in Alzhemer' s Disease. *Hum Brain Mapp* (2017) 38(3):1191–207. doi: 10.1002/hbm.23448
13. Seeley WW, Crawford RK, Zhou J, Miller BL, Greicius MD. Neurodegenerative Diseases Target Large-Scale Human Brain Networks. *Neuron* (2009) 62(1):42–52. doi: 10.1016/j.neuron.2009.03.024
14. Hafkemeijer A, Altmann-Schneider I, de Craen AJM, Slagboom PE, van der Grond J, Rombouts SARB. Associations between age and gray matter volume in anatomical brain networks in middle-aged to older adults. *Aging Cell* (2014) 13(6):1068–74. doi: 10.1111/acel.12271
15. Montembeault M, Joubert S, Doyon J, Carrier J, Gagnon JF, Monchi O, et al. The impact of aging on gray matter structural covariance networks. *Neuroimage* (2012) 63(2):754–9. doi: 10.1016/j.neuroimage.2012.06.052
16. Koini M, Duering M, Gesierich BG, Rombouts SARB, Ropele S, Wagner F, et al. Grey-matter network disintegration as predictor of cognitive and motor function with aging. *Brain Struct Funct* (2018) 0(0):0. doi: 10.1007/s00429-018-1642-0
17. Foster-Dingley JC, Hafkemeijer A, van den Berg-Huysmans AA, Moonen JEF, de Ruijter W, de Craen AJM, et al. Structural Covariance Networks and Their Association with Age, Features of Cerebral Small-Vessel Disease, and Cognitive Functioning in Older Persons. *Brain Connect* (2016) 6(9):681–90. doi: 10.1089/brain.2016.0434
18. Hafkemeijer A, Möller C, Dopper EGP, Jiskoot LC, van den Berg-Huysmans AA, van Swieten JC, et al. Differences in structural covariance brain networks between behavioral variant frontotemporal dementia and Alzheimer's disease. *Hum Brain Mapp* (2016) 37(3):978–88. doi: 10.1002/hbm.23081
19. Li K, Luo X, Zeng Q, Huang P, Shen Z, Xu X, et al. Gray matter structural covariance networks changes along the Alzheimer's disease continuum. *NeuroImage Clin* (2019) 23(October 2018):101828. doi: 10.1016/j.nicl.2019.101828
20. Seiler S, Schmidt H, Lechner A, Benke T, Sanin G, Ransmayr G, et al. Driving Cessation and Dementia: Results of the Prospective Registry on Dementia in Austria (PRODEM). *PloS One* (2012) 7(12):e52710. doi: 10.1371/journal.pone.0052710
21. Schmidt R, Ropele S, Enzinger C, Petrovic K, Smith S, Schmidt H, et al. White matter lesion progression, brain atrophy, and cognitive decline: The Austrian stroke prevention study. *Ann Neurol* (2005) 58(4):610–6. doi: 10.1002/ana.20630
22. McKhann G, Drachman D, Folstein M, Katzman R, Price D, Stadlan EM. Clinical diagnosis of Alzheimer's disease: Report of the NINCDS-ADRDA Work Group* under the auspices of Department of Health and Human Services Task Force on Alzheimer's Disease. *Neurology* (1984) 34(7):939. doi: 10.1212/WNL.34.7.939
23. Jenkinson M, Beckmann CF, Behrens TEJ, Woolrich MW, Smith SM. Fsl. *Neuroimage* (2012) 62(2):782–90. doi: 10.1016/j.neuroimage.2011.09.015
24. Douaud G, MacKay C, Andersson J, James S, Quested D, Ray MK, et al. Schizophrenia delays and alters maturation of the brain in adolescence. *Brain* (2009) 132(9):2437–48. doi: 10.1093/brain/awp126
25. Smith SM. Fast robust automated brain extraction. *Hum Brain Mapp* (2002) 17(3):143–55. doi: 10.1002/hbm.10062
26. Ashburner J, Friston KJ. Voxel-based morphometry - The methods. *Neuroimage* (2000) 11(6 I):805–21. doi: 10.1006/nimg.2000.0582
27. Andersson JLR, Jenkinson M, Smith S. Non-linear registration, aka spatial normalisation. In: . *FMRIB Technial Report TR07JA2*. UK: Oxford Cent Funct Magn Reson Imaging Brain, Dep Clin Neurol Oxford Univ Oxford (2007). p. 22.
28. Good CD, Johnsrude IS, Ashburner J, Henson RNA, Friston KJ. Frackowiak RSJ. A voxel-based morphometric study of ageing in 465 normal adult human brains. *Neuroimage* (2001) 14(1 Pt 1):21–36. doi: 10.1006/nimg.2001.0786

29. Filippini N, MacIntosh BJ, Hough MG, Goodwin GM, Frisoni GB, Smith SM, et al. Distinct patterns of brain activity in young carriers of the APOE-epsilon4 allele. *PNAS* (2009) 106(17):7209–14. doi: 10.1073/pnas.0811879106
30. Scheltens P, Leys D, Barkhof F, Huglo D, Weinstein HC, Vermersch P, et al. Atrophy of medial temporal lobes on MRI in "probable" Alzheimer's disease and normal ageing: diagnostic value and neuropsychological correlates. *J Neurol Neurosurg Psychiatry* (1992) 55:967–72. doi: 10.1136/jnnp.55.10.967
31. Fischl B. Freesurfer. *Neuroimage* (2012) 62(2):774–81. doi: 10.1016/j.neuroimage.2012.01.021
32. Morris JC, Heyman A, Mohs RC, Hughes JP, van Belle G, Fillenbaum G, et al. The Consortium to Establish a Registry for Alzheimer's Disease (CERAD). *Neurology* (1989) 39(9):1159–65. doi: 10.1212/WNL.39.9.1159
33. Chandler MJ, Lacritz LH, Hynan LS, Barnard HD, Allen G, Deschner M, et al. A total score for the CERAD neuropsychological battery. *Neurology* (2005) 65 (1):102–6. doi: 10.1212/01.wnl.0000167607.63000.38
34. R-Core-Team. A language and environment for statistical computing. *R Found Stat Comput* (2016).
35. Breiman L. Random forests. *Mach Learn* (2001) 45(1):5–32. doi: 10.1023/A:1010933404324
36. Hothorn T, Bühlmann P, Dudoit S, Molinaro A, Van Der Laan MJ. Survival ensembles. *Biostatistics* (2006) 7(3):355–73. doi: 10.1093/biostatistics/kxj011
37. Strobl C, Malley J, Tutz G. An Introduction to Recursive Partitioning An Introduction to Recursive Partitioning: Rationale. *Psychol Methods* (2009) 14 (4):323–38. doi: 10.1037/a0016973. Technical Report Number 55.
38. Strobl C, Boulesteix AL, Zeileis A, Hothorn T. Bias in random forest variable importance measures: Illustrations, sources and a solution. *BMC Bioinf* (2007) 8:25. doi: 10.1186/1471-2105-8-25
39. Strobl C, Boulesteix AL, Kneib T, Augustin T, Zeileis A. Conditional variable importance for random forests. *BMC Bioinf* (2008) 9:1–11. doi: 10.1186/1471-2105-9-307
40. Kuhn M, Wing J, Weston S, Williams A, Keefer C, Engelhardt A, et al. caret: Classification and Regression Training. (2018).
41. Zhou L, Wang Y, Li Y, Yap PT, Shen D. Alzheimer's Disease Neuroimaging Initiative (ADNI). Hierarchical anatomical brain networks for MCI prediction: Revisiting volumetric measures. *PloS One* (2011) 6(7):1–14. doi: 10.1371/journal.pone.0021935
42. Reid AT, Evans AC. Structural networks in Alzheimer ' s disease. *Eur Neuropsychopharmacol* . (2013) 23(1):63–77. doi: 10.1016/j.euroneuro.2012.11.010
43. Scheff SW, Price DA, Schmitt FA, Scheff MA, Mufson EJ. Synaptic Loss in the Inferior Temporal Gyrus in Mild Cognitive Impairment and Alzheimer Disease. *J Alzheimer's Dis* (2011) 24(3):547–57. doi: 10.3233/JAD-2011-101782
44. Jones BF, Barnes J, Uylings HBM, Fox NC, Frost C, Witter MP, et al. Differential regional atrophy of the cingulate gyrus in Alzheimer disease: A volumetric MRI study. *Cereb Cortex* (2006) 16(12):1701–8. doi: 10.1093/cercor/bhj105
45. Frisoni GB, Testa C, Zorzan A, Sabattoli F, Beltramello A, Soininen H, et al. Detection of grey matter loss in mild Alzheimer's disease with voxel based morphometry. *J Neurol Neurosurg Psychiatry* (2002) 73(6):657–64. doi: 10.1136/jnnp.73.6.657
46. Steven AE, Hyman BT, Van Hoesen GW. Neuropathologic Changes of the Temporal Pole in Alzheimer's Disease and Pick's Disease. *Arch Neurol* (1994) 51(2):145–50. doi: 10.1001/archneur.1994.00540140051014
47. Seeley WW, Crawford RK, Zhou J, Miller BL, Greicius MD. Neurodegenerative Diseases Target Large-Scale Human Brain Networks. *Neuron* (2009) 62(1):42–52. doi: 10.1016/j.neuron.2009.03.024
48. Montembeault M, Rouleau I, Provost JS, Brambati SM. Altered Gray Matter Structural Covariance Networks in Early Stages of Alzheimer's Disease. *Cereb Cortex* (2016) 26(6):2650–62. doi: 10.1093/cercor/bhv105
49. Spreng RN, Turner GR. Structural Covariance of the Default Network in Healthy and Pathological Aging. *J Neurosci* (2013) 33(38):15226–34. doi: 10.1523/JNEUROSCI.2261-13.2013
50. Fillmore PT, Phillips-Meek MC, Richards JE. Age-specific MRI brain and head templates for healthy adults from 20 through 89 years of age. *Front Aging Neurosci* (2015) 7(MAR):1–14. doi: 10.3389/fnagi.2015.00044
51. Huang CM, Lee SH, Hsiao IT, Kuan WC, Wai YY, Ko HJ, et al. Study-specific EPI template improves group analysis in functional MRI of young and older adults. *J Neurosci Methods* (2010) 189(2):257–66. doi: 10.1016/j.jneumeth.2010.03.021
52. Koini M, Duering M, Gesierich BG, Rombouts SARB, Ropele S, Wagner F, et al. Grey-matter network disintegration as predictor of cognitive and motor function with aging. *Brain Struct Funct* (2018) 0(0):0. doi: 10.1007/s00429-018-1642-0
53. Bijsterbosch J, Smith SM, Beckmann CF. *Introduction to resting state FMRI functional connectivity*. Oxford: Oxford University Press (2017).
54. Jovicich J, Czanner S, Han X, Salat D, van der Kouwe A, Quinn B, et al. MRI-derived measurements of human subcortical, ventricular and intracranial brain volumes: Reliability effects of scan sessions, acquisition sequences, data analyses, scanner upgrade, scanner vendors and field strengths. *NeuroImage [Internet]* (2009) 46(1):177–92. doi: 10.1016/j.neuroimage.2009.02.010

Conflict of Interest: The authors declare that the research was conducted in the absence of any commercial or financial relationships that could be construed as a potential conflict of interest.

frontiers in Aging Neuroscience

ORIGINAL RESEARCH
published: 12 June 2020
doi: 10.3389/fnagi.2020.00173

Neural Mechanisms of the Contextual Interference Effect and Parameter Similarity on Motor Learning in Older Adults: An EEG Study

Meysam Beik[1], *Hamidreza Taheri*[1]* *Alireza Saberi Kakhki*[1] *and Majid Ghoshuni*[2]

[1]*Motor Behavior Laboratory, Department of Motor Behavior, Faculty of Sport Sciences, Ferdowsi University of Mashhad, Mashhad, Iran,* [2]*Department of Biomedical Engineering, Islamic Azad University, Mashhad Branch, Mashhad, Iran*

The purpose of this study was to investigate the neural mechanisms of the contextual interference effect (CIE) and parameter similarity on motor learning in older adults. Sixty older adults (mean age, 67.68 ± 3.95 years) were randomly assigned to one of six experimental groups: blocked-similar, algorithm-similar, random-similar, blocked-dissimilar, algorithm-dissimilar, and random-dissimilar. Algorithm practice was a hybrid practice schedule (a combination of blocked, serial, and random practice) that switching between practice schedules were based on error trial number, ≤33%. The sequential motor task was used to record the absolute timing for the absolute timing goals (ATGs). In similar conditions, the participants' performance was near ATGs (1,350, 1,500, 1,650 ms) and in dissimilar conditions, they performed far ATGs (1,050, 1,500, 1,950 ms) with the same spatial sequence for all groups. EEG signals were continuously collected during the acquisition phase and delayed retention. Data were analyzed in different bands (alpha and beta) and scalp locations (frontal: Fp1, Fp2, F3, F4; central: C3, C4; and parietal: P3, P4) with repeated measures on the last factor. The analyses were included motor preparation and intertrial interval (motor evaluation) periods in the first six blocks and the last six blocks, respectively. The results of behavioral data indicated that algorithm practice resulted in medium error related to classic blocked and random practice during the acquisition, however, algorithm practice outperformed the classic blocked and random practice in the delayed retention test. The results of EEG data demonstrated that algorithm practice, due to optimal activity in the frontal lobe (medium alpha and beta activation at prefrontal), resulted in increased activity of sensorimotor areas (high alpha activation at C3 and P4) in older adults. Also, EEG data showed that similar conditions could affect the intertrial interval period (medium alpha and beta activation in frontal in the last six-block), while the dissimilar conditions could affect the motor preparation period (medium alpha and beta activation in frontal in the first six-block). In conclusion, algorithm practice can enhance motor learning and optimize the efficiency of brain activity, resulting in the achievement of a desirable goal in older adults.

Keywords: contextual interference effect, EEG, motor learning, optimal error, older adults, parameter similarity

OPEN ACCESS

Edited by:
Hans J. Grabe,
University of Greifswald, Germany

Reviewed by:
David Thornton,
Gallaudet University, United States
Bradley Jay Edelman,
Stanford University School of Medicine, United States
Pedro Ribeiro,
Federal University of Rio de Janeiro, Brazil

***Correspondence:**
Hamidreza Taheri
hamidtaheri@um.ac.ir

Received: *06 September 2019*
Accepted: *19 May 2020*
Published: *12 June 2020*

Citation:
Beik M, Taheri H, Saberi Kakhki A and Ghoshuni M (2020) Neural Mechanisms of the Contextual Interference Effect and Parameter Similarity on Motor Learning in Older Adults: An EEG Study. Front. Aging Neurosci. 12:173. doi: 10.3389/fnagi.2020.00173

INTRODUCTION

Motor learning is defined as the relatively permanent changes in the capacity for movement through practice or experience (Schmidt et al., 2018, p. 283). Therefore, learning may be highly dependent on practice conditions. One of the most frequent research topics in terms of the practice conditions is about how the multiple tasks or variations of a task are arranged in a practice session. This issue is examined under the contextual interference effect (CIE). The CIE states how different orders of task performance interfere with each other to affect the outcome of practice conditions. Task orders in blocked or random formations are known as low or high contextual interference. In blocked practice, the number of the same trials is repeated before shifting to the next set of different trials, while in the random practice, the performer is faced with different types of tasks, thus there is no chance to anticipate the characteristics of the next trial. The result of several studies has shown that the random practice results in poorer performance during acquisition but superior performance during retention and transfer compared to the blocked practice (Shea and Morgan, 1979; Magill and Hall, 1990; Brady, 1998). The result of studies has also indicated that older adults may benefit from this type of practice condition like younger performers (Lin et al., 2010, 2012; Pauwels et al., 2015, 2018; Sidaway et al., 2016; Chalavi et al., 2018). However, some studies did not show the superior performance of random practice during retention in older adults (de Souza et al., 2015). In this regard, other pieces of evidence showed that variables such as age, skill level, and learning style of learners can affect the CIE (Magill and Hall, 1990; Brady, 1998, 2008; Merbah and Meulemans, 2011), and optimal learning outcome is the result of interaction between the skill level of learner and task difficulty, known as challenge point framework (Guadagnoli and Lee, 2004). Computer-controlled practice based on error rate can be used to adjust the interaction between task difficulty and progress in skill level during the acquisition phase (Choi et al., 2008; Simon et al., 2008; Wilson et al., 2018; Wadden et al., 2019). Also, task similarity is another variable that may affect the CIE (Battig, 1966; Wood and Ging, 1991; Boutin and Blandin, 2010a). Similar and dissimilar tasks are defined according to the motor program- or the distance between parameters used in the same motor program (Magill and Hall, 1990; Boutin and Blandin, 2010a). There is a contradiction between similar and dissimilar conditions concerning CIE, so that some studies showed the superior performance in dissimilar conditions of random practice (Wood and Ging, 1991; Boutin and Blandin, 2010a), whereas another study revealed the superior performance in similar conditions of random practice (Boutin and Blandin, 2010b). Likely, the similar and dissimilar conditions are not themselves the reason for the discrepancy in the findings, but creating the optimal challenge point could be the possible reason. Possibly the beneficial effect of CIE can be seen in similar and dissimilar conditions both by creating the optimal challenge point using an algorithm-based practice schedule.

Motor learning causes different neurological changes in early and late phases of learning (Galván, 2010). The results of neurological studies indicate that even in a situation that the findings of younger vs. older adults are similar, they may have a different pattern of activation in their brain (Lin et al., 2012). Some of the changes in activation patterns of the brain in older adults are related to their optimal performance because it seems that these changes are as a compensation potential and neuroplasticity in the brain of older adults (Lin et al., 2012). Also, there is some evidence that the pattern of coding and retrieval in older adults is different from that of younger people. Therefore, it is likely that there are different neurological paths in younger adults compared to older counterparts, to perform a motor task (Lin et al., 2012). Given that the CIE influences motor learning, it, therefore, can be concluded that it also affects brain activities associated with effort and motor preparation (Lage et al., 2015; Frömer et al., 2016; Thürer et al., 2017; Henz et al., 2018). Some studies have shown that CIE is associated with dorsolateral prefrontal cortex (DLPFC) and primary motor area (M1) activity (Cohen et al., 2009; Wymbs and Grafton, 2009; Kantak et al., 2010; Lin et al., 2010; Lage et al., 2015). Henz et al. (2018) examined differential learning protocol and the CIE after learning a motor skill by applying electroencephalography (EEG) technique. The result indicated that the high CIE resulted in increasing the cognitive processing activities (increased beta and gamma waves in the frontal region). EEG is a brain imaging technique that has high temporal resolution and mediates spatial resolution. In this study, concerning the task, it was needed to use brain imaging techniques with a high temporal resolution to record brain activity. The studies have revealed that motor processing is often linked to beta oscillatory activity (Espenhahn et al., 2019; Schmidt et al., 2019). Learning requires plasticity and it is the balance between inhibitory and excitatory process in the brain reflected in the amplitude of frequencies, especial beta frequency (14–30 Hz) in the sensorimotor cortex (Espenhahn et al., 2019), and prefrontal cortex (PFC; Schmidt et al., 2019). In PFC, increased beta appeared at the end of the trial when working memory information needs to be erased (Schmidt et al., 2019). It was found that high CIE (i.e., random practice) results in a balance between inhibition and excitation networks in the brain (Chalavi et al., 2018). Furthermore, studies have shown that there is an optimal level of cognitive processing for optimal motor learning (Kahneman, 1973; Lin et al., 2008). Cognitive processing is related to alpha band (8–12 Hz) in the frontal lobe. The reduced alpha in frontal lobe reveals high cognitive processing and vice versa (Kropotov, 2010). However, it has been shown that random practice results in a high activation at prefrontal (e.g., DLPFC) and motor (e.g., M1) cortices (Lage et al., 2015), other studies have revealed that cognitive style and individual differences may influence EEG frequencies during information processing (Riding et al., 1997). According to the challenge point framework, individual differences in CIE can be covered by the interaction between skill level and task difficulty (Guadagnoli and Lee, 2004). Therefore, practice based on an optimal challenge point (i.e., algorithm practice) may affect EEG frequencies and motor outcomes. Although the neurological basis of contextual interference has been studied in previous research (Henz et al., 2018; for a review see Lage et al., 2015), it is hard to find a study

that addressed the brain activity in algorithm-based practice in older adults.

Two different theories attempt to describe the beneficiary high CIE: the reconstruction action plan hypothesis (forgetting-reconstructing) and the elaborative hypothesis (distinctive and meaningful processing). Concerning the first hypothesis, random practice results in forgetting and reconstruction of the action plan in working memory (Lee and Magill, 1985). The second hypothesis states that random practice results in more distinctive and deeper meaningful processing (Shea and Zimny, 1983). It appears that the emergence of these mechanisms in a practice session is different. The reconstruction of the action plan and elaborative hypotheses are formed at the first and the last practice session, respectively (Magill and Hall, 1990; Yuhua, 1994; Boutin and Blandin, 2010a). In studies conducted by Lin et al. (2008, 2010), the neural mechanisms involved in CIE were examined through transcranial magnetic stimulation (TMS) during the trial intervals. The result demonstrated that the random practice group with TMS utilized at the motor area showed performance decrement during the retention test. In another research study conducted by Cohen et al. (2009), the CIE was examined during the movement preparation using TMS. The result indicated that random practice plays a role only in movement preparation, but not in motor execution. In their study, Frömer et al. (2016) examined the effect of event-related potential (ERP) on motor preparation of CIE. The results indicated that although cognitive processing related to attention increased in high CIE during the early acquisition, the cognitive and motor processes were severely declined in delayed retention. Although the processing related to the CIE associated with the motor preparation and intertrial interval periods has been investigated in the previous studies (Lin et al., 2008, 2010; Cohen et al., 2009; Frömer et al., 2016), in the current study, we used a new practice schedule (i.e., algorithm-based practice) and evaluated the processing in a between- within the design. It is possible to evaluate the reconstruction of the action plan hypothesis (forgetting-reconstructing) and also the elaborative hypothesis in a more concise manner by using the EEG method.

Briefly, despite the neural examinations to investigate the CIE, earlier studies were not carefully designed to examine this effect based on their distinctive cognitive mechanisms for the motor preparation and intertrial interval (motor evaluation) periods. For the first time, this study was designed to compare the neurological mechanisms of both reconstruction and elaborative processing hypotheses separately, using a similarity variable. Also, to date, no study has investigated the effect of practice based on the challenge point (i.e., algorithm practice) on EEG frequencies and we examined a novel practice schedule based on the individual cognitive style on EEG bands, especially alpha and beta bands that are related to cognitive and motor processing (Kropotov, 2010; Espenhahn et al., 2019; Schmidt et al., 2019). Besides, this study adopted a between—within-group design to perform the statistical analysis in comparison with the analysis applied in the previous studies, which only used either a within-group design (Cohen et al., 2009; Wymbs and Grafton, 2009) or a between-group design (Lin et al., 2008, 2010). Therefore, the purpose of this study was to investigate the neurological foundation underlying CIE and parameter similarity on motor learning in older adults.

MATERIALS AND METHODS

Participants

Sixty healthy older adults (mean age, 67.68 ± 3.95 years; all men), right-handed (Edinburgh inventory; Oldfield, 1971), were enrolled in this study. Participants were randomly divided into six groups of blocked-similar (BS), algorithm-similar (AS), random-similar (RS), blocked-dissimilar (BD), algorithm-dissimilar (AD), or random-dissimilar (RD). Exclusion criteria were neurological disease (e.g., Parkinson), dementia [e.g., Alzheimer's disease, cognitive mild impairment; according to Montreal of cognitive assessment (MoCA with cut-off <26; Nasreddine et al., 2005)], uncorrected vision and inadequate sleep (sleep timing questionnaire; Monk et al., 2003). The written informed consent was obtained from all participants. They had no previous experience at the task and were unaware of the purpose of this study. The study protocol was approved by the Ethics Committee of Ferdowsi University of Mashhad (Code: IR.UM.REC.1397.013).

Apparatus and Procedure

Behavioral Section

The device used in this study was similar to that used by Boutin and Blandin (2010a). Hardware included a foam board 50 × 50 cm that contained nine keys with 6.5 cm diameter and 10 cm apart from each other (**Figure 1A**). The task was sequentially depressing the 2, 5, 6, 9 keys with the dominant (right) hand in Absolute Timing Goals (ATGs). ATGs were defined as the amount of time elapsed from depressing the first key (number two) to the last key (number nine). Participants had to perform three ATGs (1,350, 1,500, 1,650 ms) in a similar parameter and three ATGs (1,050, 1,500, 1,950 ms) in the dissimilar parameter. The 1,500 ms ATG was the mean of performance for the older adults based on a pilot study. The similar and dissimilar conditions were defined as a ±10% and ±30% difference from the mean ATG (1,500 ms), respectively (Boutin and Blandin, 2010a). A LabView-based (LabView, National Instrument 2018, Austin, TX, USA) custom software program was used for displaying the patterns, recording the responses, and switching the ATGs.

Participants performed all the experimental stages individually in a quiet room at the Motor Behaviour Laboratory. Every performer sat on an adjustable chair behind a table in front of the device and a monitor (**Figure 1B**). Every trial was started by releasing the Enter key of the numeric pad beside the device (**Figure 1A**). During the acquisition phase, participants performed 162 trials in 18 blocks (nine trials per block) and received delayed visual knowledge of results (KR) after accomplishing each trial. The procedure for performing one trial is presented in **Figure 2**. Each block was interspaced by 4 s rest intervals. Between every six-block of trials, there were 3 min rest to prevent fatigue. The participants were instructed to maintain the same time

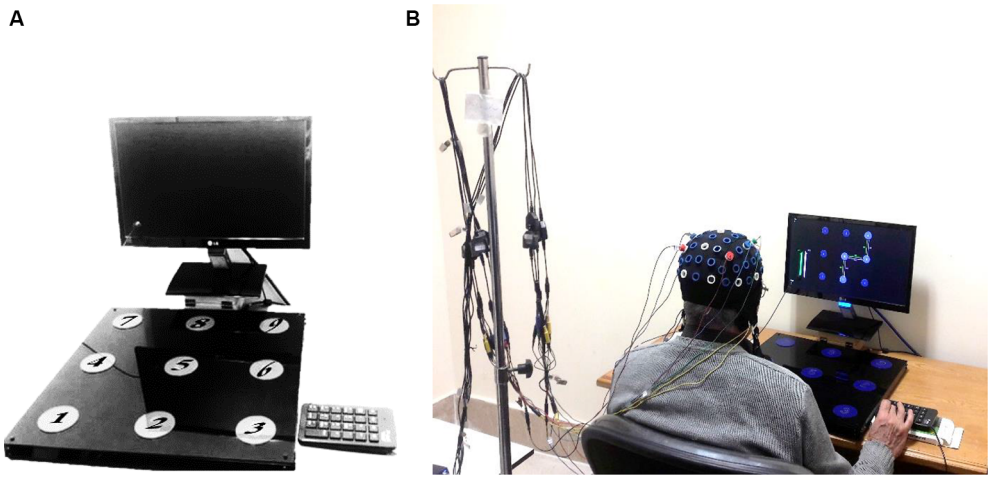

FIGURE 1 | Sequential timing device **(A)**, and procedure of experiment in progress **(B)**.

interval to move for pressing two consecutive keys to keep the relative timing fixed. Furthermore, the performers were encouraged to try their best performance in each trial as closely as to the ATGs. In a condition that participants missed a key, an error message was shown and that trial was immediately repeated.

During the acquisition, all participants practiced the tasks (ATGs) according to their grouping (see **Figure 3**). The blocked practice groups (in the similar and dissimilar conditions) performed 54 trials in each ATG (total 162 trials) in a blocked order (AAA, BBB, CCC), distributed in six blocks of nine trials. The order of practice of the ATGs was counterbalanced between the participants. The random practice groups (in the similar and dissimilar conditions) performed 18 blocks of nine trials in random order in each block with the constraints that each block included three trials of each ATG and no ATG was practiced in two consecutive trials (e.g., BCA, CAB, ACB). The algorithm practice was a combination of blocked, serial, and random practice schedules. The algorithm practice groups (in both of similarity conditions) were switched between blocked, serial- and random-practice orders (known as stages 1, 2, and 3, respectively) in forward and/or not backward (progression and/or not regression) concerning the number of error trial limitations in each block ($\leq$33%) and based on ATGs error range ($\pm$5%; **Table 1**). The algorithm practice was designed to maintain the level of functional task difficulty between a moderate to a high range. A trial was considered as an error if the difference between the performed timing with the ATG of that trial (the ideal time) was higher than $\pm$5 percent. For example, the error range for 1,500 ms ATG was between 1,425 and 1,575 ms, and if the performed timing was outside of this range (e.g., 1,420 or 1,580 ms), that trial was known as one error trial. The error limit (criterion level) was considered to be 33% of nine trials in each block. The procedure of algorithm practice was as follows. The participants started the practice with blocked order (the first block). At the end of the first block, if the number of error trials was equal or lower than three (33%), the blocked practice (stage 1) was switched to serial practice (stage 2) in the second block. If the number of error trials was higher than the criterion level (more than three trials), the first stage (i.e., blocked practice) was repeated. In the second stage, participants practiced the ATGs in the serial order and if the number of error trials was lower than—or equal to—the criterion, they moved to the third stage (i.e., random practice) in the next block. If their number of error trials was higher than the criterion, they moved to a stage that we called stage 1.5. In this stage, the practice order was blocked-serial (AABBCCABC) and this was to maintain the performers' motivation. In stage 1.5, if the number of errors was lower than—or equal to—the criterion, the participants were moved to the second stage (i.e., serial practice) in the next block, and if the number of errors was higher than the criterion, this stage was repeated. The practice order in the third stage was random. If the number of error trials was lower than—or equal to—the criterion, this stage was repeated, and if the number of errors was higher than the criterion, they moved to the second stage (see schematic representation in **Figure 4**). Note that switching the stages was depending on participants' performance (error rate at the end of each block) in the algorithm practice groups, therefore, task difficulty was individualized in regards to participant' progress (i.e., individualized optimal challenge point).

A delayed retention test was performed 24 h after the acquisition. During the retention, 12 trials with no-KR were performed. The mean ATG (1,500 ms) was used as the task during delayed retention (**Figure 3**).

EEG Recording

EEG brain activity was recorded by the 10-channel FlexComp differential amplifier and Biograph software (Version 5.0.3) developed by Thought Technology (TT) of Canada. Eight channels were used to record the EEG signals according to the international 10-20 system, placed on the scalp with two reference electrodes to the ipsilateral ears of the active electrode and two ground electrodes to the contralateral ears of the active

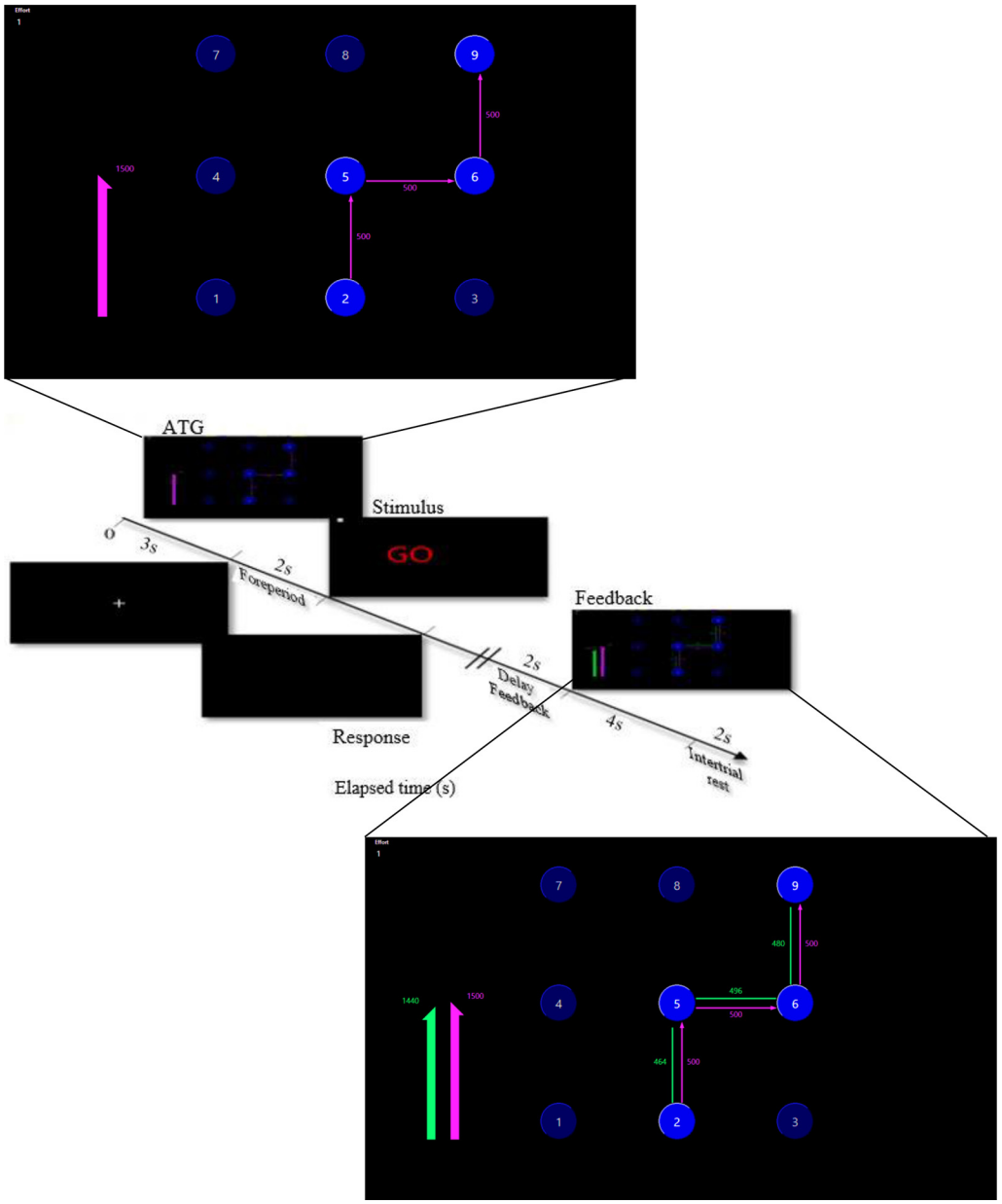

FIGURE 2 | Procedure of one trial.

electrode. One channel was also used for the TT AV-Sync sensor to determine the beginning of each section of a trial on the EEG signals. EEG data were documented in the Biograph database and processed using a custom script written in MATLAB (Version R2017b, MathWorks, USA). To collect signals, first, the scalp area was carefully scrubbed with NuPrep abrasive gel, and then the electrodes were pasted by utilizing Ten20 paste. Impedances of all electrodes were kept below 5 kΩ in all trials. The signals were amplified with a time constant of 2 s (high pass filter: 0.1 Hz; low pass filter: 64 Hz). Furthermore, a 50 Hz notch filter (for line noise) was enabled. EEG signals were continuously recorded and digitized at a sampling rate of 256 Hz. Absolute power was calculated for alpha (8–12 Hz) and beta (14–30 Hz) bands in frontal (Fp1, Fp2, F3, F4), central (C3, C4), and parietal (P3, P4) cortices in the acquisition phase and delayed retention test.

Data Analyses

Behavioral Analysis

Data analysis in the acquisition phase was performed by applying a three-way analysis of variance (ANOVA), 3 (practice schedule: blocked, algorithm, random) × 2 (similarity: similar, dissimilar) × 18 (blocks: 1–18) with repeated measures on the last

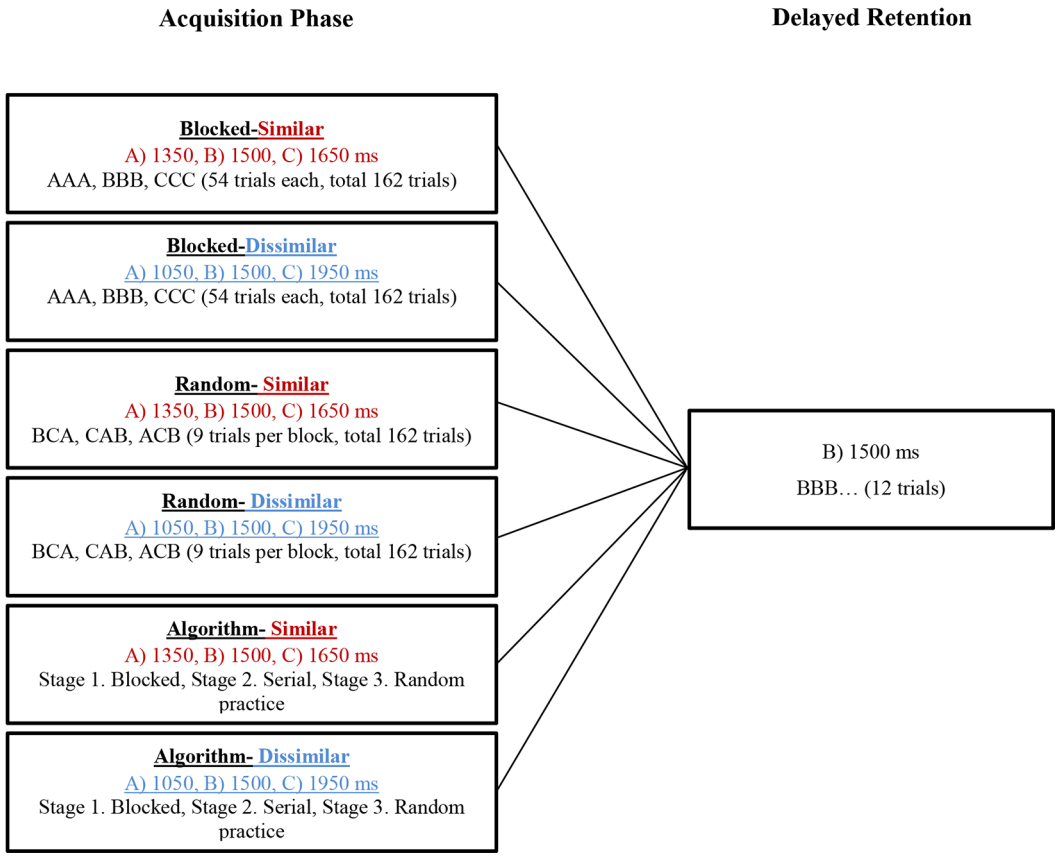

FIGURE 3 | The paradigm of the experimental groups in the acquisition phase and delayed retention. Note that algorithm practice was a combination of blocked, serial, and random practice that forward and/or not backward switching between stages was based on error rate (number of error trial ≤33% in each block based on error range of the ATGs, ±5%).

factor. Data analysis in delay retention test were also performed by univariate ANOVA, 3 (blocked, algorithm, random) × 2 (similar, dissimilar).

EEG Analysis

Data analysis in the acquisition phase were performed using three-way ANOVA, 3 (practice schedule: blocked, algorithm, random) × 2 (similarity: similar, dissimilar) × 8 (scalp location: Fp1, Fp2, F3, F4, C3, C4, P3, P4) with repeated measures on the last factor. Two periods of motor preparation and intertrial interval have been considered in data analysis during the acquisition phase, separately. The first and last six blocks of the acquisition was used to analyze the EEG signals in motor preparation and intertrial interval periods, respectively. The signals were analyzed during 2 s before movement execution in motor preparation period (Cohen et al., 2009; Frömer et al., 2016), and analyzed during 2 s immediately after the feedback in the intertrial interval period (Lin et al., 2008, 2010). Data analysis in the delayed retention test was similar to the acquisition phase performed using mixed-design ANOVA, 3 × 2 × 8 with repeated measures on the last factor in the motor preparation period.

According to the normality of data (Shapiro-Wilk test) and homogeneity of variance (Levene's test), we used the parametric test for the behavioral and EEG data (ANOVA with repeated measures). Also, Mauchly's test of sphericity was not violated, except for the main effect of the block in behavioral data that Greenhouse–Geisser correction was used. Bonferroni *post hoc* test was used to determine the means differences between the groups for both behavioral and EEG analyses. The significance level for all analyses was set at $p \leq 0.05$ using SPSS version 25 (SPSS Inc., Chicago, IL, USA).

RESULTS

Behavioral

Total Error (E)

Acquisition Phase

The ANOVA results showed that there were significant main effects for practice schedule ($F_{(2,54)} = 21.645$, $p < 0.001$, $\eta_p^2 = 0.445$), similarity ($F_{(1,54)} = 43.299$, $p < 0.001$, $\eta_p^2 = 0.445$), and block ($F_{(10.73,579.58)} = 22.827$, $p < 0.001$, $\eta_p^2 = 0.297$). In addition, there was a significant interaction effect of practice schedule × similarity ($F_{(2,54)} = 4.435$, $p = 0.016$, $\eta_p^2 = 0.141$).

TABLE 1 | The error range of absolute timing goals (ATGs) in algorithm practice schedule groups.

Group	Error range				
	1,350 ms (±67.5)	1,500 ms (±75)	1,650 ms (±82.5)	1,050 ms (±52.5)	1,950 ms (±97.5)
Algorithm-Similar	1,282.5–1,417.5 ms	1,425–1,575 ms	1,567.5–1,732.5 ms	*	*
Algorithm-Dissimilar	*	1,425–1,575 ms	*	997.5–1,102.5 ms	1,852.5–2,047.5 ms

**Lack of existence that ATG in algorithm similar/dissimilar groups.*

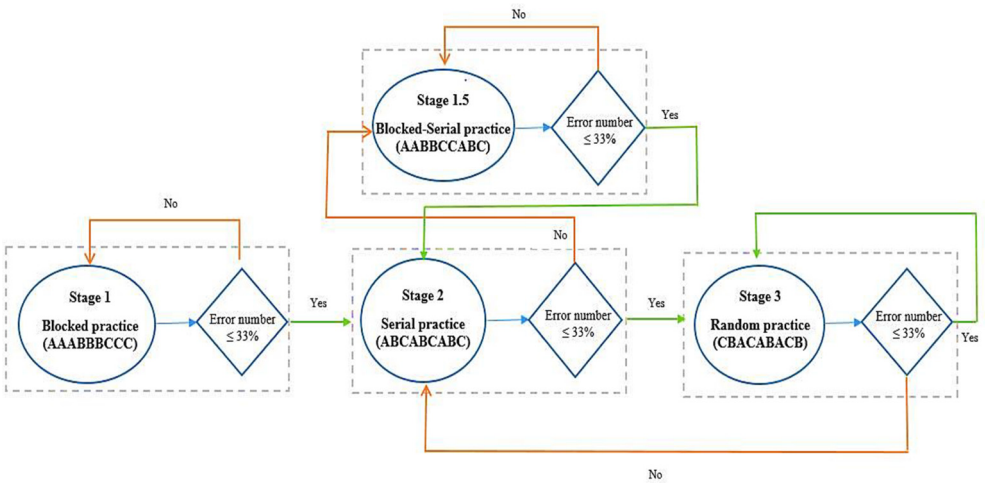

FIGURE 4 | Computer algorithm and how to change the stages in the algorithm practice schedule. Follow the arrows in regards to Yes/No.

No significant interaction was found between the block and other factors (all $F < 1$). *Post hoc* test for interaction effect showed that there were significant differences between the RD and AD groups compared to BD, BS, AS, and RS groups (all $p < 0.001$), but no significant difference was found between the RD and AD groups ($p > 0.05$). Also, there was no significant differences among BS, AS, RS, and BD groups (all $p > 0.05$). A comparison of means showed that RD group had more error than other groups (means: RD = 84.77, AD = 76.09, BD = 49.64, RS = 54.02, AS = 53.17, BS = 41.41; see **Figure 5A**).

Delayed Retention

The results of ANOVA showed that the main effects of practice schedule ($F_{(2,54)} = 63.552$, $p < 0.001$, $\eta_p^2 = 0.702$), similarity ($F_{(1,54)} = 15.077$, $p < 0.001$, $\eta_p^2 = 0.218$), were significant but the interaction effect of practice schedule × similarity ($F_{(2,54)} = 1.477$, $p = 0.237$, $\eta_p^2 = 0.052$), were not significant. The *post hoc* test for the main effect of practice schedule showed that there were significant differences between the algorithm practice compared with blocked and random practice schedules ($p < 0.001$ and $p = 0.002$, respectively). As can be seen in **Figure 5A**, a comparison of means showed that the algorithm practice had lower error than blocked and random practice (means: algorithm = 62.88 ms, random = 84.79 ms, and blocked = 128.90 ms). Also, the mean comparisons showed that similar conditions had lower error than dissimilar conditions (means: similar = 82.73 ms, dissimilar = 101.65 ms).

EEG

Acquisition Phase

Motor Preparation Period

Alpha Band: the results of ANOVA showed that there were significant main effects of practice schedule ($F_{(2,54)} = 7.855$, $p = 0.001$, $\eta_p^2 = 0.225$), similarity ($F_{(1,54)} = 5.023$, $p = 0.029$, $\eta_p^2 = 0.085$), location ($F_{(7,378)} = 11.457$, $p < 0.001$, $\eta_p^2 = 0.175$), and interaction effects of location × practice schedule ($F_{(14,378)} = 47.455$, $p < 0.001$, $\eta_p^2 = 0.637$), location × similarity ($F_{(7,378)} = 13.383$, $p < 0.001$, $\eta_p^2 = 0.199$), and location × practice schedule × similarity ($F_{(14,378)} = 3.536$, $p < 0.001$, $\eta_p^2 = 0.116$), but there was no significant effect of practice schedule × similarity ($F_{(2,54)} = 1.263$, $p = 0.291$, $\eta_p^2 = 0.045$). *Post hoc* test of interaction effect of location × practice schedule × similarity revealed that there were significant differences between the RD group and other groups in frontal lobe (all $p < 0.001$). *Post hoc* test for interaction also indicated that there were significant differences between the AD compared to other groups in C3 (all $p < 0.05$). As shown in **Figure 6A**, the mean comparisons of frontal lobe showed that the RD had less activity than other groups (means: RD = 16.01, AD = 19.78, RS = 19.89, AS = 22.77, BD = 25.56, and BS = 27.07). Also, the mean comparisons of C3 area showed that the AD group had more activity than other groups (means: AD = 31.58, RD = 27.36, RS = 22.94, AS = 22.71, BS = 18.14, and BD = 17.65).

Beta Band: the results of ANOVA showed that there were significant main effects of the practice schedule ($F_{(2,54)} = 60.240$,

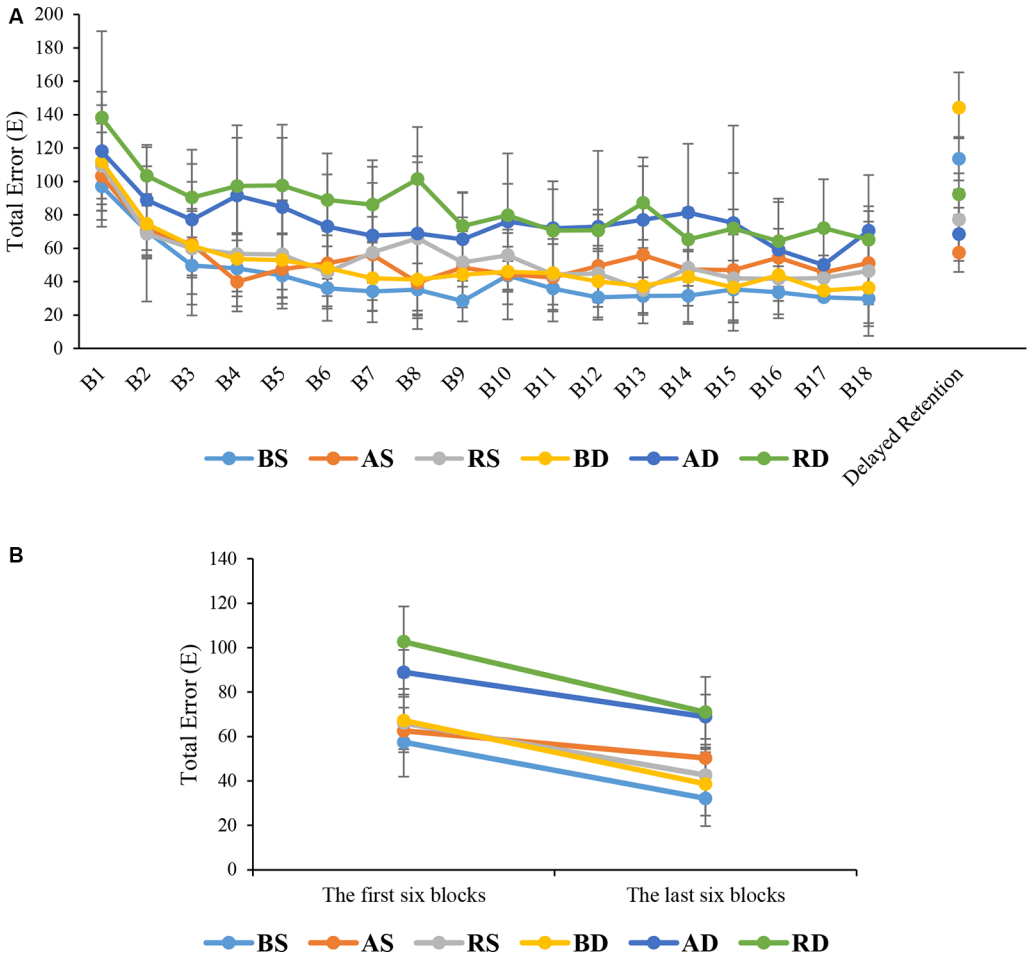

FIGURE 5 | Means and standard deviations of the total error of the groups in **(A)** different phases and **(B)** the first and last six blocks (for a direct comparison with EEG data).

$p < 0.001$, $\eta_p^2 = 0.691$), similarity ($F_{(1,54)} = 20.800$, $p < 0.001$, $\eta_p^2 = 0.278$), location ($F_{(7,378)} = 44.645$, $p < 0.001$, $\eta_p^2 = 0.453$), and interaction effects of location × practice schedule ($F_{(14,378)} = 45.273$, $p < 0.001$, $\eta_p^2 = 0.626$), location × similarity ($F_{(7,378)} = 4.566$, $p < 0.001$, $\eta_p^2 = 0.078$), and location × practice schedule × similarity ($F_{(14,378)} = 2.678$, $p = 0.001$, $\eta_p^2 = 0.090$), but no significant effect was observed for practice schedule × similarity $F < 1$. *Post hoc* test for the interaction effect for the location × practice schedule × similarity revealed that there were significant differences among the RD group and other groups in frontal lobe (all $p < 0.001$). As can be seen in **Figure 6B**, the mean comparisons showed that the RD group had more activity than other groups (means: RD = 26.99, AD = 21.98, RS = 22.25, AS = 19.03, BD = 11.12, and BS = 9.75).

Intertrial Interval Period

Alpha Band: the results of ANOVA showed that there were significant main effects of practice schedule ($F_{(2,54)} = 9.442$, $p < 0.001$, $\eta_p^2 = 0.259$), location ($F_{(7,378)} = 60.985$, $p < 0.001$, $\eta_p^2 = 0.530$), and interaction effects of practice schedule × similarity ($F_{(2,54)} = 5.303$, $p = 0.008$, $\eta_p^2 = 0.164$), location × practice schedule ($F_{(14,378)} = 91.204$, $p < 0.001$, $\eta_p^2 = 0.772$), location × similarity ($F_{(7,378)} = 22.667$, $p < 0.001$, $\eta_p^2 = 0.296$), and location × practice schedule × similarity ($F_{(14,378)} = 5.899$, $p < 0.001$, $\eta_p^2 = 0.179$), but there was no significant main effect of similarity ($F_{(1,54)} = 1.851$, $p = 0.179$, $\eta_p^2 = 0.033$). *Post hoc* test for interaction effect of location × practice schedule × similarity revealed that there were significant differences among the RS group and BS, BD, AD, and RD groups in frontal lobe (all $p < 0.001$), but no significant difference was found between RS and AS groups ($p = 0.069$). *Post hoc* test for interaction effect also indicated that the AS group performed significantly different from the other groups in C3 (all $p < 0.05$) and P4 (all $p < 0.05$). As shown in **Figure 6A**, comparison of the mean values in the frontal lobe showed that the RS group had less activity than other groups (means: RS = 13.28, AS = 15.43, RD = 18.45, AD = 19.82, BS = 26.35, and BD = 27.12).

Beta Band: the results of ANOVA showed that there were significant main effects of practice schedule ($F_{(2,54)} = 48.740$,

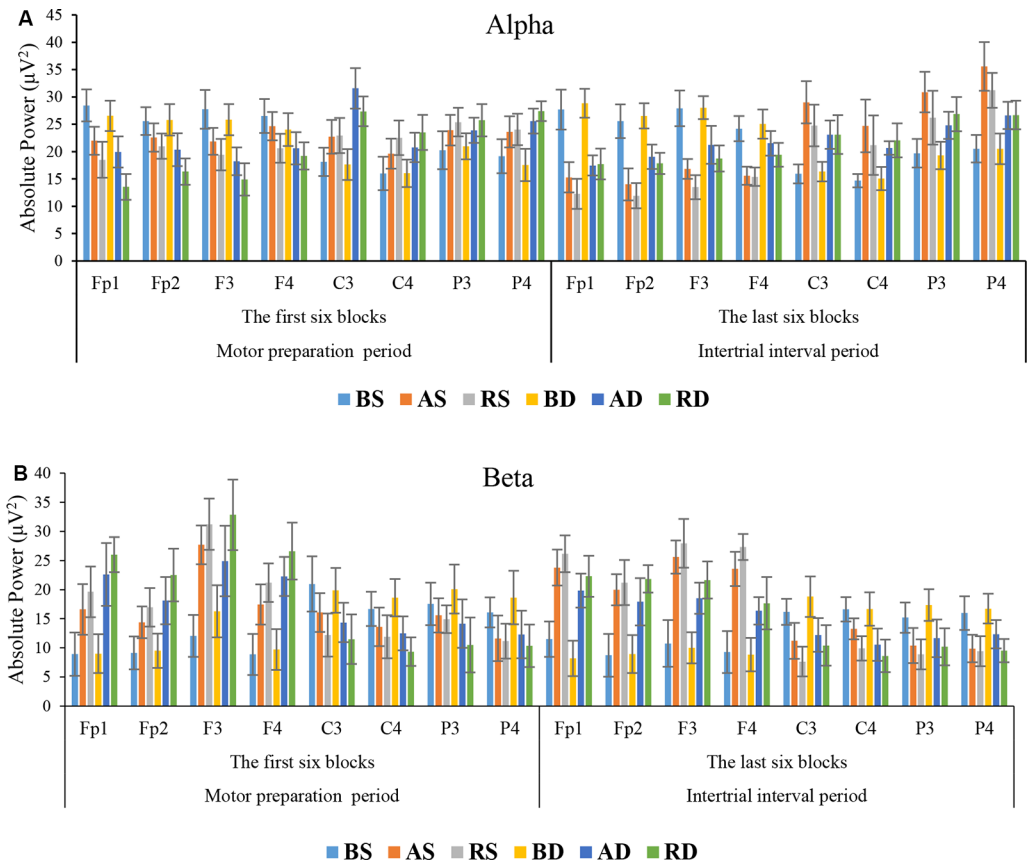

FIGURE 6 | Means and standard deviations power of the groups in **(A)** alpha band and **(B)** beta band in different scalp locations at the acquisition phase.

$p < 0.001$, $\eta_p^2 = 0.644$), similarity ($F_{(1,54)} = 22.490$, $p < 0.001$, $\eta_p^2 = 0.294$), location ($F_{(7,378)} = 60.577$, $p < 0.001$, $\eta_p^2 = 0.529$), and interaction effects of the practice schedule × similarity ($F_{(2,54)} = 7.075$, $p = 0.002$, $\eta_p^2 = 0.208$), location × practice schedule ($F_{(14,378)} = 80.347$, $p < 0.001$, $\eta_p^2 = 0.748$), location × similarity ($F_{(7,378)} = 15.538$, $p < 0.001$, $\eta_p^2 = 0.223$), and location × practice schedule × similarity ($F_{(14,378)} = 2.187$, $p = 0.008$, $\eta_p^2 = 0.075$). *Post hoc* test for interaction effect of location × practice schedule × similarity revealed that there were significant differences among the RS group and other groups in frontal lobe (all $p < 0.05$). The mean comparisons showed that the RS group had more activity than other groups (means: RS = 25.66, AS = 23.23, RD = 20.86, AD = 18.17, BS = 10.08, and BD = 9.01; see **Figure 6B**).

Delayed Retention

Alpha Band: the results of ANOVA showed that there were significant main effects of practice schedule ($F_{(2,54)} = 73.454$, $p < 0.001$, $\eta_p^2 = 0.731$), location ($F_{(7,378)} = 164.346$, $p < 0.001$, $\eta_p^2 = 0.753$), and interaction effect of location × practice schedule ($F_{(14,378)} = 18.566$, $p < 0.001$, $\eta_p^2 = 0.407$), but there were no significant effects of similarity, and interaction of location × similarity, location × practice schedule × similarity, and practice schedule × similarity, all $F < 1$. *Post hoc* test for interaction effect of location × practice schedule revealed that there were significant differences between the algorithm groups and other groups at C3 ($p < 0.001$ and $p = 0.035$, respectively) and P4 ($p < 0.001$ and $p = 0.034$, respectively). The mean comparisons showed that the algorithm groups had more activity than other groups (means at C3: algorithm = 28.22, random = 25.55, blocked = 20.29; means at P4: algorithm = 29.44, random = 27.20, blocked = 19.01; see **Figure 7A**).

Beta Band: the results of ANOVA showed significant main effects of practice schedule ($F_{(2,54)} = 3.471$, $p = 0.038$, $\eta_p^2 = 0.114$), location ($F_{(7,378)} = 11.025$, $p < 0.001$, $\eta_p^2 = 0.170$), and interaction effects of location × practice schedule ($F_{(14,378)} = 6.398$, $p < 0.001$, $\eta_p^2 = 0.192$), but the main effects of similarity ($F_{(1,54)} = 1.183$, $p = 0.182$, $\eta_p^2 = 0.033$), and interaction effects of practice schedule × similarity location × similarity all $F < 1$, and location × practice schedule × similarity were not significant ($F_{(14,378)} = 1.177$, $p = 0.291$, $\eta_p^2 = 0.042$). The *post hoc* test for interaction effect of location × practice schedule revealed significant differences between the random and algorithm practice as compared with the blocked practice in frontal lobe (all $p < 0.001$), but no significant difference was found between the random and algorithm practice schedules ($p > 0.05$). The mean comparisons indicated that the random groups had more activity

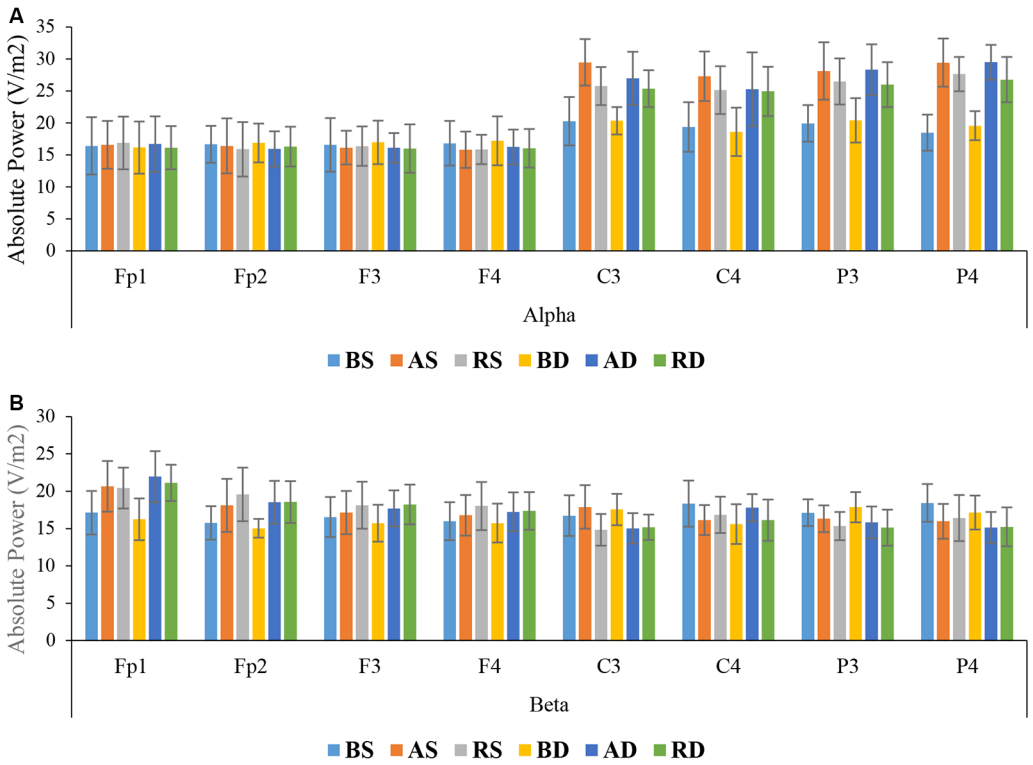

FIGURE 7 | Means and standard deviations power of the groups for **(A)** alpha band and **(B)** beta band in different scalp locations in the delayed retention test.

than other groups (means: random = 18.92, algorithm = 18.51, blocked = 16.02; see **Figure 7B**).

DISCUSSION

The purpose of this study was to investigate the neural mechanisms of CIE and parameter similarity on motor learning in older adults. The results of this study confirmed the previous findings of other studies demonstrating that high CI (random practice) can increase the activities of cognitive, sensory, and motor regions of the brain compared to blocked practice (Cross et al., 2007; Lin et al., 2008, 2010, 2013; Cohen et al., 2009; Wymbs and Grafton, 2009; Thürer et al., 2017; Henz et al., 2018). The older adults also benefit from the high CI in reducing their error during the retention test and also their cognitive, sensory, and motor areas activated more than blocked practice. In their study, Henz et al. (2018) demonstrated that random practice increased beta wave in the frontal lobe. Other studies applied TMS or fMRI reported that random practice can increase DLPFC—an area related to the cognitive processing and motor preparation—and M1 activity (for a review see Lage et al., 2015).

The results of this study indicated that algorithm practice as an optimal level of error led to an optimal level of activation in the frontal lobe (medium levels of alpha and beta activities) in motor preparation and intertrial interval (motor evaluation) periods of performing a motor task. This optimal level of activation in the frontal resulted in a maximized of sensory and motor excitation (an increase of alpha wave in parietal and central regions). The trend of the first and last six blocks for total error showed that in similar and dissimilar conditions, the algorithm practice had moderate error than other groups. These results are comparable with EEG results showing moderate alpha and beta waves in the frontal area during algorithm practice compared with other practice schedules (see **Figures 5B**, **6A,B**). Also, the total error decreased in the last six blocks in the intertrial interval and EEG results revealed the RS had a moderate activity of alpha and beta in the frontal area and maximum activity of alpha in C3 and P4 compared with the other groups. In the first six blocks in motor preparation periods, the RD had a moderate error and moderate alpha and beta activation and maximum activation of alpha at C3 (see **Figures 5B**, **6A,B**). Cognitive control of motor processing is directly associated with the increase of beta and reduction of alpha waves in the frontal lobe (Kropotov, 2010; Henz et al., 2018). Also, the increase in the alpha wave in parietal and central regions is an indicator of an increase in sensory integration and motor memory (Kanayama et al., 2015; Henz et al., 2018). In PFC, the assessment of beta band in motor preparation and intertrial interval periods showed that the random practice resulted in the highest beta activity and the algorithm based practice resulted in a moderate beta activity while the blocked practice resulted in the lowest

beta activity in this area. Studies have shown that increased beta in PFC is related to the working memory process of movement. It is suggested that this increase is an index of erased working memory (Lundqvist et al., 2018; Schmidt et al., 2019). Therefore, even though an increase in cognitive effort results in the improvement of memory coding and decoding, the studies have demonstrated that there is a desirable level of attention allocation and cognitive processes based on the task difficulties and skill level of the learner for the optimal motor learning output (Kahneman, 1973; Guadagnoli and Lee, 2004; Lin et al., 2008).

The findings obtained from the brain waves confirm the cognitive flexibility (Berry et al., 2016), cognitive load (Sweller et al., 2019), and schema (Schmidt, 1975) theories about the CIE. Our results indicated that algorithm practice optimized alpha and beta band in frontal and maximized alpha band in sensorimotor regions (at C3 and P4). The absolute power of alpha and beta in frontal areas for algorithm schedule was between the random (the highest power) and blocked (the lowest power) schedules. Also, the alpha power in sensorimotor regions (C3 and P4) was maximized during the algorithm practice compared with other schedules. These EEG results should be considered along with the error data. The results of behavioral data showed that during acquisition, the algorithm schedules resulted in an error range between the blocked (the lowest error range) and the random (the highest error range) schedules. This type of brain activation and this range of error during the algorithm schedule resulted in the lowest error range during the retention test. According to these results one can conclude that during the algorithm practice an optimal level of cognitive processing occurred, resulted in optimal motor learning during retention (Kahneman, 1973; Guadagnoli and Lee, 2004; Lin et al., 2008). Cognitive flexibility in aging is related to frontoparietal connectivity (Berry et al., 2016), and increased beta and alpha bands reflect plasticity in memory (Espenhahn et al., 2019). Lin et al. (2013) found that interleaved practice enhances skill learning due to increased frontoparietal networks. According to cognitive load theory, working memory has a limited capacity for information processing (Sweller et al., 2019). Possibly, the algorithm practice with providing optimal cognitive processing facilitated optimal cognitive load in the frontal lobe (medium alpha and beta waves). Also, the findings of this study revealed that in similar conditions, beta activity increased in frontal, and alpha activity increased in central and parietal lobes at the end of acquisition, while in dissimilar conditions, beta activity enhanced in frontal, and alpha activity enhanced in central and parietal lobes at the beginning of acquisition. According to the schema theory, there are two types of memory involved in learning a motor task: the recall memory that is in charge in producing the movement and the recognition memory that is in charge of evaluating the movement (Schmidt, 1975). The distinction between the reconstruction and elaborative processing hypotheses based on the neural mechanism can be explained by the views they adopt. Based on our findings, both mechanisms of reconstruction and elaboration emerged in different stages of practice. Both of these are cognitive processes: the reconstruction hypothesis during motor preparation and before the performance recalls the movement memory (reinforcing the recall memory) and elaborative hypothesis is in charge for evaluation between the course of trials and comparing inter-trial performances (reinforcement of recognition memory). In a study conducted by Lin et al. (2008, 2010) the TMS was applied during the interval between trials to impair M1 region in different practice arrangements. The results confirmed strongly the elaborative hypothesis due to TMS-Random practice condition, however, the reconstruction hypothesis was not supported because of the lack of enhancement of learning in TMS-Blocked practice condition. Accordingly, in other studies, TMS was applied to impair M1 during the movement preparation period and the result indicated that random practice condition showed performance decrement during the delayed retention test and consolidation of performance was detected in No-TMS and Sham-TMS groups (Cohen et al., 2009; Wymbs and Grafton, 2009). The difference in performances may be attributed to two mechanisms that can improve memory as follows. One is the space effect and the other is CIE. Therefore, it appears that contextual interference has more instability effect on memory compared to the space effect and increases the long retention and generalizability (Robertson, 2018). Blocked-TMS groups have experienced space effect to reconstruct the action plan in the M1 region, while the Random-TMS group results in interference effect for different action plans. Therefore, it may be plausible to explain why the reconstruction hypothesis of Lin et al. (2008, 2010) was less supported. The difference between space and interference effects may be due to the memory formations. Consequently, the researcher proposed the conceptual model for the CIE (**Figure 8**).

Also, two paths for motor memory encoding and retrieval in motor tasks have been discussed in the literature review, indicating the frontal to central and parietal to central pathways (Verwey et al., 2015). In other words, the excitation of the motor region takes place through two pathways. This study showed that algorithm practice optimized these pathways with an optimal activation of alpha and beta waves in frontal, and high activation of motor area (high alpha at central region) that these changes could be related to motor memory encoding (Lin et al., 2013; Henz et al., 2018). Also, the results showed that algorithm practice resulted in the activation of sensorimotor regions (high alpha power in central and parietal) that could be related to motor memory retrieval (Lin et al., 2013; Henz et al., 2018). Furthermore, our results indicated that the interaction effect of practice arrangement and similarity provides a different neurological mechanism. At the beginning of the random practice group, the highest levels of activities occurred in the frontal lobe (increase in beta power) and the algorithm-dissimilar group had the highest level of activity in the motor area (an increase of alpha power), however, at the end of practice, the random-similar group had the highest level of activity in the frontal lobe and algorithm-similar group exhibited the highest level of activity in the sensory and motor regions. In fact, in similar conditions, most of the parietal

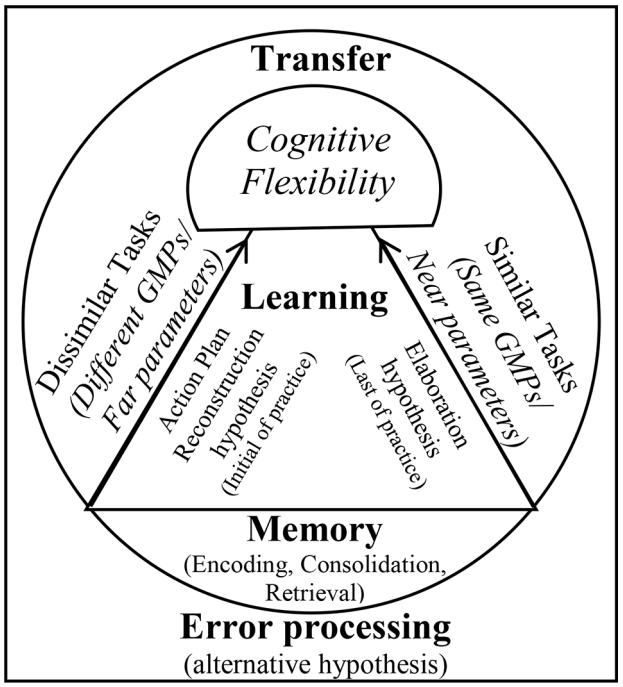

FIGURE 8 | Proposed Contextual Interference Model (CIM).

and frontal regions during the intertrial interval period were activated through the elaboration mechanism at the end of acquisition (the last six-block), resulting in a maximum level of activation in motor regions (high alpha at C3 and P4). However, in the dissimilar conditions, most of activities in frontal lobe led to the maximum level of activity of alpha band in contralateral motor region (C3) throughout reconstructing the action plan during the early phase of acquisition processes (the first six-block).

The results obtained from EEG data in this study confirmed the findings of previous studies demonstrating that restructuring action plan develops at the early stage of acquisition, while the elaborative hypothesis develops at the last stage of acquisition (Yuhua, 1994; Brady, 1998; Boutin and Blandin, 2010a), and the practice amount affects this process (Shea et al., 1990). In similar conditions, the EEG results showed that the high activation of the beta band in frontal increased at the end of the acquisition. In similar conditions due to close ATGs, the elaborative mechanism was needed. While, in dissimilar conditions due to far ATGs, high activation of beta in frontal increased at the early of acquisition (reconstructive mechanism). According to the schema theory, the parameterization of movement occurs during the practice process as a whole. However, according to the parameter remapping phenomenon, with the extension of practice, parameterization occurs separately (Rosenbaum et al., 1986; Verwey et al., 2015). Accordingly, this may be the reason for introducing a generalized parameter for similar parameters to each other in the early practice (similar conditions). EEG studies have shown that absolute timing is specified before muscle group/effector (Leuthold and Jentzsch, 2011) and absolute force (Shea and Wulf, 2005).

Also, the results of this study showed that contralateral motor region was more activated (high alpha at C3) during performing the task with the dominant (right) hand which were consistent with the findings of previous studies suggesting that motor regions were more activated in the contralateral limb of performers (alpha wave at C3; Lin et al., 2008, 2010). However, other studies reported that more activities took place in the motor region of the ipsilateral limb (Cohen et al., 2009; Wymbs and Grafton, 2009). One of the reasons for these inconsistent findings may be related to the use of dominant/non-dominant hand in these studies during the task execution, while all of the participants in these inconsistent studies were right-handed. Therefore, despite the contradictory findings in terms of the increase of activity in the ipsilateral or contralateral limb, the similarity of these studies is associated with the increase in activity of the left hemisphere of the brain and right-handedness of performers. The results of some studies have indicated that the left hemisphere of motor cortex is dominant in motor learning, particularly when the non-dominant hand is utilized, and the complexity of the movement increases when the non-dominant hand is used (Kawashima et al., 1993; Ziemann and Hallett, 2001; Suzuki et al., 2013).

Studies have shown that practice under the high CI when impairing the M1 region using TMS immediately after the acquisition phase resulted in a decrement of performance in a practice session. After one night of rest, it did not affect retention test, while disturbance using TMS before the acquisition phase resulted in performance decrement in delayed retention test even after a night sleep (Wymbs and Grafton, 2009). Therefore, it appears that high CI results in more flexible neural traces that can facilitate coding, storing, and retrieval and make motor-memory less vulnerable to interference and time passing. However, the behavioral and neural results of our study indicated that the optimal level of interference based on a performance algorithm and optimal error rate resulted in the highest efficiency in performance and brain activity.

CONCLUSION

This study showed that algorithm-based practice resulted in the performance enhancement of motor learning in elderly learners. Also, our findings demonstrated that algorithm-based practice led to an optimal activity in sensorimotor areas due to optimal cognitive processes involvement. Alpha and beta bands are related to motor performance (Espenhahn et al., 2019; Schmidt et al., 2019). This study showed that algorithm practice optimized alpha and beta band in frontal (as cognitive processing center) and maximized activation of sensorimotor regions (at C3 and P4). However, the random practice showed higher activation of alpha and beta bands in the prefrontal lobe, but evidence has revealed that optimal activation of cognitive processing results in optimal motor learning (Kahneman, 1973; Guadagnoli and Lee, 2004; Lin et al., 2008) Furthermore, EEG result revealed that task similarity affects the activation of beta at early or

late of the acquisition. In dissimilar conditions, increased beta activity in frontal lobe was observed at the early of acquisition, while in similar conditions, it was seen at the late of acquisition. Future studies need to investigate the rehabilitation and clinical applications of this type of practice to increase the efficiency of the practice.

DATA AVAILABILITY STATEMENT

The datasets generated for this study are available on request to the corresponding author.

ETHICS STATEMENT

The studies involving human participants were reviewed and approved by Ethics Committee of Ferdowsi University of Mashhad (code: IR.UM.REC.1397.013). The patients/participants provided their written informed consent to participate in this study.

AUTHOR CONTRIBUTIONS

MB, HT, and AS designed the experiment, and MB performed the experiment. All authors contributed to analyze the data and MB wrote the manuscript. All authors approved the final version of the manuscript.

ACKNOWLEDGMENTS

We thank all of the older adults who participated in this study. This research is part of Meysam Beik's dissertation.

REFERENCES

Battig, W. F. (1966). Evidence for coding processes in "rote" paired-associate learning. *J. Verbal Learn. Verbal Behav.* 5, 177–181.

Berry, A. S., Shah, V. D., Baker, S. L., Vogel, J. W., O'Neil, J. P., Janabi, M., et al. (2016). Aging affects dopaminergic neural mechanisms of cognitive flexibility. *J. Neurosci.* 36, 12559–12569. doi: 10.1523/JNEUROSCI.0626-16.2016

Boutin, A., and Blandin, Y. (2010a). Cognitive underpinnings of contextual interference during motor learning. *Acta Psychol.* 135, 233–239. doi: 10.1016/j.actpsy.2010.07.004

Boutin, A., and Blandin, Y. (2010b). On the cognitive processes underlying contextual interference: contributions of practice schedule, task similarity and amount of practice. *Hum. Mov. Sci.* 29, 910–920. doi: 10.1016/j.humov.2010.07.011

Brady, F. (1998). A theoretical and empirical review of the contextual interference effect and the learning of motor skills. *Quest* 50, 266–293.

Brady, F. (2008). The contextual interference effect and sport skills. *Percept. Mot. Skills* 106, 461–472. doi: 10.2466/pms.106.2.461-472

Chalavi, S., Pauwels, L., Heise, K.-F., Adab, H. Z., Maes, C., Puts, N. A. J., et al. (2018). The neurochemical basis of the contextual interference effect. *Neurobiol. Aging* 66, 85–96. doi: 10.1016/j.neurobiolaging.2018.02.014

Choi, Y., Qi, F., Gordon, J., and Schweighofer, N. (2008). Performance-based adaptive schedules enhance motor learning. *J. Mot. Behav.* 40, 273–280. doi: 10.3200/JMBR.40.4.273-280

Cohen, N. R., Cross, E. S., Wymbs, N. F., and Grafton, S. T. (2009). Transient disruption of M1 during response planning impairs subsequent offline consolidation. *Exp. Brain Res.* 196, 303–309. doi: 10.1007/s00221-009-1838-x

Cross, E. S., Schmitt, P. J., and Grafton, S. T. (2007). Neural substrates of contextual interference during motor learning support a model of active preparation. *J. Cogn. Neurosci.* 19, 1854–1871. doi: 10.1162/jocn.2007.19.11.1854

de Souza, M. G. T. X., Nunes, M. E. S., Corrêa, U. C., and dos Santos, S. (2015). The contextual interference effect on sport-specific motor learning in older adults. *Hum. Mov.* 16, 112–118. doi: 10.1515/humo-2015-0036

Espenhahn, S., van Wijk, B. C. M., Rossiter, H. E., de Berker, A. O., Redman, N. D., Rondina, J., et al. (2019). Cortical beta oscillations are associated with motor performance following visuomotor learning. *NeuroImage* 195, 340–353. doi: 10.1016/j.neuroimage.2019.03.079

Frömer, R., Stürmer, B., and Sommer, W. (2016). (Don't) mind the effort: effects of contextual interference on ERP indicators of motor preparation. *Psychophysiology* 53, 1577–1586. doi: 10.1111/psyp.12703

Galván, A. (2010). Neural plasticity of development and learning. *Hum. Brain Mapp.* 31, 879–890. doi: 10.1002/hbm.21029

Guadagnoli, M. A., and Lee, T. D. (2004). Challenge point: a framework for conceptualizing the effects of various practice conditions in motor learning. *J. Mot. Behav.* 36, 212–224. doi: 10.3200/JMBR.36.2.212-224

Henz, D., John, A., Merz, C., and Schöllhorn, W. I. (2018). Post-task effects on EEG brain activity differ for various differential learning and contextual interference protocols. *Front. Hum. Neurosci.* 12:19. doi: 10.3389/fnhum.2018.00019

Kahneman, D. (1973). *Attention and Effort.* Pennsylvania, PA: Citeseer.

Kanayama, N., Kimura, K., and Hiraki, K. (2015). Cortical EEG components that reflect inverse effectiveness during visuotactile integration processing. *Brain Res.* 1598, 18–30. doi: 10.1016/j.brainres.2014.12.017

Kantak, S. S., Sullivan, K. J., Fisher, B. E., Knowlton, B. J., and Winstein, C. J. (2010). Neural substrates of motor memory consolidation depend on practice structure. *Nat. Neurosci.* 13, 923–925. doi: 10.1038/nn.2596

Kawashima, R., Yamada, K., Kinomura, S., Yamaguchi, T., Matsui, H., Yoshioka, S., et al. (1993). Regional cerebral blood flow changes of cortical motor areas and prefrontal areas in humans related to ipsilateral and contralateral hand movement. *Brain Res.* 623, 33–40. doi: 10.1016/0006-8993(93)90006-9

Kropotov, J. D. (2010). *Quantitative EEG, Event-Related Potentials and Neurotherapy.* San Diego, CA: Academic Press.

Lage, G. M., Ugrinowitsch, H., Apolinário-Souza, T., Vieira, M. M., Albuquerque, M. R., and Benda, R. N. (2015). Repetition and variation in motor practice: a review of neural correlates. *Neurosci. Biobehav. Rev.* 57, 132–141. doi: 10.1016/j.neubiorev.2015.08.012

Lee, T. D., and Magill, R. A. (1985). "Can forgetting facilitate skill acquisition?" in *Differing Perspectives in Motor Learning, Memory and Control*, eds D. Goodman, R. B. Wilberg and I. M. Franks (Amsterdam: North Holland), 3–22.

Leuthold, H., and Jentzsch, I. (2011). Are temporal response features prepared in fixed order? Inferences from movement-related potentials. *Psychophysiology* 48, 633–644. doi: 10.1111/j.1469-8986.2010.01126.x

Lin, C., Chiang, M., Knowlton, B. J., Iacoboni, M., Udompholkul, P., and Wu, A. D. (2013). Interleaved practice enhances skill learning and the functional connectivity of fronto-parietal networks. *Hum. Brain Mapp.* 34, 1542–1558. doi: 10.1002/hbm.22009

Lin, C.-H., Chiang, M.-C., Wu, A. D., Iacoboni, M., Udompholkul, P., Yazdanshenas, O., et al. (2012). Age related differences in the neural substrates of motor sequence learning after interleaved and repetitive practice. *NeuroImage* 62, 2007–2020. doi: 10.1016/j.neuroimage.2012.05.015

Lin, C.-H., Fisher, B. E., Winstein, C. J., Wu, A. D., and Gordon, J. (2008). Contextual interference effect: elaborative processing or forgetting—reconstruction? A *post hoc* analysis of transcranial magnetic stimulation—induced effects on motor learning. *J. Mot. Behav.* 40, 578–586. doi: 10.3200/jmbr.40.6.578-586

Lin, C.-H., Winstein, C. J., Fisher, B. E., and Wu, A. D. (2010). Neural correlates of the contextual interference effect in motor learning: a transcranial magnetic stimulation investigation. *J. Mot. Behav.* 42, 223–232. doi: 10.1080/00222895.2010.492720

Lundqvist, M., Herman, P., Warden, M. R., Brincat, S. L., and Miller, E. K. (2018). Gamma and beta bursts during working memory readout suggest roles in its volitional control. *Nat. Commun.* 9:394. doi: 10.1038/s41467-017-02791-8

Magill, R. A., and Hall, K. G. (1990). A review of the contextual interference effect in motor skill acquisition. *Hum. Mov. Sci.* 9, 241–289. doi: 10.1016/0167-9457(90)90005-x

Merbah, S., and Meulemans, T. (2011). Learning a motor skill: effects of blocked versus random practice: a review. *Psychol. Belg.* 51, 15–48. doi: 10.5334/pb-51-1-15

Monk, T. H., Buysse, D. J., Kennedy, K. S., Potts, J. M., DeGrazia, J. M., and Miewald, J. M. (2003). Measuring sleep habits without using a diary: the sleep timing questionnaire. *Sleep* 26, 208–212. doi: 10.1093/sleep/26.2.208

Nasreddine, Z. S., Phillips, N. A., BÃ© dirian, V., Charbonneau, S., Whitehead, V., Collin, I., et al. (2005). The montreal cognitive assessment, MoCA: a brief screening tool for mild cognitive impairment. *J. Am. Geriatr. Soc.* 53, 695–699. doi: 10.1111/j.1532-5415.2005.53221.x

Oldfield, R. C. (1971). The assessment and analysis of handedness: the Edinburgh inventory. *Neuropsychologia* 9, 97–113. doi: 10.1016/0028-3932(71)90067-4

Pauwels, L., Chalavi, S., Gooijers, J., Maes, C., Albouy, G., Sunaert, S., et al. (2018). Challenge to promote change: the neural basis of the contextual interference effect in young and older adults. *J. Neurosci.* 38, 3333–3345. doi: 10.1523/jneurosci.2640-17.2018

Pauwels, L., Vancleef, K., Swinnen, S. P., and Beets, I. A. M. (2015). Challenge to promote change: both young and older adults benefit from contextual interference. *Front. Aging Neurosci.* 7:157. doi: 10.3389/fnagi.2015.00157

Riding, R. J., Glass, A., Butler, S. R., and Pleydell-Pearce, C. W. (1997). Cognitive style and individual differences in EEG alpha during information processing. *Educ. Psychol.* 17, 219–234. doi: 10.1080/0144341970170117

Robertson, E. M. (2018). Memory instability as a gateway to generalization. *PLoS Biol.* 16:e2004633. doi: 10.1371/journal.pbio.2004633

Rosenbaum, D. A., Weber, R. J., Hazelett, W. M., and Hindorff, V. (1986). The parameter remapping effect in human performance: evidence from tongue twisters and finger fumblers. *J. Mem. Lang.* 25, 710–725. doi: 10.1016/0749-596x(86)90045-8

Schmidt, R. A. (1975). A schema theory of discrete motor skill learning. *Psychol. Rev.* 82, 225–260. doi: 10.1037/h0076770

Schmidt, R. A., Lee, T. D., Winstein, C., Wulf, G., and Zelaznik, H. N. (2018). *Motor Control and Learning: A Behavioral Emphasis.* 6th Edn. Champaign, IL: Human Kinetics.

Schmidt, R., Ruiz, M. H., Kilavik, B. E., Lundqvist, M., Starr, P. A., and Aron, A. R. (2019). Beta oscillations in working memory, executive control of movement and thought and sensorimotor function. *J. Neurosci.* 39, 8231–8238. doi: 10.1523/jneurosci.1163-19.2019

Shea, C. H., Kohl, R., and Indermill, C. (1990). Contextual interference: contributions of practice. *Acta Psychol.* 73, 145–157. doi: 10.1016/0001-6918(90)90076-r

Shea, J. B., and Morgan, R. L. (1979). Contextual interference effects on the acquisition, retention and transfer of a motor skill. *J. Exp. Psychol. Hum. Learn. Mem.* 5, 179–187. doi: 10.1037/0278-7393.5.2.179

Shea, C. H., and Wulf, G. (2005). Schema theory: a critical appraisal and reevaluation. *J. Mot. Behav.* 37, 85–102. doi: 10.3200/jmbr.37.2.85-102

Shea, J. B., and Zimny, S. T. (1983). "Context effects in memory and learning movement information," in *Memory and Control of Action*, ed. R. A. Magill (Amsterdam: North-Holland), 345–366.

Sidaway, B., Ala, B., Baughman, K., Glidden, J., Cowie, S., Peabody, A., et al. (2016). Contextual interference can facilitate motor learning in older adults and in individuals with Parkinson's disease. *J. Mot. Behav.* 48, 509–518. doi: 10.1080/00222895.2016.1152221

Simon, D. A., Lee, T. D., and Cullen, J. D. (2008). Win-shift, lose-stay: contingent switching and contextual interference in motor learning. *Percept. Mot. Skills* 107, 407–418. doi: 10.2466/pms.107.6.407-418

Suzuki, T., Higashi, T., Takagi, M., and Sugawara, K. (2013). Hemispheric asymmetry of ipsilateral motor cortex activation in motor skill learning. *Neuroreport* 24, 693–697. doi: 10.1097/wnr.0b013e3283630158

Sweller, J., van Merriënboer, J. J. G., and Paas, F. (2019). Cognitive architecture and instructional design: 20 years later. *Educ. Psychol. Rev.* 31, 261–292. doi: 10.1007/s10648-019-09465-5

Thürer, B., Stockinger, C., Putze, F., Schultz, T., and Stein, T. (2017). Mechanisms within the parietal cortex correlate with the benefits of random practice in motor adaptation. *Front. Hum. Neurosci.* 11:403. doi: 10.3389/fnhum.2017.00403

Verwey, W. B., Shea, C. H., and Wright, D. L. (2015). A cognitive framework for explaining serial processing and sequence execution strategies. *Psychon. Bull. Rev.* 22, 54–77. doi: 10.3758/s13423-014-0773-4

Wadden, K. P., Hodges, N. J., De Asis, K. L., Neva, J. L., and Boyd, L. A. (2019). Individualized challenge point practice as a method to aid motor sequence learning. *J. Mot. Behav.* 51, 467–485. doi: 10.1080/00222895.2018.1518310

Wilson, R. C., Shenhav, A., Straccia, M., and Cohen, J. D. (2018). The eighty five percent rule for optimal learning. *bioRxiv* [Preprint]. doi: 10.1101/255182

Wood, C. A., and Ging, C. A. (1991). The role of interference and task similarity on the acquisition, retention and transfer of simple motor skills. *Res. Q. Exerc. Sport* 62, 18–26. doi: 10.1080/02701367.1991.10607514

Wymbs, N. F., and Grafton, S. T. (2009). Neural substrates of practice structure that support future off-line learning. *J. Neurophysiol.* 102, 2462–2476. doi: 10.1152/jn.00315.2009

Yuhua, L. (1994). Contextual interference in motor skill learning: examination of attention demands. Unpublished Doctoral Dissertation. Texas A & M University, College Station, TX, United States.

Ziemann, U., and Hallett, M. (2001). Hemispheric asymmetry of ipsilateral motor cortex activation during unimanual motor tasks: further evidence for motor dominance. *Clin. Neurophysiol.* 112, 107–113. doi: 10.1016/s1388-2457(00)00502-2

Conflict of Interest: The authors declare that the research was conducted in the absence of any commercial or financial relationships that could be construed as a potential conflict of interest.

frontiers in Psychiatry

ORIGINAL RESEARCH
published: 29 June 2020
doi: 10.3389/fpsyt.2020.00574

Aging-Dependent Genetic Effects Associated to ADHD Predict Longitudinal Changes of Ventricular Volumes in Adulthood

Natalia Vilor-Tejedor[1,2,3,4*†], *Mohammad Arfan Ikram*[5,6,7], *Gennady Roshchupkin*[6,8], *Elisabeth J. Vinke*[5,6], *Meike W. Vernooij*[5,6] *and Hieab H. H. Adams*[4,5,6*†]

[1] Centre for Genomic Regulation (CRG), The Barcelona Institute for Science and Technology, Barcelona, Spain, [2] BarcelonaBeta Brain Research Center (BBRC), Pasqual Maragall Foundation, Barcelona, Spain, [3] Department of Clinical Genetics, Erasmus Medical Center, Rotterdam, Netherlands, [4] Universitat Pompeu Fabra (UPF), Barcelona, Spain, [5] Department of Epidemiology, Erasmus Medical Center, Rotterdam, Netherlands, [6] Department of Radiology and Nuclear Medicine, Erasmus Medical Center, Rotterdam, Netherlands, [7] Department of Neurology, Erasmus Medical Center, Rotterdam, Netherlands, [8] Department of Medical Informatics, Erasmus Medical Center, Rotterdam, Netherlands

Background: Attention-Deficit/Hyperactivity Disorder (ADHD) is a childhood-onset disorder that can persist into adult life. Most genetic studies have focused on investigating biological mechanisms of ADHD during childhood. However, little is known about whether genetic variants associated with ADHD influence structural brain changes throughout adulthood.

Methods: Participant of the study were drawn from a population-based sample of 3,220 healthy individuals drawn from the Rotterdam Study, with at least two magnetic resonance imaging (MRI)-scans (8,468 scans) obtained every 3–4 years. We investigate associations of genetic single nucleotide polymorphisms (SNPs) that have previously been identified in genome-wide association studies for ADHD, and trajectories of global and subcortical brain structures in an adult population (aged 50 years and older), acquired through MRI. We also evaluated the existence of age-dependent effects of these genetic variants on trajectories of brain structures. These analyses were reproduced among individuals 70 years of age or older to further explore aging-dependent mechanisms. We additionally tested baseline associations using the first MRI-scan of the 3,220 individuals.

Results: We observed significant age-dependent effects on the rs212178 in trajectories of ventricular size (lateral ventricles, P= 4E-05; inferior lateral ventricles, P=3.8E-03; third ventricle, P=2.5E-03; fourth ventricle, P=5.5E-03). Specifically, carriers of the G allele, which was reported as protective for ADHD, had a smaller increase of ventricular size compared with homozygotes for the A allele in elder stages. Post hoc analysis on the subset of individuals older than 70 years of age reinforced these results (lateral ventricles, P=7.3E-05). In addition, the rs4916723, and the rs281324 displayed nominal significant age-dependent effects in trajectories of the amygdala volume (P=1.4E-03), and caudate volume (P=1.8E-03), respectively.

OPEN ACCESS

Edited by:
Hans J. Grabe,
University of Greifswald, Germany

Reviewed by:
Georgios Demetrios Kotzalidis,
Sapienza University of Rome, Italy
Anbupalam Thalamuthu,
University of New South Wales, Australia

***Correspondence:**
Natalia Vilor-Tejedor
natalia.vilortejedor@crg.eu
Hieab H. H. Adams
h.adams@eramusmc.nl

†ORCID:
Natalia Vilor-Tejedor
orcid.org/0000-0003-4935-6721
Hieab H. Adams
orcid.org/0000-0003-3687-2508

Specialty section:
This article was submitted to Aging Psychiatry, a section of the journal Frontiers in Psychiatry

Received: *20 October 2019*
Accepted: *05 June 2020*
Published: *29 June 2020*

Citation:
Vilor-Tejedor N, Ikram MA, Roshchupkin G, Vinke EJ, Vernooij MW and Adams HHH (2020) Aging-Dependent Genetic Effects Associated to ADHD Predict Longitudinal Changes of Ventricular Volumes in Adulthood. Front. Psychiatry 11:574. doi: 10.3389/fpsyt.2020.00574

Conclusions: To the best of our knowledge, this is the first study suggesting the involvement of protective genetic variants for ADHD on prevention of brain atrophy during adulthood.

Keywords: adulthood, aging, brain atrophy, brain trajectories, neurogenetics, rs212178, ventricle size

INTRODUCTION

Attention-Deficit/Hyperactivity Disorder (ADHD) is a childhood neurodevelopmental disorder with an estimated worldwide prevalence of 5.2% (1–3). Although it is most common in children, recent work suggests that for some individuals, ADHD first emerges in adulthood (4), and one-sixth of individuals with a childhood diagnosis continue to meet clinical criteria for ADHD in adulthood (5–7).

It is challenging to characterize the determinants of the persistence and/or occurrence of ADHD through adulthood because the normal aging process mimics some classic ADHD symptoms. However, it is well established that genetic factors explain a large part of the individual differences in the vulnerability for ADHD (75%–90% in children, 30%–50% in adults) (8–10).

Knowing which genetic variants are associated with ADHD set the interest to understand how they could act on the brain to bring about ADHD. For instance, given that structural magnetic resonance imaging (MRI) markers maybe even better suited as intermediate phenotypes than ADHD symptoms, and these measures generally show strong test-retest reliability (11–13), an increasing number of studies have attempted to examine whether genetic variants for ADHD could have distinct effects on the brain, thereby elucidating the causal pathway to disease (14–17).

Furthermore, it has been suggested that the genetic basis of the disorder may vary depending on the age (18). In line with these results, recent findings showed that genetic factors implicated in ADHD during childhood (cADHD) play different roles in adult ADHD (aADHD), which in turn, may lead to a different genetic influences across the development of these symptoms (19–22). Indeed, family genetic studies in clinical samples hinted that there may be a higher familial liability for aADHD compared with cADHD (23), which supports that aADHD symptoms may have stronger genetic liability. Therefore, examining the genetic basis of aADHD symptoms can offer reliable etiological information.

Moreover, whilst longitudinal studies are essential in characterizing differences on neuroanatomical trajectories attributed to genetic variants (20), most of ADHD studies have focused exclusively on cross-sectional associations (24–26). Also, the lack of age-proper clinical measures has constrained progress in the field.

The current study aimed to examine the associations between genome-wide significant SNPs reported in the latest genome-wide association (GWAS) meta-analysis for ADHD (27), and trajectories of global and brain subcortical structures in a sample of non-diagnosed individuals, to provide a more precise understanding of how genetic markers associated with ADHD shape brain structural variations, and how age-dependent genetic effects influence regional brain changes throughout adulthood. Moreover, due to the polygenic architecture of ADHD, where common risk alleles have small effect sizes, we also inspected associations between a composite genetic risk score (GRS) and brain structural trajectories.

MATERIALS AND METHODS

Study Population

The study sample was drawn from the Rotterdam Study, an ongoing population-based cohort study in Netherlands, which currently consists of 14,926 individuals aged 45 years or more at baseline (28). At study entry, and every 3–4 years, participants visited the dedicated research center for extensive investigations. Simultaneously, electronic data linkage with general practitioners recorded incident events or diagnoses. A total of 5,430 individuals were scanned through magnetic resonance imaging (MRI) and were eligible for this study. Individuals with only a single MRI scan, incomplete MRI-acquisitions, scans with artifacts and dementia or stroke were excluded. The Rotterdam Study has been approved by the Medical Ethics Committee of the Erasmus MC and by the Ministry of Health, Welfare and Sport of Netherlands, implementing the Wet Bevolkingsonderzoek: ERGO (Population Studies Act: Rotterdam Study). All participants provided written informed consent to participate in the study and to obtain information from their treating physicians. Data on ADHD diagnosis or symptomatology was not collected because of the study's focus on late-onset diseases.

Image Acquisition, Processing, and Selection

Magnetic Resonance Imaging scanning was done on a 1.5-T MRI scanner (Sigma Excite II; General Electric Healthcare, Milwaukee, WI, USA). Brain MRI scans included a high-resolution 3D T1-weighted fast radio frequency spoiled gradient-recalled acquisition in steady-state with an inversion recovery prepulse (FASTSPGR-IR) sequence (29). Sequence parameters were TR = 700 ms, TE = 14 ms, matrix side of 192 × 256 and flip angle = 70 with a voxel size of 1 × 1 × 1 mm. All participants were imaged on the same scanner with fixed protocol and imaging parameters. A total of 12,174 brain MR-scans have been obtained in over 5,430 individuals, as of July 2015. The T1-weighted MRI scans were used to calculate global and subcortical structures and thickness of the cerebral cortex using a standard model-based automated procedure on

Freesurfer (30) (version 5.1) image analysis suite. Quality control included the removal of outliers, as well as unusual brain volume values. We additionally excluded individuals with dementia and/or stroke. The brain measures included in the analyses were: cerebral white matter, cerebral grey matter, total intracranial volume, lateral ventricles, inferior lateral ventricles, cerebellum white matter, cerebellum cortex, thalamus, corpus callosum, caudate, putamen, pallidum, hippocampus, amygdala, accumbens area, third ventricle, fourth ventricle, and cerebrospinal fluid. The value of the brain measures used as the outcomes of the study was calculated as the average of the regional value of each hemisphere (mm3). From the total sample of individuals included in the study (N=5,430), a total of 3,220 have at least two scan measurements, 1,887 have at least three scan measurements, and 141 have four scan measurements. Further details of the MRI protocol, can be found in (29).

Genotyping Acquisition and Genetic Variant Selection

The Illumina 550K, 550K duo, and 610K arrays were used for genotyping samples with a call rate below 97.5%, gender mismatch, excess autosomal heterozygosity (>0.336), duplicates or family relations and ethnic outliers were excluded. Genetic variants were filtered by Hardy-Weinberg equilibrium ($P<10^{-6}$), allele frequency (excluding minor allele frequency (MAF < 0.001) and SNP call rate with a minimum of 98%. Genotypes were imputed using MACH/minimac software to the 1000 Genomes phase I version three-reference panel (all populations). From the imputed data (HRC version 1.1), we selected eight SNPs associated with ADHD at a genome-wide threshold of significance ($P<10^{-8}$) [**Table SM1**] (27). Four genetic variants were not included because were not available in the HRC imputations, nor were there are any variants in linkage disequilibrium, likely because the original ADHD GWAS used a custom genotyping array for psychiatric disorders. Furthermore, we constructed a genetic risk score (GRS) by multiplying the number of risk alleles by their reported odds ratio (after natural logarithm transformation) for the disease and summing this weighted allele score of each variant up into a disease risk score for ADHD.

Statistical Analysis

Longitudinal Models

We used mixed-effects models with random slopes and intercepts to calculate trajectories of volumetric MRI markers for each subject. The linear mixed models were fitted using the "lme" function within the R-package "nlme" (31). This model was selected based on previous brain trajectory assessment in the Rotterdam Study sample (32). We tested the longitudinal association between genome-wide genetic risk variants for ADHD and brain structures in fully adjusted models. A total of 3,220 individuals with at least two repeated measures of MRI-scan were included, resulting in 8,468 observations in total (**Figure 1**). Moreover, to account for possible non-linearity in brain structural trajectories, the age of the individuals at each measurement was used as the time variable of the model. Furthermore, after an exploratory analysis, splines of age with one *knot* were used in all models. Fixed effects of the model included: sex, and total intracranial volume (ICV). In addition, age-by-genotype interactions for each volume were included in the mixed-effects model to test whether age moderated genetic effects on longitudinal brain changes. The age-dependent model allows obtaining the difference in the change in average regional volume per additional year of age in spline, and the change in the slope for each spline, depending on genotypes effects. The coefficients of the interaction terms quantified the existence of possible slope differences of the trajectories explained by genotype.

Baseline Models

We used general linear models to test genetic influences on baseline differences in brain volumes. We also assessed age-dependent effects to test whether age moderated genetic effects on regional brain structures. Age-by-genotype interactions for each volume were included in the model. We used data corresponding to the first scan-acquisition of the whole sample (first observation per subject, *N*=3,220), as would be the case in a simple single observation cross-sectional study. As in the longitudinal models, splines of age with one knot were used in all models. Fixed effects included sex and ICV.

Post Hoc Analyses

In addition, we performed *post hoc* analyses to facilitate interpretation of the results. Among individuals 70 years of age or older (N=900, 2,084 observations), we tested whether regional brain volumes and/or longitudinal brain changes were associated with genetic effects or whether age moderated those genetic effects.

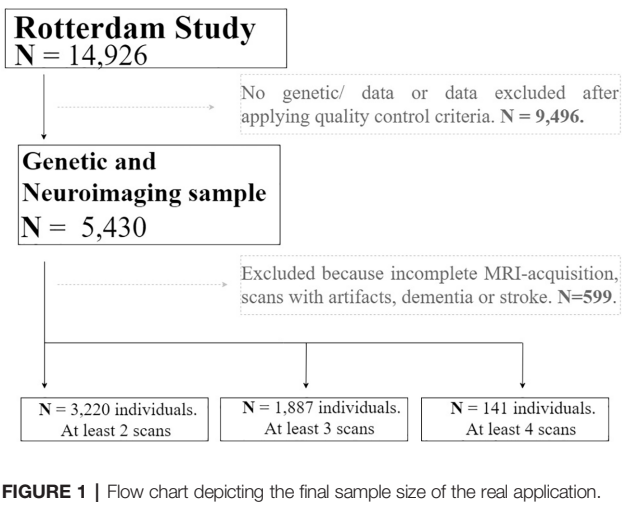

FIGURE 1 | Flow chart depicting the final sample size of the real application. Solid lines and boxes represent individuals remaining in the study. Dashed lines and boxes represent individuals excluded. Reason and number of individuals excluded is indicated in dashed boxes. *Legend: N, size of the sample.*

Multiple Comparison Correction

The weighted effects of baseline and longitudinal models were corrected for multiple comparisons. Since brain outcomes are correlated, we calculated the effective number of independent outcomes, k_{eff}, using a permutation procedure, assuming 10,000 permutations. Additionally, we used the Bonferroni method for multiple testing correction. The threshold of significance was set following the formula $\frac{k_{eff}}{n_{SNPs}}$, were k_{eff} represents the p-value threshold obtained through the permutation procedure, and n_{SNPs} the number of genetic variants assessed in the models. The resulting adjusted threshold of significance was set to p < 2E-04. All statistical analyses were performed using R version 3.3.4.

RESULTS

Descriptives

Descriptive characteristics of the subjects with at least two valid MRIs and descriptive of the brain volumetry for each scan acquisition are presented in **Table 1**. The study included 1,731 women and 1489 men between 50 and 100 years of age at baseline (65.3 ± 9.3). The distribution in the percentage of women/men is balanced in all the scan acquisitions, while the age becomes slightly higher in the last visit, as expected. **Figure S1** shows the pattern of correlation (Pearson correlation statistics) among all brain structures included in the study. Further descriptive of brain structures included in the study can be found at **Supplemental Table 2**.

Longitudinal Association Results

We observed significant age-dependent effect of the rs212178 (intron variant *LINC01572* at chromosome 16) in trajectories of ventricular size (lateral ventricles, P= 4E-05; third ventricle, P=2.5E-03; fourth ventricle, P=5.5E-03) (**Figures 2B, C** and **Supplemental Table 3**). Specifically, carriers of the protective ADHD allele G of rs212178 were associated with a less pronounced increase in lateral ventricle volumes among individuals 70 years of age or older (**Figure 3B**). Pointedly, among subjects > 70 years of age, we observed significant differences in trajectories (slope and intercept differences) for the different genotypes of rs212178 on ventricle size (lateral ventricles, P=7.3E-05) (**Figure 4** and **Supplemental Table 4**).

In addition, rs4916723 (intron variant *LINC00461* at chromosome 5), and rs281324 (intron variant *SEMA6D* at chromosome 15) displayed nominal significant age-dependent effects, which not survive multiple comparison, in trajectories of amygdala volume (P=1.4E-03) and caudate volume (P=1.8E-03), respectively.

No additional significant main effects were found after multiple comparisons correction (**Figures 2A** and **3A** and **Supplemental Tables 5** and **6**). Likewise, no significant effects were found for GRS.

Baseline Association Results

Figure 5 showed results for the adjusted age-by-SNP interaction coefficients. None of the results remained significant after multiple comparison correction. Furthermore, no age-by-GRS interaction effects were found on either brain structure of interest.

Post hoc analyses suggested patterns of age-dependent effects of the rs212178 in ventricle size (lateral ventricles, P=0.01; and fourth ventricle, P=0.009) on individuals up to 70, sustained also among individuals 70 years of age or older (lateral ventricles, P=0.03; fourth ventricle, P=0.041: third ventricle, P=0.008), which reinforce our longitudinal results [**Supplemental Tables 7–10**].

DISCUSSION

According to our knowledge, this is the first study to investigate the effects of genome-wide significant SNPs for ADHD on longitudinal brain changes and its age-dependent effects in an adult population. Our main finding suggests that carriers of the minor allele G of rs212178 (chr16, *LINC01572*) were associated with a smaller increase of ventricular volume—indirectly reflecting lower brain atrophy—during aging, compared with homozygotes for the A allele. Interestingly, the G allele of rs212178 has been reported as a protective variant of ADHD (27) (OR=0.891; P=7.68×10-9), suggesting a relationship between the protective genetic effect on ADHD and less brain atrophy across the lifespan. Moreover, nominally significant age-dependent effects were identified, in which carriers of protective ADHD variants (C allele carriers of rs4916723 and rs281324) had smaller increases in the amygdala and caudate volumes.

However, these results should be interpreted considering its limitations, especially, due to the unavailability of a replication sample. First, in the present study, only a single variant was suggested affecting longitudinal changes on ventricle volumes with a small effect size. We can hypothesize a lack of statistical power in our analysis, but also the existence of a pleiotropic effect that could involve multiple different effects of genes to ADHD (20). Second, there are still many genetic variants contributing to the heritability of ADHD which remained undiscovered, and that therefore were not included in the models of the study. Third, we should be cautious because although ventricular size can represent accumulation of brain atrophy, it might also

TABLE 1 | Participant characteristics.

	N	Age (m at each scan ± SD; years)	Sex distribution (W/M)(%)	TIV (m ± SD; mm3)
scan 2	3,220	65.3(9.3)	1,731/1,489 (53.8%)	1,486,432 (161,510)
scan 3	1,887	64.5(7.3)	989/898 (52.4%)	1,491,226 (158,878)
scan 4	141	74.8(3.9)	59/82 (41.8%)	1,468,570 (174,479)

Mean (m) and standard deviation (SD) are shown for continous variables. TIV, total intracranial volume; W, women; M, men.

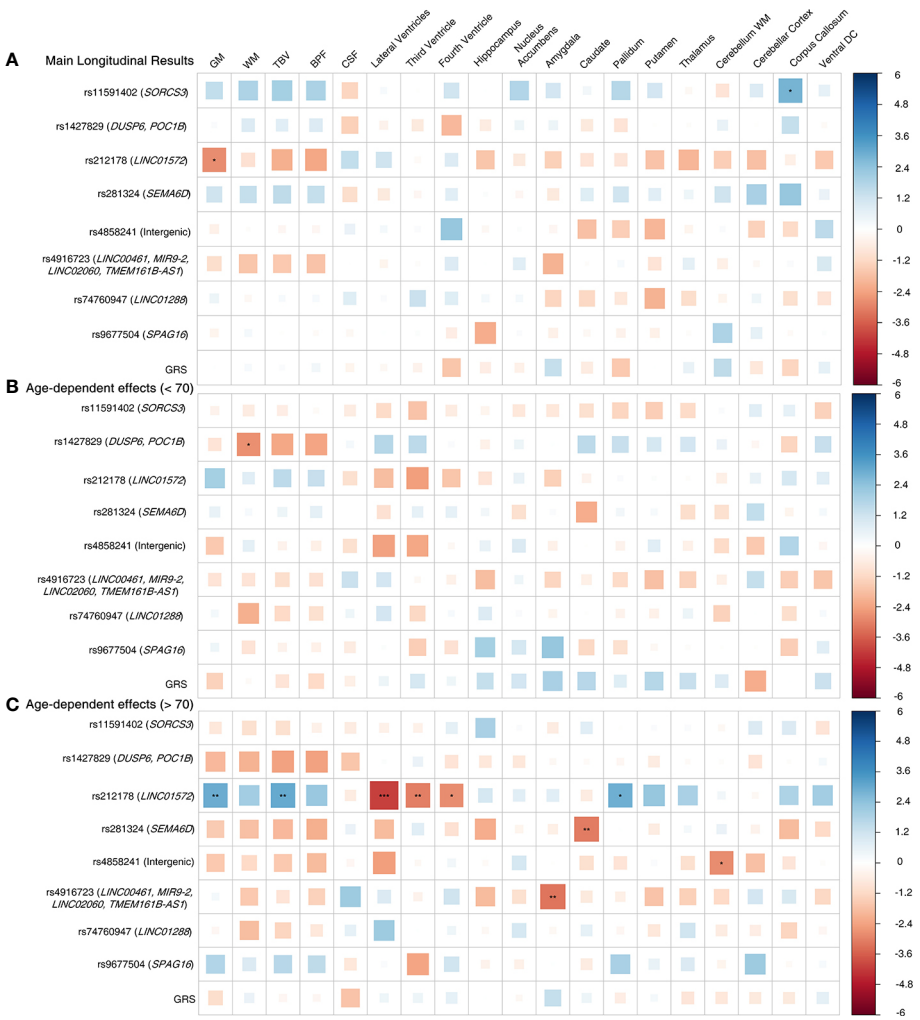

FIGURE 2 | Longitudinal design whole sample. **(A)** Main genetic results. **(B)** Age-by-SNP results, spline 1. **(C)** Age-by-SNP results, spline 2***Pvalue = 0.0002 (Bonferroni correction); **Pvalue = 0.003 (BH correction); *Pvalue = 0.05 (nominal p-value). Color scale represents the normalized effect sizes. Legend: GM, Grey Matter; WM, White Matter; TBV, Total Brain Volume; BPF, Brain Parenchymal Fraction; CSF, Cerebrospinal Fluid; DC, Diencephalon; GRS, Genetic Risk Score.

indirectly reflects a loss of brain tissue in other regions, which could confuse our results. Fourth, we should take into account that, in general, brain volume measurements are only a crude simplification of the complex anatomical brain changes, and often ignore the fact that longitudinal changes are not uniform across a brain structure. Finally, the study sample belongs to the general population; thus, the significant effects identified in this study do not necessarily imply a causal relationship with the clinical presentation of ADHD symptoms, but instead may represent a proxy for the potential causes that underlie their internal physiopathology.

Nevertheless, the present study identified intraindividual changes in brain structures using longitudinal data, which include at least two scanner acquisitions per individual. This provides a more valid measure of the brain structural change than extrapolating an estimate of change from separate individuals across a range of ages using cross-sectional designs. Furthermore, compared to the cross-sectional design, the longitudinal design can provide increased statistical power by reducing the confounding effect of between-subject variability and provide unique insights into the temporal dynamics of the underlying biological process of neurodevelopmental domains (33). Moreover, we considered the statistical interaction between genetic variations and age because of the implications for the shape of the distribution of onset age in risk analyses, which improves the understanding of the degree and direction of change over time (34, 35).

Progressive enlargement of the ventricular system is a common finding in several neurologic and psychiatric disorders including dementia (36), Parkinson's disease (37), multiple sclerosis (38, 39), schizophrenia (40) and it has been extensively discussed in the context of brain cerebral atrophy and cognitive impairment (41). Interestingly, ventricular enlargement has been suggested as a neuroimaging-based

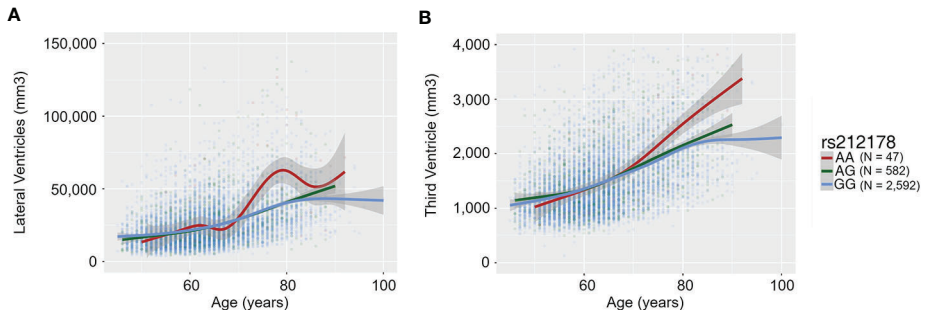

FIGURE 3 | Trajectory differences of ventricle sizes between rs212178 genotypes In red, green and blue, the average trajectory of AA, AG, and GG genotypes, respectively. The x-axis represents the age at time of the scan (years), the left y-axis represents the value of the ventricle size (mm3): **(A)** *Lateral ventricles* **(B)** *Third ventricle*.

FIGURE 4 | Longitudinal design, subset of individuals older than 70 years. **(A)** Main results. **(B)** Age-by-SNP results. ***Pvalue = 0.0002 (Bonferroni correction); **Pvalue = 0.003 (BH correction); *Pvalue = 0.05 (nominal p-value). Color scale represents the normalized effect sizes. Legend: GM, Grey Matter; WM, White Matter; TBV, Total Brain Volume; BPF, Brain Parenchymal Fraction; CSF, Cerebrospinal Fluid; DC, Diencephalon; GRS, Genetic Risk Score.

biomarker in normal aging (42, 43), which may herald the cognitive decline associated with the onset and progression of Alzheimer's disease (44–46). In this line, our results also suggested that age-related changes in G-allele carriers of rs212178 are important on prevention of brain atrophy during adulthood.

Although the rs212178 SNP was located within the *LINC01572*, fine-mapping results showed that the LD region was close to the protein coding zinc finger homeobox 3 (*ZFHX3*) gene. Thus, we cannot discard that this SNP may be responsible for regulation of the *ZFHX3* gene. This gene encodes cardio-enriched transcription factors, and regulates myogenic and neuronal differentiation (47). In addition, is highly expressed in human stem cell-derived cardio myoblasts and it has been reported as a one of the major atrial fibrillation (AF) susceptibility-conferring genes and an important regulatory factor which modifies circadian function (48–51). Indeed, several studies have reported ventricular enlargement

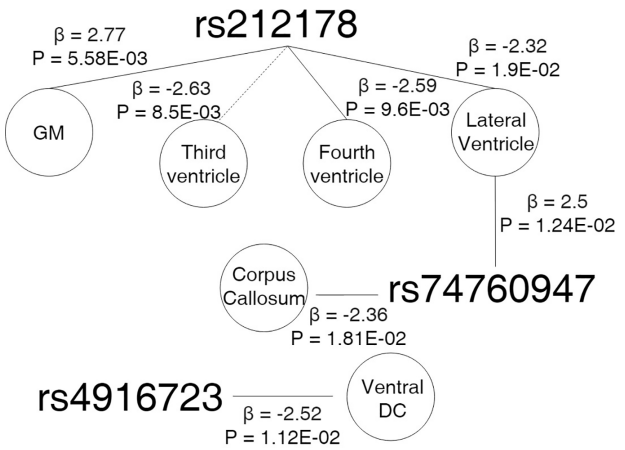

FIGURE 5 | Cross sectional design. Age-by-genotype results. Straight lines represents a nominally significant age-by-SNP interaction at the first spline. Dotted lines represents a significant age-by-SNP interaction at the second spline. Parallel dotted lines represents a significant age-by-genotype interaction term in both splines. Legend: GM, Grey Matter; DC, Diencephalon; β, Effect size; P, p-value.

associated with AF and other related cardiovascular phenotypes (52–54). This is in agreement with some other studies consistently suggesting that ventricular dysfunction and AF reduce cerebral blood flow exerting negative influences on cognitive function along in the aging process (55, 56). Hence, our findings might add to the current evidences relating similar genetic mechanisms of ventricular enlargement, aging, and adult ADHD through cardio metabolic pathways.

Finally, our results suggested the involvement of protective genetic ADHD factors and amygdala and caudate volume trajectories. These associations did not survive multiple testing correction, and therefore need to be replicated before further conclusions can be drawn. However, both brain regions have been well-described in the literature, and several meta-analyses have elucidated their involvement in ADHD (21, 57–59). Moreover, smaller caudate and amygdala volumes have been reported to be associated with cognitive deficits, the inhibition of attentional domains, and motor function constraints (60–63). Thus, our results may also suggest the existence of indirect causal effects on the biological mechanisms underlying the lifespan trajectories of ADHD symptoms, which may be mediated through impacts on brain structures.

To sum up, results obtained showed that specific effects of genetic variants associated with ADHD in adulthood are quite modest to elucidate longitudinal brain changes, but could suggest signs of brain atrophy. Such research furthers our understanding of the extent to which and how brain volume trajectories are genetically determined. Hence, research in imaging genetic field may greatly benefit from longitudinal designs, which represent a potential form to increase the statistical power to detect significant causal factors affecting structural brain changes.

DATA AVAILABILITY STATEMENT

Due to patient privacy, individual level genetic data cannot be made publicly available. Researchers who wish to use data of the Rotterdam Study must obtain approval from the Rotterdam Study Management Team. They are advised to contact the PI of the Rotterdam Study, MI (m.a.ikram@erasmusmc.nl).

ETHICS STATEMENT

The studies involving human participants were reviewed and approved by The Rotterdam Study has been approved by the Medical Ethics Committee of the Erasmus MC and by the Ministry of Health, Welfare and Sport of Netherlands, implementing the Wet Bevolkingsonderzoek: ERGO (Population Studies Act: Rotterdam Study). The patients/participants provided their written informed consent to participate in this study.

AUTHOR CONTRIBUTIONS

NV-T and HA conceived the original idea of the study. NV-T performed the computations. EV contributed improving the R scripts and verified the analytical methods. NV-T wrote the manuscript in consultation with HA and MV. HA supervised the project. All authors contributed to the article and approved the submitted version.

FUNDING

NV-T is funded by a post-doctoral grant, Juan de la Cierva Programme (FJC2018-038085-I), Ministerio de Ciencia, Innovación y Universidades – Spanish State Research Agency, and of a European Molecular Biology Organization (EMBO) Short-Term Fellowship (#8576). Her research has received additional support of "la Caixa" Foundation (LCF/PR/GN17/10300004) and the Health Department of the Catalan Government (Health Research and Innovation Strategic Plan (PERIS) 2016-2020 grant# SLT002/16/00201), the EU COST Action 15120 Open Multiscale Systems Medicine (OpenMultiMed) and Centro de Investigación Biomédica en Red de Epidemiología y Salud Pública (CIBERESP). HA was supported by ZonMW grant numbers 916.19.15 and 916.19.151.

The generation and management of GWAS genotype data for the Rotterdam Study are supported by Netherlands Organization of Scientific Research NWO Investments (no. 175.010.2005.011, 911-03-012). This study is funded by the Research Institute for Diseases in the Elderly (014-93-015; RIDE2), Netherlands Genomics Initiative (NGI)/Netherlands Organization for Scientific Research (NWO) project no. 050-060-810. All CRG authors acknowledge the support of the Spanish Ministry of Science, Innovation and Universities to the EMBL partnership,

the Centro de Excelencia Severo Ochoa and the CERCA Programme/Generalitat de Catalunya.

ACKNOWLEDGMENTS

The Rotterdam Study is funded by Erasmus Medical Center and Erasmus University, Rotterdam, Netherlands Organization for the Health Research and Development (ZonMw), the Research Institute for Diseases in the Elderly (RIDE), the Ministry of Education, Culture and Science, the Ministry for Health, Welfare and Sports, the European Commission (DG XII), and the Municipality of Rotterdam. This research is supported by the Dutch Technology Foundation STW (12723), which is part of the NWO, and which is partly funded by the Ministry of Economic Affairs. This project has received funding from the European Research Council (ERC) under the European Union's Horizon 2020 research and innovation programme (project: ORACLE, grant agreement No: 678543).

SUPPLEMENTARY MATERIAL

The Supplementary Material for this article can be found online at: https://www.frontiersin.org/articles/10.3389/fpsyt.2020.00574/full#supplementary-material

REFERENCES

1. Faraone SV, Asherson P, Banaschewski T, Biederman J, Buitelaar JK, Ramos-Quiroga JA, et al. Attention-deficit/hyperactivity disorder. *Nat Rev Dis Prim* (2015) 1:15020. doi: 10.1038/nrdp.2015.20
2. Thomas R, Sanders S, Doust J, Beller E, Glasziou P. Prevalence of Attention-Deficit/Hyperactivity Disorder: A Systematic Review and Meta-analysis. *Pediatrics* (2015) 135:e994–e1001. doi: 10.1542/peds.2014-3482
3. Willcutt EG. The Prevalence of DSM-IV Attention-Deficit/Hyperactivity Disorder: A Meta-Analytic Review. *Neurotherapeutics* (2012) 9:490–9. doi: 10.1007/s13311-012-0135-8
4. Agnew-Blais JC, Polanczyk GV, Danese A, Wertz J, Moffitt TE, Arseneault L. Evaluation of the Persistence, Remission, and Emergence of Attention-Deficit/Hyperactivity Disorder in Young Adulthood. *JAMA Psychiatry* (2016) 73:713. doi: 10.1001/jamapsychiatry.2016.0465
5. Caye A, Rocha TBM, Anselmi L, Murray J, Menezes AMB, Barros FC, et al. Attention-Deficit/Hyperactivity Disorder Trajectories From Childhood to Young Adulthood. *JAMA Psychiatry* (2016) 73:705. doi: 10.1001/jamapsychiatry.2016.0383
6. Faraone SV, Biederman J, Mick E. The age-dependent decline of attention deficit hyperactivity disorder: a meta-analysis of follow-up studies. *Psychol Med* (2006) 36:159–65. doi: 10.1017/S003329170500471X
7. Moffitt TE, Houts R, Asherson P, Belsky DW, Corcoran DL, Hammerle M, et al. Is Adult ADHD a Childhood-Onset Neurodevelopmental Disorder? Evidence From a Four-Decade Longitudinal Cohort Study. *Am J Psychiatry* (2015) 172:967–77. doi: 10.1176/appi.ajp.2015.14101266
8. Brikell I, Kuja-Halkola R, Larsson H. Heritability of Attention-Deficit Hyperactivity Disorder Across The Lifespan. *Eur Neuropsychopharmacol* (2019) 29:S757–8. doi: 10.1016/J.EURONEURO.2017.06.106
9. Li Z, Chang S, Zhang L, Gao L, Wang J. Molecular genetic studies of ADHD and its candidate genes: A review. *Psychiatry Res* (2014) 219:10–24. doi: 10.1016/j.psychres.2014.05.005
10. Middeldorp CM, Hammerschlag AR, Ouwens KG, Groen-Blokhuis MM, Pourcain BS, Greven CU, et al. A Genome-Wide Association Meta-Analysis of Attention-Deficit/Hyperactivity Disorder Symptoms in Population-Based Pediatric Cohorts. *J Am Acad Child Adolesc Psychiatry* (2016) 55:896–905.e6. doi: 10.1016/j.jaac.2016.05.025
11. Huang L, Huang T, Zhen Z, Liu J. A test-retest dataset for assessing long-term reliability of brain morphology and resting-state brain activity. *Sci Data* (2016) 3:160016. doi: 10.1038/sdata.2016.16
12. Maclaren J, Han Z, Vos SB, Fischbein N, Bammer R. Reliability of brain volume measurements: A test-retest dataset. *Sci Data* (2014) 1:140037. doi: 10.1038/sdata.2014.37
13. Madan CR, Kensinger EA. Test-retest reliability of brain morphology estimates. *Brain Inf* (2017) 4:107–21. doi: 10.1007/s40708-016-0060-4
14. Dark C, Homman-Ludiye J, Bryson-Richardson RJ. The role of ADHD associated genes in neurodevelopment. *Dev Biol* (2018) 438:69–83. doi: 10.1016/J.YDBIO.2018.03.023
15. Hayman V, Fernandez TV. Genetic Insights Into ADHD Biology. *Front Psychiatry* (2018) 9:251. doi: 10.3389/fpsyt.2018.00251
16. Vilor-Tejedor N, Alemany S, Forns J, Cáceres A, Murcia M, Macià D, et al. Assessment of Susceptibility Risk Factors for ADHD in Imaging Genetic Studies. *J Atten Disord* (2019) 23:671–81. doi: 10.1177/1087054716664408
17. Vilor-Tejedor N, Alemany S, Cáceres A, Bustamante M, Mortamais M, Pujol J, et al. Sparse multiple factor analysis to integrate genetic data, neuroimaging features, and attention-deficit/hyperactivity disorder domains. *Int J Methods Psychiatr Res* (2018) 27:e1738. doi: 10.1002/mpr.1738
18. Bidwell LC, Gray JC, Weafer J, Palmer AA, de Wit H, MacKillop J. Genetic influences on ADHD symptom dimensions: Examination of a priori candidates, gene-based tests, genome-wide variation, and SNP heritability. *Am J Med Genet B Neuropsychiatr Genet* (2017) 174:458–66. doi: 10.1002/ajmg.b.32535
19. Chang Z, Lichtenstein P, Asherson PJ, Larsson H. Developmental Twin Study of Attention Problems. *JAMA Psychiatry* (2013) 70:311. doi: 10.1001/jamapsychiatry.2013.287
20. Faraone SV, Larsson H. Genetics of attention deficit hyperactivity disorder. *Mol Psychiatry* (2019) 24:562–75. doi: 10.1038/s41380-018-0070-0
21. Franke B, Michelini G, Asherson P, Banaschewski T, Bilbow A, Buitelaar JK, et al. Live fast, die young? A review on the developmental trajectories of ADHD across the lifespan. *Eur Neuropsychopharmacol* (2018) 28:1059–88. doi: 10.1016/j.euroneuro.2018.08.001
22. Luo Y, Weibman D, Halperin JM, Li X. A Review of Heterogeneity in Attention Deficit/Hyperactivity Disorder (ADHD). *Front Hum Neurosci* (2019) 13:42. doi: 10.3389/fnhum.2019.00042
23. Franke B, Faraone SV, Asherson P, Buitelaar J, Bau CHD, Ramos-Quiroga JA, et al. The genetics of attention deficit/hyperactivity disorder in adults, a review. *Mol Psychiatry* (2012) 17:960–87. doi: 10.1038/mp.2011.138
24. Durston S. Imaging genetics in ADHD. *Neuroimage* (2010) 53:832–8. doi: 10.1016/j.neuroimage.2010.02.071
25. Klein M, Onnink M, van Donkelaar M, Wolfers T, Harich B, Shi Y, et al. Brain imaging genetics in ADHD and beyond – Mapping pathways from gene to disorder at different levels of complexity. *Neurosci Biobehav Rev* (2017) 80:115–55. doi: 10.1016/j.neubiorev.2017.01.013
26. Vilor-Tejedor N, Cáceres A, Pujol J, Sunyer J, González JR. Imaging genetics in attention-deficit/hyperactivity disorder and related neurodevelopmental domains: state of the art. *Brain Imaging Behav* (2017) 11:1922–31. doi: 10.1007/s11682-016-9663-x
27. Demontis D, Walters RK, Martin J, Mattheisen M, Als TD, Agerbo E, et al. Discovery of the first genome-wide significant risk loci for attention deficit/hyperactivity disorder. *Nat Genet* (2019) 51:63–75. doi: 10.1038/s41588-018-0269-7
28. Ikram MA, Brusselle GGO, Murad SD, van Duijn CM, Franco OH, Goedegebure A, et al. The Rotterdam Study: 2018 update on objectives, design and main results. *Eur J Epidemiol* (2017) 32:807–50. doi: 10.1007/s10654-017-0321-4
29. Ikram MA, van der Lugt A, Niessen WJ, Koudstaal PJ, Krestin GP, Hofman A, et al. The Rotterdam Scan Study: design update 2016 and main findings. *Eur J Epidemiol* (2015) 30:1299–315. doi: 10.1007/s10654-015-0105-7
30. Fischl B, Salat DH, van der Kouwe AJW, Makris N, Ségonne F, Quinn BT, et al. Sequence-independent segmentation of magnetic resonance images. *Neuroimage* (2004) 23:S69–84. doi: 10.1016/j.neuroimage.2004.07.016

31. Pinheiro J, Bates D, DebRoy S, Sarkar D, R Core Team. (2014). *nlme: Linear andNonlinear Mixed Effects Models. R package version 3*. pp. 1–117.
32. Vinke EJ, de Groot M, Venkatraghavan V, Klein S, Niessen WJ, Ikram MA, et al. Trajectories of imaging markers in brain aging: the Rotterdam Study. *Neurobiol Aging* (2018) 71:32–40. doi: 10.1016/j.neurobiolaging.2018.07.001
33. Bernal-Rusiel JL, Greve DN, Reuter M, Fischl B, Sabuncu MR. Alzheimer's Disease Neuroimaging Initiative. Statistical analysis of longitudinal neuroimage data with Linear Mixed Effects models. *Neuroimage* (2013) 66:249–60. doi: 10.1016/j.neuroimage.2012.10.065
34. Pfefferbaum A, Rohlfing T, Rosenbloom MJ, Chu W, Colrain IM, Sullivan EV. Variation in longitudinal trajectories of regional brain volumes of healthy men and women (ages 10 to 85years) measured with atlas-based parcellation of MRI. *Neuroimage* (2013) 65:176–93. doi: 10.1016/j.neuroimage.2012.10.008
35. Fjell AM, Walhovd KB, Fennema-Notestine C, McEvoy LK, Hagler DJ, Holland D, et al. One-Year Brain Atrophy Evident in Healthy Aging. *J Neurosci* (2009) 29:15223–31. doi: 10.1523/JNEUROSCI.3252-09.2009
36. Carmichael OT, Kuller LH, Lopez OL, Thompson PM, Dutton RA, Lu A, et al. Cerebral Ventricular Changes Associated With Transitions Between Normal Cognitive Function, Mild Cognitive Impairment, and Dementia. *Alzheimer Dis Assoc Disord* (2007) 21:14–24. doi: 10.1097/WAD.0b013e318032d2b1
37. Mak E, Su L, Williams GB, Firbank MJ, Lawson RA, Yarnall AJ, et al. Longitudinal whole-brain atrophy and ventricular enlargement in nondemented Parkinson's disease. *Neurobiol Aging* (2017) 55:78–90. doi: 10.1016/j.neurobiolaging.2017.03.012
38. Dalton CM, Miszkiel KA, O'Connor PW, Plant GT, Rice GPA, Miller DH. Ventricular enlargement in MS: one-year change at various stages of disease. *Neurology* (2006) 66:693–8. doi: 10.1212/01.wnl.0000201183.87175.9f
39. Martola J, Stawiarz L, Fredrikson S, Hillert J, Bergström J, Flodmark O, et al. Rate of ventricular enlargement in multiple sclerosis: a nine-year magnetic resonance imaging follow-up study. *Acta Radiol* (2008) 49:570–9. doi: 10.1080/02841850802039898
40. Kempton MJ, Stahl D, Williams SCR, DeLisi LE. Progressive lateral ventricular enlargement in schizophrenia: A meta-analysis of longitudinal MRI studies. *Schizophr Res* (2010) 120:54–62. doi: 10.1016/j.schres.2010.03.036
41. Missori P, Currà A. Progressive cognitive impairment evolving to dementia parallels parieto-occipital and temporal enlargement in idiopathic chronic hydrocephalus: a retrospective cohort study. *Front Neurol* (2015) 6:15. doi: 10.3389/fneur.2015.00015
42. Preul C, Hund-Georgiadis M, Forstmann BU, Lohmann G. Characterization of cortical thickness and ventricular width in normal aging: A morphometric study at 3 Tesla. *J Magn Reson Imaging* (2006) 24:513–9. doi: 10.1002/jmri.20665
43. Kwon YH, Jang SH, Yeo SS. Age-related changes of lateral ventricular width and periventricular white matter in the human brain: a diffusion tensor imaging study. *Neural Regener Res* (2014) 9:986–9. doi: 10.4103/1673-5374.133152
44. Nestor SM, Rupsingh R, Borrie M, Smith M, Accomazzi V, Wells JL, et al. Ventricular enlargement as a possible measure of Alzheimer's disease progression validated using the Alzheimer's disease neuroimaging initiative database. *Brain* (2008) 131:2443–54. doi: 10.1093/brain/awn146
45. Thompson PM, Hayashi KM, de Zubicaray GI, Janke AL, Rose SE, Semple J, et al. Mapping hippocampal and ventricular change in Alzheimer disease. *Neuroimage* (2004) 22:1754–66. doi: 10.1016/j.neuroimage.2004.03.040
46. Apostolova LG, Green AE, Babakchanian S, Hwang KS, Chou YY, Toga AW, et al. Hippocampal Atrophy and Ventricular Enlargement in Normal Aging, Mild Cognitive Impairment (MCI), and Alzheimer Disease. *Alzheimer Dis Assoc Disord* (2012) 26:17–27. doi: 10.1097/WAD.0b013e3182163b62
47. Berry FB, Miura Y, Mihara K, Kaspar P, Sakata N, Hashimoto-Tamaoki T, et al. Positive and Negative Regulation of Myogenic Differentiation of C2C12 Cells by Isoforms of the Multiple Homeodomain Zinc Finger Transcription Factor ATBF1. *J Biol Chem* (2001) 276(27):25057–65. doi: 10.1074/jbc.M010378200
48. den Hartogh SC, Wolstencroft K, Mummery CL, Passier R. A comprehensive gene expression analysis at sequential stages of in vitro cardiac differentiation from isolated MESP1-expressing-mesoderm progenitors. *Sci Rep* (2016) 6:19386. doi: 10.1038/srep19386
49. Michael Parsons AJ, Brancaccio M, Sethi S, Mallon AM, Hastings MH, Nolan PM, et al. The Regulatory Factor ZFHX3 Modifies Circadian Function in SCN via an AT Motif-Driven Axis In Brief Article The Regulatory Factor ZFHX3 Modifies Circadian Function in SCN via an AT Motif-Driven Axis. *Cell* (2015) 162:607–21. doi: 10.1016/j.cell.2015.06.060
50. Zhai C, Cong H, Liu Y, Zhang Y, Liu X, Zhang H, et al. Rs7193343 polymorphism in zinc finger homeobox 3 (ZFHX3) gene and atrial fibrillation: an updated meta-analysis of 10 case-control comparisons. *BMC Cardiovasc Disord* (2015) 15:58. doi: 10.1186/s12872-015-0044-y
51. Benjamin EJ, Rice KM, Arking DE, Pfeufer A, van Noord C, Smith AV, et al. Variants in ZFHX3 are associated with atrial fibrillation in individuals of European ancestry. *Nat Genet* (2009) 41:879–81. doi: 10.1038/ng.416
52. Therkelsen SK, Groenning BA, Svendsen JH, Jensen GB. Atrial and ventricular volume and function in persistent and permanent atrial fibrillation, a magnetic resonance imaging study. *J Cardiovasc Magn Reson* (2005) 7:465–73. doi: 10.1081/jcmr-200053618
53. Kazui T, Henn MC, Watanabe Y, Kovács SJ, Lawrance CP, Greenberg JW, et al. The impact of 6 weeks of atrial fibrillation on left atrial and ventricular structure and function. *J Thorac Cardiovasc Surg* (2015) 150(6):1602–8. doi: 10.1016/j.jtcvs.2015.08.105
54. Chatterjee NA, Shah RV, Murthy VL, Praestgaard A, Shah SJ, Ventetuolo CE, et al. Right Ventricular Structure and Function Are Associated With Incident Atrial Fibrillation. *Circ Arrhythmia Electrophysiol* (2017) 10(1):e004738. doi: 10.1161/circep.116.004738
55. Bursi F, Rocca WA, Killian JM, Weston SA, Knopman DS, Jacobsen SJ, et al. Heart disease and dementia: A population-based study. *Am J Epidemiol* (2006) 163(2):135–41. doi: 10.1093/aje/kwj025
56. Leeuwis AE, Smith LA, Melbourne A, Hughes AD, Richards M, Prins ND, et al. Cerebral blood flow and cognitive functioning in a community-based, multi-ethnic cohort: The SABRE study. *Front Aging Neurosci* (2018) 10:279. doi: 10.3389/fnagi.2018.00279
57. Frodl T, Skokauskas N. Meta-analysis of structural MRI studies in children and adults with attention deficit hyperactivity disorder indicates treatment effects. *Acta Psychiatr Scand* (2012) 125:114–26. doi: 10.1111/j.1600-0447.2011.01786.x
58. Greven CU, Bralten J, Mennes M, O'Dwyer L, Van Hulzen KJE, Rommelse N, et al. Developmentally stable whole-brain volume reductions and developmentally sensitive caudate and putamen volume alterations in those with attention-deficit/hyperactivity disorder and their unaffected siblings. *JAMA Psychiatry* (2015) 72:490–9. doi: 10.1001/jamapsychiatry.2014.3162
59. Hoogman M, Bralten J, Hibar DP, Mennes M, Zwiers MP, Schweren LSJ, et al. Subcortical brain volume differences in participants with attention deficit hyperactivity disorder in children and adults: a cross-sectional mega-analysis. *Lancet Psychiatry* (2017) 4:310–9. doi: 10.1016/S2215-0366(17)30049-4
60. Hanakawa T, Goldfine AM, Hallett M. A common function of basal ganglia-cortical circuits subserving speed in both motor and cognitive domains. *eNeuro* (2017) 4 (6):ENEURO.0200-17.2017. doi: 10.1523/ENEURO.0200-17.2017
61. Brown P, Marsden CD. What do the basal ganglia do? *Lancet* (1998) 351:1801–4. doi: 10.1016/S0140-6736(97)11225-9
62. Sagaspe P, Schwartz S, Vuilleumier P. Fear and stop: A role for the amygdala in motor inhibition by emotional signals. *Neuroimage* (2011) 55:1825–35. doi: 10.1016/j.neuroimage.2011.01.027
63. Etkin A, Gyurak A, O'Hara R. A neurobiological approach to the cognitive deficits of psychiatric disorders. *Dialogues Clin Neurosci* (2013) 15(4):419–29.

Conflict of Interest: The authors declare that the research was conducted in the absence of any commercial or financial relationships that could be construed as a potential conflict of interest.

frontiers in Aging Neuroscience

ORIGINAL RESEARCH
published: 23 July 2020
doi: 10.3389/fnagi.2020.00194

Maintenance vs. Manipulation in Auditory Verbal Working Memory in the Elderly: New Insights Based on Temporal Dynamics of Information Processing in the Millisecond Time Range

Katarzyna Jablonska[1†], Magdalena Piotrowska[2†], Hanna Bednarek[1], Aneta Szymaszek[2], Artur Marchewka[3], Marek Wypych[3] and Elzbieta Szelag[2]*

[1]Faculty of Psychology, SWPS University of Social Sciences and Humanities, Warsaw, Poland, [2]Laboratory of Neuropsychology, Nencki Institute of Experimental Biology of the Polish Academy of Sciences, Warsaw, Poland, [3]Laboratory of Brain Imaging, Nencki Institute of Experimental Biology of the Polish Academy of Sciences, Warsaw, Poland

OPEN ACCESS

Edited by:
Hans J. Grabe,
University of Greifswald, Germany

Reviewed by:
Deana Davalos,
Colorado State University, United States
Edward Nęcka,
Jagiellonian University, Poland
Leah Fostick,
Ariel University, Israel

***Correspondence:**
Elzbieta Szelag
e.szelag@nencki.edu.pl

[†]These authors have contributed equally to this work

Received: 11 December 2019
Accepted: 03 June 2020
Published: 23 July 2020

Citation:
Jablonska K, Piotrowska M, Bednarek H, Szymaszek A, Marchewka A, Wypych M and Szelag E (2020) Maintenance vs. Manipulation in Auditory Verbal Working Memory in the Elderly: New Insights Based on Temporal Dynamics of Information Processing in the Millisecond Time Range. Front. Aging Neurosci. 12:194. doi: 10.3389/fnagi.2020.00194

Working memory (WM) is a limited-capacity cognitive system that allows the storage and use of a limited amount of information for a short period of time. Two WM processes can be distinguished: maintenance (i.e., storing, monitoring, and matching information) and manipulation (i.e., reordering and updating information). A number of studies have reported an age-related decline in WM, but the mechanisms underlying this deterioration need to be investigated. Previous research, including studies conducted in our laboratory, revealed that age-related cognitive deficits are related to decreased millisecond timing, i.e., the ability to perceive and organize incoming events in time. The aim of the current study was: (1) to identify in the elderly the brain network involved in the maintenance and manipulation WM processes; and (2) to use an fMRI task to investigate the relation between the brain activity associated with these two processes and the efficiency of temporal information processing (TIP) on a millisecond level reflected by psychophysical indices. Subjects were 41 normal healthy elderly people aged from 62 to 78 years. They performed: (1) an auditory verbal *n*-back task for assessing WM efficiency in an MRI scanner; and (2) a psychophysical auditory temporal-order judgment (TOJ) task for assessing temporal resolution in the millisecond domain outside the scanner. The *n*-back task comprised three conditions (0-, 1-, and 2-back), which allowed maintenance (1- vs. 0-back comparisons) and manipulation (2- vs. 1-back comparisons) processes to be distinguished. Results revealed the involvement of a similar brain network in the elderly to that found in previous studies. However, during maintenance processes, we found relatively limited and focused activations, which were significantly extended

Abbreviations: ACC, anterior cingulate cortex; aPFC, anterior prefrontal cortex; ATOT, auditory temporal-order threshold; BG, basal ganglia; dlPFC, dorsolateral prefrontal cortex; IFG, inferior frontal gyrus; IPL, inferior parietal lobule; ISI, interstimulus interval; MFG, middle frontal gyrus; ROI, region of interest; RT, reaction time; SFG, superior frontal gyrus; SMA, supplementary motor area; SPL, superior parietal lobule; TIP, temporal information processing; TOJ, temporal-order judgment; vlPFC, ventrolateral prefrontal cortex; WM, working memory.

during manipulation. A novel result of our study, never reported before, is an indication of significant moderate correlations between the efficiency of WM and TIP. These correlations were found only for manipulation but not for maintenance. Our results confirmed the hypothesis that manipulation in the elderly is a dynamic process requiring skilled millisecond timing with high temporal resolution. We conclude that millisecond timing contributes to WM manipulation in the elderly, but not to maintenance.

Keywords: working memory, temporal information processing, auditory *n*-back task, fMRI, maintenance and manipulation processes

INTRODUCTION

Working memory (WM) is involved in almost every cognitive task and plays a crucial role in complex cognition in humans. It allows one to successfully keep and manipulate information in mind over a short period of time (Baddeley, 2000; Cowan, 2008). Because of the important role of such moment-to-moment processing in mental activity, impairments in WM function can be a major barrier to independent living. One of the possible causes of a decline in WM efficiency may be the neurodegenerative processes associated with normal aging, known also as "healthy aging" (for a summary see Fakhri et al., 2013; Nyberg et al., 2014; Eriksson et al., 2015). Many people with advancing age report problems in processing information in rapidly changing contexts. Evidence indicates that WM consists of two different processes: *maintenance* for temporary storage in a readily accessible state and *manipulation* for the online information processing required for the guidance of subsequent behavior. Accordingly, maintenance has been defined as storage (including rehearsal), monitoring, and matching information in WM, whereas manipulation refers to the reorganization and updating of each memory set (Fletcher and Henson, 2001; Veltman et al., 2003).

As these processes differ in their sensitivity to advancing age, one may observe individual differences in WM. On this matter, Dixon and de Frias (2007) and Lindenberger et al. (2013) reported an increase in individual differences in WM in the elderly in comparison with those observed in young adults presumably reflecting the contribution of general cognitive domains—such as sustained and executive attention or short- and long-term memory—to WM efficiency (Conway et al., 2005; Jaeggi et al., 2010). This leads to the question: why is WM better preserved in some elderly people than in others?

The main objective of the present study is to understand such individual differences in elderly subjects with reference to temporal information processing (TIP). The rationale for this approach comes from a number of literature studies, including studies conducted in our laboratory, which indicate that TIP in the millisecond range sets a frame for our mental activity and determines human behaviors (e.g., Szelag et al., 2011; Bao et al., 2013, 2014; Nowak et al., 2016). Many mental functions, including WM, may be characterized by their specific temporal dynamics in the millisecond domain; hence, patterning in time is considered to be one of the characteristic features of our working brains (Lewandowska et al., 2010; Radua et al., 2014; Nowak et al., 2016). One may assume, therefore, that TIP constitutes a neural basis for mental activity in both normal and pathological conditions, including cognitive declines in healthy aging (e.g., Szymaszek et al., 2009; Teixeira et al., 2013). Accumulated data have also indicated age-related deterioration in TIP (e.g., Fitzgibbons and Gordon-Salant, 1994; Kolodziejczyk and Szelag, 2008; Szymaszek et al., 2009; Kumar and Sangamanatha, 2011; Nowak et al., 2016).

The temporal dynamics of the processes underlying WM are supported by the original Scalar Expectancy Theory (Treisman, 1963; Treisman et al., 1990; Meck, 2005; Matthews and Meck, 2016). These authors assumed that TIP is associated with the operation of three mental stages, i.e., internal clock, memory (WM and reference memory), and decision processes. Thus, individual differences in timing might reflect alterations within these stages. This suggests that cognitive functions cannot be understood without their temporal frame. Despite the fact that WM studies require efficient TIP and vice versa, the interface of timing and WM has been rarely studied in the existing literature (Lewandowska et al., 2010; Radua et al., 2014; Üstün et al., 2017).

Given the importance of TIP for our mental activity, the present study focuses on relationships between WM and TIP in advanced age. Both these functions seem to deteriorate in the elderly. Based on neuroimaging data (see below), these relationships seem to be of great importance for understanding individual differences in WM—in particular, why some people have more efficient WM than others. One might hypothesize that the two WM processes, i.e., maintenance and manipulation, are differentially vulnerable to TIP (see below for more explanation).

Neuroanatomical Representation of WM and TIP

Recent neuroimaging data have indicated the involvement of several brain areas in WM tasks, stressing that a key role is played by the *prefrontal cortex* (PFC; Ragland et al., 2002; Tisserand and Jolles, 2003; Raz et al., 2005; Fuster, 2009; Fakhri et al., 2013; Lindenberger et al., 2013; D'Esposito and Postle, 2015; Luis et al., 2015). In particular, three regions of the lateral PFC—*ventrolateral* (vlPFC), *dorsolateral* (dlPFC), and *anterior* (aPFC)—are consistently reported to be involved (Fletcher and Henson, 2001). The involvement of more posterior areas has been also postulated, i.e., the *premotor*, *parietal*, *cingulate* and *superior temporal gyrus*, and *supplementary motor area* (SMA). Furthermore, some authors indicated the role of the *basal ganglia* (BG) and *cerebellum*, as well as regions specialized for processing particular modalities (see the meta-analysis of 24 previous

studies by Veltman et al., 2003; Owen et al., 2005; D'Esposito and Postle, 2015; Luis et al., 2015; for the recent overview see also Eriksson et al., 2015). Some studies have found that brain activity during WM is vulnerable to attentional load, the type of information to be maintained, as well as perceptual and long-term memory representations. Hence, the neurocognitive architecture of WM results also from the specific complex interactions within a given task (e.g., Jaeggi et al., 2010; Eriksson et al., 2015; summarized in Box 1; Luis et al., 2015).

Another support for the "WM–TIP" relation comes from the neural underpinnings of timing, which indicate the involvement of many brain areas in TIP (for a recent review see Merchant et al., 2013). One approach assumes that the main core timing mechanism interacts with context-dependent areas. This hybrid model suggests a partially distributed timing mechanism, integrated by core structures such as *cortico-thalamo-BG* circuits and areas that are selectively engaged in a given task (Buhusi and Meck, 2005; Coull et al., 2011; Matthews and Meck, 2014). Such diffuse timing representation is in agreement with the earlier report by Rao et al. (2001), who indicated the involvement of nontemporal processes during timing tasks, reflected by activations in the dlPFC (related to WM or comparison functions), posterior parietal cortex, and anterior cingulate cortex (ACC, which controls modulatory attention), as well as the BG providing the subcortical "timekeeper" system. These results are supported by numerous and more recent fMRI studies, which have consistently identified several key timing areas: the right inferior frontal cortices, in particular, the inferior prefrontal cortex, dlPFC, ACC, SMA, and nonfrontal brain regions such as the inferior parietal lobules (IPLs), cerebellum, and BG (Coull and Nobre, 2008; Szelag et al., 2009; Allman and Meck, 2012; Merchant et al., 2013). The functional contribution of these areas to the timing network is still a matter of debate.

The theoretical dissociation of the processes underlying WM is based on neuroimaging data indicating the neuroanatomical segregation of maintenance and manipulation processes. This distinction between the activations obtained for these two processes seems important in the context of studying the role of TIP in WM. We hypothesize that TIP is more important for processing information within WM than for maintenance because of the more dynamic mental process involved in reordering and updating. Therefore, analyses of brain activity during each of these two processes may provide a better understanding of the role of TIP in WM.

Neuroanatomical Representation of Maintenance and Manipulation Processes

The early approach to this distinction (Smith et al., 1998; Veltman et al., 2003) was based on a comparison of brain activity between the traditional item-recognition tasks (e.g., the Sternberg WM task)—classified as pure storage tasks (involving rehearsal and storage)—and the *n*-back task (characterized more as a manipulation task involving processing and updating). Based on such comparisons, Smith et al. (1998) indicated that the dlPFC is activated whenever a WM task requires processing. In contrast, the traditional item-recognition tasks (which can be considered as storage tasks) did not produce any sign of dlPFC activation.

On the other hand, Veltman et al. (2003) indicated the functional rather than neuroanatomical distinction between maintenance (increased primarily on the Sternberg task) and manipulation (increased on the *n*-back task) processes, given the evidence that both these tasks resulted in a very similar pattern of task-related activations in the bilateral dlPFC, left vlPFC, bilateral parietal cortex, as well as in the cerebellum and SMA.

The other approach to explaining the neuroanatomy of WM processes comes from studies exploring *n*-back tasks. Over the years, these tests have been frequently used as continuous-recognition measures that present stimulus sequences, such as letters, pictures, syllables, etc. (e.g., Miller et al., 2009; Jaeggi et al., 2010). The subjects' task is to judge for each item in the sequence whether it matches the one presented *n*-items before. Participants must maintain and update a dynamic rehearsal set while responding to each item. Behavioral data using the *n*-back task have demonstrated that the reason for the "2-back" condition being more difficult than the "1-back" is that these conditions involve different processes associated with WM. Specifically, the "1-back" task is based more on maintenance, whereas "2-back" uses manipulation resources.

Recent neuroimaging studies have indicated the involvement of several brain areas in these two conditions (D'Esposito et al., 1999; Rypma and D'Esposito, 1999; Tsukiura et al., 2001; Ragland et al., 2002). Using the *n*-back task, a few contrasts may be designed to reveal activation changes reflecting maintenance vs. manipulation demands (Ragland et al., 2002). Specifically, the "1- vs. 0-back" contrast reveals changes related to WM maintenance (controlling for perceptual and motor components) while minimizing the role of the central executive system and updating (manipulation) resources. On the other hand, the "2- vs. 0-back" contrast shows activation changes reflecting the addition of central executive components (monitoring and manipulation) to the online maintenance demands. On the contrary, the "2- vs. 1-back" contrast diminishes the effect of maintenance demands (involved in both 1- and 2-back tasks) and allows the gauging of WM manipulation resources, given the difficulty of the task. The application of these three contrasts allows the identification of the involvement of specific brain areas in different WM processes.

Both the existing theoretical models and the results of neuroimaging studies have compared the specific functions, i.e., maintenance of sensory information vs. manipulation for which the central executive components are required (Petrides, 1994; D'Esposito et al., 1998). Whereas the former WM processes involve the vlPFC (BA 44, 45, and 47), the latter ones activate the dlPFC (BA 9 and 46). This functional dissociation, however, appears rather to be relative than absolute (Ragland et al., 2002).

Experimental Aim

The present study addresses the question of whether individual differences in brain activity in normal healthy elderly subjects during maintenance and manipulation of information in WM are related to the efficiency of TIP evidenced in psychophysical indices. We hypothesize that WM and millisecond timing are interrelated and may share a similar neuroanatomical basis. However, fluctuations in cognitive efforts to perform more

difficult WM tasks may influence this relationship. Our study has the following two aims:

(1) To identify in elderly subjects the brain structures engaged in maintenance (storage, monitoring, and matching) of presented auditory verbal material, as well as in the manipulation (reorganization and updating) of such material, using the standard *n*-back auditory task.
(2) To investigate the relationship between the efficiency of millisecond TIP and WM by examining both behavioral indices and brain activity in the two WM processes. Taking into account that maintenance is reflected more in storage and manipulation in dynamic processing, we hypothesize that TIP is related mostly to manipulation but not to maintenance. The relationships between TIP and manipulation could provide a new insight into individual differences in WM in the elderly.

To avoid any cross-modal interference that might obscure the observed relationships, both the TIP and WM measurements applied here employ the perception of auditory stimuli.

MATERIALS AND METHODS

Participants

Forty-one normal healthy elderly adults (37 women and four men), aged from 62 to 78 years (M = 67.1, SD = 3.7) took part in the study. They were recruited through local advertisements at various community centers, senior clubs, and Universities of the Third Age in the Warsaw area. All participants had between 11 and 18 years of education and were right-handed Polish native speakers. They reported no neurological or psychiatric disorders, head injuries, systemic diseases, or the use of medications affecting the central nervous system. The above-mentioned inclusion and exclusion criteria were verified in an interview with each subject individually. Furthermore, hearing level was screened using pure-tone audiometry (Audiometer MA33, MAICO; ANSI, 2004). The tested frequencies were selected to encompass the frequency spectrum of the presented auditory stimuli, which included 250, 500, 750, 1,000, 1,500, 2,000, and 3,000 Hz. All subjects had normal hearing level, assessed with pure-tone average (PTA), i.e., $\leq$25 dB HL at 500, 1,000, and 2,000 Hz (Carhart, 1971; Kung and Willcox, 2007).

The Mini-Mental State Examination (MMSE; Folstein et al., 2001) and the Geriatric Depression Scale (GDS; Sheikh and Yesavage, 1986) were used to screen for dementia and depression. A score of 27 or more points on the MMSE (M = 28.93, SD = 1.01) and a score of 5 or fewer points on the GDS (M = 2.61, SD = 1.75) were inclusion criteria. The study was approved by the Ethical Commission at the University of Social Sciences and Humanities (permission no 1/2017, registered as 2 /I/ 16–17) and was in line with the Declaration of Helsinki. All participants signed a written informed consent form prior to the study.

Experimental Paradigms

Each participant completed two experimental paradigms performed in separate sessions. These paradigms comprised: (1) an auditory *n*-back fMRI task; and (2) a psychophysical auditory temporal-order judgment (TOJ) task.

Auditory *n*-Back fMRI Task

A simple block design with two experimental *n*-back conditions (1- and 2-back) and one control condition (0-back) was applied (**Figure 1**). The auditory stimuli were 30 consonant–vowel syllables lasting 300 ms each. The successive syllables were separated by 1,700-ms silent intervals. Each syllable was built from one of six consonants (B, D, G, L, M, Z), followed by one of five vowels (A, E, O, U, Y). An additional syllable (WO) was created for the control condition (0-back). The strings of syllables were delivered binaurally through MRI compatible headphones, using Presentation® software (Version 18.0, Neurobehavioral Systems, Inc., Berkeley, CA, USA[1]).

The subjects were asked to listen to presented strings of syllables and to press a button with their right thumb in response to a target syllable (**Figure 1**). Depending on the condition, the target was the predefined syllable WO (0-back), a syllable matching the previous one (1-back), or a syllable matching the one before the previous syllable (2-back). Subjects were instructed to suppress their reactions to nontarget syllables. A written instruction for the current task was displayed permanently on the screen as a reminder.

The study comprised three sessions. Each session consisted of six blocks: four experimental (1- and 2-back conditions repeated twice) and two control blocks with 0-back condition. During each session, the blocks were presented in pseudo-random order. The example order of blocks in session 1 was as follows: 0-, 1-, 2-, 1-, 0-, and 2-back. Each block lasted 60 s and consisted of 30 trials (five targets and 25 nontargets). Each trial comprised one syllable presentation. The whole study comprised 540 trials.

Measures of behavioral performance on the 0-, 1-, and 2-back conditions were accuracy of performance (reflected in the percentage of correct responses to target syllables in each condition) and reaction time (RT), measured from the onset of the presented syllable to the onset of the subject's button press for the correct target identification. The percentage of correct responses and the mean RTs from each condition were submitted to data analysis.

To familiarize subjects with the task proper, each participant took part individually in a training session performed outside the scanner. In this session, subjects were presented with 0-, 1-, and 2-back conditions and practiced the detection of a target syllable by pressing a button. After completion of each condition, feedback on correctness achieved was provided. The introductory session was continued until a criterion of 75% correct responses was achieved. Then, the fMRI experiment started. No feedback on performance was provided during the fMRI session.

The MRI procedure was conducted in the Laboratory of Brain Imaging at the Nencki Institute of Experimental Biology using a 3-T Siemens MAGNETOM Trio system (Siemens Medical Solutions). Prior to the task, participants were asked to complete an MRI safety questionnaire.

[1] www.neurobs.com

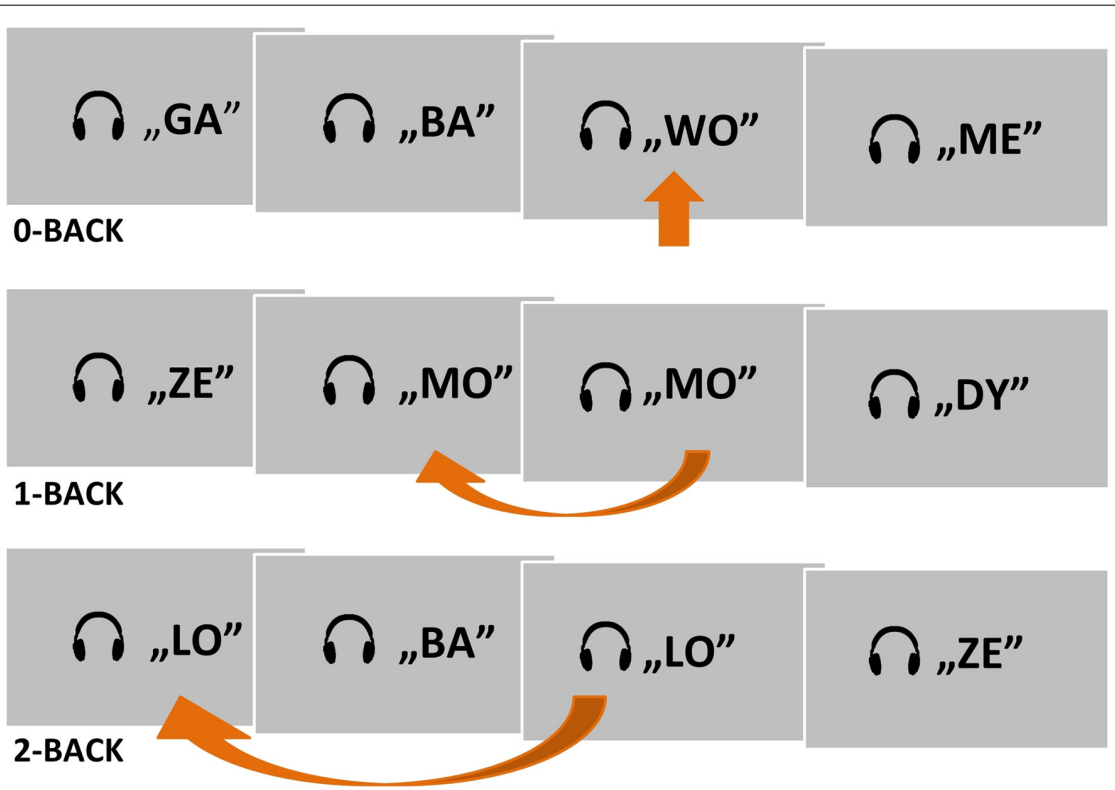

FIGURE 1 | A schema of the two experimental conditions (1- and 2-back) and one control condition (0-back) used in the auditory *n*-back fMRI task. Target situations are indicated by arrows.

Psychophysical Auditory Temporal-Order Judgment Task

To study the efficiency of TIP in auditory perception, we applied the TOJ task using the psychophysical procedure described in our previous studies (e.g., Szymaszek et al., 2009; Szelag et al., 2018). Some of the results presented here have been previously published in a study that focused on sequencing abilities in different TOJ tasks (Szelag et al., 2018).

Participants were presented with pairs of 10-ms sinusoidal tones with a rise-and-fall time of 1 ms. The stimuli were generated with a Realtek ALC3246 sound controller and Waves MaxxAudio Pro software. They were delivered binaurally at a comfortable listening level through Philips SHP8500 headphones. Each pair consisted of two tones (a low 400-Hz tone and a high 3,000-Hz tone) separated by a short interstimulus interval (ISI)—the time gap between the offset of the first stimulus and the onset of the second stimulus. Two tones within each pair were adjusted to equal loudness on the basis of isophones. A warning signal was delivered 1 s prior to each pair of stimuli in order to focus the participants' attention on the task. They were asked to report verbally the order of two sounds within the presented pair, i.e., to judge whether the order of tones was high–low or low–high.

The TOJ task consisted of two parts. Part 1 comprised 20 trials (presented tone pairs). The two tones in each pair were separated by fixed ISIs, changing in steps of 27 ms in the range from 240 to 1 ms, in a decreasing (n = 10) and then increasing (n = 10) order. On the basis of these predefined 20 trials, the ISI value of the first trial in part 2 of the TOJ task was computed according to an algorithm based on maximum likelihood estimation (Treutwein, 1997). Part 2 consisted of 50 trials. The ISI in each trial was adjusted according to an adaptive algorithm, depending on the correctness achieved in the previous response (see Szelag et al., 2018 for a more detailed description).

On the basis of 70 completed trials (20 trials in part 1 and 50 trials in part 2) an auditory temporal-order threshold (ATOT) was calculated (in milliseconds) for each subject (see Szelag et al., 2018). The ATOT reflected the index of TIP efficiency and was defined as the shortest time gap between two paired tones presented in rapid succession at which a subject could identify their temporal order (i.e., their before–after relation) with at least 75% correctness (Szelag et al., 2011, 2014, 2015a,b; Bao et al., 2013, 2014).

In order to familiarize participants with the TOJ task, prior to the task proper, they were instructed by the experimenter and performed a few practice trials. After each response, feedback on correctness was given. During the proper task, no feedback on correctness was given.

The TOJ task was conducted in a soundproof room in the Laboratory of Neuropsychology at the Nencki Institute of Experimental Biology.

fMRI Data Acquisition and Preprocessing

MRI data were collected on a Siemens 3-T Trio MRI scanner using a 12-channel coil. High-resolution (1 × 1 × 1 mm voxels) T1-weighted anatomical images were acquired with the following parameters: repetition time (TR) = 2,530 ms, echo time (TE) = 3.32 ms, flip angle = 7°, 176 1-mm thick slices, field of view (FOV) = 256 × 256 mm. Functional images (3 × 3 × 3 mm voxels) were acquired using an echo planar imaging pulse sequence with the following parameters: TR = 2,000 ms, TE = 30 ms, flip angle = 90°, 36 interleaved slices with 0.5-mm gap, FOV = 216 × 216 mm. Additionally, a field map was acquired to allow for field inhomogeneity distortion correction, with TE1/TE2/TR = 4.5/6.96/600.

MRI data were preprocessed and analyzed in SPM12[2]. Data from each subject underwent the same preprocessing steps (motion correction and unwarping, coregistration of the T1 image to mean EPI image, and segmentation of the T1 image to different tissues). The fMRI data were normalized to MNI space with 2 × 2 × 2-mm voxels using a standard SPM12 algorithm and smoothed with a 6-mm Gaussian kernel.

STATISTICAL ANALYSES

n-Back Behavioral Data and Psychophysical TOJ Indices

The behavioral data from the *n*-back task (accuracy of performance and mean RT), as well as psychophysical TOJ indices (reflected in ATOT values), were analyzed using IBM® SPSS® Statistics 25. As the distribution of data deviated from the Gaussian (according to the Shapiro–Wilk test), nonparametric statistical methods were used. First, to test whether there were differences in the behavioral measures obtained in 0-, 1-, and 2-back conditions, the Friedman test followed by the Wilcoxon signed-rank test were applied. Next, to investigate correlations between the efficiency of WM and TIP, two-tailed Spearman's rank correlations were used. To control for the effect of subjects' age on these relationships, partial correlations were performed.

n-Back fMRI Data Analysis

There were two steps in the fMRI data analysis. First, we identified brain areas engaged in maintenance (storage) or manipulation (updating) of the presented material. Second, we investigated the correlations between brain activity during the WM task and psychophysical indices of TIP efficiency.

Identification of Brain Structures Engaged in WM Maintenance or Manipulation Processes

The fMRI data analysis was performed with SPM12 software, within the general linear model (GLM) framework. At a single-subject level, design matrices with 0-, 1- and 2-back conditions and additional head movement regressors and regressors of motion affected volumes (acquired with the ART toolbox[3]) were estimated. Images were regarded as artifactual when mean image intensity *z*-threshold was above 9, movement threshold was above 2 mm, or rotation threshold was above 0.02 rad. As a result, on average, 5.05 images per person were identified as outliers (between 0 and 57; however, in no case did it exceed 10% of all images, thus no subject was excluded due to excessive motion). Subsequently, a group-level full factorial model with one within-subjects factor—"task" (0-, 1-, 2-back)—was computed. For whole brain analyses, a gray matter mask of 0.20 probability was applied. Familywise error (FWE) $p < 0.05$ threshold at voxel level was set to correct for multiple comparisons. To indicate brain structures engaged in maintenance and manipulation processes, three *t*-contrasts were computed within the model: 1- vs. 0-back, 2- vs. 1-back, and 2- vs. 0-back (see "Introduction" section for a description of these contrasts). The xjView toolbox[4] was used to generate tables of activated regions. All activation peaks were labeled using the Talairach Atlas labels (Lancaster et al., 2000). Structural images of each subject were assessed by a radiologist to exclude brain pathology.

Correlations Between Brain Activity in WM and Psychophysical Indices of TIP Efficiency

We created regions of interest (ROIs) on the basis of two *t*-contrasts from the group-level model: 1- vs. 0-back and 2- vs. 1-back based on clusters surviving the FWE correction (Poldrack, 2007). The 2- vs. 0-back contrast was not considered in correlation analysis because of the engagement of both WM processes (maintenance and manipulation). In total, 26 functional ROIs were created. Eight ROIs (**Table 1**) were built on the basis of the 1- vs. 0-back comparison (reflecting maintenance in WM) and 18 on the basis of the 2- vs. 1-back comparison (reflecting manipulation in WM). Additionally, a sphere ROI was built in the visual cortex in the occipital lobe (20 mm in diameter; the MNI coordinates of the center were *x*, 10; *y*, −80; *z*, 20) as an ROI for statistical control for correlation analyses (Poldrack, 2007). This control ROI exhibited a lack of any activation either in 1- vs. 0-back or 2- vs. 1-back comparisons.

Finally, the correlation analyses for these ROIs were conducted between mean brain activity extracted from 1- vs. 0-back and 2- vs. 1-back contrasts and obtained ATOT values. The MarsBaR toolbox was used to export brain activity[5]. To avoid inflated effects due to multiple comparisons, two-tailed Spearman's rank correlations were applied with adjusted *p*-value cutoff. The cutoff was computed separately for the 1- vs. 0-back and 2- vs. 1-back comparisons, following Bonferroni correction, i.e., dividing a standard *p*-value of 0.05 by the number of performed correlations (Bland and Altman, 1995). As a result, for 1- vs. 0-back, a *p*-value of 0.006 (0.05/9 performed correlations) was used, whereas for the 2- vs. 1-back, a *p*-value of 0.003 (0.05/19 performed correlations) was used.

RESULTS

Behavioral Indices of WM Task

The behavioral data obtained in each *n*-back condition are presented in **Figure 2**. It displays the accuracy of performance

[2]http://www.fil.ion.ucl.ac.uk/spm/software/spm12/
[3]https://www.nitrc.org/projects/artifact_detect
[4]http://www.alivelearn.net/xjview/
[5]http://marsbar.sourceforge.net/

TABLE 1 | Peak level activations in each cluster related to maintenance (1- vs. 0-back), manipulation (2- vs. 1-back), and maintenance with manipulation processes (2- vs. 0-back).

Cluster peak, hemisphere	Brodmann area (BA)	No. of voxels	*t*-value	*p*-value (FWE)	MNI coordinates		
					x	*y*	*z*
1- vs. 0-back (maintenance)							
Middle frontal gyrus, L	6	74	6.069	0.001	−26	0	56
Middle frontal gyrus, R	6	18	5.840	0.001	44	4	56
Inferior parietal lobule, R	7	75	5.905	0.001	40	−40	40
Superior parietal lobule, L	7	19	5.888	0.001	−12	−70	54
Superior frontal gyrus, R	6	43	5.785	0.002	26	4	54
Inferior frontal gyrus, L	13	13	5.412	0.009	−30	22	8
Inferior frontal gyrus, L	44	10	5.256	0.016	−44	6	22
Medial frontal gyrus, L	8	14	5.366	0.010	−4	16	50
2- vs. 1-back (manipulation)							
Insula, L	13	282	8.814	<0.0005	−30	24	2
Precuneus, R	7	255	8.320	<0.0005	10	−70	52
Cerebellum, L	–	251	8.134	<0.0005	−28	−66	−28
Cerebellum, R	–	65	6.590	<0.0005	28	−64	−30
Cerebellum, L	–	48	6.197	<0.0005	−12	−78	−26
Cerebellum, R	–	49	6.019	0.001	10	−74	−28
Middle frontal gyrus, R	9	754	7.856	<0.0005	38	40	32
Middle frontal gyrus, R	6	668	7.806	<0.0005	26	6	52
Middle frontal gyrus, L	6	451	7.189	<0.0005	−26	2	54
Middle frontal gyrus, L	46	207	6.660	<0.0005	−42	46	10
Middle frontal gyrus, L	9	284	6.428	<0.0005	−40	30	30
Inferior parietal lobule, R	40	984	7.768	<0.0005	48	−48	46
Inferior parietal lobule, L	40	1,083	7.111	<0.0005	−38	−44	40
Inferior frontal gyrus, R	13	308	7.304	<0.0005	32	28	2
Inferior frontal gyrus, L	6	69	6.448	<0.0005	−38	2	36
Medial frontal gyrus, L	8	535	7.280	<0.0005	−2	24	48
Superior frontal gyrus, L	6	42	6.149	<0.0005	−8	12	56
Superior frontal gyrus, L	10	10	5.540	0.005	−24	48	0
2- vs. 0-back (maintenance with manipulation)							
Insula, L	13	3,379	11.349	<0.0005	−30	24	2
Inferior parietal lobule, R	40	1,963	10.340	<0.0005	38	−46	42
Inferior parietal lobule, L	40	2,058	9.579	<0.0005	−38	−44	40
Superior frontal gyrus, R	6	1,259	10.225	<0.0005	26	4	54
Superior frontal gyrus, L	6	1,120	8.471	<0.0005	−6	10	56
Cerebellum, L	–	334	8.980	<0.0005	−30	−68	−26
Cerebellum, R	–	192	8.141	<0.0005	28	−64	−30
Cerebellum, R	–	90	7.128	<0.0005	10	−76	−26
Cerebellum, L	–	44	6.310	<0.0005	−12	−76	−26
Inferior frontal gyrus, R	13	599	8.835	<0.0005	32	28	2
Middle frontal gyrus, R	9	717	8.310	<0.0005	38	38	30
Caudate, R	48	17	5.683	0.003	14	−2	14
Caudate, L	48	26	5.663	0.003	−16	0	16
Medial frontal gyrus, L	32	25	5.391	0.009	−6	28	34

Presented p- and t-values were obtained with familywise error (FWE) correction at a voxel (peak) level. Regions were labeled using the Talairach Atlas labels. The x, y, and z Montreal Neurological Institute (MNI) coordinates were used for the left–right, anterior–posterior, and inferior–superior dimensions, respectively. In some structures, more peak activations were observed, but in each cluster, only one peak was indicated.

(**Figure 2A**) and the mean RT (**Figure 2B**) in 0-, 1-, and 2-back conditions.

The Friedman test revealed significant differences between the accuracy of performance in these three conditions ($\chi^2_{(41,2)} = 35.30$, $p < 0.001$). The accuracy in the 2-back condition was significantly lower than in the other two conditions ($p < 0.001$; Wilcoxon tests). There were also significant differences between mean RTs in the 0-, 1-, and 2-back conditions ($\chi^2_{(41,2)} = 48.20$, $p < 0.001$; Friedman test). The mean RT was higher in the 2-back condition than in the 0- and 1-back conditions ($p < 0.001$; Wilcoxon tests).

Psychophysical Indices of TIP

In the present study, the median ATOT value was 89 ms. This is consistent with the results of our previous studies where ATOT values in elderly participants were between 60 and 100 ms (Szymaszek et al., 2009; Szelag et al., 2018).

Correlations Between Behavioral Indices of WM and ATOT Values

To investigate the "WM–TIP" relationship, partial correlations between *n*-back behavioral indices (in 0-, 1-, and 2-back conditions) and ATOT were conducted, controlling for age. Only in the 2-back condition did the results show

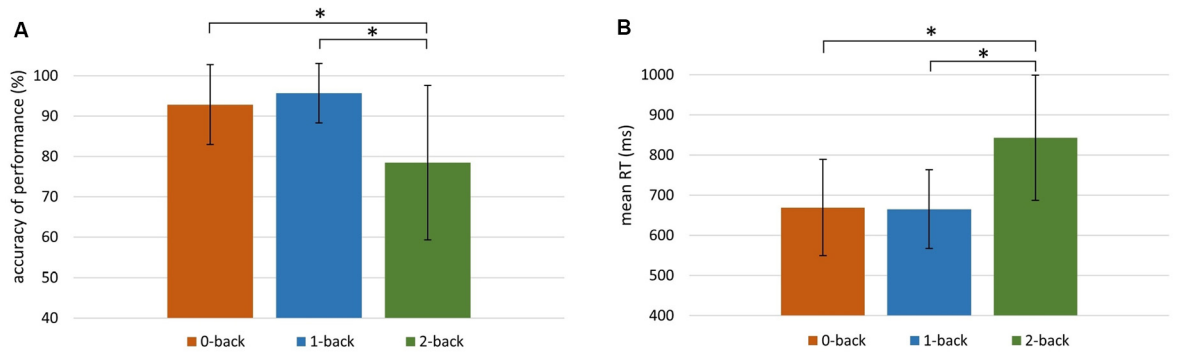

FIGURE 2 | Behavioral indices of working memory (WM) efficiency in the 0-, 1-, and 2-back conditions. **(A)** Accuracy of performance (%) in 0-back: $M = 92.83$, $SD = 9.92$; 1-back: $M = 95.66$, $SD = 7.33$; 2-back: $M = 78.41$, $SD = 19.18$. **(B)** Mean reaction time (RT) in 0-back: $M = 669$ ms, $SD = 121$ ms; 1-back: $M = 665$ ms, $SD = 98$ ms; 2-back: $M = 843$ ms, $SD = 156$ ms. Significant differences ($p < 0.001$) are indicated with an asterisk.

significant correlations between ATOT values and accuracy ($rho = -0.37$, $p < 0.05$; **Figure 3A**), as well as between ATOTs and mean RTs ($rho = 0.47$, $p < 0.01$; **Figure 3B**). This indicates that better performance on the WM task (reflected in higher accuracy and shorter mean RT) was accompanied by more efficient TIP (lower ATOT values). In 0- and 1-back conditions, these correlations were nonsignificant.

fMRI Results of the *n*-Back Task

The results of the group analysis are presented in **Table 1** and **Figures 4A–C**.

Direct comparison of brain activity in the 1- vs. 0-back condition (**Figure 4A**) showed regions engaged mostly in WM maintenance processes (for a more detailed discussion of maintenance/manipulation processes, see "Introduction" section). The comparison revealed activations in bilateral MFG (BA 6), right IPL (BA 7), left superior parietal lobule (SPL; BA 7), right superior frontal gyrus (SFG; BA 6), and left inferior frontal gyrus (IFG; BA 13 and 44), indicating the engagement of the vlPFC, as well as the left medial frontal gyrus (BA 8).

On the other hand, the areas involved mainly in manipulation processes were identified by contrasting the 2- and 1-back conditions (**Figure 4B**). This comparison showed, in general, stronger and wider activations than those observed in the 1- vs. 0-back comparison (maintenance). These activations comprised the left insula (BA 13), right precuneus (BA 7), bilateral cerebellum, and MFG (BA 6, 9, and 46), indicating the involvement of the dlPFC, bilateral IPL (BA 40), and IFG (BA 6 and 13), as well as the left medial frontal gyrus (BA 8) and left SFG (BA 6 and 10).

The 2- vs. 0-back comparison (reflecting maintenance with manipulation; **Figure 4C**) also revealed a widespread network of fronto-parieto-cerebellar activations, comprising the left insula (BA 13), bilateral IPL (BA 40), SFG (BA 6), and cerebellum, as well as the right IFG (BA 13) and MFG (BA 9), bilateral caudate (BA 48), and left medial frontal gyrus (BA 32).

Correlations Between Brain Activity in WM and the Efficiency of TIP

To investigate the relationships between the efficiency of TIP and brain activity in WM processes (maintenance/manipulation), we calculated correlations between ATOT values and mean activation extracted from ROIs (the ROI selection is described in "Statistical Analyses" section). The results revealed moderate negative correlations with some frontal brain regions, as well as the insula, engaged in manipulation processes (2- vs. 1-back). Correlations were found in the bilateral MFG (BA 6, 9, and 46), left medial frontal gyrus (BA 8), left insula (BA 13), and left SFG (BA 6). This indicates that more efficient TIP (reflected in lower ATOTs) was related to stronger activations only in the above regions during the WM manipulation process (**Figure 5**). In contrast, no significant correlations in regions related to maintenance (1- vs. 0-back) were observed. The outcomes of the correlation analyses are presented in **Table 2**.

DISCUSSION

Summary of Results

Using the auditory verbal *n*-back task, we found evidence in elderly people of the activity of a WM brain network comprising mainly the prefrontal cortex (MFG, SFG, IFG), IPL, and SPL, as well as the insula, precuneus, and cerebellum. The relevant result from the present study was the indication of similar brain networks that differ in the range and intensity of activity for the two WM processes, i.e., maintenance (reflected in 1- vs. 0-back comparisons) and manipulation (2- vs. 1-back). For maintenance, the activity was lower and more focused in comparison to that found for manipulation, which was characterized by higher and more spread-out activity (**Table 1**). These effects corresponded to behavioral data that indicated the lower accuracy of performance and longer RT in the 2-back condition than in the 1- or 0-back conditions, confirming that the 2-back condition (based mainly on manipulation) is more difficult than two other conditions studied here (see **Figure 2**).

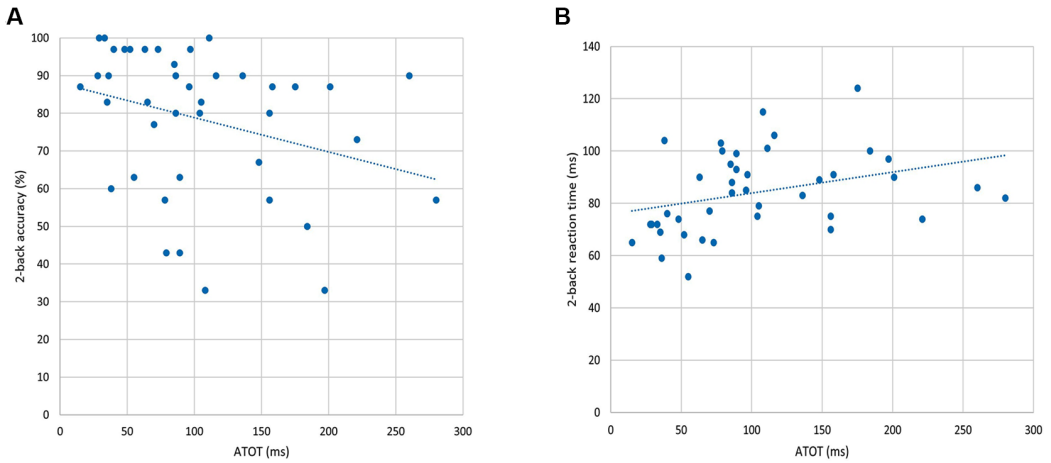

FIGURE 3 | Correlations between behavioral indices from the 2-back condition and auditory temporal-order threshold (ATOT) values: **(A)** accuracy of performance and **(B)** mean RT.

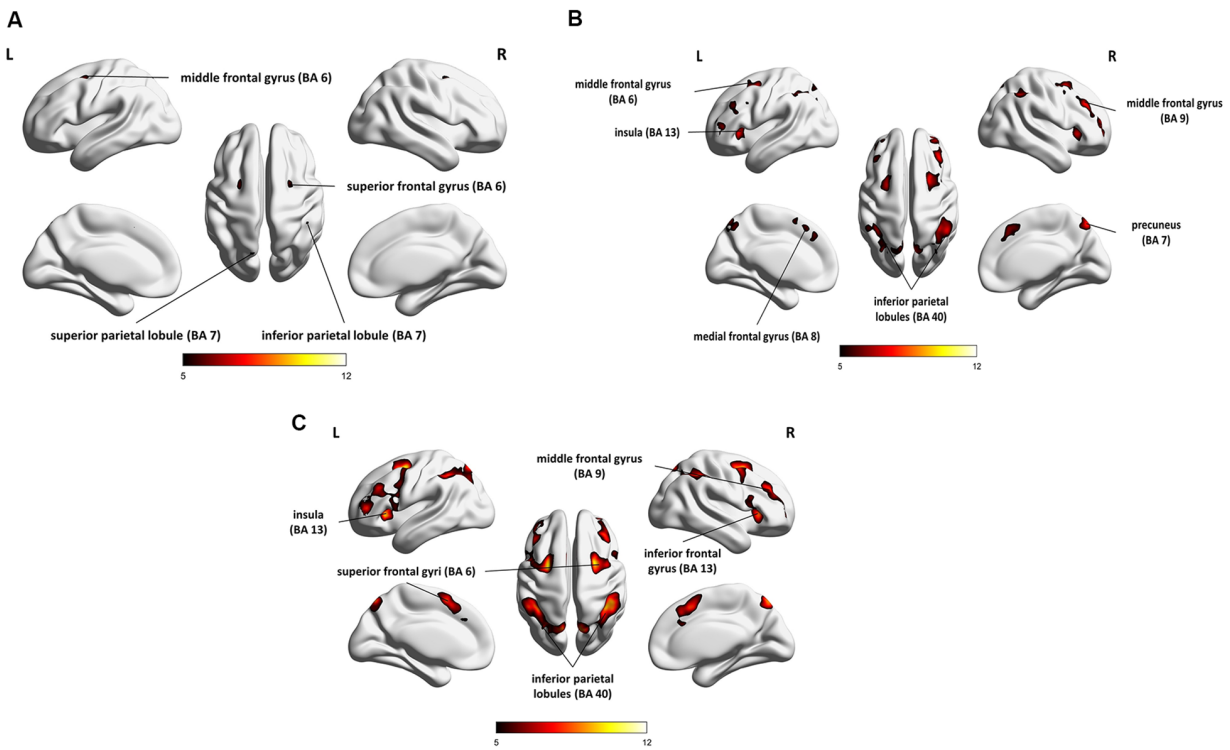

FIGURE 4 | Whole-brain statistical parametric maps representing brain activation specific to: **(A)** maintenance (1- vs. 0-back), **(B)** manipulation (2- vs. 1-back), and **(C)** maintenance with manipulation (2- vs. 0-back). A voxel-level familywise error (FWE) correction was applied ($p < 0.05$) with a cluster extent threshold of 10. L, left hemisphere; R, right hemisphere.

Our results also provided a new, previously unstudied, insight into the "WM–TIP" relation evidenced in both behavioral data and brain activity. We observed moderate significant correlations between psychophysical indices of TIP (ATOT values) and behavioral 2-back performance (accuracy and RTs; **Figure 3**), as well as brain activity during manipulation processes (2- vs. 1-back comparisons; **Table 2**). The better temporal resolution (i.e., lower ATOT) was accompanied by better performance on the 2-back task and stronger activations in regions engaged in manipulation. In contrast, these correlations proved nonsignificant in 1- and 0-back conditions and in maintenance processes, indicating a weaker contribution of

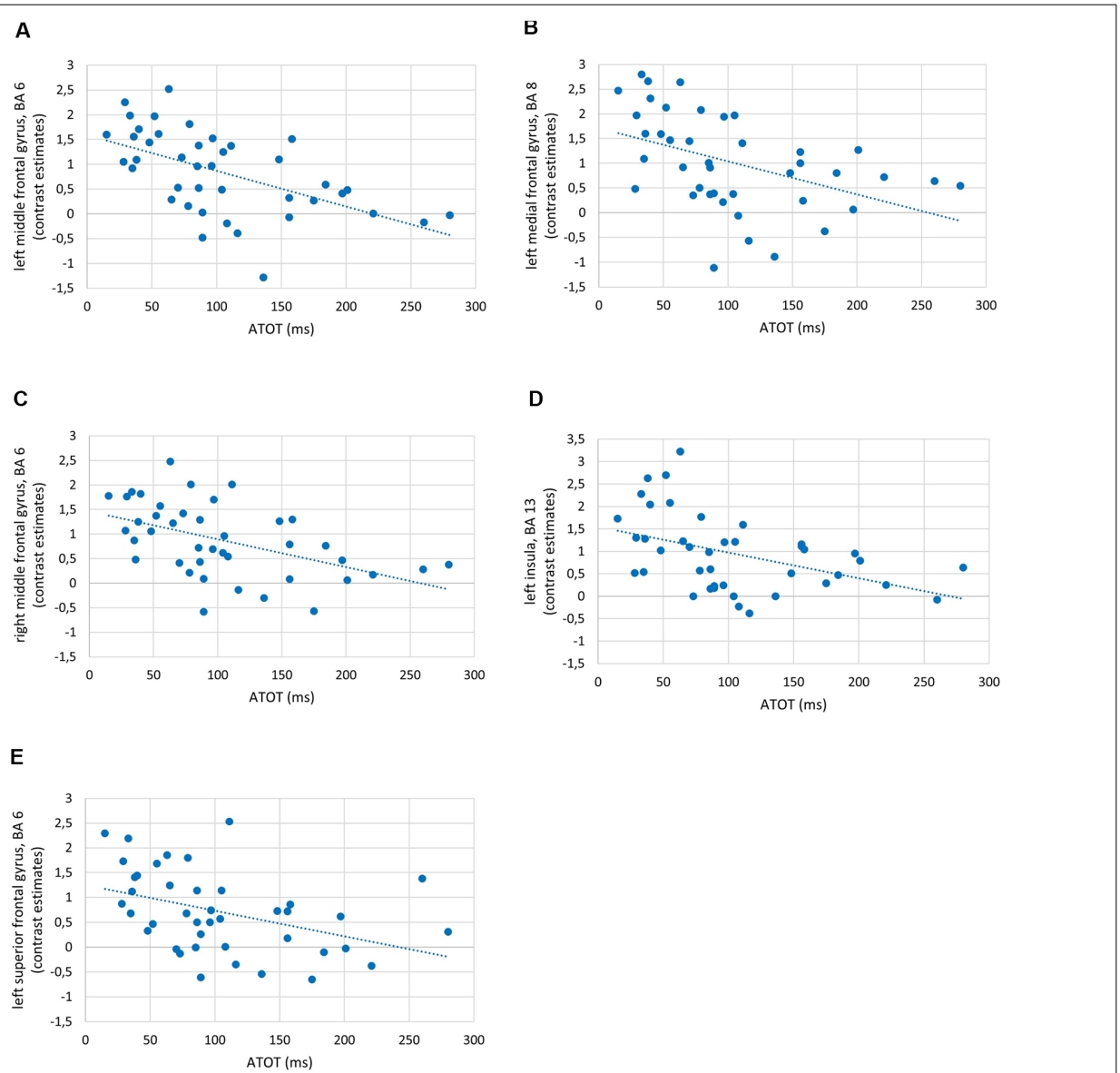

FIGURE 5 | Examples of correlations between temporal-order threshold (ATOT) values and brain activity in regions of interest (ROIs) with peak level activation in **(A)** left middle frontal gyrus (MFG), BA 6; **(B)** left medial frontal gyrus, BA 8; **(C)** right MFG, BA 6; **(D)** left insula, BA 13; and **(E)** left superior frontal gyrus (SFG), BA 6.

temporal resolution to maintenance. Such correlations allowed the identification of some brain areas within the WM network, which are also strongly related to temporal resolution.

Brain Network Supporting WM

Maintenance

The brain network engaged in maintenance reported here (**Figure 4A**) is similar to that reported in previous studies (Tsukiura et al., 2001; Ragland et al., 2002; Crottaz-Herbette et al., 2004; Narayanan et al., 2005) and comprised fronto-parietal regions, including the bilateral MFG (BA 6), right SFG (BA 6), left IFG (BA 13, 44), and left medial frontal gyrus, as well as the right IPL (BA 7) and left SPL (BA 7). It should be noted that the network reported in the above studies was independent of the subjects' age (remaining similar across the lifespan from 18 to 53 years), target modality (visual, auditory), and the procedure used.

A similar brain network as evidenced in our study for maintenance, comprising the left hemispheric premotor cortex (BA 6), SFG (BA 8), and precentral gyrus (BA 44), was previously reported using different procedures. For example, Narayanan et al. (2005) used an item recognition task and found that increasing memory load (task difficulty) was related to increasing activity in the dlPFC and vlPFC. Moreover, the parietal activations in the IPL and SPL (BA 7) evidenced by us indicate the contribution of information storage, which has

TABLE 2 | Correlations (*rho* and *p*-values) between temporal information processing (TIP) and brain activity in regions of interest (ROIs) reflecting working memory (WM) manipulation (2- vs. 1-back) and maintenance (1- vs. 0-back).

Cluster peak, hemisphere	Brodmann area (BA)	No. of voxels	MNI coordinates			*Rho*	*p*
			x	*y*	*z*		
2- vs. 1-back (manipulation)							
Middle frontal gyrus, L	**6**	**451**	**−26**	**2**	**54**	**−0.616**	**<0.0005**
Middle frontal gyrus, L	**46**	**207**	**−42**	**46**	**10**	**−0.583**	**<0.0005**
Medial frontal gyrus, L	**8**	**535**	**−2**	**24**	**48**	**−0.579**	**<0.0005**
Middle frontal gyrus, R	**6**	**668**	**26**	**6**	**52**	**−0.561**	**<0.0005**
Middle frontal gyrus, R	**9**	**754**	**38**	**40**	**32**	**−0.550**	**<0.0005**
Insula, L	**13**	**282**	**−30**	**24**	**2**	**−0.529**	**<0.0005**
Superior frontal gyrus, L	**6**	**42**	**−8**	**12**	**56**	**−0.520**	**0.001**
Middle frontal gyrus, L	**9**	**284**	**−40**	**30**	**30**	**−0.457**	**0.003**
Inferior frontal gyrus, R	13	308	32	28	2	−0.450	0.004
Superior frontal gyrus, L	10	10	−24	48	0	−0.441	0.004
Inferior parietal lobule, L	40	1,083	−38	−44	40	−0.426	0.006
Inferior parietal lobule, R	40	984	48	−48	46	−0.372	0.018
Precuneus, R	7	255	10	−70	52	−0.359	0.023
Cerebellum, R	–	49	10	−74	−28	−0.303	0.057
Cerebellum, R	–	65	28	−64	−30	−0.279	0.081
Inferior frontal gyrus, L	6	69	−38	2	36	−0.261	0.103
Cerebellum, L	–	48	−12	−78	−26	−0.256	0.111
Cerebellum, L	–	251	−28	−66	−28	−0.245	0.127
Control ROI	18	4,120	10	−80	20	−0.141	0.386
1- vs. 0-back (maintenance)							
Middle frontal gyrus, L	6	74	−26	0	56	−0.203	0.209
Inferior parietal lobule, R	7	75	40	−40	40	0.027	0.868
Superior parietal lobule, L	7	19	−12	−70	54	−0.047	0.772
Middle frontal gyrus, R	6	18	44	4	56	−0.167	0.302
Superior frontal gyrus, R	6	43	26	4	54	0.027	0.871
Inferior frontal gyrus, L	13	13	−30	22	8	−0.281	0.079
Medial frontal gyrus, L	8	14	−4	16	50	−0.131	0.421
Inferior frontal gyrus, L	44	10	−44	6	22	0.156	0.335
Control ROI	18	4,120	10	−80	20	−0.277	0.084

The p-value cutoff with Bonferroni correction for 2- vs. 1-back was 0.003, and for 1- vs. 0-back, it was 0.006 (for further explanation, see "Materials and Methods" section). Significant correlations are in bold.

been frequently observed in the literature (Awh et al., 1996; Jonides et al., 1998). Our results also indicate the contribution of the vlPFC (reflected in BA 44 activations) to maintenance, which is congruent with the findings of Owen (1997) and D'Esposito et al. (1998).

On the other hand, some reports also suggest activity in the dlPFC, specifically in the right MFG, during maintenance (BA 9, 46; Tsukiura et al., 2001), which was not observed in our study. This disagreement between our data and those obtained by Tsukiura et al. (2001) may be due to the more complicated procedure used, causing more complex maintenance processes with an associated delay in the subjects' reaction. It is possible that the complex task used by Tsukiura et al. (2001) may activate a larger network of structures than the relatively simple task used in our study.

Manipulation

Although in our study the brain network engaged in maintenance and manipulation processes was nearly the same, the network involved in manipulation was characterized by higher and more spread-out activity (**Figures 4A,B**). This probably reflects the more complex processes required for manipulation, which involves the permanent reorganization and updating of analyzed material.

In line with previous studies, the manipulation-specific regions in our study were the bilateral MFG (BA 6, 9, 46), IFG (BA 6, 13) and IPL (BA 40), left SFG (BA 6, 10) and insula (BA 13), and also the bilateral cerebellum. These results support the broad engagement of the core WM system in the fronto-parietal network during manipulation (Tsukiura et al., 2001; Ragland et al., 2002; Veltman et al., 2003; Schmidt et al., 2009; Barbey et al., 2013). In agreement with the traditional functional division between maintenance and manipulation, our results suggest that activity in the dlPFC (BA 9 and 46), but not in vlPFC (BA 44, 45, 47), is involved in manipulation.

It is also important to emphasize the involvement of the cerebellum in the WM network in our study. Cerebellar activations during WM tasks have also been reported in previous studies (Luis et al., 2015); therefore, our results support the involvement of the fronto-parieto-cerebellar network in WM. Interestingly, the contribution of motor system network was indicated in both verbal and nonverbal WM performance (Liao et al., 2014). Cooper et al. (2012) suggested that cerebellum plays an integrative role in processing of motor information and pointed out importance of these integrative processes also in executive functions and other cognitive tasks. Cerebellum involvement was observed not only in WM but also in various TIP tasks

(Ben-Yehudah et al., 2007). The activations in the cerebellar cortex in the elderly reported in our study may be due to the contribution of compensatory mechanisms supporting more complex processing during manipulation, which may be more difficult for elderly subjects, taking into account age-related decline.

To sum up, our results are generally in line with previous reports that used the *n*-back task in elderly subjects, supporting the engagement of the broad fronto-parieto-cerebellar network in WM processes (Owen et al., 2005; Luis et al., 2015).

Functional Hemispheric Asymmetry in Verbal WM in the Aging Brain

According to the literature (Owen et al., 2005), the type of material used in the *n*-back task in the present study (syllables) may primarily activate left hemispheric regions. The language-dominant hemisphere usually exhibits stronger involvement in memory processing of verbal material (Bradshaw and Nettleton, 1981; Gazzaniga, 2000; Weber et al., 2007; Hellige, 2008). It may be supported by electrical neuroimaging analyses of auditory evoked potentials recorded while the participants completed the TOJ task (Bernasconi et al., 2010, 2011). They showed the engagement of the left, but not right, posterior perisylvian regions activity as a predictor of accurate behavioral performance of auditory TOJ task and early encoding phases of paired stimuli critical for the perception of their order. However, in our study, despite the syllable processing required (i.e., typical verbal material), there was no clear lateralization pattern in either maintenance or manipulation processes—we observed left, bilateral, and right activations of brain structures (**Figure 4**). As stated above, the observed left hemispheric activity is consistent with previous findings (Owen et al., 2005) and confirms that lateralization is determined by the type of presented material. As we also found bilateral and right hemispheric activations in verbal stimuli processing, two possible explanatory mechanisms may be proposed for the observed hemispheric asymmetry pattern.

First, despite the general left hemispheric dominance in language, there is also much evidence in the literature regarding the contribution of the right hemisphere (Hellige, 2001, 2008). This lateralization pattern may result from the involvement of global holistic processing in language processing. In our study, it may support the phonological sequential analysis of presented syllables, which may be also processed as whole acoustic patterns without the need for linguistic coding (Zatorre and Samson, 1991; Hellige, 2001; Lindell, 2006).

Second, the observed bilateral activations may be associated with age-related reduced hemispheric asymmetry. Previous research revealed that elderly adults demonstrate reduced material-relevant activity and engagement of additional, nonspecific brain areas in comparison to young adults performing the same task (Cabeza, 2002; Mattay et al., 2002). This extra activity is interpreted as a neurocognitive compensatory mechanism underlying the dedifferentiation hypothesis of hemispheric asymmetry (Dennis and Cabeza, 2008). Accordingly, brain areas become less specialized with increasing age, leading to decreased activity in task-relevant regions, accompanied by increased activity in less specialized brain areas. Therefore, bilateral and right hemispheric activations in our study could result from an interplay of such compensatory mechanisms. Thus, to meet the demands of the maintenance and manipulation processes, additional engagement of cross-hemispheric counterparts is observed in the elderly.

The "WM–TIP" Relationship

The Role of TIP in WM Processes

As mentioned in "Introduction" section, previous studies have suggested that TIP plays an important role in numerous cognitive functions, such as language, attention, learning, executive processes, and WM (Pöppel, 1997; Poeppel, 2003; Szymaszek et al., 2009; Ulbrich et al., 2009; Nowak et al., 2016). Because of the specific temporal dynamics of these functions, it can be assumed that they are rooted in a defined time template creating the neural frame for our mental activity. Despite pronounced individual differences, experimental data have indicated that proper temporal ordering is controlled by a hypothetical internal clock (pacemaker counter or oscillator device), likely operating at a high oscillation rate, within a window of some tens of milliseconds (Treisman, 1963; Treisman et al., 1990; Pöppel, 1997; VanRullen and Koch, 2003; Rammsayer and Brandler, 2007; Troche and Rammsayer, 2009; Binder, 2015).

The temporal dynamics of WM are emphasized in the classic Scalar Expectancy Theory (see articles cited in "Introduction" section), which assumes that TIP is attributable to the operation of WM. Despite these facts, studies on the neural basis of WM have often ignored the underlying time frame in which the specific WM processes are embedded.

WM and TIP are fundamental properties of mental activity and commonly believed to interact with each other. The influences of many other factors are an important aspect of this interaction. Our paradigm employed context-specific processes, i.e., auditory perception of exposed syllables, phonological processing, rehearsal resources, and executive properties (comparison, decision-making, motor reaction, or suppression of some reactions). In the subject sample studied here, we confirmed the existence of individual differences in TIP and WM efficiency, evidenced in behavioral data (**Figure 3**). The question is: *what mechanisms coexist and cooperate with such multifactorial WM resources?*

Clock Functions Differentiate WM Processes

The novel value of the present study is the observation of a large difference, never reported before, between two different WM processes (maintenance/manipulation) in relation to their TIP properties. Both the behavioral data (**Figure 3**) and brain activity registered in the scanner (**Figure 5**) indicated a strong contribution of TIP to manipulation, but not to maintenance (**Table 2**). *Why are temporal dynamics incorporated differently in these two processes?*

In the 1-back condition, involving mostly maintenance (storage and rehearsal), the incoming information is collected by integrating information over intervals of ∼2-s duration,

referring to the last syllable followed by the button press (or the suppression thereof), while minimizing the role of updating permanent resources. In the 0-back condition, such integration intervals were much longer because the predefined target syllable (here WO) remained unchanged during the whole trial.

In contrast, the necessity of manipulation in the 2-back condition (permanent reorganizing and updating) incorporated the strong temporal dynamics in a millisecond frame during relatively long intervals. Such integration intervals were not only longer than those in the 1-back condition but also required more advanced phonological analysis in order to distinguish between phonemes in processed consonant–vowel syllables. In such processing, skilled millisecond timing (proper temporal resolution) is crucial for decoding the initial stop consonants which, in many languages, are limited in time up to ∼40 ms. In such short intervals, rapid formant transitions characteristic to the initial consonants must be decoded. During this phonological processing, high temporal resolution is necessary for the proper identification and correct ordering of consonants and vowels in the presented syllables (Poeppel, 2003; Szelag et al., 2014). Additionally, in the 2-back condition, the information was collected and analyzed by integrating information in real time. This relies on continuous online updating and comparison with the syllable before–last, accompanied by a tentative suppression of the last syllable. Such manipulation transcended the storage required for maintenance by the dynamic processing of information with a precision of some tens of milliseconds. As a consequence, manipulation caused the 2-back condition to be more difficult than the 1- or 0-back ones (**Figures 2**, **3**).

To understand better the "WM-TIP" relationships, it should be clarified whether they may be also evidenced using other temporal processing tasks. The previous studies, including studies conducted in our laboratory, indicated the heterogeneity of temporal ordering ability measured with various TOJ tasks. In these studies, the obtained absolute threshold values were strongly stimulus-dependent, procedure-related, and influenced by perceptual strategies used by participants (Szymaszek et al., 2009; Ulbrich et al., 2009; Fostick and Babkoff, 2017; Szelag et al., 2018). Furthermore, these threshold values depended on peripheral sensory mechanisms, corresponding to shorter transduction time for auditory than visual stimuli at the level of receptive cells in each modality system (Kanabus et al., 2002).

The question is whether the relationship reported here may be also observed using other tasks addressing millisecond TIP. Although the present experiment cannot answer this question directly, we are of the opinion that the binaural presentation of two tones differing in pitch applied here may reflect properties of the hypothetical internal clock (see the Scalar Expectancy Theory, Matthews and Meck, 2016). Further experimental studies are necessary to clarify these issues.

These considerations lead to another question that could be answered in our recently running research project, whether the "WM-TIP" relationships are characteristic selectively for millisecond TIP or also for other temporal levels, namely, several hundred millisecond or multisecond domains. There is some evidence that the interval timing (addressed usually multisecond level) and WM can originate from the same oscillatory brain activity and may share common cognitive properties, such as attentional or executive resources (for the recent review see Gu et al., 2015). These common properties were reviewed from behavioral, anatomical, pharmacological, and neuropsychological perspectives.

On this background, the novel value of our study is the indication of some dissociation in WM processes, indicating the temporal constraints of manipulation but rather not of maintenance processes. Accordingly, our finding gives a new light on relationships between WM and TIP, which are critical components of cognition.

Correlations Between ATOT and Behavioral and Neuroimaging WM Indices

In terms of individual resources in TIP, persons characterized by better temporal resolution (lower ATOT in our study) could follow the updating in real time more accurately and with shorter RT, as evidenced in **Figure 3**. It is important to stress that the above processing was important for the 2-back condition, which mostly required manipulation, but not for the 1- and 0-back conditions, which mostly involved maintenance (compare above).

As the behavioral WM indices corresponded strongly to brain activity, we observed in parallel significant moderate negative correlations between temporal resolution evidenced by psychophysical TIP indices (ATOT values) and brain activity in 2- vs. 1-back comparisons (**Figure 5**). In other words, for manipulation, better temporal resolution (lower ATOT) was accompanied by higher activity (corresponding to more neural resources involved). Such activity comprised (**Table 2**) mostly the dlPFC (specifically, MFG: bilateral BA 9 and left BA 46), accompanied by the bilateral MFG (BA 6), left medial frontal gyrus (BA 8), SFG (BA 6), and insula (BA 13). In contrast, less skilled TIP (lower temporal resolution) was related to less efficient manipulation, evidenced in lower activity in these areas, accompanied by lower accuracy of performance with longer RTs (**Figures 3**, **5**).

In contrast, in maintenance (1- vs. 0-back comparisons), such correlations proved nonsignificant (**Table 2**) probably because of a weak contribution of temporal dynamics to storage processes.

To explain correlations between TIP and brain activity in WM, one should refer to general age trends in functional brain activation during WM performance. As stated in "Introduction" section, both WM and TIP decline in advanced age. The pattern of activations in aging brain is not easily interpretable, as some studies report underactivation of task-relevant brain areas, whereas others find overactivation relative to younger adults (e.g., Reuter-Lorenz, 2002; for the recent overview see Nagel and Lindenberger, 2015). Accordingly, underactivation is interpreted as a sign of structural, neuromodulatory, and hemodynamic response declines. Overactivation, on the other hand, is reported as a form of larger activation in elderly. The reduction in processing efficiency in elderly may lead to compensatory reactions, which occur in a response to deficient processing. The activation of additional regions may function as an aid to preserve WM (and probably other cognitive functions) because of age-related losses (Park and Reuter-Lorenz, 2009).

Considering these evidence, we are of the opinion that TIP may support WM processes, especially during manipulation, which involves more complex resources than the maintenance. The stronger activity in manipulation may reflect the contribution of more efficient TIP into WM to support such age-related WM losses. Further studies are needed to explain these issues in detail.

Brain Activity Overlaps in WM and TIP

Support for the "WM–TIP" relation in manipulation reported here can be found in studies on the neuroanatomy of TIP. Considering the broad neural network activated in WM manipulation identified in this study (**Table 1**), we found selected areas within this WM network that are strongly related to the effectiveness of temporal ordering (**Figure 5**, **Table 2**). These areas do not only concern WM function but are thought to also reflect the cognitive demands of the TIP network reported in the literature on the neuroanatomy of TIP. Based on the meta-analysis provided by Lewis and Miall (2003), supported by subsequent reports (Lewis and Miall, 2006; Lewandowska et al., 2010; Kotz and Schwartze, 2011), PFC (both dorso- and ventrolateral), pre-SMA, frontal pole, and parietal network activity were often reported in TIP. Referring to the diverse timing representation model proposed by Grondin (2010) and Merchant et al. (2013), assuming a partially shared timing mechanism, the dlPFC activity may reflect the contribution of nontemporal resources such as WM and comparison functions during TIP tasks (Rao et al., 2001; Livesey et al., 2007), irrespective of stimulus modality (Pastor et al., 2006) or task difficulty (Livesey et al., 2007). On the other hand, insular activation has also been observed in literature studies on paradigms involving auditory TIP, phonological processing, and sound detection (Craig, 2002, 2009).

To sum up, our results are in agreement with the partially shared timing theoretical model that assumes that TIP depends on the interaction of multiple areas, including main core TIP areas and context-dependent areas. The interaction between these two types of areas controls the specific performance of the task (Merchant et al., 2013). On the basis of our neuroimaging data, it may be concluded that the neural network responsible for the updating during dynamic manipulation of resources in WM is also sensitive to temporal ordering in the millisecond time window.

The data reported here may have not only the theoretical relevance but also the practical importance. They support the thesis that accurate WM manipulation processes require accurate TIP resources. Thus, the application of specific training in TIP may result in a transfer of improvement from time domain to WM domain *via* improvement of WM manipulation, but not maintenance, resources (Szelag et al., 2015a,b; Szymaszek et al., 2018). It would provide a new light on neurorehabilitation of subjects suffering from declined WM functions.

Finally, it would be interesting for future studies to investigate whether in traditional item-recognition WM tasks (e.g., the Sternberg task), often classified as storage tasks (Veltman et al., 2003), correlations between the efficiency of TIP and WM could be also observed. As some previous studies postulated the involvement of the dlPFC mainly during manipulation processes, in which the pure storage of information is less engaged (Marvel and Desmond, 2012), one might anticipate a lack of significant correlations between the efficiency of WM and TIP in these item-recognition tasks.

Final Remarks

The relationships observed here contribute to the existing literature some important new data on the neural network controlling WM, supporting the differentiation between processes engaged in the *n*-back task. The most important result of this study is the indication of the divergent involvement of TIP in maintenance and manipulation WM processes. We identified for the first time the contribution of temporal properties to brain activity—but only in manipulation processes, which require the continuous reorganization and updating of incoming information. It appears that this relation cannot work for processes that rely more heavily on storage maintenance.

DATA AVAILABILITY STATEMENT

The datasets generated for this study are available on request to the corresponding author.

ETHICS STATEMENT

The studies involving human participants were reviewed and approved by Ethical Commission at the University of Social Sciences and Humanities (permission no. 1/2017, registered as 2 /I/ 16-17). The patients/participants provided their written informed consent to participate in this study.

AUTHOR CONTRIBUTIONS

KJ and MP: subject recruitment, acquisition, analysis, and interpretation of data. HB and AS: interpretation of data and manuscript writing. AM and MW: analysis and interpretation of fMRI data. ES: conceptualization and study design, analysis and interpretation of data, manuscript writing, and responsibility for the final version of manuscript.

FUNDING

This research was supported by the National Science Centre (Narodowe Centrum Nauki, NCN), Poland, grant number 2015/17/B/HS6/04182. The project was realized with the aid of CePT research infrastructure purchased with funds from the European Regional Development Fund as part of the Innovative Economy Operational Programme 2007–2013.

ACKNOWLEDGMENTS

We thank Anna Bombinska for her technical assistance during the data collection phase.

REFERENCES

Allman, M. J., and Meck, W. H. (2012). Pathophysiological distortions in time perception and timed performance. *Brain* 135, 656–677. doi: 10.1093/brain/awr210

ANSI. (2004). *ANSI s3.6–2004. American National Standard Specification for Audiometers*. New York, NY: American National Standard Institute.

Awh, E., Jonides, J., Smith, E. E., Schumacher, E. H., Koeppe, R. A., and Katz, S. (1996). Dissociation of storage and rehearsal in verbal working memory: evidence from positron emission tomography. *Psychol. Sci.* 7, 25–31. doi: 10.1111/j.1467-9280.1996.tb00662.x

Baddeley, A. (2000). The episodic buffer: a new component of working memory? *Trends Cogn. Sci.* 4, 417–423. doi: 10.1016/s1364-6613(00)01538-2

Bao, Y., Fang, Y., Yang, T., Wang, L., Szymaszek, A., and Szelag, E. (2014). Auditory perception of temporal order: a comparison between tonal language speakers with and without non-tonal language experience. *Acta Neurobiol. Exp.* 74, 98–103.

Bao, Y., Szymaszek, A., Wang, X., Oron, A., Pöppel, E., and Szelag, E. (2013). Temporal order perception of auditory stimuli is selectively modified by tonal and non-tonal language environments. *Cognition* 129, 579–585. doi: 10.1016/j.cognition.2013.08.019

Barbey, A. K., Koenigs, M., and Grafman, J. (2013). Dorsolateral prefrontal contributions to human working memory. *Cortex* 49, 1195–1205. doi: 10.1016/j.cortex.2012.05.022

Ben-Yehudah, G., Guediche, S., and Fiez, J. A. (2007). Cerebellar contributions to verbal working memory: beyond cognitive theory. *Cerebellum* 6, 193–201. doi: 10.1080/14734220701286195

Bernasconi, F., Grivel, J., Murray, M. M., and Spierer, L. (2010). Interhemispheric coupling between the posterior sylvian regions impacts successful auditory temporal order judgment. *Neuropsychologia* 48, 2579–2585. doi: 10.1016/j.neuropsychologia.2010.05.004

Bernasconi, F., Manuel, A. L., Murray, M. M., and Spierer, L. (2011). Pre-stimulus beta oscillations within left posterior sylvian regions impact auditory temporal order judgment accuracy. *Int. J. Psychophys.* 79, 244–248. doi: 10.1016/j.ijpsycho.2010.10.017

Binder, M. (2015). Neural correlates of audiovisual temporal processing-comparison of temporal order and simultaneity judgments. *Neuroscience* 300, 432–447. doi: 10.1016/j.neuroscience.2015.05.011

Bland, J. M., and Altman, D. G. (1995). Multiple significance tests: the Bonferroni method. *Br. Med. J.* 310:170. doi: 10.1136/bmj.310.6973.170

Bradshaw, J., and Nettleton, N. (1981). The nature of hemispheric specialization in man. *Behav. Brain Sci.* 4, 51–63. doi: 10.1017/s0140525x00007548

Buhusi, C. V., and Meck, W. H. (2005). What makes us tick? Functional and neural mechanisms of interval timing. *Nat. Rev. Neurosci.* 6, 755–765. doi: 10.1038/nrn1764

Cabeza, R. (2002). Hemispheric asymmetry reduction in older adults: the HAROLD model. *Psychol. Aging* 17, 85–100. doi: 10.1037//0882-7974.17.1.85

Carhart, R. (1971). Observations on relations between thresholds for pure tones and for speech. *J. Speech Hear. Disord.* 36, 476–483. doi: 10.1044/jshd.3604.476

Conway, A. R., Kane, M. J., Bunting, M. F., Hambrick, D. Z., Wilhelm, O., and Engle, R. W. (2005). Working memory span tasks: a methodological review and user's guide. *Psychon. Bull. Rev.* 12, 769–786. doi: 10.3758/bf03196772

Cooper, F. E., Grube, M., Von Kriegstein, K., Kumar, S., English, P., Kelly, T. P., et al. (2012). Distinct critical cerebellar subregions for components of verbal working memory. *Neuropsychologia* 50, 189–197. doi: 10.1016/j.neuropsychologia.2011.11.017

Coull, J. T., and Nobre, A. C. (2008). Dissociating explicit timing from temporal expectation with fMRI. *Curr. Opin. Neurobiol.* 18, 137–144. doi: 10.1016/j.conb.2008.07.011

Coull, J. T., Cheng, R. K., and Meck, W. H. (2011). Neuroanatomical and neurochemical substrates of timing. *Neuropsychopharmacology* 36, 3–25. doi: 10.1038/npp.2010.113

Cowan, N. (2008). What are the differences between long-term, short-term, and working memory? *Prog. Brain Res.* 169, 323–338. doi: 10.1016/s0079-6123(07)00020-9

Craig, A. D. (2002). How do you feel? Interoception: the sense of the physiological condition of the body. *Nat. Rev. Neurosci.* 3, 655–666. doi: 10.1038/nrn894

Craig, A. D. (2009). Emotional moments across time: a possible neural basis for time perception in the anterior insula. *Philos. Trans. R. Soc. Lond. B Biol. Sci.* 364, 1933–1942. doi: 10.1098/rstb.2009.0008

Crottaz-Herbette, S., Anagnoson, R. T., and Menon, V. (2004). Modality effects in verbal working memory: differential prefrontal and parietal responses to auditory and visual stimuli. *NeuroImage* 21, 340–351. doi: 10.1016/j.neuroimage.2003.09.019

Dennis, N. A., and Cabeza, R. (2008). "Neuroimaging of healthy cognitive aging," in *The Handbook of Aging and Cognition*, 3rd Edn. eds F. Craik and T. Salthouse (New York, NY: Psychology Press), 10–63.

D'Esposito, M., Aguirre, G. K., Zarahn, E., Ballard, D., Shin, R. K., and Lease, J. (1998). Functional MRI studies of spatial and nonspatial working memory. *Cognit. Brain Res.* 7, 1–13. doi: 10.1016/s0926-6410(98)00004-4

D'Esposito, M., and Postle, B. R. (2015). The cognitive neuroscience of working memory. *Annu. Rev. Psychol.* 66, 115–142. doi: 10.1146/annurev-psych-010814-015031

D'Esposito, M., Postle, B. R., Ballard, D., and Lease, J. (1999). Maintenance versus manipulation of information held in working memory: an event-related fMRI study. *Brain Cogn.* 41, 66–86. doi: 10.1006/brcg.1999.1096

Dixon, R. A., and de Frias, C. M. (2007). Mild memory deficits differentially affect 6-year changes in compensatory strategy use. *Psychol. Aging* 22, 632–638. doi: 10.1037/0882-7974.22.3.632

Eriksson, J., Vogel, E. K., Lansner, A., Bergström, F., and Nyberg, L. (2015). Neurocognitive architecture of working memory. *Neuron* 88, 33–46. doi: 10.1016/j.neuron.2015.09.020

Fakhri, M., Sikaroodi, H., Maleki, F., Ghanaati, H., and Oghabian, M. A. (2013). Impacts of normal aging on different working memory tasks: implications from an fMRI study. *Behav. Neurol.* 27, 235–244. doi: 10.3233/BEN-2012-110234

Fitzgibbons, P. J., and Gordon-Salant, S. (1994). Age effects on measures of auditory duration discrimination. *J. Speech Hear. Res.* 37, 662–670. doi: 10.1044/jshr.3703.662

Fletcher, P. C., and Henson, R. N. A. (2001). Frontal lobes and human memory: insights from functional neuroimaging. *Brain* 124, 849–881. doi: 10.1093/brain/124.5.849

Folstein, M. F., Folstein, S. E., and Fanjiang, G. (2001). *MMSE: Mini-Mental State Examination Clinical Guide.* Lutz, FL: Psychological Assessment Resources.

Fostick, L., and Babkoff, H. (2017). Auditory spectral versus spatial temporal order judgment: threshold distribution analysis. *J. Exp. Psychol. Hum. Percept. Perform.* 43, 1002–1012. doi: 10.1037/xhp0000359

Fuster, J. M. (2009). Cortex and memory: emergence of a new paradigm. *J. Cogn. Neurosci.* 21, 2047–2072. doi: 10.1162/jocn.2009.21280

Gazzaniga, M. S. (2000). Cerebral specialization and interhemispheric communication: does the corpus callosum enable the human condition? *Brain* 123, 1293–1326. doi: 10.1093/brain/123.7.1293

Grondin, S. (2010). Timing and time perception: a review of recent behavioral and neuroscience findings and theoretical directions. *Atten. Percept. Psychophys.* 72, 561–582. doi: 10.3758/app.72.3.561

Gu, B. M., van Rijn, H., and Meck, W. H. (2015). Oscillatory multiplexing of neural population codes for interval timing and working memory. *Neurosci. Biobehav. R.* 48, 160–185. doi: 10.1016/j.neubiorev.2014.10.008

Hellige, J. B. (2001). *Hemispheric Asymmetry: What's Right and what's Left.* Cambridge, MA and London: Harvard University Press.

Hellige, J. B. (2008). "Interhemispheric interaction in the lateralized brain," in *Handbook of the Neuroscience of Language*, eds B. Stemmer and H. A. Whitaker (Amsterdam: Academic Press), 257–266.

Jaeggi, S. M., Buschkuehl, M., Perrig, W. J., and Meier, B. (2010). The concurrent validity of the N-back task as a working memory measure. *Memory* 18, 394–412. doi: 10.1080/09658211003702171

Jonides, J., Schumacher, E. H., Smith, E. E., Koeppe, R. A., Awh, E., Reuter-Lorenz, P. A., et al. (1998). The role of parietal cortex in verbal working memory. *J. Neurosci.* 18, 5026–5034. doi: 10.1523/JNEUROSCI.18-13-05026.1998

Kanabus, M., Szelag, E., Rojek, E., and Pöppel, E. (2002). Temporal order judgement for auditory and visual stimuli. *Acta Neurobiol. Exp.* 62, 263–270.

Kolodziejczyk, I., and Szelag, E. (2008). Auditory perception of temporal order in centenarians in comparison with young and elderly subjects. *Acta Neurobiol. Exp.* 68, 373–381.

Kumar, U., and Sangamanatha, A. V. (2011). Temporal processing abilities across different age groups. *J. Am. Acad. Audiol.* 22, 5–12. doi: 10.3766/jaaa.22.1.2

Kung, B. C., and Willcox, T. O. Jr. (2007). "Examination of hearing and balance," in *Neurology and Clinical Neuroscience*, ed. A. H. V. Schapira (Philadelphia: Mosby), 318–327.

Kotz, S. A., and Schwartze, M. (2011). Differential input of the supplementary motor area to a dedicated temporal processing network: functional and clinical implications. *Front. Integr. Neurosci.* 5:86. doi: 10.3389/fnint.2011.00086

Lancaster, J. L., Woldorff, M. G., Parsons, L. M., Liotti, M., Freitas, C. S., Rainey, L., et al. (2000). Automated Talairach atlas labels for functional brain mapping. *Hum. Brain Mapp.* 10, 120–131. doi: 10.1002/1097-0193(200007)10:3<120::aid-hbm30>3.0.co;2-8

Lewandowska, M., Piatkowska-Janko, E., Bogorodzki, P., Wolak, T., and Szelag, E. (2010). Changes in fMRI BOLD response to increasing and decreasing task difficulty during auditory perception of temporal order. *Neurobiol. Learn. Mem.* 94, 382–391. doi: 10.1016/j.nlm.2010.08.005

Lewis, P. A., and Miall, R. C. (2003). Distinct systems for automatic and cognitively controlled time measurement: evidence from neuroimaging. *Curr. Opin. Neurobiol.* 13, 250–255. doi: 10.1016/s0959-4388(03)00036-9

Lewis, P. A., and Miall, R. C. (2006). A right hemispheric prefrontal system for cognitive time measurement. *Behav. Processes* 71, 226–234. doi: 10.1016/j.beproc.2005.12.009

Liao, D. A., Kronemer, S. I., Yau, J. M., Desmond, J. E., and Marvel, C. L. (2014). Motor system contributions to verbal and non-verbal working memory. *Front. Hum. Neurosci.* 8:753. doi: 10.3389/fnhum.2014.00753

Lindell, A. K. (2006). In your right mind: right hemisphere contributions to language processing and production. *Neuropsychol. Rev.* 16, 131–148. doi: 10.1007/s11065-006-9011-9

Lindenberger, U., Burzynska, A. Z., and Nagel, I. E. (2013). "Heterogeneity in frontal lobe aging," in *Principles of Frontal Lobes Function*, 2nd Edn. eds D. T. Stuss and R. T. Knight (New York, NY: Oxford University Press), 609–627.

Livesey, A. C., Wall, M. B., and Smith, A. T. (2007). Time perception: manipulation of task difficulty dissociates clock functions from other cognitive demands. *Neuropsychologia* 45, 321–331. doi: 10.1016/j.neuropsychologia.2006.06.033

Luis, E. O., Arrondo, G., Vidorreta, M., Martínez, M., Loayza, F., Fernández-Seara, M. A., et al. (2015). Successful working memory processes and cerebellum in an elderly sample: a neuropsychological and fMRI study. *PLoS One* 10:e0131536. doi: 10.1371/journal.pone.0131536

Marvel, C. L., and Desmond, J. E. (2012). From storage to manipulation: how the neural correlates of verbal working memory reflect varying demands on inner speech. *Brain Lang.* 120, 42–51. doi: 10.1016/j.bandl.2011.08.005

Mattay, V. S., Fera, F., Tessitore, A., Hariri, A. R., Das, S., Callicott, J. H., et al. (2002). Neurophysiological correlates of age-related changes in human motor function. *Neurology* 58, 630–635. doi: 10.1212/wnl.58.4.630

Matthews, W., and Meck, W. H. (2014). Time perception: the bad news and the good. *Wiley Interdiscip. Rev. Cogn. Sci.* 5, 429–446. doi: 10.1002/wcs.1298

Matthews, W., and Meck, W. H. (2016). Temporal cognition: connecting subjective time to perception, attention, and memory. *Psychol. Bull.* 142, 865–907. doi: 10.1037/bul0000045

Meck, W. H. (2005). Neuropsychology of timing and time perception. *Brain Cogn.* 58, 1–8. doi: 10.1016/j.bandc.2004.09.004

Merchant, H., Harrington, D. L., and Meck, W. H. (2013). Neural basis of the perception and estimation of time. *Annu. Rev. Neurosci.* 36, 313–336. doi: 10.1146/annurev-neuro-062012-170349

Miller, K. M., Price, C. C., Okun, M. S., Montijo, H., and Bowers, D. (2009). Is the n-back task a valid neuropsychological measure for assessing working memory? *Arch. Clin. Neuropsychol.* 24, 711–717. doi: 10.1093/arclin/acp063

Nagel, I. E., and Lindenberger, U. (2015). "Adult age differences in working memory: evidence from neuroimaging," in *Working Memory and Ageing*, eds R. H. Logie and R. G. Morris (London and New York, NY: Psychology Press), 129–155.

Narayanan, N. S., Prabhakaran, V., Bunge, S. A., Christoff, K., Fine, E. M., and Gabrieli, J. D. (2005). The role of the prefrontal cortex in the maintenance of verbal working memory: an event-related FMRI analysis. *Neuropsychology* 19, 223–232. doi: 10.1037/0894-4105.19.2.223

Nowak, K., Dacewicz, A., Broczek, K., Kupisz-Urbanska, M., Galkowski, T., and Szelag, E. (2016). Temporal information processing and its relation to executive functions in elderly individuals. *Front. Psychol.* 7:1599. doi: 10.3389/fpsyg.2016.01599

Nyberg, L., Andersson, M., Kauppi, K., Lundquist, A., Persson, J., Pudas, S., et al. (2014). Age-related and genetic modulation of frontal cortex efficiency. *J. Cogn. Neurosci.* 26, 746–754. doi: 10.1162/jocn_a_00521

Owen, A. M. (1997). The functional organization of working memory processes within human lateral frontal cortex: the contribution of functional neuroimaging. *Eur. J. Neurosci.* 9, 1329–1339. doi: 10.1111/j.1460-9568.1997.tb01487.x

Owen, A. M., McMillan, K. M., Laird, A. R., and Bullmore, E. (2005). N-back working memory paradigm: a meta-analysis of normative functional neuroimaging studies. *Hum. Brain Mapp.* 25, 46–59. doi: 10.1002/hbm.20131

Park, D. C., and Reuter-Lorenz, P. (2009). The adaptive brain: aging and neurocognitive scaffolding. *Annu. Rev. Psychol.* 60, 173–196. doi: 10.1146/annurev.psych.59.103006.093656

Pastor, M. A., Macaluso, E., Day, B. L., and Frackowiak, R. S. J. (2006). The neural basis of temporal auditory discrimination. *NeuroImage* 30, 512–520. doi: 10.1016/j.neuroimage.2005.09.053

Petrides, M. (1994). Frontal lobes and behaviour. *Curr. Opin. Neurobiol.* 4, 207–211. doi: 10.1016/0959-4388(94)90074-4

Poeppel, D. (2003). The analysis of speech in different temporal integration windows: cerebral lateralization as 'asymmetric sampling in time'. *Speech Commun.* 41, 245–255. doi: 10.1016/s0167-6393(02)00107-3

Poldrack, R. A. (2007). Region of interest analysis for fMRI. *Soc. Cogn. Affect. Neurosci.* 2, 67–70. doi: 10.1093/scan/nsm006

Pöppel, E. (1997). A hierarchical model of temporal perception. *Trends Cogn. Sci.* 1, 56–61. doi: 10.1016/S1364-6613(97)01008-5

Radua, J., del Pozo, N. O., Gómez, J., Guillen-Grima, F., and Ortuño, F. (2014). Meta-analysis of functional neuroimaging studies indicates that an increase of cognitive difficulty during executive tasks engages brain regions associated with time perception. *Neuropsychologia* 58, 14–22. doi: 10.1016/j.neuropsychologia.2014.03.016

Ragland, J. D., Turetsky, B. I., Gur, R. C., Gunning-Dixon, F., Turner, T., Schroeder, L., et al. (2002). Working memory for complex figures: an fMRI comparison of letter and fractal n-back tasks. *Neuropsychology* 16, 370–379. doi: 10.1037/0894-4105.16.3.370

Rammsayer, T. H., and Brandler, S. (2007). Performance on temporal information processing as an index of general intelligence. *Intelligence* 35, 123–139. doi: 10.1016/j.intell.2006.04.007

Rao, S. M., Mayer, A. R., and Harrington, D. L. (2001). The evolution of brain activation during temporal processing. *Nat. Neurosci.* 4, 317–323. doi: 10.1038/85191

Raz, N., Lindenberger, U., Rodrigue, K. M., Kennedy, K. M., Head, D., Williamson, A., et al. (2005). Regional brain changes in aging healthy adults: general trends, individual differences and modifiers. *Cereb. Cortex* 15, 1676–1689. doi: 10.1093/cercor/bhi044

Reuter-Lorenz, P. A. (2002). New visions of the aging mind and brain. *Trends Cogn. Sci.* 6, 394–400. doi: 10.1016/s1364-6613(02)01957-5

Rypma, B., and D'Esposito, M. (1999). The roles of prefrontal brain regions in components of working memory: effects of memory load and individual differences. *Proc. Natl. Acad. Sci. U S A* 96, 6558–6563. doi: 10.1073/pnas.96.11.6558

Schmidt, H., Jogia, J., Fast, K., Christodoulou, T., Haldane, M., Kumari, V., et al. (2009). No gender differences in brain activation during the N-back task: an fMRI study in healthy individuals. *Hum. Brain Mapp.* 30, 3609–3615. doi: 10.1002/hbm.20783

Sheikh, J. I., and Yesavage, J. A. (1986). "Geriatric depression scale: recent findings and development of a short version," in *Clinical Gerontology: A Guide to Assessment and Intervention*, ed. T. L. Brink (New York, NY: Oxford University Press), 165–173.

Smith, E. E., Jonides, J., Marshuetz, C., and Koeppe, R. A. (1998). Components of verbal working memory: evidence from neuroimaging. *Proc. Natl. Acad. Sci. U S A* 95, 876–882. doi: 10.1073/pnas.95.3.876

Szelag, E., Dreszer, J., Lewandowska, M., and Szymaszek, A. (2009). "Cortical representation of time and timing processes", in *Neuronal Correlates of thinking*, eds E. Kraft, B. Guylas and E. Pöppel (Berlin: Springer Verlag), 185–196.

Szelag, E., Dacewicz, A., Szymaszek, A., Wolak, T., Senderski, A., Domitrz, I., et al. (2015a). The application of timing in therapy of children and adults with language disorders. *Front. Psychol.* 6:1714. doi: 10.3389/fpsyg.2015.01714

Szelag, E., Szymaszek, A., and Oron, A. (2015b). "Aphasia as a temporal information processing disorder," in *Time Distortions in Mind: Temporal Processing in Clinical Populations*, eds A. Vatakis and M. J. Allman (Leiden and Boston: Brill), 328–355.

Szelag, E., Jablonska, K., Piotrowska, M., Szymaszek, A., and Bednarek, H. (2018). Spatial and spectral auditory temporal-order judgment (TOJ) tasks in elderly people are performed using different perceptual strategies. *Front. Psychol.* 9:2557. doi: 10.3389/fpsyg.2018.02557

Szelag, E., Lewandowska, M., Wolak, T., Seniow, J., Poniatowska, R., Pöppel, E., et al. (2014). Training in rapid auditory processing ameliorates auditory comprehension in aphasic patients: a randomized controlled pilot study. *J. Neurol. Sci.* 338, 77–86. doi: 10.1016/j.jns.2013.12.020

Szelag, E., Szymaszek, A., Aksamit-Ramotowska, A., Fink, M., Ulbrich, P., Wittmann, M., et al. (2011). Temporal processing as a base for language universals: cross-linguistic comparisons on sequencing abilities with some implications for language therapy. *Restor. Neurol. Neurosci.* 29, 35–45. doi: 10.3233/rnn-2011-0574

Szymaszek, A., Dacewicz, A., Urban, P., and Szelag, E. (2018). Temporal dysfunction as a core deficit in voicing contrast perception in children with SLI: the effect of training based on time processing. *Front. Hum. Neurosci.* 12:213. doi: 10.3389/fnhum.2018.00213

Szymaszek, A., Sereda, M., Pöppel, E., and Szelag, E. (2009). Individual differences in the perception of temporal order: the effect of age and cognition. *Cogn. Neuropsychol.* 26, 135–147. doi: 10.1080/02643290802504742

Teixeira, S., Machado, S., Flávia, P., Velasques, B., Silva, J. G., Sanfim, A. L., et al. (2013). Time perception distortion in neuropsychiatric and neurological disorders. *CNS Neurol. Disord. Drug Targets* 12, 567–582. doi: 10.2174/18715273113129990080

Tisserand, D. J., and Jolles, J. (2003). On the involvement of prefrontal networks in cognitive ageing. *Cortex* 39, 1107–1128. doi: 10.1016/s0010-9452(08)70880-3

Treisman, M. (1963). Temporal discrimination and the indifference interval: implications for a model of the "internal clock". *Psychol. Monogr.* 77, 1–31. doi: 10.1037/h0093864

Treisman, M., Faulkner, A., Naish, P. L., and Brogan, D. (1990). The internal clock: evidence for a temporal oscillator underlying time perception with some estimates of its characteristic frequency. *Perception* 19, 705–742. doi: 10.1068/p190705

Treutwein, B. (1997). YAAP: yet another adaptive procedure. *Spat. Vis.* 11, 129–134.

Troche, S. J., and Rammsayer, T. H. (2009). The influence of temporal resolution power and working memory capacity on psychometric intelligence. *Intelligence* 37, 479–486. doi: 10.1016/j.intell.2009.06.001

Tsukiura, T., Fujii, T., Takahashi, T., Xiao, R., Inase, M., Iijima, T., et al. (2001). Neuroanatomical discrimination between manipulating and maintaining processes involved in verbal working memory; a functional MRI study. *Brain Res. Cogn. Brain Res.* 11, 13–21. doi: 10.1016/s0926-6410(00)00059-8

Ulbrich, P., Churan, J., Fink, M., and Wittmann, M. (2009). Perception of temporal order: the effects of age, sex, and cognitive factors. *Neuropsychol. Dev. Cogn. B Aging Neuropsychol. Cogn.* 16, 183–202. doi: 10.1080/13825580802411758

Üstün, S., Kale, E. H., and Çiçek, M. (2017). Neural networks for time perception and working memory. *Front. Hum. Neurosci.* 11:83. doi: 10.3389/fnhum.2017.00083

VanRullen, R., and Koch, C. (2003). Is perception discrete or continuous? *Trends Cogn. Sci.* 7, 207–213. doi: 10.1016/s1364-6613(03)00095-0

Veltman, D. J., Rombouts, S. A., and Dolan, R. J. (2003). Maintenance versus manipulation in verbal working memory revisited: an fMRI study. *NeuroImage* 18, 247–256. doi: 10.1016/s1053-8119(02)00049-6

Weber, B., Fliessbach, K., Lange, N., Kügler, F., and Elger, C. E. (2007). Material-specific memory processing is related to language dominance. *NeuroImage* 37, 611–617. doi: 10.1016/j.neuroimage.2007.05.022

Zatorre, R. J., and Samson, S. (1991). Role of the right temporal neocortex in retention of pitch in auditory short-term memory. *Brain* 114, 2403–2417. doi: 10.1093/brain/114.6.2403

Conflict of Interest: The authors declare that the research was conducted in the absence of any commercial or financial relationships that could be construed as a potential conflict of interest.

frontiers in Aging Neuroscience

HYPOTHESIS AND THEORY
published: 24 July 2020
doi: 10.3389/fnagi.2020.00185

Dysfunction of the Blood-Brain Barrier—A Key Step in Neurodegeneration and Dementia

Christian R. Noe[1], Marion Noe-Letschnig[2], Patricia Handschuh[3], Chiara Anna Noe[4] and Rupert Lanzenberger[3]**

[1]Department of Medicinal Chemistry, University of Vienna, Vienna, Austria, [2]ProFem GmbH, Vienna, Austria, [3]Neuroimaging Lab (NIL), Department of Psychiatry and Psychotherapy, Medical University of Vienna, Vienna, Austria, [4]Department of Otorhinolaryngology, University Clinic St. Poelten, St. Poelten, Austria

The vascular endothelium in the brain is an essential part of the blood-brain-barrier (BBB) because of its very tight structure to secure a functional and molecular separation of the brain from the rest of the body and to protect neurons from pathogens and toxins. Impaired transport of metabolites across the BBB due to its increasing dysfunction affects brain health and cognitive functioning, thus providing a starting point of neurodegenerative diseases. The term "cerebral metabolic syndrome" is proposed to highlight the importance of lifestyle factors in neurodegeneration and to describe the impact of increasing BBB dysfunction on neurodegeneration and dementia, especially in elderly patients. If untreated, the cerebral metabolic syndrome may evolve into dementia. Due to the high energy demand of the brain, impaired glucose transport across the BBB *via* glucose transporters as GLUT1 renders the brain increasingly susceptible to neurodegeneration. Apoptotic processes are further supported by the lack of essential metabolites of the phosphocholine synthesis. In Alzheimer's disease (AD), inflammatory and infectious processes at the BBB increase the dysfunction and might be pace-making events. At this point, the potentially highly relevant role of the thrombocytic amyloid precursor protein (APP) in endothelial inflammation of the BBB is discussed. Chronic inflammatory processes of the BBB transmitted to an increasing number of brain areas might cause a lasting build-up of spreading, pore-forming β-amyloid fragments explaining the dramatic progression of the disease. In the view of the essential requirement of an early diagnosis to investigate and implement causal therapeutic strategies against dementia, brain imaging methods are of great importance. Therefore, status and opportunities in the field of diagnostic imaging of the living human brain will be portrayed, comprising diverse techniques such as positron emissions tomography (PET) and functional magnetic resonance imaging (fMRI) to uncover the patterns of atrophy, protein deposits, hypometabolism, and molecular as well as functional alterations in AD.

Keywords: blood-brain barrier (BBB), GLUT1, dementia, Alzheimer's disease, amyloid precursor protein (APP), inflammation, positron emission tomography (PET), glucose

OPEN ACCESS

Edited by:
Mohamad Habes, The University of Texas Health Science Center at San Antonio, United States

Reviewed by:
Ana I. Duarte, University of Coimbra, Portugal
Behrooz Hooshyar Yousefi, University of Marburg, Germany

****Correspondence:***
Christian R. Noe
christian.noe@univie.ac.at
Rupert Lanzenberger
rupert.lanzenberger@meduniwien.ac.at

Received: *19 November 2019*
Accepted: *27 May 2020*
Published: *24 July 2020*

Citation:
Noe CR, Noe-Letschnig M, Handschuh P, Noe CA and Lanzenberger R (2020) Dysfunction of the Blood-Brain Barrier—A Key Step in Neurodegeneration and Dementia. Front. Aging Neurosci. 12:185. doi: 10.3389/fnagi.2020.00185

INTRODUCTION

The human brain's activity is driven by about 86 billion neurons and 85 billion glial cells, mostly astrocytes (Azevedo et al., 2009) that are connected by a highly complex axonal network. Once embedded and stabilized in this network, neurons are maintained for a lifetime. The points of axonal contact are the synapses, where neuronal signals are transmitted by neurotransmitters from neuron to neuron, molecule by molecule (Jessell and Kandel, 1993). Glia cells of the brain do not only support and isolate neurons but are of utmost importance for metabolic functions. The maintenance of the continuous activity of this communication system by synthesis, release, and reuptake of neurotransmitters is a tremendous energetic effort for both neurons and glial cells (Habbas et al., 2015; Santello et al., 2019). The decline in metabolic activity during aging also includes a reduced capacity for the synthesis of neurotransmitters, which means that the general decline in cognitive activity in elderly people is to be considered a "natural" process. Consequently, physical and mental decline is directly related to the exhaustion of synaptic vesicles due to a lack of metabolites (Ivakhnitskaia et al., 2018).

Beyond that, neuronal cells are endowed with synaptic plasticity, which allows the strengthening of pre-existing axonal connections and the formation of new ones as a reaction to new, repetitive, or intense impulses (Draganski et al., 2004; Bruel-Jungerman et al., 2007). Stem cell transformation into neurons has recently become a further element of this system (Selvaraj et al., 2012). Neuronal plasticity equally requires an efficient and continuous supply with nutrients and metabolites. The reduced synthetic capacity for metabolites going along with aging is not limited to neurotransmitters, but also affects the components (e.g., phospholipids) of the neuronal cell membrane. Phospholipids are needed to strengthen neuronal connections within the process of synaptic plasticity. Therefore, also synaptic plasticity is weakening with age (Power and Schlaggar, 2017). Reduced neuronal plasticity can either be of transient or permanent character, depending on whether new impulses are set by enduring activity or not. Mental activity means "training impulses" for neurons to preserve neuronal stability and to induce neuronal growth *via* synaptic stability (Power and Schlaggar, 2017). If certain pre-existent neuronal pathways are not used anymore, the inter-synaptic communication pathway can get lost, resulting in irreversible memory loss. This explains why both mental and physical activity is of utmost importance for aging people (Draganski et al., 2004). However, it must be borne in mind that this "normal" impairment or loss of "unused" inter-neuronal connections does not correspond to the massive decline in inter-axonal communication processes going along with neuronal cell death, as seen in the course of dementia, in particular in Alzheimer's disease (AD; Guillon et al., 2017; Power and Schlaggar, 2017).

The term dementia describes a pathology or a syndrome that is characterized by an increasing loss of cognitive, social, and emotional abilities (Cunningham et al., 2015). This process is associated with an abnormal level of cellular decline within the brain that exceeds regular aging (Simić et al., 1997). Since dementia is usually linked to higher age, the relevance of mental disorders is constantly growing. At present, cardiovascular disease (in the narrower sense, cardiac failure, and stroke) is the leading cause of death worldwide (Roth et al., 2017). Nevertheless, dementia as a cause of death has been gaining importance progressively in recent years. Among other causes, this can be traced back to demographic change with a higher average life expectancy in industrial as well as developing countries. A wide range of manifestations of neurodegeneration has been defined, with AD representing the most frequent one (60%; Alzheimer's Association, 2017). Between 2000 and 2016, the mortality caused by AD has doubled, reaching the position of the fifth-leading cause of death (World Health Organization, 2018).

A variety of mechanisms can cause neurodegeneration. Overlaps between diverse forms of dementia may further complicate diagnostics (Iadecola, 2010). In some cases, responsible triggers have been identified. Nevertheless, there are significant gaps that need to be closed regarding the etiology of neurodegeneration, especially in the case of AD. Regarding their pathomechanism, an increasing number of commonalities have been identified across the diverse forms of dementia and cardiovascular diseases (Ashraf et al., 2016). Such a commonality also appears with diabetes mellitus, which is not only associated with vascular comorbidities but is also known to increase the risk of AD (Arvanitakis et al., 2004; Pilon, 2016). Several forms of dementia are associated with pathological vascular alterations (O'Brien and Thomas, 2015), thus linking neurodegeneration and cardiovascular disease. In this context, the role of the blood-brain barrier (BBB) in neurodegeneration has recently gained growing attention (Weiss et al., 2009; Blonz, 2017; Yamazaki and Kanekiyo, 2017) and will be the main focus of this article.

THE CEREBRAL METABOLIC SYNDROME—A COHERENT CONCEPT FOR PREVENTING AND TREATING NEURODEGENERATION

The Blood-Brain Barrier

Atherosclerosis is one of the well-known results of dysfunctional endothelial tissue within the vessel walls. The pathophysiological consequences of unfavorable lifestyle habits (e.g., overeating, smoking, lack of exercise) and other, endogenous factors (e.g., genetic vulnerability) are summarized under the term "metabolic syndrome" (MS), which describes the cluster of obesity, elevated blood lipid levels, hypertension and impaired glucose tolerance (Grundy et al., 2004). It represents the common pathologic starting point for secondary diseases like diabetes mellitus, myocardial infarction, and stroke. Its growing global prevalence comes along with the continuous increase of obesity due to the mentioned unfavorable living conditions and eating habits. Summing up these conditions into one clinical picture has proven its worth in respect to prevention and therapy (Mendrick et al., 2018).

The brain as the central controlling structure of the body, its strict separation from the remaining physiological

systems—especially the blood system—is reasonable. This separation is ensured by a specific structure of the vascular endothelium in the brain. Induced by factors released by brain astrocytes, vascular endothelial cells express intercellular adhesion molecules (most importantly, claudin and occludin) that connect them *via* tight junctions (Neuhaus et al., 2008; Weiss et al., 2009). The resulting tight cerebral vascular endothelium and additional components are building up the BBB, separating brain tissue from the blood. This tight barrier exhibits a high electric resistance and does not allow peri-cellular transport (Neuhaus et al., 2012; Novakova et al., 2014) into the brain. Apart from passive diffusion of lipophilic molecules, any transport into and out of the brain's nervous tissue is exclusively transporter-mediated (Kniesel and Wolburg, 2000; Wolburg and Lippoldt, 2002; Ecker and Noe, 2004; Shah et al., 2012). Bearing this in mind, it is evident that the impairment of membranous fluidity and functionality going along with atherosclerosis might harm brain cells even more than peripheral ones. Insufficient supply of nutrients and metabolites into the brain over the BBB is the primary cause for a process, which might be called cerebral metabolic syndrome. This finding is crucial for and consistent with increasingly upcoming hypotheses, relating dementia to metabolic dysfunction or energy deficits of the brain (Jurcovicova, 2014; Szablewski, 2017). In contrast to atherosclerosis and the related metabolic syndrome, the fundamental consequences of BBB impairment have only recently become the focus of broader attention (Noe, 2009; Yamazaki and Kanekiyo, 2017). A synoptic mechanistic view towards metabolic syndrome and cerebral metabolic syndrome to define potential commonalities is still missing, although they might appear as the first signs of pathophysiological processes, leading to neurodegeneration as a potentially life-threatening syndrome.

The Energy Supply of the Brain

The plethora of physiological brain activities explains the high energy demand of the brain. Not surprisingly, the brain is by far the largest consumer of glucose, physiologically the main energy source of most organisms. About 200 g of glucose are needed per day just to sustain the brain's basal metabolism (Peters, 2011). This amount corresponds to about 25–50% (Reinmuth et al., 1965) of available (mobilizable) glucose within the organism (Fehm et al., 2006). Due to the steadily high demand for glucose, it is evolutionarily implicated that the glucose-transport into the brain—to a large extent—does not depend on the insulin system (Thorens and Mueckler, 2010), which is a signaling system that is directing blood glucose into tissues upon demand. As a result of insulin signaling, cells express glucose transporters (GLUT4), which then transport glucose into the cell. In contrast to these, GLUT1 (**Figure 1**) glucose transporters at the BBB are independent of insulin signaling. They secure the continuous transport of glucose across the BBB (Shah et al., 2012).

There is convincing evidence that also the efficiency of GLUT1 transporters might be affected by a loss of membrane fluidity (Pifferi et al., 2005; Deng et al., 2015; Winkler et al., 2015). It might even be speculated that the up-regulation of blood glucose levels could be triggered by an impairment of BBB transport. Nevertheless, it is broadly assumed that the adequate energy supply of the brain is warranted in any case (Fehm et al., 2006). Thereby, various pathways can be activated, including the utilization of lactate and ketone bodies in case of acute hypoglycemia, for instance (Morris, 2005; van Hall et al., 2009).

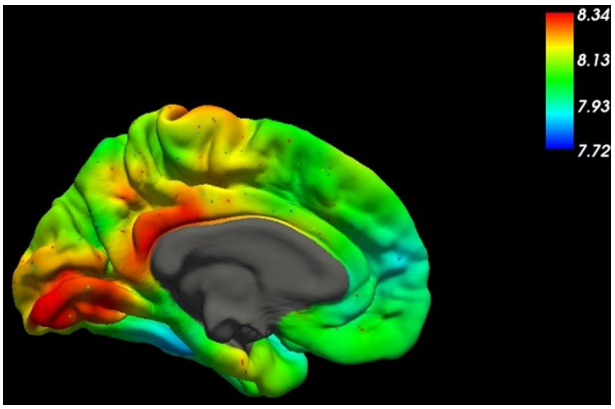

FIGURE 1 | This figure shows the spatial distribution of the mRNA expression of SLC2A1, the gene coding for the glucose transporter GLUT1, across the medial surface of the human brain (Gryglewski et al., 2018). Higher concentrations are indicated by red colors in the table.

The mentioned loss of membrane fluidity is caused by various pathophysiological mechanisms, all harming the transport function and stability of the BBB. Therefore, cerebral glucose availability in obese people tends to be impaired despite chronic hyperbolic nutrition (Wardzinski et al., 2018). High blood sugar levels in diabetic patients do not guarantee an adequate supply of glucose to the brain. Life-threatening situations, which may occur in cases of severe hypoglycemia, and which are a frequent and well-known danger in diabetic patients, point to the possibility that the maintenance of a physiological level of glucose in the brain is by no means self-fulfilling in any case.

Inadequate glucose availability in the brain is an important element of impaired function going along with cerebral metabolic syndrome. However, the consequences go far beyond mere impairment. Apoptosis—the controlled dismantlement of a cell from the inside—is usually initiated within mitochondria, which control the energetic metabolism of a cell (Hengartner, 2000; Martinvalet et al., 2005). With glucose being the main energy source of the brain, one may assume that a permanent and adequate availability of glucose in the brain is crucial to delay mitochondrial apoptotic processes. Lack of glucose has been directly associated with neuronal cell death (Mergenthaler et al., 2013). A permanent deficit in glucose availability renders a brain more vulnerable to neurodegenerative processes.

Definition

We propose to use the term "cerebral metabolic syndrome," by widening the definition of the "metabolic syndrome." Both syndromes are related to endothelial dysfunction of blood vessels, usually starting from a loss of endothelial membranous fluidity. In the case of cerebral metabolic syndrome, this dysfunction is focused on the BBB. In its first manifestation, it describes

a clinical situation by which a reduced neuronal capacity evolves into symptoms such as mental fatigue, obliviousness, stress aversion, or depression. However, focused on BBB pathophysiology, the concept goes far beyond a mere description of aging deficits. Impairment, dysfunction, and destruction of the BBB system is not the only causative for the clinical picture of improper aging, but also onset and/or aggravation of dementia.

The cerebral metabolic syndrome may also go along with hypertension and impaired glucose tolerance, which are the main consequences of metabolic syndrome. However, the syndromes will lead to different secondary diseases, unless treated timely. In the case of metabolic syndrome, hypertension is related to myocardial infarction and/or stroke (Isomaa et al., 2001), while impaired glucose tolerance is the prodromal stage of diabetes (Mendrick et al., 2018). In the case of the cerebral metabolic syndrome, however, hypertension and glucose intolerance additionally point to a potentially impaired transport function of nutrients and metabolites into the brain across the BBB. Increased blood pressure and elevated blood sugar levels are also indicators signaling impending neurodegeneration and dementia.

Over the last two decades, there has been a shift, from reductionist towards systemic approaches, favoring synoptic views. According to this, all specific types of dementia may be considered as part of one group of brain diseases and may be expected to have certain features in common. Further, the systemic approach implies that brain functions should be interpreted concerning the rest of the body, considering them as part of an interdependent system. The BBB, as a bidirectional interface between the central nervous system and the periphery, serves as an integral element in this context. The cerebral metabolic syndrome is combining a certain number of clinical pictures into one conceptual system, thus providing a frame for systemic approaches in understanding and treatment of neurodegeneration. Defining the clinical picture of the metabolic syndrome has been particularly helpful because it connects individual lifestyles to severe, life-threatening diseases. In times of genetic determinism, the concept of metabolic syndrome helped to point out the individual responsibility for personal health. Thereby, the main focus on preventing obesity is needed, which is a primary factor for metabolic syndrome and a health problem increasingly affecting young people (Dominguez and Barbagallo, 2016). In the case of the cerebral metabolic syndrome, aggravation of metabolic deficits in elderly people by impaired function of their BBB is the major cause of disease. The opportunity of linking lifestyle to life-threatening diseases might trigger the feeling of responsibility for personal health, also on the field of neurodegeneration. This is one of the major justifications for defining cerebral metabolic syndrome.

Diagnosis of Cerebral Metabolic Syndrome

Considering the overlap of both syndromes, most diagnostic parameters in use for the metabolic syndrome are applicable for the cerebral metabolic too (Grundy et al., 2005). Despite these methods, various diagnostic tools exist, which allow for determining mental performance, cognitive deficits, and other symptoms. Mental testing is in the focus of cerebral metabolic syndrome diagnostics.

The lost neuronal function can hardly be replaced (Power and Schlaggar, 2017). Therefore, therapy of neurodegeneration is to start as soon as first clear signals come up or before. Most of the diagnostic methods in use to detect loss of mental functions are of empirical character (Fleming et al., 1995), however, brain imaging methods (that will be discussed later on) have gained widespread attention over the last decades. A standardized set of diagnostic methods still is to be set up for the cerebral metabolic syndrome. This set might include the screening for biomarkers, predicting the risk of developing dementia later on. The diagnostic tools will have to include the possibility to examine metabolic functions, such as the brain's energy supply in general, and the impairment of BBB functioning, specifically. Existing metabolic parameters, such as homocysteine (Derosa et al., 2006) and other metabolites, as well as enzymes and coenzymes, should be screened and adjusted to serve as predictors for pathologic processes. Given the rapidly evolving field of imaging methods, further development in this area will hopefully lead to sufficient prediction accuracy in diagnosing the cerebral metabolic and sequelae with high specificity and sensitivity (Aisen et al., 2017).

Prevention

Given its life-threatening sequelae, the prevention of metabolic syndromes is a central goal, both in the peripheral and the cerebral case. With both syndromes, dietetic measures, as well as physical exercise, are particularly important. Measures include diets to maintain vascular membrane fluidity. Increased use of fats with a high content of specific unsaturated fatty acids, e.g., omega-3 fatty acids, avoidance of trans-fats, and cholesterol-rich food are known to support membrane fluidity both in younger and older people (Gammone et al., 2018). In the classification of the individual nutritional status, the definition of the body mass index (BMI) has proven to be a helpful marker to control dietary measures and to foster health competency within the population (Afshordel et al., 2015; Cass, 2017). With cerebral metabolic syndrome, the improvement of physical fitness should be complemented by measures to maintain mental fitness. Cognitive training to promote and preserve neuronal plasticity is of special interest, also to prevent a cerebral metabolic syndrome in elderly people (Meeusen, 2014).

In the prevention of cerebral metabolic syndrome, specific attention should be attributed to brain nutrition, most of all, to the energy supply of the brain by providing sufficient glucose. While in most tissues, energy can also be provided by other sources, mainly other carbohydrates such as fructose, mannose, and lactose, the main consumers of glucose—brain tissue and erythrocytes—entirely dependent on the supply of molecular glucose (Mergenthaler et al., 2013). Due to the lack of a nucleus, erythrocytes cannot express enzymes to utilize other sources than glucose. The brain, on the other hand, depends on the active transport of glucose over the BBB, because its relatively high energy demand cannot be covered by alternative metabolic pathways on the long-term impact (Hajjawi, 2013).

DEMENTIA

From Cerebral Metabolic Syndrome to Dementia

The risk of developing a specific type of dementia depends on genetic as well as epigenetic factors, including lifestyle and nutrition habits. By now, several genes could be identified that are known to be involved in AD, but none of them is exclusively accountable for this type of dementia (Broadstock et al., 2014). The disease rather originates from a combination of a dysfunctional genomic network, including impaired alleles of receptors, transporters or enzymes, and specific lifestyle parameters. Extensive ongoing research on neurodegeneration has generated a wealth of new knowledge and will certainly add new targets and novel drugs for therapy. Due to its strict obligation for active transport, the BBB provides—beyond GLUT1—a series of potentially dysfunctional receptors and transporters. They are determinants for the course of neurodegeneration (Baumgart et al., 2015) and might serve as drug targets.

Nevertheless, in our opinion, it cannot be expected that a reductionist concept leading to one perfect drug-target will appear to provide the "total" solution for AD. Indeed, the evaluation of holistic concepts seems to be a promising approach. The cerebral metabolic syndrome, particularly the impaired function of the BBB, is proposed as the starting point of this path, where dementia could be interpreted as a consequence of cerebral metabolic syndrome (Iadecola, 2010). Thereby, neurodegeneration might be induced by an overall impairment of BBB functioning, including loss of fluidity as well as (partly genetically determined) deficits of receptors and transporters in the BBB. Inflammation (Heneka et al., 2015) or infections (Holmes et al., 2003) of BBB tissue could aggravate vascular dementia (VD) and induce AD. Not only the endothelial transport capacity will be disturbed in the course of such processes, but also the integrity of the BBB is threatened by apoptotic procedures, thus carrying neurodegeneration into deeper compartments of the brain.

The Choline System and Apoptosis

Cellular survival is largely modulated by apoptosis and autophagy, which has gained increased attention in anti-aging and neurodegenerative research recently (Gump and Thorburn, 2011). In the human body, millions of new cells arise every day. At the same time, millions of them decay. This type of cellular death is an efficient, controlled process called apoptosis. It guarantees the disposal of dying cells without disturbing ongoing, physiologic processes within the organism (Kerr et al., 1972; Elmore, 2007). Brain cells, especially neurons, are highly durable and cannot be simply reproduced. They are part of a highly complex network with an individual set of connections to other neurons. Neuronal cell loss is, therefore, mostly irreversible damage (Okouchi et al., 2007). The status of cerebral metabolic syndrome supports apoptotic processes and cellular decay due to inflammation.

It has long been known that the pathogenesis of AD comes along with a deficiency in acetylcholine. Therefore, the therapy of AD includes the administration of acetylcholinesterase inhibitors (Ladner and Lee, 1998), substances that are meant to prevent the breakdown of acetylcholine. It is known that these drugs improve the current state of concerned patients, though they lack an effect on disease progression (Bartolini et al., 2003). Acetylcholine is formed by acetylation of choline. It is well known that choline is also a structural moiety of phosphatidylcholine, which is the major component of the lipid bilayer of cell membranes. A lack of choline can mean both a lack of acetylcholine—the deficient neurotransmitter in AD—and a lack of the membrane constituent phosphatidylcholine (Hollenbeck, 2012).

In the course of apoptotic dismantling, the cell shrinks, splitting cellular DNA into typical fragments. At the end of this internal process, parts of the inner layer of the cell membrane that are rich in the phospholipid phosphatidylserine change their position. They flip to the outer surface of the apoptotic cell, replacing phosphatidylcholine rich epitopes. Now, instead of choline, the amino acid serine is the polar rest of the outer cell membrane (Fadok et al., 1992; Ravichandran, 2011). These phosphatidylserine epitopes at the outside are the signals tagging the cell as "disposable." Thereby, a well-known cascade of final steps of apoptotic cell death is induced, attracting macrophages to internalize the tagged apoptotic cell (Ravichandran, 2011).

The cross-relation of both acetylcholine and phosphatidylcholine deficiency has not been considered sufficiently up to now. We hypothesize that the choline-related impairment of cell metabolism, which results in a cellular acetylcholine-deficiency, will at the same time have an impact on the composition of the cell membrane, increasing there the relative share of the phosphatidylcholine-precursors phosphatidylserine and phosphatidylethanolamine. While the acetylcholine-deficiency can be held accountable for emerging neurological deficits of AD, the lack of phosphatidylcholine—due to the same metabolic defect—impairs neuronal plasticity. Above all, it directly triggers the induction of the apoptotic cascade. This might explain why the administration of acetylcholinesterase inhibitors or acetylcholine receptor agonists improves physiologic deficits only temporarily (Rogers et al., 2000; Ferreira-Vieira et al., 2016).

In terms of chemical reactions, the biosynthesis of choline (Bremer et al., 1960) starts with the decarboxylation of the amino acid serine to ethanolamine, followed by the quaternization of ethanolamine, which is affected by methylation with three methyl groups. Thereby, the choline molecule receives its typical pH-independent polar charge. This sequence of steps is relevant both in acetylcholine- and phosphatidylcholine-biosynthesis (Hollenbeck, 2012). The provision of methyl- and methylene-groups (one carbon building blocks) is the task of a complex metabolic system, the choline system. Among others, it comprises the coenzymes folic acid (B9) and cobalamin (B12), as well as the amino acid methionine, which are substrates of closely interacting enzymes. In this context, S-adenosylmethionine, formed from methionine (Mato et al., 1997), plays a major role. Adenosylation activates the methyl group of methionine for methylation. In the course of this process, homocysteine is

generated from methionine, a marker for both the ongoing active methylation and for the dysfunction of the methylation cycle. The dysfunction of the choline system may cause severe deficits. It plays an important role both in embryonal development and in the process of aging. It may be speculated that an insufficient biosynthesis of choline directly triggers apoptotic cellular loss in all cells of the body, a phenomenon that is known to be accelerated in patients with AD (Campoy et al., 2016; Bekdash, 2018).

Cellular availability of the components of the choline system depends on their active transport across the vascular endothelium. Any loss of membrane fluidity will, therefore, harm the system. However, the situation is by far aggravated in the brain, where the tight BBB will potentiate the effects of endothelial transport deficits. This is also true for the amino acids and coenzymes of the choline system (Fadok et al., 1992; Hollenbeck, 2012; Bekdash, 2018). We hypothesize that a dysfunctional blood-brain might trigger apoptotic processes also by preventing adequate availability of methyl groups, required both for the biosynthesis of acetylcholine and phosphatidylcholine. In any case, both impaired glucose transport—inducing mitochondrial apoptosis—and an impaired choline system—speeding up apoptotic processes by macrophage attraction—are directly related to cellular apoptosis and will render neuronal cells more susceptible to neurodegenerative processes in general (Okouchi et al., 2007). They are candidates for a rational interpretation of neuronal cell death in normal aging processes and VD.

Vascular Dementia

A steadily decreasing function of BBB endothelial cells may support the pathological process of a slowly proceeding dementia. However, increasing vascular deficits may equally end up in a local mechanic deconstruction of a brain vessel leading to VD. There, ischemic or hemorrhagic infarcts may affect multiple brain areas (Iadecola, 2010) due to occlusion of vessels or due to the loss of microvascular tightness. The situation is different with AD, which is diagnosed per definition by the appearance of amyloid plaques.

A HYPOTHESIS ON THE ETIOLOGY OF ALZHEIMER'S DISEASE

The Amyloid Precursor Protein (APP)

Although a wide range of approved medicines is available for palliative therapy of neurodegeneration, the present pharmacotherapeutic situation is far away from satisfactory given the rising prevalence of dementia (Ladner and Lee, 1998; Ferreira-Vieira et al., 2016). For more than 30 years, AD has been one of the central areas of academic and industrial research. However, no significant breakthrough regarding therapeutic approaches has been achieved so far (Salloway et al., 2008). The most characteristic pathologic features of AD are the amyloid plaques found in the brain (Gouras et al., 2010). It is almost self-evident to assume that exactly these plaques impair the functionality of cells and cause cell death in the long-term. Up to now, all efforts to develop drugs that aim to dissolve these plaques and remove them from the brain have not yet been successful. This also holds true for those immunotherapies that target APP (Sigurdsson et al., 2001; Solomon and Frenkel, 2010) and Tau, the second pathophysiological protein in AD. Currently, a disappointment on the slow progress is visible in industrial research, which has led to the cancellation of research activities performed by major pharmaceutical companies in this field (Broadstock et al., 2014). While the diagnosis of neurodegeneration is well established, a reasonable approach to counteract neurodegeneration, above all AD, is still lacking.

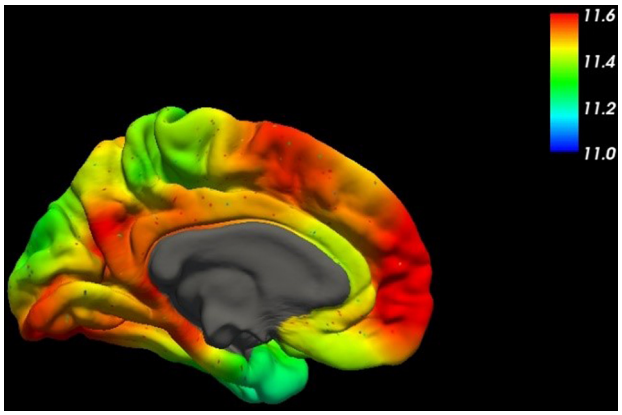

FIGURE 2 | This figure shows the spatial distribution of the mRNA expression of the amyloid-β precursor protein (APP) across the human brain (mesial surface) using high-resolution mapping techniques of the human whole-brain transcriptome (Gryglewski et al., 2018).

Genetic investigations have revealed significant APP mutations causally linked to a familial predisposition for AD (Cuyvers and Sleegers, 2016). However, an exclusive role of genetic factors could only be shown for a low percentage of all AD patients—a subset of less than 10% so far (Zhang et al., 2011).

For all the other cases, a rather complex etiology is to be assumed with amyloid plaques as a common marker. Even though amyloid plaques are probably rather remnants of a devastating pathophysiologic process than elicitors, the central role of the precursor protein APP (**Figure 2**) in AD remains unquestioned (Goate et al., 1991).

Inflammation of BBB Cells

Already in 1989 (Braak et al., 1989), a detailed study on the presence of cerebral amyloid tangles in deceased patients appeared (Braak and Braak, 1991). These investigations were also beneficial concerning understanding the etiology of AD. Two remarkable correlations have emerged from this research. First, the plaques could be found scattered across the whole study population; they were not limited to patients suffering from AD. Second, an age-dependent increase in plaque formation could be identified. These findings shed doubt on the assumption that the amyloid plaques are the primary mandatory cause of dementia. Probably these results were relevant for upcoming concepts, which relate AD to inflammatory processes of the brain (Neuhaus et al., 2011; Hommet et al., 2014; Blonz, 2017). Although treatment of

inflammation seems to be a manageable task, the situation is different and by far more complex with chronic inflammation of unproven origin (Dominy et al., 2019). Although sporadic success has been shown for the inflammation concept over the years, it has remained a therapeutic outsider approach, also because a lifelong preventive drug therapy for a disease with an unpredictable out-brake prognosis cannot be justified (Holmes, 2013).

To understand the inflammation hypothesis of AD, certain physiologic assumptions need to be outlined. To begin with, cell membranes consist of lipid bilayers. The most remarkable fatty acid positioned within the phosphocholine membrane is the polyunsaturated arachidonic acid (AA; Yeagle, 1985). This integral component of the membrane triggers a cellular alert system, which acts as a kind of primordial immune system. Any disturbance of membrane integrity leads to cleavage of AA esters in the membrane by the enzyme phospholipase A2. The release of AA induces a cascade of metabolites. Cyclooxygenases and lipoxygenase oxidize this acid to yield prostaglandins, prostacyclins, thromboxanes, and leukotrienes. In higher organisms, the AA system represents the main player in inflammatory processes (Moncada and Vane, 1979).

Regarding the role of the BBB in neurodegeneration, thromboxane, which activates and attracts thrombocytes, deserves specific attention. Any lesion of a vascular membrane potentially leads to inflammation and attracts thrombocytes, which attach to the membrane *via* adhesion molecules to cover the membrane lesions (Moncada and Vane, 1979). A further task of thrombocytes is to support wound healing. Apoptosis of damaged endothelial cells is part of this process, which ends with the shedding of thrombocytes.

Like high blood sugar in the context of diabetes, APP—due to its connection to AD—is also generally perceived as fundamentally "evil." However, from an evolutionary point of view, it is implausible that a frequently occurring protein would remain conserved in the case of exclusively carrying out a severely pathologic function. Comparably little attention has been paid to the physiological role of APP in prior investigations. In the context of inflammation of the BBB, it is remarkable that the largest amounts of APP in the whole body appear in thrombocytes (Bush et al., 1990). Interestingly, also APP plays a role in this thrombocyte adhesion process. It is cleaved at the end of this process by the enzyme β-secretase, leaving back the neurotoxic Aβ42-amyloid-fragment in the vascular cell membrane (Bush et al., 1990; Vassar et al., 1999). The functional role of APP in this context has not yet been fully clarified. It is physiological in wound healing as part of the AA system. However, it is at the same time pathophysiological in neurodegeneration. We hypothesize that the formation of Aβ42 fragments going along with cleavage of thrombocytes from an inflamed BBB is a key step in the etiology of AD.

A series of diseases of the CNS, such as multiple sclerosis (Minagar and Alexander, 2003) or viral encephalitis (Dallasta et al., 1999) is caused by inflammatory processes in the brain of different origins. In connection with the inflammatory hypotheses of AD, altered permeability of the BBB or its disruption has been proposed to allow access to inflammation in the brain. Considering inflammation of BBB tissue itself as the starting point of the disease goes beyond that; providing several new aspects and tracing back inflammation hypotheses of AD to the inflammation of the BBB. Inflamed or infected endothelial cells themselves transfer the processes from the periphery to the CNS *via* their direct contact with pericytes, glia cells, and neurons. The focus on the BBB and its inflammation provide a clear mechanistic link between APP and neurodegeneration (Heneka and O'Banion, 2007). Beyond membrane stiffness and other factors, inflammation easily adds to the concept of BBB dysfunction as a key factor to transform a cerebral metabolic syndrome into neurodegeneration (Heneka and O'Banion, 2007; Bennani-Baiti et al., 2015; Heneka et al., 2015; Gleizes et al., 2016).

The Infection-Inflammation Interplay

Disease patterns of dementia cannot be explained by sporadically occurring, heavy infections, but suggest chronic processes in any case. Although chronic inflammation can be associated with various severe diseases with underlying factors ranging from a genetic disposition to immunological problems, there is no convincing explanation for the chronic inflammatory processes in dementia lasting for years (Dunn et al., 2005; Chitnis and Weiner, 2017). At this point, a remarkable correlation within the AA system deserves attention. This system is not only involved in the induction of inflammation in higher organisms but can also be found in microorganisms, where it is strongly involved in cell-cell interaction. If microorganisms are present in blood or tissue, they might be easily attracted by thromboxane—released from an endothelial lesion—in the same way as thrombocytes are attracted. Remarkably, they will trigger further inflammation of the cell membrane through the activation of phospholipase or their AA system. For instance, in the case of chlamydia (that has been detected in atherosclerotic plaques), their attachment to the vascular endothelium takes place *via* the action of adhesion molecules, just like in thrombocyte-attachment. Bacteria can trigger inflammatory processes, just like any other trigger of inflammation (Ramirez, 1996).

Each infection starts with the adhesion of the micro-organism to a cell membrane, usually followed by invasion. Brain infection is frequently preceded by an infection of the BBB. Chronic brain infection is one of the theories to explain the etiology of AD (Holmes, 2013), with several microorganisms proposed as candidates. There are recent reports on promising results with anti-infective treatment (Tzeng et al., 2018). However, the search for the reason of chronification in dementia remains the same, both with infection and inflammation (Dominy et al., 2019). An ongoing interplay between inflammation and infection starting from the BBB provides a good explanation for long term maintenance of inflammation (Holmes, 2013). It does not matter whether microorganisms are the immediate inflammation trigger or just opportunistic colonizers of inflamed tissue and plaques. Even a treated infection might reappear if the

chronic inflammation remains because persisting quiescent microorganisms can be re-activated by prostaglandins and thromboxane to carry on the chronic process. The parallel course of inflammation and infection in a latent or chronic disease is well-known and described on an empirical basis. The mechanistic explanation linking these processes based on the AA system was therapeutically implemented for the first time with recurrent vulvovaginal candidiasis (RVVC), where in combination with a constant dose of the antifungal, the disease could be suppressed only by simultaneous treatment with a non-steroidal anti-inflammatory drug (NSAID) in a dose-dependent manner (Noe-Letschnig, 2019).

Membrane Pore Formation and Cell Death

Within the concept of the cerebral metabolic syndrome, chronic inflammation, and/or infection of the BBB aggravate the process leading both to VD and AD. While infarcts terminate pathologic processes in VD, the situation is different for AD, where amyloid plaques appear. It is known that chronic inflammation can lead to serum amyloid A protein (SAA) induced AA amyloidosis, where repetitive phases of cell death accumulate remnants of apoptotic cells. Also, AD belongs to the class of amyloidoses, with amyloids formed from Aβ42 fragments, which are generated from their precursor protein APP *via* proteolysis (Braak et al., 1989; Bush et al., 1990; Hommet et al., 2014).

The drugs memantine and amantadine are structurally very similar, both exhibiting a ball-like shape. Nevertheless, they are used in different indications: Memantine is used in the treatment of AD (Wang and Reddy, 2017), while the primary therapeutic indication of amantadine is influenza A. Amantadine has also been used in the treatment of Morbus Parkinson (MP; Stromberg et al., 1970). Both drugs make use of a similar mechanism of pharmacologic action: They are—apart from other reported mechanisms—rather unspecific blockers of membrane channels, preventing the uncontrolled influx of protons and ions. Memantine is delaying neuronal apoptosis by interfering with excitotoxic cellular calcium influx *via* glutamatergic N-methyl-D-aspartate (NMDA) receptors (Neuhaus et al., 2011), while amantadine is blocking the matrix protein 2 of influenza 1 virus, which weakens infected cells by proton influx, thus disturbing the electrochemical potential (Bischofberger et al., 2009). The identical channel blocking mode of the pharmacologic action of these both drugs points to a potential role of APP and its Aβ42 fragments in driving damaged cells into apoptosis. The Aβ42 fragment is one of the main plaque-components in the brains of AD patients (Magalhaes et al., 2018). There has been extensive work to investigate how Aβ42 exerts its toxic function (Younkin, 1998). It is known that it tends to form oligomers. The formation of membranous pores to disturb the cell potential and pore-forming in microbial infection are known (Borlikova et al., 2013; Brown and Bevan, 2016). Because of the infection-inflammation interplay, we hypothesize that cleaved membrane sequences of both microbial origin and human APP origin can equally contribute to the apoptotic disturbance of the electrochemical potential of infected neurons.

Chronic Infection Ending up in Amyloids

At this point, the hypothesis emerges that the physiological role of APP in thrombocytes might consist of supporting apoptosis of damaged cells *via* the formation of pores. These pore-forming domains will rest in the membrane after cleavage of APP by β-secretase. In the course of a chronic infection-inflammation process, they accumulate and are set free from disintegrating membranes during apoptosis, thus becoming infectious β-amyloid fragments, which on the one hand, may aggregate as remnants to the known amyloid plaques, or on the other hand, integrate into surrounding cell membranes. Consequently, chronic inflammation-infection of the BBB could be the prerequisite for the massive, long-lasting build-up of infectious, pore-forming β-amyloid fragments, explaining the dramatic progression of the disease. With infectious Aβ42, a new quality of disease is emerging. The inflammatory-infectious process cannot be eliminated anymore by just terminating inflammation and infection.

At this stage, genetic predisposition matters, because the tendency of Aβ42 towards protein aggregation depends on the sequence of amino acids favoring aggregation-prone β-sheet formation. Equally, the type of microbial infection might play a role. Since APP is a player in thrombocyte action in general, physiological mechanisms to prevent infectious Aβ42 formation or to remove it from the body must exist. At present, it is not known why and when a chronic inflammation, particularly in the case of Aβ42, turns into an uncontrollable process. While according to the cerebral metabolic syndrome concept, prevention and treatment of early AD is a feasible task to be solved, unfortunately, the reversion of the auto-dynamic infection by Aβ42, which is the prerequisite to stop AD at later stages, has not yet been achieved (Deyts et al., 2019).

Recently, the efflux of disease driving metabolites from the brain across the BBB has received increased attention (Poetsch et al., 2010a). Therapeutic concepts to prevent and resolve Aβ42 oligomerization are a promising approach in this direction, albeit far from the therapeutic implementation (Poetsch et al., 2010b). Removal of undesirable metabolites and deposits, including Aβ42 fragments, is a valid therapeutic concept. Amongst others, P-glycoprotein at the BBB has become a target of research related to the export of amyloid peptides (Neuhaus et al., 2010; Saidijam et al., 2018). Current concepts also consider an important role of the glymphatic system of the brain (Smith and Verkman, 2018).

GENDER DIFFERENCES IN ENDOTHELIAL DYSFUNCTION AND DEMENTIA

AD and other types of dementia are reported to be more frequent in women than in men. Although several limitations in prevalence and incidence studies, as well as geographical and methodological differences, need to be taken into account, there is evidence supporting the hypothesis of a greater biological risk of dementia in women including elevated tauopathy and faster brain atrophy (Buckley et al., 2019). The most striking

gender-dependent biological risk factors for disadvantageous endothelial characteristics among women will be outlined in this paragraph.

Regarding the risk of dementia, microvascular defects, and certain metabolic conditions like obesity, diabetes, or high cholesterol levels seem to have a more significant pathologic impact on women than on men (Azad et al., 2007). Women show a greater risk of diabetic complications, including myocardial infarction, depression, and coronary heart disease. These complications *per se* represent some of the most evident risk-factors for AD (Kautzky-Willer et al., 2016). Further, genetic preconditions like, e.g., Apolipoprotein E ε 4 genotype status, seem to have a more pronounced (harmful) effect on hippocampal atrophy and cognitive decline in women compared to men (Fleisher et al., 2005). Thereby, the risk of conversion from physiological cognition to mild cognitive impairment, as well as from mild cognitive impairment to AD, seems to be elevated in women (Altmann et al., 2014). Besides genetic and metabolic risk factors, several hormonal studies implicate a neuroprotective role of estrogen (Petanceska et al., 2000; Rosario et al., 2011). However, inconclusive data on estrogen replacement therapy in postmenopausal women has aroused interest in other hormones of the hypothalamic-pituitary-gonadal axis that cross the BBB, e.g., gonadotropins, suggesting higher gonadotropin levels as a potential cause for AD (Webber et al., 2005). Finally, the prevalence of major depression is twice as high in women as in men (Rai et al., 2013). In this context, stress and its molecular counterpart, namely cortisol, as well as the receptor binding of corticotropin-releasing factor (CRF) has been discussed (Rosinger et al., 2020) to play a major role in the pathophysiology of depression and AD.

DIAGNOSIS OF DEMENTIA

The Requirement for Early Diagnosis

The diagnosis of dementia has traditionally been clinical. Scores for mental activity have been dominant in AD diagnosis but will determine the diagnosis only in a stage of manifest disease. Despite their potential to reveal AD at early stages and to differentiate between subtypes of dementia, neuroimaging methods do not belong to the standard repertoire of routine screening procedures (Teipel et al., 2018), unless a family history of early-onset dementia is known. Over the years, also a series of clinical metabolic parameters in blood and liquor have been established (Vos et al., 2015; Wiltfang, 2015; Frölich et al., 2017). Genetic analyses aim to predict the risk of developing such a disease. Despite these diagnostic modalities, also neuroimaging techniques are available to reveal cerebral metabolic deficits, functional impairment, and protein deposits. Currently, molecular neuroimaging with positron emission tomography (PET) and ^{11}C-radioligands are mainly research tools and restricted to a few medical centers in most of the countries, however, these tools provide unique opportunities in the (ultra)early diagnosis of AD to foster the investigation and implementation of causal therapeutic strategies in the pathogenesis of AD, especially regarding inflammatory processes at the BBB. The massive financial investments in the development and clinical establishment of ^{18}F-radioligands for the quantification of β-amyloid plaques and tau proteins using PET are showing high confidence in this cutting-edge technology, triggering new evidence-based early diagnosis approaches and the systematic development of clinically useful prediction markers in AD.

Positron Emission Tomography (PET) as a Diagnostic Tool in Dementia

Brain imaging methods provide a straightforward way for diagnostics in the otherwise not easily accessible brain. To reveal distinct patterns of atrophy, hypometabolism, or pathologic accumulation of β-amyloid plaques in diverse neurodegenerative disorders involving dementia, various neuroimaging modalities exist. Especially, PET plays a crucial role in the diagnosis and differentiation of relevant pathophysiologic entities. In this regard, diverse target points evolved. FDG-PET, targeting specific brain areas with pathologic glucose hypometabolism, uses fluorodeoxyglucose ([^{18}F]-FDG) as a radioligand. Amyloid-PET scans need β-amyloid-specific tracers to visualize Aβ-40 and Aβ-42 deposits (Berndt et al., 2008). Regarding the imaging of inflammatory processes in AD and other pathologies linked to dementia, translocator-protein (TSPO)-tracers (Hommet et al., 2014) are used. Moreover, the efflux transporter P-glycoprotein (P-gp), limiting substrate compounds at the BBB, and maintaining the homeostasis of the brain can be examined with [^{11}C]-verapamil (Hendrikse et al., 1998). P-gp is known to be frequently affected by neurodegeneration. Further approaches comprise, among others, the challenging visualization of tau protein (Villemagne et al., 2012) or targeting metabotropic glutamate receptors ([^{18}F]-FPEB; Bélanger et al., 2008), the fatty acid amide hydrolase (e.g., [^{11}C]-MK-3168) and acetylcholine esterases (e.g., [^{11}C]-PMP; Iyo et al., 1997).

FDG-PET is known to highlight the distribution of hypometabolic brain regions in diverse types of dementia (Foster et al., 2007). Particularly [^{18}F]-FDG PET is a valuable diagnostic tool to optimize the early and differential diagnosis of various pathologies comprising dementia (Mosconi et al., 2008). A meta-analysis, including 119 studies on diagnostic modalities in general, and 27 studies investigating the specific role of FDG-PET (Bloudek et al., 2011), could reveal the diagnostic superiority of FDG-PET compared to clinical diagnostic tools, CT, SPECT, and MRI. Compared to non-demented controls, a sensitivity of 90% and a specificity of 89% could be shown. Distinguishing patients with AD from patients suffering from other forms of dementia, FDG-PET reached a sensitivity of 95% and a specificity of 78% (Bloudek et al., 2011). Since glucose is both tracer and target of analysis, FDG-PET seems to be a perfect approach to develop methods for diagnosis of a cerebral metabolic syndrome and to detect early signs of metabolic impairment in the brain.

Despite the accuracy of FDG-PET concerning cerebral metabolic alterations in patients with dementia, the

differentiation of AD and other entities (e.g., frontotemporal dementia) remains challenging. Due to anatomic overlaps with regards to hypometabolic brain regions in various types of dementia and β-amyloid fragments specifically characterizing AD, targeting these β-amyloid plaques is helpful to identify individuals with AD (Rabinovici et al., 2011). Therefore, various tracers can be used (e.g., [^{11}C]-PiB; Klunk et al., 2004 and [^{18}F]-Florbetapir; Berndt et al., 2008; Clark et al., 2011).

Diagnosis of Neuroinflammation by PET

As described earlier, neuroinflammatory processes play a major role in multiple neurodegenerative diseases. Neuronal decline due to inflammation is triggered by the activation of microglia, inducing the production of free radicals (Klegeris and McGeer, 2000), the stimulation of T cells (Togo et al., 2002), and thereby the release of pro-inflammatory cytokines (e.g., IL-6, IL-1β, and TNF-α; Swardfager et al., 2010). In this sense, complement activation by β-amyloid (Rogers et al., 1992) and tau protein (Holmes and Diamond, 2014; Stancu et al., 2019) seem to play a crucial role. This pattern might be triggered by infections, like herpes simplex virus (Hogestyn et al., 2018), helicobacter pylori (Doulberis et al., 2018), or chlamydia pneumoniae (Lim et al., 2014), as intensely discussed in the last two decades. One way to identify these processes *via* PET is targeting the translocator protein-18 kDa (TSPO) with a large group of more than 80 suitable tracers, however, (R)-[^{11}C]-PK11195 remains the most frequently used ligand in clinical practice (Damont et al., 2013). TSPO is known to be upregulated in the presence of neurodegenerative pathologies and is associated with microglial activation. Establishing and validating methods to detect inflammatory processes specifically at the microvascular endothelium of the BBB will be a challenging, but certainly rewarding task.

Magnetic Resonance Imaging (MRI)

It is evident that imaging methods currently represent the gold standard approach in diagnosing brain diseases beyond clinical evaluation and specific liquor/blood parameters. In this context, also the potential of imaging methods beyond PET, such as MRI, is of importance. In that respect, structural MRI is a frequently applied diagnostic tool to assess structural changes like generalized brain atrophy (Fox et al., 1999) and e.g., hippocampal atrophy (Kesslak et al., 1991) as well as microvascular alterations in the diseased brain (Christov et al., 2008). Although not established in clinical practice, functional MRI (fMRI) provides an evidentially effective possibility to record network connectivity changes, detect relevant cortical hubs (Buckner et al., 2009) and uncover functional impairment both in the resting (Greicius et al., 2004; Supekar et al., 2008) as well as the task performing brain (De Marco et al., 2017). Therefore, it can be expected that future investigations might pave the way for the clinical implementation of fMRI as an elementary low-cost (compared to PET) diagnostic tool, also for early stages of cognitive impairment and AD.

Other Diagnostic Methods

The importance of early diagnosis in the case of dementia is already known in principle, with a broad repertoire of various methods already available and constantly evolving. The need to distinguish between transient cognitive impairment and progressive forms of dementia as soon as the first symptoms occur is challenging. In the context of the cerebral metabolic syndrome and the upcoming option for a causal therapy of early dementia, it is to be expected that the scope of potential differential methods for diagnosis might become rather broad, ranging from smelling tests (Devanand et al., 2000) and pupillometry (Fotiou et al., 2000) to polymerase chain reaction PCR (Goate et al., 1991).

CONCLUSION

Increased consideration of the role of brain metabolism in dementia as presented here, favors synoptic approaches in diagnosis and systemic therapy of dementia. Within the concept of the cerebral metabolic syndrome, a plethora of findings of dementia that have emerged over the last decades can be interpreted in a much broader and coherent context when compared to the target-specific approaches of conventional pharmaceutical research.

The focus on the impairment of the BBB plays a central role in the development of cerebral metabolic syndrome and its sequelae. Within this concept, the etiology of dementia is rather based on metabolic than on genetic factors. Deficiency in glucose and nutrients inside the brain weaken the neuronal metabolism and provoke disease progression. Just as in the case of the general metabolic syndrome, preventive measures are of special importance to hold back pathological processes at the beginning of the disorder. Support to the choline metabolism may further specifically inhibit apoptotic processes and help to delay the progression of dementia.

Beyond membrane stiffness induced by nutritional behavior and a harmful lifestyle (e.g., smoking), chronic inflammation and/or infections of the BBB can be considered as the main reasons for its dysfunction. Nevertheless, both treatment of AD with anti-inflammatory drugs and/or with anti-infectives could not provide a therapeutic breakthrough, hitherto. The thrombocyte protein APP links the inflammation of the BBB directly to neurodegeneration. Its physiological role in inflammatory processes is to be further clarified in general. The chronification of inflammatory processes at the BBB *via* inflammation-infection interplay promotes apoptotic processes and amyloid deposition. The understanding of this mechanism needs to be deepened. In this context, self-supported autoinfection by Aβ42-fragments of APP will play an important role. In addition to prevention and early therapy, termination of the Aβ42 induced apoptotic process is an indispensable final step to complete the option for a causal therapy of AD, even at later stages (Poksay et al., 2017).

Given the growing prevalence of dementia in the aging population, an appropriate lifestyle is a key factor in preventing

the outbreak of neurodegeneration. The cerebral metabolic syndrome points towards the essential criteria to maintain mental health. Health competency and self-awareness among the general population need to be promoted to call attention towards the personal responsibility to preserve mental health.

It seems a feasible task to treat neurodegeneration effectively shortly. Early diagnosis is a key prerequisite for successful causal therapeutic intervention (Poetsch et al., 2010a). In contrast to all the stagnating efforts in conventional AD research, the definition of the cerebral metabolic syndrome will contribute to widening the view and open up the way for preventive and therapeutic concepts that can be implemented swiftly.

AUTHOR CONTRIBUTIONS

All authors of the manuscript were involved in the manuscript conception, revised several versions, and approved the final version. All authors contributed to the article and approved the submitted version.

ACKNOWLEDGMENTS

We wish to thank several people for providing their expertise and a basis for the scientific discourse, namely, Dr. Michael Berger and Dr. Inge Schuster.

REFERENCES

Afshordel, S., Hagl, S., Werner, D., Rohner, N., Kogel, D., Bazan, N. G., et al. (2015). Omega-3 polyunsaturated fatty acids improve mitochondrial dysfunction in brain aging—impact of Bcl-2 and NPD-1 like metabolites. *Prostaglandins Leukot. Essent. Fatty Acids* 92, 23–31. doi: 10.1016/j.plefa.2014.05.008

Aisen, P. S., Cummings, J., Jack, C. R. Jr., Morris, J. C., Sperling, R., Frolich, L., et al. (2017). On the path to 2025: understanding the Alzheimer's disease continuum. *Alzheimers Res. Ther.* 9:60. doi: 10.1186/s13195-017-0283-5

Altmann, A., Tian, L., Henderson, V. W., and Greicius, M. D. (2014). Sex modifies the APOE-related risk of developing Alzheimer disease. *Ann. Neurol.* 75, 563–573. doi: 10.1002/ana.24135

Arvanitakis, Z., Wilson, R. S., Bienias, J. L., Evans, D. A., and Bennett, D. A. (2004). Diabetes mellitus and risk of Alzheimer disease and decline in cognitive function. *Arch. Neurol.* 61, 661–666. doi: 10.1001/archneur.61.5.661

Ashraf, G. M., Chibber, S., Mohammad, Zaidi, S. K., Tabrez, S., and Ahmad, A. (2016). Recent updates on the association between Alzheimer's disease and vascular dementia. *Med. Chem.* 3, 226–237. doi: 10.2174/1573406411666151030111820

Alzheimer's Association. (2017). 2017 Alzheimer's disease facts and figures. *Alzheimers Dement.* 13, 325–373. doi: 10.1016/j.jalz.2017.02.001

Azad, N. A., Al Bugami, M., and Loy-English, I. (2007). Gender differences in dementia risk factors. *Gend. Med.* 4, 120–129. doi: 10.1016/s1550-8579(07)80026-x

Azevedo, F. A., Carvalho, L. R., Grinberg, L. T., Farfel, J. M., Ferretti, R. E., Leite, R. E., et al. (2009). Equal numbers of neuronal and nonneuronal cells make the human brain an isometrically scaled-up primate brain. *J. Comp. Neurol.* 5, 532–541. doi: 10.1002/cne.21974

Bartolini, M., Bertucci, C., Cavrini, V., and Andrisano, V. (2003). β-Amyloid aggregation induced by human acetylcholinesterase: inhibition studies. *Biochem. Pharmacol.* 65, 407–416. doi: 10.1016/s0006-2952(02)01514-9

Baumgart, M., Snyder, H. M., Carrillo, M. C., Fazio, S., Kim, H., and Johns, H. (2015). Summary of the evidence on modifiable risk factors for cognitive decline and dementia: a population-based perspective. *Alzheimers Dement.* 11, 718–726. doi: 10.1016/j.jalz.2015.05.016

Bekdash, R. A. (2018). Choline, the brain and neurodegeneration: insights from epigenetics. *Front. Biosci.* 23, 1113–1143. doi: 10.2741/4636

Bélanger, M. J., Krause, S. M., Ryan, C., Sanabria-Bohorquez, S., Li, W., Hamill, T. G., et al. (2008). Biodistribution and radiation dosimetry of [^{18}F]F-PEB in nonhuman primates. *Nucl. Med. Commun.* 10, 915–919. doi: 10.1097/mnm.0b013e3283060c72

Bennani-Baiti, B., Toegel, S., Viernstein, H., Urban, E., Noe, C. R., and Bennani-Baiti, I. M. (2015). Inflammation modulates RLIP76/RALBP1 electrophile-glutathione conjugate transporter and housekeeping genes in human blood-brain barrier endothelial cells. *PLoS One* 10:e0139101. doi: 10.1371/journal.pone.0139101

Berndt, U., Stanetty, C., Wanek, T., Kuntner, C., Stanek, J., Berger, M., et al. (2008). Synthesis of a ^{18}F fluorobenzothiazole as potential amyloid imaging agent. *J. Labelled Comp. Radiopharm.* 51, 137–145. doi: 10.1002/jlcr.1476

Bischofberger, M., Gonzalez, M. R., and van der Goot, F. G. (2009). Membrane injury by pore-forming proteins. *Curr. Opin. Cell Biol.* 21, 589–595. doi: 10.1016/j.ceb.2009.04.003

Blonz, E. R. (2017). Alzheimer's disease as the product of a progressive energy deficiency syndrome in the central nervous system: the neuroenergetic hypothesis. *J. Alzheimers Dis.* 60, 1223–1229. doi: 10.3233/jad-170549

Bloudek, L. M., Spackman, D. E., Blankenburg, M., and Sullivan, S. D. (2011). Review and meta-analysis of biomarkers and diagnostic imaging in Alzheimer's disease. *J. Alzheimers Dis.* 26, 627–645. doi: 10.3233/jad-2011-110458

Borlikova, G. G., Trejo, M., Mably, A. J., Mc Donald, J. M., Sala Frigerio, C., Regan, C. M., et al. (2013). Alzheimer brain-derived amyloid β-protein impairs synaptic remodeling and memory consolidation. *Neurobiol. Aging* 5, 1315–1327. doi: 10.1016/j.neurobiolaging.2012.10.028

Braak, H., and Braak, E. (1991). Neuropathological stageing of Alzheimer-related changes. *Acta Neuropathol.* 82, 239–259. doi: 10.1007/BF00308809

Braak, H., Braak, E., Bohl, J., and Lang, W. (1989). Alzheimer's disease: amyloid plaques in the cerebellum. *J. Neurol. Sci.* 93, 277–287. doi: 10.1016/0022-510x(89)90197-4

Bremer, J., Figard, P. H., and Greenberg, D. M. (1960). The biosynthesis of choline and its relation to phospholipid metabolism. *Biochim. Biophys. Acta* 43, 477–488. doi: 10.1016/0006-3002(60)90470-4

Broadstock, M., Ballard, C., and Corbett, A. (2014). Latest treatment options for Alzheimer's disease, Parkinson's disease dementia and dementia with Lewy bodies. *Expert Opin. Pharmacother.* 15, 1797–1810. doi: 10.1517/14656566.2014.936848

Brown, A. M., and Bevan, D. R. (2016). Molecular dynamics simulations of amyloid β-peptide (1–42): tetramer formation and membrane interactions. *Biophys. J.* 111, 937–949. doi: 10.1016/j.bpj.2016.08.001

Bruel-Jungerman, E., Rampon, C., and Laroche, S. (2007). Adult hippocampal neurogenesis, synaptic plasticity and memory: facts and hypotheses. *Rev. Neurosci.* 18, 93–114. doi: 10.1515/revneuro.2007.18.2.93

Buckley, R. F., Waller, M., Masters, C. L., and Dobson, A. (2019). To what extent does age at death account for sex differences in rates of mortality from Alzheimer disease? *Am. J. Epidemiol.* 188, 1213–1223. doi: 10.1093/aje/kwz048

Buckner, R. L., Sepulcre, J., Talukdar, T., Krienen, F. M., Liu, H., Hedden, T., et al. (2009). Cortical hubs revealed by intrinsic functional connectivity: mapping, assessment of stability, and relation to Alzheimer's disease. *J. Neurosci.* 6, 1860–1873. doi: 10.1523/jneurosci.5062-08.2009

Bush, A. I., Martins, R., Rumble, B., Moir, R., Fuller, S., Milward, E., et al. (1990). The amyloid precursor protein of Alzheimer's disease is released by human platelets. *J. Biol. Chem.* 26, 15977–15983. doi: 10.1016/0197-4580(90)90886-5

Campoy, F. J., Vidal, C. J., Muñoz-Delgado, E., Montenegro, M. F., Cabezas-Herrera, J., and Nieto-Ceron, S. (2016). Cholinergic system and cell proliferation. *Chem. Biol. Interact.* 259, 257–265. doi: 10.1016/j.cbi.2016.04.014

Cass, S. P. (2017). Alzheimer's disease and exercise: a literature review. *Curr. Sports Med. Rep.* 16, 19–22. doi: 10.1249/JSR.0000000000000332

Chitnis, T., and Weiner, H. L. (2017). CNS inflammation and neurodegeneration. *J. Clin. Invest.* 127, 3577–3587. doi: 10.1172/JCI90609

Christov, A., Ottman, J., Hamdheydari, L., and Grammas, P. (2008). Structural changes in Alzheimer's disease brain microvessels. *Curr. Alzheimer Res.* 5, 392–395. doi: 10.2174/156720508785132334

Clark, C. M., Schneider, J. A., Bedell, B. J., Beach, T. G., Bilker, W. B., Mintun, M. A., et al. (2011). Use of florbetapir-PET for imaging β-amyloid pathology. *JAMA* 3, 275–283. doi: 10.1001/jama.2010.2008

Cunningham, E. L., McGuinness, B., Herron, B., and Passmore, A. P. (2015). Dementia. *Ulster Med. J.* 84, 79–87.

Cuyvers, E., and Sleegers, K. (2016). Genetic variations underlying Alzheimer's disease: evidence from genome-wide association studies and beyond. *Lancet Neurol.* 15, 857–868. doi: 10.1016/s1474-4422(16)00127-7

Dallasta, L. M., Pisarov, L. A., Esplen, J. E., Werley, J. V., Moses, A. V., Nelson, J. A., et al. (1999). Blood-brain barrier tight junction disruption in human immunodeficiency virus-1 encephalitis. *Am. J. Pathol.* 6, 1915–1927. doi: 10.1016/s0002-9440(10)65511-3

Damont, A., Roeda, D., and Dolle, F. (2013). The potential of carbon-11 and fluorine-18 chemistry: illustration through the development of positron emission tomography radioligands targeting the translocator protein 18 kDa. *J. Labelled Comp. Radiopharm.* 56, 96–104. doi: 10.1002/jlcr.2992

De Marco, M., Duzzi, D., Meneghello, F., and Venneri, A. (2017). Cognitive efficiency in Alzheimer's disease is associated with increased occipital connectivity. *J. Alzheimers Dis.* 57, 541–556. doi: 10.3233/jad-161164

Deng, D., Sun, P., Yan, C., Ke, M., Jiang, X., Xiong, L., et al. (2015). Molecular basis of ligand recognition and transport by glucose transporters. *Nature* 526, 391–396. doi: 10.1038/nature14655

Derosa, G., Cicero, A. F., D'Angelo, A., Gaddi, A., Ciccarelli, L., Piccinni, M. N., et al. (2006). Effects of 1 year of treatment with pioglitazone or rosiglitazone added to glimepiride on lipoprotein (A) and homocysteine concentrations in patients with type 2 diabetes mellitus and metabolic syndrome: a multicenter, randomized, double-blind, controlled clinical trial. *Clin. Ther.* 28, 679–688. doi: 10.1016/j.clinthera.2006.05.012

Devanand, D., Michaels-Marston, K. S., Liu, X., Pelton, G. H., Padilla, M., Marder, K., et al. (2000). Olfactory deficits in patients with mild cognitive impairment predict Alzheimer's disease at follow-up. *Am. J. Psychiatry* 157, 1399–1405. doi: 10.1176/appi.ajp.157.9.1399

Deyts, C., Clutter, M., Pierce, N., Chakrabarty, P., Ladd, T. B., Goddi, A., et al. (2019). APP-mediated signaling prevents memory decline in Alzheimer's disease mouse model. *Cell Rep.* 27, 1345.e6–1355.e6. doi: 10.1016/j.celrep.2019.03.087

Dominguez, L. J., and Barbagallo, M. (2016). The biology of the metabolic syndrome and aging. *Curr. Opin. Clin. Nutr. Metab. Care* 19, 5–11. doi: 10.1097/MCO.0000000000000243

Dominy, S. S., Lynch, C., Ermini, F., Benedyk, M., Marczyk, A., Konradi, A., et al. (2019). Porphyromonas gingivalis in Alzheimer's disease brains: evidence for disease causation and treatment with small-molecule inhibitors. *Sci. Adv.* 5:eaau3333. doi: 10.1126/sciadv.aau3333

Doulberis, M., Kotronis, G., Thomann, R., Polyzos, S. A., Boziki, M., Gialamprinou, D., et al. (2018). Review: impact of helicobacter pylori on Alzheimer's disease: what do we know so far? *Helicobacter* 23:e12454. doi: 10.1111/hel.12454

Draganski, B., Gaser, C., Busch, V., Schuierer, G., Bogdahn, U., and May, A. (2004). Neuroplasticity: changes in grey matter induced by training. *Nature* 427, 311–312. doi: 10.1038/427311a

Dunn, N., Mullee, M., Perry, V. H., and Holmes, C. (2005). Association between dementia and infectious disease: evidence from a case-control study. *Alzheimer Dis. Assoc. Disord.* 19, 91–94. doi: 10.1097/01.wad.0000165511.52746.1f

Ecker, G. F., and Noe, C. R. (2004). *In silico* prediction models for blood-brain barrier permeation. *Curr. Med. Chem.* 11, 1617–1628. doi: 10.2174/0929867043365071

Elmore, S. (2007). Apoptosis: a review of programmed cell death. *Toxicol. Pathol.* 35, 495–516. doi: 10.1080/01926230701320337

Fadok, V. A., Voelker, D. R., Campbell, P. A., Cohen, J. J., Bratton, D. L., and Henson, P. M. (1992). Exposure of phosphatidylserine on the surface of apoptotic lymphocytes triggers specific recognition and removal by macrophage. *J. Immunol.* 148, 2207–2216.

Fehm, H., Kern, W., and Peters, A. (2006). The selfish brain: competition for energy resources. *Prog. Brain Res.* 153, 129–140. doi: 10.1016/S0079-6123(06)53007-9

Ferreira-Vieira, T. H., Guimaraes, I. M., Silva, F. R., and Ribeiro, F. M. (2016). Alzheimer's disease: targeting the cholinergic system. *Curr. Neuropharmacol.* 14, 101–115. doi: 10.2174/1570159x13666150716165726

Fleisher, A., Grundman, M., Jack, C. R. Jr., Petersen, R. C., Taylor, C., Kim, H. T., et al. (2005). Sex, apolipoprotein E epsilon 4 status and hippocampal volume in mild cognitive impairment. *Arch. Neurol.* 6, 953–957. doi: 10.1001/archneur.62.6.953

Fleming, K. C., Adams, A. C., and Petersen, R. C. (1995). Dementia: diagnosis and evaluation. *Mayo Clin. Proc.* 70, 1093–1107. doi: 10.4065/70.11.1093

Foster, N. L., Heidebrink, J. L., Clark, C. M., Jagust, W. J., Arnold, S. E., Barbas, N. R., et al. (2007). FDG-PET improves accuracy in distinguishing frontotemporal dementia and Alzheimer's disease. *Brain* 130, 2616–2635. doi: 10.1093/brain/awm177

Fotiou, F., Fountoulakis, K., Tsolaki, M., Goulas, A., and Palikaras, A. (2000). Changes in pupil reaction to light in Alzheimer's disease patients: a preliminary report. *Int. J. Psychophysiol.* 37, 111–120. doi: 10.1016/s0167-8760(00)00099-4

Fox, N. C., Scahill, R. I., Crum, W. R., and Rossor, M. N. (1999). Correlation between rates of brain atrophy and cognitive decline in AD. *Neurology* 52, 1687–1689. doi: 10.1212/wnl.52.8.1687

Frölich, L., Peters, O., Lewczuk, P., Gruber, O., Teipel, S. J., Gertz, H. J., et al. (2017). Incremental value of biomarker combinations to predict progression of mild cognitive impairment to Alzheimer's dementia. *Alzheimers Res. Ther.* 9:84. doi: 10.1186/s13195-017-0301-7

Gammone, M. A., Riccioni, G., Parrinello, G., and D'Orazio, N. (2018). Omega-3 polyunsaturated fatty acids: benefits and endpoints in sport. *Nutrients* 11:46. doi: 10.3390/nu11010046

Gleizes, C., Kreutter, G., Abbas, M., Kassem, M., Constantinescu, A. A., Boisrame-Helms, J., et al. (2016). β cell membrane remodelling and procoagulant events occur in inflammation-driven insulin impairment: a GLP-1 receptor dependent and independent control. *J. Cell. Mol. Med.* 20, 231–242. doi: 10.1111/jcmm.12683

Goate, A., Chartier-Harlin, M.-C., Mullan, M., Brown, J., Crawford, F., Fidani, L., et al. (1991). Segregation of a missense mutation in the amyloid precursor protein gene with familial Alzheimer's disease. *Nature* 349, 704–706. doi: 10.1038/349704a0

Gouras, G. K., Tampellini, D., Takahashi, R. H., and Capetillo-Zarate, E. (2010). Intraneuronal β-amyloid accumulation and synapse pathology in Alzheimer's disease. *Acta Neuropathol.* 119, 523–541. doi: 10.1007/s00401-010-0679-9

Greicius, M. D., Srivastava, G., Reiss, A. L., and Menon, V. (2004). Default-mode network activity distinguishes Alzheimer's disease from healthy aging: evidence from functional MRI. *Proc. Natl. Acad. Sci. U S A* 101, 4637–4642. doi: 10.1073/pnas.0308627101

Grundy, S. M., Brewer, H. B. Jr., Cleeman, J. I., Smith, S. C. Jr., and Lenfant, C. (2004). Definition of metabolic syndrome: report of the National Heart, Lung, and Blood Institute/American Heart Association conference on scientific issues related to definition. *Circulation* 109, 433–438. doi: 10.1161/01.cir.0000111245.75752.c6

Grundy, S. M., Cleeman, J. I., Daniels, S. R., Donato, K. A., Eckel, R. H., Franklin, B. A., et al. (2005). Diagnosis and management of the metabolic syndrome. An american heart association/national heart, lung, and blood institute scientific statement. Executive summary. *Cardiol. Rev.* 13, 322–327. doi: 10.1161/01.ATV.0000111245.75752.C6

Gryglewski, G., Seiger, R., James, G. M., Godbersen, G. M., Komorowski, A., Unterholzner, J., et al. (2018). Spatial analysis and high resolution mapping of the human whole-brain transcriptome for integrative analysis in neuroimaging. *NeuroImage* 176, 259–267. doi: 10.1016/j.neuroimage.2018.04.068

Guillon, J., Attal, Y., Colliot, O., La Corte, V., Dubois, B., Schwartz, D., et al. (2017). Loss of brain inter-frequency hubs in Alzheimer's disease. *Sci. Rep.* 7:10879. doi: 10.1038/s41598-017-07846-w

Gump, J. M., and Thorburn, A. (2011). Autophagy and apoptosis: what is the connection? *Trends Cell Biol.* 21, 387–392. doi: 10.1016/j.tcb.2011.03.007

Habbas, S., Santello, M., Becker, D., Stubbe, H., Zappia, G., Liaudet, N., et al. (2015). Neuroinflammatory TNFα impairs memory *via* astrocyte signaling. *Cell* 7, 1730–1741. doi: 10.1016/j.cell.2015.11.023

Hajjawi, O. S. (2013). Glucose transport in human red blood cells. *Am. J. Biomed. Life Sci.* 1, 44–52. doi: 10.11648/j.ajbls.20130103.12

Hendrikse, N. H., Schinkel, A. H., de Vries, E. G., Fluks, E., Van der Graaf, W. T., Willemsen, A. T., et al. (1998). Complete *in vivo* reversal of P-glycoprotein pump function in the blood-brain barrier visualized with positron emission tomography. *Br. J. Pharmacol.* 124, 1413–1418. doi: 10.1038/sj.bjp.0701979

Heneka, M. T., Carson, M. J., Khoury, J. E., Landreth, G. E., Brosseron, F., Feinstein, D. L., et al. (2015). Neuroinflammation in Alzheimer's disease. *Lancet Neurol.* 14, 388–405. doi: 10.1016/S1474-4422(15)70016-5

Heneka, M. T., and O'Banion, M. K. (2007). Inflammatory processes in Alzheimer's disease. *J. Neuroimmunol.* 184, 69–91. doi: 10.1016/j.jneuroim.2006.11.017

Hengartner, M. O. (2000). The biochemistry of apoptosis. *Nature* 407, 770–776. doi: 10.1038/35037710

Hogestyn, J. M., Mock, D. J., and Mayer-Proschel, M. (2018). Contributions of neurotropic human herpesviruses herpes simplex virus 1 and human herpesvirus 6 to neurodegenerative disease pathology. *Neural Regen. Res.* 13, 211–221. doi: 10.4103/1673-5374.226380

Hollenbeck, C. B. (2012). An introduction to the nutrition and metabolism of choline. *Cent. Nerv. Syst. Agents Med. Chem.* 12, 100–113. doi: 10.2174/187152412800792689

Holmes, C. (2013). Review: systemic inflammation and Alzheimer's disease. *Neuropathol. Appl. Neurobiol.* 39, 51–68. doi: 10.1111/j.1365-2990.2012.01307.x

Holmes, B. B., and Diamond, M. I. (2014). Prion-like properties of Tau protein: the importance of extracellular Tau as a therapeutic target. *J. Biol. Chem.* 289, 19855–19861. doi: 10.1074/jbc.r114.549295

Holmes, C., El-Okl, M., Williams, A., Cunningham, C., Wilcockson, D., and Perry, V. (2003). Systemic infection, interleukin 1β and cognitive decline in Alzheimer's disease. *J. Neurol. Neurosurg. Psychiatry* 74, 788–789. doi: 10.1136/jnnp.74.6.788

Hommet, C., Mondon, K., Camus, V., Ribeiro, M. J., Beaufils, E., Arlicot, N., et al. (2014). Neuroinflammation and β amyloid deposition in Alzheimer's disease: *in vivo* quantification with molecular imaging. *Dement. Geriatr. Cogn. Disord.* 37, 1–18. doi: 10.1159/000354363

Iadecola, C. (2010). The overlap between neurodegenerative and vascular factors in the pathogenesis of dementia. *Acta Neuropathol.* 120, 287–296. doi: 10.1007/s00401-010-0718-6

Isomaa, B., Almgren, P., Tuomi, T., Forsén, B., Lahti, K., Nissén, M., et al. (2001). Cardiovascular morbidity and mortality associated with the metabolic syndrome. *Diabetes Care* 4, 683–689. doi: 10.2337/diacare.24.4.683

Ivakhnitskaia, E., Lin, R. W., Hamada, K., and Chang, C. (2018). Timing of neuronal plasticity in development and aging. *Wiley Interdiscip. Rev. Dev. Biol.* 7:e305. doi: 10.1002/wdev.305

Iyo, M., Namba, H., Fukushi, K., Shinotoh, H., Nagatsuka, S., Suhara, T., et al. (1997). Measurement of acetylcholinesterase by positron emission tomography in the brains of healthy controls and patients with Alzheimer's disease. *Lancet* 9068, 1805–1809. doi: 10.1016/s0140-6736(96)09124-6

Jessell, T. M., and Kandel, E. R. (1993). Synaptic transmission: a bidirectional and self-modifiable form of cell-cell communication. *Cell* 72, 1–30. doi: 10.1016/s0092-8674(05)80025-x

Jurcovicova, J. (2014). Glucose transport in brain—effect of inflammation. *Endocr Regul.* 48, 35–48. doi: 10.4149/endo_2014_01_35

Kautzky-Willer, A., Harreiter, J., and Pacini, G. (2016). Sex and gender differences in risk, pathophysiology and complications of type 2 diabetes mellitus. *Endocr. Rev.* 37, 278–316. doi: 10.1210/er.2015-1137

Kerr, J. F., Wyllie, A. H., and Currie, A. R. (1972). Apoptosis: a basic biological phenomenon with wide-ranging implications in tissue kinetics. *Br. J. Cancer* 26, 239–257. doi: 10.1038/bjc.1972.33

Kesslak, J. P., Nalcioglu, O., and Cotman, C. W. (1991). Quantification of magnetic resonance scans for hippocampal and parahippocampal atrophy in Alzheimer's disease. *Neurology* 41, 51–54. doi: 10.1212/wnl.41.1.51

Klegeris, A., and McGeer, P. L. (2000). Interaction of various intracellular signaling mechanisms involved in mononuclear phagocyte toxicity toward neuronal cells. *J. Leukoc. Biol.* 67, 127–133. doi: 10.1002/jlb.67.1.127

Klunk, W. E., Engler, H., Nordberg, A., Wang, Y., Blomqvist, G., Holt, D. P., et al. (2004). Imaging brain amyloid in Alzheimer's disease with Pittsburgh Compound-B. *Ann. Neurol.* 3, 306–319. doi: 10.1002/ana.20009

Kniesel, U., and Wolburg, H. (2000). Tight junctions of the blood-brain barrier. *Cell. Mol. Neurobiol.* 20, 57–76. doi: 10.1023/a:1006995910836

Ladner, C. J., and Lee, J. M. (1998). Pharmacological drug treatment of Alzheimer disease: the cholinergi hypothesis revisited. *J. Neuropathol. Exp. Neurol.* 57, 719–731. doi: 10.1097/00005072-199808000-00001

Lim, C., Hammond, C. J., Hingley, S. T., and Balin, B. J. (2014). Chlamydia pneumoniae infection of monocytes *in vitro* stimulates innate and adaptive immune responses relevant to those in Alzheimer's disease. *J. Neuroinflammation* 11:217. doi: 10.1186/s12974-014-0217-0

Magalhaes, T. N. C., Weiler, M., Teixeira, C. V. L., Hayata, T., Moraes, A. S., Boldrini, V. O., et al. (2018). Systemic inflammation and multimodal biomarkers in amnestic mild cognitive impairment and Alzheimer's disease. *Mol. Neurobiol.* 7, 5689–5697. doi: 10.1007/s12035-017-0795-9

Martinvalet, D., Zhu, P., and Lieberman, J. (2005). Granzyme A induces caspase-independent mitochondrial damage, a required first step for apoptosis. *Immunity* 22, 355–370. doi: 10.1016/j.immuni.2005.02.004

Mato, J., Alvarez, L., Ortiz, P., and Pajares, M. A. (1997). S-adenosylmethionine synthesis: molecular mechanisms and clinical implications. *Pharmacol. Ther.* 73, 265–280. doi: 10.1016/s0163-7258(96)00197-0

Meeusen, R. (2014). Exercise, nutrition and the brain. *Sports Med.* 44, S47–S56. doi: 10.1007/s40279-014-0150-5

Mendrick, D. L., Diehl, A. M., Topor, L. S., Dietert, R. R., Will, Y., La Merrill, M. A., et al. (2018). Metabolic syndrome and associated diseases: from the bench to the clinic. *Toxicol. Sci.* 162, 36–42. doi: 10.1093/toxsci/kfx233

Mergenthaler, P., Lindauer, U., Dienel, G. A., and Meisel, A. (2013). Sugar for the brain: the role of glucose in physiological and pathological brain function. *Trends Neurosci.* 36, 587–597. doi: 10.1016/j.tins.2013.07.001

Minagar, A., and Alexander, J. S. (2003). Blood-brain barrier disruption in multiple sclerosis. *Mult. Scler.* 9, 540–549. doi: 10.1191/1352458503ms965oa

Moncada, S., and Vane, J. (1979). Arachidonic acid metabolites and the interactions between platelets and blood-vessel walls. *N. Engl. J. Med.* 300, 1142–1147. doi: 10.1056/nejm197905173002006

Morris, A. A. M. (2005). Cerebral ketone body metabolism. *J. Inherit. Metab. Dis.* 28, 109–121. doi: 10.1007/s10545-005-5518-0

Mosconi, L., Tsui, W. H., Herholz, K., Pupi, A., Drzezga, A., Lucignani, G., et al. (2008). Multicenter standardized 18F-FDG PET diagnosis of mild cognitive impairment, Alzheimer's disease, and other dementias. *J. Nucl. Med.* 49, 390–398. doi: 10.2967/jnumed.107.045385

Neuhaus, W., Freidl, M., Szkokan, P., Berger, M., Wirth, M., Winkler, J., et al. (2011). Effects of NMDA receptor modulators on a blood-brain barrier *in vitro* model. *Brain Res.* 1394, 49–61. doi: 10.1016/j.brainres.2011.04.003

Neuhaus, W., Mandikova, J., Pawlowitsch, R., Linz, B., Bennani-Baiti, B., Lauer, R., et al. (2012). Blood-brain barrier *in vitro* models as tools in drug discovery: assessment of the transport ranking of antihistaminic drugs. *Pharmazie* 67, 432–439. doi: 10.1002/jps.21371

Neuhaus, W., Plattner, V. E., Wirth, M., Germann, B., Lachmann, B., Gabor, F., et al. (2008). Validation of *in vitro* cell culture models of the blood-brain barrier: tightness characterization of two promising cell lines. *J. Pharm. Sci.* 12, 5158–5175. doi: 10.1002/jps.21371

Neuhaus, W., Stessl, M., Strizsik, E., Bennani-Baiti, B., Wirth, M., Toegel, S., et al. (2010). Blood-brain barrier cell line PBMEC/C1–2 possesses functionally active P-glycoprotein. *Neurosci. Lett.* 2, 224–228. doi: 10.1016/j.neulet.2009.11.079

Noe, C. R. (2009). *In vitro* blood brain barrier (BBB) models and their application in drug research. *Eur. J. Pharm. Sci.* 38:S7.

Noe-Letschnig, M. (2019). Rezidivierende vulvovaginalcandidose. *Gyn. Aktiv.* 48:9.

Novakova, I., Subileau, E. A., Toegel, S., Gruber, D., Lachmann, B., Urban, E., et al. (2014). Transport rankings of non-steroidal antiinflammatory drugs across blood-brain barrier *in vitro* models. *PLoS One* 9:e86806. doi: 10.1371/journal.pone.0086806

O'Brien, J. T., and Thomas, A. (2015). Vascular dementia. *Lancet* 386, 1698–1706. doi: 10.1016/S0140-6736(15)00463-8

Okouchi, M., Ekshyyan, O., Maracine, M., and Aw, T. Y. (2007). Neuronal apoptosis in neurodegeneration. *Antioxid. Redox Signal.* 9, 1059–1096. doi: 10.1089/ars.2007.1511

Petanceska, S. S., Nagy, V., Frail, D., and Gandy, S. (2000). Ovariectomy and 17β-estradiol modulate the levels of Alzheimer's amyloid β peptides in brain. *Exp. Gerontol.* 35, 1317–1325. doi: 10.1016/s0531-5565(00)00157-1

Peters, A. (2011). The selfish brain: competition for energy resources. *Am. J. Hum. Biol.* 23, 29–34. doi: 10.1002/ajhb.21106

Pifferi, F., Roux, F., Langelier, B., Alessandri, J. M., Vancassel, S., Jouin, M., et al. (2005). (n-3) polyunsaturated fatty acid deficiency reduces the expression of both isoforms of the brain glucose transporter GLUT1 in rats. *J. Nutr.* 135, 2241–2246. doi: 10.1093/jn/135.9.2241

Pilon, M. (2016). Revisiting the membrane-centric view of diabetes. *Lipids Health Dis.* 15:167. doi: 10.1186/s12944-016-0342-0

Poetsch, V., Bennani-Baiti, B., Neuhaus, W., Muchitsch, E. M., and Noe, C. R. (2010a). Serum-derived immunoglobulins alter amyloid β transport across a blood-brain barrier *in vitro* model. *Pharmazie* 65, 267–273. doi: 10.1691/ph.2010.9319

Poetsch, V., Neuhaus, W., and Noe, C. R. (2010b). Serum-derived immunoglobulins neutralize adverse effects of amyloid-β peptide on the integrity of a blood-brain barrier *in vitro* model. *J. Alzheimers Dis.* 21, 303–314. doi: 10.3233/jad-2010-090769

Poksay, K. S., Sheffler, D. J., Spilman, P., Campagna, J., Jagodzinska, B., Descamps, O., et al. (2017). Screening for small molecule inhibitors of statin-induced APP C-terminal toxic fragment production. *Front. Pharmacol.* 8:46. doi: 10.3389/fphar.2017.00046

Power, J. D., and Schlaggar, B. L. (2017). Neural plasticity across the lifespan. *Wiley Interdiscip. Rev. Dev. Biol.* 6:e216. doi: 10.1002/wdev.216

Rabinovici, G. D., Rosen, H. J., Alkalay, A., Kornak, J., Furst, A. J., Agarwal, N., et al. (2011). Amyloid vs FDG-PET in the differential diagnosis of AD and FTLD. *Neurology* 23, 2034–2042. doi: 10.1212/wnl.0b013e31823b9c5e

Rai, D., Zitko, P., Jones, K., Lynch, J., and Araya, R. (2013). Country- and individual-level socioeconomic determinants of depression: multilevel cross-national comparison. *Br. J. Psychiatry* 202, 195–203. doi: 10.1192/bjp.bp.112.112482

Ramirez, J. A. (1996). Isolation of Chlamydia pneumoniae from the coronary artery of a patient with coronary atherosclerosis. *Ann. Intern. Med.* 125, 979–982. doi: 10.7326/0003-4819-125-12-199612150-00008

Ravichandran, K. S. (2011). Beginnings of a good apoptotic meal: the find-me and eat-me signaling pathways. *Immunity* 35, 445–455. doi: 10.1016/j.immuni.2011.09.004

Reinmuth, O., Scheinberg, P., and Bourne, B. (1965). Total cerebral blood flow and metabolism: a new method for the repeated serial measurement of total cerbral blood flow using iodoantipyrine (1131) with a report of determination in normal human beings of blood flow, oxygen consumption, glucose utilization and respiratory quotient of the whole brain. *Arch. Neurol.* 12, 49–66. doi: 10.1001/archneur.1965.00460250053007

Rogers, J., Cooper, N. R., Webster, S., Schultz, J., McGeer, P. L., Styren, S. D., et al. (1992). Complement activation by β-amyloid in Alzheimer disease. *Proc. Natl. Acad. Sci. U S A* 21, 10016–100120. doi: 10.1073/pnas.89.21.10016

Rogers, S. L., Doody, R. S., Pratt, R. D., and Ieni, J. R. (2000). Long-term efficacy and safety of donepezil in the treatment of Alzheimer's disease: final analysis of a US multicentre open-label study. *Eur. Neuropsychopharmacol.* 10, 195–203. doi: 10.1016/s0924-977x(00)00067-5

Rosario, E. R., Chang, L., Head, E. H., Stanczyk, F. Z., and Pike, C. J. (2011). Brain levels of sex steroid hormones in men and women during normal aging and in Alzheimer's disease. *Neurobiol. Aging* 32, 604–613. doi: 10.1016/j.neurobiolaging.2009.04.008

Rosinger, Z. J., De Guzman, R. M., Jacobskind, J. S., Saglimbeni, B., Malone, M., Fico, D., et al. (2020). Sex-dependent effects of chronic variable stress on discrete corticotropin-releasing factor receptor 1 cell populations. *Physiol. Behav.* 219:112847. doi: 10.1016/j.physbeh.2020.112847

Roth, G. A., Johnson, C., Abajobir, A., Abd-Allah, F., Abera, S. F., Abyu, G., et al. (2017). Global, regional, and national burden of cardiovascular diseases for 10 causes, 1990 to 2015. *J. Am. Coll. Cardiol.* 70, 1–25. doi: 10.1016/j.jacc.2017.04.052

Saidijam, M., Karimi Dermani, F., Sohrabi, S., and Patching, S. G. (2018). Efflux proteins at the blood-brain barrier: review and bioinformatics analysis. *Xenobiotica* 48, 506–532. doi: 10.1080/00498254.2017.1328148

Salloway, S., Mintzer, J., Weiner, M. F., and Cummings, J. L. (2008). Disease-modifying therapies in Alzheimer's disease. *Alzheimers Dement.* 4, 65–79. doi: 10.1016/j.jalz.2007.10.001

Santello, M., Toni, N., and Volterra, A. (2019). Astrocyte function from information processing to cognition and cognitive impairment. *Nat. Neurosci.* 22, 154–166. doi: 10.1038/s41593-018-0325-8

Selvaraj, V., Jiang, P., Chechneva, O., Lo, U. G., and Deng, W. (2012). Differentiating human stem cells into neurons and glial cells for neural repair. *Front. Biosci.* 17, 65–89. doi: 10.2741/3916

Shah, K., Desilva, S., and Abbruscato, T. (2012). The role of glucose transporters in brain disease: diabetes and Alzheimer's disease. *Int. J. Mol. Sci.* 13, 12629–12655. doi: 10.3390/ijms131012629

Sigurdsson, E. M., Scholtzova, H., Mehta, P. D., Frangione, B., and Wisniewski, T. (2001). Immunization with a nontoxic/nonfibrillar amyloid-β homologous peptide reduces Alzheimer's disease-associated pathology in transgenic mice. *Am. J. Pathol.* 159, 439–447. doi: 10.1016/s0002-9440(10)61715-4

Simić, G., Kostovic, I., Winblad, B., and Bogdanović, N. (1997). Volume and number of neurons of the human hippocampal formation in normal aging and Alzheimer's disease. *J. Comp. Neurol.* 379, 482–494. doi: 10.1002/(sici)1096-9861(19970324)379:4<482::aid-cne2>3.0.co;2-z

Smith, A. J., and Verkman, A. S. (2018). The "glymphatic" mechanism for solute clearance in Alzheimer's disease: game changer or unproven speculation? *FASEB J.* 32, 543–551. doi: 10.1096/fj.201700999

Solomon, B., and Frenkel, D. (2010). Immunotherapy for Alzheimer's disease. *Neuropharmacology* 59, 303–309. doi: 10.1016/j.neuropharm.2010.04.004

Stancu, I. C., Cremers, N., Vanrusselt, H., Couturier, J., Vanoosthuyse, A., Kessels, S., et al. (2019). Aggregated Tau activates NLRP3-ASC inflammasome exacerbating exogenously seeded and non-exogenously seeded Tau pathology *in vivo*. *Acta Neuropathol.* 137, 599–617. doi: 10.1007/s00401-018-01957-y

Stromberg, U., Svensson, T. H., and Waldeck, B. (1970). On the mode of action of amantadine. *J. Pharm. Pharmacol.* 22, 959–962. doi: 10.1111/j.2042-7158.1970.tb08487.x

Supekar, K., Menon, V., Rubin, D., Musen, M., and Greicius, M. D. (2008). Network analysis of intrinsic functional brain connectivity in Alzheimer's disease. *PLoS Comput. Biol.* 4:e1000100. doi: 10.1371/journal.pcbi.1000100

Swardfager, W., Lanctôt, K., Rothenburg, L., Wong, A., Cappell, J., and Herrmann, N. (2010). A meta-analysis of cytokines in Alzheimer's disease. *Biol. Psychiatry* 68, 930–941. doi: 10.1016/j.biopsych.2010.06.012

Szablewski, L. (2017). Glucose transporters in brain: in health and in Alzheimer's disease. *J. Alzheimers Dis.* 55, 1307–1320. doi: 10.3233/jad-160841

Teipel, S., Kilimann, I., Thyrian, J. R., Kloppel, S., and Hoffmann, W. (2018). Potential role of neuroimaging markers for early diagnosis of dementia in primary care. *Curr. Alzheimer Res.* 15, 18–27. doi: 10.2174/1567205014666170908093846

Thorens, B., and Mueckler, M. (2010). Glucose transporters in the 21st Century. *Am. J. Physiol. Endocrinol. Metab.* 298, E141–E145. doi: 10.1152/ajpendo.00712.2009

Togo, T., Akiyama, H., Iseki, E., Kondo, H., Ikeda, K., Kato, M., et al. (2002). Occurrence of T cells in the brain of Alzheimer's disease and other neurological diseases. *J. Neuroimmunol.* 124, 83–92. doi: 10.1016/s0165-5728(01)00496-9

Tzeng, N. S., Chung, C. H., Lin, F. H., Chiang, C. P., Yeh, C. B., Huang, S. Y., et al. (2018). Anti-herpetic medications and reduced risk of dementia in patients with herpes simplex virus infections-a nationwide, population-based cohort study in taiwan. *Neurotherapeutics* 15, 417–429. doi: 10.1007/s13311-018-0611-x

van Hall, G., Strømstad, M., Rasmussen, P., Jans, Ø., Zaar, M., Gam, C., et al. (2009). Blood lactate is an important energy source for the human brain. *J. Cereb. Blood Flow Metab.* 29, 1121–1129. doi: 10.1038/jcbfm.2009.35

Vassar, R., Bennett, B. D., Babu-Khan, S., Kahn, S., Mendiaz, E. A., Denis, P., et al. (1999). β-Secretase cleavage of Alzheimer's amyloid precursor protein by the transmembrane aspartic protease BACE. *Science* 5440, 735–741. doi: 10.1126/science.286.5440.735

Villemagne, V. L., Furumoto, S., Fodero-Tavoletti, M., Harada, R., Mulligan, R. S., Kudo, Y., et al. (2012). The challenges of tau imaging. *Future Neurol.* 4, 409–421. doi: 10.2217/fnl.12.34

Vos, S. J., Verhey, F., Frolich, L., Kornhuber, J., Wiltfang, J., Maier, W., et al. (2015). Prevalence and prognosis of Alzheimer's disease at the mild cognitive impairment stage. *Brain* 138, 1327–1338. doi: 10.1093/brain/awv029

Wang, R., and Reddy, P. H. (2017). Role of glutamate and NMDA receptors in Alzheimer's disease. *J. Alzheimers Dis.* 57, 1041–1048. doi: 10.3233/jad-160763

Wardzinski, E. K., Kistenmacher, A., Melchert, U. H., Jauch-Chara, K., and Oltmanns, K. M. (2018). Impaired brain energy gain upon a glucose load in obesity. *Metabolism* 85, 90–96. doi: 10.1016/j.metabol.2018.02.013

Webber, K. M., Casadesus, G., Perry, G., Atwood, C. S., Bowen, R., and Smith, M. A. (2005). Gender differences in alzheimer disease: the role of luteinizing hormone in disease pathogenesis. *Alzheimer Dis. Assoc. Disord.* 19, 95–99. doi: 10.1097/01.wad.0000165512.90864.3f

Weiss, N., Miller, F., Cazaubon, S., and Couraud, P. O. (2009). The blood-brain barrier in brain homeostasis and neurological diseases. *Biochim. Biophys. Acta* 1788, 842–857. doi: 10.1016/j.bbamem.2008.10.022

Wiltfang, J. (2015). Cerebrospinal fluid markers in early diagnosis of Alzheimer dementia. *Ther. Umsch.* 72, 271–278. doi: 10.1024/0040-5930/a000675

Winkler, E. A., Nishida, Y., Sagare, A. P., Rege, S. V., Bell, R. D., Perlmutter, D., et al. (2015). GLUT1 reductions exacerbate Alzheimer's disease vasculo-neuronal dysfunction and degeneration. *Nat. Neurosci.* 18, 521–530. doi: 10.1038/nn.3966

Wolburg, H., and Lippoldt, A. (2002). Tight junctions of the blood-brain barrier: development, composition and regulation. *Vascul. Pharmacol.* 38, 323–337. doi: 10.1016/s1537-1891(02)00200-8

World Health Organization. (2018). *The Top 10 Causes of Death. 24.05.2018. Report No*. Geneva: World Health Organization.

Yamazaki, Y., and Kanekiyo, T. (2017). Blood-brain barrier dysfunction and the pathogenesis of Alzheimer's disease. *Int. J. Mol. Sci.* 18:1965. doi: 10.3390/ijms18091965

Yeagle, P. L. (1985). Cholesterol and the cell membrane. *Biochim. Biophys. Acta* 822, 267–287. doi: 10.1016/0304-4157(85)90011-5

Younkin, S. G. (1998). The role of A β 42 in Alzheimer's disease. *J. Physiol.* 92, 289–292. doi: 10.1016/s0928-4257(98)80035-1

Zhang, Y. W., Thompson, R., Zhang, H., and Xu, H. (2011). APP processing in Alzheimer's disease. *Mol. Brain* 4:3. doi: 10.1186/1756-6606-4-3

Conflict of Interest: RL received conference speaker honoraria within the last 3 years from Bruker BioSpin MR, Heel, and support from Siemens Healthcare regarding clinical research using PET/MR. CRN, MN-L, and RL are shareholders of the start-up company BM Health GmbH since Feb. 2019. MN-L was employed by the company ProFem GmbH.

The remaining authors declare that the research was conducted in the absence of any commercial or financial relationships that could be construed as a potential conflict of interest.

frontiers in Aging Neuroscience

ORIGINAL RESEARCH
published: 12 November 2020
doi: 10.3389/fnagi.2020.498978

The Neural Correlates of Visual and Auditory Cross-Modal Selective Attention in Aging

Franziska Rienäcker[1], Pascal W. M. Van Gerven[2], Heidi I. L. Jacobs[3,4], Judith Eck[5], Caroline M. Van Heugten[1,3] and Maria J. S. Guerreiro[6]*

[1] Department of Neuropsychology and Psychopharmacology, Faculty of Psychology and Neuroscience, Maastricht University, Maastricht, Netherlands, [2] Department of Educational Development and Research, Faculty of Health, Medicine and Life Sciences, School of Health Professions Education (SHE), Maastricht University, Maastricht, Netherlands, [3] Department of Psychiatry and Neuropsychology, Faculty of Health, Medicine and Life Sciences, School of Mental Health and Neuroscience, Maastricht University, Maastricht, Netherlands, [4] Division of Nuclear Medicine and Molecular Imaging, Department of Radiology, Massachusetts General Hospital/Harvard Medical School, Boston, MA, United States, [5] Department of Cognitive Neuroscience, Faculty of Psychology and Neuroscience, Maastricht University, Maastricht, Netherlands, [6] Biological Psychology and Neuropsychology, Institute for Psychology, University of Hamburg, Hamburg, Germany

OPEN ACCESS

Edited by:
Hans J. Grabe, University of Greifswald, Germany

Reviewed by:
Stephanie Rosemann, University of Oldenburg, Germany
Noam Alperin, University of Miami Health System, United States

***Correspondence:**
Franziska Rienäcker
franziska.rienacker@maastrichtuniversity.nl

Received: *18 September 2019*
Accepted: *27 October 2020*
Published: *12 November 2020*

Citation:
Rienäcker F, Van Gerven PWM, Jacobs HIL, Eck J, Van Heugten CM and Guerreiro MJS (2020) The Neural Correlates of Visual and Auditory Cross-Modal Selective Attention in Aging. Front. Aging Neurosci. 12:498978. doi: 10.3389/fnagi.2020.498978

Age-related deficits in selective attention have been demonstrated to depend on the sensory modality through which targets and distractors are presented. Some of these investigations suggest a specific impairment of cross-modal auditory selective attention. For the first time, this study is taking on a whole brain approach while including a passive perception baseline, to investigate the neural underpinnings of selective attention across age groups, and taking the sensory modality of relevant and irrelevant (i.e., distracting) stimuli into account. Sixteen younger (mean age = 23.3 years) and 14 older (mean age = 65.3 years), healthy participants performed a series of delayed match-to-sample tasks, in which participants had to selectively attend to visual stimuli, selectively attend to auditory stimuli, or passively view and hear both types of stimuli, while undergoing 3T fMRI. The imaging analyses showed that areas recruited by cross-modal visual and auditory selective attention in both age groups included parts of the dorsal attention and frontoparietal control networks (i.e., intraparietal sulcus, insula, fusiform gyrus, anterior cingulate, and inferior frontal cortex). Most importantly, activation throughout the brain did not differ across age groups, suggesting intact brain function during cross-modal selective attention in older adults. Moreover, stronger brain activation during cross-modal visual vs. cross-modal auditory selective attention was found in both age groups, which is consistent with earlier accounts of visual dominance. In conclusion, these results do not support the hypothesized age-related deficit of cross-modal auditory selective attention. Instead, they suggest that the underlying neural correlates of cross-modal selective attention are similar in younger and older adults.

Keywords: selective attention, sensory modality, aging, whole-brain fMRI, top-down modulation

INTRODUCTION

Selective attention enables a person to attend to relevant stimuli in the environment while ignoring irrelevant stimuli. The strong need for this ability becomes apparent by considering the limited human processing capacity (Miller, 1956). Because an individual can only attend to a limited portion of the environment, incoming stimuli need to be filtered. In contrast to bottom-up attentional modulation, which happens when an individual's attentional focus is passively drawn toward environmental, incoming stimuli, selective attention requires active selection, that is, facilitation of relevant and suppression of irrelevant stimuli, which is referred to as "top-down" attentional modulation. This modulation takes place at two levels: (1) relevant stimuli are enhanced over other stimuli to facilitate processing of those stimuli and (2) processing of irrelevant stimuli is inhibited to avoid distraction. Research into healthy cognitive aging has primarily focused on the latter mechanism: inhibition. A variety of common cognitive challenges in old age, such as memory decline, are thought to be the result of deficits in the inhibition of task-irrelevant information. This so-called inhibitory deficit hypothesis was originally proposed by Hasher and Zacks (1988). Since then, many studies have offered support for the notion that older individuals are less effective at inhibiting irrelevant information than their younger counterparts (e.g., Zacks and Hasher, 1994; Lustig et al., 2001).

Notably, the majority of studies investigating selective attention in aging employed visual tasks with visual distraction, whereas only a small number of studies involved auditory targets and distractors. Only a few studies employed cross-modal selective attention paradigms (for a review, see: Guerreiro et al., 2010; Van Gerven and Guerreiro, 2016), for instance visual or auditory tasks with distraction from the other modality. This is remarkable, as in most everyday situations relevant and irrelevant stimuli are conveyed through multiple modalities. At least three studies investigated performance of younger and older participants on a working memory task that involved all possible combinations of visual and auditory attention and distraction (Guerreiro and Van Gerven, 2011; Guerreiro et al., 2013; Rienäcker et al., 2018). In all of these studies, older adults were specifically impaired in conditions of auditory selective attention with visual distraction. This suggests that the inhibitory deficit hypothesis applies to cross-modal auditory selective attention.

The neural correlates of this specific age-related deficit have however remained unclear. In the unimodal visual domain, Gazzaley and colleagues have shown age-related impairments in the neural suppression of irrelevant stimuli in visual category-selective cortical areas. On the other hand, enhancement of relevant information has been found to be intact in healthy older, as compared to younger participants (Gazzaley et al., 2005b). Looking beyond sensory brain areas, Geerligs et al. (2014) demonstrated an involvement of the dorsal attention network (DAN) and the frontoparietal control network (FPCN)—including the dorsolateral prefrontal cortex (DLPFC), parts of the parietal cortex, the rostrolateral prefrontal cortex (RLPFC), and the cerebellum—in age-related selective attention. Compared to younger participants, older participants demonstrated increased activation of these areas during unimodal visual attention—as well as increased connectivity to somatosensory regions—during the detection of relevant target stimuli.

In the domain of cross-modal selective attention, functional magnetic resonance imaging (fMRI) and electroencephalogram (EEG) studies comparing top-down modulation across age groups, have revealed brain responses that appear to be unaffected by normal aging (e.g., Mishra and Gazzaley, 2013; Guerreiro et al., 2014). Mishra and Gazzaley (2013) demonstrated age-equivalent early event-related potentials (ERPs)—such as the P1 and N1—in visual and auditory cortices during cross-modal selective attention. Guerreiro et al. (2015) investigated top-down modulation during both uni- and cross-modal visual and auditory distraction in category-specific brain areas in a sample of healthy younger and older adults. The employed memory task, which involved relevant and irrelevant, visual, and auditory information (adapted from Gazzaley et al., 2005a), showed age-independent visual enhancement, as well as, and most importantly, age-independent suppression of visual cortical processing during auditory selective attention, relative to a perceptual baseline condition. These results are consistent with earlier accounts of age-equivalent enhancement and suppression of auditory and visual information in cross-modal paradigms (Mishra and Gazzaley, 2013; Guerreiro et al., 2014), but stand in stark contrast with earlier uni-modal selective attention studies that found clear age-differences in visual suppression (e.g., Gazzaley et al., 2005b).

Further evidence for age effects in cross-modal selective attention come from a small proportion of neuroimaging studies that have also looked beyond sensory-specific cortical areas. These studies indicate a different pattern, depending on modality. For example, Townsend et al. (2006) studied cortical modulation during cross-modal auditory and visual distraction in younger and older adults. Using a whole-brain analysis, they demonstrated similar brain areas to be involved in cross-modal auditory attention across age groups, which is in line with the aforementioned region of interest (ROI) results on cross-modal selective attention (e.g., Guerreiro et al., 2014). In older adults, however, more widespread areas of the inferior frontal gyrus, the left insula, and left fusiform gyrus were recruited during cross-modal visual attention. Different patterns across modalities have also been demonstrated in early ERP components. The P1 and N1 components are commonly modulated by attentional processes. Top-down neural modulation, reflected by these components, was found to be unaffected by aging in auditory distraction conditions (Čeponienė et al., 2008). Moreover, in older participants, P1 and N1 components were diminished in visual distraction conditions, as compared to younger participants. In sum, the results of these cross-modal paradigms looking beyond sensory and category specific cortical regions point toward an important role of sensory modality in age-related differences in selective attention.

In contrast to the aforementioned ROI studies, most whole-brain investigations did not use a passive perceptual baseline, that is, they did not base their estimations of neural modulation on a comparison between selective attention conditions and a passive viewing or listening baseline, but directly compared

brain activation across groups or conditions. This might be less favorable, as it does not allow for any interpretation regarding the direction of activation differences (i.e., enhancement or suppression relative to baseline).

In sum, there is little research into the neural underpinnings of cross-modal selective attention deficits in aging. Research that is available is methodologically diverse and results are contradictory. Neuroimaging investigations focusing on sensory-specific brain responses have demonstrated age-equivalent top-down modulation during cross-modal visual and auditory selective attention (Mishra and Gazzaley, 2013; Guerreiro et al., 2014, 2015). This may imply that the earlier observed sensory-specific performance deficits (e.g., Guerreiro et al., 2013) are the result of age-related differences in the modulation of other, higher-order, cortical regions. Studies undertaking a whole-brain approach indeed point toward possible age differences in cross-modal attentional modulation, depending on sensory modality, however, without employing a perceptual baseline. Therefore, the aim of the current study was to investigate cortical activity beyond sensory areas, in response to cross-modal visual and auditory selective attention, relative to a perceptual baseline, a combination of conditions that has never been investigated before. We aimed to examine whether this activity differs between age groups, and if these differences are modulated by sensory modality. Based on previous studies investigating cross-modal selective attention (Townsend et al., 2006; Čeponienė et al., 2008; Mishra and Gazzaley, 2013), we hypothesized that, similar to unimodal visual selective attention, frontoparietal areas are involved in cross-modal selective attention, that activity in these areas is more widespread in older individuals, and that this age-effect might depend on the sensory modality of the distraction.

GENERAL METHODS

Participants

Data of 16 younger (aged 20–29 years, $M = 23.3$, $SD = 3.0$, 9 women) and 14 older participants (aged 60–71 years, $M = 65.3$, $SD = 4.1$., 10 women) was employed for this study (Guerreiro et al., 2015). There was no significant association between age group and sex, $\chi^2(1) = 0.74$, $p = .389$, indicating that sex distribution did not differ between younger and older adults. All participants were right-handed, free of major physical or psychiatric illnesses, and reported having normal or corrected-to-normal vision and hearing. Older participants were cognitive healthy, as indicated by a score of 18 or higher on the Cognitive Screening Test (De Graaf and Deelman, 1991). In total, 17 younger and 21 older participants went through the testing procedure. Data of one younger and seven older participants were excluded because of excessive head movement (> 3.5 mm) during scanning, resulting in a final sample of 16 younger and 14 older participants. Recruitment was done through advertisements on local bulletin boards. This study was approved by the Ethics Review Committee Psychology and Neuroscience. Written informed consent was obtained from all participants before testing.

Task and Procedure

Younger and older participants were asked to perform a working memory-based selective attention task, developed by Gazzaley et al. (2005a) and adapted by Guerreiro et al. (2015), while undergoing fMRI (see **Figure 1**).

All task conditions involved a sequential presentation of stimuli from four categories: faces, scenes, voices, and music. Face stimuli (neutral portrait pictures of male and female adults) and scene stimuli were presented in black-and-white, at a resolution of 225 × 300 pixels, in the center of a computer screen. The screen was projected via a mirror to be visible from inside the MRI scanner. Voice stimuli included Portuguese trisyllabic words, recorded by male and female native speakers. In order to prevent semantic processing of the words, only participants without understanding of the Portuguese language were included. Music stimuli were recorded at a sampling rate of 44 kHz and presented with normalized amplitude with a duration of 800 ms.

All participants performed five tasks—two visual attention tasks, two auditory attention tasks, and a perceptual baseline task—in a counterbalanced order. The setup of the trials was identical for each of these conditions. During a cue period, two stimuli of each of four categories (faces, scenes, voices, and music) were sequentially presented in a pseudo-random order, whereby each was shown for 800 ms, followed by an inter-stimulus interval of 200 ms. After presentation of these eight stimuli, and following a 4000 ms delay period, a probe stimulus from the relevant category was displayed, to which a response had to be given during a 2000 ms response interval. Each condition—which was presented in separate experimental runs—consisted of 24 such trials. The conditions only differed in the instructions given. During the four selective attention conditions (remember faces, remember scenes, remember voices, and remember music), one stimulus category presented in the cue period had to be attended to, while the other three had to be ignored. During the presentation of the probe stimulus from this category, the participant was asked to indicate whether or not this stimulus had been shown in the cue period. Participants were instructed to respond as accurately as possible with a button press (yes/no). In the perceptual baseline condition, participants were asked to passively view and listen to the stimuli, without attempting to memorize any of them. Subsequently, an arrow pointing left or right was displayed instead of a probe stimulus. Participants were instructed to give a left/right response, based on the direction of this arrow.

Analysis of Behavioral Data

Behavioral data were analyzed using IBM SPSS Statistics version 22. Accuracy data (in %) of all conditions was submitted to a 2 (Age Group: younger, older) × 5 (Condition: passive baseline, remember scenes, remember faces, remember voices, remember music) repeated-measures analysis of variance (ANOVA). Age Group was the between- and Condition the within-groups factor. Results were considered significant at $p < 0.05$. A Greenhouse-Geisser correction was applied if the assumption of sphericity was violated. To correct for multiple comparisons, a Bonferroni correction was applied.

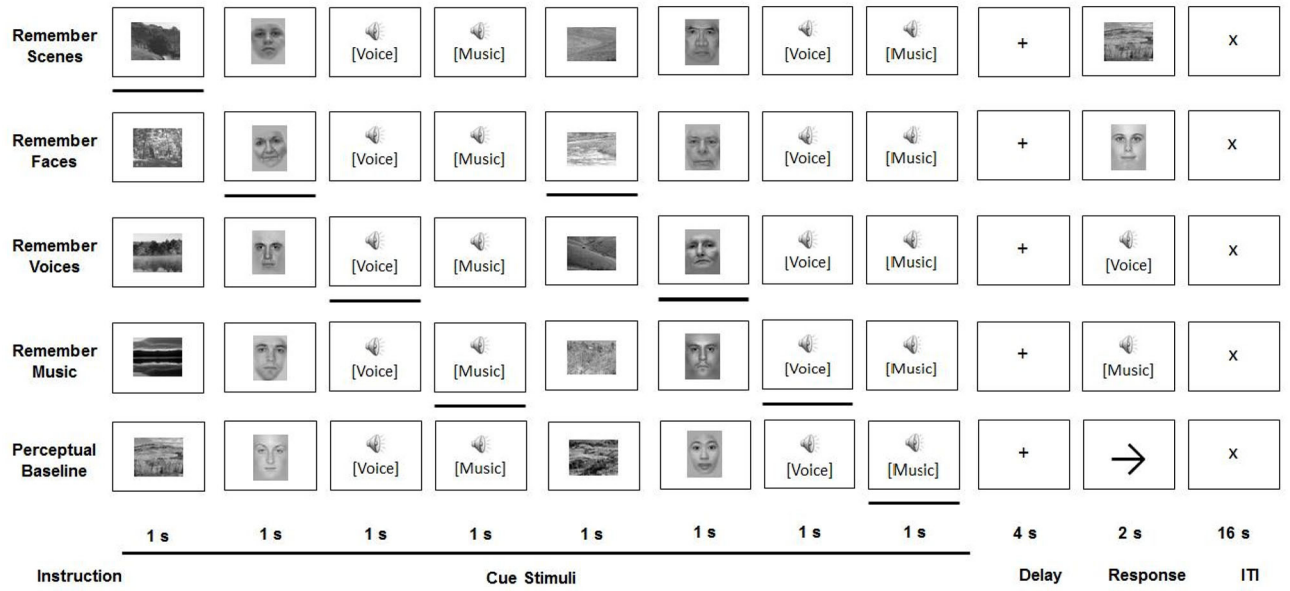

FIGURE 1 | Experimental paradigm.

MRI Acquisition

All participants underwent 3-T (f)MRI scanning in a Siemens Allegra head scanner (Siemens Allegra, Erlangen, Germany) at the Maastricht Brain Imaging Center (M-BIC), employing a quadrature birdcage coil.

T1-weighted anatomical images were recorded with an ADNI MPRAGE sequence, covering the whole brain (192 sagittal slices; matrix size = 256 × 256; voxel dimensions = 1 × 1 × 1 mm; repetition time [TR] = 2250 ms; echo time [TE] = 2.6 ms; flip angle [FA] = 9°). Anatomical images were recorded after two of the five selective attention task conditions, to allow participants to rest in between. T2* 2D-functional images were acquired with an EPI sequence (TR = 2000 ms; TE = 30 ms; FA = 90°; slice thickness = 3.5 mm; 32 axial slices; matrix size = 64 × 64; field of view = 224 × 224).

A significant concern in fMRI studies, especially those involving the presentation of auditory stimuli, is that the acoustic noise generated by standard EPI sequences may render participants unable to adequately perceive the auditory stimuli, rendering the interpretation of neural responses problematic (e.g., Peelle, 2014). Although the use of sparse imaging has been proposed to bypass this problem, we used a standard EPI sequence for two interrelated reasons: The present paradigm constituted a replication and extension of the paradigm originally developed by Gazzaley et al. (2005a), so not only did we want to keep it as close to the original as possible, but also modifying it for use with a sparse sequence would have led to a prohibitively long task duration, considering our five experimental conditions. To ensure, however, that participants were able to adequately perceive the auditory stimuli, we adjusted the intensity of the auditory stimuli prior to task performance to equalize the perceived loudness across participants. This was done by presenting a sample of voice and music stimuli while participants were in the scanner with earplugs and headphones and the EPI sequence was running, in order to replicate the background noise throughout the tasks. The intensity of the auditory stimuli was increased or decreased until a hearing level was reached that was both audible and comfortable for each participant.

fMRI Data Analysis

In contrast to the previously published work (Guerreiro et al., 2015), this investigation takes on a whole brain approach instead of a specific ROI approach. This enables the detection of activation (differences) in cross-modal selective attentional modulation in brain areas beyond the previously investigated sensory and category selective regions of interest. This is an important addition, as attention processes are known to involve especially prefrontal and parietal areas.

All acquired (f)MRI data were analyzed with BrainVoyager, version 20.6.2.3266 (BVQX 3.6.2) (Brain Innovation, Maastricht, the Netherlands). Pre-processing of functional data included head motion correction, temporal high-pass filtering, spatial smoothing (6 mm), and slice scan time correction using sinc interpolation. The first two functional volumes were discarded. Functional data were co-registered with the intra-session structural data set and transformed into Montreal Neurological Institute (MNI) space.

Functional data were analyzed with a single-subject general linear model (GLM) with separate predictors for the cue, delay, and response period for each of the experimental conditions and runs (e.g., passive baseline: cue, remember faces: delay, etc.). All regressors were convolved with a double gamma hemodynamic response function before entering them in the model. Confounding predictors included movement parameters

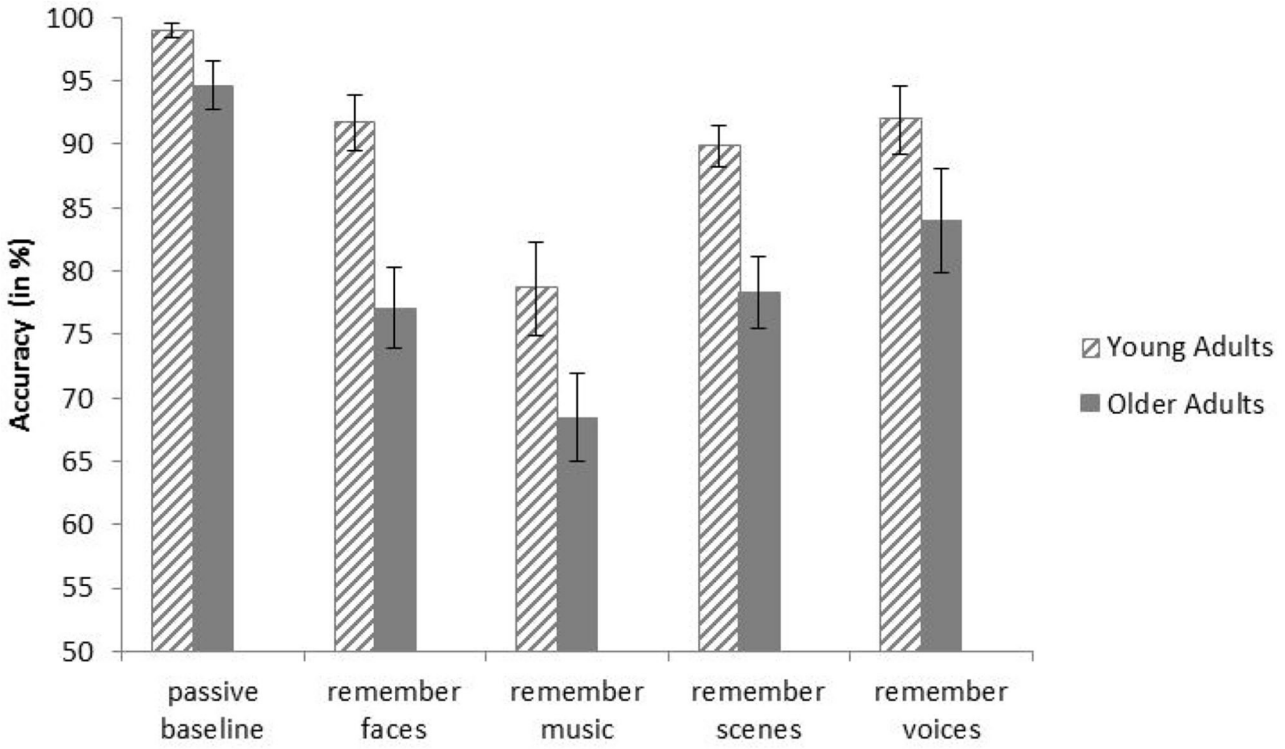

FIGURE 2 | Mean accuracies of younger and older adults in all conditions of the behavioral task. Error bars indicate one standard error of the mean.

of all directions, as well as predictors for trials with incorrect responses. For the subsequent group analyses, multi-subject random effects GLMs were computed with predictors of the cue period at a whole-brain level, involving contrasts for: cross-modal visual attention vs. passive baseline [remember faces (RF) + remember scenes (RS) > passive baseline (PB)], cross-modal auditory attention vs. passive baseline (remember music (RM) + remember voices (RV) > PB), and cross-modal visual attention vs. cross-modal auditory attention (RF + RS > RM + RV). All active conditions include cross-modal, as well as uni-modal attention and distraction. Taking together both visual, and both auditory categories (i.e., RF + RS and RM + RV), we expect that uni-modal enhancement and suppression is canceled out, to remain with an index of cross-modal attention only. All specified contrasts were balanced and compared between and across age groups. The obtained statistical maps were Bonferroni-corrected at $p < 0.05$ (two-sided). Peak activations were extracted from each cluster. The MNI coordinates of the cluster peaks were associated with anatomical and functional brain regions with guidance of the Yale BioImage Tal/MNI to Brodmann tool (based on Lacadie et al., 2008).

RESULTS

Behavioral Results

There was a significant main effect of Age Group on task accuracy (% correct responses), $F_{(1, 28)} = 18.18$, $p < 0.001$, $\eta_p^2 = 0.39$, indicating that the younger participants were significantly more accurate than the older participants ($M = 90.20\%$, $SD = 5.15$, and $M = 80.48\%$, $SD = 7.29$, respectively). Furthermore, there was a main effect of Condition, $F_{(3.01, 84.40)} = 21.80$, $p < 0.001$, $\eta_p^2 = 0.44$. Pairwise comparisons revealed that, across age groups, participants were significantly more accurate in the baseline condition than in all selective attention conditions ($ps < 0.001$). There was no significant interaction between Age Group and Condition, $F_{(3.01, 84.40)} = 1.16$, $p = .330$, $\eta_p^2 = 0.04$, indicating that the condition effect was independent of Age Group. Means and standard errors of both age groups and all conditions are displayed in **Figure 2**.

fMRI Results

Cross-Modal Visual Selective Attention

Across age groups, higher activation during visual attention conditions relative to the perceptual baseline was observed in the left supplementary motor area, the premotor cortex, lateral parietal cortex, parts of the inferior frontal gyrus, right insula, left fusiform gyrus, and the left occipital visual association cortex (VAC) (see **Figure 3**). For all cluster peaks, associated Brodmann areas (BAs), and MNI coordinates, see **Table 1**.

The contrast Young Adults [RF + RS > PB] > Older Adults [RF + RS > PB] revealed no differences between age groups, suggesting that top-down modulation in the setting of cross-modal visual selective attention was the same for younger and older adults. Single-subject data corroborated this notion in

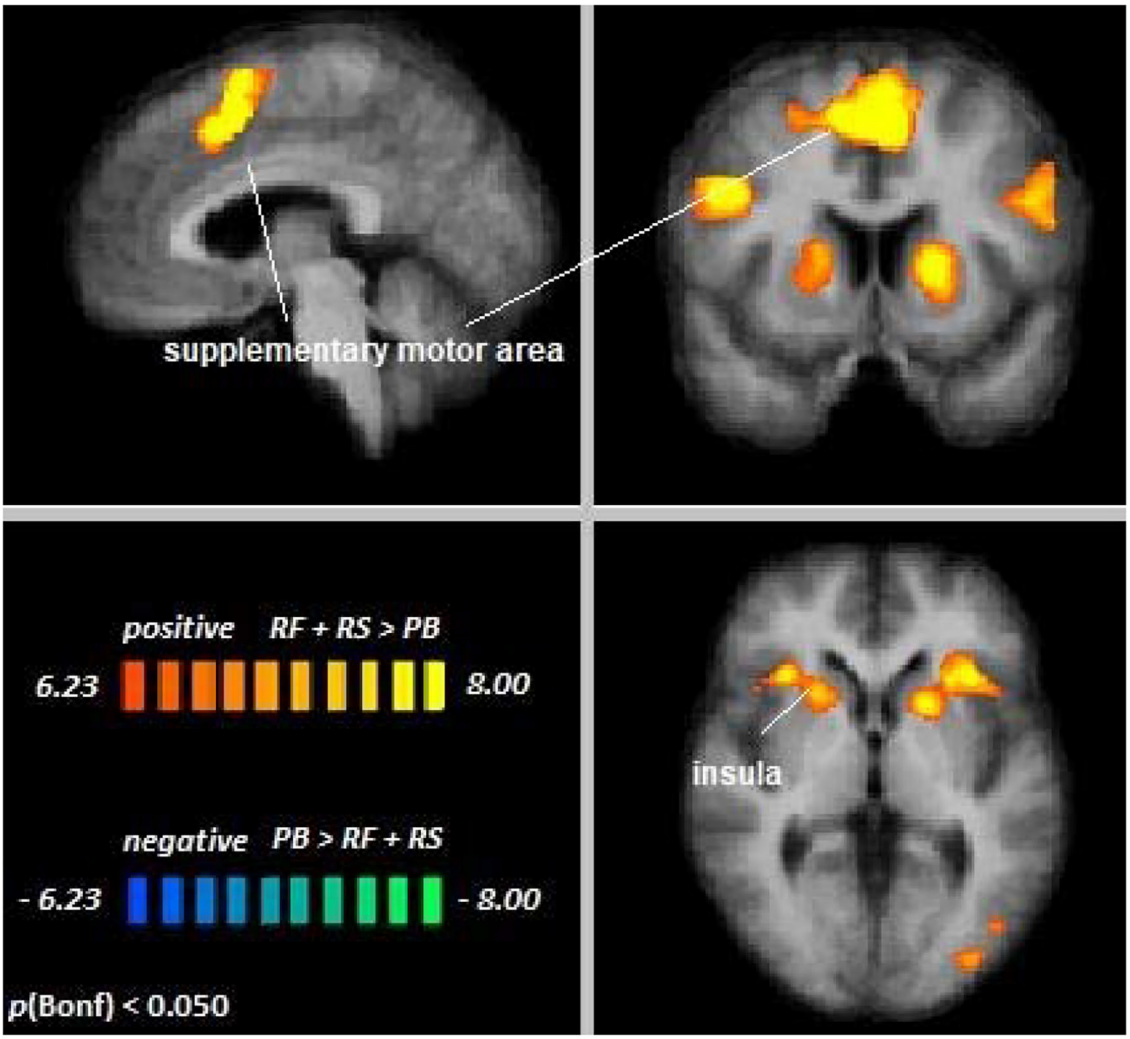

FIGURE 3 | Remember faces and remember scenes vs. passive baseline. An overview of significant clusters for the contrast RF + RS > PB. Sagittal, coronal, and axial planes are shown at $x = 3$, $y = 6$, $z = 2$. Active clusters indicate voxels with increased activation in visual selective attention conditions relative to baseline.

the regions showing significant attentional modulation during cross-modal visual attention (see **Supplementary Figure 1**).

Cross-Modal Auditory Selective Attention

Across age groups, higher activation during auditory attention conditions relative to the perceptual baseline was observed in the right supplementary motor area, left inferior frontal gyrus, left putamen, and right insula, whereas lower activation was observed in the anterior cingulate cortex (see **Figure 4**). For all cluster peaks, associated BAs, and MNI coordinates, see **Table 2**.

The contrast Young Adults [RM + RV > PB] > Older Adults [RM + RV > PB] revealed no differences between age groups, suggesting that top-down modulation in the setting of cross-modal auditory selective attention was the same for younger and older adults. Single-subject data confirmed this notion in the regions showing significant attentional modulation during cross-visual auditory attention (see **Supplementary Figure 2**).

Differences in Cross-Modal Selective Attention Across Modalities

Across age groups, higher activation during cross-modal visual selective attention relative to cross-modal auditory selective attention was observed in the right fusiform gyrus, the extrastriate cortex, premotor cortex, posterior cingulate cortex, and left thalamus (see **Figure 5**). For all cluster peaks, associated BAs, and MNI coordinates, see **Table 3**.

The contrast Young Adults [RF + RS > RM + RV] > Older Adults [RF + RS > RM + RV] revealed no differences between age groups, suggesting that differences in top-down modulation across modalities were the same for younger and older adults. Single-subject data corroborated this notion in the regions showing significant differences in attentional modulation across sensory modalities (see **Supplementary Figure 3**).

TABLE 1 | Cluster location and peaks across age groups (RF + RS > PB).

Location	Hemisphere	BA	MNI coordinates			Peak *t*	Size
			x	*y*	*z*		
Supplementary motor area	LH (medial)	6	0	11	49	12.39	26511
Intraparietal sulcus (IPS)	LH	7	−21	−67	52	12.34	20930
	RH	7	21	−61	58	11.25	9095
Inferior frontal gyrus	LH	45	−33	20	7	12.24	6237
Premotor cortex	LH (lateral)	6	−45	−1	37	11.75	5561
Insula	RH	13	33	23	4	9.90	3284
Angular gyrus	RH	39	33	−76	22	8.78	11330
Fusiform gyrus	LH	37	−51	−64	−8	8.54	3927
Occipital VAC	LH	19	−36	−85	−2	7.47	720

LH, left hemisphere; RH, right hemisphere; BA, Brodmann area; RF, remember faces; RS, remember scenes; PB, passive baseline; VAC, visual association cortex. ps < 0.0001, Bonferroni correction was applied. Clusters are displayed, sorted by t value, cluster sizes in number of 1 mm^3 voxels.

DISCUSSION

The aim of the current investigation was to identify cortical areas involved in visual and auditory cross-modal selective attention and understand how activation patterns in these areas differ with age or sensory modality. Findings from previous studies provided inconsistent results, possibly due to methodological differences. By incorporating a perceptual baseline condition, we have now been able to show recruitment of several brain regions known to be involved in attentional regulation, such as the frontoparietal, and fronto-subcortical areas of the frontoparietal control network, the dorsal attention network, and the salience network. A variety of brain regions, including visual specific, as well as visual unspecific areas, such as the posterior cingulate cortex, have moreover been found to be more heavily recruited under conditions of cross-modal visual, as compared to auditory selective attention in both age groups. Recruitment of brain resources during cross-modal selective attention did not differ across age groups, suggesting age-independent top-down modulation during cross-modal selective attention.

Independent of age, large areas of the left and right supplementary motor cortex, the inferior frontal cortex, and the insula have been demonstrated to show increased activation during visual and auditory attention relative to a perceptual baseline condition. Activation in the premotor and motor areas may reflect response planning in anticipation of the button press that was required by the tasks (cf. Nachev et al., 2008). In contrast to the perceptual baseline, participants may have prepared for a motor response already during the stimulus presentation. Moreover, during conditions of visual selective attention, activation of regions commonly related to visual processing, such as the occipital visual association cortex (VAC) and the bilateral intraparietal sulcus (IPS), was found to be enhanced relative to the perceptual baseline. Especially the insula and IPS have been established as important players in various, predominantly visual, attentional processes and as nodes in the FPCN and the salience network (Corbetta and Shulman, 2002). The current results suggest that this role extends to cross-modal visual and auditory selective attention. The anterior cingulate cortex was also observed to be affected by top-down modulation during auditory selective attention, demonstrating lower activation in the auditory selective attention conditions than in the perceptual baseline condition, possibly reflecting default mode network deactivation during the active task conditions. When directly comparing cross-modal visual and auditory selective attention, our results suggest that visual processing might require more brain resources than auditory processing. That is, no cortical area has been observed to be more involved in auditory than in visual selective attention, but visual selective attention seems to more heavily rely on a variety of brain areas, as indicated by positive activation clusters resulting from the visual > auditory comparison. These areas include the bilateral premotor cortex, the posterior cingulate cortex, and regions related to visual attentional processing (i.e., the right fusiform gyrus, occipital extrastriate areas, thalamus, and posterior cingulate cortex), representing important nodes of several neural networks related to bottom-up and top-down selective attention (Leech and Sharp, 2014). In light of these results, attention networks might be more heavily used in visual than in auditory selective attention. This finding is in accordance with the visual dominance hypothesis. That is, visual processing has repeatedly been found to be dominant over auditory (and tactile) processing, on a behavioral, as well as neurophysiological level (Posner et al., 1976; Colavita and Weisberg, 1979). In line with this, recent research has found healthy young participants to enhance top-down processing of visual selective attention in several brain regions in the presence of auditory distraction, whereas processing of relevant auditory stimuli was suppressed by irrelevant visual stimuli (Yan et al., 2015). The present results substantiate this account of visual dominance in the context of cross-modal selective attention and offer a possible neural underpinning of the previously observed behavioral findings (e.g., Posner et al., 1976).

Contrary to our expectations, top-down modulation during cross-modal visual and auditory selective attention did not differ between age groups. Instead, our results suggest that top-down modulation during cross-modal visual and auditory selective attention is intact in older adults. This is consistent with earlier ROI results (Guerreiro et al., 2015), which demonstrated that older adults effectively enhance cortical processing of relevant visual information and suppress cortical processing of irrelevant visual information in the setting of auditory selective attention in a visual category-selective brain area (the parahippocampal place area). These accounts of age-equivalent top-down processing stand in contrast with reports of increased recruitment of cortical resources in aging, possibly representing a compensatory mechanism (Geerligs et al., 2014; Grady et al., 2016). Čeponienė et al. (2008), as well as Townsend et al. (2006), found age-independent brain responses during attention to one modality, but age-related differences in brain responses during attention to the other, representing a modality specific asymmetry depending on whether relevant or irrelevant information is visual or

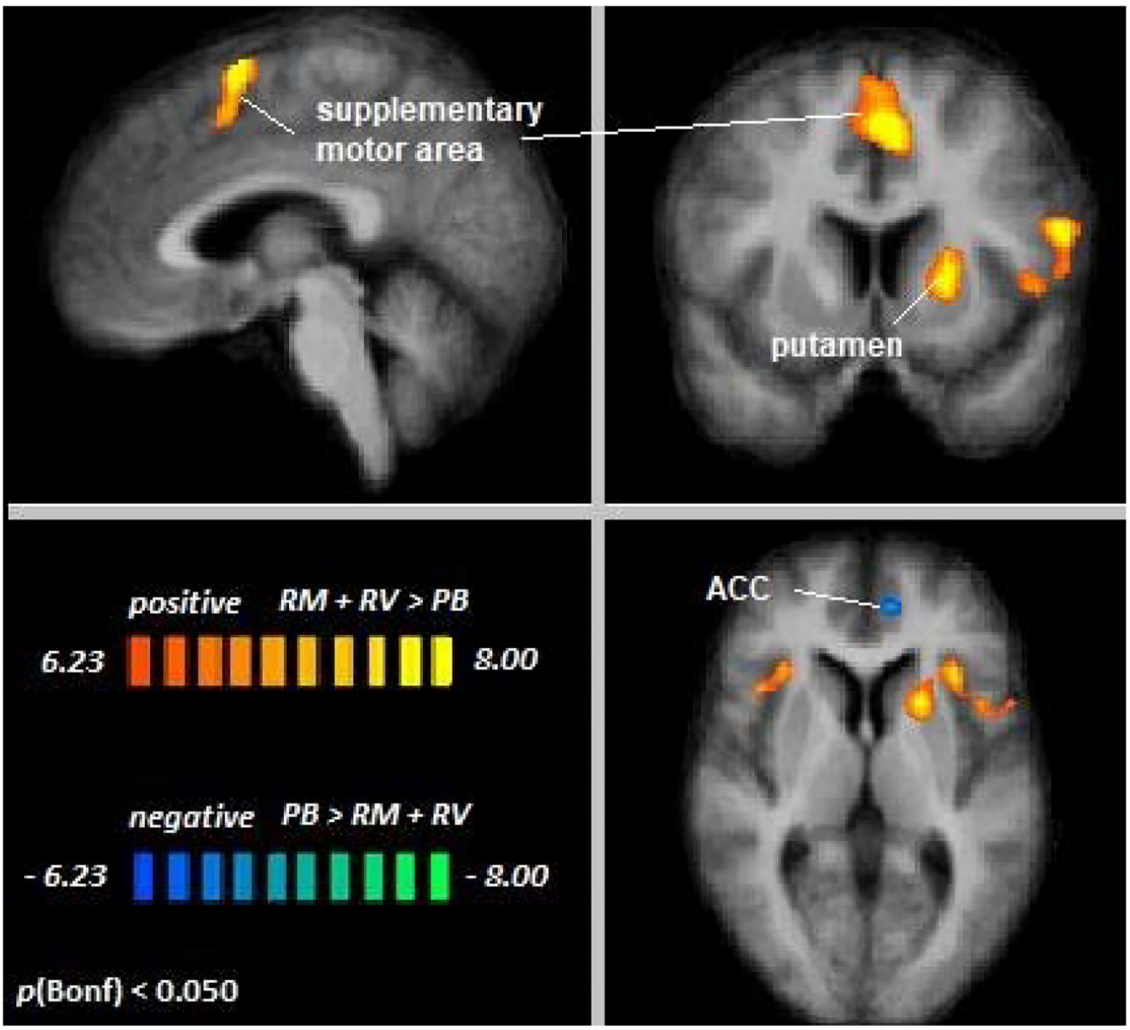

FIGURE 4 | Remember music and remember voices vs. passive baseline. An overview of significant clusters for the contrast RF + RS > PB. Sagittal, coronal, and axial planes are shown at $x = 3$, $y = 6$, $z = 2$. Orange to yellow clusters indicate voxels with greater activation in auditory selective attention conditions relative to baseline. Blue to green clusters reveal voxels with lower activation in auditory selective attention conditions relative to baseline.

TABLE 2 | Cluster location and peaks across age groups (RM + RV > PB).

			MNI coordinates				
Location	**Hemisphere**	**BA**	***x***	***y***	***z***	**Peak *t***	**Size**
Supplementary motor area	RH (medial)	6	3	8	61	10.42	6160
Inferior frontal gyrus	LH	44	−57	11	16	9.32	2027
Putamen	LH	49	−21	11	4	8.54	1432
Insula	RH	13	33	23	4	7.34	393
Anterior cingulate cortex	LH	32	−9	47	4	−7.30	401

LH, left hemisphere; RH, right hemisphere; BA, Brodmann area; RV, remember voices; RM, remember music; PB, passive baseline. ps < 0.0001, Bonferroni correction was applied. Clusters are displayed, sorted by t value, cluster sizes in number of 1 mm^3 voxels.

auditory. While, in line with this, the current results do support differential processing of visual and auditory cross-modal selective attention, previously reported age differences have not been replicated.

The observed lack of age differences in the present results may be explained by the following three notions. First, research focusing on unimodal visual selective attention suggests an important dissociation between enhancement and suppression in selective attention (Gazzaley et al., 2005a; Haring et al., 2013). Haring et al. (2013) demonstrated that younger and older participants did not differ in their overall modulation (as measured with EEG) between "ignore" and "attend" conditions. However, in comparison to younger participants, older individuals did not suppress activation below baseline in the "ignore" condition, but did enhance activation in the

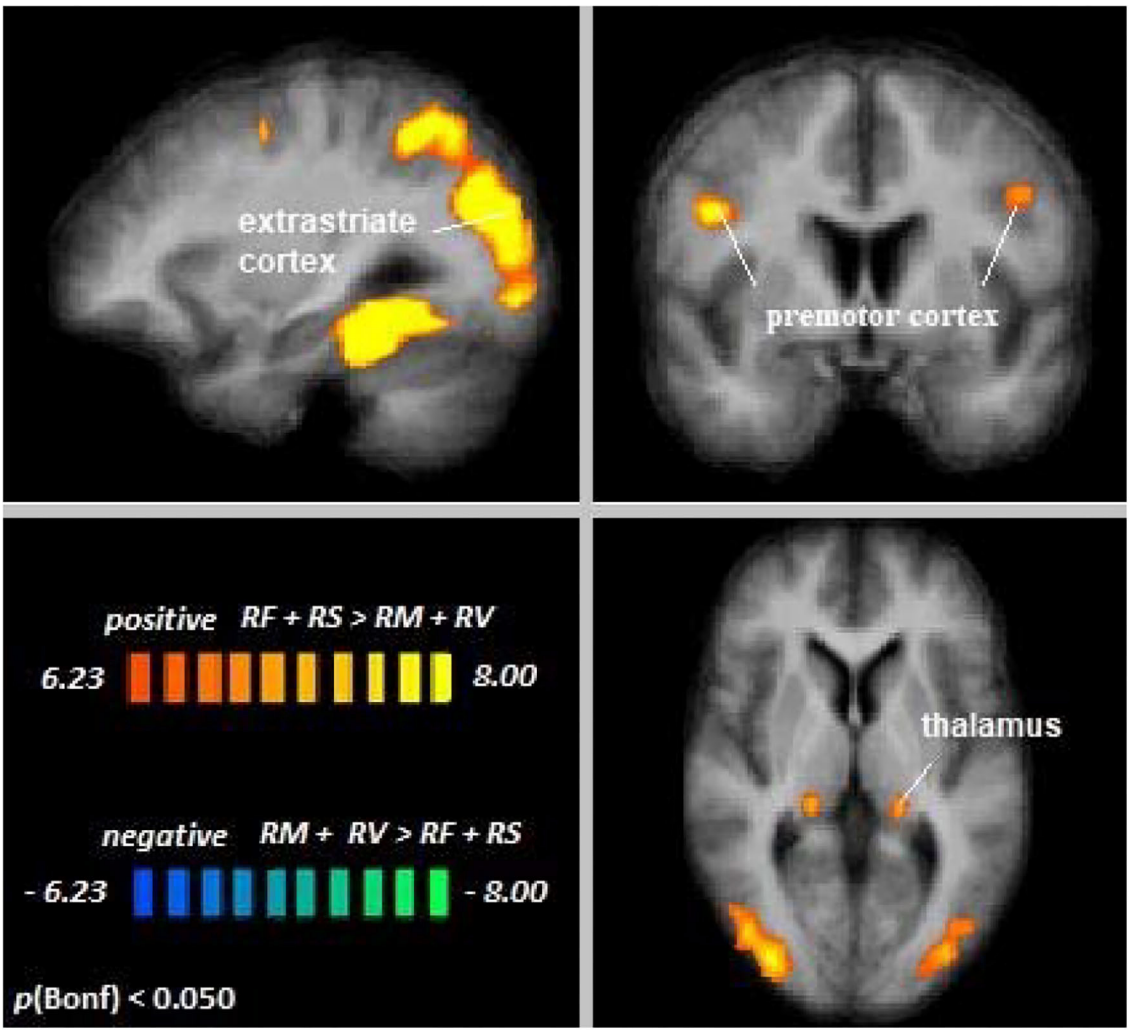

FIGURE 5 | Remember faces and remember scenes vs. remember music and remember voices. An overview of significant clusters for the contrast RF + RS > RM + RV. Sagittal, coronal, and axial planes are shown at $x = 3$, $y = 6$, $z = 2$. Active clusters show voxels with increased activation in visual relative to auditory selective attention conditions.

"attend" conditions. Similar patterns were observed by Gazzaley et al. (2005b). While it is still unclear whether these results also apply to cross-modal selective attention, the findings suggest a dissociation between enhancement and suppression in selective attention. The current study can only give a common index of cross-modal selective attention, including both mechanisms, especially concerning higher-order, sensory-unspecific brain areas. Therefore, it may be beneficial for future investigations to employ a paradigm that allows independent analysis of these processes.

A second factor that may be important to explore in more detail is age. Recent work indicated that sub-groups of older adults may differ in overall neural modulation, depending on whether they are at the higher or lower end of the age range (Manan et al., 2018). Brain activation during unimodal auditory selective attention was increased in adults until the age of 47, possibly reflecting a compensation mechanism, but decreased for adults beyond that age. This was interpreted as a result of advanced neural disintegration, possibly due to age-related cerebral volumetric changes. Combining "compensators" and "deteriorators" in one group may dilute these associations and could result in an overall unchanged index of neuronal modulation between younger and older participants. Future studies should therefore adopt a lifespan approach to investigate nonlinear relationships between attention and neural recruitment.

A third and final explanation for the absence of age differences in the present results is related to the behavioral results. Increased cortical recruitment, possibly reflecting a compensatory mechanism, has been reported in older adults with high or age-unaffected cognitive performance (Cabeza et al., 2002; Eyler et al., 2011). While older adults

TABLE 3 | Cluster location and peaks across age groups (RF + RS > RM + RV).

Location	Hemisphere	BA	MNI coordinates			Peak *t*	Size
			x	*y*	*z*		
Fusiform gyrus	RH	37	36	−40	−17	14.87	36780
Extrastriate cortex	LH	19	−36	−85	22	14.25	36433
Premotor cortex	RH	6	48	5	28	9.80	1052
	LH		−45	2	31	7.23	331
Posterior cingulate cortex	RH	23	15	−52	10	8.50	591
Thalamus	LH	n/a	−18	−31	1	8.09	498

LH, left hemisphere; RH, right hemisphere; BA, Brodmann area; RF, remember faces; RS, remember scenes; RM, remember music; RV, remember voices. ps < 0.0001, Bonferroni correction was applied. Clusters are displayed, sorted by t value, cluster sizes in number of 1 mm^3 voxels.

in this study generally demonstrated lower performance in all conditions, including the perceptual baseline control task, this age-related effect did not interact with condition. Older adults were not disproportionately affected in the selective attention conditions as compared to baseline. These age differences are therefore more likely to reflect generalized mental slowing, which is well documented in the aging literature (Salthouse, 1985; Krail and Salthouse, 1994). Consequently, our finding that neural modulation during cross-modal selective attention does not differ between older and younger individuals most likely does not merely reflect an inability of older participants to employ compensatory mechanisms.

An important limitation to our study may be the sample size. However, inspection of probabilistic maps of all comparisons, showing similar activation patterns and no regions that stand out in any age group, may point toward true age-independent attentional modulation, and not merely insufficient power for detecting age-related differences. Moreover, age group effects of attentional modulation have been detectable in previous studies with as little as ten participants per age group (Townsend et al., 2006). Nevertheless, it is warranted that our findings of age-equivalent top-down modulation during cross-modal selective attention be further substantiated with larger samples.

In conclusion, the present study provided more insight into the neural basis of cross-modal visual and auditory selective attention by demonstrating that key brain regions that have been extensively documented to be involved in, mainly visual, unimodal selective attention are also recruited for cross-modal visual and auditory selective attention. In addition, we have shown patterns of activity that suggest dominance of visual over auditory processing at the neural level. Most importantly, however, we have demonstrated that top-down modulation in the setting of cross-modal selective attention is independent of age, which suggests intact neural functioning of this crucial cognitive function in older age.

DATA AVAILABILITY STATEMENT

The datasets analyzed in this manuscript are not publicly available. Requests to access the datasets should be directed to franziska.rienacker@maastrichtuniversity.nl.

ETHICS STATEMENT

The studies involving human participants were reviewed and approved by Ethics Review Committee Psychology and Neurosciences (ERCPN), Maastricht University. The patients/participants provided their written informed consent to participate in this study.

AUTHOR CONTRIBUTIONS

MG and PV designed the experimental paradigm. MG gathered the fMRI and behavioral data. FR executed the analyses and wrote the manuscript. MG, PV, HJ, and CV contributed to the conception of the study, interpretation of the results, and preparation of the manuscript. MG, JE, and HJ supported the fMRI analyses. All authors contributed to the article and approved the submitted version.

SUPPLEMENTARY MATERIAL

The Supplementary Material for this article can be found online at: https://www.frontiersin.org/articles/10.3389/fnagi.2020.498978/full#supplementary-material

REFERENCES

Cabeza, R., Anderson, N. D., Locantore, J. K., and McIntosh, A. R. (2002). Aging gracefully: compensatory brain activity in high-performing older adults. *NeuroImage* 17, 1394–1402. doi: 10.1006/nimg.2002.1280

Čeponienė, R., Westerfield, M., Torki, M., and Townsend, J. (2008). Modality-specificity of sensory aging in vision and audition: evidence from event-related potentials. *Brain Res.* 1215, 53–68. doi: 10.1016/j.brainres.2008.02.010

Colavita, F. B., and Weisberg, D. (1979). A further investigation of visual dominance. *Percep. Psychophy.* 25, 345–347. doi: 10.3758/BF03198814

Corbetta, M., and Shulman, G. L. (2002). Control of goal-directed and stimulus-driven attention in the brain. *Nat. Rev. Neurosci.* 3, 201–215. doi: 10.1038/nrn755

De Graaf, A., and Deelman, B. G. (1991). *Cognitieve Screening Test.* Lisse: Swets en Zeitlinger.

Eyler, L. T., Sherzai, A., Kaup, A. R., and Jeste, D. V. (2011). A review of functional brain imaging correlates of successful cognitive aging. *Biol. Psychiatry* 70, 115–122. doi: 10.1016/j.biopsych.2010.12.032

Gazzaley, A., Cooney, J. W., McEvoy, K., Knight, R. T., and D'Esposito, M. (2005a). Top-down enhancement and suppression of the magnitude and speed of neural activity. *J. Cogn. Neurosci.* 17, 507–517. doi: 10.1162/0898929053279522

Gazzaley, A., Cooney, J. W., Rissman, J., and D'Esposito, M. (2005b). Top-down suppression deficit underlies working memory impairment in normal aging. *Nat. Neurosci.* 8, 1298–1300. doi: 10.1038/nn1543

Geerligs, L., Saliasi, E., Maurits, N. M., Renken, R. J., and Lorist, M. M. (2014). Brain mechanisms underlying the effects of aging

on different aspects of selective attention. *NeuroImage* 91, 52–62. doi: 10.1016/j.neuroimage.2014.01.029

Grady, C., Sarraf, S., Saverino, C., and Campbell, K. (2016). Age differences in the functional interactions among the default, frontoparietal control, and dorsal attention networks. *Neurobiol. Ag.* 41, 159–172. doi: 10.1016/j.neurobiolaging.2016.02.020

Guerreiro, M. J. S., Anguera, J. A., Mishra, J., Van Gerven, P. W. M., and Gazzaley, A. (2014). Age-equivalent top-down modulation during cross-modal selective attention. *J. Cogn. Neurosci.* 26, 2827–2839. doi: 10.1162/jocn_a_00685

Guerreiro, M. J. S., Eck, J., Moerel, M., Evers, E. A. T., and Van Gerven, P. W. M. (2015). Top-down modulation of visual and auditory cortical processing in aging. *Behav. Brain Res.* 278, 226–234. doi: 10.1016/j.bbr.2014.09.049

Guerreiro, M. J. S., Murphy, D. R., and Van Gerven, P. W. M. (2010). The role of sensory modality in age-related distraction: A critical review and a renewed view. *Psychol. Bull.* 136, 975–1022. doi: 10.1037/a0020731

Guerreiro, M. J. S., Murphy, D. R., and Van Gerven, P. W. M. (2013). Making sense of age-related distractibility: the critical role of sensory modality. *Acta Psychol.* 142, 184–194. doi: 10.1016/j.actpsy.2012.11.007

Guerreiro, M. J. S., and Van Gerven, P. W. M. (2011). Now you see it, now you don't: Evidence for age-dependent and age-independent cross-modal distraction. *Psychol. Ag.* 26, 415–526. doi: 10.1037/a0021507

Haring, A. E., Zhuravleva, T. Y., Alperin, B. R., Rentz, D. M., Holcomb, P. J., and Daffner, K. R. (2013). Age-related differences in enhancement and suppression of neural activity underlying selective attention in matched young and old adults. *Brain Res.* 1499, 69–79. doi: 10.1016/j.brainres.2013.01.003

Hasher, L., and Zacks, R. T. (1988). "Working memory, comprehension, and aging: a review and a new view," in *Psychology of Learning and Motivation,* G. H. Bower, eds. (San Diego, CA: Academic Press), 193–225. doi: 10.1016/S0079-7421(08)60041-9

Krail, R., and Salthouse, T. A. (1994). Processing speed as a mental capacity. *Acta Psychol.* 86, 199–225. doi: 10.1016/0001-6918(94)90003-5

Lacadie, C. M., Fulbright, R. K., Arora, J., Constable, R. T., and Papademetris, X. (2008). "Brodmann Areas defined in MNI space using a new tracing tool in bioimage suite," in *Proceedings of the 14th Annual Meeting of the Organization for Human Brain Mapping*, (Melbourne, VIC) 771.

Leech, R., and Sharp, D. J. (2014). The role of the posterior cingulate cortex in cognition and disease. *Brain* 137, 12–32. doi: 10.1093/brain/awt1762

Lustig, C., Hasher, L., and Tonev, S. T. (2001). Inhibitory control over the present and the past. *Eur. J. Cogn. Psychol.* 13, 107–122. doi: 10.1080/095414401256215

Manan, H. A., Yusoff, A. N., Franz, E. A., and Mukari, S. Z.-M. S. (2018). Effects of aging and background babble noise on speech perception processing: an fMRI study. *Neurophysiology* 49, 441–452. doi: 10.1007/s11062-018-9707-5

Miller, G. A. (1956). The magical number seven, plus or minus two: some limits on our capacity for processing information. *Psychol. Rev.* 63, 81–97. doi: 10.1037/h0043158

Mishra, J., and Gazzaley, A. (2013). Preserved discrimination performance and neural processing during crossmodal attention in aging. *PLoS ONE.* 8:e81894. doi: 10.1371/journal.pone.0081894

Nachev, P., Kennard, C., and Husain, M. (2008). Functional role of the supplementary and pre-supplementary motor areas. *Nat. Rev. Neurosci.* 9, 856–869. doi: 10.1038/nrn2478

Peelle, J. E. (2014). Methodological challenges and solutions in auditory functional magnetic resonance imaging. *Front. Neurosci.* 8:253. doi: 10.3389/fnins.2014.00253

Posner, M. I., Nissen, M. J., and Klein, R. M. (1976). Visual dominance: an information-processing account of its origins and significance. *Psychol. Rev.* 83, 157–171. doi: 10.1037/0033-295X.83.2.157

Rienäcker, F., Jacobs, H. I. L., Van Heugten, C. M., and Van Gerven, P. W. M. (2018). Practice makes perfect: high performance gains in older adults engaged in selective attention within and across sensory modalities. *Acta Psychol.* 191, 101–111. doi: 10.1016/j.actpsy.2018.09.005

Salthouse, T. A. (1985). "Speed of behavior and its implications for cognition," in. *The Handbooks of Aging. Handbook of the Psychology of Aging, 2nd ed,* J. E. Birren, K. W. Schaie, eds. (New York, NY: Van Nostrand Reinhold Co), 400–426.

Townsend, J., Adamo, M., and Haist, F. (2006). Changing channels: an fMRI study of aging and cross-modal attention shifts. *NeuroImage* 31, 1682–1692. doi: 10.1016/j.neuroimage.2006.01.045

Van Gerven, P. W. M., and Guerreiro, M. J. S. (2016). Selective attention and sensory modality in aging: curses and blessings. *Front. Hum. Neurosci.* 10:147. doi: 10.3389/fnhum.2016.00147

Yan, T., Geng, Y., Wu, J., and Li, C. (2015). Interactions between multisensory inputs with voluntary spatial attention: an fMRI study. *NeuroReport* 26, 605–612. doi: 10.1097/WNR.0000000000000368

Zacks, T., and Hasher, L. (1994). "Directed ignoring: inhibitory regulation of working memory," in *Inhibitory Processes in Attention, Memory, and Language,* D. Dagenbach and T. H. Carreds. (San Diego, CA: Academic Press), 241–264.

Conflict of Interest: The authors declare that the research was conducted in the absence of any commercial or financial relationships that could be construed as a potential conflict of interest.

frontiers in Aging Neuroscience

ORIGINAL RESEARCH
published: 21 April 2021
doi: 10.3389/fnagi.2021.513605

DHCR24 Knock-Down Induced Tau Hyperphosphorylation at Thr181, Ser199, Thr231, Ser262, Ser396 Epitopes and Inhibition of Autophagy by Overactivation of GSK3β/mTOR Signaling

Xiaojing Bai[1], *Junfeng Wu*[1], *Mengqi Zhang*[1], *Yixuan Xu*[1], *Lijie Duan*[1], *Kai Yao*[1], *Jianfeng Zhang*[1], *Jimei Bo*[1], *Yongfei Zhao*[1], *Guoxiong Xu*[2] *and Hengbing Zu*[1]*

[1] *Department of Neurology, Jinshan Hospital, Fudan University, Shanghai, China,* [2] *The Research Center for Clinical Medicine, Jinshan Hospital, Fudan University, Shanghai, China*

Accumulating evidences supported that knock-down of DHCR24 is linked to the pathological risk factors of AD, suggesting a potential role of DHCR24 in AD pathogenesis. However, the molecular mechanism link between DHCR24 and tauopathy remains unknown. Here, in order to elucidate the relationship between DHCR24 and tauopathy, we will focus on the effect of DHCR24 on the tau hyperphosphorylation at some toxic sites. In present study, we found that DHCR24 knock-down significantly lead to the hyperphosphorylation of tau sites at Thr181, Ser199, Thr231, Ser262, Ser396. Moreover, DHCR24 knock-down also increase the accumulation of p62 protein, simultaneously decreased the ratio of LC3-II/LC3-I and the number of autophagosome compared to the control groups, suggesting the inhibition of autophagy activity. In contrast, DHCR24 knock-in obviously abolished the effect of DHCR24 knock-down on tau hyperphosphrylation and autophagy. In addition, to elucidate the association between DHCR24 and tauopathy, we further showed that the level of plasma membrane cholesterol, lipid raft-anchored protein caveolin-1, and concomitantly total I class PI3-K (p110α), phospho-Akt (Thr308 and Ser473) were significantly decreased, resulting in the disruption of lipid raft/caveola and inhibition of PI3-K/Akt signaling in silencing DHCR24 SH-SY5Y cells compared to control groups. At the same time, DHCR24 knock-down simultaneously decreased the level of phosphorylated GSK3β at Ser9 (inactive form) and increased the level of phosphorylated mTOR at Ser2448 (active form), leading to overactivation of GSK3β and mTOR signaling. On the contrary, DHCR24 knock-in largely increased the level of membrane cholesterol and caveolin-1, suggesting the enhancement of lipid raft/caveola. And synchronously DHCR24 knock-in also abolished the effect of DHCR24 knock-down on the inhibition of PI3-K/Akt signaling as well as the overactivation of GSK3β and mTOR signaling. Collectively, our data strongly supported DHCR24 knock-down lead to tau hyperphosphorylation and the inhibition of autophagy by a lipid raft-dependent PI3-K/Akt-mediated GSK3β and mTOR signaling. Taking

OPEN ACCESS

Edited by:
Hans J. Grabe,
University of Greifswald, Germany

Reviewed by:
Deep R. Sharma,
Albert Einstein College of Medicine, United States
Ravi Manjithaya,
Jawaharlal Nehru Centre for Advanced Scientific Research, India

****Correspondence:***
Hengbing Zu
hbzyy666@163.com

Received: *20 November 2019*
Accepted: *26 February 2021*
Published: *21 April 2021*

Citation:
Bai X, Wu J, Zhang M, Xu Y, Duan L, Yao K, Zhang J, Bo J, Zhao Y, Xu G and Zu H (2021) DHCR24 Knock-Down Induced Tau Hyperphosphorylation at Thr181, Ser199, Thr231, Ser262, Ser396 Epitopes and Inhibition of Autophagy by Overactivation of GSK3β/mTOR Signaling. Front. Aging Neurosci. 13:513605. doi: 10.3389/fnagi.2021.513605

together, our results firstly demonstrated that the decrease of plasma membrane cholesterol mediated by DHCR24 deficiency might contribute to the tauopathy in AD and other tauopathies.

Keywords: DHCR24, hyperphosphorylation, autophagy, PI3-K, GSK3β, mTOR, Alzheimer's disease 3/, Cholesterol

INTRODUCTION

Previous studies found that there is a significant reduction in the expression of new gene in specific vulnerable brain regions in Alzheimer's disease (AD) patients, which was named selective AD indicator 1 (Seladin-1), or 3β-hydroxysterol-Δ24 reductase (DHCR24) (Greeve et al., 2000; Waterham et al., 2001). In the past more than 10 years, increasing data suggested that the downregulation of DHCR24 expression could was induced by many AD-related risk factors, including genetic, β-amyloid protein (Aβ), aging, intermittent low or high blood glucose, hyperglycemia, hyperinsulinemia, diabetes mellitus, chronic inflammation, oxidative stress, obesity, metoblic syndrome, and growth factor insufficiency (e.g., insulin, IGF-1), etc. (Greeve et al., 2000; Livonen et al., 2002; Giannini et al., 2008; Kuehnle et al., 2008; McGrath et al., 2009; Khuda et al., 2010; Vanmierlo et al., 2010; Berisha et al., 2011; Shih et al., 2011; Sharpe et al., 2012; Ing et al., 2014; Kleinridders et al., 2014; Orre et al., 2014; Sassi et al., 2014; Bing et al., 2015; Kazkayasi et al., 2016; Najem et al., 2016; Dhana et al., 2018; Lemche, 2018). Accumulating evidences supported that the downregulation of DHCR24 is linked to the pathological risk factors of both sporadic and familiar AD, suggesting a potential role of DHCR24 in AD pathogenesis. Moreover, studies indicate that DHCR24 transcription is selectively down-regulated in brain regions vulnerable to Alzheimer's disease in the transgenic mouse model of AD (Livonen et al., 2002; Vanmierlo et al., 2010; Orre et al., 2014). Besides, in AD patients, it has been reported that DHCR24 transcription and protein expression were selectively down-regulated in the brain areas affected in AD (Greeve et al., 2000; Livonen et al., 2002; Liang et al., 2008). Thus, it seems that DHCR24 is likely to establish a new direct link between the familial and sporadic AD. Nevertheless, the potential role of DHCR24 in Alzheimer disease and other neurodegenerative diseases is still unknown (Greeve et al., 2000; Livonen et al., 2002; Sharpe et al., 2012; Zerenturk et al., 2013). Iivonen et al. found that the downregulation of DHCR24 might be associated with hyperphosphorylated tau in AD mouse model, but the molecular mechanism behind this association remains unknown (Livonen et al., 2002). Tauopathy is regarded as one of the most characterized pathology in AD and other tauopathies, which is recognized as linkage to hyperphosphorylated tau, immunohistochemically detected paired helical filament tau, and neurofibrillary tangles (Alonso and Cohen, 2018). Therefore, to elucidate a molecular mechanism link between DHCR24 and tauopathy will help to clarify the role of DHCR24 in the pathogenesis of AD and other tauopathies.

DHCR24 is known as the key synthetase in cholesterol synthesis, which catalyzes the final step of cholesterol synthesis via the Bloch pathway, or converts lanosterol to cholesterol at the first step in the Kandutsch-Russell pathway (Drzewińska et al., 2009; Segatto et al., 2019). DHCR24 mutation results in Deficient/defective of DHCR24 activity, low cholesterol, high desmosterol levels, and disturbance of cholesterol-rich lipid-rafts in brain (Waterham et al., 2001; Zerenturk et al., 2013). Moreover, recent studies suggested that activities of DHCR24 enzyme can obviously affect membrane lipid raft organization and dynamics, which are key factors for signaling processes for cellular responses (Crameri et al., 2006; Lu et al., 2006; Matthews et al., 2008; Gao et al., 2011). Therefore, the present investigation is to explore *whether the* downregulation of DHCR24 may induce an abnormality of membrane lipid raft-dependent PI3-K/Akt signaling, including downstream glycogen synthase kinase-3β (GSK3β) and mammalian target of rapamycin (mTOR) signaling, which are involved in the abnormal hyperphosphorylation of some tau sites in tauopathy. In our experiment, we will focus on the effect of DHCR24 on the tau hyperphosphorylation at some sites such as Thr181, Ser199, Thr231, Ser262, Ser256, Ser396, and autophagy, in order to elucidate the relationship between DHCR24 downregulation and tauopathy.

MATERIALS AND METHODS

Primary antibodies against DHCR24 (#2033), AKt (#4691), Phospho-Akt (T308) (#13038), Phospho-Akt (Ser473) (#4060), PI3 Kinase p110α (#4249), GSK-3β (#12456), Phospho-GSK-3β(Ser9) (#5558), mTOR (#2983), Phospho-mTOR (#2971),Tau (#46687), Phospho-Tau (Thr181) (#12885), Phospho-Tau (Ser199) (#29957), Phospho-Tau (Ser396) (#9632), LC3B (#3868), P62/SQSTM1 (#23214), GAPDH (#2118), secondary antibodies anti-rabbit IgG, HRP-linked antibody (#7074), Anti-rabbit IgG (H+L) (#5366), Anti-mouse IgG, HRP-linked antibody (#7076) were purchased from Cell Signaling Tech (USA), Primary antibodies against Caveolin-1 (ab2910), Phospho-Tau (Ser262) (ab131354) were purchased from British abcam Company, Primary antibodies against Phospho-Tau (Thr231) (4137) was purchased from China ABclonal Company. Primers were purchased from Sangon Biotech (Sangon Biotech, China). Propidium Iodide (abs9105), Methyl-β-cyclodextrin (abs42021762), Filipin III (abs42018484) were purchased from China Absin Company.

Cell Culture

SH-SY5Y cells were obtained from Chinese Academy of Sciences (Shanghai, China) and kept in DMEM F12 (Corning, USA) with 10% fetal bovine serum (Gibco, USA). Following ATCC protocols, all cells were cultured in a 5% CO2 humidified incubator at 37°C.

Lentivirus Transfection and Screening of a Stable SH-SY5Y Cell Line

With regard to lentivirus transfection, lentivirus at multiplicity of infection (MIO) about five mediated DHCR24 shRNA, DHCR24 cDNA, and NC infected into the SH-SY5Y cells. At 48 h after infection, the medium was replaced with fresh complete growth medium containing the appropriate concentration of puromycin (6 μg/mL). At 3 to 4 days after infection, the selected cells were used for experiments. Note: ShRNA target sequence was as follow: (5'-GCATCATCCCTGCCAAGAAGT-3'); The empty vector sequence was as follow: (5'-TTCTCCGAACGTGTCACG T-3'), cDNA sequence was as follow: (5'-ATGGAGCCCGCCGT GTCGCTGGCCGTGTGCGCGCTGCTCTTCCTGCTGTGGG TGCGCCTGAAGGGGCTGGAGTTCGTGCTCATCCACCAG CGCTGGGTGTTCGTGTGCCTCTTCCTCCTGCCGCTCTCG CTTATCTTCGATATCTACTACTACGTGCGCGCCTGGGTG GTGTTCAAGCTCAGCAGCGCTCCGCGCCTGCACGAGCA GCGCGTGCGGGACATCCAGAAGCAGGTGCGGGAATGG AAGGAGCAGGGTAGCAAGACCTTCATGTGCACGGGGC GCCCTGGCTGGCTCACTGTCTCACTACGTGTCGGGAAG TACAAGAAGACACACAAAAACATCATGATCAACCTGAT GGACATTCTGGAAGTGGACACCAAGAAACAGATTGTCC GTGTGGAGCCCTTGGTGACCATGGGCCAGGTGACTGCC CTGCTGACCTCCATTGGCTGGACTCTCCCCGTGTTGCCT GAGCTTGATGACCTCACAGTGGGGGGCTTGATCATGGG CACAGGCATCGAGTCATCATCCCACAAGTACGGCCTGT TCCAACACATCTGCACTGCTTACGAGCTGGTCCTGGCT GATGGCAGCTTTGTGCGATGCACTCCGTCCGAAAACTC AGACCTGTTCTATGCCGTACCCTGGTCCTGTGGGACGC TGGGTTTCCTGGTGGCCGCTGAGATCCGCATCATCCCT GCCAAGAAGTACGTCAAGCTGCGTTTCGAGCCAGTGCG GGGC CTGGAGGCTATCTGTGCCAAGTTCACCCACGAGT CCCAGCGGCAGGAGAACCACTTCGTGGAAGGGCTGCTC TACTCCCTGGATGAGGCTGTCATTATGACAGGGGTCAT GACAGATGAGGCAGAGCCCAGCAAGCTGAATAGCATT GGCAATTACTACAAGCCGTGGTTCTTTAAGCATGTGGA GAACTATCTGAAGACAAACCGAGAGGGCCTGGAGTAC ATTCCCTTGAGACACTACTACCACCGCCACACGCGCAG CATCTTCTGGGAGCTCCAGGACATTATCCCCTTTGGCA ACAACCCCATCTTCCGCTACCTCTTTGGCTGGATGGTG CCTCCCAAGATCTCCCTCCTGAAGCTGACCCAGGGTGA GACCCTGCGCAAGCTGTACGAGCAGCACCACGTGGTGC AGGACATGCTGGTGCCCATGAAGTGCCTGCAGCAGGCC CTGCACACCTTCCAAAACGACATCCACGTCTACCCCAT CTGGCTGTGTCCGTTCATCCTGCCCAGCCAGCCAGGCC TAGTGCACCCCAAAGGAAATGAGGCAGAGCTCTACATC GACATTGGAGCATATGGGGAGCCGCGTGTGAAACACTT TGAAGCCAGGTCCTGCATGAGGCAGCTGGAGAAGTTTG TCCGCAGCGTGCATGGCTTCCAGATGCTGTATGCCGAC TGCTACATGAACCGGGAGGAGTTCTGGGAGATGTTTGA TGGCTCCTTGTACCACAAGCTGCGAGAGAAGCTGGGTT GCCAGGACGCCTTCCCCGAGGTGTACGACAAGATCTGC AAGGCCGCCAGGCACTGA-3').

Real-Time PCR Analysis

Total RNA was extracted using RNAiso Plus (Takara, Japan) according to the manufacturer's instructions. Reverse transcription was performed using a PrimeScript™ RT Master Mix (Takara, Japan) with specific primers (see **Table 1**). Reaction conditions were followed as 37°C 15 min, 85°C 5 s, 4°C 30 min. PCR amplification was performed at 95°C 10 min, followed by 95°C 5 s and 60°C 31 s for 40 cycles using SYBR Green Master. Assays were conducted in triplicate and were repeated at least three times. The amount of DHCR24 normalized to an endogenous control GAPDH given by 2-ΔΔCt, in which threshold cycle (Ct) was obtained using Sequence Detection Software V1.4 (7,300 Real Time PCR System, Applied Biosystems, USA).

TABLE 1 | The PCR primer sequences.

gene	Sequence
DHCR24	
Forward primer	5′-3′ AGTCCAGTTCCCCGTTTA
Reverse primer	5′-3′ CTTACCCAGCACCTTCAA
GAPDH	
Forward primer	5′-3′ ACGGATTTGGTCGTATTGGG
Reverse primer	5′-3′ CGCTCCTGGAAGATGGTGAT

Immunofluorescence Staining

SH-SY5Y cells seeded in twelve-well-plate were incubated for 12-20 h, followed by washing three times with PBS, then fixed with 4% paraformaldehyde at room temperature for 30 min, followed by washing three times with PBS.0.5% Triton X-100 was adopted to permeate cells for 20 min. Cells were blocked with 5% bovine serum Albumin (BSA) in PBS at room temperature for 1 h, then incubated with the primary antibody at 4°C overnight followed by three times washing with PBS. Samples were incubated in secondary antibody in the dark for 1 h followed by stained with DAPI (0.5 μg/mL) for 5 min at room temperature. Finally, cells were observed and the fluorescent images were captured by a confocal microscope (Leica sp5, Germany).

Western Blot Analysis

After designated treatment, lysates were generated by placing the cells in SDS lysis buffer containing a cocktail of protease and phosphatase inhibitors. BCA was performed to determine total protein concentrations, which were normalized to 1 mg/mL for all samples. Samples were then prepared in sample buffer and heated to 100°C for 8 min. Equal amounts of lysates were fractionated using 8–12% sodium dodecyl sulfate polyacrylamide gels and were then electrotransferred onto nitrocellulose membranes. Gels were run at a constant voltage (80V) for 2–3 h for maximum separation. Wet transfer was performed for 120 min at constant current (250 mA) using polyvinylidenedifluoride membrane presoaked in methanol. The membrane was blocked in 5% milk in 0.2% TBST. The membrane was then washed three times in TBST for 10 min each. After overnight incubation at 4°C with the primary antibodies [DHCR24 1:1000, Akt 1:1000, Phospho-Akt 1:1000, mTOR 1:1000, Phospho-mTOR 1:1000, LC3B 1:1000, P62/SQSTM1 1:1000, PI3-K 1:1000, GSK3β 1:1000, Phospho-GSK3β 1:1000, Tau 1:1000, Phospho-Tau 1:1000, Caveolin-1 1:500, GAPDH 1:5000] the blots were washed and exposed for 1 h at room temperature to corresponding HRP-conjugated

secondary antibodies. Chemiluminescent (Bio-Rad, Hercules, CA, USA) detection was then used to detect the expression of each protein; GAPDH level served as internal loading controls.

Cholesterol Labeling With Filipin III and Analysis

Cells were grown on coverglass bottom dishes. In order to allow a better visualization of intracellular cholesterol pools, cells were treated with 10 mM methyl-β-cyclodextrin (MβCD, China Absin Company) for 30 min at 37°C to remove cholesterol from the plasma membrane. Cells were then fixed for 10 min at RT with 4% paraformaldehyde in phosphate-buffered saline (PBS). Cells were incubated with a solution of filipin (0.1 mg/ml, China Absin Company) for 30 min. Finally, after two washes, cells were counterstained with propidium iodide (PI, 0.35 μg/ml in PBS; China Absin Company) for 5 min. Acquiring images with a confocal laser scanning microscope equipped with a 380 nm optically pumped semiconductor laser (Leica sp5, Germany). Whole-cell cholesterol staining with filipin did not require MβCD treatment.

Transmission Electron Microscopy (TEM) Analysis

SH-SY5Y cells were treated by stationary liquid which contained 3% glutaraldehyde and 0.22 mmol/L sucrose phosphate buffer for 4 h, then rinsed three times with 0.1 M phosphoric acid rinsing solution for 10–15 min, and fixed with 1% citric acid for 2 h. Next, stepwise ethanol dehydration, followed by epoxy resin embedding, overnight in a 30°C oven, then in a 60°C oven for 12 h. Using an ultra-thin slicer, 50-to 100-nm-thick slices were cut. Using uranium acetate and lead nitrate double staining, a transmission electron microscopy (Hitachi HT7700, Japan) was used to examine autophagosomes in SH-SY5Y cells.

Statistical Analysis

Statistical analysis was performed using SPSS statistical software. All data were expressed as mean ± SD from at least three independent experiments. *P*-values were determined using one-way ANOVA. Significance was defined as $P < 0.05$.

RESULTS

ShRNA-Mediated Knock-Down and cDNA-Mediated Knock-in of DHCR24 Gene Expression in SH-SY5Y Cells

To explore the influence of DHCR24 on tauopathy in Alzheimer's disease, a transient knock-down of DHCR24 by lentivirus-mediated shRNA (knock-down group) and knock-in of DHCR24 by lentivirus-mediated cDNA (knock-in group) in the SH-SY5Y cell line was performed. DHCR24 shRNA, DHCR24 cDNA were well-expressed in SH-SY5Y cells, as indicated by GFP (green) under fluorescence microscopy (**Figure 1A**). Transduced cells that survived puromycin selection were followed by qPCR and Western blot analysis. Compared to vector control group (negative control group, NC) and no treatment group (untransfected SH-SY5Y cells), the level of DHCR24 of knock-down group were significantly reduced, and the level of DHCR24 of knock-in group were significantly increased (**Figures 1B–F**). As mentioned above, the knock-down of DHCR24 by shRNA-lentivirus and knock-in of DHCR24 by cDNA-lentivirus were validated in SH-SY5Y cells.

DHCR24 Knock-Down Induced Hyperphosphorylation of Tau at Thr181, Ser199, Thr231, Ser262, and Ser396

So far, it is still not to elucidate the potential relationship between DHCR24 and tau hyperphosphorylation. Increasing data supported that the hyperphosphorylation of tau at several sites, such as Thr181, Ser199, Thr231, Ser262, Ser356, and Ser396, which are tightly associated with tauopathy in AD and other tauopathies (Sengupta et al., 1998; Duka et al., 2013; Neddens et al., 2018). Thus, we examined whether the DHCR24 knock-down could induce the tau hyperphosphorylation at some toxic sites, such as Thr181, Ser199, Thr231, Ser262, Ser356, and Ser396. In present study, total tau and phosphorylated tau (p-tau) at residues Thr181, Ser199, Thr231, Ser262, Ser356, and Ser396 were assessed by western blot, respectively. Compared with the no treatment or negative control group, we found that the level of four phosphorylated tau, including tau sites at Thr181, Ser199, Thr231, Ser262, and Ser396, are markedly increased by DHCR24 knock-down in SH-SY5Y cells (**Figures 2A,B,E,F,I,J,M,N,Q,R**). Moreover, the increase in phosphorylation relative to controls was highest at Thr231 and Ser262. Conversely, after DHCR24 knock-in in human neuroblastoma SH-SY5Y cells, we showed that the level of the above five phosphorylated tau are obviously lowered compared to the control group (**Figures 2C,D,G,H,K,L,O,P,S,T**). By contrast, the level of p-tau at Ser356 showed no significant difference in four different groups (data not shown). To sum up, we firstly demonstrated that DHCR24 knock-down induced the abnormal hyperphosphorylation of tau at Thr181, Ser199, Thr231, Ser262, and Ser396.

DHCR24 Knock-Down Obviously Induced the Inhibition of Autophagy

To further uncover the role of autophagy in the tauopathy induced by DHCR24 knock-down, we examined the regulation of autophagic activity in the knock-down or knock-in of DHCR24 by transmission electron microscope (TEM) and western blot analysis. Autophagy is an intracellular degradation pathway essential for cellular and energy homoeostasis, involving in the clearance of misfolded proteins and damaged organelles (Lee et al., 2013; Zare-Shahabadi et al., 2015). Nevertheless, with the tauopathy progression, autophagy mediates tau clearance and homeostasis mechanism. Autophagy deficits are regarded as major contributors to the pathogenesis of tauopathy (Yang and Klionsky, 2010; Lee et al., 2013; Zare-Shahabadi et al., 2015). Furthemore, p62, also well-known as sequestosome 1 (SQSTM1) in humans, is a scaffold protein. It interacts with phagophores through the LC3-interacting domain and with the ubiquitinated protein aggregates through the ubiquitin-associated domain. It sequesters the target cargo into inclusion bodies by its PB1 domain. P62 can directly interact with LC3

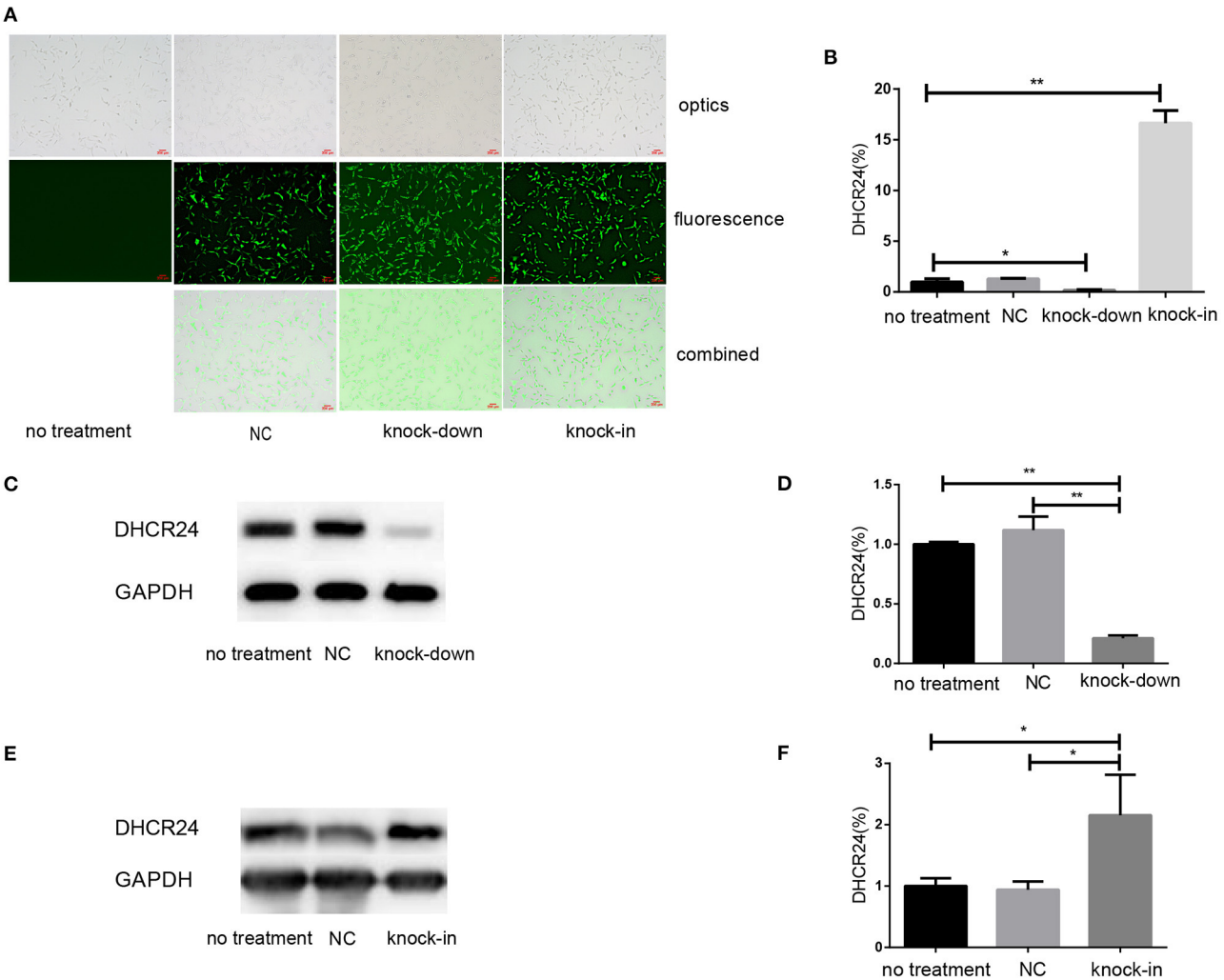

FIGURE 1 | Illustration of SH-SY5Y cells transfected with DHCR24 shRNA-lentivirus and DHCR24 cDNA-lentivirus. The SH-SY5Y cells were transfected with the lentivirus-delivered DHCR24 shRNA, DHCR24 cDNA and lentiviral vector, and used as knock-down group, knock-in group, vector control group (Negative control group, NC) respectively. The untransfected SH-SY5Y cells were used as the no treatment group. **(A)** DHCR24 shRNA, DHCR24 cDNA and lentiviral vector were well-expressed in the SH-SY5Y cells, as indicated by GFP (green) under fluorescence microscopy. Scale bars = 200 μm; **(B)** qPCR analyses were performed and displayed a five-fold lower expression of the DHCR24 shRNA transgenes and a 15-fold higher expression of the DHCR24 cDNA transgenes. Western blot was performed to analyze the knock-down **(C,D)** and knock-in **(E,F)** of DHCR24. All the data are presented as mean ± SD of at least three individual experiments (**B–F**; $n = 3$). $^{*}P < 0.01$, $^{**}P < 0.001$; vs. the no treatment and NC group (**C**, **Figure 2E**, **Figures 6A,Q** share one loading control).

for autophagosome formation (Yang and Klionsky, 2010; Zare-Shahabadi et al., 2015; Zhang et al., 2017). Thus, p62 and LC3-I/LC3-II are key markers of autophagy. In experiments, as shown in **Figures 3E,F**, compared with the control groups, we found that the accumulation of p62 was rapidly increased by DHCR24 knock-down in SH-SY5Y cells, suggesting the weakness of autophagy activity. In contrast, the p62 protein level was significantly decreased in the DHCR24 knock-in SH-SY5Y cells, leading to the enhancement of autophagy activity compared to the control groups (**Figures 3G,H**). Moreover, the ratio of LC3-II/LC3-I in DHCR24 knock-down SH-SY5Y cells was significantly decreased, suggesting the weakness of autophagy (**Figures 3A,B**). On the contrary, the DHCR24 knock-in obviously increased the ratio of LC3-II/LC3-I, resulting in the enhancement of autophagy in SH-SY5Y cells (**Figures 3C,D**). Collectively, our data strongly suggested that the DHCR24 knock-down lead to the inhibition of autophagic activity in SH-SY5Y cells.

In addition, to further study the change f autophagosomes, SH-SY5Y neuroblastoma cells were analyzed by transmission electron microscopy. As shown in **Figures 3I,J** typical autophagosomes of SH-SY5Y cells were observed by transmission electron microscope in control group, knock-down and knock-in groups. It can be seen from the TEM images

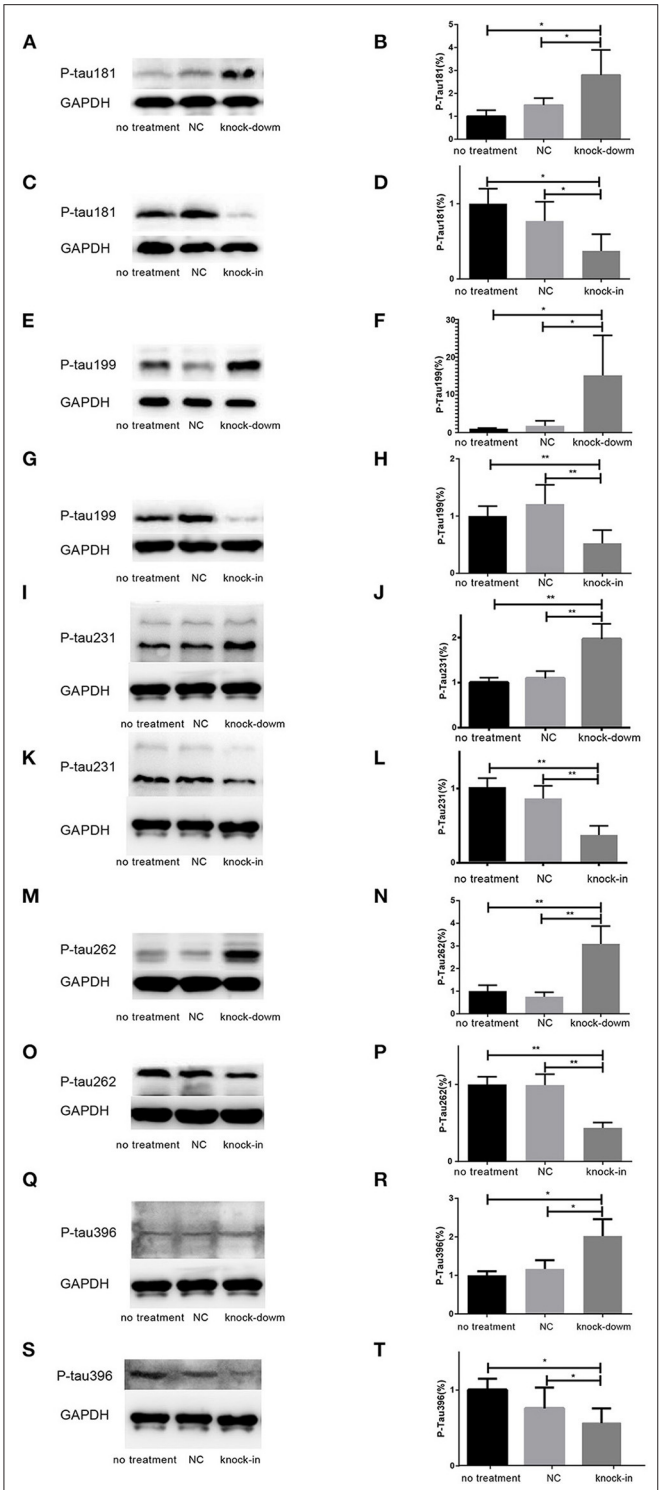

FIGURE 2 | DHCR24 knock-down induced hyperphosphorylation of Tau protein at Thr181, Ser199, Thr231, Ser262, and ser396 in SH-SY5Y cells. **(A,B,E,F,I,J,M,N,Q,R)** Representative western blots of phosphorylated tau at residues Thr181, Ser199, Thr231, Ser262, and Ser396 from DHCR24 knock-down SH-SY5Y cells. **(C,D,G,H,K,L,O,P,S,T)** Representative western blots of phosphorylated tau at residues Thr181, Ser199, Thr231, Ser262, and Ser396 from DHCR24 knock-in SH-SY5Y cells. All the data are presented as mean ± SD of at least three individual experiments ($n = 3$).*$P < 0.05$, **$P < 0.01$; vs. the no treatment and NC group (**Figures 2I**,**Q**,**3E** share one loading control).

of autophagosome that most of the autophagosome had the characteristics of double layer or multilayer membrane and inclusions, which could be identified from the other cell structure (shown in **Figure 3I**). Moreover, double layer or multilayer membrane and inclusions are the characteristics of the autophagosome structure which contains organelles and other cytoplasm components. Additionally, the qualitative analysis of autophagosome was made based on the data from transmission electron microscope. We found that DHCR24 knock-down decreased autophagosome numbers in DHCR24 knock-down SH-SY5Y cells compared to the control groups. On the contrary, DHCR24 knock-in increased autophagosome numbers compared to the control groups. However, TEM analysis revealed that there was no statistically significant difference in the number of autophagosome between the no treatment and negative control group (**Figure 3I**). Consequently, the results of TEM analysis also further revealed DHCR24 knock-down markedly decreased the formation and accumulation of autophagosome (**Figure 3J**), suggesting the inhibition of autophagic activity in SH-SY5Y cells. Taking together, our findings strongly supported that the DHCR24 knock-down lead to the inhibition of autophagy.

DHCR24 Knock-Down Lead to the Decrease of Plasma Membrane and Intracellular Cholesterol Level

As a major constituent of cellular membranes, cholesterol is essential in providing the membrane with its mechanical and structural properties, but also critical in the formation of membrane lipid-raft domains (Caveolae) (Matthews et al., 2008; Zerenturk et al., 2013). DHCR24 is known as a synthetase heavily involved in cholesterol synthesis, controlling the cholesterol synthesis in the brain (Greeve et al., 2000; Drzewińska et al., 2009). Filipin III is naturally fluorescent and specifically binds to free cholesterol, and it labels total cellular cholesterol, especially the plasma membrane. In addition, to visualize intracellular cholesterol pools, we treated live cells with methyl-β-cyclodextrin (MβCD), a molecule able to deplete cholesterol from the plasma membrane (Zidovetzki and Levitan, 2007). Intracellular and plasma membrane cholesterol were labeled and analyzed, respectively, by Filipin III staining. In our study, whole-cell and intracellular cholesterol were stained with filipin III and analyzed by a confocal laser scanning microscope. We found that fluorescence intensity of plasma membrane and intracellular cholesterol in the DHCR24 knock-down group was obviously weaker than that of no treatment group and vector group cells, suggesting the decrease of plasma membrane and intracellular cholesterol level (**Figures 4A,B**). In contrast, as shown in **Figures 4C,D**, immunofluorescence intensity analysis revealed that the level of plasma membrane and intracellular cholesterol were markedly increased in the DHCR24 knock-in group cells compared to the control group cells, suggesting the increase of plasma membrane and intracellular cholesterol level. Together, we verified that DHCR24 knock-down obviously lead to the decrease of plasma membrane cholesterol and intracellular cholesterol level.

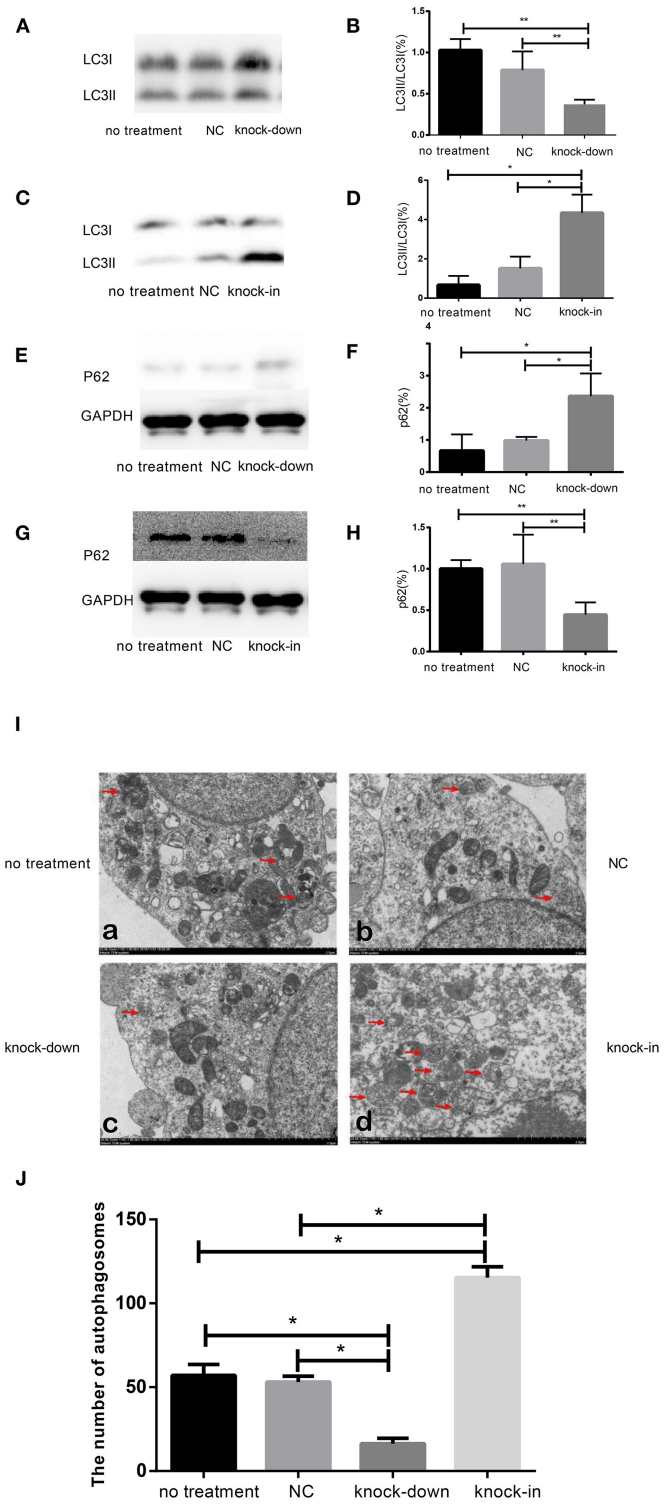

FIGURE 3 | DHCR24 knock-down obviously induced the inhibition of autophagy in SH-SY5Y cells. **(A,B,E,F)** Representative western blots of LC3 and p62 from DHCR24 knock-down SH-SY5Y cells. **(C,D,G,H)** Representative western blots of LC3 and p62 from DHCR24 knock-in SH-SY5Y cells. **(I)** Transmission electron microscopy showed the autophagosomes (red arrow). Scale bar = 2.0 μm. **(J)** Quantitation analyses of autophagosomes for **(I)**. All the data are presented as mean ± SD of at least three individual experiments ($n = 3$).*$P < 0.05$, **$P < 0.01$; vs. the no treatment and NC group (**Figures 2I**,**Q**,**3E** share one loading control; **Figures 2K**,**S**,**3G** share one loading control).

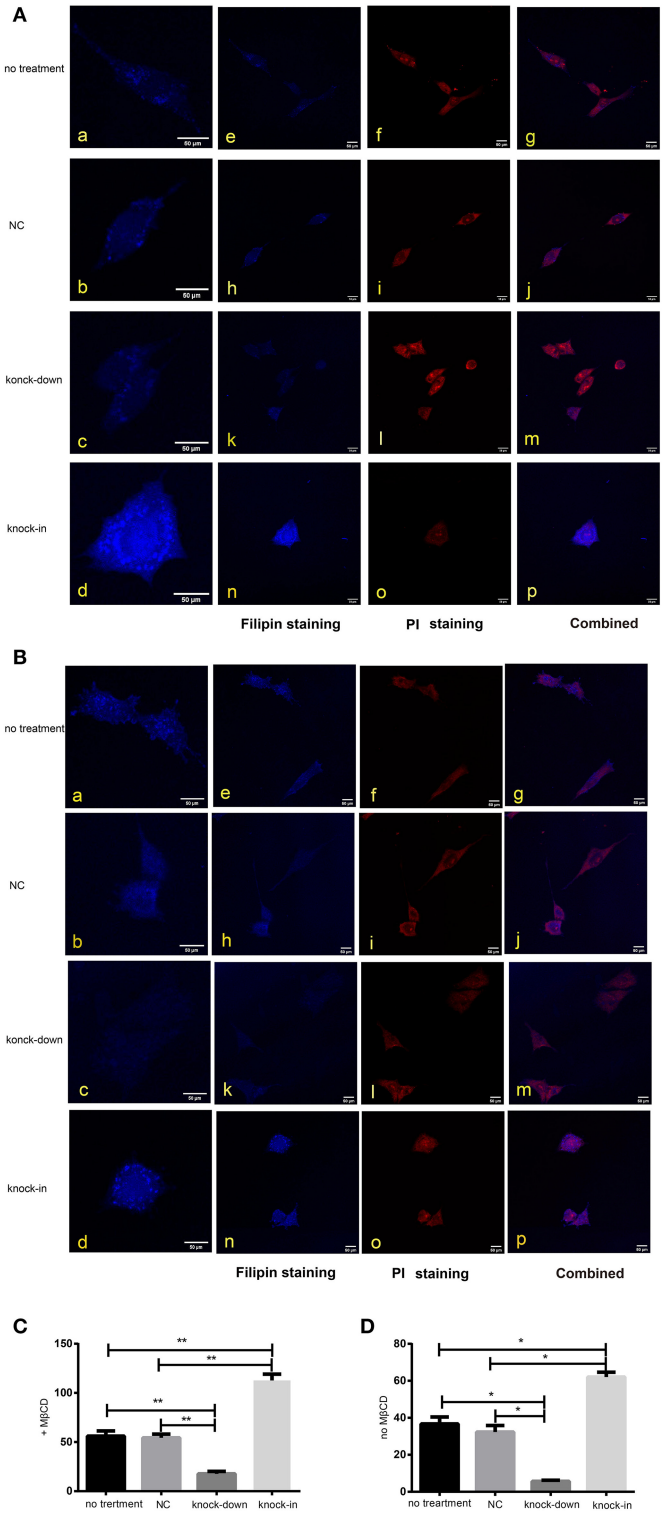

FIGURE 4 | DHCR24 knock-down lead to the decrease of plasma membrane and intracellular cholesterol level. Whole-cell and intracellular cholesterol stained with filipin. **(A)** Filipin stained cholesterol in the intracellular compartments. Cells were treated with MβCD (methyl-β-cyclodextrin) before fixation and filipin staining. The cells in blue were stained with filipin, and in red were stained with PI (propidium iodide), the final column shows a merged image of the two channels. **(B)** Whole-cell cholesterol staining with filipin on fixed SH-SY5Y cells. Filipin stains cholesterol in the plasma membrane and in intracellular compartments. Scale bar = 50 μm. (a–d) of **(A,B)** were the zoomed picture of each group. Filipin intensity of cholesterol in the intracellular compartments **(C)** and cholesterol in whole-cell **(D)** were measured using Image J Software. All the data are presented as mean ± SD of at least three individual experiments ($n = 3$). *$P < 0.05$, **$P < 0.01$; vs. the no treatment and NC group.

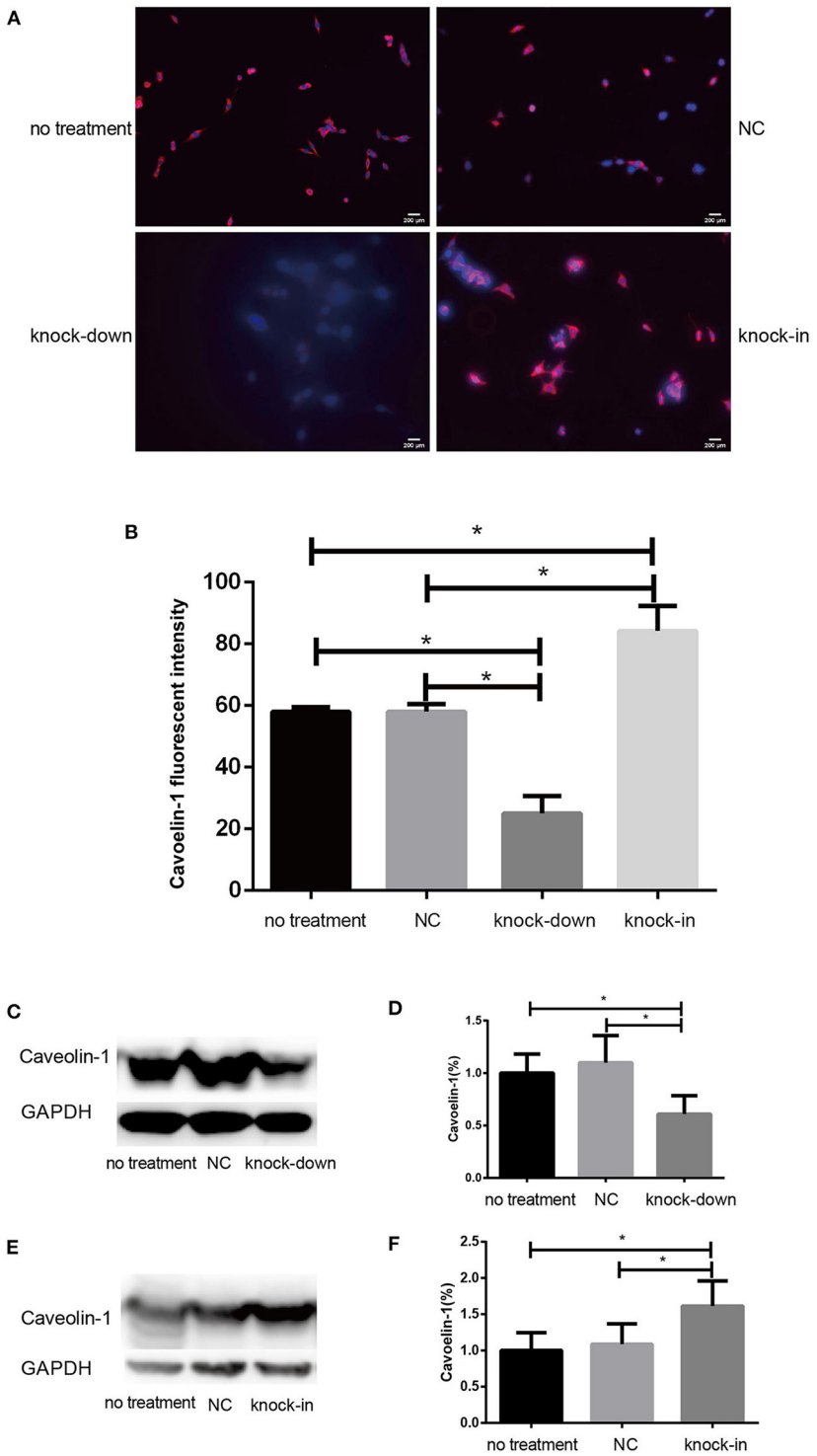

FIGURE 5 | DHCR24 knock-down lead to downregulation of caveolin-1 in plasma membrane caveolae in SH-SY5Y cells. **(A)** Immunofluorescence studies showing staining of caveolin-1 in SH-SY5Y cells. Scale bar=200 μm. **(B)** The fluorescence intensities of caveolin-1 were quantified and presented as the mean of IOD of Caveolin-1 immunofluorescence intensity. **(C,D)** Western blots of caveolin-1 from DHCR24 knock-down SH-SY5Y cells. **(E,F)** Western blots of caveolin-1 from DHCR24 knock-in SH-SY5Y cells. All the data are presented as mean ± SD of at least three individual experiments ($n = 3$). *$P < 0.05$, **$P < 0.01$; vs. the no treatment and NC group. caveolin-1, in red-fluorescence; DAPI, in blue-fluorescence (**Figures 2M**, **5C** share one loading control).

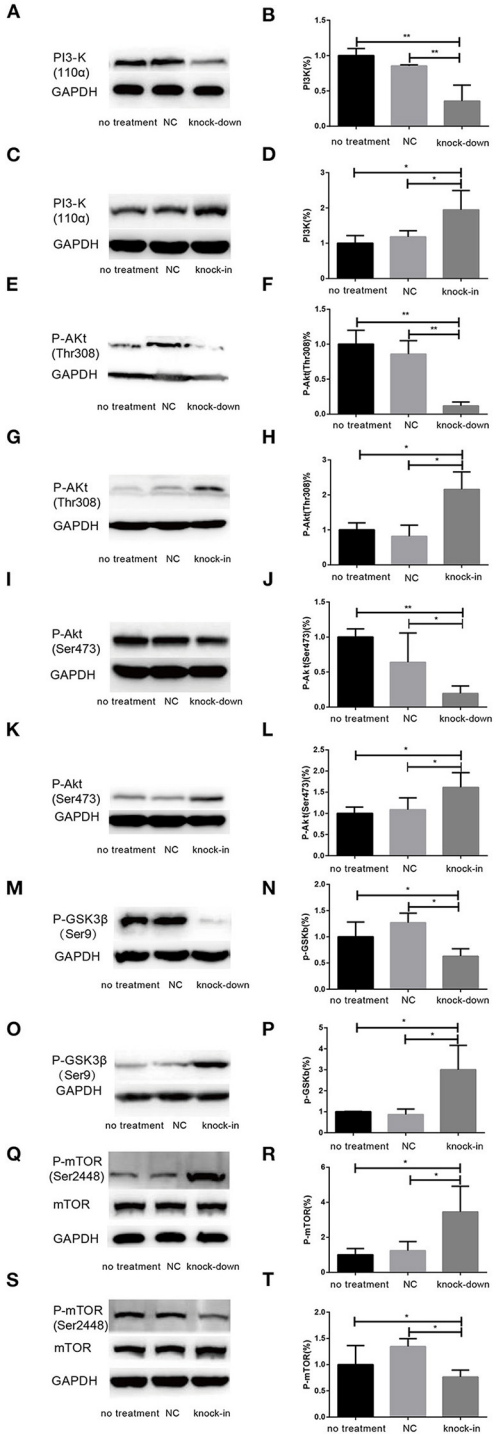

FIGURE 6 | DHCR24 knock-down induced the overactivation of GSK3β/mTOR signaling via PI3K/Akt pathway. **(A,B,E,F,I,J,M,N,Q,R)** Representative western blots of total PI3-K, p-Akt at Ser473, p-Akt at Thr308, p-GSK3β at Ser9, total mTOR, p-mTOR at Ser2448 from DHCR24 knock-down SH-SY5Y cells. **(C,D,G,H,K,L,O,P,S,T)** Representative western blots of total PI3-K, p-Akt at Ser473, p-Akt at Thr308, p-GSK3β at Ser9, total mTOR, p-mTOR at Ser2448 from DHCR24 knock-in SH-SY5Y cells. All the *(Continued)*

FIGURE 6 | data are presented as mean ± SD of at least three individual experiments ($n = 3$). $^{*}P < 0.05$, $^{**}P < 0.01$; vs. the no treatment and NC group (**Figures 1C**, **2E**, **6A**,**Q** share one loading control).

DHCR24 Knock-Down Lead to Inhibition of PI3-K/Akt Signaling in a Membrane Lipid Raft-Dependent Manner

Consistent with our findings analyzed by Filipin III staining, some data suggest that the knock-down or deficiency of DHCR24 lowers cholesterol level of neuronal cell membrane and leads to cholesterol depletion in lipid rafts of cell membranes (Lu et al., 2006; Matthews et al., 2008; Gao et al., 2011). The cellular cholesterol biosynthesis is critical for the activation and maintenance of the PI3-K/Akt cell survival cascade (Lu et al., 2006; Gao et al., 2011). In this study, we examined a possible role of caveolin-1 related lipid raft in the PI3-K/Akt signal transduction in SH-SY5Y cells. In present study, western blot analysis showed that the expression of caveolin-1 protein was markedly lowered in DHCR24 knock-down SH-SY5Y cells compared to control groups, and concomitantly its fluorescence intensity of cell caveolin-1 in DHCR24 knock-down group was weaker than that of control group cells by immunofluorescence analysis, suggesting the disruption of membrane lipid-raft/caveolae in SH-SY5Y cells (**Figures 5A–D**). Conversely, as shown in DHCR24 knock-in group, immunofluorescence and western blot analysis revealed that DHCR24 knock-in significantly upregulated the expression of caveolin-1 protein in the caveolae fraction of the SH-SY5Y cells, suggesting the enhancement of caveolae in SH-SY5Y cells (**Figures 5A,B,E,F**). Based on our findings, we confirmed that DHCR24 knock-down could simultaneously decrease of plasma membrane cholesterol and caveolin-1 in the lipid-raft/caveolae. According to previous data and our study, we demonstrated that DHCR24 knock-down impaired the plasma membrane lipid raft structure and function which is mediated by the depletion of cholesterol and caveolin-1.

Additionally, Cholesterol and caveolin-1 are essential components of caveolae (Chini and Parenti, 2004). Caveolae, cholesterol-rich lipid-raft microdomains of plasma membrane, has been known to modulate the function of lipid raft-dependent protein kinases, such as PI3-K kinase (Chini and Parenti, 2004; Lu et al., 2006; Matthews et al., 2008; Gao et al., 2011). Here, we further evaluate the activation of PI3-K and Akt induced by the knock-down or knock-in of DHCR24 in SH-SY5Y cells. In our experiments, we found that level of total Akt was similar among the four groups (data not shown, see **Supplementary Data**). As shown in **Figure 6**, compared with the no treatment and negative control group, the level of total I class PI3-K (p110α), Phospho-Akt (Thr308) and Phospho-Akt (Ser473) were significantly decreased by DHCR24 knock-down in SH-SY5Y cells, leading to the inhibition of Akt kinase (**Figures 6A,B,E,F,I,J**). Conversely, as shown in **Figure 6**, the level of total PI3-K, p-Akt (Thr308) and p-Akt (Ser473) were obviously increased in DHCR24-in

SH-SY5Y cells, suggesting the activation of Akt kinase, which is similar to the previous study (Lu et al., 2006). To sum up, above data further demonstrated that DHCR24 knock-down impaired the lipid raft organization of caveolae and thereby inhibited the activation of PI3-K/Akt survival signaling via lipid raft dependent manner.

DHCR24 Knock-Down Induced the Overactivation of GSK3β/mTOR Signaling via PI3K/Akt Signaling

As a downstream substrate of PI3-K/Akt Signaling, GSK3β is a Ser/Thr kinase that is active in its non-phosphorylated form, and negatively regulated its activity mainly by Akt kinase (Buller et al., 2008; Bhaskar et al., 2009). So, quantitative analysis of the total GSK3β and phospho-GSK3β (Ser9) was also detected by western blot in different groups. In the study, by DHCR24 knock-down in SH-SY5Y cells, western blot analysis indicated that the level of total GSK3β was similar among the different groups (data not shown, see **Supplementary Data**). In contrast, compared with the control groups, the level of GSK3β phosphorylated at Ser9 was significantly lowered in the DHCR24 knock-down group (**Figures 6M,N**). Conversely, compared with the control group, the level of Phospho-GSK3β (Ser9) was markedly increased in DHCR24 knock-in group (**Figures 6O,P**). GSK3β is inactive when phosphorylated at Ser9; and the level of GSK3β phosphorylated at Ser9 inversely correlate with its activity (Buller et al., 2008; Bhaskar et al., 2009). Concomitantly, with the inhibition of PI3-K/Akt signaling (**Figures 6A,B,E,F,I,J**), DHCR24 knock-down decrease the level of p-GSK3β (Ser9), strongly suggesting the activation of GSK3β kinase in SH-SY5Y cells. In summary, our outcomes suggested that DHCR24 knock-down obviously increase the activity of GSK3β signaling through PI3-K/Akt signaling.

Abnormal activation of mTOR signaling have been recently implicated in the pathophysiology of AD and other neurodegenerative disease, including such as autophagy, tauopathy, and Aβ metabolism (Buller et al., 2008; Bhaskar et al., 2009; Zare-Shahabadi et al., 2015). However, in DHCR24 knock-down SH-SY5Y cells the implication of mTOR signaling still remains unknown. Further, we found that DHCR24 knock-down significantly and simultaneously decreased the level of phosphorylated GSK3β at Ser9 (inactive form) and increased the level of phosphorylated mTOR at Ser2448 (active form), and concomitantly phosphorylated Akt at Ser308/Ser473 were also significantly decreased in SH-SY5Y cells when compared with control cells, as shown in **Figures 6E,F,I,J,M,N,Q,R**. On the contrary, as shown in **Figure 6**, DHCR24 knock-in significantly increased the level of phosphorylated Akt at Ser308/Ser473 and increased the level of phosphorylated GSK3β at Ser9, and concomitantly decreased the level of phosphorylated mTOR at Ser2448 (**Figures 6G,H,K,L,O,P,S,T**). Thus, our results showed the activation of mTOR signaling in knock-down DHCR24 SH-SY5Y cells in comparison to control cells. However, mTOR integrates multiple signaling pathways, such as upstream components Akt and GSK3β. As a major downstream target of the PI3-K/Akt/mTOR pathway, the Akt activation usually lead to the increase of p-mTOR (Ser2448), and conversely the Akt inactivation can induce the decrease of p-mTOR (Ser2448) (Buller et al., 2008; Bhaskar et al., 2009). Moreover, GSK3β activation can also promote phosphorylated activation of mTOR (Ser2448) (Buller et al., 2008; Bhaskar et al., 2009). So, our data supported the activation of mTOR signaling could result from the stimulation of GSK3β signaling, and do not depend on the stimulation of PI3K/Akt signaling. Therefore, our results suggested that the knock-down of DHCR24 promoted the activation of mTOR signaling via PI3-K/Akt/GSK3β.

DISCUSSION

In present study, in SH-SY5Y cells, we found that silencing DHCR24 facilitated abnormal hyperphosphorylation of the tau sites, including Thr181, Ser199, Thr231, Ser262, and Ser 396. Conversely, the DHCR24 knock-in could abolish hyperphosphorylation of these p-tau sites. Very importantly, our results are tightly consistent with previous studies showing that Thr181, Ser199, Thr231, Ser262, and Ser 396 are major phosphorylation sites of p-tau in the progression of AD (Duka et al., 2013; Wang et al., 2013; Neddens et al., 2018). In Alzheimer disease, tau was hyperphosphorylated at over 80 epitopes of p-Tau (Wang et al., 2013). The accumulating data supported that the altered phosphorylation of some tau sites, such as Tau site at Thr181, Ser199, Thr231, Ser262, and Ser422, can lead to generate a gain of toxic function for tau (Wang et al., 2013; Neddens et al., 2018). P-tau could self-assemble into soluble aggregates of oligomeric tau, paired helical filaments (PHF), straight filaments (SF), or neurofibrillary tangles (NFT), and also convert tau into a prion-like protein, which are critical events in the pathological progression of AD (Duka et al., 2013; Moszczynski et al., 2015; Alonso and Cohen, 2018). Furthermore, it appears that phosphorylation of tau at Thr231 and Ser262 is critically involved in their self-assembly into PHF because phosphorylation of Thr231 and Ser262 appears to be necessary for the conversion of normal tau to pathological tau (Ikura et al., 1998; Alonso and Cohen, 2018; Alonso et al., 2018). Collectively, the abnormal hyperphosphorylation of tau not only lead to the loss of its normal function but also the gain of a toxic activity. Based on previous data, we confirmed that the altered phosphorylation of these tau sites induced by DHCR24 knock-down might be a critical event. In a word, we found that the abnormal phosphorylation of several toxic tau sites was obviously induced by DHCR24 downregulation. Therefore, our findings for the first time unraveled a relationship between DHCR24 downregulation and tauopathy.

Noticeably, in our study, *immunofluorescence and western blot analysis revealed* that the cholesterol level of plasma membrane and the expression level of membrane lipid raft-anchored caveolin-1, the principal structural protein of caveolae, were markedly lowered in SH-SY5Y cells with silencing DHCR24. Conversely, DHCR24 knock-in significantly increased the level of plasma membrane cholesterol and lowered the expression of membrane caveolin-1. Concomitantly, we found that the level of total class I PI3-K, Phospho-Akt (Ser473) and Phospho-Akt

(Thr308) were also markedly lowered by DHCR24 knock-down in SH-SY5Y cells. In contrast, the DHCR24 knock-in obviously increased the expression level of total class I PI3-K and the Phospho-Akt (Ser473 and 308), leading to the enhancement of PI3-K/Akt signaling. Thus, we considered that the decrease of PI3-K expression induced by DHCR24 knock-down could directly inhibited the phosphorylation activation of Akt, leading to the inhibition of PI3-K/Akt signaling. In addition, previous study suggested that brain cholesterol deficiency induced by silencing DHCR24 was associated with reduce of membrane cholesterol and altered membrane cholesterol-rich lipid-raft composition including the dysfunction of caveolae in cholesterol-rich lipid-raft microdomains, resulting in the markedly Akt inactivation, which is partly consistent with our outcomes (Lu et al., 2006). And cholesterol-rich caveolae in membrane lipid-rafts control a great variety of biological functions through their regulation of enzymes, receptors, neurotransmitter (Lynch and Mobley, 2000; Chini and Parenti, 2004). Moreover, it has been demonstrated that the main activation of Akt is done by PDK1 at cellular membranes and initiated by lipid raft-dependent kinases of the class I PI3K family (Lynch and Mobley, 2000; Chini and Parenti, 2004; Gao et al., 2011). To sum up, as the decline of cholesterol biosynthesis and caveolin-1 expression induced by DHCR24 knock-down, the disruption of lipid rafts/*caveolae* may lead to the alteration of raft-dependent functional protein kinase, such as PI3-K kinase (**Figure 7**). Together, DHCR24 knock-down lead to the decrease of cholesterol synthesis, the reduction of plasma membrane cholesterol and alteration of membrane lipid raft structure and function, and then induced the inhibition of PI3-K/Akt signaling.

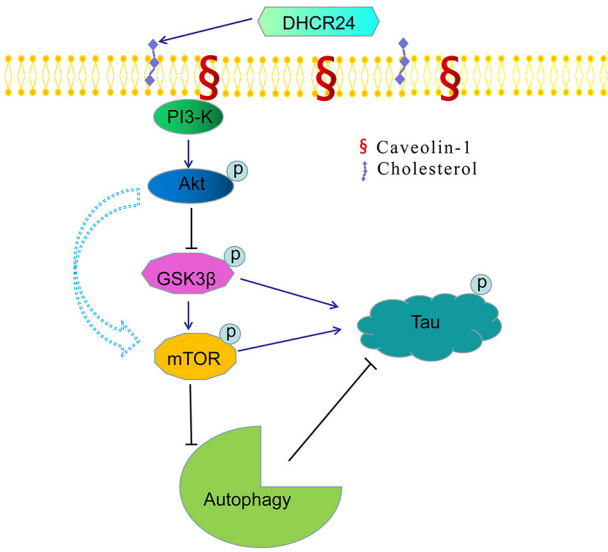

FIGURE 7 | A bridge connecting cholesterol and AD: knock-down of DHCR24 mediated disregulation of cholesterol homeostasis in regulating tau hyperphosphorylation and autophagy. DHCR24 knock-down could lead to the abnormality of membrane lipid raft structure and function, then in turn resulting in the inhibition of lipid raft-dependent PI3-K/Akt signaling. Moreover, it also enhanced the activation of GSK3β and mTOR signaling by lipid raft-dependent PI3-K/Akt signaling. In addition, DHCR24 knock-down obviously induced tau hyperphosphorylation and inhibition of autophagy by the overactivation of GSK3β and mTOR signaling via lipid raft-dependent PI3-K/Akt signaling, which are involved in the pathogenesis of AD.

In present paper, we also further showed that the DHCR24 knock-down could induce overactivation of GSK3β and mTOR kinase activity by the inhibition of PI3-K/Akt. Conversely, the DHCR24 knock-in could promote the activation of PI3-K/Akt signaling, and simultaneously inhibition of GSK3β and mTOR signaling. Furthermore, GSK3β was one of the first identified substrates of the heavily studied oncogenic kinase Akt, phosphorylation by which inhibits GSK3β activity. Akt activation is highly dependent on the class I PI3-K, and in turn promte the GSK3β at Ser9 phosphorylation and inhibition of GSK3β activity (Buller et al., 2008; Bhaskar et al., 2009). Obviously, in present study, overactivation of GSK3β signaling could be dependent on the inhibition of PI3-K/Akt. Thus, we firstly confirmed that DHCR24 knock-down induced the overactivation of GSK3β signaling through PI3-K/Akt pathway. Besides, it has been confirmed that mTOR activation is controlled by a variety of upstream components, including PI3-K/Akt and GSK3β (Bhaskar et al., 2009). In PI3-K/Akt/mTOR pathway manner, active p-Akt promotes the activation of mTOR through phosphorylation of the tuberous sclerosis complex 2 (TSC2), and active GSK3β has also been shown to phosphorylate mTOR and induce the activation of mTOR (Buller et al., 2008; Bhaskar et al., 2009). In present experiment, with the inhibition of PI3-K/Akt signaling by DHCR24 knock-down, leading to the inhibition of Akt signaling and the enhancement of GSK3β signaling, so the activation of mTOR signaling could be activated by the enhancement of GSK3β signaling through the inhibition of PI3-K/Akt pathway, but could be not directly dependent on inactive p-Akt. To sum up, mechanistically, the overactivation of mTOR was mediated by GSK3β through the inhibition of PI3-K/Akt pathway. Collectively, we showed that DHCR24 knock-down could induce the enhancement of GSK3β/mTOR signaling axis by PI3-K/Akt pathway.

In addition, the alteration of GSK3β and mTOR signaling plays a crucial role in tauopathy, which directly or indirectly participated in regulation of tau phosphorylation (Balaraman et al., 2006; Buller et al., 2008). In our study, we found that the silencing DHCR24 could induce the inhibition of PI3-K/Akt, simultaneously leading to the overactivation of GSK3β and mTOR kinase activity, as well as concomitantly the hyperphosphrylation of tau at Thr181, Ser199, Thr231, Ser262, and Ser 396 in SH-SY5Y cells (**Figures 2**, **6**). On the contrary, the DHCR24 knock-in could simultaneously reversed the effects of silencing DHCR24 on the inhibition of PI3-K/Akt signaling, overactivation of GSK3β and mTOR signaling, and the hyperphosphrylation of tau at Thr181, Ser199, Thr231, Ser262, and Ser 396 in SH-SY5Y cells (**Figures 2**, **6**). Previous data suggest that the GSK3β is one of main tau kinases, which nearly could phosphorylate tau at almost all the sites (Balaraman et al., 2006; Alejandra et al., 2010; Hernandez et al., 2013; Llorens-Marítin et al., 2014). Moreover, GSK3β participate in the phosphorylation of tau at multiple sites, which appear to be required to convert it into the pathological protein. These

sites include four clusters amino terminal to the microtubule binding domains, i.e. Thr181, Ser199/Thr205, Thr212/Thr217, Thr231/Ser235, Ser262, and Ser396/Ser422 regions (Alejandra et al., 2010; Llorens-Marítin et al., 2014; Alonso and Cohen, 2018; Alonso et al., 2018). Additionally, mTOR, another tau kinase, is involved in the regulation of tau phosphorylation. However, the mechanism of tauopathy mediated by mTOR is still unclear. Firstly, evidences suggest that activation of mTOR induces p-tau production and aggregation by GSK3β, and autophagy by mTOR (Caccamo et al., 2010; Yang and Klionsky, 2010; Zare-Shahabadi et al., 2015). Secondly, it has been reported that the activation of mTOR enhanced the expression levels of p70S6K and p4E-BP1 which further lead to the tauopathy (Caccamo et al., 2010; Cai et al., 2015). Additionally, the hyperphosphorylated tau is found to be attenuated by rapamycin, a potential inhibitor of mTOR (Caccamo et al., 2010; Spilman et al., 2010; Cai et al., 2015). Thus, we firstly confirmed that DHCR24 knock-down lead to the hyperphosphorylation of tau protein, at least partly, by the enhancement of GSK3β/mTOR signaling axis through PI3-K/Akt pathway.

Dysfunction of autophagy mechanism has been proposed to play a critical role in AD and other neurodegenerative disorders (Zare-Shahabadi et al., 2015; Zhang et al., 2017; Chang et al., 2018). Moreover, autophagy-lysosome defects occur early in the pathogenesis of AD and have been proposed to be a significant contributor to the disease process (Zare-Shahabadi et al., 2015; Zhang et al., 2017). Here, we have demonstrated that DHCR24 knock-down simultaneously increased the expression of P62 protein and lowered LC3II/LC3I ratio, leading to autophagy suppression in SH-SY5Y cells. Concomitantly, DHCR24 knock-down also increased the overactivation GSK3β/mTOR signaling (**Figures 3**, **6**). On the contrary, DHCR24 knock-in markedly promoted autophagy activity, and simultaneously lead to the inhibition of GSK3β/mTOR signaling in SH-SY5Y cells. LC3 and p62 are main markers for autophagy activity. P62/SQSTM1 is a multidomain protein that interacts with the autophagy machinery as a key adaptor of target cargo. P62 can directly interact with LC3 for autophagosome formation (Zhang et al., 2017). Further, the conversion of LC3-I to LC3-II denotes autophagy stimulation and autophagosome formation (Zare-Shahabadi et al., 2015). In addition, in our study, transmission electron microscope analysis revealed that the DHCR24 knock-down decreased autophagosome numbers in silencing SH-SY5Y cells compared to the blank or vector groups, suggesting the inhibition of autophagy (**Figure 3**). In contrast, DHCR24 knock-in reversed the effect of DHCR24 knock-down the decrease of autophagosomes. Furthermore, the autopagy-mediated dysfunction of tau protein and amyloid-β protein degradation mechanisms has been proposed to play a pivotal role in AD (Yang and Klionsky, 2010; Lee et al., 2013; Cai et al., 2015). Accordingly, with the tau hyperphosphorylation induced by DHCR24 knock-down in SH-SY5Y cells, the inhibition of autophagy could further cause the disturbance of homeostasis in p-tau clearance and deposition, involving in pathological process of tauopathy. Therefore, our outcomes strongly indicated that the DHCR24 knock-down obviously lead to the inhibition of autophagy through GSK3β/mTOR signaling axis.

Noteworthily, Ledesma et al. revealed that the neuronal membrane cholesterol have a significant reduction, the loss of neuronal membrane cholesterol and anomalous raft microdomains, which contribute to excessive amyloidogenesis in AD patients (Abad-Rodriguez et al., 2004; Ledesma et al., 2012). Besides, some data suggest there is a reduction in cholesterol in brain in aging and AD mice (Jacob et al., 2009; Ledesma et al., 2012; Llorens-Marítin et al., 2014; Mauricio et al., 2014). Generally speaking, in adult brain, differentiated neurons gradually lose their *de novo* synthetic ability and mainly rely on lipoprotein-conjugated cholesterol produced by Astrocytes (Dietschy and Turley, 2004). Thus, in the adult CNS cholesterol is mainly synthesized and regulated by astrocyte. The astrocyte meets neuronal cholesterol demands by secreting cholesterol-apolipoprotein complexes (Dietschy and Turley, 2004). Furthermore, some studies support that cholesterol synthetic genes in astrocytes were obviously down regulated in aging, diabetes and AD mice brain, suggesting the disruption of brain cholesterol biosynthesis and reduction in cholesterol synthesis in brain (Kleinridders et al., 2014; Orre et al., 2014; Lana et al., 2016; Boisvert et al., 2018; Han et al., 2020). It appears that there is an overall inhibition of cholesterol synthesis in astrocytes in neurodegenerative disorders, leading to the decrease of cholesterol synthesis and loss of cholesterol in brain. Very interestingly, in mice with knockout of SREBP2 in astrocytes, the loss of astrocyte cholesterol synthesis disrupted neuronal function and cognitive defects (Heather et al., 2017). Conversely, another important study showed that the loss of cholesterol in the hippocampus of aged mice produced a strong cognitive deficit, and cholesterol replenishment improved hippocampal cholesterol-loss-dependent cognitive decline (Mauricio et al., 2014). Similarly, DHCR24-deficient mouse brains had reduced levels of membrane cholesterol, and increased APP β-cleavage and Aβ production by disorganized cholesterol-rich lipid rafts, which showed similar reduction of membrane cholesterol than that reported in the AD patients (Abad-Rodriguez et al., 2004; Crameri et al., 2006; Ledesma et al., 2012). Based on our study and previous data, we propose that the decrease of plasma membrane cholesterol might tightly correlates with tauopathy and amyloid-beta pathology in AD and other neurodegenerative disorders.

In conclusion, in present study, our results further showed that DHCR24 could control the rate of cholesterol synthesis and cholesterol homeostasis by the Bloch pathway and/or K-R pathway. As a synthetase heavily involved in cholesterol synthesis, DHCR24 knock-down significantly lead to a reduction of cholesterol in plasma membrane and intracellular compartments, resulting in the cholesterol loss in SH-SY5Y cells. Furthermore, the decrease of plasma membrane cholesterol mediated by DHCR24 deficiency might contribute to the tauopathy in AD and other tauopathies, at least partly by membrane lipid raft-mediated signaling mechanism (**Figure 7**). Taken together, our outcomes provided convincing evidence supporting the importance of DHCR24 in the context of neurodegenerative disorders, highlighting the therapeutic potential and value in researching its activity further.

DATA AVAILABILITY STATEMENT

The raw data supporting the conclusions of this article will be made available by the authors, without undue reservation, to any qualified researcher.

AUTHOR CONTRIBUTIONS

HZ designed the study and wrote the manuscript. XB contributed to the experimental work about tau phosphorylation and autophagy. JW and MZ contributed to the transfection work of SH-SY5Y cells. YX, LD, and KY provided their experimental assistance and TEM work. JZ and JB contributed to analysis of data. YZ and GX provided their technical assistance. All authors have read the manuscript and provided the input.

FUNDING

This work was supported by research Grants 201740209 from the Shanghai Health and Medical Development Foundation, JSZK2015A05 from the Shanghai Jinshan District Key Medical Foundation, Shanghai, China, and JYQN-JC-202007 from the Jinshan Hospital, Fudan University, Shanghai, China.

SUPPLEMENTARY MATERIAL

The Supplementary Material for this article can be found online at: https://www.frontiersin.org/articles/10.3389/fnagi.2021.513605/full#supplementary-material

REFERENCES

Abad-Rodriguez, J., Ledesma, M. D., Craessaerts, K., Perga, S., Medina, M., Delacourte, A., et al. (2004). Neuronal membrane cholesterol loss enhances amyloid peptide generation. *Cell Biol.* 167, 953–960. doi: 10.1083/jcb.200404149

Alejandra, D. A., John, D. C., Bin, L., Christopher, P. C, Alaniz, M. E., Grundke-Iqbal, I. (2010). Phosphorylation of tau at Thr212 Thr231 and Ser262 combined causes neurodegeneration. *J. Biol. Chem.* 285, 30851–30860. doi: 10.1074/jbc.M110.110957

Alonso, A. D., and Cohen, L. S. (2018). Our tau tales from normal to pathological behavior. *J. Alzheimers Dis.* 64, S507–S516. doi: 10.3233/JAD-179906

Alonso, A. D., Cohen, L. S., Corbo, C., Morozova, V., ElIdrissi, A., and Phillips, G., et al. (2018). Hyperphosphorylation of tau associates with changes in its function beyond microtubule stability. *Front. Cell Neurosci.* 12:338. doi: 10.3389/fncel.2018.00338

Balaraman, Y., Limaye, A. R., Levey, A. I., and Srinivasan, S. (2006). Glycogen synthase kinase 3beta and Alzheimer's disease: pathophysiological and therapeutic significance. *Cell Mol. Life Sci.* 63, 1226–1235. doi: 10.1007/s00018-005-5597-y

Berisha, S. Z., Serre, D., Schauer, P., Kashyap, S. R., and Smith, J. D. (2011). Changes in whole blood gene expression in obese subjects with type 2 diabetes following bariatric surgery: a pilot study. *PLoS ONE* 6:e16729. doi: 10.1371/journal.pone.0016729

Bhaskar, K., Miller, M., Chludzinski, A., Herrup, K., Zagorski, M., and Lamb, B. T. (2009). The PI3K-Akt-mTOR pathway regulates Abeta oligomer induced neuronal cell cycle events. *Mol. Neurodegener.* 4:14. doi: 10.1186/1750-1326-4-14

Bing, L., Wu, J., Zhang, J., Chen, Y., Hong, Z., and Zu, H. (2015). DHT inhibits the Aβ25-35-induced apoptosis by regulation of seladin-1, survivin, XIAP, bax, and bcl-xl expression through a rapid PI3-K/Akt signaling in C6 glial cell lines. *Neurochem. Res.* 40, 41–48. doi: 10.1007/s11064-014-1463-3

Boisvert, M. M., Erikson, G. A., Shokhirev, M. N., and Allen, N. J. (2018). The aging astrocyte transcriptome from multiple regions of the mouse brain. *Cell Rep.* 22, 269–285. doi: 10.1016/j.celrep.2017.12.039

Buller, C. L., Loberg, R. D., Fan, M. H., Zhu, Q., Park, J. L., Vesely, E., et al. (2008). A GSK3/TSC2/mTOR pathway regulates glucose uptake and GLUT1 glucose transporter expression. *Am. J. Physiol. Cell Physiol.* 295, C836–C843. doi: 10.1152/ajpcell.00554.2007

Caccamo, A., Majumder, S., Richardson, A., Strong, R., and Oddo, S. (2010). Molecular interplay between mammalian target of rapamycin (mTOR), amyloid-beta, and tau: effects on cognitive impairments. *J. Biol. Chem.* 285, 13107C−13120C. doi: 10.1074/jbc.M110.100420

Cai, Z., Chen, G., He, W., Xiao, M., and Yan, L. J. (2015). Activation of mTOR: a culprit of alzheimer's disease? *Neuropsychiatr. Dis. Treat.* 11, 1015–1030. doi: 10.2147/NDT.S75717

Chang, H. Y., Sang, T. K., and Chiang, A. S. (2018). Untangling the Tauopathy for Alzheimer's disease and parkinsonism. *J. Biomed. Sci.* 25:54. doi: 10.1186/s12929-018-0457-x

Chini, B., and Parenti, M. (2004). G-protein coupled receptors in lipid rafts and caveolae: how, when and why do they go there? *J. Mol. Endocrinol.* 32, 325–338. doi: 10.1677/jme.0.0320325

Crameri, A., Biondi, E., Kuehnle, K., Lütjohann, D., Thelen, K. M., Perga, S., et al. (2006). The role of seladin-1/DHCR24 in cholesterol biosynthesis, APP processing and Abeta generation *in vivo*. *EMBO J.* 25, 432–443. doi: 10.1038/sj.emboj.7600938

Dhana, K., Braun, K. V. E., Nano, J., Voortman, T., Demerath, E. W., Guan, W., et al. (2018). An epigenome-wide association study of obesity-related traits. *Am. J. Epidemiol.* 187, 1662–1669. doi: 10.1093/aje/kwy025

Dietschy, J. M., and Turley, S. D. (2004). Thematic review series: brain Lipids. Cholesterol metabolism in the central nervous system during early development and in the mature animal. *J. Lipid Res.* 45, 1375–1397. doi: 10.1194/jlr.R400004-JLR200

Drzewińska, J., Pułaski, L., Soszyński, M., Bartosz, G. (2009). Seladin-1/DHCR24: a key protein of cell homeostasis and cholesterol biosynthesis. *Postepy Hig. Med. Dosw.* 63, 318–330.

Duka, V., Lee, J. H., Credle, J., Wills, J., Oaks, A., Smolinsky, C., et al. (2013). Identification of the sites of tau hyperphosphorylation and activation of tau kinases in synucleinopathies and Alzheimer's diseases. *PLoS ONE* 8:e75025. doi: 10.1371/journal.pone.0075025

Gao, X., Lowry, P. R., Zhou, X., Depry, C., Wei, Z., Wong, G. W., et al. (2011). PI3K Akt signaling requires spatial compartmentalization in plasma membrane microdomains. *Proc. Natl. Acad. Sci. U.S.A.* 108, 14509–14514. doi: 10.1073/pnas.1019386108

Giannini, S., Benvenuti, S., Luciani, P., Manuelli, C., Cellai, I., Deledda, C., et al. (2008). Intermittent high glucose concentrations reduce neuronal precursor survival by altering the IGF system: the involvement of the neuroprotective factor DHCR24 (Seladin-1). *J. Endocrinol.* 198, 523–532. doi: 10.1677/JOE-07-0613

Greeve, I., Hermans-Borgmeyer, I., Brellinger, C., Kasper, D., Gomez-Isla, T., Behl, C., et al. (2000). The human DIMINUTO/DWARF1 homolog seladin-1 confers resistance to Alzheimer's disease-associated neurodegeneration and oxidative stress. *J. Neurosci.* 20, 7345–7352. doi: 10.1523/JNEUROSCI.20-19-07345.2000

Han, X., Zhang, T., Zhang, T., Liu, H., Mi, Y., and Gou, X. (2020). Astrocyte senescence and Alzheimer's disease: a review[J]. *Front. Aging Neurosci.* 12:148. doi: 10.3389/fnagi.2020.00148

Heather, A., Ferris, R. J., Perry, G. V., Moreira, G. I., Shulman, J. D., Horton, C., and Ronald, K. (2017). Loss of astrocyte cholesterol synthesis disrupts neuronal function and alters whole-body metabolism. *Proc. Natl. Acad. Sci. U.S.A.* 114, 1189–1194. doi: 10.1073/pnas.1620506114

Hernandez, F., Lucas, J. J., and Avila, J. (2013). GSK3 and tau: two convergence points in Alzheimer's disease. *J. Alzheimer's Dis.* 33, S141–S144. doi: 10.3233/JAD-2012-129025

Ikura, Y., Kudo, T., Tanaka, T., Tanii, H., Grundke-Iqbal, I., Iqbal, K., et al. (1998). Levels of tau phosphorylation at different sites in Alzheimer disease brain. *Neuroreport* 9, 2375–2379. doi: 10.1097/00001756-199807130-00041

Ing, N. H., Forrest, D. W., Riggs, P. K., Loux, S., Love, C. C., Brinsko, S. P., et al. (2014). Dexamethasone acutely down-regulates genes involved in steroidogenesis in stallion testes. *J. Steroid. Biochem. Mol. Biol.* 143, 451–459. doi: 10.1016/j.jsbmb.2014.07.003

Jacob, R., Hascalovici, J. V., Soliman, K., Christina, A., Holcroft, H, Z., Wei, S., et al. (2009). Brain sterol dys-regulation in sporadic AD and MCI: Relationship to heme oxygenase-1. *J. Neurochem.* 110, 1241–1253. doi: 10.1111/j.1471-4159.2009.06213.x

Kazkayasi, I., Ismail, M. A., Parrado-Fernandez, C., Björkhem, I., Pekiner, C., Uma, S., et al. (2016). Lack of insulin results in reduced seladin-1 expression in primary cultured neurons and in cerebral cortex of STZ-induced diabetic rats. *Neurosci. Lett.* 633, 174–181. doi: 10.1016/j.neulet.2016.09.018

Khuda, I. I., Koide, N., Noman, A. S., Dagvadorj, J., Tumurkhuu, G., Naiki, Y., et al. (2010). Seladin-1 is a novel lipopolysaccharide (LPS)-responsive gene and inhibits the tumour necrosis factor-α production and osteoclast formation in response to LPS. *Immunology* 131, 59–66. doi: 10.1111/j.1365-2567.2010.03274.x

Kleinridders, A., Ferris, H. A., Cai, W., and Kahn, C. R. (2014). Insulin action in brain regulates systemic metabolism and brain function. *Diabetes* 63, 2232–2243. doi: 10.2337/db14-0568

Kuehnle, K., Crameri, A., Kälin, R. E., Luciani, P., Benvenuti, S., Peri, A., et al. (2008). Prosurvival effect of HCR24/Seladin-1 in acute and chronic responses to oxidative stress. *Mol. Cell Biol.* 28, 539–550. doi: 10.1128/MCB.00584-07

Lana, M., Osborn, Willem, K.amphuis, Wytse, J., and Wadman, E.lly M., Hol. Astrogliosis: (2016). An integral player in the pathogenesis of Alzheimer's disease. *Prog. Neurobiol.* 144, 121–141. doi: 10.1016/j.pneurobio.2016.01.001

Ledesma, M. D., Martin, M. G., and Dotti, C. G. (2012). Lipid changes in the aged brain: effect on synaptic function and neuronal survival. *Prog. Lipid Res.* 51, 23–35. doi: 10.1016/j.plipres.2011.11.004

Lee, M. J., Lee, J. H., and Rubinsztein, D. C. (2013). Tau degradation: the ubiquitin-proteasome system versus the 3 autophagy-lysosome system. *Prog. Neurobiol.* 105, 49–59. doi: 10.1016/j.pneurobio.2013.03.001

Lemche, E. (2018). Early life stress and epigenetics in late-onset Alzheimer's dementia: a systematic review. *Curr. Genomics* 19, 522–602. doi: 10.2174/1389202919666171229145156

Liang, W. S., Dunckley, T., Beach, T. G., Grover, A., Mastroeni, D., Ramsey, K., et al. (2008). Altered neuronal gene expression in brain regions differentially affected by Alzheimer's disease: a reference data set. *Physiol. Genomics* 33, 240–256. doi: 10.1152/physiolgenomics.00242.2007

Livonen, S., Hiltunen, M., Alafuzoff, I., Mannermaa, A., Kerokoski, P., Puoliväli, J., et al. (2002). Seladin-1 transcription is linked to neuronal degeneration in Alzheimer's disease. *Neuroscience* 113, 301–310. doi: 10.1016/S0306-4522(02)00180-X

Llorens-Marítin, M., Jurado, J., Hernández, F., Ávila, J. (2014). GSK3β a pivotal kinase in Alzheimer disease. *Front. Mol. Neurosci.* 7:46. doi: 10.3389/fnmol.2014.00046

Lu, X., Kambe, F., Cao, X., Yoshida, T., Ohmori, S., Murakami, K., et al. (2006). DHCR24-knockout embryonic fibroblasts are susceptible to serum withdrawal-induced apoptosis because of dysfunction of caveolae and insulin-Akt-Bad signaling. *Endocrinology* 147, 3123–3132. doi: 10.1210/en.2005-1426

Lynch, C., and Mobley, W. (2000). Comprehensive theory of Alzheimer's disease. The effects of cholesterol on membrane receptor trafficking. *Ann. N. Y. Acad. Sci.* 924, 104–111. doi: 10.1111/j.1749-6632.2000.tb05568.x

Matthews, L. C., Taggart, M. J., and Westwood, M. (2008). Modulation of caveolin-1 expression can affect signalling through the phosphatidylinositol 3-kinase/Akt pathway and cellular proliferation in response to insulin-like growth factor I. *Endocrinology* 149, 5199–5208. doi: 10.1210/en.2007-1211

Mauricio, G., Martin, T. A., Alejandra, K., Cesar, V., Silvia, A., Menchón, I., S.alas, et al. (2014). Constitutive hippocampal cholesterol loss underlies poor cognition in old rodents. *EMBO Mol. Med.* 6, 902–917. doi: 10.15252/emmm.201303711

McGrath, K. C., Li, X. H., Puranik, R., Liong, E. C., Tan, J. T., Dy, V. M., et al. (2009). Role of 3beta-hydroxysteroid-delta 24 reductase in mediating antiinflammatory effects of high-density lipoproteins in endothelial cells. *Arterioscler. Thromb. Vasc. Biol.* 29, 877–882. doi: 10.1161/ATVBAHA.109.184663

Moszczynski, A. J., Gohar, M., Volkening, K., Leystra-Lantz, C., Strong, W., and Strong, M. J. (2015). Thr175-phosphorylated tau induces pathologic fibril formation via GSK3beta-mediated phosphorylation of Thr231 *in vitro*. *Neurobiol. Aging* 36, 1590–1599. doi: 10.1016/j.neurobiolaging.2014.12.001

Najem, D., Bamji-Mirza, M., Yang, Z., and Zhang, W. (2016). Aβ-induced insulin resistance and the effects of insulin on the cholesterol synthesis pathway and Aβ secretion in neural cells. *Neurosci. Bull.* 32, 227–238. doi: 10.1007/s12264-016-0034-9

Neddens, J., Temmel, M., Flunkert, S., Kerschbaumer, B., Hoeller, C., Loeffler, T., et al. (2018). Phosphorylation of different tau sites during progression of Alzheimer's disease. *Acta Neuropathol. Commun.* 6:52. doi: 10.1186/s40478-018-0557-6

Orre, M., Kamphuis, W., Osborn, L. M., Jansen, A. H. P., Kooijman, L., Bossers, K., et al. (2014). Isolation of glia from Alzheimer's mice reveals inflammation and dysfunction. *Neurobiol. Aging.* 35, 2746–2760. doi: 10.1016/j.neurobiolaging.2014.06.004

Sassi, C., Guerreiro, R., Gibbs, R., Ding, J., Lupton, M. K., Troakes, C., et al. (2014). Investigating the role of rare coding variability in Mendelian dementia genes (APP, PSEN1, PSEN2, GRN, MAPT, and PRNP) in late-onset Alzheimer's disease. *Neurobiol. Aging* 35, 2881. e1–2881. doi: 10.1016/j.neurobiolaging.2014.06.002

Segatto, M., Tonini, C., Pfrieger, F. W., Trezza, V., and Pallottini, V. (2019). Loss of mevalonate/cholesterol homeostasis in the brain: a focus on autism spectrum disorder and rett syndrome. *Int. J. Mol. Sci.* 20:3317. doi: 10.3390/ijms20133317

Sengupta, A., Kabat, J., Novak, M., Wu, Q., Grundke-Iqbal, I., and Iqbal, K. (1998). Phosphorylation of tau at both Thr 231 and Ser 262 is required for maximal inhibition of its binding to microtubules. *Arch. Biochem. Biophys.* 357, 299–309. doi: 10.1006/abbi.1998.0813

Sharpe, L. J., Wong, J., Garner, B., Halliday, G. M., and Brown, A. J. (2012). Is seladin-1 really a selective Alzheimer's disease indicator? *J. Alzheimers Dis.* 30, 35–39. doi: 10.3233/JAD-2012-111955

Shih, P. H., Wu, C. H., Yeh, C. T., and Yen, G. C. (2011). Protective effects of anthocyanins against amyloid β-peptide-induced damage in neuro-2A cells. *J. Agric. Food Chem.* 59, 1683–1689. doi: 10.1021/jf103822h

Spilman, P., Podlutskaya, N., Hart, M. J., Debnath, J., Gorostiza, O., Bredesen, D., et al. (2010). Inhibition of mTOR by rapamycin abolishes cognitive deficits and reduces amyloid-beta levels in a mouse model of Alzheimer's disease. *PLoS ONE* 5:e9979. doi: 10.1371/journal.pone.0009979

Vanmierlo, T., Bloks, V. W., van Vark-van der Zee, L. C., Rutten, K., Kerksiek, A., Friedrichs, S., et al. (2010). Alterations in brain cholesterol metabolism in the APPSLxPS1mut mouse, a model for Alzheimer's disease. *J. Alzheimers Dis.* 19, 117–127. doi: 10.3233/JAD-2010-1209

Wang, J. Z., Xia, Y. Y., Grundke-Iqbal, I., and Iqbal, K. (2013). Abnormal hyperphosphorylation of tau: sites, regulation, and molecular mechanism of neurofibrillary degeneration. *J. Alzheimers Dis.* 33(Suppl. 1), S123–S139. doi: 10.3233/JAD-2012-129031

Waterham, H. R., Koster, J., Romeijn, G. J., Hennekam, R. C., Vreken, P., Andersson, H. C., et al. (2001). Mutations in the 3beta-hydroxysterol Delta24-reductase gene cause desmosterolosis, an autosomal recessive disorder of cholesterol biosynthesis. *Am. J. Hum. Genet.* 69, 685–694. doi: 10.1086/323473

Yang, Z., and Klionsky, D. J. (2010). Mammalian autophagy. Core molecular machinery and signaling regulation. *Curr. Opin. Cell Biol.* 22, 124–131. doi: 10.1016/j.ceb.2009.11.014

Zare-Shahabadi, A., Masliah, E., Johnson, G. V., and Rezaei, N. (2015). Autophagy in Alzheimer's disease. *Rev. Neurosci.* 26, 385–395. doi: 10.1515/revneuro-2014-0076

Zerenturk, E. J., Sharpe, L. J., Ikonen, E., and Brown, A. J. (2013). Desmosterol and DHCR24: unexpected new directions for a terminal step in cholesterol synthesis. *Prog. Lipid Res*. 52, 666–680. doi: 10.1016/j.plipres.2013.09.002

Zhang, Y., Chen, X., Zhao, Y., Ponnusamy, M., and Liu, Y. (2017). The role of ubiquitin proteasomal system and autophagy-lysosome pathway in Alzheimer's disease. *Rev. Neurosci*. 28, 861–868. doi: 10.1515/revneuro-2017-0013

Zidovetzki, R., and Levitan, I. (2007). Use of cyclodextrins to manipulate plasma membrane cholesterol content: evidence, misconceptions and control strategies. *Biochim. Biophys. Acta* 1768, 1311–1324. doi: 10.1016/j.bbamem.2007.03.026

Conflict of Interest: The authors declare that the research was conducted in the absence of any commercial or financial relationships that could be construed as a potential conflict of interest.

Advantages of publishing in Frontiers

OPEN ACCESS
Articles are free to read for greatest visibility and readership

FAST PUBLICATION
Around 90 days from submission to decision

HIGH QUALITY PEER-REVIEW
Rigorous, collaborative, and constructive peer-review

TRANSPARENT PEER-REVIEW
Editors and reviewers acknowledged by name on published articles

Frontiers
Avenue du Tribunal-Fédéral 34
1005 Lausanne | Switzerland

Visit us: www.frontiersin.org
Contact us: frontiersin.org/about/contact

REPRODUCIBILITY OF RESEARCH
Support open data and methods to enhance research reproducibility

DIGITAL PUBLISHING
Articles designed for optimal readership across devices

FOLLOW US
@frontiersin

IMPACT METRICS
Advanced article metrics track visibility across digital media

EXTENSIVE PROMOTION
Marketing and promotion of impactful research

LOOP RESEARCH NETWORK
Our network increases your article's readership